Number 1 Volume 20 1956

BULLETIN

of the

Academy of Sciences of the USSR

- Physical Series -

(Izvestiia Akademii Nauk SSSR)
(Seriia fizicheskaia)

Reproduction rights reserved

by

Columbia Technical Translations
5 Vermont Avenue
White Plains, New York

Single Issues

$20

Annual Subscription

$210

Digitized by the Internet Archive
in 2024

https://archive.org/details/russian-academy-of-sciences-physics-bulletin_1956_20_part-1

TRANSACTIONS OF THE THIRD ALL-UNION CONFERENCE ON
THE PHYSICS OF COSMIC RAYS
(Continued from Vol. 19, Nos. 5 & 6)

ON THE ORIGIN OF COSMIC RAYS

- V.L.Ginzburg

Some specific ideas as to the origin of cosmic rays were developed in 1953, primarily on the basis of radio-astronomical data. It is superfluous here to describe in detail the various concrete results and the general model for the generation and evolution of cosmic rays in the Galaxy, for these are presented in Refs. 1 and 2. We shall, therefore, only note that it is the writer's thesis that cosmic rays are generated primarily in the envelopes of novae and supernovae and, possibly, other similar variable stars. The acceleration of the particles is accomplished by a statistical mechanism which is incomparably more effective in the envelopes of such stars than in interstellar space. Emerging from the envelopes of the novae (and similar variable stars) into interstellar space, the cosmic particles (hereinafter in using this term we refer only to the particles that make up cosmic rays) are scattered by interstellar magnetic fields. As a result they, like the rarefied intergas, come to occupy a quasi-spherical region (subsystem) whose radius is of the order of the Galactic radius ($R \sim 10^{23}$ cm). In wandering in interstellar space the cosmic particles gain practically no energy, since the statistical acceleration mechanism, proposed by Fermi, is ineffective for many reasons (see below). As for energy losses, deceleration by magnetic fields, leading to cosmic radio emission, would appear to operate primarily for electrons. For protons and nuclei such losses are negligibly small; for them the dominant losses are those due to nuclear collisions (we take no account of ionization losses, since we are here considering only sufficiently fast particles).

As has been shown by the author,[2] the available data either support the above picture or do not contradict it. Many questions of detail, however, can be answered only after further experimental and theoretical investigations. The aim of the present paper is to consider the results of several new studies that have appeared during the year and a half preceding this Conference (end 1954).

1

The premise mentioned above, that cosmic rays form (in contradistinction to the basic stellar population of the Galaxy) a quasi-spherical subsystem of about 10^{23} cm radius was arrived at by analyzing the intensity distribution of cosmic radio emission in the meter band with reference to the galactic coordinates. However, since we are located within the Galaxy, we necessarily encounter certain difficulties in separating the extra-galactic component of the cosmic radio emission. True, I.S.Shklovski and G.G.Getmantsev have concluded that the extra-galactic radiation can be reliably separated, and that the cosmic electrons (and, therefore, also the protons) form a quasi-spherical subsystem, yet it would undoubtedly be desirable to have more direct proofs. At present such proof, and in our opinion it is convincing proof, has been given by the study[3] of the radio isophotes of the Great Nebula in Andromeda (nebula M31). This nebula is a galaxy similar to our own and in view of its proximity has served as the object of many studies that have shed light also on the structure of our own Galaxy, investigation of which as a whole, for example in the visual part of the spectrum, is difficult for us because of the absorption of light by interstellar matter. Measurements at a wavelength of 3.7 meters have shown that the dimensions of nebula M31 in the radio region are substantially larger than in the optical region and that the visible nebula is surrounded by what may be called a "radio corona", that is, by a region emitting intense radio radiation. The intensity distribution of radio emission is identical with that to be expected in the case of the quasi-spherical cosmic ray distribution that is deduced from the data on radio emission in our own Galaxy. Thus it is shown that the character of the distribution of radio emission in the Galaxy is not related to the extra-galactic background, which obviously could not account for the characteristics of the distribution in M31. Furthermore, the character of the deduced distribution (the presence of an isotropic component in the galactic radio emission) has at the present time but one explanation, and this is related to the assumption that the radiation comes from magnetically decelerated electrons occupying a quasi-spherical region which encompasses our stellar Galaxy. Further support for this point of view may be forthcoming from measurements of the polarization of cosmic radio emission, but it may be considered well founded even now (see also below).

Without going into the details of other new results of radio astronomy (such as the work of I.S.Shklovski[18] on the nature of discrete sources of radio emission), we note that in Refs. 1 and 2 radio emission by novae was considered possible, but had not yet been experimentally observed at the time. It seems that radio emission has recently been discovered[4] from Nova Aquilae 1918, which is also indirect confirmation of our hypothesis that cosmic rays are generated not only in supernovae, but in novae as well. In addition, analysis of the distribution of cosmic radio emission throughout the sky leads to evidence[5] that the sources of primary cosmic rays occupy a region having the shape of a very flat spheroid of radius roughly equal to the distance of the sun from the center of the Galaxy. This distribution is in agreement with the data on the distribution of novae, and is not in conflict with the sparse data on the distribution of supernovae.

An argument against the assumption, made by some investigators, that the sources of cosmic rays are concentrated near the center of the Galaxy is furnished by the results of Ellis et al[6] on the latitude cutoff in the cosmic ray spectrum. Attempts[7] were made to explain the high-altitude cutoff by assuming that cosmic rays are generated in the region of the galactic center and that, therefore, the less penetrating component (protons with $cp < 10^9$ ev) cannot reach the earth as a result of ionization losses. An alternate point of view, relating the high-latitude cutoff to the influence of the solar magnetic field, is sometimes considered disproved because of the lack of evidence for a sufficiently great solar magnetic moment. As we have noted earlier[1], the assumption that the high-latitude cutoff is a result of ionization losses is open to serious objections and is in contradiction with radio astronomical data on the concentration and spectrum of cosmic electrons in the Galaxy. On the other hand, the magnetic cutoff may be caused not by the field of the sun proper but by the magnetic field of the whole solar system (see Ref. 1, p. 156). The work of Ellis et al[6] supports these conclusions, since it shows that the high-latitude cutoffs in the spectra of protons and multiply-charged particles (nuclei) occur at equal values of the magnetic rigidity, which is convincing proof of the magnetic character of the cutoff.

2

An extremely important problem for the theory of the origin of cosmic rays is interpretation of the changes in the composition and spectrum of cosmic particles during their wandering in interstellar space. Unfortunately, the solution of this problem is rendered difficult by lack of data on the probability of the various nuclear transformations as well as of reliable data on the primary flux of Li, Be, and B nuclei. However, even the results that have been reported[8] allow us to draw certain deductions with respect to the evolution of protons as well as the generation of electrons in interstellar space.

In Ref. 2, as in some other works, it was assumed that the cross section for the destruction of a fast proton is $2.5 \cdot 10^{-26}$cm^2, i.e., less than the "geometric cross section" ($4 \cdot 10^{-26}$cm^2), and also less than the cross section $\pi \left(\frac{\hbar}{m_\pi c} \right)^2 \approx 6 \cdot 10^{-26}$cm^2. This difference in the cross sections was introduced in connection with the possibility of non-catastrophic proton collisions. According to Ref. 8, in each collision of a proton of 10^9–10^{12} ev energy with an N or O nucleus, the proton loses about 30% of its energy and, thus, after n collisions its energy becomes $E_n \sim (0.7)^n E_0$, where E_0 is its energy prior to the first collision. Therefore, $E \sim 0.1 E_0$ after 6 or 7 collisions with N or O nuclei, and possibly even after 10 to 15 collisions with other protons. At the same time $E \sim \frac{1}{2} E_0$ after 2 collisions with a nucleus and, probably, after 3 or 4 collisions with another proton (on the average 1.5 to 2 collisions between nucleons may occur within an N or O nucleus). It follows that in calculating the energy losses due to collisions in interstellar space a cross section two to four times smaller than the geometric cross section ("an interaction cross section") must be used, i.e., a cross section no smaller than about 10^{-26}cm^2. This means that there is no reason to increase the value of the lifetime of the cosmic protons that was used in the energy calculations of Ref. 2 ($T = 4 \cdot 10^8$ years) by more than a factor of two; in view of the approximate nature of all the other data, this makes but little difference, especially since in taking account of the collisions in interstellar space in time T is reduced (see Ref. 2, Table II). Thus we can continue to use the value $T \approx 4 \cdot 10^8$ years (this corresponds to traversal of a 67 g/cm^2 thickness of hydrogen, since the concentration n of hydrogen atoms is taken as 0.1). This time may be considered to be the time it takes for a proton to lose a significant fraction of its energy (about 1/2 to 2/3), which is the important factor in energy balance calculations.* As for the lifetime of the cosmic particle itself, it is in no sense a universal constant, since it depends on the initial and final energy of the particle.**

In any case, the lifetime of the particles is not particularly relevant, since in treating the question of changes in the spectrum of cosmic protons we need merely use the time between collisions, or in other words, a cross section of the order of $4 \cdot 10^{-26}$cm^2.

---

*Note added in proof: This assertion is contradicted in an article by Terletski[19] that appeared after the present article was submitted. However, the corresponding conclusions of that author are unsubstantiated and mistaken, as is clear from what is said in the text of our article. Neither can Terletski's article as a whole withstand criticism, since it attempts to maintain Fermi's theory[15] without any serious modifications, which is impossible (see Refs. 12, 16, 17 and Section 3 of the present paper). We take this opportunity to note that some parts of this article are developed and presented in more detail in Ref. 20; Ref. 21 also bearing on this subject.

**It is clear from this in particular that a "number-of-particles" balance calculation is less reliable than an energy balance calculation. This fact has already been emphasized by the author elsewhere[1].

In what follows, in order not to introduce unnecessary complications, this cross section will be taken as equal to that for the average energy loss, since the possible difference by a factor of two is not particularly meaningful in view of the accuracy attainable at the present time, and, moreover, experimental data on the cross sections in hydrogen are lacking.

While it may be readily admitted that where energy losses are concerned the non-catastrophic character of proton-proton collisions is unimportant, it might be thought that it is of great import when we come to determining the spectrum. Yet in Ref. 2, as in most other investigations that take no special account of the role of secondary protons and other secondary particles, it is concluded that the spectrum of the cosmic particles injected into interstellar space (nuclei, protons and electrons) is about constant and, on the average, of the form

$$N(E) = \frac{K}{E^{\gamma}}, \tag{1}$$

where, for not excessively high energies, $\gamma \approx 2$–2.5 (for more details see Refs. 1 and 9) and E is the total energy per nucleon or electron.* This neglect of the change brought about in the spectrum by nuclear collisions in interstellar space is based essentially on the assumption that these collisions hardly change the spectrum, since the energy of the secondary products is proportional to that of the primary particles. Thus, if the energy of a secondary particle $E_2 = \delta E_1$, where E_1 is the energy of the primary particle, and δ depends only slightly or not at all on E_1 and E_2, then the spectrum of the secondary products is identical with the primary spectrum. This result follows directly from the fact that the transformation $E_2 = \delta E_1$ is simply a scale change, and the exponent γ cannot be altered by such a transformation. An interval of the primary spectrum $N_1(E_1)dE_1$ is transformed into an interval $N_2(E_2)dE_2$ of the secondary spectrum, i.e., we have $sN_1(E_1)dE_1 = N_2(E_2)dE_2$, where s is the number of secondary particles produced in the collision. From this (and the equality $E_2 = \delta E_1$) we obtain,

$$N_2(E_2) = \frac{s}{\delta} N_1\left(\frac{E_2}{\delta}\right); \tag{2}$$

in the case of (1) with $\gamma = 2$,

$$N_2(E) = \frac{s\delta K}{E^2}. \tag{3}$$

This result, of course, is true also if we consider the losses to be continuous and given by the law

$$\frac{dE}{dt} = -aE, \tag{4}$$

since the case (4) is the same as the previous one at the limit $\delta \to 0$.**

---

*The quantity N(E)dE is the concentration of particles in the interval dE; by definition $N(E > E_0) = \int_{E_0}^{\infty} N(E)dE$ is the integral spectrum.

**If (4) is valid, then the conclusion that the spectrum is constant can be derived by a method similar to that used on p. 366 of Ref. 2, as well as on the basis of equation (10) below. It should be noted that if (4) or (5) are valid, the spectrum does not generally remain constant if there exist other mechanisms slowing down or accelerating the particles. For the theory here developed, however, it is assumed that there are no such mechanisms for fast protons.

The production of secondary particles with energies proportional to that of the primary particle would seem entirely natural and, therefore, our assumption that the spectrum as a whole is not altered as a result of collisions in interstellar space is logical. Obviously final clarification of this question will be possible only when adequate experimental data on the spectrum of the secondary particles become available. For protons, as has been said, such data, within certain limits, are available and approximately support the relation

$$E_2 = \delta E_1, \tag{5}$$

for collisions of protons with light nuclei with an average value of $\delta \approx 0.3$ and $s \approx 1$ (i.e., one fast particle remains after the collision). For proton-proton collisions the value of δ may be about half the above. Thus the data of Vernov et al[8], pertaining to the principal part of the spectrum ($E \leqslant 10^{12}$ ev) substantiate the assumption that the proton spectrum remains constant even in the case of nuclear collisions.

The results of Vernov et al also allow us to reach certain conclusions as to the quantity and spectrum of the electrons produced as a result of collisions of primary protons with the particles of interstellar medium. Thus, we can presumably assume that for $E \leqslant 10^{12}$ ev (that is, for most of the primary protons) about 30% of the energy of the primary particle is expended on meson production. We may suppose that one third of these mesons are π° mesons, which give rise to gamma-rays that subsequently leave the Galaxy[2]. Of the remainder, about 20% of the energy probably goes into the production of $\pi^\pm$ mesons, about 10% into $\mu^\pm$ mesons and finally about 5% of the primary particle energy goes into electrons and positrons. In addition, there are some indications that only one secondary meson is a fast one and, therefore, that on the average only one electron or positron ($s \sim 1$) with an appreciable energy is produced per collision. However, the distribution of energy among the secondary electrons is not particularly important, since only the product $s\delta \approx 5 \cdot 10^{-2}$ enters into (3).

The number of secondary electrons and positrons produced per unit time in a unit volume, obviously, is given by (see (3))

$$Q = \int_0^\infty q_e(E)\,dE, \quad q_e(E_e) = \frac{s\delta K}{TE_e^2} = \frac{s\delta}{T} N_p(E_e), \tag{6}$$

where s and δ pertain to the secondary electrons and $N_p(E_e)$ is expression (1) for the protons; i.e., the concentration of protons with energy E_e per unit energy interval (the limits 0 and ∞ in this integral are, of course, merely conventional).

In contrast to protons and nuclei, electrons and positrons lose energy in moving through interstellar space as a result of deceleration by the magnetic fields:

$$\frac{dE_e}{dt} = -bE_e^2 = -\frac{2c}{3}\left(\frac{e^2}{mc^2}\right)^2 H^2 \left(\frac{E_e}{mc^2}\right)^2 = -0{,}98 \cdot 10^{-3} H^2 \left(\frac{E_e}{mc^2}\right)^2 \text{ ev sec}^{-1} \tag{7}$$

These losses lead to a change in the electron spectrum, so that for them $\gamma = 3$. The calculation is presented in Ref. 2. In a similar way it is easy to show that the spectrum of electrons with $q_e(E_e)$, when calculated by relation (6) with the losses (7) taken into account, is of the form

$$N_e(E_e) = \frac{1}{bE_e^2}\int_{E_e}^\infty q_e(E)\,dE = \frac{s\delta K}{bTE_e^3}. \tag{8}$$

It is simpler, however, to obtain the same result by using the continuity equation in "energy space", i.e., the equation

$$\frac{\partial N(E)}{\partial t} + \operatorname{div} j(E) = \frac{\partial N}{\partial t} + \frac{\partial j}{\partial E} = q,$$

where $j(E)$ is the flux of particles whose energy passes through the value E in unit time (see, for example, Ref. 10). If we take into account only the systematic acceleration, then

$$\frac{dE}{dt} = \varphi(E) \tag{9}$$

and, clearly,

$$j(E) = N(E)\frac{dE}{dt} = N(E)\,\varphi(E),$$

that is,

$$\frac{\partial N}{\partial t} + \frac{\partial}{\partial E}[\varphi(E)N] = q(E). \tag{10}$$

If, in addition, there occur collisions which knock the particles out of the energy interval under consideration, this equation takes on the form

$$\frac{\partial N}{\partial t} + \frac{N}{T} + \frac{\partial}{\partial E}[\varphi(E)N] = q(E), \tag{11}$$

where T is mean free path time, and $N = N(E,t)$. Equation (11) is a particular case of the analogous equation previously used by Logunov and Terletski,[11] wherein both the diffusion in interstellar space and the possibility of the fluctuation of particle energies were taken into account. In our case we can disregard these two effects, and can, therefore, make use of equation (11), which we have rederived for this purpose.

In the steady state ($\partial N/\partial t = 0$), we have, for electrons, taking (7) into account,

$$\frac{N_e}{T_e} - \frac{\partial}{\partial E_e}(bE_e^2N_e) = q_e(E_e) = \frac{s\delta K}{TE_e^2}, \tag{12}$$

whence

$$N_e(E_e) = \frac{e^{-\frac{1}{bT_eE_e}}}{bE_e^2}\int_{E_e}^{\infty} q_e(E)\,e^{\frac{1}{bT_eE}}dE. \tag{13}$$

For electrons in the Galaxy, the time T_e is determined by radiation losses in hydrogen; for which $T_e \sim 10^{16}$ sec (see Ref. 2). Also for $E_e = 10^9$ ev and $H = 10^{-5}$, we have $bE_e = 4\cdot 10^{-16}$, i.e., when $E_e > 10^9$ ev, $(bE_eT_e)^{-1} \ll 1$, and solution (13) becomes (8); obviously (8) is obtained directly from (12) when $T_e \rightarrow \infty$. The integral spectrum of the secondary electrons, according to (8), is

$$N_e(E > E_e) = \int_{E_e}^{\infty}\frac{s\delta K}{bTE^3}dE = \frac{s\delta K}{2bTE_e^2} = \frac{s\delta N_p(E > E_e)}{2bTE_e}, \tag{14}$$

where $N_p(E > E_e) = \int_{E_e}^{\infty} N_p(E)\,dE$ is the integral spectrum of the protons (the density of protons with $E > E_e$); in integrating it is assumed that s = const.

Putting $s\delta \sim 5\cdot 10^{-2}$, $T \sim 10^{16}$, $E_e \sim 10^9$eV, we obtain $N_e(E > E_e) \sim 6\cdot 10^{-3}N_p(E > E_e)$, i.e., we see that the number of secondary electrons of energy $E_e > 10^9$ ev is of the order of 0.6% of the protons (when we take into account that $\gamma > 2$, we obtain a lower value; see below). As is known[1,2,9], experiments give just this figure (0.6%) for the upper limit of the number of electrons (clearly, the exact agreement of these values is fortuitous). Thus even if the primary sources of cosmic rays emitted no electrons, a sufficient number of electrons could be produced by nuclear collisions to explain the observed cosmic radio emission (see Ref. 2). Yet, the accuracy of the data is not great enough to permit excluding the possibility, which we shall now consider, that the secondary electrons and positrons make up only a quarter, or even merely a tenth of the total number of electrons in the Galaxy. It would seem quite possible that fast electrons are generated in the cosmic-ray sources, since it is difficult to conceive of a particle-accelerating mechanism which is entirely ineffective for electrons; in addition, and this is more important, radio-astronomical data indicate the presence of relativistic electrons in the envelopes of novae and supernovae. As the envelopes diffuse, these electrons must enter interstellar space. However, these electrons on the whole must have energies $E_e < 10^9$ ev, and hence at $E_e > 10^9$ ev, the secondary electrons and positrons will play a relatively more important role than at lower energies.

The very important and interesting question of what fraction of the electronic component of the primary cosmic rays is made up of secondary particles as against particles accelerated in the source can, in principle, be answered by experiment. The point is that secondary light particles must comprise equal numbers of electrons and positrons. In the case of acceleration in stellar envelopes, on the other hand, only electrons should be observed, since there is no reason to suppose that there is a significant number of positrons in stellar envelopes (see, however, Ginzburg, Pikel'ner and Shklovski[21]). The experimental observation of the electron-positron component of cosmic rays outside the atmosphere of the earth is one of the outstanding problems of cosmic ray physics, as we have already noted elsewhere[1,2].

The above considerations lead to another conclusion, which we believe to be quite important. Let us assume that magnetic fields in the Galaxy are very weak or absent ($H \ll 3\cdot 10^{-6}$ oersted). In this case the losses caused by magnetic deceleration will be insignificant, and we may neglect the second term in (12), then

$$N_e(E_e) = \frac{s\delta K T_e}{T E_e^2}, \quad N_e(E > E_e) = \frac{s\delta K T_e}{T E_e} = \frac{s\delta T_e}{T} N_p(E > E_e). \tag{15}$$

For $T_e \sim T$ and $s\delta \sim 5\cdot 10^{-2}$, this gives $N_e(E > E_e) \sim 5\cdot 10^{-2} N_p(E > E_e)$ which is definitely in contradiction to the experimental data (see above, as well as Refs. 1 and 2). In (15) T means the time for interaction, which is probably 1.5 to 2 times less than the time (of the order of 10^{16} sec) it takes for a total energy loss. The time $T_e \sim 10^{16}$ is also the energy dissipation time for electrons, so that a somewhat longer electron lifetime should enter into (15). The value of $s\delta \sim 5\cdot 10^{-2}$ can likewise hardly be made smaller in spite of the fact that there are no direct data for hydrogen. In addition, it was assumed in (15) that $\gamma = 2$ for protons, whereas at $E \sim 10^{11}$-10^{12} ev, actually $\gamma = 2.5$. Using $\gamma = 2.5$, instead of (6) and (15) we have

$$q_e(E_e) = \frac{s\delta^{1,5} K}{T E_e^{2,5}}, \quad N_e(E > E_e) = \frac{s\delta^{1,5} T_e}{T} N_p(E > E_e). \tag{15a}$$

For $s \sim 1$ and $\delta \sim 5\cdot 10^{-2}$, we obtain from (15a) that $N_e(E > E_e) \approx 10^{-2} N_p(E > E_e)$.

Thus even with the artificial assumption, which contradicts radio astronomical data, that the accelerating mechanism in the primary sources is ineffective for electrons[12], but without taking into account the loss due to magnetic deceleration, we could expect to observe in the primary cosmic ray flux about 1 to 5% electrons with $E_e > 10^9$ ev; observations, however, show that the proportion of such electrons is less than 0.6%. The disparity here is not large enough to be entirely convincing, but as the data become more precise it should become possible to secure further convincing arguments in favor of the existence of interstellar magnetic fields, wherein the electrons lose energy which is converted into radiation at radio frequencies.

With respect to nuclear collisions in interstellar space, we note two minor points. In addition to unstable particles, antiprotons can be produced in nucleonic collisions, and these should reach the earth. Evaluations[13], however, show that the number of antiprotons is no greater than 0.1% of the number of protons, according to the available data. With respect to the nuclear component of primary cosmic radiation there is little new recent data, and here we shall refer only to the work of Stix[14], in which the value obtained for the ratio of the concentration N_L of Li, Be and B nuclei to the concentration N_H of all other nuclei with $Z \geqslant 6$ was N_L/N_H 0.37. This result does not contradict the assumption that the primary component of cosmic rays comprises a large proportion of Li, Be and B nuclei, as should be the case if equilibrium is attained between light and heavy ($Z \geqslant 6$) nuclei. Indeed, for equilibrium

$$\frac{\eta N_H}{T_H} = \frac{N_L}{T_L}, \text{ i.e., } \frac{\eta N_H}{l_H} = \frac{N_L}{l_L}, \tag{16}$$

where T_H and T_L are the lifetimes (for transformation to a different nucleus) of nuclei with $Z \geqslant 6$ and those with Z = 3, 4 or 5, respectively, $l_H = cT_H$ and $l_L = cT_L$ are the respective mean free paths and η is the fraction (relative number) of Li, Be and B nuclei produced in the disruption of nuclei with $Z \geqslant 6$.

According to the best data available $\eta = 0.22$, and since nuclei with Z 6 are primarily C, N and O nuclei, we may suppose that T_H is nearly equal to T_L, or, more specifically, $T_L/T_H \approx 1.5$ to 1.7 (see Table 10 in Ref. 9). From this we obtain $N_L/N_H = \eta T_L/T_H = 0.33$-$0.38$, which does not contradict the experimental values[14]. In order to answer the question of whether equilibrium exists between light nuclei (Li, Be and B) and heavy ones, the ratio N_L/N_H in primary flux as well as the values of η, l_H and l_L must be found with greater accuracy. (We note that in the work of Stix[14], as well as in some of the other literature, the basic attempt was not to find the equilibrium value of N_L/N_H, but to determine the distance χ that the nuclei travel in interstellar space. In doing so, it is assumed that the N_H nuclei are not recreated in space. Therefore $dN_H/d\chi \neq 0$, whereas for equilibrium $dN_H/d\chi = dN_L/d\chi = 0$ and equation (16) follows. In previous communications by the author and others[20, 21], new experimental data are presented for the ratio N_L/N_H, and it is shown that in calculating the equilibrium value of this ratio it is important to take into account the diffusion of the nuclei, which has not been done to the present time.) The determination of these values with greater accuracy is more important because if our point of view[2] is correct, then we should expect the value of the ratio N_L/N_H to be close to if not equal to the equilibrium one.

As for the energy spectra of the nuclei with different values of Z, if the fragments carry off an amount of energy proportional to the energy of the primary particle, as is most natural to suppose, the secondary particle spectrum, in particular that of the protons, should coincide with the spectrum of the primary nuclei. This is what is observed experimentally.

In summary, we may say that all available data on the secondary cosmic particles that are produced in interstellar space either support or do not contradict (where the data are inadequate or ambiguous) the theory of the origin of cosmic rays as here presented.

3

As has been noted in the introduction, we consider the acquisition of energy by the cosmic particles in interstellar space as practically negligible or non-existent. This conclusion[2] is based on the following argument. In the Fermi theory of interstellar acceleration[15], the exponent γ in the spectrum equation (1) is defined by the relation

$$\gamma = 1 + \frac{1}{\alpha T}, \tag{17}$$

where T is the mean free path time for nuclear interaction[*] and α is the coefficient in the equation for the statistical acceleration

$$\frac{dE}{dt} = \alpha E \approx \frac{u^2 c}{c^2 l} E, \tag{18}$$

(here u is the velocity of the regions of interstellar gas that transport the magnetic fields, l is the characteristic dimension of the regions with a quasi-homogeneous magnetic field, and the velocity v of the particles along the lines of force is set about equal to c).

In order to obtain the experimental value γ = 2–3 (we are considering a wide energy interval), we must set

$$\alpha T \approx 1 \tag{19}$$

in (17). In addition, if for protons $\alpha T_p \sim 1$, then (since α is independent of Z) we have for Fe nuclei $\alpha T_n = \alpha T_p \frac{T_n}{T_p} \approx \frac{1}{20} \alpha T_p \approx 1/20$, and $\gamma_{Fe} \approx 20$ (from a more careful calculation we obtain even $\gamma_{Fe} \approx 40$). Experiment[1,2,9] shows, however, that at an energy of $E \leqslant 3 \cdot 10^{10}$ ev per nucleon (and according to some data, also for $E \leqslant 10^{12}$ ev), the exponent γ is the same for the proton spectrum as for the nuclear one. This is the first difficulty encountered by the theory of interstellar acceleration. The second is that the kinetic energy at which the particles must be injected is very large because α is so small (according to (19) $\alpha \approx 5 \cdot 10^{-17}$ sec^{-1}); for Fe nuclei this injection energy is about $3 \cdot 10^{11}$ ev (see Ref. 2). For protons the injection energy is about 10^8 ev, but since the proton and nuclear spectra are identical and nuclei are known to be produced in large quantities (see Ref. 2), it is clear that the interstellar accelerating mechanism is ineffective at least up to energies of the order of 10^{12} ev.

At higher energies the assumption as to the effectiveness of this mechanism does not conflict with the direct experimental data, since the composition of the primary component at high energies (the percent of nuclei in the primary flux) is unfortunately not known at present. Indirect considerations, however, indicate that the interstellar acceleration mechanism is ineffective even at the highest energies. The primary spectrum has no "break" at large energies, whereas if the accelerating mechanisms were entirely different, at say, $E < 10^{12}$ ev (acceleration in the primary sources) and at $E > 10^{12}$ ev (interstellar acceleration), the matching of the spectra would be purely fortuitous. Furthermore astrophysical data in no way conflict with the assumption that α may be so small that interstellar acceleration is ineffective (that is, $\alpha T \ll 1$ and $\gamma \gg 1$). Finally, there is no necessity for assuming an interstellar acceleration in general, since even the fastest of the cosmic particles ($E \sim 10^{18}$ ev) can have been accelerated to their velocity in the envelopes of supernovae.

---

[*] This result, which was derived by Fermi[15] and the author[2] by different means, follows immediately from (11) if we put q = 0, $\varphi = \alpha E$ (see Fradkin[9] and Shklovski[18]) and $\partial N/\partial t = 0$. In taking account of secondary processes, i.e., when secondary protons are produced, $q(E) \neq 0$ in (11), and q itself depends on N. In this case we may, with some approximation, be able to use equation (11) with q = 0, but with other values of α and T. In the general case, in particular for calculating the fluctuations[11] and taking account of the secondary particles, the exponent γ is determined primarily by the value of αT and depends essentially on this parameter, since with $\alpha = 0$ there is no acceleration at all.

All these arguments force us to reject the interstellar accelerating mechanism (see Ref. 2). It has been necessary to emphasize this in the present article, because in two recent publications[12, 16] attempts are made to retain this mechanism by modifying it. It is, however, easy to see that the new form of the theory of interstellar acceleration also meets with some very serious difficulties and, in our opinion, does not correspond to reality. A criticism of this variant of the theory is contained in another article by the author;[17] hence we shall only summarize it briefly in the present report.

In order to overcome the noted difficulties encountered by the older variant of the interstellar acceleration theory,[15] it is assumed[12, 16] that the lifetime T of cosmic particles in the Galaxy is determined not by nuclear collisions, but by the time it takes the particles to escape from the Galaxy, which is the same for protons and nuclei and equal to about 10^6–10^7 years. In order to retain relation (19) the coefficient α must be

$$\alpha \sim 10^{-14}\ \mathrm{sec}^{-1} \tag{20}$$

(for $T = 4 \cdot 10^6$ years, $\alpha = 5 \cdot 10^{-15}$; see Ref. 17). The value in (20) is about 100 times larger than the previous value[2] $\alpha \approx 5 \cdot 10^{-17}$ and is favorable from the point of view of lowering the injection energy. But, on the other hand, the value $\alpha \sim (u^2/c^2)(c/l) \approx 10^{-14}$ is definitely in conflict with the expression

$$T \sim \frac{R^2}{6D} \gtrsim \frac{R^2}{cl} \tag{21}$$

for the time of diffusion (escape) of the particles from the Galaxy ($R \gtrsim 3 \cdot 10^{22}$ cm is the galactic radius, $D \sim (l v)/3 \lesssim (lc)/3$ is the diffusion coefficient). When the reflection of the particles from the "boundary" of the Galaxy is taken into account (that is, from the region in which the magnetic field falls off sharply), the above contradiction becomes even more serious. But without taking this into account, even for $R \sim 3 \cdot 10^{22}$ cm we have $l \gtrsim R^2/cT \sim 3 \cdot 10^{20}$ cm, $\alpha \lesssim u^2 c/c^2 l \sim 10^{-31}$ 2, and in order to obtain the value $\alpha \sim 10^{-14}$ it is necessary that u be greater than $2 \cdot 10^3$ km/sec.

At the same time, it follows from the astrophysical data[1] that in the clouds of interstellar gas u is of the order of 10 km/sec, and that in the most rarefied regions $u \sim 50$ km/sec. Therefore the modified Fermi mechanism (Ref. 12, 16) is closely tied to the assumption that the interstellar magnetic field is quasi-homogeneous along the arms of the galactic spiral[16]. But this assumption, as has been shown by Pikel'ner,[1] is not necessary for the explanation of the data on the interstellar polarization of light,[16] and is thus quite hypothetical. Moreover the volume of the spiral arms is only a small part of the total volume occupied by cosmic rays. Therefore even if the field along the spiral arms is quasi-homogeneous, there is, after all, no reason to assume that it is quasi-homogeneous everywhere. The latter assumption is, in particular, not in agreement with the fact that the primary cosmic radiation is isotropic, and it contradicts several other considerations which indicate that the magnetic field in the Galaxy is chaotic. It is even more important to note that for the field configuration suggested in the modified Fermi theory,[16] the acceleration no longer takes place according to the typical statistical mechanism, but as a result of unique "type a collisions"[15, 16]. The question of how probable these are in the Galaxy is still completely unanswered. Furthermore, the value $\alpha \sim 10^{-4}$ is in contradiction with the fact that there does not exist in the Galaxy a significant number of electrons with $E > 10^9$ ev (Refs. 2 & 17). (We take this opportunity to add to our previous remarks in Ref. 17 the observation that for $\alpha \sim 10^{-14}$ a magnetic field $H \sim 8 \cdot 10^{-6}-10^{-5}$ cannot completely decelerate secondary electrons and positrons, which should, therefore, be observed even if the primary sources are ineffective for accelerating electrons). If, among the particles of the primary component, there is a significant number of Li, Be, and B nuclei, which is extremely probable, then the value $T \sim 4 \cdot 10^6$ years contradicts also this fact (if we do not assume that the primary sources emit an extremely and implausibly large number of Li, Be and B nuclei). Finally, because of the escape of cosmic particles from the Galaxy, there must be 100 times as many particles generated in the primary sources, according to the modified theory,[12, 16] as was indicated in Ref. 2. Therefore, in spite of the fact that according to this modification most of the energy comes from interstellar space, the energy of the injectors must, within one or two orders of magnitude, be $Q \sim 10^{40}$ erg/sec, just as when no account is taken of the interstellar acceleration or of escape from the Galaxy.[1,2] It follows from this, first that the whole question of primary sources of cosmic rays remains as vital as before. In our opinion this question can be satisfactorily answered only by admitting that these sources are novae and supernovae. Second, in the modified interstellar acceleration theory the turbulent energy of interstellar matter should be entirely transformed to cosmic ray energy in a time on the order of $4 \cdot 10^6$ years, and this means that there should exist some very powerful unknown mechanism for agitating interstellar matter, which interferes with the cessation of chaotic motion (for more details see Ref. 17). As a consequence of all that has been said, it is clear that the modified theory of the origin of cosmic rays,[12,16] if it is at all possible to say that it does not contradict experiment, can be reconciled with it only at the cost of many completely ill-founded and improbable assumptions. In addition, the question of the primary sources remains just as acute in this theory as when the process of energy gain in interstellar space is ignored. We therefore feel that the articles of Morrison et al[12] and of Fermi[16] change nothing in what has already been said[2] about the state of the theory of the origin of cosmic rays.* In addition to this, the many considerations discussed above substantiate the model for the origin of cosmic rays previously developed by the author,[2] and briefly described at the beginning of this article.

P.N.Lebedev Physical Institute of the
Academy of Sciences of the USSR

---

*It should be noted that in the previous article[2] the author not only did not ignore, but on the contrary, emphasized the possible influence of the escape of cosmic particles from the Galaxy. This factor is undoubtedly important, but we do not consider it to be the principal factor determining the lifetime of cosmic particles. In any case, taking it into account does not make the theory of interstellar acceleration any more acceptable.

REFERENCES

1. Trudy 3-go soveshchaniia po voprosam kosmogonii. Proiskhozhdenie kosmicheskikh luchei. (Transactions of the 3rd Conference on Problems of Cosmogony. Origin of cosmic rays.) M. 1954.
2. V. L. Ginzburg, Usp. fiz. nauk, 51, 343 (1953); Fort. Phys., 1,659 (1954).
3. J. E. Baldwin, Nature, 174, 320 (1954).
4. J. G. Bolton, G. J. Stanley & O. B. Slee, Austr. J. Phys. 7,110 (1954).
5. G. G. Getmantsev, Uch. zapiski GGU (Scientific records of Gor'ki State University), 27, 23 (1954).
6. R. A. Ellis, M. B. Gottlieb & J. A. VanAllen, Phys. Rev.,95, 147 (1954).
7. C. Y. Fan, Phys. Rev., 82, 211 (1951).
8. S. N. Vernov, N. L. Grigorov, G. T. Zatsepin & A. E. Chudakov, Izv. AN SSSR, Ser. fiz., 19, 493 (1955).
9. M. I. Fradkin, Usp. fiz. nauk, 53, 305 (1954).
10. L. E. Gurevich, Osnovy fizicheskoi kinetiki (Basic physical kinetics) M. - L., 1940.
11. A. A. Logunov & Ia. P. Terletski, Izv. AN SSSR, Ser. fiz. 17,19 (1953).
12. P. Morrison, S. Olbert & B. Rossi, Phys. Rev., 94, 440 (1954).
13. M. I. Fradkin, Zhur. eksp. i teor. fiz., 29, 147 (1955).
14. T. H. Stix, Phys. Rev., 95, 782 (1954).
15. E. Fermi, Phys. Rev., 75, 1169 (1949).
16. E. Fermi, Ap. J. 119, 1 (1954).
17. V. L. Ginzburg, Doklady AN SSSR, 99, 703 (1954).
18. I. S. Shklovski, Doklady AN SSSR, 98, 353 (1954).
19. Ia. P. Terletski, Doklady AN SSSR, 101, 59 (1955).
20. V. L. Ginzburg, Trudy 5-go soveshchaniia po voprosam kosmogonii. (Transactions of the 5th Conference on Problems of Cosmogony.) M., 1956.
21. V. L. Ginzburg, S. B. Pikel'ner & I. S. Shklovski, Astr. Zhurn.,(Journal of Astronomy), 32, 503 (1955).

* * * * * * *

ON THE SPECTRUM OF PRIMARY PROTONS

- Ia.P.Terletski

It is almost universally accepted that cosmic rays are protons or ions of the heavier elements which have been ejected into space by stellar sources and then accelerated further while diffusing through the magnetized interstellar medium which is in turbulent motion.[1-5] It has not yet been established what type of star is the principal source nor is there a definitive characterization of the nature and motion of the interstellar medium. However, there is no doubt that the power-function form of the primary particle energy spectrum is largely due to the diffusion of the particles in the magnetized, ionized medium in turbulent motion.

In contrast to Fermi,[2] who based his explanation of the shape of the energy spectrum on the concept of acceleration of the particles owing to encounters with magnetized clouds (see, for example, Ref. 6), in our work[3,4,7,8] we investigated a diffusion equation of the form

$$\frac{\partial f}{\partial t} - D\Delta f + \frac{\partial}{\partial E}[\alpha E f] - \frac{\partial^2}{\partial E^2}[\alpha E^2 f] + \frac{1}{T} f - \frac{\partial}{\partial E}(\beta E^2 f) = Q, \qquad (1)$$

where $f = f(E, r, t)$ is the particle distribution function in space and in energy; $\alpha = \frac{1}{\tau}\left(\frac{u}{c}\right)^2$; c is the velocity of light; u is the mean velocity of the turbulent pulsations; τ is the mean time of transit of a particle through a pulsation region; T is the mean free path time of a particle prior to its encounter with a proton of the interstellar gas; $D = c^2\tau/3$ is the coefficient of spatial diffusion; β is a coefficient defining the loss of energy by electromagnetic radiation in the magnetic field; $Q = Q(E, r, t)$ is the intensity of the primary cosmic ray sources and Δ is the Laplace operator. The term taking into account ionization losses has been omitted in the above version of the diffusion equation.

We have investigated the solutions of equation (1) for a point source of particles emitted with a given energy E_0 for two cases, namely, when the diffusion coefficient D is independent of energy[7] and when D is linearly dependent on the energy.[3,4] Our results for the first case differ little from Fermi's. The energy spectrum obtained is a power function: $f \sim E^{-\gamma}$ However, as in Fermi's theory, the exponent $\gamma = 1 + (\alpha T)^{-1}$ depends strongly on the numerical value of $\alpha T = \frac{T}{\tau}\left(\frac{u}{c}\right)^2$. This may be construed as a shortcoming of the theory, since agreement with the observed spectrum, in this case, is explained by the fortuitous coincidence of a number of different and entirely independent parameters entering into αT. The stationary solution for the second case (that is, on the assumption that $D = yE$, where y is a constant) was found in the form

$$f(E, r) \sim E^{-2,5} e^{-\frac{\beta}{\alpha}E}, \tag{2}$$

provided the conditions

$$E \gg E_0, \quad r \ll 2\sqrt{\frac{y}{\alpha}E} \quad \text{and} \quad \alpha T \gg 1. \tag{3}$$

were fulfilled.

In the energy range 10^{10}–10^{20} ev, the exponent in the expression (2) hardly differs from unity and the solution obtained agrees well with the observed distribution ($\gamma = 2$–3). According to this assumption, then, the exponent of the energy spectrum at sufficiently high values of αT is $\gamma = 2.5$, i.e., is independent of αT, which obviates the above mentioned shortcoming of Fermi's theory.

However, the assumption that $D = yE$ can be justified only for a restricted energy range. As Logunov has shown, D is constant at low energies, while at sufficiently high energies, $D \sim E^2$. The condition that $r \ll 2\sqrt{(y/\alpha)E}$ limits the theory to the case of a rather close grouping of the primary cosmic ray sources. For these reasons expression (2) cannot yet be regarded as a definitive solution of the problem of the spectrum of the primary component.

We will now discuss another vital defect which is common to both Fermi's theory and that of equation (1). In both cases it is assumed that in the collision of a proton, accelerated by the interstellar fields, with a stationary proton of the interstellar gas the former particle losses all its energy while the latter does not gain enough to begin to be accelerated by the interstellar fields. In other words, it is assumed that nucleon-nucleon collisions lead only to the loss of fast protons. In actual fact, in a collision between an ultra-relativistic proton and a stationary one either both particles acquire relativistic energies (when the collision is nearly inelastic) or one of the protons retains an ultra-relativistic energy (when the collision is nearly elastic). In any case, one or both particles can be accelerated anew by the interstellar fields. It is necessary to take this into account in a more complete theory.*

Let us assume that as the result of an encounter of a proton of energy E with a proton of the interstellar gas an average energy $a_0 E$ is expended on the production of π mesons, and that the final energies of the colliding protons are $a_1 E$ and $a_2 E$. It is clear that

$$\frac{dE}{T}\left\{\frac{1}{a_1} f\left(\frac{E}{a_1}\right)+\frac{1}{a_2} f\left(\frac{E}{a_2}\right)\right\} \tag{4}$$

protons will enter the energy interval E to E+dE per unit time as a result of collisions of higher-energy protons. Obviously, too,

$$a_1 + a_2 + a_0 = 1. \tag{5}$$

If we wish to take into account the formation of n nucleon-antinucleon pairs as a result of the collisions, instead of (4) and (5), we must write

$$\frac{dE}{T}\sum_{k=1}^{2n+2}\frac{1}{a_k} f\left(\frac{E}{a_k}\right) \quad \text{and} \quad \sum_{k=1}^{2n+2} a_k = 1 - a_0. \tag{6}$$

Restricting the discussion to the simplest case (4), we can write the equation for the distribution function in the form

$$\frac{\partial f(E)}{\partial t} - D\Delta f(E) + \frac{\partial}{\partial E}[\alpha E f(E)] - \frac{\partial^2}{\partial E^2}[\alpha E^2 f(E)] +$$

$$+\frac{1}{T}\left\{f(E)-\frac{1}{a_1} f\left(\frac{E}{a_1}\right)-\frac{1}{a_2} f\left(\frac{E}{a_2}\right)\right\}-\frac{\partial}{\partial E}[\beta E^2 f(E)] = Q(E). \tag{7}$$

For the sake of brevity the arguments r and t have been omitted above. It is clear that in taking more accurate account of the destruction and creation of fast protons in nucleonic collisions, the terms in the braces should be written in the form of integrals.

Let us consider the simplest solution of equation (7). We assume that the sources are uniformly distributed in space and emit particles of energies not exceeding E_0. In this case we can assume f to be independent of r and set $Q = 0$ in the energy region $E > E_0$. We note further that the term

$\frac{\partial}{\partial E}[\beta E^2 f]$, which allows for the radiation loss, is significant only at sufficiently high energies ($E > E_m = \alpha/\beta$) and may be omitted when $E < E_m$.

Let us consider the stationary solutions of equation (7) in the energy interval $E_0 < E < E_m$ in the light of the above assumptions. In this case (7) can be simplified to

$$\alpha T\left\{\frac{\partial}{\partial E}[E f(E)] - \frac{\partial^2}{\partial E^2}[E^2 f(E)]\right\} + f(E) - \frac{1}{a_1} f\left(\frac{E}{a_1}\right) - \frac{1}{a_2} f\left(\frac{E}{a_2}\right) = 0. \tag{8}$$

This equation has a solution of the type

$$f(E) = AE^{-\gamma}, \tag{9}$$

where A is an arbitrary constant and γ is defined by

$$-(\alpha T)(\gamma-1)^2 + 1 - a_1^{\gamma-1} - a_2^{\gamma-1} = 0. \tag{10}$$

---

*Fermi[2] noted that it was necessary to allow for the loss of energy not being complete, but he never considered the influence of this effect on the energy spectrum.

When $\alpha T \geqslant 0$ equation (10) has real roots only in the region $\gamma > 1$, since $a_1 < 1$ and $a_2 < 1$.

If the condition $\alpha T \ll 1$ holds, equation (10) will have two real roots: $\gamma_1 \to \infty$ and γ_2 defined by the equation

$$1 - a_1^{\gamma_2 - 1} - a_2^{\gamma_2 - 1} = 0. \qquad (11)$$

As a_0 increases from 0 to 1, in view of condition (5) γ_2 varies from 2 to 1. Hence for $\alpha T \ll 1$ and $a_0 \to 0$ the exponent γ in the expression (9) tends to the value 2. The second root of equation (10), $\gamma_1 \to \infty$, may be disregarded in this case.

The condition $a_0 \to 0$ may be taken as a realistic approximation in the given energy interval. According to the experimental data,[9] presented to the Conference by Grigorov, in interactions between primary protons of energies up to 30 Bev and stationary protons only a small part of the energy (not more than 30%) goes for meson production while the remaining energy is shared very unequally by the participating nucleons.

It is clear that in the $a_0 \to 0$ case the exponent γ is independent of the numerical value of αT when $\alpha T \ll 1$. However, the deduced value of γ is somewhat smaller than the experimentally observed one ($\gamma \leqslant 2$ instead of $\gamma = 2$–3).

When αT is large (at an arbitrary a_0) the real roots of equation (10) approach each other, becoming virtually identical somewhere in the $\gamma \geqslant 2$ region. At still larger values of αT equation (10) has no real roots in general.

Thus, for arbitrary values of αT, greater than zero and smaller than some critical number, there exist two solutions of equation (8), one with an exponent γ close to 2 and the other with an exponent γ exceeding 2 and tending to infinity as $\alpha T \to 0$. The latter solution corresponds to the solution obtained from Fermi's theory when this is extended to take fluctuations into account.[3]

In his thesis Iu. A. Popov also investigated the solution of equation (8) for the case of an instantaneous point source having a given energy. A nova or supernova, for example, may be such a source. He obtained a solution in the form

$$f = \frac{Q_0}{2\pi E_0} \frac{e^{-\frac{r^2}{4Dt}}}{(4\pi Dt)^{3/2}} \int_{-\infty}^{+\infty} e^{i\mu \ln E/E_0 - \alpha\mu^2 t + \frac{t}{T}(e^{i\mu\Delta_1} + e^{i\mu\Delta_2} - 1)}\, d\mu, \qquad (12)$$

where $\Delta_1 = \ln \frac{1}{a_1}$, $\Delta_2 = \ln \frac{1}{a_2}$, r is the distance to the source, and t is the time elapsed since the eruption of the source.

Analysis of the integral in (12) shows that for some interval of the parameter values, the energy spectrum is described by a power law. For example, when $a_1 = 0.1$, $a_2 = 0.6$, $a_0 = 0.3$ and $\alpha = 5 \cdot 10^{-18}$ sec^{-1} and $t = 10^{18}$ sec, we obtain the following results:

$\gamma = 2.2$ for $E \approx 10^{10}$ ev,
$\gamma = 2.5$ for $E \approx 10^{12}$ ev,
$\gamma = 2.8$ for $E \approx 10^{15}$ ev.

If we take the distance from the source to be $L \approx 10^{23}$ cm and $D \approx 10^{28}$ cm^{2}sec^{-1}, then $t = L^2/6D \approx 10^{18}$ sec. The results of these calculations will be given in greater detail in a separate article.

Thus taking account of the fast protons that remain after proton-proton collisions leads to qualitatively new solutions of the equation characterizing the diffusion cosmic ray particles in the interstellar medium. One of the solutions of equation (7), under certain general assumptions concerning the parameters entering into it, yields a distribution close to the observed distribution of cosmic ray protons in energy. Any theory of the origin of cosmic rays must take into account the fast protons produced in proton-proton collisions.

In the light of what has been said above it is clear that some recent estimates[10, 11] of the balance of the creation and destruction of cosmic ray particles in the Galaxy cannot be accepted as correct. The authors of Refs. 10 and 11 used these estimates to revive the hypothesis that the entire primary component of the cosmic rays is produced in the flare-ups of novae and supernovae.[12-15] These estimates are based, however, on an incorrect assumption regarding the total loss of energy by cosmic ray protons in their collision with the protons of the interstellar gas and, consequently, an unjustified neglect of the "multiplication" of fast particles, which we have taken into account in equation (4).

"M.V.Lomonosov"
Moscow State University

REFERENCES

1. Ia. P. Terletski, Usp. fiz. nauk, 44, 46 (1951).
2. E. Fermi, Phys. Rev., 75, 1169 (1949).
3. Ia. P. Terletski & A. A. Logunov, Zhur. eksp. i teor. fiz., 23, 682 (1952).
4. A. A. Logunov & Ia. P. Terletski, Izv. AN SSSR, Ser. fiz., 17, 119 (1953).
5. P. Morrison, S. Olbert & B. Rossi, Phys. Rev., 94, 440 (1954).
6. C. Y. Fan, Phys. Rev., 79, 912 (1950).
7. Ia. P. Terletski & A. A. Logunov, Zhur. eksp. i teor. fiz., 21,567 (1951).
8. A. A. Logunov & Ia. P. Terletski, Zhur. eksp. i teor. fiz., 26,129 (1954).
9. S. I. Brikker, N. L. Grigorov, I. V. Rybin & F. D. Savin, Doklady AN SSSR 86, 1089 (1952).
10. I. S. Shklovski, Doklady AN SSSR, 90, 983 (1953).
11. V. L. Ginzburg, Usp. fiz. nauk, 51, 343 (1953).
12. F. Zwicky, Proc. Nat. Acad. Sci. Wash., 25, 338 (1939).
13. F. M. Hoyl, [?] 106, 384 (1947).
14. D. Ter Haar, Rev. Mod. Phys., 22, 119 (1950).
15. L. Spitzer, Phys. Rev., 76, 583 (1949).

DIFFUSION AND ACCELERATION OF CHARGED PARTICLES IN A MAGNETIZED INTERSTELLAR MEDIUM

- A.A.Logunov and Ia.P.Terletski

The diffusion of charged particles in a magnetized interstellar medium is of paramount importance in interpreting the properties of primary cosmic radiation. Charged particles, emitted from sources in space, undergo a whole series of changes while traversing the interstellar medium. The mechanism of the passage of charged particles through the magnetized interstellar medium is analogous to the diffusion of particles in a gaseous medium.

In the ensuing discussion we assume that the interstellar magnetic field varies chaotically from one region of space to another. Let us denote the mean "dimension" of the homogeneous sections of the general magnetic field through L and the mean radius of curvature of the particle trajectories through R_k. Let us see how the diffusion coefficient depends on the particle energy. If the energy of the particle is such that $R_k \ll L$, then, in view of the chaotic structure of the magnetic field the motion of the particles through it will be characterized by wandering. Here, we can assume that the mean free path of the particles will be equal to the mean "dimension" of the homogeneous sections of the field and, consequently, in the given energy interval the particle diffusion coefficient will be constant.

When the energy of the particles is such that $R_k \gg L$, then, in view of the fact that the scattering is mainly forward, in order to establish the energy dependence of the diffusion coefficient we must evaluate the "transport mean free path" for particles moving in the magnetized medium. This "transport mean free path", λ, is the mean distance a particle will be displaced after traversing an infinite number of chaotically distributed homogeneous sections of the magnetic field. It is given by

$$\lambda = L(1 + \overline{\cos\theta_k} + \overline{\cos\theta_k}^2 + \ldots) = \frac{L}{1 - \overline{\cos\theta_k}},$$

where θ_k is the mean angle through which the particle is deflected in traversing one homogeneous section of the field.

Since the radius of curvature of a particle trajectory in a magnetic field H is

$$R_k = \frac{cp}{eH\sin\varphi},$$

where φ is the angle between the momentum of the particle and the magnetic field direction, we have

$$\overline{\theta_k^2} \approx \frac{L^2e^2H^2\overline{\sin^2\varphi}}{c^2p^2}.$$

Whence

$$\lambda \approx \frac{c^2p^2}{Le^2H^2}$$

while for the region of ultra-relativistic particle energies we have

$$\lambda \approx \frac{E^2}{Le^2H^2},$$

Consequently, the diffusion coefficient

$$D \approx \frac{cE^2}{Le^2H^2}.$$

If we assume that the diffusion coefficient is essentially a monotonic function of the energy, we can readily establish the nature of the energy dependence in the region of intermediate energies as well.

Next we turn to the process of acceleration of particles in the magnetized interstellar medium. The mechanism of the acceleration of charged particles in a magnetized interstellar medium was first examined by Fermi.[1] His analysis showed that particles could be accelerated in the medium, but inasmuch as the acceleration of high-energy particles was not considered, the analysis in Ref. 1 was incomplete. More detailed treatment of the acceleration process comprising the regions of both low and high particle energies has confirmed Fermi's original idea. In considering the acceleration process in the magnetized interstellar medium, we assume, where necessary, that the mean magnetic energy density is comparable with the mean kinetic energy density of the medium. In the case when the magnetic energy density is less than the kinetic energy density, the acceleration process under consideration will still occur; however, in this case there will prevail a more appreciable acceleration due to eddy fields, induced by the increasing strength of the general magnetic field.[2]

A detailed analysis (see Ref. 3) of the acceleration of charged particles moving in a magnetized medium leads to the following results:

1. When $R_k \ll L$, the acceleration of the particles obeys the law:

$$\frac{d\overline{E}}{dt} \approx \frac{1}{\tau}\left(\frac{u}{c}\right)^2 \overline{E},$$

which is identical with that given by Fermi.

When $R_k \gg L$, the expression describing the acceleration has the form

$$\frac{d\overline{E}}{dt} \approx \frac{\overline{Z^2e^2u^2H^2}}{E}\,\tau,$$

where τ is the mean time a particle spends in a homogeneous section of the magnetic field. A distinctive feature of this expression is that the extent of the acceleration depends on the charge of the particle. This feature, taken in conjunction with data on the absorption of particles in the medium, may make it possible to determine the cut-offs in the protonic and ionic component spectra.

Using the above equations for the acceleration laws and the values of the diffusion coefficient, one can deduce equations for the particle distributions both in space and in energy.[2]

However, not enough is known at present regarding the sources of cosmic radiation, the distribution of these sources and the way they behave for us to be able to reduce the problem of the cosmic ray spectrum to a specific boundary problem.

"M.V.Lomonosov"
Moscow State University

REFERENCES

1. E. Fermi, Phys. Rev., 75, 1169 (1949).
2. A. A. Logunov & Ia. P. Terletski, Izv. AN SSSR, Ser.fiz., 17, 119 (1953).
3. A. A. Logunov & Ia. P. Terletski, Zhur. eksp. i teor. fiz., 26, 129 (1954).

ON THE NATURE OF THE VARIATION OF COSMIC RAYS*

- L.I.Dorman

Introduction

Over the last two decades continuous measurements of the intensity of cosmic rays (hereinafter abbreviated - cr) have been made at several different stations - unfortunately, not distributed uniformly over the earth; during the last few years intensity of the neutron component has also been recorded at most stations. These measurements, the accuracy of which over an hour of recording attains several tenths of one percent, show that the intensity of cosmic rays is not entirely constant in time. A large number of different types of variations have been brought out; it has been found that the amplitude of some differs from that of others by almost four orders of magnitude: from several hundred percent to a few hundredths of one percent (see Table 1). However, until recently the investigators have been limited for the most part to collection of experimental facts and establishing empirical correlations between the cr variations and diverse other effects and phenomena.

This is due primarily to the fact that certain difficulties are encountered in attempting to clarify the nature of the cr variations and the character of the mechanisms involved in the relationships between these variations and the different geo- and helio-physical phenomena affecting cr intensity. Of these the principal difficulties are the following:

1. The observed variations in the intensity of the hard cr component (the principal component at sea level) are greatly subject to distortion by meteorological factors, which until very recently it has been impossible to discount quantitatively.

2. The primary cr component, interacting with the nuclei of air atoms, is increasingly transformed with the atmospheric depth. Hence observed variations in cr intensity, even when entirely free of the influence of meteorological factors, do not truly reflect the variations of the primary component. Furthermore, even if we could measure the variations of the primary component directly in the stratosphere we would still not know the energy spectrum of the variation, i.e., the dependence of the variation on the energy of the particles. The third principal difficulty follows therefrom.

3. The deflecting influence of the earth's magnetic field on the trajectories of charged cr particles differs for particles of different energy. Hence without knowing the spectrum of the variation we cannot determine the location of the "source", responsible for the variations in intensity, relative to the earth.

As a result of the investigations described in Refs. 1-5 the first difficulty has finally been largely overcome. Now, knowing the temperature profile in the atmosphere above the point of observation, we can accurately calculate the variation in the mu-meson component due to meteorological factors. The residual variations will therefore be essentially variations of the primary component.

Further, as will be shown below, we can establish the nature of the connection between variations of different cr components observed at different altitudes and different points on the earth (secondary variations), on the one hand, and variations in different portions of the energy spectrum of the primary component at the boundary of the atmosphere (primary variations), on the other hand. In this manner the second difficulty can be overcome, which in turn permits obviating the third difficulty as well.

---

* The questions touched upon are discussed in greater detail in the author's thesis listed under Ref. 65.

1. Correlation between the primary and secondary variations of cosmic rays

The way to establish a correlation between the primary and secondary variations of cr can be found if we make use of the vast experimental material accumulated on the geomagnetic effects associated with the different cr components.

Let us consider a cr component i (mu mesons, neutrons, stars, soft component, total ionizing component and the like) recorded at a geomagnetic latitude λ and a pressure altitude h_0. In general its global intensity can be characterized by

$$N^i_\lambda(h_0) = \int\limits_{\varepsilon^{min}_\lambda}^{\infty} D(\varepsilon)\, m^i(\varepsilon, h_0)\, d\varepsilon, \tag{1}$$

where $D(\varepsilon)$ is the differential energy spectrum of the primary component (principally protons), $m^i(\varepsilon, h_0)$ is the multiplicity,^{6} i.e., the number of particles of type i recorded at altitude h_0 and generated in the events initiated by one primary particle of total initial energy ε; $\varepsilon^{min}_\lambda$ is the effective geomagnetic cut-off, at the point of observation for protons vertically incident on the atmospheric boundary. When variations of some type j (diurnal, 27-day, decreased during magnetic storms, increases during large solar flares, etc.) are observed after elimination of meteorological effects (i.e., the data are reduced to a multiplicity $m^i(\varepsilon, h_0)$ constant in time) they will be due to variations of $D(\varepsilon)$. The relative change in intensity will be

$$\frac{\delta_j N^i_\lambda(h_0)}{N^i_\lambda(h_0)} = \frac{1}{N^i_\lambda(h_0)} \int\limits_{\varepsilon^{min}_\lambda}^{\infty} \delta_j D(\varepsilon) \cdot m^i(\varepsilon, h_0)\, d\varepsilon = \int\limits_{\varepsilon^{min}_\lambda}^{\infty} W^i_\lambda(\varepsilon,\ h_0) \cdot \frac{\delta_j D(\varepsilon)}{D(\varepsilon)}\, d\varepsilon, \tag{2}$$

wherein we shall term

$$W^i_\lambda(\varepsilon, h_0) = \frac{D(\varepsilon) \cdot m^i(\varepsilon, h_0)}{N^i_\lambda(h_0)} \tag{3}$$

the density of the correlation coefficient between the primary and secondary variations. Thus if the values of this coefficient are known and we have given the relative variation of the spectrum of primary particles $\frac{\delta_j D(\varepsilon)}{D(\varepsilon)}$ (say on the basis of some hypothesis being tested) we can use (2) to determine the secondary variations $\frac{\delta_j N^i_\lambda(h_0)}{N^i_\lambda(h_0)}$ and then, comparing these with results of observation prove or disprove the assumed hypothesis. Moreover, knowing $W^i_\lambda(\varepsilon, h_0)$, we can with sufficient accuracy for our purposes solve the inverse problem, i.e., determine the energy spectrum of the variation of the primary component from the secondary variations of different components, characterized by different correlation coefficients. The accuracy of such determinations will be all the higher the greater the number of different experimental data on the secondary variations of the given type utilized in the calculations.

Differentiating expression (1) with respect to the lower limits of the interval and taking (3) into account, we obtain

$$W^i_\lambda(\varepsilon^{min}_{\lambda'}, h_0) = -\frac{1}{N^i_\lambda(h_0)} \cdot \frac{\partial N^i_{\lambda'}(h_0)}{\partial \varepsilon^{min}_{\lambda'}}. \tag{4}$$

When we are concerned with primary particles subject to the influence of the

Table 1

Variations of Cosmic Rays (amplitude in %)

Type of variation	$\lambda = 50°$				$\lambda = 0°$		Origin*	Mechanism (nature of variation)*
	Hard comp. at sea level	Neutron comp. at sea or mountain level	Ionization at high altitudes	Hard comp. underground, 60 m.w.e.	Hard comp. at sea level	Neutron comp. at sea or mountain level		
Seasonal	$2 \div 4$	—	—	—	—	—	Atmospheric	Instability of π & μ mesons and absorption in the atmosphere (separated with the aid of the theory of meteorological effects).
Diurnal (masking effect of extra-atmospheric origin). .	$\sim 0{,}15$	—	—	—	$\sim 0{,}15$	—		
11-year	~ 2	—	—	—	~ 2	—	Extra-atmospheric	Class 1 (acceleration, deceleration and scattering of cosmic rays solar corpuscular streams transporting "frozen" magnetic fields).
Annual	$0{,}5 \div 1$	—	—	—	$0{,}5 \div 1$	—		
27-day	$\sim 0{,}3$	~ 1	—	—	$\sim 0{,}35$	—		
Solar day	$\sim 0{,}3$	$\sim 0{,}6$	$\leqslant 1 \div 2$	$\sim 0{,}05$	$\sim 0{,}35$	$\sim 0{,}43$		
Semi-diurnal	$\sim 0{,}03$	—	—	$\leqslant 0{,}02$	$\sim 0{,}03$	—		
Decrease during magnetic storms	$\leqslant 10$	—	~ 22	$< 0{,}5$	$\leqslant 10$	—		
Increase during large solar flares	$10 \div 40$	~ 550	—	$< 0{,}5$	$< 0\ 5$	—		Class 2 (generation of cr of several Bev energy on the sun, apparently by a statistical acceleration mechanism).
Increase during small solar flares	$\sim 0{,}3$**	$\sim 0{,}6$	$\leqslant 10$	—	—	—		
Sidreal day (existence open to question)	$\leqslant 0{,}02$	—	—	$\leqslant 0{,}02$	$< 0{,}02$	—		Class 3 (possible non-uniform distribution of sources; diffusion from the Galaxy, etc.).

---

*See "Conclusions" regarding the last two columns.

**The increase in intensity of the hard component during small solar flares is apparently of atmospheric origin (see Ref. 1 and below under Section 6). If this is the case the opposite effect should be oberved underground.

earth's magnetic field, i.e., particles of energies to $\mathcal{E}_0 = 15$ Bev, the right hand part of (4) can readily be evaluated from experimental data for the latitude effect (in a manner analogous to the calculations of Neher[6] and Simpson[7]). In the region of higher energies we take recourse to extrapolation. Bearing in mind that at higher energies the energy spectrum of the primary component and the multiplicity of generated particles are characterized by power functions,[8] we can set

$$W_\lambda^i(\varepsilon, h_0)_{\varepsilon>\varepsilon_0} = k\left(\frac{\varepsilon}{\varepsilon_0}\right)^{-a+\frac{b}{\varepsilon/\varepsilon_0}}, \tag{5}$$

where the second term in the exponent permits taking into account the possible weak dependence of the exponent on the energy; the constants k, a and b are determined from the conditions of normalizing the density of the correlation coefficient and the conditions of matching, at $\varepsilon = \varepsilon_0$, the extrapolated curve with the curve computed according to (4) on the basis of latitude effect data. The results of such calculations for some of the principal cr components for geomagnetic latitudes 50, 30 and 0° are presented in Figs. 1-3.

To applying this method one must have available data on the variation at different latitudes of the intensity of different cr components having markedly different primary-secondary correlation coefficients. The availability of such data at present cannot be described as highly satisfactory. Nevertheless we shall attempt to carry through the evaluations on the basis of currently available data. The internal consistence of the results leads us to believe that the principal attributes of the variation of cr are in the main correctly characterized. From the point of view of this analysis the greatest wealth of experimental data is available for the diurnal variation and the effect of the large solar flare of November 19, 1949. We shall examine these in the following sections.

2. The nature of diurnal variations of cosmic rays

Having examined the several different simpler forms of $\frac{\delta D(\varepsilon)}{D(\varepsilon)}$ (the primary variation), we found with the aid of (2), the case which best satisfies the available experimental data on the average (for several years) diurnal variation of different cr components at different altitudes and latitudes. Then

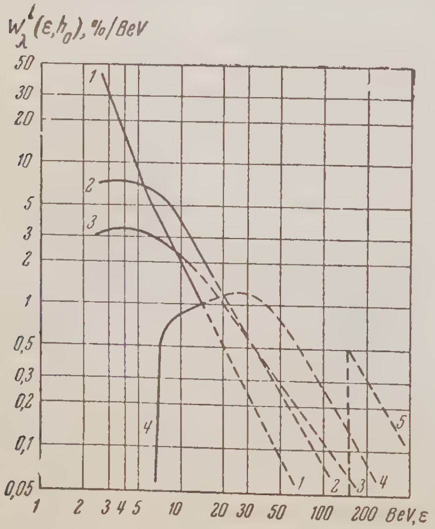

Fig. 1. Density of correlation coefficients at geomagnetic latitude $\lambda = 50°$ for the following cr components: 1) ionizing component in the stratosphere at great altitudes (computed according to Ref. 9), 2) neutron component at sea level (computed according to Ref. 7) 3) ionizing at mountain altitudes (computed according to Ref. 10 for 4300 m), 4) hard component at sea level (computed from the latitude effect taking the influence of meteorological factors into account - Ref. 5), 5) hard component at 60 m.w.e. (computed by extrapolation of curve 4 into the region of high energies on the basis of the further assumption that the pi meson carries off 15% of the energy of a primary particle in the first interaction of the particle with an air atom - Ref. 11). The solid curves are computed according to equation (4); the dash-line curves, are extrapolated according to equation (5).

from the determined energy spectrum of this primary variation, utilizing the results of Malfors[12] and Brunberg[13], we found the effective direction in which the particles must arrive in order to produce the observed diurnal variations. We obtained the following results.

1. The energy spectrum of the variation is described by

$$\frac{\delta D(\varepsilon)}{D(\varepsilon)} = \begin{cases} a(\bar{\Phi})\,\varepsilon^{-1}, & \text{when } \varepsilon > (7{,}5 \pm 0{,}5)\ \text{Bev,} \\ 0, & \text{when } \varepsilon < (7{,}5 \pm 0{,}5)\ \text{Bev.} \end{cases} \qquad (6)$$

The coefficient $a(\bar{\Phi})$ is given in the form of a curve in Fig. 4, where $\bar{\Phi}$ is the angle between the plane of the ecliptic and the effective direction of motion from infinity of the particles producing the diurnal variations. The value of $\bar{\Phi}$ is determined in each specific case by the geomagnetic latitude of the point of observation and the type of the recorded component (it is computed in the first approximation by means of (6) with a constant a and the curves in Figs. 1–3 according to the conventional formula for a weighted average; the distribution of $\bar{\Phi}(\varepsilon)$ is given in Refs. 12 & 13).

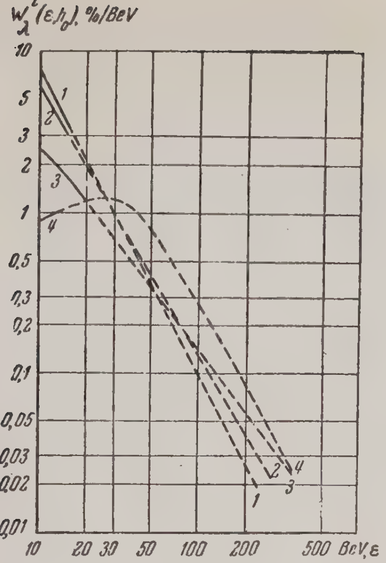

Fig. 2. Density of connection coefficients at geomagnetic latitude λ = 30°. Designations as in Fig. 1.

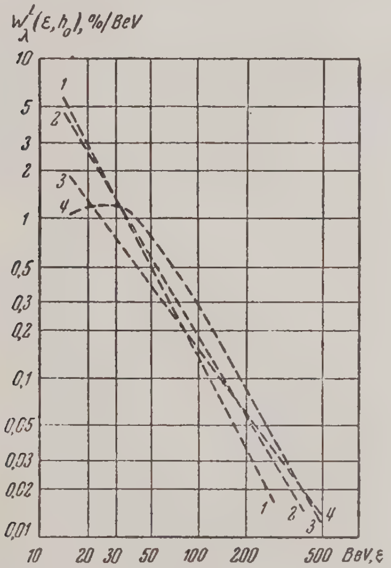

Fig. 3. Density of connection coefficients at the geomagnetic equator (λ = 0°). Designations as Fig. 1.

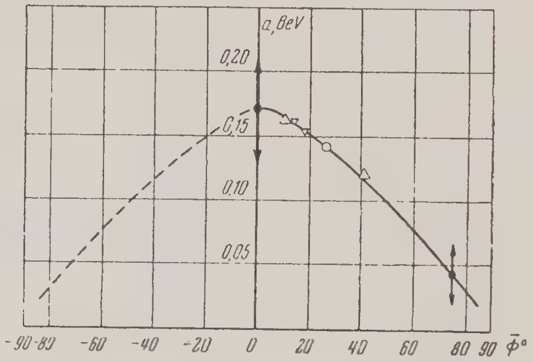

Fig. 4. Curve for $a(\bar{\Phi})$. The markings Δ, ∇, ○ & ↕ identify the results of calculations based on data for the observed diurnal variain the northern hemisphere (with the corresponding uncertainties associated with the inaccuracy of the data); the dash-line curve is a mirror image of the solid curve.

In this manner we find that the effective source of the additional flux of cr responsible for the increase in the intensity of cr in the daytime is located to the left of the sun (for an observer in the northern hemisphere) at an angle of 82 ± 8° to the earth-sun line and participates, together with the earth, in the annual revolution about the sun.

The results of calculations of the amplitude and phase of the diurnal variations on the basis of the deduced properties of this source, are in satisfactory agreement with the experimental results obtained for ten different cases of observation (Table 2). Thus the widely discussed distribution of the diurnal cr variations over the surface of the earth and their dependence on the direction of the arrival of the particles, the altitude of observation and the type of component recorded all fall into a single consistent pattern.

The deduced properties of the source permit us to reject immediately the hypothesis explaining the diurnal variations through the azimuthal effect in the general magnetic field of the sun, which gives variations only in the $\mathcal{E} \lesssim$ 5-6 Bev energy region,[14-19] or through direct emission of cr by the sun.[20-22]

From this point of view a somewhat more credible hypothesis is that of Elliot and Dolbear[23] to the effect that diurnal variations are produced by a mechanism of acceleration and slowing-down of cr on their way to the earth through corpuscular streams which, according to Alfven,[24] are polarized in moving through the solar magnetic field. According to Alfven, the particles crossing the corpuscular beam undergo an energy change of

$$\delta\varepsilon = 300\,\frac{u}{c}\,Hl\,\mathrm{eV}, \tag{7}$$

where u is the velocity of the stream ($\sim 10^8$ cm/sec), l is the width of the stream ($\sim 10^{12}$-10^{13} cm), H is the intensity of the general magnetic field of the sun near the earth's orbit ($H \lesssim 10^{-6}$ oersted) and c is the speed of light. Then the energy spectrum of the variation is

$$\frac{\delta D(\varepsilon)}{D(\varepsilon)} \approx \pm \frac{\Omega}{2\pi}(1+\gamma)\frac{\delta\varepsilon}{\varepsilon}. \tag{8}$$

Here the plus and minus signs correspond to streams passing to the left and right of the sun, if the direction of the solar field coincides with that of the earth. Here Ω is the solid angle under which the stream is viewed from the earth and γ is the exponent in the expression defining the energy spectrum of the undisturbed primary component.

Although (8) gives the correct location of the source relative to the earth-sun line and essentially the correct dependence of the variation on the particle energy, the Elliot-Dolbear[23] hypothesis encounters the following difficulties: a) the diurnal variations expected in conformity with (8) — as computed by means of (2) on the assumption that the intensity of the magnetic field of the sun at its surface does not exceed a few oersted[25,26] — prove to be some two orders of magnitude smaller than the observed variations; b) inasmuch as according to (8), in contrast to (6), particles of all energies are subject to variation, calculations by means of equation (2) give a value of 1:5 for the ratio of the amplitude of the diurnal variations of the hard and neutron components at sea level and 50° latitude; this is in marked conflict with the experimental value of 1:2 (obtained taking meteorological corrections into account - see Table 2).

In order to overcome these difficulties without sacrificing the basic idea of the hypothesis (i.e., that the diurnal variations are caused by corpuscular streams) we must accept the assumption that the streams are characterized by a high conductivity and hence can transport "frozen" magnetic fields.[24,27,59] Here, in addition to the influence of the electric field (arising in the fixed system of coordinates due to the motion of the corpuscular stream with a "frozen" in magnetic field relative to this system) an appreciable effect on the primary cr is also exerted by the "frozen" in field, which leads to scattering of low-energy particles (Fig. 5). If the stream is not incident on the earth, the magnetic field, due to the isotropy of cr, cannot produce any changes in the intensity of cr on the earth. The electric field, altering the energy of the particles traversing the corpuscular

Table 2

Variations of Cosmic Rays Expected on the Basis of (6) and Experimentally* Observed

Type of component	Amplitude						Time of maximum (local time), hours					
	λ = 0°		λ = 50°		λ = 80°		λ = 0°		λ = 50°		λ = 80°	
	Expected	Experimental	Expected	Experimental	Expected	Experimental	Expected	Experimental	Expected	Experimental	Expected	Experimental
Ionization at high altitudes	0,69	no data	0,41	1	0,11	no data	11,3	no data	15,3	no data	16,4	no data
Ionization at sea level	0,35	0,3±0,1**	0,49	no data	0,13	no data	12,8	13±0,5**	15,1	no data	16,3	no data
Neutron component at sea level	0,41	0,43±0,1	0,58	0,6±0,1	0,13	no data	11,4	12±1	14,5	14±0,5	16,1	no data
Hard component at sea level	0,33	0,3±0,1	0,30	0,3±0,1	0,09	0,1±0,03	13,3	13±0,5	14,9	15±0,5	15,9	16±1
Hard component underground (60 m.w.e.) .	0,06	no data	0,03	0,05±0,02	0,01	no data	16,0	no data	16,5	16±1	16,8	no data
Hard component at sea level:												
32° S	—	—	0,3	~ 0,3	—	—	—	—	15,9	16±0,5	—	—
32° N	—	—	0,3	~ 0,3	—	—	—	—	13,4	13±0,5	—	—

---

* The experimental data on the hard component have been corrected approximately for the influence of meteorological factors according to the procedures outlined in Ref. 1-4.

**Data pertain to ionization produced by the hard component.

stream, will lead to variations of the form described by (8), where $\delta\varepsilon$ is determined by the relationship (7), in which H is now understood to be the intensity of the magnetic field "frozen" into the stream. However, particles having an energy

$$\varepsilon \lesssim 300\,Hl, \qquad (9)$$

the trajectories of which in the stream have a radius of curvature less than l will be unable to cross the full width of the stream, so that for them the variation described by (8), due to the electric field, will not obtain. Thus, assuming

$$300\,Hl \approx 7{,}5 \cdot 10^{9}\ \text{ev}, \qquad (10)$$

(for which the field H must equal about 10^{-5} oersted with $l \approx 2\cdot10^{12}$ cm) we qualitatively satisfy the properties of the source (6).

For full qualitative agreement (we omit here details of the calculations connected with integrating the effect over all elements of a stream and averaging over all the streams, emitted with equal probability in all directions from the sun[65]) there must be simultaneous emission from the sun of 5–10 streams on the average and the number of such streams must increase somewhat with the helio-latitude (Fig. 6). If the normal to the plane of the ecliptic component of the magnetic field "frozen" into

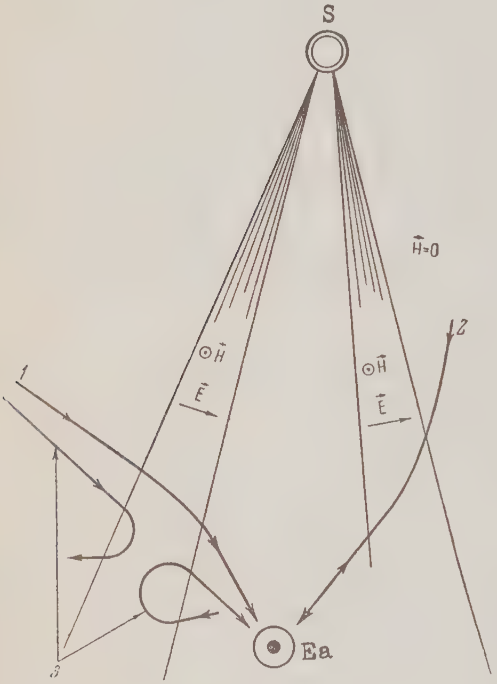

Fig. 5. Scheme of acceleration, slowing down and scattering of cr particles in corpuscular streams transporting "frozen" in magnetic fields not incident on the earth. S – sun; Ea – earth. 1) high-energy particles accelerated in passing through the field E in the stream (the direction of the "frozen" magnetic field coincides with that of the earth's field); 2) high-energy particles losing part of their energy in passing through the stream; 3) low-energy particles scattered in the "frozen" magnetic field.

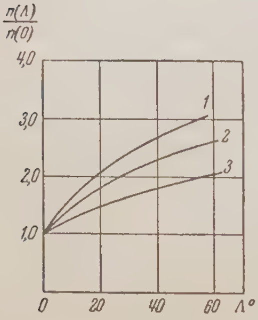

Fig. 6. Approximate helio-latitude dependence of the number of emitted streams carrying weak (H 10^{-5} oersted near the earth) "frozen" magnetic fields. Curves 1, 2 and 3 are plotted on the assumption that the angular width of the streams equals approximately 8, 15 and 30°, respectively. Ordinates: ratio of the number of streams emitted at the helio-latitude Λ to the number emitted at the helio-equator.

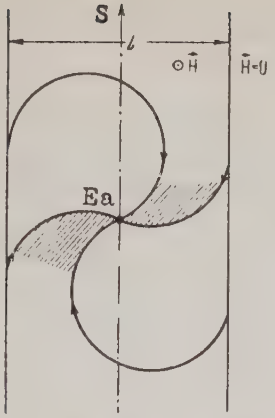

Fig. 7. Effect of scattering and deflection (curling) of particles by a "frozen" magnetic field when the stream falls on the earth (field normal to the plane of the drawing). S - to sun; Ea - earth. Hatched area - region of forbidden directions for particles with a radius of path curvature $l/4 < \rho < l/2$ where l is the width of the stream.

the stream is directed on the average in the same direction as the intensity of the earth's field, we obtain agreement with the results of the analysis of the experimental data on the second point as well. We have already spoken of the direction of arrival of the primary particles producing the diurnal variation at the beginning of this section.

If the intensity of the field "frozen" into the stream decreases in inverse proportion to the square of the distance from the sun (or more slowly), the expected value of the field intensity near the surface of the sun is 1 oersted. Hence it may be assumed that primarily the general magnetic field of the sun is "frozen" into streams of the discussed type.

The properties of the corpuscular streams requisite to explaining the principal characteristics of the diurnal cr variations are in agreement with the current concepts regarding the nature of the corpuscular streams eminating from the sun or in any case not in conflict with such concepts.

When the corpuscular streams strike the earth they give rise, according to our current concepts, to geomagnetic disturbances and polar auroras. In connection with the additional curling of the particle paths in the "frozen" magnetic fields of the streams (Fig. 7) the effective source of the diurnal variations is "displaced" clockwise towards the earth-sun line, which should lead to a shift of the maximum in the diurnal cr variation into the ante meridian hours. In connection with the marked increase in the effective solid angle Ω at these times there should also be observed an increase in the amplitude of the diurnal variations. Such shifts in the diurnal variations of cr during geomagnetic disturbances have actually been observed.[23,28,29]

3. On the variation in the intensity of cosmic rays during magnetic storms

When the corpuscular streams are incident on the earth, in addition to acceleration and deceleration of cr particles induced by the electric field there is also scattering of particles of relatively low energies by the "frozen" in magnetic field which leads to a further decrease in the intensity of the cr on the earth. Calculations carried out on the assumption that the earth is in the center of the corpuscular beam and that the "frozen" magnetic field is homogeneous show that the energy spectrum of the variation must have the form

$$\frac{\delta D(\varepsilon)}{(\varepsilon)} \approx f \begin{cases} -1, & \text{when } \varepsilon < 300\, H \frac{l}{4}, \\ -\frac{2}{\pi} \arcsin\left(\frac{300\, Hl}{2\varepsilon} - 1\right), & \text{when } 300\, H \frac{l}{4} < \varepsilon < 300\, H \frac{l}{2}, \\ 0, & \text{when } \varepsilon > 300\, H \frac{l}{2}. \end{cases}$$

Here f is a factor, equal to about 0.1-0.3, which is dependent upon the fraction of the particles moving perpendicularly to the magnetic lines of force and on the degree of homogeneity of the field. We determined the magnitude of this factor from comparison with experiment.

It follows from (11) that only particles having an energy

$$\varepsilon \leqslant 300\, H \frac{l}{2}. \qquad (12)$$

will be subject to the aforementioned variations. Insofar as this corresponds to energies inferior to 3-4 Bev in streams of the described type, the variation of the diurnal cr effect with the earth in the path of the corpuscular beam should not be accompanied by a decrease of any of the cr components at the equator or of the hard component at sea level at all latitudes. However, numerous experimental data show that in many cases (mainly during strong geomagnetic disturbances - great and very great magnetic storms) there is a noticeable decrease in the intensity of the cr components. At the same time the diverse mechanisms propose in the literature to explain the decrease in cr intensity during magnetic storms encounter serious, if not insuperable difficulties.

Thus, for example, the mechanism proposed by Chapman[30], associating this decrease with the existence of an equatorial ring current (postulated in the theory of magnetic storms[31]), according to Treiman's calculations[32] could act only when the radius of this ring is smaller than 1.3 times the radius of the earth. The expected (computed) decrease in the intensity proved to be only a few tenths or hundredths of the observed decrease. Furthermore, at latitudes where the latitude effect for a given component is absent with this mechanism, there should be observed no change in the intensity of this component; this too is in marked conflict with experimental data. (By way of example, one can cite the numerous data evincing a decrease during magnetic storms in the intensity of the hard component at sea level at geomagnetic latitudes 50° (Cheltenham, Md.) and 80° (Godhavn), whereas the latitude cutoff for the hard component occurs at 35-40° - Ref. 5)

On the other hand if the radius of the current ring exceeds 1.3 earth radii, according to Treiman[32] there should be an increase rather than a decrease in the cr intensity during magnetic storms, which is also in contradiction to the experimental data. (The radius of the ring is determined by the properties of the stream emitted by the sun and according to Chapman[31] equals some 3-5 earth radii; this value for the radius of the ring is substantiated by the results of spherical analysis of the field of magnetic storms.[33])

Alfven's hypothesis[24] on the effect of the electric field of the corpuscular streams on primary Cr (discussed above as regards its application to the diurnal variation) fares no better in the light of experimental data on the variation in the intensity of cr during magnetic storms. The expected changes in the intensities of cr, computed by means of our correlation coefficients, proved to be 2-3 orders of magnitude smaller than the observed changes; furthermore in accord with this hypothesis one should expect an increase rather than a decrease in cr intensity during storms.* Despite the conclusions reached by Trumpy,[34] the hypothesis cannot be salvaged by taking into account scattering of the particles by the electric field of the stream.*

---

*In a communication published after the closing date of the Conference on Cosmic Rays, Brunberg and Dattner[35] attempt to overcome these difficulties by recourse to a number of artificial assumptions regarding the nature of the general magnetic field of the sun and by taking into account the particle trajectories in this field. However, under these assumptions particles having energies less than 15-20 Bev could not reach the earth at all and to explain their presence on the earth it is necessary to make the further assump- that such particles are of purely solar origin and this in turn leads to even more serious difficulties.[36]

Table 3

Expected decreases in the intensity of different cosmic ray components during magnetic storms⊛

Intensity of the magnetic field near the earth assuming a stream width $l = 2 \cdot 10^{12}$ cm (in oersteds)	Decrease in cosmic ray intensity, %												
	λ = 50°				λ = 0°				Underground				
	Ionization at top of atmos.	Ionization at mt. altitudes	Neutron comp. at sea level	Hard comp. at sea level	Ionization at top of atmos.	Ionization at mt. altitudes	Neutron comp. at sea level	Hard comp. at sea level	10 m.w.e.	22 m.w.e.	45 m.w.e.	117 m.w.e.	400 m.w.e.
$0{,}5 \cdot 10^{-5}$	0,00	0,00	0,00	0,00	0,00	0,00	0.00	0,00	0,00	0,00	0,00	0,00	0,00
$1{,}0 \cdot 10^{-5}$	0,42	0,04	0,08	0,00	0,00	0.00	0,00	0,00	0,00	0,00	0.00	0,00	0,00
$3{,}0 \cdot 10^{-5}$	17,5	3,05	6,9	0,02	0,00	0.00	0,00	0,00	0,00	0,00	0,00	0,00	0,00
$5 \cdot 10^{-5}$	21,7	6,14	12,8	0,38	0.00	0,00	0,00	0.00	0.00	0,00	0,00	0,00	0,00
$1 \cdot 10^{-4}$	25,0	7.75	19,3	3,05	4,63	1,80	3,63	1,32	0,00	0,00	0,00	0,00	0,00
$2 \cdot 10^{-4}$	26,8	11,4	23,4	9,05	15,1	6,89	12.9	7,80	~3	0,00	0,00	0,00	0,00
$5 \cdot 10^{-4}$	27,7	15,2	26,4	18,8	21,9	12,1	19,8	18,2	~15	~14	~11	0,00	0,00
$2{,}5 \cdot 10^{-3}$	28,3	20,1	28,8	26,8	25,5	19,0	25,3	26,8	~25	~24	~22	~14	0,00

⊛The values in the table are computed in the light of the mechanism of scattering of cr particles by the magnetic fields "frozen" into the corpuscular streams on the assumption that f in eq.(11) is independent of the latitude and has a constant value of 0.3.

The failure of these hypotheses where interpretation of the observed decrease in the intensity of cr during magnetic storms is concerned prompts us to re-examine the possibilities of the mechanism of the scattering of cr particles by the magnetic fields "frozen" into corpuscular streams. Table 3 shows the results of calculations, made by means of eq. (2) (using the correlation coefficients of Figs. 1-3), for the case of the energy spectrum, described by (11), of the expected variations in intensity of different cr components at different latitudes with the earth in the path of corpuscular beams transporting "frozen" magnetic fields of different intensities (for definiteness of the calculations the width of the beam in the vicinity of the earth was taken equal to $2 \cdot 10^{12}$ cm). In order to verify the mechanism in question thoroughly, it is necessary to have data on the variations of the different cr components at different latitudes. Experimental data** available at present can be summarized from this point of view as follows:

1. Noticeable (1% or over) variations in the intensity of the hard cr component at sea level observed simultaneously at several points on the earth are apparently produced only by great or very great magnetic storms. Approximately 88% of such storms give rise to such noticeable variations. (There have, however, been observed cases when even very strong storms produced no noticeable change in the intensity - for example, the storm of August 21, 1937.[29]) At the same time only 8% of the moderate storms - to say nothing of

---

*In Ref. 34 the perturbing effect of the stream is examined on the assumption that the stream is infinite in extent in the plane of the particle's motion. But it would appear that even if the extent of the stream is regarded as finite,[65] the results of the calculations remain much the same as Alfven's.[24]

**To apply the method of correlation coefficients it is also important to know the intensity variations of the neutron component during magnetic storms. Unfortunately such data are not available in the literature.

weak storms - are accompanied by such changes in intensity and as a rule such changes are not world-wide.[37]

2. The variation in the intensity of the hard cr component at sea level during magnetic storms appears to be virtually independent of the latitude (more accurately speaking the effect at 50° latitude is only some 1.1 times greater than at the equator[38]).

3. Underground (at 60 m.w.e.) there is no noticeable change in the intensity of cr during magnetic storms.[39]

4. There is information on one case[40] (July 26, 1946) where during a very strong magnetic storm, following a solar flare-up, the cr intensity at about 20 km decreased by 22%, while at sea level the decrease amounted to some 7-8%.[29]

Comparison of our calculated results (Table 3) with the cited experimental data shows that the scattering by "frozen" magnetic field mechanism can wholly explain the now available experimental facts if we assume that great and very great magnetic storms are produced by corpuscular streams transporting "frozen" magnetic fields having intensities of about $2 \cdot 10^{-4}$ oersted near the earth (further assuming a stream width near the earth of $2 \cdot 10^{12}$ cm and $\beta \approx 0.3$), which value corresponds to an intensity of some tens of oersteds at the surface of the sun. In connection with this it may be expected that the local fields associated with sun spots and other solar formations may also be "frozen" into streams of this type.

The dependence of the magnitude of variations in the cr intensity during magnetic storms on the geomagnetic latitude is determined by the direction and distribution of the "frozen" field in the stream. Thus a detailed study of this distribution may make it possible to deduce more information on the electromagnetic properties of corpuscular streams.

4. On the nature of the 11-year, 1-year and 27-day variations in the intensity of cosmic rays and on day-to-day variations

Inasmuch as the geomagnetic activity is closely associated with the incidence of the corpuscular streams on the earth (accompanied by a decrease in the cr intensity), there must be a correlation between the cr intensity and some index characterizing the magnetic activity.

With an increase in the magnetic activity (increase in the number of beams striking the earth) there must be a corresponding decrease in the cr intensity. Experimental data[38-40] tend to confirm this and on the basis of such data Neher and Forbush[41] have deduced ratios for the amplitudes of the day-to-day variations of the different cr components; these are a) 7:1 for the ratio of the ionizing component at high altitudes (Bismarck) to the hard component at sea level (Cheltenham, Md.)*; b) 3:1 for the ratio of the neutron component at mountain altitudes (Climax and Sacramento Peak) to the hard component at sea level (Cheltenham)**; c) 1.1:1 for the ratio of the hard component at latitude 50° (Cheltenham) to the hard component at the equator (Huancayo).

It will be seen from Table 3 that in order to explain the observed ratios we must assume that the streams, producing the variations in cr intensity, carry "frozen" magnetic fields having a strength on the order of $1\text{-}2 \cdot 10^{-4}$ oersted in the vicinity of the earth (assuming a stream width of $2 \cdot 10^{12}$ cm). Inasmuch as the variations of the hard component, connected with such magnetic effects, have an amplitude of one or a few percent, it follows from Table 3 that for these streams $f \approx 0.1-0.2$. With increased solar activity the number of corpuscular streams emitted from the sun and incident on the earth increases, which leads to a more intense scattering of particles of relatively low energies and, consequently, to a decrease in the cr intensity on the earth.* The decrease in the intensity of the hard component should be approximately the same at the equator and at middle latitudes. However, although the investigations of Refs. 45 and 46 do give the correct qualitative dependence for the variation, the amplitude at the equator turns out to be greater than at the middle latitudes (5.8 and 2.4%, respectively).**

---

*Comparable results for these same components - 10:1 and 6:1 have been obtained in Refs. 42 and 43.

**This value is comparable with the ratio of 5:1 found in Ref. 44 for the amplitudes of the 27-day variations of the same components.

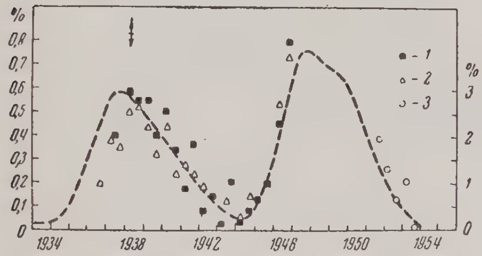

Fig. 8. Changes in the amplitude of the 27-day variations in the hard and neutron cr components with the solar activity cycle (according to Ref. 48). Abscissa: time in years; ordinates: amplitude of 27-day variations in percent (left hand scale pertains to the Carnegie Institute ionization chamber data; the right hand scale, to neutron detector data. 1) averaged ionization chamber data for Huanacayo and Cheltenham; 2) averaged neutron detector data for Huanacayo and Christchurch. Double-arrow indicates maximum probable uncertainty of the experimental points. The dash line curve gives the relative number of sunspots R (Zürich data).

Inasmuch as the geomagnetic activity generally attains a peak during the equinoctial periods,[31] we may well expect a decrease in the intensity of cosmic rays at these periods (the so-called annual variation). However, the expected amplitude of the annual variation of the hard cr component amounts to only a few tenths of a percent, so that it will be difficult to detect against the background of the seasonal variations (several percent), due to meteorological factors.[1]

Inasmuch as there is observed a tendency to a 27-day periodicity of the geomagnetic activity associated with the rotation of the sun about its axis and a relatively great persistence of the active (stream-emitting) areas on the sun, in the light of the aforementioned particle-scattering mechanism we might expect the 27-day variations to be in counter-phase with the variations in solar activity. Variation with the requisite amplitude ratios of the different cr components has actually been observed.[29,46] Further evidence in favor of the aforementioned mechanism is the fact that during the period of maximum solar activity (i.e., when a number of corpuscular beams is maximal) the 27-day variations attain their greatest amplitude, while during the minimal activity period they virtually vanish (Refs. 46

---

*It may be noted that the magnetic fields "frozen" into the streams may be the reason for the latitude cut-off at high altitudes. In the investigations of Ref. 72 it was suggested that the reason for the cut-off may be the existence of a solar-system magnetic field; a like role may be played by the magnetic fields of corpuscular streams. However, in the latter case the scattering process will not be stationary and appreciable fluctuations in the intensity of low energy cr particles should be observed at high latitudes; this has been substantiated experimentally.[40] Furthermore, if this is the case the latitude at which the latitude-effect cut-off is observed should increase with with declining solar activity (i.e., with a decreasing number of corpuscular streams).

**According to Ref. 47, published after the Conference, the experimental data utilized in Refs. 45 and 46 comprise equipment errors. If these errors are allowed for, the decreases in intensity at the equator and middle latitudes become equal to those predicted by theory.

and 48 - see Fig. 8).

(We note that the 27-day variation mechanism in which the variation is associated with the supposed 27-day variation of the heliomagnetic latitude of the earth due to the non-coincidence of the magnetic dipole of the sun with its axis of rotation, proposed by Vallarta et al[49], must be rejected. This mechanism can at best produce variations in the intensity of particles having energies under 5-6 Bev. If this should be the operative mechanism there should be no 27-day variations in any cr component at the equator. Moreover at 50° latitude the variation in the hard component should be hundreds of times smaller than that of a neutron component. This is of course at sharp variance with the experimental data.)

5. On the nature of the correlation between diurnal variation and geomagnetic activity

When the earth is in the path of a corpuscular stream, transporting a "frozen" magnetic field, together with the aforementioned decrease in cr intensity there appear additional diurnal variations due to the acceleration and deceleration of the cr particles on their way to the earth by the electric field of the stream (Fig. 9). In view of the scattering of low energy particles by the "frozen" magnetic field the additional daily variations will be associated with particles of higher energies than in the case of "normal" diurnal variations. Hence these additional diurnal variations during magnetic storms may be expected to attain an appreciable magnitude even deep underground. The results of calculations of the additional diurnal variations for different components and different "frozen" magnetic field intensities (carried out on the assumptions that the earth is at the center of a stream, carrying a homogeneous field, that the width of the stream near the earth is $2 \cdot 10^{12}$ cm and that its velocity $u = 2 \cdot 10^{8}$ cm/sec) are given in Table 4. These calculations were based on values of the correlation coefficients obtained by extrapolation (see equ. (5)) and are, therefore, only approximate.

The hour of the peak in the diurnal variations and their distribution over the surface of the earth depend on the direction of the field in the stream. When the lines of force are perpendicular to the plane of the ecliptic, the source of the variations (in view of the deflection of the particles in the field - see Fig. 7) will appear to be nearly in the direction of the sun and the flux of particles emitted by it will be symmetrical relative to the plane

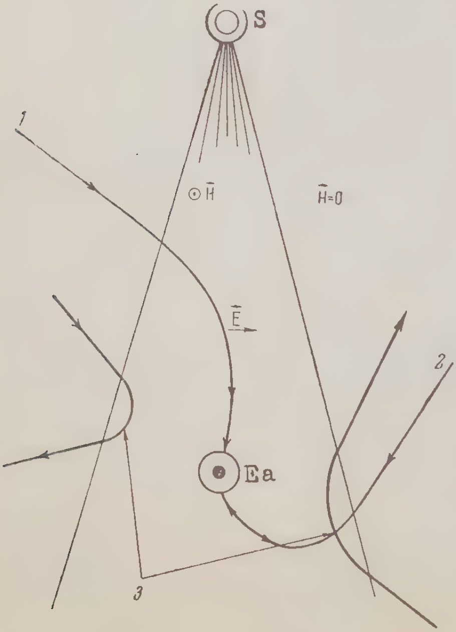

Fig. 9. Diagram illustrating the acceleration, deceleration and scattering of cr particles in a corpuscular stream, transporting a "frozen" magnetic field, incident on the earth. S - sun; Ea - earth. 1) high-energy particles accelerated in passing through field E in the stream (the direction of the "frozen" magnetic field coincides with the earth's field), 2) high-energy particles losing part of their energy in traversing the stream, 3) particles of lower energies, scattered in the "frozen" magnetic field and therefore not reaching the earth.

of the ecliptic. Consequently, the distribution of these additional diurnal variations over the earth will be approximately symmetrical relative to the equator. If the direction of the field of the stream is parallel to that of the earth's field, the source will lie in the same direction of the sun; if the direction of the stream's field is opposite to that of the earth, the source will appear to be in opposition to the sun. Consequently, in the former case the amplitude of the diurnal variations will be increased while the time of the maximum will be shifted into the ante-meridian hours, with the extent of the shift differing for different cr components. In the latter case the inverse effects will obtain.

Table 4

Expected amplitude of additional diurnal variations in the intensity of different cosmic ray components, due to the electric field associated with the corpuscular streams incident on the earth (computed on the assumption that the velocity of the streams $u = 2 \cdot 10^8$ cm/sec)

Intensity of the magnetic field near the earth (Oc) with stream width = $2 \cdot 10^{12}$ cm	Amplitude of change in cr intensity, %											
	$\lambda = 50°$				$\lambda = 0°$				Underground			
	Ionization at top of atmos.	Ionization at mt. altitudes	Neutron comp. at sea level	Hard comp. at sea level	Ionization at top of atmos.	Ionization at mt. altitudes	Neutron comp. at sea level	Hard comp. at sea level	22 m.w.c.	45 m.w.c.	117 m.w.c.	400 m.w.c.
$0{,}5 \cdot 10^{-5}$	0,62	0,21	0,35	0,07	0,13	0,04	0,08	0,07	0,021	0,013	0,006	0,002
$1{,}0 \cdot 10^{-5}$	1,24	0,42	0,70	0,15	0,26	0,08	0,16	0,14	0,043	0,027	0,011	0,004
$3{,}0 \cdot 10^{-5}$	0,53	0,61	0,80	0,44	0,77	0,22	0,48	0.42	0,122	0,080	0,033	0,010
$5 \cdot 10^{-5}$	0,34	0,56	0,56	0,70	1,22	0,36	0,76	0,70	0,21	0,13	0,06	0,02
$1 \cdot 10^{-4}$	0,18	0,47	0,30	0,91	1,00	0,64	0,67	0,92	0,43	0,27	0,11	0,04
$2 \cdot 10^{-4}$	0,10	0,38	0,17	0,70	0,58	0,55	0,40	0,77	0,87	0,53	0,22	0,07
$5 \cdot 10^{-4}$	0,05	0,31	0,08	0,39	0,26	0,43	0,19	0,49	0,88	1,23	0,56	0,18
$2{,}5 \cdot 10^{-3}$	0,01	0,18	0,02	0 12	0,11	0,35	0,08	0,18	0,30	0,44	0,91	0,88

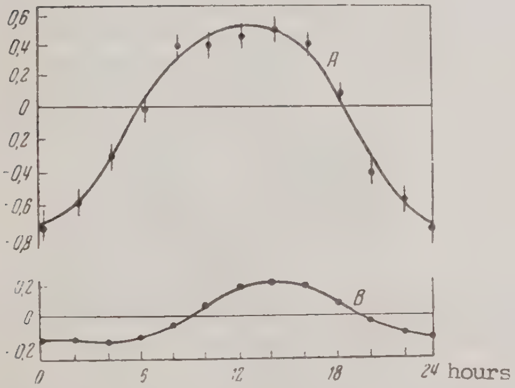

Fig.10. Changes in the diurnal variation of the hard component during the very great magnetic storms of Jan.24,1949 and July 26,1946. A- Curve during period of the magnetic storms; B- average curve for 360 days. Ordinates: cr intensities in percent relative to the normal value; abscissae: local time in hours.

If the lines of force of the field of the stream are parallel to the plane of the ecliptic, the induced electric field will be normal to the plane of the ecliptic, so that the energy of the particles moving parallel to the plane of the ecliptic will not change. Let us assume, for example, that the field in the stream is oriented in the direction of the rotation of the earth about the sun. Then the electric field will be directed from north to south and consequently positive particles moving from the north will be accelerated, while those arriving from the south will be slowed down. In view of the curling effect of the magnetic field "frozen" into the stream, the particles arriving from the north will approach the earth along a vertical not at the North Pole but at some point between it and the equator on the meridian for which the local solar time is noon. In connection with this, if we take into account the additional deflection of the particles by the earth's magnetic field, we must expect the maximum of the additional diurnal variations to occur during the morning hours.

If the magnetic field in the stream is directed in the opposite sense, analogous reasoning leads us to the conclusion that the time of the maximum of the diurnal variations will remain the same but that the source of the additional radiation will now appear to lie between the directions to the South Pole and the sun.

The experimental data (Refs. 23, 28, 29 and 50) now available are in agreement with the expected attributes of the additional diurnal variations. Moreover, simultaneous measurement of the decrease in the intensity of cr and the increase in the diurnal variations during magnetic storms makes it possible to determine in principle not only the electromagnetic properties of the corpuscular streams but also their velocity relative to the earth. For example, as a result of analysis, with the aid of Table 3, of the decrease in intensity of cr during the magnetic storms of January 24, 1949 and July 26, 1946 we find that the intensity of the magnetic field $H \approx 2 \cdot 10^{-4}$ oersted. From Table 4 it will be seen that at this field intensity, the additional diurnal variations of the hard component at sea level and 50° latitude, assuming the stream velocity to be $2 \cdot 10^8$ cm/sec, should have an amplitude of $\lesssim 0.7\%$ (the $\lesssim$ stems from the fact that we assumed that the earth is in the center of the corpuscular beam and that all the particles traversing it undergo the maximum possible change in energy $\delta\varepsilon$ determined by (7)). Since there has been observed[29] an increase in the amplitude of the diurnal variations amounting to 0.4% with a simultaneous displacement of the time of the maximum into the morning hours (Fig. 10), the expected velocity of the stream is

$$u \gtrsim \frac{0.4\%}{0.7\%} \cdot 2.10^8 \text{ cm/sec} = 1.2 \cdot 10^8 \text{ cm/sec}$$

This value is close to the velocity of the stream that produced the July 26, 1946 storm as determined from the time difference between the beginning of the solar flare and the start of a magnetic storm ($1.6 \cdot 10^8$ cm/sec).

It is interesting to note that the additional diurnal variations to be expected* underground at a depth of 60 m.w.e. are very appreciable: several tenths of a percent (see Table 4). These variations should be relatively easy to detect against the background of the relatively small "normal" diurnal variations, characterized by an amplitude one order of magnitude smaller. Available experimental data[39] are not in conflict with this conclusion.

6. On the nature of the variations of cosmic rays during large and small solar flares

Analysis by the method of correlation coefficients of the experimental data[51-55] on the increase in intensity of different cr components at different points on the earth during the great solar flare[56] of November 19, 1949 yielded the following information on the properties of the source.

1. The energy spectrum of the variations remote from the earth, where the influence of the geomagnetic field on the particle trajectories may be neglected, is characterized by

$$\frac{\delta D(\varepsilon)}{D(\varepsilon)} = \begin{cases} 11\text{-}12, & \text{when } \varepsilon < 12\text{-}13 \text{ Bev}, \\ 0, & \text{when } \varepsilon > 12\text{-}13 \text{ Bev}, \end{cases} \tag{13}$$

---

*At the same time there should be no decrease in the cr intensity at this depth when a stream with fields having an intensity of about $2 \cdot 10^{-4}$ oersted is incident on the earth. This is in agreement with the measurements (Ref. 39) made during magnetic storms similar to that of July 26, 1946.

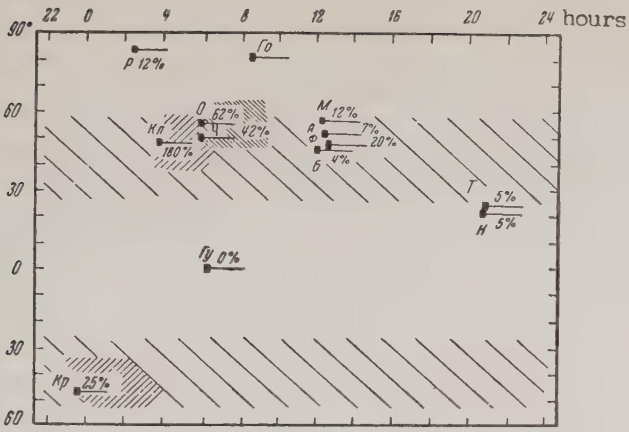

Fig. 11. Areas upon which particles of energies to 10 Bev, emitted by the sun should be incident, as computed in Ref. 57. Ordinates: geomagnetic latitudes. Abscissae: local time in hours at instant of solar flare of Nov. 19, 1949. Closer hatching indicates greater amplitude of increase (assuming cr stream to be homogeneous). The cited experimental data favor the assumption that the additional cosmic radiation originates in the sun. Observation points: A - Amsterdam, Б - Banner, Ч - Cheltenham, Кр - Christchurch, Кп - Climax, Ф - Freiburg (Frederickshaven), Го - Godhavn, Гу - Huancayo, M - Manchester, H - Nagoya, O - Ottowa, P - Resolute, T - Tokyo.

i.e., the variations are produced by an additional flux of particles having energies under a certain effective energy, equal to 12-13 Bev. This flux is some 10-12 times greater than the flux of the undisturbed primary component in the same energy region. The energy spectrum of these particles is approximately the same as that of the undisturbed, normal component.

2. The source of this additional flux is located in or nearly in the direction of the sun.

3. The particle flux decreases exponentially with time (about e times in 3 hours).

These deduced properties of the source substantiate the assumptions upon which the investigations of Ref. 57 are based and thus help interpret the distinctive features of the distribution of the intensity peaks of the different components over the surface of the earth (Fig. 11).

The deduced spectrum of the variations (13) explains the great increase in the neutron component (almost 5.5 times[55]) compared with the rise in the hard component (under 100%[51-54]) and the complete absence of any effect at the equator[51] and underground at 60 m.w.e.[39] Thus we have here a clear case of the generation and emission by the sun of positive* particles of relatively low energy. Among the different mechanisms of cr generation proposed in the literature, on the basis of our analysis we are inclined to give preference to the statistical mechanism suggested for the envelopes of the sun and stars (particularly novae and supernovae) by Ginzburg.[58] This mechanism provides for a natural explanation of all the principal required properties of the source of variations without coming into conflict with the results of observations of chromospheric eruptions and solar magnetic fields.[56-59] It is necessary that the chromospheric eruptions should comprise formations having dimensions on the order of $2 \cdot 10^7$ cm, moving with velocities of $3 \cdot 10^7$ cm/sec and transporting magnetic fields of an intensity exceeding at least 2 oersteds.

If such chromospheric formations occupy a volume greater than 0.02-0.002 the total volume of the source (having dimensions on the order of 10^{10} cm, located in the upper part of the chromosphere and in the corona) their kinetic energy will be great enough to produce the required stream of particles. It is calculated that during the flare of November 19, 1949 a total of about 10^{32} particles having energies between 1.5 and 12.5 Bev were emitted by the sun.

---

*This follows from the deflection of the particles in the earth's magnetic field.

Since during the last two decades there have been four such flares on the visible side of the sun, the mean flux of particles emitted from the sun due to such flares amounts to about $1.5 \cdot 10^{24}$ particles per sec.

There is apparently also some generation and emission of particles of moderate energies during small solar flares. Evidence in favor of this is furnished by analysis of the ~0.6% increase in the intensity of the neutron component observed during small solar flares[57] (Fig. 12). At the same time the observed ~0.3% increase in the intensity of the hard component[60] (Fig. 13) is apparently of meteorological origin[1] (otherwise one should expect the neutron component to increase by some tens percent). However, in the case of small flares the flux of particles is some 2-3 orders of magnitude weaker than in the case of the large flare of Nov. 19, 1949. In view of the fact that there are many such small flares (hundreds per annum) the mean cr flux due to them may be comparable to that due to great flares. Thus we can assume that the sun generates some $3 \cdot 10^{24}$ particles per sec, having an energy of a few Bev. This value of the particle flux makes the hypothesis of the solar or stellar origin of all cosmic radiation (or of its low energy portion) implausible.[36]

If the sun has even a very weak permanent magnetic field (intensity at the poles ~1 oersted*), there must exist some special conditions for the emitted particles to escape

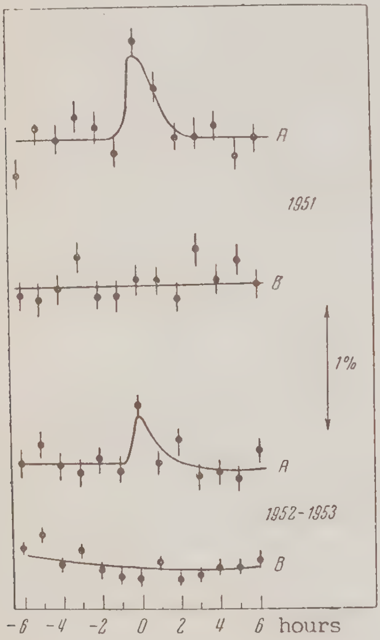

Fig. 12. Variation of the intensity of the neutron component at Climax (Lat.48°N) during small solar flares in 1951 and 1952-3. A- effect of flares occurring at times when low energy (a few Bev) particles emitted by the sun arrived vertically at the boundary of the atmosphere over Climax (3-7 hours local solar time); B - curve characterizing cases when Climax was outside this zone. Ordinates variations in cr intensity in percent relative to balance value. Abscissae: time in hours prior to and after beginning of flare (results obtained by the method of superposition of epochs).

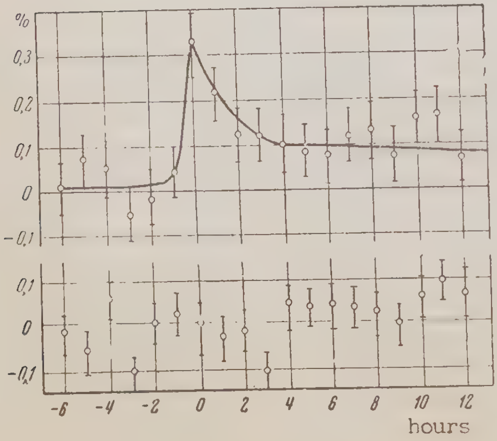

Fig. 13. Average change in intensity of the hard component at Manchester at time of radio fadeout (closely correlating with solar flares. Upper curve plotted on the basis of 35 cases of radio fadeout during daytime hours (9 to 16 hours local time); lower curve based on 69 cases of fadeout during night hours (16 to 9 hours local Manchester time). Ordinates: change in intensity in percent relative to average value. Abscissae: hours prior to and after interruption of radio communications.

---

*This value for the intensity of the general magnetic field of the sun appears to be most plausible. Virtually all recent investigations including that of Ref. 61, which appeared after the Conference, lead to this value.

(otherwise the particles curling in the field will return to the sun). Such a special condition, for example, could be the formation of a "tunnel" in the region of the forbidden directions in the dipole field due to the influence of local fields (for instance, fields associated with sun spots[62]). The emergence of particles from the sun is also possible as a consequence of their "capture" by the magnetic fields "frozen" into the corpuscular streams with a subsequent ejection together with these streams to a considerable distance from the sun. It is conceivable that the great difference in the fluxes of particles generated during great and small flares (some 2-3 orders of magnitude) is due not only to differences in the conditions of generation but also to differences in the conditions governing their escape or ejection.

7. On the sidereal-day variations in cosmic rays

If cr are of extra-galactic origin, then due to rotation of the Galaxy there should be observed a sidereal-day variation with an amplitude of about 0.17% and a maximum at 13 hours 20 min sidereal time.[63,64] However, the results[23] obtained by averaging data for almost ten years show a variation of the hard component at sea level characterized by an amplitude not exceeding 0.02% and a maximum at about 5 hours sidereal time. Measurements[39] underground (60 m.w.e.) indicate no sidereal periodicity within the limits of the experimental error (0.02%). A like result is obtained at 846 m.w.e. (error - 0.5%)[66] and at 1600 m.w.e. (experimental error - 017%)[67]. Measurements[68] of extensive air showers also indicate the absence of sidereal variations for primary particles of 10^{16} ev energy within ± 0.6% and for $(2-5)\cdot 10^{16}$ ev particles within ± 1%. Thus we can say that, despite the experimental errors involved, the results of measurements rather convincingly indicate the absence of a cr variation effect due to rotation of the Galaxy.

It may be noted that sidereal-day variations can also occur even in the case when cosmic radiation has an intra-galactic origin. Variations in this case could be due to non-uniform distribution of the cr sources and to absorption and diffusion of cosmic radiation in the Galaxy. Rough evaluations, analogous to those by Cocconi,[69] show that in order to explain the already available data for the upper bound of the sidereal variations of high-energy cr we must postulate the existence of a general galactic magnetic field having an intensity of 10^{-5}-10^{-6} oersted (on the assumption that the properties of magnetic fields are such as described in Ref. 70); such a field is necessary to reduce the diffusion of the particles from the Galaxy, for otherwise the expected amplitude of the sidereal variation would conflict with the experimental data. In addition we must assume that the cr sources are not concentrated at the center of the Galaxy but are more uniformly distributed throughout it (Ginzburg's[58] hypothesis regarding generation of cr by supernovae and novae apparently gives the most satisfactory distribution of sources, a distribution which is in agreement with that obtained by Getmantsev[71] as a result of an analysis of the distribution of non-thermal radio radiation). For more precise calculations we still need more accurate data both on the sidereal-day variations in cr and on certain astrophysical factors characterizing the diffusion and absorption of cr in inter-stellar space.

Conclusions

1. The method of correlation coefficients in conjunction with the theory of allowing for the effect of meteorological factors makes possible a consistent analysis of the variations of the different cr components at different latitudes, altitudes above sea level and depths underground for the purpose of bringing out the basic attributes of the sources of variation: the energy spectrum and direction of the source. This narrows down the various possible speculations and makes it feasible to successively check the diverse extant

hypotheses regarding the origin and causes of different types of cr variations. Where before we had an apparent multitude of experimental data, which appeared to be a simple accumulation of unrelated facts, we now have an entirely different situation. The available data find a perfectly natural explanation from a unified point of view and it even turns out that to make effective use of the indicated methods we still lack experimental data free of the influence of meteorological factors. As a result of the program of the International Geophysical Year 1957-1958 we can expect the experimental material to be greatly enriched and can hope that further development and application of the method of correlation coefficients in conjunction with the theory of taking account of the influence of meteorological factors will yield even more reliable results. From this point of view we attach particular importance to the complex measurements at different latitudes, longitudes and altitudes of the variations in the different cr components characterized by different correlation coefficients: the mu-meson component at sea level and underground, the neutron component at sea level and mountain altitudes and the ionizing component, also the frequency of extensive air showers and the frequency of star-production in the stratosphere.

2. Application of the described method to the analysis of published experimental data already (despite the insufficiency of such data) makes it possible to assert that all the hitherto observed variations in cr of extra-atmospheric origin can be divided into two classes (see Table 1): a) variations due to acceleration, deceleration and scattering of cr particles by solar corpuscular streams transporting "frozen" magnetic fields (diurnal, 11-day year, 1-year, 27-day, half-day, day-to-day variations, variations during magnetic storms, 27-day variations in the diurnal periodicity, changes in the diurnal variations associated with magnetic activity, etc.) and b) variations due to the generation and emission of particles of low-energy by the sun (cr variations during large and small solar flares).

Incidentally it follows from the above that at high altitudes there should be observed two types of fluctuations: fluctuations decreasing slowly and fluctuations decreasing rapidly with increasing atmospheric depth.

Generally speaking we cannot preclude the existence of yet a third class of variations: variations due to non-uniform distribution of cr sources in the Galaxy and absorption and diffusion of the galactic cosmic radiation (sidereal-day variations).

3. Investigations of the variations in cr lead to a number of important deductions regarding certain geo-, helio- and astrophysical factors: a) the electromagnetic properties of corpuscular streams; the "freezing" of magnetic fields into such corpuscular streams; a rather sharp separation of the streams into two types, those transporting weak (about 10^{-5} oersted near the earth) and those transporting strong (10^{-4} oersted) magnetic fields, associated, respectively, with high-latitude and low-latitude formations on the sun; the relative weak dependence of the former type (carrying weak fields) and the strong dependence of the latter type (carrying strong fields) on the degree of solar activity, etc., b) some of the characteristics of the turbulent motions in solar chromospheric eruptions and the magnitudes of the magnetic fields "frozen" into the prominences; c) the nature of the general magnetic field of the Galaxy and the distribution of cr sources within it.

In connection with the International Geophysical Year program, it is to be hoped that the results of observations of cr taken together with the data obtained on visible and radio frequency radiation will be a more effective tool in the study of these factors.

In conclusion I wish to express my deep gratitude to Prof. E. L. Feinberg

for his continuous interest in the work and his valuable suggestion and advice and to Technician N.Vlasova for her assistance in carrying out the numerical calculations.

Scientific Research Institute
for Terrestrial Magnetism

References

1. L.I.Dorman, A.I.Kuz'min, G.V.Tianutova, E.L.Feinberg, et al, Zhur. eksp. i teor. fiz., 26, 537 (1954).
2. E.L.Feinberg, Doklady AN SSSR, 53, 421 (1946).
3. L.I.Dorman, Doklady AN SSSR, 94, 438 (1954).
4. L.I.Dorman, Doklady AN SSSR, 95, 49 (1954).
5. L.I.Dorman, Zhur. eksp. i teor. fiz., 26, 504 (1954).
6. Physics of Cosmic Rays, G. Wilson, Ed. in Rus. Trans., M. - 1954.
7. J.A. Simpson, W.H. Fonger & S.B.Treiman, Phys. Rev., 90, 934 (1953).
8. I.L.Rozental' & D.S. Chernavski, Usp fiz. nauk., 52, 185 (1954).
9. J.A. Van Allen, Nuovo Cim., 10, 630 (1953).
10. D.V. Skobel'tsyn, Kosmicheskie luchi (cosmic rays - M. 1936.
11. N.L. Grigorov, Thesis, Moscow State University, 1954.
12. K.G. Malmfors, Ark. Mat. Astr. Fys. 32A, No 8 (1945).
13. E.A. Brunberg, Tellus, 5, 135 (1953); E.A. Brunberg & A. Dattner, Tellus, 5, 269 (1953).
14. L. Janossy, Zs. f. Phys. 104, 430 (1937).
15. H. Alfven, Phys. Rev., 72, 88 (1947).
16. E.O. Kane, T.J.B.Stanley & J.A.Wheeler, Rev. Mod.Phys., 21, 51 (1949).
17. K. Dwight, Phys. Rev., 78, 40 (1950).
18. S.B. Treiman, Rev., 93, 544 (1954).
19. J. Firor, F. Jory & S.B. Treiman, Phys. Rev., 93, 551 (1954).
20. V. Sarabhai & R.P. Kane, Phys. Rev., 90, 204; 91, 688; 92, 415 (1953).
21. V. Sarabhai & R.P. Kane, Proc. Ind. Acad. Sci., A37, 287 (1953).
22. V. Sarabhai, V.D. Desai & D. Venkatesan, Phys. Rev.., 96,469 (1954).
23. H. Elliot & D.W.N. Dolbear, J. Atm. Terr. Phys., 1, 205 (1951).
24. H.Alfven, Cosmic electrodynamics, (Rus. trans.) M.,1952.
25. H.W. Babcock, Ap. J., 117, 387 (1953).
26. H.W. Babcock & T.G.Cowling, M. N., 113, 353 (1953).
27. S.B.Pikel'ner, Usp astr. nauk, 6, 281 (1954).
28. Y. Sekido & S. Ioshida, Rep. on Ionosph. Res., Japan, 4, 37 (1950).
29. Physics of Cosmic Rays, G. Wilson, Ed. in Rus. Trans., M. - 1954.
30. S. Chapman, Nature, 190, 423 (1937).
31. S. Chapman & J.Bartels, Geomagnetism.-Clarendon press, Oxford, 1940.
32. S.B. Treiman, Phys. Rev., 89, 130 (1953).
33. N.P. Ben'kova, Trudy NIIZM, (Transactions, Scientific Research Institute for Terrestrial Magnetism.)
34. B. Trumpy, Physica, 19, 645 (1953).
35. E.A. Brunberg & A. Dattner, Tellus, 6, 254 (1954).
36. V.L. Ginzburg, Usp fiz. nauk, 51, 343 (1953).
37. E.S. Glokova, Trudy NIIZM, (Transactions, Scientific Research Institute for Terrestrial Magnetism.)
38. S.E. Forbush, Phys. Rev., 54, 975 (1938).
39. I.V. McAnuff, See Physics of Cosmic Rays, Wilson Ed. M. - 1954.
40. H.V. Neher, V.Z. Peterson & E.A. Stern, Phys. Rev., 90, 655 (1953).

41. H.V. Neher & S.E. Forbush, Phys. Rev., 87, 889 (1952).
42. A.T. Biehl & C.V.Montgomery, Rev. Mod. Phys., 20, 336 (1948).
43. W.P. Jesse, Phys. Rev., 58, 281 (1940).
44. W.H. Fonger, Phys. Rev., 91, 351 (1953).
45. E.G. Roka, Zs. f. Naturf., 5a, 517 (1950).
46. E.S. Glokova, Izv. AN SSSR, ser. fiz., 17, 136 (1953).
47. S.E. Forbush, J. Geoph. Res. 59, 525 (1954).
48. V.P. Meyer & J.A. Simpson, Phys. Rev., 96, 1085 (1954).
49. M.S. Vallarta & O.Godart, Rev. Mod. Phys., 11, 180 (1939).
50. J.W. Firor, W.H. Fonger & J.A. Simpson, Phys. Rev., 94, 1031 (1954).
51. S.E. Forbush, T.B. Stinchcomb & M. Shein, Phys.Rev., 79, 501 (1950).
52. D.C. Rose, Phys. Rev., 78, 181 (1950).
53. A.Ehmert, J. Atm. Terr. Phys., 1, 39 (1950); H.Salow, J. Atm. Terr. Phys., 1, 40 (1950); A. Sittkus, J. Atm. Terr. Phys., 1, 40 (1950).
54. A.Dauvillier, C. R., 229, 1096 (1949).
55. N.Adams, Phil. Mag., 41, 503 (1950).
56. M.A. Ellison & M. Conway, Observatory, 70, 77 (1950).
57. J. Firor, Phys. Rev., 94, 1017 (1954).
58. V. L. Ginzburg, Doklady AN SSSR, 92, 727 (1953).
59. V. A. Ambartsumian, E.R. Mustel', A.B. Severnyi & V.V.Sobolev, Teoreticheskaia astrofizika (Theoretic Astrophysics) M., 1952.
60. D.W.N.Dolbear, H.Elliot & D.I.Dawton, J.Atm.Terr.Phys.,1, 187 (1951).
61. H.W.Babcock & H.D.Babcock, Nature, 175, 296 (1955).
62. S.E.Forbush, P.S.Gill & M.S.Vallarta, Rev.Mod.Phys., 21, 44 (1949).
63. A.H.Compton & J.A.Getting, Phys. Rev., 47, 817 (1935).
64. M.S.Vallarta, C.Graef & S.Kusaka, Phys. Rev., 55, 1 (1939).
65. L.I.Dorman, Thesis, NIIZM (Scientific Research Inst. for Terrestrial Magnetism) M. - 1955.
66. N. Sherman, Phys. Rev., 89, 25 (1953).
67. C.P.Barrett, G.Cocconi, Y.Eisenberg & K.Greisen, Phys.Rev.,95, 1571 (1954).
68. T.E.Cranshaw & W.Galbraith, Phil.Mag.,45,1109 (1954).
69. G. Cocconi, Phys. Rev., 83, 1193 (1951).
70. S.B.Pikel'ner, Trudy 3-go soveshchaniia po voprosam kosmogonii. (Transactions of the Third Conference on Problems of Cosmogony) Pub. AN SSSR, M.1954.
71. G.G.Getmantsev, Uch. zap. (Scientific Records Gor'ki State Univ., Phys. ser., 27, 23 (1954).
72. V.L.Ginzburg & M.I.Fradkin, Doklady AN SSSR, 92, 531 (1953); V.L.Ginzburg, G.G.Getmantsev & M.I.Fradkin, Trudy 3-go soveshchaniia po voprosam kosmogonii, (Transactions of the Third Conference on Problems of Cosmogony) Pub. AN SSSR,M.1954

SOME RESULTS OF AN INVESTIGATION OF THE VARIATIONS IN THE HARD COMPONENT OF COSMIC RAYS

- E.S.Glokova

Currently investigation of the variations in primary cosmic radiation is attracting the attention of geo- and astro-physicists. As shown in Dorman's contribution[1], knowing the variation in the different secondary components, we can determine the variation in the spectrum of the primary rays and deduce some of the properties of the source of variation.

In elucidating the variation in intensity of the meson component, due to variations in the primary cosmic rays (hereinafter cr), it is important to allow for meteorological effects.

Our present investigation was concerned with two problems:

1. Verification on the basis of extensive experimental material of the theory of the temperature effect, developed by Soviet physicists[2], and thus clarification of the potentialities of the theory for separating and investigating the variations in the intensity of the meson component, associated with primary cr.
2. Obtaining a comprehensive picture of the correlation between the observed variations and the magnetic and solar activity.

In the investigation we made use of the data obtained in the NIIZM (Scientific Research Institute for Terrestrial Magnetism) as well as the data published by the Carnegie Institute for three cr stations.[3] The latitude and longitude of the stations and the years of observation are shown in Table 1. Hereinafter the stations will be designated by the corresponding numbers in parentheses: (1), (2), (3) and (4).

Table 1

Station	Coordinates, °			Altitude above sea level, meters	Interval comprised in data
	Geomag. latitude	Geographic			
		Lat.	Long.		
(1) Huancayo . . .	0,6 S	12 S	75 W	3350	1937—1946
(2) Cheltenham . .	50,1 N	37 N	77 W	100	1937—1946
(3) Godhavn . . .	79,9 N	69 N	54 W	100	1941—1946 1947—1950
(4) Moscow	52 N	56 N	37 O	100	1951—1952

In all the examined cases the role of the temperature effect was carefully evaluated. The temperature corrections were computed according to the equation

$$\frac{\delta N_\mu}{N_\mu}=\int_0^{h_0} W(h)\,\delta T(h)\,dh,$$

where $\delta N_\mu/N_\mu$ is the change in the intensity of cr due to the temperature effect; $\delta T(h)$ is the temperature fluctuation as a function of the atmospheric depth h; $W(h)$ is a function depending on the regularities governing the generation and absorption of mesons in the atmosphere: $W(h)=W_\mu(h)+W_\pi(h)$. The dependence of $W(h)$ on the atmospheric depth for the global intensity is shown in Fig. 1. In preparing the curve the integration was carried out from the boundary of the atmosphere to the level of observation h_0.

To take the temperature effect into account fully one must know the variation in temperature all the way to altitudes of 30-35 km at which the generation of mesons begins. Only part of the temperature effect, however, can be computed on the basis of the available aerological data obtained by means of sonde balloons. However, the layer of the atmosphere in which the fluctuation

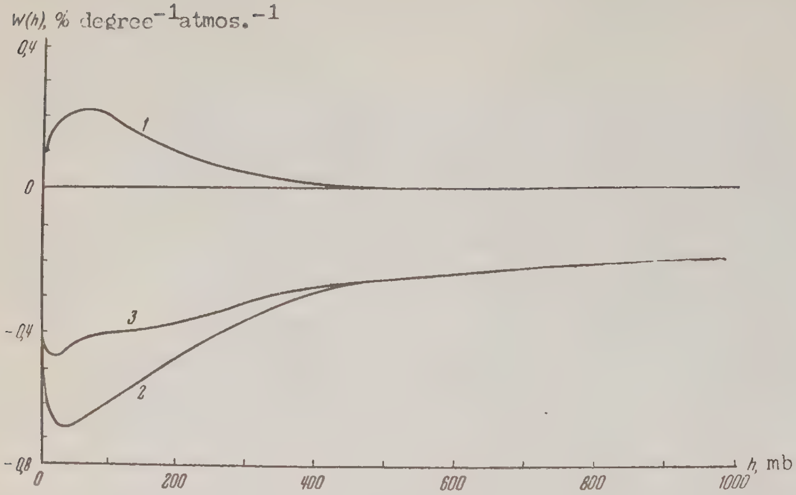

Fig. 1. Curve of the function $W(h)$: 1) $W_{\pi}(h)$, 2) $W_{\mu}(h)$, 3) $W(h) = W_{\pi} + W_{\mu}(h)$

in temperature with altitude is known comprises approximately 9/10ths of the total weight of the atmosphere so that correct exclusion of this part of the temperature effect should at least greatly facilitate interpretation of the remaining variations.

Analysis of the methods of utilizing aerological data for computing temperature corrections showed that the data on air temperatures as now recorded by means of radiosondes are not sufficiently accurate as compared with the present accuracy of recording cr intensities. More or less satisfactory results can be expected only through statistical processing of the aerological material, so as to minimize the influence of chance errors in individual radiosonde flights.

Our earlier processing of the data published by the Carnegie Institute showed that the intensity J of cr decreases several percent with increasing solar activity in the 11-year cycle and

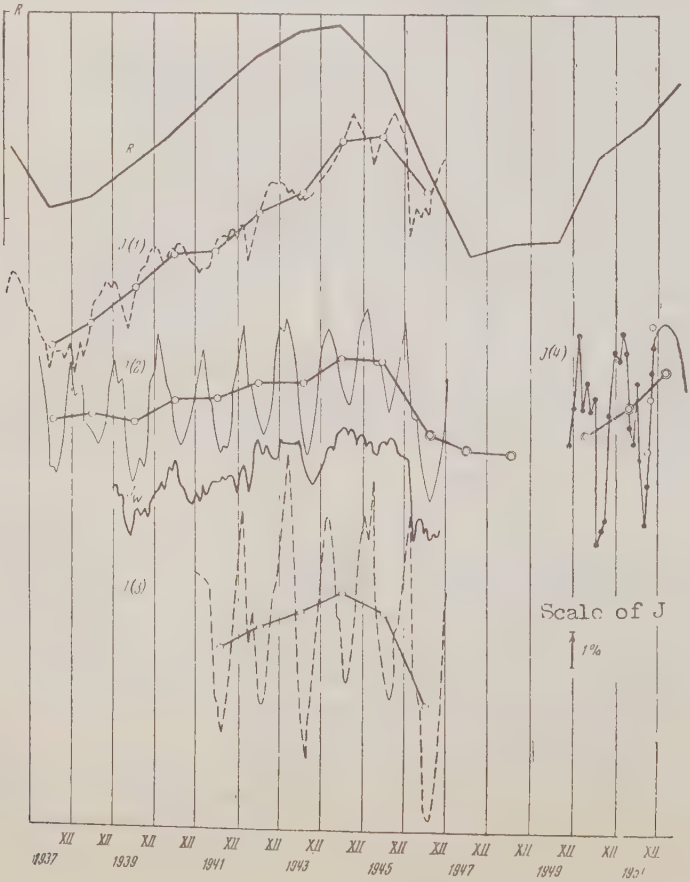

Fig.2. Variations of the mean monthly and mean annual variations in the intensity of cosmic rays from 1936 to 1951: J(1), J(2), J(3) and J(4) - variations at stations (1), (2), (3) and (4) (see Table 1); J_W - variation at station (2) after subtraction of temperature effect; R - variation in relative number of sun spots. Arrow indicates scale and direction of positive axis.

that certain known variations (27-day, diurnal and day-to-day) undergo regular changes with the solar cycle.[4] The changes in the intensity J over the period 1937 to 1946 are shown in Fig. 2. The curve for station (2) has been extended on the basis of the Moscow data up to 1952. The figure shows a) periodic variations in J during two solar activity cycles, b) regular seasonal variations at high latitude stations (the amplitude of these variations increases with latitude), c) large fluctuations in J at the equatorial station (1) (these are not seasonal in nature).

Introduction of temperature corrections* to the mean monthly values for station (2) (curve J_W in Fig. 2) did not bring out any periodic variations but did iron out the regular annual variations. It brought out variations at station (2) that largely duplicate the variations at station (1). Thus introduction of temperature corrections into the data of station (2) was instrumental in bringing out world-wide variations.

Seasonal variations were excluded by yet another method, namely, by averaging the data over 12 consecutive months by the so-called method of "sliding means".[6] The resultant smoothed out curves for the three stations are presented in Fig. 3. In addition to cyclic variations, they also exhibit variations with shorter periods whose maxima and minima virtually coincide with all three stations. We have called these world-wide fluctuations, which have an appreciable 2-3-year quasi-periodic component, long-period fluctuations. Analysis of the different indices characterizing magnetic and solar activities showed that during this interval the international magnetic index C exhibited similar fluctuations. The fluctuations of the horizontal component of the geomagnetic field are appreciably less pronounced, while corresponding fluctuations in the relative number of sun spots R are hardly evident. The short-term, irregular fluctuations of J, remaining after exclusion of the long-period and cyclic variations, also exhibit a world-wide nature and a definite correlation with the magnetic activity. This correlation is more pronounced for station (2) than for station (1), since temperature corrections were made to the data of station (2).

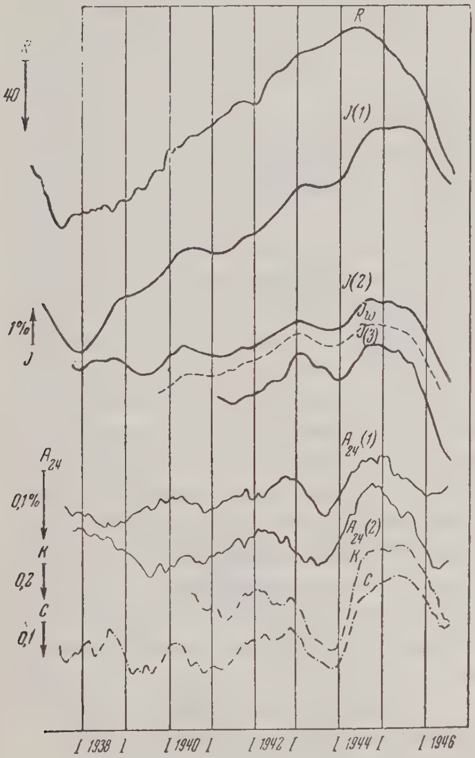

Fig. 3. Cyclic and long-period variations in J after smoothing of the curves by the method of "sliding means" (see Ref. 6): C and K) magnetic activity indices; A_{24}) amplitude of the diurnal J wave. Arrows indicate scale and direction of positive axes. Uncertainty in determining A_{24} equals ± 0.015%.

In averaging the data over several years (in connection with determining the mean annual variation) we detected at station (2) a residual mean annual variation J_W similar to the mean annual variation of the magnetic activity (Fig. 4). At the equatorial station (1) the mean annual variation in J exhibits less similarity with the curve for C; this may be attributed to the influence of small seasonal variations of atmospheric origin at this station. For all the examined variations there is a clear negative correlation with a magnetic activity: J decreases when the magnetic activity increases. It is known that J also decreases during magnetic storms.

---

*Temperature corrections were made only to the data of station (2). They were computed on the basis of the aerological data given in Ref. 5. Account was taken of temperature fluctuations up to the 100 and 50 mb isobars.

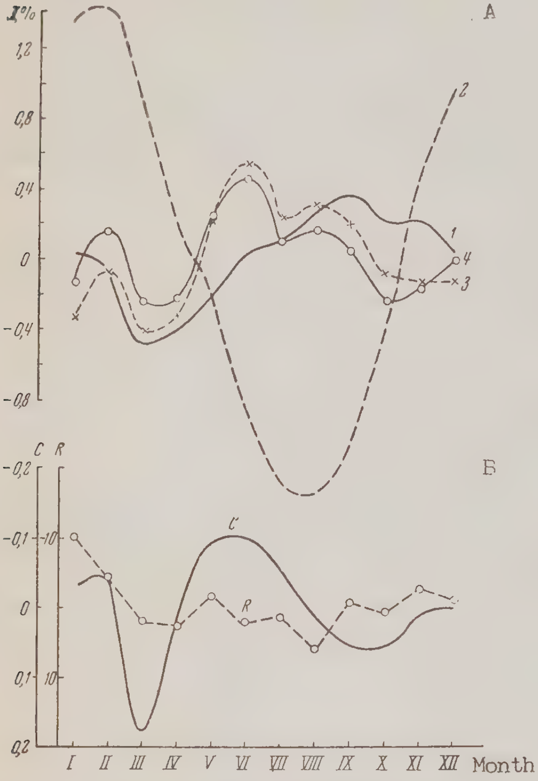

Fig. 4. Mean annual variations: A - cr intensity: 1) J(1); 2) J(2); 3) $J_W(2)$ with temperature fluctuations to the 100 mb isobar taken into account; 4) $J_W(2)$ with temperature to the 50 mb isobar taken into account. B - magnetic index C - relative number of sun spots R.

However the cyclic and long-period variations in J are definitely not simply the overall ultimate effect of magnetic storms. Although the number of magnetic storms during years of intense solar activity is appreciably higher than during years of low activity, the number of magnetic storms accompanied by an appreciable effect in cr (greater than 1% relative to the total intensity) does not exceed 10 even during the years of maximum solar activity.[7] Thus this effect is virtually not reflected in the mean annual values of J.

The above facts indicate that the correlation between the variation in cr intensity and magnetic activity is manifest not only during the periods of magnetic storms or short-term magnetic disturbances but definitely has a more general character.

The examined variations, including the decrease in J during magnetic storms, have yet another common characteristic, namely, an equal fluctuation amplitude at the equatorial station (1) and at station (2) located at geomagnetic latitude 50°N. At station (3) the amplitude of the variations is apparently greater. The ratios of the amplitudes of the fluctuations at the different stations in relation to the amplitude at station (1) (taken as unity) for the different types of cr variations are listed in Table 2.

Table 2

Nature of variation	Station		
	(1)	(2)	(3)
Long period	1	0,96 ± 0,03	1,30
Effect of magnetic storms . .	1	1,12 ± 0,08	1,2 ± 0,1
Irregular	1	1,1 ± 0,1	—
27-day	1	1,0 ± 0,1	—
Changes in spread of mean diurnal values	1	1,0 ± 0,1	1,3 ± 0,15

Thus there is reason to assume that all the examined variations of the same nature can be classified as variations associated with the magnetic activity. We shall call variations of this type M-variations.

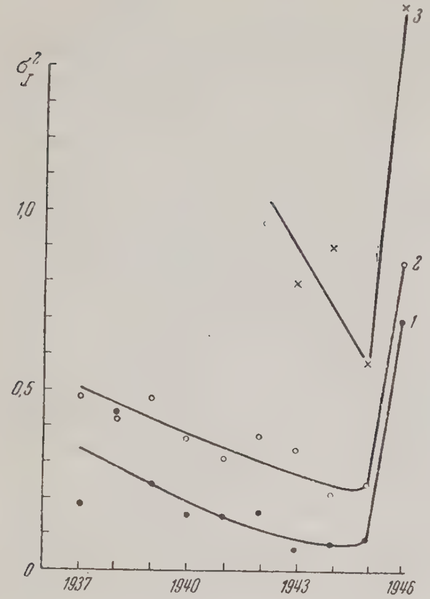

Fig. 5. Variation in the scattering σ^2 of the mean diurnal values of J from 1937 to 1947 at stations (1), (2) and (3).

We showed in Ref. 4 that the decrease in cr intensity with increasing solar activity is accompanied by an increased spread of the mean diurnal values relative to the mean monthly ones, i.e., by intensified day-to-day fluctuations in J.

As may be seen in Fig. 5 the increase in the spread or scattering σ^2 from years with a low to years with a high solar activity is virtually the same at stations (1) and (2). This may be interpreted as an indication that the increase in the fluctuation of cr intensity during years of strong solar activity is due to intensification of the M-variations.

In addition to the M-variations in the intensity of cr there are observed occasional "flare-ups", which are undoubtedly connected with solar activity. The "flare-ups" have a latitude dependence markedly different from the M-variations. They are not observed at the equator. Apparently in these cases there is an additional incoming flux of low-energy cr particles, accelerated in the vicinity of the sun.[1] The correlation between the scattering of the mean diurnal values at the different stations and the solar activity indicates that at high latitudes the influx of particles from the sun has no noticeable effect on the fluctuations of the mean diurnal value of the meson component.

Our analysis of the data brought out the following facts concerning the 27-day variations in cr intensity:

1. The 27-day variations are world-wide in character and depend on the phase of the 11-year solar cycle. They are clearly evident during years of strong solar activity and virtually undetectable in years of weak activity.[4]

2. In years of strong solar activity the 27-day variations exhibit a pronounced negative correlation with the corresponding variations in magnetic activity. The amplitude of the mean 27-day wave in 1937-8 fell off by half after subtraction of the data pertaining to revolutions of the sun during which effective magnetic storms were observed. This would indicate that the 27-day variations in the intensity of cr are of the same nature as the other M-variations.

The main reason why a different nature was formerly[8] ascribed to the 27-day variations is that in processing the data by the method of superposition of epochs different shapes of the magnetic activity and the cr intensity curves resulted. With this method of processing the magnetic activity curve exhibits narrow peaks at 27-28 day intervals, the heights of which fall off rapidly with time. On the other hand, the cr intensity curves are sinusoidal with an approximately constant amplitude.[9] Analysis of the aerological data obtained for Moscow showed that the rhythmic fluctuations of the mean temperature of the atmosphere have an appreciable influence on the results of processing variations in cr intensity by the method of superposition of epochs. After appropriate corrections for the temperature effect are made the 27-day variations in J become more clearly evident and accord more closely with the magnetic activity curves.

A correlation with the magnetic activity is also apparent in the case of diurnal J variations. The amplitude of the diurnal variations in J increases with decreasing general cr intensity and increasing magnetic activity. The nature of this correlation can be seen in Fig. 3. It should be borne in mind that the amplitude of the observed diurnal variations is small so that any error due to statistical fluctuations becomes relatively important. Hence one cannot expect to find as great a similarity for curves A and J as for the J curves at different stations. However, the correlation is obvious for the larger variations. It indicates that the diurnal variations comprise a component associated with the M-variations of the general cr intensity.

As is known the phase of the diurnal variations also exhibits a world-wide shift.[4] At present the world-wide shift in the phase of the diurnal variations on the basis of the data of different stations has been traced up to 1954. Since 1947 there is evident a continuous displacement in time of the peak of the diurnal wave towards earlier hours. The fact that there is such a phase displacement is very important in developing the theory of diurnal variations. However, the results of any evaluations of the amplitude of the mean diurnal wave of extra-atmospheric origin and the magnitude of the shift of its peak are greatly dependent on the role in the observed diurnal variations played by the variations due to the temperature effect. We evaluated the extent of the temperature effect in the troposphere on the diurnal variations in cr intensities observed at Moscow. We found that the temperature fluctuations in 1951-2 tended to partially compensate the diurnal waves of other origins. The introduction of temperature effect corrections resulted in a two-fold increase in the apparent amplitude of the diurnal wave and virtually did away with the observed seasonal difference in amplitude (Fig. 6 and 7). However, in view of the uncertainty in determining the diurnal fluctuations of temperature in the atmosphere the resultant mean diurnal fluctuations in J cannot be regarded as wholly

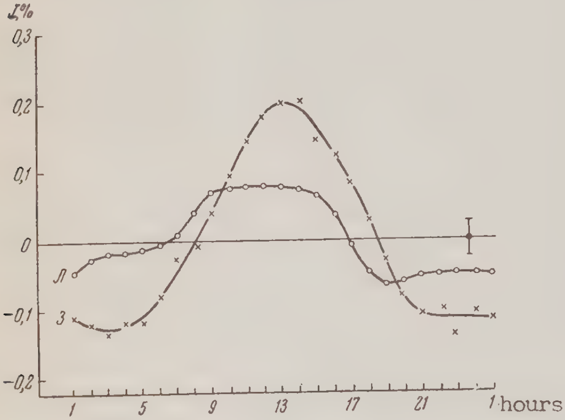

Fig. 6. Mean diurnal variation in J (in percent) in winter and summer at Moscow in 1951-2.

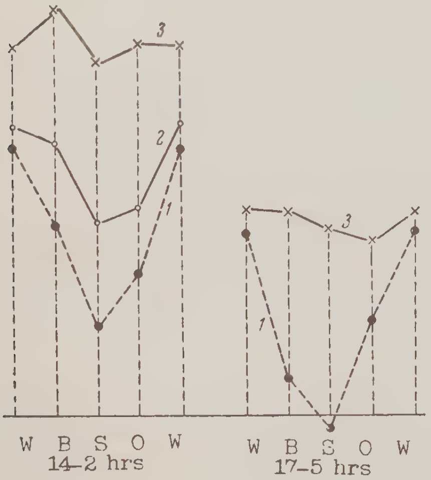

Fig. 7. Differences between values of J (cr intensity) at 14 and 2 hours (left) and at 17 and 5 hours local time (right): 1) before correction for the temperature effect, 2) after temperature corrections taking into account temperature fluctuations from observation level to the 800 mb isobar, 3) after temperature correction taking into account temperature fluctuations up to the 300 mb isobar. W - winter, B - spring, S - Summer and O - autumn.

and exclusively due to variations in primary cr intensity.

Thus, as the result of processing a large amount of observational data and introducing corrections for the temperature effect we brought to light some new experimental facts and obtained a general picture of the variation in the intensity of the meson component, due to variation in the intensity of primary cr. The deduced data are in agreement with the theory of the origin of cr variations, developed by Dorman.[1]

Conclusions

1. The Feinberg-Dorman theory of the temperature effect makes it possible to allow correctly for variations in cr intensity due to temperature fluctuations. The accuracy with which this can be done at present is determined by the accuracy of the available aerological data.
2. All world-wide variations (except "flare-ups") observed in the form of variations in the intensity of the meson component, belong to the same class or type. The processes giving rise to these variations are associated with the corpuscular streams responsible for magnetic storms and disturbances. This type of variation includes cyclic and long-term variations, annual changes in cr intensity during magnetic storms, world-wide irregular fluctuations from day-today and, apparently, 27-day variations.
3. There is good experimental evidence that the extra-atmospheric component in the diurnal variations can also be attributed to the processes that are responsible for the M-variations in the general intensity of cosmic radiation.

Scientific Research Institute
for Terrestrial Magnetism.

REFERENCES

1. L.I.Dorman, Preceding article in present issue of Bulletin.
2. E.L.Feinberg, Doklady AN SSSR, 53, 421 (1946); L.I.Dorman Doklady AN SSSR, 94, 433 (1954); Doklady AN SSSR, 95, 47 (1954).
3. Carnegie Inst., Washington, 175 (1948).
4. E.S.Glokova, Izv. AN SSSR, Ser. fiz., 17, 137 (1953).
5. Monthly Weather Review, Washington, 1949.
6. Spravochnik po peremennomu magnitnomu poliu SSSR, (Handbook on the Variable Magnetic Field for the USSR), V.I.Afanas'evoi, Editor, M.-L. 1954.
7. E.S.Glokova, Trudy NIIZM (Transactions Scientific Research Institute for Terrestrial Magnetism) 8, 59 (1952).
8. E.Roka, Zsf. Natur., 5a, 517 (1950).
9. Physics of cosmic rays, Wilson, Editor, IL, M., 1954.

VARIATION IN THE INTENSITY OF COSMIC RADIATION AT HIGH ALTITUDES

- Iu.I.Logachev & Iu.G.Shafer

Until now there have been no direct investigations of the variations in cosmic radiation at high altitudes: what information we had on the subject has been a "by-product" of other investigations. However, such indirect investigations have yielded certain data on the regularities of the variations at high altitudes. Thus the experiments of Biehl, Neher and others[1,2], devoted to investigation of the latitude effect at high altitudes showed that in the case of ascents from the same location on the intensity of cosmic radiation varies by some 5-10% from flight to flight when these are made at intervals of several days (Fig.1). On the other hand, the data obtained during the ascent and descent of the same flight are, as a rule, in close agreement, which indicates that the changes in intensity are slow. Neher[2] showed that the altitude dependence of the variations differs little from the altitude dependence of the basic cosmic radiation. This would indicate that if the observed variations are produced by variations in the primary radiation the primary flux must change over the entire energy spectrum, since obviously variations in a narrow range of the spectrum could not otherwise yield an altitude dependence largely duplicating the altitude dependence of the basic radiation.[3]

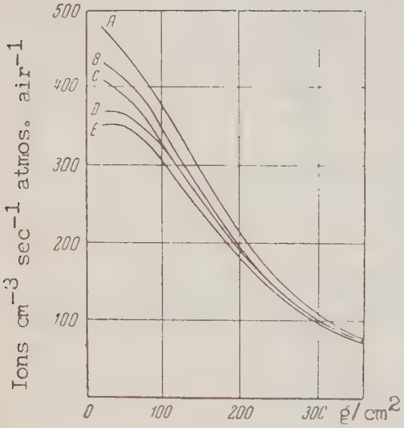

Fig. 1. Results of measurements of cosmic ray intensity at latitude 56°N. A) Aug. 21, 1940; B) Aug. 6, 1951; C) Aug. 3, 1951; D) June 26 to July 5, 1938; E) at 60° Lat. in 1937.

That these variations are produced by the primary radiation is indicated by the close correlation between the variations in the different components at different altitudes and latitudes. The pertinent data obtained by Neher and Forbush[4] are reproduced in Fig. 2.

On the other hand, a number of investigators[5-7] note that there are also observed cases of increases or decreases in cosmic ray intensity that become unnoticeable at altitudes corresponding to a pressure of 100 g/cm^2. The results of these investigations lead us to conclude that these rapidly attenuated variations are associated with low energy primary particles. Such increases in intensity are frequently observed at the time of solar flares, which proves that these variations are of solar origin and are due to fluctuations in the low energy region of the primary spectrum.

Our observations were made at a pressure altitude of 300 g/cm^2 by means of an unshielded counter telescope. For better monitoring of the operation of the equipment the apparatus was separated into two entirely independent channels; coincidences of the results from the two channels served as a criterion for the proper operation of all the equipment.

Twenty two flights were made with this equipment; in all flights the intensity registered in one of the channels coincided with that recorded in the other two within 0.1%. The overall measurement error is evaluated to be about 0.3%, the major part of the error being due to the uncertainty in the altitude indications.

Ours were the first experiments of comparable accuracy carried out expressly for the purpose of investigating the fluctuations in cosmic ray intensity. In 1942-49 Biehl and Neher[8] using similar equipment studied the

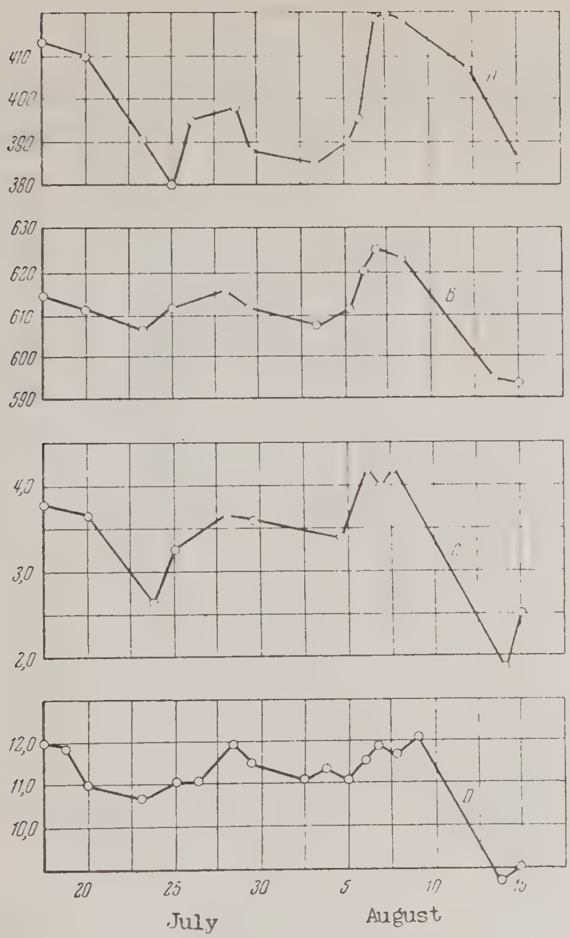

Fig. 2. Simultaneous variations in the intensity of different cosmic ray components: A) total ionization (ions cm^{-3} sec^{-1} atm^{-1} of air) at 50 g/cm^2 altitude (56°N); B) intensity of the neutron component in relative units at mountain altitude (48°N); C) deviations from normal intensity of hard component at sea level in % (50°N); D) deviations from normal ionization at mountain altitude in % (0°).

latitude effect at the same altitude (30,000 feet). As a result of several flights carried out under identical conditions, it was found that the intensity varies by 5-10% from flight to flight; these fluctuations can be attributed only to variations in the intensity of primary radiation (i.e., cannot be explained by apparatus and similar errors).

The results of our experiments are shown in Fig. 3, where the horizontal scale is laid off in successive flight numbers and the vertical scale in percent intensity relative to the normal value. It will be seen that the maximum deviation does not exceed 2%. In the same figure we show the variations in global intensity of the hard component at sea level as measured in Moscow and Iakutsk with an accuracy of within 0.2%. The fluctuations in intensity at these two points amount to about 1%. The measured intensity values were corrected for meteorological effects according to Dorman[3]; it may be noted that the necessary temperature correction to the intensity at 300 g/cm^2 pressure altitude proved to be very small.

Comparing the respective data we found the following altitude - to-ground correlation coefficients: 0.43 ± 0.2 for Moscow and 0.78 ± 0.1 for Iakutsk. This appreciable difference in the correlation coefficients is explained by the following. No observations were being made at Moscow during the period of large fluctuations in intensity at 300 g/cm^2 altitude; on the other hand, for small deviations the correlation may not be close, since in this case the measurement errors are comparable to the magnitude of the fluctuations. In Iakutsk the measurements were continuous and large fluctuations in intensity make an appreciable contribution to the correlation coefficient. Furthermore, it may be assumed that the errors in evaluating the temperature corrections at Iakutsk were appreciably smaller than for Moscow since radiation errors in temperature measurements at Iakutsk were minimal (the measurements were made at night), and interpolations of the radiosonde temperature measurements at Iakutsk are more accurate due to the greater stability of the atmosphere over that region.

Thus, there is close correlation between the intensity variations at

300 g/cm^2 pressure altitude in the region of Moscow and the variations at sea level at Iakutsk. This indicates that all variations are produced by the same changes in the primary radiation.

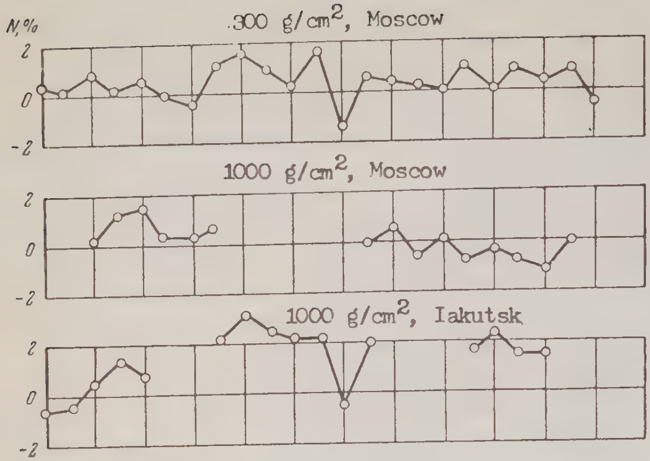
300 g/cm^2, Moscow

1000 g/cm^2, Moscow

1000 g/cm^2, Iakutsk

Fig. 3. Variations in the total intensity of cosmic rays at 300 g/cm^2 pressure altitude and simultaneous fluctuations in the global intensity of the hard component measured at Moscow and Iakutsk at ground level.

Our measurements were made during a year of minimum solar activity whereas those of Neher were carried out during a year close to the 11-year cycle maximum. That we detected only minor variations may be explained by assuming that their magnitude changes with changes in solar activity. This assumption identifies the sun as the cause of the variations that change little with the altitude of observation and that are consequently associated with fluctuations in the intensity of the primary radiation over the major part of its energy spectrum. As has been noted above, the intensity variations characterized by rapid attenuation with increasing atmospheric depth are also apparently produced by the sun. Thus it may be said that all variations in cosmic ray intensity that have so far been observed at high altitudes are probably connected with solar activity or are produced by it.

The experimental data on the variations in cosmic ray intensity at high altitudes cited above are in agreement with the general picture of the origin of cosmic ray variations and fluctuations presented in Dorman's report[9] and examined in detail in his thesis[3].

Further investigation of cosmic ray variations at high altitudes should be of great interest and may be expected to yield valuable information on the nature of corpuscular streams, various processes occurring on the sun and other astrophysical factors.

"M.V.Lomonosov" Moscow State University
and
Iakutsk Branch of the USSR Academy of Sciences

REFERENCES

1. A.T.Biehl, R.A.Montgomery, H.V.Neher, W.H.Pickering & W.C.Roesch, Rev. Mod. Phys., 20, 360 (1948).
2. H.V.Neher, V.Z.Peterson & E.A.Stern, Phys. Rev., 90, 655 (1952).
3. L.I.Dorman, Thesis, NIIZM, M., 1955.
4. H.V.Neher, G.E.Forbush, Phys. Rev., 87, 889 (1952).
5. N.L.Grigorov, Thesis, Moscow State University,1954.
6. M.A.Pomerantz, Phys. Rev., 81, 731 (1951).
7. J.J.Lord, A.W.Elston & M.Schein, Phys. Rev., 79, 540 (1950).
8. A.T.Biehl, H.V.Neher, Phys. Rev., 83, 1169 (1951).
9. L.I.Dorman, Present issue of the Bulletin.

CLOSING ADDRESS

- S.N.Vernov

Our Conference has completed its work. We have heard much that is new and interesting in the field of high-energy physics. The reports presented and ensuing discussions also indicate the paths that further investigations should follow.

The Conference was begun with reports on the most thoroughly studied range of cosmic radiation, that having energies of the order of 10^{10} ev. Diverse experimental methods have been used for the study of the interactions of cosmic ray particles with atomic nuclei at these energies. Thanks to these extensive experiments it has been possible to elucidate the characteristics of particle collisions at energies exceeding the π-meson production threshold energy by more than an order of magnitude. There may be some argument as to how one should interpret the structure of nucleons. However, the fact that the major part of the primary particle's energy in nuclear collisions is retained by one of the secondary nucleons speaks in favor of a complex nucleon structure and makes it possible to approach the study of nucleonic structure by investigating high-energy encounters.

The Conference heard a large number of theoretical reports and the special lecture of Academician L.D.Landau. There can be no doubt that the systematic development of the theory of processes occurring at high energy on the basis of thermodynamic and hydrodynamic concepts and comparison of the predictions of theory with experiment are highly important. I feel, however, that the hypothesis of the transfer of 100% of the primary energy to the Fermi-system has not been justified. It would be more logical in this case to be guided by the empirical results of experiment.

Results of investigations of extensive air showers, produced by the interaction of ultra-high energy particles with atomic nuclei, have shown that the new technique based on use of correlated hodoscopes consisting of many thousands of counters actually makes it possible to study elementary processes at energies of 10^{14}-10^{16} ev. We cannot emphasize too much the importance of further investigations in this direction and, particularly, along the lines of observation of extensive air showers simultaneously at the surface of the ground and underground. As we have heard, the first successful attempts along this line were made by the staff of the Georgian SSR Academy of Sciences. In order to clarify the nature of elementary events at energies to 10^{16} ev, in addition to extensive experimentation, theoretical analysis of the known processes is also necessary. Here the course to be followed has been chartered by Academician D.V.Skobel'tsyn. Without profound theoretical analysis we cannot form any definite conclusions about so complex a phenomenon as extensive air showers. We may have reason to expect to find in the composition of extensive air showers (or at any rate in some of them) a type of particle having an energy greatly exceeding that of all other known particles. If this should be true the interpretation of the experimental data will be much simpler.

Unfortunately the untimely death of N.V.Shostakovich has made it impossible to discuss fully certain problems regarding new particles, particularly those having a mass of about 600 m_e. We have heard here of new experimental methods, such as the newly developed liquid bubble chambers.

From reports and discussions on the origin of cosmic rays and fluctuations in the intensity of cosmic radiation, certain plausible assumptions can now be made. Such data may prove helpful in studying the corpuscular streams emitted by the sun.

In the name of the organizing committee I would like to thank our astrophysicist colleagues A.I.Lebeninski, S.B.Pikel'ner and I.S.Shklovski for participating in our Conference.

Proceedings of the Meeting of the Department of Physical-Mathematical Sciences of the USSR Academy of Sciences (Moscow, 26-27 April 1955)

(Session on Semiconductors)

OPENING ADDRESS

- A. F. Ioffe

The Board of the Department of Physical-Mathematical Sciences of the USSR Academy of Sciences has decided to devote this meeting of the Department to problems having to do with semiconductors. The selection of this topic is justified by the rapidly growing importance of semiconductors to solid state physics and its technical applications. The problems involved will be considered at this session.

Semiconductors constitute the link between metals and dielectrics. The theory of semiconductors was developed on the basis of the zone theory of metals and to this day bears evidences of its origin.

In some respects semiconductors are simpler than metals: the use of the one-electron approximation is better founded and Fermi statistics may frequently be replaced by the classical Boltzmann statistics in treating semiconductors. On the other hand, the semiconductors are more complex and diversified. We need only mention the complex structure of the zone spectrum, the existence of excitons and polarons, the frequently decisive role played by volume charges, the statistics of holes and electrons and of the great diversity of properties which now form the basis of almost twenty branches of technology.

During my own, almost thirty-year, period of activity in the field many significant advances have been made in study of semiconductors. Quantum concepts regarding zones, effective mass, electrons and holes, and the chemical potential, and on passing from Boltzmann statistics to the statistics of degenerate electrons have entered current usage not only of the physicist but also of the engineer and chemist. The kinetic equation has been extended to many of the diverse processes occurring in different semiconductors. Theory and experiment have uncovered new electron states in solids: polarons and excitons. The study of boundary and transition layers, such as those at the separation between two bodies and those associated with changes in properties inside the semiconductor, has seen great development.

New technological possibilities have been opened up by the profounder development of physical theory. Rectifiers are being made with ratings in the hundreds of amperes at potentials of hundreds of volts and efficiencies above 95%, thus solving the problem of rectifying heavy alternating currents. Semiconducting diodes and triodes successfully replace vacuum tubes, leading to a new era in electronics. Photoelectric tubes, thermistors and photoresistors are becoming the basic components in automation, communications and remote control. Finally, before our very eyes, semiconductors are invading the domain of engineering, -- in power engineering, for example, thermoelectric elements transform heat to electric energy without the use of machinery; together with photoelectric tubes they are making it possible to utilize not only solar energy but the energy of radiation from radioactive substances, as well.

This importance of semiconductors imposes especially high requirements on the state of theory and its substantiation by experiment.

It seems to me that current semiconductor theory has already passed beyond the boundaries marked by its original hypotheses. Assuming that an electron moving in the periodic field of a lattice traverses without collision tens of interatomic distances, the theory treats its motion as that of a plane wave and, by analogy with free motion, introduces the concepts of mean velocity, acceleration, and effective mass. But in many if not most semiconductors, the length of the mean free path turns out to be shorter than the period of the lattice and but a fraction of the wavelength; the uncertainty in the value of the kinetic energy is ten or a hundred times greater than the value of the energy itself. Under such circumstances the kinetic equation loses its meaning, and the theory is left "hanging in mid-air."

To be sure, it is possible to increase appropriately the effective mass by a factor of several thousand, but what is one to do with the self-consistent field and with the adiabatic approximation if the mass of an electron is equal to that of an ion?

The theory deduces the zone structure of the electron energy spectrum from the periodicity of the crystal lattice. But the spectrum persists even after melting, when the periodicity of long range order has vanished! This implies that the deduction is based on false premises.

There are also direct disagreements between theory and experiment, for example, in matters of the temperature dependence of mobility, the variation of the thermoelectromotive power at low temperatures, the influence of magnetic fields, of effective mass, etc.

The status of experiment, too, leaves much to be desired: the number of semiconductors which have been studied is too small to allow of broad generalizations. We know nothing about dipole or molecular substances or about how various types of bonds — covalent, ionic, metallic — are interrelated.

The properties of semiconductors are studied in isolation from each other: we study the scattering of electrons by thermal vibrations without regard to the spectrum of these vibrations or the scattering of phonons by these vibrations. No account is taken of the character of these vibrations, their anharmonicity, which determines the thermal conductivity and thermal expansion.

No one has yet become interested in the mechanical properties of semiconductors. For example, in connection with thermal conductivity I will show* how tightly interwoven are the thermal, electric and optical properties of semiconductors.

The indicated shortcomings of both theory and experiment show that the study of semiconductors is only in its birth as an independent field of knowledge. Until now semiconductors have been merely an "extrapolation" of metals. Is it not the time to approach them from another point of view, for example, from that of the concepts on which the theory of plasma is founded?

---

* See the paper by A. V. Ioffe and A. F. Ioffe. "Thermal conductivity of semiconductors,"

Development of theory and experiment, as well as more rigorously founded generalizations, will create the basis on which the many technical potentialities of semiconductors can be more richly and more quickly realized. Electronics and automation, energetics and measurement techniques will all receive new momentum.

The present meeting does not have as its aim to embrace all sides of the semiconductor problem. That is the objective of the conference which we expect to hold in Leningrad next October.

THERMAL CONDUCTION IN SEMICONDUCTORS

- A. V. Ioffe and A. F. Ioffe

Two mechanisms are involved in heat transfer in semiconductors: thermal-movement waves (phonons) and electrons. The thermal conduction coefficient can be represented in the form of a sum:*

$$\varkappa = \varkappa_{\text{ф}} + \varkappa_{\text{эл}}. \tag{1}$$

The electronic component in the right half of (1) is directly related to the electric conductivity :

$$\varkappa_{\text{эл}} = L\sigma, \tag{2}$$

where the values of L are

$$L_{\text{n-d}} = 2\left(\frac{k}{e}\right)^2 T, \tag{2a}$$

for the non-degenerate electrons of the atomic crystal lattices and

$$L_{\text{deg}} = 3{,}3\left(\frac{k}{e}\right)^2 T. \tag{2b}$$

for electron concentrations corresponding to the degenerate state.

If $\varkappa$ is given in cal/cm/sec/deg and σ in mho/cm, we have at room temperatures, with sufficient accuracy

$$L_{\text{n-d}} = 1\cdot 10^{-6} \text{ and } L_{\text{deg}} = 1.6\cdot 10^{-6}$$

Hence, if the specific electric conductivity does not exceed 100 mho/cm, the electronic component of the thermal conduction will be less than 10^{-4} cal/cm/sec/deg and can be neglected. Once σ exceeds 1000 mho/cm, $\varkappa_{\text{эл}}$ usually becomes comparable to $\varkappa_{\text{ф}}$.

The semiconductor thermal-conduction measurements described below were made at room temperatures using a previously described instrument, since improved, having a probable error of 2-5% (depending on the value of $\varkappa$).**

The relationship between $\varkappa_{\text{эл}}$ and σ (eq. 2), known as the Wiedemann-Franz law, applies not only to metals, on which Wiedemann and Franz experimented, but also to semiconductors. This law was substantiated by Iu. A. Dunaev and Iu. P. Maslakovets for lead sulfide with non-degenerate electrons, by E. D. Deviatkova for degenerate electrons, and by our own experiments for a semiconductor, the conductivity of which, ranging from 1000 to 4500 mho/cm, embraced both cases. Fig. 1 shows that at a constant value $\varkappa_{\text{ф}} = 2.3 \times 10^{-3}$ cal/cm/sec/deg, obtained by extrapolating to $\sigma = 0$, $\varkappa_{\text{эл}}$ increases linearly with σ, and L assumes the values predicted by theory: about 10^{-3} cal/cm/sec/deg per 1000 mho/cm at $\sigma < 2500$ mho/cm and $1.5\cdot 10^{-3}$ cal/cm/sec/deg at $\sigma > 3500$. This increase in the value of L corresponds to the degeneracy boundary at concentrations on the order of 10^{19} per cm^3.

That $\varkappa_{\text{ф}}$ and $\varkappa_{\text{эл}}$ are additive is far from obvious: such an assumption would disregard the scattering of thermal waves (phonons)

---

* Translator's note. Key to subscripts: ф - phonon; эл - electron.

** The low temperature measurements were made by E.D.Deviatkova, while the high temperature ones were made by P.V.Gul'tiaev. The speed of sound and the mobility of the electrons were determined by A.G.Ostroumov.

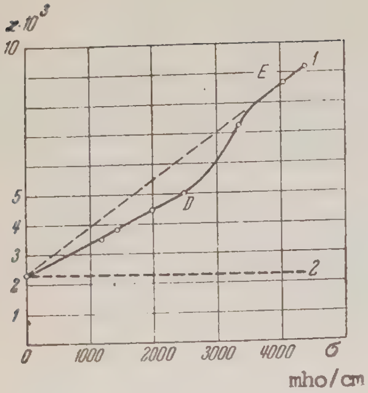

Fig. 1. Variation of thermal conduction with electric conductivity. 1) Conduction $\varkappa = \varkappa_{\text{ф}} + \varkappa_{\text{эл}}$; 2) conduction $\varkappa_{\text{ф}}$; D - beginning of degeneracy, E - degenerate electron system.

from electrons. That such scattering is possible is evidenced by the applicability of the Wiedemann-Franz law to light as well as heavy metals. It will be shown below that it is natural to assume that in the absence of free electrons the measured thermal conduction would be on the order of several tens of cal/cm/sec/deg, as compared with the several thousands that can be expected for the crystal lattice of a heavy metal. Yet this difference is not reflected in the experimentally-obtained values of thermal conduction of metals. From the applicability of (1) to metals, it would follow that the ratio $\varkappa/\sigma$ should be almost twice as large for light metals as for heavy ones.

This contradiction is reminiscent to some extent of the specific-heat paradox of the classical theory of metals with that difference, naturally, that in the evaluation of the thermal conduction we do not take into account the thermal conduction of the crystal lattice, while in the case of the specific heat of metals it was necessary to ignore the specific heat of the electrons.

Attempts to attribute the small differences in the coefficient L for different metals to the contribution of the thermal conduction of the lattice did not lead to conclusive results. No extant theory is capable of adequately describing both mechanisms of thermal conduction in metals. However, it appears logical to ascribe the minor role of phonon thermal conduction to the scattering of phonons from free electrons. If we assume that the additional thermal conduction of the lattice results in variations in the factor L, the contribution of the phonon thermal conduction becomes not more than 0.01 cal/cm/sec/deg. In other words, scattering of phonons by electrons introduces a thermal "resistance" of not less than 100 cm/sec/deg/cal. It vanishes completely only upon transition to the superconducting state, when $\varkappa = \varkappa_{\text{ф}}$ and $\varkappa_{\text{эл}} = 0$.

The electron concentration in semiconductors usually does not exceed 10^{20} per cm^3 while in metals it amounts to 10^{22} per cm^3. One can, therefore, assume the thermal resistance introduced by scattering from the electrons of the semiconductor attains a value of several units. At a thermal conduction of $\varkappa = 5 \times 10^{-3}$ cal/cm/sec/deg and the thermal resistance of $1/\varkappa$ = 200 cm/sec/deg/cal, this amounts to only a few percent. But in semiconductors having a thermal resistance measuring only few units or tons of units, the effect of scattering from the conduction electrons may become noticeable.

The above rough estimate of the role of the scattering of phonons by electrons does not take into account the differences in the interactions of the phonons with metal electrons, which have kinetic energies of several electron volts, on one hand, and with semiconductor electrons, which have kinetic energies on the order of some hundredths of an electron volt, on the other.

As Debye showed back in 1914, the phonon component of the theral conduction can be expressed, by analogy with the coefficient of diffusion in gases, as

$$\varkappa_\Phi = {}^1/_3 \,(\text{or } {}^1/_4)\, c v \bar{\lambda}, \tag{3}$$

where c is the specific heat per unit volume, v the velocity of propagation of the thermal waves (phonons) and $\bar{\lambda}$ is the mean free path of the phonons. The value of $\bar{\lambda}$ depends on the extent to which the thermal vibrations are anharmonic and on the intensity of these vibrations, which can be expressed as $\int_0^T c\,dT.$

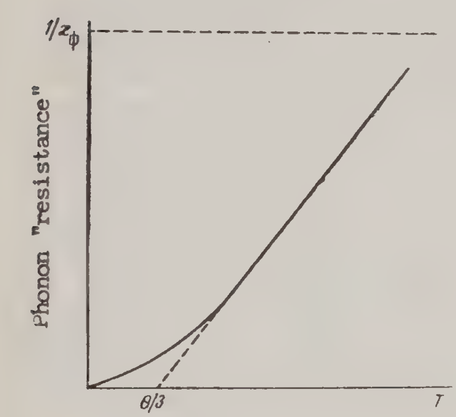

Fig. 2

At temperatures above the Debye temperature, at which the average heat energy is equally distributed among the degrees of freedom, we can assume that

$$\frac{1}{\bar{\lambda}} = A \int_0^T c\,dT, \tag{4}$$

and the degree of anharmonicity A is independent of the temperature.

Let us provisionally start out with the spectrum of the thermal vibrations of a continuous solid body, for which the number of vibrations in an interval $d\nu$ is proportional to ν^2, and for our unit of temperature take the Debye temperature θ. Values of the integral (4) for this case are fully tabulated, while for temperatures above θ, the integral may be written as

$$\left(\int_0^T c\,dT\right)_{T>\theta} = c\left(T - \frac{\theta}{3}\right). \tag{5}$$

we have, consequently, under these conditions

$$\frac{1}{\varkappa_\Phi} = \frac{3A}{v}\left(T - \frac{\theta}{3}\right). \tag{6}$$

The dependence of $1/\varkappa_\Phi$ on T is shown in Fig. 2.

As expected, eq.(6) is valid as long as the body can be regarded as a continuum. When $\bar{\lambda}$ approaches the lattice constant a, $1/\varkappa_\Phi$ no longer increases as expected from (6). We were unable to carry $\varkappa_\Phi$ down to values at which $\bar{\lambda} < a$. The corresponding limiting value of $\varkappa_\Phi$ is tentatively indicated by the dotted line in Fig. 2.

The applicability of the Debye equations to thermal conduction is substantiated by the following facts:

Where $\bar{\lambda}$ can be estimated in advance, as in amorphous bodies or, at low temperatures in powders as well, the value of $\varkappa_\Phi$, as computed from the kinetic theory of gases agrees well with the experimental results. In powders at low temperatures $\bar{\lambda}$ **is actually determined** by the size of the individual grains. For glass $v = 5 \times 10^5$, $c = 0.3$, and $\varkappa_\Phi = 2.5 \times 10^{-3}$, and consequently $\bar{\lambda} \approx 5$ to 7 Å, which corresponds to the molecular spacing.

Insofar as c and v in glass change little with temperature above the Debye temperature, $\varkappa_\Phi$ is temperature independent; at low temperatures, where c is proportional to T^3, $\varkappa$ is also proportional to T^3.

The further development of the theory of phonon thermal conduction by Peierls and others does not yield an answer to our problem of evaluating the thermal conduction and of relating it to other parameters, characterizing the properties of the material. Yet the variation of is large : from 0.5 cal/cm/sec/deg for diamond to

0.0005 cal/cm/sec/deg for sulphur. Until recently, experimental investigations were devoted predominantly to the variation of $\varkappa_\Phi$ with temperature.

It can be predicted from elementary considerations that, other conditions being equal, thermal conduction decreases with the temperature θ of the material, i.e., with the frequency of the atomic vibrations, which are dependent upon the atomic weight and the modulus of elasticity (or the speed of sound); $\varkappa_\Phi$ will be smallest for crystal lattices whose thermal vibrations are most anharmonic. The first deduction that can be drawn from the above considerations is that $\varkappa_\Phi$ will decrease with increasing atomic weight in substances having the same type of lattice. This deduction is confirmed both by published data on thermal conduction and by the results of our experiments. Thus the values of the thermal conduction $\varkappa_\Phi$ come to several tenths of a calorie/cm/sec/deg for elements in the top two lines of the periodic table, drop to several hundredths for elements in the middle portion of the table and to a few thousandths for the elements at the bottom of the table. The results of our experiments are shown in Fig. 3 where values of log $\varkappa_\Phi$ as a function of the average atomic weight $\bar{A}$ of the components of the investigated material. The lines join substances of the same crystal-chemical type: 1) diamond type lattices, 2) compounds formed by elements of the 3rd and 5th groups, 3) oxides of 2nd-group elements, and 4) ionic lattices of alkali halides. There is no doubt that $\varkappa_\Phi$, as a rule, decreases with increasing $\bar{A}$. Aiken has shown that $\varkappa_\Phi$ decreases with decreasing hardness in crystals of the same type.

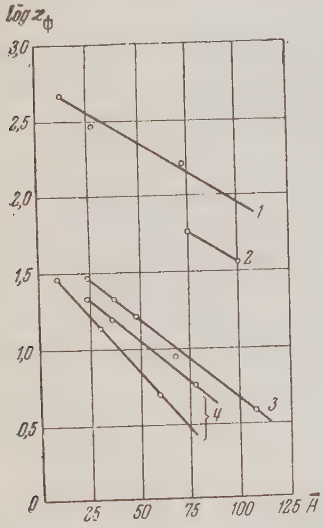

Fig. 3

Thermal conduction is of decisive importance where the quality of thermocouples is concerned: the smaller $\varkappa_\Phi$, the higher the efficiency. It is, therefore, important to find means for selecting semiconductors having a low $\varkappa_\Phi$ and for reducing $\varkappa_\Phi$ where it is excessive. Here the mobility of the electrons must also be taken into account. The higher the ratio of electron mobility to thermal conduction, the more suitable the semiconductor for use in thermocouples. Aiken already noted that the presence of defects or of impurity atoms in the crystal lattice decreases $\bar{\lambda}$ and consequently $\varkappa_\Phi$, as well. This is shown in Fig. 4, where $1/\varkappa_\Phi$ is plotted against impurity-atom concentrations in Ge and Si.

The effect of impurities can be evaluated quantitatively: each impurity introduces an added phonon scattering center having a cross section pa^2, where a is the lattice period.

In the case of Ge, $\bar{\lambda}$ = 200Å or approximately 35 a. In germanium, at room temperatures, 3% of the atoms in the path of a phonon participate in the scattering. The addition of yet another 3% of extraneous atoms, each causing a like scattering, should reduce $\varkappa_\Phi$ by half or double $1/\varkappa_\Phi$.

In the case of lead telluride, on the other hand, where $\bar{\lambda}$ = 15Å = 3 a, at least 30% of impurity atoms would be needed to reduce the thermal conduction by one half; this difference is clearly evident from a comparison of Figs. 4 and 5.

There are, however, impurities that cause more effective scattering. Thus, for example, 7% of Te reduces the thermal conduction

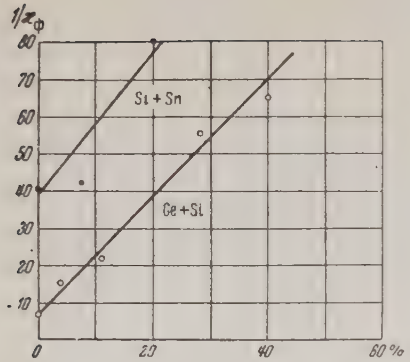

Fig. 4

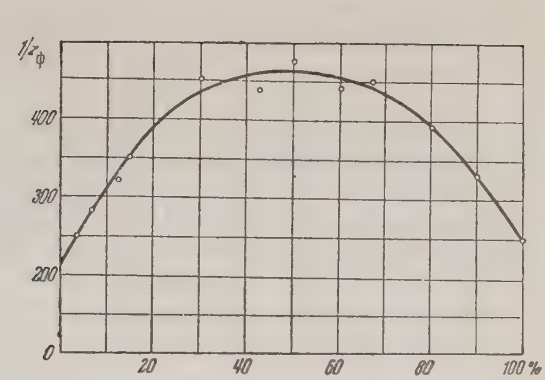

Fig. 5. Variation of the thermal resistance of solid solutions of PbSe in PbTe with the PbSe concentration (in per cent).

of GaSb from $60 \cdot 10^{-3}$ to $12 \cdot 10^{-3}$. In this case $p > 1$, although there may be defects for which the average value of $p < 1$. Thus, the effect of impurities depends not only on their concentrations, but also on how they enter into the structure of the material. Apparently inclusion impurities deforming the lattice by several atomic distances are characterized by a higher scattering cross section than substitution impurities.

It would be interesting to investigate impurities in a wide range of concentrations, particularly solid solutions of isomorphic substances. The variation of the thermal resistance of a solid solution of PbSe in PbTe with the PbSe concentration is shown in Fig. 5.

The solid line curve describes the equation proposed by Nordheim for metal alloys:

$$\frac{1}{\varkappa_\Phi} = \frac{1}{\varkappa_0} + \frac{1}{\varkappa_0}(1 - x)xp\frac{\overline{\lambda}_0}{a}, \qquad (7)$$

where x is the concentration. In the case of solutions of Bi_2Te_3 and Sb_2Se_3 the solubility of both components is limited to a certain range.

It has also been found that in approximately half of the solutions investigated the substance becomes "amorphous" with respect to phonon scattering, while $\overline{\lambda}$ approaches the interatomic distance a; here $\varkappa_\Phi$ in such cases is close to $2 \cdot 10^{-3}$ and independent of temperature (straight line in Fig. 6, based on measurements by P. V. Gul'tiaev). Even for solutions of Si in Ge the value of $\varkappa_\Phi$ drops from $145 \cdot 10^{-3}$ to $8 \cdot 10^{-3}$ (by a factor of 20) and $\overline{\lambda}$ approaches 6A — the lattice period.

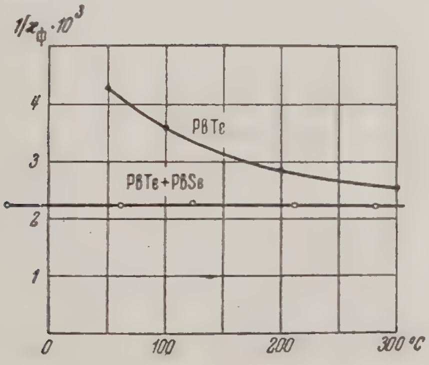

Fig. 6

In solid solutions, where the mean free path of the phonons is reduced to the value of the lattice constant, the mobility of the electrons still remains high, and their mean free path is on the order of tens of atomic distances. A solid solution that is nearly amorphous as regards phonons still maintains its periodic properties where the electrons are concerned.

There is reason to think that this difference may be due to the difference in wavelengths. The wavelength of the principal mass of phonons is on the order of 10^{-8}-10^{-7} cm; consequently each irregularity in atomic dimensions produces scattering. The electron wavelength, on the other hand, is on the order of 20 lattice constants; for such wavelengths the periodicity of the long range order is of paramount importance, while local variations of the structure will have little more effect than fluctuations in the thermal motion. Thus the reduced mobility in the PbSe-PbTe alloy (compared with the pure substances) corresponds to a temperature increase from 300 to 380°K, whereas for thermal conduction the corresponding temperatures would be 300 to 750°K.

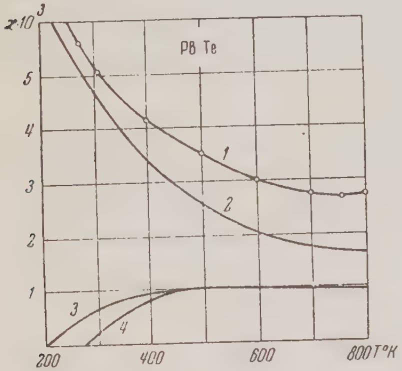

Fig. 7. Comparison of the different thermal conduction mechanisms: 1) $\varkappa$ - measured value, 2) $\varkappa_0$ - extrapolated value on assumption of linearity of the temperature dependence of $\varkappa_ф$ and applicability of the equation $\varkappa_ф = \varkappa - L\sigma$, 3) $\Delta\varkappa = \varkappa - \varkappa_0$; 4) $\varkappa_{exc}$ - computed on the assumption of heat transfer by excitons.

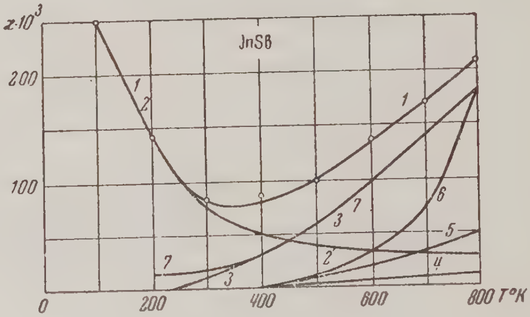

Fig. 8. Comparison of the different mechanisms of the additional thermal conduction in pure specimens: 1) $\varkappa$ - measured value, 2) $\varkappa_0$ - extrapolated assuming the variation of $\varkappa_ф$ with temperature to be linear and $\varkappa_ф = \varkappa - L\sigma$ to be applicable, 3) $\Delta\varkappa = \varkappa - \varkappa_0$, 4) $\Delta\varkappa_{eh}$ - computed assuming heat transfer by bipolar diffusion of electrons and holes, 5) $\Delta\varkappa_{exc}$ - calculated assuming heat transfer by excitons, 6) $\Delta\varkappa_{en.pr.}$ - computed assuming heat transfer by phonons entrained (carried along) by the electron-hole stream; the value of $\Delta\varkappa$ at 800°K is adjusted to fit the experimental value, 7) $\Delta\varkappa_{en.exc.}$ - measured, due to entrainment of phonons by excitons.

Let us now turn to the electron portion of the thermal conduction. It would seem to be fully covered by the Wiedemann-Franz law. Subtracting $L\sigma$ from the total value of $\varkappa$ we should obtain the expected linear temperature variation for $\varkappa_ф$ (eq. (2) and Fig. 2).

However, E. D. Deviatkova noted already several years ago that once the intrinsic conductivity becomes manifest, the use of the Wiedemann-Franz Law to account for $\varkappa_{эл}$ does not make the re-calculated curve a straight line; there remains a residual thermal conduction $\Delta\varkappa$, which increases with the intrinsic electric conductivity.

In 1954 the Swiss physicist Busch noted a similar deviation in an In-Sb alloy; the reported deviation exceeds the correction based on the Wiedemann-Franz law by a factor of about 100 (Fig. 8).

Reminder. Key to subscripts: ф - phonon; эл- electron.

Gul'tiaev extended the measurements of Deviatkova into the region of higher temperatures and confirmed the deviation from the straight line of Fig. 2 to the side of higher thermal conduction values.

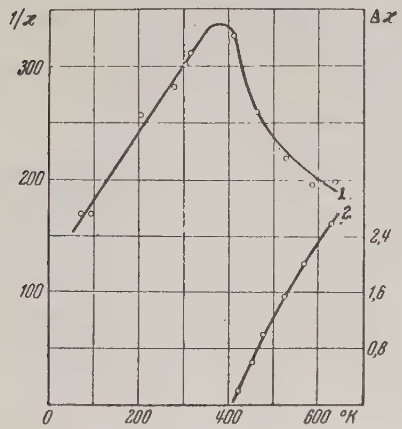

Fig. 9. 1) Variation of thermal resistance with temperature in Bi_2Te_3; 2) variation of increment in the thermal conduction in Bi_2Te_3.

An even greater increase in the thermal conduction is evinced in Bi_2Te_3, according to the measurements of Deviatkova and Gul'tiaev (Fig. 9). Judging from the temperature range in which the increase in thermal conduction is observed, it may be assumed that here, too, it is connected with the appearance of intrinsic conductivity.

Thus, the appearance (simultaneously with the intrinsic conductivity of a semiconductor) of an elevated thermal conduction, exceeding the value of $L\sigma$ given by the Wiedemann-Franz law (2), is not an isolated phenomenon. This phenomenon does not invalidate, but on the contrary, supplements the aforementioned experiments confirming the applicability of the Wiedemann-Franz law to semiconductors, inasmuch as these experiments pertain to impurity conductivity, in which only current carriers of the same polarity (either electrons or holes) participate. Deviations from this law appear in the temperature range where the intrinsic conductivity, which involves carriers of both polarities, may be expected to become pronounced and even to predominate. The connection between the current carried by the charges and the temperature equalization effected by them becomes quite different when both holes and electrons participate simultaneously in the flow of current or in the diffusion.

As long as only electrons or only holes are present, their flow from the hot to the cold region produces an electric field counterbalancing the diffusion. A static equilibrium is established in which every section of the body is traversed by an equal number of electrons in both directions; although equal in number the electrons differ as regards kinetic energy. This is the process by which the temperature becomes equalized by free charges of the same polarity.

A different situation obtains when the charges are of both polarities, for the joint diffusion of holes and electrons (bipolar diffusion) does not transfer any charge and, therefore, does not produce a counteracting field. If the charges have different mobilities, the faster charges, moving ahead of the general diffusion, produce an electric field E, which accelerates the charges of lower mobility and slows down the faster moving ones to a uniform diffusion rate. As in the analogous case of diffusion in electrolytes, the intensity of this field is:

$$E = \frac{kT}{e}\frac{1}{n}\frac{dn}{dx}\frac{u_- - u_+}{u_- + u_+} = \frac{\Delta\varepsilon}{2Te}\frac{u_- - u_+}{u_- + u_+}\frac{dT}{dx}. \tag{8}$$

The thermal emf produced in this case is $\alpha = \frac{\Delta\varepsilon}{2Te} \times \frac{u_- - u_+}{u_- + u_+}$, compared with $\frac{\Delta\varepsilon}{2Te}$ in the case of impurity conductivity.

The bipolar-diffusion field is due only to the difference in the carrier mobilities. Hence, if $u_- = u_+$, $E = 0$ and $\alpha = 0$.

An equation for $\varkappa_{\text{эл}}$ in the simultaneous presence of holes and electrons was published by Davydov and Shmushkevich as early as 1940, and by Price in 1954. They took into account not only the different conditions of motion of the charges, but also the fact that the electron-hole pairs, while moving from the hot (high concentration) end to the cold end, combine and liberate an energy $\Delta\varepsilon$.

The Davydov-Shmushkevich equation can be written in the following form:

$$\varkappa_{\text{эл}} = L(\sigma_+ + \sigma_-) + 2L\frac{\sigma_+\sigma_-}{\sigma_+ + \sigma_-}\left(\frac{\Delta\varepsilon}{2kT} + 2 + r\right)^2. \qquad (9)$$

Here σ_+ and σ_- are the specific electric conductivities produced by the holes and electrons separately, $\Delta\varepsilon$ – the width of the "forbidden" zone, and r – the exponent in the expression for the mean free path of the free charges as a function of their energy ε, i.e., in the expression $l \sim \varepsilon^r$.

In the particular case of atomic lattices having one acoustic branch of the thermal vibrations, $r = 0$. The additional thermal conduction, produced by the flow of electron-hole pairs is

$$\Delta\varkappa_{\text{pr}} = 2L\frac{\sigma_+\sigma_-}{\sigma_+ + \sigma_-}\left(\frac{\Delta\varepsilon}{2kT} + 2 + r\right)^2.$$

The value of the factor in front of the parentheses depends on the ratio σ_+/σ_-.

When $\sigma_+ = \sigma_-$, the factor in front of the parentheses of the second term in (9) becomes $L\sigma$ or $1/2\, L(\sigma_+ + \sigma_-)$; and

$$\varkappa_{\text{эл}} = L(\sigma_+ + \sigma_-)\left[1 + \frac{1}{2}\left(\frac{\Delta\varepsilon}{2kT} + 2\right)^2\right]. \qquad (9a)$$

As long as the ratio of the two specific conductivities does not exceed 1.5-2.0, the above factor changes little. But if σ_+ is much greater or much smaller than σ_- the factor in front of the second term parentheses assumes a value close to $2L\sigma_i$, where σ_i is the lesser of the two conductivities. For example, for the alloy InSb, where the mobility ratio u_-/u_+ is approximately 80 in the intrinsic conductivity region, when $n_- = n_+$, $\sigma_-/\sigma_+ = 80$, and eq. (9) becomes:

$$\varkappa_{\text{эл}} = L(\sigma_+ + \sigma_-)\left[1 + \frac{1}{40}\left(\frac{\Delta\varepsilon}{2kT} + 2\right)^2\right]. \qquad (9b)$$

Within the range of attainable temperatures, the intrinsic conductivity $\sigma_+ + \sigma_-$ and with it $\varkappa_{\text{эл}}$ become quite large, provided $\Delta\varepsilon$ does not exceed 0.6 ev. The second term in the brackets in eq. (9a) attains values approaching 70; in other words, the coefficient L becomes some 70 times larger in the intrinsic conductivity region than is indicated by the Wiedemann-Franz law.

In the case of InSb with $\Delta\varepsilon \approx 0.3$ ev, eq. (9b) calls for L to increase by a factor of only 2, while Busch's measurements give a nearly 100-fold increase for L.

However, the effect of bipolar diffusion of free charges discussed above is not the only process capable of leading to an increase of the thermal conduction. The manifestation of intrinsic conductivity may, for example, also be accompanied by the formation of excitons.

Excitons were introduced into semiconductor theory by Ia. I. Frenkel' in 1931. They were used by Zhuze and Ryvkin to explain the nature of the internal photo-effect in cuprous oxide. The spectra of the excitation of excitons by light in cuprous oxide and cadmium sulfide were studied by E. F. Gross, while the order of magnitude of the mean free path of non-localized excitons was evaluated by A. I. Anselm.

If excitations of this type can be produced in a crystal lattice under the influence of light, they can also be produced by thermal motion. The exciton concentration N can be represented in this case as a function of the temperature and of a certain excitation energy $\Delta\varepsilon$, determined by the conditions of static equilibrium.

One can expect the non-localized excitons, each of which can be considered as formed of a coupled hole and electron, to diffuse freely from the hot portions of the body into the cold ones, without carrying any charge. The number of excitons diminishes along the way while the energy $\Delta\varepsilon'$ expended on their excitation is liberated, i.e., converted into heat and radiated.

Under these assumptions, the additional thermal conduction $\Delta\varkappa_{\text{exc}}$ of the excitons can be expressed, in analogy with $\Delta\varkappa_{\text{pr}}$ for the intrinsic conductivity, as:

$$\Delta\varkappa_{\text{exc}} = \frac{k^2}{e^2}\sigma T \frac{N}{n}\frac{U}{u}\left[\frac{\Delta\varepsilon'}{kT}+2\right]^2, \tag{10}$$

where N is the exciton concentration, $U = \frac{e}{kT}D$ (D is the exciton diffusion coefficient), and n and u are the same quantities pertaining to free charges.

According to the theory developed by Anselm, U and u are of the same order of magnitude.

G. E. Pikus obtained the following expression for $\Delta\varkappa_{\text{exc}}$:

$$\Delta\varkappa_{\text{exc}} = ND\left(\frac{\Delta\varepsilon'}{kT}+2\right)^2, \tag{10a}$$

where $N = 2\frac{(2\pi m^* kT)^{3/2}}{h^3}e^{-\frac{\Delta\varepsilon'}{kT}}$.

In the case of InSb, where, according to Busch's data, the electrons are presumably already in the degenerate state, N should be much greater than n. In this case, the exciton thermal conduction according to (10) may be appreciably greater than given by equation (9b), which would explain Busch's results.

We should consider two more processes capable of increasing the thermal conduction of semiconductors in the temperature region where the intrinsic conductivity becomes noticeable.

Bipolar diffusion of holes and electrons presupposes a continuous flow of these charges from the hot to the cold portions of the body. If, as assumed, phonons are scattered from the electrons, the interaction of the electrons and holes with the phonons should lead to the phonons being entrained (pulled along) by the stream of charges. This effect will be all the stronger the more frequent the interactions of electrons with phonons and, hence, the shorter the free path and the lower the mobility u. Hence we may expect to have an additional thermal conduction due to the entrainment of the photons by the electrons and holes:

$$\Delta\varkappa_{\text{en.pr}} \sim \frac{n}{e} \sim \frac{n}{u}T^{1/2}. \tag{11}$$

Assuming that in the intrinsic conductivity region the flow of electrons and holes is accompanied by a flow of excitons, we should expect entrainment of the phonons by the excitons as well. The additional thermal conduction due to this effect will be

$$\Delta\varkappa_{\text{en.exc}} \sim \frac{N}{D}. \tag{12}$$

Finally, as the temperature increases the transfer of energy by heat radiation becomes noticeable. The contribution to the thermal conduction introduced by the radiant energy has been computed by Hensel:

$$\Delta\varkappa_{\text{excess}} = \frac{16}{3}\frac{a\xi}{k}T^3, \qquad (13)$$

where ξ is the square of the index of refraction, k the infrared absorption coefficient, and a the coefficient in tne expression $u = aT^4$ for the radiant energy density u of a black body (the quantity k is related to the concentration n of the free charges).

Conclusions

Summarizing, it can be stated that equations (1) and (2) are approximately valid only for impurity conductivity, and only as long as $n < 10^{20}/\text{cm}^3$. At higher values of n the scattering of phonons by the current carriers becomes pronounced, and $\varkappa$ can no longer be divided into the independent components $\varkappa_{\text{ф}}$ and $\varkappa_{\text{эл}}$, i.e., the value of $\varkappa$ becomes greater than the sum of $\varkappa_{\text{ф}}$ and $\varkappa_{\text{эл}}$.

The appearance of intrinsic conductivity of the semiconductor due to the simultaneous participation of electrons and holes in the current, leads to a series of new effects which alter the relationship between $\varkappa_{\text{эл}}$ and σ.

We discussed the additional thermal conduction due to the diverse processes that may accompany bipolar diffusion at high temperatures:

a) diffusion stream of electron-hole pairs;
b) exciton stream;
c) entrainment of phonons by the pair stream;
d) entrainment of phonons by the exciton stream;
e) heat transfer by radiant energy.

All these processes are jointly capable of changing the value of L in equation (2a) and (2b) by a factor of tens and hundreds. Any of the processes listed can become predominant in certain cases, depending on the properties of the semiconductor.

The only additional thermal conduction for which all tne data needed for a quantitative evaluation are available is $\Delta\varkappa_{\text{pair}}$, due to the electron-hole pair stream, where the Davydov and Shmushkevich equation can be used.

In the case of the exciton stream, if the excitons are produced in thermal equilibrium, we are still unable to determine their concentration as a function of temperature, and only for a few cases (Cu_2O, CdS, and PbTe) can we get some idea of their energy levels and the magnitude of $\Delta\varepsilon'$ from the absorption spectra.

So far we have not determined the absolute value of the entrainment of phonons by electron-hole pairs and excitons.

There are still not enough experimental facts to permit defining the true causes of the increase in thermal conduction at high temperatures and establishing a relationship between this phenomenon and the intrinsic conductivity.

Analyzing all the thermal-conduction data accumulated to date, we can state that the relationship $\left(\frac{1}{\varkappa_{\text{ф}}}\right)_{T>\theta} = \frac{3A}{v}\left(T - \frac{\theta}{3}\right)$ (see Fig. 2) is valid for insulating crystals, so long as $\bar{\lambda} < a$. The presence of extraneous (impurity) scattering centers introduces an additional term S into the expression for $1/\varkappa_{\text{ф}}$. In this case the extrapolation of the straight line $\left(\frac{1}{\kappa_\Phi}\right)_{T>\theta} = f(T)$ should intercept the horizontal axis at $T < \theta/3$, and sometimes also at $T < 0$. If the scattering by the impurities exceeds substantially the scattering from phonons, the value of $1/\kappa_\Phi$ in the expression $\frac{1}{\kappa_\Phi} = \frac{3A}{\theta}\left(T - \frac{\theta}{3}\right) + B$ changes little as T is increased, as can be seen from Fig. 6.

For semiconductors having impurity conductivity, equation (6) and the graphic dependence shown in Fig. 2 are just as valid as for insulators, provided κ_Φ is defined, taking the electric conductivity into account, as

$$\kappa_\Phi = \kappa - L\sigma T$$

However, with the appearance of intrinsic conductivity the temperature dependence of κ_Φ changes radically: the curve $1/\kappa_\Phi = f(T)$ deviates toward lower values of $1/\kappa$. This is clearly seen in Figs. 7, 8, and 9.

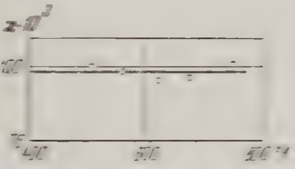

Fig. 10

Fig. 10 shows the results of measurements by Gul'tiaev, obtained for a sample of InSb containing so great an amount of impurities that impurity scattering predominates even at high temperatures. The scattering of phonons from the impurities apparently predominates over scattering by thermal-motion fluctuations. Therefore, κ is practically independent of T, as in the case of solid solutions (Fig. 6). The rise in thermal conduction at high temperatures, noted by Busch, is not observed at all in this case.

Plotted at the bottom of Figs. 7 and 8 are the values of $\Delta\kappa$ computed as the difference between the value extrapolated from the curve of Fig. 2 and the value of κ_Φ measured at a given temperature. The dotted lines show the calculated values of $\Delta\kappa$ with one of the points for $\Delta\kappa_{exc}$ adjusted to coincide with the value of $\Delta\kappa$. The agreement between the theoretical and experimental curves would indicate that this mechanism is probably responsible for the observed effect. The value of $\Delta E'$ for the excitons was determined for PbTe from the absorption spectrum near the natural absorption boundary. For all other materials, $\Delta E'$ was assumed to be 0.1-0.2 ev less than ΔE.

The above data are still inadequate, however, to permit us to draw any definite conclusions regarding the relative importance of the roles played by different effects contributing to the increase in thermal conduction.

It can be stated that the energy transfer by electron-hole pairs, as evaluated by Davydov and Shmushkevich, cannot in itself account for the measured values of $\Delta\kappa$. This justifies our turning to other effects, particularly to those involving excitons, in attempting to interpret the experimental data. We are continuing to study the thermal conduction in other semiconducting materials with a narrow forbidden band and hope, on the basis of our results, to give a more convincing analysis of the processes of heat transfer in semiconductors in the near future.

Institute of Semiconductors at the
Academy of Sciences of the USSR

THERMOELECTRIC GENERATORS

- A. F. Ioffe

The problem of using thermoelectric elements for converting heat energy into electricity was raised by Raleigh as long ago as 1885. However, a practical solution of the problem had to await the availability of semiconductors having substantial thermoelectromotive forces.

Some 25 years ago I predicted that through the use of semiconductors it would be possible to prepare thermoelectric elements with efficiencies far exceeding those obtainable with metals. This prediction has been realized and it is now possible to consider the generation of electrical energy from heat as a serious engineering problem.

Let us examine processes taking place in a thermoelectric couple from the energy point of view, when a quantity of heat Q_1 is brought every second to the hot junction at the absolute temperature T_1, while from the cold junction at T_0 there is removed an amount of power Q_0. Let us express the thermoelectromotive coefficient by α, the internal resistance of the couple by r, and the external resistance of the useful load by R. In addition, let K be the thermal conductivity of the branches of the thermoelectric couple and I be the current in the closed circuit whose resistance is r + R. We shall express all these quantities, including the thermal conductivity, in electrical units. Then, in accord with the well known laws of thermoelectric effects:

$$Q_1 = \alpha_1 I T_1,$$
$$Q_0 = \alpha_0 I T_0,$$

the useful power

$$W = I^2 R,$$

and the thermal flux along the branches of the thermocouple

$$Q_m = K(T_1 - T_0).$$

Assuming that of the heat I^2r generated in the thermoelectric element by the current I half is returned to the hot junction, the efficiency can be expressed in the form

$$\eta = \frac{I^2 R}{\alpha_1 T_1 I + k(T_1 - T_0) - {}^1/_2 I^2 r}. \qquad (1)$$

The next step is to find the conditions under which η attains its maximum value. This condition is obtained by differentiating with respect to the appropriate variable and setting the derivative equal to zero. In this way it is possible to establish the optimal relation between the cross sections S_1 and S_2 of the two branches, the values of the specific resistances ρ_1 and ρ_2 and the thermal conductivities $\varkappa_1$ and $\varkappa_2$ of the thermocouple materials.

$$\frac{S_1^2}{S_2^2} = \frac{\rho_1}{\rho_2}\frac{\varkappa_2}{\varkappa_1}. \qquad (2)$$

Let us set R/r = m. Then the expression (1) can be brought into the form

$$\eta = \frac{T_1 - T_0}{T_1} \frac{\frac{m}{m+1}}{1 + \frac{kr}{\alpha^2}\frac{m+1}{T_1} - \frac{1}{2}(T_1 - T_0)\frac{1}{m+1}}. \qquad (3)$$

Here η is determined, aside from the temperatures T_1 and T_0, only by the ratio $R/r = m$ and the quantity

$$z = \frac{\alpha^2}{kr} = \frac{(\alpha_1 + \alpha_2)^2}{(\sqrt{\varkappa_1\rho_1} + \sqrt{\varkappa_2\rho_2})^2}, \qquad (4)$$

characterizing the properties of the semiconductors comprising the thermocouple. Neither the geometric dimensions, as long as they satisfy the requirement (2), nor the particulars of construction, enter into the expression for the efficiency.

As far as the ratio R/r is concerned, its optimum value is

$$\left(\frac{R}{r}\right)_{\text{opt}} = M = \sqrt{1 + \frac{1}{2} z (T_1 + T_0)}\,. \qquad (5)$$

The greatest efficiency which can be attained with semiconductors, having a given value of z at the temperatures T_1 and T_0 at the junctions, is

$$\eta_{\text{opt}} = \frac{T_1 - T_0}{T_1} \frac{M - 1}{M + \frac{T_0}{T_1}}. \qquad (6)$$

The first factor in this expression is the efficiency of a reversible engine, while the second gives the reduction in efficiency caused by the thermal conductivity $\varkappa$ and the resistance ρ.

We note that the product $\varkappa\rho$ cannot be made as small as desired since the thermal conductivity of the semiconductor consists of $\varkappa_\Phi$ - the thermal conductivity of the crystal lattice, determined by the scattering of thermal waves (phonons), and by $\varkappa_e$ - the thermal conductivity determined by the free electrons, and related by the Wiedemann-Franz law with the specific resistance:

$$\varkappa = \varkappa_\Phi + \varkappa_e; \qquad (7)$$

$$\varkappa_e = L \frac{1}{\rho}, \qquad (8)$$

where L, at room temperatures, has a value close to 4.3×10^{-6} for the nondegenerate case, and close to 7.1×10^{-6} for the degenerate case. For this reason the minimum value of $\varkappa\rho$ even when $\varkappa_\Phi$ can be neglected in comparison with $\varkappa_e$, will be

$$\varkappa\rho > 4{,}3 \cdot 10^{-6}. \qquad (9)$$

If we take

$$\alpha_1 = \alpha_2 = 200 \cdot 10^{-6}\ \text{V/degree}$$

then $z < 10 \cdot 10^{-3}$.

Taking $T_1 = 600^\circ K$ and $T_0 = 300^\circ K$, we would obtain

$$\eta_{\text{opt}} < 24\%,$$

or at $T_1 = 900^\circ K$ and $T_0 = 300^\circ K$.

$$\eta_{\text{opt}} < 37\%.$$

For the semiconductors which have so far been studied z has a value not exceeding $3 \cdot 10^{-3}$.

Further, if we take for $\alpha_1 = \alpha_2$ the value $170 \cdot 10^{-6}$ following from the theory of non-degenerate semiconductors, then with $T_1 = 600^\circ K$,

$T_0 = 300^\circ K$ and $z = 1.5 \times 10^{-3}$.,

$$\eta_{opt} = 8.2\%.$$

In the accompanying figure η_{opt} is plotted as a function of for different values of T_1 (in $^\circ K$).

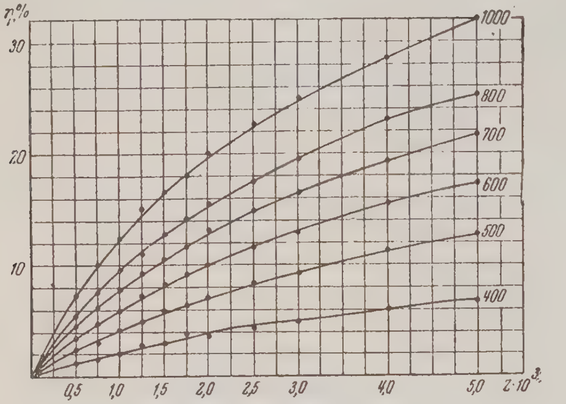

Fig. 1

Let us turn now to the problem of maximizing the value of z_0. Three constants characterizing the semiconductor - α, $\varkappa$ and ρ - enter into this quantity.

Let us first examine the case when $\varkappa_\Phi$ does not depend on the electrical variables, and $\varkappa_\Phi \gg \varkappa_e$. Then the requirement for $z = z_{max}$ reduces to the condition for a maximum value of α^2/ρ and a minimum of $\varkappa_\Phi$. We find that α and ρ, or α and $\sigma = 1/\rho$ related by the following expression deduced by N. L. Pisarenko for atomic lattices with nondegenerate carriers of current of the same polarity.

$$\alpha = \frac{k}{e}\left[2 + \ln\frac{2(2\pi m^* kT)^{3/2}}{h^3 n}\right]. \tag{10}$$

The magnitude n (the concentration of free electrons) entering into the equation (10) is related with the electrical conductivity σ by

$$\sigma = nue, \tag{11}$$

where u is the mobility of the current carriers (electrons or holes).

It is easy to show that the maximum value of $\alpha^2\sigma$ is obtained when

$$\alpha = 2\frac{k}{e} = 172 \cdot 10^{-6} \text{ v/degree} \tag{12}$$

$$\sigma = 4u. \tag{13}$$

Moreover the equation (10) for α remains valid in going from atomic lattices to any other, except that constant 2 in the brackets may take on values from 1 to 4.

If, however, $\varkappa_e$ is commensurate with $\varkappa_\Phi$, then the condition that $(\alpha^2\sigma)$ be maximal does not follow from the requirement for z_{max}. In this case it is more convenient to determine the condition for the minimum value of $1/z$

$$\frac{1}{z} = \frac{\varkappa_\Phi + \varkappa_e}{\alpha^2\sigma} = \frac{\varkappa_\Phi}{\alpha^2\sigma} + \frac{L}{\alpha^2}. \tag{14}$$

The optimum value of α in this more general case is

$$\alpha_{opt} = 172\left(1 + \frac{\varkappa_e}{\varkappa_\Phi}\right) \cdot 10^{-6} \text{ v/degree} \tag{12a}$$

The expression (12a) relates to nondegenerate current carriers.

In the case of degeneracy the particular Pisarenko equation (10) must be replaced by the general one:

$$\alpha = \pm \frac{k}{c}\left(\frac{r+2}{r+1} \cdot \frac{F_{r+1}(\mu^*)}{F_r(\mu^*)} - \mu^*\right), \tag{15}$$

where $F_r(\mu^*)$ and $F_{r+1}(\mu^*)$ are the Fermi integrals:

$$F_r(\mu^*) = \int_0^\infty \frac{x^r\,dx}{e^{x-\mu^*}+1};$$

μ^* being the reduced chemical (Gibbs) potential; x is the reduced energy of the carrier, and r is the exponent in the well known formula for the energy dependence of the mean free path.

For the same values of σ in the degenerate case, α is larger than follows from equation (10).

The integrals occurring in (15) have been tabulated and the calculation of α_{opt} does not involve any difficulties. Similarly it is not difficult to determine the value α_{opt} corresponding to z_{max} graphically. It is somewhat larger than the value of α_{opt} for the nondegenerate case.

Introduction of impurities into the semiconductor or departure from stoichiometric proportions of the components, opens a way for the variation of n and α without greatly influencing the mobility u.

An increase in z may also be obtained by a reducing $\varkappa_\Phi$ or, more accurately speaking, by lowering the ratio $\varkappa_\Phi/u$. It is feasible to lower this ratio through the introduction of appropriate admixtures and the formation of solid solutions, since the scattering of phonons and of electrons obeys different laws.

A thermoelectric battery is characterized not only by its efficiency but also by the power obtainable per cm^2 of surface or per cm^3. At a given efficiency, the power is determined by the density of the heat flux q through a cm^2 of battery surface per second,

$$q = \varkappa \frac{T_1 - T_0}{l}, \tag{16}$$

where l is the distance between the hot and the cold junctions, or the thickness of the semiconductor layer in the battery. At given $\varkappa$ and $(T_1 - T_0)$ the power per cm^2 is

$$W_{sur} = \eta q = \eta\varkappa (T_1 - T_0)\frac{1}{l}, \tag{17}$$

while the electric power produced per cm^3 of the semiconductor is

$$W_{vol} = \eta\varkappa (T_1 - T_0)\frac{1}{l^2}. \tag{18}$$

Thus, for example, with η = 8% and q = 200,000 $kcal/m^2/hr$ = 11.6 W cm^2 and l = 0.5 cm

$$W_{sur} = 0.93\ w/cm^2 = 9.3\ kw/m^2,$$
$$W_{vol} = 1.86\ w/cm^3 = 1860\ kw/m^3.$$

If we take the specific weight of the semiconductor to be d = 5 the gross weight of the "battery" to be equal to that of the thermoelectric couple we get the following specific power per 1 kg of battery:

$$W_{sp} = 0.2\ kw/kg.$$

With $l = 0.3$ cm, we get

$$W_{sp} = 0.5 \text{ kw/kg}.$$

We have described the semiconducting materials of the thermoelectric element with the aid of the constants α, $\varkappa$ and ρ, not taking into account their dependence on the temperature. One should use, instead, their mean values in the temperature range from T_0 to T_1; these can be determined in the following way:
the thermal conductivity coefficient:

$$\bar{\varkappa} = \frac{2}{\frac{1}{\varkappa_1} + \frac{1}{\varkappa_0}}; \qquad (19)$$

the thermoelectromotive coefficient:

$$\bar{\alpha} = \frac{1}{2}(\alpha_1 + \alpha_0); \qquad (20)$$

the temperature dependence of the specific resistance of the semiconductors $\rho(T)$ is characterized by

$$\rho T^m = \text{const}. \qquad (21)$$

Hence

$$\bar{\rho} = \frac{1}{m} \ln \frac{T_1}{T_0} (\rho_1 - \rho_0). \qquad (22)$$

For realization of the battery, in addition to the hole and electron semiconductors, forming the branches of the thermoelectric couple, it is also necessary to have metallic bridging elements to connect them. These must have a high electric conductivity, and must not produce additional resistance at the boundaries with the semiconductors. With a specific electric conductivity for the branches of 1000/ohm cm and a length of 0.5 cm, the resistance of the bridge including the contact resistance should not exceed 10^{-5} ohm/cm. The coefficient of thermal expansion of the bridge material must be close to that of the semiconductors.

Finally, we must not overlook the steep temperature gradient (600°/cm in our case), and the resultant flexure of the thermoelectric battery. The radius R of flexure of a flat battery strip of material with a linear expansion coefficient β equals

$$R = \frac{l}{\beta (T_1 - T_0)}. \qquad (23)$$

Taking $\beta = 2 \cdot 10^{-5}$, $l = 0.5$ cm and $(T_1 - T_0) = 300°$, we get $R = 83$ cm, while with $l = 0.3$ cm, $R = 50$ cm.

Hence, if we pass an alternating current through a battery or a separate thermoelectric strip, we can make it vibrate, and thus generate elastic waves in the surrounding medium.

Institute of Semiconductors of the
Academy of Sciences of the USSR

THERMOELECTRIC COOLING [Peltier Effect]

- L. S. Stil'bans, E. K. Iordanishvili
and T. S. Stavitskaia

The present article is devoted to a brief exposition of the theory of thermoelectric cooling developed by A. F. Ioffe[1] and the report of the experimental results obtained in experiments carried out by the Institute of Semiconductors of the USSR Academy of Sciences in 1953-4.

In the investigation we made use of the experience gained in the laboratories of Iu. P. Meslakovtsev and G. I. Shmelev incident to the development of semiconductor thermocouples for thermoelectric generators.

1. Theory

Thermoelectric generators are based on the Seebeck effect. If in a circuit consisting of two different conductors the junction points are maintained at different temperatures there develops an emf

$$E = \alpha(T_1 - T_0),$$

where α is a thermoelectromotive coefficient which in general depends on the temperature.

Thermoelectric cooling is based on the opposite effect, known as the Peltier effect. If the two conductor circuit is connected to an outside emf source, heat will be liberated at one junction and absorbed at the other. The quantity of heat liberated (or absorbed) per sec is $Q_\pi = \Pi I$, where I is the current and Π is the Peltier coefficient, which is related to the thermoelectromotive coefficient by $\Pi = \alpha T$.

If the junction at which heat is liberated is maintained at a constant temperature, the absorbing junction will be cooled to the point where the heat flowing from the surrounding medium plus the heat conducted in by the branches of the thermocouple becomes equal to the absorbed Peltier heat. The temperature difference between the junctions reaches a maximum when the cold junction is completely isolated thermally; in this case the thermocouple cools only itself.

On the other hand, if the cold junction is in thermal contact with some object, subject to cooling, the temperature differential will of course be smaller. Such an object may be the interior of a "refrigerator" or some apparatus. In this case the thermocouple operates as a refrigerating machine in which the cooling agent (freon) is replaced by electronic gas.

The principal parameter characterizing a refrigerating machine is the cooling coefficient

$$k = \frac{Q}{W},$$

where Q is the amount of heat removed per unit time and W is the power expended. In the case of thermoelectric cooling

$$Q = \Pi I - {}^1/_2 I^2 R - \varkappa (T_0 - T_1), \tag{1}$$

where R is the resistance and $\varkappa$ is the heat conductivity of the thermocouple. The power expended on cooling

$$W = V \cdot I = [\alpha (T_0 - T_1) + IR] \cdot I. \tag{2}$$

As may be seen from the above expressions the cooling coefficient of a thermocouple is a function of the current. Equating the derivative $\partial k/\partial I$ to zero we can find the optimum value of the current and the corresponding value of the cooling coefficient. Straightforward computations give

$$k_0 = \frac{T_1}{T_0 - T_1} \frac{\sqrt{1+M} - \frac{T_0}{T_1}}{\sqrt{1+M} + 1}, \tag{3}$$

here

$$M = \frac{T_0 + T_1}{2} z \quad \text{and} \quad z = \frac{(\alpha_1 + \alpha_2)^2}{\left(\sqrt{\frac{\varkappa_1}{\sigma_1}} - \sqrt{\frac{\varkappa_2}{\sigma_2}}\right)^2}, \tag{4}$$

where α_1 and α_2, σ_1 and σ_2, and $\varkappa_1$ and $\varkappa_2$ are, respectively, the thermoelectromotive coefficients, the specific electric conductivities and the heat conductivities of the thermocouple branches. Hereinafter we will assume that the coefficients and conductivities of the two branches are equal and will accordingly drop the subscripts. Then

$$z = \frac{\alpha^2 \sigma}{\varkappa} \tag{5}$$

Expression (3) shows that under given operating conditions (given values of T_0 and T_1) the cooling coefficient is wholly determined by the quantity z, characterizing the quality of the thermocouple: with $z \longrightarrow \infty$, we have $k_0 \to \frac{T_1}{T_0 - T_1}$ or the cooling coefficient of an ideal refrigerating machine; with $z \to 0$, $k_0 \to 0$ (regardless of T_1 and T_0).

The maximum reduction in temperature attainable with $k_0 = 0$ (when the cold junction is under conditions of ideal thermal isolation), according to (3), is determined by the value of z. With $k_0 = 0$.

$$\left(\frac{T_0}{T_1}\right)_{max} = \sqrt{1 + T_{av} z},$$

or

$$(T_0 - T_1)_{max} = \frac{1}{2} T_1^2 z,$$

or

$$T_1 = \frac{\sqrt{1 + 2T_0 z} - 1}{z}.$$

We must consequently determine the conditions under which the value of z is maximal.

The parameters (α, σ and $\varkappa$) entering into z are not independent; they are all functions of the concentration n of free electrons (or holes).

The qualitative dependence is presented in Fig. 1: the electric conductivity σ is roughly proportional to n. The thermoelectomotive force, on the contrary, tends to zero when $n \to \infty$ and to infinity when $n \to 0$. The heat conductivity of a substance is comprised of the heat conductivity of the crystal lattice $\varkappa_{lat}$ and the electronic heat conductivity $\varkappa_e$ which is proportional, in the first approximation, to the concentration of current carriers.

The maximum of the quantity $\alpha^2\sigma$ in the denominator in the expression for z, lies in the vicinity of carrier concentration $\sim 10^{19}$ cm^{-3}, i.e., a concentration some 10^3 times lower than the concentration in metals.

The magnitude of the electronic heat conductivity is small as compared with that of the lattice so that the maximum of z is displaced only slightly relative to the maximum of $\alpha^2\sigma$ into the region of lower electron concentrations.

In metal and metal alloys z is very small inasmuch as the thermoelectromotive coefficient is nearly zero and the electron heat conductivity is comparatively large; in dielectrics, on the other hand, $z = 0$ because $\sigma \sim 0$.

These considerations explain why the efficiency of metallic couples is low and why neither thermoelectric generators nor thermoelectric coolers have found practical application until recently.

Through suitable "selection" of the electron concentration the efficiency of thermocouples can be increased manifold.

To formulate these considerations qualitatively we must express α, σ and $\varkappa$ through the electron concentration or, what is more convenient, through chemical potentials. The corresponding expressions are the following:

$$\left.\begin{aligned} n &= \frac{4\pi (2mkT)^{3/2}}{h^3}, \\ \alpha &= \pm \frac{k}{e}\left[\frac{r+2}{r+1}\,\frac{F_{r+1}(\mu^*)}{F_r(\mu^*)} - \mu^*\right], \\ \varkappa_e &= \frac{16\pi m^* l_0(T)}{3h^3}(kT)^{r+2}\left[(r+3)F_{r+2}(\mu^*) - \frac{(r+2)^2 F_{r+1}^2(\mu^*)}{(r+1)F_r(\mu^*)}\right], \\ \sigma &= \frac{16\pi m^* l_0(T)\, e^{r}}{3h^3}(kT)^{r+1} F_r(\mu^*), \end{aligned}\right\} \qquad (6)$$

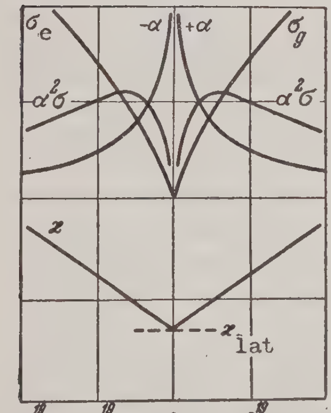

Fig. 1

where, $\mu^* = \frac{\mu}{kT}$; r is the exponent in the expression for the length l of the electron free path: $l(\varepsilon, T) = l_0(T)\,\varepsilon^r$; ε is the electron kinetic energy;

$$F_r(\mu^*) = \int_0^\infty f x^r\,dx,\quad x = \frac{\varepsilon}{kT} \quad \text{and} \quad f(x) = \frac{1}{e^{x-\mu^*}+1}$$

is the Fermi distribution function.

The Fermi integrals have been tabulated and the problem of finding the value of μ^* corresponding to maximum value of z can be solved numerically. However, the problem can be approached in a different, more convenient way. If we assume that the optimum value of μ^* lies in the region wherein classical statistics applies (i.e., that $\mu^* < -2$) the expressions for α, σ and $\varkappa$ are greatly simplified:

$$\left.\begin{aligned} & n = \frac{2(2\pi m^* kT)^{3/2}}{h^3} e^{\mu^*}, \quad \sigma = eun, \\ & \alpha = \pm\frac{k}{e}(r+2-\mu^*) = \pm\frac{k}{e}\left(r+2+\ln\frac{2(2\pi m^* kT)^{3/2}}{h^3 n}\right) \\ & \text{and} \\ & \varkappa = (r+2)\left(\frac{k}{e}\right)^2 Teun. \end{aligned}\right\} \qquad (7)$$

If the condition

$$\frac{\partial z}{\partial n} = 0 \qquad (8)$$

actually yields $\mu^* < -2$ our initial assumption will be validated.

If we substitute the approximations of (7) in expression (5), the condition (8) will give us a transcendental equation for determining n or μ^* that can be solved graphically. We can make a further simplification, namely, assume that at the optimum electron concentration, the electron heat conductivity constitutes only a small fraction of the heat conductivity of the lattice (which, generally speaking, follows directly from the graphical solution of eq. (8)), solve for the maximum value of $(\alpha^2\sigma)$, and then correct by the method of successive approximations.

The condition that $\frac{\partial(\alpha^2\sigma)}{\partial n} = 0$ gives

$$\left.\begin{aligned} \mu_0^* &= r, \\ {}_0 &= \pm 2\,\frac{k}{e} = \pm 172 \quad \mu\ \text{v/degree}, \\ n_0 &= \frac{2\,(2\pi m^* kT)^{3/2}}{h^3}\,e^r = 2{,}5\cdot 10^{19}\left(\frac{m^*}{m_0}\right)^{3/2}\left(\frac{T}{T_0}\right)^{3/2} e^r, \\ z_{max} &= 1{,}2\cdot 10^{-7}\,\frac{u}{\varkappa}\left(\frac{m}{m_0}\,\frac{T}{T_0}\right)^{3/2} e^r, \end{aligned}\right\} \qquad (9)$$

where m_0 is the free electron mass and T_0 is room temperature (293°K).

Setting $u = 1000$ cm^2 v^{-1} sec^{-1}, $\varkappa_{lat} = 2\cdot 10^{-2}$ W cm^{-1} degree^{-1}, $m = m_0$ and $T = T_0$, we obtain $z = 2\cdot 20^{-3}$ degree^{-1}, which agrees with the experimentally observed values.

The equation for n_0 in (9) shows that to retain optimal conditions for z in a wide temperature range the current carrier concentration should vary little with temperature ($n_0 \sim T^{3/2}$). This requirement is not met by ordinary semiconductors in which the carrier concentration varies exponentially with the temperature, but is fairly well satisfied by semimetals in which n is independent of the temperature.

We will not dwell here on the corrections connected with taking into account the electronic heat conductivity and the degeneracy of the electron gas. All the calculations were also carried out according to the exact equations given at the beginning of this article. We will only note 1) that taking these factors into account yields a value of α_0 varying between the limits of 170 and 400 µv degree^{-1} depending on the value of r and the rating $u/\varkappa_{lat}$ and 2) in the vicinity of its maximum value z varies as the square root of the difference $(n - n_0)$ and hence, as calculations show a 50% deviation from n_0 results in only a 6% decrease in the value of z.

Thus the conditions for n_0 and α_0 are not critical and the deduced expression is sufficiently accurate for qualitative evaluations and in many cases for quantitative calculations as well.

The above analysis shows that the problem of finding suitable materials for thermocouples reduces essentially to 1) finding substances characterized by a maximum value of the ratio $u/\varkappa_{lat}$ and means for further increasing this ratio and 2) creating carrier concentrations satisfying conditions (8) in these substances.

There are two ways in which the last can be achieved:

1. A number of semiconductors having a carrier concentration of 10^{16} cm^{-3} or lower can be converted into semimetals with a carrier concentration of 10^{19} cm^{-3} by introducing appropriate acceptor

and donor impurities. This expedient, however, proves to be ineffective where lowering the carrier concentration is concerned: in the case of substances having concentrations of about 10^{20}-10^{21} cm^{-3} such acceptor and donor admixtures do not enter into the lattice in sufficient quantities. Nevertheless, there are a number of substances characterized by a favorable value of the ratio $u/\varkappa_{lat}$.

2. In this case it is usually possible to attain the desired result by combining hole and electron semimetals (or even metals) having similar lattices. Such binary (or pseudo-binary) systems give a positive or negative thermocouple arm, depending upon which of the components is present in excess.

According to the theory of A. F. Ioffe, which has by now been confirmed by a wealth of experimental material, a minimal heat conductivity should be exhibited by substances with a high heat content, i.e., a low Debye temperature and highly anharmonic lattice vibrations (manifested in a large thermal expansion coefficient). These requirements are generally met by compounds and alloys of the heavier elements of the middle groups in the periodic table.

As V. P. Zhuze showed on the basis of an analysis of a large amount of experimental data these compounds (the bonds which are intermediate between valence and metallic bonds) are also characterized by a high carrier mobility; they are consequently among the most advantageous substances for thermocouple use from the point of view of having a high $u/\varkappa_{lat}$ ratio.

A further appreciable enhancement of the $u/\varkappa_{lat}$ ratio can be attained, as A. V. Ioffe and A. F. Ioffe have shown, by introducing neutral admixtures, effective where scattering of short-wave thermal lattice vibrations is concerned and ineffective where dispersion of the 10-times longer electronic waves is concerned.

The temperature dependence of z is also determined by the variation of $u/\varkappa_{lat}$ with temperature, namely, by $z \sim T^{3/2}(u/\varkappa_{lat})$. If we disregard the case when $T < \theta$, which at present is of no practical interest, we have $\varkappa_{lat} \sim 1/T$ in the case of scattering of phonons from phonons and $\varkappa \approx$ const. in the case of scattering from lattice defects. Both these laws have been substantiated by the investigations of Deviatkova and Gul'tiaev.

Studies, in the laboratory of Maslakovets, of the temperature dependence of the carrier mobility in a number of semi-conductor materials used in thermocouples gave a $u \sim T^{-3}$ law for PbS, PbSe, PbTe, and Bi_2Te and a $u \sim T^{-3/2}$ law for SbZn and some other compounds. At low temperatures when the dominant role is played by scattering from the impurity ions the mobility varies in accord with the $u \sim T^{3/2}$ law.

Thus we can have the different cases of temperature dependence for z listed in Table 1.

At present cases 3, 4 and 5 have been realized. The most promising for thermoelectric generators (batteries) appears to be case 2; the most promising for refrigerators is case 6.

The values of z characterizing thermocouples now used are by no means the best possible values: for example, for a negative thermocouple arm of PbTe we have

$$\alpha_1 \approx 170 \mu v \text{ degree}^{-1},\ \sigma_1 = 1000 \text{ ohm}^{-1} \text{ cm}^{-1},\ \varkappa \approx 7 \cdot 10^{-3} \text{ cal cm}^{-1} \cdot \text{sec}^{-1} \text{ degree}^{-1} \text{ and } z_1 \approx 1 \cdot 10^{-3} \text{ degree}^{-1};$$

for the positive arm

$$\alpha_2 = 170,\ \sigma_2 = 1000,\ \varkappa_2 = 4\cdot 10^{-3} \text{ and } z_2 = 1.8\cdot 10^{-3} \text{ degree}^{-1};$$

so that

$$z_{ave} = 1.2\cdot 10^{-3} \text{ degree}^{-1}$$

which gives $(T_0 - T_1)_{max} = 50°$ for a refrigerator and an efficiency of about 6% for a generator.

At present it is entirely feasible, using newly developed materials, to realize $z \approx 2.5\cdot 10^{-3}$ degree^{-1}, i.e., to increase the efficiency of thermocouples nearly two-fold.

Table 1

Temperature dependence	Ideal lattice $\varkappa \sim \frac{1}{T}$	Defective lattice $\varkappa = \text{const}$
Scattering from ions $u \sim T^{3/2}$	1. $z \sim T^4$	2. $z \sim T^3$
Atomic lattice $u \sim T^{-3/2}$	3. $z \sim T$	4. $z = \text{const}$
$u \sim T^{-3}$.	5. $z \sim T^{-1/2}$	6. $z \sim T^{-3/2}$

2. Comparison of theory with experiment

In Fig. 2 we have juxtaposed the theoretical and experimental curves for the dependence of $\alpha^2\sigma$ on T for three samples of lead telluride with different carrier concentrations, corresponding to the optimum value for n_0 at different temperatures. The long-dash curves are the theoretical curves computed according to the approximate equations; the short-dash curve is computed according to the exact equations (taking degeneracy into account); the solid lines are the curves based on experimental data.

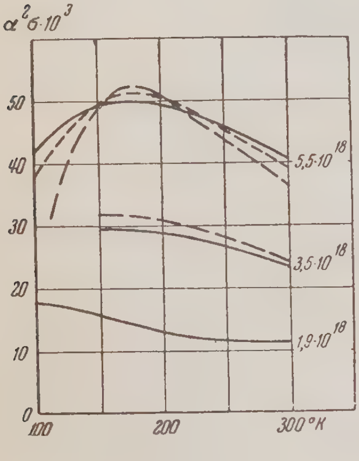

Fig. 2

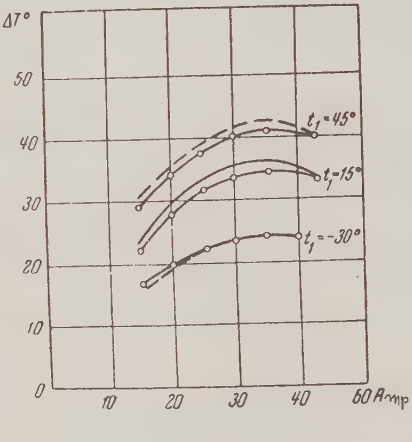

Fig. 3

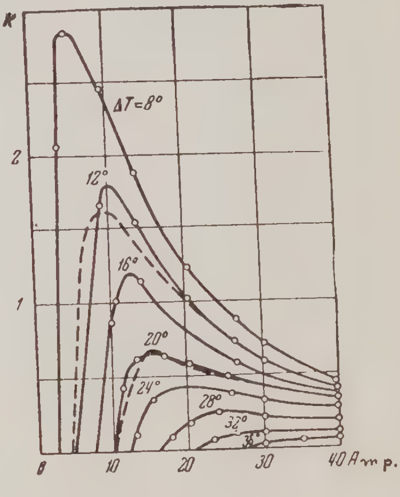

Fig. 4

Fig. 3 gives the variation of the temperature differential between the thermocouples with the current; the dash-lines are the theoretical curves. Fig. 4 gives the variation of the cooling coefficient with the current at temperature differentials of 8, 12, 16, 20, 24, 28, 32 and 36°C; the dash-lines are the theoretical curves. Lastly, Fig. 5 shows the dependence of the cooling coefficient on the temperature differential (again the dash-line is the theoretical curve).

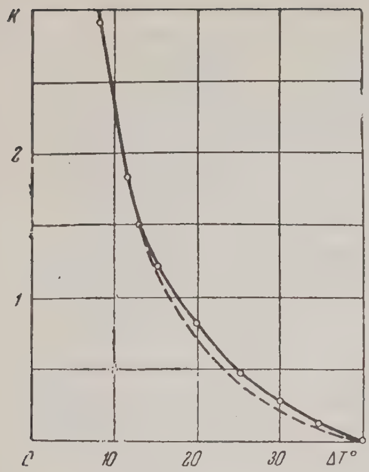

Fig. 5.

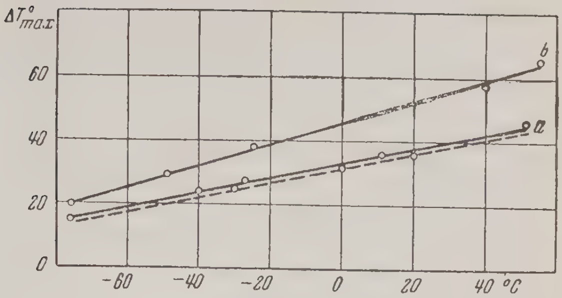

Fig. 6. Dependence of the maximum cooling on the temperature of the hot junction: a) single-stage assembly; b) two-stage assembly.

One can obtain greater cooling with a given cooling coefficient or a greater cooling coefficient with a given temperature differential by using successive cooling (multiple stage assemblies). At the present, however, the use of more than 3 stages does not appear to be expedient.

We can conclude from the above figures that the basic postulates of the theory lead to satisfactory agreement with experiment. Table 2 gives the values of maximum cooling obtained in the neighborhood of room temperatures. For purposes of comparison we also give the data obtained by foreign investigators: Justi[2] and Goldsmid and Douglas[3]. The dependence of the optimum cooling T_{max} on the temperature of the hot junction(s) for single and two-stage assemblies is shown in Fig. 6 (the dash-line is the theoretical curve for a single-stage unit).

Table 2

Maximum temperature reduction, °C

	T_0	T_1	$(T_0-T_1)_{max}$
One stage . . .	34	—14	48
Two stages . . .	47	—14	61
Three stages. .	25	—45	70
Justi (Ref.3). .	10	—14	24
Goldsmid & . . . Douglas (R.6)	12	—14	26

3. Practical application

1. At the end of 1953 the Institute of Semiconductors in cooperation with the Leningrad Refrigeration Institute constructed a small model of a domestic refrigerator with a cooled volume of about 10 liters. The thermo-assembly consumed 25 watts power and provided an air temperature of 4°C in the cabinet at an outside air temperature of 27°C. The cooling coefficient of the assembly was 20% at a junction temperature differential of 40°. Tests of the refrigerator brought out a number of design shortcomings as a result of which the effective temperature reduction (23°) was approximately only half the junction differential.

At the present time our Institute in cooperation with the Leningrad Refrigeration Institute is working on the development of a 60 liter refrigerator in the design of which the above-mentioned shortcomings, on the one hand, and the latest advances in thermocouples, on the other hand, are being taken into account. It is hoped that the cooling coefficient will be increased to 30%.

2. In collaboration with the Main Geophysical Observatory we have developed an instrument for measuring air humidity on the basis of the dew point; this instrument has a number of advantages over conventional hygrometers and psychrometers, particularly in the region of sub-zero temperatures and on moving objects.

3. The Institute is collaborating with a number of industrial research institutes in applying thermo-electric cooling to reducing and stabilizing the temperature of radio and other electronic components. Some of the developments in this field are already being used in practice.

In conclusion the authors wish to thank Academician A. F. Ioffe under whose supervision the present investigation was carried out.

Institute of Semiconductors of the
Academy of Sciences of the USSR

REFERENCES

1. A.F.Ioffe, Energeticheskie osnovy termobatarei iz poluprovodnikov. - (Energetic fundamentals of semi-conductor thermobatteries), M. 1956.
2. E. Justi, Kältetechnik, 6, 150 (1953).
3. H.Y. Goldsmid & R.W. Douglas, Brit. J. of Appl. Phys., 3, 386 (1954).

* * * * * *

EXCITON EXCITATION SPECTRUM IN SOLIDS

- E. F. Gross

It is well known that crystals exhibit wide regions or bands of a continuous spectrum, the so-called principal or self-absorption spectrum; in these regions the absorption coefficient attains exceptionally high values (10^5-10^6 cm^{-1}). On the long-wave side the continuous absorption region generally has an edge (limit), which is very sharp in some crystals. The location of the edge depends on the material of the crystal and is known to be determined by the width of the forbidden zone in the crystal.

The principal absorption in many substances is associated with the internal photoelectric effect. This photoelectric effect is induced principally by wavelengths corresponding to the absorption edge. This is clearly shown, for example, by Fig. 1 which depicts the absorption curve a and the curve b for the spectral distribution of the internal photoelectric effect in the cuprous oxide crystal, as given by A. V. Ioffe and A. F. Ioffe.[1] This empirical rule was established by Gudden and Pohl[2] back in 1923. However, until today, the reason for the sharp decrease in photosensitivity in the region of the primary absorption band still remains unclear. Gudden[3] considered this effect puzzling. As is known, Frenkel in 1931 introduced[4] the concept of the exciton for explaining light absorption in the primary band without the rise of photoconductivity.

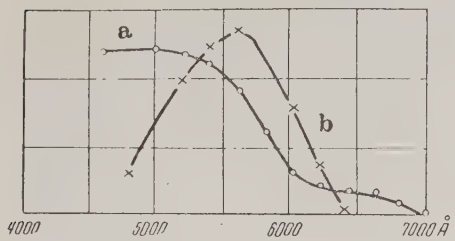

Fig. 1. a) absorption curve, b) spectral distribution of photoconductivity in a Cu$_2$O crystal, after A. V. Ioffe and A. F. Ioffe[1].

In connection with this effect we initiated a systematic investigation of crystal absorption spectra at the Physico-Technical Institute of the Academy of Sciences with the objective of obtaining detailed data on electron energy levels in crystal lattices.

We elected to start with a cuprous oxide (Cu$_2$O) crystal. This choice was based on the following considerations. The electrical properties of cuprous oxide, the "classic" semiconductor, had already been thoroughly investigated. In recent years (1947-1950) Zhuze and Ryvkin[5] had carried out at the Physico-Technical Institute a very thorough study of the photoelectric properties of these crystals coming to the conclusion that the photoconductivity of Cu$_2$O was due to impurities. In connection with this work Zhuze and Ryvkin[6] were the first to note the role of excitons in the internal photoelectric effect. For the external photoelectric effect the exciton mechanism had been previously proposed by Apker and Taft.[7]

Depending on the location of electronic energy levels, the light absorption in crystals may occur in different spectral regions. According to the photoconductivity studies of Zhuze and Ryvkin[5,6], light absorption in Cu$_2$O crystals should be associated with the electron transitions schematically shown in Fig. 2. The difference in energy between levels for transitions of types a and b is relatively larger than for transitions of types c and d. The energy of the c and d transitions is small and, accordingly, the light absorption associated with them can be expected to take place in the long wavelength (infrared) region of the spectrum. The light absorption associated with the a and b transitions should be observed near the long-wave edge of the absorption band (for Cu$_2$O near 6300 A).

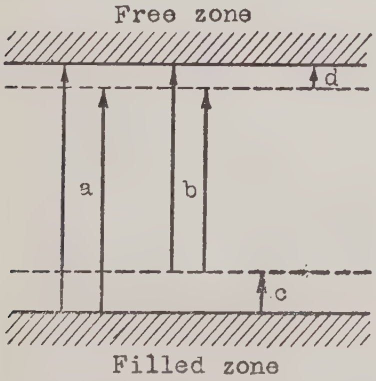

Fig. 2. Scheme of electron levels in Cu$_2$O crystal according to photoconductivity data of Zhuze and Ryvkin[5,6].

Light absorption in Cu$_2$O has been studied little. The visible region of the spectrum was studied by A. V. Ioffe and A. F. Ioffe,[1] by Pigarev and Golub,[8] and by Mönch.[9]

In order to study the long-wave absorption edge in detail in our experiments we used spectral instruments with a dispersion approximately 10 times greater (25 A/mm in the neighborhood of 6300 A) than that used in earlier investigations. The high dispersion of the instruments allowed observation of the Cu$_2$O crystal absorption limit on a magnified scale. By virtue of this it was possible to detect a phenomenon which had escaped observation with low dispersion instruments.

Our initial experiments in studying the absorption edge of cuprous oxide were made at room temperature (20°C) with coarse crystal plates of various thicknesses (from several tens to several hundreds of microns). In these experiments, carried out by the author and N. A. Karryev, it was discovered[10] that the self-absorption edge of Cu_2O crystals has a complex structure. Light absorption near the edge does not increase continuously with decreasing wavelength but has a step-like character. Two sharp boundaries are observed at which the absorption curve exhibits a break and forms a "step." These boundaries at 20°C are located: 1) at 6371 A (1.945 ev) and 2) 6284 A (1.942 ev), so that the width of the step is about 87 A (0.027 ev).

Light absorption in the region of the step is relatively low. Beyond the edge of the step (6284 A), on the short-wave side, absorption begins to increase rapidly and the absorption curve rises steeply. All these effects are clearly discernible in the microphotograph of the absorption spectrum in the region of the edge shown in Fig. 3.

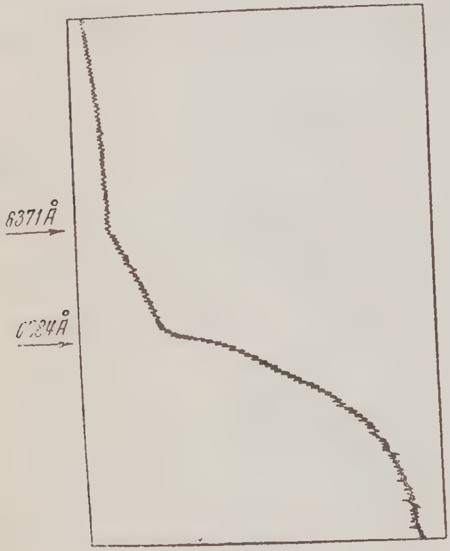

Fig. 3. Microphotograph of the "step" at the edge of the absorption curve of Cu_2O crystals at 20°C.

Another interesting phenomenon can be observed at both sides of the step: in front of each boundary of the step (on the long-wave side) a narrow, light line can be seen against the absorption background. These lines adjoin the boundaries where the sharp breaks in the absorption curve are observed. Thus these lines are located at 6271 A and 6284 A, and constitute narrow emission lines.*

As the temperature of the crystal is lowered, the absorption edge of the Cu_2O crystal, together with the step and its sharp boundaries, is displaced toward the short wavelength side. Absorption of light in the step interval depends strongly on the temperature and decreases (apparently according to an exponential law) very rapidly with cooling of the crystal. The breaks in the absorption curve at the step edges are shifted but remain sharp down to the temperature of liquid nitrogen (77.3°K). At 77.3°K the edges of the step are located: 1) at 6164 A (2.010 ev) and 2) 6086 A (2.034 ev). The distance between the two boundaries, i.e., the width of the step, at 77.3°K equals 78 A (0.024 ev). That is, the width of the step varies little with temperature. Absorption in it, however, is attenuated to such an extent that it becomes hardly noticeable at 77.3°K.

The results described above were obtained independently by Hayashi and Katsuki.[12] These Japanese investigators report that they observed only the absorption edges in the absorption spectrum of cuprous oxide.

* Bright lines at the edges of the step were also observed by Nikitin and coworkers.[11]

We succeeded in advancing further in the study of the structure of the edge in the absorption spectrum of Cu_2O, and discovered a new interesting phenomenon. As the temperature is lowered, the edge of the principal absorption of crystal Cu_2O, together with the region of step absorption, as noted above, is shifted toward the short-wave side (into the orange region) and a very narrow absorption line emerges against the greatly weakened continuum background of the step.[13] At 77.3°K, this line becomes extremely sharp and thin, so that its width becomes comparable with that of the narrow lines in atomic spectra. Its location is strongly dependent on the temperature, and on cooling of the Cu_2O crystal, together with the step, is displaced to the short-wave side. At 77.3°K, this line is located at 6125.3 A (Table 1, n = 1).

Lowering the temperature not only reduces the light absorption coefficient in the step region but also weakens the continuous spectrum beyond the step so that the beginning of the region of strong absorption is displaced toward the short-wave side more rapidly than the step itself. As the continuous spectrum is weakened with decreasing temperature, a series of separate absorption lines in the yellow region of the spectrum, located ahead of the strong absorption edge, is gradually revealed. At 77.3°K these lines become extremely narrow. We succeeded in detecting five such narrow lines, whose separation decreased with increasing frequency; that is, six lines in all, the first line being the one against the background of the step. The location of the lines is materially dependent on the temperature: the whole series of lines is displaced into the short wavelength region as the crystal is cooled. The location of all of the six of the observed lines at 77.3°K is shown in Table 1 (n from 1 to 6). In Fig. 4 is shown a spectrogram of the yellow series of absorption lines in Cu_2O.

With increase of temperature to 0°C the lines broaden and become less noticeable against the continuous spectrum background which increases greatly in intensity and moves in from the short-wave side as the temperature rises. The line broadening is asymmetric, being greater in the long wavelength region of the spectrum. The short wavelength side of the lines remains sharper.

Table 1

Location of the yellow exciton series lines in the absorption spectrum of Cu_2O at 77.3°K

Quantum numbers n	Wave-length λ_n, A	Energy ev	Frequency ν_n, см$^{-1}$	$\Delta\nu_n$, см$^{-1}$	
				Obs.	Comp.
1	6125,3	2,0234	16325,7	1134,3	785
2	5792,7	2,1396	17263,2	196,8	196,3
3	5756,6	2,1530	17371,2	88,8	87,2
4	5743,8	2,1578	17410,1	49,9	49,1
5	5738,1	2,1599	17427,5	32,5	31,4
6	5734,1	2,1615	17439,4	20,6	21,8
.	.	.	.	.	.
.	.	.	.	.	.
.	.	.	.	.	.
∞	5727,4	2,1640	17460	0	0

The increasingly closer narrow lines merge at the boundary at which the continuous absorption spectrum begins. The continuum boundary is located at about 5727.4 A (in Table 1, n = ∞). The discrete lines against the continuous spectrum, form a sequence having the appearance of the series observed in atomic (ionic) line absorption spectra near the series limits.

We attempted to determine the regularity in the spacing of the narrow lines in the absorption spectrum of Cu_2O. It turned out that the frequencies of the new lines satisfy the simple serial relationship:

$$\nu_n = A - \frac{B}{n^2} = \nu_\infty - \frac{B}{n^2} = 17460 - \frac{785}{n^2}\ \text{см}^{-1};\ n = 1, 2, 3, 4, 5, 6 \ldots \qquad (1)$$

where n is the quantum number and A and B are constants, with A = being the series limit ($n = \infty$), that is, corresponding to the red limit of photodissociation of the system of charges in the crystal lattice, which is responsible for this line series in the spectrum of Cu_2O.

In Table 1 are given the experimentally determined values of the frequencies of the lines in the series together with the observed and the computed values of the differences $\Delta\nu_n$ between the frequency ν_∞ of the series limit and the frequencies ν_n of the lines of the series:

$$\Delta\nu_n = \nu_\infty - \nu_n = \frac{B}{n^2};\ n = 1, 2, 3, 4, 5, 6.$$

As may be seen, the agreement between the observed and the calculated values is very good. The only exception is the divergence between the wave numbers for the first line of the series ($n = 1$) which stands out in the list of differences.

The relationship (1) and Table 1 show that the series of lines observed in the Cu_2O crystal spectrum have a hydrogenic character. The continuous spectrum beyond the line series must be associated with the break-away of the electrons resulting from the photodissociation of the system of charges responsible for the line series in the crystal spectrum.

The existence of sharp absorption lines in crystals at low temperatures has been repeatedly observed, for example, in molecular crystals (Obreimov and Prikhot'ko[14,15], Shpol'ski[16]), in alkali-halide salts, both colored and with metallic impurities, for example, in KI-Tl (Yuster and Delbec and Pringsheim[17]), in salts of the rare earths, etc.

However, hitherto no group of lines satisfying the series regularity has been observed in crystals.

The researches described above establish the new interesting fact that series of narrow lines with a large number of members, regularly converging towards a series limit, can be observed in solids and that these series are analogous to those which are observed for free atoms and ions.

There naturally arises the question: how does a hydrogen-like series arise in the crystal lattice of cuprous oxide and by what is it caused? The location of the series of lines in the spectrum directly next to the long wavelength edge of the self-absorption spectrum of the lattice and the large absorption coefficient in the lines of the series, both indicate that the effect is associated with the main cuprous oxide lattice and not with local distortions or departures from stoichiometric proportions.* The serial regularity (1) of

---

* It is known that in the crystal of cuprous oxide there is ordinarily an excess of oxygen which may be eliminated by prolonged heating in

(footnote continued on following page)

a hydrogenic atom in the succession of the lines shows that the system of electric charges in the crystal responsible for the series is bound by Coulomb forces.

All of these considerations led us to the idea that the hydrogenic series of narrow lines in cuprous oxide is caused by the absorption of light associated with the excitation of excitons in the Cu_2O lattice.

The concept of the exciton as an excited lattice state that can move or wander in the crystal was introduced by Frenkel[4] in 1931.

After Frenkel's work, excitons and their properties were studied by Wannifer[18], Mott[19], Slater and Shockley[20], Franck and Teller[21], and Seitz[22]. Recently various properties of excitons have been investigated by Seitz[23,24], as well as by Heller and Marcus[25], Anse'lm and Firsov[26], Samoilovich and Korenblit[27], Samoilovich and Kononova[28], Davydov[29], Dykman and Pekar[30] and Dykman[31].

Wannier[18] and Mott[19] considered the exciton as a quasi-hydrogen atom in which an electron and a hole, bound by Coulomb forces, rotate about their common center of mass.

Bound excited states of an electron and a hole are characterized by the discrete energy levels of a hydrogenic atom. The absorption spectrum of such a system must therefore consist of discrete lines** corresponding to transitions of the system under the influence of light to different excited states of the exciton. In these states the exciton is not a current carrier. Photoconductivity develops when light of higher frequency can dissociate an exciton and bring about transition to the state consisting of a free electron and hole, wherein both of them become current carriers.

It follows that the discrete energy levels of the excited states of the exciton must be located below the boundary of the free zone and that the red limit of photodissociation of the exciton must coincide with its lower boundary (determined from optical data***). Hence it can be seen that the discrete light absorption lines associated with transitions of electrons to exciton states must be located in the spectrum on the red side of the principal absorption edge and must come together at the limit of the series which is at the absorption edge.

It follows from theoretical considerations that the frequencies of the absorption spectrum of the exciton must exhibit the serial regularity characteristic of hydrogenic atoms:

$$\nu_n = \nu_\infty - \frac{R'}{n^2},$$

where ν_n is the frequency of the nth absorption line in the exciton spectrum; ν_∞ is a constant having the value of the frequency of the series limit in the exciton absorption spectrum, which corresponds to the photodissociation energy of the exciton; n is a quantum number, assuming integral values 1,2,3,...; and R' is a quantity described by the relationship

---

* (continued from previous page) vacuum at high temperatures. In spite of such treatment of a Cu_2O crystal the series of absorption lines persisted in the spectrum of Cu_2O. This shows that the origin of the series is not attributable to the excess of oxygen in the crystal.

** The possibility of the existence of narrow lines in absorption spectra of crystals was also shown by Peierls[32].

*** The zone boundary as determined from spectroscopic data may not coincide with the value obtained by thermal means.

$$R' = \frac{R(\mu / m)}{n_0^4},$$

where R is the Rydberg constant, n_0 is the index of refraction, m is the electron mass in vacuum, and μ is the reduced effective mass of the exciton:

$$\frac{1}{\mu} = \frac{1}{\mu_1} + \frac{1}{\mu_2}$$

(μ_1 and μ_2 are the effective masses of the electron and hole).

If we turn now to the experimental results described above, we find that the observed facts are in very good agreement with the concepts regarding the exciton. Furthermore, the results of experiments permit the determination for Cu_2O, from the value of the constant for the B exciton series, of the reduced mass of the exciton μ, and from it to calculate either the effective mass μ_1 of the electron or the effective mass μ_2 of the hole, if one or the other of these masses is known. Taking $\mu_2 \approx 1$* and $n_0 = 2.5$, we get from the data on the exciton spectrum the value $\mu_1 = 0.4$.

Thus from the exciton spectrum we obtain a reasonable value for the effective mass, indicating good agreement between theory and experiment.

On the basis of the above considerations we can conclude that the hydrogenic series of narrow lines observed by us[10,13] in the yellow region of the absorption spectrum of cuprous oxide crystals is the optical spectrum of excitons and constitutes a direct proof of the existence of excitons in the crystal lattice.

The above results were obtained in the spring of 1951**. Several months later the existence of the hydrogen-like series of narrow lines in solids, experimentally established by us[10,13] in crystals of cuprous oxide, was confirmed by the work of the Japanese physicists, Hayashi and Katsuki[33] who observed a series of lines in the yellow part of the spectrum of cuprous oxide but erroneously attributed the series to the polaron (self-trapped electron). In 1954 our experiments were repeated in France, and substantiated by the results of Nikitine and his co-workers[11].

The excitation of excitons by quanta of light in a crystal lattice can be represented schematically as shown in Fig. 5. In contrast to the hydrogen atom, in order to create an exciton, it is necessary to expend a certain energy ν_1, the energy of exciton formation in the state $n = 1$.*** Theory does not give the value

---

* The value $\mu_2 = 1$ can be taken as the average of the value $\mu_2 = 1.5-1.8$ obtained from F-center data for the Cu_2O crystal and the value $\mu_2 = 0.5$ obtained from an investigation of the thermoelectromotive force and the Hall effect. These data were kindly communicated to us by C. I. Pekar and V. P. Zhuze.

** The results of these investigations were reported on September 19, 1951, at the Physico-Technical Institute of the Acad. of Sci. of the USSR in Leningrad, and on December 12, 1951, at the Physico-Technical Institute of the Acad. Sci. of the Ukrainian SSR in Kiev.

*** If the number of excitons in the state with quantum number $n = 1$ were sufficiently large, then it would be possible to observe a

(footnote continued on following page)

of this energy, but ν_1 can be determined experimentally from the exciton spectrum just as the quantity ν_∞ can be obtained from the photodissociation of the exciton. For cuprous oxide $\nu_1 = 2.023$ ev, $\nu_\infty = 2.164$ ev. The frequency of the first member of the exciton series determines the minimal energy of exciton formation. The exciton may be formed in higher, excited states, but for this higher energies are necessary (Fig. 5).

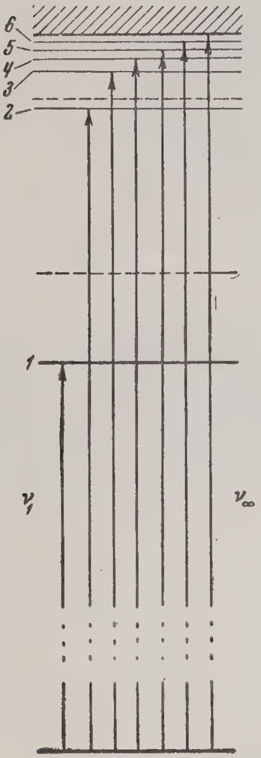

Fig. 5. Diagram of exciton formation in a crystal lattice.

From the comparison of the values of $\Delta\nu_n$ for the exciton spectrum with the values for the spectrum of hydrogen, given in the last column of Table 1, it is clear that a significant departure from similarity to hydrogen occurs for the first member of the exciton series ($n = 1$). It follows that the Coulomb law for the interaction of the electron and hole in the crystal, regarded as a dielectric medium, proposed by Mott[19] - $V = e^2/rn_0^2$ - does not hold for the smaller exciton orbits. The corresponding exciton energy levels lie deeper than those of hydrogen, which are shown in Fig. 5 by dashed lines.

According to the ideas of Frenkel[4], a crystal can contain two basic types of excitons which he called "free" and "adhering". These two types of excitons have been recently investigated by Davydov[29] for molecular crystals ("free" and "localized" excitons) and by Dykman and Pekar[30], and Dykman[31], for ionic crystals ("non-polarizing" and "polarizing" excitons).

The narrowness not only of the first, but also of the other lines of the yellow exciton series in Cu_2O crystals indicates that the exciton in the crystal of Cu_2O migrates through the crystal, i.e., it is a free, "non-polarizing" exciton.

For further study of the discovered effect, we felt it would be of interest to extend the investigation into the region of continuous absorption by cuprous oxide, beyond the limit of the series of narrow exciton lines. Investigation of this region presents great difficulties because of the large absorption coefficient. Nevertheless, even in our first experiments, using very long exposures, we discovered[13] non-homogeneities in the continuous absorption spectrum of Cu_2O beyond the limit of the yellow series of the exciton. The strong continuous absorption, beginning immediately beyond the series limit, gradually grows somewhat weaker as we go into the short wavelength region and attains a broad minimum, located in the vicinity of 5500 A (2.25 ev) at 77.3°K. This indicates some non-homogeneity in the structure of the free zone in

---

*** (continued from preceding page) series of transitions from the state with $n = 1$ into the excited states with the quantum numbers $n = 2,3,4,\ldots$ This series of lines, similar to the Lyman series in hydrogen, should lie in the infrared part of the spectrum. It is possible that in certain crystals having a very narrow forbidden zone the concentration of thermally excited excitons may be sufficiently large for this "infrared series" of the exciton to be observable.

Cu_2O crystals. Accordingly, together with B. P. Zakharchenia, we undertook[34] a new investigation of this phenomenon using thin plates. By careful polishing we obtained plates of cuprous oxide with a thickness of only about 20 μ.

In the absorption spectrum of thin plates of Cu_2O at the temperature of liquid nitrogen (77.3°K), beyond the absorption minimum on the short wavelength side of the yellow series, there appears a new "green" series of narrow lines converging on the short-wave side to a limit beyond which a continuous spectrum is again observed.[34] We succeeded in distinguishing four lines of the second series in the spectrograms. Light absorption in the lines of this second, green series is significantly greater than in lines of the yellow series; moreover, these lines are wider. Measurements showed that these lines also conform to a serial regularity characteristic of hydrogen atoms:

$$\nu_n = \nu_\infty - \frac{B}{n^2} = 18507 - \frac{1246}{n^2}\ \text{cm}^{-1};\ n = 2, 3, 4, 5, \ldots \quad (2)$$

We could not, however, detect at 77.3°K either visually or on the spectrograms, a line which could be interpreted as the first member of the green series.

The section of the spectrum in which both series appear, with the green series magnified, is shown in Fig. 6.

In Table 2 are given the frequencies ν_n of the lines of the green series as well as the differences $\Delta\nu_n$ between the frequencies ν_n of the observed lines and the frequency ν_∞ of the series limit:

$$\Delta\nu_n = \nu_\infty - \nu_n = 18507 - \nu_n.$$

The differences $\Delta\nu_n$ obtained experimentally are compared in Table 2 with the values calculated from relationship (2):

$$\Delta\nu_n = \frac{B}{n^2} = \frac{1246}{n^2},\ n=2, 3, 4, 5, \ldots$$

As can be seen, the frequencies of the second series also agree well with the serial regularity for hydrogenic atoms.

We assume that the second hydrogenic series in cuprous oxide, just as the first series, is produced by excitons in the Cu_2O lattice crystal.

It is interesting to note that the difference in the limit frequencies of the yellow and green exciton series $\delta\nu$ = 0.131 ev, coincides within the limits of the experimental error with the energy of one of the infrared absorption bands of Cu_2O[10] (0.138 ev).

The green series in cuprous oxide was also observed by Hyashi and Katsuki[33] who attribute it to the exciton. Hyashi and Katsuki associate the yellow (first) series with the polaron (self-trapped electron), which we believe is erroneous in view of the following considerations.

1) The dissociation energy of the polaron is of the order of some tenths of an electronvolt[36], and hence the absorption spectrum of the polaron should be located in the infrared region and not in the visible region, as is the yellow series, which has an exciton energy of about 2 ev.

2) By its polarization nature, the polaron is closely related to lattice vibrations and, therefore, the optical spectrum of its

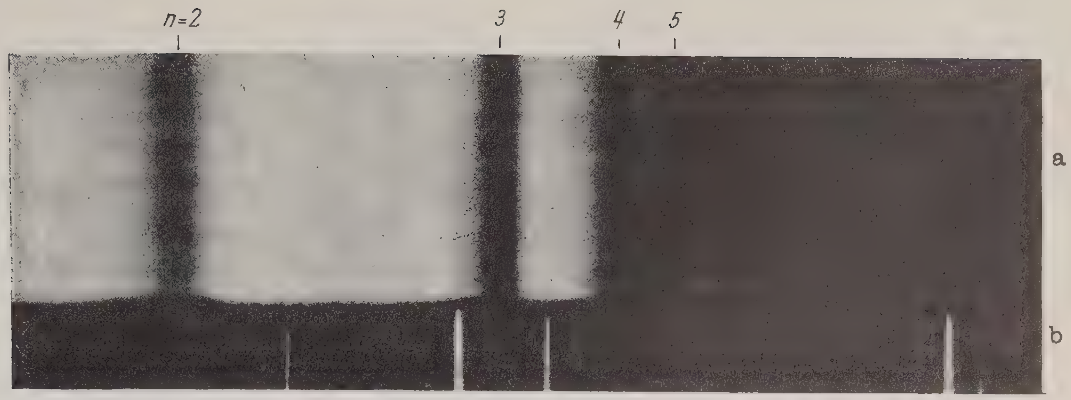

Fig. 4. Spectrograms: a) the yellow exciton series in Cu_2O crystal at 77.3°K; b) iron spectrum (for comparison).

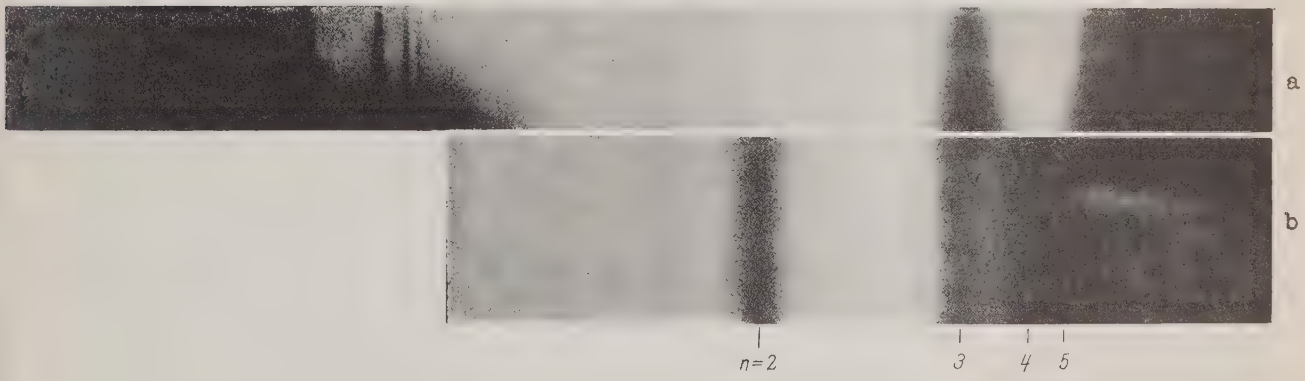

Fig. 6. Spectrograms: a) yellow and green series in Cu_2O crystal and b) green series to enlarged scale, at 77.3°K.

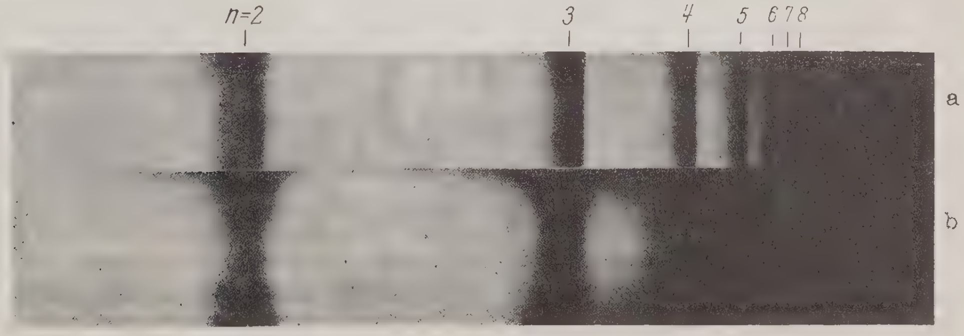

Fig. 8. Spectrograms of the yellow exciton series in Cu_2O crystal at a) 1.3°K, b) 77.3°K.

excitation must consist primarily of a single wide band (as in the case of F-centers[24,26]), and not of several narrow lines as in the yellow series.

3) As the temperature is lowered the absorption of light caused by polarons must fall off very rapidly since the concentration of polarons in the crystal decreases according to an exponential law.[36] Nothing of the kind is observed for the yellow series of Cu_2O.

Table 2

Location of the green exciton series lines in the absorption spectrum of Cu_2O at 77.3°K

Quantum numbers n	Wave-length, λ_n, A	Energy, ev	Frequency ν_n, cm^{-1}	$\Delta\nu_n$, cm^{-1}	
				Obs.	Comp.
1	—	—	—	—	1246
2	5496	2,255	18195	312	311
3	5444	2,277	18369	138	138
4	5426	2,284	18429	78	77
5	5419	2,287	18454	53	50
.		.	.	.	.
∞	5404	2,294	18507	0	0

In subsequent experiments carried out jointly with Zakharchenia and Reinov we subjected the crystal of cuprous oxide to much deeper cooling in liquid helium and increased the dispersion of the prism spectrograph to 7 A/mm in the vicinity of 5800 A. In cooling the crystal of cuprous oxide to the temperature of liquid helium, 4.2°K, the lines of the yellow as well as of the green series became considerably narrower than at the temperature of liquid nitrogen and both series of lines were displaced toward the short-wave side of the spectrum.[37] A new edge (step) where the continuous absorption exhibits a jump was discovered at 5841 A (2.1219 ev), and another very weak line was detected in this step at 5817 A (2.1306 ev). We assume that this line is the first member (n = 1) of the green exciton series.

The frequencies of the lines of the yellow as well as of the green series at 4.2°K (except for the first members) satisfy the hydrogenic serial regularities:

for the yellow series $$\nu_n = 17523{,}3 - \frac{780{,}7}{n^2};\ n = 1, 2, 3, \ldots \qquad (1')$$

for the green series, $$\nu_n = 18587 - \frac{1200}{n^2};\ n = 1, 2, 3, \ldots \qquad (2')$$

At the temperature of liquid helium we discovered[37] an additional seven weak narrow absorption lines located between the lines of the yellow exciton series, as shown in Fig. 7. The frequencies of the new lines are listed in Table 3.

In addition, experiments were undertaken to study the absorption spectrum of the Cu_2O crystal with a spectrograph having a diffraction grating, and yielding a dispersion close to 4 A/mm. Furthermore, the Cu_2O crystal was cooled to even lower temperatures, i.e. to the temperatures attained by evaporating liquid helium at low pressures.

At the temperature 1.3°K, at which the lines of the exciton spectrum become even more narrow, it was possible to observe that some members of the exciton series, beginning with the second,

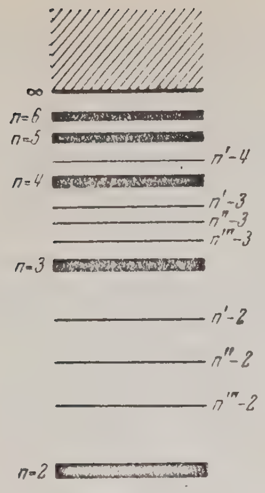

Fig. 7. Location of the weak new absorption lines between the members of the yellow exciton series at 4.2°K.

exhibit a fine structure.[38] Thanks to the narrowing of the lines and the great weakening of the continuous spectrum, we were able to observe the higher members of the yellow exciton series in the neighborhood of the series limit up to and including the ninth member.* The spectrogram of the yellow exciton series at 1.3°K is shown in Fig. 8,a. In the same figure (8,b) is the spectrogram of the same series, obtained with the same 160 μ thick Cu_2O plate at 77.3°K. From these spectrograms it is clear to what extent the continuous spectrum, superimposed on the series, is weakened in going from 77.3°K to 1.3°K and how much narrower the lines are at 1.3°K.

In the second column of Table 4 are shown the measured frequencies of the members of the yellow exciton series at 1.3°K. The wave numbers refer to the centers of the lines, without taking the fine structure into account.

The narrowing of the absorption lines 1.3°K makes it feasible to measure the lines of the series, particularly of the higher members, $n = 7$ and $n = 8$, with relatively high accuracy. It is possible to use measurements of these members, for which the hydrogenic regularity should be closely observed, for computing** the constants ν_∞ and R for the yellow series. The following expression is obtained

$$\nu_n = 17524{,}5 - \frac{710{,}5}{n^2};\ n = 1, 2, 3, \ldots$$

The frequencies of the members of the yellow series calculated using this formula, are listed in the third column of Table 4. The differences $\Delta\nu$ between the observed and the calculated frequency values show the departure from hydrogenic behavior of the members of the yellow series. It is seen from Table 4 that deviations are noticeable not only for the first member of the series $n = 1$, but also for other members of the series: $n = 2, 3, 4, 5$, and that the deviation diminishes with increasing quantum numbers.

---

* The dimensions of the exciton orbits corresponding to the higher members of the series ($n = 10$) experimentally obtained at 1.3°K are of interest. For such large quantum numbers the radii of the orbits in the crystal are enormous. Taking $\mu_1 = \mu_2 = m$, we obtain for the radius of the electron and hole orbits in the exciton

$$r_{n\,\mathrm{exc}} = 2r_{1\mathrm{H}} n^2 n_0^2 \approx n^2 n_0^2 \text{ Å},$$

where r_1 is the radius of the first orbit in a hydrogen atom, while n_0 is the index of refraction of the crystal.

Assuming $n_0^2 \approx 6$ and $n = 10$, we get

$$r_{10\,\mathrm{exc}} = 600 \text{ Å}.$$

** The calculations were carried out by B. P. Zakharchenia.

It follows that the smaller the exciton orbit, the greater is the departure from similarity to hydrogen. On the one hand, this deviation may be due to the fact that neglecting the microstructure of the crystal and treating it, macroscopically, as a medium with a certain dielectric constant is an allowable procedure only for large exciton orbits; on the other hand, the deviations for small orbits may be explained by the fact that a hole in the crystal is not a point charge.

At 1.3°K we discovered[38] still other new lines located between $n = 4$ and $n = 5$, and between $n = 5$ and $n = 6$ members of the series, in addition to the lines previously observed[37] at 4.2°K. Furthermore, because of the line narrowing at 1.3°K, several of the weak lines we had previously observed between the members of the yellow series split into several very fine lines. All the new lines located between the members of the yellow exciton series, observed at 4.2°K and 1.3°K, are listed in Table 3.*

Table 3

Location of the new lines in the exciton spectrum of Cu_2O at 4.2°K and 1.3°K

Line designation	$T = 4{,}2°$ K Wavelength A	Frequency cm⁻¹	$T = 1{,}3°$ K Wavelength A	Frequency cm⁻¹
$n'''—2$	5758,7	17365,0	5758,8	17367,1
$n''—2$	5753,2	17381,6	5752,5	17383,7
$n'—2$	5746,3	17402,5	5745,1	17406,1
$n'''—3$	5731,8	17446,5	5731,8	17446,5
$n''—3$	5729,0	17455,0	5729,5	17453,5
			5728,0	17458,1
$n'—3$	5726,5	17462,7	5727,3	17460,2
			5726,5	17462,7
			5726,0	17464,2
			5725,4	17466,0
$n'—4$	5719,8	17483,1	5719,3	17484,7
			5718,1	17488,3
			5714,7	17498,7
			5713,9	17501,2

From what has been said above, it is clear that the light absorption spectrum in a crystal of cuprous oxide has a complex character and comprises a large number of absorption lines. This indicates a complex crystal structure with a multiplicity of electronic energy levels in the vicinity of the free zone at 0.4 ev.

It is well known that the splitting of atomic spectrum lines in magnetic and electric fields can be used to advantage in the analysis of complex spectra. Accordingly, we undertook to investigate the influence of an external electric field on the lines of the exciton series in cuprous oxide. These investigations, interesting in themselves, could be expected to be of help in understanding the complex spectrum of cuprous oxide and interpreting the new lines discovered at the temperature of liquid helium.

A considerable Stark effect in the exciton spectrum was to be expected in view of its hydrogenic nature and the large electron and hole orbits.

In applying an electric field to the Cu_2O crystal we actually discovered[35,39] new effects, leading to very large changes in the exciton spectrum.

---

* In the vicinity of the first member of the series $n = 1$, at the temperature of liquid helium, we noticed a diffuse line at 6039 A (2.0523 ev).

In the first stage of our experiments we studied the yellow exciton series at the temperature of liquid nitrogen (77.3°K). For obtaining the Stark effect, we used two voltages: 20 and 70 kv.

Table 4

Location of the members of the yellow exciton series of Cu_2O at 1.3°K

Quantum numbers n	Frequency ν_n, см$^{-1}$		$\Delta\nu$, см$^{-1}$
	Obs.	Comp.	
1	16406,8	16814,0	407,2
2	17331,3	17346,9	15,6
3	17438,3	17445,6	7,3
4	17477,3	17480,1	2,8
5	17494,4	17496,1	1,7
6	17504,5	17504,8	0,3
7	17510,0	17510,0	0
8	17513,4	17513,4	0
9	17515,8	17515,8	0
.	.	.	
.	.	.	
.	.	.	
∞		17524,5	

The effect of homogeneous and non-homogeneous electric fields on the exciton was investigated with the electrode arrangement shown in Fig. 9. The spectrograms of the Stark effect for the exciton obtained in an inhomogeneous field, created with the aid of a sharp-point electrode (Fig. 9,b) are similar to the well known Stark effect spectrograms obtained by Lo Surdo's method.[40]

We succeeded in detecting the Stark effect in five members of the yellow exciton series (n = 1,2,3,4,5).

As in the hydrogen atom, the changes in the exciton spectrum under the influence of a gradually increasing electric field become noticeable first only in the higher members of the series, those with large values of the quantum number n. As the field intensity is increased the effect extends to all members of the series.

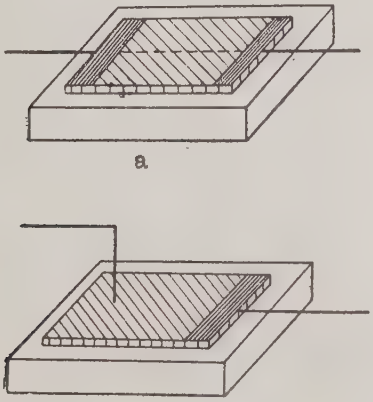

a

b

Fig. 9. The electrode arrangement for study of the Stark effect in Cu_2O crystals: a) linear electrodes for obtaining a "homogeneous" electric field, b) point electrode for obtaining a non-homogeneous field.

Among the members of the series with n = 5, 4 and 3, we discovered the appearance of line components in the electric field; as the field is increased the separation between the components increases, the lines broaden and are shifted into the red or the violet part of the spectrum. In addition, under the influence of the electric field, new lines, not observed in the absence of the field, appear in the exciton spectrum.

We established that these new lines were identical with the weak lines we had observed in the Cu_2O spectrum at the temperature of liquid helium. With increase of the field these lines grow in intensity and are shifted toward the red or the violet regions. They behave like "forbidden" lines in the Stark effect. We assume, therefore, that they are associated with some forbidden transitions between electronic energy levels, appearing under the influence of the electric field.

At present, it is difficult to identify the energy levels between which these forbidden transitions occur. Probably the existence of these levels is connected with the fact that the exciton energy level structure is not entirely hydrogen-like.

Deviation from hydrogenic character in the exciton structure must lead to the removal of degeneracy with respect to the number l (determining the orbital angular momentum) and the appearance of new levels in the exciton energy scheme. The appearance of new forbidden lines in the exciton spectrum between the members of the yellow series must then be associated with violations of the selection rules: $\Delta l = \pm 1$.

In very strong non-homogeneous fields in the vicinity of the pointed electrode (Fig. 9,b) we were able to determine the effect of the field on the first members of the exciton series ($n = 2$ and $n = 1$). The $n = 2$ line is weakened and displaced toward the red end of the spectrum. Even in strong fields the $n = 2$ weak line does not split, but only increases in intensity, indicating that it is connected with a forbidden electronic transition. The absence of splitting in an electric field, even though such splitting should be readily noticeable because of the line's extreme narrowness, confirms its assignment to the S-level with the quantum number $n = 1$.

In addition to the above-mentioned changes in the exciton spectrum under the influence of a gradually increasing electric field, we discovered another very interesting phenomenon. With increasing field strength, the higher members of the exciton series, together with their components, are broadened and, together with their satellites (the new lines), weaken in intensity and gradually disappear: first the $n = 5$ member of the series, then, at higher voltages, the $n = 4$, and, at still higher voltages the $n = 3$. Simultaneously with the disappearance of each member from the series limit side, the continuous spectrum moves into the place of vanishing series members and their components. We observed that, at sufficiently strong fields, of the entire exciton series there remained only the first two members: $n = 1$ and $n = 2$.* We interpret this disappearance of the higher members of the exciton series under the influence of the electric field as being due to the electron being removed by the field from the energy levels of the exciton, i.e., to ionization (dissociation) of the exciton by the electric field.

This effect in the exciton is similar to the ionization of the hydrogen atom in a strong electric field, first predicted by Oppenheimer,[41] and discovered in the hydrogen atom by Rausch and Traubenberg.[42] The theory of the effect for hydrogen was developed by Lanczos.[43] The possibility of disruption of excitons by an electric field was investigated by Seitz.[44] In order to observe the ionization of the hydrogen atom, as shown by the experiments of Rausch and Traubenberg, fields of the order of 10^6 v/cm are necessary. The magnitude of the critical field for exciton ionization is reduced, as our experiments have shown, to about 10^4 v/cm, in consequence of the influence of the dielectric constant of the crystal and the large orbits of the electron and hole.

---

* From external effects, the disappearance of the higher members of the exciton series with increase of the field might be interpreted as the result of the Cu_2O crystal heating by electrical currents (increasing with increasing field intensity). However, this is not the case. By special experiments it was established that the disappearance of the higher members of the series, to $n = 3$ inclusive, under the influence of heating is connected with a very pronounced shift of the entire line series, including the first and second members; this shift is not observed in an electric field.

The observed changes in the exciton spectrum occurring under the influence of an increasing electric field are shown schematically in Fig. 10.

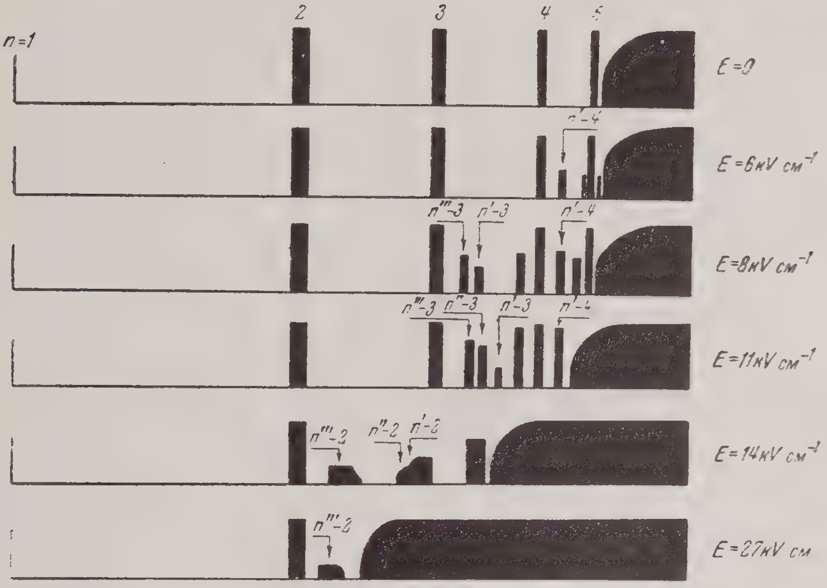

Fig. 10. Scheme of shifts in the yellow exciton series in the spectrum of a Cu_2O crystal, occurring under the influence of an increasing electric field at 77.3°K.

The quantitative determination of the exciton line shifts in electric fields is very difficult because measurement of the field intensity effective inside the crystal involves large errors. Having selected plates of cuprous oxide in which the electric field was relatively homogeneous* and the Stark splitting uniform over the entire width of the spectrograph slit, we carried out quantitative measurements of the exciton line displacements as functions of the mean electric field E determined from the potential difference and the distance between the electrodes (Table 5). The data of Table 5 can give some idea of the magnitudes of exciton line shifts, but not of the law characterizing the displacements in the field (linear or quadratic).**

From the foregoing it is clear that a careful and thorough study of the absorption of light in Cu_2O reveals effects indicating appreciable departures of the exciton spectrum in Cu_2O crystals from the spectrum characteristic of hydrogen:

1) Deviation of the frequencies of the first members of the yellow series from the hydrogenic regularity described by formula (1); these deviations decrease with increasing quantum number n (Table 4).

---

* Insofar as is attainable in Cu_2O crystals with the electrodes shown in Fig. 9,a.

** The influence of an electric field on the absorption spectrum has also been investigated by Kaliniak and Feodorovich.[45]

Table 5

Shift of exciton lines in Cu_2O in electric fields

$n = 3$		$n''' - 3$		$n = 4$		$n' - 4$	
E, kV см$^{-1}$	$\Delta\lambda$, Å	E, kV см$^{-1}$	$\Delta\lambda$, Å	E, kV см$^{-1}$	$\Delta\lambda$, A	E, kV см$^{-1}$	$\Delta\lambda$, Å
10	0,4	9	0	7	1,0	7	0
14	1,2	12	—0,7	12	1,8	10	—0,5
18	2,1	14	—1,1	13	2,0	12	—0,9

2) The appearance between the members of the yellow series at liquid helium temperatures of new weak lines with frequencies which do not conform with the regularity (1).

3) Stark effect in exciton lines which shows that the behavior of the yellow series in an electric field is different from the behavior of the line spectrum of the hydrogen atom.

On the basis of the as yet rather scant experimental material available, it seems to us that the exciton must be regarded as a system closer to a complex atom than to the hydrogen atom. The complex structure of the exciton, and consequently, the structure of the absorption edge depends on the substance, - on the atoms and ions forming the crystal lattice - and is apparently related to the crystal structure. The exciton excitation spectrum can, therefore, be more complex and hence more similar to the spectrum of a complex atom (or ion) than to the simple spectrum of the hydrogen atom. This becomes manifest in the spectra of cuprous oxide and other investigated crystals.

The concept of an exciton as a hydrogen-like system consisting of a hole and an electron must be regarded as only the first approximation to reality, as one giving only the general characteristics of this quasi-particle.

Leningrad Physico-Technical Institute of
the Academy of Sciences of the USSR

REFERENCES

1. A.V.Ioffe & A.F.Ioffe, Zhur. eksp. i teor. fiz., 6, 737 (1936).
2. B.Gudden & R.Pohl, Zs. f. Phys., 17, 331 (1923); 18,199 (1923).
3. B.Gudden, Lichtelektrische Erscheinungen - Berlin, 1928.
4. J.Frenkel, Phys. Rev., 37,17,1276 (1931); Ia.I.Frenkel', Zhur. eksp. i teor. fiz., 6, 647 (1936); Phys. Z. Sow. Union, 9, 158 (1936).
5. V.P.Zhuse & S.M.Ryvkin, Zhur. eksp. i teor. fiz., 20, 152 (1950).
6. V.P.Zhuse & S.M.Ryvkin, Sbornik posviashchennyi semidesiatiletiiu akademika A.F.Ioffe, (Symposium in honor of the 70 anniversary of Academician Ioffe, M. 1950; Doklady AN SSSR, 76, 241 (1951); Izv. AN SSSR Ser. fiz., 16, 93 (1952).
7. L.Apker & E.Taft, Phys. Rev., 79, 964 (1950); 81, 698 (1951);82,814 (1951).
8. M.Pigarev & S.Golub, Sow. Phys., 6, 603 (1934).
9. G.Mönch, Zs. f. Phys., 78, 728 (1932).
10. E.F.Gross & N.A.Karryev, Doklady AN SSSR, 84, 261 (1952).

11. S.Nikitine, G.Perny & M.Sieskind, C.R., 238, 67 (1954); S.Nikitine, L.Couture, M.Sieskind & G.Perny, C.R., 238, 1786 (1954); S.Nikitine, M.Sieskind & G.Perny, C.R., 238, 1987 (1954); S.Nikitine, R.Reiss & G.Perny, C.R., 240, 505 (1955); S.Nikitine, C.R., 240, 1415 (1955).

12. M.Hayashi & K.Katsuki, J.Phys. Soc., Japan, 5, 381 (1950).

13. E.F.Gross & N.A.Karryev, Doklady AN SSSR, 84, 471 (1952).

14. I.V.Obreimov & A.F.Prikhot'ko, Sow. Phys., 1, 203 (1932); 9, 34, 48 (1936); I.V.Obreimov, A.F.Prikhot'ko & K.G.Shabaldas, Zhur. eksp. i teor. fiz., 6, 1062 (1930); I.V.Obreimov & K.G.Shabaldas, J. of Phys., 7, 168 (1943).

15. A.F.Prikhot'ko, J. of Phys., 8, 257 (1944); Zhur. eksp. i teor. fiz., 19, 383 (1949); I.V.Obreimov, A.F.Prikhot'ko & I.V.Rodnikova, Zhur. eksp. i teor. fiz., 18, 409 (1948).

16. E.V.Shpol'ski & L.A.Klimova, Izv. AN SSSR, Ser. fiz., 18, 673 (1954). (Trans. in Bulletin No. 6, Vol. 18, p. 357.

17. P.H.Yuster & C.J.Delbec, J. Chem. Phys. 21, 892 (1953); P.Pringsheim, Zs. f. Phys. 136, 573 (1954).

18. G.H.Wannier, Phys. Rev., 52, 191 (1937).

19. N.F.Mott, Proc. Roy. Soc., 167, 384 (1938).

20. J.Slater & W.Shockley, Phys. Rev., 50, 705 (1936).

21. J.Franck & E.Teller, J. Chem. Phys., 6, 859 (1938).

22. F.Seitz, Trans. Faraday Soc., 35, 74 (1939); F.Seitsz, J. Chem. Phys., 6, 150 (1938); F.Seitz, The Modern Theory of Solids - New York, 1940.

23. F.Seitz, Imperfections inNearly Perfect Crystals, p. 25 - New York, 1952; F.Seitz, Rev. Mod. Phys. 23, 328 (1951).

24. F.Seitz, Rev. Mod. Phys., 26, 27 (1954).

25. W.R.Heller & A.Marcus, Phys. Rev., 84, 808 (1951).

26. A.I.Ansel'm & Iu.A.Firsov, Zhur. eksp. i teor. fiz., 28, 151 (1955).

27. A.G.Samoilovich & L.L.Korenblit, Doklady AN SSSR, 101, 55 (1955).

28. A.G.Samoilovich & M.V.Kononova, Doklady AN SSSR, 101, 55 (1955).

29. A.S.Davydov, Izv. AN SSSR, Ser. fiz. 12, 608 (1948); Teoriia pogloshcheniia sveta v molekuliarnykh kristallakh, (Theory of light absorption in molecular crystals, Kiev, 1951.

30. I.M.Dykman & S.I.Pekar, Trudy In-ta fiziki, (Transactions of the Physics Institute of the Ukr. SSR Ac. of Sciences) No. 3, 92 (1952).

31. I.M.Dykman, Trudy In-ta fiziki (Transactions of the Physics Institute of the Ukr. SSR Ac. of Sciences) No. 5, 48 (1954).

32. R.Peierls, Ann. d. Phys. 13, 905 (1932).

33. M.Hayashi & K.Katsuki, J. Phys. Soc., Japan, 7, 599 (1952).

34. E.F.Gross & B.P.Zakharchenia, Doklady AN SSSR, 90, 745 (1953).

35. E.F.Gross, B.P.Zakharchenia & N.M.Peinov, Doklady AN SSSR, 97, 57 (1954).

36. S.I.Pekar, Issledovaniia po elektronnoi teorii kristallov, (Contributions of the electronic theory of crystals). M., 1951.

37. E.F.Gross, B.P.Zakharchenia & N.M.Peinov, Doklady AN SSSR, 92, 265 (1953).

38. E.F.Gross, B.P.Zakharchenia & N.M.Reinov, Doklady AN SSSR,99,231 (1954).

39. E.F.Gross, B.P.Zakharchenia & N.M.Reinov, Doklady AN SSSR, 97, 221 (1954).

40. A.LoSurdo, Rend. d. Linc., 22, 665 (1913).

41. J.R.Oppenheimer, Phys. Rev. 31, 66 (1928).

42. V.Rausch & H.Traubenberg, Zs. f. Phys. 54, 307 (1929); 56, 254 (1929); 62, 289 (1930); 71, 291 (1931).

43. C.Lanczos, Zs. f. Phys., 62, 518 (1930); 68, 204 (1931).

44. F.Seitz, Phys. Rev., 76, 1376 (1949).

45. A.A.Kaliniak & L.G.Fedorovich, Doklady AN SSSR, 96, 1137 (1954).

TRANSACTIONS OF THE CONFERENCE ON X-RAY SPECTROSCOPY (Moscow, January 25-26, 1955).

The Conference on X-Ray Spectroscopy, called by the Commission on Röentgenography at the Crystallographic Institute of the USSR Academy of Sciences, was held January 25-26, 1955 in Moscow.

The Conference heard the following reports:

1. G.S.Zhdanov, Opening address.
2. N.V.Troneva & I.B.Borovski (MGU), Certain problems relating to the classification of complex x-ray emission spectra.
3. T.I.Kakushadze (Georgian Pedogogical Inst.), On the electronic configuration of lantanides.
4. R.L.Barinski (Lab. for the Mineralogy and Geochemistry of Rare Elements, USSR Acad. of Sc.), The fine structure of the absorption and emission spectra of thorium in compounds.
5. K.I.Narbutt (IGN), On the structure of x-ray emission lines of ions in solution.
6. M.A.Blokhin (RGU), Investigation of the distribution of the density of electronic states in a solid and the width of the internal atomic levels.
7. S.A.Nemnonov (Ural Branch of the Ac. of Sc.), On the nature of the asymmetry of the $K\alpha_{1,2}$-lines of the transition elements of the iron group and its dependence on the concentration of certain alloying elements.
8. S.M.Karal'nik (Kiev State Univ.), X-ray spectra and the inter-atomic bond in metals and alloys.
9. V.A.Kazantsev (Kuibyshev Ind. Inst.), Investigation of the x-ray spectra of metallic alloys (Mn-Ni system).
10. A.V.Sokolov (Ural Branch of Ac. of Sc.), On the absorption and emission of x-rays by ferromagnetic metals.
11. V.P.Bykov & I.B.Borovski (MGU), The RSKU-53 x-ray spectrograph.
12. V.A.Kazantsev (Kuibyshev Ind.Inst.), Design of two x-ray tubes for spectrum analysis.
13. K.I.Narbutt & E.M.Fridman (IGN), A high-energy sealed-off x-ray tube for spectrum analysis.
14. M.A.Blokhin & A.N.Gusatinski (RGU), Selection of optimum specimen density for investigation of x-ray absorption spectra.
15. E.E.Vainshtein & I.D.Shevaleevski (Geochemical Inst. of the Ac. of Sc.), Characteristics of the ($W_1 - W_2$) diagram and its use in determining relative intensity of x-ray spectral lines.
16. K.I.Narbutt, E.E.Vainshtein, A.B.Gil'varg & L.M.Beliaev (IGN, Geochemical Inst. and Crystallographic Inst. of the Ac. of Sc.), The new RSD-2 x-ray vacuum spectrograph.

Nine of these reports are published below.

Translator's note: Some of the titles listed above differ somewhat from the titles used over the reports below.

MGU = Moscow State University; IGU = Institute of Geological Sciences of the USSR Academy of Sciences; RGU = Rostov State University.

INVESTIGATION OF THE X-RAY SPECTRA OF ALLOYS OF THE Mn-Ni SYSTEM

- V.A.Kazantsev

In a series of experiments carried out in 1952, we investigated the behavior of the K $_5$ emission bands as well as of other lines of the K group the spectra of manganese and nickel incident to magnetic transformations of in the Mn-Ni system.

The results of these experiments show that magnetic transformations ocurring both due to changes in the composition of the alloy and to transition through the Curie point (although these are fundamentally different factors) have the same effect on the behavior of the $K\beta_5$ emission bands of Mn and Ni atoms. Transition of the alloys to the paramagnetic state is accompanied by a shift of the $K\beta_5$ band of nickel towards the side of higher energies and a shift of the $K\beta_5$ of Mn in the opposite direction. The shape, width and intensity of the $K\beta_5$ bands of both components are affected by magnetic transformation.

The data obtained in 1952, however, proved insufficient for a more or less complete interpretation of the behavior of the spectra incident to both types of magnetic transformation. In view of this we undertook a further investigation of the K absorption edge for manganese in the same alloy samples and under the same conditions. It may be noted that in obtaining the emission spectra the temperature of the specimen in the para- and ferromagnetic states was maintained constant to within ± 20°C. In obtaining the absorption spectra the temperature of the alloy was monitored by means of a thermocouple, which fully insured that the specimens were in the desired magnetic state.

The behavior of the K absorption edge of Mn incident to magnetic transformations under the influence of temperature (i.e., transition to the paramagnetic state) turned out to be entirely unexpected.

As the temperature was increased from 20 to 180° (up to the transformation temperature) the K edge of Mn shifted towards the side of higher energies. With further increase in the temperature up to 300° (transition through the Curie point) the absorption edge, on the contrary, was markedly displaced to the side of lower energies, coming to a position intermediate between those observed at 20° and 180°. This was substantiated by numerous repetitions of the experiments. The maximum measurement error was ± 0.5 ev, whereas the shift of the absorption edge amounted to 3.8-4.2 ev.

Far from helping explain the influence of magnetic transformation of alloys on their x-ray spectra, the observed behavior of the K absorption edge made doubtful the physical interpretation of the behavior of the $K\beta_5$ bands of Mn and Ni proposed earlier by the writer.

Investigation of the K absorption edge for Ni in the same specimens and under the same conditions yielded new results. The results obtained on the K edges and $K\beta_5$ bands of nickel and manganese in alloys of the Mn-Ni system are described below.

K Absorption Edge of Nickel

1. As the temperature is increased from 20 to 180° (up to the magnetic transformation point) the center of the 3d absorption band remains unchanged (within ± 0.5 ev). The width of this band also remains constant at 16 ± 0.5 ev (without corrections for focusing).
2. The center of the 4sp absorption band is shifted some 2 ev to the side of higher energies as the temperature is increased from 20 to 180°.
3. With further increase in temperature (transition through the Curie point) the width of the 3d band, as before, remains unaltered (16.5 ± 0.5 ev)

but its center is appreciably (3 ± 0.5 ev) shifted towards higher energies.

4. The width of the entire 4sp absorption band increases gradually and continuously from 17 to 24.2 ev (error ± 0.8 ev) as the temperature is increased from 20 to 300°.

5. In passing through the Curie point (180–300°) the center of the 4sp absorption band is shifted by 2 ± 0.5 ev towards higher energies; its overall displacement in the 20—300° temperature interval amounts to 4 ± 0.5 ev.

6. With increasing temperature the upper part of the 4sp band shifts continuously but slowly towards higher temperatures; the overall displacement from 20 to 300° amounts to only 8 ± 0.8 ev. The displacement in the pretransformation interval (20–180°) is equal to the displacement in the 180–300° range: 4 ± 0.8 ev.

7. The full width of the K absorption edge of nickel (3d + 4sp) changes entirely at the expense of the 4sp absorption band (its upper branch).

Thus, the experimental data may be summarized as follows:

Between 20 and 180° the 3d absorption band is not subject to influence of temperature. The 4sp band, on the contrary, is affected by the temperature: with increasing temperature it is shifted into the region of higher energies and its width increases gradually.

In passing through the Curie point the center of the 3d absorption band is noticeably shifted towards higher energies (the band width remains unchanged); while, at the same time, the 4sp band continues to shift just as without magnetic transformation (i.e., by 2 ± 0.5 ev).

We can conclude therefrom that the 3d band is subject to the influence of magnetic transformations but not to temperature, whereas the 4sp band is subject to the influence of temperature but not of magnetic transformations.

K Absorption Edge of Nickel

1. As the temperature rises from 20 to 180° the K absorption edge for Mn as a whole is displaced to the side of high energies: the center of the 3d band is shifted by 4.6 ± 0.5 ev and the center of the 4sp band by 3.8 ± 0.5 ev.

2. With further temperature increase to 300° (transition through the Curie point) with Mn absorption edge as a whole shifts in the opposite direction: towards lower energies. The shift of the 3d band amounts to 2.3 ev; that of the 4sp band to 1.5 ev.

3. The total width of the 3d band behaves in an analogous manner: at 20° its width is 7.9 - 0.6 ev, by 180° it increases to 10.6 ev. With further temperature rise (through the Curie point) the width of this band begins to decrease (by about 8.2 ev) and becomes equal to the width at 20°, within the limits of the experimental error.

4. The behavior of the full width of the 4sp band is the inverse of that of the 3d absorption band: at first the width decreases (15.6 — 13.7 ev) with rising temperature and then, in passing through the Curie point increases to about 14.6 ev.

5. It is interesting to note that the variation in the width of the 3d absorption band is appreciably greater than the variation of the 4sp band.

Kβ_5 Atomic Bands of Manganese and Nickel

Our earlier experiments[1,2] showed that the effects of magnetic transformation despite certain experimental difficulties can definitely be detected by means of instruments having a dispersion of 7–8 XE/mm.

In view of this it was necessary to enhance the resolution of the instrument in photographing the $K\beta_5$ emission lines of nickel. The manganese spectra were photographed as before on an instrument having a dispersion of 7.42 XE/mm. The $K\beta_5$ bands of nickel, however, were photographed in the new experiments on a high transmission factor spectrograph with a bent quartz crystal (R = 1020 mm; Cauchois method), using a vacuum tube.

We utilized the second order of reflection. This somewhat increased the exposure time but made it possible to attain a dispersion of 3.92 XE/mm, i.e., to enhance the effective resolution more than two-fold. The linear dispersion on the microphotograms was thereby brought to 0.486 XE/mm (instead of the former 1.1 XE/mm).

The $K\beta_5$ band spectra of nickel were also obtained in the first order (dispersion 7.8 XE/mm). Excellent agreement was observed between the spectra in the first and second orders.

We investigated the behavior of the shape, width, intensity and wavelength of the $K\beta_5$ bands of Mn and Ni incident to magnetic transformation of the alloy both under the influence of changes in composition and in passing through the Curie point. The following results were obtained.

1. In the case of changes in composition the transition to the paramagnetic state is accompanied by an increase of 2.2 ev in the energy of the $K\beta_5$ photon of nickel and a 1.17 ev decrease in the energy of the $K\beta_5$ photon of manganese (measurement error ± 0.3 ev).

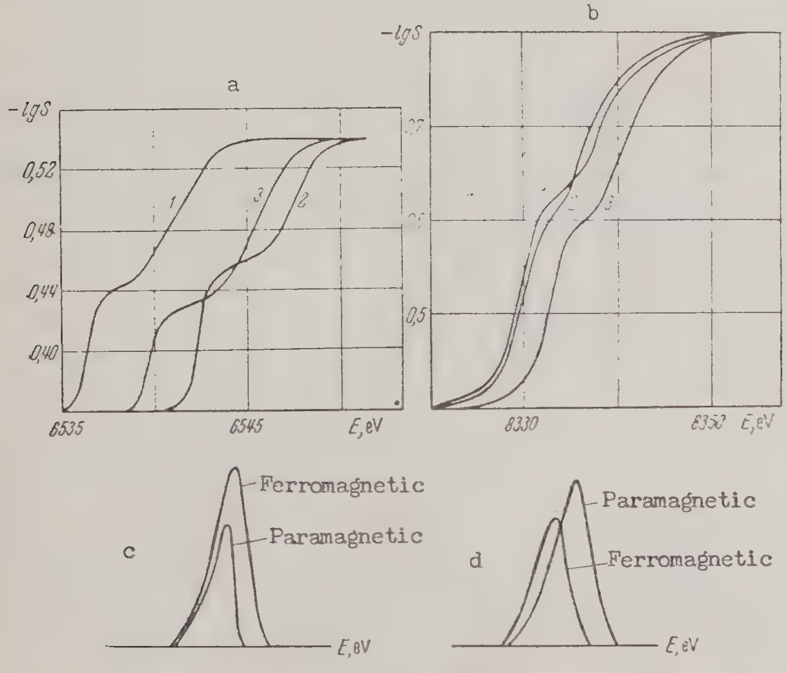

Fig. 1. a – Displacement of the K absorption edge of manganese under the influence of temperature. b – Displacement of the K edge of nickel under the influence of temperature. In both cases 1, 2 and 3 are the absorption edges obtained at 20, 180 and 300° respectively. Magnetic transformation of the alloy occurs in the 180–300° interval. c and d – Behavior of the shape of the $K\beta_5$ bands of Mn and Ni, respectively, incident to magnetic transformation under the influence of temperature.

2. In the case of magnetic transformation due to transition through the Curie point the energy of the $K\beta_5$ nickel photon increases by 2.8 ev while that of the manganese photon decreases by 1.52 ev.

3. The width of the $K\beta_5$ band of nickel increases slightly (14.0 → 15.0 ev), While that of manganese decreases appreciably (13.6 → 11.2 ev).

4. The asymmetry index of the $K\beta_5$ nickel band remains almost unaltered (1.1 → 1.2); the increase for manganese is somewhat greater (1.2 → 1.7).

5. The peak intensity I_m of nickel increases from 1.0 to 1.63, while for manganese it decreases from 1.51 to 0.73.

6. Transition of the alloy to the

paramagnetic state is accompanied by an increase in the integral intensity of the Kβ_5 band of nickel (1.0 → 1.26) and a decrease in that of manganese (1.0 → 0.78).

7. The shape of the Kβ_5 bands of both components undergoes an appreciable change.

Figure 1 illustrates the behavior of the K absorption edges and of the shape, width and position of the Kβ_5 emission bands of Mn and Ni incident to magnetic transformations of the alloy. From an examination of the figure it will be obvious that transition of the alloy to the paramagnetic state is accompanied by a displacement of the K absorption edge and the Kβ_5 band of nickel towards the short-wave side of the spectrum.

It will be noted, too, that in the 20-180° interval (where there is no magnetic transformation) the absorption edge of nickel remains stationary, while the K edge of manganese is shifted towards higher energies. In the presence of magnetic transformation (180 — 300°) the absorption edge of nickel is displaced towards higher energies while the K edge of manganese returns to the interval of lower energies. The behavior of the Kβ_5 manganese band in this case conforms to the behavior of the absorption edge: it also shifts into the region of lower energies.

The changes in the shape and width of the Kβ_5 bands of Mn and Ni, as well as the variations in their intensity, are clearly discernible in the figure.

Interpretation of the K 5 Emission Bands and K Absorption Edges

The following facts stand out in the experimental results. There is a profound analogy between the behavior of the Kβ_5 emission bands and the 3d absorption bands of the Mn and Ni atoms under the influence of magnetic transformations: the center of the short-wave branch of the Kβ_5 band is displaced to the same side as the 3d absorption band and both displacements are of the same order of magnitude (within the limits of the experimental error).

There is a like similarity in the behavior of the widths of the Kβ_5 emission and 3d absorption bands of the Mn and Ni atoms. The changes of the different characteristics of the Kβ_5 bands and K absorption edges of the two elements (quality, I_{max}, shape of the Kβ_5 bands and position of the K edges) proceed in opposite directions and, as a rule, are equal in order of magnitude.

The cited data are evidence of a definite correlation between the behavior of the spectra of Mn and Ni, a correlation indicating that a transition to the paramagnetic state, regardless of whether it occurs under the influence of temperature or that of change in composition involves both atomic systems forming the crystal lattice of the alloy.

This opens the way to a physical interpretation of the magnetic transformation effect; that is, in view of the above we can reasonably assume that in all probability the magnetic transformation is a result of a redistribution of the occupied and unoccupied 3d- and 4sp-states of the atoms in the crystal lattice.

To arrive at a clear concept of the mechanism of magnetic transformation we must carefully analyze the behavior of the investigated spectra. We must also bear in mind a commonly known experimental fact: increases in temperature are accompanied by expansion of the crystal lattice and this, of course, directly affects the separation of the atoms and, consequently, the interaction between them. Increase in the number of Mn atoms in the Ni lattice (without increasing the temperature) is also accompanied by expansion of the lattice. There is, however, no reason to assume that prior to attainment of the paramagnetic state the lattices expand equally in both cases. It would be more correct to assume that increase in the number of Mn atoms in the Ni lattice, as the alloy approaches the paramagnetic state, leads to the same interaction of the atomic systems as develops under the influence of temperature.

Evidence in favor of the latter assumption is the fact that the characteristics of the paramagnetic state spectra regardless of whether the state is reached as a result of increased temperature of change in composition are wholly identical.

Modern quantum theory is not sufficiently developed to permit of a full quantitative treatment of the behavior of the spectra of atoms in the molecules of chemical compounds and metallic alloys. Only in individual cases is it now possible to give a correct qualitative interpretation of the behavior of certain spectra.[3,4] For the Mn-Ni alloy system, however, we now have an adequate amount of data obtained through investigations of the system by magnetic, electric and other methods. In particular, studies of the x-ray spectra of both Ni and Mn atoms, should greatly facilitate the matter of physical interpretation of the magnetic transformations of the alloys of this system.

If we use the hypothesis regarding the behavior of the energy levels of valence electrons in a metal lattice, proposed earlier by the writer, the behavior not only of the K absorption edges of Mn and Ni but of their $K\beta_5$ bands as well becomes comprehensible. Without recourse to this hypothesis it appears impossible to explain the behavior of the width and intensity of the spectra, or even of the wavelengths of the characteristic points of these spectra, under the influence of temperature.

The underlying concepts of the hypothesis are the following: it is assumed that the atomic energy levels in the metal lattice are somewhat compressed* (brought nearer each other) by virtue of the mutual repulsion of the 3d and 4sp electrons of neighboring atoms. In heating there is some separation of the atoms, in consequence of which the electronic repulsion decreases and the energy levels "retreat" from the nucleus. Simultaneously the overlapping and width of the levels are reduced.

In line with this hypothesis the observed behavior of the K absorption edges and $K\beta_5$ bands can be interpreted as follows:

Under the influence of rising temperature the crystal lattice of the alloy expands and the distance between atoms increases. This effect should be accompanied by a decrease in the wavelength or an increase in the energy of the K absorption edge and $K\beta_5$ band with increasing temperature. As we noted the K edge of Mn in the ferromagnetic region is actually displaced to the side of higher energies. The investigated alloys contain a relatively small amount of Mn so that the basic Ni lattice structure is retained. The alloy is a solid substitutional solution, consequently each Mn atom is more or less surrounded by Ni atoms; due to the influence of these, the 3d and 4sp electron states of Mn are disturbed to a much greater degree than the 3d and 4sp states of Ni. This should obviously lead to an increase in the width of the 3d absorption band and hence of the $K\beta_5$ band of Mn. This is substantiated by experiment. At the same time this serves as an indication that the disturbing effect predominates over the effect of narrowing of the levels during expansion of the lattice. The Ni atoms are much less subject to disturbance and, consequently, their spectra must remain virtually unaltered. This, too, is confirmed by experiment: with increasing temperature the K absorption edge of Ni does remain stationary in the energy scale and its width, too, remains constant.

---

*This as we know is not in conflict with experimental data: the $K\beta_5$ photon energy in metal vapors is known to be greater than in a solid state.

With further increase in the temperature the changes in the $K\beta_5$ band and K absorption edge of Mn should continue, i.e., they should continue to shift to the side of higher energies, while their increase in width should slow down or stop owing to the decrease in overlapping and narrowing of the bands. There should also be a change in the Ni spectrum. In fact the changes in the spectra of both components (Mn and Ni) should be in the same direction.

However, in the temperature interval where magnetic transformation takes place the K absorption edges and $K\beta_5$ bands do not behave in this manner: actually the K edges as well as the $K\beta_5$ bands of Ni and Mn are observed to shift in opposite directions. The widths and intensities of the edges and bands also behave in a contrary manner. In view of this it must be assumed that at temperatures corresponding to magnetic transformation there occur processes that differ radically from those normally produced by temperature changes.

In order to explain the observed behavior of the spectra incident to magnetic transformation of alloys we must make the assumption that prior to attainment of the Curie temperature the effect of "retreat" from the nucleus and disturbance of the 3d and 4sp electron states may become so appreciable and the coupling of the corresponding electrons with their nuclei in Mn so weak that one or more electrons (on the average per a certain number of atoms) go over into the overlapping 3d and 4sp states of the Ni atoms. At the same time there occurs a compensation of the atomic magnetic moments and the alloy goes over into the paramagnetic state.

Incident to this the K edge and $K\beta_5$ band of Mn should shift sharply into the region of lower energies and, on the contrary, the K edge and $K\beta_5$ band of Ni should be displaced towards higher energies. The width of the $K\beta_5$ band and the absorption edge as well as the intensity of the $K\beta_5$ band of Mn should decrease. Those of Ni in contrast should increase. This is precisely the behavior of the $K\beta_5$ bands and K edges observed experimentally.

The above appears to us to be the most plausible explanation of the behavior of the atomic spectra of Mn and Ni in their binary alloys and the probable mechanism of magnetic transformation in alloys of this system.

Kuibyshev Industrial Institute

REFERENCES

1. V. A. Kazantsev, Trudy KII (Transactions of the Kubiekev Industrial Institute, 6, 87 (1955).
2. V. A. Kazantsev, Thesis, Rostov State University,1952.
3. I. V. Sorokin, Thesis, Moscow State University, 1946.
4. M. A. Blokhin, Zhur. eksp. i teor. fiz., 9, 1515 (1939).

ON THE ABSORPTION AND EMISSION OF X-RAYS BY FERROMAGNETIC METALS

- A.V.Sokolov

1. On the one hand a knowledge of the density of valence electron levels is of great value in investigating the soft x-ray absorption and emission spectra of metals. On the other hand, by studying the fine structure of the absorption edges one can get detailed information about the higher electronic energy levels of a metal.

Until now theoretical treatments of these questions have been made on the basis of the one-electron zone theory of metals, which disregards interactions between the electrons. However, for ferromagnetic metals, whose electrons form a single quantized system with strong interaction, treatment of these questions in the framework of the one-electron model is particularly inappropriate since the very occurrence of ferromagnetism is a result of electronic interaction.

It would appear desirable to develop a theory or model which a) would be a multi-electron theory and b) would combine the features of the theory taking account of the complete symmetry of the crystal lattice (space symmetry groups) and of the theory which takes the influence of near neighbors into account. We do not yet have such a combined theory.

In a preliminary attempt to take account of electronic interactions in calculating the density of states and describing the absorption and emission of x-rays, we have used the model of exchange interaction between the outer s-electrons and the inner d-electrons in transition metals, proposed by Vonsovski.[1] Turov and Vonsovski[2] have given strong arguments for this model on the basis of Bogoliubov's multi-electron theory[3]. This model has made it possible to offer a qualitative interpretation of the "anomalous" electrical, optical, galvanomagnetic and thermomagnetic properties of ferromagnetic metals.

According to this model the electrons in a ferromagnetic metal are provisionally divided into groups: 1) "inner electrons" (d-electrons, corresponding to electrons of the unfilled d-shell in isolated atoms of transition elements in the iron group) which are primarily responsible for ferromagnetism, and 2) "outer" electrons (3-electrons, corresponding to the valence 4s-electrons of the same atoms) which are responsible for conduction. The separation of the electrons into these two groups is admittedly an artificial convention, inasmuch as these electrons, forming a single quantum mechanical system, actually interact strongly with each other. Although we refer here to the sub-systems of d- and s-electrons, we are really talking about the two branches of the energy spectrum of the single electronic system of a ferromagnetic metal, i.e., the Bose spectrum of elementary excitations - "ferromagnons" - associated with the inner electrons and mainly responsible for the ferromagnetic effects, and the Fermi spectrum of elementary excitations or conduction electrons which are, in principle, responsible for the various conduction effects. We call these quasi-particles on the second branch conduction electrons or s-electrons in order to emphasize their genetic connection with the conduction electrons of the one-electron theory, although one must bear in mind their essential difference from the latter. These quasi-particles are essentially elementary excitations whose existence follows from a quite general formulation of the problem of the motions of the electron system, i.e., from the general Hamiltonian, taking interaction between electrons into account. Moreover, the existence of these particles follows from the field theory of collective interactions.[11]

On the other hand, although, due to the electronic interactions and the field properties of matter, these quasi-particles have energies, masses, etc. differing from those of the metal electrons of one-electron theory, they obey Fermi statistics and, like "ordinary" electrons, are the principal current carriers. According to this model, we consider the system of elementary excitations of the second branch in a ferromagnetic to be a mixture of two "gases" of elementary excitations which correspond to the two possible spin orientations. The energy of an s-electron in the effective mass approximation is

$$E = \alpha - \alpha' \overrightarrow{y\sigma} + (\beta + \beta' \overrightarrow{y\sigma})\, k^2, \tag{1}$$

where α, α', β and β' are parameters, dependent on the exchange integrals of the s- and d-electrons and the transfer integrals of the s-electrons, y is the mean relative atomic magnetic moment of a d-electron, $\vec{\sigma}$ is the s-electron spin vector, and k is the electron quasi-momentum.

2. According to the zone theory of metals,[12] the expression for density of states is

$$n(E) = \pm \frac{m^2}{8\pi^3\hbar^4 |g|} \int\limits_{-E_g}^{E-V_{000}-E_g} \frac{\Gamma d\Gamma}{\sqrt{\Gamma^2 - |V_g|^2}}, \tag{2}$$

where E is the energy of an electron in the metal, $E_g = \frac{\hbar^2}{2m}\pi^2 g^2$ is the kinetic energy of an electron moving perpendicularly to the reflecting plane and undergoing a Bragg reflection, V_g is the Fourier coefficient in the expansion describing lattice potential, and the variable of integration is

$$\Gamma = E - V_{000} - E_g - \frac{\hbar^2}{2m}(\varkappa_2^2 + \varkappa_3^2), \tag{3}$$

where $\varkappa_2$ and $\varkappa_3$ are the components of the electron quasi-momentum, resolved parallel to the zone boundary, while the component $\varkappa'_1 = -\pi|g| + \varkappa_1$ is directed parallel to the vector g of the reverse lattice. The plus sign is to be taken for states of the upper band and the minus sign for the lower band.

3. In the case of ferromagnetic metals equation (1) is replaced by

$$n_\pm(E, y) = \pm \frac{m_\pm^2}{8\pi^3\hbar^4 |g|} \int \frac{\Gamma_\pm d\Gamma_\pm}{\sqrt{\Gamma_\pm^2 - |V_g|^2}}. \tag{4}$$

We note that the limits of integration in equation (4) differ from the limits in equation (3). Here n_+ and n_- are the densities of states corresponding, respectively, to right and left spin orientations. It follows that the next expression is valid:

$$n(E, y) = n_+(E, y) + n_-(E, y). \tag{5}$$

If we consider only the temperature region near the Curie point $(y \ll 1)$, we may expand $\Gamma_\pm$ in terms of y and retain only terms up to second order. We finally obtain the following relationship for the total density of "conduction electron" states in ferromagnetic metals

$$n(E, y) = n_+(E, y) + n_-(E, y) \approx \frac{m_1^2}{4\pi^2\hbar^4 |g|}(1 + A^2y^2) \int \frac{\Gamma d\Gamma}{\sqrt{\Gamma^2 - V_g^2}}, \tag{6}$$

where $A = \beta'/\beta$ is a quantity of order unity or less. The limits of integration in (6) are the same as in (3).

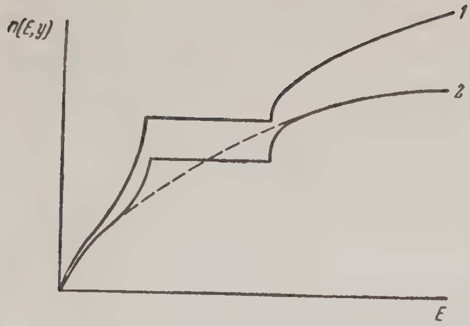

Fig. 1

The forms of the functions $n(E,y)$ (curve 1) and $n(E,0)$ (curve 2) are shown in Fig. 1 [$n(E,0)$ is $n(E,y)$ with $y=0$]. We note that the deviation of the curves given here from the curve for free electrons (dash-line) is determined only by the two planes g and $-g$, whereas we should actually consider at least six planes. Accordingly, these deviations must be multiplied by the number of pairs of equivalent surfaces bounding the lower band.

It is clear from equation (6) and Fig. 1 that the curve $n(E, y)$ lies above the curve $n(E,0)$. Hence it follows that if we take several equivalent planes into account the jump in the density $n(E, y)$ of the conduction electron states of a ferromagnetic near the Curie point will be sharper than in the absence of magnetization. At $y=0$ the expression for the density of states of the conduction electrons in a ferromagnetic coincides exactly with that for ordinary metals.

4. The expression for the density of states can readily be brought to the form

$$n(E, y) = n(E, 0)(1 + A^2y^2). \qquad (7)$$

The most important feature of this expression is that the density of conduction electron states is a quadratic function of the spontaneous magnetization. The spontaneous magnetization in turn is a function of the temperature, so that the density of electronic states, (being dependent on y) must show an anomalous variation with temperature. As the equations show, with increasing magnetization of the ferroelectric, the density of conduction-electron states increases. We may conclude, therefore, that the band of s-electron levels becomes narrower. This is in agreement with the fact that, in the first approximation, the spins of the system of d-electrons in a ferromagnetic are strongly coupled, while the orbital moments cancel each other so that there obtains an effect analogous to the Paschen-Back effect. Namely the strong internal "magnetic field" due to the exchange interaction of s- and d-electrons acts to simplify rather than to complicate the picture of the s-electron levels, i.e., to produce a narrowing of the band.

Starting with equation (7) it is easy to obtain an expression for the ferromagnetic "anomaly" of the density of electronic states in ferromagnetics

$$\frac{n(E, y) - n(E, 0)}{n(E, 0)} = A^2y^2. \qquad (8)$$

This quantity is proportional to the square of the spontaneous magnetization. It would be very desirable to carry out an experimental verification of the theoretical deductions following from this equation.

In the above we have shown, using the exchange model of the inner and outer electrons in a ferromagnetic, that the density of states must depend on the spontaneous magnetization. Near the ferromagnetic Curie point this dependence is a straightforward quadratic one. We have also obtained the ferromagnetic "anomaly" of the density of electronic states in ferromagnetic metals.[13]

5. A theoretical investigation of the absorption and emission of x-rays by ferromagnetic metals has been carried out in the framework of this model.[14] It follows from the theory that the emission and absorption of x-rays must

depend on the value of the spontaneous magnetization of the ferromagnetic metal. Near the Curie point this dependence is quadratic. Calculations also show that the intensity curve $F(E, y)$ for K-radiation in a ferromagnetic must be shifted somewhat above the curve in the absence of magnetization (see Fig. 2, wherein the intensity curve for free electrons is indicated by the dash-line). The nature of the x-ray spectrum must undergo a marked change incident to passage through the ferromagnetic transition point. Since changes in the magnetic structure of the crystal are involved in the ferromagnetic transformation, we have here a concrete illustration of the influence of structural (energetic) inhomogeneities on the structure of the x-ray spectrum. This opens the way to establishing a qualitative correlation between the shape of the x-ray spectrum and the structural state of the crystal.

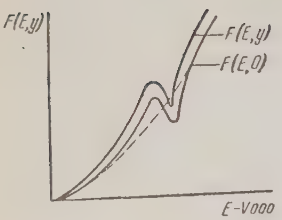

Fig. 2

It may be asked: in what direction should one develop theoretical investigations of the x-ray spectra of metals? It seems to us that it is now time to construct a more complete and comprehensive theory of metallic x-ray spectra. For example, instead of having two theories of the fine structure of x-ray absorption spectra in metals, namely Kronig's theory which is based on the Bloch one-electron model of a metal which takes account of the periodicity of the crystal lattice and of general quantum mechanical principles, and Kostarev's theory in which the absorption of x-rays is treated as an atomic process on which only atoms in the immediate neighborhood have a significant influence, one would like to have a single theory which would take into account both the complete symmetry of the lattice and of the influence of the near neighbors. We remark in passing that the one-electron zone theory not only neglects electronic interactions but also fails to take account of the angular dependence of the potential in an actual crystal lattice.

Thus, the first problem is that of constructing a more consistent one-electron theory of x-ray spectra, taking account of both the immediate neighborhood and the angular dependence of the potential in a crystal lattice.

Study of the x-ray spectra of metals and alloys, particularly the fine structure, along with investigation of other physical and chemical properties of metals, may ultimately lead to a more correct theory of the metallic state.

In recent years attention has been given both at home and abroad to the development of theories which describe the electrons and the lattice of the metal in a single scheme, and take account of the interactions between the electrons, i.e., theories that consider the metal as a whole. These are the theories of quasi-particles and collective interactions. In so far as the latter is a field theory the symmetry of the crystal should not, in it, be considered phenomenologically, as in the usual quantum theory of metals, but should follow automatically from the symmetry properties of the appropriate fields.

Therefore, the next problem is the construction of a multiple electrc theory of x-ray spectra which will take into account both the symmetry of the crystal lattice and the influence of nearest neighbors.

Finally we must strive to create a more consistent theory of x-ray spectra based on the field theory of collective interactions in which the symmetry of the crystal lattice must follow automatically from the symmetry of the fields.

In conclusion, we want to emphasize that we do not claim the above calculations to be a quantitative description of the emission and absorption of x-rays by ferromagnetic metals, inasmuch as they are based on a simplified model of a ferromagnetic. Nevertheless there is no reason to doubt the validity of our qualitative conclusions regarding the dependence of the absorption and emission of x-rays by ferromagnetic metals on the spontaneous magnetization.

Institute of the Physics of Metals of the
Ural Branch of the U.S.S.R. Academy of Sciences

REFERENCES

1. S. V. Vonsovski, Zhur. eksp. i teor. fiz., 16, 981 (1946).
2. S. V. Vonsovski & E. A. Turov, (?), 24, 419 (1953).
3. N. N. Bogoliubov, Lektsii z kvantofoi statistiki (Lecture on quantum statistics, Kiev, 1949.
4. S. V. Vonsovski, Zhur. eksp. i teor. fiz., 18, 219 (1948).
5. S. V. Vonsovski, Izv. AN SSSR, ser. fiz., 11, 463 (1947).
6. S. V. Vonsovski & A. V. Sokolov, Zhur. eksp. i teor. fiz., 19, 615, 703 (1949).
7. S. V. Vonsovski & A. V. Sokolov, Doklady AN SSSR, 76, 197 (1951).
8. A. V. Sokolov & A. Z. Veksler, Doklady AN SSSR, 81, 27, (1951).
9. A. V. Sokolov & A. Z. Veksler, Zhur. eksp. i teor. fiz., 25, 215 (1953).
10. S. V. Vonsovski & K. P. Rodionov, Doklady AN SSSR, 75, 643 (1950).
11. D. Bohm & D. Pines, Phys. Rev., 82, 625 (1951); D. Pines, D. Bohm, Phys. Rev., 85, 338 (1952).
12. A. Wilson, Quantum theory of metals. In Russian trans. M - 1941
13. A. V. Sokolov & S. M. Tsupis, Zhur. eksp. i teor. fiz., 28, 321 (1955).
14. A. V. Sokolov, Zhur. eksp. i teor. fiz., 28, 326 (1955).

* * * * * * *

ON THE STRUCTURE OF X-RAY EMISSION LINES OF IONS IN SOLUTION

- K.I.Narbutt

In a recent investigation[1] of the x-ray absorption spectra of ions in solution we were able to bring out the influence of a number of factors on the fine structure of the principal x-ray absorption edge in the ionic spectrum. In particular we established the following.

1. The nature of the solvent exerts an appreciable influence on the x-ray absorption spectrum of the solution. Varying the solvent leads a) to an appreciable change in the width of the principal absorption peak, b) to a shift of up to 18 ev in the position of the broad diffuse maximum, c) to a shift in the location of the principal absorption peak and d) to a change in the distance between the principal and the following peak.

2. There is a correlation between the width of the principal absorption peak and the magnitude of the dipole moment of the solvent molecules. The effect of broadening of the principal peak with increasing dipole moment can in a general way be interpreted on the basis of a Stark effect for the zinc ions in the molecular field of the solvent.

3. In the case of a number of complex zinc ions there is a clear relation between the type of ion involved and the x-ray spectrum of the zinc atom.

It was obviously of interest to determine how these different effects and factors are reflected in the x-ray emission spectrum. The present investigation was undertaken to this end.

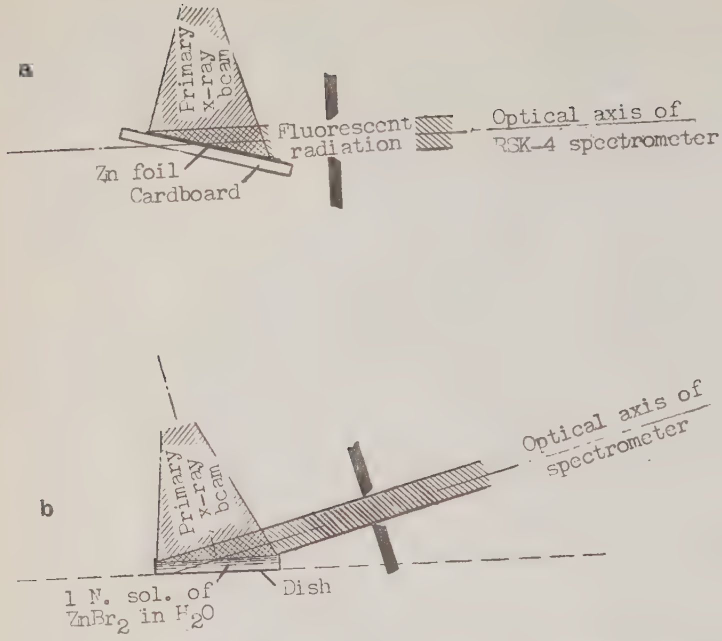
a
Primary x-ray beam
Fluorescent radiation
Optical axis of RSK-4 spectrometer
Zn foil
Cardboard
b
Primary x-ray beam
Optical axis of spectrometer
1 N. sol. of $ZnBr_2$ in H_2O
Dish

Fig. 1. Excitation of fluorescence spectra of solutions

The x-ray emission spectra of solutions were obtained by the method of secondary excitation. The basic apparatus consisted of the fluorescence x-ray spectrometer, developed earlier by the writer[2], and a high intensity sealed-off x-ray tube[3] capable of being operated at 200 ma and 50 kv. It may be noted that only the use of so powerful an x-ray tube made it possible to obtain the emission spectra of solutions. The x-ray tube, housed in a shielding jacket, was mounted horizontally on the spectrometer so that the primary beam was directed downward. The investigated specimen - the secondary emitter (Fig. 1, a) - was located in the primary beam at an angle to the optical axis of the spectrometer. This arrangement is very convenient in a case of solid specimens. In the case of solutions, however, certain difficulties are encountered so that to obtain the spectra of solutions we employed the following expedient: the entire spectrometer was tilted so that the flat dish with 2 mm high edges (filled with the specimen solution) would be horizontal in space and oriented at an angle relative to the analyzer of the spectrometer. Thus, the fluorescent emission of the solution was obtained directly from the open surface of the liquid (Fig. 1, b). The spectra were recorded both by the ionization method (Geiger counter) and photographically. The latter method had to be used in recording the spectra of most solutions in view of the fact that evaporation from the open surface resulted in some variation in the intensity of emission. It proved necessary to add solution periodically to the open container. The resultant changes in intensity hampered ionization recording but did not interfere with photographic

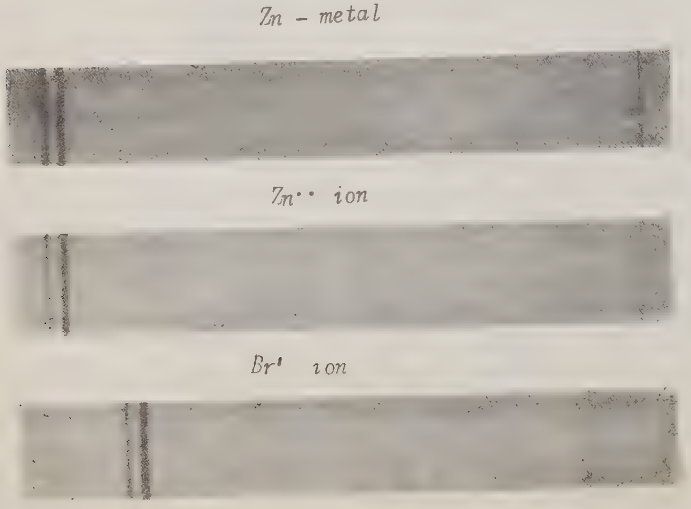

Fig. 2. Reproduction of the fluorescence K spectra of metallic zinc and Zn ions. The $K\alpha_{1,2}$ and $K\beta_1$ lines are shown.

recording. In view of this the spectra of solids were recorded by the ionization method, the spectra of liquid solutions by the photographic method. The exposure time for solutions ran to 4-6 hours. The photographs were made in the second order of reflection from the (10$\bar{1}$0) plane of a quartz crystal; the dispersion was 5 XE/mm.

Figure 2 shows the emission spectra of the aqueous solution of $ZnBr_2$ and of metallic zinc obtained by the fluorescence method. The line locations in both cases were determined with reference to the $L\alpha_{1,2}$ doublet of Au which were imposed on the spectrograms for this purpose. There was no noticeable displacement of the lines of the solution relative to the lines of the metal. There is, however, a very clear difference where the shape and width of the lines are concerned (the broadening of the solution line compared to the metal line is clearly apparent even in the reproduction.

The microphotograms of the spectra are given in Fig. 3. It will be seen that the solutions lines are appreciably broadened and asymmetric. This holds for the bromine ion lines as well. At the same time the lines of metallic zinc, as has been noted before, are entirely symmetric and much narrower than the solution lines.

Next we undertook a systematic investigation of the width and shape of the $K\alpha_{1,2}$ lines of Zn ions as a function of the nature of the solvent. The same substance (zinc chloride) was dissolved in water, acetone, methyl alcohol, glycerin and formic acid. The resultant spectrograms were measured on a photometer, the width of the $K\alpha_1$ line at the height of the $K\alpha_2$ peak was evaluated and the asymmetry index determined. The results are listed in Table 1.

For purposes of com-

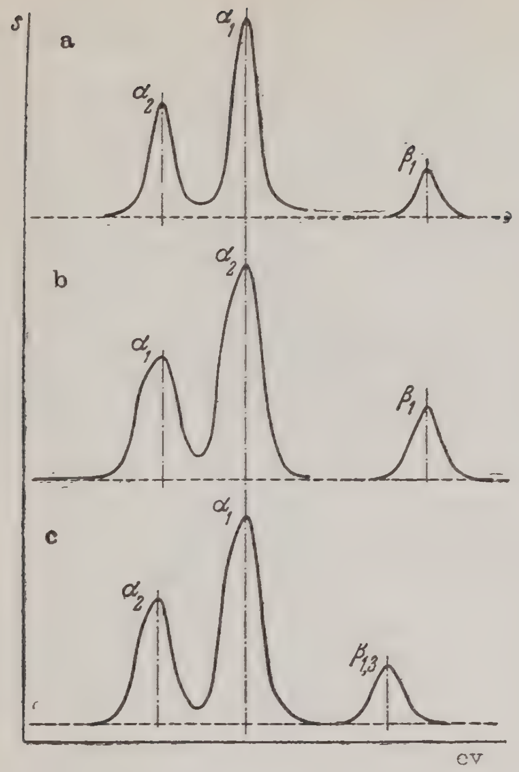

Fig. 3. Microphotograms of the K spectra of metallic zinc and Zn ions: a) emission K spectrum of the metal; b) emission K spectrum of Zn'' ions; c) emission K spectrum of Br' ions (1 N solution of $ZnBr_2$ in H_2O).

Table 1

Solvent for $ZnCl_2$	Width of $K\alpha_1$ line, ev	Asymmetry index of $K\alpha_1$ line
Water	6,3	1,28
Acetone	5,4	1,15
Methyl alcohol	5,4	1,41
Glycerin	5,6	1,18
Formic acid	6,3	1,00

Table 2

Compound	Width of $K\alpha_1$ line, ev	Asymmetry index of $K\alpha_1$ line
Zn-metal	3,6	1,00
ZnO	3,4	0,97
ZnS	3,7	0,94
$Zn(CH_3COO)_2$	3,4	1,08
$ZnCl_2$	3,4	1,04
$ZnBr_2$— anhydrous	3,6	1,05
$ZnBr_2$— hydrate	3,6	0,90
$ZnSO_4 \cdot nH_2O$	3,6	0,93

parison we obtained the emission K spectra of a number of solid compounds of zinc. The resultant data are listed in Table 2.

We can draw a number of conclusions from the data in Tables 1 & 2:

1. The width of the $K\alpha_1$ line of ions in solution is 1.5-1.8 times greater than the width of the line for solid compounds.

2. The $K\alpha_1$ line of ions in solution is highly assymetric; the asymmetry index k depends on the nature of the solvent, but in any case $k \geqslant 1$.

3. The asymmetry index of the $K\alpha_1$ line of most solid compounds is close to unity, the exceptions being hydrated salts and zinc sulfide for which $k < 1$.

To explain the observed effects, here, as in the case of absorption spectra,[1] we must assume a Stark effect in the molecular field of the solvent. The observed dependence of the asymmetry index on the nature of the solvent indicates that this assumption is plausible. At the same time the broadening of the spectral lines is approximately equal in all solvents. This indicates that the line broadening is connected not so much with the nature of the solvent as with the ionization in general. Inasmuch as the $K\alpha_1$ and $K\alpha_2$ lines are associated with electron transitions from the L_{II}- and L_{III}—levels to the K-level, it must be admitted that the ionization process leads to splitting of these levels.

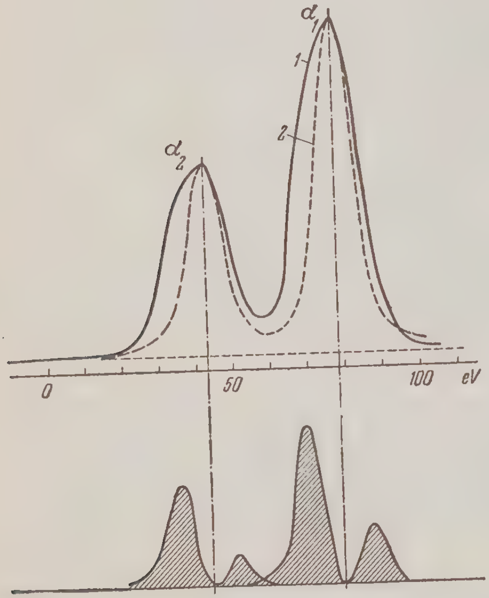

Fig. 4. Comparison of the shapes of the $K\alpha_1$ and $K\alpha_2$ lines of metallic zinc and Zn ions.

In Fig. 4 the contour of the $K\alpha_1$ and $K\alpha_2$ lines of metallic zinc (curve 2) is subtracted from the contour of the Zn ion (solution) lines (curve 1). The difference is represented by the shaded profiles in the lower part of the figure. The subtraction discloses the appearance of two additional components in the Zn ion doublet.

A different interpretation is possible, namely, one based on the presence of two states in the solution: $Zn^{\cdot\cdot}$ ions and undissociated molecules. If we assume further that two somewhat different positions of the $K\alpha_1$ line correspond to these different states, the observed data may be taken to represent the superposition of the two components. This would explain the observed line broadening. Furthermore, since the intensity of the two components will change, depending on the degree of dissociation, we can expect the asymmetry index of the total line to vary accordingly. Further investigation should show which of the interpretations is correct. In this connection it is important to investigate the dependence of the line shape on the concentration of the solution.

Institute of Geological Sciences of the
Academy of Sciences SSSR

REFERENCES

1. K. I. Narbutt, Zhur. eksp. i teor. fiz., 26, 208 (1954).
2. K. I. Narbutt, Izv. AN SSSR, ser. fiz., 17, 249 (1953).
3. K. I. Narbutt & E. M. Fridman, See present issue of the Bulletin.

AN X-RAY TUBE FOR SPECTRUM ANALYSIS

- V.A.Kazantsev

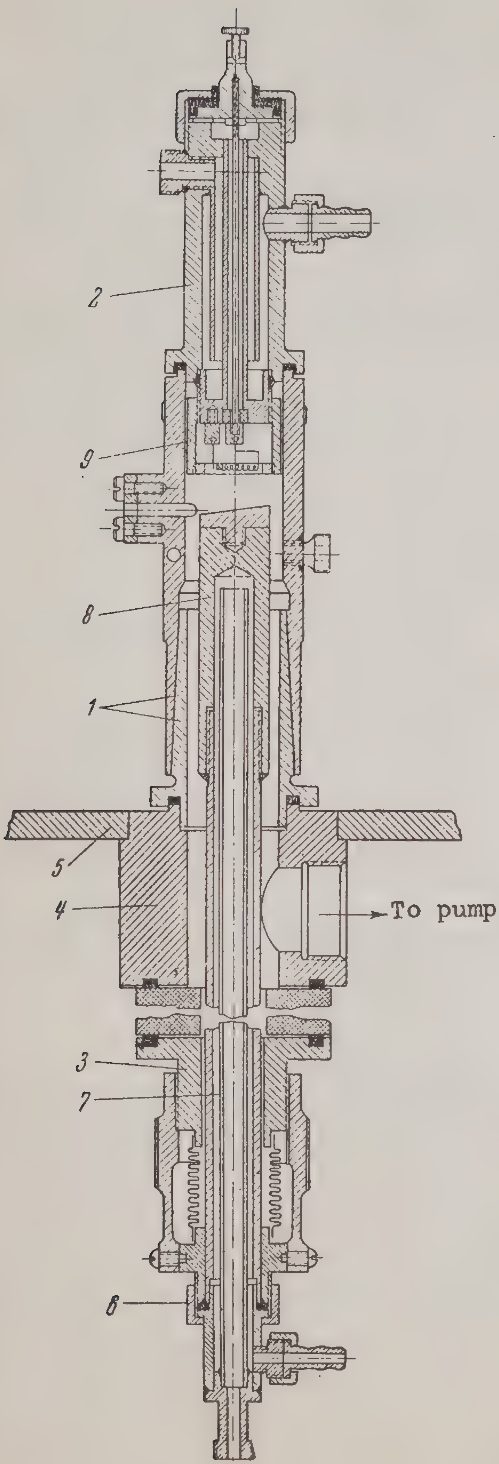

The accompanying drawing shows a longitudinal section through the proposed tube. The tube consists of four main units: the case 1, cathode 2, anode 3 and tee fitting 4, which connects the first three parts. The tube is designed for vertical installation: cathode up, anode down.

Shock safety of the tube is assured by location of the anode (which is the element operated at high potential) below the level of the base plate 5 and suitable shielding with iron sheets, covering all openings in the base.

The anode is adjusted at the time of assembly and until such time as it needs repair or replacement need not be demounted. The lower part of the anode, which is connected to the anode housing 3 by means of the collar nut 6, can be removed together with the cooling water tube 7. This makes it possible to clean out the interior of the anode tube 8 (washout mineral deposits with acid solution).

The case 1 incorporates a tapered sleeve as shown in the illustration. (It should be noted that the notion that the vacuum is impaired by sleeve lubricant is erroneous.) This makes the tube very convenient for rapid analysis since the cathode section can be easily lifted out to replace the specimen and oxidize the cathode. This operation does not effect the adjustment of the tube. The body of the tube is readily detached from the cathode 2 which facilitates thorough cleaning of the inside surfaces of the tube as frequently as necessary. The enumerated design features make for faster analysis and consequently reduce the operating costs per analysis.

Adjustment of the shape and size of the focal spot is made by means of the focusing cap 9. This cap is not made in the shape of a hollow cylinder as usual but rather in the form of a cup with a removable bottom. A suitable assortment of cup bottoms with different openings makes it possible to obtain focal spots of diverse shapes and sizes. There is no need to alter the shape of the cathode filament; it is linear in all cases.

The line focal spot can be brought out either perpendicularly or parallel to the crystal by simply turning the entire cathode 90°. In this way one can obtain narrow angular intervals of high intensity as well as wide intervals with normal intensity (crystal and line focus parallel) and a very uniform distribution of the continuous spectrum background over the entire angular range. This feature makes the tube suitable for absorption analysis.

With a wide focus the tube can be operated at 50-60 ma and 60 kv.

The safety of the tube as regards high voltage greatly reduces operator fatigue and hence enhances productivity. The safety features also make the tube suitable for use by students.

The simplicity of design and operating convenience of the tube recommended it for use by geological agencies employing spectrum analysis of ores and minerals.

The operation of a prototype tube in the laboratories of Rostov State University over a period of four years has demonstrated that the tube is convenient and dependable both for chemical analyses and for investigating the fine structure of spectra.

Tubes of this type have been produced in 1954 by the experimental equipment workshop of Rostov State University; it is now being installed in short wave x-ray spectrographs.

"V.M.Molotov"
Rostov State University

SELECTION OF OPTIMUM SPECIMEN DENSITY FOR THE INVESTIGATION OF X-RAY ABSORPTION SPECTRA

- M. A. Blokhin and A. N. Gusantinski

1. Introduction

In the present article we shall examine the question of the optimum superficial density of specimens for the investigation of x-ray absorption spectra, using ionization and photographic recording. Optimum superficial density is understood to mean the density assuring maximum contrast, i.e., greatest difference between the directly observed quantities to either side of the absorption edge. In the case of investigation of the fine structure maximum contrast is understood to mean the greatest fluctuation of the directly observed quantities.

In case of ionization recording (by means of ionization chambers, proportional amplifiers, counter tubes, etc.) as well as recording by means of a scintillation crystal and photomultiplier, the x-ray intensity in a wide interval is virtually directly proportional to the measured quantity: the ionization current, number of pulses, etc. In this case we need only insure the maximum relative difference in the intensities $(I_1 - I_2)/I_o$ of the spectrum in passing from one side to the other of the absorption edge or in the case of fine structure studies a maximum fluctuation of the relative intensity I/I_o in the investigated region.

In the case of photographic recording, the directly observed quantity is the deflection d of the instrument connected to the photometer, i.e., the "spot" of the galvanometer, the electrometer pen or the like. In this case the condition for maximum contrast is that for which we obtain the greatest relative deflection difference $(d_2 - d_1)/d_o$ where d_o is a deflection when the analyzing light beam is traversing an unexposed section of the spectrogram and d_1 and d_2 are the respective deflections at the long wave and short wave sides of the absorption edge. Or, in the case of fine structure investigations the contrast is determined by d/d_o.

We note here that in a number of earlier investigations[1] the problem of optimum density has been analyzed either incompletely or on the basis of erroneous premises.

2. Ionization recording

The optimum superficial density $m_{o.i}$ of the absorbing substance, insuring a maximum intensity difference across the absorption edge has been defined by Sandström[2] and is given by the following equation

$$m_{o.i} = 2{,}30 \frac{\log S}{\tau_{m,2}(1 - S^{-1})}, \tag{1}$$

here $S = \tau_{m,2}/\tau_{m,1}$ is the absorption jump and $\tau_{m,1}$ and $\tau_{m,2}$ are the mass-absorption coefficients on the long- and short-wave sides of the absorption edge.

For the optimum superficial density in the fine structure region Palacios[3] found

$$m_{o.i} = \frac{1}{\tau_m}, \tag{2}$$

where τ_m is the mean value of the mass-absorption coefficient for the given region.

Both Sandström and Kurylenko (from whose publication[3] the equation (2) is taken), as well as a number of other writers used equations (1) and (2) for photographic recording; this, as will be shown below, is incorrect. Equations (1) and (2) provide for obtaining the maximum contrast of the relative intensities or the quantities directly proportional thereto and are therefore applicable only to ionization recording.

In investigation of specimens of complex composition the mass-absorption coefficients must be determined according to the following formula:

$$\tau_m = \frac{1}{100} \sum_i C_i \tau_{m,i},$$

where C_i is the gravimetric concentration of the individual elements in percent and $\tau_{m,i}$ are the mass-absorption coefficients of the constituent elements.

The dependence of the relative intensity difference on the superficial density of a specimen of complex composition is illustrated in Fig. 1, where by way of illustration we give the computed values for $(I_1 - I_2)/I_o$ for the specific case of the K edge of Cu-Zn alloys of varying composition. The figures at the curves indicate the percent Zn by weight. The optimum superficial densities $M_{o.i}$ corresponding to the maxima of these curves are listed in Table 1, where we also list the values of superficial density of the zinc alloy

$$m_{o.i} = 0{,}01 C_{Zn} M_{o.i},$$

corresponding to the given values of $M_{o.i}$ and the values of the ratio

$$(I_1 - I_2)_{m_{o.i}} / (I_1 - I_2)_{8,32},$$

This ratio indicates the factor by which the contrast is reduced if the presence of the second component is neglected in the calculation.

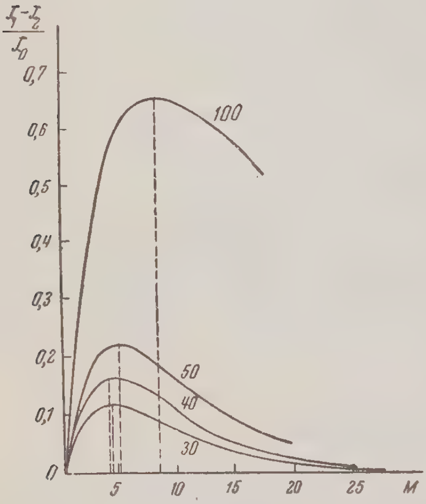

Fig. 1. Variation of $(I_1 - I_2)/I_o$ with M (in mg/cm^2) for the K edge of zinc in Cu-Zn alloys. Figures at curves indicate zinc content in per cent.

Table 1

C_{Zn}, %	$M_{o.i}$, mg/cm^2	$m_{o.i}$, mg/cm^2	$\frac{(I_1-I_2)m_{o.i}}{(I_1-I_2)_{8,32}}$
100	8,32	8,32	1,0
50	5,1	2,55	3,0
40	4,33	1,74	6,4
30	4,4	1,32	27

It will be seen from the last column of Table 1 that if the superficial density for a given element is selected on the basis of a calculation for the pure element the actual contrast obtained may be a fraction of the maximum possible value. It will also be seen that the optimum density $m_{o.i}$ of the element in a specimen of complex composition falls off rapidly with decreasing concentration of the element in the specimen. It follows that the optimum density for the pure element is no standard to go by in investigation substance of complex composition, contrary to widely held, but obviously erroneous views on the subject.

3. Photographic recording in the absence of an interfering background

The problem of selecting the optimum exposure time in photographing absorption spectra has been examined by one of the present authors.[4] We shall hereinafter assume that the optimum superficial density is sought on the basis of maximum contrast of the quantities measured on the microphotometer, presuming an optimal exposure for each superficial density.

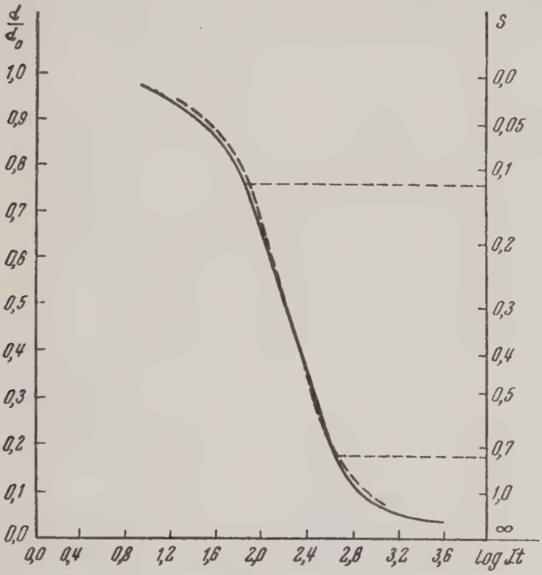

Fig. 2. Variation of d/d_o with log It according to experimental data for the $L\alpha_1$ line of Pb. Ordinate scale at right laid off in values of photographic density s.

In Ref. 4 a curve for d/d_o vs log It was plotted on the basis of theoretical data. In the present investigation the dependence was studied experimentally. The resultant curve (reproduced in Fig. 2) proved to be virtually linear in the wide range of plate densities: 0.14 to 0.74. Thus in this interval the contrast on the microphotogram, i.e., the relative difference in deflections of the recording unit of the microphotometer, is directly proportional to the logarithm It:

$$\frac{d_2-d_1}{d_0} \sim \log I_1 t - \log I_2 t = \log \frac{I_1}{I_2}.$$

Consequently, maximum contrast in this case requires a maximum ratio of intensities across the absorption edge; this ratio equals

$$\frac{I_1}{I_2} = \exp\left[(\tau_{m,2} - \tau_{m,1})\, m\right], \quad (3)$$

whence it follows that the contrast increases continuously and indefinitely with the superficial density and has no optimum value. Naturally the optimum exposure time increases with the superficial density. (The optimum exposure time, as shown in Ref. 4, is the time with which the absorption edge is located symmetrically to both sides of the line on the microphotogram, characterized by a photographic density s = log 2 ≈ 0.30.) Thus having selected the maximum allowable exposure time for the given analysis, we should select a superficial density at which the central line of the absorption edge on the microphotogram will have a photo-density s ≈ 0.30.

4. Photographic recording in the presence of an interfering background

An interfering background is here understood to mean any and all radiation that impinges on the photographic film during exposure and produces blackening but does not contribute to the absorption "jump" in the investigated region of the spectrum. This background may consist of scattered radiation, higher order spectra, etc. Part of this background radiation passes through the absorber (specimen) and is reduced as the thickness of the absorber is increased. The other part of this radiation may impinge on the film without traversing the absorber; the intensity of this part will obviously be independent of the absorber thickness. As is known the most contrasty absorption spectra are obtained in the first order, provided the potential on the x-ray tube is too low to excite the second order spectra. In this case the intensity of the background will be independent or weakly dependent on the superficial density of the absorber. For our calculation let us assume that the background intensity I_b is entirely independent of the absorber thickness. In this case the intensity ratio I_1/I_2 will be

$$\frac{I_1}{I_2} = \frac{I_b + I_0 \exp(-\tau_{m,1} m)}{I_b + I_0 \exp(-\tau_{m,2} m)} = \frac{a + \exp(-\tau_{m,1} m)}{a + \exp(-\tau_{m,2} m)}, \qquad (4)$$

where $a = I_b/I_o$ is constant. The condition for maximum contrast will be given by

$$\frac{d(I_1/I_2)}{dm} = 0,$$

from which we can readily derive the following equation for determining the optimum value of $m_{o.p}$:

$$\exp(\tau_{m,2} m_{o.p}) - S \exp(\tau_{m,1} m_{o.p}) = \frac{S-1}{a}, \qquad (5)$$

whereas before $S = \tau_{m,2}/\tau_{m,1}$. Knowing m for the given absorber and having computed $\tau_{m,1}$ and $\tau_{m,2}$ and measured I_1/I_2 from the test microphotogram we can readily evaluate a by means of (4). Equation (5) can be solved graphically to find the optimum superficial density $m_{o.p}$. When $a = 0$ we have $m_{o.p} = \infty$. When $a = \infty$, it will readily be seen that $m_{o.p}$ is defined by equation (1). Hence for intermediate values $0 < a < \infty$ we have

$$m_{o.p} > 2{,}30 \frac{\log S}{\tau_{m,2}(1 - S^{-1})}, \qquad (6)$$

i.e., in any case $m_{o.p}$ exceeds the value of the optimum density computed after Sandström, the excess being greater for weaker background values. This explains why in earlier investigations in which photo recording was employed experimental selection of the optimum superficial density always led to values exceeding $m_{o.p}$ as computed according to equation (1).

For investigating the fine structure of the absorption spectrum the optimum surface density $m_{o.p}$ can be found from equation (5) if we set

$$\tau_{m,2} = \tau_{m,1} + \Delta\tau_{m,1},$$

where $\Delta\tau_{m,1}$ is very small. In this case

$$S - 1 = (\Delta\tau_{m,1})/\tau_{m,1}.$$

Assuming furthermore that to a close approximation

$$\exp(\Delta\tau_{m,1} m_{o.p}) \approx 1 + \Delta\tau_{m,1} m_{o.p},$$

we obtain instead of (5):

$$m_{o.p}\tau_m = 1 + \frac{1}{a} \exp(-\tau_m m_{o.p}), \qquad (7)$$

where τ_m is the mean value of the mass-absorption coefficient in the investigated spectral region. The magnitude of a, as before, can be found from (4) if the value of I_1/I_2 has been measured for some density m. Then solving equation (5) graphically we find the optimum value of $m_{o.p}$. In the absence of background ($a = 0$), we obtain $m_{o.p} = \infty$, i.e., there is no optimum thickness; the contrast fluctuation continues to increase indefinitely with m. At $a = \infty$ equation (7) yields a value of $m_{o.p}$ in full agreement with (2). Thus for investigation of the fine structure of absorption spectra by photographic recording we have

$$m_{o.p} > \frac{1}{\tau_m}.$$

5. Experimental verification

For our experimental verification of the dependence of the contrast on the superficial density of the absorber when the spectrum is recorded photographically we selected the L_{II} absorption edge of lead in $Pb(NO_3)_2$. The computed value of the absorption jump in the vicinity of the L_{II} edge of lead was 1.4. An absorption edge with so small a jump was selected on purpose since it is in precisely such cases that the matter of selecting the optimum superficial density is highly important. The lead nitrate was mixed in known proportions by weight with spectroscopic carbon and the mixture was tightly packed into a holder frame 1.7 mm deep. In each case the frame was weighed before and after packing. This insured a uniform distribution of the mixture over the entire area of the frame (6 x 5 mm) and an accurately determined value of the superficial density. Tungsten oxide was thoroughly rubbed into the surface of the copper anode of the x-ray tube in order to enhance the general intensity of the continuous spectrum. The tube was operated at 28 kv, a potential at which the second order of reflection is not excited.

The exposure for each specimen was selected on the basis of the following considerations. As was noted under Section 3 above the curve for d/d_o vs log It has a virtually linear interval in the region of photographic densities from 0.14 to 0.74. It follows that the maximum contrast will not be reduced by variations in exposure so long as the entire absorption edge remains within the indicated density range. Hence in the case of small absorption jumps there is no need to adhere rigidly to the rule calling for the central line of the absorption edge to have a photographic density of 0.30: it is sufficient to have an exposure such that all points of the absorption edge will have densities between 0.14 and 0.74 on the spectrogram, i.e., in the straight-line portion of the curve. This requirement was used as a guide in selecting the exposure and photographing the absorption spectra of the specimens with different superficial densities.

The experimental results are listed in Table 2. To give these results general meaning instead of the superficial density M of the specimen (lead nitrate in this case) we give the ratio of the actual density M to $M_{o.i}$, the optimum superficial density as computed according to equation (1). In substituting the numerical values in (1), both S and $\tau_{m.2}$ were computed for the composition of the lead nitrate molecule. $M_{o.i}$ was found to equal 10.3 mg per cm^2. In row 2 of the Table the degrees of contrast of the edge are also given in relative units, i.e., in the form of the ratio of $(d_1 - d_2)_M$ to the amplitude of the edge at the optimum density $M_{o.i}$ as computed according to equation (1). All photometric determinations were referred to a constant value of d_o.

Table 2

$M/M_{o.i}$	0,88	1,00	1,36	2,52
$(d_1 - d_2)_M/(d_1 - d_2)_{M_{o.i}}$	0,95	1,00	1,16	2,17

As may be seen from the table, the contrast on the microphotogram increases with increasing superficial density and there is no difficulty in obtaining a contrast value twice that obtainable with the calculated "optimum ionization" density $M_{o.i}$. It is clear, therefore, that in the case of photographic recording the value of $M_{o.i}$ as computed according to equation (1) is definitely not the optimum value.

In order to elucidate the part played by an interfering background in the specific case of the L_{II} edge of lead in lead nitrate we computed, using eq. (5), the values of the relative background a, corresponding to the given value of the ratio of the optimum density $M_{o.p}$ for photographic recording to the optimum density $M_{o.i}$ as computed according to eq. (1). For convenience in computation eq. (5) was brought to the following form

$$\exp\left(\frac{\ln S}{1 - S^{-1}}\,k\right) - S\exp\left(\frac{\ln S}{S-1}\,k\right) = \frac{S-1}{a}, \qquad (8)$$

where $k = M_{o.p}/M_{o.i}$. The computed values of k for different values of $a = I_b/I_o$ with S = 1.40 are listed in Table 3.

Table 3

a	0	0.01	0.05	0.10	0.30	1.0	4,0	∞
k	∞	3.6	2,6	2.2	1.6	1,3	1,1	1,0

As simple calculations show the degree of contrast $(d_1 - d_2)_{M_{o.p}}$ is directly proportional to k. Inasmuch as commonly the background intensity amounts to 5-15% of the "useful" intensity, the optimum superficial density $M_{o.p}$ in photographic recording - as may be seen from Table 3 - should be 2-2.5 times greater than for ionization recording. This will result in a like 2-2.5-fold increase in the contrast of the absorption edge on the microphotogram.

It is interesting to note that in investigating the pure element the intensity ratio I_1/I_2 at the optimum superficial density $m_{o.i}$ defined by eq. (1) equals the abosrption jump S:

$$\left(\frac{I_1}{I_2}\right)_{m=m_{o.i}} = \frac{m,2}{\tau_{m,1}} = S.$$

In the case of ionization recording this corresponds to the greatest contrast. In the case of photographing recording the maximum attainable contrast is obtained with an intensity ratio $(I_1/I_2)_m > m_{o.i}$, appreciably exceeding the absorption jump value.

Conclusions

1. Equations (1) and (2) assure maximum contrast of the absorption edge only in the case of ionization recording or recording by means of a photomultiplier.

2. In the case of specimens of complex composition the values of the absorption coefficient and absorption jump substituted in eq. (1) and (2) must be computed for the entire specimen rather than for the investigated element alone.

3. In the case of photographic recording the contrast of the absorption spectrum on the microphotogram increases continuously with the surface density and its maximum value is limited only by the interfering background.

4. The optimum surface density for photographic recording can be determined by graphic solution of eq. (5) or (7) for the principal edge or for the fine structure as the case may be.

5. The relative intensity of the interfering background $a = I_b/I_o$ can be found from by means of eq. (4) by first measuring the ratio I_1/I_2 for the case of some absorber (specimen) having a known density m.

6. In view of the fact that the intensity of the interfering background may decrease with increasing specimen density m, the exact value of the optimum density $m_{o.p}$ can be found only by the method of "approximation and error:" by preparing an absorber with a superficial density as computed from eq. (5) or (7), computing the new value of a for the given specimen and repeating the entire process until the asymptotic value of $m_{o.p}$ is found.

7. The contrast of the absorption spectrum rises rapidly with decreasing intensity of the interfering background. Hence in planning an experiment all possible measures should be taken to reduce the background intensity. If the background intensity is successfully reduced to a negligible value, the onerous work of determining the optimum superficial density by "approximation and error" can be dispensed with: in this case one need only select the greatest density at which the optimum exposure will not exceed the allowable time under the given experimental conditions.

8. For practical purposes the exposure is optimal if all points in the investigated spectral region have a photographic density s between the limits $0.14 < s < 0.74$.

These limits pertain to the films we used. They can be determined accurately for any other given material by plotting a curve for d/d_o vs log It; the limits are then defined by the ends of the straightline section of the curve.

"V. M. Molotov" Rostov State University.

REFERENCES

1. E.E.Vainshtein, Zavodsk. labor. (The Factory Laboratory), 13, 424 (1947); 16, 962 (1950); K.I.Narbutt, R.L.Barinski & E.E.Vainshtein, Doklady AN SSSR, 82, 567 (1952).
2. A.Sandström, Thesis, Uppsala, 1935.
3. C.Kurylenko, Thesis, Paris, 1939.
4. M.A.Blokhin, Izv. AN SSSR, Ser. fiz., 17, 224, 1953.

* * * * * * *

X-RAY SPECTRA AND THE ELECTRONIC STRUCTURE OF THORIUM IN $Th(NO_3)_4$ AND ThO_2

- R. L. Barinski

Investigations of x-ray absorption spectra of uranium have substantiated the fact (already known from optical, magnetic and chemical studies) that uranium belongs in the new group of rare earth elements: the actinides.[1] However, the question of the ancestor of this group (thorium or actinium) is still open[2] and apparently cannot be resolved by the methods now commonly employed by investigators. In this respect use of the x-ray spectroscopic method of studying the electronic structure of atoms of a substance in a solid state appears to be particularly promising.

In the present investigation we studied the M_{IV} and M_V absorption and emission spectra of thorium in two solid crystalline compounds: $Th(NO_3)_4$ and ThO_2. The investigation was carried out on a vacuum x-ray spectrograph with a bent quartz crystal (lattice constant d = 3.33 A; R = 500 mm). The dispersion of the instrument in the vicinity of the M_{IV} and M_V absorption edges of Th was 10 XE/mm (9 ev/mm). The continuous spectrum was obtained from an x-ray tube with a tungsten anode at a potential of 10 kv and currents up to 50 ma. The emission spectrum of Th was obtained by the method of primary excitation; to this end the powdered specimens were rubbed into the ribbed surface of the aluminum anode. The spectra were recorded photographically on very fine-grain positive motion picture film; the exposure varied between 1.5 and 10 hours. The spectrograms were processed visually on an MF-2 microphotometer. Five spectrograms were obtained for each of the investigated spectra. The same section of the spectrogram was examined 3-5 times at different settings of the microphotometer and the resultant density curves were averaged. Finally the averages for the five results were used for plotting the spectral curve.

The specimens for the absorptions photographs were prepared by mixing the thoroughly powdered and screened material with zapon-lac (a cellulose nitrate varnish). The thickness was varied between 1 and 5 mg/cm^2.

The M_{IV} and M_V absorption spectra of Th in $Th(NO_3)_4$ and the last emission lines of Th in this compound (hatched) are shown in Fig. 1. It will be seen that both absorption spectra are characterized by an exceptional intensity of the absorption line on the side of lower energies. The absorption line in the M_V edge has a width of about 11 ev and exhibits a clear, fine structure. In contrast, the absorption line in the M_{IV} edge shows no fine structure and is narrower.

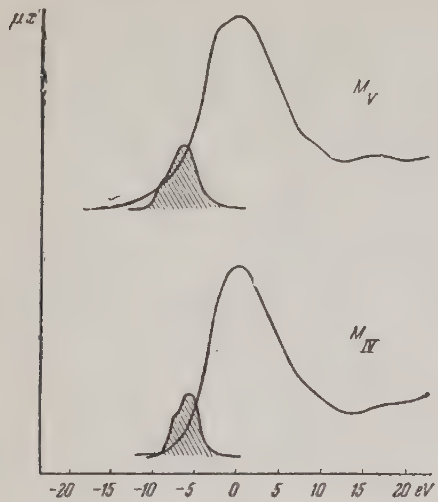

Fig. 1. M_{IV} and M_V absorption spectra of Th in $Th(NO_3)_4$ and the last emission lines of Th in the same compound (hatched). Vertical scale laid off in units proportional to the absorption coefficient and line intensity.

From an analysis of the absorption curves (Fig. 1), taking the selections rules into account, it follows that the absorption lines in the M_{IV} and M_V edges are associated with dipole transitions of 3d electrons to the excited 5f-levels of Th in $Th(NO_3)_4$, with which the region of unoccupied states of the Th atoms in the crystal begins, while the entire section of the edge beyond the absorption line is due to the capture of 3d electrons by the p-symmetry levels (apparently the 7p level). The fact that the absorption lines in the M_{IV} and M_V spectra are located energetically below all the other unoccupied levels of the Th atoms in the crystal indicates that it is most "advantageous" for the electrons in the atoms immediately neighboring the Th atoms to fill the 5f-states rather than any of the others. The narrowness of the absorption lines (which, however, are somewhat wider than the M_{IV} and M_V lines in the absorption spectrum of U - Ref. 1) proves that the 5f-levels are only weakly affected by the neighboring atoms in the compound; the disturbing effect is even weaker than in the case of the d-levels in the transition elements.[3]

Apparently the selection rules for the total momentum j, too, are violated to a lesser degree than in the case of transition elements, as follows from the differences in the fine structure and widths of the absorption lines in the respective M_{IV} and M_V edges. These differences can be understood in the light of the selection rule for the quantum number j: $\Delta j = 0, \pm 1$. Thus the 5f-states in a free atom are subdivided into two groups in accordance with the values of j; those with $j = 5/2$ and those with $j = 7/2$. Electron transitions from the M_V level ($j = 5/2$) in the process of absorption are allowed in the region of states with different values of j, while the corresponding transitions from the M_{IV} level ($j = 3/2$) to the sublevel with $j = 7/2$ are forbidden by the selection rules ($\Delta j = 2$). This is manifest in the weakening of the corresponding component of the absorption line, which naturally leads to narrowing of the line with an effacement of the fine structure.

Thus the presence in the Th atoms in $Th(NO_3)_4$ of low-lying excited 5f-states, located in a relatively narrow energy interval, electron transitions to which are subject to the selection rules for transitions in a free atom and, as will be seen below, little subject to the influence of the chemical bonds, proves that Th, just as U, can be classified with the elements of the new rare earths group. On the other hand, the wider spread in energy of the 5f-levels of Th as compared with U and their subdivision into groups indicate that the 5f-levels of Th in the compound crystal are in a more highly excited state than in U, which is to be expected.

The emission lines of Th in Th$(NO_3)_4$, arising in transitions of valence electrons to the M_{IV} and M_V levels of the atom, are appreciably narrower (~3 ev) than the corresponding lines of U (10 ev) and have approximately the same structure in both spectra.

A method of comparing x-ray spectral data with the results of studies of optical absorption by transition element atoms in solids was proposed in Ref. 4. Applying this method to the M_{IV} and M_V spectra of Th in Th$(NO_3)_4$, it can be shown that the limits of discrete optical absorption in this compound are located at 4000 A and 1200 A and the continuum begins at 900 A. The fact that the long-wave absorption limit in Th$(NO_3)_4$ lies beyond the visible region of the spectrum apparently explains the white color of this compound.

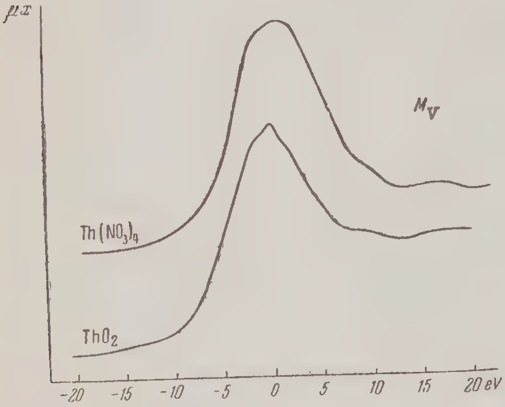

Fig. 2. M_V absorption spectra of Th in Th$(NO_3)_4$ and ThO$_2$. Vertical scale laid off in units proportional to the absorption coefficient.

The M_V absorption spectra of Th in Th$(NO_3)_4$ and ThO$_2$ are reproduced in Fig. 2. It will be seen that the two spectra differ somewhat as regards fine structure. The absorption line in the ThO$_2$ spectrum has a more complex structure compared to the line in the Th$(NO_3)_4$ spectrum and is displaced about 1 ev towards the long-wave side relative to the latter. The section of the spectrum beyond the absorption line is somewhat more intense in the case of ThO$_2$. The widths of both absorption lines are virtually equal (11 ev).

It is evident from the above that there is little difference between the structures of the excited 5f-levels of Th in ThO$_2$ and Th$(NO_3)_4$. The greater density of the free p-states in the former compound and the lower energy of the 5f-level centroid give reason to assume that the ionic bonds in ThO$_2$ are weaker than in Th$(NO_3)_4$. By analogy with uranium compounds[1] we may say that the type of bond in this group approaches the "uranyl bond." As regards other characteristics, the M_V spectra of Th in both Th$(NO_3)_4$ and ThO$_2$ are similar to the corresponding spectra of tetravalent uranium.

Laboratory of the Minerology and
Geochemistry of Rare Elements of
the Academy of Sciences of the USSR

REFERENCES

1. I.B.Borovski & R.L.Barinski, Doklady AN SSSR, 72, 31 (1950); Izv. AN SSSR, Ser. fiz., 15, 225 (1951).
2. J.J.Katz & E.Rabinowitch, The Chemistry of Uranium, part 1 (1951). In Russian trans. M.-1954.
3. R.L.Barinski, Doklady AN SSSR, 83, 381 (1952).
4. R.L.Barinski, E.E.Vainshtein & K.I.Narbutt, Doklady AN SSSR, 83,199 (1952)

A HIGH-ENERGY SEALED-OFF X-RAY TUBE FOR SPECTRUM ANALYSIS

- K. I. Narbutt and E. M. Fridman

There are many different designs of x-ray tubes for fluorescence analysis. A common characteristic of these tubes is two-piece, demountable construction, generally necessitating continuous evacuation. A number of designers, seeking to increase the intensity of the fluorescent emission even provide for introducing the specimen into the working space (inside the vacuum) thereby losing the principal advantages of the fluorescence method. Sealed-off x-ray tubes have not generally been accepted by our scientists for fluorescence analysis in view of the fact that the medical and industrial type tubes of domestic manufacture are not suitable for this purpose and that no special fluorescence analysis tubes are being produced. Yet the use of sealed-off tubes in x-ray spectroscopy practice is desirable since they do away with the necessity of maintaining and operating vacuum equipment.

On the other hand, the low intensity of the fluorescence spectrum requires a powerful source of primary radiation in order to bring the intensity of the spectra to values at which recording difficulties are obviated. Recently developed[1] wide-aperture bent crystals for x-ray spectrographs now make it possible to use x-ray tubes with a wide focus. The possibility of utilizing a wide focus in turn makes it easier to solve the problem of designing a powerful primary radiation source for fluorescent analysis.

Fig. 1 shows a preliminary design drawing of the x-ray tube for spectrum analysis being developed in the Institute of Geological Sciences of the USSR Academy of Sciences. In the figure 1 is a metallic case of cubical shape with an extended "quarter;" a milled recess in the case serves as the working space; in cross section it has the form of a 55 x 16 mm rectangle with rounded corners.

The working space houses a powerful cathode designed to give a wide electron beam. A cylindrical anticathode 2 with a tungsten reflector 3, in the form of an extended 45 x 8 mm rectangle, is welded inside the tube body to the case 1. A slit for the exit of the x-rays is milled in the wall of the case parallel to the anticathode. The slit is covered with a window 4 of Lindeman steel. The window also has the form of an elongated rectangle corresponding to the shape and dimensions of the focal spot and is welded to the case 1. Both the case 1 and the anticathode 2 are cooled by circulating water. The cathode is mounted on the glass cylinder (envelope) sealed to the case 1. The tube must be operated with a grounded positive (case 1 is grounded).

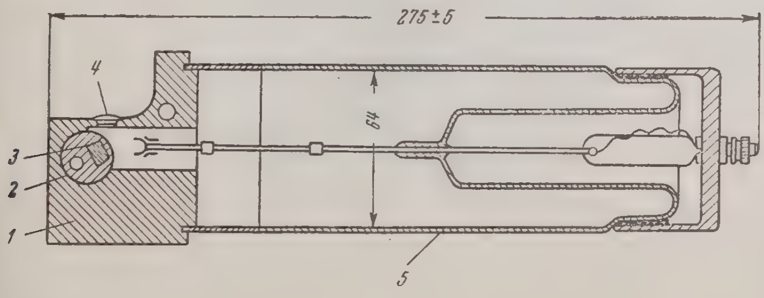

Fig. 1. Initial design drawing for the high-energy sealed-off x-ray tube for spectrum analysis.

A prototype model of the tube fabricated in the shops of the Institute is shown in Fig. 2 a (this model is operated under continuous evacuation). Tests on the model showed that the design is suitable for obtaining high-energy x-ray beams with a tube operated at up to 50 kv and 200 ma.

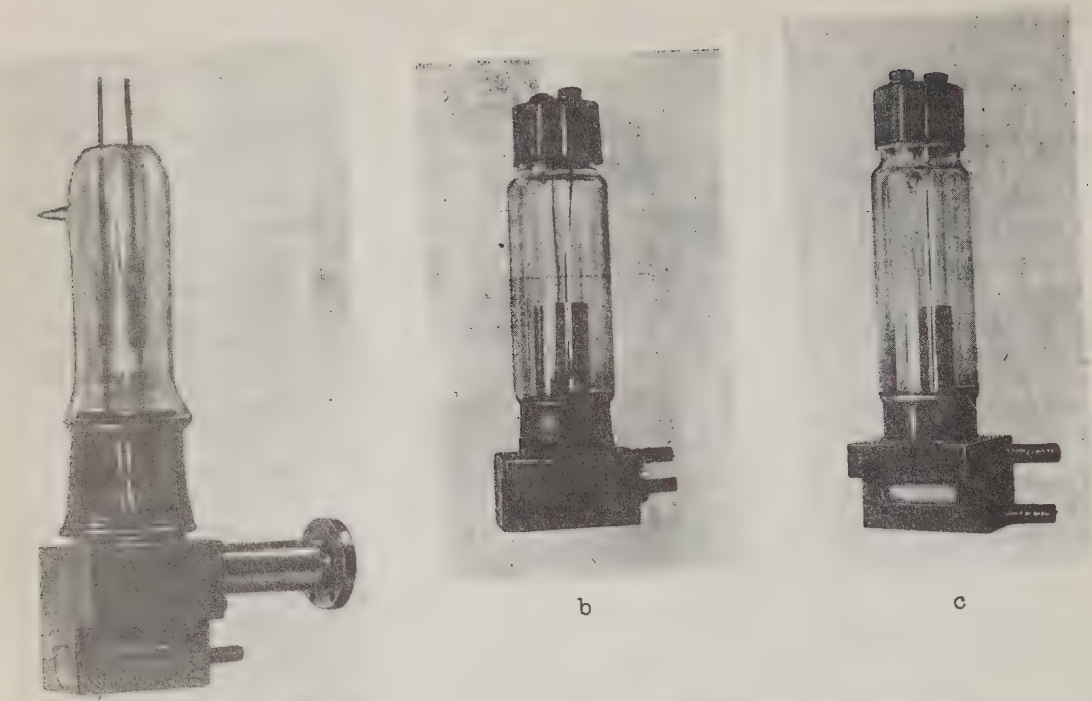

a

b

c

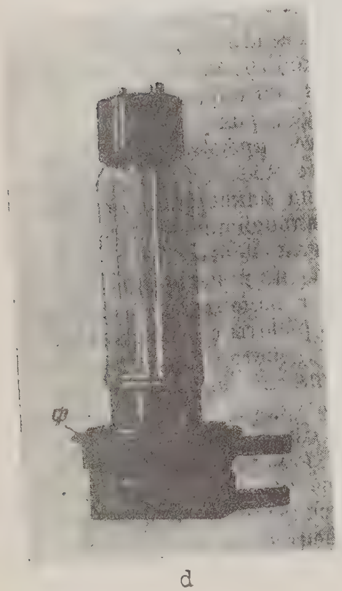

d

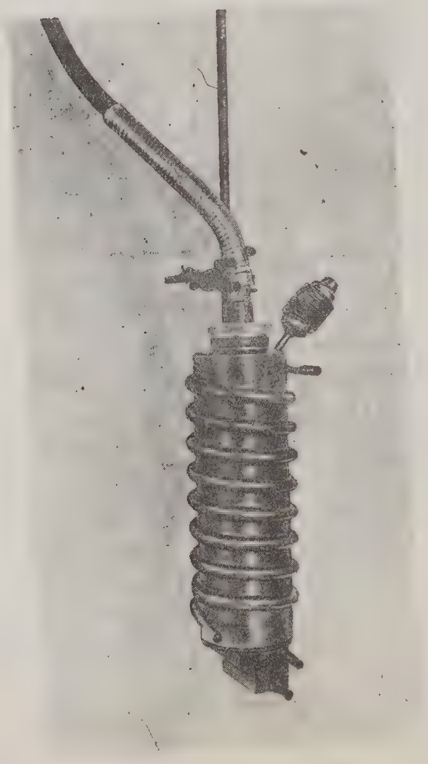

Fig. 2. a) Preliminary sectional model of tube; b) initial sealed-off model; c) model with improved cooling; d) final version of the sealed-off x-ray tube.

Fig. 4. The BFV-70 x-ray tube for spectrum analysis in the water-cooled, oil-filled protective housing.

Further work on the development on the tube for spectrum analysis was carried out by E. M. Fridman at the tube manufacturing plant. This was necessary, first, because realization of the sealed-off tube, in accordance with the design sketch, required the use of industrial electro-vacuum equipment (not available at the Institute) and, second, because the intention was not so much to fabricate a prototype but to develop ways and means for commercial production of these tubes.

As a result of this work there was developed the first satisfactory sample of a sealed-off x-ray tube for spectrum analysis; this is pictured in Fig. 2,b. Tests showed that at highest power operation (50 kv and 200 ma) the casing heated appreciably (to 100°). In view of this the case designed was modified with a view to increasing the cooling. The model with improved cooling is shown in Fig. 2,c. Tests showed that the modification resulted in reduction of the peak load operating temperature.

Further tests showed that certain other modifications in the initial design were desirable. These changes were primarily for the purpose of insuring greater shock and x-ray safety (there was some scattered radiation through the glass envelope). The case of the tube was equipped with a flange (Φ in Fig. 2,d) and the shape of the cathode contacts was changed. These modifications made it possible to enclose the tube in a protective oil-filled housing which simultaneously shields the personnel from high voltage and scattered rays. Fig. 3 shows the drawing of the final design of the tube. The anode portion of the tube consists of a massive copper casing 1 having the shape of a parallelepiped; the cooling water channels are drilled into the casing. The anode 2, hard soldered to the casing, has a tungsten reflector in the form of a rectangular plate set at an angle of 60° to the principal axis to the tube. The exit window is covered by a filter 3 formed by a 1 mm thick vacuum tight beryllium plate. The distance from the focus to the exit window is under 11 mm which makes it possible to bring the sample close to the focus. Water, circulating through the channels in the copper casing at the rate of 6-7 liters per minute, insures proper cooling of both the casing and the target. For the purpose of mounting the tube in the protective housing, the casing is provided with a welded on flange 4, to which also is welded the Kovar ring 5 serving for sealing the metal casing to the glass of the envelope 7. The cathode 6 is sealed to the other end of the envelope and incorporates a linear tungsten filament spiral designed to give a high emission (about 200 ma).

The cathode part of the tube is enclosed in a carbolite (resin) base 8, having two brass prongs. The tube gives a very wide primary x-ray beam which is only slightly absorbed in the exit window by virtue of the fact that the latter is made of beryllium.

The use of a wide focus (38 x 5 mm) and intensive water cooling of the anode and casing insures dissipation of very high energies at the cathode. The allowable load for prolonged operation is 200 ma at 50 kv_{max} (or 150 ma at 70 kv_{max}).

The maximum allowable anode voltage is 70 kv for continuous operation with the tube in air or oil when using a pulsed rectified voltage. The tube has the following filament characteristics: filament current not over 7.4 amp, filament voltage 13 v. The tube is fully shock-proof since the casing is grounded and has partial shielding cutting down the non-useful x-ray radiation. For complete ray-proofing the glass part must be covered with a special protective

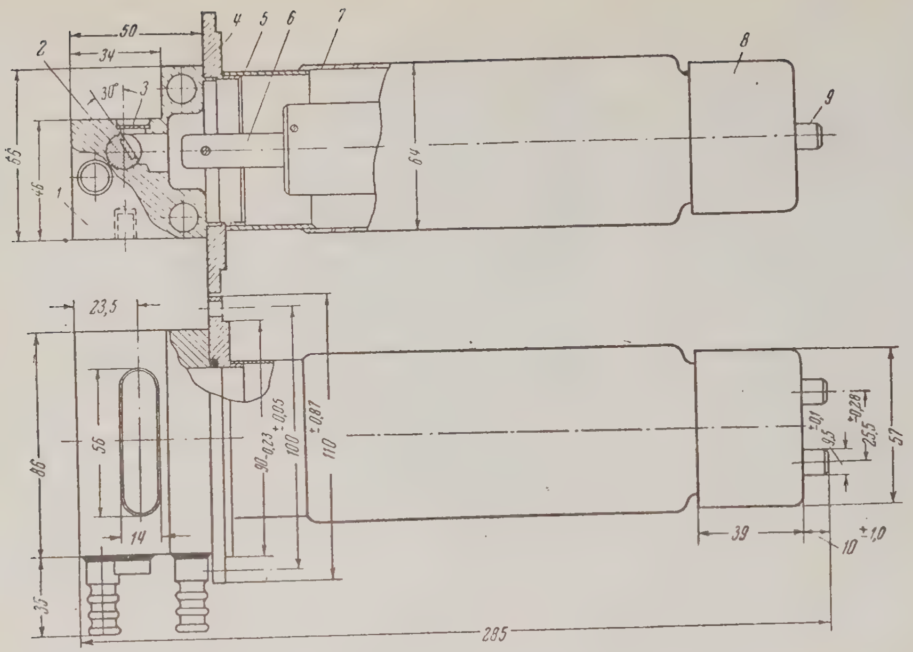

Fig. 3. Diagram of powerful sealed-off x-ray tube (type BFB-70) for spectrum analysis.

housing. The special oil-filled housing developed at the Institute is shown, with the tube in place, in Fig. 4. The high voltage is brought in by means of a special cable connector with the coupling inside the housing. The tube is attached to the housing by means of a rectangular flange seating on a rubber gasket and retained by six bolts. The space between the metallic housing and the tube itself is filled with transformer oil. A bellows oil expansion chamber makes it possible to use the tube either in the vertical or horizontal position. The walls of the protective housing are cooled by circulating water forced through a helical tube welded to the housing walls.

Tests of the tube for spectrum analysis with the protective housing in place gave excellent results.

In addition to providing protection against high-voltage and scattered x-rays the housing substantially improved the electric performance of the tube. Inside the housing the tube operates evenly and quietly without any corona effects, hissing or irregular discharges.

In the first half of 1954 a special commission appointed by the Ministry for the Radio-Technical Industry carried out state tests on a number of these spectrum-analysis tubes; part of the tests were made at the manufacturing plant and part at the chemical laboratory of the Institute. The tubes passed all the tests satisfactorily and the tube was assigned the official designation BFV-70 (БФВ-70) and the appropriate technical reports were sent to the Ministry for the Radio Engineering Industry.

Use of this x-ray tube for spectrum analysis on the earlier developed[2] RSK-4 x-ray spectrometer demonstrated the high efficiency of this tube for fluorescence analysis. We need only mention that the sensitivity in x-ray spectrum analysis, using this tube, can be brought to 0.01%. It proved easy to obtain the fluorescence spectra of solutions. The fact that this tube permits doing away with the complex and troublesome vacuum equipment required with not sealed tubes should prove of inestimable advantage in x-ray spectrum analysis work.

The use of a sealed-off x-ray tube of the BFV-70 type in conjunction with a RSK-4 type spectrometer greatly extends the potentialities of fluorescence analysis.

It may be noted that this x-ray tube can also be used as a continuum source for photographing x-ray absorption spectra. At present application of the BFV-70 tube for this purpose is limited to cases in which the presence of the characteristic lines of tungsten is not objectionable. However, it is perfectly feasible to manufacture these tubes with different anticathodes specifically for absorption analysis. In addition the BFV-70 tube has found application in radiation chemistry. It is to be hoped that the decision will soon be taken to put the BFV-70 x-ray tube into production in order to make it generally available to x-ray spectroscopists.

Institute of Geological Sciences of the
Academy of Sciences of the SSSR

REFERENCES

1. K.I.Narbutt, A.B.Gil'varg, E.E.Vainshtein & L.M.Beliaev, Zavodsk. labor., (The Factory Laboratory), 17, 1485 (1951).
2. K.I.Narbutt, Izv. AN SSSR, Ser. fiz., 17, 249 (1953).

* * * * *

INVESTIGATION OF THE DISTRIBUTION OF THE DENSITY OF ELECTRONIC STATES IN A SOLID AND THE WIDTH OF THE INTERNAL ATOMIC LEVELS

- M. A. Blokhin

1. Definition of the Problem

The problem of finding the true shape of x-ray spectra from their experimentally observed, distorted shape has, at present, been worked out only for emission lines having a classical, dispersion-curve shape. Such lines, for example, are the $K\alpha_1$ and $K\alpha_2$ emission lines of the non-transition elements. As Brogren[1] has shown, the distortions introduced by a double crystal spectrometer are closely characterized by the classical dispersion curve. These distortions can be found directly by recording the reflection curve in the position (1, -1). If the experimental line contour, recorded in position (1, +1), is dispersional,* the true shape of the line will also be dispersional and its width at half-maximum can be determined from the difference between the lines widths obtained in the positions (1, +1) and (1, -1). Pertinent data are now available for many lines; however, these data require revision since the corrections for the distortions introduced by a double-crystal spectrometer have, for the most part, been calculated on the assumption of a Gaussian shape of the reflection curves obtained in positions (1, −1) and (1, +1). The true shape in such cases was determined as the difference of the squares of the contour widths, recorded in positions (1, +1) and (1, −1), which, according to Brogren,[1] is incorrect.

---

* Hereinafter "dispersional" is understood to mean having the shape of the classical dispersion curve. Translator.

The problem of finding the true line shape in the general case has been solved in principle by Smith.[2] However, the method proposed by Smith has not been developed to the point where it can be used in practice.

In a number of investigations[3,4] devoted to finding the true shape of the lines of optical spectra and, in particular, of Raman spectra, the problem has been solved as far as practical application is concerned only in the case of certain simple line shapes (dome-shaped contours) and simple forms of distortion. The developed methods do not permit of practical solution of the problem in the case of complex contours, such as those characteristic of emission and absorption x-ray spectra associated with the outer levels of atoms, molecules and solids, particularly where elements of the transition groups are concerned.

Ornstein and Wyk[5] give a method of determining the true shape of a line having any contour, but only for the case of distortions introduced by an echelon. These authors also give a method of solving the problem with any distortions known in analytic form, but only in cases when the true shape is close to the Doppler intensity distribution. Thus, these methods cannot be utilized for establishing the true line shape of x-ray spectra in the general case.

The relation between the experimental line shape $F(x)$ distorted due to the finite resolving power of the apparatus (spectrograph, microphotometer, etc.) and the true shape of the spectrum $f(x)$ is established by the following integral equation

$$F(x) = \int_{-\infty}^{\infty} f(t)\,\varphi(x-t)\,dt, \tag{1}$$

where $\varphi(x-t)$ is the distortion function.

This equation can also be used for establishing the relationship between the true shape of the spectrum $f(x)$ and the distribution of the densities of electronic states $N(x)$ in a solid, molecules, and the like:

$$f(x) = \int_{-\infty}^{\infty} N(t)\,P(t)\,\psi(x-t)\,dt, \tag{2}$$

where $P(x)$ is the transition probability and $\psi(x-t)$ is distribution function for the electronic states of the inner atomic level.

This last function can be approximated by the dispersion function. The distortions introduced by a bent crystal spectrograph and the slit of the microphotometer (or of the counter in the case of ionization recording) are commonly very close to the dispersional form. In this case the function $N(x)P(x)$ can be found from the experimental curve through solution of the equation:

$$F(x) = \int_{-\infty}^{\infty} N(t)\,P(t)\,\chi(x-t)\,dt, \tag{3}$$

where $\chi(x-t)$ is the dispersion function with a width at half-maximum equal to the sum of the widths of both the dispersion functions $\varphi(x-t)$ and $\psi(x-t)$.

In solving the integral equation (1), one must first find the function $\varphi(x-t)$, which must be determined from experimental data obtained on the same instruments.

2. Determination of the Distortion Function

For determining the distortion function it is preferable to select a standard reference line, whose true shape $f_c(x)$, according to the indications of the double-crystal spectrometer, is dispersional. The width of this line must also be known from the same data. The selected standard line should be one located as close as possible to the investigated region of the spectrum (in the same order of reflection). This line must be recorded on the same spectrogram as the investigated spectrum. In the case of ionization recording, the shapes of the standard line and the investigated spectrum must be measured (or recorded) in the course of the same experiment.

Let us designate the known width at half-maximum of the standard line by γ_c. If the observed contour of this line proves to be close to the classical (dispersion curve) with a half-width $\gamma_э$, the distortion function will also be dispersional with a half-width

$$\gamma = \gamma_э - \gamma_c. \tag{4}$$

The normalization condition is

$$\int\limits_{-\infty}^{\infty} \varphi(u)\,du = 1, \tag{5}$$

whence we get

$$\varphi(x-t) = \frac{1/\pi\gamma}{1+\left(\frac{x-t}{\gamma}\right)^2}. \tag{6}$$

If the observed experimental shape $F_c(x)$ of the standard line cannot be approximated by a dispersion function, the form of the distortion, too, will not be dispersional. In the general case the distortion may be asymmetric. In this case equation (1) can be used to find the distortion function from the graphically given function $F_c(x)$ and the function $f_c(x)$ known in analytic form:

$$f_c(x) = \frac{S/\pi\gamma_c}{1+(x/\gamma_c)^2}, \tag{7}$$

where S is the area under the $F_c(x)$ curve:

$$S = \int\limits_{-\infty}^{\infty} F_c(x)\,dx. \tag{8}$$

The value of S is found by measuring the area under the curve; in this case the solution of (1) relative to $\varphi(x-t)$ yields the normalized value of the function.

Where the investigated spectrum is an emission band, it will be characterized by a finite width Δ. Outside this interval the intensity of the spectrum is commonly less than the experimental error and hence for practical purposes may be assumed to be zero. Let us select our origin on the x-axis at the middle of the interval Δ. Inasmuch as the width of the standard reference line will usually be appreciably smaller than the width of the emission band, we can with adequate accuracy set

$$S = \int_{-\Delta/2}^{\Delta/2} F_c(x)\,dx; \tag{9}$$

$$F_c(x) = \int_{-\Delta/2}^{\Delta/2} f_c(t)\,\varphi(x-t)\,dt. \tag{10}$$

To find $\varphi(x-t)$ let us expand all three functions comprised in (10) in trigonometric series, taking Δ equal to the half-period of these functions. In the second half period let us extend these functions so that they will have third order symmetry; here $f_c(t)$ will be an even function. We will then have

$$f_c(t) = \sum_h A_h^c \cos\frac{h\pi}{\Delta}\,t, \tag{11}$$

$$F_c(x) = \sum_k \left(B_k^c \cos\frac{k\pi}{\Delta}\,x + b_k^c \sin\frac{k\pi}{\Delta}\,x\right), \tag{12}$$

$$\varphi(x-t) = \sum_l \left[C_l \cos\frac{l\pi}{\Delta}(x-t) + c_l \sin\frac{l\pi}{\Delta}(x-t)\right], \tag{13}$$

where h, k, and l are odd integers. The coefficients A_h^c can, with sufficient accuracy (with $\Delta \gg \gamma_c$) be found by means of the formula

$$A_h^c = \frac{2S}{\Delta}\left[\exp\left(-\frac{h\pi\gamma_c}{\Delta}\right) - \frac{2h\gamma_c}{\Delta}\,\mathrm{si}\,\frac{h\pi}{2}\right]. \tag{14}$$

The coefficients B_k^c and b_k^c can be found by the commonly known methods of graphic harmonic analysis from the experimental spectral distribution curve for the intensities of the standard line. The origin on the x-axis should be taken at the point of the maximum intensity of the standard line as recorded by means of the double-crystal spectrometer.

Substituting (11), (12) and (13) in (10), we find

$$C_k = \frac{2}{\Delta}\cdot\frac{B_k^c}{A_k^c} \quad \text{and} \quad c_k = \frac{2}{\Delta}\cdot\frac{b_k^c}{A_k^c}. \tag{15}$$

This solves the problem of finding the distortions introduced by the given apparatus.

In order to evaluate the accuracy attainable when a finite number of the coefficients A_h^c, B_k^c and b_k^c is evaluated, the described method was applied to a case when the given analytic function $F_c(x)$ permitted finding the analytic expression for the distortion function $\varphi(x-t)$. An asymmetric form of the function $F_c(x)$ was selected:

$$F_c(x) = \frac{400}{3}\left[\frac{1}{1+\left(\frac{x}{2}\right)^2} + \frac{0{,}5}{1+\left(\frac{x+1}{2}\right)^2}\right]. \tag{16}$$

The dispersion curve, equal to that of the above function in area and simulating the "true shape" of the standard line, was taken in the form

$$f_c(t) = \frac{400}{1+t^2}. \tag{17}$$

In this case the distortion function has the form

$$\varphi(x-t) = \frac{2}{3\pi}\left[\frac{1}{1+(x-t)^2} + \frac{0{,}5}{1+(1+x-t)^2}\right], \tag{18}$$

where condition (5) is fulfilled.

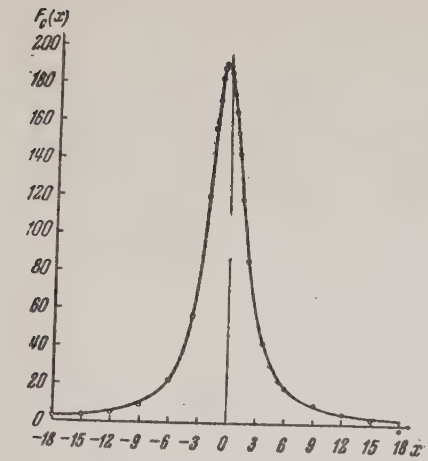

Fig. 1. Curve of the function $F_{\text{c}}(x)$. The points represent the results of synthesis of the series (12) using the amplitudes found by graphic harmonic analysis

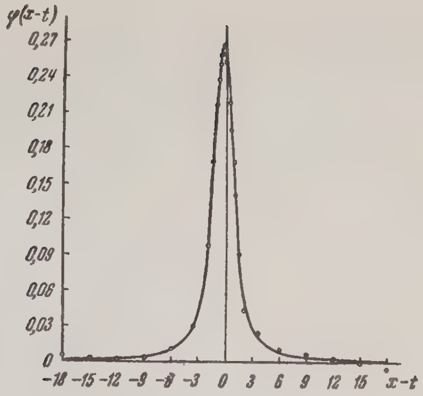

Fig. 2. Curve of the function $\varphi(x-t)$. Points represent the results of synthesis of series (13) using the amplitudes found according to (15).

The curve for $F_{\text{c}}(x)$, plotted on the basis of (16), is shown in Fig. 1. The graphic harmonic analysis of this curve in the interval $\Delta = 36$ was carried out by the method of Chebyshev.[6] We found the first thirteen pairs of amplitudes B_k^{c} and b_k^{c} for odd values of k from 1 to 25. The amplitudes A_k^{c} were calculated for the same values of k according to equation (8) with $S = 400\pi$. Using the values of C_k and c_k, found from (15), we synthetized the series (13) at a number of points. These points are shown in Fig. 2 together with curve plotted on the basis of the exact analytic expression (18) for $\varphi(x-t)$. As may be seen, even with so small a number of calculated amplitudes the agreement is satisfactory.

3. Determination of the True Shape of the Emission Spectrum in the General Case

We now turn to the problem of finding the true shape $f(x)$ of a spectrum whose distorted shape $F(x)$ has been determined experimentally. We will assume that the distortion $\varphi(x-t)$ has been found in the above described manner and is defined by the coefficients C_l and c_l of series (13). Let us represent the function $F(x)$ by the trigonometric series

$$F(x) = \sum_k \left(B_k \cos \frac{k\pi}{\Delta} x + b_k \sin \frac{k\pi}{\Delta} x \right), \tag{19}$$

where Δ is the interval utilized above in which the function $F(x)$ is given graphically. Outside this interval the values of the functions $F(x)$ and $f(x)$ do not exceed the experimental error and can therefore be assumed equal to zero. We select the symmetry of $F(x)$ to be identical to that of $F_{\text{c}}(x)$. We take the interval Δ to be equal to the half-period of $F(x)$. In this case the amplitudes of the even number harmonics are zero. We take the origin on the x-axis at the center of the interval Δ. We find the coefficients B_k and b_k by graphic harmonic analysis.

We represent the true shape of the spectrum by the series

$$f(t) = \sum_h \left(A_h \cos \frac{h\pi}{\Delta} t + a_h \sin \frac{h\pi}{\Delta} t \right), \tag{20}$$

in which the amplitudes of the even number harmonics are also equal to zero. Substituting (19), (20) and (13) in the integral equation

$$F(x) = \int_{-\Delta/2}^{\Delta/2} f(t)\,\varphi(x-t)\,dt, \tag{21}$$

we find

$$A_k = \frac{2}{\Delta}\frac{b_k c_k + B_k C_k}{c_k^2 + C_k^2} \quad \text{and} \quad a_k = \frac{2}{\Delta}\frac{b_k C_k - B_k c_k}{c_k^2 + C_k^2}. \tag{22}$$

Synthesis of the series (20) with the amplitudes from (22) permits us to plot the curve giving the true shape of the spectrum.

The described method makes it possible to find any shape of distortion of the x-ray spectrum and to utilize it for re-establishing the true shape. Obviously the re-established shape will be all the more accurate and closer to the true shape, the higher the resolution of the apparatus. Thus the distortion can be of any shape but not of any width. That is, if some details of the spectrum are smeared out due to insufficient resolving power and do not exceed the experimental errors (connected with quantum nature of the radiation, graininess of the film, etc.), these details cannot be brought out in re-establishing the true shape of the spectrum.

It should be borne in mind that the functions $F(x), f(t)$ and $\varphi(x-t)$ were replaced above by the periodic functions (19), (20) and (13), which coincide with the former only over one-half the period, i.e., in the interval Δ. Outside this interval the curves representing the series (19), (20) and (13) were artificially extended so as to satisfy the requirements of symmetry and orthogonality of the functions $f(t)$ and $\varphi(x-t)$ in the interval Δ. This leads to a distortion of the determined curve of $f(x)$ near the boundaries of the interval (at $-\Delta/2$ and $\Delta/2$). However, if this interval is selected so that near the boundaries (inside the interval) the curve of $F(x)$ has small ordinates over sections not narrower than the width of the function $\varphi(x-t)$, the edge distortions will be insignificant.

4. Determination of the True Shape of the Emission Spectrum in the Case of Dispersional Distortion

Let the distortion function $\varphi(x-t)$ have the form (6) and a known half-width γ. On solving equation (1) we assume that the functions $F(x)$ and $f(x)$ virtually vanish outside the interval 0 to Δ. Then

$$F(x) = \frac{1}{\pi\gamma}\int_0^{\Delta} \frac{f(t)\,dt}{1+\left(\frac{x-t}{\gamma}\right)^2}. \tag{23}$$

Let us represent function $F(x)$ by a trigonometric series, letting the interval equal a quarter period. Let us extend the curve representing the experimentally determined shape of the spectrum outside the interval 0 to Δ so that $F(x)$ will be an odd number function, having third order symmetry, with a period 4Δ. Then

$$F(x) = \sum_k b_k \sin \frac{k\pi}{2\Delta} x, \qquad (24)$$

where $k = 2n + 1$, $n = 0, 1, 2, \ldots$ The coefficients b_k can be found by one of the methods of graphic harmonic analysis.

Let us represent the distortion function $\varphi(x-t)$ also in the form of a trigonometric series with a period 4Δ, extending this function artificially in the remaining part of the period so that it will be an even number function having third order symmetry. Then

$$\frac{1}{1+\left(\frac{x-t}{\gamma}\right)^2} = \pi\gamma\varphi(x-t) = \sum_{l=1}^{\infty} C_l \cos \frac{l\pi}{2\Delta}(x-t), \qquad (25)$$

where $l = 2n + 1$. With $\Delta \gg \gamma$, the coefficients C_l can be found with sufficient accuracy by means of the equation

$$C_l = \frac{\pi\gamma}{\Delta}\left[\exp\left(-\frac{l\pi\gamma}{2\Delta}\right) - \frac{l\gamma}{\Delta} \operatorname{si} \frac{l\pi}{2}\right]. \qquad (26)$$

Let us represent the true shape of the spectrum, i.e., the function $f(t)$, by the series

$$f(t) = \sum_h a_h \sin \frac{h\pi}{2\Delta} t, \qquad (27)$$

where $h = 2n + 1$. The function $f(t)$ has the same period and order of symmetry as $F(x)$.

Let us substitute (24), (25) and (27) in (23). Integrating (in view of orthogonality considerations) from 0 to 2Δ, we find

$$a_h = \frac{\pi\gamma}{\Delta}\frac{b_k}{C_k}. \qquad (28)$$

This expression gives the solution of integral equation (23) with respect to $f(x)$. Arbitrary increase of the integration interval and artificial choice of the symmetry of the function leads to a bilateral distortion of the function $f(x)$ at the edges. However, if the function $f(x)$ has small values near the limits of the interval (0 to Δ) at distances not less than 2γ and provided $\Delta \gg \gamma$, the edge effect will introduce a noticeable distortion only in parts of the line close to the limits of the interval (0 to Δ).

5. Determination of the True Shape of the Absorption Spectrum

The presence of an edge (distortion) effect makes it impossible to apply the above method directly to correcting the shape of an absorption spectrum, since in this case the ordinates of the functions $f(x)$ and $F(x)$ will have large values at one of the boundaries of the interval Δ. Let us divide the area under $F(x)$ into two parts (Fig. 3 a), partitioned by the arc tangent curve

$$F_1(x) = \frac{F_0}{\pi}\left(\frac{\pi}{2} - \operatorname{arctg}\frac{x-\alpha}{\gamma_1}\right), \qquad (29)$$

where F_0 is the ordinate of the upper asymptote of the $F(x)$ curve and γ_1 and α are arbitrary constants, the selected values of which will depend on the magnitude of the section of the $F(x)$ curve being corrected. The parameter γ_1 must in any case be greater than the half-width of the distortion function. If the latter is dispersional, we must have $\gamma_1 > \gamma$. In this case the section of the area under the $F(x)$ curve, located in Fig. 3,a to the left of $F_1(x)$, may be corrected directly: after correction it will be bounded by the curve

$$f_1(x) = \frac{F_0}{\pi}\left(\frac{\pi}{2} - \operatorname{arctg}\frac{x-\alpha}{\gamma_1-\gamma}\right). \quad (30)$$

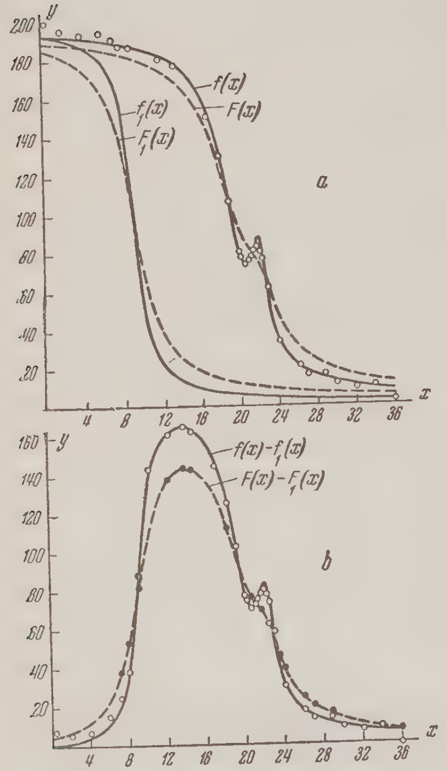

Fig. 3. a) curves $F(x)$, $f(x)$, $F_1(x)$ and $f_1(x)$; circles indicate determined values of the function $f(x)$; b) curves $F(x)-F_1(x)$ and $f(x)-f_1(x)$; points show the results of synthesis of the series approximating the function $F(x)-F_1(x)$; the circles indicate the results of synthesis of the series of odd harmonics with amplitudes as determined according to (28).

If the distortion function $\varphi(x-t)$ departs from the dispersional shape, then by selecting the abscissa α of the inflection point of (29) at a sufficiently great distance from the absorption edge we can nevertheless approximate $\varphi(x-t)$ by means of (6) and construct $f_1(x)$ on the basis of (30); this will obviate any appreciable distortion of the $f(x)$ in the vicinity of the edge.

In order to correct the area under the $F(x)$ curve enclosed between $F(x)$ and $F_1(x)$, we find the difference between these functions graphically (Fig. 3,b). The resultant curve has small ordinates near both limits of the interval Δ and therefore can be corrected by one of the methods described above, without involving an appreciable edge effect. Thus the problem of correcting the absorption spectrum has been reduced essentially to a problem fully analogous to that encountered in the case of emission spectra. Adding the ordinates of the corrected difference of the functions $f(x)-f_1(x)$ to the ordinates of $f_1(x)$, we obtain the corrected shape of the absorption spectrum $f(x)$ in Fig. 3,a.

It must be noted that inasmuch as the distortion function lies on the intensity distribution curve, correction of the absorption spectrum for the finite resolution of the apparatus must also be carried out over the absorption spectrum intensity distribution curve.

In order to demonstrate the accuracy of the proposed method and evaluate the edge effects we carried out correction calculations for an artificial curve simulating the absorption spectrum of transition elements and having the "thickening," characteristic of these elements at the principal absorption edge. Choice of an artificial curve made it possible to find the exact shape of the corrected curve analytically for purposes of checking. Moreover, use of an artificial curve obviated possible experimental errors which, after correction, might still produce an appreciable deviation of the corrected curve from the true shape of the spectrum.

The curve $F(x)$ (Fig. 3,a) represents the following function:

$$F(x) = \frac{200}{\pi}\left(\frac{\pi}{2} - \operatorname{arctg}\frac{x-19}{3}\right) + \frac{25}{1+\left(\frac{x-22}{2}\right)^2}. \tag{31}$$

The corrected shape of this curve is defined by the function

$$f(x) = \frac{200}{\pi}\left(\frac{\pi}{2} - \operatorname{arctg}\frac{x-19}{2}\right) + \frac{50}{1+(x-22)^2}, \tag{32}$$

where the distortion function $\varphi(x-t)$ is taken in the form of equation (6) with a half-width $\gamma = 1$. The auxiliary function $F_1(x)$ was selected according to (29) with $\alpha = 9$ and $\gamma_1 = 2$. The corrected form of this function was determined from (30). The curve of the difference $F(x)-F_1(x)$ (Fig. 3,b) was expanded by the method of Chebyshev to the 49th harmonic. After correction of this curve by the method described under Section 4 above, we found the amplitudes a_k. Synthesis of the series (27) with $\Delta = 36$ yielded, as may be seen from Fig. 3,b, an entirely satisfactory approximation of the true curve, except for narrow sections at the limits.

Graphic addition of the ordinates of $f(x)-f_1(x)$ to the ordinates of the plot of function $f_1(x)$ gave the points for the corrected function $f(x)$, which are shown in Fig. 3,a.

6. Finding the Distribution Curve for the Density of the Electronic States

The method outlined in Section 1 can be used to find the distribution curve for the densities of the occupied electronic states - or more accurately, of the product $N(x)P(x)$, where $x = E$, the electron energy - from the emission band data. In the case when the distortion can be approximated by a dispersion curve, the experimental data can be processed directly by means of equation (3). However, in the case of the distribution of the densities of the unoccupied electron states this processing must be divided into two successive operations. First, one must establish the true form of the curve characterizing the intensity distribution of the absorption spectrum from the experimental absorption curve. Then, having found (from the true absorption curve) the true distribution curve for the absorption coefficient, one must first determine the width of the inner level.[7,8] Here it must be noted that determination of the width of the inner level from the uncorrected experimental absorption curve with subsequent correction for the instrument distortion by simple subtraction of the parameter – 2 – of the distortion function (as had been done in Ref. 8) can give the correct value of the true width of the inner level only in the case when the absorption edge is characterized by an arc tangent curve. In the case of the complex absorption curves, characteristic of transition group elements, this procedure is inadmissible and for this reason the data given in Ref. 8 must be regarded as inaccurate.

Having determined the half-width γ_i of the inner level from the corrected absorption curve, we can treat the shape of this level as a distortion function having a dispersional shape and reapply the method of processing to the absorption curve. This will give us the function N(E)P(E) for the energy region free of electrons.

7. Distribution of the Densities of Electronic States in Metallic Nickel

In order to find the curves characterizing the distribution of electronic states in metallic nickel, we processed the data on the Kβ_5 emission band and the K absorption edge of nickel given in Ref. 8. The experimental curves were obtained on a double-crystal spectrometer and are reproduced in Fig. 4. After converting the absorption curve to an intensity curve and correcting this for distortion of dispersional form with a width 2γ = 0.73 ev, we plotted the corrected absorption curve. From this curve we found the width of the K-level using the method employed for this purpose in Ref. 8. We obtained a value of 1.6 ev for the full width of the K-level (instead of 1.9 ev in Ref. 8). We found the curve for N(E)P(E) for the unoccupied region from the corrected absorption curve for a value of γ_i = 0.8 ev. This curve is also shown in Fig. 4. In processing the intensity curve we determined the amplitudes to the 69th harmonic; in processing the corrected absorption curve the amplitudes were determined to the 49th harmonic.

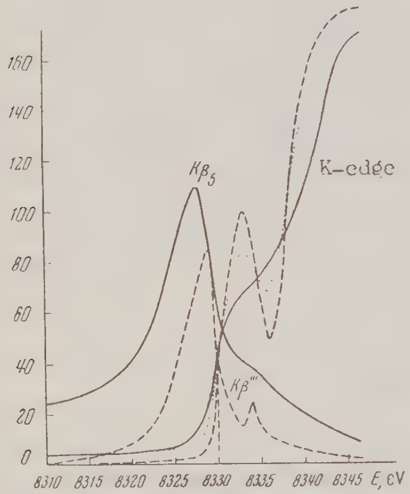

Fig. 4. Solid curves represent the shape of the Kβ_5 emission band of metallic nickel and its K absorption edge. The dotted line shows the corrected absorption curve. The dash lines are the curves for N(E)P(E). (Vertical scale arbitrary.)

The correction of the shape of the emission band was carried out simultaneously for the total width of the inner level and the distortion of the double-crystal spectrometer:

$$2(\gamma_i + \gamma) = 2.33 \text{ ev}.$$

In processing this curve we determined the amplitudes to the 69th harmonic. In the final N(E)P(E) curve for the filled part of the distribution of states there remains the clearly discernible Kβ''' satellite, which of course has no meaning in the N(E)P(E) curve. However, between the point of inflection of this curve on the side of higher energies and the point of inflection of the N(E)P(E) curve for the unoccupied states there proved to be a break amounting to 0.7 ev. In view of the considerations, set forth by Kostarev,[9] regarding the displacement of the emission spectrum relative to the absorption spectrum, this break is only apparent. Consequently the N(E)P(E) curve for the occupied states shown in Fig. 4 was shifted 0.7 ev to the side of higher energies in plotting. In addition, all the ordinates of this curve have been arbitrarily multiplied by 0.282 in order to equalize the ordinates of the inflection points of the two curves. The common abscissa of these points corresponds to the Fermi surface.

If we assume that the filled part of the distribution corresponds to the 3d band of nickel and that the pronounced peak in the unoccupied part of the distribution corresponds to the same 3d band, the steep rise in the curve after the peak must correspond to the 4sp band, the P(E) transition associated with which is characterized by a very high probability. A striking feature of the curves in the light of this interpretation is the great width of the 3d band in comparison with the calculated width. According to the calculations of Slater[10] the width of the entire 3d band of nickel should be about 5 ev; while according to the more exact calculations of Fletcher[11,12] the theoretical width is 2.7 ev. Yet as may be seen from Fig. 4 the actual width of this band would appear to be 15-20 ev. Furthermore, the shape of this band predicted from theory, with two peaks in the occupied part[10,11], is not realized. Somewhat closer to the actual shape of the band is the curve given by Fletcher[11] for the ferromagnetic state. Fletcher shows the second peak in the unoccupied part of the band. All this is indicative of the inadequacy of the present day state of the electronic theory of metals and, in particular, of the shortcomings of the one-electron model.

8. Determination of the Widths of the K-Level in Transition Elements of the Iron Group

It is worth calling particular attention to the shape of the unoccupied part of the 3d band and its relatively small width. Approximation of the rise of the absorption curve (to the first inflection point) by an arc tangent curve does not give the correct value of the width of the K-level. It follows, therefore, that the N(E)P(E) curves shown in Fig. 4 are only first approximations and require revision. At present there appears to be no reliable method capable of giving the true width of the K-level of elements of the transition group. However, by determining the width of the K-level for non-transition elements with atomic numbers $Z \geqslant 30$ and $\leqslant 20$, one can evaluate the width for the transition elements of the iron group by interpolation, bearing in mind that according to Zinn[13] the width of the K-levels must be proportional to Z^4.

Zinn shows a theoretical curve for the dependence of the width of the K-level on the atomic number together with points based on experimental data for different elements with atomic numbers from 25 to 53. The experimental points fall on the theoretical curve, except in the region of the transition elements of the iron group where there is appreciable scattering of the points from which it appears that the width of the K-level in these elements is more or less constant. In view of what has been said above, these results must be attributed to incorrect determination of the width of the K-level of the transition group elements.

"V. M. Molotov" Rostov State University

REFERENCES

1. G. Brogren, Phys. Rev.. 96. 589 (1954).
2. L.P. Smith, Phys. Rev., 46, 343 (1934).
3. V.M. Chulanovski & A.V. Timoreva, Izv. AN SSSR, Ser. fiz., 11, 376 (1947).

4. M.M. Sushchinski, Zhur. eksp. i teor. fiz., 25, 87 (1953).
5. L.S. Ornstein & W.R. van Wyk, Zs. f. Phys., 78, 743 (1932).
6. P.L. Kalantarov, Teoria peremennykh tokov, (Alternating current theory), 1940.
7. F.K. Richtmyer, S.W. Barnes & E. Ramberg, Phys. Rev., 46, 843 (1934).
8. W.W. Beeman & H. Friedman, Phys. Rev., 56, 392 (1939).
9. A.I. Kostarev, Zhur. eksp. i teor. fiz., 22, 628 (1952).
10. J.C. Slater, Phys. Rev., 49, 537 (1936).
11. G.C. Fletcher & E.P. Wohlfarth, Phil. Mag., 42, 106 (1951).
12. G.C. Fletcher, Proc. Phys. Soc. (London), 65A, 192 (1952).
13. W.H. Zinn, Phys. Rev., 46, 659 (1934).

* * * * * *

THE NEW RSD-2 X-RAY VACUUM SPECTROGRAPH

- K. I. Narbutt, E. E. Vainshtein,
A. B. Gil'varg and L. M. Beliaev

The acceptance and use of the methods of x-ray spectrum analysis by industrial and scientific laboratories is predicated on continuous and marked improvement of x-ray spectroscopic equipment, particularly enhancement of the transmission characteristics and resolving power of spectrographs. In a previous communication[1] we set forth some of the results of an experimental investigation of the bending of crystals in the crystal holder of focusing x-ray spectrographs, an investigation which made it possible to develop a technique for bending large crystals and thereby improved the transmission factor of x-ray instruments. Subsequently this investigation served as the basis for the development of the high-energy RSK-3 x-ray spectrograph[2] for the short wave region of the spectrum with photographic recording; the results of the investigation were also utilized by one of the present authors in designing a universal-type x-ray spectrometer.[2]

The RSD-2 (РСД-2) spectrograph which we shall describe in the present article is the next in a series of new instruments of enhanced transmission and resolution to be developed on the basis of the aforementioned investigation.[1] This spectrograph is designed for work in the long-wave region of the x-ray spectrum, the region in which the K series lines of the elements from K to Cu and the L series lines of the elements from Ag through Ta are commonly studied.

The new spectrograph can be used both for conventional elementary analysis and for scientific investigations connected with the study of the fine structure of emission lines and absorption edges.

Our aims in designing the RSD-2 spectrograph were the following:

1. To increase the power of the spectrograph so as to increase the speed of analyses by an appreciable factor.

2. To enhance the dispersion and resolving power of the instrument, at the same time making the analyzer a stable unit. To

this end it appeared appropriate a) to utilize the experience[1,2] gained in producing crystal holders with a bent crystal mounted in optical contact with the holder, b) increase the radius of curvature of the crystal and utilize the method of oblique planes proposed by Protopopov,[4] and c) realize the method of improved focusing, known as the method of Johanson.[5]

3. To provide for controlling the dimension of the focal spot and for convenient adjustment of the size, shape and position of the spot.

4. To provide for accurate and standard positioning of the anticathode incident to replacement of the specimens.

5. To simplify and accelerate the process of loading the film, preferably without the necessity of darkening the x-ray room.

6. To take into account in designing the rocking mechanism of the desirability of eliminating the non-uniform sensitivity of the instrument in different parts of the spectrum, connected with the geometric conditions of focusing.

7. To design the spectrograph as an integral unit with the high voltage supply. This integral construction would do away with the need for the separate purchase and installation of high voltage equipment and would thus provide purchasers with a complete and self-contained x-ray analysis instrument.

Description of the Instrument

A general view of the RSD-2 spectrograph and a diagram of the main chamber are shown in Fig. 1. In the figure T is the source of x-rays, K is the crystal holder and S is the film holder located on the focal circle. As may be seen in the general view, the stand of the instrument has been utilized for housing the electric equipment and vacuum unit. I is the main housing of the spectrograph, II is the central chamber (camera chamber) and III is the x-ray tube. To the right of this unit can be seen the control panel, mounting the vacuum valves and electric switches. The electric grounding unit and the vacuum gauge are mounted on the vertical panel in front of the operator.

A. The X-Ray Tube

The x-ray tube is shown in Fig. 2; it is made in the form of a separate assembly and connected with the crystal holder chamber by means of a large diameter sylphon 3. The steel casing 1, cooled by running water, has three openings: the upper one receives the cathode K, the lower the anode A, mounted on the insulator 2, while the side opening serves for access to the replaceable anticathode and during operation is closed by the cover B which has a viewing window.

The design of the cathode provides for both adjustment of the cathode as a whole relative to the anticathode and of the depth of the filament in the focusing cup. These adjustments are made by rotating the rings 6 and 7 and are accomplished by electrostatic focusing of the electron beam. The design of the anode provides for easy and rapid replacement of the anticathodes, which are made in the form of 40 x 25 x 4 mm metal plates. These plates (Fig. 3) are clamped between the teeth of the anode cap 8 and the tip 9. The latter can be moved by means of the knurled collar 10. Unscrewing the collar frees the anticathode; screwing it down clamps

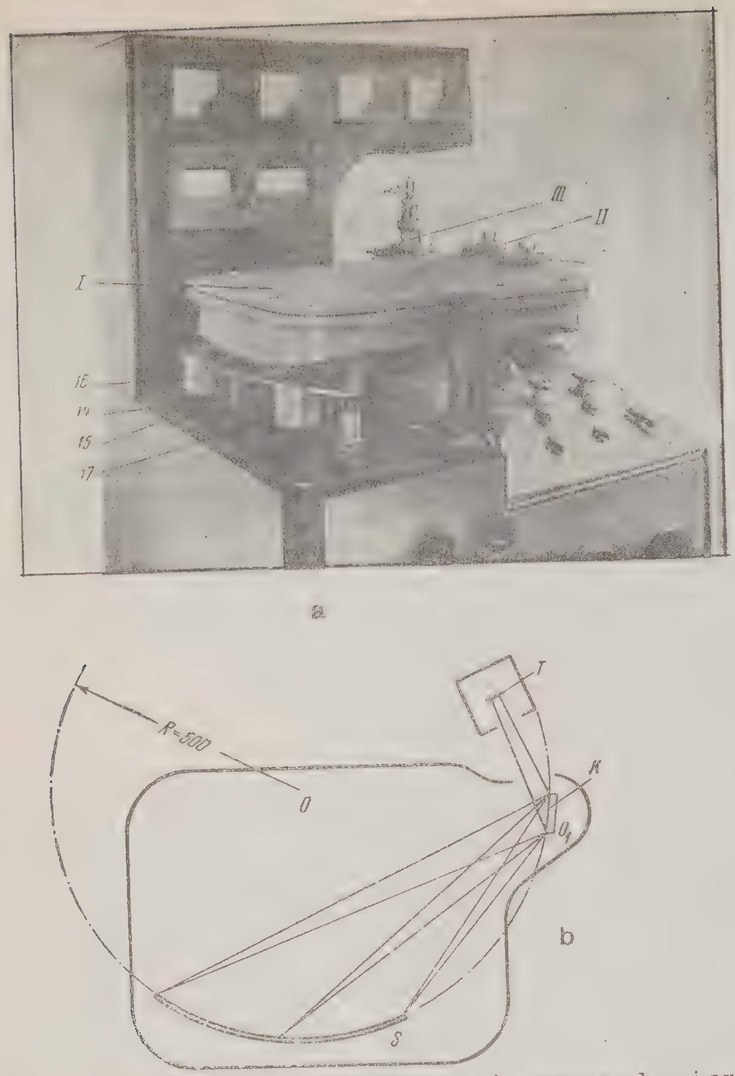

Fig. 1. RSD-2 Spectrograph: a) general view, b) diagram

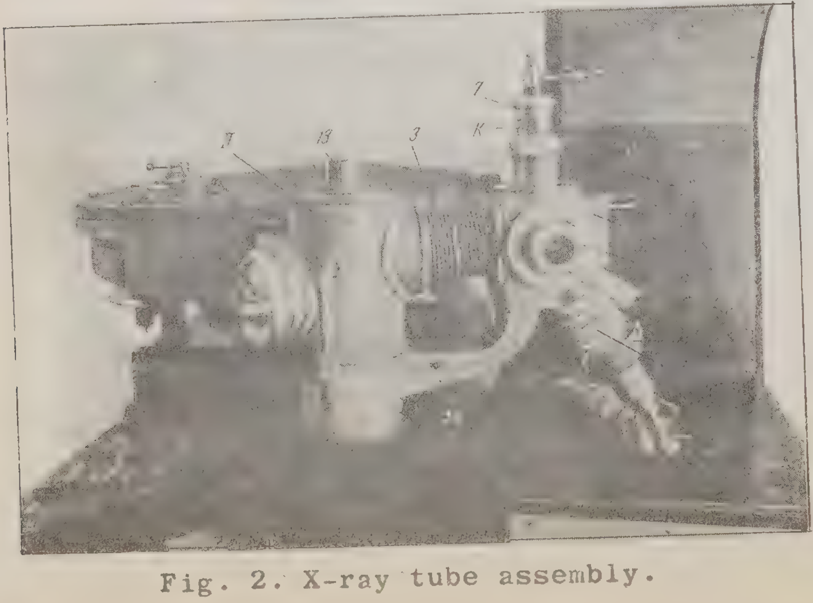

Fig. 2. X-ray tube assembly.

the anticathode against the teeth of the anode cup. Hence, the height of the anticathode in a working position, regardless of wear and erosion, is always determined only by the location of the teeth of the anode cup, the position of which therefore need only be adjusted once and for all. The cooling of the anticathode is accomplished by heat conduction through the tip 9 which is water cooled. The cathode K and cover B are attached to the tube casing by means of iris-type latches operated by levers (12 in Fig. 2).

As was noted above the casing of the x-ray tube is connected to the central chamber II by means of a sylphon. The wall of the x-rays as well as a sleeve for connecting the vacuum line. The shape and size of the focal spot are observed through the viewing tube 13 (Fig. 2) mounted on the cover of chamber II.

The x-ray tube assembly is mounted on the arm 14, rotating about the vertical axis of the central chamber II. The other end of the arm serves as an angle indicator the angles being read on scale 15 (Fig. 1,a). The limiting stops 16 and 17 serve to set the rocking interval; pressure of the end of arm 14 actuates mercury switches, mounted in the limiting stops, reversing the rocking mechanism. In this manner the rocking of the x-ray tube relative to the crystal is made automatic in the set angular interval.

The arm 14 is rotated about its vertical axis by means of a cam, driven by a motor through an appropriate worm gear and Cardan shaft linkage. The rocking cam assembly is designed so that the angular motion is non-uniform, i.e., dependent on the reflection angle.

It may be worth dwelling briefly upon the reason for this non-uniform rocking motion. In a focusing x-ray spectrograph of conventional design, in order to maintain a constant intensity over the entire working range of reflection angles one must maintain an optimum relation between the dimensions of the focus and the size of the crystal, i.e., vary the size of the focal spot in an appropriate manner. In working with a spectrograph having a constant focus x-ray tube the intensity of the x-ray lines will decrease as the reflection angle is increased. Let us turn to the simple diagram of a spectrograph shown in Fig. 4: K is the crystal bent along the circumference of a cylinder of radius R, θ is the angle of reflection, P is the x-ray source and F is the image of the source. It is known that in order to obtain the image of a monochromatic point source by means of a crystal bent in this manner both the source and image must be on the circumference of a circle having a radius equal to half the radius of curvature of the crystal. For a point source the conditions for constant intensity of the source for each of the spectral lines in the investigated narrow wavelength interval are fulfilled automatically. However, for a number of reasons and primarily to enhance the useful radiation energy, it is necessary in practice to use a focus of finite size, which is located inside the image circle and is equivalent to an imaginary source of enhanced luminosity on the circle PKF.

It can readily be seen that for a given length of the exposed section of the crystal the condition for identical source intensity for each of the spectral lines is fulfilled only provided the quantity

$$d\omega = \frac{S_\theta}{(r - a)^2}$$

or what amounts to the same thing, the ratio

$$\frac{S_\theta}{(\sin\theta - a/R)^2}$$

remains constant in the selected interval of reflection angles. In the above expressions a is the distance between the crystal and the focus of the x-ray tube and therefore constant for a given instrument, $r = R \sin\theta$ and S_θ is the optimal size of the focal spot for the given reflection angle.

The aforesaid means that to provide identical exposure conditions for different lines in a given range of reflection angles the size of the focal spot in a Johanson spectrograph must be varied according to a trigonometric law (i.e., cannot remain constant as is the case in many present day instruments). Failure to provide the necessary variation results in a non-uniform sensitivity, that is, in a decrease in sensitivity with an increasing reflection angle. In other words, in a constant focal spot Johanson spectrograph the effective section of a reflecting crystal is reduced in the sense that a proper exposure is not obtained at the greater reflection angles.

It will be seen from the above expressions that the intensity of the spectral lines at small values of a/R (other conditions being equal) will fall off with increasing θ approximately as $1/\sin^2\theta$. In a general case, if a/R is sufficiently large the attenuation in line intensity as a function of the angle obeys a somewhat more complex law. The above theoretical analysis is substantiated by experiment.

It follows from what has been said above that:

1. For any given value of the effective section of the crystal in a Johanson spectrograph (in which the source is not on the image circle and is of finite dimensions) there is a certain optimum size of the focal spot for each reflection angle.
2. The optimum size of the focal spot varies (in the first approximation) as $1/\sin^2\theta$ and in general depends on the parameters of the instrument.
3. In working with a spectrograph having a constant focus x-ray tube the intensity of the x-ray lines will decrease with increasing reflection angle.
4. For the purpose of obtaining a uniform sensitivity response when using a Johanson type spectrograph it is expedient to vary the rocking rate of the tube in such a manner that the exposure time at each reflecting position will be proportional to $(\sin\theta - a/R)^2$.

B. Crystal Holder and Crystal

The crystal and crystal holder of the RSD-2 spectrograph are shown in Figs. 5 and 6. The main part of the crystal holder is a glass segment whose concave cylindrical surface is formed to optical-precision standards. Both the face of the crystal holder and the crystal proper, which is mounted in optical contact with the holder, were ground and polished on a device especially designed and built for this purpose. The radius of the curvature of the cylindrical surface of the crystal holder is 500 mm. The oriented quartz plate used as an analyzer in the instrument, in accordance with the Johanson method, was first ground on both sides to a radius of 1000 mm. Hence the radius of curvature of the bent crystal used in the RSD-2 spectrograph is twice that in instruments produced in the past by the experimental mechanical plant of the Petroleum Institute of the Academy of Sciences. This together with the focusing conditions utilized assures an appreciably greater dispersion and resolving power as compared with earlier spectrographs of this type. A further increase in the dispersion and resolution was obtained by cutting the surface of the crystal on an oblique angle relative to its reflecting planes (after Protopopov[4]). The crystal plate used in the described holder was cut so that the crystallographic planes $(10\bar{1}0)$ utilized for reflection would be at an angle of 10° to the tangent at the center of the plate. The dimensions of the effective (working) surface of the bent crystal are 10 x 50 mm.

In addition to the above-described "forced deflection" crystal

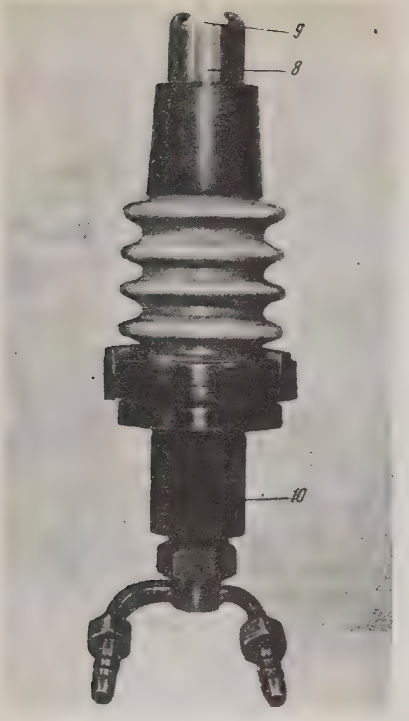

Fig. 3. Anode

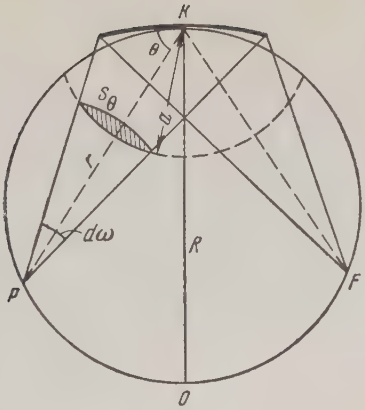
K
θ
S_θ
α
r
dω
R
P
F
O

Fig. 4.

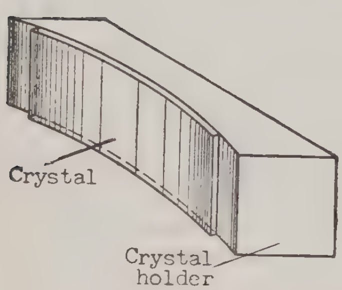
Crystal
Crystal holder

Fig. 5. Glass segment crystal holder.

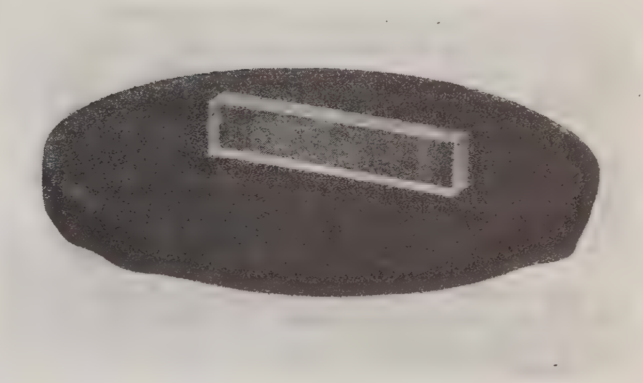

Fig. 6. Crystal holder with crystal mounted in optical contact.

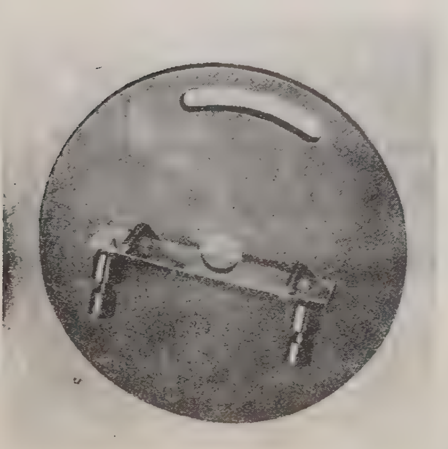

Fig. 7. Four-support crystal holder.

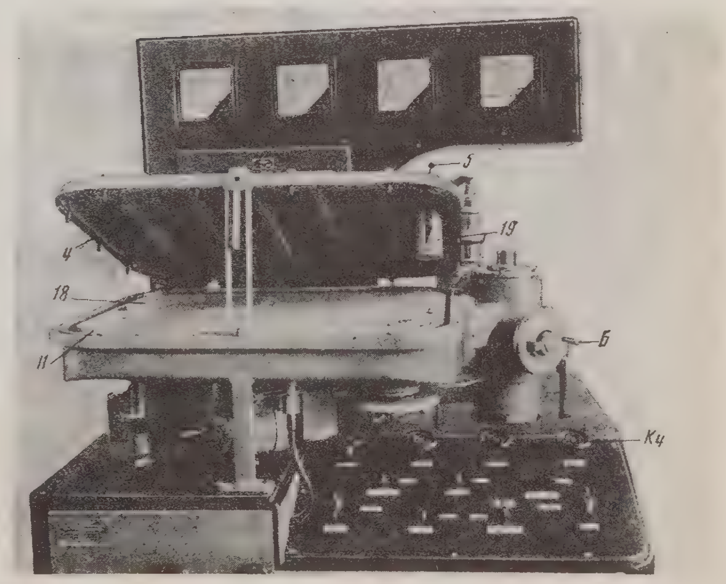
5
19
4
18
11
6
Ky

Fig. 8. Spectrograph with cover open.

holder (Figs. 5 and 6), we also prepared and successfully used a crystal holder with free bending of the crystal, in conformity with a design proposed some years ago by one of the present authors.[6] With this method of bending the analyzer the crystal plate is deformed on four parallel supports as shown in Fig. 7. In this case to conform with the requirements of the Johanson system it was necessary to use a quartz plateground on both sides to a radius of 1000 mm rather than a plane-parallel crystal plate. When carefully fabricated this four support holder results in an analyzer fully comparable in quality to that obtained with the optical contact crystal holder described above.

C. Film Holder and Film Feed

For the purpose of reducing the time expended on loading and removing the film from the spectrograph we provided the instrument with a magazine holding an appreciable length of film, a film feed mechanism and a special cassette for extracting the exposed film. Any motion picture film having the requisite sensitivity in the 2000-5000 XE region can be used in the magazine.

For loading the instrument, the chamber cover 4 is raised and the magazine 18 removed (see Fig. 8). The magazine is loaded with motion picture film in a dark room, and then replaced in the chamber. The end of the film is threaded into the feed drum and the cover closed and locked. The film is fed into cassette 19 by actuating an external control. The exposed film is cut off by a knife operated by handle 5. The feeding and cutting operations can be performed in full daylight.

The arc of the film holder 11, extending along the focal circle, has two slots. The upper slot serves for the passage of the defracted rays; the lower slot is covered by a transparent wavelength scale. Behind this is a small lamp which is turned on for an instant to print the wavelength scale on the film. Impressing the scale directly on the spectrogram greatly facilitates subsequent interpretation of the spectrum.

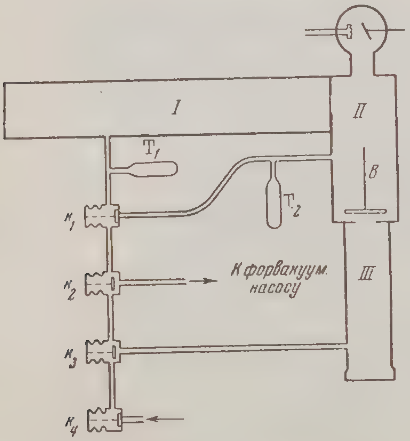

Fig. 9. Vacuum system of the spectrograph: I) housing, II) central chamber, III) high-vacuum pump, B) high-vacuum valve, T_1) and T_2) manometric type LG-2 tubes, K_1-K_4) valves.

D. Vacuum System and Auxiliary Equipment

The vacuum system consists of a forepump, a high-vacuum oil pump, four valves and the appropriate fittings and metal tubing. The vacuum installation is diagramed in Fig. 9.

The spectrograph operates on the "divided vacuum" principle, i.e., a forevacuum is maintained in the spectrograph housing while a high-vacuum is maintained only in the central chamber II and in the x-ray tube. There is a divider of black paper installed between the central chamber and the housing. The "divided vacuum" arrangement has proved satisfactory; it simplifies the problem of maintaining a high-vacuum in the x-ray tube and yet does not introduce any additional undesirable absorption losses. The instrument is equipped with a thermoelectric vacuum gauge with two sensing elements, one of which measures the vacuum in the central chamber, the other the vacuum in the housing I.

The electric equipment consists of the high-voltage supply unit (comprising a high-voltage transformer), a filament supply transformer and two kenotrons. The high-voltage unit is housed in an iron tank filled with transformer oil and located in the back part of the instrument stand. The potentiometers controlling the high-voltage and the filament voltage are mounted in the front part of the stand. The equipment provides for operation at voltages up to 30 kv and current values up to 60 ma.

Institute of Crystallography,
Institute of Geological Sciences and
Institute of Geochemistry and Analytic Chemistry
of the
Academy of Sciences of the USSR

REFERENCES

1. E.E.Vainshtein, K.I.Narbutt & A.B.Gil'varg, Trudy In-ta kristallographii, (Proceedings of the Institute of Crystallography) 6, 206 (1951).
2. K.I.Narbutt, A.B.Gil'varg, E.E.Vainshtein & L.M.Beliaev, Zavodsk. labor., (Factory Laboratory), 17, 1425 (1951).
3. K.I.Narbutt, Inventor certificate No. 443615/1992, 1952.
4. V.Protopopov, Zavodsk. labor. (Factory Laboratory), 14, 196 (1948).
5. T.Johanson, Zs. f. Phys. 82, 507 (1933).
6. A.B.Gil'varg, Doklady AN SSSR, 72, 489 (1950).

Bulletin of the Academy of Sciences of the USSR - Physical Series
Volume 20, Number 1, 1955

Table of Contents

Transactions of the Third All-Union Conference on the Physics of Cosmic Rays
(Continued from Vol. 19, Nos. 5 & 6)

	Page Orig.	Page Trans.
On the origin of cosmic rays - V.L.Ginzburg	5	1
On the spectrum of primary protons - Ia.P.Terletski	17	12
Diffusion and acceleration of charged particles in a magnetized interstellar medium - A.A.Logunov & Ia.P.Terletski	22	17
On the nature of the variation of cosmic rays - L.I.Dorman	24	19
Some results of an investigation of the variations in the hard component of cosmic rays - E.S.Glokova	47	41
Variation in the intensity of cosmic radiation at high altitudes - Iu.I.Logachev & Iu.G.Shafer	55	48
Closing address - S.N.Vernov	59	51

Proceedings of the Meeting of the Department of Physical-Mathematical Sciences
of the USSR Academy of Sciences (Moscow, 26-27 April 1955)
(SESSION ON SEMICONDUCTORS)

	Page Orig.	Page Trans.
Opening address - A.F.Ioffe	63	52
Thermal conduction in semiconductors - A.V.Ioffe & A.F.Ioffe	65	55
Thermoelectric generators - A.F.Ioffe	76	66
Thermoelectric cooling (Peltier Effect) - L.S.Stil'bans, E.K.Iordanishvili & T.S.Stavitskaia	81	71
Exciton excitation spectrum in solids - E.F.Gross	89	78

Transactions of the Conference on X-Ray Spectroscopy
(Moscow, 25-26 January 1955)

	Page Orig.	Page Trans.
Investigation of the x-ray spectra of alloys of the Mn-Ni system - V.A.Kazantsev	107	97
On the absorption and emission of x-rays by ferromagnetic metals - A.V.Sokolov	113	103
On the structure of x-ray emission lines of ions in solution - K.I.Narbutt	118	107
An x-ray tube for spectrum analysis - V.A.Kazantsev	122	111
Selection of optimum specimen density for the investigation of x-ray absorption spectra - M.A.Blokhin & A.N.Gusatinski	125	113
X-ray spectra and the electronic structure of thorium in $Th(NO_3)_4$ and ThO_2 - R.L.Barinski	133	120
A high-energy sealed-off x-ray tube for spectrum analysis - K.I.Narbutt & E.M.Fridman	136	123
Investigation of the distribution of the density of electronic states in a solid and the width of the internal atomic levels - M.A.Blokhin	142	127
The new RSD-2 x-ray vacuum spectrograph - K.I.Narbutt, E.E. Vainshtein, A.B.Gil'varg & L.M.Beliaev	152	138

Translated in 1956 by
Columbia Technical Translations
5 Vermont Ave., White Plains, N.Y.

Reprinted in 1960

Number 2 Volume 20 1956

BULLETIN

# of the

Academy of Sciences of the USSR

- Physical Series -

(Izvestiia Akademii Nauk SSSR)
(Seriia fizicheskaia)

Reproduction rights reserved

by

Columbia Technical Translations
5 Vermont Avenue
White Plains, New York

Single Issues

$20

Annual Subscription

$215

Transactions of the Second Conference on Piezoelectricity
(Moscow, 26-29 April 1955)

NEW FERROELECTRICS AND ANTIFERROELECTRICS OF THE OXY-OCTAHEDRAL TYPE

- G.A.Smolenski

In recent years there has been a great increase of interest in ferroelectrics: crystals in which there occur phase transitions of the first or second order from the disordered to the ordered polarized state at a certain temperature.

The discovery by Vul and Gol'dman of ferroelectric properties in barium titanate, which crystallizes in a simple perovskite lattice and is characterized by good mechanical strength and thermal stability, played an important part in the development of our concepts concerning ferroelectric effects and in fact has served as the basis of many investigations of ceramic ferroelectrics and led to the development of a new group of ceramic materials.

For some time after the discovery of the ferroelectric properties of barium titanate it was thought that $BaTiO_3$ is the only ferroelectric material among crystals with perovskite structure since the separation between the Ti and O ions in the barium titanate lattice is greater than the sum of their radii. It was shown in 1948-1950, however, that $BaTiO_3$ is only one of many ferroelectrics with a perovskite structure. At present we know of a number of new ferroelectric substances crystallizing with the structure of perovskite, ilmenite, pyrochlore and rhenium trioxide. Recently antiferroelectrics with a perovskite structure have been discovered. In antiferroelectrics the ions are aligned so that the net spontaneous polarization equals zero.

All these ferroelectrics and antiferroelectrics are characterized by a structure in which the oxygen ions surrounding the smaller cation form an octahedron, hence one may logically call them ferroelectrics and antiferroelectrics of the oxy-octahedral type.

1. Ferroelectric Properties of the Titanates of Bivalent Metals (Sr, Cd and Pb)

A. Rushman and Streivens[1] by extrapolating the curve expressing the dependence of the Curie point of (Ba-Sr) TiO_3 solid solutions, which have a perovskite structure, on the strontium titanate concentration showed that $SrTiO_3$ is in all probability a ferroelectric with a Curie point at 15-35°K. However, no fully convincing proof of ferroelectric properties was given. The variation of the Curie point of the investigated solid solutions with the $SrTiO_3$ concentration at high concentrations is not linear, consequently extrapolation in this region could lead to an erroneous deduction. In view of this it appeared desirable to investigate the properties of strontium titanate at very low temperatures. We carried out such an investigation in 1949.[2,3] We studied two specimens of polycrystalline strontium titanate, prepared from chemically pure grades of titanium dioxide and strontium carbonate and sintered at 1460-1500° (held 3 hours at a maximum temperature). The dielectric constant of the specimens at room temperature attained 275. The temperature dependence of the dielectric constant of one $SrTiO_3$ specimen is shown in Fig. 1; it will be seen that the curve has a maximum. In addition clear hysteresis loops were obtained at low temperatures. From this we concluded that strontium titanate with perovskite structure is a ferroelectric with a Curie point between 20-30°K. We did not succeed in determining the exact Curie point. The measurements were made only at the normal boiling points and the triple points of nitrogen and hydrogen and

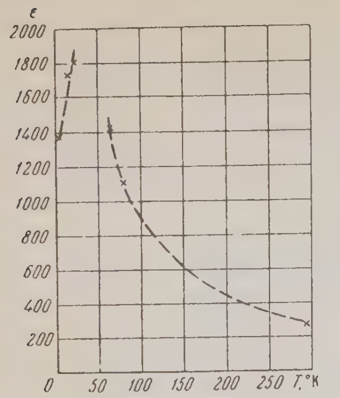

Fig. 1. Temperature dependence of the initial dielectric constant of a sample of strontium titanate (f = 10^6 cps).

at the temperature of boiling of helium at normal and reduced pressure.

Subsequent investigations of $SrTiO_3$, carried out by V.I.Odelevski, also showed that the dielectric constant as a function of the temperature has a peak at about 30°K. In 1950 Hulm[4] published a communication in which he asserted that strontium titanate is not ferroelectric. Hulm prepared his samples of sufficiently pure grades of strontium carbonate and titanium dioxide and sintered them for 3 hours at 1400°. Apparently, however, Hulm's specimens had an appreciable porosity and consequently their dielectric constant at low temperatures did not exceed 1300.

This difference in results can be understood if we allow for the fact that the Curie point in ferroelectrics depends on the impurities present and on the firing procedure employed. Thus, for example, the Curie point of different samples of barium titanate varies over an appreciable range (70-130°). Inasmuch as the Curie point of $SrTiO_3$ is rather close to absolute zero, it is entirely possible that spontaneous polarization fails to develop in some samples. In view of this it would be expedient to investigate at very low temperatures a series of samples of strontium titanate prepared of different raw materials and processed in different ways.

B. Early in our work we investigated polycrystalline samples of $CdTiO_3$, having an appreciable open porosity and obtained as a result of prolonged (10-25 hours) roasting at relatively low temperatures (1050-1180°). X-ray studies showed that these samples had a well-pronounced perovskite structure. Measurements of the dielectric constant of these samples at low temperatures were carried out in 1949.[2,3] The results of these measurements are shown in Fig. 2. It is obvious that the dielectric constant has a maximum in the 50-60°K temperature interval. In addition to determining the temperature dependence of the dielectric constant for a number of the cadmium titanate samples, we obtained hysteresis loops, characteristic of ferroelectrics, for a number of the samples.

On the basis of these measurements we concluded that cadmium titanate is a ferroelectric with a Curie point at 50-60°K.

Later we prepared polycrystalline specimens of cadmium titanate with a low porosity. The dielectric constant of these at room temperature attained 250. The temperature dependence of the dielectric constant of one such specimen down to 55°K is shown in Fig. 2. It will be seen that the dielectric constant increased sharply in the 55-60°K interval, which is characteristic of ferroelectrics in the vicinity of the Curie point. The Curie-Weiss constants for cadmium titanate at $T > \theta°$ proved to be appreciably smaller than in barium titanate and did not exceed 40,000-55,000°K.

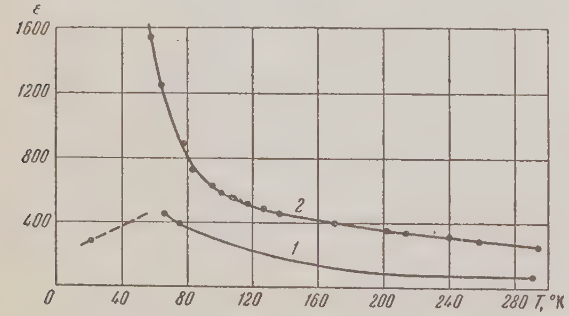

Fig. 2. Temperature dependence of the initial dielectric constant of cadmium titanate at 10^6 cps: 1) sample sintered at 1100°; 2) sample sintered at 1300°.

It is important to remember in sintering cadmium titanate that it undergoes thermal dissociation at high temperatures with resultant impairment of the lattice. Hence, specimens sintered at excessively high temperatures show weak or no ferroelectric properties. In this connection it may be noted that Matthias[5] also investigated $CdTiO_3$ but failed to detect ferroelectric properties in his specimens. In all probability this was because he used specimens with a deformed lattice obtained as a result of sintering at excessively high temperatures. In 1952, Odelevski confirmed our conclusions regarding the ferroelectric characteristics of cadmium titanate.

C. In an early investigation[1] of ferroelectrics with perovskite structure it was shown that the Curie point and the tetragonality of the unit cells in solid solutions of lead titanate in barium titanate increase with increasing $PbTiO_3$ concentration. On the basis of these data one may assume that lead titanate is a ferroelectric with a high Curie point. This was first suggested by Jonker and van Santen[6] who investigated the temperature dependence of the dielectric constant of $(Ba-Pb)TiO_3$ and $(Sr-Pb)TiO_3$ solid solutions. However, they did not extend their investigation to solid solutions with a high lead titanate content and to the pure material since the conductivity of lead titanate increases rapidly with the temperature. Thus it was not determined in this study whether lead titanate is or is not a ferroelectric.

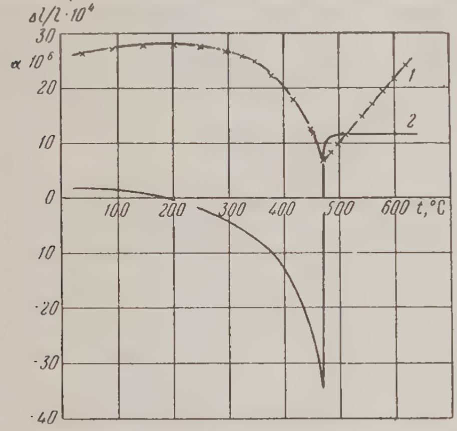

Fig. 3. Temperature dependence of the relative change in length (1) and of the coefficient of linear expansion (2) of a sample of lead titanate.

To answer this question one must establish whether the phase transition characteristic of ferroelectrics occurs in lead titanate. In investigating the temperature dependence of the linear expansion coefficient of polycrystalline lead titanate in 1948 we showed that at about 500° there occurs a phase transformation analogous to that in barium titanate. This proved that $PbTiO_3$ is a ferroelectric.[2,3,7 & 8]

The temperature dependence of the relative elongation of a sample of lead titanate is shown in Fig. 3. The temperature dependence of the coefficient of linear expansion α was determined graphically from the $\Delta l/\sqrt{l} = f(t)$ curve and is also shown in Fig. 3. The $\alpha = f(t)$ curves for lead and barium titanate are similar. Obviously their anomalous shape is due to the fact that in heating both the volume and the linear dimensions of a ferroelectric change not only due to the usual thermal dilation but also because of deformations connected with the decrease in spontaneous polarization. The volume of the specimen may decrease due to decreasing spontaneous polarization as in the present case (positive volumetric electrostriction) or it may increase (negative electrostriction).

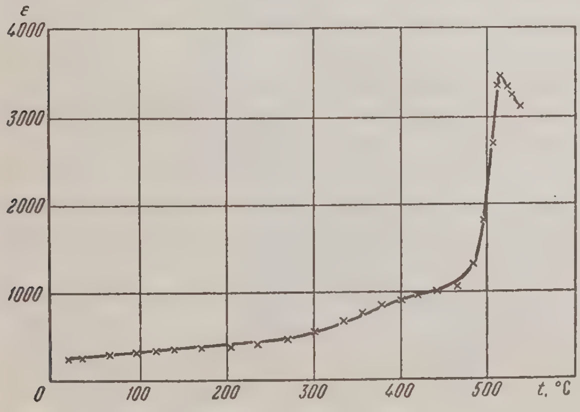

Fig. 4. Temperature dependence of the initial dielectric constant of a lead titanate specimen prepared with a mineralizer (2% boron oxide) (f = 10^6 cps).

Later we prepared samples of lead titanate with a mineralizer. These samples had a lower conductivity at high temperatures and lower porosity. The temperature dependence of the dielectric constant of a lead titanate specimen prepared with boron oxide

(2% by weight) and sintered for 4.5 hours at 1080° is shown in Fig. 4.

Our conclusion that lead titanate is a ferroelectric was confirmed by subsequent investigations. In the investigations of Shirane et al[9-11] it was established that a phase transition occurs at about 500°. Above 500° the crystal has a cubic structure; below 500° a tetragonal one.[9] In lead titanate, as in barium titanate, there is elongation along one axis (c) which apparently becomes the polar axis and contraction along the other two axes. The phase transition energy in lead titanate is appreciably greater (1150 cal/mol) than in barium titanate.[10] The temperature dependences of the linear expansion coefficient and the dielectric constant, according to the data of Shirane and Hoshino[11], are similar to those found in our investigations (Figs. 3 & 4).

In contrast to the case of barium titanate no low temperature phase transitions are observed in lead titanate down to −195° (see Fig. 3).

A single crystal of barium titanate was grown and investigated by Beliaev and Khodakov.[12] Recently Fesenko succeeded in detecting a domain network in lead titanium single crystals.[13]

In investigating lead titanate we did not succeed in observing hysteresis loops. This is explained by the fact that at high temperatures the conductivity of the specimens is rather high; at low temperatures (remote from the transition temperature) the domains are no longer reoriented in attainable fields.

2. Phase Transitions in Lead Zirconate

We first observed phase transitions in lead zirconate in 1948.[2,7,8] The first lead zirconate specimens, prepared of technical grade zirconium dioxide, were sintered at a relatively low temperature (1000–1100°) for periods of up to 24 hours. As a result there were obtained rather porous specimens with a dielectric constant of about 25 at room temperature and about 260 at the transition temperature. Later we prepared better polycrystalline specimens of lead zirconate; these were also prepared of the technical grade dioxide but were fired in an atmosphere of lead oxide and as a result had virtually no open porosity.[3] The temperature dependence of the dielectric constant of one of these specimens is shown in Fig. 5. The Curie-Weiss law

$$\varepsilon = \frac{C_w}{T - \theta'} = \frac{1{,}15 \cdot 10^5}{T - 228}$$

holds above the transition point.

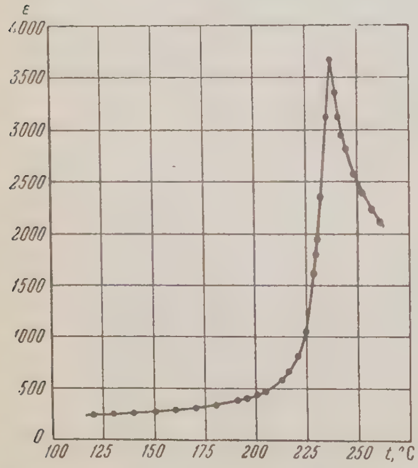

Fig. 5. Temperature dependence of the dielectric constant of a lead zirconate constant sintered in a lead oxide atmosphere ($f = 10^6$ cps).

A phase transition has also been observed in lead zirconate by Roberts.[14]

With decreasing temperature the total polarization in lead zirconate increases at first and then falls off (Fig. 6). As the temperature is decreased the hysteresis loops become increasingly flatter and "degenerate". The spontaneous polarization in lead zirconate attains about $18 \cdot 10^6$ coulomb/cm², which is twice as high as the spontaneous polarization in barium titanate. The above value of the spontaneous polarization must be regarded as only a rough approximation since the maximum of the total polarization is observed at temperatures close to the phase transition points.

For some lead zirconium specimens the hysteresis loops at 200–220° have the shape characteristic of antiferroelectrics (Fig. 7).

However, when the field intensity is increased the loops assume the shape common to ferroelectrics. As the field is decreased the hysteresis loops again narrow down. This effect is reproduced in repeated heating and cooling. The distortion of the hysteresis loops is apparently due to antiparallel arrangement of the domains. We base this deduction on the fact that at high field intensities the hysteresis loops assume the shape usual for ferroelectrics. In this case the polarization processes are characterized by an appreciable relaxation time, which apparently is necessary for the reorientation of the domains.

Interesting results were obtained in studying the temperature dependence of the expansion coefficient of lead zirconate.[8] These are shown in Fig. 8, from which it will be seen that in lead zirconate prepared from technical grade raw materials there are two close temperature transitions: the first, at the higher temperature, is accompanied by positive spontaneous volume electrostriction; the second, by appreciable negative electrostriction. It should be noted

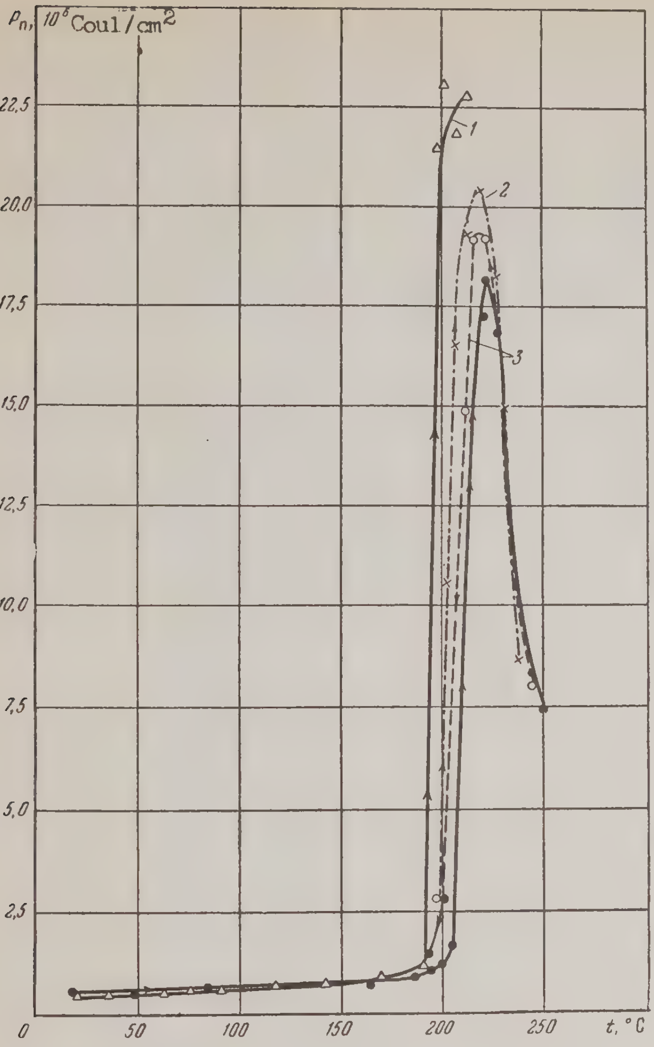

Fig. 6. Temperature dependence of the total polarization of some specimens of lead zirconate at different field intensities (in kv/cm): 1) E = 19.7; 2) E = 23.6; 3) E = 21.2.

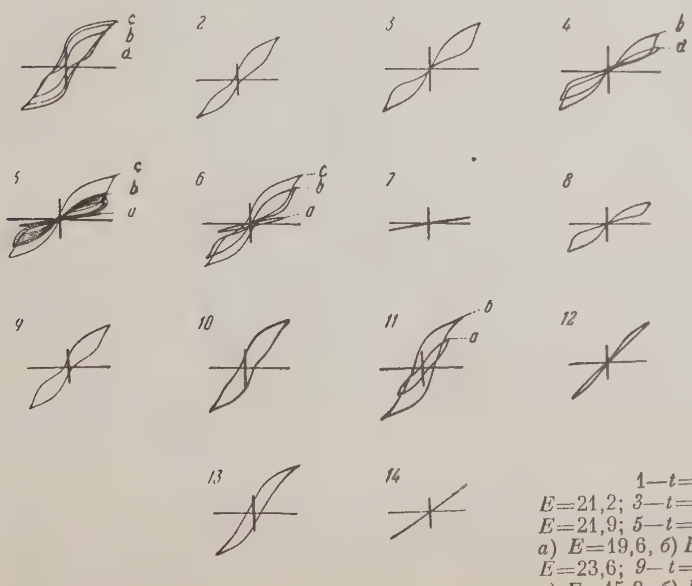

Fig. 7. Hysteresis loops of one of the lead zirconate specimens at different temperatures (°C) and different field intensities (kv/cm):

1—$t=212,5^\circ$, а) $E=21,2$, б) $E=24,7$, в) $E=28,3$; 2—$t=213,5^\circ$, $E=21,2$; 3—$t=206,5^\circ$, $E=21,90$; 4—а) $t=203,5^\circ$, $E=21,9$; б) $t=204,5^\circ$, $E=21,9$; 5—$t=198,5^\circ$, а) $E=22,1$, б) $E=25,9$, в) $E=28,3$; 6—$t=202,5^\circ$, а) $E=19,6$, б) $E=25,4$; в) $E=28,3$; 7—$t=199,5^\circ$, $E=23,6$; 8—$t=202,5^\circ$, $E=23,6$; 9—$t=208,5^\circ$, $E=23,6$; 10—$t=213,5^\circ$, $E=23,6$; 11—$t=220,5^\circ$, а) $E=15,8$, б) $E=23,6$; 12—$t=232,5^\circ$, $E=23,6$; 13—$t=228,5^\circ$, $E=23,6$; 14—$t=238^\circ$, $E=23,6$

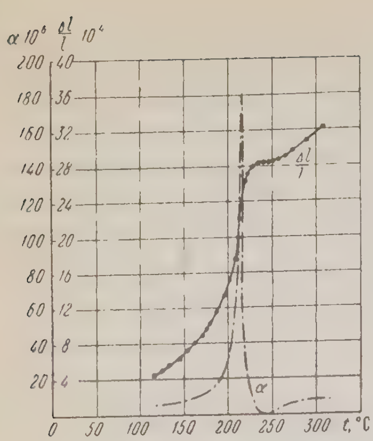

Fig. 8. Temperature dependence of the relative change in length $\Delta l/l$ and the linear expansion coefficient α of a specimen of lead zirconate prepared of technical grade materials.

that hysteresis loops were observed only in the interval between the two transitions. In lead zirconate with a minimum impurity content there is observed only one phase transition and no hysteresis loops are apparent.[15] However, in cooling the phase transition in pure lead zirconate separates into two distinct transitions and an inflection point appears in the $\varepsilon(T)$ curve.[16] Apparently supercooling is more pronounced at the second (lower temperature) transition. This assumption is substantiated by the case of barium titanate.

The transition in pure lead zirconate from the polarized to the non-polarized state is probably a first order transition. This conclusion is supported by the appreciable electrostriction, the rather high transition energy (440 cal/mol),[17] the sharp change in the dielectric constant and its temperature hysteresis (4°) at the transition point and by the linear dependence of the polarization on the field intensity above the transition point.

Roberts[18] determined the piezoelectric modulus (constant) d_{33} of lead zirconate; its value at room temperatures is very small, some 2–3 orders smaller than for barium titanate. We obtained analogous results.[3]

In order to clarify the nature of the phase transitions in lead zirconate a number of solid solutions containing it were investigated: $(Pb\text{-}Ba)ZrO_3$, $(Pb\text{-}Ba)(Zr\text{-}Ti)O_3$, $(Sr\text{-}Pb)ZrO_3$ and $Pb(Ti\text{-}Zr)O_3$.

Shirane, on the basis of experimental data, suggests that lead zirconate with a minimal impurity content is an antiferroelectric.[17,19–23] In addition Shirane is of the opinion that the low temperature, polarized phase in the solid solutions $(Pb\text{-}Ba)ZrO_3$ and $Pb(Zr\text{-}Ti)O_3$ is antiferroelectric, while in the solid solutions $(Pb\text{-}Sr)TiO_3$ both polarized phases are antiferroelectric. Shirane notes the following characteristics of lead zirconate and the corresponding phases of its solid solutions: 1) the absence of hysteresis loops, 2) the presence of superstructure (unit cell 4a x 4a x c), 3) decrease in the volume of the crystal incident to cooling at the transition point (negative volume electrostriction), 4) displacement of the transition point into the region of lower temperatures under the influence of a biasing dc field, 5) increase in the reversible permittivity in the region of the phase transition, 6) anomalous (for ferroelectrics) hysteresis loops at high field intensities and 7) the absence of a discharge current in the region of the phase transition when a specimen to which a dc voltage has been previously applied is heated. On the basis of x-ray studies Shirane states that there is an antiparallel displacement of the lead ions in lead zirconate.

It is possible that there is an antiparallel ion shift in lead zirconate. However, it still remains unclear why the volume electrostriction is negative, why the period of the superstructure lines is 4a rather than 2a and why a piezoelectric effect is observed.

It may be noted that the absence of hysteresis loops and a number of the other peculiarities of lead zirconate can also be explained by assuming that the transition in it is a first order transition in which the domains are not oriented in attainable fields.

The superstructure lines appearing in x-ray spectrograms of lead zirconate can also be explained by assuming that the zirconate ions are shifted simul-

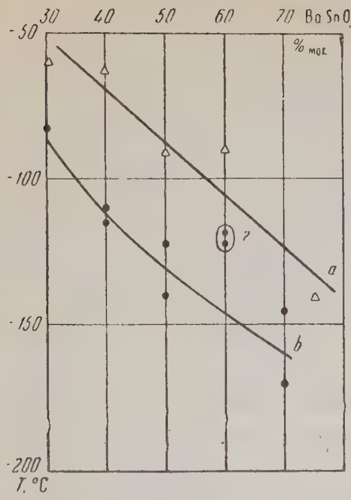

Fig. 9. Variation of the temperature of the maximum dielectric constant of (Ba-Pb)SnO_3 solid solutions with the barium stannate concentration: a) first lot of samples sintered at 1120-1150° for 1 hour; b) second lot of samples prepared with mineralizer (2% H_2SiO_3) fired to 1120-1150° but not held at the peak temperature for any length of time.

taneously towards 2 or 3 oxygen ions along 4 or 6 nonorthogonal axes.[20] In the direction of the net spontaneous polarization the dipole moments of the unit cells arrange themselves in a herringbone pattern in the domains. The observed negative volume electrostriction is apparently due to deformations connected with the ion shift.

Recently single crystals of lead zirconate were successfully grown.[24] Optical studies of the single crystals showed that there is an appreciable difference between the domain structures of barium titanate and lead zirconate.

3. Ferroelectric Properties of (Ba-Pb)SnO_3 Solid Solutions

Unlike lead zirconate and titanate, lead stannate does not exist as an independent chemical compound.[25,26] However, with a certain concentration (not less than 30%) of barium stannate one can obtain (Ba-Pb)SnO_3 solid solutions with a perovskite structure.[27]

The temperatures corresponding to maximum values of the dielectric constant in the specimens of two batches of (Ba-Pb)SnO_3 solid solutions, as determined from the $\varepsilon = f(t)$ curves, are shown in Fig. 9. The phase transition temperature, i.e., the temperature of the maximum dielectric constant, decreases with increasing concentration of barium stannate, which is not a ferroelectric. As may be seen in Fig. 9 there is an appreciable scattering of the data for different samples. This is largely explained by the complexity of the process of preparing specimens containing lead ions.

In the region of temperatures corresponding to the maximum values of the dielectric constant there occurs a change in the linear expansion coefficient, which is further indication of

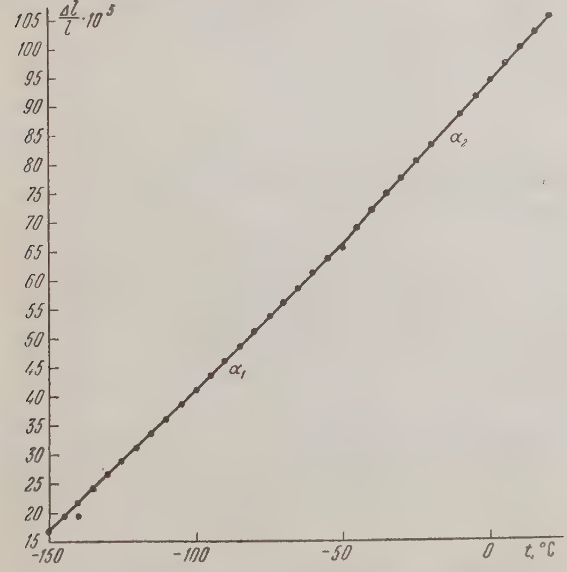

Fig. 10. Temperature dependence of the relative change in length for specimens of the first lot of the ($Ba_{0.3}$-$Pb_{0.7}$) SnO_3 solution ($\alpha_1 = 5.1 \cdot 10^{-6}$ degree^{-1}; $\alpha_2 = 5.6 \cdot 10^{-6}$ degree^{-1}).

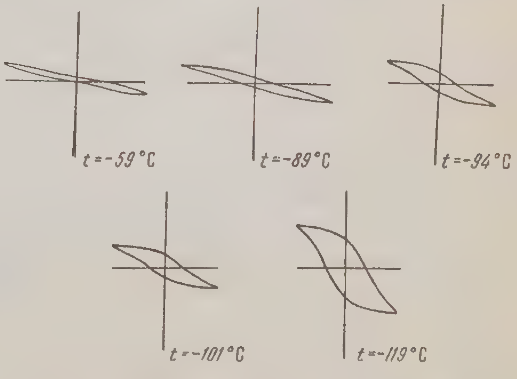

Fig. 11. Hysteresis loops in ($Ba_{0.3}$-$Pb_{0.7}$)SnO_3 specimen with a biasing field of 25 kv/cm at different temperatures.

the occurrence of a phase transition (Fig. 10). True, as in the number of other solid solutions, this transition is "smeared out".

The hysteresis loops obtained in investigating the $(Ba_{0.3}-Pb_{0.7})SnO_3$ solid solution are shown in Fig. 11. The spontaneous polarization of the solid solution at -119° attains $12.8 \cdot 10^{-6}$ coulomb/cm^2. The loops for some specimens were distinctly narrowed in the middle.

4. Ferroelectric Properties of Lead Metatantalate

We have previously shown that one can expect spontaneous polarization to appear at a certain temperature in compounds of the ANb_2O_6 and ATa_2O_6 type.[28] Recently Goodman[29] found that $PbNb_2O_6$ is a ferroelectric with a transition point at 570°. Hence it was natural to expect the manifestation of ferroelectricity in lead tantalate as well.

The temperature dependences of the dielectric constant and the dielectric loss tangent in weak fields observed in lead tantalate are shown in Fig. 12. The transition from the non-polarized to the polarized state occurs at 260°.[30] The hysteresis loops are shown in Fig. 13. The spontaneous polarization of lead tantalate is about $2.5 \cdot 10^{-6}$ coulomb/cm^2.

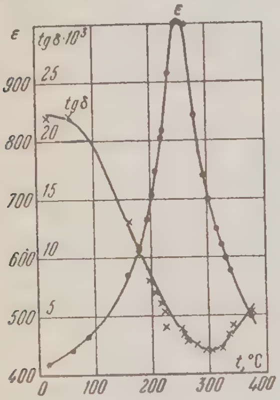

Fig. 12. Temperature dependences of the dielectric constant and the dielectric loss tangent in lead tantalate (f = 10^6 cps.).

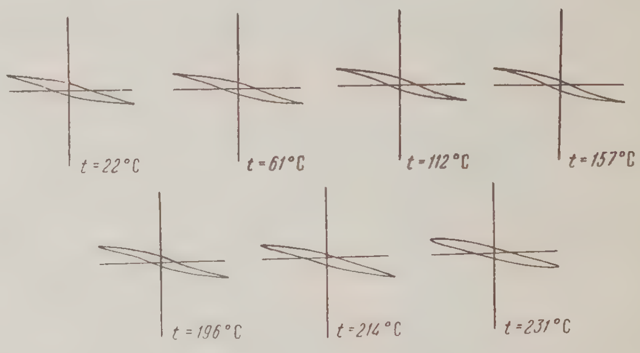

Fig. 13. Hysteresis loops in lead tantalate with a biasing field of 25 kv/cm at different temperatures.

5. Conditions for the Existence of Spontaneous Polarization and the Nature of a High Permittivity

Other investigators have detected ferroelectric and antiferroelectric properties in the number of compounds in addition to those discussed above.

Data on the phase transition temperatures, the structure and the lattice parameters of a number of new ferroelectrics and antiferroelectrics are listed in Table 1. Antiparallel displacement of the metal ions is observed in $PbZrO_3$, $PbHfO_3$, $NaNbO_3$ and WO_3.

We can draw the following deductions from an examination of the properties and behavior of the known ferroelectrics and the antiferroelectrics: all known ferroelectrics crystallize in a structure in which comparatively small cations, having a large charge, are octahedrally surrounded by oxygen ions; the cations inside the oxygen octahedron, i.e., the central ions, have the structure of a noble gas atom after removal of the s- and d-electrons; ions of this type are formed from atoms with an unfilled next-to-the-last shell.[28] It should be noted that the bonds between the oxygen ions and the central ion are not purely ionic but more or less intermediate in character. Hence, some of the electrons are shared.

Table 1

Chemical formula	Structure	Lattice parameters, A (at 20°C)	Transition temperatures, °C
$BaTiO_3$	Perovskite		120, 0, —70
$SrTiO_3$	»	$a = 3,897$	—250?
$CdTiO_3$	»	$a = c = 3,784$, $b = 3,800$, $\beta = 91°10'$	—210
$PbTiO_3$	»	$a = 3,896$, $c/a = 1,063$	500
$PbZrO_3$	»	$a = 4,150$, $c/a = 0,998$	235
$(Ba, Pb)\ SnO_3$	»		
$NaTaO_3$	»	$a = 5,5239$, $b = 3,8831$, $c = 5,4778$	475?
$KTaO_3$	»	$a = 3.9885$	—260
$NaNbO_3$	»	$a = 2 \times 3,921$, $b = 4 \times 3,885$, $\beta = 90°40'$ $c = 2 \times 3,921$	640, 480, 360
$KNbO_3$	»	$a = 4,045$, $b = 3,984$, $\beta = 90°21'$ $c = 4,045$	435, 225, —10
$PbHfO_3$	»	$a = 4,136$, $c/a = 0,91$	215, 163
$LiTaO_3$	Ilmenite ?	$a = 4,136$, $\alpha = 56°30'$	>450
$LiNbO_3$	»	$a = 5,47$, $\alpha = 55°43'$	>450
WO_3	Rhenium trioxide	$a = 7,274$, $b = 7,501$, $\beta = 89°56'$, $c = 3,824$	740?, —50
$Cd_2Nb_2O_7$	Pyrochlore	—	—90, —190
$PbNb_2O_6$		—	570
$PbTa_2O_6$		—	260
$NaVO_3$		—	380?

Crystals, the central ions of which do not satisfy the above conditions, are not ferroelectric. An example is furnished by lanthanum aluminate. The aluminum ion has the structure of a noble gas atom, a small ionic radius and a comparatively large charge, but it is formed from an atom with a filled next-to-the-last shell. Consequently, as experiments show, lanthanum aluminate with perovskite structure does not possess ferroelectric characteristics; furthermore this crystal has a relatively low dielectric constant (~ 17) which increases little with rising temperature.

Thus, on the basis of the available experimental data, we can already tentatively formulate the necessary conditions for the existence of spontaneous polarization in crystals. The only crystals that exhibit ferroelectric and antiferroelectric properties are those in which the oxygen octahedrons are wholly or in part occupied by cations having the electronic structure of a noble gas after removal of the s- and d-electrons, a large charge and a small ionic radius.

In Table 2 we list the cations with the electronic structure of a noble gas atom and the hydrogen ion together with the radii (in angstroms) for the coordination number 6. The ions with the structure of the noble gas, after removal of the s- and d-electrons from the atom, appear in the framed section of the table. The central ions of known ferroelectrics and antiferroelectrics are printed in heavy type.

As may be seen from the table the Hf^{4+}, V^{5+}, Cr^{6+}, Mo^{6+}, Mn^{7+}, Tc^{7+} and Re^{7+} ions have small radii and large charges. From this it was concluded that if there should exist crystals in which these ions occupy the oxygen octahedrons these crystals may exhibit ferroelectric attributes. In 1950 there was compiled a list of compounds, specifically of compounds of the $A(TaO_3)_2$ and $A(NbO_3)_2$ type, where A is a bivalent metal, in which one could expect spontaneous polarization at certain temperatures.

Subsequent studies of other investigators substantiated our hypothesis regarding the appearance of spontaneous polarization in crystals with a central Hf^{4+} or V^{5+} ion.[31,32]

An exception to the above is presented by certain crystals containing Pb^{2+} ions. In these crystals spontaneous polarization may appear even when the oxygen octahedrons are occupied by ions not having the electronic structure of a noble gas, for example, Sn^{4+} ions. This is apparently explained by the influence of the strongly polarizable lead ions on the nature of the bonds in these crystals. This influence also serves to explain why lead titanate has a higher Curie point than barium titanate, despite the fact that the lead ion has a smaller radius than the barium ion.

Table 2

Series	Group						
	I	II	III	IV	V	VI	VII
	Valence						
	+1	+2	+3	+4	+5	+6	+7
1	[H]						
2	Li 0,78	Be 0,31	B 0,20				
3	Na 0,98	Mg 0,76	Al 0,57	Si 0,39			
4	K 1,33	Ca 1,06	Sc 0,83	Ti 0,64	V 0,4	Cr 0,3—0,4	Mn 0,46
5	Rb 1,49	Sr 1,27	Y 1,06	Zr 0,77	Nb 0,69	Mo 0,62	Tc 0,56
6	Cs 1,65	Ba 1,43	La 1,22	Hf 0,84	Ta 0,68	W 0,62	Re
7	Fr	Ra 1,52	Ac	Th 1,20	Pa	U	

Lanthanides (+3)

Ce	Pr	Nd	Pm	Sm	Eu	Cd	Tb	Dy	Ho	Er	Tu	Yb	Lu
1,18	1,16	1,15		1,13	1,13	1,11	1,10	1,05	1,04	1,04	1,04	1	0,99

The conditions for the appearance of spontaneous polarization are fulfilled in crystals having a sufficiently large internal field coefficient and partially covalent bonds. In such semipolar compounds the elastic binding coefficient is probably comparatively small, while the anharmonicity of the vibrations of the central ions is rather pronounced.

The internal field and, consequently, the internal field coefficient are largely determined by the arrangement of oxygen octahedrons relative to each other. It is known that the octahedrons can touch each other at the apexes, edges or faces. One of the most favorable structures for the manifestation of spontaneous polarization is the perovskite structure in which the octahedrons touch at the apexes. As Skanavi[33] was the first to show the arrangement of ions obtaining in perovskite results in a strong internal field. If the octahedrons have common edges the internal field coefficient is reduced; it is reduced to an even greater extent when the octahedrons have common faces. In general, the decrease is the greater, the greater the number of common elements the adjoining octahedrons have.

The size of the octahedrons also plays an important role. We have already noted that the larger the octahedron, the smaller the elastic binding coefficient and the higher the Curie point (with the same central ion). In a

Table 3

Chemical formula	Structure	ε	Temp. coef. of ε $TK_{\varepsilon} \cdot 10^6$
$CaTiO_3$	Perovskite	150÷180	—(1500÷1800)
$CaSnO_3$	»	14÷17	110
$SrSnO_3$	»	15	?
$BaSnO_3$	»	17÷20	?
$CaZrO_3$	»	25	50
$SrZrO_3$	»	30	100
$BaZrO_3$	»	40÷43	—(160÷300)
$SrCeO_3$	»	27	40
$BaCeO_3$	»	28	180
$BaTa_2O_6$	?	132	—160
$Cd_2Ta_2O_7$	Pyrochlore	113	—960
$Pb_2Ta_2O_7$	»	114	—340

perovskite type crystal the ions with a coordination number 12, given a sufficiently great radii, may force the oxygen ions further apart and thereby increase the size of the octahedron.

The above considerations are valid not only for ferroelectrics but for all crystals with a high dielectric constant in general. Actually only those crystals in which (with a sufficient size of the octahedron) the central ion has the electronic structure of a noble gas after removal of the s- and d-electrons have a dielectric constant above 40 and a negative temperature coefficient of the dielectric constant (Table 3). The above considerations should be of help in seeking new materials with a high dielectric constant.

Matthias[34-36] also attempted to formulate the conditions for the appearance of spontaneous polarization. According to this author spontaneous polarization appears in crystals in which there are metal-oxygen octahedrons having a high polarizability. Moreover, according to Matthias, the electronic structure of central ions must be that of a noble gas atom and the radius of the ion must be 0.6-0.7 A. However, as we have just shown, the above condition as regards central atoms is incomplete, while the condition for the radii is mistaken.

Matthias explains the absence of spontaneous polarization in $LaAlO_3$ by the small dimensions of the aluminum ion. We cannot agree with this explanation. It is clear that the smaller the central ion the lower will be the value of the coefficient of elastic binding with the oxygen ions and, consequently, the higher the Curie point. Furthermore, we cannot agree with Matthias regarding the character of the bonds in ferroelectrics; he assumes that the closed shell of the central ion makes for ionic bonds in the crystal. Our view that the bonds between the central ion and the oxygen ions in ferroelectrics are of an intermediate nature is in agreement with the views of Vousden[37] and Megaw[38]. With respect to $KTaO_3$ and $NaTaO_3$, Vousden notes that despite the high polarizability and large size of the K ion as compared with the Na ion the transition temperature of $KTaO_3$ is much lower than the transition temperature of $NaTaO_3$. This can be explained only by differences in the covalent character of the bonds in these crystals.

Megaw believes that the d-electrons play an important part in the formation of the covalent bonds. For this reason the transition temperatures of the niobates of the alkaline metals are higher than the transition temperatures of the tantalates. The niobium and tantalum ions in the ground state have the electronic configurations $4d^45S$ and $5d^36S^2$, respectively. Consequently there is a greater possibility of a formation of d-electron bonds in niobium as compared with tantalum.

Conclusions

In recent year many new ferroelectrics and antiferroelectrics with a structure of perovskite, ilmenite, rhenium trioxide and pyrochlore have been discovered.

Analysis and generalization of the experimental data have made it possible to establish that spontaneous polarization can appear in crystals in which the oxygen ion octahedrons are wholly or partially occupied by cations, having the structure of a noble gas after removal of the s- and d-electrons, a large charge and a small ionic radius. An exception is formed by the crystals containing Pb^{2+} ions, which is apparently to be explained by the influence of the strongly polarizable lead ions on the character of the bond in these crystals.

The conditions formulated above apply not only to ferroelectrics but also to non-ferroelectric crystals characterized by a high dielectric constant.

Institute of the Chemistry of Silicates of the
Academy of Sciences of the USSR.

References

1. D.F.Rushman & M.A.Streivens, Trans. Farady Soc., A42, 231 (1946).
2. G.A.Smolenski, Doklady AN SSSR, 70, 405 (1950).
3. G.A.Smolenski, Doklady AN SSSR, 85, 985 (1952).
4. J.K.Hulm, Proc. Phys. Soc., 63, 1184 (1950).
5. J.K.Hulm, B.T.Matthias & E.A.Long, Phys. Rev., 79, 885 (1950).
6. G.H.Jonker & J.H.vanSanten, Chemisch Werkblad, 43, 672 (1947).
7. G.A.Smolenski, Zhur. tekh. fiz., 20, 137 (1950).
8. G.A.Smolenski, Zhur. tekh. fiz., 21, 1045 (1951).
9. G.Shirane, S.Hoshino & K.Suzuki, Phys. Rev., 80, 1105 (1950).
10. G.Shirane & E.Sawaguchi, Phys. Rev., 81, 458 (1951).
11. G.Shirane & S.Hoshino, J. Phys. Soc. Japan, 6, 265 (1951).
12. I.N.Beliaev & A.L.Khodakov, Zhur. eksp. i teor. fiz., 22, 376 (1952).
13. E.G.Fesenko, Doklady AN SSSR, 88, 785 (1953).
14. S.Roberts, J. Amer. Cer. Soc., 33, 63 (1950).
15. G.Shirane, E.Sawaguchi & A.Takada, Phys. Rev., 80, 485 (1950).
16. G.Shirane, E.Sawaguchi & Y.Takagi, Phys. Rev., 84, 476 (1951).
17. G.Shirane, Phys. Rev., 84, 854 (1951); 86, 219 (1952).
18. S.Roberts, Phys. Rev., 83, 1078 (1951).
19. G.Shirane, E.Sawaguchi & Y.Takagi, J. Phys. Soc. Japan, 6, 208 (1951).
20. E.Sawaguchi, H.Maniwa & S.Hoshino, Phys. Rev., 83, 1078 (1951).
21. G.Shirane & A.Takada, J. Phys. Soc. Japan, 7, 5 (1952).
22. G.Shirane, K.Suzuki & A.Takada, J. Phys. Soc. Japan, 7, 12 (1952).
23. G.Shirane & S.Hoshino, Acta Cryst. 7, 203 (1954).
24. F.Jona, G.Shirane & R.Pepinski, Phys. Rev., 94, 1407 (1954); 97,1584(1955).
25. G.G.Urazov, Speranskaia & Gulianitskaia. Tezisy dokladov i vystuplenii na III Vsesoiuznom sveshchanii po fiziko-khimicheskomu analizu (Summary of reports presented at the 3rd All-Union conference on physico-chemical analysis. M. 1955.
26. Iu.N.Venevtsev, Thesis, MIFI, M., 1955.
27. G.A.Smolenski, A.I.Agranovskaia, A.M.Kalinina & G.M.Fedotova, Zhur. tekh. fiz., 25, 2134 (1955).
28. G.A.Smolenski & N.V.Kozhevnikova, Doklady AN SSSR, 76, 519 (1951).
29. G.Goodman, J. Am. Cer. Soc., 36, 368 (1953).
30. G.A.Smolenski & A.I.Agranovskaia, Doklady AN SSSR, 97, 237 (1954).
31. G.Shirane & R.Pepinsky, Phys. Rev., 91, 812 (1953).
32. S.Sawada & S.Nomura, J. Phys. Soc. Japan, 6, 192 (1951).
33. G.I.Skanavi, Fizika dielektrikov (Physics of dielectrics), M., 1948.
34. B.T.Matthias, Phys. Rev., 75, 1771 (1949).
35. B.T.Matthias, Science, 113, 591 (1951).
36. B.T.Matthias, Helv. Phys. Acta, 23, 167 (1950).
37. P.Vousden, Acta Cryst., 4, 373 (1951).
38. H.D.Megaw, Acta Cryst., 5,739 (1952); 7, 187 (1954).

X-RAY ANALYSIS OF FERROELECTRIC SOLID SOLUTIONS WITH PEROVSKITE STRUCTURE

- Iu.N.Venevtsev & G.S.Zhdanov

Ferroelectrics are substances that exhibit spontaneous electric polarization (reversible in normally attainable fields) in a certain temperature interval. Ferroelectrics are now being intensively studied and ever more widely used in many branches of technology. Soviet scientists have played an important part in developing the theory of ferroelectricity, discovering new ferroelectric materials and finding technical applications for them in engineering and industry.

Both for theoretical and practical purposes it is important to establish the conditions under which spontaneous polarization develops in crystals. X-ray studies, particularly of the geometry and magnitude of the ionic shifts in the lattice, can contribute greatly to the solution of this problem. The causes of the ion displacements and the associated deformations of the lattice are closely related to the interactions between the particles composing the crystal. Unfortunately, the nature of the chemical interactions in ferroelectrics and similar compounds is still inadequately known.

In view of their relatively simple structure and a number of other factors, the more important ferroelectric solid solutions, which crystallize in a perovskite lattice, are actually the most convenient subjects for investigation of the influence of the size, polarizability and other attributes of the solid solution ions on the ferroelectric properties of the material.

We carried out an x-ray investigation of the structure of the two systems: $PbTiO_3$-"$PbSnO_3$" and $PbZrO_3$-"$PbSnO_3$". In the former lead titanate is a ferroelectric; in the latter the lead zirconate is an antiferroelectric.*

There are conflicting data in the literature[2,3] regarding the best conditions for obtaining the component common to these systems — lead stannate -- as well as regarding its properties. Our investigations showed that a specimen of "$PbSnO_3$" composition obtained by sintering in air of mixtures of PbO and SnO_2 at temperatures from 800° to about 1050° does not consist of a single compound but rather of two phases: Pb_2SnO_4 and SnO_2. This indicates that Naray-Szabo[2] is mistaken when he claims to have obtained a single compound of the composition $PbSnO_3$ with a perovskite type structure and that Coffeen's data[3] on the beginning of formation and the temperature of the decomposition of $PbSnO_3$ are ill-founded. After heating of Pb_2SnO_4 to temperature above 1050°, x-ray photographs of the material showed the presence of only SnO_2.**

When mixtures of PbO and SnO_2 (in proportions for Pb_2SnO_4 or $PbSnO_3$) are loaded into a furnace preheated to above 1050° there are obtained products consisting of a new phase X and tin dioxide in different proportions. The presence of the X phase has also been detected in the multiphase region of the $PbTiO_3$-"$PbSnO_3$" system.

In view of the dual-phase nature of "$PbSnO_3$" the investigated systems were actually three component systems. In our study we investigated specimens belonging in each section of the three-phase diagram.

---

*The work was carried out in contact with the research group, under G.A. Smolenski, studying the electric properties of silicates in the laboratory of the Institute of the Chemistry of Silicates of the USSR Academy of Sciences. Most of the ceramic specimens for x-ray analysis were prepared in this laboratory. The dielectric properties of the specimens we studied were investigated by Smolenski, Agranovskaia, Kalinina & Fedotova.[1]

**According to the data of Urazov, Speranskaia & Gulianitskaia,[4] in the PbO-SnO_2 system at 780-830° the only reaction occurring in the solid phase is that leading to the formation of Pb_2SnO_4. This compound melts incongruently at 1060°.

The following results were obtained for the $PbTiO_3$-"$PbSnO_3$" system.*

1. It was established that when the "$PbSnO_3$" content is between 0 and 75 mol % we have the solid solution $Pb(Ti-Sn)O_3$, while in the 75-100 mol % range of concentrations there obtains a four-phase region comprising the following phases: $Pb(Ti-Sn)O_3$, X, $(Sn-Ti)O_2$ and Pb_2SnO_4; (in preparing the specimens the final sintering temperature was reduced from 1060 to 1000° with increasing "$PbSnO_3$" content).

2. In the region of the solid solution we carried out an accurate determination of the unit cell parameters. With "$PbSnO_3$" concentrations up to 55% the unit cell remains tetragonal; the ratio c/a decreases with increasing "$PbSnO_3$" content. At concentrations above 55% the cell becomes rhombohedral and retains this symmetry to the solid solution boundary. As the "$PbSnO_3$" content is increased the rhombohedral distortion of the cell decreases. The volume of the unit cell of $Pb(Ti-Sn)O_3$ grows with increasing "$PbSnO_3$" content since the radius of the Sn^{4+} ion (0.67 A) is greater than the radius of Ti^{4+}(0.64 A).

These results indicate that the conclusions in Refs. 5 and 6 to the effect that at "$PbSnO_3$" concentrations above 50% the cell remains tetragonal and only the c/a ratio falls off sharply are erroneous.

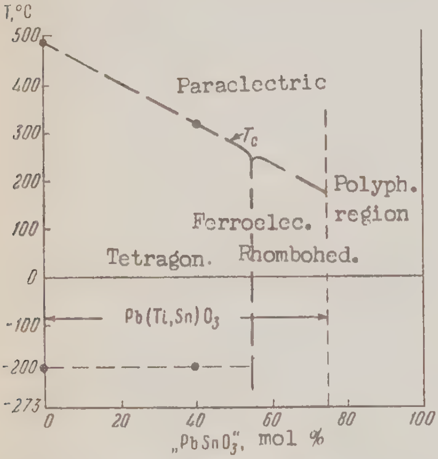

Fig. 1. Phase diagram of the $Pb(Ti-Sn)O_3$ solid solution.

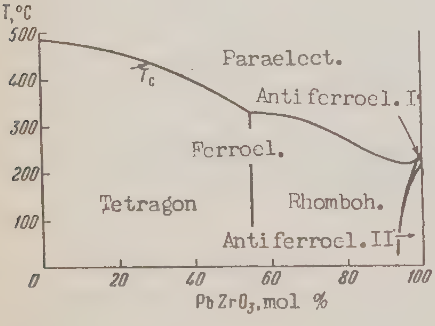

Fig. 2. Phase diagram of the $Pb(Ti-Zr)O_3$ solid solution after Sawaguchi.[7]

3. X-ray photographs at -183° of pure $PbTiO_3$ and of a sample containing 40% "$PbSnO_3$" indicated the absence of phase transitions in these specimens in the interval from room temperature to that of liquid oxygen. We established a Curie point for the specimen containing 40% "$PbSnO_3$": 320 ± 5°.

It is clear therefore that the Curie temperature is lowered with increasing concentration of tin ions in a solid solution. The transition of the tetragonal modification to the rhombohedral one and the lowering of the Curie point with increasing "$PbSnO_3$" content demonstrate the similarity of the changes in the properties of the solid solutions $Pb(Ti-Sn)O_3$ and $Pb(Ti-Zr)O_3$ (see Figs. 1 & 2). The similarity of the influence of Zr^{4+} and Sn^{4+} ions in replacing Ti^{4+} ions in $PbTiO_3$ is explained by the fact that the radius of the Zr^{4+} ion (0.82 A), like that of Sn^{4+}, is greater than the radius of the displaced Ti^{4+} ion (see below).

The phase diagram of the $Pb(Ti-Sn)O_3$ system differs from the diagram of the $Ba(Ti-Sn)O_3$ solid solution established by Smolenski and Isupov.[8] This is due to the difference between the atomic shift mechanisms in $PbTiO_3$ and $BaTiO_3$, a factor which has been neglected hitherto.

Nomura & Sawada[5] and Nomura[6] give no information on the similarity of the phase diagram for $Pb(Ti-Sn)O_3$ to the diagram for $Pb(Ti-Zr)O_3$ and offer no discussion of the differences in the mechanism of atomic shifts in $BaTiO_3$ and $PbTiO_3$.

---

*T.N.Shendrik participated in the preliminary investigation at room temperature of the specimens in this group.

The following results were obtained for the $PbZrO_3$-"$PbSnO_3$" system.

1. It was confirmed that $PbZrO_3$ has a "fagot" structure, composed of a series of barium titanate type subcells. The antiferroelectric state of lead zirconate is manifested in x-ray photographs by the appearance of superstructure lines. The relatively strong superstructure lines conform to the indications of the structure model proposed by Sawaguchi, Maniwa and Hoshino[9], corresponding to the space group $D_{2h}(9)$. Displacement of the lead ions along one of the diagonals of the plane (001), established in Ref. 9, distorts the symmetry of the subcells from the tetragonal to the monoclinic.

2. We established that in this system there exists a large solid solution region extending to a "$PbSnO_3$" content of 75%. In the heterogeneous region for specimens sintered at high temperatures ($\sim 1180^\circ$) there exist two solid solutions $Pb(Zr-Sn)O_3$ and $(Sn-Zr)O_2$.

3. In the entire region of the solid solution, monoclinic symmetry of the subcells persists at room temperatures and the solid solution is antiferroelectric. The volume of the unit cell decreases linearly with increasing "$PbSnO_3$" content.

This indicates that the nature of the superstructure in a solid solution remains the same as in pure lead zirconate.

4. High temperature x-ray photographs of a specimen containing 70% "$PbSnO_3$" showed that a phase transition occurs at $180 \pm 10^\circ$. The monoclinic antiferroelectric modification is transformed to a rhombohedral ferroelectric modification. Establishing the temperature of the transition from the rhombohedral to the cubic modification by x-ray analysis proved to be difficult since the rhombohedral distortion is very small and vanishes gradually with increasing temperature. Hence the Curie point for this specimen was determined only approximately: $290 \pm 25^\circ$.

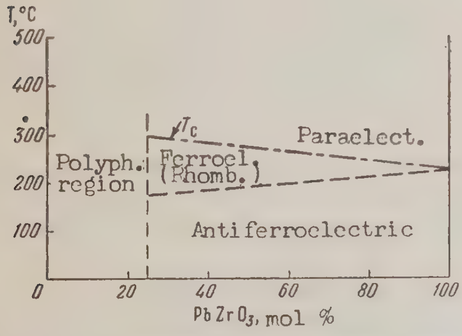

Fig. 3. Phase diagram of the $Pb(Zr-Sn)O_3$ solid solution.

This system comprises three different regions: an antiferroelectric, a ferroelectric and a paraelectric. The phase diagram of the $Pb(Zr-Sn)O_3$ solid solution (Fig. 3) exhibits certain similarities with part of the diagram of $Pb(Zr-Ti)O_3$ (Fig. 2).

On the basis of the results obtained by Smolenski and Isupov[8] and Sawaguchi[7] and other investigators we conclude that the phase diagram of $Ba(Ti-Zr)O_3$ is similar to the diagram of $Ba(Ti-Sn)O_3$. At the same time the diagram of $Pb(Ti-Zr)O_3$, a solid solution which is analogous to $Ba(Ti-Zr)O_3$, differs in character from the above. In the case of the $(Ba-Pb)TiO_3$ solid solution in the region of 10-25% concentrations of $PbTiO_3$, as Suzuki's data[10] show, the parameters of the unit cell vary anomalously with the temperature. These effects can readily be explained if we accept that different atomic shift mechanisms operate in $BaTiO_3$ and $PbTiO_3$.

Analysis of the experimental data on x-ray studies of solid solutions and on the structure of different ferroelectric and antiferroelectric materials have made it possible to evolve a system of classifying the known ferroelectrics and antiferroelectrics of the $BaTiO_3$ type on the basis of a new principle taking into account the type of ferroelectro-active cation: A or B, as listed in Table 1. In Table 1 we also give the values of the geometric factor $t = (A - O)/\sqrt{2(B - O)}$ (see Ref. 11).

These values were computed on the basis of the latest data on ionic radii[12] and taking into account the correction for the coordination number.

Table 1

Classification of ferroelectrics and antiferroelectrics of the barium titanate group according to the type of active cation

Type of polarization	Type of active cation	ABO_3	R_A, Å	R_B, Å	t, (R_o=1,36Å)	T_C, °K
Ferro-electric	B	$BaTiO_3$ $KNbO_3$	1,38 1,33	0,64 0,66	1,03 1,00	393 708
		$KTaO_3$ $PbTiO_3$ $SrTiO_3$	1,33 1,26 1,20	0,66 0,64 0,64	1,00 0,98 0,96	13 773 20?
Antiferro-electric	A	$PbHfO_3$ $PbZrO_3$ $NaNbO_3$ $NaTaO_3$	1,26 1,26 0,98 0,98	0,78 0,82 0,66 0,66	0,92 0,90 0,86 0,86	488 508 913 748
Ferro-electric	A	$CdTiO_3$	0,99	0,64	0,87	55÷60

The ferroelectric $CdTiO_3$ has been separated from the others in the table, for above the Curie point it has a pseudomonoclinic cell. The mechanism of polarization in this compound is as yet unknown.

All the compounds can be classified into two groups depending on the type of the active cation (A or B). $BaTiO_3$ and $KNbO_3$ belong to the first group in which the shifts are produced by the B-type ion; all the other listed compounds fall into the second group in which the cation is of the A type. Unlike $BaTiO_3$, which belongs in the first group, $PbTiO_3$ falls into the second group with most of the other compounds.

Displacements of both the A and B ions, which occur along the axes of the second, third and fourth order, lead to a reduction of the initial values of the coordination numbers, from 12 for the A ions and 6 for the B ions to the values listed in Table 2.

Table 2

Change of the coordination number incident to displacement of the cations along the symmetry axes of the initial cell.

Type of shifted ion	Direction of displacement		
	C_2	C_3	C_4
A	1+4	3	4
B	2	3	1

The value of the factor t, when it differs appreciably from unity, allows us to determine which of the cations is primarily responsible for the atomic shifts. The determination becomes ambiguous when t differs but little from the boundary value t = 1. It is impossible to compute the factor with an error of less than 0.01-0.02 since the ionic radii can be determined only to within about 1%.

Smolenski and Agranovskaia[13] observed spontaneous polarization in (Pb-Ba)SnO_3 solid solutions over a wide range of concentrations. This polarization is associated with the presence of lead ions in the solid solution and intensification of the covalent nature of the bond between the B type metal ion and the oxygen ions which, according to these authors, leads to displacement of the tin ions. In order to elucidate the atomic shift mechanism in this solid solution we carried out a geometric analysis and made use of certain supplementary experimental data. The t factor for $BaSnO_3$ proved to be very close to unity, so that it is impossible to judge of the type of cation displacement in this compound on the basis of the factor. It is known from experimental data[3] however that $BaSnO_3$ is not a ferroelectric and in forming a solid solution with $BaTiO_3$ yields a phase diagram similar to that for the $Ba(Ti-Zr)O_3$ solid solution. The t factor for $BaZrO_3$ equals 0.94 and consequently the zirconium ion is "crowded" in the $BaZrO_3$ lattice. These data indicate that it is impossible for the tin ion to be displaced in the initial barium stannate structure. If the compound $PbSnO_3$ existed, the computed value of the t factor (0.97) for it shows that the lead ions would be freer in a structure of this compound; that is, the lead ions could shift just as they shift in lead titanate ($t = 0.98$). In the $(Pb-Ba)SnO_3$ solid solution the spontaneous polarization is due to the displacement of the lead ions. Computations for $CeAlO_3$ lead to a value of $t = 0.92$, which indicates that the cerium cations are relatively free to shift.

It has recently been reported[14] that $CeAlO_3$, as well as $CeCrO_3$ has a high dielectric constant. The dielectric constant for $CeAlO_3$ at 276° is 1796.

The difference between the atomic shift mechanisms in perovskite type compounds with $t > 1$ and $t < 1$ must be taken into account in elucidating the factors favoring the appearance of spontaneous polarization and affecting the Curie points. The Curie points, as the data listed in Table 1 indicate, are not directly dependent on the value of the t factor. It is also necessary to examine the energy states of the displaced ions. The polarizability of the ions and the distance between them are also important in this respect. Direct comparison of the Curie points of ferroelectrics and antiferroelectrics is meaningful only when the shifted cations are of the same type.

The entire question of the Curie point has until now generally been examined without taking into account the type of the atomic shifts. Megaw[15] and Smolenski[16,17] explain the higher Curie point of lead titanate as compared with barium titanate by enhancement of the covalent nature of the bonds in the former. Von Hippel[18] attempts to relate the Curie points of different titanates with a strength of the bonds between the oxygen and bivalent metal ions A; to evaluate the strength of the bonds he proposes to utilize the melting points of the simple oxides PbO, BaO etc. In doing so he puts the oxides of the alkaline earth metals in a common series with lead oxide which we feel is a doubtful procedure. There is a direct dependence between the strength of the bonds and the melting point only in the case of isomorphous substances. Lead oxide has an entirely different structure from that of the alkaline earth metal oxides.

Lead ions are displaced in both lead titanate - a ferroelectric - and in lead zirconate - an antiferroelectric. The cell parameters of these compounds differ appreciably due to the difference in the size of the zirconium and titanium ions. These ions also have different polarizability values ($0.80 \cdot 10^{-24}$ and $0.27 \cdot 10^{-24}$ cm^3, respectively). In considering the properties of these compounds it may be of interest to examine the attributes of some of their solid solutions and the data listed in Table 1. In the solid solutions $Pb(Ti-Sn)O_3$, $Pb(Zr-Sn)O_3$ and $Pb(Ti-Zr)O_3$ the Curie point goes down with increasing size of the central B type cation. Hence the difference in the Curie temperatures of lead titanate and lead zirconate is due mainly to the lattice parameters of these compounds. The difference in polarizability of zirconium and titanium ions plays only a secondary role in this case.

The situation is entirely different where $PbTiO_3$ and $SrTiO_3$ are concerned. The high polarizability of the lead ion results in a high Curie point for lead titanate while strontium titanate does not exhibit spontaneous polarization down to the very lowest temperatures.

Table 3

Factors affecting the Curie point, T_C

ABO_3	$\alpha_A \cdot 10^{24}$, см^3	a_0, Å	t	T_C, °K
$SrTiO_3$ . .	1,42	3,90$_{18°C}$	0,96	20?
$PbTiO_3$ . .	4,32	3,96$_{500°C}$	0,98	773
$PbZrO_3$ . .	4,32	4,15$_{230°C}$	0,90	508
$BaZrO_3$ . .	1,69	4,19$_{18°C}$	0,94	—
$SrZrO_3$ . . .	1,42	4,10$_{18°C}$	0,88	—

Why one cannot use only geometric considerations, specifically the t factor, is illustrated by the case of the zirconates of strontium, barium and lead. For all the zirconates $t < 1$ (see Table 3) and consequently, one may expect displacement of the A type ion. However, spontaneous polarization is observed only in lead zirconate. The factor favoring the appearance of spontaneous polarization in this compound is the large value of the polarizability of the ions in lead zirconate, in particular of the lead ions. Sawaguchi[7] has already called attention to this circumstance. Thus in a group of isomorphous substances the Curie point will be higher, the smaller the unit cells and the greater the polarizability of the shifted cation.

In $Ba(Ti-Sn)O_3$ and $Ba(Ti-Zr)O_3$ the tin and zirconium are constrained from shifting and consequently the Curie point in these solid solutions is depressed even though the polarizability of the zirconium ion is higher than that of the titanium ion.

Of great importance in understanding the appearance of spontaneous polarization is the question of the interaction between the particles forming the crystal. Small distortions of symmetrical crystal structures, distortions connected with small shifts of the atoms in the unit cells are determined by the nature of the interaction between the particles. These shifts can lead to the appearance of electric dipole moments where the ions are joined by ionic or iono-covalent bonds. Light can be thrown on the polymorphism of ferroelectric substances by crystallo-chemical analysis of the structure of the simple oxides entering into the composition of the complex ferroelectric oxides. In the low temperature modifications of ferroelectrics the structural changes observed in a number of cases occur in the direction of an approach to the structural configurations prevailing in the simple oxides. For it to be possible for the small structural deformations to occur under the influence of temperature changes the initial lattice of the complex oxide must have a certain "openness" or deformability. At sufficiently high temperatures the most symmetric modification is attained by virtue of the high energy of the thermal motion of the particles. As the temperature is reduced the particles can approach closer to each other. The energy of this interaction with the cation free to shift inside the oxygen polyhedron decreases with decreasing coordination number of the cation, i.e., with displacement of the cation from the symmetric position. The subsequent processes occurring during the phase transition rearrangement may be extremely complex. We should call attention here to the deformation of the valence angles of some bonds in the direction of realization of more stable configurations, in particular, the configurations established by crystallo-chemical data.

There can be no doubt that investigation of the structure of ferroelectrics must play an important part in the development of the theory of ferroelectricity.

We desire to thank G.A.Smolenski for making available the investigated specimens.

References

1. G.Smolenski, A.I.Agranovskaia, A.M.Kalinina & T.M.Fedotova, Zhur. tekh. fiz., 25,2134 (1955).

2. I.Naray-Szabo, Müeguetemi Közlemnyek, 1,30 (1947).

3. W.W.Coffeen, J. Am. Cer. Soc., 36,207 (1953).

4. G.G.Urazov, Speranskaia & Gulianitskaia, Tezisy dokladov i vystuplenii na III Vsesoiuznom soveshchanii po fiziko-khimicheskomu analizu (Summary of reports presented at the 3rd All-Union conference on physico-chemical analysis). M. 1955.

5. S.Nomura, S.Sawada, Rep. Inst. Sci., Technol. Univ., Tokyo, 7,83 (1953).

6. S.Nomura, J. Phys. Soc. Japan, 10,112 (1955).

7. E.Sawaguchi, J. Phys. Soc. Japan, 8,615 (1953).

8. G.A.Smolenski & V.A.Isupov, Doklady AN SSSR, 96, 53 (1954).

9. E.Sawaguchi, H.Maniwa & S.Hoshino, Phys. Rev., 83,1078 (1951).

10. K.Suzuki, J. Phys. Soc. Japan, 6,340 (1951).

11. V.M.Goldschmidt, T.Barth &.G.Lunde, Skrifter Norske Videnskaps Akad., Oslo, J. Mat. Natur. Klasse, 7,21 (1925).

12. G.B.Boki, Vvedenie v kristallokhimiiu (Introduction to crystal chemistry) M. 1954.

13. G.A.Smolenski & A.I.Agranovskaia, Doklady AN SSSR, 97,237 (1954).

14. L.Keith &. R.Roy, Amer. Miner., 39, 1-2, 1 (1954).

15. H.D.Megaw, Acta Cryst., 7,187 (1954).

16. G.A.Smolenski, Zhur. tekh. fiz., 20,137 (1950).

17. G.A.Smolenski, Thesis, Institute of the Chemistry of Silicates of the USSR Academy of Sciences, 1954.

18. A.vonHippel, ZS. f. Physik, 133,158 (1952).

NON-LINEAR PROPERTIES OF FERROELECTRICS

- T.N.Verbitskaia

Ferroelectrics, which include ferroceramics, are unique in having a high dielectric constant that is sharply dependent on the temperature and field intensity and exhibiting ferroelectric hysteresis loops and a piezoelectric effect.

Ferroceramics are used to make new types of miniature ceramic capacitors, which are distinguished for high values of specific capacity. They are used for low and high voltages in the range of both low and radio frequencies. Owing to their high piezoelectric properties, ferroelectrics are extensively used in diverse acoustic equipment. Ceramic ferroelectrics are used as radiators and receivers of ultrasonic oscillations, in piezoelectric meters and for other purposes.

Recently there has been much interest in the non-linear properties of ferroelectrics; namely, that the dielectric polarization P and the dielectric constant ε are non-linear functions of the field intensity in the ferroelectric region. As the applied ac field is increased, the dielectric constant $\varepsilon = f(E_\sim)$ first increases to a limiting(saturation) value and then diminishes.

The behavior of the ferroelectrics in an electric field is in many respects analogous to the behavior of ferromagnetics in a magnetic field. Under the influence of an electric field ferroelectrics exhibit saturation and hysteresis, just as magnetic materials do under the influence of a magnetic field.

The polarization vs electric-field intensity curve of ferroelectrics has the same character as the magnetic induction vs the magnetic field strength curve for ferromagnetics. This curve cannot be described even approximately by a linear equation.

The non-linear characteristics of ferroelectrics and ferromagnetic materials, despite the difference in the physical processes responsible for these characteristics, make these materials capable of replacing vacuum tubes in various electronic circuits.

Vacuum tubes have a relatively limited service life and are very sensitive to overloads, shocks and vibration. This reduces the reliability of the equipment in which the vacuum tubes are employed. Non-linear elements of ceramic materials have very high mechanical strength; in consequence such elements have a longer life and give more dependable service than can vacuum tubes. In addition, ferroceramic and magnetic elements are cheaper and simpler in construction and can be used to miniaturize equipment.

The behavior and applicability of circuits with non-linear elements are studied by means of the analytic methods used for the design of electric circuits containing non-linear elements. In the case of ferroelectrics the analysis is based on the assumption that the typical curve showing the dependence of the charge of a non-linear capacitor on the field intensity can be approximated by different functions. The most accurate representation of the experimental dependence of the charge on the field intensity for ferroelectrics is given by a hyperbolic sine function.[2,3] Solution of the differential equation for the dependence of the charge on the field intensity makes it possible to determine the optimum operating conditions under which non-linear elements can be used in many practical circuits.

The Russian and foreign literature contains many articles devoted to the use of ferroelectrics in diverse types of radio equipment and instruments. The circuits investigated in greatest detail, both theoretically and experimentally, are those of dielectric amplifiers. The mathematical analysis of the fundamental dielectric-amplifier circuit has been carried out, and the amplification factor and other parameters have been determined.[3] Dielectric voltage and power amplifiers for high and for low frequencies as well as dc amplifiers have been developed.[4] There exist two-, three-, and multi-stage amplifiers having high gain factors and a considerable output power.

The practical realization of tubeless electric and radio apparatus and equipment employing non-linear ferroelectric materials became possible only after the development of ferroceramic materials characterized by pronounced non-linear properties.[5]

1. Non-linear Properties of Ferroelectrics at Normal Temperatures

Among the known ferroelectrics, the three whose electric characteristics have been most fully studied at the present time are Rochelle salt, barium titanate and the ceramic material T-7500. The field dependences of the polarization P and the dielectric constant ε for these have been established. The characteristics $P = f(E)$ and $\varepsilon = f(E)$ are similar for all ferroelectrics. With increasing field intensity the polarization of the ferroelectric increases and reaches saturation at some value. The dielectric constant, which may be defined as the polarization divided by the field intensity, first increases with the field intensity, reaches a maximum, and then falls off. The degree of non-linearity of individual ferroelectrics is determined by the value of the ac field intensity at which the change in the slope of the $P = f(E)$ and $\varepsilon = f(E)$ curves is observed. To evaluate the non-linearity one establishes the value of the ac field intensity E_{max} at which the dielectric constant of the ferroelectric reaches its maximum value. For some ferroelectrics the value of the field intensity E_{max} corresponding to the maximum value of ε is small (under a few hundred volts per cm). Foremost among such materials is Rochelle salt, which thus far is unsurpassed for its high non-linear qualities in weak fields.

For other ferroelectrics, including barium titanate, considerably stronger fields are required for the dielectric constant to reach its maximum value.

In weak fields the dielectric constant of barium titanate varies much less than that of Rochelle salt; the T-7500 ceramic occupies an intermediate position in this respect.

To establish the degree of non-linearity of various ferroelectrics, in addition to the value of E_{max}, it is also necessary to know the extent of the variation of the dielectric constant over the 0 to E_{max} range of fields.

Rochelle salt. The dielectric constant of Rochelle salt (Figure 1) in very weak fields (a few volts per cm) is only on the order of several hundreds. At a field intensity E_{max} of about 100 v/cm, ε attains a value close to 20,000. Thus the variation of the dielectric constant in weak fields is more than 1:20 (Ref. 6). This is the great advantage Rochelle salt has over other ferroelectrics for use as a non-linear element in weak fields. However, Rochelle salt retains its ferroelectric properties, including its high non-linearity, only in a relatively narrow temperature range, from -15° to $+25.5^{\circ}$, i.e., between its upper and lower Curie points.

Rochelle salt has poor mechanical strength and a low decomposition temperature (55°). In addition, the non-linear properties of Rochelle salt are affected by even minor mechanical deformations of

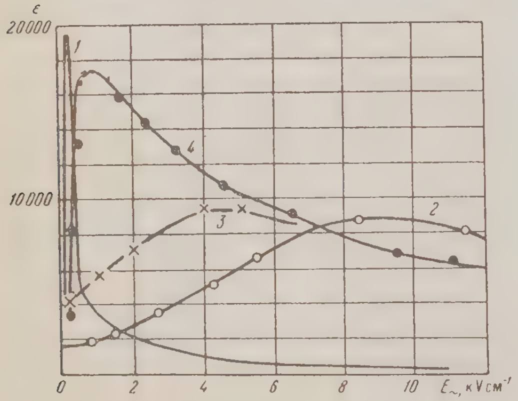

Fig. 1. Variation of the dielectric constant with the ac field intensity: 1) Rochelle salt, 2) $BaTiO_3$ (after B.M.Vul), 3) T-7500 and 4) Varikond VK-1.

the crystal. Rochelle salt crystals are brittle and readily soluble in water. All this makes it impractical to use Rochelle salt crystals as non-linear elements, in spite of their favorable non-linear properties.

Barium Titanate. Barium titanate, as we know, was the first ceramic material with high ferroelectric properties discovered in the Soviet Union. According to data of Vul and Gol'dman[7], the dielectric constant of barium titanate depends on the ac field intensity; as the latter is increased, ε increases gradually and reaches a maximum at a relatively high field intensity (8-10 kv/cm). Our measurements indicated that the dielectric constant of barium titanate reaches a maximum at approximately 6 kv/cm. Our own specimens, which had a Curie point of 120°C, were not identical with those used by Vul and Gol'dman.

Comparing the dependences $\varepsilon = f(E_{\sim})$ in weak fields for Rochelle salt and for barium titanate, one can readily see that the variation of the dielectric constant with the field is considerably more pronounced in Rochelle salt than in barium titanate. The value of E_{max} for barium titanate is many times greater than that for Rochelle salt. The dielectric constant of barium titanate changes by not more than 4-5 fold in the 10 v/mm to E_{max} field range. The value of the field intensity E_{max} for barium titanate is rather high, which operates against the use of this dielectric in circuits in which the voltage is applied for a prolonged time.

The advantages of barium titanate over Rochelle salt are that the ceramic retains its non-linear properties over a wide temperature range from 120° down to very low sub-zero temperatures and has a high mechanical strength with consequent resistance to vibration, impact, and shock. The ceramic is also easier to mount. Many practical uses of barium titanate, based on its non-linear properties and its high electrical and mechanical durability, have been reported. Vologodin proposed the use first of Rochelle salt, and then of barium titanate for frequency multiplication. Demichev and Fogel' showed that it is possible to use barium titanate for sonic and supersonic generators. They realized a static frequency converter with a capacity of 200 kv (water-cooled).[8,9] Skanavi and Neiman developed a voltage stabilizer incorporating barium-titanate capacitors.[10]

Whenever barium titanate is used as the non-linear element in electric and radio circuits, rather high voltages must be employed. The practical need is for new ceramic ferroelectrics, having much more pronounced non-linear properties in weak fields. This is particularly important where non-linear elements intended for various radio circuits are concerned.

Material T-7500. The designation of the ceramic T-7500, like that of a number of other ceramic materials, is based on the value of its dielectric constant, i.e., the dielectric constant of T-7500 is 7500 at the Curie point (35--40°). T-7500 retains its ferroelectric properties from this temperature down to low negative ones. At room temperatures the dielectric constant is about 4,000-5,000. At temperatures 20-30° above the Curie point T-7500 no longer exhibits ferroelectric properties.[13,14]

T-7500 is used for various miniaturized ceramic capacitors, where stability of the capacitance value is not critical: for example, when only a certain lower capacitance value must be maintained. T-7500 is used to manufacture low-voltage capacitors in the form of thin-wall tubes and wafers as well as high-voltage "barrel" capacitors. The low-voltage capacitors are used in filter and low-frequency blocking circuits at effective ac voltages up to 150 and dc voltages to 250 v, in television apparatus, in decoupling circuits, and different UHF circuits. The nominal rating of such capacitors may range from one to several tens of thousands $\mu\mu f$.

Ceramic fixed high-voltage capacitors are used in filters at effective dc voltages up to 12 kv in the 5-70° ambient temperature interval. The nominal rating of such a capacitor measuring 20 mm in thickness and diameter sheathed is 500 μμf at 20°.

At room temperatures T-7500 exhibits more pronounced non-linearity than barium titanate; the dielectric constant reaches a maximum at E_{max} = 4-5 kv/cm. However, the ratio of the maximum value of ε to the initial value measured at E = 10 v/mm does not exceed 2-2.5. This is probably due to the Curie point of T-7500 being close to room temperature, and at the same time to the initial values of the dielectric constant being rather high: 3,000-5,000. The limiting values of ε do not exceed 7,000-8,000 both when temperature is raised to the Curie point, and when the field intensity is increased to E_{max} (these high values of dielectric constant are obtained only when high purity raw material is used).

Aging - an effect to which T-7500 is particularly subject[13,14] - makes the values of the dielectric constant of this material unstable with time. Nor do the non-linear properties of T-7500 remain constant with time. An aged specimen has a considerably higher E_{max} than a fresh one. The dielectric constant at the maximum is lower in the aged material. The curves showing the dependence of the "reversible" dielectric constant on the dc biasing field $\varepsilon = f(E_=)$ are different for fresh and aged specimens. In the former case an increase in the biasing field causes the dielectric constant to diminish noticeably, starting with rather weak fields. In the second case the ε vs. dc field curve has a maximum.

The relatively low non-linearity of T-7500 and the noticeable change in dielectric constant with time (aging) limit the use of this material for non-linear circuit elements. There is still need for new ceramic materials with stable and favorable non-linear properties.

Varikond VK-1. The non-linear properties of ferroelectrics depend on their composition and the structure of their crystal lattice. Our research on the effect of the composition on the electric properties of ferroelectrics led to the development of a material having sharply pronounced non-linear properties. This material was named Varikond VK-1. By virtue of its high non-linear properties, Varikond VK-1 is suitable for use in non-linear elements, the capacity of which does not remain constant with varying field intensity. The dependence of the dielectric constant on the intensity of the ac field for Varikond VK-1 and several other ferroelectrics is shown in Fig. 1.

The dielectric constant of Varikond VK-1 varies greatly in weak ac fields and reaches its maximum at approximately 1,000 v/cm. The $\varepsilon = f(E_\sim)$ curve for Varikond VK-1 is quite similar in form to that obtained for Rochelle salt, but differs noticeably from analogous curves for T-7500 and barium titanate.

The shape of the ferroelectric hysteresis loops is further evidence of the highly non-linear properties of Varikond VK-1.

In the case of barium titanate and T-7500, the charge vs field intensity curves hardly deviate from a straight line in fields up to 1500 v/cm. On the other hand, the onset of saturation is quite noticeable in Varikond VK-1 well below this field intensity.

As the ac field intensity is increased from its initial value of 1 v/mm to E_{max}, the dielectric constant of Varikond VK-1 increases by more than 6 times and attains a maximum value of about 15,000-20,000.

In mass production of Varikond VK-1 elements, i.e., when the ceramic is made up in large batches, both the initial and maximum values of ε are reduced; however, the $\varepsilon_{max}/\varepsilon_{initial}$ ratio remains comparatively high (not less than 4-5).

In order to use ferroceramic elements in different radio components and evaluate their non-linearity, in addition to the $\varepsilon = f(E_\sim)$ characteristic, it is essential to know the dependence of the dielectric constant on a dc biasing field applied simultaneously with the ac field (i.e., the so-called reversible dielectric constant). This characteristic, $\varepsilon = f(E_=)$, is very important in selecting the best material for the production of the non-linear elements of dielectric amplifiers and similar components. Hitherto in studying the reversible characteristics of ferroelectrics whose dielectric constant varies little with the ac field intensity (for example, barium titanate) the effect of the ac field has often been neglected. In the case of Varikond VK-1, however, the form of the variation of the dielectric constant with the dc biasing field depends to a very considerable extent on the intensity of the ac field. The reversible characteristic has the steepest slope when the peak ac voltage $E_\sim = E_{max}$. In both weaker and stronger fields the slope of the reversible characteristic is reduced. Effective control of the slope of the reversible characteristic by means of an external ac field became possible only after development of ferroelectrics with sharply pronounced dependence of the dielectric constant on the ac field intensity.

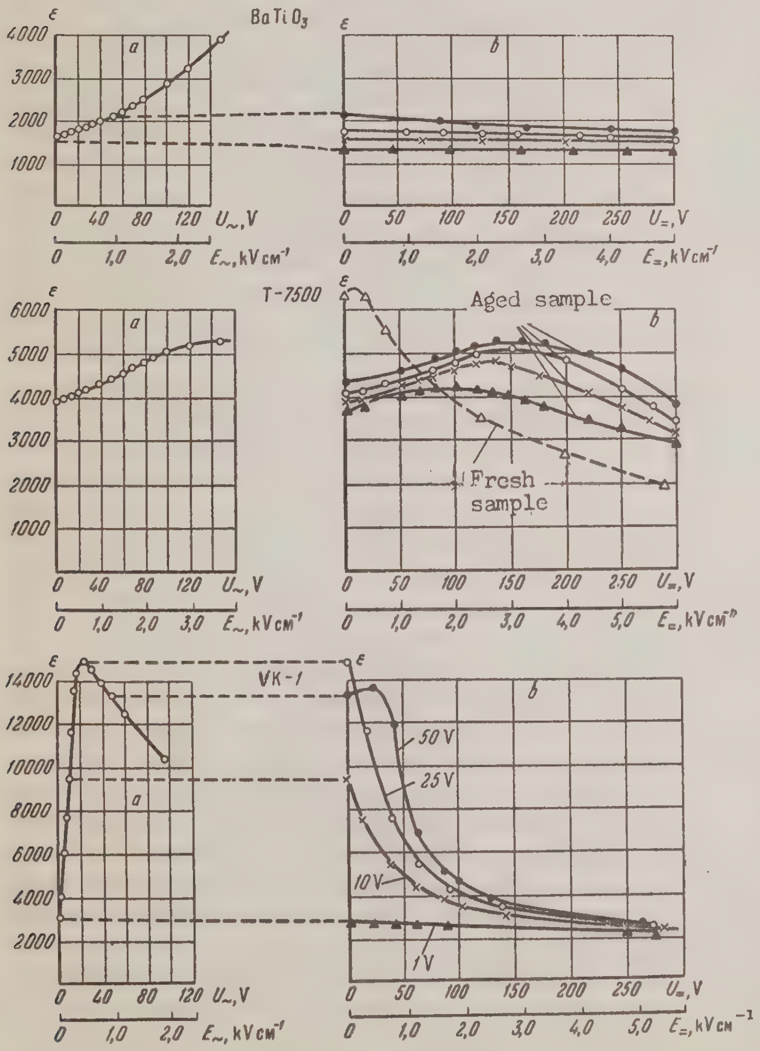

Fig. 2. Variation of the dielectric constants of barium titanate, ceramic T-7500 and Varikond VK-1 with the intensity of a) the ac field and b) the dc biasing field.

Figure 2 shows variations of the dielectric constant with the ac and dc biasing field intensities for three materials: barium titanate, T-7500, and Varikond VK-1. Comparison of these curves brings out clearly the exceptionally high non-linearity of Varikond VK-1. For barium titanate in ac fields up to 1 kv/cm, an increase in the dc biasing field from zero to 4-5 kv/cm reduces the dielectric constant only slightly (3-5 %). For freshly-prepared specimens of T-7500 under similar conditions, the reversible dielectric constant may diminish by a factor of three, but the slope of the reversible characteristic does not remain constant with time: incident to aging the character of the variation of the reversible dielectric constant changes: $\varepsilon = f(E_=)$ curve develops a smeared-out maximum (Figure 2b). The reversible dielectric constant of Varikond VK-1 undergoes a considerably greater change in weak ac fields. In an ac field of an intensity equal to E_{max}, the reversible dielectric constant of Varikond falls off by a factor of 4-5, the corresponding change in the dc biasing field being from 0 to 2-3 kv/cm. Further increase in the dc field causes no noticeable additional change in the dielectric constant. Increasing the alternating field above the value of E_{max} or reducing it below this value reduces the slope of the reversible characteristic.

If the non-linear elements are made in the form of thin wafers or tubes with 0.1-0.5 mm thick walls, an ac field intensity of a few tens or even a few volts will suffice to insure a sufficiently steep reversible characteristic.

2. Non-Linear Properties of Varikond VK-1 at Different Temperatures

Non-linear elements can be used in many radio components only if their non-linear properties remain constant over a wide temperature range. It is known, however, that the dielectric constant of ferroelectrics varies with temperature, particularly near the Curie point. These variations are greatest when the ferroelectric is in a relatively weak field.

In a strong field the behavior is different. Here by "strong field" we mean a field equal to or greater than E_{max} for the given material.

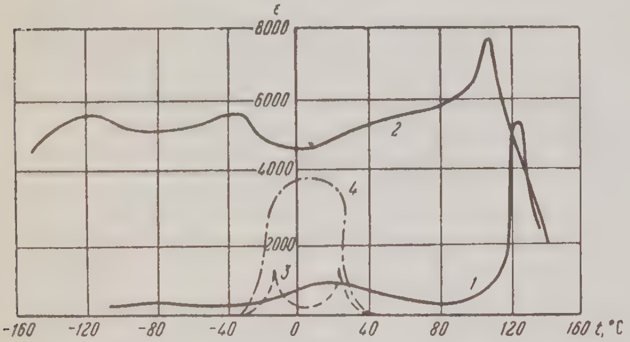

Fig. 3. Temperature dependence of the dielectric constant of barium titanate: 1) $E_\sim = 6$ v/mm and 2) $E_\sim = 600$ v/mm; of Rochelle salt: 3) $E_\sim = 0.5$ v/mm, 4) $E_\sim = 50$ v/mm.

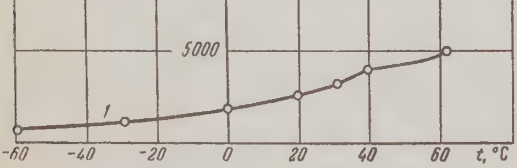

Fig. 4. Temperature dependence of the dielectric constant of Varikond VK-1 in different fields: 1) E = 10 v/mm and 2) E = 200 v/mm.

The temperature dependence of the dielectric constant of Rochelle salt has one smeared-out strong-field maximum at intensities E = 50 v/mm, instead of the two near the two Curie points observed in weak fields. E_{max} of Rochelle salt is close to 10 v/mm. This smeared-out maximum extends to the entire 15-24.5° interval corresponding to the ferroelectric region (Fig. 3). Within this interval the value of the dielectric constant remains high, approximately 4200. The data for Rochelle salt are taken from Ref. 6.

In the case of barium titanate the temperature dependence in strong fields is also smoothed out. In a weak field (6 v/mm) the curve of the temperature dependence of the dielectric constant of barium titanate exhibits three maxima at temperatures corresponding to the three phase transitions of the crystal lattice. The value of the dielectric constant in weak fields and at below-zero temperatures does not exceed a few hundred, while at the point of the principal phase transition, at 120 degrees, it attains several thousand. In strong fields (E_{max} of barium titanate is approximately 500-800 v/mm), ε_{max} at the temperatures of the second and third phase transitions of barium titanate becomes comparable with ε_{max} at 120° (Fig. 3, curve 2). In the entire temperature range from -180 to +120 degrees the dielectric constant of barium titanate remains high in fields on the order of 600 v/mm. The deviation from the mean value of 5000 does not exceed 20% in the temperature range from +80 to -60 degrees.

Varikond VK-1 exhibits a marked difference in the character of the temperature dependence of the dielectric constant in strong as compared with weak fields (Fig. 4). In the weak fields (E = 10 v/mm - curve 1 in Figure 4) there is a monotonic increase in the dielectric constant with rising temperature from -60 to +60 degrees; the value of ε increases by a factor of 8-10.

In the strong-field region (E_{max} of Varikond VK-1 is approximately 100 v/mm) the dielectric constant of Varikond changes considerably less over the above temperature range (Figure 4, curve 2). The average value of the dielectric constant is close to 16,000 and intermediate values do not differ by more than 20% from this average.

An examination of the curves of Figure 4 shows that Varikond VK-1 retains its ferroelectric properties over a wide range of temperatures. We established that Varikond remains ferroelectric with sharply pronounced non-linear properties all the way down to -195°. Figure 5a shows the variation of ε with the ac field intensity measured for Varikond at 60, 20, and -60°. In all cases E_{max} remains under 250 v/mm.

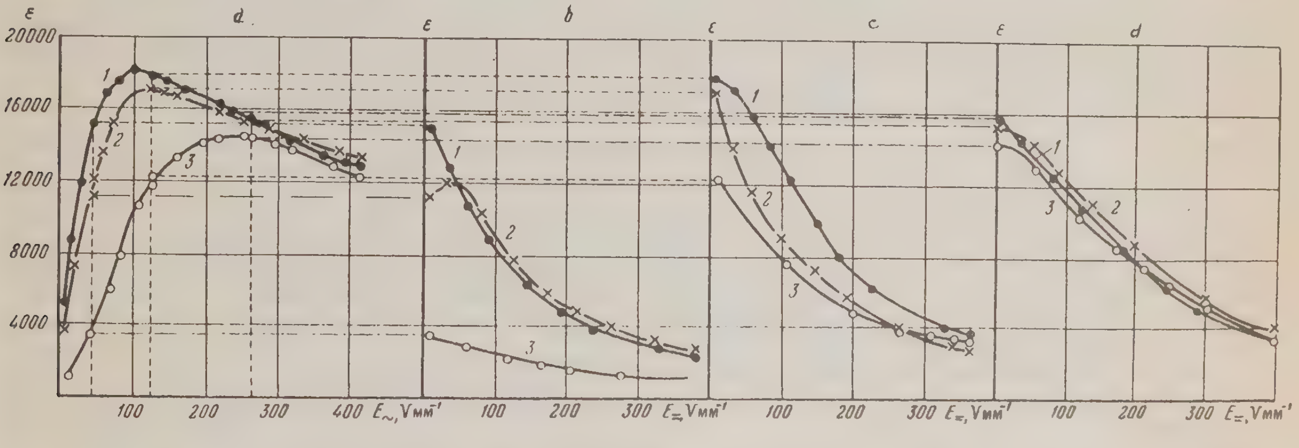

Fig. 5. Variation of the dielectric constant of Varikond VK-1 with the intensity of a) the ac field, and dc biasing field with b) $E_\sim = 40$ v/mm, c) $E_\sim = 120$ v/mm d) $E_\sim = 260$ v/mm at different temperatures: 1) t = 60°, 2) t = 20°, 3) t = -60°.

The persistence of the non-linear properties of Varikond VK-1 over a wide temperature range favors its use in non-linear elements for apparatus subjected to wide temperature fluctuations. By selecting an appropriate ac field intensity (approximately 200 v/mm for Varikond) it is possible to obtain reversible characteristics that differ relatively little from each other over a wide temperature range (-60 to +60°).

In that case when the value of the ac field intensity is less than E_{max} - for example, $E_\sim = 40$ v/mm - the dielectric constant has different values below and above 0°C. Moreover the slopes of the reversible dielectric constant curves measured in such weaker fields are quite different at 60, 20 and -60° (Fig. 5b).

If the ac field is quite strong - for example, $E_\sim = 120$ v/mm or $E_\sim = 260$ v/mm - the values of the dielectric constant at 60, 20 and -60° are nearly equal and the slopes of the reversible characteristics $\varepsilon = f(E_=)$ at the three temperatures are similar (Figures 5c and 5d).

Thus, by applying an ac field of 120 v/mm and higher to non-linear elements made of Varikond VK-1, one can obtain reversible dielectric constant characteristics that change little in a wide temperature range. Because of the favorable non-linear properties of Varikond VK-1, this material can be used to replace vacuum tubes in various types of radio equipment. The fact that it retains good non-linear properties over a wide temperature range extends the potentialities of Varikond even further.

Non-linear Varikond elements were used to construct frequency multipliers, low- and high-frequency and dc dielectric amplifiers and voltage stabilizers. Non-linear Varikond elements have been used to generate frequency-modulation pulses, a very considerable frequency deviation being obtained.

The dependence of the dielectric constant on the dc biasing field makes it possible to regulate the frequency of oscillating circuits as well as the value of the alternating current in such circuits by controlling the dc voltage. Non-linear Varikond elements can be used to tune the input circuit of receivers, to obtain variable selectivity in intermediate-frequency stages and to trim various filters.

Worthy of attention, too, are the possible applications of non-linear elements in automation equipment, computers and the like. By applying appropriate electric fields the ceramic material can be brought to either of the two states associated with ferroelectric hysteresis. The steepness of the hysteresis curve of Varikond makes it a promising material for memory cells of computers.

Above, we have mentioned only a few applications of Varikond. Further study of its properties and theoretical and experimental investigations of electronic and electrical components with Varikond non-linear elements will undoubtedly open new fields of usefulness for this ceramic material.

References

1. B.M.Bul, Elektrichestvo, (Electricity), 3,12 (1946).
2. L.A.Bessonov, Perekhodnye protsessy v nelineinykh electricheskikh tsepiakh so stal'iu (Transients in non-linear electric circuits in steel).M.-L.,1951.
3. G.Penney, I.Horsch & E.Lack, Trans. AIEE, 72,1,68 (1953).
4. T.N.Verbitskaia, Report NII MRTP, 1954.
5. T.N.Verbitskaia, Doklady AN SSSR, 100,29 (1955).
6. W.P.Mason, Piezoelectric crystals and their application to ultrasonics. (In Russian trans. M. 1952).
7. B.M.Bul & I.M.Gol'dman, Doklady AN SSSR, 19,179 (1945).
8. V.P.Vologdin, Elektrichestvo, (Electricity), 8,28 (1946).
9. V.P.Vologdin, Reports of the NII TVCh, 1947, 1950, 1951.
10. G.I.Skanavi & M.D.Neiman, Elektrichestvo, (Electricity), 7,43 (1949).
11. D.M.Kazarnovski, Elektrichestvo, (Electricity), 2,40 (1954).
12. D.M.Kazarnovski, Elektrichestvo, (Electricity), 10,68 (1953).
13. N.P.Bogoroditski & T.N.Verbitskaia, Zhur. tekh. fiz., 22,1920 (1952).
14. T.N.Verbitskaia, Thesis, NII MRTP, 1952.

STABILITY OF THE PIEZOELECTRIC EFFECT IN POLYCRYSTALLINE BARIUM TITANATE

- I.P.Kozlobaev

Polycrastalline specimens of barium titanate can become piezoelectric only after polarization in a strong, constant electric field. After removal of the field, polycrystalline barium titanate remains polarized, i.e., a certain amount of ordering persists in the spatial distribution of the electric moments in the specimen. Conditions are thus created for the appearance of the piezoelectric effect in polycrystalline specimens. Investigations have shown that the effective piezoelectric modulus (constant) $\bar{d}_{33}$ of polycrystalline barium titanate is approximately two orders of magnitude larger than the d_{11} and d_{33} moduli of tourmaline and is of the same order of magnitude as the anomalous piezoelectric modulus d_{14} of Rochelle salt (45° X-cut at 4°C).

For practical applications, aside from the magnitude of the piezoelectric effect, the length of time that the piezoelectric properties persist in an element and their invariability in time are important.

To study the stability of the piezoelectric effect, special investigations were undertaken on a large group of specimens; some of the tests begun on April 14, 1949 are still continuing. On one series of specimens, measurements were made at short time intervals after application of a strong electric field. The first measurement was made immediately after removal of the polarizing field, the measurement itself lasting 5-7 minutes. The results of these measurements are shown in Fig. 1, where the various curves are as follows: 1) piezoelectric modulus $\bar{d}_{31}$, polarization time, one hour; 2) piezoelectric modulus $\bar{d}_{33}$, polarization time, one hour; 3) piezoelectric modulus $\bar{d}_{33}$, polarization time, 1.5 hrs; 4) dielectric constant ε, which had the same value with polarization time of 1 and 1.5 hrs.

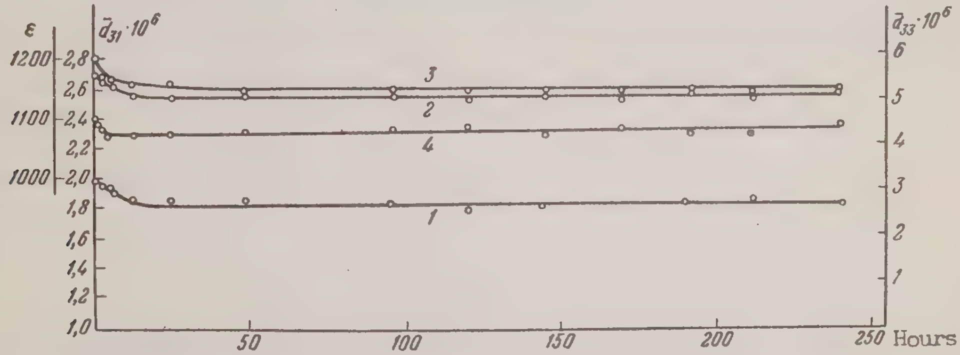

Fig. 1

From Fig. 1 it can be seen that, after polarization, the magnitudes of the piezoelectric moduli and dielectric constant decrease during the first 7-10 hours to 80-90% of their initial value. Measurements carried out on the same sample during this time interval give the maximum spread in observed values. In some samples individual values deviate by up to 10% from average value. Some 7-10 hours after removal of the polarizing field, the piezoelectric effect attained comparative stability, which then persisted for a protracted period without further substantial change. This observation is substantiated by tests on several series of specimens, systematic measurements on which have extended over a six-year period (Fig. 2-4).

In Fig. 2 are given results of measurements of the effective piezoelectric moduli $\bar{d}_{33}$ and $\bar{d}_{31}$ for a group of specimens stored at normal room conditions: curves 1 and 2 are for specimens with unshorted electrodes; curves 3 and 4 pertain to specimens with shorted electrodes.

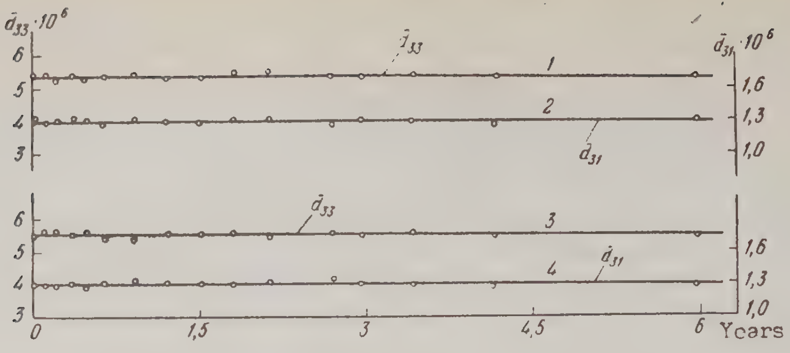

Fig. 2

The piezoelectric modulus $\bar{d}_{33}$ is computed from measurements with a ballistic galvanometer, while $\bar{d}_{31}$ -- from extreme fluctuations of dynamic measurements. No particular precautions were taken in storing these specimens. Data obtained over a period of six years indicate that specimens with shorted and unshorted electrodes show no appreciable difference as regards their piezoelectric moduli. At the beginning of the experiments (April 1949) we had $\bar{d}_{33} = 5.55\cdot 10^{-6}$ e.s.u. and $\bar{d}_{31} = 1.31\cdot 10^{-6}$ e.s.u., while approximately six years later (April 1955), we found $\bar{d}_{33} = 5.49\cdot 10^{-6}$ e.s.u. and $\bar{d}_{31} = 1.30\cdot 10^{-6}$ e.s.u. That is, the effective piezoelectric constants remained unchanged within the limits of the measurement error (± 0.1).

In large-scale use of piezoelectric elements of polycrystalline barium titanate, the piezoelectric transducers are exposed to different environments. In view of this we ran a series of experiments on the stability of the piezoelectric effect under diverse conditions.

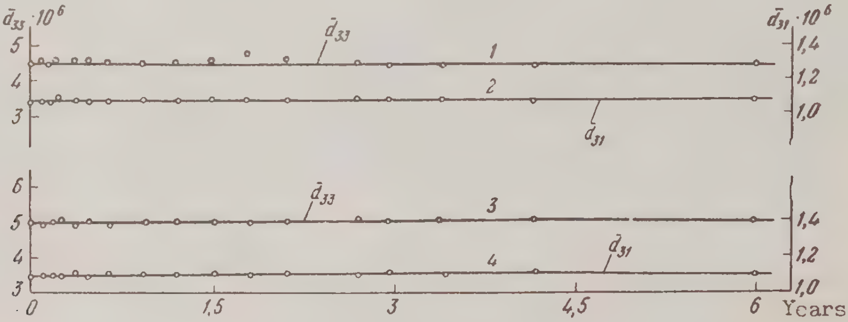

Fig. 3

On October 3, 1949, one lot of the piezoelectric elements prepared in September 1949 was placed in a humidity chamber at a relative humidity of 100%, while a second lot was immersed in water. Neither the first nor the second lot was given any special protection. Measurements were made at different time intervals. Before each measurement water droplets were blotted off with filter paper. The results of the measurements of the piezoelectric moduli $\bar{d}_{33}$ and $\bar{d}_{31}$ are given in Fig. 3: curves 1 and 2 are for the specimens kept in water vapor; curves 3 and 4 are for the specimens immersed in water. Over a time span of more than five years no noticeable changes in the values of the effective piezoelectric moduli were observed.

In Fig. 4 are shown the results of systematic measurements on three groups of specimens (all 2 mm thick) subjected to electrical loads. One of the groups (curves 1 and 2), during working days, was kept in an alternating field of 2 v/cm intensity and a frequency of 1000-1200 cps, obtained by means of a vibrator, for a period of 10-13 hours per day. The second group (curves 3 and 4) was placed in alternating field of 600 v/cm obtained via transformer from the regular power line (50 cps) for the same daily period. The third group (curves 5 and 6) was kept in a 1100 v/cm field of the same frequency (power line) for like periods.

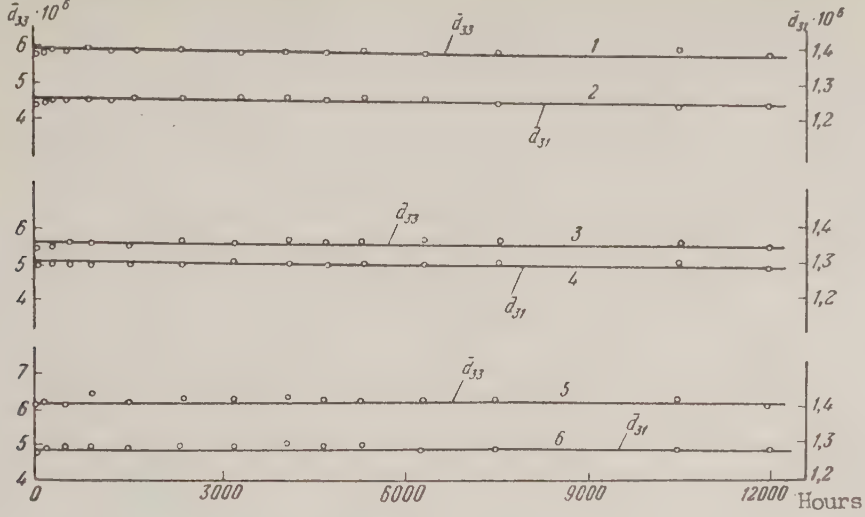

Fig. 4

Since October 1949, the specimens have been under the described electrical loads for a total of more than 12000 hours without any protection from atmospheric influences. The following data have been obtained for the third group: $\bar{d}_{33} = 6.06\cdot10^{-6}$ e.s.u., $\bar{d}_{31} = 1.27\cdot10^{-6}$ e.s.u. (October 22, 1949) and $\bar{d}_{33} = 6.09\cdot10^{-6}$ e.s.u., $\bar{d}_{31} = 1.27\cdot10^{-6}$ e.s.u. (April 15,1955). We also studied the effects of prolonged thermal loading. The change in the effective piezoelectric constant $\bar{d}_{33}$ under prolonged heating is shown in Fig. 5.

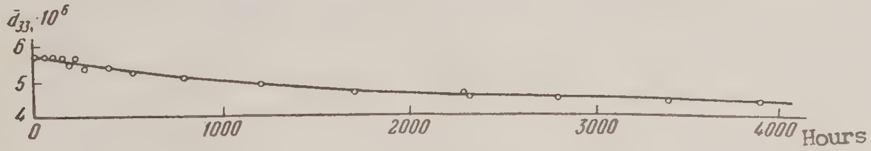

Fig. 5

A group of specimens was placed in a thermostat which was maintained at 73° for 10-13 hours during working days. The temperature was kept constant within ± 1%. Before the beginning of the experiment on August 17, 1950, the mean value of the effective modulus was $\bar{d}_{33} = 5.61\cdot10^{-6}$ e.s.u., while after the specimens had been exposed to heat for more than 4000 hours, on April 25, 1952, the value $\bar{d}_{33} = 4.36\cdot10^{-6}$ e.s.u. was obtained. In comparing the initial and final values of the piezoelectric constant it is necessary to bear in mind that the temperature regulator twice failed to break the heater circuit and the specimens were heated up to 83-85°C. These periods of high heating occurred some 2300 hours after the start of the experiment and lasted 2.5-3 hours each.

To investigate the influence of short duration thermal changes on the piezoelectric effect in polycrystalline barium titanate, the following experiment was made. One group of specimens was placed in boiling water for 60 min., and a second group was suspended in steam over boiling water for the same period. Measurements before heating yielded $\bar{d}_{33} = 6.15\cdot10^{-6}$ e.s.u. and $\bar{d}_{33} = 6.16\cdot10^{-6}$ e.s.u. for the two groups, while after heating the respective values were $\bar{d}_{33} = 6.11\cdot10^{-6}$ e.s.u. and $\bar{d}_{33} = 6.13\cdot10^{-6}$ e.s.u.

The results of extensive observations on these specimens (Fig. 6) show that short periods of heating do not change the magnitude of the piezoelectric effect and do not alter the rate of its decrease with time, provided that the maximum temperature of exposure is kept 10-12° below the Curie point. In all experiments, in addition to the piezoelectric moduli we measured the dielectric constant. Within the limits of experimental error, the value of the dielectric constant remained unchanged in all cases.

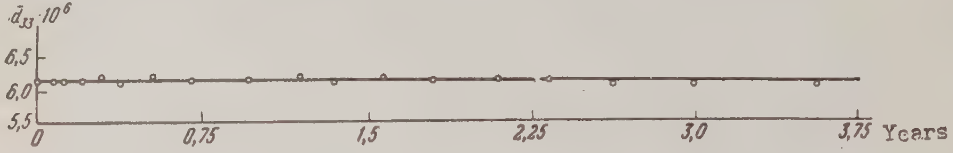

Fig. 6

When the maximum heating temperature was very close to the Curie point, or was equal to it, and the sample was maintained at such a temperature for only 10-30 minutes, then on cooling to room temperature the piezoelectric effect was partially retained. The magnitude of the piezoelectric moduli of such samples fell off by a factor of 1.5-2 relative to the initial values. The dielectric constant decreased by 5-7%.

One group of specimens was heated during 45 minutes from room temperature to 140° (17° above the Curie point) and then cooled to room temperature over a period of 90 minutes. Measurements before heating gave $\bar{d}_{33} = 6.52\cdot10^{-6}$ e.s.u. and $\bar{d}_{31} = 2.19\cdot10^{-6}$ e.s.u. and $\varepsilon = 1251$, while after heating and cooling the measurements showed $\bar{d}_{33} = 2.2\cdot10^{-7}$ e.s.u., $\bar{d}_{31} = 0.71\cdot10^{-7}$ e.s.u. and $\varepsilon = 1080$. In a group of specimens heated to 25° above the Curie point no piezoelectric effect was observed after cooling to room temperature.

Stability studies show that the piezoelectric effect in polycrystalline specimens of $BaTiO_3$ is preserved reasonably well over a long time. External conditions (except strong electric fields > 3 kv/cm) have no noticeable effect on the magnitude of the piezoelectric effect. This is of extreme importance in practical applications of piezoelectric transducers made of polycrystalline barium titanate.

Voronezh State University

EFFECT OF PRESSURE ON THE DIELECTRIC PROPERTIES OF FERROELECTRIC CERAMICS

- I.A.Izhak

The first investigation of the influence of pressure on the permittivity of barium titanate was that of B.M.Vul and L.F.Vereshchagin[1] who showed that the dielectric constant of polycrystalline barium titanate increases with increasing hydrostatic pressure and that its mean relative change over a pressure range of 300 to 2000 atm amounts to 1.2^{-5} per kg/cm^2.

In spite of the fact that some studies of the effect of pressure on the dielectric properties or barium titanate were initiated immediately after the discovery of its ferroelectric properties, little subsequent attention was devoted to this subject.

During the past decade only four articles on the influence of pressure on the dielectric properties of barium titanate and other ferroelectrics have appeared in print. Merz[2] and Forsbergh[3] investigated the effect of hydrostatic and two-dimensional pressure on the Curie temperature of single crystals of barium titanate. Takagi et al[4] studied the effect of unilateral compression on the phase transition temperature of polycrystalline barium titanate. These investigators also observed the effect of pressure on the dielectric hysteresis loops. Shirane and Sato[5] report on the effect of hydrostatic pressure and unilateral compression on the dielectric constant of solid solutions of barium titanate and strontium titanate.

In all these investigations the dielectric constants were measured in weak high-frequency fields. Siniakov and Izhak[6] were the first to study the effect of pressure on the dielectric constant in strong low-frequency fields. They found that it is mainly the spontaneous polarization that is sensitive to pressure and that the relative change in ε as a function of pressure is considerably greater in strong fields than in weak ones. The present article deals with a continuation of the investigations described in Ref. 6. The primary purpose of the present study was to explore the possibility of using ceramics as capacitative pressure sensing elements. In addition we attempted to verify experimentally some of the predictions of the thermodynamic theory of ferroelectrics.

I

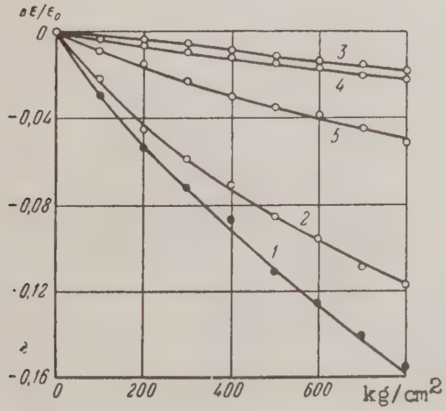

Fig. 1. Pressure dependence of relative change in the dielectric constant. E – 7 v/cm, f – 10^6 cps, t – 20°. 1) $BaTiO_3$, 2) $BaTiO_3$ + 2%BaO, 3) $BaTiO_3$ + + 3%Al_2O_3, 4) $BaTiO_3$ + 4%$PbTiO_3$, 5) $BaTiO_3$ + 5% Pb_3O_4.

Let us start by summarizing the experimental results which showed that under appropriate conditions ferro- and piezoelectric ceramics can be used in various devices as pressure sensitive elements.

Fig. 1 presents the pressure dependence of the relative change in ε for various types of such ceramics. The curves were obtained in a high-frequency (10^6 cycle) weak field (7 v/cm). The fact that the curves extend down from the zero line indicates that the permittivity decreases with increasing pressure. Analogous data obtained in a strong (3.2 kv/cm) low-frequency (50 cps) field are plotted in Fig. 2. It can be seen that the pressure sensitivity of the ceramics depends on their composition. Such ingredients as Al_2O_3, Pb_3O_4 and $PbTiO_3$ decrease the effect of pressure on ε. The pressure dependence of the dielectric constant for the same type of ceramics is stronger in a strong field. It can be seen from Figs. 1

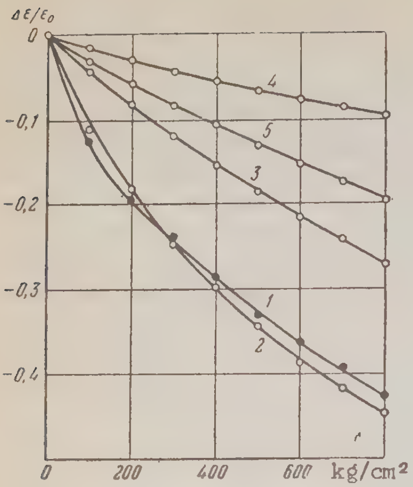

Fig. 2. E - 32 kv/cm, f - 50 cps, t - 20°. Ceramics as in Fig. 1.

and 2 that the dependence of dielectric constant on pressure, especially for $BaTiO_3$ and $BaTiO_3$ + 2% BaO specimens is non-linear. This non-linearity may be corrected by applying a biasing field. Fig. 3 shows the pressure dependences of ε for barium titanate obtained in a low-frequency field of 1 kv/cm with different biasing fields. We see that as the strength of the biasing field is increased the curve straightens out; at the same time, the sensitivity to pressure grows weaker.

Fig. 4 shows the dependence of the relative change in ε for various types of ceramics at a pressure of 600 kg/cm² on the intensity of the low-frequency field. The data of this figure indicate that for every type of ceramics there exists a certain field value for which the pressure sensitivity is a maximum. Tests have shown that the most pressure-sensitive ceramics are those with the weakest saturation fields and with the strongest field — dependence of ε. The field for which the relative change in ε with pressure attains its maximum coincides roughly with the saturation field. The maximum relative change in ε at a pressure of 600 kg/cm² comes to 35-40%. No comparable change in ε with pressure had been observed hitherto because the research had been done in weak fields.

Thus, by a proper choice of the composition of ceramic and of the electric field intensity, it is possible to increase the pressure sensitivity of ceramic elements.

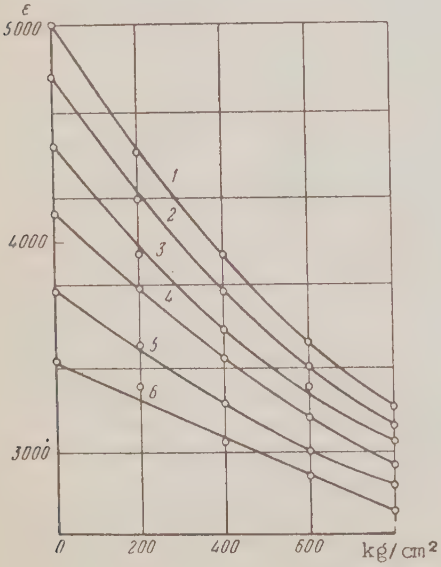

Fig. 3

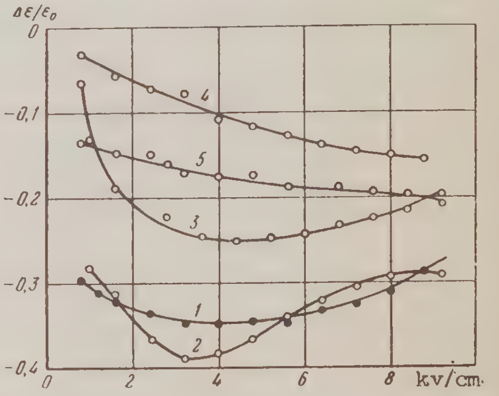

Fig. 4

Fig. 3. Pressure dependence of the dielectric constant of barium titanate in different dc biasing fields superimposed on a 1 kv/cm 50 cps alternating field. t = 20°. 1) E = 0, 2) 2 kv/cm, 3) 3 kv/cm, 4) 4 kv/cm, 5) 5 kv/cm, 6) 6 kv/cm.

Fig. 4. Dependence of relative change in dielectric constant on the intensity of the low frequency (50 cps) field; t = 20°, p = = 600 kg/cm². Ceramics same as numbers 1) through 5) in Fig. 1.

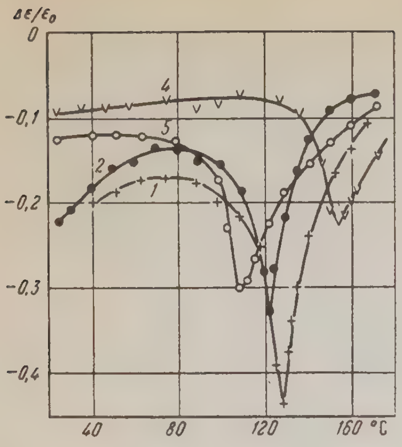

Fig.5. Temperature dependence of the relative change in dielectric constant of different ceramics at p = = 600 kg, E = 1 kv/cm and f = 50 cps. 1-5) as in Fig.1.

Fig. 5 shows the temperature dependences of the relative change in ε for various kinds of ceramics at a pressure of 600 kg/cm^2, observed in a low-frequency field of 1 kv/cm. It can be seen that the materials with the smallest relative change in ε are distinguished by the greatest temperature stability. Fig. 6 shows the analogous dependences for barium titanate made with 2% excess of BaO at a pressure of 600 kg/cm^2, observed in a low-frequency field of 1 kv/cm with different dc biasing fields. It will be seen that the temperature stability of the ceramic can be improved by superimposing a biasing field, although this also reduces the pressure sensitivity.

For conditions where there are no strong variations in temperature, the lack of temperature stability is no drawback to the use of ceramics as capacitive pressure sensing elements.

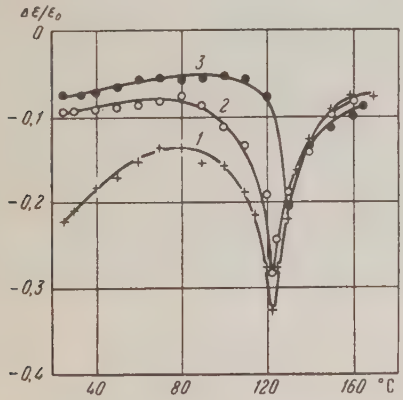

Fig. 6. Temperature dependence of the relative change in dielectric constant of BaTiO$_3$ + 2% BaO in a 1 kv/cm 50 cycle ac field with different biasing fields. 1) E = 0; 2) 1.5 kv/cm; 3) 3 kv/cm.

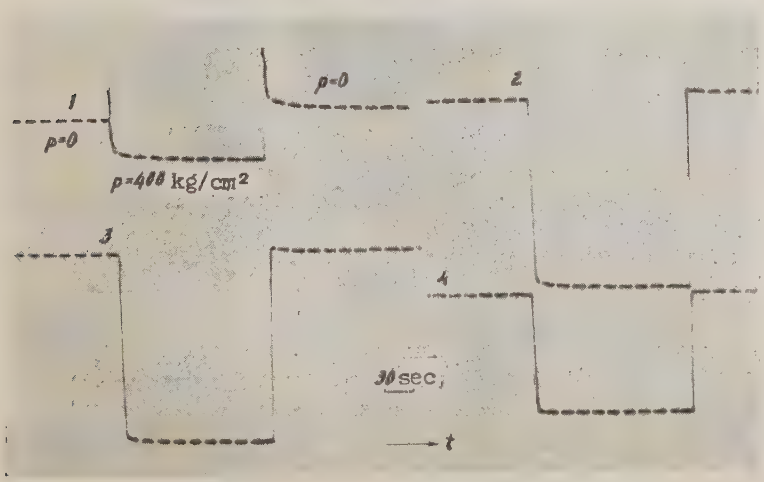

Fig.7. Variation of ε with time in BaTiO$_3$ + 2% BaO incident to pressure changes in different low-frequency fields: 1) 0.15 kv/cm, 2) 2.6 kv/cm, 3) 3.8 kv/cm, 4) 7.2 kv/cm. All measurements at t=20°C.

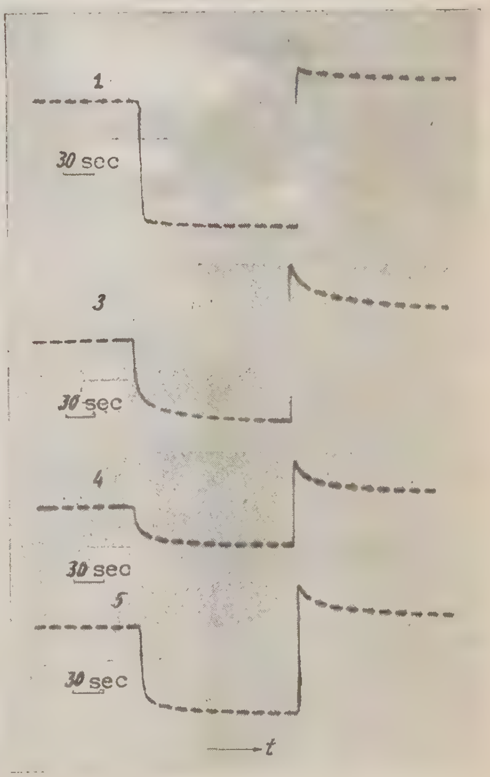

Fig. 8. E = 2.6 kv/cm, t = 20°. 1-5) Materials as in Fig. 1.

Moreover, as can bee seen from the presented data, their temperature stability can be improved by adjusting the composition and by applying a dc biasing field.

When a ceramic specimen is subjected to varying pressure, a certain lag is observed in the establishment of the equilibrium value of ε. Our experiments show that this lag depends on the composition of the ceramic and the intensity of the electric field. Fig. 7 shows the variation of ε with time observed for specimens of one type of ceramic ($BaTiO_3$ + 2% BaO) in different low-frequency fields when a pressure of 400 kg/cm^2 was applied and removed. Fig. 8 shows the analogous variation for various kinds of ceramics, but at a constant field intensity. From these graphs it can be seen that the rate at which the equilibrium value of ε is established depends on the composition of the ceramic and increases with increasing field intensity. The lag in attaining the equilibrium value of ε may be almost completely eliminated by making a proper selection of the composition of the ceramic and the field intensity.

Summing up the above, we conclude that ferro- and piezoelectric ceramics may find one further application, namely, as a material for capacitive sensing elements for gaging constant or slowly varying pressures.

II

We checked the fitness of barium titanate for use as the pressure sensing element in several simple instrument circuits.

1. The simplest circuit is the one shown in Fig. 9. Its principal components are: the transducer (pressure element) C_x, resistor R, detector D, and microammeter A. A potential of 560 volts from a transformer was supplied to the series circuit comprised of C_x and R. The ceramic element had an area of 0.25 cm^2 and a thickness of 0.2 cm. The resistance of R was 5 kΩ. When a pressure of 600 kg/cm^2 was applied, the ammeter pointer deflected over more than a third of the scale; the reading showed good reproducibility as long as the voltage on the circuit remained constant. Where sensing elements with a greater area are used, a less sensitive ammeter can be employed, since the current through such elements will be greater.

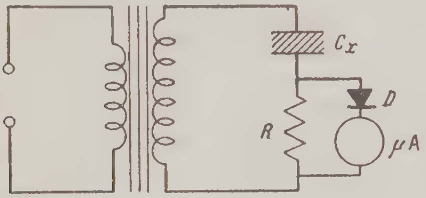

Fig. 9

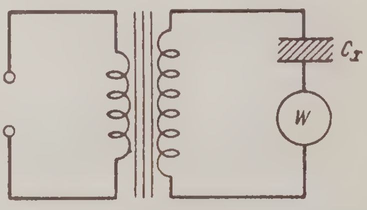

Fig. 10

2. For measuring slowly varying pressures a circuit with a loop oscillograph (Fig. 10) can be recommended. This circuit differs from that in Fig. 9 in that the resistor, detector and microammeter are replaced by the vibrator of the loop oscillograph W. Since the capacitance depends on the size of the sensing element, the requisite current for any vibrator can be obtained through proper selection of the sensing element size. Oscillograms recorded by means of a circuit of this type show good reproducibility (Fig. 11).

3. The arrangement shown in Fig. 12 has the advantage that it permits varying the measurement range. In this circuit a standard capacitor C_0, having a known rating, is connected in series with the ceramic capacitor element C_x. When pressure is applied to C_x its capacitance is reduced, causing a decrease in the voltage across C_0 and hence a corresponding change in the indication of the vacuum tube voltmeter V.

Whereas in the previous two circuits the current requisite for the indicators employed is obtained through selection of the capacitance of the sensing

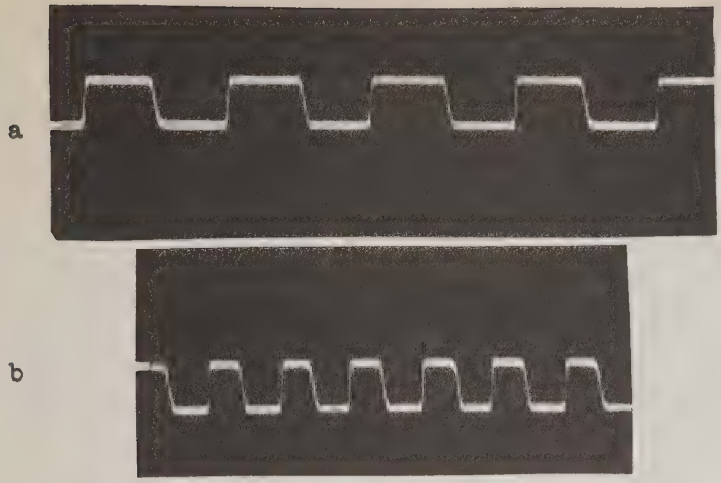

Fig. 11. Periodic variation in pressure to 600 kg/cm^2; a) 3 per min, b) 6 per min.

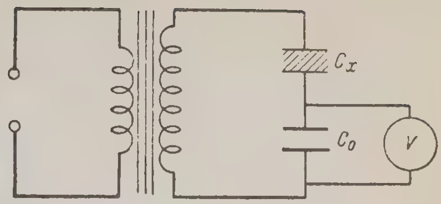

Fig. 12

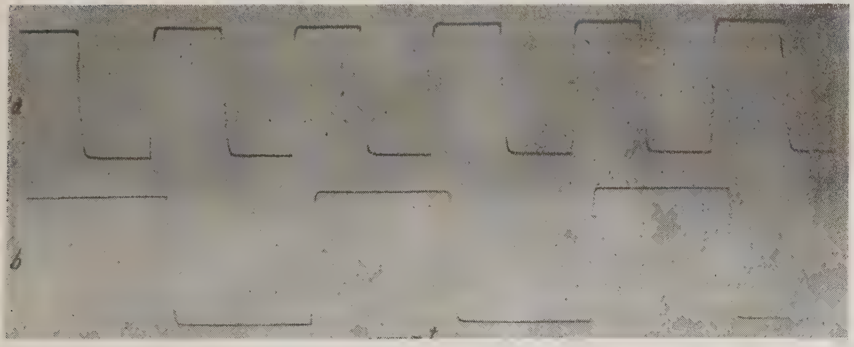

Fig. 13. Periodic pressure of 400 kg/cm^2; a) 3 per min, b) 1.5 per min.

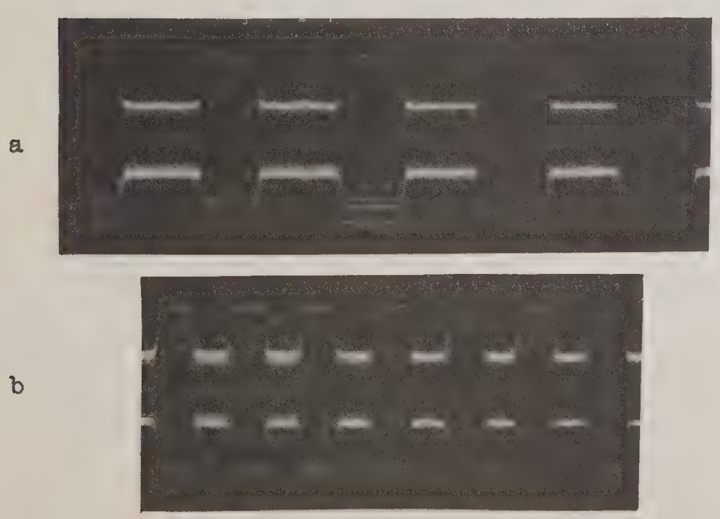

Fig. 14. Periodic pressure of 600 kg/cm^2; a) 3 per min, b) 1.5 per min.

element, in the circuit of Fig. 12 the sensitivity (range) can be varied by changing the capacitance of C_0 and switching the scale of the voltmeter. We used a circuit of this type in our laboratory for investigating the pressure dependence of the dielectric constant.

4. As pictured, the circuit of Fig. 12 does not permit of photographic recording. It can easily be adapted to this purpose however, by shunting a high resistance (about 100 kiloohms) across the microammeter of the voltmeter; an appropriate voltage can then be taken off the resistor and applied to a recording galvanometer. A record of the effect of periodic pressure obtained in this manner is shown in Fig. 13. The excellent reproducibility is evident.

5. If we replace the microammeter in the circuit of the VKS-7 vacuum tube voltmeter[7] used in the circuit of Fig. 12 with the vibrator of a loop oscillograph, then instead of the envelope of the 50 cycle oscillations shown in Fig. 11 we obtain a clear single curve such as that shown in Fig. 14. Here again it

will be seen that the reproducibility is good.

While the last circuit is more complicated than that shown in Fig. 10, it allows of recording several processes on a single film strip.

Naturally there are other circuits in which ceramic pressure sensing elements can be used.

Our experiments were the first in this direction, but they have already proved that ferroelectric ceramic pressure sensing elements have a number of advantages over other pressure elements in the way of simplicity of production, mechanical sturdiness, good reproducibility of results and wide applicability in diverse devices and automatic installations, wherever there are large constant or slowly changing pressures. Their sensitivity, inertness and temperature stability depend on the composition of the ceramic and the intensity of the electric field. In this respect the best of the tested ceramics was pure barium titanate at a field intensity of 4 kv/cm.

III

Thermodynamic theory leads to the deduction that elastic stresses have an orienting effect on the spontaneous polarization of ferroelectrics.[8]

Thus, for ferroelectrics with positive volume electrostriction ($BaTiO_3$ and $PbTiO_3$), under unilateral compression, the spontaneous polarization occurs in the direction perpendicular to the axis of compression, or, in case of expansion, in the direction of the axis of elongation.

If this conclusion is correct, we should expect ε to increase in a direction perpendicular to the axis of compression and to decrease along the axis of compression due to the effect of pressure on the spontaneous polarization.

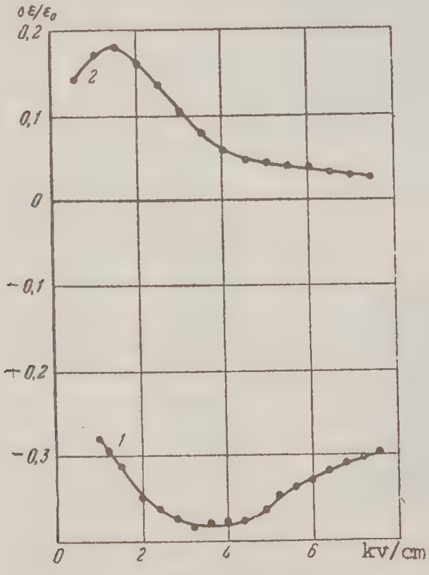

Fig. 15

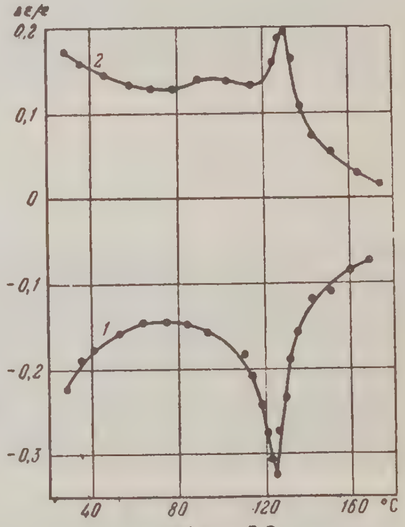

Fig. 16

Fig. 15. Variation in dielectric constant of $BaTiO_3$ + 2% BaO in the directions normal and parallel to axis of compression with pressure. 50 cps; 600 kg/cm^2; 20°.

Fig. 16. Same as Fig. 15 but with biasing dc field of 1 kv/cm.

We made the pertinent measurements, the results of which are shown in Fig. 15 and 16. Curves 1 show an increase in ε in the direction perpendicular to the axis of compression, while curves 2 show a decrease in the direction of the axis of compression. As can be seen from these data, the prediction of thermodynamic theory as to the orienting effect of pressure on the spontaneous polarization is qualitatively confirmed in a wide range of fields and temperatures.

However, it is not possible to attribute the observed behavior solely to the orienting effect of pressure on spontaneous polarization, since some variation of ε with pressure is also observed above the Curie point, where there is no spontaneous polarization.

Another deduction from theory -- that the Curie point is shifted to the side of higher temperatures under unilateral compression[8] -- has already been experimentally confirmed in an earlier investigation.[6]

Dnepropetrovsk State University

References

1. B.M.Bul & L.F.Vereshchanin, Doklady AN SSSR, 48, 662 (1945).
2. W.J.Merz, Phys. Rev., 78, 52 (1950).
3. P.W.Forsbergh, Phys. Rev., 93, 686 (1954).
4. J.Takagi, E.Sawaguchi & T.Akioka, J. Phys. Soc. Japan, 3, 270 (1948).
5. G.Shirane & K.Sato, J. Phys. Soc. Japan, 6, 20 (1951).
6. E.V.Siniakov & I.A.Izhak, Doklady, AN SSSR, 100, 243 (1955).
7. A.K.Balikhin, Radioizmereniia (Radio measurements), M. 1949.
8. L.P.Kholodenko & M.Ia.Shiokobokov, Zhur. eksp. i teor. fiz., 21,1250(1951).

FUSION OF BARIUM TITANATE BY CONDUCTION CURRENTS

- N.S.Novosil'tsev, O.I.Prokopalo & A.F.Iatsenko

In the present report we give the results of an investigation of the dependence of the conductivity of titanate ceramics on the temperature and the electric field intensity. The power dissipated in the specimen under different conditions is evaluated. It is shown in the case of barium titanate specimens fused by conduction current that after resolidification the density approaches the theoretical value and the dielectric constant increases, particularly at the Curie point.

Barium titanate and similar ceramics sintered in a resistance furnace at 1300-1400° usually have a density lower than the value calculated from x-ray data on the structure of single crystals. The theoretical density of $BaTiO_3$ should be about 6.24 g/cm^3. When a ceramic is fired without a flux an appreciably lower density is obtained. Fluxes improve the mechanical properties of the ceramic body and, in particular, increase the density. However, the dielectric constant and dielectric loss are structure-sensitive properties. Hence, an increase in the extraneous binding flux-layers between the individual crystals is highly undesirable.

In many cases, as, for example, when barium titanate is used as a piezotransducer for generating ultrasound, it is important to have a vacuum-tight material. One may expect to obtain monolithic and dense ceramic material through melting and solidification.

Here, however, we encounter practical difficulties. First, $BaTiO_3$ has a high melting point: according to the literature[1] and our data nearly 1700°. Experiments with other titanates and their solid solutions show that they, too, have high melting points. Second, it is difficult to find a suitable crucible material. The molten titanate attacks all practical refractory materials: it is absorbed by chromomagnesite and corundum and fuses with mullite, quartz and carborundum.

1. Conductivity of Titanate Ceramics at High Temperatures

Our investigation of the variation of the electric resistance of barium titanate ceramic specimens with the temperature and other factors showed that one can create conditions under which the current flowing through the ceramic will be heavy enough not only to maintain the specimen at high temperature but also, if desired, to cause melting.

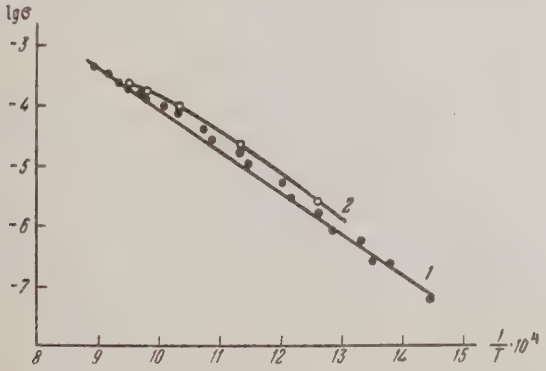

Fig. 1. Variation of the conductivity of $BaTiO_3$ specimens with the sintering temperature: 1) rising temperature, 2) falling temperature.

The dependence of the conductivity on the sintering temperature of a barium titanate ceramic specimen is shown in Fig. 1. The specimens were prepared without flux. The sintering temperature from sample to sample varied within 20°. This variation does not affect the character of the conductivity vs temperature curve: the curve of Fig. 1 is representative for all specimens.

The measurements were made with dc current with a field gradient of 55 v/cm. In each case readings were made 5 seconds after application of the voltage. It will be seen that all measurements made during the temperature rise fit a straight line. The activation energy of the charge carriers computed from the slope of this curve proved to be 1.4 ev.

Measurements made during cooling yield somewhat higher values of conductivity (Fig. 1), which shows that there is some temperature hysteresis. In the case of specimens heated to 350-400° and then cooled to room temperature the final conductivity is some 1-2 orders of magnitude higher than the initial conductivity. The slow return to the initial value continues for weeks.

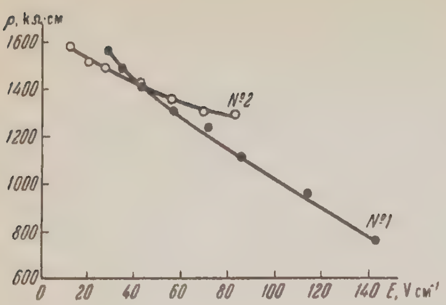

Fig. 2. Dependence of the specific resistance of two BaTiO3 specimens on the electric field gradient.

In order to verify the applicability of Ohm's law to the ceramics we measured the specific resistance. The resistance vs voltage curves obtained for the two specimens at 500° are shown in Fig. 2. The curves for both specimens show a decrease in specific resistance with increasing field gradient (specimen No. 1 was sintered at a 20° higher temperature than specimen No. 2). This falling-off of the resistance at 500° cannot be attributed to self-heating (resistance heating by the current). For appreciable self-heating the initial temperature must be raised to at least 800-900°. As can readily be computed from the data of Fig. 2 with $E = 140$ v/cm and $\rho = 800$ kΩ, the dissipated power is only 0.025 watt/cm^3 or 0.006 cal/sec/cm^3.

The curves of Figs. 1 & 2 are based on measurements made 5 seconds after application of the voltage. The current through the barium titanate specimen may undergo appreciable variations with time. The character of the variations depends on the initial temperature, the applied voltage and the graininess of the sample. The size of the constituent crystals obviously determines their volume to surface area ratio. The amount of material with a defective lattice, which in such ceramics plays the role of the intrinsic vitreous phase, depends on this ratio.

The variation of current with time at different temperatures for a fine-grain specimen is shown in Fig. 3. In all cases the initial current value was taken as unity in plotting the curves. As may be seen, at 470° the decrease in current due to high-voltage polarization is rather slow; at 550° high-voltage polarization proceeds somewhat more rapidly. At an initial temperature of 600° the polarization process is further accelerated, but beginning with the 20th second the influence of a new factor becomes apparent: the current stops falling off and begins to increase. This factor is self-heating. As we go to higher temperatures the self-heating increases and becomes more effective.

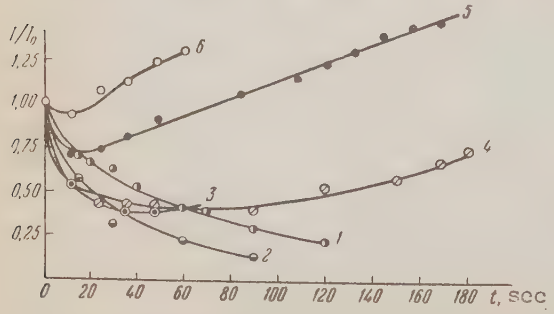

Fig. 3. Variation of current with time: 1) at 470°, 2) at 550°, 3) at 600°, 4) at 650°, 5) at 700° and 6) at 760° (initial temperatures).

It will be seen from the curves that increasing the temperature from 470° to 760° raises the conductivity by almost three orders of magnitude. Further increase in temperature results in a vigorous and non-uniform (over the volume) evolution of heat. One can no longer speak of the temperature as having a uniform value for all parts of the specimen. Obviously the current density in different parts of the specimen differs. Low-resistance "bridges" are formed at various points and here the current and heat evolution are markedly higher.

From the point of view of the tech-

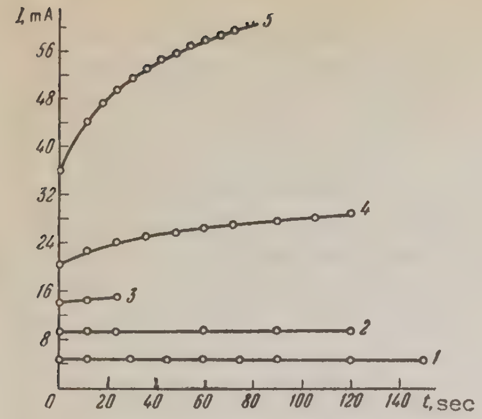

Fig. 4. Variation of current with time for sample No. 1 at 700° with different field intensities: 1) 28 v/cm, 2) 57 v/cm, 3) 85 v/cm, 4) 110 v/cm and 5) 170 v/cm.

nology of fusing ceramic specimens by means of current, the question arises whether it would not be possible to replace the initial thermal heating by an appropriate increase of the field gradient (applied voltage).

The curves given in Fig. 4 give an affirmative answer to this question — in principle; practice shows, however, that this is not expedient. The curves of Fig. 4 were obtained on a specimen sintered at a reduced temperature. The measurements were made on the specimen mounted in a thermostatic chamber at 700°. The first readings, as in the other cases, were made 5 seconds after application of the voltage. From a comparison of the curves it is obvious that at low field gradients the self-heating is not sufficient for development of the current-increase process. As the field gradient is increased, the self-heating increases and the current grows. From the data in Fig. 4 one can readily compute the energy given off with different field gradients at any instant.

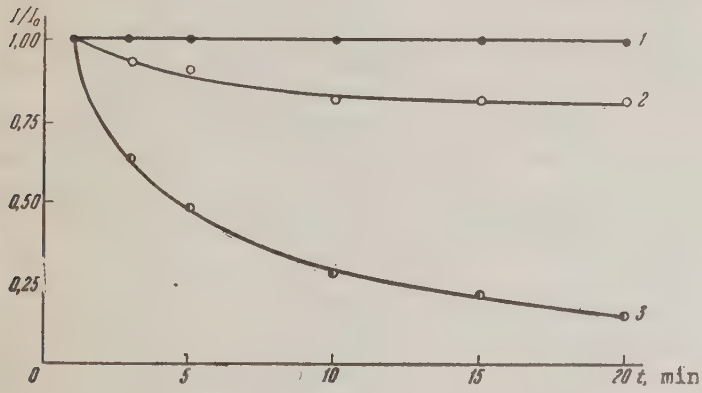

Fig. 5. Time dependence of current: 1) at 300°, 2) at 200° and 3) at 80°.

At moderate temperatures (80-300°) and weak gradients (55 v/cm) we observe the usual falling-off of the current with time owing to high-voltage polarization. Curves for the variation of current with time at temperatures in this range are shown in Fig. 5. In plotting the curves, the current measured at 1 minute after application was taken as unity (I_0).

Analysis of the variation with time of the processes of polarization and depolarization at different temperatures, in conjunction with other data, led us to the conclusion that the nature of the processes producing high-voltage polarization in barium titanate ceramic is different at low (20-200°) as against high temperatures (500-600°).[2 & 3] At low temperatures the high-voltage polarization may be attributed to displacement of the charges in micro-regions. In this case the potential distribution in the specimen between electrodes remains linear. At higher temperatures the elementary charges are displaced greater distances; they accumulate in the pre-electrode regions, as is the case in almost all dielectrics at elevated temperatures.

2. Melting Titanate Ceramic by Commercial Frequency (50 cps) Current

In attempting to fuse titanates by means of alternating current it is important to bear in mind that ceramic specimens which may differ little as regards losses at radio frequencies, may differ greatly at low frequencies. This was investigated in detail for titanium dioxide specimens in our laboratory.[4] Where melting of $BaTiO_3$ is concerned the additional evolution of heat due to low-frequency losses can only be helpful.

As noted above, great difficulties are encountered in attempting to fuse barium titanate by furnace heating in a crucible. As the heat is conducted to the barium titanate through the walls of the crucible, the material adjacent to the crucible walls melts first. The molten barium titanate dissolves and breaks down most refractory crucibles.

When the ceramic is melted by conduction current the difficulty of the crucible material is obviated. In this case the surface of the specimen is at a lower temperature than the interior so that the heating and melting occur primarily inside the specimen. The outer, relatively cold parts of the specimen here play the part of the container, thus insuring high purity of the barium titanate melt.

In electro-melting the barium titanate bar must be preheated. In our experiments this was accomplished by mounting the specimen with the electrodes attached in a nichrome furnace which could be heated to 1000°. The voltage was applied to the specimen from the regular power line and regulated by means of an auto-transformer. After the preliminary heating (necessary to bring down the resistance) the current through the specimen attains several amperes and at this point the resistance furnace can be switched off. The power dissipated in the sample, amounting to several hundred watts, is sufficient to maintain the necessary high temperature and melt the ceramic material.

The current must not be allowed to rise beyond a certain value in order to avoid melting of the surface layers with consequent escape of the molten interior matter. One can readily select a regime for a specimen of any size or shape at which the interior region will be melted while the surface remains hard.

In order to insure high purity it is important to avoid over-heating at the points of electrode contact. Experiments showed that with proper choice of the shape and material of the electrodes the most intensive heating occurs several millimeters in from the electrodes. With sufficiently massive electrodes the barium titanate does not fuse at the points of contact.

3. Some Properties of Melted Barium Titanate

When a ceramic material is melted by conduction current the outside dimensions of the sample remain unaltered; inside, however, shrinkage cavities appear due to consolidation of the material. Molten barium titanate has a fairly high viscosity so that the shrinkage cavities do not coalesce into a single large cavity. Nevertheless in case a surface crack forms the molten material seeps through.

When the molten material solidifies there is an appreciable reduction of the specific volume. This is apparent from the visible pores observed in solidified flows.

In order to check the degree of consolidation, we cut samples from different parts of fused and solidified specimens. The samples from well-fused regions showed a density of 5.6-5.8 g/cm^3 while samples from regions near the surface had a density of 5.3-5.4 g/cm^3.

The approach to the theoretical density attained is substantiated by dielectric measurements. Samples cut from well-melted regions had a dielectric constant at room temperature some 15-20% higher than not fused samples. The difference in the dielectric constant at the Curie point attained 50%.

The $BaTiO_3$ specimens obtained by conduction current melting are more transparent than the ceramics prepared in the usual way.

References

1. W.O.Statton, J. Chem. Phys., 19,1,33 (1951).
2. N.S.Novosil'tsev, Zhur. tekh. fiz., 20,808 (1950).
3. O.I.Prokopalo, Thesis, Rostov State University, 1953.
4. I.N.Beliaev, N.S.Novosil'tsev, A.L.Khodakov & M.S.Shul'man, Zhur. tekh. fiz., 11,547 (1951).

SOME PHYSICAL PROPERTIES OF ROCHELLE SALT CRYSTALS EXPOSED TO RADIOACTIVE IRRADIATION

- I.S.Zheludev & V.A.Iurin

Historically, Rochelle salt - potassium sodium tartarate - is the first representative of the class of materials known as ferroelectrics: solid dielectrics exhibiting spontaneous electric polarization in a certain temperature interval. One of the characteristic features of ferroelectrics is the non-linear dependence of the polarization on the intensity of the external electric field. The polarization curves of the X-cut of Rochelle salt in an alternating field are widely known; these curves have the appearance of hysteresis loops (Fig. 1, a) and are commonly termed normal ferroelectric hysteresis loops in the literature.

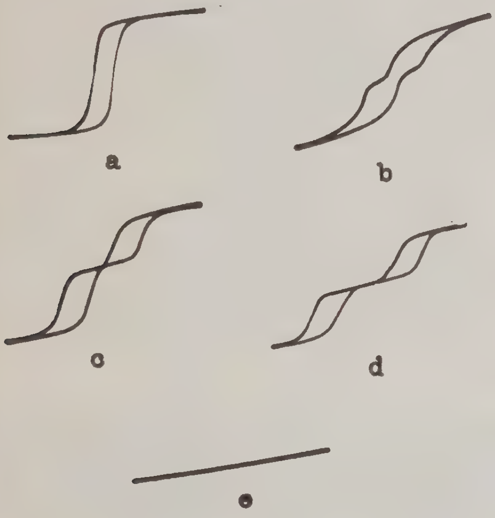

Fig. 1. Hysteresis loops in Rochelle salt (temperature 19°, frequency 50 cps, maximum field intensity for all specimens 1390 v/cm: a) not irradiated, maximum polarization $17.9 \cdot 10^{-8}$ coulomb/cm^2; b) after 30 min irradiation; c) after 1 hour irradiation; d) after 2 hours irradiation; e) after 13 hours irradiation. The vertical scales for the different specimens are different.

Together with Proskurnin and Baberkin[1] we discovered anomalous (as regards the hysteresis loops) polarization in crystals of Rochelle salt exposed to radioactive radiation. X-cut specimens of Rochelle salt measuring 20 x 10 x 1.5 mm with silver foil electrodes attached thereto were exposed to a Co^{60} radioactive source; the dosage received by the crystal amounted to about 10^5 roentgen per hour.

The hysteresis loops of specimens exposed to different amounts of radiation are reproduced in Fig. 1, b,c,d and e. It will be seen that even after a short irradiation time (Fig. 1, b) the hysteresis loop begins to differ from the normal (Fig. 1, a), i.e., narrows somewhat at low field intensities. The narrowing is enhanced as the irradiation time is increased, to the point where sections with linear polarization appear (Fig. 1, c & d). Further exposure to radiation leads to polarization analogous to that of a linear dielectric (Fig. 1, e).

We felt it would be of interest to investigate the effect of a dc biasing field on the shape of the anomalous hysteresis loops. The distortion of the hysteresis loops, as the intensity of the dc biasing field is increased, is shown in Fig. 2; curve *a* shows the loop in the absence of a biasing field; as the biasing voltage is applied and increased, at first the upper branch of the loop is deformed - b & c in Fig. 2. At a biasing field intensity equal to the peak value of the ac field this branch disappears entirely, while the other branch remains unchanged (if we neglect the elongation of the linear section in the saturation field - Fig. 2, c). Further increase in the dc field strength begins to distort the second branch as well (2, d), until at an intensity equal to twice the amplitude of the ac field the crystal is polarized just as a linear dielectric (2, e).

As is known,[2] polarization processes in ferroelectrics are closely associated with rearrangement and reorientation of the domain structure. In order to establish the influence of irradiation on a domain structure of Rochelle salt we photographed this structure in irradiated and not irradiated samples

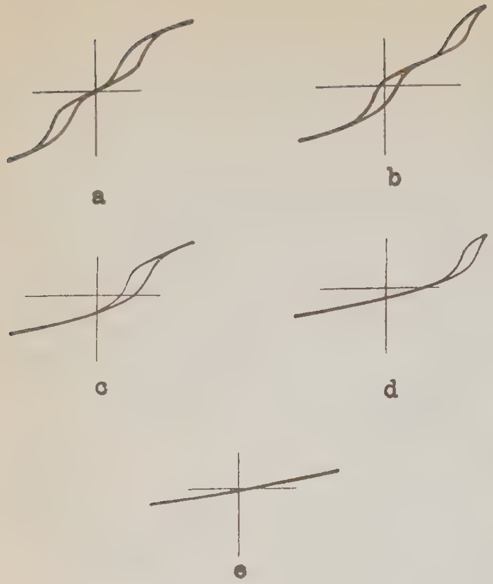

Fig. 2. Hysteresis loops in Rochelle salt in a dc biasing field (temperature 20.5°, frequency 50 cps, maximum field intensity in all cases 1100 v/cm, irradiation time 3 hours): a) in the absence of a biasing field (maximum polarization $13.5 \cdot 10^{-8}$ coulomb/cm^2); b) in 467 v/cm dc biasing field; c) in 1100 v/cm dc field; d) in 1530 v/cm dc field; e) in 2150 v/cm dc field. Vertical scale is the same for all loops.

cut from the same growth pyramid.

The domain structure photographs are shown in Fig. 3; a is for the not irradiated specimen; b, c and d are for specimens irradiated for 30 minutes, 3 hours and 13 hours, respectively. The photographs and observed data do not permit of drawing definitive conclusions regarding the nature of the changes in the domain structure produced by radiation. For this purpose it is apparently necessary to observe the domain structure of the same specimen under the influence of increasing irradiation. However, the most important of the observed facts is that not only the weakly irradiated but also the specimens exposed to prolonged radiation, i.e., the specimens that exhibit either anomalous (Fig. 3,c) of virtually no hysteresis loops (3,d) have a clearly discernible domain structure. It is interesting to note that the specimen which received the heaviest

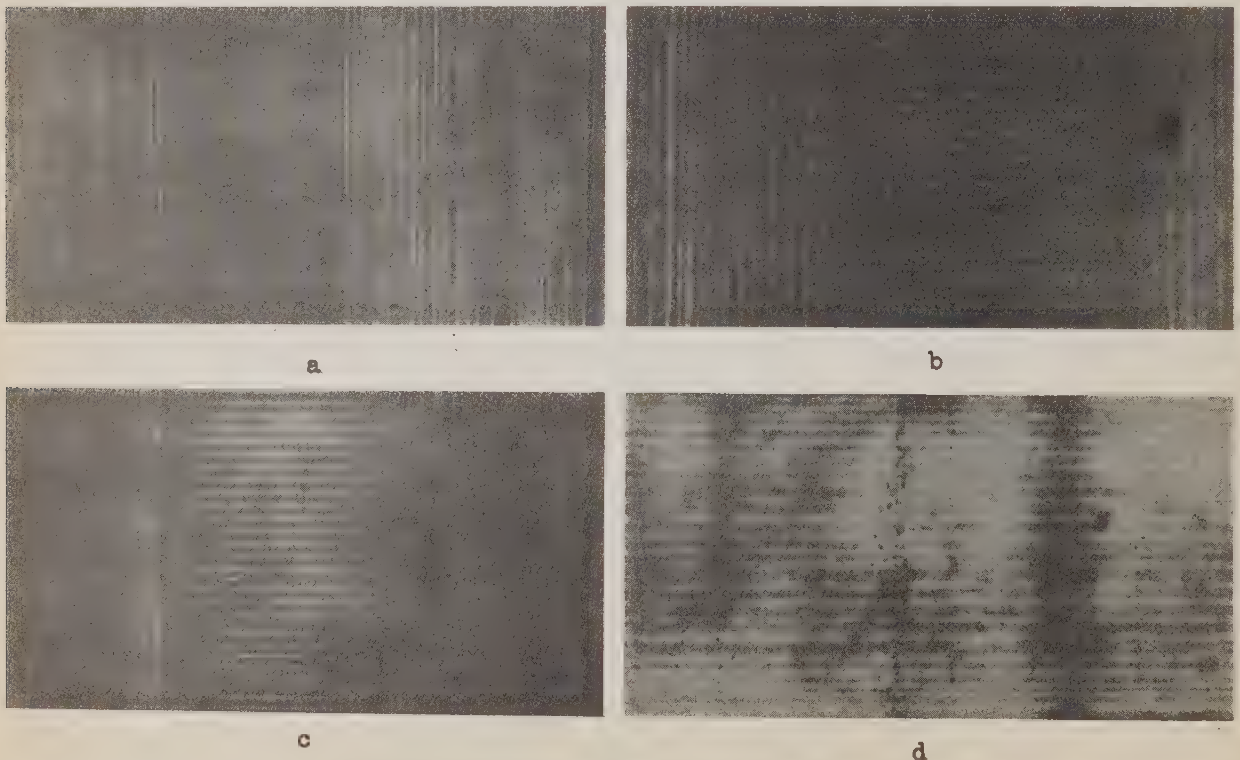

Fig. 3. Domain structure of Rochelle salt (t = 19°): a) not irradiated; b) irradiated 30 min; c) irradiated 3 hours; d) irradiated 13 hours.

dose of radiation (Fig. 3,d) shows a fairly large number of defects in crystal structure: rows of dark spots oriented perpendicularly to the domain boundaries.

Investigation of the piezo-effect in Rochelle salt samples exposed to radioactive radiation is also of interest. We made approximate determinations of the piezoelectric constant g_{14} of such specimens by the static method by means of an electrometer. It was established that within the limits of the experimental error irradiated specimens having an anomalous polarization including a linear section (Fig. 1,e) do exhibit a piezo-effect and have almost the same value of the constant g_{14} as the non-irradiated specimens.

In addition to the above experimental data on the physical properties of irradiated Rochelle salt, we might note that (as was established in the experiments of Ref. 1) Rochelle salt undergoes appreciable decomposition under the influence of γ-radiation: gases (H_2, CO, CO_2 CH_4) are evolved in the amount of about 5 molecules per 100 ev and the crystal yellows. The total number of dissociated anions $(C_4H_4O_6)^{--}$ is not great; even with an amount of irradiation resulting in the complete loss of ferroelectric properties (Fig. 1,e) only one molecule out of several thousand is decomposed. The charges of the ion pair involved are neutralized, which apparently produces a strain in the crystal lattice.

The polarization process, characterized by the anomalous hysteresis loops of Fig. 1,d, is commonly associated with the polarization theoretically predicted by Kittel[3] and investigated by other authors[4-8] in antiferroelectric crystals. In such crystals the ions are arranged in rows, with those in one row spontaneously polarized in one direction and those in the neighboring row in the opposite direction.

At the same time, as has been indicated by Anliker, Känzig and Peter[9], an antiferroelectric state is possible for very small ferroelectric crystals since in them the ratio of the surface (layer) energy to the volume energy is so great that the surface energy has an appreciable effect on the thermodynamic state of the crystal.

On the basis of the above concepts the following explanation of the observed anomalous polarization effect in irradiated specimens appears plausible. As was noted, a small fraction of the Rochelle salt molecules undergoes decomposition as a result of irradiation. Obviously, this decomposition leads to the loss of spontaneous polarization by some of the unit cells. Thus irradiation leads to an increase of the interstitial layer between domains (and at the same time to an increase in the energy of this layer) and to the formation of atomic or ionic inclusions between the individual cells within a given domain. These two factors are apparently the ones responsible for the polarization of irradiated specimens being similar to the polarization of antiferroelectrics (Fig. 1,c & d). As for the linear polarization observed in strongly irradiated specimens (Fig. 1,e), in view of the above interpretation it may be assumed that in these samples two anomalous hysteresis loops may be observed at sufficiently high field intensities.

The above interpretation is not in conflict with the presence of the domain structure in irradiated specimens since the fraction of broken-up molecules in relation to the total number is very small (on the order of 1 to 1000). There is no difficulty either in explaining the presence and magnitude of the piezo-effect in irradiated specimens since structurally Rochelle salt undergoes only minor alterations incident to irradiation. (We note that the possibility of a piezo-effect in some antiferroelectrics is not excluded.) From this point of view irradiated Rochelle salt may be regarded as not a true antiferroelectric (inasmuch as structurally it is not one) but rather as a ferroelectric material in the antiferroelectric state.

Obviously the antiferroelectric state of Rochelle salt (as, apparently, of other ferroelectrics) can be obtained not only by irradiation but in other ways as well. The transforming agency must give rise to the distortions, defects or inclusions in the ferroelectric, required for the transition to the antiferroelectric state.

Institute of Crystallography of the
Academy of Sciences of the USSR.

References

1. I.S.Zheludev, M.A.Proskurnin, V.A.Iurin & A.S.Baberkin, Doklady AN SSSR, 103,207 (1955).
2. M.A.Chernysheva, Doklady AN SSSR, 81,1065 (1951).
3. C.Kittel, Phys. Rev., 82, 729 (1951).
4. M.H.Cohen, Phys. Rev., 84,369 (1951).
5. Y.Takagi, Phys. Rev., 85,315 (1952).
6. G.Shirane, E.Sawaguchi & Y.Takagi, Phys. Rev., 84,476 (1951).
7. W.P.Mason, Phys. Rev., 88,480 (1952).
8. G.A.Smolenski & V.Kh.Kozlovski, Zhur. eksp. i teor. fiz., 26,684 (1954).
9. M.Anliker, W.Känzig & M.Peter, Helv. Phys. Acta, 25,474 (1952).

ON CERTAIN PHYSICAL PROPERTIES OF ROCHELLE SALT CRYSTALS

- I.Ia.Eisner

In their researches, I.V. and B.V.Kurchatov, M.A.Eremeev and P.P.Kobeko[1-4] investigated Rochelle salt crystals obtained from solutions with isomorphic admixtures, in which the potassium of Rochelle salt was replaced by NH_4, Rb, Cs and Tl. The influence of certain non-isomorphic impurities on the electric properties of Rochelle salt crystals was investigated by Thorp and Buckley.[5]

In our investigation we studied the influence of admixtures on the dielectric constant and dielectric loss in Rochelle salt crystals. We investigated the possibility of obtaining Rochelle salt crystals from its solution in the presence of boric acid under conditions of mutual saturation. The habit of the obtained crystals differs from the habit of crystals of pure Rochelle salt. The (210) shape prevails among the crystals obtained under these conditions (Fig. 1).

We also obtained crystals of Rochelle salt with an admixture of copper ions. These crystals were grown in solutions of a complex compound of Rochelle salt and copper prepared from a mixture of copper sulphate and Rochelle salt. The habit of these crystals also differs from that of the pure salt. Here, too, the (210) shape predominates (Fig. 2).

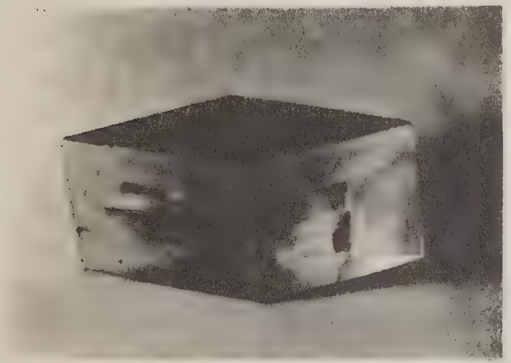

Fig. 1. Rochelle salt crystal with boron ions.

Fig. 3. Rochelle salt crystal with molybdenum.

Fig. 2. Rochelle salt crystal with copper.

We also grew crystals of Rochelle salt from its solutions with admixtures of salts comprising certain elements of the sixth group of the periodic table. A spectroscopic investigation of the resultant crystals failed to show the presence of any elements of this group other than molybdenum. In view of this, in further studies we grew crystals only from Rochelle salt solutions containing different concentrations of ammonium molybdate. The habit of these crystals differs markedly from that of the pure salt. The crystals are greatly elongated in the direction of the Z-axis. Again the (210) shape predominates but the third pinacoid in these crystals is weakly developed as compared with the Rochelle crystals with admixtures of B or Cu ions (Fig. 3).

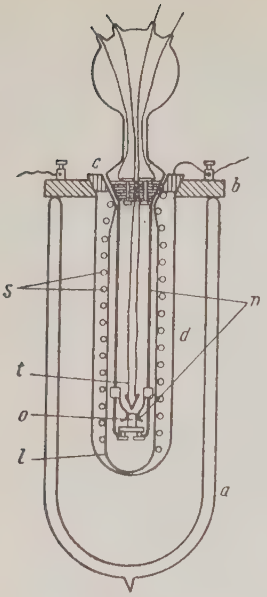

Fig. 4. Diagram of apparatus for determining ε and tan δ of Rochelle salt crystals: a) Dewar flask, b & c) insulating covers, d) glass vessel with alcohol, s) electric heater, l) tube, n) crystal holder, o) crystal, and t) thermocouple.

X-cut plates of uniform thickness of 0.2 cm were prepared from all the investigated crystals. Gold-foil electrodes were applied to the cut plates. The resultant "capacitors" were kept in a drying chamber with a solid desiccating agent for a period of 2-3 hours and then immediately transferred to the special glass "holder" tube (Fig. 4). Inside the tube the crystal plate fitted into a special brass crystal holder equipped with spring contacts. During the measurement no desiccant was used in the tube.

The dielectric constant and dielectric loss tangent of the pure Rochelle salt and of the crystals with impurities were measured in ac fields (50 cps) at different intensities up to 20 v/cm. The measurements were made by means of an ac bridge. Below we give the data obtained in the 10 to 15 v/cm interval.

The temperature dependence of the dielectric constant in the interval from -20 to +40° for the pure crystals shows two maxima, $\varepsilon' = 5130$ and $\varepsilon'' = 5175$ at 23.8° and at -15.5°, respectively (Fig. 5). At the same time the variation of the loss tangent exhibits to rather flat maxima: tan $\delta_1 = 0.33$ at $t_1' = 19.5°$ and tan $\delta_2 = 0.34$ at $t_2' = -4°$. Thus the loss tangent curve attains both maxima in the temperature interval corresponding to spontaneous polarization. At temperatures near the Curie point the loss tangent falls off (in jumps), while at temperatures beyond the Curie points it rapidly tends to values under 0.001.

The temperature variation of the dielectric constant of crystals with an admixture of boron ions is similar to the variation for the pure salt. The dielectric constant passes through to two maxima $\varepsilon' = 736$ and $\varepsilon'' = 735$ at +18.5 and -12.5°, respectively (Fig. 6). The dielectric loss tangent for these crystals in the spontaneous polarization region is some 10-30 times smaller than for the pure salt at the same temperature.

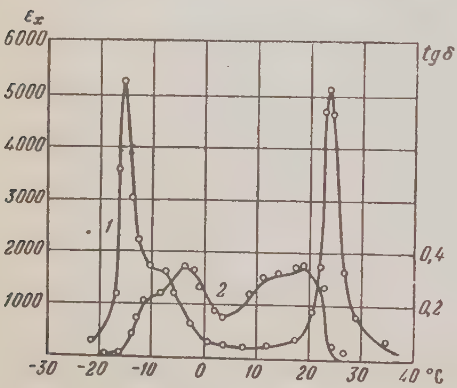

Fig. 5. Temperature dependence of 1) dielectric constant and 2) dielectric loss tangent for pure Rochelle salt.

The temperature variation of the dielectric constant of Rochelle salt crystals with an admixture of copper ions also exhibits

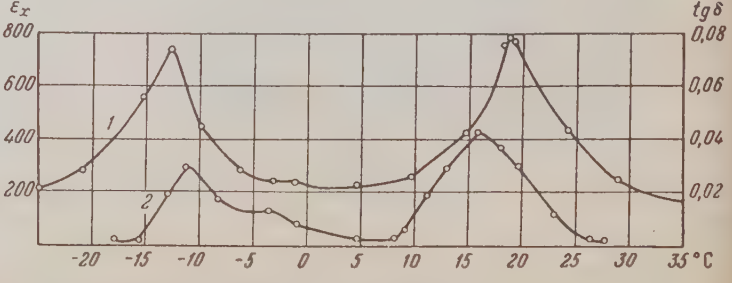

Fig. 6. Temperature dependence of 1) dielectric constant and 2) loss tangent for Rochelle salt with admixture of B ions.

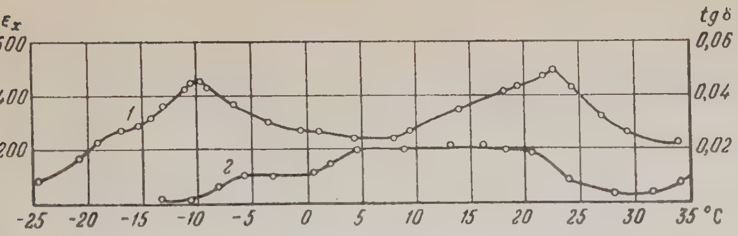

Fig. 7. Temperature dependence of 1) dielectric constant and 2) loss tangent for Rochelle salt with admixture of Cu ions.

two maxima, $\varepsilon' = 527$ and $\varepsilon'' = 457$, at 22.8° and -10°. In this case the dielectric loss tangent has only one wide maximum ($\tan\delta = 0.02$) in the spontaneous polarization interval (Fig. 7).

The temperature dependence of the dielectric constant of Rochelle salt with molybdenum as the impurity was investigated on crystals grown from solutions containing 0.3, 1 and 1.4% ammonium molybdate. The temperature characteristics of the investigated crystals (Fig. 8) are reminiscent of the characteristics of the pure salt. Thus the curve for the crystals shows two maxima: $\varepsilon' = 1909$ and $\varepsilon'' = 2400$ at 4.8° and -9.5°, respectively (Fig. 9). With increasing ammonium molybdate concentration the Curie points of the crystals draw closer together, i.e., the upper Curie point shifts to the side of lower temperatures; the lower Curie point, to the side of higher temperatures.

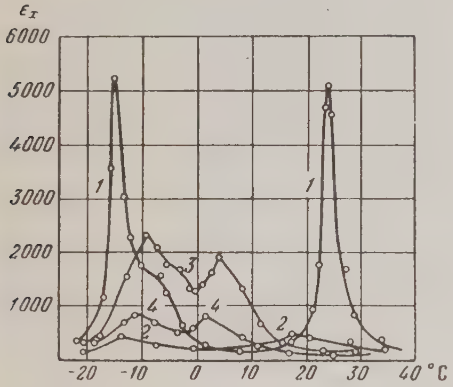

Fig. 8. Temperature dependence of the dielectric constant of Rochelle salt grown from a solution with admixtures of $(NH_4)_6O_{24} \cdot 4H_2O$. Ammonium molybdate concentrations: 1) 0%, 2) 0.3%, 3) 1%, and 4) 1.4%.

We also investigated the dielectric constant and loss tangent of Rochelle salt crystals (pure and with admixtures) at room temperature in a 50 cps alternating field as a function of the field intensity in the 20 to 60 v/cm interval. In this interval the dielectric constant of the pure salt increases with the voltage, while dielectric constants of the crystals with B, Cu and Mo impurities remain virtually constant. The dielectric loss tangent of the pure salt increases 0.012, while the tangents of the crystals with impurities increase only some 0.0002-0.0008 per v/cm (Fig. 10).

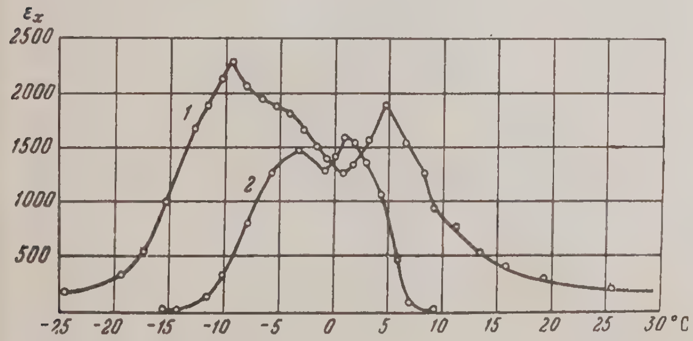

Fig. 9. Temperature dependence of the dielectric constant and the loss tangent of Rochelle salt grown from the solution containing 1% ammonium molybdate: 1) dielectric constant, 2) loss tangent (each division on the vertical scale equals 0.06).

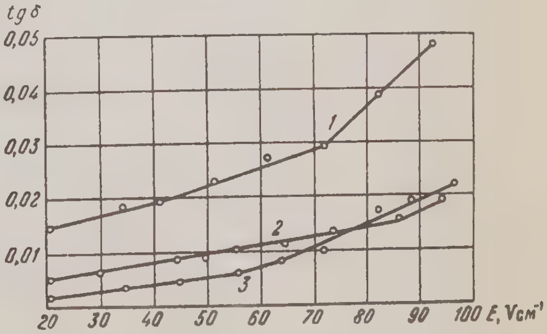

Fig. 10. Field dependence of the dielectric loss tangent: 1) Rochelle salt with B ions, 2) with Cu ions, 3) with Mo ions.

Conclusions

1. The presence of B, Cu and Mo impurity ions in Rochelle salt crystals results a) in a modification of the crystal habit and b) in a change of the dielectric properties.

2. The dielectric constant of crystals of Rochelle salt containing B, Cu and Mo ions shows temperature variations characteristic of other ferroelectrics.

3. The Curie points of Rochelle salt crystals with impurity ions are shifted closer together so that the region of spontaneous polarization is narrowed.

4. The temperature variation of the dielectric loss tangent of Rochelle salt is a significant characteristic. The loss tangent curve shows two maxima, shifted closer together in relation to the dielectric constant maxima.

5. The dielectric loss tangents of crystals with impurities have maxima in the region of spontaneous polarization; the maximum values are smaller than the loss tangent values for the pure salt.

6. With increasing field intensity the dielectric constant and the loss tangent in the region between Curie points vary to an appreciably greater extent in the crystals of the pure salt as compared with the crystals containing impurity ions.

L'vov Pedagogical Institute

References

1. M.A.Eremeev & B.V.Kurchatov, Zhur. eksp. i teor. fiz., 1,201 (1931).
2. M.A.Eremeev, P.P.Kobeko, B.V.Kurchatov & I.V.Kurchatov, Zhur. eksp. i teor. fiz., 2,102 (1932).
3. B.V.Kurchatov & I.V.Kurchatov, Zhur. eksp. i teor. fiz., 2,319 (1932).
4. M.A.Eremeev & B.V.Kurchatov, Zhur. eksp. i teor. fiz., 2,329 (1932).
5. I.H.Thorp & H.E.Buckley, Acta Cryst., 2, 333 (1949).

AN INVESTIGATION OF NEW PIEZOELECTRIC CRYSTALS

- V.A.Koptsik

In recent years scientific and technical applications of electromechanical transducers employing piezoelectric crystals have greatly expanded.

Since the discovery of the piezoelectric effect by the brothers Pierre and Jacques Curie (1880) until today, crystals of more than 500 compositions have been qualitatively shown to exhibit piezoelectric properties (Refs. 1-9).

Despite the large number of crystals in which the piezoelectric effect has been observed qualitatively, complete quantitative determinations of the piezoelectric constants have been carried out only for 30 substances, while practical use is made of crystals of not more than 10 substances.

The reason for this is that electro-technological applications of piezoelectric crystals are determined by many factors; among the more important of these are the symmetry of the crystals, their mechanical and chemical stability, the magnitudes of the electrical and elastic parameters, the time and temperature stability of the latter, as well as the possibilities of preparing specimens with the requisite structure or of growing large, homogeneous single crystals susceptible of subsequent cutting, etc.

The choice of a piezoelectric crystal depends on the specific nature of the problem involved. The employment of piezoelectric crystals as ultrasonic radiators, in addition to other relevant conditions, is principally affected by the magnitude of the piezoelectric constants d and the temperature coefficients of these constants. The values of the coefficients g and h determine the possibility of using piezoelectric crystals as ultrasonic receivers and pressure sensing devices in electroacoustical apparatus and in high-frequency electronics.

In Fig. 1 are shown the values of the electrical and elastic parameters of the piezoelectric crystals now used in engineering.[10] A study of this chart shows that there is still a real need for new and better piezoelectric crystals.

For a majority of applications, the characteristic of piezoelectric crystals to be initially considered is the electromechanical coupling coefficient k. Crystals with a coefficient $k < 10\%$ have no advantages over crystals already in use and, with the single exception of frequency stabilization applications, are of no practical interest.

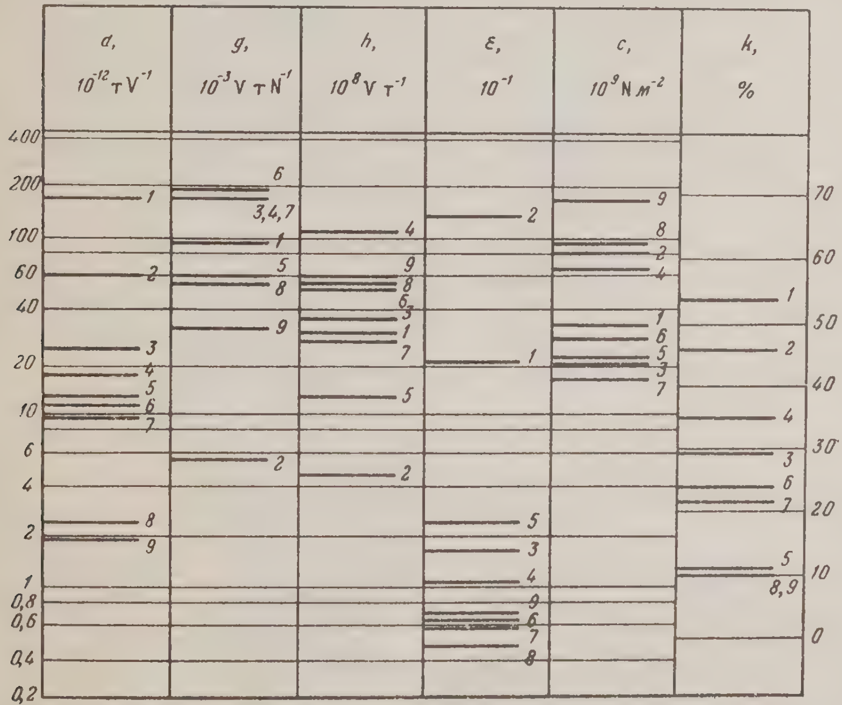

Fig. 1. Electrical and elastic parameters of piezoelectric crystals used in piezoelectric technology in practical units at 20°C: 1) 45° X-cut of Rochelle salt, 2) polarized barium titanate ceramic, 3) 45° Z-cut of ammonium orthophosphate, 4) Y-cut of lithium sulphate, 5) 45° Z-cut of potassium orthophosphate, 6) 45° Z-cut of potassium tartarate, 7) 45° Z-cut of ethyldiamine tartarate, 8) X-cut of quartz, 9) X-cut of tourmaline.

Unfortunately we have few data on the strength of the piezoelectric effect in the crystals that have been qualitatively studied. It follows that it would be desirable to make such an evaluation for all known piezoelectric crystals (small specimens are adequate for this purpose).

The next step would be growing small single crystals of substances having promising coupling coefficients and evaluation of their electrical and elastic parameters as well as of their chemical and mechanical stability. Such an evaluation would lead to the clarification of the potential technical value of the crystals; the practical possibilities of using the more promising ones would then depend on subsequent studies of the temperature, frequency and time dependence of their parameters, as well as on finding simple conditions under which sufficiently large homogeneous single crystals could be grown and processed.

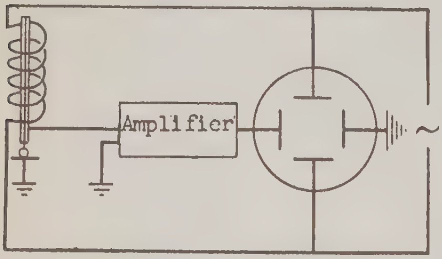

Fig. 2. Circuit for qualitative detection of the piezoelectric effect in crystals.

With the objective of carrying through such a research program we assembled an apparatus for the qualitative detection of the piezoelectric effect in crystal grains, and the simultaneous evaluation of the electromechanical coupling coefficient.

The apparatus consisted of mechanical and electrical oscillators, an amplifier and cathode ray tube indicator (Fig. 2).

The measurement procedure was the following.[11] An electrical voltage is generated in the crystal or grain (the dimensions of which can be of the order of some tenths of a millimeter) by mechanically induced strains with a frequency in the audio range. This voltage, after appropriate amplification, is applied to the horizontal plates of the oscilloscope; the vertical plates are fed a sweep signal with the frequency of the mechanical vibrations. In case the crystal is piezoelectric an ellipse will be observed on the screen of the cathode-ray tube; the width of this ellipse along the horizontal axis is proportional to the electromechanical coupling constant.

More than 250 substances were studied using this procedure. The piezoelectric effect was detected in crystals of 65 substances; the results are shown in Table 1 where, for each substance, we give the chemical formula, the electromechanical coupling coefficient and the type of symmetry. The substances marked with an asterisk (*) are those whose crystals are known piezoelectrics.

Table 1

Crystals in which a piezoelectric effect was detected

Name	Chemical Formula	Symmetry	Coupling Coefficient,%
1. Mellite	$Al_2C_{12}O_{22}\cdot 18H_2O$	$D_4^{3,7}$	10
2. Cancrinite	$3Na_2Al_2O_4\cdot Si_2O_4\cdot 2CaCO_3$	C_6^6	20
3. Polybasite	$Sb_2S_3\cdot 8(Ag, Cu)_2S$	D_3^2	10
4. Eucryptite	$Li(AlSiO_4)$	$D_6^{4,5}$	10
5. Potassium Aluminum Sulphate	$K(AlSiO_4)$	D_6^6	10
6. Niobium oxide	Nb_2O_5	C_{2V}^7	10
7. Vanadium oxide	V_2O_5	C_{2V}^7	10

Table 1 (continued)

Name	Chemical Formula	Symmetry	Coupling Coefficient,%
8. Oxyfluoroniobate potassium, monohydrate	$K_2NbOF_5 \cdot H_2O$	---	10
9. Sodium hexaniobate	$Na_{14}Nb_{12}O_{37} \cdot 32H_2O$	---	10
10* Nickel sulphate, heptahydrate	$NiSO_4 \cdot 7H_2O$	D_2^4	10
11. Cadmium iodide	CdI_2	C_{2V}^4	10
12. Chromium chloride	$CrCl_3$	$D_3^{3,5}$	10
13. Chromium anhydride	CrO_3	D_2^5	10
14. Nickel triethylenediamine (II)—nitrate	$(NiEn_3)(NO_3)_2$	---	10
15. Ammonium tetrathiocyanonickelate triamine	$(NH_4)_2\ Ni\ (SCN)_4 \cdot 3NH_3$		10
16. Ammonium tetrathiocyanonickelate tetraamine	$(NH_4)_2\ Ni(SCN)_4 \cdot 4NH_3$	C_{3i}	10
17. Ethylenediamine aminochlorobromonitroplatinochloride	$Pt(EnNH_3Cl)NO_2Br\ Cl$	---	10
18. Tribromoethylene platinate potassium monohydrate	$K\ PtBr_3C_2H_4 \cdot H_2O$	C_2^2	10
19. Hydroxitetraaminonitroso ruthenium—chloride	$Ru(NH_3)_4NO \cdot OH\ Cl_2$	C_2^3	10
20. Calcium ethyl lactate	$C_2H_5(C_3H_5O_3)_2Ca$	---	10
21. Ammonium malate	$C_4H_4O_5(NH_4)_2$	---	10
22. Cobalt citrate, hydrate	$Co_3\ C_6H_5O_7\ {}_2 \cdot xH_2O$	---	10
23. Zinc α-oxybutyrate	$(C_4H_7O_3)_2Zn$	---	10
24. Salt of *d*-α phenylethylamine with l-borneol bisulphate	$C_{18}H_{29}O_4NS$	---	10
25. Salt of *l*-α phenylethylamine with l-borneol bisulphate	$C_{18}H_{29}O_4NS$	---	10
26. Diketopiperazidine	$C_4H_6O_2N_2$	C_2	10
27. Crystalviolet, nonohydrate	$C_{25}H_{31}ON_3 \cdot 9H_2O$	C_{3V}^4	10
28. β-*d*-glucosan	$C_6H_{10}O_5$	D_2^4	10
29.* Sucrose	$C_{12}H_{22}O_{11}$	C_2	10
30.* Glucose·sodium chloride, monohydrate	$(C_6H_{12}O_6)_2 \cdot NaCl \cdot H_2O$	D_2^4	10
31. Arabinose	$C_4H_9O_4 \cdot CHO$	D_2^4	10
32. *d*-Sorbose (hexose)	$C_6H_{12}O_6$	D_2	10
33.* *l*-Xylose	$C_5H_{10}O_5$	D_2^4	10
34.* *l*-Rhamnose	$C_6H_{12}O_5 \cdot H_2O$	C_2^2	20
35.* Lactose	$C_{12}H_{22}O_{11} \cdot H_2O$	C_2	10
36. Levulose	$CH_2OH(CHOH)_2$	---	10
37. 1,8—Dinitronaphthalene	$C_{10}H_6(NO_2)_2{}^{1,8}$	D_2^4	10

Table 1 (continued)

Name	Chemical Formula	Symmetry	Coupling Coefficient,%
38. Trithioformaldehyde	$C_3H_6S_3$	C_{2v}^7	10
39. Acenaphthene	$C_{12}H_{10}$	C_{2v}^2	10
40. Triphenylmethane	$(C_6H_5)_3CH$	—	10
41. m-Dinitrobenzol	$C_6H_4(NO_2)_2$	C_{2v}^9	10
42. Coumarin	$C_9H_6O_2$	C_{2v}^5	10
43. β -Indonyl-propione-nitryl	$C_{11}H_9N_2$	—	10
44. Maleic anhydride	$(:CH\cdot CO)_2O$	—	10
45. Camphoric acid	$C_{18}H_{14}(CO_2H)_2$	C_2	10
46.* Urotropine	$C_6H_{12}N_4$	T_d^4	10
47.* Histidine	$C_6H_9O_2N_3$	D_2?	10
48. 3,4(3'-pentalidine)-5, 5-tetramethylene pyrazoline	$C_{15}H_{11}N_2$	—	10
49. *d*-α- Phenylthylamine sulphate	$C_6H_5(CH_2)NH_2\cdot H_2SO_4$	—	10
50. *l*-*p*-chrolo-α-phenylthylamine salt of *l*-bornyl sulfuric acid	$C_{18}H_{24}O_4NSCl$	—	10
51. Barium salt of *l*-bornyl sulfuric acid	$C_{10}H_{18}O_4SBa$	—	10
52.* Acetamide	CH_3CONH_2	C_{3v}^6	10
53. Quinoic acid	$C_{30}H_{46}O_5$	C_2^2	10
54.* *l*-Glutamic acid	$C_5H_9O_4N$	D_2^4	10
55. *l*-Glutamic acid, hydrochloride	$C_5H_9O_4N\cdot HCl$	D_2	10
56. *d*-Oxystearic acid	$C_{18}H_{36}O_3$	—	10
57. Aspartic acid	$C_4H_7O_4N$	C_2^2	10
58.* Asparagine monohydrate	$C_4H_8O_3N_2\cdot H_2O$	D_2^4	10
59. Malic acid	$C_4H_6O_5$	—	10
60.* Tartaric acid	$C_4H_6O_6$	C_2^2	10
61. Toluquinone	$O:C_6H_3(CH_3):O$	—	10
62. Diphenyl ester	$(C_6H_5)_2O$	—	10
63. *l*-Tyrosine chlorohydrate	$C_9H_{11}O_3N\cdot HCl$	C_2^2	10
64. Sulfanilic acid	$NH_2C_6H_4SO_3H$	—	10
65. Congo blue	$C_{32}H_{24}O_6N_6S_2$	—	10

For crystals of 52 substances the piezoelectric effect was detected for the first time.

Further investigation of the crystals of Cancrinite $3Na_2Al_2O_4\cdot ScO_2\cdot 2CaCO_3$ and of l-Rhamnose $C_6H_{12}O_6\cdot H_2O$ would appear to be worthwhile.

The data of Table 1 substantiate the validity of the statistical criterion for the existence of the piezoelectric effect we formulated earlier:[9,12] a sufficient condition for the existence of piezoelectric effect in dielectric crystals is the presence in the crystal structure of permanent dipoles and their appropriate distribution in accordance with the laws of space group symmetry.

$$D_2^4,\ C_2^2,\ C_{3v}^5,\ D_{2d}^{12},\ C_1^1,\ C_{2v}^9,\ D_4^{4,8},\ D_3^{4,6},\ C_{6v}^4,\ T_d^2,$$
$$T^4,\ D_2^3,\ D_3^2,\ C_s^4,\ S_4^2,\ C_3^4,\ C_{2v}^5,\ D_{2d}^3,\ C_{3v}^6,\ C_6^6,$$
$$C_{2v}^{20},\ C_2^3,\ D_6^6,\ D_2^5,\ C_{3v}^2,\ C_{2v}^{17},\ C_4^{2,4},\ D_4^{3,7},\ C_{2v}^1,\ C_{2v}^2,$$
$$T_d^{3,4},\ D_4^2,\ C_{2v}^7,\ C_{2v}^4,\ D_3^{3,5},\ D_6^{5,4},\ C_{3v}^4,\ D_6^{2,3},\ C_4^5,\ C_6^{2,3}.$$

Among the total of 180 crystals for which the space group is known more than 60% belong in the symmetry groups listed in the first line above, about 15% in the groups in the second line, 10% in groups in the third line and less than 10% in the last-listed groups.

This criterion, therefore, can be used for searching for new piezoelectric crystals among crystalline dielectrics.

Until now not enough attention has been paid to the fact that every true piezoelectric must posses permanent dipoles localized in the crystal structure in accordance with the laws for the selected space symmetry groups. Yet this follows from simple considerations.[9, 12 & 13]

An electric field polarizes the material, creating new dipole moments or changing the magnitude and orientation of the existing ones. In both cases the dimensions of the body change owing to displacement of the electrons and nuclei to a new equilibrium position.

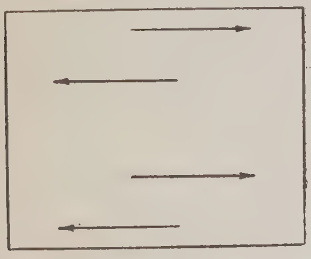

Fig. 3. Centro-symmetric localization of dipole components in the unit cell.

Mechanical stresses also change the dimensions of the body, but they act directly on the particles as a whole and not on their charges. For this reason dipole moments cannot be created by mechanical stresses in crystals which do not contain dipole components or in crystals with a centro-symmetric arrangement of the dipoles (Fig. 3). This irreversible electromechanical effect is called electrostriction, and occurs in all solid dielectrics.

Piezoelectricity, however, is characterized by coupling of the direct and of the inverse effects. For this reason it must be associated with the existence of dipole moments and their acentric localization in the crystal structure (Fig. 4).

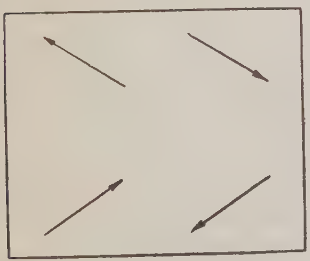

Fig. 4. Acentric localization of the dipole components in the unit cell of a crystal.

That this is the case is shown by a crystallochemical study we have made of the known piezoelectric structures.[9] The dipole moments are localized in the piezoelectrics on discrete groups of particles constituting the crystal: molecules, radicals, complex anions or pairs of reciprocally polarized particles. For this reason piezoelectric crystals are found only among those particular space symmetry groups which permit of a stable acentric arrangement of the dipole particles or particle groupings. Piezoelectric crystals were found only in 43 of the 129 space groups, homeomorphic with the piezoelectric symmetry groups.

The limitation in the number of space groups follows from the fact that the symmetry relations of dipoles in the structure of a piezoelectric crystal require that no center of symmetry be present in the unit cell and, for special dipole arrangements, the absence of symmetry planes or axes of any kind. Generally speaking, stable dipole structures can be bound only by helical axes and by grazing reflection planes (possibly in combination with ordinary symmetry planes and axes (Fig. 5). In this way the criterion for the existence of the piezoelectric effect (the absence of a center of symmetry) can be made more rigorous.

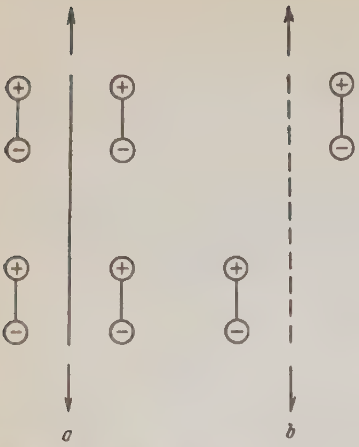

Fig. 5. The effect of space group symmetry elements on space localized dipoles in the unit cell of a crystal: a) effect of planes and axes of symmetry, b) effect of grazing reflection planes and helical axes.

With the objective of elucidating further the connection between crystal structure and piezoelectric properties, it would be desirable to determine – experimentally and through calculations on the basis of the crystal structure – the constants for a number of structurally and chemically related (isotopic and isomorphic) substances, which might include:

a) the series of derivatives of tartaric acid consisting of 64 piezoelectrically active compounds;

b) the series of compounds with a deformed lattice of the perovskite type, consisting of 10 piezoelectrically active compounds;

c) the series of orthophosphates and orthoarsenates with the general formula MH_2RO_4, where M = NH_4, Na, K, Rb or Te; and R = P or As;

d) the series of compounds with structure of the type of pyrochlore or fluorspar, with the general formula $M'_2M''_2O_7$, where M' = Cd, Pb or In and M'' = Nb, Ta, Ti or Zr;

e) the series of chlorates, bromates and iodates with the general formula MXO_3 where M = H, NH_4, Li, Na, K, Rb, Cs, Tl or Ag and X = Cl, Br or I;

f) the series of metaderivatives of benzene with the general formula $C_6H_4R'R_3$, where R' = NO_2, NH_2, OH or COOH and R_3 = Cl, Br, I, NO_2, NH_2 or OH;

g) the series of sulphates, selenates and chromates with the general formula $MRO_4 \cdot 7H_2O$, where M = Mg, Ni, Co or Zn and R = S, Se or Cr;

h) the series of sulphites, selenites and chromites with the general formula $MRO_3 \cdot 6H_2O$, where M = Mg, Ni, Co or Zn and R = S, Se or Cr;

i) the series of the three isostructural substances: $NH_4B_5O_8 \cdot 4H_2O$, $KB_5O_8 \cdot 4H_2O$ and $PbB_5O_8 \cdot 4H_2O$;

j) the series of the two isostructural substances: SiO_2(quartz) and $AlPO_4$;

k) the series of the two isostructural substances: $Li_2SO_4 \cdot H_2O$ and $Li_2SeO_4 \cdot H_2O$.

Carrying out this program of studies would make it possible to allow separately for the effect on piezoelectric properties of the chemical nature of the particles and of the symmetry of their relative arrangement in the structure of the crystal.

Regularities in the variation of the piezoelectric parameters of series of compounds having the same symmetry actually are observed, as can be demonstrated, for example, in the case of the series of compounds of the type $MRO_4 \cdot 7H_2O$, having the symmetry D_2^4 (Table 2).[10]

Table 2

Piezoelectric and structural parameters of crystals of the $MRO_4 \cdot 7H_2O$ series

Material	*a*, Å	*b*, Å	c, Å	$d_{14} \cdot 10^8$	$d_{25} \cdot 10^8$	$d_{36} \cdot 10^8$
$MgSO_4.7H_2O$ . . .	11,89	12,01	6,86	—6,18	— 8,16	—11,5
$NiSO_4.7H_2O$ . . .	11,86	12,08	6,81	—5,98	— 8,84	— 9,63
$ZnSO_4.7H_2O$ . . .	11,85	12,09	6,83	—5,70	—10,5	— 9,2

Conclusions

1) Conditions for electrotechnical application of piezoelectric materials have been characterized and a procedure for testing new piezoelectric crystals developed.

2) The existence of 52 new compounds having piezoelectric properties has been established and their electromechanical coupling coefficients have been evaluated.

3) Confirmation was obtained of the new criterion established by the author, which gives sufficient conditions for the existence of the piezoelectric effect in dielectric crystals.

4) It was shown that every true piezoelectric must have permanent dipoles localized in the crystal structure in accordance with selected space group symmetries.

5) A program is proposed for further investigation of isostructural and isomorphic series of piezoelectric compounds for the purpose of clarifying in greater detail the relation between piezoelectric properties and the crystal structure.

The author wishes to thank the individuals who supplied him with specimens of crystals for study and A.F.Solov'ev for assistance in the experimental work.

"M.V.Lomonosov"
Moscow State University

References

1. W.G.Cady, Zh.P.F. (J. Appl. Phys.?) 7,107 (1930).
2. A.Hettich & H.Steinmetz, ZS. F. Phys. 76,688 (1932).
3. A.Scheibe, Piezoelektrizität des Quarzes. - Dresden - Leipzig, 1938.
4. E.E.Flint, Sb. rabot rentg. lab. (Collected reports of the X-ray laboratory) Institute for Mineral Raw Materials, M.-L. 1939.
5. W.L.Bond, Bell. Syst. Techn. J., 22,145 (1943).
6. M.Bruzau, Electr. Comm., 29,445 (1946).
7. P.H.Egli, Am. Miner., 33, 622 (1948).
8. W.P.Mason, Piezoelectric crystals and their application to ultrasonics - (in Russ. trans), M. - 1952.
9. V.A.Koptsik, Pervoe soveshchanie po kristallokhimii (Transactions of the First Conference on Crystal Chemistry), IONKh AN SSSR, M. -1954.
10. F.Spitzer, Arch. Elektr. Ubertrag., 5,544 (1951).
11. J.Jitaka, Acta Cryst., 6,663 (1953).
12. V.A.Koptsik, Elektrichestvo (Electricity), 6,85 (1953).
13. A.Hippel, Zs. f. Phys., 133,158 (1952).

THE PIEZOELECTRIC PROPERTIES OF WOOD AND CELLULOSE MATERIALS

- V.A.Bazhenov

The discovery by Shubnikov[1] of a piezoelectric effect in wood initiated extensive investigation of this interesting effect in different varieties of wood and wood products. After we established that the piezoelectric properties of wood are related to the structure of its oriented component, cellulose,[2,3] the investigation was extended to wood pulp and other cellulose materials.

Diverse piezoelectric elements and testing procedures have been devised for the purpose of investigating the symmetry of the piezoelectric texture (structure or grain) and determining the piezoelectric moduli and the manner in which these are affected by different factors.[1]

For qualitative investigations of wood and other materials good results have been obtained with piezoelectric elements deformed in bending and made in the form of square (5 x 5 cm) or round (5 cm dia) plates or laminae. In the case of single elements the plates were equipped with metal electrodes: one a sheet of foil cemented to the element, the other a metal plate. This asymmetry assured an unambiguous value of the stress in the deformed plate and accordingly, an unambiguous electric effect (by virtue of deflection of the neutral axis). In the case of "bimorph" elements, consisting of two cemented together laminae with their structural axes at right angles, symmetric foil electrodes were employed. Such electrodes were attached to wood sheets, films and oriented cardboard by means of a paste made of beeswax and rosin (2:1); they were attached to laminae of viscose filaments by means of BF-2 cement, which was also used for consolidating the filaments in preparing the laminae. The piezoelectric elements laid on two end supports were deformed by a force applied at the midpoint by means of a small lever press.[3] Naturally the various materials were dried to a constant weight and the tests were carried out with due protection against warping and other distortions.

A string galvanometer was used to measure the voltage induced by the application and removal of the deforming loads; the capacity of the charge-accumulating systems was measured by means of a conventional capacity bridge. Tests of elements cut in different manners and oriented in different positions on the supports yielded a complete picture of the piezo-effect and made it possible to determine experimentally the symmetry of the piezoelectric texture (structure). The qualitative investigations were supplemented by quantitative measurements. The quantitative measurements were basic in our investigation of the symmetry of the piezoelectric structure; they made it possible to find the true values of the piezoelectric moduli. The test procedure varied according to the properties and form of the investigated material. In investigating wood the piezoelectric elements were for the most part cut in the form of cubes (2.0, 2.5 and 3.0 cm on edge) and stressed in compression. The electrodes were formed on appropriate faces by a coating of aquadag (graphite lubricant).

The procedure followed in testing these elements has been described earlier;[3] instead of presses the cubes were compressed by means of a materials testing machine (for example, the IM-4P); automatic loading was used and the stress-strain diagram was recorded as usual in testing materials; a synchronous record of the polarization process, as indicated by the electrometer, was imposed on the stress-strain diagram. In addition to wood, the same set-up was used for testing elements cut of oriented viscose filaments consolidated into blocks with BF-2 cement.

In investigating films and laminar materials, the piezoelectric elements were stressed in tension. Here the greatest difficulty was presented by the choice of electrodes, for the use of foil electrodes would have the effect of replacing the investigated material by a different laminated material of unknown structure, while the use of painted-on electrodes involved the danger of penetration of the conducting material into the films and sheets, which would be equivalent to an unknown reduction in the thickness of the tested sheets.

A solution was found in the set-up pictured in the accompanying illustration. This design has no attached electrodes, i.e., parts of the set-up itself serve as contact electrodes. The sheet or film specimen a is laid on the smooth horizontal metal plate b; one end of it is clamped to the plate by means of the bar c which is attached to the base plate by the two screws d. The other end of the sheet, held in the clamp e, extends beyond the plate; this clamp is connected by the rope g, passing over pulley f with the weight platform h. When under tension the test sheet was held tightly against the surface of the plate by virtue of the fact that the top of the pulley was slightly below the surface of the plate. A small polished metal bar i was laid on top of the test sheet; it served as the electrode and was connected by means of a shielded cable to the electrometer. The capacity of the charged piezoelectric system, as usual, was measured by means of a capacity bridge.

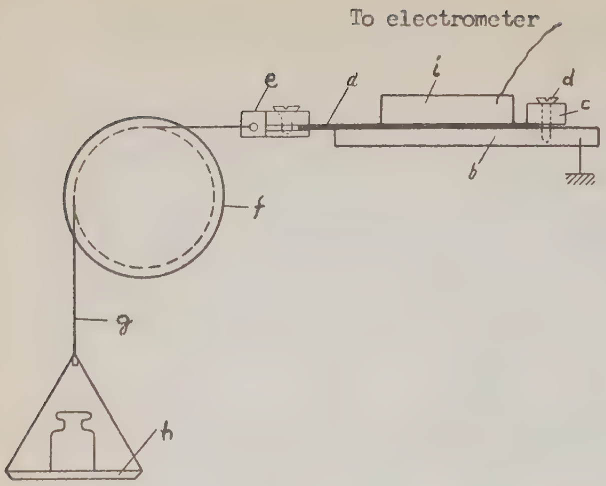

Set-up for testing piezoelectric elements stressed in tension.

Tests showed that the static charge due to friction in the case of unwarped, reasonably flat specimens was so small that it was not detected by the electrometer, while the piezoelectric effect with its characteristic alternations of polarity was readily observed.

In concluding this section on procedure, it may be noted that both the described set-ups for quantitative studies of the piezoelectric effect operated in a fully satisfactory manner as regards both reliability and speed so that we were able to test about a thousand piezoelectric elements of different varieties of wood alone.

We now turn to a summary of the experimental results.

1. In testing cubic specimens (3 cm on edge) the electrostatic potential obtained is of the order of 100 volts with a capacity of the charge system equal to 12-15 μμf. So appreciable a piezoelectric effect made it feasible not only to make reliable determinations of the piezoelectric moduli of different varieties of wood but also to establish the relation between these moduli and the structure and other physical and mechanical properties of wood that are of interest in wood technology.

Of considerable interest is the inverse proportionality between the piezoelectric modulus and the elastic modulus observed in wooden piezoelectric elements (in the direction of compression). Hard varieties have a lower piezoelectric modulus as compared with soft woods. There also appears to be a direct relationship between the piezoelectric modulus and the volumetric weight, although in some varieties this is partially masked by the influence of the modulus of elasticity and other factors.

The values of the piezoelectric modulus d_{14} for a few of the woods investigated in greatest detail are listed in Table 1. The piezoelectric moduli of other materials, expressed in percent of the modulus of alder wood tested in the form of sheets (veneer) under tensile loading, are listed in Table 2.

Table 1

Piezoelectric modulus d_{14} of different varieties of wood

Wood	$d_{14} \cdot 10^8$ Abs. e.s.u.
Beech	0.307
Birch	0.595
Oak	0.588
Aspen	0.583
Pine	0.610

Table 2

Piezoelectric moduli of cellulose materials in percent of the modulus of alder

Material	Piezoelectric modulus,%
Alder wood (veneer)	100.0
Cellophane	3.7
Celluloid	27.2
Paper of wood pulp	12.8
Oriented viscose filaments "set" in hardened BF-2 cement	78.5
White sulphite cellulose	11.4
Paper of cotton fiber	10.0

The values of the piezoelectric moduli vary under the influence of different factors (in addition to the aforementioned, the degree of the orientation of the structure, the amount of cellulose therein, and the density of packing). It is entirely possible that if all these factors could be taken fully into account the differences between the moduli for different varieties would vanish.

2. A very appreciable piezoelectric effect was detected in specially prepared sheets of oriented fibrous wood cellulose, prepared by the sulphite process from fine chips cooked in ceramic perforated tubes enclosed in iron-screen shields. In contrast to this, we note the entire absence of a piezoelectric effect in non-oriented sheets laid by hand from the same cellulose after thorough stirring of the fibrous mass. The contrasting results are convincing proof of the decisive role played by orientation of the fibers where the piezoelectric effect is concerned.

The small piezoelectric effect detected in certain cellulose and paper sheets indicates that piezoelectric properties can appear when the fibers are partially oriented in one of the predominant directions, in this case, along the length of the sheet. The reason for such orientation lies in the technological nature of the continuous paper or cellulose sheet fabrication process; the fibers are oriented in the flow of pulp much as are logs floating in a stream.

It is interesting to note that the piezoelectric properties of fibrous cellulose materials exhibit the same $\infty:2$ symmetry as wood. We also detected a piezoelectric effect and the $\infty:2$ piezoelectric structure symmetry in papers made of pure cotton cellulose.

3. As a matter of principle we deemed it desirable to investigate the possibility of piezoelectric effects in cellulose entirely free of fibrous structure. To this end we tested hydrocellulose materials: cellophane films (with the glycerine extracted beforehand) as well as viscose filaments amalgamated in structures with different degrees of orientation.

In the case of cellophane we detected a small but distinct piezoelectric effect corresponding to the same $\infty : 2$ structural symmetry. In oriented viscose filaments the piezoelectric effect was appreciably greater and had the same symmetry. In a sense, cellophane echoed the properties of oriented paper and cardboard of fibrous cellulose while viscose filaments reflected the properties of materials of oriented fibrous cellulose.

Cellophane, being a molecular "paper" formed of randomly interwoven long molecules, still has some orientation as a result of the continuous flow technology of its fabrication; this applies to an even stronger degree of oriented viscose filaments. Obviously, the greater the number of molecules that happen to be turned parallel or nearly parallel to some one direction (the direction of flow), the greater will be the degree of structural orientation and the more pronounced the piezoelectric effect.

4. A piezoelectric effect with the $\infty : 2$ symmetry was also detected in nitrocellulose (celluloid) films, which is to be expected in the light of current concepts regarding the structure of cellulose molecules.

The fact that the piezoelectric structural symmetry $\infty : 2$ proved to be the same in both fibrous materials and those devoid of fibrous structure served as the basis for a theoretical generalization of the experimental results of our researches.

Conclusions

1. The "grains" of the piezoelectric structure (grain) of cellulose are linear chains of polar molecules consisting of β-d-glucose groups.

2. The conditions of orientation of molecules from a solution or suspension, in which they are mixed at random, are such that when they are arranged more or less in parallel in the direction of the flow of the solidifying liquid, half of the polar molecules will have their polar axes oriented in one direction. These conditions fully correspond to the method of obtaining the first kind of $\infty : 2$ type structure described in the familiar Theorem IV of Shubnikov.[1]

3. A $\infty : 2$ molecular structure is not characterized by a lattice-like arrangement of molecules, but is rather a porous structure capable of being filled by molecules of other substances. In individual cases the penetration of polar molecules into this porous structure is accompanied by their orientation in the $\infty : 2$ symmetry which has piezoelectric properties. Thus we established experimentally that soaking ash wood with xylol results in a more than two-fold increase of the piezoelectric modulus d_{14} of the wood. If the xylol is subsequently eliminated the modulus returns to its initial value. We interpret this result as being due to the orientation of the polar xylol molecules in the porous structure of the oriented component of wood: cellulose.

4. We believe that the porosity of the cellulose structure stems from the fact that each cellulose molecule, through its individual radicals, interacts (probably through the agency of hydrogen bonds - see Ref. 4) with a number of the neighboring molecules, thereby precluding dense packing.

As for the possible applications of piezoelectricity of wood, cellulose and its derivatives, it may be noted that it offers a new means of investigating the structure of these materials and, in particular, for constructing a steric model of cellulose molecules. In many cases the piezoelectric effect can serve as the criterion for the orientation in various anisotropic cellulose substances. We have already used it for studying the structure of paper and different films.

In conclusion I wish to thank A.V.Shubnikov for his advice in connection with the investigations and F.F.Sadovski for his help in preparing the equipment and carrying out the experiments.

Forestry Institute of the
Academy of Sciences of the USSR

References

1. A.V.Shubnikov, P'ezoelektricheskie tekstury (Piezoelectric textures) M.-1946.

2. V.A.Vazhenov & V.P.Konstantinova, Doklady AN SSSR, 71,283 (1950).

3. V.A.Vazhenov, Trudy In-ta lesa AN SSSR (Transactions of the Wood Institute of the SSSR), 9,281 (1953).

4. N.I.Nikitin, Khimiia drevesiny (Chemistry of Wood), M.-1951.

THERMAL-MECHANICAL OSCILLATIONS (FLUCTUATIONS) OF PIEZOELECTRIC CRYSTALS

- K.V.Goncharov and V.A.Krasil'nikov

It is known that the spectrum of the equilibrium thermal electric oscillations (fluctuations) of electric impedances is determined by Nyguist's formula, which can be derived from classical thermodynamics taking into account the statistical law for equipartition of energy over the degrees of freedom.[1-3]

The applicability of Nyguist's formula to various conductors has been verified by many authors.[4-7] At the same time, measuring the thermal noise in conductors is one of the most precise methods of determining Boltzmann's constant.

Johnson[4] and Neitzert[5] note the correspondence of the equilibrium thermal noise distribution in conductors, loaded by the capacitance of the input stage of an amplifier, with the premises of theory. In view of the uniform nature of the spectral distribution, it was not necessary to effect a successive spectral analysis of the thermal fluctuations in conductors over a wide frequency range. (Measurements were usually made at fixed frequencies).

We investigated the spectra of the thermal electric oscillations in electromechanical transducers, cut in the form of bars of metallized piezocrystals of Rochelle salt (various cuts), ammonium phosphate and barium titanate ceramic. The spectra of these specimens exhibited the specific characteristics having strongly-accentuated components at anti-resonance frequencies. The oscillations of the charges on the electrodes, although random, comprise certain predominant frequencies, and their spectra possess very abrupt heterogeneities.

These specific characteristics of the spectrum of the thermal electric oscillations of piezocrystals are a consequence of the piezoelectric effect in the crystals, as a result of which the resonance of the mechanical thermal vibrations has a corresponding reflection in the electric oscillations.

In principle, the apparatus used for studying thermal noise in piezoelectrics is similar to that used for investigating thermal noise in conductors. The apparatus consists of a preamplifier, an amplifier and an analyzer with an appropriate measuring instrument. Unfortunately, the necessity of continuously tuning the analyzer over a wide frequency range resulted in an appreciable reduction in the accuracy of measurement at this stage of the investigation.

A distinctive feature of the preamplifying part of the installation stemmed from the necessity of eliminating the leakage resistor from the control grid circuit, since otherwise the thermal e.m.f. arising in this resistor would substantially distort the spectral characteristics of the piezoelectric thermal noise; moreover, this resistance represents a load for the thermal e.m.f.'s produced within the piezocrystal.

On the whole, a piezocrystal, shunted by a resistance, is a more involved system with a more complicated dependence of the resistive component of the impedance, Re $Z(\omega)$ and, consequently, of the mean square of the thermal noise voltage in the system:

$$\overline{u^2(\omega)} = \frac{2}{\pi} kT \operatorname{Re} Z(\omega),$$

where k is Boltzmann's constant and T is absolute temperature.

Figure 1 shows a graph of the spectral characteristics for the thermal noise of one 45° X-cut specimen of Rochelle salt (dimensions: 8.12 x 0.62 x 0.86 cm^3); the thermal noise characteristics of various conductors are given in the figure for calibration purposes. The thermal noise characteristic was obtained by means of an analyzer, employing the principle of selective amplification with negative feedback, and with continuous tuning in the 2-250 kc range, accomplished by the use of variable resistors and feedback circuit. This characteristic describes quite exactly the spectral composition of thermal noise in piezoelectrics at low frequencies, but at higher frequencies, due to the constant width of the relative pass band $\Delta\omega_0/\omega_0 = 0.04$, the resolution may prove to be inadequate and some smearing of the higher order resonance peaks may occur.

We evaluate the intrinsic thermal noise of the preamplifier as equivalent to that of a 500 ohm resistance.

Measurements of the equilibrium thermal noises in conductors and their spectra served to check the apparatus. The characteristics obtained in these test measurements were used as calibration curves in evaluating the thermal noises of the piezoelectric specimens.

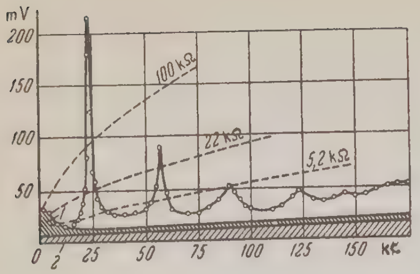

Fig. 1. Typical thermal noise characteristic of a piezoelectric 45° X-cut bar of Rochelle salt: 1) noise due to conduction, 2) thermal noise of the amplifier.

The values of Boltzmann's constant were calculated on the basis of the mean squares of the voltages on the amplifying channel output with different resistances (conductors) on the input and at different frequency settings, using the following equation

$$\overline{U^2_{\text{out}}} = \frac{2}{\pi} kT \int_0^\infty R K^2_{\text{tot}}(\omega)\, d\omega,$$

where $K_{\text{tot}}(\omega)$ — is the overall gain of the installation including the preamplifier, amplifier and RC-analyzer, defined by

$$K_{\text{tot}}(\omega) = \frac{A}{\sqrt{1 + (2K_0 + K_0^2)\cos^2\psi}};$$

$$\operatorname{tg}\psi = \frac{2}{uQ},$$

here $u = \frac{\omega}{\omega_0} - \frac{\omega_0}{\omega}$, and Q is the Q-factor of the feedback mesh.

Integrating, we obtain (provided that $\omega_0 \gg \frac{\Delta\omega Q}{\pi K_0}$):

$$\overline{U^2_{\text{out}}} = 4kTR\frac{\omega_0}{K_0}A^2.$$

The resultant mean value of Boltzmann's constant was found to be 15% less than the true value; in view of this the error in all measurements, with the present apparatus, was assumed to be no less than ±15-20%.

It follows from the semi-phenomenological theory of equilibrium thermal fluctuations that the sources of thermal electromotive forces are concentrated where losses in the electrical impedance occur, i.e., where $\operatorname{Re} Z(\omega) \neq 0$.

The semi-phenomenological theory does not require elucidation of the nature and mechanism of the processes occuring in the electric impedances; consequently the theoretical results, in particular Nyguist's formula, can be applied to electric circuits comprising energy losses of various types (losses in current as well as in the electric field), losses by electromagnetic radiation

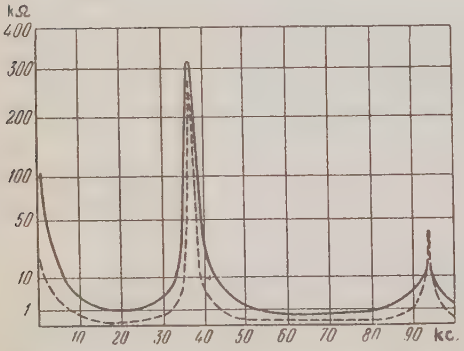

Fig. 2. Measured dependence of Re Z(ω) for one 45° X-cut specimen of Rochelle salt (dash line); solid line -- thermal noise characteristic for the same specimen.

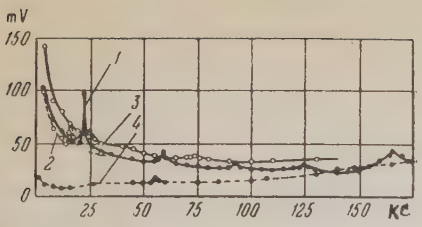

Fig. 3. Thermal noise characteristics of different piezoelectric crystals: 1) di-H ammonium phosphate, 2) Rochelle salt, Y-45°-cut, 3) Rochelle salt, Z-45° cut, 4) barium titanate.

or due to energy dissipation in a piezoelectric transducer in the form of acoustic radiation.

Oscillograph measurements indicated that the resistance of a piezo-crystal is reactive at almost all frequencies and has the same sign as ordinary capacitance; the reactance changes sign in the narrow frequency interval between resonance and antiresonance. In the neighborhood of the antiresonance frequency there is a sharp jump of the resistive component of the impedance; for a metallized bar of Rochelle salt (45° X-cut – $4.70 \times 0.44 \times 0.73$ cm^3) this rise amounts to about 300 KΩ at room temperature.

A comparison of the measured Re $Z(\omega)$ dependences with the thermal noise characteristics showed (see Fig. 2) that, within the limits of the probable error, the Nyguist formula is applicable to piezoelectrics.

An evaluation of the results obtained for 15 different specimens (see Fig. 3) also substantiates the equilibrium character of the noise in all the specimens. As calculations made on the basis of an equivalent circuit and by means of the rigorous equation for the frequency dependence of the impedance of a piezo-bar:

$$Z = \frac{1}{j_{\omega} C_{\xi}\left(1 + \varkappa^2 \frac{\operatorname{th} z}{z}\right)},$$

where for the case of a free piezo-bar

$$z = jx + y = \frac{(j\omega + \alpha)\, l_2}{2c_E} *$$

show, the maximum value of the resistive component of the impedance is

$$\operatorname{Re} Z_{max} = \frac{1}{2\alpha C_m} \approx \frac{4\varkappa^2}{\pi^2 m^2 \alpha C_{\xi}} = \frac{32\, l_1 l_2 \varkappa^2 \rho}{\pi^3 t_3 \varepsilon_{\xi}} \cdot \frac{1}{F},$$

where $C_m = \frac{1}{2} C_{\xi}\left(1 + \varkappa^2 + \frac{\omega_m^2 l_2^2}{4c_E^2 \varkappa^2}\right)$ is the reduced piezocrystal capacity corresponding to the m^{th} oscillatory degree of freedom; $m = 1, 3, 5\ldots$, ω_m is the antiresonance frequency of the m^{th} harmonic.

The dependence of the heights of the peaks of the thermal noise characteristics on the geometric dimensions of the tested specimens agrees with the derived formula. This is easily seen from the diagram of Fig. 4; here the horizontal scale is laid off in

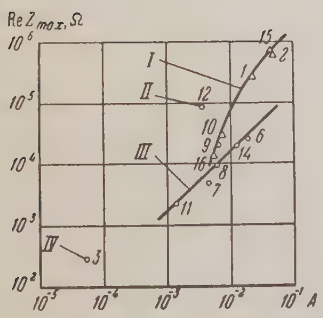

Fig. 4. Diagram of the spectral peak values for the tested specimens: I) 45° X-cut of Rochelle salt, II) di-H ammonium phosphate, III) 45° Y- and 45° Z-cuts of Rochelle salt, IV) barium titanate.

---

* c_E is the velocity of sound in the metallized crystal, l_2 is the length of the piezoelectric bar, C_{ξ} is capacitance of the piezocrystal with a constant bias; $\alpha = \frac{F\omega^2}{2Y_E}$ is the attenuation constant for sound waves, Y_E is the modulus of elasticity in a constant field E, F is the coefficient of internal friction; the constant is related to the electro-mechanical coupling λ by $\varkappa^2(1-\lambda^2) = \lambda^2$.

values of $A = \frac{32\, l_1 l_2 \lambda^2 \rho}{\pi^3 l_3 \varepsilon_\xi (1-\lambda^2)} \cdot \frac{C_\xi}{C_\xi + C_{in}}$, while the corresponding values of Re Z_{max}, taken from the thermal noise characteristics for different specimens are the ordinates.

The factor $\frac{C_\xi}{C\xi + C_{in}}$ is here introduced to take account of the capacitance C_{in}, introduced by the input stage of the amplifier. The values of ε_ξ and of the electromechanical coupling λ for the 45° X-cut of Rochelle salt were taken in accordance with our measurements, carried out by the antiresonance method (at 20°, $\lambda^2 = 0.38$).

The area under the thermal noise curve for piezoelectric crystals may be of interest in certain cases; as follows from Nyguist's formula

$$\overline{U}^2 = \frac{2}{\pi} kT \int_0^\infty \operatorname{Re} Z d\omega = \frac{kT}{\pi} \int_{-\infty}^{\infty} Z(jx + y)\, d\omega = \frac{kT}{j\pi C_\xi} \int_{y-j\infty}^{y+j\infty} \frac{dz}{z + \varkappa^2 \operatorname{th} z}.$$

The function under the integral has a series of poles $z_m = jx_m$ on the X-axis, which correspond to antiresonance frequencies of different harmonics.

Replacing integration over the axis by integration over the contour and invoking Cauchy's integral theorem, we obtain

$$\int_{y-j\infty}^{y+j\infty} \frac{dz}{z + \varkappa^2 \operatorname{th} z} = 2\pi j \sum_m sub \frac{1}{z + \varkappa^2 \operatorname{th} z},$$

whence it follows that if the corresponding residues are evaluated the mean square of the thermal noise voltage on the electrodes of a free metallized piezo-bar, that is a distributed system, can be represented in the form of the summation

$$\overline{U}^2 = \sum_m^\infty \overline{U}_m^2 = kT \sum_m^\infty \frac{1}{C_m}.$$

Thus the mean square of the voltage, which is numerically equal to the area under the thermal noise characteristic $u^2(\omega)$, — with uniform distribution of the energy over the degrees of freedom — is independent of the magnitude of the losses in the piezo-bar but is strongly dependent on the value of the electro-mechanical coupling coefficient. With increased attenuation, the spectral thermal noise characteristic becomes smeared out but the area under it remains unchanged.

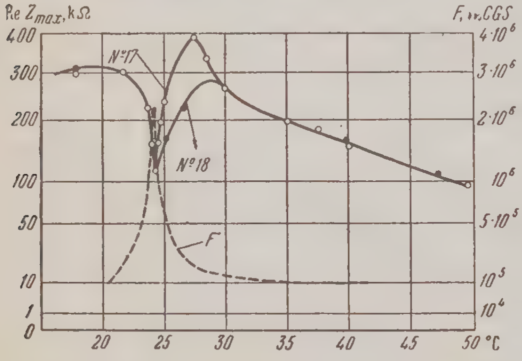

Fig. 5. Temperature dependence of the height of the peak of the thermal noise characteristic of two 45° X-cut specimens of Rochelle salt; F — temperature dependence of the internal friction coefficient.

The described procedure can be used for studying the internal friction in piezoelectrics; in particular, if the measurements are carried out for higher harmonics of the natural frequency one can obtain the frequency dependence of the internal friction coefficient F. Obviously, this can be accomplished only with high-frequency equipment having a high sensitivity and high resolution.

The peaks of all the orders in the spectral characteristic of the 45° X-cut bar of Rochelle salt are shifted to the left as the temperature approaches the Curie point, as might be expected in view of the fact that the corresponding resonant frequencies are noticeably reduced in the vicinity of the Curie point.

On the basis of the characteristics recorded at different temperatures in the 10 to 50° range, we plotted (Fig. 5) the temperature dependence of the internal friction coefficient F, which rises sharply in the 45° X-cut of Rochelle salt as the Curie point is neared. The temperature dependence of the coefficient F shown in Fig. 5 by the dash line was computed taking into account the temperature dependences of the dielectric constant and the electro-magnetic coupling coefficient. The solid lines in the same figure represent the temperature dependences of Re Z_{max} for two different specimens.

In addition to the RC-analyzer, an electronic spectrograph has been used for observing the thermal noise of piezoelectric crystals. In this the spectra are analyzed by means of a quartz crystal filter with modulation of the frequency by a heterodyne oscillator. A photograph of the screen of the cathode-ray tube of the spectrograph is reproduced in Fig. 6.

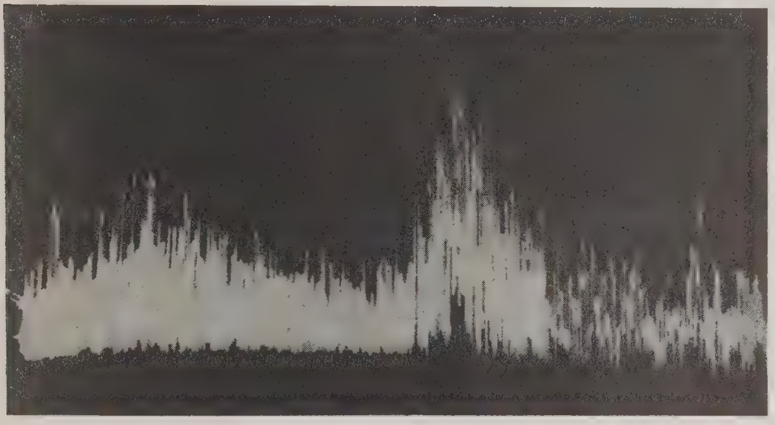

Fig. 6. Oscillogram of the thermal noise spectrum of a 45° X-cut bar of Rochelle salt at 28°. Frequency marker at 20 kc.

In actual piezoelectric transducers - radiators and receivers - in addition to the internal friction a number of other factors affect the width of the thermal noise peaks. Radiation loss and losses in the crystal holder also contribute to smearing out of the spectral characteristics of transducers. The height of the peak in the thermal noise characteristic of an actual piezoelectric transducer may be appreciably lower than the height observed by us for freely suspended specimens. Nevertheless, the intrinsic thermal noise in piezoelectric receivers can largely determine their sensitivity threshold. Generally, the operating frequencies of piezoelectric receivers coincide with the frequencies of the thermal noise peaks. There can be no doubt that minimizing thermal noise in piezo-receivers will play an important part in further improvement of amplifying equipment.

It is of interest to note that the spectral thermal noise characteristics of piezoelectric receivers and radiators are similar in shape to the frequency characteristics of their sensitivities. It would seem, therefore, that determination of the thermal noise characteristics would offer a rapid and easy approach to determining the sensitivity characteristics of piezoelectric transducers. The procedure outlined above may thus be of help in connection with the design of new piezoelectric transducers.

Department of Physics of
"M.V.Lomonosov" Moscow State University

References

1. V.L.Ginzburg, Usp. fiz. nauk, 46, 348 (1952).
2. G.S.Gorelik, Usp fiz. nauk, 44, 33 (1951).
3. H.Nyguist, Phys. Rev., 29, 614 (1927); 32, 110 (1928).
4. J.Johnson, Phys. Rev., 32, 97 (1928).
5. C.Neitzert, Physics, 5, 292 (1934).
6. E.Ia.Pumper, Doklady AN SSSR, 46, 41 (1949): Zhur. eksp. i teor. fiz., 18, 1112 (1948).
7. V.S.Troitski, A.G.Liubina & A.V.Zolotov, Zhur. eksp. i teor. fiz., 25, 455 (1953).
8. A.M.Bonch-Bruevich, Primenenie elektronnykh lamp v eksperimental'noi fizike (Applications of vacuum tubes in experimental physics) M.-L. 1954.

NEW PARAMETERS OF QUARTZ CRYSTALS AND AN ENGINEERING METHOD OF DESIGNING QUARTZ OSCILLATORS

- E.I.Kamenski

Although quartz crystal oscillators are widely used in modern radio equipment and there are many articles and monographs on crystal stabilization and control, there are virtually no publications, in the USSR or abroad, giving an accurate yet simple engineering design procedure for quartz crystal exciters. Consequently the development of new crystal exciters and new types of quartz resonators is carried out in what must be termed a very primitive manner. Commonly the operating regime and the frequency of the oscillator and the crystal resonator parameters required to assure these are not calculated but determined experimentally. This is due to the fact that industrial control methods employed in the fabrication of quartz plates are far from perfect and that there is no engineering method of designing and calculating the exact parameters of crystal oscillators. Hence quality inspection and acceptance tests for crystal plates amount to little more than checks of the generated frequency and amplitude of the exciter, with virtually no quality control of the quartz plate parameters. This situation naturally leads to difficulties in the electronic components industry when it comes to designing and mass producing new quartz crystal stabilized radio equipment.

The purpose of the present investigation was development of a new engineering design procedure for quartz crystal exciters and new inspection and control methods which would provide not only for rapid determination of the plate parameters in production but also standardized, operationally dependable final components.

1. Operating Parameters of Quartz Crystals

Let us first see whether it is feasible to utilize the conventional equivalent parameters of crystals for purposes of industrial quality control and engineering design. As we know[1] the equivalent parameters cannot be measured with the accuracy requisite for insuring the exact specified frequency of the oscillator and are not readily amenable to standardization where multiple frequency operation is concerned. Inasmuch as the insufficiently accurate measurements of the equivalent parameters are useless for predicting the operating frequency of the exciter, they are commonly not checked at all in the process of crystal plate production. Numerous attempts have been made to provide for more effective quality control of quartz plates, particularly during the years of the Second World War when crystals were being made in great numbers. Different quantities and factors were suggested to serve as such control parameters: the Q-factor, the figure of merit, the performance index PI, the impedance diameter ID, etc. However, none of these quantities assured a sufficiently convenient and effective quality control of the plates in process of production or provided for making simple design calculations for crystal oscillators.

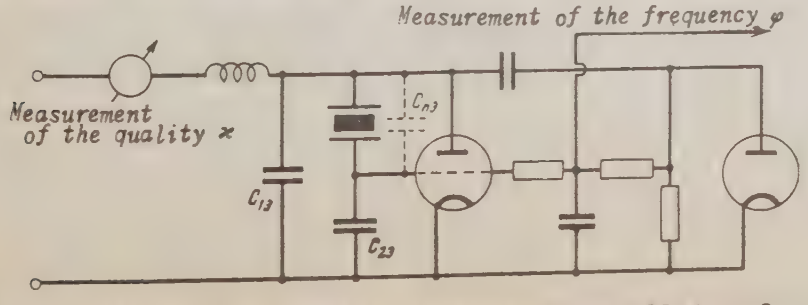
Measurement of the frequency φ
Measurement of the quality $\varkappa$
C_{n3}
C_{13}
C_{23}

Fig. 1. Diagram of special "standard" oscillator for measuring the frequency and quality of crystal plates.

We here propose the following new "operating" or working parameter which we shall designate as the crystal frequency φ, the cut coefficient K_{cp}, the quality $\varkappa$ (not to be confused with Q) and the capacitance C_0.

We define the first quantity, the crystal frequency, as the frequency yielded by the quartz plate when tested in a "standard" oscillator, having the specially designed circuit pictured in Fig. 1, operating without grid current. Assuming that the frequency of oscillation of the standard crystal oscillator is independent of the resistances in the circuit and the parameters of the tube, we find that the frequency φ is related to the subsequent resonant frequency of the crystal $f_{\text{к}} = \frac{1}{2\pi\sqrt{L_{\text{к}}C_{\text{к}}}}$ by the expression*

$$\varphi = f_{\text{к}}\left(1 + 0{,}5\,\frac{C_{\text{к}}}{C_0 + C_{\text{сх. э}}}\right), \tag{1}$$

where C_K is the equivalent capacitance of the crystal, C_0 is its usual "static" capacitance, while C_{cx} is the capacitance equivalent to the circuit connected in parallel with the crystal in the standard oscillator.

We introduce the quantity $K_{cp} = C_K/C_0$; after substituting and factoring, we get

$$\varphi = f_{\text{к}}\left(1 + K_{\text{ср}}\,\frac{0{,}5}{1 + \frac{C_{\text{сх}}}{C_0}}\right). \tag{2}$$

We can write an analogous equation for the frequency f of any crystal oscillator, using the appropriate equivalent capacitance C_{cx}:

$$f = f_{\text{к}}\left(1 + K_{\text{ср}}\,\frac{0{,}5}{1 + \frac{C_{\text{сх}}}{C_0}}\right). \tag{2a}$$

It will be seen from equations (2) and (2a) that knowing the frequency φ we can uniquely determine the natural oscillating frequency of the crystal in any operating generator. The relationship connecting the frequencies f and φ that also takes into account the active parameters of the circuit and tube has the form

$$f = \varphi\,[1 + K_{\text{ср}}F_1], \tag{3}$$

where F_1 is a function that depends not only on the capacitance but also on the other parameters of the circuit and crystal. The quantity K_{cp}, entering into (3), is another highly important parameter of the crystal, a parameter which determines the frequency instability of the crystal oscillator incident to changes of the oscillator circuit parameters. It has been shown[2] that the magnitude of the ratio of the equivalent to the static capacitance of the crystal depends only on the electromechanical coupling coefficient K and is characterized by

$$\frac{C_{\text{к}}}{C_0} = \frac{8}{\pi^2}\cdot\frac{K^2}{1 - K^2}. \tag{4}$$

Usually the electromagnetic coupling coefficient K is assumed to be constant for a given angle of cut; K_{cp} under the same conditions is also theoretically constant. In practice, however, the value of K_{cp} depends not only on the angle of the cut but also on the quality of the surfaces and the presence of inclusions and other defects in the crystal; consequently the actual value is always somewhat lower than the theoretical one. Hence, even for the same angle of cut, K_{cp} can vary to some extent. The actual value of K_{cp}, necessary for computing the design frequency of an oscillator incorporating the crystal can easily be measured by means of an instrument developed by the writer[3] and is usually of the order of 10^{-3}. Calculations show that for most circuits employed in practice F_1 is always appreciably smaller than unity. The frequency correction defined by the term $K_{cp}F_1$ in (3) is always very small. For most actual circuits this correction is on the order of 10^4-10^{-5} and, consequently, the frequency of a crystal oscillator can be calculated to an accuracy of 1 in 10^5-10^6 if the values of K_{cp} and F_1 are determined within a few percent, which can readily be done even under mass production conditions.

---

*Here and below the subscript $_{K}$ stands for "quartz crystal". (Translator)

The third operating parameter mentioned is the quality $\varkappa$. It may be defined as the control resistance yielded by the tested crystal in the same standard oscillator. In an earlier article[3] it was shown that the control resistance R_y of any crystal oscillator, having a circuit reducible to the basic Hartley circuit, can be defined by an equation of the form

$$R_y = \varkappa F_2, \tag{5}$$

where F_2 is a function dependent on the type of circuit, the circuit parameters and the capacitance C_o. This expression shows that the quality of the crystal uniquely determines the amplitude of the oscillating voltage U_c on the grid as well as the amplitudes of the first harmonics of the control grid and plate (anode) currents $I_{c(1)}$ and $I_{a(1)}$, the relationship between the former and the latter being

$$U_c = \varkappa F_2 [I_{a(1)} - F_3 I_{c(1)}], \tag{6}$$

where F_2 and F_3 are functions dependent on the operating parameters of the oscillator circuit and the crystal capacitance C_o. By means of this equation (using the method outlined in Ref. 4) one can find the voltage U_o and the grid and plate current cut-off angles θ and θ_c.

The fourth operating parameter determining the characteristics of the oscillator is the static capacitance C_o. Knowing the operating parameters of the crystal and the values of the functions F_1, F_2 and F_3 (the method of determining these will be described below), we can readily calculate the frequency and the other operating characteristics of any oscillator incorporating this crystal.

From the measured values of the operating parameters, φ, K_{cp}, $\varkappa$ and C_o we can also easily determine the equivalent parameters of the crystal C_K, L_K, r_K and C_o. In order to find the relationships linking the operating and equivalent parameters of crystal plates, let us examine the generalized crystal oscillator circuit and the equivalent electric circuit pictured in Fig. 2, a and c. The capacitance C_{KB} in Fig. 2, c represents the total capacitance comprised in the Z's replacing the crystal. This capacitance is

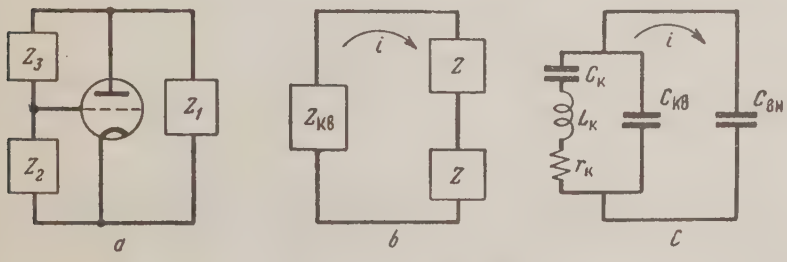

Fig. 2. Generalized and equivalent circuits of a quartz crystal oscillator.

$$C_{KB} = C_o + C_p \tag{7}$$

where C_p is the combined capacitance of the circuit and tube connected parallel to the crystal, disregarding the capacitances comprised in the other Z's. The capacitance C_{BH} replaces both Z's serving for coupling to the tube. This replacement is allowable inasmuch as in a quartz crystal oscillator the Z's, replacing the crystal at the oscillation frequency are always inductive in character, hence the sum of the Z's, serving for coupling with the tube, must always be capacitative. Let us evaluate the impedance Z_0 obtained in going around the oscillator mesh:

$$Z_0 = Z_1 + Z_2 + Z_3 \tag{8}$$

Inasmuch as the self-sustaining oscillations always occur at a frequency ω close to the around-the-mesh resonant frequency $\omega_{o\kappa}$, Z_0 can be written in the form

$$Z_0 = r(1 + i\alpha), \tag{9}$$

where the detuning relative to $\omega_{o\kappa}$ is

$$\alpha = \frac{x}{r}. \tag{10}$$

In crystal oscillator circuits in practical use, the attenuation is determined principally by the resistance of the crystal. To simplify the equations, we shall neglect the resistances of the other components of the oscillating circuit. Let us designate the impedance of the circuit element, defining the piezo-admittance of the crystal, through Z_K, where

$$Z_{\text{К}} = r_{\text{К}} + ix_{\text{К}}. \tag{11}$$

Further let us designate the lumped capacitance shunting the piezo-admittance of the crystal through C_{CB}, where

$$C_{\text{СВ}} = C_{\text{КВ}} + C_{\text{ВН}}. \tag{12}$$

Determining the around the circuit impedance of the oscillator circuit and making the appropriate substitutions, we obtain the following complex expression:

$$r(1 + i\alpha)(1 + \omega C_{\text{КВ}} x_{\text{К}} + i\omega C_{\text{КВ}} r_{\text{К}}) = r_{\text{К}} \frac{C_{\text{СВ}}}{C_{\text{ВН}}} + i\left[x_{\text{К}} \frac{C_{\text{СВ}}}{C_{\text{ВН}}} - \frac{1}{\omega C_{\text{ВН}}}\right]. \tag{13}$$

Taking the sum of the real terms and neglecting the term since it is small compared to unity, we obtain the following formula for r:

$$r(1 - \omega C_{\text{КВ}} x_{\text{К}}) = r_{\text{К}} \frac{C_{\text{СВ}}}{C_{\text{ВН}}}. \tag{14}$$

The self-sustaining oscillation frequency ω is always close to ω_o, i.e., to the frequency of the parallel resonance of the tank circuit C_K, L_K, r_K with the capacitance C_{CB} shunted across it (Fig. 2, c). At the resonant frequency ω_o, we have

$$x_{\text{К}0} - \frac{1}{\omega_0 C_{\text{СВ}}} = 0, \tag{15}$$

where $x_{\text{К}0}$ is the reactance corresponding to the piezo-admittance of the crystal at the frequency ω_o. Inasmuch as both ω and ω_o are far from ω_κ (the natural resonant frequency of the piezo-crystal) and at the same time close to each other, we can assume that $x_{\text{К}0} \approx x_{\text{К}}$. Then, making use of (41), (15) and (12), we can deduce an expression for determining the resistance of the crystal circuit at the self-sustaining oscillation frequency:

$$\boxed{r = r_{\text{К}} \left(\frac{C_{\text{СВ}}}{C_{\text{ВН}}}\right)^2}. \tag{16}$$

This very important relationship coincides with the relationship $r = r_{\text{к}} K_{\varepsilon}^2$. obtained by Shembel' and valid for all Hartley type circuits and, consequently, for our standard oscillator circuit. Applying equation (13) to the standard oscillator we can find the expressions relating the quality $\varkappa$ of the crystal with the usual equivalent parameters of a crystal. According to our definition the quality is numerically equal to the control resistance of the standard oscillator, which, according to Evtianov[6] for the capacitative type circuit in question, equals

$$\varkappa = \frac{1}{\omega^2 C_{1\text{э}} C_{2\text{э}} r}, \tag{17}$$

where r is the effective resistance of the circuit at the frequency of self-sustaining oscillation and the indices э indicate that the capacitances are taken for the standard oscillator. Invoking the fact that for the standard oscillator $C_{\text{кв. э}} = C_{3\text{э}}$ and the circuit capacitance

$$C_{\text{вн. э}} = \frac{C_{1\text{э}} C_{2\text{э}}}{C_{1\text{э}} + C_{2\text{э}}}, \tag{18}$$

we find that the overall capacitance $C_{\text{св, э}} = C_{\text{кв. э}} + C_{\text{вн. э}}$ is given by

$$C_{\text{св. э}} = \frac{C_{1\text{э}} C_{2\text{э}} + C_{2\text{э}} C_{3\text{э}} + C_{3\text{э}} C_{1\text{э}}}{C_{1\text{э}} + C_{2\text{э}}}. \tag{19}$$

Substituting in (17), we obtain

$$\varkappa = \frac{1}{\omega^2 r_k} \cdot \frac{C_{1\text{э}} C_{2\text{э}}}{(C_{1\text{э}} C_{2\text{э}} + C_{2\text{э}} C_{3\text{э}} + C_{3\text{э}} C_{1\text{э}})^2}. \tag{20}$$

The second term in this equation can be represented in the form of the square of a certain equivalent capacitance

$$C_{\varkappa} = \frac{C_{1\text{э}} C_{2\text{э}} + C_{2\text{э}} C_{3\text{э}} + C_{3\text{э}} C_{1\text{э}}}{\sqrt{C_{1\text{э}} C_{2\text{э}}}}. \tag{21}$$

Hereinafter we shall term this capacitance $C_{\varkappa}$ the "effective capacitance" of the quartz crystal plate. Substituting from (21) in (20), we obtain a very simple expression relating the quality with the equivalent parameters of the crystal and the parameters of the standard oscillator circuit:

$$\boxed{\varkappa = \frac{1}{\omega^2 C_{\varkappa}^2 r_{\text{к}}}}. \tag{22}$$

Equation (21) can readily be brought to the form

$$C_{\varkappa} = \frac{\sqrt{C_{1\text{э}} C_{2\text{э}}}}{C_{\text{вн. э}}} (C_{\text{вн. э}} + C_{\text{п. э}} + C_0). \tag{23}$$

Inasmuch as all the parameters of the standard oscillator circuit are constant and determine only the quantities we have selected for evaluating the quality and frequency, by substituting the numerical values of these parameters (deduced by the writer in Ref. 3) — $C_{1\text{э}}$ = 39.2 μμf, $C_{2\text{э}}$ = 122.6 μμf and $C_{\text{п. э}}$ = 3 μμf — we obtain the following simple equation for finding the effective capacitance of the crystal:

$$\boxed{C_{\varkappa} = 2{,}32\,(C_0 + 33)}, \tag{24}$$

wherein all the capacitances are in micromicrofarads.

To simplify the relationships connecting the operating parameters with the equivalent parameters of the crystals, let us introduce the quantity $x_{\varkappa}$

or "effective impedance" of the crystal

$$x_\varkappa = \frac{1}{\omega C_\varkappa}. \tag{25}$$

Using equations (22) and (25), we get

$$\boxed{r_\text{к} = \frac{x_\varkappa^2}{\varkappa}}. \tag{26}$$

On the basis of our definition of the cut coefficient K_{cp}, we have

$$\boxed{C_\text{к} = K_\text{cp} C_0}. \tag{27}$$

Invoking expressions (2), (24) and (25) and expressing the frequency $f_\text{к}$ in terms of the equivalent parameters of the crystal, we obtain

$$\boxed{L_\text{к} = \frac{x_\varkappa^2 (C_\varkappa + 1{,}16\, K_\text{cp} C_0)^2}{K_\text{cp} C_0}}. \tag{28}$$

Let us now deduce the relationships connecting our operating parameters with the Q of the crystal and the "performance index" PI, proposed by Fair and used in the U.S.A. Replacing the equivalent by the corresponding operating parameters in the expression $Q = 1/(\omega C_K r_K)$ and simplifying, we get

$$Q = \frac{1}{K_\text{cp}} \cdot \frac{\varkappa}{x_\varkappa} \cdot \frac{C_\varkappa}{C_0}. \tag{29}$$

According to the definition given by Fair,[7] the performance index

$$PI = \frac{1}{\omega^2 (C_0 + C_\text{cx})^2 r_\text{к}} = \frac{1}{\omega^2 C_\text{cв}^2 r_\text{к}}. \tag{30}$$

When, using (22), we find

$$PI = \varkappa \left(\frac{C_\varkappa}{C_\text{cв}} \right)^2. \tag{31}$$

As is known, the magnitude of C_{CB} depends on the type of operating circuit used. This dependence makes the PI a less objective parameter and gives rise to certain additional difficulties in measuring it and in employing it for control purpose in the mass production of crystal plates. On the other hand the operating parameters can be readily and simply measured on the Kvarts-2 (Quartz-2) instrument (described in Ref. 3) with an accuracy adequate for both production quality control and engineering design of crystal oscillators.

The feasibility of direct measurement and their independence of the type and characteristics of the test crystal oscillator circuit are the outstanding advantages of our "operating" parameters as compared with both the conventional equivalent parameters and the various indices, such as the "performance index" and the "impedance diameter", that have been proposed in the past.

The use of the operating parameters for inspection and quality control of crystal plates will make it possible to set up uniform technical specifications for the production of quartz crystal plates, check all plates on a single set-up and do away with the present onerous procedure of measuring the frequency and voltage amplitude of each plate in different oscillator circuits. At the same time use of the operating parameters should also facilitate the introduction of new and better methods of tuning and frequency adjustment of resonators, since by referring to the operating parameters it should be possible to effect the final frequency adjustment (grinding, etc.) of plates intended for different oscillators and other crystal controlled components with the aid of one and the same standard oscillator.

2. Engineering Design of Crystal Exciters

Present design and computation procedures cannot be termed "engineering" methods, for they are far too complicated and yet do not insure the requisite technical accuracy inasmuch as they do not take into account a number of important factors encountered in actual oscillators. The complexity of present design procedures is due, first, to the inclusion of minor factors that have little influence on the end result and, second, to the poor choice of the basic frequency with reference to which the initial equations are set up. In developing an engineering procedure, let us start by establishing the group of circuits that are to be provided for by our design procedure and evaluating all the factors that must be taken into account to assure the requisite accuracy; then let us determine the most advantageous basic frequency on which to base our design equations. Analysis of the crystal oscillators commonly used in radio equipment shows that virtually all of them have circuits which can be reduced to the basic Hartley oscillator circuit. Hence for our reference circuit, let us take the one pictured in Fig. 2. In view of the general characteristics of circuits of this type, in setting up the equations we can neglect the plate reactance and the influence of all the resistances in the circuit with the exception of the resistance of the crystal itself; at the same time it is essential to take into account the grid current and the grid and plate self-bias. The simplest initial equations are obtained if we construct them with respect to the resonant frequency obtained by going around the mesh consisting of the impedances Z_1, Z_2 and Z_3. Replacing Z_0 by the value in (9), we obtain relationships by means of which one can design and calculate any oscillator circuit that is reducible to the generalized Hartley oscillator:

$$U_c(1+i\alpha) = -\frac{Z_1Z_2}{r}\left[I_{a\,(1)} + \frac{Z_3+Z_1}{Z_1} I_{c\,(1)}\right]. \tag{32}$$

The design equations for finding the control resistance and the detuning (frequency difference) are readily obtained by separating the real and imaginary parts of (32):

$$U_c = \mathrm{Re}\left[-\frac{Z_1Z_2}{r}\left(I_{a\,(1)} + \frac{Z_3+Z_1}{Z_1} I_{c\,(1)}\right)\right], \tag{33}$$

$$\alpha = \mathrm{Im}\left[-\frac{z_1z_2}{rR_y}\cdot\frac{I_{a\,(1)} + \frac{Z_3+Z_1}{Z_1} I_{c\,(1)}}{I_{a\,(1)} - KI_{c\,(1)}}\right]. \tag{34}$$

Equation (33) is easily brought to a more convenient form, analogous to (6):

$$U_c = R_y\left(I_{a\,(1)} - KI_{c\,(1)}\right). \tag{35}$$

In equations (33), (34) and (35) Re and Im designate the real and imaginary parts of the expression in the brackets, $R_y = \varkappa F_2$ is the control resistance of the oscillator and $K = F_3$ is a coefficient taking into account the influence of the grid current on the operation of the oscillator. The values of R_y, K and α can readily be found by means of equations (33) and (34) if we substitute therein all the known values of Z, replace the complex Z, equivalent to the crystal, by means of the relationship

$$\frac{x_\varkappa^2}{\varkappa}\left(\frac{C_{\text{CB}}}{C_{\text{BH}}}\right)^2(1+i\alpha) = Z_1 + Z_2 + Z_3,$$

deduced from (8), (16) and (26), and discard all negligibly small quantities. This was the method employed by the present writer in Ref. 3 to evaluate the values of R_y, K and α for five of the most commonly used oscillator circuits. The computed values were checked by a different, more complicated calculating

Table 1

SUMMARY OF EQUATIONS FOR THE ENGINEERING DESIGN OF CRYSTAL GENERATORS

Circuit	Capacitance C_{BH}	Control resistance $R_y = \varkappa F_2$	Coefficient $K = F_3$	Detuning α
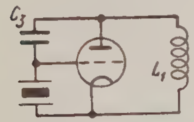	$\frac{C_3}{1-\omega^2 L_1 C_3}$	$\varkappa\omega^2 L_1 C_{\text{BH}} \left(\frac{C_x}{C_{\text{CB}}}\right)^2$	$\frac{1}{\omega^2 L_1 C_{\text{BH}}}$	$-\frac{x_1}{R_y}$
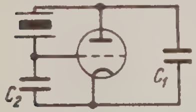	$\frac{C_1 C_2}{C_1 + C_2} = C_{12}$	$\varkappa \frac{C_{\text{BH}}}{C_1 + C_2} \left(\frac{C_x}{C_{\text{CP}}}\right)^2$	$\frac{C_1}{C_2}$	$\frac{x_2}{R_y} \cdot \frac{i_c}{i_a - \frac{C_1}{C_2} i_c}$
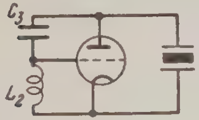	$\frac{C_3}{1-\omega^2 L_2 C_3}$	$\gamma\omega^2 L_2 C_{\text{BH}} \left(\frac{C_x}{C_{\text{CB}}}\right)^2$	$\omega^2 L_2 C_{\text{BH}}$	$-\frac{x_3}{R_y} \cdot \frac{i_a - i_c}{i_a - \omega^2 L_2 C_{\text{BH}} i_c}$
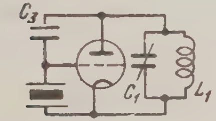	$\frac{C_3(1-\omega^2 L_1 C_1)}{1-\omega^2 L_1 (C_3 + C_1)}$	$\varkappa \frac{\omega^2 L_1 C_{\text{BH}}}{1-\omega^2 L_1 C_1} \left(\frac{C_x}{C_{\text{CB}}}\right)^2$	$\frac{1-\omega^2 L_1 C_1}{\omega^2 L_1 C_{\text{BH}}}$	$\frac{x_1}{R_y(1+\omega^2 L_1 C_1)}$
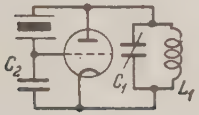	$\frac{C_2(\omega^2 L_1 C_1 - 1)}{\omega^2 L_1 (C_1 + C_2) - 1}$	$\varkappa \frac{\omega^2 L_1 C_{\text{BH}}}{\omega^2 L_1 (C_1 + C_2) - 1} \left(\frac{C_x}{C_{\text{CB}}}\right)^2$	$\frac{\omega^2 L_1 C_1 - 1}{\omega^2 L_1 C_2}$	$\frac{x_2}{R_y} \cdot \frac{i_c}{i_a - \frac{C_1}{C_2} i_c}$

Note: $x_1 = \omega L_1$, $x_2 = \frac{1}{\omega C_2}$, $x_3 = \frac{1}{\omega C_3}$, $\omega \approx 2\pi\varphi$.

procedure and proved to be in excellent agreement with the latter. The results are listed in Table 1, from which it can be seen that the frequency of an oscillator with the crystal located between the grid and plate is independent of the magnitude of the grid and plate currents of the tube. The calculations also show that in an oscillator with the crystal located between the plate and grid the control resistance is entirely independent of the frequency and the detuning produced by the tube equals zero when there is no grid current. This is why an oscillator of this type was selected for the standard oscillator to be used for measuring the operating parameters of quartz crystals.

To calculate the frequency of the crystal exciter and its frequency instability, let us deduce the general equation defining the relation between the frequency of self-oscillation, the frequency $f_{o.\text{к}}$ determined by going around the mesh and the usual, readily determined frequency f_o, i.e., the frequency of parallel resonance of the crystal with all the reactances connected in parallel to it. To this end let us turn to the imaginary part of (13):

$$\alpha(1-\dot{\omega}C_{\text{кв}}x_{\text{к}})\,r_{\text{к}}\left(\frac{C_{\text{св}}}{C_{\text{пп}}}\right)^2+r_{\text{к}}\omega C_{\text{кв}}\left(\frac{C_{\text{св}}}{C_{\text{вн}}}\right)^2=x_{\text{к}}\frac{C_{\text{св}}}{C_{\text{вн}}}-\frac{1}{\omega C_{\text{вн}}}. \qquad (36)$$

Using expression (15), combining terms and dividing by $C_{\text{CB}}/C_{\text{BH}}$, we get

$$\alpha r_{\text{к}}=x_{\varkappa}-\frac{1}{\omega C_{\text{св}}}-r_{\text{к}}^2\omega C_{\text{кв}}\frac{C_{\text{св}}}{C_{\text{вн}}}. \qquad (37)$$

At a frequency $\omega=\omega_{\text{о.к}}$, the detuning $\alpha = 0$. Whence we get

$$x_{\text{к.о.к}}-\frac{1}{\omega_{\text{о.к}}C_{\text{св}}}-r_{\text{к}}^2\omega_{\text{о.к}}C_{\text{кв}}\frac{C_{\text{св}}}{C_{\text{пп}}}=0, \qquad (38)$$

where $x_{\text{к.о.к}}$ is the reactance of the impedance Z_K at the frequency $\omega_{\text{о.к}}$. Let us denote the difference between $\omega_{\text{о.к}}$ and ω_0 through $\Delta\omega_0$, i.e., let

$$\Delta\omega_0=\omega_{\text{о.к}}-\omega_0. \qquad (39)$$

Let us find the reactance in the impedance Z_K at $\omega_{\text{о.к}}$:

$$x_{\text{к.о.к}}=(\omega_0+\Delta\omega_0)\,L_{\text{к}}-\frac{1}{(\omega_0+\Delta\omega_0)\,C_{\text{к}}}. \qquad (40)$$

Using (15) and discarding the small second order terms, we obtain

$$x_{\text{к.о.к}}=\frac{1}{\omega_0C_{\text{св}}}\left(1+\frac{\Delta\omega_0}{\omega_0}\right)+\frac{2\Delta\omega_0}{\omega_0}\cdot\frac{1}{\omega_0C_{\text{к}}}. \qquad (41)$$

Substituting (41) in (38), expressing $\omega_{\text{о.к}}$ in terms of ω_0 and simplifying, we obtain

$$\frac{2\Delta\omega_0}{\omega_0}\cdot\frac{1}{\omega_0}\left(\frac{1}{C_{\text{к}}}+\frac{1}{C_{\text{св}}}\right)=r_{\text{к}}^2(\omega_0+\Delta\omega_0)\,C_{\text{кв}}\frac{C_{\text{св}}}{C_{\text{вн}}}. \qquad (42)$$

From this, discarding small quantities, multiplying through and dividing by C_K and introducing the crystal damping $\delta_{\text{к}}=\omega_0C_{\text{к}}r_{\text{к}}$, we obtain the following expression for the shift of the resonant frequency $\omega_{o.\text{к}}$ relative to ω_o, applicable to all Hartley type crystal oscillators:

$$\frac{\Delta\omega_0}{\omega_0}=\frac{C_{\text{кв}}C_{\text{св}}}{2C_{\text{к}}C_{\text{вн}}}\delta_{\text{к}}^2. \qquad (43)$$

In order to determine the self-oscillation frequency ω, let us find the relationship between the frequency shift $\Delta\omega$ and the relative detuning α for our compound circuit. Expressing $x_{\text{к}}$ in terms of $x_{\text{к.о.к}}$ and $\Delta\omega$, we obtain the following expression analogous to (41):

$$x_{\text{к}}=x_{\text{к.о.к}}\left(1+\frac{\Delta\omega}{\omega_{\text{о.к}}}\right)+\frac{2\Delta\omega}{\omega_{\text{о.к}}}\cdot\frac{1}{\omega_{\text{о.к}}C_{\text{к}}} \qquad (44)$$

from which, by means of similar substitutions and manipulations, we obtain

$$\alpha r_{\text{к}} = \frac{2\Delta\omega}{\omega_{\text{о.к}}}\left(\frac{1}{\omega_{\text{о.к}}C_{\text{к}}} + \frac{1}{\omega_{\text{о.к}}C_{\text{св}}}\right). \tag{45}$$

Again, discarding the small quantities and introducing $\delta_{\text{к}}$, we get

$$\alpha = \frac{2\Delta\omega}{\omega_{\text{ок}}\delta_{\text{к}}}. \tag{46}$$

Making use of the relationships (43) and (46) for "in-design" and standard oscillators, we obtain the following general formula for the frequency of self-sustaining oscillation of any quartz crystal oscillator, having a circuit reducible to the generalized Hartley one:

$$\boxed{f = \varphi\left\{1 + \frac{K_{\text{ср}}}{2}\left[\frac{C_0}{C_{\text{св}}} - 2{,}32\frac{C_0}{C_{\varkappa}} + \frac{C_0}{C_{\varkappa}}\cdot\frac{x_{\varkappa}^2}{\varkappa^2}\left(\frac{C_{\text{кв}}C_{\text{св}}}{C_{\text{вн}}C_{\varkappa}} - \frac{C_0+3}{69{,}6} + \alpha\frac{\varkappa}{x_{\varkappa}}\right)\right]\right\}}. \tag{47}$$

Comparing (3) with (47), we see that the value of the function F_1 is the same for all Hartley type circuits; this function is characterized by

$$F_1 = 1{,}16\frac{C_0}{C_{\varkappa}}\left[\frac{33 - C_{\text{сх}}}{C_{\text{св}}} + 0{,}432\frac{x_{\varkappa}^2}{\varkappa^2}\left(\frac{C_{\text{кв}}C_{\text{св}}}{C_{\text{вн}}C_{\varkappa}} - \frac{C_0+3}{69{,}6} + \alpha\frac{\varkappa}{x_{\varkappa}}\right)\right]. \tag{47a}$$

Formula (47) can be rewritten in a different form, by making use of (40) and introducing the capacitances $C_{\text{сх}}$ and $C_{\text{сх.э}}$ = 33 μμf,

$$f = \varphi\left\{1 + 1{,}16\,K_{\text{ср}}\frac{C_0}{C_{\varkappa}}\cdot\frac{33 - C_0}{C_{\text{св}}} + \frac{1}{2Q}\cdot\frac{x_{\varkappa}}{\varkappa}\left(\frac{C_{\text{кв}}C_{\text{св}}}{C_{\text{вн}}C_{\varkappa}} - \frac{C_0+3}{69{,}6}\right) + \frac{\alpha}{2Q}\right\}. \tag{48}$$

In this expression the first term depends only on the crystal parameter φ, the second term gives the deviation of the frequency due to the difference between the capacitances of the design and standard oscillators, the third term gives the frequency deviation due to the resistance of the crystal and the last term the frequency shift due to the detuning introduced by the tube of the oscillator.

It should be noted that usually in Hartley type oscillator circuits, which are characterized by the fact that in them the oscillation frequency is close to the frequency of parallel resonance of the crystal with all the reactance connected thereto, the second term, which is independent of the Q of the crystal, is appreciably greater than the third and fourth terms. Hence for a given set of circuit parameters, the principal part of the frequency instability due to changes in the capacitances associated with the tube proves to be virtually independent of the Q of the crystal. However, the frequency instability due to variations of the effective parameters of the tube, i.e., the instability resulting from changes in the plate and cathode voltages of the tube, is always inversely proportional to the Q of the crystal (the influence of the dynamic capacitance of the tube is taken into account in evaluating ΔC_{CB}).

To deduce design formulas and determine the frequency instability incident to the variations of the various destabilizing factors we found the partial derivatives with respect to these factors, expressing the total instability in the form

$$\Delta f = \frac{\partial f}{\partial\varphi}\Delta\varphi + \frac{\partial f}{\partial\varkappa}\Delta\varkappa + \frac{\partial f}{\partial C_0}\Delta C_0 + \frac{\partial f}{\partial C_{\text{св}}}\Delta C_{\text{св}} + \frac{\partial f}{\partial S}\Delta S + \frac{\partial f}{\partial S_{\text{с}}}\Delta S_{\text{с}}. \tag{49}$$

The results of the calculations are listed in Table 2. For evaluating $(\partial f/\partial S)\Delta S$ for the case of a capacitative Hartley oscillator we utilized the empirical formula obtained by the writer in Ref. 3 for the coefficient

$$\gamma_1\theta = \frac{\frac{R_{\text{с}}}{R_{\text{у}}} + 1{,}84F_3}{S\left[R_{\text{с}} + 1{,}1R_{\text{а}}F_3\right]}, \tag{50}$$

where R_c is the grid and R_a the plate resistance of the crystal oscillator.

Table 2

Equations for computation of frequency instability

Parameters causing instability	Frequency deviation
Crystal frequency	$\frac{\partial f}{\partial \varphi}\Delta\varphi = \Delta\varphi$
Quality of crystal	$\frac{\partial f}{\partial \varkappa}\Delta\varkappa = -\varphi K_{\text{cp}}\frac{C_0}{C_\varkappa}\cdot\frac{x_x^2}{\varkappa^2}\left(\frac{C_{\text{кв}}C_{\text{св}}}{C_{\text{вн}}C_\varkappa} - \frac{C_0+3}{69{,}6} + \frac{\varkappa}{x_\varkappa}\alpha\right)\frac{\Delta\varkappa}{\varkappa}$
Capacit. of crystal	$\frac{\partial f}{\partial C_0}\Delta C_0 = \varphi\ \frac{K_{\text{cp}}}{2}\left[\frac{(C_{\text{св}}-C_0)\,C_0}{C_{\text{св}}^2} - \frac{33C_0}{C_\varkappa^2}\cdot 2{,}32\right]\frac{\Delta C_0}{C_0}$
Capacit. of circuit	$\frac{df}{\partial C_{\text{св}}}\Delta C_{\text{св}} = -\varphi\frac{K_{\text{cp}}}{2}\cdot\frac{C_0}{C_{\text{св}}}\cdot\frac{\Delta C_{\text{св}}}{C_{\text{св}}}$
Grid-plate trans-conductance	$\frac{\partial f}{\partial S}\Delta S + \frac{\partial f}{\partial S_c}\Delta S_c = \varphi\ \frac{K_{\text{cp}}}{2}\cdot\frac{C_0}{C_\varkappa}\cdot\frac{x_\varkappa}{\varkappa}\left[\frac{\partial\alpha}{\partial S}\Delta S + \frac{\partial\alpha}{\partial S_c}\Delta S_c\right]$
Transconductance in the particular case of a capacitative Hartley osc.	$\frac{\partial f}{\partial S_c}\Delta S_c = \varphi\ \frac{K_{\text{cp}}}{2}\cdot\frac{C_0}{C_\varkappa}\cdot\frac{x_\varkappa}{\varkappa}\times$ $\times\left[\frac{S_c\gamma_1(\theta)}{\omega C_2} - \frac{1}{\omega C_1}\left(\gamma(\theta)S - \frac{1}{R_y}\right)\right]\frac{\Delta S_c}{S_c}$

Calculation of the instability by means of the listed equations permits determining beforehand what variations in the circuit, tube and crystal parameters can be allowed in view of the specified frequency stability; they are therefore very useful in designing exciters. It is also essential in the course of designing to determine whether the selected parameters will assure an allowable operating regime of the crystal. In the case of high-frequency crystals the most important criterion as regards the operating conditions is the power dissipated in the crystal; this can readily be evaluated by means of the following equation deduced by the writer in Ref. 3:

$$P_{\text{кв}} = \frac{U_{\text{кв}}^2}{2\varkappa}\left(\frac{C_{\text{св}}}{C_\varkappa}\right)^2. \qquad (51)$$

Norms for the dissipated power for different types of crystals can be deduced on the basis of the allowable temperature rise. The temperature rise at different dissipated power values is measured by means of a thermocouple and the norms for the allowable power can then be established on the basis of the resultant curves. Examples of such experimental temperature rise vs dissipated power curves for two types of crystals are shown in Fig. 3. In the case of high-frequency crystals the norms are determined almost entirely by the allowable frequency drift. Thus if the temperature coefficient of frequency of a given crystal is 2-1.5·10^{-6} and the allowable frequency shift due to the temperature rise is 1 part in 2·10^5, the permissible temperature rise will obviously be on the order of 10-15°. From the curves of Fig. 3 we find that for

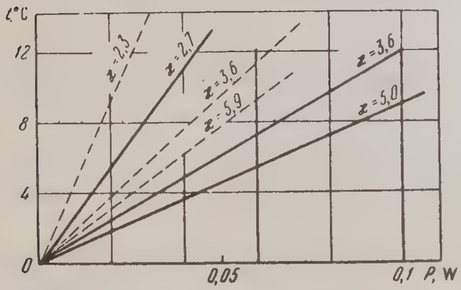

Fig. 3. Dependence of the temperature rise on the dissipated power for normal and miniature crystals. Solid lines - rectangular plates, S = 2.1 cm^2; dash lines - circular plates, S = 1.5 cm^2.

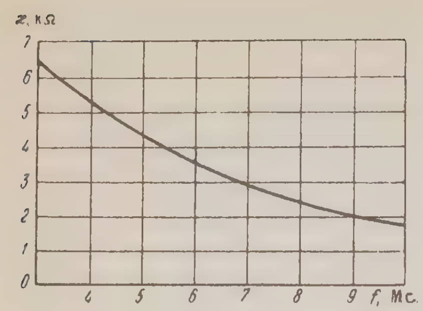

Fig. 4. "Quality norms for mass-produced high-frequency crystals.

this drift in the case of average quality crystals with $\varkappa = 4$ kΩ the allowable power will be about 0.1 watts for rectangular plates having an area $S = 2.1$ cm^2 or about 0.06 watts for circular plates with $S = 1.5$ cm^2.

The experimentally obtained provisional quality norms for mass-produced high-frequency crystals are shown in Fig. 4. Adherence to these norms will assure satisfactory operation of exciters employing modern electronic tubes and provide for mass production of relatively small crystal plates with a minimum of technical difficulties.

In conclusion we note that for complete characterization of serially produced crystal resonators one must know not only the operating parameters of the crystals but also their behavior with aging and temperature changes. The writer hopes that the proposed operating parameters will also prove useful in working with crystal plates vibrating in higher harmonic modes and in the design of another interesting group of circuits, namely those operating at frequencies close to the series resonance of the crystal.

3. Measurement of the Operating Parameters

Inasmuch as the methods of measuring the frequency φ and capacitance C_0 are generally known, we gave primary attention to developing convenient procedures for measuring the quality and the cut coefficient and determining the parameters of the standard oscillator. The writer showed earlier (Ref. 3) that when the oscillator employs a tube with an exponential characteristic $i_a = A \exp(\alpha E_c)$, when the voltage amplitude on the tube grid is small and the crystal sub-circuit is not shunted by any other resistances, the quality of the crystal can be found by means of the equation

$$\varkappa = \frac{1}{aI_{a.0}}, \tag{52}$$

where $I_{a.0}$ is a constant component of the oscillator plate current.

A more precise calibration characteristic for the measuring instrument can be obtained by introducing a number of corrections allowing for the facts that the amplitude of the voltage on the grid has a finite value, that the tube characteristic is not an ideal exponential curve and that the crystal circuit is shunted by a certain resistance.

In order to take into account the fact that the amplitude of the voltage on the grid has a finite value, let us express the plate current of the tube (provisionally assuming it to have a purely exponential characteristic) in terms of a Fourier series with coefficients in the form of Bessel functions:

$$i_a = A \exp(-\beta a U_c)\,[I_0(aU_c) + 2I_1(aU_c)\cos\omega t + \ldots], \tag{53}$$

where $I_0(aU_c)$ and $I_1(aU_c)$ are Bessel functions of the zero and first orders of the purely imaginary argument and $\beta = E_c/U_c$ is a coefficient characterizing the transformation of the ac voltage on the grid to the biasing voltage, produced by the circuit. Using this relationship we deduced a more accurate formula for determining the quality of the crystal:

$$\varkappa = \frac{1}{aI_{a.0}} \cdot \frac{aU_c I_0(aU_c)}{2I_1(aU_c)}\,. \tag{54}$$

We also deduced formulas for the other corrections, taking account of the deviation of the actual characteristic of the tube from the ideal exponential and the influence of the resistances introduced by the circuit components shunting the crystal. All these corrections were taken into account in calculating the calibration curves of the instruments used for measuring the operating parameters of crystals.

An experimental study showed that the calibration curves (scales) so computed are sufficiently accurate and that the crystal parameters measured in this manner are very close to the values of the same parameters determined by other methods.

On the basis of these studies and tests we are designing a set of measuring instruments - the Kvarts-2, Kvarts-3 and Kvarts-6 [Kvarts = Quartz] - which will provide for rapid measurement of the operating parameters of quartz crystal resonantors operating in the frequency range from 1.5 kc to 15 Mc with an accuracy of 1 in 10^5-10^6 as regards frequency and within 2-5% as regards cut coefficient, 3-10% as regards quality and 2-5% as regards capacitance. A description of these instruments will be given in a future article.

The outlined design procedure has been used for a number of specific projects and in all cases the calculated (predicted) values proved to be in close agreement with the experimental ones.

Conclusions

The results of the present investigation are the following:

1. We have found new "operating parameters" for quartz crystal plates on the basis of which one can evaluate the suitability of the crystals for operation in any particular oscillator circuit.
2. We have deduced expressions for calculating the frequency and other characteristics of crystal oscillators, taking into account the influence of the plate current and self-bias of the circuit tube, and developed a simple and yet sufficiently accurate engineering design procedure for oscillators, capable of predicting the operating regime, frequency and frequency instability of the circuit.
3. We have developed a procedure for measuring the operating parameters and designed appropriate instruments for measuring both the new operating parameters and the conventional equivalent parameters of crystal plates. Work with the new instruments under laboratory conditions showed that measurement of the operating parameters is useful and desirable both in developing new types of oscillators and in connection with the serial production of crystal plates. Use of the new parameters and instruments not only simplifies but also improves inspection and quality control of quartz plates in mass production; it also permits doing away with the present far from perfect methods of acceptance-inspection.
4. We determined the operating parameters of a series of typical shortwave quartz plates in the 3-10 Mc frequency range and established tentative, preliminary norms (standards) for such plates. Design calculations backed by tests for a number of exciters of the types now widely used in radio equipment showed that in some cases the size of the crystal plates used in these components can be substantially reduced without impairing the characteristics of the equipment.

References

1. E.A.Gerber, Proc. IRE, 41,9,1103 (1953).

2. W.P.Mason, Piezoelectric crystals and their application to ultrasonics (in Russian translation), M. 1952.

3. E.Kamenski, Thesis, NII MRTP (Scientific Research Institute of the Ministry of the Radio Engineering Industry), 1955.

4. S.Evtianov, E.Kamenski & V.Esin, Radiotekhnika, 2,36(1954).

5. B.Shembel', Zhur. tekh. fiz., 17, 349 (1947).

6. S.Evtianov, Radioperedaiushchie ustroistva, (Radio transmitting equipment), M. 1950.

7. G.E.Fair, Bell Sys. Tech. J., 24, 2 (1945).

PARASITIC VIBRATIONS OF PIEZOELECTRIC PLATES WITH A FUNDAMENTAL LONGITUDINAL MODE

- E.G.Bronnikova

Introduction

A piezoelectric resonator having a multi-frequency characteristic in addition to the fundamental mode vibrates at a number of other, secondary frequencies. This is, of course, an undesirable feature which operates against the use of many cuts of piezoelectric crystals in crystal filters and oscillators. Attenuation or suppression of the parasitic resonances can be achieved in different ways in different specific cases.

There are comparatively few reports on parasitic vibrations and their suppression in the otherwise very extensive literature on piezoelectricity. As a result of collation and generalization of all available data on the subject and extensive experimental research in the Central Scientific Research Laboratory of Piezotechnology of the Ministry of the Radio Engineering Industry on resonators with artificially grown crystals it has become possible to establish the best sequence for analyzing parasitic vibrations and evolve methods for their suppression.

In the present article we shall give the results of a theoretical and experimental investigation of the parasitic oscillations of resonators employing potassium tartrate crystals with a fundamental longitudinal mode. Resonators with this mode of vibration are most commonly used in piezoelectric filters in the 40-200 kc frequency range.

1. Multi-frequency Characteristic of Resonators

The principal types of vibrations of piezoelectric plates are classified as shear, flexural and longitudinal. All the different complex vibrations exhibited by crystals are essentially comprised of these types and their harmonics in different combinations. The type of vibrations excited in a given piezoelectric plate depends on its piezoelectric and elastic properties which are determined primarily by the cut, i.e., by the orientation of the plate faces relative to the crystallographic axes of the parent crystal.

A single frequency of vibration is characteristic only of long thin bars, having a length appreciably greater than the other two dimensions.

The plates used usually in fabricating piezoelectric resonators are commonly nearly as wide as they are long and are characterized by the fact that several types of vibration are excited in them simultaneously. Consequently the equations for determining the resonant frequency, derived for thin long bars:

for longitudinal (extentional) vibrations

$$f_{lo} = \frac{1}{2l}\sqrt{\frac{1}{S_{ii}\rho}} \qquad (1)$$

for shear vibrations (space shear)

$$f_{sh} = \frac{1}{2b}\sqrt{\frac{C_{ii}}{\rho}}, \qquad (2)$$

(where l and b are respectively the length and width of the plate, ρ is the density of the crystal, and where C_{ii} is the modulus of elasticity and S_{ii}^{*} is the coefficient of flexibility in the direction of vibration) are only approximations for the relatively wide plates actually used.

---

*In the present article we shall use S_1, S_2, etc. to denote strain coefficients and s_{ii} and s_{ik} to designate the coefficients of flexibility.

In practice the resonant frequency, the temperature coefficient of frequency and the equivalent parameters of a resonator depend also on the other geometric dimensions of the plate.

Figs. 1 and 2 show the variations of the resonant frequency of the fundamental vibrations in length as a function of the width to length ratio in XY-cut quartz plates and in YX-cut plates of ethylenediamine tartrate. The greater the relative width of the plate, the more the actual resonant frequency deviates from the theoretical one computed according to equation (1). The dependence of the resonant frequency and the equivalent parameters of a resonator on the dimensions not included in equation (1) stems from coupling between the different modes.

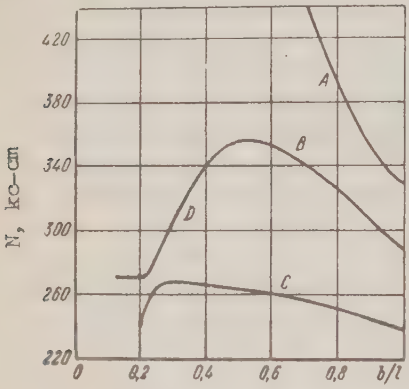

Fig. 1. Variation of the frequency of an XY-cut quartz plate with the width/length ratio. N - frequency constant. Type of vibrations: A) along the width; B) space shear; C) longitudinal; D) flexural produced by shear vibrations.

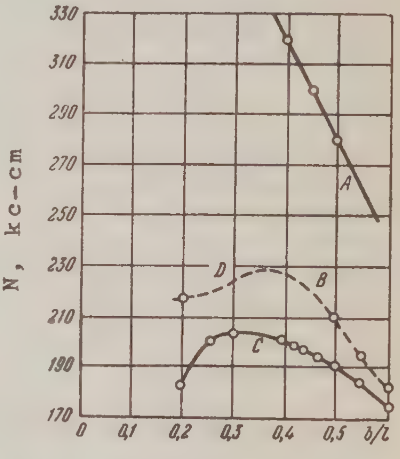

Fig. 2. Variation of frequency of a YX-cut crystal of ethylenediamine tartrate with the width/length ratio. Curve designations as Fig.1.

2. Reasons for Resonators Having Many Frequencies

There are two principal reasons for the multiple frequency characteristic of resonators.

The first reason for a resonator having many resonant frequencies is that an alternating electric field applied to a crystal plate produces six different modes in the general case of complete asymmetry of the crystal. All six are excited directly by the applied field and may exist regardless of whether there is any coupling between them. The modes of vibration excited in a particular kind of crystal are determined by the piezoelectric strain tensor.

The second reason for multiple frequencies is elastic coupling between the different types of vibration. Where such coupling is present, excitation of one mode by the applied electric field gives rise to one or more other modes that are normally not excited directly by the applied field.

One can judge whether there is coupling between the different vibrations in the case of a given plate (cut) from the value of the coefficients of flexibility S_{ik}, where $i \neq k$. To indicate the extent of coupling of the individual deformations with the mechanical stresses through the coefficient of flexibility, in Fig. 3 (next page) we give the piezoelectric strain tensor for a crystal characterized by complete asymmetry. The deformations resulting from the different mechanical stresses are shown in the same figure. The arrows indicate the direction of the deforming forces, while the deformed plates are indicated by the dash lines.

$$\begin{array}{c|cccccc} & T_1 & T_2 & T_3 & T_4 & T_5 & T_6 \\ \hline S_1 & S^{L}_{11} & S^{T}_{12} & S^{T}_{13} & S^{L'}_{14} & S^{T'}_{15} & S^{T'}_{16} \\ S_2 & S^{T}_{12} & S^{L}_{22} & S^{T}_{23} & S^{T'}_{24} & S^{L'}_{25} & S^{T'}_{26} \\ S_3 & S^{T}_{13} & S^{T}_{32} & S^{L}_{33} & S^{T'}_{34} & S^{T'}_{35} & S^{L'}_{36} \\ S_4 & S^{L'}_{14} & S^{T'}_{24} & S^{T'}_{34} & S^{S}_{44}(\perp x) & S^{S}_{45} & S^{S'}_{46} \\ S_5 & S^{T'}_{15} & S^{L'}_{25} & S^{T'}_{35} & S^{S'}_{45} & S^{S}_{55}(\perp y) & S^{S'}_{65} \\ S_6 & S^{T'}_{16} & S^{T'}_{26} & S^{L'}_{36} & S^{S'}_{46} & S^{S'}_{56} & S^{S}_{66}(\perp z) \end{array}$$

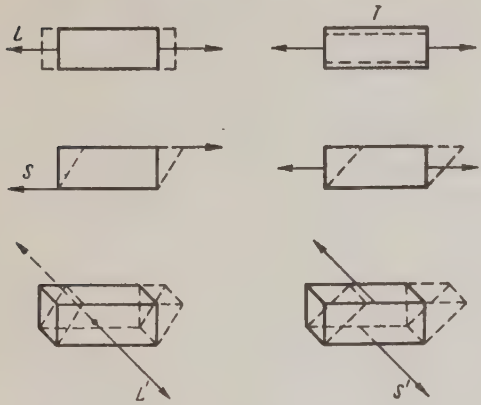

Fig. 3

3. Analysis of the Frequencies Excited

We shall carry out our analysis for the specific case of the principal and rotated cuts of a potassium tartrate crystal.

The two cuts of this crystal having a zero temperature coefficient in the region of room temperatures are the XZ $t_{37.5^{\circ}}$ and XZ $t_{45^{\circ}}$ cuts. Resonators with plates of this cut are now being used in the USSR in the individual channel filters of 12-channel high-frequency telephone systems instead of quartz plate resonators.

The two XZ cuts are characterized by a large number of parasitic vibrations, the exact causes of which have not yet been fully elucidated. With a view to eliminating the parasitic vibrations associated with the fundamental mode and obtaining elements suitable for commercial purposes, the Laboratory carried out an extensive experimental research project aimed at determining the best plate dimensions where the resonant characteristics are concerned.

While the particular project was successful, the procedure in general cannot be recommended for further development of resonators since it is very time-consuming and requires the preparation of a large number of experimental resonators.

It is more expedient to determine the causes of the parasitic resonances before attempting to eliminate them.

Let us begin our analysis of the multiple-frequency characteristic of a potassium tartrate crystal with an examination of the tensors of the coefficients of piezoelectric strain (3) and the coefficients of flexibility (4)

$$\begin{array}{c|cccccc} & T_1 & T_2 & T_3 & T_4 & T_5 & T_6 \\ \hline P_1 & 0 & 0 & 0 & d_{14} & 0 & d_{16} \\ P_2 & d_{21} & d_{22} & d_{23} & 0 & d_{25} & 0 \\ P_3 & 0 & 0 & 0 & d_{34} & 0 & d_{36} \end{array} \qquad (3)$$

$$\begin{array}{c|cccccc} & T_1 & T_2 & T_3 & T_4 & T_5 & T_6 \\ \hline S_1 & S_{11} & S_{12} & S_{13} & 0 & S_{15} & 0 \\ S_2 & S_{12} & S_{22} & S_{23} & 0 & S_{25} & 0 \\ S_3 & S_{13} & S_{23} & S_{33} & 0 & S_{35} & 0 \\ S_4 & 0 & 0 & 0 & S_{44} & 0 & S_{46} \\ S_5 & S_{15} & S_{25} & S_{35} & 0 & S_{35} & 0 \\ S_6 & 0 & 0 & 0 & S_{46} & 0 & S_{66} \end{array} \qquad (4)$$

Here P_1, P_2 and P_3 are the components of the polarization in the direction of the X, Y and Z axes, respectively, $T_1,\dots,T_6$ are the components of the mechanical stresses acting along the X, Y and Z and the shear axes and $S_1,\dots,S_6$ are the corresponding elongation and shear strains.

If the electric field is directed along the X axis (X cut), there will be excited in the plate shear vibrations in the plane of the plate (low-frequency shear vibration) and thickness-shear vibrations (high-frequency shear type vibrations), determined by the piezoelectric moduli d_{14} and d_{16}.

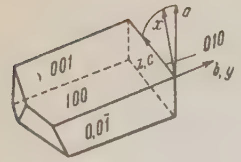

Fig. 4. Designations of cuts as per Standards on Piezoelectric Crystals.[5]

Although, in view of the fact that the coefficient S_{46} is present (i.e., is not zero), there is coupling between the two modes, it can be neglected owing to the great frequency difference between the two modes.

In a YX-cut plate (see second row of the piezoelectric strain coefficient matrix) an electric field will excite longitudinal vibrations along the length and along the width (moduli d_{21} and d_{23}), and shear vibrations in the plane of the plate (d_{25}) and thickness-shear vibrations (d_{22}). There is elastic coupling between all these modes. The longitudinal vibrations along the length produce transverse vibrations and shear vibrations in the XZ plane (S_{13} and S_{15}); the transverse longitudinal vibrations give rise in turn to longitudinal vibrations and shear vibrations in the XZ plane; the shear vibrations produce longitudinal vibrations along the length and width (S_{15} and S_{35}).

Thus, even if only one of the modes were excited by the applied field, all the other modes would develop because of the elastic couplings.

In the case of a Z-cut, as in the case of the X-cut, the external field produces shear vibrations in the plane of the plate (d_{36}) which are not coupled with any other mode.

As noted above, two cuts rotated about the X axis — XZ t_{45° and XZ $t_{37.5^\circ}$ -- are suitable for practical applications. Hence we will pursue the analysis for the specific case of the XZ $t_{37.5^\circ}$ cut.

When the plate is rotated about the X axis, there develop in it, in addition to the shear vibrations mentioned above, longitudinal vibrations along the length and width, which interact with each other.

The interaction between the modes is characterized by the so-called coupling coefficient K, the equation for which can be derived from the equivalent circuit of a crystal vibrating in two modes.

As we know the equivalent electric network of a piezoelectric resonator vibrating in one mode close to resonance is the familiar tank circuit LCCo pictured in Fig. 5, a. When there are several modes of vibration but with no elastic coupling between them (or when the coupling is negligibly weak), the equivalent circuit may be represented in the form shown in Fig. 5, b. The number of LC branches is determined by the piezoelectric strain tensor corresponding to the given direction of the field. The resonant frequencies and the parameters of the equivalent electric network are found by means of the equations appropriate to each type of vibration.

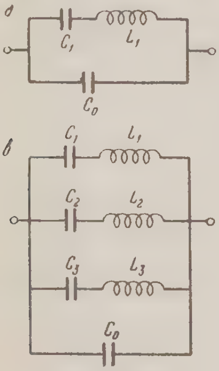

Fig. 5

When there is elastic coupling between the modes, the equivalent network, as Mason[1] has shown, can be represented in the form of two resonance voltage circuits coupled by a capacitance $C_{M.c.}$. The coupling of the two electric circuits through the capacitance is equivalent to the elastic coupling between two mechanical systems (Fig. 6).

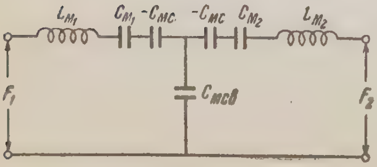

Fig. 6

The expression for the coupling coefficient, taking into account the interaction between the two modes of vibration, is

$$K = \frac{\sqrt{C_{\text{M}_1} C_{\text{M}_2}}}{C_{\text{M.c}}} = \frac{S_{ik}}{\sqrt{S_{ii} S_{kk}}}, \tag{5}$$

where C_{M_1}, C_{M_2} and $C_{\text{M.c}}$ are the capacitances of the equivalent circuit, S_{ii} and S_{kk} are the coefficients of flexibility for the isolated vibrations and S_{ik} is the coefficient for the coupled vibrations.

In our case (XZ $t_{37.5^\circ}$ cut) the expressions for the coupling coefficients are of the form

$$K^2_{\text{l-s}} = \frac{S'^2_{34}}{S'_{33} S'_{44}}, \tag{6}$$

$$K^2_{\text{l-w}} = \frac{S'^2_{32}}{S'_{33} S'_{22}}, \tag{7}$$

$$K^2_{\text{w-s}} = \frac{S'^2_{24}}{S'_{22} S'_{44}}. \tag{8}$$

where the K's in the listed order are the coupling coefficients between the longitudinal vibrations along the length and the shear vibrations, the longitudinal vibrations along the length and transverse longitudinal vibrations and, finally, transverse longitudinal vibrations and the shear vibrations; S'_{ii} and S'_{ik} are the coefficients of flexibility of the plate in longitudinal and shear vibrations of the rotated cut.

These coefficients can be determined for different cut angles in terms of the principal flexibility coefficients S_{33}, S_{32}, S_{22} and S_{44} and the directional cosines by means of the equations given by Cady. (See Ref. 2).

The values of the principal coefficients of flexibility characterizing the Z-cut were determined in the Central Scientific Research Laboratory of Piezotechnology. The values at 20° C are the following

$S_{33} = 2.17 \cdot 10^{-12}$ cm^2/dyne,
$S_{32} = 0.39 \cdot 10^{-12}$ cm^2/dyne,
$S_{44} = 9.74 \cdot 10^{-12}$ cm^2/dyne,
$S_{22} = 3.50 \cdot 10^{-12}$ cm^2/dyne.

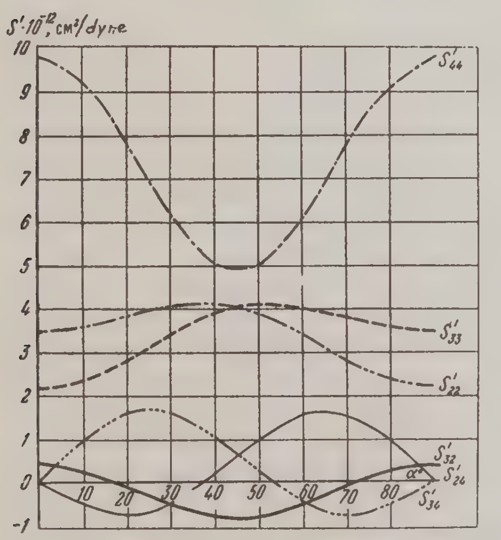

Fig. 7. Coefficients of flexibility of different cuts of potassium tartrate rotated about the X axis; α - angle of rotation from the Y-axis.

The curves showing the variation of the coefficients of flexibility S'_{ik} and S'_{ii} with the angle of rotation about the X axis (from 0 to 90°) are plotted in Fig. 7. It will be seen that the XZ t_{45° and XZ $t_{37.5^\circ}$ cuts used for constructing resonators have flexibility coefficients, coupling the longitudinal vibrations with the shear vibrations (S'_{34}) and the transverse vibrations (S'_{32}) different from zero.

Let us determine which mode of vibration interacts most strongly with the longitudinal vibrations of the XZ $t_{37.5^\circ}$ cut plates. To this end we compare the values of the coupling coefficients as calculated according to equations (6) and (7):

$$K_{\text{l-s}} = 0.274 \text{ and } K_{\text{w-s}} = 0.189.$$

Obviously, the shear vibrations exert a stronger effect on the longitudinal vibrations than do the transverse vibrations.

Let us see how the frequency constant of the longitudinal vibrations changes due to the influence of the shear vibrations. To this end let us compute the resonant frequencies of the longitudinal and shear modes, taking into account the coupling between them (K_{1-s}), by means of the following equations given by Mason:

$$\omega_1^2 = \frac{1}{2}\left[(\omega_{01}^2 + \omega_{02}^2) + \sqrt{(\omega_{01}^2 - \omega_{02}^2) + 4K^2\omega_{01}^2\omega_{02}^2}\right], \qquad (9)$$

$$\omega_2^2 = \frac{1}{2}\left[(\omega_{01}^2 + \omega_{02}^2) - \sqrt{(\omega_{01}^2 - \omega_{02}^2) + 4K^2\omega_{01}^2\omega_{02}^2}\right]. \qquad (10)$$

Here ω_{01} and ω_{02} are the resonant frequencies of the separate isolated vibrations and K is the coupling coefficient.

Equations (9) and (10) can be transformed so as to comprise the parameters determining the frequencies; we obtain

$$f_1^2 = \frac{1}{2}\left[\left(\frac{A^2}{l^2} + \frac{B^2}{b^2}\right) - \sqrt{\left(\frac{A^2}{l^2} - \frac{B^2}{b^2}\right) + 4K^2\frac{A^2B^2}{l^2b^2}}\right], \qquad (11)$$

$$f_2^2 = \frac{1}{2}\left[\left(\frac{A^2}{l^2} + \frac{B^2}{b^2}\right) + \sqrt{\left(\frac{A^2}{l^2} - \frac{B^2}{b^2}\right) + 4K^2\frac{A^2B^2}{l^2b^2}}\right], \qquad (12)$$

where A^2 and B^2 depend on between which modes the coupling is being considered. In our case, for the coupling between the shear and longitudinal modes

$$A^2 = \frac{1}{4S'_{33}(1 - K_{1-s}^2)\rho}, \qquad (13)$$

$$B^2 = \frac{1}{4S'_{44}(1 - K_{1-s}^2)\rho}, \qquad (14)$$

where b is the width and l is the length of the plate.

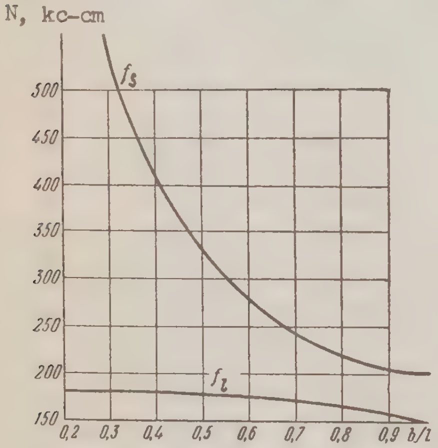

Fig. 8

By varying the ratio b/l from 0.1 to 1 we obtain a series of resonant frequency values. The values of the frequency constant of the longitudinal vibrations for different width/length ratios are shown in Fig. 8, where we have also plotted the corresponding calculated curve for the shear vibrations.

The variation of the frequency constant of the longitudinal vibrations, computed taking into account the influence of the transverse vibrations, with the width-length ratio is shown in Fig. 9.

Actually, of course, all three modes of vibration interact with each other. However, for practical purposes it is sufficient to take into account only the coupling of the longitudinal vibrations with the shear vibrations, inasmuch as this coupling is the strongest. This may be seen from a comparison of the calculated curves with the experimental ones. Fig. 10 shows the frequency spectrum of XZ $t_{37.5^\circ}$ cut plates as a function of the width/length ratio, obtained on the basis of tests. The lower curve C corresponds to the resonant frequency of the longitudinal mode. This curve shows a good fit with the lower curve of Fig. 8, calculated taking into account only the influence of the shear vibrations. The upper curve A corresponds to the resonance curve of the coupled transverse vibrations (longitudinal type along the width) calculated as described above and shown in Fig. 9 (f_w).

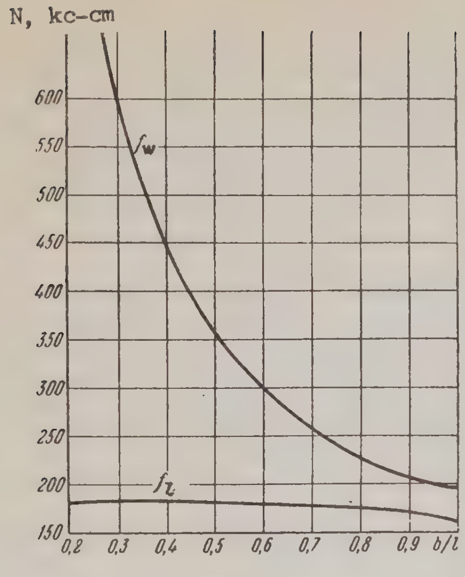

Fig. 9

Curve B pertains to the shear vibrations coupled with the longitudinal vibrations. The right-hand part of this curve is close to the right-hand part of the corresponding theoretical curve (f_s in Fig. 8).

It may be assumed that the left-hand part of the same curve (section D) in Fig. 10 pertains to the flexural vibrations that are coupled with the fundamental longitudinal mode through the shear constant, as in the case of XY-cuts of quartz and YZ cuts of ethylenediamine tartrate crystals (see Figs. 1 and 2, section D). That these are flexural vibrations in the plane of the plates is indicated by the fact that their frequency is directly proportional to the width of the plate (a characteristic feature of this mode of vibration). Vibrations of this type cannot be calculated owing to the lack of a flexibility coefficient corresponding to the flexural vibrations. Mason[1] and Sykes[3] note the similarity of the deformations produced by the even number harmonics of shear modes and the odd number harmonics of the flexural vibrations.

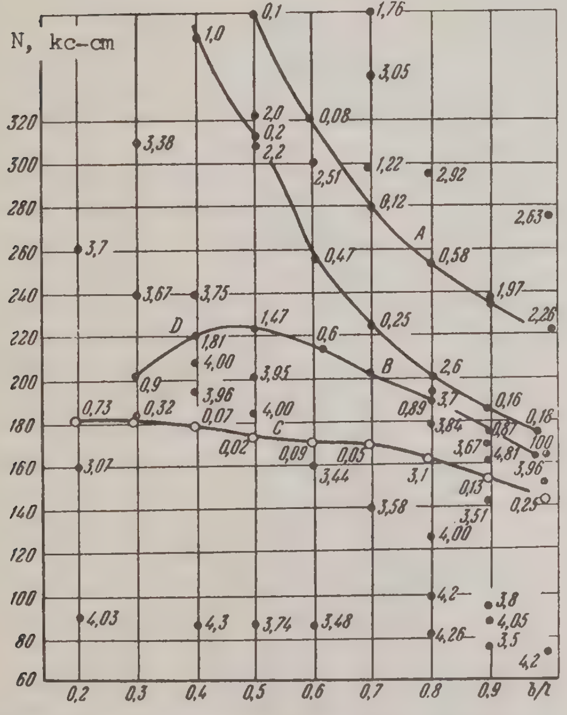

Fig. 10. Frequency spectra of the XZ $t_{37.5^\circ}$ cut of a potassium tartrate crystal as a function of the width/length ratio. N is the frequency constant.

Fig. 10 shows the spectrum of the resonant frequencies recorded by means of rather sensitive measuring equipment for resonators incorporating XZ $t_{37.5^\circ}$ cut potassium tartrate plates having a thickness of 1 mm and different width to length ratios. The relative effectiveness in nepers is indicated by the figures at each resonance point.

For purposes of evaluation we took the maximum effectiveness of resonance to be that corresponding to the minimum attenuation introduced by the resonator into the circuit (equivalent to the minimum resistance of the resonator). Curves were obtained by connecting the points of approximately equal values of the effectiveness. They were drawn through points for relatively high values: 0.1 to 1.5 nepers.

Evaluation of the effectiveness of the parasitic resonances and the shape of the calculated theoretical resonance curves helped resolve some of the complexities of the frequency spectrum of the potassium tartrate plates.

It is obvious that theoretically one can take account of only the stronger parasitic vibrations influencing the fundamental mode, that is, of the shear and flexural vibrations and the transverse vibrations. In addition to these stronger modes, the plates perform many other less effective vibrations, represented in Fig. 10 by the points with values from 3 to 7 nepers. The exact nature of these vibrations has not yet been determined; however, it may be assumed that these are higher order harmonic flexural modes.

There is no mention in the literature of this type of weak parasitic vibrations in quartz and ethylenediamine tartrate crystal resonators. They can scarcely be detected in resonators, but they do become evident in measurement of the attenuation characteristics of filters and do distort the filter characteristic curve when they come within or near the pass band.

4. Methods of Suppressing Parasitic Vibrations

There are several accepted methods of suppressing parasitic vibrations of resonators designed to vibrate in the fundamental longitudinal mode. The method used in any particular case will depend on the causes giving rise to the parasitic vibrations. The most common cause is coupling between the fundamental longitudinal vibrations (along the length) and the space-shear vibrations, which not only have harmonics but are also accompanied by flexural vibrations with their harmonics.

In order to eliminate the parasitic resonances due to elastic couplings, the cut of the crystal must be chosen so that the coefficient of flexibility linking the principal mode with the undesirable parasitic vibrations would be reduced to zero.

Among X-cut quartz plates with different angles of rotation about the X-axis, we found one — the XY $t_{18.5°}$ cut — for which the S'_{24} coefficient coupling the longitudinal vibrations along the length with the space-shear vibrations in the plane of the plate equals zero. This quartz crystal cut is free of parasitic vibrations and has long been used in making resonators for wide-band filters employed in 12- and 24-channel high-frequency telephone networks. This method of eliminating parasitic modes, however, can only be used when the parasite-free cut also has acceptable electric characteristics.

Thus, for example, the XZ $t_{52°}$ cut of potassium tartrate for which the coefficient S'_{34}, coupling the longitudinal vibrations with the low-frequency type space-shear vibrations, is zero (see Fig. 7) cannot be employed because the mean temperature coefficient of resonators incorporating such plates is $50 \cdot 10^{-6}$ degree^{-1} in the 5 to 35°C temperature interval.

The second method of eliminating parasitic resonances consists of selecting the width to length ratio so that the undesirable resonances will be shifted outside the working frequency band. To this end it is expedient to plot the frequency

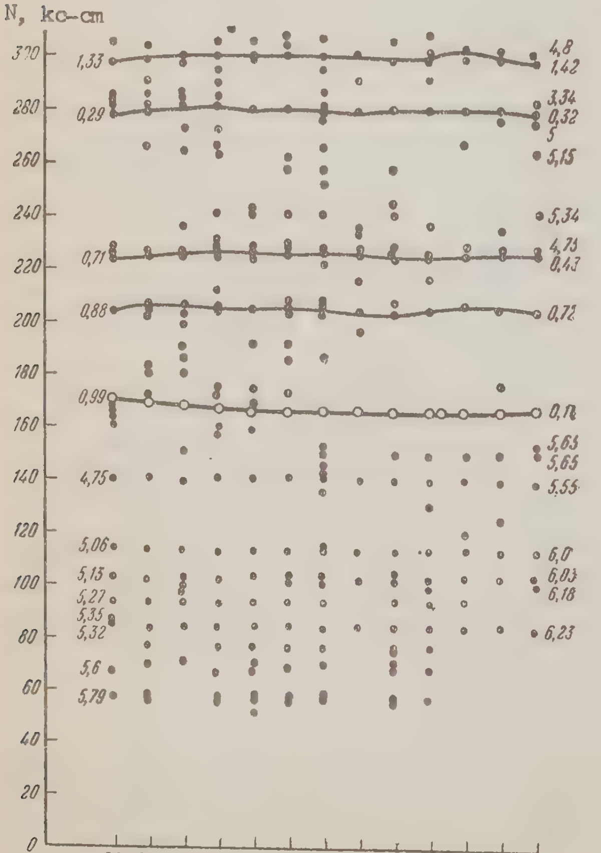

Fig. 11. Frequency spectrum of XZ $t_{37.5°}$ cut plates with different thickness to length ratios.

spectra $f = f(b/l)$ and $f_1 = f'(t/l)$ in order to locate the zones relatively free of parasitic vibrations. This is the only effective procedure in cases when, as in the case of the XZ $t_{37.5}°$ cut of potassium tartrate, the given plate has a number of weak parasitic modes in addition to the strong ones.

The spectrum of potassium tartrate plates having a constant thickness (1 mm) and different width/length ratios was given in Fig. 10. The spectrum of plates of the same cut and a constant width/length ratio of 0.7 as a function of the thickness to length ratio is shown in Fig. 11. The 0.7 width/length ratio was found to be the optimum one as regards freedom from parasitic resonances from an analysis of the spectrum of Fig. 10.

As examination of Fig. 11 shows that there are a few thickness/length ratios at which the parasitic resonances are relatively far removed from the principal frequency (7-8 kc). These are the ratios (0.12, 0.13, 0.14, etc.) that should be tried in designing resonators incorporating XZ $t_{37.5}°$ cut potassium tartrate crystals.

Further studies aimed at determining the causes of the weaker parasitic vibrations are indicated; it is also necessary to investigate the influence of the mounting and supports on the frequency and effectiveness of the different parasitic resonances.

Conclusions

Investigations of the parasitic vibrations of resonators employing potassium tartrate crystals vibrating in a fundamental longitudinal mode (along the length), carried out in the Central Scientific Research Laboratory of Piezotechnology, lead to the following preliminary conclusions:

1. Making use of the tensors of the piezoelectric strain coefficients and the coefficients of flexibility, it is feasible to analyze and identify the coupled vibrations occurring in a given type and cut of piezoelectric plate.
2. In the case of potassium tartrate plates the frequency spectrum of cuts rotated about the X-axis is due to longitudinal vibrations along the length (the fundamental mode) and the following parasitic vibrations, coupled with the fundamental mode and modifying its frequency and the parameters of the plate: low-frequency type shear vibrations (in the plane of the plate), transverse "longitudinal type" vibrations and flexural vibrations.
3. In addition to the above vibrations characterized by an effectiveness close to that of the fundamental mode, such X-cut plates have other weaker parasitic vibrations of low effectiveness. When these weaker vibrations have a frequency in or near the pass band of the filter they can distort the frequency characteristic of the filter incorporating the plate. There is reason to assume that these weaker vibrations are high order harmonics of thickness flexural vibrations.
4. The aforesaid is applicable to the XZ $t_{37.5}°$ and XZ $t_{45}°$ cuts of potassium tartrate crystals now being used in telephone system channel filters.
5. The only practical method of obtaining resonators relatively free of the undesirable parasitic modes is by proportioning the plates, i.e., selecting the optimum width/length and thickness/length ratios on the basis of plots of the frequency spectra $f = f(b/l)$ and $f_1 = f'(t/l)$. In addition, in order to obtain the specified value of the equivalent inductance of the resonator the applied electrodes must be made of a certain specific length.

References

1. W.P.Mason, BSTJ, 13,405 (1934).
2. W.G.Cady, Piezoelectricity (In Russian trans., M. 1949).
3. R.A.Sykes, BSTJ, 23,52 (1944).
4. W.P.Mason, Phys. Rev., 70,705 (1946).
5. Standards on Piezoelectric Crystals, V, 1949, Proc. IRE, 37,1378 (1950).

CONTRIBUTION TO THE THEORY OF A COMPOSITE PIEZOELECTRIC VIBRATOR*

– V.A.Solov'ev and I.G.Mikhailov

Investigation of the mechanical properties of high-polymers requires making measurements in a wide range of frequencies. However, the 10^4-10^5 cps range is virtually unexplored since it is unattainable by the conventional ultrasonic methods used for frequencies above 10^6 cps, on the one hand, and by usual sonic and subsonic procedures, on the other. The only practical method for studying polymers in this frequency band is the resonance method involving the use of a composite piezoelectric oscillator. In this method a bar of the investigated material is cemented to a suitable piezoelectric bar in which the required vibrations (longitudinal, torsional or other) are excited. Then the resonant frequency and the Q-factor of the composite vibrator are determined in an appropriate manner; in practice it is usually most convenient to measure the equivalent electric impedance. This method of exciting and measuring vibrations is very simple and convenient. Where the piezoelectric crystal is of simple geometry (bar or plate) one can easily take into account and allow for its contribution to the parameters of the composite vibrator; this is not true, however, for other variants of the resonance method, particularly at high frequencies. In fact where high-loss polymers and other materials are concerned the usual resonance methods are generally unsuitable in view of the low Q of these materials, for in a composite vibrator the major fraction of the vibrating mass is comprised by the piezocrystal, characterized by a low loss and a high Q.

Below we shall examine the theory of the composite vibrator method and compare the different variants of the method primarily from the point of view of their applicability to investigations of high-polymers.

Let us examine the case of a piezo-crystal bar of length l and cross section S=bd (see accompanying figure). The electrodes are attached to the wide side faces of the bar and there is a potential difference V between them. The potential difference produces an homogeneous field in the bar of intensity

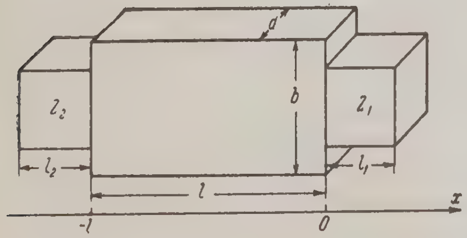

$$\mathrm{E} = \frac{V}{d}\,.$$

We can write the fundamental equations of elastic and piezoelectric theory in the form

$$f = E\frac{\partial u}{\partial x} - e\mathrm{E}\ , \tag{1}$$

$$\mathrm{P} = e\frac{\partial u}{\partial x} + \varkappa\mathrm{E}. \tag{2}$$

where f is the mechanical stress, u is the displacement, $\frac{\partial u}{\partial x}$ is the strain, P is the polarization, E = E' + iE" is the complex modulus of elasticity, $\varkappa$ is the polarizability and e is the piezoelectric coefficient.

We are dealing here with a one-dimensional model, i.e., the case when the deformation can be described by a single component of the displacement , dependent only on the x coordinate. The geometric significance of u, f and the coefficients in (1) and (2) is determined by the type of the vibrator. In some cases, for example, when the bar vibrated in a torsional mode, the electric field is inhomogeneous and has highly complex configuration; in such cases, equations (1) and (2) must be regarded as averaged expressions and the parameters entering into them must be determined experimentally. The one-dimensional model permits of determining the basic properties of the vibrator theoretically, but the theoretical results should be verified experimentally for every specific case. Unfortunately this is not always done in practice.

---

*The present article comprises the main part of the report, "Certain Problems Connected with the Theory of Piezoelectric Transducers". The full report also touches on problems having to do with the emission of ultrasound.

Inasmuch as the field E is independent of x, our wave equation has the usual form

$$\rho \frac{\partial^2 u}{\partial t^2} = E \frac{\partial^2 u}{\partial x^2}, \tag{3}$$

where ρ is the density. The solution with a sinusoidal process of frequency ω is of the form

$$u = (Ae^{-ikx} + Be^{ikx})\, e^{i\omega t}. \tag{4}$$

Here the complex wave number $k = \omega/v - i\alpha = \omega \sqrt{\frac{\rho}{E}}$, where v is the speed of sound and α is the absorption coefficient. In the case of not excessively high losses, $v = \sqrt{E'/\rho}$ and $\alpha = \omega E''/2\rho v^3$.

Let us introduce the specific acoustic impedance of the medium:

$$\mathfrak{z} = R + iX = \sqrt{\rho E} \approx \rho v + iE''/2v \text{ (for } E'' \ll E').$$

The amplitudes A and B must be determined from the boundary conditions at the ends of the bar.

Let our piezoelectric bar be loaded at both ends (at $x = 0$ and $x = -l$) with "test" bars, having total mechanical impedances Z_1 and Z_2. These impedances are determined by the ratio of the forces acting on the end face of the bar to the rate of displacement of the face:

$$Z_1 = \left.\frac{f_1 S_1}{\dot{u}_1}\right|_{x=0} \quad \text{and} \quad Z_2 = \left.\frac{f_2 S_2}{\dot{u}_2}\right|_{x=-l}.$$

We note that in view of the difference in the selected positive directions for f and u, the signs of Z_1 and Z_2 will depend on choice of the positive direction for the x-axis. At equal loads $Z_1 = -Z_2$. The magnitudes of Z_1 and Z_2 will be determined by the acoustic impedances of the attached bars, their cross sections and the boundary conditions at their free ends.

The boundary conditions at the bar interfaces require equality of the displacements u and the stresses f at each point of the contacting surfaces. In the one-dimensional model these conditions have to be averaged over the cross sections of the bars. The only case examined hitherto in the literature is the one when the cross sections of the main bar and the load bars are identical:

$$S = S_1 = S_2.$$

In this case use of the one-dimensional model is more or less justified, although even here experimental verification is indicated. In working on high-polymers we had to use specimen test-bars of smaller cross section ($S_1 < S$). It is doubtful whether one can justifiably use the one-dimensional model for such a vibrator inasmuch as in this case the "interfaces" of the bars are deformed. Actually the one-dimensional approximation is allowable only in the following two cases:

1. The interface is virtually not deformed, i.e., it moves as a rigid piston, so that the total force acting on the surface is transferred from bar to bar. The boundary conditions can then be described by

$$[u - u_1]_{x=0} = 0; \quad [u - u_2]_{x=-l} = 0, \tag{5}$$

$$\left[\left(E\frac{\partial u}{\partial x} - e\mathrm{E}\right)S - Z_1 \dot{u}_1\right]_{x=0} = 0; \quad \left[\left(E\frac{\partial u}{\partial x} - e\mathrm{E}\right)S - Z_2 \dot{u}_2\right]_{x=-l} = 0 \tag{6}$$

(we have equated the mean displacements and the total forces on both sides of the interfaces).

2. The free end face of the bar is deformed in such a manner that the stresses on the contacting surface are virtually unaffected. In this case condition (6) is replaced by the following condition, specifying equality of the average stresses on the contact surfaces:

$$\left[E\,\frac{\partial u}{\partial x} - e\mathrm{E} - \frac{Z_1}{S_1}\,\dot{u}_1\right]_{x=0} = 0; \quad \left[E\,\frac{\partial u}{\partial x} - e\mathrm{E} - \frac{Z_2}{S_2}\,\dot{u}_2\right]_{x=-l} = 0. \tag{7}$$

Both boundary condition variants are, of course, purely theoretical and have not been validated experimentally. However, we attempted to utilize the one-dimensional model for one particular case of a composite vibrator: for the case when both the piezoelectric bar and the investigated high-polymer bar are close to resonance. The interface is then (almost) in the loop of the displacements and in the node of the stresses and deformations, so that the errors introduced by deformations of the surface may be assumed to be small. We carried out a series of tests in which the cross section S_1 of the specimens was varied from 1 S to 0.3 S and found that the results of measurement, within the limits of the scattering of values common to measurements on high-polymers (about 1% as regards the speed of sound and 10-15% as regards absorption) are satisfactorily described by the one-dimensional model with the boundary conditions defined by (5) and (6). The results of these tests are given in Ref. 2. We note that dependable verification was obtained only for longitudinal vibrations. While it would appear that the one-dimensional approximation is also applicable in the case of torsional vibrations (equation (6) is replaced, in this case, by the condition of equality of moments), this still requires further verification.

Some authors have made use of the boundary conditions (5) and (6) without analyzing them, since they based their discussion on the analogy of the composite vibrator with a long line, which is essentially a one-dimensional system. In the investigation of Ref. 3 specimens of small cross section ($S_1 < S$) were employed in studying polymers in a vibrator of a different type (namely, in a symmetric vibrator, see below), when the resonance frequencies of the bars did not coincide. The authors of Ref. 3 do not state whether they checked the independence of their results from the cross section of the specimens. We tried this method on a specimen of polymethyl metacrylate and obtained a negative result: the speed of sound proved to be 7% and the absorption over $1\frac{1}{2}$ times lower than the values obtained in measurements with a sample adjusted exactly in resonance with the piezoelectric crystal (the latter measurements were made with $S_1 = S$ and may, therefore, be regarded as reliable.

Substituting the value of u from (4) and the analogous expressions for u_1 and u_2 in the boundary condition expressions (5) and (6), we find the amplitude of the elongation of the piezoelectric crystal:*

$$s = u(0) - u(-l) = \frac{\varepsilon V}{i\omega} \cdot \frac{-4\mathfrak{z}\,S\sin^2 y/2 + i\,(Z_2 - Z_1)\sin y}{i\,(\mathfrak{z}^2 S^2 - Z_1 Z_2)\sin y + \mathfrak{z}S\,(Z_2 - Z_1)\cos y}, \tag{8}$$

where $\varepsilon = \frac{S}{d}\,e = be$ and $y = kl$. The effective current through the piezocrystal equals

$$I = \frac{d}{dt}\int\limits_{-l}^{0} \frac{D}{4\pi}\,b\,dx = i\omega\,\frac{(1 + 4\pi\varkappa)\,bl}{4\pi d}\,V + \varepsilon \cdot i\omega s, \tag{9}$$

or

$$I = i\omega C_0 V + \varepsilon^2 V\,\frac{-4\mathfrak{z}\,S\sin^2 y/2 + i\,(Z_2 - Z_1)\sin y}{i\,(\mathfrak{z}^2 S^2 - Z_1 Z_2)\sin y + \mathfrak{z}S\,(Z_2 - Z_1)\cos y}, \tag{10}$$

---

*The applicability of the equation derived below to the general case where $S_1 \neq S_2 \neq S$ must be verified experimentally for each particular case.

where C_0 is the capacitance of the contracted (i.e., not vibrating) crystal.

Equation (10) is simplified in the two cases of greatest interest to us: 1) when the piezocrystal is vibrating close to resonance $(y \approx (2N+1)\pi)$, and the loads Z_1 and Z_2 are not excessively great and 2) when the loads are symmetrical $(Z_1 = -Z_2)$. Then

$$I = \left(i\omega C_0 + \frac{4\varepsilon^2}{Z + Z_2 - Z_1}\right)V, \tag{11}$$

where $Z = -2i\mathfrak{z} S \operatorname{ctg} y/2$ is the total mechanical impedance of the non-loaded crystal.

The above derivation of the equations for the vibrations of a bar has commonly been used for deducing the equation for thickness vibrations of a plate (in this case the field is directed along the x-axis and $\varepsilon = e(S/l)$; all the other expressions remain unchanged). As Andreev (see Ref. 4 for details) has shown, however, the thickness vibrations of a plate are essentially different from the vibrations of a bar. In a plate, the induction $D = E + 4\pi P$ must be constant, while E is a function of x. It can be shown, however, that in the cases of interest to us here the final result can be brought to the form of (11) with the same values of the constants. The only difference is that a term $i\frac{4\varepsilon^2}{\omega C_0}$ is added to the mechanical impedance of the vibrator, in consequence of which the resonant frequency of the vibrator is reduced. In the case of quartz for which ε is small this reduction is extremely small; hence the resultant reduction apparently introduced no substantial error into the results of investigations in which a quartz plate was used instead of a bar (see below).

The composite vibrator method has been employed in three principal variants:

1. The piezoelectric crystal loaded on one side, the lengths of the crystal and of the specimen bar chosen arbitrarily.

2. The piezocrystal loaded symmetrically by two specimens of equal but arbitrarily chosen length.

3. The piezocrystal loaded on one side, but the specimen length selected so that its resonant frequency would be approximately equal to the frequency of the piezocrystal.

Variant 1 (Refs. 5 & 6). One-side loading; $-Z_2 = 0$.* Z_1 in the case of a bar free at the other end is described by

$$Z_1 = -i\mathfrak{z}_1 S_1 \operatorname{tg} w, \tag{12}$$

where $w = k_1 l_1$. Substituting in (8), we get

$$i\omega s = \varepsilon V \frac{-2(1/\cos y - 1) - \frac{\mathfrak{z}_1 S_1}{\mathfrak{z} S}\operatorname{tg} w \operatorname{tg} y}{i(\mathfrak{z} S \operatorname{tg} y + \mathfrak{z}_1 S_1 \operatorname{tg} w)}. \tag{13}$$

In the absence of losses $(\mathfrak{z} = R$ and $\mathfrak{z}_1 = R_1)$ is observed at a frequency ω_0 satisfying the following condition

---

* This is not quite true inasmuch as there are always some losses (radiation, at the support points, etc.) which could be taken into account approximately by assigning a value to Z_2 differing from zero. However, these losses can be lumped with the losses due to internal friction in the piezocrystal material. Although this may be questionable in Variant 1, it is certainly admissible in Variants 2 & 3 wherein formula (11) is applicable and the impedances of all the loads are additive.

$$RS \operatorname{tg} y_0 + R_1 S_1 \operatorname{tg} w_0 = 0,$$

where $y_0 = \omega_0 l/v = \pi\omega_0/\omega_k$, and $w_0 = \omega_0 l_1/v_1 = \pi\omega_0/\omega_1$.

Denoting the natural resonant frequencies of the piezocrystal and specimen through ω_k and ω_1, the resonance condition becomes

$$m\omega_k \operatorname{tg} \frac{\omega_0}{\omega_k}\pi + m_1\omega_1 \operatorname{tg} \frac{\omega_0}{\omega_1}\pi = 0, \tag{14}$$

where m and m_1 are the masses of the respective bars. If the losses are not particularly large, the resonant frequency is still approximated by (14). Near this resonance $(n = \omega - \omega_0 \ll \omega_0)$

$$\dot{s} = \varepsilon V \frac{\operatorname{tg}^2 y_0 - 2\,(1/\cos y_0 - 1)}{i\left(\frac{m}{\cos^2 y_0} + \frac{m_1}{\cos^2 w_0}\right)n + XS\left(\frac{y_0}{\cos^2 y_0} - \operatorname{tg} y_0\right) + X_1S_1\left(\frac{w_0}{\cos^2 w_0} + \operatorname{tg} w_0\right)} \tag{15}$$

(in the above we invoked the relationship $i\mathfrak{z}S\,(y - y_0) = imn + y_0XS$). Substituting in (9) we find an expression for the current analogous to the formula for the current flowing at frequencies close to resonance in a network consisting of an rLC series circuit shunted across a capacitance C_0. Through appropriate radio-engineering procedures we can readily determine the resonant frequency ω_0 of the rLC branch (mechanical) and its resistance r at resonance. From similar measurement with the crystal not loaded, we can find ω_k and X and then, making use of (14) and (15), calculate the resonant frequency ω_1 and the loss X_1 in the specimen.

Variant 2 (Refs. 7 & 3). Load: two identical bars of length l_1 and mass m_1 Here

$$Z_2 = -Z_1 = i\mathfrak{z}_1 S_1 \operatorname{tg} w.$$

Since the loading is symmetrical, we can use equation (11). We obtain

$$i\omega s = \frac{4\varepsilon V}{\mathbf{Z_V}} = \frac{4\varepsilon V}{-2i\mathfrak{z}S \operatorname{ctg} y/2 + 2i\mathfrak{z}_1S_1 \operatorname{tg} w}. \tag{16}$$

The resonance condition is

$$RS \operatorname{ctg} \frac{y_0}{2} = R_1S_1 \operatorname{tg} w_0,$$

where $y_0 = \omega_0 l/v = \pi\omega_0/\omega_k$ and $w_0 = \omega_0 l_1/v_1 = \pi\omega_0/2\omega_1$ (ω_1 is the resonant frequency of the entire bar of length $2l_1$).

In the same notation

$$m\omega_k \operatorname{ctg} \frac{\omega_0}{\omega_k}\frac{\pi}{2} = 2m_1\omega_1 \operatorname{tg} \frac{\omega_0}{\omega_1}\frac{\pi}{2}. \tag{17}$$

Near resonance the mechanical impedance of the entire vibrator is

$$\mathbf{Z_V} = i\left(\frac{m}{\sin^2 y_0/2} + \frac{2m_1}{\cos^2 w_0}\right)n + \left(\frac{y_0}{\sin^2 y_0/2} + \operatorname{ctg} y_0/2\right)XS + 2\left(\frac{w_0}{\cos^2 w_0} - \operatorname{tg} w_0\right)X_1S_1. \tag{18}$$

Further calculations are carried out with the aid of the equivalent network.

This variant has been used primarily for obtaining low frequencies by means of a thin piezoelectric plate. The specimen ("load") bars in this case are of comparatively great length $l_1 \gg l$, and from (17) we have

$$\omega_0 = \frac{\omega_1}{1 + 2m_1\omega_1^2 / m\omega_k^2} \tag{19}$$

(an approximation applicable when $2m_1\omega_1^2 / m\omega_k^2 \ll 1$).

For the mechanical impedance of the vibrator we have

$$Z_V = \frac{4}{\pi^2}\left(\frac{\omega_k}{\omega_0}\right)^2 \left\{ i\left(m + \frac{m^2\omega_k^2}{4m_1^2\omega_1^2}2m_1\right)n + \pi\left(\frac{\omega_1}{\omega_k}XS + \frac{m^2\omega_k^2}{4m_1^2\omega_1^2}\cdot 2X_1S_1\right)\right\}. \tag{20}$$

In the investigation described in Ref. 3, a vibrator of this type ("resonance stack") was utilized in turn for studying high-loss materials. The "stack" was loaded with two additional symmetrical specimens, the impedances of which were

$$Z_4 = -Z_3 = i\mathfrak{z}_3S_3 \operatorname{tg} k_3l_3.$$

In this case, instead of (12), we have

$$Z_1 = -i\mathfrak{z}_1S_1 \operatorname{tg} w \frac{\mathfrak{z}_1S_1 + iZ_3 \operatorname{ctg} w}{\mathfrak{z}_1S_1 - iZ_3 \operatorname{tg} w}. \tag{21}$$

This expression is substituted in (11). The behavior of the vibrator near resonance is characterized by the same equivalent network, but the actual calculations are very complicated.

Variant 3. Length of the specimen is selected beforehand so that the resonant frequencies of the crystal bar and sample will be nearly (within 5-10%) identical. Then

$$y_0 \approx (2N+1)\pi \quad \text{and} \quad w_0 \approx N_1\pi \quad (N, N_1 = 0, 1, 2, \ldots),$$

and the mechanical impedance of the vibrator

$$Z_V = i(m + m_1)n + (2N+1)\pi XS + N_1\pi X_1S_1, \tag{22}$$

where n is the detuning with respect to the resonant frequency ω_0 of the entire vibrator

$$\omega_0 = \frac{\omega_k m + \omega_1 m_1}{m + m_1}. \tag{23}$$

These equations can be derived as a particular case of (14) and (15), but it is easier to substitute expression (22) directly in (11). The formulas for the parameters of the equivalent network in this case are so simple that it is worthwhile giving them here:

$$L = \frac{m}{8\varepsilon^2}, \quad C = \frac{1}{\omega_0^2 L} \quad \text{and} \quad r = \frac{(2N+1)\pi XS + N_1\pi X_1S}{4\varepsilon^2}. \tag{24}$$

Most of the investigators, working by the resonance method, have used the third version (see Refs. 8-12 and the bibliography in Ref. 1). We have also utilized this variant and consider it to be the most convenient for the following reasons.

In the first variant the nodal plane of the vibrations of the vibrator does not coincide with the nodal plane of the piezocrystal; in consequence of this the clamping points have to be changed for each test. This is not only onerous but also may give rise to errors. The second and third variants are free of this shortcoming. The equations involved in the first and second variants are complicated. As regards accuracy of the final results, the third method is superior, for the quantity measured in this case is essentially the small difference between the frequencies of the piezocrystal and the specimen.

In investigating materials characterized by high losses (polymers) it is important for the composite vibrator to have as high a Q-factor as possible. When the piezocrystal and sample bars are of approximately the same size the Q proves to be highest in the third variant. The Q in the first and second variants can be enhanced by using bars considerably shorter than a quarter wavelength. However, it is difficult to take advantage of this in the case of polymers since with longitudinal vibrations the length of the sample becomes comparable to the transverse dimensions and the modes of vibration become very complex. In the case of torsional vibrations Kornfel'd[6] worked with very short specimens.

The possibility of obtaining low frequencies without recourse to very long (and expensive) piezocrystal bars is one of the great advantages of the second variant. However, in a "resonance stack" the mechanical and equivalent electrical impedances are increased in the ratio of $\frac{4}{\pi^2}\left(\frac{\omega_k}{\omega_0}\right)^2$ compared to the values for an all piezoelectric crystal bar (it must be noted, however, that this is partially compensated for by the higher value of the dielectric constant for the plate). This higher impedance makes measurements more difficult. Where the circuitry and equipment for measuring such high impedances accurately are available, the "resonance stack" may prove very convenient. In particular, it can be used to advantage instead of an ordinary piezocrystal for studying polymers.[3] When a "stack" is used, it is best to use samples whose resonant frequency coincides with that of the "stack". In this case equation (21) reduces to

$$Z_1 = -i\mathfrak{z}_1 S_1 \operatorname{tg} w_0 + Z_3/\cos^2 w_0, \tag{25}$$

i.e., Z_3 becomes an additive term in (16) and the calculations become as simple and straightforward as in Variant 3.

Lastly, as was noted above, in working with polymers it proved necessary to use specimens of small cross section ($S_1 < S$) in order to increase Q of the vibrator and enhance the ratio between the longitudinal and transverse dimensions. By using such specimens we were able to investigate polymers with a very high loss (X_1 of the order of 10^4 g sec^{-1} cm^{-2}) and a low speed of sound (to 300 m/sec). We have shown above that any substantial improvement of the method, particularly extension of the limits of its applicability, is apparently feasible only for the third variant.

Some investigators who have used the third variant (see Ref. 10, for example) assert that in this variant the influence of the cement joining the sample to the piezocrystal is minimal, owing to the fact that in this case the cement (joint) is located in a node. This is erroneous. Analysis of the applicable equations shows the effect of a very thin layer of cement is virtually independent of where it is located along the length of the vibrator. The cement in all cases lowers the frequency of the vibrator by an amount proportional to its mass (if anything the reduction in the case of the third variant is somewhat greater) and has no influence on the attenuation.

"A.A.Zhdanov" Leningrad State University

References

1. W.G.Cady, Piezoelectricity (in Russian trans) M. 1949.
2. I.G.Mikhailov & V.A.Soloviev, Akust. zhur. (Acoustic Journ.)1,343 (1955).
3. N.S.Ageeva, I.P.Zhukov, M.A.Isakovich, A.L.Sosedova, Iu.M.Sukharevski, Zhur. tekh. fiz., 22, 1029 (1952).
4. N.N.Andreev, Trydy Vsesoiuznogo zaochnogo energeticheskogo in-ta (Transaction of the All-Union Power Engineering Correspondence Inst) No. 1,5 (1951).
5. S.L.Quimby, Phys. Rev., 25, 558 (1925).

6. M.O.Kornfel'd, Zhur. eksp. i teor. fiz., 13, 116 (1943); Doklady AN SSSR, 38, 312 (1943).
7. S.L.Quimby, Phys. Rev., 39, 345 (1932).
8. J.Zacharias, Phys. Rev., 44, 116 (1933).
9. L.Balamuth, Phys. Rev., 45, 715 (1934).
10. S.Siegel & S.L.Quimby, Phys. Rev., 49, 663 (1936).
11. J.S.Rinehart, Appl. Phys., 12, 811 (1941).
12. S.V.Subrahmanyam, J. Chem. Phys., 22, 1562 (1954).

PIEZOELECTRIC RESONATORS WITH CRYSTALS HAVING DEFECTS IN STRUCTURE

- M.I.Iaroslavski

At present only defect-free crystals (or, more accurately speaking, crystals or parts of crystals not containing any visible inhomogeneities) are used for cutting crystal bars and plates for resonators. However, all or almost all natural crystals contain greater or smaller regions of inhomogeneous structure. Twins, cracks, gas-liquid inclusions and other flaws can generally be found in any crystal. Hence the size of the "perfect" part of a natural crystal which can be used for piezo-elements is usually small compared to the total volume of the crystal.

Very often the sizes of the individual structural defects are small compared with the dimensions of the fabricated element. It is natural to assume in such cases that the defects will not affect the properties of the resonator as an electronic component. This assumption has been put forward and checked by a number of investigators.[1-4] However, for the most part these have been qualitative experiments, in the sense that specific plates with some particular defect have been tested in a particular oscillator or filter circuit, the investigators contenting themselves with determining whether the given construction met the applicable technical specifications. With this approach, the problem must be solved anew for each specific type of circuit, if not for every defective crystal plate.

To determine the possibility of using crystals with different specific inhomogeneities in any oscillator or filter circuits one must investigate the influence of such defects on independent parameters of quartz resonators, i.e., parameters related to quantities independent of the circuit in which these parameters are measured.

Such parameters are the equivalent "dynamic" capacitance C_q, the equivalent inductance L_q and the equivalent resistance R_q as well as the "static" capacitance of the crystal and crystal holder C_o (the parameters of the familiar electric circuit equivalent to a piezoelectric resonator - Fig. 1).

In addition, the requirement formulated above is satisfied by the "operating" parameters of a quartz resonator introduced by Kamenski[5], the static capacitance of a crystal and crystal holder C_o and the "quality" of the resonator $\varkappa$.* The latter is given by the equation

$$\varkappa = \frac{1000}{R_q \cdot f^2 \cdot F(C_0)},$$

where R_q is the equivalent resistance of the resonator, $F(C_o)$ is a function dependent on the magnitude of C_o and the parameters of the oscillator in which $\varkappa$ is measured, and f is the frequency at which the crystal is excited in the oscillator. The "quality" $\varkappa$, measured in kilo-ohms, is directly proportional to the activity of the

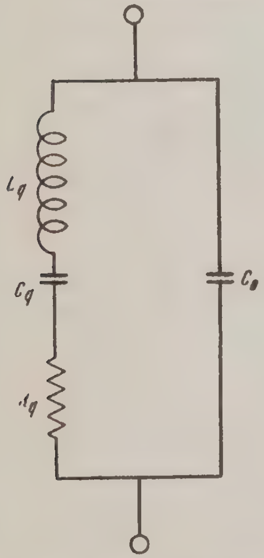

Fig. 1. Equivalent circuit of a piezoelectric resonator: R - equivalent resistance, L_q-equivalent inductance, C_q-equivalent "dynamic" capacitance and C_o-static capacitance of crystal and crystal holder.

---

*The third "operating" parameter - the frequency φ of a standard oscillator stabilized by the investigated crystal, does not enter into the present discussion.

For definitions of these "operating" parameters see article by Kamenski in the present issue of the Bulletin. Translator.

Table 1. Test data on quartz resonators with X-cut bars for 200 kc

Characteristics of crystals	R_q, Ohms	C_q, $\mu\mu f$	Q^{*}_{equ}	Temp. coef. of frequency (20–50°), x 10^{-6}
Reference resonators with crystals of defect-free quartz (10)	350–750	0.0102–0.0122	92,800–194,100	–0.6 – +0.8
With gas-liquid inclusions (10)	350–650	0.0105–0.0124 (0.0156 in one)	92,800–250,000	–0.7 – +0.6
With solid inclusions(6)	350–750 (2200 in one^h)	0.0111–0.0123	91,000–194,500 (11,000 in one^h)	–0.8 – +0.3
With cracks (16)	550–4500	0.0100–0.0128	13,400–128,400	–3.5 – +0.05
With twins and gnarls	450^b–1100	0.0111^b–0.0500	14,450–102500^b	–0.8 – +0.05

*Equivalent Q. h) bar with inclusions of hematite crystals up to 2 mm in section. b) with Brazilian twins.

Table 2. Test data on quartz resonators with AT-cut plates for 500 kc

Characteristics of crystals	R_q, Ohms	C_q, $\mu\mu f$	Q_{equ}	Temp. coef. (20–50°)	Activity,** ma
Reference resonators with defect-free quartz crystals (11)	90–380 (900 in one)	0.0183–0.0302	76,000–116,500	$0-2\cdot10^{-6}$ $(6.6\cdot10^{-6})$*	3.0–5.6
With gas-liquid inclusions (6)	100–160	0.0282–0.0300	106,000–153,000	$(0.6-2)\cdot10^{-6}$ $(5\cdot10^{-6})$* & $(5\cdot10^{-5})$*	4.8–5.5 5.2
With rutile inclusion (1)	85	0.0310	120,500	$0.66\cdot10^{-6}$	
With Brazilian twins (1)	450	0.0270	26,200	$2.6\cdot10^{-6}$*	3.4
With Dauphine twins (5)	Vibrations not excited				
With crack (1)					

---

*Values obtained for one specimen in each case; no attempt was made to grind the side faces in order to reduce the temperature coefficient.

**Activity = grid current (in ma) in Pierce oscillator employing a 6C2C tube.

Table 3. Test data on quartz resonators with BT-cut plates for 5 Mc

Characteristics of crystal	$\varkappa$("quality" of the plate), kilo-ohms	R_q, Ohms	Temp. coef. (20-90°)	Activity, (cf.Table 2) ma	No. passing serviceability test (-60 to +80°)
Reference, standard resonators with defect-free quartz(10)	4.5-6.7	11.6-16.5	$(2.2-3.7)\cdot 10^{-6}$	0.8-1.2	8 resonators
With gas-liquid inclusions (26 resonators)	Group I (15) 5.1-8.6 Group II (11) 3.8 & under	Group I 9.0-14.7 Group II 38.8 & over	$(0.1-1.9)\cdot 10^{-6}$ in 9 of the group $(2.2-6.3)\cdot 10^{-6}$ in 9 of Gps. I & II (8 not measured)	Group I 0.9-1.2 Group II 0.8 & under	14 resonators of Group I
With "azure rays" (14)	5.4-8.0	6.9-10.7	$(0.7-1.5)\cdot 10^{-6}$; $3.35\cdot 10^{-6}$ in one	Over 1 ma	Not tested
With carbonate flake inclusions(6)	5.3-7.6; 4.4 in one	8.1-14.1	$(0.7-1.4)\cdot 10^{-6}$	Over 0.9; 0.5 in one	Not tested
With Dauphiné twins and gnarls (11)	1.95-3.4 in 3; 6.2-7.3 in 3; could not be measured in 5	Under 16.2 in 4 and over 26 in 7	$1.8\cdot 10^{-6}$ in one; over $2.6\cdot 10^{-6}$ in other ten	Over 0.9 in 4; under 0.6 in 7	2 resonators

crystal in oscillator circuits.

We measured the above listed parameters in 139 oscillator-type crystals; these included 48 vacuum resonators designed for a frequency of 200 kc with X-cut bars (vibrating in flexure in the second harmonic), 67 resonators having frequencies of about 5Mc with BT-cut quartz plates and 24 resonators having a frequency of 500 kc with AT-cut plates. Ten plates of each type were prepared of defect-free quartz.

The same standard resonator circuit was employed in all cases. No special measures were taken to increase the activity, decrease the temperature coefficient or otherwise alter the characteristics of the plates with defects. It proved unnecessary to make any special calculations of the frequency of these plates. For the most part the "defective" crystals in the test resonators contained gas-liquid and solid (pyrite, hematite, gersdorffite and rutile) inclusions. A certain number of resonators were made with crystals containing "gnarls" and Dauphiné twins.

The tests were made by comparing the parameters of resonators with single-crystal plates with the parameters of resonators incorporating the crystals having the different defects in structure.

In addition to the values of the equivalent and "operating" parameters (the "operating" parameters were measured only for the 5000 kc resonators), we also determined the temperature coefficient of frequency and the activity of each crystal in a Pierce circuit. Further, we carried out serviceability tests in the -60° to +90° temperature range on some of the resonators in typical oscillator circuits.

The results of the tests and measurements are listed in Tables 1, 2 & 3.

The following conclusions may be drawn from the test data:

1. In the case of crystal bars of the X-cut (5° and -18.5°) group, intended for frequencies up to 200 kc, the presence of an appreciable accumulation of gas-liquid and small solid inclusions (hematite, pyrite, gersdorffite and rutile crystals not exceeding 0.2-0.3 mm in cross section) has no discernible effect on the parameters of the resonator.

2. As a rule the parameters of such bars are adversely affected by the presence of even fine cracks, Dauphiné twins and "gnarls".

3. Similarly the defects enumerated under 1 above do not affect the parameters of resonators with AT-cut plates (thickness-shear vibrations), at least at frequencies from 500 kc. What has been said above under 2 applies equally to these plates.

4. Inclusions begin to have an adverse effect on the parameters of high-frequency plates having thicknesses on the order of 0.3-0.4 mm or less.

We did not test any 5000 kc resonators with crystals containing inclusions of such minerals as pyrite, hematite, gersdorffite and rutile. Inclusions of such minerals in quartz plates under 0.5 mm thick must undoubtedly have a highly adverse effect on the resonator parameters. It was noted, however, that fine flakes (apparently carbonates) scattered throughout the crystal do not have a harmful effect on the properties of the resonator (Table 3).

The effect of gas-liquid inclusions in plates of resonators operating in the 5000 kc frequency band differs, depending on the size of the inclusions and on the section of the plate wherein they occur. The quality of the plates is most severely affected when accumulations of large (relative to the plate thickness) inclusions are concentrated near the center of the plate. Virtually no deterioration of the resonator parameters was observed in cases where small gas-liquid inclusions were located at or near the corners of the plate.

5. Although in some cases plates with Dauphiné twins may show satisfactory characteristics as far as the values of equivalent and "operating" parameters are concerned the temperature coefficients of such crystals are appreciably

Fig. 2

Fig. 3

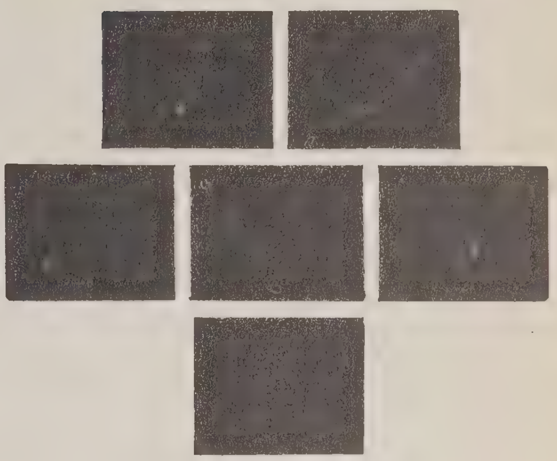

Fig. 4

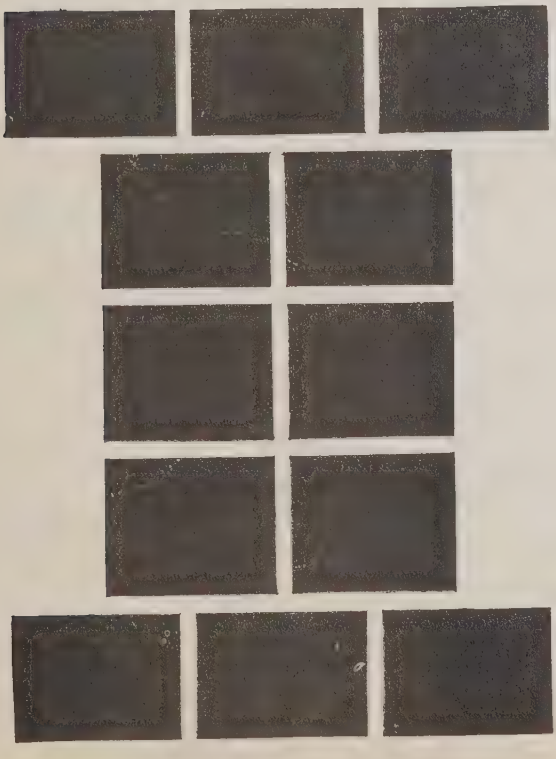

Fig. 5

Sketches of quartz plates with different defects:

Fig. 2. AT cut for 500 kc with gas-liquid inclusions.

Fig. 3. AT cut for 500 kc with Brazilian twin.

Fig. 4. BT cut for 5 Mc resonator; the parameters of these plates were appreciably impaired by the accumulations of gas-liquid inclusions near the center.

Fig. 5. BT cut plates for 5 Mc resonators the parameters of which are in no way inferior to those of defect-free plates.

Number 3 Volume 20 1955

BULLETIN

of the

Academy of Sciences of the USSR

- Physical Series -

(Izvestiia Akademii Nauk SSSR)
(Seriia fizicheskaia)

Reproduction rights reserved

by

Columbia Technical Translations
5 Vermont Avenue
White Plains, New York

Single Issues

$20

Annual Subscription

$215

Transactions of the Fifth All-Union Conference on Nuclear Spectroscopy

FORBIDDEN β-SPECTRA OF Rb^{86}, Sr^{90}, Y^{90} and Tl^{204}

- E.E.Berlovich, D.M.Khai and A.V.Savateev

In solving the problem of β-interaction, i.e., in determining experimentally which form of interaction (scalar, vector, tensor, axial-vector or pseudoscalar) or linear combination thereof is applicable in a given case, an important part is played by elucidation of the shape of the forbidden β-spectra. Such investigations are also of interest in connection with study of the nuclear shell model.

In the present work we studied the shape of the forbidden spectra of Rb^{86}, Sr^{90}, Y^{90} and Tl^{204}. All these nuclei have an even mass number and for them the transitions to the ground state of the daughter nucleus occur between even-even and odd-odd nuclei (or vice versa). According to the nuclear shell model,[1] even-even nuclei must be assigned spin 0 and even parity. The characteristics of odd-odd nuclei cannot be determined as unambiguously by means of the shell model. However, in many cases the configurations of the odd-odd nuclei involved in the investigated transitions are characterized by a spin value of 2 and odd parity. For such transitions the shell model predicts a unique shape of the β-spectrum, corresponding, according to the Gamow-Teller selection rules, to a first forbidden transition ($\Delta J = 2$, yes). According to the theory of forbidden β-spectra,[2] the "uniqueness" of their shape stems from the fact that only one matrix element - associated with axial-vector and tensor interactions of the nucleons with the electron-neutrino field - is involved. These transitions are characterized by a large value of log ft (about 8-9).

The investigations were carried out on the high transmission wedge-type spectrometer with improved focusing described earlier.[3] A distinctive feature of the experimental procedure was the use of a scintillation counter as the β-particle detector. As will be shown below, the problem of determining correctly the shape of the β-particle energy distribution by means of such a detector involves certain experimental difficulties. However, replacement of the conventional gas-discharge counter by a scintillation counter is desirable in a number of cases; for example, in separating the partial β-spectra by the method of coincidences,[4] since the short luminescence time of the phosphor makes it possible to reduce the resolving time of the coincidence circuit. Although the coincidence method was not actually utilized in the experiments described below, development of the scintillation detector was essential in connection with the general research program of our laboratory.

I. Experimental Procedure

1. Spectrometer

In view of the particular importance attached to correct rendition of the shape of the β-spectra, the large angles of our high-transmission spectrometer[3] were reduced somewhat by installing additional diaphragms (baffles) in the path of the beam in the source, deflection and counter chambers in order to minimize possible scattering of the electrons from the chamber walls. The transmission factor of the modified spectrometer was 0.6%. The resolution, as determined by the width at half-height of internal conversion lines, was 1.6% (the F line in the spectrum of active thorium, corresponding to the 238 kev γ-rays, and the line of Ba^{137} corresponding to 661 kev γ-rays.

2. Detector

A. Crystal and light conductor. A brass diaphragm, 3 mm thick with a 6 mm

pulses recorded on the potential on the FEU-19 at a given electron energy has the form of a rising curve which flattens in the region of saturation and then again begins to rise sharply. The initial rise in the curve is connected with increasing recording efficiency. The sharp rise after the plateau is probably connected with non-linear distortions (cut-off and differentiating) in the amplifier in the case of high pulses. It proved necessary to investigate the count vs potential curves over a wide range of voltages for different electron energies and to establish the minimum value of the voltage at which saturation is attained for the entire electron energy range in question.

The voltage supply unit for the photomultiplier was assembled of BSG-70 dry cells. The potential was monitored and regulated by means of a suitable compensating circuit.

F. Fatigue of the photomultiplier. With light pulses above a certain intensity incident on the FEU-19, beginning with only a few tens of thousands of pulses per minute, the counting rate falls off for several minutes and reaches a stable value only after ten or more minutes. This effect is connected with the familiar fatigue of the last dynodes (where the currents are greatest); it is due to the reduction of the secondary emission coefficient which results in a decrease of the height of the output pulses. Where the crystal is irradiated by radiation of constant intensity, the effect, even though it may be appreciable in absolute magnitude (see Ref. 5 for example), can be obviated as far as the experimental results are concerned by starting measurements after a sufficient lapse of time, i.e., after the stable counting rate is attained.

However, in β-spectrum work the intensity of irradiation of the crystal varies from point to point and hence the effect of fatigue can distort the shape of the soft part of the spectrum; the pulse amplitudes may be reduced below the response threshold of the recording circuit.

With a view to obviating the fatigue effect we reduced the potential on the last dynodes, thereby reducing the currents in these stages. A typical voltage divider employed in the experiments had the following resistance ratios:

$$\frac{r_1}{r_4 - r_{12}} = 3{,}5; \quad \frac{r_2}{r_4 - r_{12}} = 3{,}2; \quad \frac{r_3}{r_4 - r_{12}} = 0{,}2; \quad \frac{r_{13} - r_{15}}{r_4 - r_{12}} = 0{,}7.$$

G. Cooling of the photomultiplier. In order to provide for the possibility of radically reducing the dark current background we developed a system of refrigeration for the FEU-19.

The arrangement consisted of a special copper collar (with a slit for the leads) with phosphor bronze liners that fitted over the tube envelope. A 20 mm diameter copper rod was screwed into a threaded bushing soldered to the copper collar; the rod passed freely through the magnetic shields and its other end was immersed in a Dewar containing liquid nitrogen. The collar was held by means of an asbestos gasket in a thick cylinder of Plexiglas bolted to a flange on the inner iron shielding cylinder. Except for the part immersed in the liquid nitrogen, the entire length of the copper rod was wrapped in asbestos cord. The temperature of the photocathode must be maintained above the solidification point of oil. To prevent condensation on the tube socket, the socket section of the photomultiplier was surrounded by a heavy copper ring conducting heat from the shielding cylinders. The background of some individual FEU-19 photomultipliers was reduced by a factor of several tens by the described method of cooling.

However, refrigeration was not employed in experiments described below.

3. Certain properties of the recording installation

In view of the importance of eliminating all effects which might distort the experimental shape of the β-spectra we investigated the influence of bremsstrahlung and Čerenkov radiation on the scintillation counter.

coordinates are shown in Fig. 2. It will be seen that the shape of the hard component clearly corresponds to a forbidden transition and is well rectified by means of an α-type correction factor. For small values of Z this factor is given approximately by[2]

$$\alpha = p^2 + q^2 = (E^2 - 1) + (E_0 - E)^2, \tag{1}$$

where and q are respectively the electron and neutrino momenta, E is the electron energy and E_0 is the total energy of the β-decay in m_0c^2.

This factor corresponds to a first forbidden β-transition with a total angular momentum change of two units and a change in parity.

The end-point energy of the hard component as determined from the rectified Fermi plot is 1785 ± 20 kev. This gives a value of log ft = 8.40.

The forbidden shape of this spectrum was first noted by Zaffarano, Kern and Mitchell[7] while the fact that it belongs to spectra of the α-type (unique) was established by Muether and Ridgway[8] and confirmed by Dmitriev and Zarubin[9] in an investigation carried on the Ketron.

Our results as regards the shape of this spectrum and its end-point energy are in agreement with the data of the last two investigations (Refs. 8 and 9). The end point of the soft component, separated by subtracting the rectified and extrapolated hard component from the total spectrum was found to be 715 ± 25 kev.

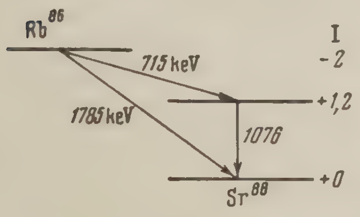

Fig. 1. Decay scheme of Rb^{86}.

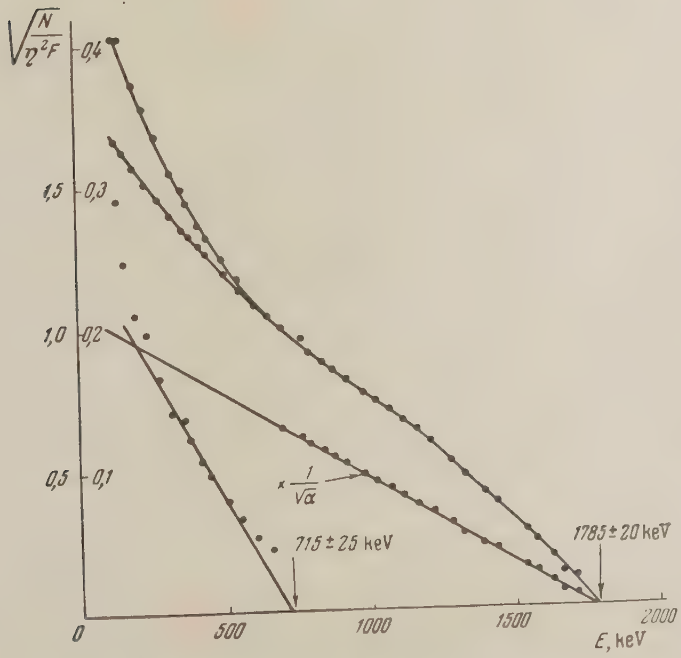

Fig. 2. Kurie plot of the β-spectrum of Rb^{86}.

As follows from the measurements of Ref. 5, the half-life of the excited state of Sr^{86} must be under 10^{-10} sec. From a comparison of this value with the theoretical curves of Moszkowsky[10] it may be concluded that the γ-radiation in the transition to the ground state must be either M1, which corresponds to a one-unit change in spin, or E2, in which case the spin change equals 2. The parity in both cases remains unchanged.

In the scheme shown in Fig. 1 we indicate the possible spins and parities of all three levels involved in the $Rb^{86} \rightarrow Sr^{86}$ transition, following from the unique shape of the hard β-spectrum (ΔJ = 2, yes) and the experimental evaluation of the lifetime of the excited state of Sr^{86}.

It may be noted, too, that the initial points of the soft component of the β-spectrum in Fig. 2 rise above the straight line, in conformity with the results of earlier investigations. Dmitriev and Zarubin, who investigatec this section of the spectrum in greate detail than the other authors mentione suggest as one possible explanation o this deviation the existence in the spectrum of Rb^{86} of a third component having an end-point energy of 230-250 kev.

In connection with this it must noted, however, that the Rb^{86} sources commonly used contain some impurities which can distort the results to some extent. In the region of low energie one can readily observe a very intens β-spectrum with an end-point energy o about 160-170 kev. The fact that it

Harmful bremsstrahlung can develop as the result of the radiation loss of electrons slowed down in the brass diaphragm located at the focus of the instrument near the crystal. In order to evaluate the magnitude of the effect we mounted brass plates 3 and 1.5 mm thick in front of the 6 mm slit in the diaphragm and observed the pure count due to bremsstrahlung radiation originating in these plates due to 950 and 1450 kev electrons (the background, measured separately with a thick aluminum absorber intercepting the beam, was subtracted to obtain the pure count). The results of these measurements are listed in Table 1.

Table 1

Electron energy, Kev	Thickness of plate, mm	Number of pulses per minute in % of the number of electrons
950	3	0,30
950	1,5	0,35
1450	3	0,51
1450	1,5	0,98

Thus bremsstrahlung originating in a 1.5 mm thick brass plate due to 1450 kev electrons yields a count of about 1% relative to the total number of electrons. During actual measurements, of course, there is no matter in the region of the slit and the bremsstrahlung can arise only in the material of the diaphragm itself (3 mm thick). In view of the fact that in this case the conditions for recording bremsstrahlung are less favorable (the matter of the diaphragm is not immediately in front of the crystal), the actual effect of the diaphragm will be less than the values indicated in the table for the 3 mm thick plate: we evaluated it to be about 0.2-0.3% relative to the number of incident 1450 kev electrons. In studying the spectra in the region of very high energies the brass diaphragm can be covered with a layer of Plexiglas.

Čerenkov radiation can arise in the Plexiglas lining of the chamber and in the Plexiglas sheets covering the diaphragms and can penetrate through the small openings in the foil covering the crystal and the front face of the light conductor. However, direct tests for detection of Čerenkov radiation with the crystal and foil removed, i.e., with the electrons incident directly on the light conductor, showed that the effect of this radiation is negligibly small even when the potential of the trigger is set appreciably closer to the self-excitation threshold than in the normal experimental conditions employed.

II. Results of Measurements

1. Spectrum of Rb^{86}

The decay scheme of Rb^{86}, established by Zaffarano, Kern and Mitchell[7] and confirmed by other investigators[8,9], is shown in Fig. 1. There can be no doubt regarding the existence of two components: a hard one associated with transitions to the ground level of Sr^{86} and a soft component connected with transitions to the excited 1.081 kev level of Sr^{86}. Dmitriev and Zarubin[9] discuss the possible existence of yet a third component with an energy of approximately 230-250 kev in view of the break in the Fermi plot for the soft (711 kev) component; there is some evidence pointing to the existence of this third component in the measurements of Refs. 7 and 8.

In the present investigation we were interested primarily in the hard component which, according to the data of Refs. 8 and 9, has a unique shape. In elaborating the decay scheme we also utilized the results of our measurements of the lifetime of the excited state of Sr^{86} (Ref. 5).

The source used in the present experiments consisted of a 15 x 2 mm strip of aluminum foil having a superficial density of 1.3 mg/cm^2 with a coating of neutron-irradiated RbCl. The thickness of the active material, which was applied by evaporation from an aqueous solution, did not exceed 0.2 mg/cm^2. The foil strip with the source was attached to two transverse strips of aluminum foil held in an aluminum holder, mounted in an appropriate position in the spectrometer.

The results of the Rb^{86} β-spectrum measurements plotted in the usual Fermi

is due to impurities is evident from the change in its relative intensity with time.

Moreover, rubidium compounds often contain admixtures of cesium, the only stable isotope of which, Cs^{133}, has a large cross section for activation by slow neutrons, yielding the β- and γ-emitter Cs^{134}. In the investigations of Refs. 7 and 8 the Rb sample was purified in an ion exchange column.

To check for the presence of cesium impurities we studied the γ-radiation from old rubidium samples, stored for over half a year and hence virtually free of 19-day Rb^{86}.

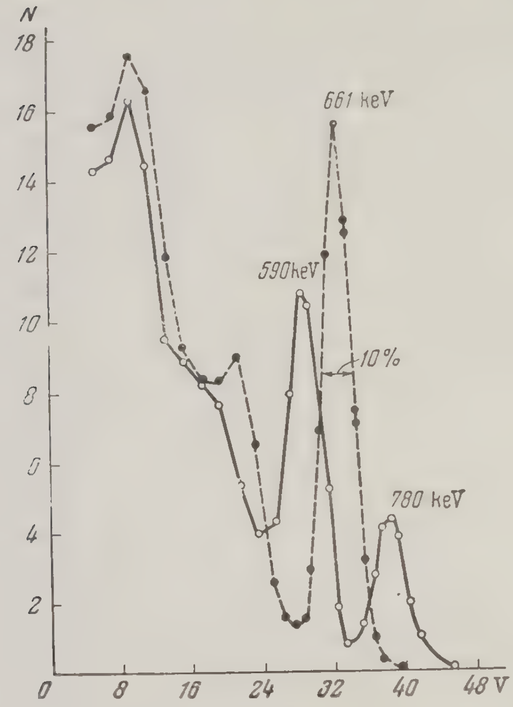

Fig. 3. Gamma-line spectrum of old sample of rubidium source. Dash-line - 661 kev reference γ-line of Cs^{137}. Solid line - γ-line of impurities in rubidium sample.

Fig. 3 shows the spectrum (solid line) obtained for one of these old samples by means of a scintillation γ-spectrometer with an NaI(Tl) crystal and a 12-stage "Dzaliuzi" ("Jalousie") type photomultiplier developed by G.S.Vil'grube. This photomultiplier yields good resolution of the γ-lines and has linear characteristics over a wide range of energies and voltages. The energies of the photopeaks were determined with reference to the peak of the 661 kev γ-line of Cs^{137} shown by the dash-line in Fig. 3 and were found to be 590 and 780 kev. Apparently the first peak corresponds to the unresolved 570 and 605 kev γ-lines and the second to the 797 kev γ-line of Cs^{134}. The 1081 kev line associated with Rb^{86} is, of course, not present in this spectrum.

An admixture of Cs^{134} can obviously distort the 710 kev component of the β-spectrum of Rb^{86} inasmuch as the more intense component of its β-spectrum has a close end-point energy (657 kev).

In principle the 6% component of the β-spectrum of Cs^{134} with end-point energy 210 kev can be the cause of the curvature observed in the soft region of the β-spectrum of Rb^{86}. In practice the apparent distortion will depend on the amount of active Cs^{134} present. We note, however, that a certain deviation was also observed in the investigations of Refs. 7 and 8 in which the Rb^{86} sources were carefully purified. Hence the question of the existence of the third component in the β-spectrum of Rb^{86} is still open.

2. Spectra of Sr^{90} and Y^{90}

The radioactive isotope Sr^{90} with a half-life of 19.9 years is one of the members of the radioactive chain beginning with Br^{90}, that is produced by the bombardment of U^{235} with slow neutrons. Sr^{90} is separated chemically from the disintegration products together with Sr^{89} ($T = 54.5$ days). After decay of the latter, Sr^{90} can be obtained together with its daughter Y^{90} which is formed in the ground state. Y^{90} with a half-life of 2.54 days decays to the stable nucleus Zr^{90} in the ground state.

The nuclear shell model[1] predicts the exact values of the spins and parities of all three nuclei. Both the even-even nuclei, Sr^{90} and Zr^{90}, have a total angular momentum of zero and even parity.

The odd-odd nucleus Y^{90} contains 39 protons and 51 neutrons; the configuration

is $p_{1/2}$ for protons and $d_{5/2}$ for neutrons. Consequently, the spin of this nucleus in the ground state equals two (inasmuch as the spins of the odd proton and odd neutron which belong to differend Schmidt groups are subtracted[1]) and the parity is odd.

Thus, both the $Sr^{90} \rightarrow Y^{90}$ and $Y^{90} \rightarrow Zr^{90}$ transitions are first forbidden transitions with a change of spin of two units and change of parity; both β-spectra should have the unique α-type shape.

However, the first investigations of Sr^{90} and Y^{90} showed no significant deviation of that β-spectrum from the shape given by the Fermi equation. Meyerhof[11] in his investigation used a 180° type spectrometer with a resolution of 3% and sources about 1 mg/cm^2 thick in which the Sr^{90} and Y^{90} were in secular equilibrium. He obtained a straight line Kurie plot with end-point energies of 0.61 and 2.3 Mev for Sr^{90} and Y^{90} respectively.

Jensen and Laslett[12] measured the β-spectra of these isotopes on a lens spectrometer using both a combined $Sr^{90} + Y^{90}$ source and Sr^{90} enriched sources; they obtained curved Kurie plots which were satisfactorily rectified by the α correction factor. In this investigation particular attention was given to the quality of the source and accurate determination of the corrections for scattering in the counter window; the investigators used the exact expression for the Coulomb function. The reported end-point energies are 0.53 and 2.23 Mev for Sr^{90} and Y^{90} respectively.

Braden, Slack and Shull[13] used both a mixed $Sr^{90} + Y^{90}$ source and separated sources. The sources were prepared by evaporation from solution on to a thin Zapon film. The samples were aged to permit the 55-day activity of Sr^{89} to die out. The measurements were made on a double-focusing spectrometer with a resolution of 1%. The end-points of the Sr^{90} and Y^{90} spectra determined from the Kurie plots, which were satisfactorily rectified by the α correction factor, were 0.53 and 2.24 Mev, respectively.

Langer and Price[14], investigating the β-spectrum of a preparation containing the mixture of Sr^{89} and 10% $Y^{90} + Sr^{90}$, rectified the hard part of the spectrum by means of the α-factor and determined the end-point of the Y^{90} spectrum, obtaining a value of 2.18 Mev. The purpose of this study was investigation of the β-spectrum of Sr^{89} (1.463 Mev) and the end-point of the Y^{90} spectrum.

Laslett, Jensen and Paskin[15] found that a more satisfactory rectification of the Sr^{90} and Y^{90} spectra is obtained by using the more precise form of the α correction factor. They give end-point values of 0.54 and 2.24 Mev.

Lastly, Moreau and Iorba[16] separated Y^{90} from a mixture of Sr^{90} and Y^{90} for the purpose of measuring the Y^{90} spectrum. The end-point value obtained from the Kurie plot (not shown in the report) rectified by the α-factor proved to be 2.270 Mev.

Thus the β-spectra of Sr^{90} and Y^{90} have been studied by many investigators which is not surprising since studies of these spectra began immediately after discovery of unique α-type spectra by Langer and Price[17] in their investigation of Y^{91}.

Nevertheless, in almost all the experimental curves one can find some deviation of the experimental points from the straight lines obtained after making the α-factor correction. The most satisfactory fit to a straight line is obtained in the measurements of Laslett, Jensen and Paskin[15].

In our measurements we used samples of Sr^{90} with a very high specific activity separated from the uranium disintegration produce and cooled for a sufficient time to insure a Sr^{89} content under 1%.

The source material was applied in the form of an ultra-thin layer to a strip of aluminum foil 1 μ thick (0.27 mg/cm^2). As in all the experiments described in the present report good conductivity between the foil strips forming the support and the aluminum holder was insured by application of aquadag at all contact points.

The activity of the samples was such that with the transmission factor of the spectroscope it was possible to obtain a very high statistical accuracy (average 0.5%) at each experimental point in a relatively short time. The number of experi-

mental points was appreciably greater than in previous investigations.

The results of our measurements for Sr^{90} and Y^{90} are shown in Kurie coordinates in Fig. 4, where the entire energy region above 540 kev pertains to Y^{90}. The lower curve was obtained as a result of introducing the α correction. As may be seen the points fall well on a straight line. The small upward deviation in the soft region of the Y^{90} spectrum may be explained by the presence of a minor amount of Sr^{89}, the spectrum of which has a peak in this region. The end-point of the Y^{90} spectrum is at 2280 ± kev.

Fig. 5 shows the spectrum of Sr^{90} obtained by subtraction of the Y^{90} spectrum (determined by extrapolation of the rectified Kurie plot into the soft region) from the common Sr^{90} + Y^{90} spectrum. The forbidden shape of the Sr^{90} spectrum and the satisfactory rectification of the plot by the α-factor correction are evident.

The results of spectroscopic investigations of Sr^{90} and Y^{90} obtained by different authors are summarized in Table 2.

The values of log ft for the $Sr^{90} \rightarrow Y^{90}$ and $Y^{90} \rightarrow Zr^{90}$ transitions are 9.80 and 8.02 respectively. In evaluating the first of these account was taken of the factor $2J_f + {}^1/_2 J_i + 1$, since in this case the total spin of the daughter nucleus is greater than the spin of the parent nucleus.

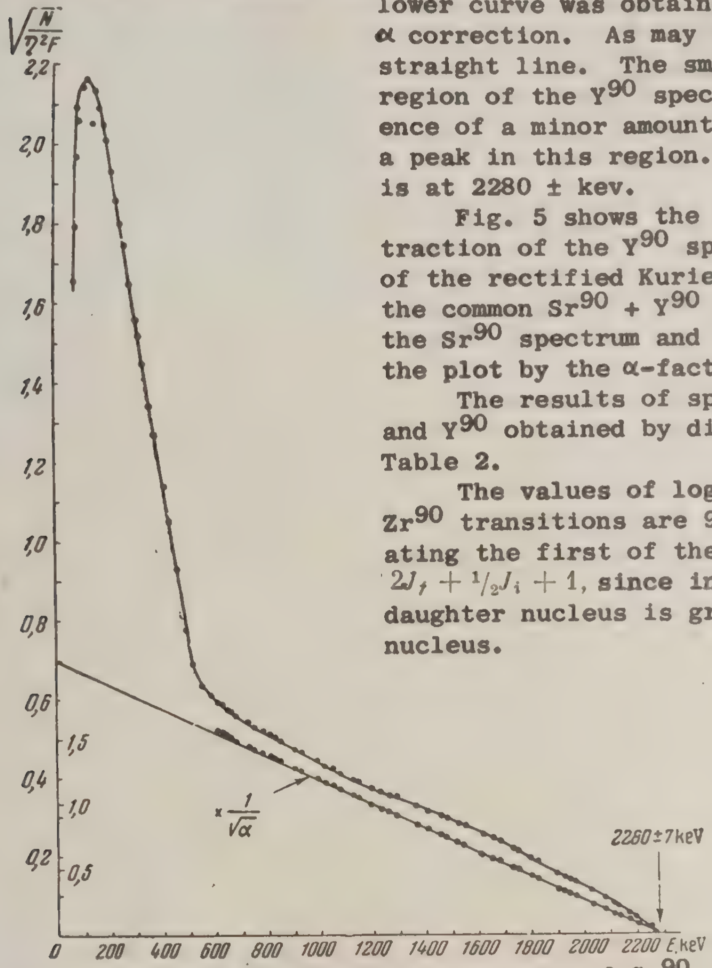

Fig. 4. Kurie plot for the β-spectrum of Sr^{90} + Y^{90}.

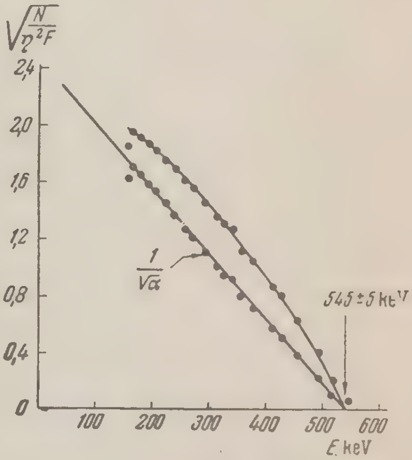

Fig. 5. Kurie plot for the β-spectrum of Sr^{90}.

Table 2

Investigators and reference number	Year	Sr^{90} End-point, kev	Sr^{90} Shape	Y^{90} End-point, kev	Y^{90} Shape
Nedzel (18)	1944	-	-	2200	-
Bothe (19)	1946	-	-	2100	-
Meyerhof (11)	1948	610 ± 10	Allowed	2350 ± 30	Allowed
Jensen & Laslett (12)	1949	537	α-type	2230	α-type
Braden, Slack & Shull (13)	1949	531	α-type	2250	α-type
Langer & Price (14)	1949	-	-	2180 ± 7	α-type
Laslett, Jensen & Paskin (15)	1950	540	α-type	2240	α-type
Moreau & Iorba (16)	1952	-	-	2270 ± 20	α-type
Our data	1954	545 ± 5	α-type	2270 ± 7	α-type

3. Spectrum of Tl^{204}

Examination of the emission of Tl^{204} is of particular interest: a) the numbers of protons and neutrons in this nucleus are close to the magic numbers 82 and 126 and consequently both the proton and neutron shells are nearly filled; according to the predictions of the shell model,[1] at high orbital momentum quantum numbers, the pairing effect should be particularly strong and lead to the appearance of small values of angular momentum instead of the large values that might normally be expected; b) there is great divergence between the results of different investigations (including the most recent ones); this divergence is largely due to experimental difficulties in measuring the relatively soft β-spectrum of nuclei with a large Z.

Saxon and Richards[20] investigated the shape of the β-spectrum of Tl^{204}. These investigators used samples that had been cooled for two years, chemically purified and converted to thallium chloride. The resultant Kurie plot departed from a straight line. Correction for the 2% spectrometer resolution did not substantially change the shape of the spectrum while introduction of the α-correction factor rectified only the hard portion of the spectrum; below about 350 kev there remained an appreciable deviation upwards. Agreement between the results obtained with sources of two different thicknesses lead these authors to conclude that the electron excess in the soft part of the spectrum is not due to scattering in the source and that the rise cannot be attricuted to a soft partial β-component in view of the absence of the difference γ-ray, established by Fajans and Voight[21]. The authors feel that it is not impossible that the $Tl^{204} \rightarrow Pb^{204}$ is a second forbidden transition ($\Delta J = 2$, no; scalar and axial vector interactions).

Lidofsky, Macklin and Wu[22] investigated the spectrum of Tl^{204} in a solenoid spectrometer using both chemically deposited and vacuum evaporated sources. The spectra obtained with the chemically deposited source could not be rectified by either the approximate or by the exact α-factor. The spectrum of the thin evaporated source yielded a straight line down to about 150 kev after introduction of the exact α correction factor.

These authors also investigated the γ-radiation and found a ~70 kev line which they identified by the method of critical absorbers as x-ray radiation of Hg. This indicated the presence of a K-capture branch evaluation of which lead to the value of $N_K/N_\beta \approx 2\text{-}3\%$.

Mateosian and Smith[23] investigated the radiation of Tl^{204} by introducing radioactive thallium into a NaI crystal together with non-active thallium, used as the activator, and measuring the pulse height spectrum with a photomultiplier. Correcting by means of the exact α-factor, they obtained a straight line Kurie plot down to ~150 kev in agreement with the results of Lidofsky, Macklin and Wu[22].

Juasa, Laberrigue-Frolow & Feuvrais[24] used a lens spectrometer with a resolution of 3% to investigate the β-spectrum from sources obtained by evaporation of $TlCl_3$ and having superficial densities of 160, 100 and 10 μg/cm^2; their counter had a window transparent to electrons of energy >2.5 kev. Introduction of the exact α-correction yielded a straight line Kurie plot to ~170 kev. In addition, these authors investigated the spectrum of Auger electrons, which together with x-rays, accompany K-capture in Tl^{204}.

Knight, Braid and Richardson[25] used a spectrometer with a resolution of 3% and thin sources (the effective thickness of the thinnest source taking into account the orientation of the source relative to the particle trajectories in the spectrometer was 100 μg/cm^2. In contrast to the results of Refs. 22-24, after introduction of the exact α-correction, these investigators obtained a small systematic deviation at energies below 400 kev. However, in view of the smallness of the electron excess (under 5%) the authors leave the reality of the deviation open to question.

In our experiments we used sources prepared by electrolytic deposition on aluminum foil (1.3 mg/cm^2) as well as by vacuum evaporation. The thickness of the

active deposits amounted to about 100-120 μg/cm^2. Examination of the electrolytically deposited sources under a binocular microscope failed to disclose any noticeable inhomogeneities. Fig. 4 shows the conventional Kurie plot (upper curve) obtained for this source and the plot (lower curve) obtained after introduction of the exact α-correction factor:

$$\alpha = (E_0 - E)^2 + A(Z, E)\,[E^2 - 1]. \quad (2)$$

The values of the function A(Z,E) were taken from Davidson[26].

The straight line section of the curve intercepts the horizontal axis at 765 ± 5 kev.

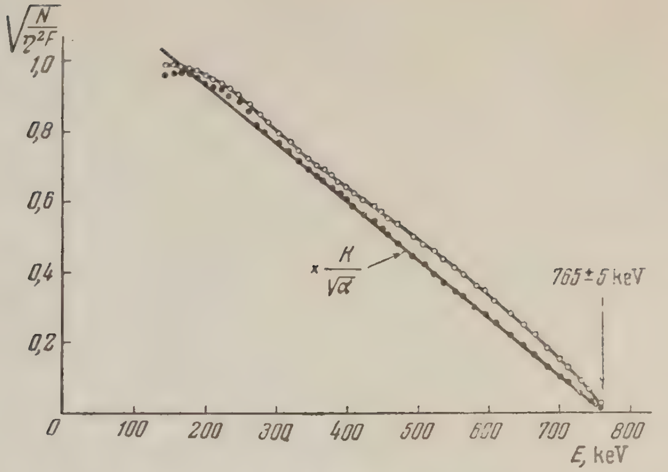

Fig. 6. Kurie plot for β-spectrum of Tl^{204}

It will be seen that the points fall noticeably above the straight line at energies under 320 kev. A similar but smaller upward deviation of the points in the same energy region was observed for the source prepared by evaporation under vacuum. Control experiments with sources 200-400 mg/cm^2 thick gave no noticeable change in the shape of the plots. The fact that the effect persisted for thinner and more homogeneous sources is evidence that the deviation is presumably not connected with scattering. Introduction of corrections for screening in accordance with the equations of Ref. 27 resulted in an enhancement of the divergence.

Summarizing of the results of all investigations of the β-spectrum of Tl^{204}, we can safely state that in virtually all cases we observed a departure from the unique α-type shape. In our investigations of Refs. 20 and 25 and in our study this departure is manifest at energies under 350 kev (or even 400 kev in Ref. 25), while in investigations of Refs. 22-24 the deviation is apparent below 150-170 kev.

The absence of γ-rays of noticeable intensity (established in Refs. 21 and 22) precludes explaining the break in the β-spectrum by the presence of a soft component associated with transitions to an excited level of Pb^{204}, although such a level at about 374 kev is manifest in K-capture by the Bi^{204} nucleus.[28]

Smith[29], analyzing the measurements of Saxon and Richards[20], showed that the observed shape of the spectrum is consistent with the assumption of a second forbidden transition with a spin change of two and no change of parity (T, S, V and A interactions). This is not impossible in view of the large value of $\log ft$ (9.6 according to Saxon and Richards). However, it does lead to a parity assignment for the ground state of the odd-odd Tl^{204} nucleus that is in conflict with the predictions of shell model theory.

It may be noted that both alternatives correspond to a small value of spin for Tl^{204} and are in line with the predictions of the shell model regarding the filling in pairs of nuclear shells at large values of l : neither the odd proton nor the odd neutron appear in the shells with large values of l ($h_{11/2}$ for protons and $i_{13/2}$).

We investigated the electromagnetic radiation from Tl^{204} by means of a scintillation spectrometer. The resultant curve obtained with an absorber filtering out the β-rays is shown by the solid line in Fig. 7. The dash-dot line in the figure is the record of the electromagnetic radiation from an Hg^{203} source made for calibration purposes. The first line (peak) of the spectrum represents x-rays from the Tl^{203} atom (the energy of the K$_\alpha$ line is 73 kev). The spectral

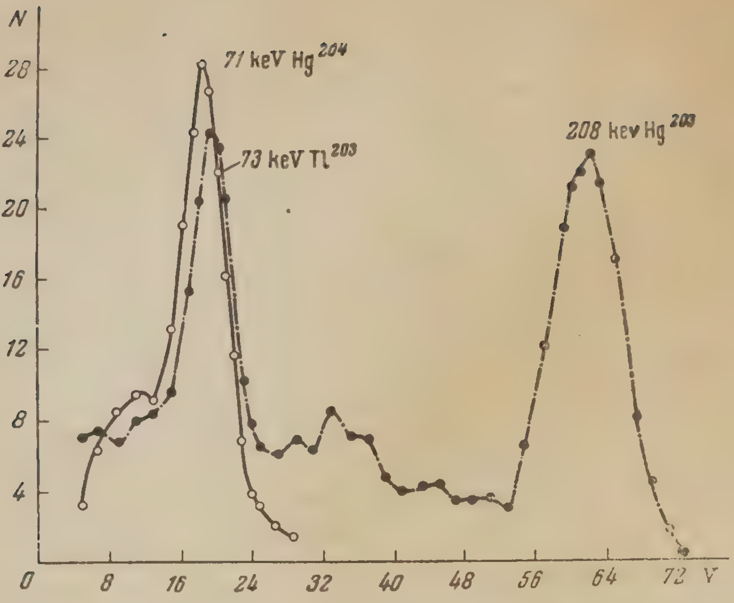

Fig. 7. Electromagnetic radiation spectrum of Tl^{204}. Dash-dot line - calibration line of Hg^{203}; the x-ray line of the Tl^{203} atom and the gamma line of the Tl^{203} nucleus. Solid line - x-ray line of the Hg^{204} atom.

Table 3

Investigation	Year	End-point energy, kev	Deviation from α-type shape, kev	K/β, %
Ref. 20	1949	783±10	Below 350	—
Ref. 22	1952	765	Below 150	2–3
Ref. 23	1952	765±10	Below 150	1,5±0,5
Ref. 24	1954	765±10	Below 170	4±1 6±2
Ref. 25	1954	766±1	Below 400	—
Our data	1955	765±5	Below 320	5,0±0,5

line of the Tl^{204} source is slightly displaced to the side of lower energies and represents the x-ray radiation of Hg^{204} forming as a result of K-capture (K_α line energy 71 kev).

We measured the intensity of the K-capture branch in the spectrum of Tl^{204}. To this end we compared the number of pulses produced in a cesium iodide crystal by β- and γ-rays under identical geometric conditions. In these measurements the response threshold of the electronic circuit was set at the lower limit. The efficiency of the crystal as regards recording of x-rays was computed on the basis of the known geometric conditions, the absorption coefficient being determined from the data of Ref. 30.

Our measurements showed that the intensity of the K-capture branch amounts to 5.0 ± 0.5% per β-particle.

The results of spectrometric investigations of Tl^{204} are summarized in Table 3.

Note added in proof. In a recent communication Juasa et al[31] report deviation (after all corrections) of the Kurie plot of Tl^{204} from a straight line at energies under ~ 400 kev.

Leningrad Physical-Technical Institute of the Academy of Sciences of the USSR.

References

1. M.Mayer, Phys. Rev., 78, 16 (1950); Phys. Rev., 78, 22 (1950); M.Mayer, S.Moszkowsky & L.Nordheim, Rev. Mod. Phys., 23, 315 (1951); L.Nordheim, Rev. Mod. Phys., 23, 322 (1951).
2. E.Greuling, Phys. Rev., 61, 568 (1942); E.Konopinski & G.Uhlenbeck, Phys. Rev., 60, 308 (1941); R.Marshak, Phys. Rev., 61, 431 (1942).
3. E.Berlovich, Izv. AN SSSR, Ser. fiz., 18, 589 (1954). (Trans. in Bulletin Vol. 18, No. 5, p. 274).
4. E.Berlovich, Izv. AN SSSR, Ser. fiz., 16, 314 (1952).
5. E.Berlovich, Izv. AN SSSR, Ser. fiz., 19, 343 (1955). (Trans. in Bulletin Vol. 19, No. 3, p. 305).
6. T.Livshitz, Usp. fiz. nauk., 50, 365 (1953).
7. D.Zaffarano, B.Kern & A.Mitchell, Phys. Rev., 74, 682 (1948).
8. H.Muether & S.Ridgeway, Phys. Rev., 80, 750 (1950).
9. A.Dmitriev & P.Zarubin, Izv. AN SSSR, Ser. fiz., 18, 580 (1954). (Trans. in Bulletin, Vol. 18, No. 5, p. 264).
10. S.Moszkowsky, Phys. Rev., 83, 1071 (1951).
11. W.Meyerhof, Phys. Rev., 74, 621 (1948).
12. E.Jensen & L.Laslett, Phys. Rev., 75, 1949 (1949).
13. C.Braden, L.Slack & F.Shull, Phys. Rev., 75, 1964 (1949).
14. L.Langer & H.Price, Phys. Rev. 76, 641 (1949).
15. L.Laslett, E.Jensen & A.Paskin, Phys. Rev., 79, 412 (1950).
16. J.Moreau & J.Iorba, C.R., 235, 38 (1952).
17. L.Langer & H.Price, Phys. Rev., 75, 1109 (1949).
18. V.Nedzel, Rev. Mod. Phys., 18, 513 (1946).
19. W.Bothe, ZS. f. Natur. 1,179 (1946).
20. D.Saxon & I.Richards, Phys. Rev., 76, 982 (1949).
21. K.Fajans & A.Voight, Phys. Rev., 60, 619 (1941).
22. Z.Lidofsky, P.Macklin & C.Wu, Phys. Rev., 87, 391 (1952).
23. E.Mateosian & A.Smith, Phys. Rev., 88, 1186 (1952).
24. T.Juasa, J.Laberrigue-Frolow & L.Feuvrais, C.R., 238, 1500 (1954).
25. J.Knight, T.Braid & H.Richardson, Proc. Phys. Soc., Sec. A., 67, 881 (1954).
26. J.Davidson, Phys. Rev., 82, 48 (1951).
27. J.Reitz, Phys. Rev., 77, 10 (1951).
28. M.Goldhaber & R.Hill, Rev. Mod. Phys., 24, 179 (1952).
29. A.Smith, Phil. Mag., 43, 915 (1952).
30. C.Davisson & R.Evans, Rev. Mod. Phys., 24, 79 (1952).
31. T.Juasa, J.Laberrigue-Frolow & L.Feuvrais, J.Phys. et rad., 16, 1, 39 (1955).

RADIATION OF Sb^{124}

- A.V.Zolotavin, E.P.Grigor'ev & M.A.Abroian

The radioactive isotope Sb^{124} ($T = 60$ days) was discovered in 1937.[1] Since then it has been the subject of almost fifty investigations. Five components, associated with first forbidden transitions, have been distinguished in the β-spectrum,[2-4] while the γ-spectrum comprises at least ten separate γ-lines.[2-9] According to a number of investigators[10-13] the spin and parity of the first excited level of Te^{124} are 2+. However, such questions as the composition, relative intensity and multipole order of the γ-transitions and the nature of the β-transitions still require further elucidation. Investigation of the radiation of Sb^{124} is also of interest in view of the fact that the first excited level of Te^{124} is classed as a so-called collective level.[14,15]

1. Procedure and conditions of measurement

We investigated the radiation of Sb^{124} on a double-focussing β-spectrometer having a central ray radius of 14 cm and a solid angle equal to 0.65% of 4π.[9] The magnetic field distribution in this spectrometer provides for precise focussing of the plane electron beam.[16] In the plane of symmetry the magnetic field is described by[9,17]

$$H(\rho) = H_0 \frac{1}{\rho}\left[1 + \frac{1}{2}(\rho - 1) - \frac{3}{8}(\rho - 1)^2 + \frac{3}{16}(\rho - 1)^3 - \frac{15}{256}(\rho - 1)^4 - \frac{3}{512}(\rho - 1)^5 + \cdots\right]^*,$$

where ρ is the distance from the axis of the field in equilibrium orbit units.

The receiving slit of the spectrometer is curved in conformity with the shape of the source image. The relative "instrument" line half-width is 0.42% with a 1 mm wide source. In the investigation of the β-spectrum of antimony, the relative half-width of the lines varied between 0.37 and 0.60%, depending on the width of the source and slit, while in the photoelectron observations, it varied between 0.6 and 1.2%, depending on the width and thickness of the target.

In order to insure an unambiguous relationship between the current in the magnet windings and the magnetic field between the polepieces we utilized the initial magnetization curve for reference and calibration purposes; to this end the magnet was demagnetized in accordance with a standard procedure prior to each series of measurements. The intensity of the residual field between the polepieces did not exceed 0.05 oersted; the field was monitored by means of a suitable coil located in the spectrometer on the extension of the equilibrium orbit (central ray) - see Fig. 1.

With this method of calibration and control of the spectrometer field the relative shift in the positions of the conversion lines, studied in different series of measurements and with different sources, did not exceed 0.10%. The calibration curve of the spectrometer was established by observing the A, B, Bb, E, F, G, H, I, J, L, M, P, X (K and L) conversion lines and the principal Auger electron lines of Th(B + C + C' + C"), the 609, 1120, 1416 and 1766 kev lines of RaC and the 661 kev line of Cs^{137}.

In our spectrometer, with a strong field in the instrument, low-energy electrons, moving along an epitrochoidal spiral in the inhomogeneous field, can enter the detector.[9] In order to "push back" the beginning of the entry of such electrons into the region of energies above 2 Mev special diaphragms oriented at small angles to the focal planes were installed in the spectrometer. (D in Fig. 1). In investigating spectra with end-point energies ⩾ 2 Mev it was necessary to take additional measures to obviate such penetration of the undesirable Compton electrons (see under Section 2 below).

---

*In equation (3) given in Refs. 9 & 17 the factor in front of the term $(\rho - 1)^3$ should be 1/8 rather than 3/16.

The collodion film window over the counter chamber passed electrons having energies from 5-10 kev. Recording of coincidences started with 15-20 kev. The background of the first counter was 10-12 pulses per min; the coincidence background was 3-4 pulses per min and was independent of the magnetic field intensity. The source was thoroughly grounded in all experiments.

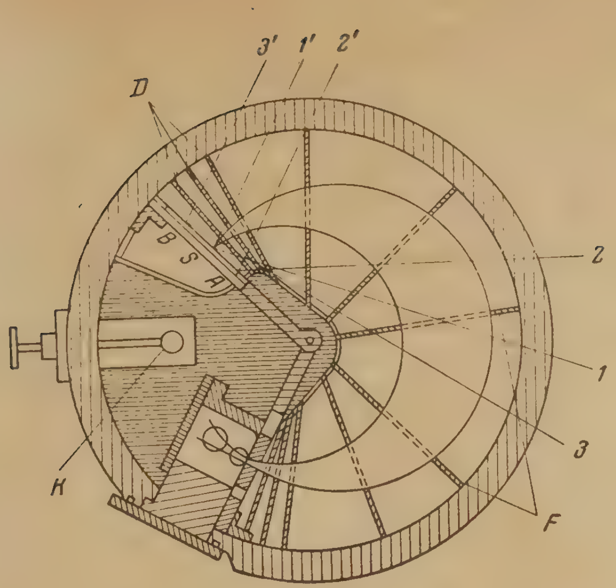

Fig. 1. Diagram of β-spectrometer: F) diaphragms (baffles) defining the beam, D) diaphragms limiting the penetration of low-energy electrons into the counter with strong fields in the spectrometer, S) position of source at focus, A & B) extreme side positions of source (recoil electrons can reach the counter from the regions defined by the angles 1S1', 2A2' and 3B3'), K) field measuring coil.

2. β-spectrum of Sb^{124}

In investigating the β-spectrum of Sb^{124} we utilized a number of different sources with superficial densities ranging from 5 to 500 $\mu g/cm^2$ prepared on supports of collodion and aluminum 50 to 1500 $\mu g/cm^2$ thick. Sources of greater thickness were utilized in the preliminary measurements[9] and in a number of special experiments. The sources were prepared by vacuum sputtering of the metallic radioactive antimony. Two-three series of β-spectrum and conversion line measurements were made with each source. The shape of the continuous spectrum was determined by comparing the data obtained for sources having superficial densities of 5, 50, 100 and 500 $\mu g/cm^2$. The general spectrum based on 600 experimental points is shown in Fig. 2 (next page). The statistical error for the ordinate values is estimated to be 0.5%, except for the beginning and end of the spectrum, where the measurement error is greater. The complex nature of the spectrum is clearly evident.

In order to resolve the spectrum into components it is necessary to know the shape of these components, in particular the shape of the hard component; we investigated this thoroughly paying particular attention to the following.

First, we provided conditions under which low-energy electrons were prevented from entering the detector with strong fields in the instrument ($H\rho > 7000$ Gauss-cm). To this end, in addition to the measures outlined above, the support was made appreciably wider than the source (to trap the electrons moving along the epitrochoidal paths at the beginning of their trajectories) and the pressure in the instrument was increased somewhat above normal (to 10^{-2} mm Hg). Under these conditions no increase in the number of counts was observed even far beyond the ends of the spectrum. That the increase in pressure did not distort the shape of the hard β-spectrum was proved by the fact that the number of coincidences at a given setting was the same, within the limits of the experimental error, at the normal and elevated pressures.

Second, we measured the dependence of the counter background on the magnetic field strength with the source moved away from the focus to a position at which the electrons of the spectrum proper did not reach the receiving slit (points A and B in Fig. 1). Such tests permit evaluating the distortions of the β-spectrum introduced by Compton electrons formed in the walls and baffles by γ-rays from the

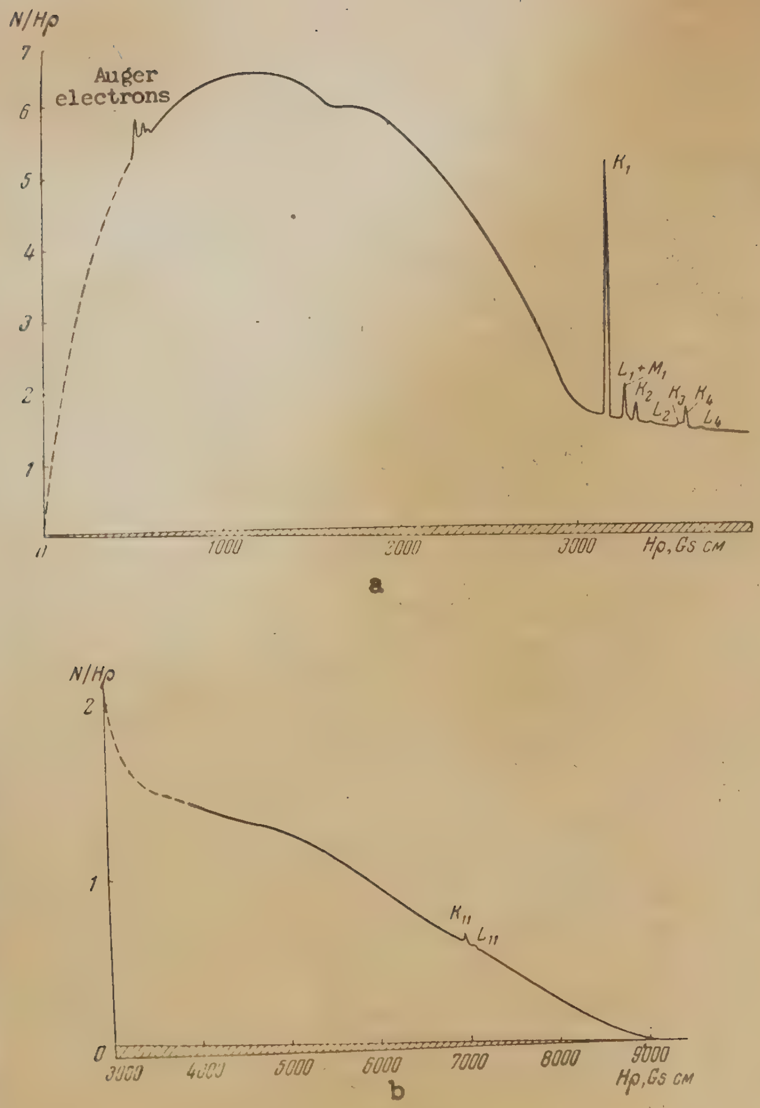

Fig. 2. β-spectrum of Sb^{124} in H coordinates: a) to 4000 Gauss-cm; b) 4000-9300 Gauss-cm. The curve is based on 600 experimental points. Ten conversion lines (see Table 2) and the group of Auger electrons (K-series) appear in the spectrum. The background, due to recoil and scattered electrons, is indicated by the shaded wedges along the horizontal axis.

source and by electrons of the spectrum scattered from the walls of the spectrometer in the immediate vicinity of the source. This procedure for taking account of the background was proposed by Dzhelepov.[18]

The shape of the hard component can also be distorted by recoil electrons produced by 2090 kev γ-quanta in the edges of the apertures in the first diaphragms. However, according to our evaluation, this distortion cannot exceed 0.1% at energies under 1850 kev and must be appreciably smaller at higher energies.

We did not investigate electron scattering in the channel of the spectrometer but obviously it must be minor in the given energy region.

The Kurie plot for the hard component of the β-spectrum is not linear (curve C = = 1 in Fig. 3), from which we conclude that the associated transition is a forbidden one. A detailed analysis of the shape of the hard component was carried by L.N.Zyrianova. This analysis was carried out by comparing the experimental correction factor

$$C_{exp} = \frac{N\delta}{\varepsilon p F (\varepsilon - \varepsilon_0)^2}$$

with the theoretical factor computed for a unique transition (ΔJ = 2, yes) and for a mixture of S + T interactions (ΔJ = 1, yes) and an end-point energy of 2311 ± 6 kev.

The electronic wave functions used in the computations were evaluated taking into account the screening of the Coulomb field and the effect of finite dimensions of the nucleus, as proposed by Sliv[19]. It was found that the theoretical factor C_{un} for an unique transition differs greatly from the experimental one, from which it may be concluded that the hard component is not an unique spectrum (see Curve C_{un} in Fig. 3). Good agreement, however, was found between the experimental and theoretical correction factors for the mixture of interactions (S + T, ΔJ = 1, yes) (curve C_{ST} in Fig. 3).

We resolved the β-spectrum of Sb^{124} into components on the basis of this assumption; with the hard component subtracted, the Kurie plots of the other compo-

Table 1

End-point energies, intensities and shapes of the Sb^{124} β-spectrum components

lg τf[4]	Kern et al[2]			Langer et al[4]			Our data						Moreau[20]		
							1953 r.			1954 r.					
	$E_{e.p.}$ kev	%	Shape*	$E_{e.p.}$ kev	%	Shape*	$E_{e.p.}$ kev	%	Shape*	$E_{e.p.}$ kev	%	Shape*	$E_{e.p.}$ kev	%	Shape*
7,0	480	18	F	240±10	14	F	208±15	11	F	202±15	9	F	250±20	9	
7,8	650	44	»	610±20	49	»	608±10	49	"	608±10	49	"	615±10	53	
9,2	1000	9	»	966±10	9	»	930±15	5	F**	930±15	4	F**	946±20	9	
10,2	1690	8	»	1620±10	7	»	1585±10	9	un	1590±10	10	F	1600±20	7	
10,5	2370	8	»	2317±5	21	S+T	2300±10	26	un	2311±6	28	S+T	2305±10	22	S+T

* F = Fermi, un = unique and S - T = mixture of scalar and tensor interactions.

** A Fermi shape was assumed in resolving the spectrum into components.

fact that these investigators in plotting the hard component failed to take into account the effect of finite nuclear size and of screening in evaluating the wave functions determining the spectrum shape and, second, by the failure of these investigators to evaluate the background due to Compton recoil electrons, which is present to some degree in all spectrometers. It may be noted that despite the fact that different investigators used different resolving procedures, there is close agreement in every case as regards the intensity of the 608 kev end-point energy line.

For the purpose of determining the probability of β-decay of Sb^{124} with direct transition to the ground state of Te^{124} we carried out a series of measurements with a very strong source (total activity about 3 mc). The measurements indicated that the probability of the corss-over transition is less than 10^{-5}.

3. Internal conversion electron spectrum of Sb^{124}

The observed conversion spectrum of Sb^{124} comprised ten lines corresponding to transition of energies 603 (K, L + M), 646 (K, L), 714 (K), 723 (K, L), 969 k (K) and 1693 k (K, L) kev and a group of Auger electrons (K-series).

The conversion lines are shown against the background of the β-spectrum in Fig. 2 and separately in Fig. 5 (714 and 723 kev γ-transitions) and Fig. 6 (1693 kev transition). We verified the fact that the 714 kev γ-transition pertains to Sb^{k24} by decay-period measurements. To this end we made two measurements of the ratio of the number of conversion electrons corresponding to the 714 and 723 kev transitions (as given by the ratio of the areas under the respective peaks) separated by an interval of 60 days. The ratio was found to be 3.8 ± 0.3 and remained constant within the limits of the experimental error.

Towards the completion of these experiments and those concerned with measurement of the photoelectron spectrum we received the publication containing Ref. 7 in which it is reported that this γ-line (714 kev) was apparently observed by Metzger.

The L conversion lines (except for the one associated with the 603 kev γ-ray) are very weak; consequently we are unable to deduce any information regarding the multipole

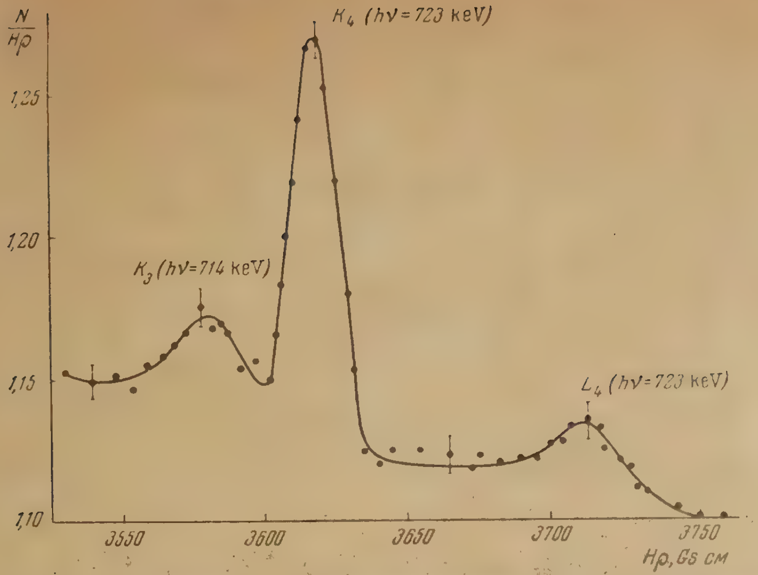

Fig. 5. Conversion lines associated with the 714 and 723 kev γ-transitions. The vertical scale, as in all other conversion spectra, is in relative units.

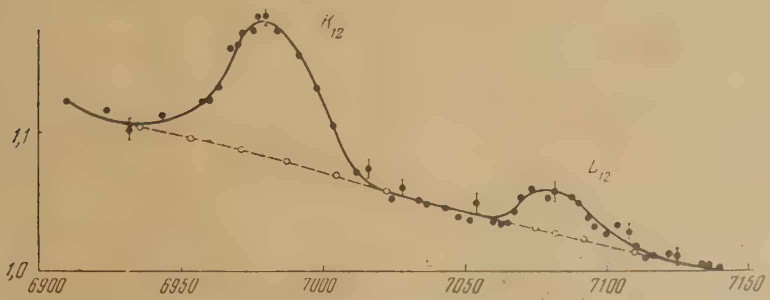

Fig. 6. Conversion lines associated with the 1693 kev γ-transition. The line numbers are taken from the photoelectron experiments; the β-spectrum (circle points) is the computed, theoretical spectrum.

order of the radiation from our measurements.

The conversion spectra had been studied by many experimenters.[2,3,5,9 &21] The latest and most complete investigation is that of Tomlinson, Ridqway & Gopalakrishnan.[22] Our data, together with that of other investigators, are listed in Table 2.

It will be seen that there is good agreement between our values and those of Tomlinson et al. In our experiments the relative numbers of conversion electrons were measured for different sources and then averaged. We obtained a value of 6.1 ± 0.5 for the K/(L + M) ratio for the 603 kev nuclear transition which agrees within the limits of the experimental error with the data of other investigators and substantiates the electric quadrupole identification given by Tomlinson et al.

According to our evaluation the K/(L+M) ratio for the 1693 kev transition is 4.2 ± 1.5. The large error inherent in the evaluation precludes identification of the multipole order of this transition.

Table 2

Energy and relative intensity of conversion lines of Sb^{124}

Shell and line No.*	Tomlinson et al[22]		Our data		
	$h\nu$, keV	Relative number of conversion electrons	$h\nu$, keV	Relative number of conversion electrons	Number of conversion electrons per decay
K_1	604	1,00	602,3 ± 1.2	1.00	$3,57\cdot10^{-3}$
L_1	604	0,13	603,2 ± 1.6	0,164	
M_1	604	0.054	603,4 ± 1,6		
K_2	648		645,8 ± 1,6	0,074	$2,64\cdot10^{-4}$
L_2			646,0 ± 2.0		
K_3			714 ± 2,5	0,026	$0,92\cdot10^{-4}$
K_4	725	0,078	723,4 ± 1,6	0,078	$2,77\cdot10^{-4}$
L_4			723 ± 2,0		
K_5			969 ± 2,0	~0,006	~$2,2\cdot10^{-5}$
K_{11}	1697	0,034	1693,6 ± 3,0	0,029	$1,0\cdot10^{-4}$
L_{11}			1691,2 ± 5,0	0,007	

---

* Line numbers taken from photo-conversion experiments.

We were able, from the results of our measurements, to determine the number of conversion electrons per disintegration; the computed values are listed in the last column of Table 2. For computing these we utilized the β-spectrum records and our measurements of the 603 kev conversion line with 5 and 50 μg/cm^2 sources. We evaluate the error in determining the energy of the intense lines as 0.2%.

We made a search for conversion electrons associated with the γ-transitions of energies close to 319 and 395 kev, i.e., transitions which might occur between higher excited levels of Te^{124}. We failed to detect any such lines. In view of the sensitivity of our instrument it may be assumed that the upper limit for these transitions is $5 \cdot 10^{-5}$ conversion electrons per disintegration.

We also evaluated the number of conversion electrons for the γ-transition of energy 970 kev. The number of conversion electrons per disintegration proved to be $(2.2 \pm 1.5) \cdot 10^{-5}$.

4. Photoelectron spectrum of Sb^{124}

We used the photoelectric method for investigating the γ-rays accompanying the decay of Sb^{124}. We employed a photoelectron radiator having axial symmetry. The first experiments with such a photoelectron radiator were carried out by Ellis and Aston.[23] More recently the method has been successfully used by Bashilov, Anton'eva and Dzhelepov.[24,25]

In our experiments the radioactive antimony sample was placed in a copper capillary tube having walls of sufficient thickness (1100 mg/cm^2) to stop all β-spectrum electrons. The radiators in the form of semicylinders 3 mm in diameter were clipped over the tube. The dimensions of the assembly were close to those of the focus of the electron beam in the spectrometer. The target materials used were Th, Pb and Pt. The photoelectron spectrum was measured with radiators of Th (3 mg/cm^2) and of Pb (18 mg/cm^2). The relative half-width of the photoline was 0.8-1.2%

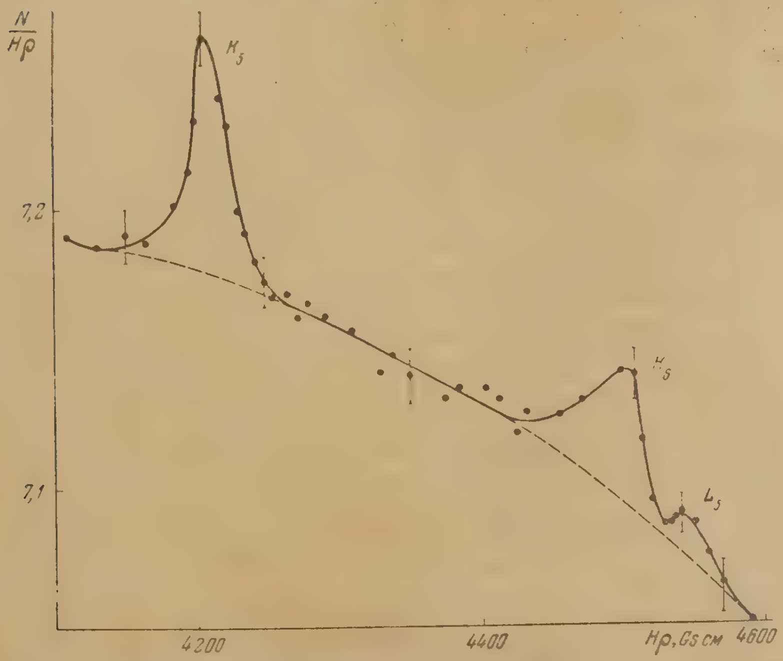

Fig. 7. Photoelectron spectrum with Th radiator from γ-rays of 970 kev (K_5 and L_5) and 1047 kev (K_6) energy.

In these experiments we observed the photoelectron lines from γ-rays having energies from 603 to 2088 kev (see Table 3). The experimental curves obtained as a result of these measurements (with the exception of the photopeaks for the 603-723 kev γ-rays) are presented in Figs. 7, 8 & 9. The photoelectron lines associated with the 603, 646, 714 and 723 kev photons were also studied using a 3 mg/cm^2 platinum radiator. In contrast with the other experiments, in these measurements a narrow (1 mm) radiator was used so that the relative half-width of the photolines was 0.6%. The experimental curve is shown in Fig. 10. The Compton electron spectrum was recorded with no radiator in place. Two series of measurements were made with each radiator, approximately $6 \cdot 10^5$ pulses being accumulated for each experimental point.

Table 3

Energies and relative intensities of the gamma-rays from Sb^{124}

Line No.	Recoil electrons		Photoelectrons						Scintillation spectrometer			
	Gromov et al[5]		Kern et al[2]		Langer et al[4]		Our data		Lu et al[7]		Lazar[6]	
	$h\nu$, keV	Relat. intens.	$h\nu$, keV	Relat. intens.	$h\nu$, keV	Relat. intens.	$h\nu$, keV	Relat. intens.	$h\nu$, keV	Relat. intens.	$h\nu$, keV	Relat. intens.
1	597 ± 5	1,82*	603	1,31	603 ± 3	–	603 ± 1,2	1.94	603		605	2,19
2			650	0,11	641 ± 5	– –	646 ± 2	0,12	–		—	
3				0,34	– –		714 ± 3	0,075	–		—	
4	711 ± 7	0,22*	714		716 ± 5	–	723 ± 2	0,20	718		720	– –
5	958 ± 10	0,066			–		970 ± 2	0,050			990	0,118
6	1052 ± 10	0,044					1047 ± 3	0,040			– –	
7	—						1298 ± 4	0,025				
8		0,17			–		1326 ± 4	0,040			. . .	0,136
9	1347 ± 14				.		1361 ± 5	0,060	.			
10					– –		1370 ± 4		1360		1380	
11	1691 ± 14	1,00	1708	1,00	1680 ± 10	–	1691 ± 3	1,00	1690		1710	1,00
12	2070 ± 21	0,10	2062	0,086	2090 ± 10		2088 ± 4	0,13	2060	–	2110	0,217

---

* These values are taken from Ref. 26 wherein the data of Ref. 5 are processed.

The relative intensities of the γ-rays were evaluated on the basis of the experimental data on the assumption that the spectral sensitivity of the instrument with the given radiator geometry (axial symmetry) is determined in the energy region above 500 kev exclusively by the photoelectric absorption coefficient . The values of the coefficient were taken from Ref. 27.

The results of the energy and intensity measurements with different radiators are in good agreement; they are listed together with date of other investigators in Table 3.

Here the following must be noted:

1. The K_3 and L_2 photoelectron lines obtained in measurements with the Pt radiator partially overlap. To find the area under the K_3 peak we resolved these lines: to determine the area under L_2 we used the known area under the separate peak K_2 and the ratio of the areas under L_1 and K_1 computed from the experimental data. For the analysis we utilized the experimental shape of the lines for the given source.

2. The photolines associated with the transitions of energies 1298, 1326, 1361 and 1370 kev were investigated with thorium and lead radiators (Fig. 8). The position of the lines in the energy scale obtained in both series of measurements corresponds to the binding energies of Th and Pb. The width of the K_9-K_{10} doublet is greater than the width of the single lines in both curves. The energy of the unresolved K_9 line was determined by separating the peak into its components. The results of our analysis of the experimental data are listed in Table 4. (Page 279)

3. We evaluate the statistical error in determining the relative intensities of the stronger γ-transitions (over 8%) as several percent (to 5%); the statistical errors for the weak transitions are obviously greater: for example, the error for the 1298 kev transition may be as great as 50%. Taking into account the dependence of the spatial distribution of the photoelectrons could

modify the listed relative intensity values. We believe, however, that in the narrow energy region in question, in particular in the 603-723 kev γ-quanta energy interval of interest to us here, this dependence cannot appreciably affect the deduced values.

Comparison of our data on the relative intensities of the γ-transitions (particularly of the strong 603 and 1694 kev transitions) with the data obtained on the Ritron[26] indicates that the spectral sensitivity of our spectrometer in the given energy region does not differ from that assumed in Ref. 26 for computing the intensities by more than 10-15%. The difference in relative intensities obtained for the γ-lines in the 603-723 kev interval can be explained by the appreciable scattering of electrons (in the target, the counter windows and the gas filling the instrument) in the Ritron. It may be noted that the value deduced from our photoelectron experiments for the ratio between the intensities of the 603 and 1693 kev γ-transitions (1.94 ± 0.10) is consistent with the decay scheme for Sb^{124}.

It will be noted that the β-transition with the end-point energy of 608 kev and an intensity of 50 ± 5% goes to the 2296 kev level of Te^{124}. This level in turn decays by the emission of quanta having energies of 1693 and 970 kev and relative intensities of 1.00 and 0.046, respectively. Inasmuch as no other transitions to and from this level with an intensity exceeding 0.5% are observed the intensity of the 1693 kev γ-transition must be 48 ± 5%. Two γ-transitions

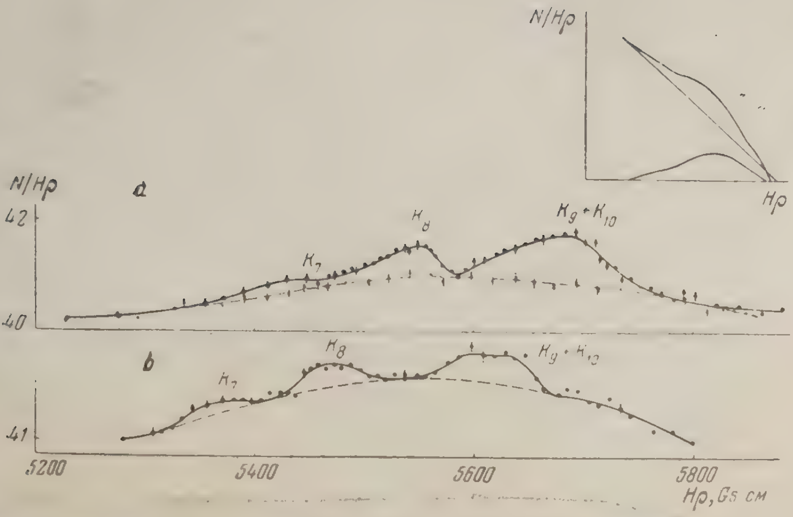

Fig. 8. Photoelectron spectrum in the 5200-5790 Gauss-cm region with thorium and lead radiators: a) Pb(18mg/cm^2), b) Th(3mg/cm^2). The recoil electron spectrum indicated by crosses was measured separately. For convenience of representation the curves are plotted according to the scheme shown in the upper right hand corner; a straight line was drawn approximately parallel to the recoil electron spectrum and then the ordinates shown in the main curve were determined as the difference between the ordinates of the spectrum and of the straight line.

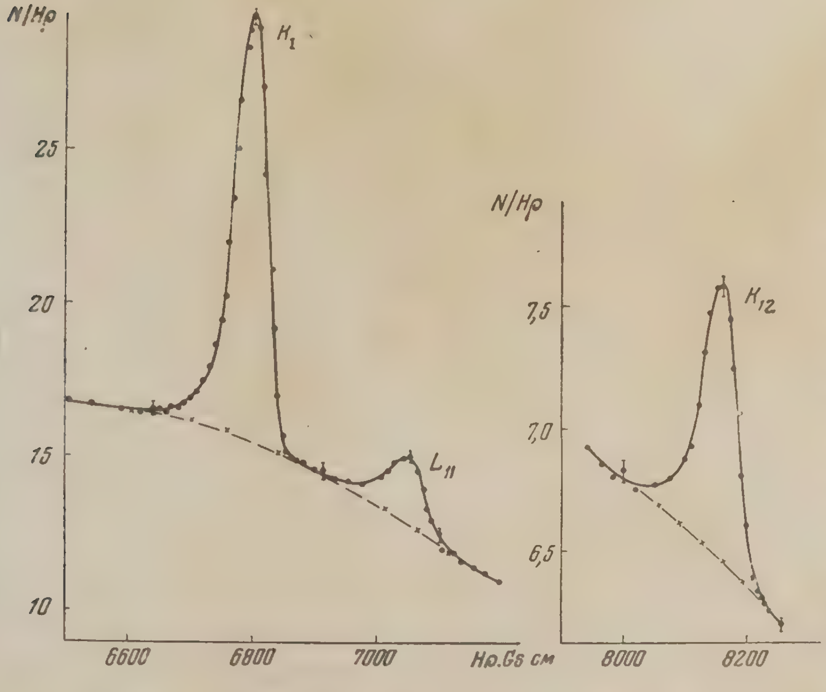

Fig. 9. Photoelectron lines obtained with lead radiator. At left for 1693 kev γ-rays; at right for 2088 kev γ-rays. Crosses indicate recoil electron spectrum.

Table 4

Determination of γ-transition energies ($h\nu$ = 1298-1370 kev)

Lines	Th (E_k = 109 keV)			Pb (E_k = 87.6 keV)			$\overline{h\nu}$, keV
	$H\rho$, Gs cm	E, keV	$h\nu$, keV	$H\rho$, Gs cm	E, keV	$h\nu$, keV	
K_7	5140	1189	1298	5480	1209	1297	1298
K_8	5510	1218	1327	5580	1238	1326	1326
K_9	5626	1252	1360	5703	1273	1361	1361
K_{10}	5660	1261	1369	5740	1284	1370	1370

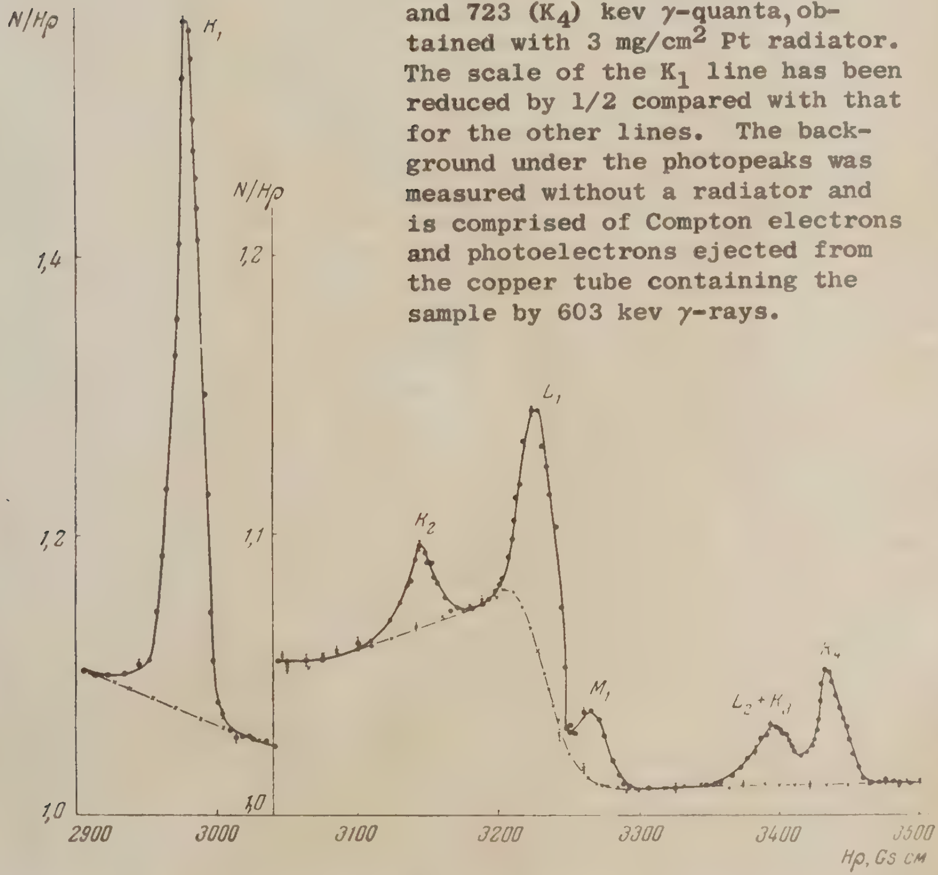

Fig. 10. Photoelectron lines, associated with the 603 (K_1,L_1 & M_1) 646 (K_2 & L_2) 714 (K_3) and 723 (K_4) kev γ-quanta, obtained with 3 mg/cm^2 Pt radiator. The scale of the K_1 line has been reduced by 1/2 compared with that for the other lines. The background under the photopeaks was measured without a radiator and is comprised of Compton electrons and photoelectrons ejected from the copper tube containing the sample by 603 kev γ-rays.

— 603 and 1326 kev — go to the ground level of Te^{124}. Since the intensity of the 1326 kev transition amounts to about 2% of the intensity of the 603 kev transition the intensity of the latter may be evaluated at 98%. Transitions from the upper levels to the ground state amount to no more than 0.5%.[8] It follows from the above figures that the intensity ratio of the 603 and 1693 kev transitions equals 2.08 ± 0.15.

We have excluded from the above analysis the low intensity γ-transitions of 1047 and 1298 kev energy which do not fit into the proposed decay scheme.

For a rigorous evaluation of the intensity of the above mentioned γ-transitions one must determine, experimentally or by calculation, the angular distribution of these photoelectrons observed in our experiments. P. Zarubin[31] determined the angular dependence in the case of the Ketron by investigation of the photoelectron spectra of isotopes for which the relative γ-transition intensities are known. Zarubin found that to judge the relative intensities of the γ-transitions in the Ketron β-spectrometer it is essential to take into account the angular distribution of photoelectrons produced by quanta of energies at least to 2 Mev. However, inasmuch as in the Ketron experiments a flat radiator was employed and the statistical error was about 20%, it would be incorrect to compare Zarubin's data with our results.

We searched the β-spectrum in the 250-450 kev interval and failed to detect any photolines in this region. In view of the sensitivity of our instrument we can safely conclude that there are no γ-transitions having intensities in excess of 0.5% in this energy region.

To summarize, in our investigation of the γ-spectrum of Sb^{124} we have discovered three new γ-lines with energies of 714, 1298 and 1361 kev, and have substantiated the results of Ref. 6 regarding the presence of γ-lines of 970, 1047 and 1326 kev energy and the results of Refs. 5 and 7 regarding the existence of a 1370 kev line.

We did not study the spectrum regions below 200 kev and between 1400 and 1600 and between 1700 and 2000 kev in detail since we are planning to study these intervals more exhaustively later, utilizing special, more favorable conditions.

5. Decay scheme for Sb^{124}

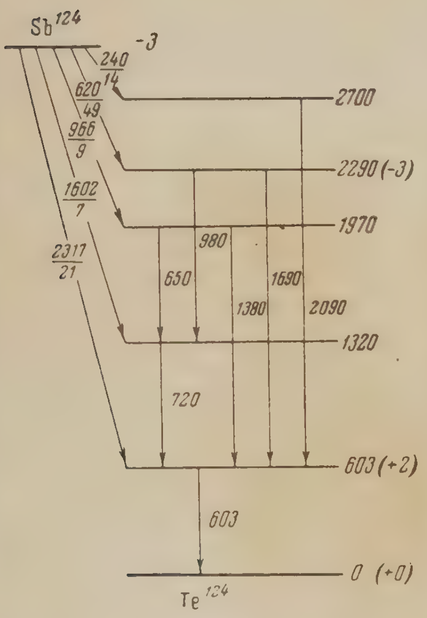

Fig. 11. Decay scheme for Sb^{124} based on the data of Refs. 4,6 & 29. The figures over the bars indicate the energy of the transition, those under the bar, the corresponding intensity in percent. The spin and parity assignment for the 2700 kev level of Te^{124} is 3-.

The decay scheme for Sb^{124} based on the data in the literature is shown in Fig. 11. The scheme is based on the following experimental data:

1. γ-γ coincidence studies indicate a) that the 1690 and 2090 kev γ-rays are in cascade with the 603 kev rays[4,28,29] and b) that the 650, 720 and 603 kev γ-rays form a triple cascade.[30]

2. β-γ coincidence studies show that a) the β-decay with 2317 kev end-point energy leads to the first excited level of Te^{124} (Refs. 11 & 31) and b) the 620 kev end-point energy β-decay yields coincidences with the 1690 kev γ-quanta.[4]

3. Observations of β-γ (Refs. 10, 11, 12, 32 & 33) and γ-γ (Refs. 13) angular correlation indicate that the ground state of Sb^{124} should be assigned spin 3 and odd parity of the wave function and that the corresponding assignments for the first and fourth excited levels of Te^{124} are 2+ and 3-, respectively. These spin and parity assignments for the levels of Te^{124} also follow from evaluations of the internal conversion coefficients for the 603 kev and 1690 kev transitions: $\alpha_K = 4.2 \cdot 10^{-3}$ (Ref. 34) and $\alpha_K < 5 \cdot 10^{-4}$ (Ref. 21), respectively.

4. The energies of the γ-quanta with $h\nu = 980 \approx 1690 - 720$ kev and $h\nu = 1370 = 720 + 650$ kev dictate the location of these transitions in the decay scheme.

The results of our measurements make it possible to refine and elaborate the above decay scheme.

A. Energy relationships. The γ-lines discovered by observation of photoelectrons in the 1326-1370 kev interval correspond to the following energy relationships between them and the energies of the well-known γ-transitions:

$$h\nu_{1326} = h\nu_{603} + h\nu_{723},$$
$$h\nu_{1361} = h\nu_{2088} - h\nu_{723},$$
$$h\nu_{1370} = h\nu_{646} + h\nu_{723}.$$

These relationships uniquely identify the locations of these γ-transitions in the new decay scheme of Fig. 12.

Thus it becomes obvious that there is a cross-over γ-transition from the second excited level to the ground state of Te^{124}.

The γ-transition of 970 kev energy also corresponds to the relationship

$$h\nu_{970} = h\nu_{1693} - h\nu_{723}.$$

The energy of the 714 kev γ-line, determined in our experiments from observation of internal and external conversion electrons, fits the following relationship:

$$h\nu_{714} = h\nu_{2088} - (h\nu_{723} + h\nu_{646}).$$

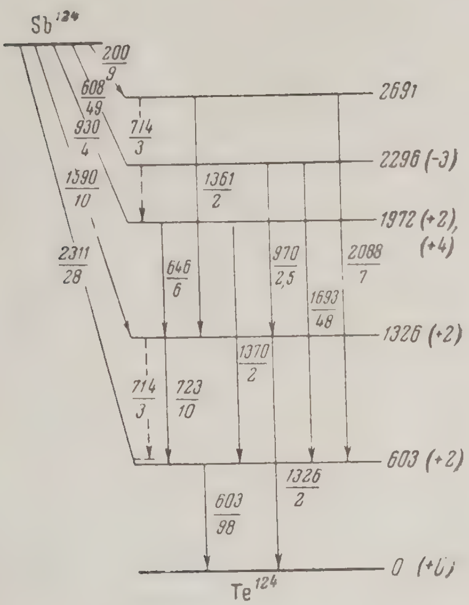

Fig. 12. Decay scheme for Sb^{124} elaborated on the basis of our data. Quantum characteristics of ground state of Sb^{124} and the 2691 kev level of Te^{124}: 3-.

In view of this relationship this line should be located between the 2691 and 1973 kev levels. In view of certain considerations (see below) such placement of this transition may not be entirely consistent. The 1047 and 1298 kev transitions do not fit into the proposed scheme. If they do pertain to the decay of Sb^{124} it must be assumed that there exist two or more as yet undetected low-intensity transitions. It is also not impossible that these γ-transitions belong to some unknown impurities having a period close to that of Sb^{124}.

B. Intensity of γ-transitions. It follows from the proposed decay scheme (Fig. 12) that the sum of the intensities I of the 603 and 1326 kev γ-transitions amounts to one quantum per disintegration. In view of the relative intensity of these transitions (Table 3), we find that I_{603} = 0.98 quanta per disintegration. From this figure we can determine the absolute intensities of the γ-transitions; the results of our calculations are listed in Table 5. For purposes of comparison we also list the absolute intensity values from Refs. 5 and 26. We calculated the number of quanta per disintegration in this investigation in the light of the scheme of Fig. 12 on the basis of two alternate assumptions:

1) I_{603} = 0.98 quanta per disintegration (column 3) or
2) I_{1693} = 0.48 quanta per disintegration (column 4).

Inasmuch as the conditions of measurement in the Ritron in the 603 kev energy region were such that there was presumably appreciable scattering of electrons and that there may, therefore, have been an appreciable error in determining the number of recoil electrons (i.e., the background), we feel it more reasonable to compare our absolute intensity values with the results (based on Refs. 5 & 6), computed on the basis of the second assumption, i.e., with the values of column 4, Table 5.

The difference between the comparable absolute intensities is somewhat greater than the assumed statistical errors and may be due to the dependence of the angular distribution of photoelectrons in our instrument on the γ-ray energy and possibly to an appreciable scattering of electrons in the 500-700 kev energy interval in the Ritron. Moreover the 603, 646 and 714+723 kev lines were not resolved in the Ritron experiments. The intensities of the γ-transitions are indicated in Fig. 12, under the bars in percent (i.e., per 100 disintegrations).

It will be noted that a consistent intensity balance (within the limits of the experimental error) is obtained in all cases except for that of the 1326 kev level. We note that placement of the 714 kev transition between the 1326 and 603 kev levels reduces the discrepancy at the 1326 level.

C. Conversion coefficient and multipole order of the transitions. We can now evaluate the conversion coefficients

$$\alpha_{K_i} = \left(\frac{n_e}{n_\gamma}\right)_i,$$

where n_e is the number of conversion electrons per disintegration (Table 2) and n_γ

is the number of quanta per disintegration (Table 5). The results are listed in column 2 of Table 6.

Table 5

Number of γ-quanta per disintegration

$h\nu$, keV	Compton electrons (Refs. 5 & 26)			Our data	
	relative intensity	quanta per decay		relative intensity	quanta per decay
1	2	3	4	5	6
603	1,82	0,98	0,87	1,94	0,98
646	—	—	—	0,12	0,06
714	—	—	—	0,075	0,036
723	0,19	0,102	0,096	0,20	0,104
970	0,066	0,036	0,032	0,046	0,023
1047	0,044	0,024	0,020	0,040	0,020
1298	0,170	0,091	0,082	0,025	0,012
1326				0,040	0,020
1361				0,070	0,035
1370					
1694	1,00	0,54	0,48	1,00	0,48
2088	0,10	0,054	0,048	0,135	0,067

The experimental conversion coefficient for the 603 kev transition is somewhat smaller than the theoretical value of $4.26\cdot10^{-3}$ for an E2 transition.[35]

We note that similar, less-than-theoretical values of the coefficient for the 603 kev transition were obtained in two other spectroscopic investigations: $(3.63 \pm 0.40)\cdot10^{-3}$ (Ref. 21) and $3.4\cdot10^{-3}$ (Ref. 4).

We can, with justification, equate the experimental value for α_K to the theoretical value, since the fact that the 603 kev transition is an E2 transition is well established, and re-evaluate the other conversion coefficients accordingly. The values of the conversion coefficients corrected in this manner are listed in column 3 of Table 6. Comparison of the resultant α_K values with the theoretical ones from Ref. 35 (columns 4-7 in Table 6) leads to the multipole order assignments listed in column 8.

The indicated multipole orders of the 723 and 646 kev transitions show that the 1326 and 1972 kev levels are characterized by even parity. Of the possible spins consistent with the multipole orders for the 723 kev transition (E2, E2+M1 or M1) we must assign a spin of 0, 2 or 4 to the 1326 kev level, in view of the experimental rule of Glaubman[36] (substantiated by the calculations of Talmi[37]) which states that in even-even nuclei levels with even parity have even spins. Of the three

Table 6

Conversion coefficients and multipole order of transitions

$h\nu$, keV	$\alpha_K\cdot10^3$ (experimental)	$\alpha_K\cdot10^3$ (corrected)	Theoretical values of $\alpha_K\cdot10^3$ from Ref. 35				Assignment
			E1	E2	M1	E3	
1	2	3	4	5	6	7	8
603	3,70±0,30	4,26±0,30	1,92	4,26	5,60	>8,0	E2
646	4,40±0,60	5,0 ±0,6	1,28	3,52	4,80	>7,0	E2+M1; M1
714	2,50±0,80	2,9 ±0,8	1,05	3,00	3,62	6,22	E2; E2 + M1;
723	2,66±0,40	3,1 ±0,4		2,93	3,55		M1;
1693	0,20±0,03	0,23±0,03	0,22	0,44	>0,6	—	E1

possible spins (0, 2 or 4) we must select 2 inasmuch as there is observed a crossover transition from the 1326 kev level to the ground state (0+).

From our data regarding the multipolarity of the 646 kev transition (E2+M1 or M1) and Glaubman's rule it follows that the spin of the 1972 kev level is probably 2 rather than 4.

The 3- assignment for the 2296 kev level established on the basis of γ-γ angular correlation measurements is consistent with our data on the multipole order of the 1693 kev transition (E1).

D. Features of the decay scheme. It is worth calling attention to certain distinctive features of the proposed decay scheme for Sb^{124}.

Let us consider the excited levels of Te^{124}: 2296 (3-), 1326 (2+) and 603 kev (2+). There are observed γ-transitions from the 2296 kev level to the other two levels, having energies of 1693 ± 3 and 970 ± 2 kev and relative intensities of 1.00 ± 0.05 and 0.040 ± 0.010, respectively. These values indicate unambiguously that the levels between which these transitions occur differ as regards character. The single particle nuclear model indicates that the ratio of intensities of these transitions should be given by the relationship:

$$\frac{I_{1693}}{I_{970}} \approx \left(\frac{h\nu_{1693}}{h\nu_{970}}\right)^{2l+1}_{l=1} = (1,74)^3 = 5,3.$$

The experimentally determined intensity ratio for these transitions is 20 ± 8.

We find a similar inconsistency for the γ-transitions from the 1972 kev (2+, 4+) level to the 1326 (2+) and 603 kev (2+) levels. The respective energies and relative intensities of the γ-transitions are 1370 ± 4 and 646 ± 2 kev and 0.04 ± ± 0.02 and 0.12 ± 0.01. Thus the intensity ratio is 0.33 ± 0.21, whereas calculations on the basis of the single particle model yield

$$\frac{I_{1370}}{I_{646}} \approx \left(\frac{h\nu_{1370}}{h\nu_{646}}\right)^{2l+1}_{l_{min}=1} = (2,12)^3 = 9,5.$$

Another distinctive feature of the decay scheme for Sb^{124} is the "suppression" of the 608 kev end-point energy β-transition to the 2296 kev level of Te^{124}: from spin and parity considerations (3- ⟶ 3-) this should be an allowed transition, while on the basis of log ft = 10.5 (Ref. 4) and the intensity value it would appear to be a forbidden transition.

We assume that an explanation of this inconsistency, as well as of the discrepancy in intensity ratio values mentioned above, must be sought in the different character of the levels as reflected in the collective nuclear model.[15]

The energy of the 714 kev γ-ray indicates that this transition may occur between the 2691 and 1973 kev levels. However, it is not impossible that this transition proceeds between the 1326 and 603 kev levels, in parallel with the 723 kev transition. In this case there should be a γ-line of 9 ± 2 kev energy (the uncertainty is evaluated from the difference between the conversion and photoelectron peaks).

To check this a search was made for a γ-line of 9 kev energy. At the suggestion of B.S.Dzhelepov the method of changing scatterers was employed. The results of these measurements are shown in Fig. 13 in the form of a counting rate for scattered γ-rays vs the Z number of the reflecting substances. The reflection maximum occurs at Z = 27 which indicates that there is a γ-line of energy 7.7 ± 0.6 kev in the γ-radiation from Sb^{124}. Although this result speaks in favor of our assumption, we do not feel justified in drawing a definitive conclusion since the experiments were preliminary in character and require further verification. The experiments were carried out by A.G.Dmitriev and P.P.Zarubin, whom we take this opportunity to thank.

In conclusion we also want to express our sincere gratitude to B.S.Dzhelepov for discussion of many problems connected with the investigation and for his interest and aid in the work, to L.K.Peker and L.A.Sliv for discussion of individual

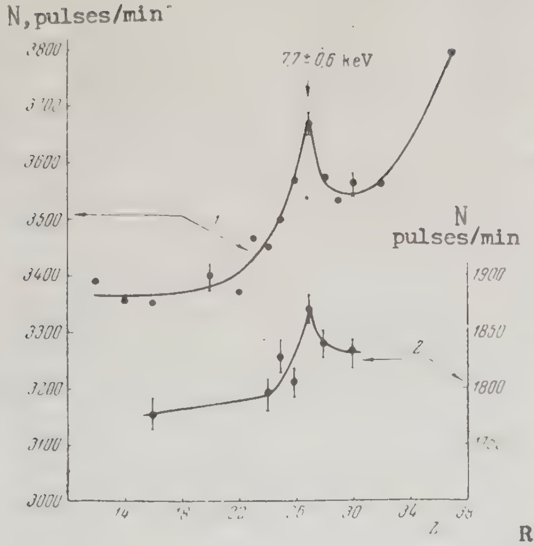

Fig. 13. Counting rate of γ-quanta from Sb^{124} reflected from foil of different pure materials with different values of Z and the same superficial density. The reflection peak occurs at Z = 27.

questions and to L.N.Zyrianov for carrying out the analysis of the shape of the hard β-component, computing the C_{un} and C_{ST} correction factors and for deducing the exact expression for the function $F(\varepsilon Z)$. We also desire to thank E.Kulakovsky, V.Bolysheva, V.Suslenko and B.Kratsika for their aid in individual experiments.

Physical Scientific Research Institute of
Leningrad State University

References

1.J.Livingood & G.Seaborg, Phys. Rev., 52, 135 (1937).
2.B.Kern, J.Zaffarno & A.Mitchell, Phys. Rev., 73, 1142 (1948).
3.C.Cook & L.Langer, Phys. Rev., 73, 1149 (1948).
4.L.Langer, N.Lazar & R.Moffat, Phys. Rev., 91, 338 (1953).
5.K.Gromov, B.Dzhelepov et al, Doklady ANSSSR, 86, 255 (1952).
6.N.Lazar, Phys. Rev., 95, 292 (1954).
7.D.Lu, W.Kelly & M.Wiedenbeck, Phys. Rev., 95, 1533 (1954).
8.W.Mayers & A.Wattenberg, Phys. Rev., 75, 992 (1949).
9.A.V.Zolotavin, Izv. AN SSSR, Ser. fiz., 18, 127 (1954).
10.E.Darby & W.Opechowski, Phys. Rev., 83, 676 (1951).
11. D.Stevenson & M.Deutsch, Phys. Rev., 83, 1202 (1951).
12.R.Kloepper, E.Lennox & M.Wiedenbeck, Phys. Rev., 88, 695 (1952).
13. J.Krauschaar & M.Goldhaber, Phys. Rev., 89, 1081 (1952).
14.K.Ford, Phys. Rev., 90, 587 (1953).
15.A.Bohr & B.Mottelson, Kgl. Danske Videnskab Selskab Mat.-fys. Medd., 27, No. 16 (1953).
16.P.P.Pavinski, Iaz. AN SSSR, Se. fiz., 18, 175 (1954).
17. A.V.Zolotavin & V.S.Sadkovski, Izv. AN SSSR, Ser. fiz, 18, 215 (1954).
18. B.S.Dzhelepov, Thesis, Radium Inst. USSR Acad. of Sciences, 1949.
19. L.A.Sliv, Zhur. eksp. i teor. fiz., 17, 1049 (1947).
20. J.Moreau, C.R., 239, 800 (1954).
21. D.Hatchinson & M.Wiedenbeck, Phys. Rev., 88, 699 (1952).
22. E.Tomlinson, S.Ridgway & K.Gopalakrishnan, Phys. Rev., 91, 484 (1953).
23. C.Ellis & G.Aston, Proc. Roy. Soc., A 129, 180 (1930).
24. A.A.Bashilov, N.M.Anton'eva, M.V.Blinov et al, Izv. AN SSSR, Ser. fiz., 18, 43 (1954).
25.A.A.Bashilov, N.M.Anton'eva, D.A.Broder & B.S.Dzhelepov, Izv. AN SSR, Ser. fiz., 17, 468 (1953).
26. Iu.V.Khol'nov, Thesis, Radium Inst. USSR Acad. of Sciences, 1952.
27. C.Davisson & R.Evans, Rev. Mod. Phys., 24, 79 (1952).
28. S.Johansson & S.Almquist, Ark. f. Fysik. 5, 427 (1952).
29. F.Metzger, Phys. Rev., 90, 328 (1953).
30. L.Langer & J.Starner, Phys. Rev., 93, 253 (1954).
31. J.Beister & M.Wiedenbeck, Phys. Rev., 79, 169 (1950).
32. P.P.Zarubin, Thesis, Leningrad State Univ., 1953.
33. Morita, Masato, Imada, Masami, Progr. Theoret, Phys., 10, 641 (1953).
34. F.Metzger, Phys. Rev., 86, 435 (1952).
35. M.Rose, Goertzel, Spinrard, Harr & Strong, Phys. Rev., 83, 79 (1951).
36. M.Glaugman, Phys. Rev., 90, 1000 (1953).
37. J.Talmi, Phys. Rev., 90, 101 (1953).

ON ANALYSIS OF THE SHAPE OF THE β-SPECTRUM OF RaE

- L.N.Zyrianova

Recent measurements of the spin of RaE (Ref. 1) indicate that the RaE(Bi^{210}) → Po^{210} transition is of the 1- → 0+ type, i.e., that the β-spectrum of RaE is a first forbidden one with $\Delta J = 1$. In contrast to most other first forbidden β-spectra of this type, having an "allowed" shape, the β-spectrum of RaE is not described by Fermi's equation. However, analysis of the shape of this spectrum on the assumption of a combination of S and T interactions has made it possible to explain[2-4] the strong energy dependence of the RaE electron distribution as a result of compensation of the large, energy-independent terms in the expression for the decay probability, due to interference between the contributing elements. In the investigations referred to above the analyses of the RaE spectrum shape were carried out taking into account a purely coulomb nuclear field. Yet it is known[5,6] that the electron wave functions, involved in computing the decay probability in the case of first forbidden transitions, are altered when more refined expressions for the atomic potential are used and particularly when the finite size of nuclei is taken into consideration. It may be assumed that, in view of the strong compensation or interference of the terms entering into the decay probability equation in the case of RaE, this modification of the electron wave functions will have an appreciable effect on the shape of the theoretical spectrum of RaE. Below we give the results of comparisons of the experimental data with the theoretical shape of the β-spectrum of RaE evaluated on the basis of different assumptions regarding the proton distribution in the nucleus and regarding the size of the nuclear radius.

Analysis of the shape of forbidden β-spectra is commonly carried out by comparing the theoretical correction (or "shape") factor C, characterizing the deviation of the spectrum from the "allowed" shape, with the experimentally determined factor

$$C_{\text{exp}} = \frac{N\delta}{EpF(E_0 - E)^2} \tag{1}$$

(in the usual notation of β-decay theory).

By way of experimental data for our analysis we have taken the results recently reported by Plassmann & Langer.[3] The theoretical correction factor for first forbidden β-spectra with $\Delta J = 1$ in the case of S + T interaction can be written in the following form:[7,8]

$$C'_{ST} = g_T^2 \left|\int [\vec{\sigma}\,\mathbf{r}]\right|^2 (T_1 + y^2T_2 - 2yT_3 + x^2S - 2xQ_1 + 2xyQ_2),$$

where

$$x = i\,\frac{g_S}{g_T} \cdot \frac{\int \beta\mathbf{r}}{\int \beta[\vec{\sigma}\,\mathbf{r}]}, \quad y = \frac{\int \beta\vec{\alpha}}{\int \beta[\vec{\sigma}\,\mathbf{r}]},$$

$$T_1 = \frac{1}{6}K^2L_0 + \frac{1}{2}L_1 + M_0 - \frac{2}{3}KN_0, \quad T_2 = L_0,$$

$$T_3 = \frac{1}{3}KL_0 - N_0,$$

$$S = \frac{1}{3}K^2L_0 + 2L_1 + M_0 + \frac{2}{3}KN_0,$$

$$Q_1 = L_1 - M_0,$$

$$Q_2 = \frac{1}{3}KL_0 + N_0.$$

In these expressions L_0, L_1, M_0 and N_0 are combinations of electronic radial wave functions; $\int \beta[\vec{\sigma}\,\mathbf{r}]$, $\int \beta\mathbf{r}$ and $\int \beta\vec{\alpha}$ are nuclear matrix elements (in the notation

of Ref. 7) and K = E_o - E.

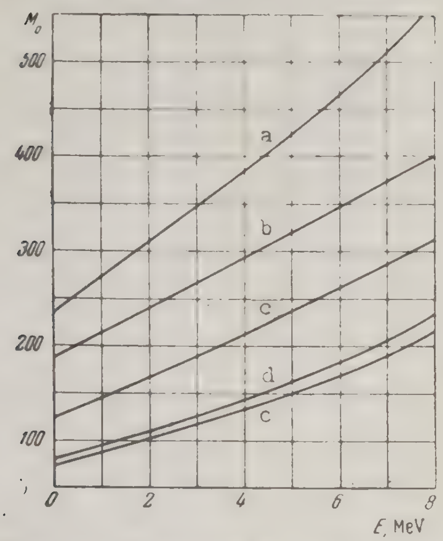

Fig. 1. Function M_o with Z=83 for different assumptions regarding the nature of the electric field inside the nucleus.

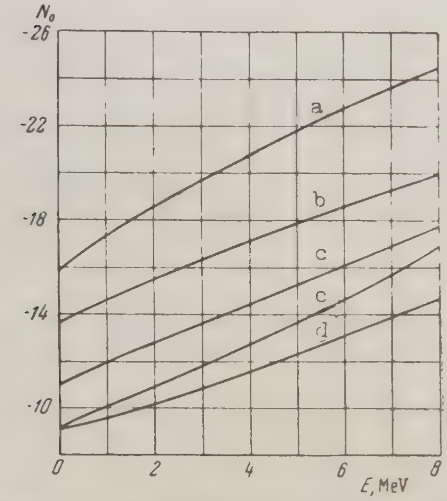

Fig. 2. Function N_o with Z=83 for different assumptions regarding the nature of the electric field inside the nucleus.

The curves of Fig. 1 show the behavior of the function M_o with Z = 83 as calculated for the following variants: a) M_o for a purely coulomb field, evaluated at the nuclear surface; b) M_o, at the nuclear surface, evaluated taking into account the finite size of the nucleus by the method of Ref. 5 on the assumption of uniform distribution of protons over the volume of the nucleus with $r_o = 1.2 \cdot 10^{-3}$ cm; c) under the same assumption as in (b) but with $r_o = 1.5 \cdot 10^{-13}$ cm; d) M_o computed, taking into account the finite size of the nucleus, on the assumption of a constant potential in the nucleus; e) M_o computed using the electronic wave functions of (b) averaged over the nuclear volume.

The corresponding curves for the function N_o, computed on the basis of the same assumptions are shown in Fig. 2. We are not reproducing the curves for L_o and L_1 inasmuch as the corrections for the effect of finite nuclear size in the case of these functions is much smaller than for M_o and N_o.

In conformity with the data of Refs. 3 & 4, we found that when the electronic wave functions for a coulomb field are used, the best agreement of the theoretical with the experimental correction factor C is obtained with $x > 0.3$ for the series of the parameters x and $y_1 = y\left(\frac{\alpha Z}{2R}\right)^{-1}$ represented by curve a in Fig. 3. If we use the values for an arbitrarily chosen point on this curve, for example, $x = 0.5$ and $y_1 = 1.8$, to calculate the C factor taking finite nuclear size into account (i.e., use the functions L, M and N evaluated according to the variants (b), (c) and (e) above), the results obtained will diverge appreciably from the experimental data. The results of our calculations are shown in Fig. 4, wherein the key letters at the curves refer to the evaluation variants for the functions L, M and N described above. Curve a fits the experimental curve for the factor C.

Our analysis showed that use of the (b) variant of the functions L_o, M_o, N_o and L_i makes it feasible to secure agreement of the theoretical C factor with the experimental curve with values of $x > 0.9$; the paired values of x and y_1 resulting in agreement in this case are given by curve b of Fig. 3.

Use of the wave functions characterized by the variant (c) allows of explaining the experimental shape of the β-spectrum of RaE only at energies exceeding 250 kev. At lower energies no combination of x and y_1 leads to complete linearization of the Kurie plot. The relation between the values of x and y_1 resulting in rectification of the Kurie plot at energies above 250 kev is shown by curve c in Fig. 3.

The correction factor C evaluated with electronic wave functions averaged over the nuclear volume (variant (e)) allows of explaining the shape of the β-spectrum of RaE only at energies exceeding 40C kev. The values of the parameters x and y_1 corresponding to this case are represented by curve e in Fig. 3.

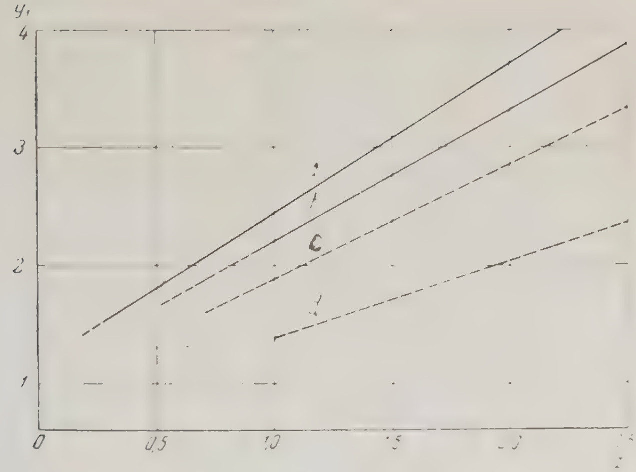

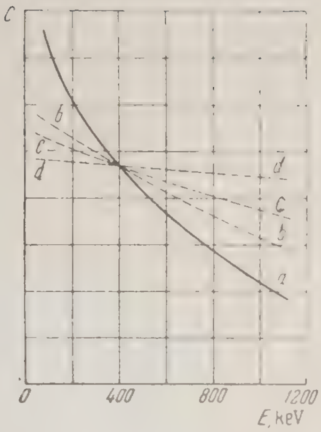

Fig. 3. Relations between the parameters x and y_1 at which the theoretical correction factor C for RaE agrees with the experimental data.

Fig. 4. Variation of the theoretical factor C with x = 0.5 and y_1 = 1.8 for different variants of the functions L, M and N.

Thus, taking account of the effect of finite nuclear size leads to an appreciable change in the parameters x and y that serve as an index to the change of state of the nucleus in the β-transition. This deduction is in conflict with the conclusion of Yamada[2] who found that taking account of the finite size of the nucleus is of little import where the spectrum of RaE is concerned.

In connection with attempts to determine the relative sign of g_S and g_T (Ref. 4), it may be noted that the use of the more exact electronic wave functions will not affect the sign of the nuclear parameters x and y yielding agreement with experiment. Calculations have shown that taking the effect of screening into account does not noticeably influence the theoretical shape of the β-spectrum.

The writer is indebted to L.A.Sliv for his interest in the work and discussion of the results.

Physical Scientific Research Institute of
Leningrad State University

References

1. R.W.King, Rev. Mod. Phys., 26, 327 (1954).
2. M.Yamada, Prog. Theo. Phys., 10, 252 (1953).
3. E.A.Plassmann & L.M.Langer, Phys. Rev., 96, 1593 (1954).
4. G.E.Lee-Whiting, Phys. Rev., 97, 463 (1955).
5. L.A.Sliv, Zhur, teor. i eksp. fiz., 17, 1049 (1947).
6. M.E.Rose & D.K.Holmes, Phys. Rev., 83, 190 (1951).
7. E.J.Konopinski & G.Uhlenbeck, Phys. Rev., 60, 308 (1941).
8. A.M.Smith, Phys. Rev., 82, 955 (1951).

CALCULATION OF PROBABILITY OF PAIR CONVERSION IN THE CASE OF O—O NUCLEAR TRANSITIONS

- L.N.Zyrianova & V.A.Krutov

Relativistic calculations of the shapes of the spectra and of the total coefficients of pair conversion taking into account the Coulomb field have been carried out for electric dipole and quadrupole (Ref. 1) and for the magnetic dipole transitions of nuclei (Ref. 2); Yukava and Sakata (Ref. 3) have carried out calculations of the shape of the positron spectrum for the O—O transition of RaC'. However, in view of the fact that such calculations are very cumbersome, in all the above mentioned investigations the shape of the positron spectrum was determined only for the case of Z = 84 and for only one or two transition energies; the curves given in the investigations are based on a small number of points and are arbitrarily extrapolated at the ends. For other elements and transition energies the calculations for the probability of pair conversion have been carried out only in the Born (non-relativistic) approximation. Yet in experimental determinations of the energy and other characteristics of nuclear transitions it is obviously of interest to know the exact theoretical spectrum shape.

In the case of O—O transitions the values of the electron and positron wave functions are important only in the region inside the nucleus where calculations of the probability of pair formation are concerned. Hence using the already available tables of relativistic wave function for intranuclear particles, we can determine the shape of the positron conversion spectra and evaluate the total probability of pair formation for radiationless nuclear transitions.

The differential probability of formation of a conversion pair per unit time in a O—O nuclear transition has the following form in the system of relativistic units

$$W_\pi(E_+)\,dE_+ = 2\pi\alpha \left| \int \psi_-^* Q_0 \psi_+ \,d\tau \right|^2 dE_+, \qquad (1)$$

where α is the fine structure constant, Q_0 is the transition potential, E_+ is the total energy of the positron, ψ_+ and ψ_- are the normalized (to a unit energy interval) solutions of the Dirac equation for an electron of the continuous spectrum with positive and with negative total energy, respectively. The integration comprises summation over the initial and final states.

A feature of O—O nuclear transitions is spherical symmetry of the transition potential and the possibility of reducing the potential to a form in which it differs from zero only in a region having the dimensions of a nucleus.[3] Hence, after integrating in equation (1) over the angular variables of the wave functions we can express the distribution of positrons in energy in the following form

$$W_\pi(E_+)\,dE_+ = 4\pi\alpha \left\{ \left| \int_0^R Q_0(r)\,(f_0^- f_0^+ + g_0^- g_0^+)\,r^2 dr \right|^2 + \left| \int_0^R Q_0(r)\,(f_{-2}^- f_{-2}^+ + g_{-2}^- g_{-2}^+)\,r^2 dr \right|^2 \right\} dE_+, \qquad (2)$$

where R is the nuclear radius, and f and g are the radial components of the wave function of the particle with j = 1/2 in the notation of Ref. 5.

In our numerical calculations of the pair production probability we used for f and g the wave functions of electrons in the coulomb field of the nucleus and the wave functions found, taking into account finite nuclear size, by the method of Sliv[6] for the uniform proton distribution nuclear model. It is impossible to carry out the calculations directly by means of equation (2) since the specific form of the potential $Q_0(r)$, which depends on the details of the nuclear structure, is at present unknown. However, if we accept that at small values of r ($r \leqslant R$) and at not excessively high transition energies the entire dependence of the functions f and g on the particle energy can be expressed in the form of a factor not containing r, then calculation of the shape of the positron spectrum in the case of O—O nuclear transitions can be carried out by replacing the radial components of f and g by their values on the surface of the nucleus:

$$\left.\begin{aligned} W_\pi(E_+)\,dE_+ &= 4\pi\alpha\left|\int\limits_0^R Q_0(r)\,r^2dr\right|^2 F(E_+,Z)\,dE_+, \\ F(E_+,Z) &= (f_0^- f_0^+ + g_0^- g_0^+)^2_{r=R} + (f^-_{-2} f^+_{-2} + g^-_{-2} g^+_{-2})^2_{r=R}. \end{aligned}\right\} \quad (3)$$

where

The shape of the positron spectrum is now determined by the function $F(E_+,Z)$.

In calculating the total probability of pair formation, replacement of the functions of $f(r)$ and $g(r)$ by $f(R)$ and $g(R)$ is not justified in the case where the wave functions for a pure coulomb field are used, since with $j = 1/2$ these functions have a singularity at the origin. However, if we do take into account the finite size of the nucleus, then bearing in mind that in this case the components g_0 and f_{-2} change little over the nucleus and neglecting the variation inside the nucleus of the components f_0 and g_{-2}, which make an insignificant contribution to the transition probability, we can write the following expression for the total probability of pair formation

$$\left.\begin{aligned} W_\pi &= 4\pi\alpha\left|\int\limits_0^R Q_0(r)\,r^2\,dr\right|^2 S, \\ S &= \int\limits_1^{\Delta W-1} F(E_+,Z)\,dE_+, \end{aligned}\right\} \quad (4)$$

where

ΔW is the transition energy in m_0c^2.

Evaluations show the difference between the results obtained using equation (4) and calculations based on replacing f and g by the mean values of these functions over the volume of the nucleus does not exceed 20% with $Z \leqslant 84$ and $\Delta W \leqslant 5$.

We carried out numerical calculations of the pair formation probability according to equations (3) and (4).

The number of known 0—0 nuclear transitions is relatively small. From the point of view of the strong influence of the nuclear field on the shape of the positron spectrum, the 1416 kev 0—0 transition of RaC' is of particular interest. The results of our calculations of the shape of the positron spectrum for this transition are shown in Fig. 1. Curve 1 gives the shape of the RaC' spectrum calculated on the assumption of a pure coulomb nuclear field. Curve 3 represents the results of Yukava and Sakata[3] obtain under the same assumption (curves 3 and 1 have been shifted to make the maximum ordinates coincide). The difference between the curves is due to the rough approximations made by Yukava and Sakata in their calculations. The ratio of the areas under curves 3 and 1 which is equivalent to the ratio of the total probabilities equals 0.73; that the result of Yukava and Sakata is an overestimate has already been noted in the literature.[7]

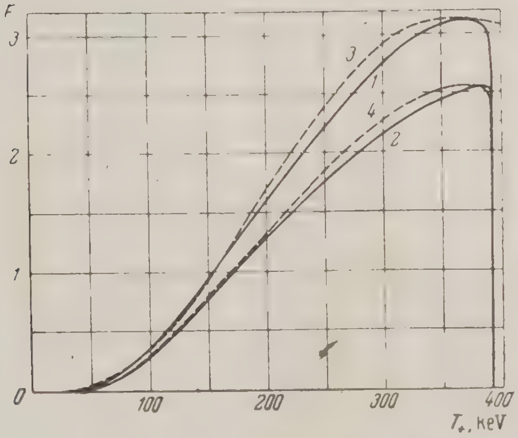

Fig. 1. Shape of the positron spectrum for the 1416 kev 0--0 transition of RaC'. T_+ is the kinetic energy of the positron.

Curve 2 represents the shape of the positron spectrum of the 0—0 transition of RaC' calculated taking into account the finite size of nuclei. Curve 4 is the curve for a pure coulomb field (i.e., curve 1 has been shifted to bring its maximum into coincidence with the maximum of curve 2).

From a comparison of curves 4 and 2 it can be seen that the shape of the positron spectrum calculated taking into account finite nuclear size differs little from

the shape of the spectrum computed on the assumption of a pure coulomb nuclear field.

The ratio of the areas under curves 2 and 1 equals 0.8, i.e., taking into account the finite size of the nucleus leads to an appreciable reduction of the calculated total pair formation probability.

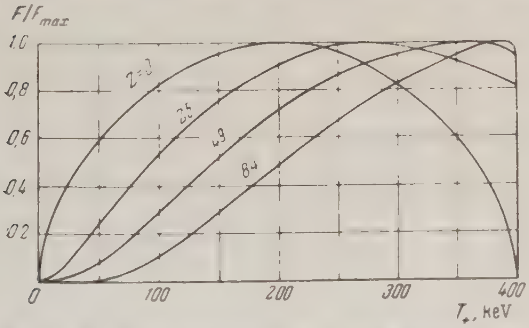

Fig. 2. Dependence of the shape of the positron spectrum on Z at a transition energy $\Delta W = 1422$ kev.

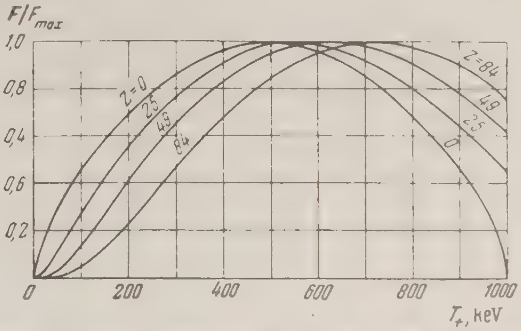

Fig. 3. Dependence of the shape of the positron spectrum on Z at $\Delta W = 2022$ kev.

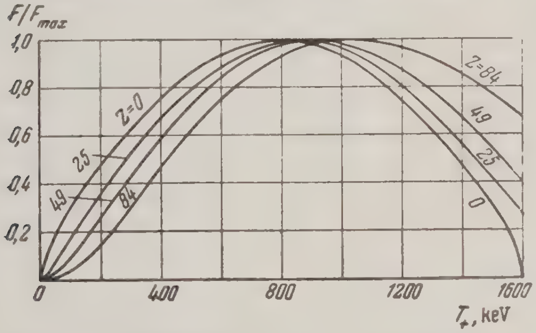

Fig. 4. Dependence of the shape of the positron spectrum on Z at $\Delta W =$ $= 2622$ kev.

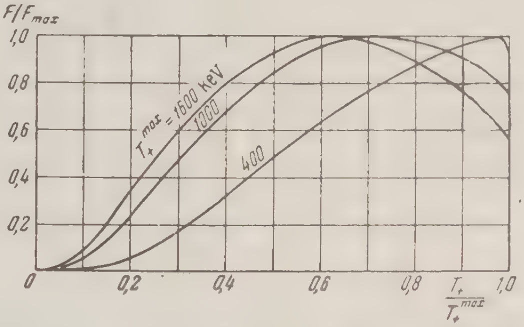

Fig. 5. Dependence of the shape of the positron spectrum on the transition energy with Z = 84.

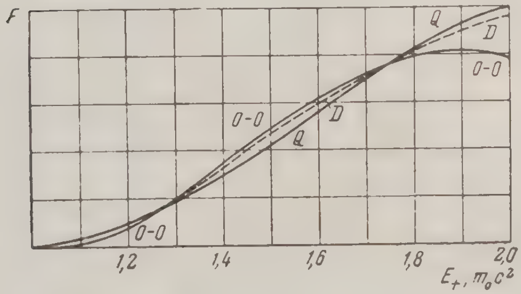

Fig. 6. Shape of the positron spectrum with Z = 84 and $\Delta W =$ $= 3\,m_0c^2$ for a 0—0 transition, and E1 transition (curve D) and an E2 transition (curve Q).

Curves showing the shape of the positron spectra as calculated taking into account finite nuclear size for different values of Z and 0—0 transition energies are shown in Figs. 2, 3, 4 and 5. We note that, in view of the unavailability of satisfactory theoretical data on the shape of positron spectra, in analyses of experimental data it is common to use extrapolations of the curves of Jaeger and Hulme,[1] calculated for one value of Z and one transition energy, for the purpose of obtaining the shape of the spectra for other transition energies. As may be seen from the figures, however, in the case of 0—0 nuclear transitions the spectrum shape is actually strongly dependent on the energy of the transition.

The shapes of the conversion positron spectra with Z = 84 and $\Delta W = 3\,m_0c^2$ for transitions of different multipole orders are juxtaposed in Fig. 6. The curves D and Q are based on the data of Jaeger and Hulme.[1] It will be seen that except at the ends the dependence of the spectrum shape on the multipole order is weak. It must be noted that the curves of Jaeger and Hulme were extrapolated over an appreciable length (the last calculated point is at $1.75\,m_0c^2$).

Areas S under positron spectra in relativistic units

ΔW, keV	Z			
	0	25	49	84
1422	0,104	0,132	0,239	0,946
2022	2,41	2,98	5,29	21,8
2622	13,6	16,5	28,3	103

The areas S under the positron spectra, which are proportional to the total curve formation probability, are listed in the accompanying table.

The data in the table indicate that the validity of the Born approximation for calculating the total pair conversion probability is limited to a much narrower range in the case of 0—0 transitions as compared with transitions of other multipole orders. It is known that the total pair conversion coefficients are determined by the equations of the Born approximation in the case of E1 and E2 transitions within 15-20% even at high values of Z. An explanation of this fact has recently been given by Horton and Phibbs[8] who showed that for continuous spectrum to continuous spectrum transitions the condition for the validity of the first Born approximation is $\left|\frac{\alpha Z}{\beta_{\pm}}\right|^2 \ll 1$ rather than the commonly accepted condition $\left|\frac{\alpha Z}{\beta_{\pm}}\right| \ll 1$ ($\beta_{\pm}$ is the mean velocity of the electron or positron in relativistic units). These authors further assert that this result is valid for the case of 0--0 nuclear transitions as well.

However, as can be seen from Fig. 7, the ratio of the total pair formation probability computed taking into account the nuclear field $W_\pi(Z)$ to the total pair formation probability for the same nucleus calculated in the Born approximation increases so rapidly with increasing Z in the case of 0—0 transitionsthat even at Z = 25 use of the Born approximation leads to larger errors than when the Born approximation is used for the E2 transition with Z = 84 (with the same transition energy).

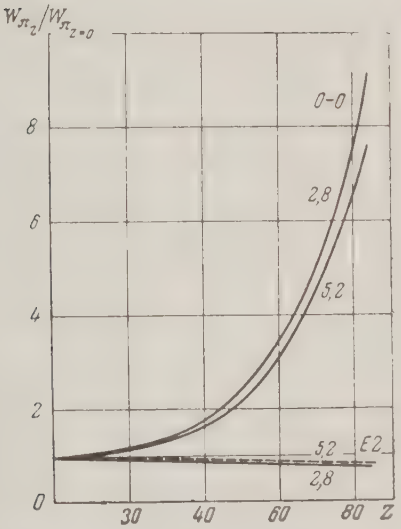

Fig. 7. Ratio of the total pair formation probability, calculated taking into account the nuclear field, to the total pair formation probability calculated in the Born approximation. The figures at the curve give the transition energies in m_oc^2.

In order to find the total conversion pair formation probability we must know the value of $\left|\int_0^R Q_0(r) r^2 dr\right|$. Rough evaluations of the matrix element for the 0--0 transition were carried out by Drell and Rose[9] by comparison with experimental data. On the basis of these evaluations one can write

$$\left|\int_0^R Q_0(r)\, r^2 dr\right| = \frac{1}{24}\,\rho\alpha^{5/2} A^{2/3}, \qquad (5)$$

where A is the mass number of the nucleus, ρ is a dimensionless parameter the numerical value of which, according to Drell and Rose for 0—0 transitions in O^{16}, Ge^{72} and RaC' lies between 1/4 and 1/9.

Accepting this evaluation of equation (5) we obtain for the total pair formation probability in 0—0 transitions

$$W_\pi = \rho^2 \frac{\pi\alpha^6}{144} A^{4/3} S \frac{m_0c^2}{h} \quad \text{sec}^{-1}, \qquad (6)$$

where the value of S should be taken from the accompanying table.

The authors want to express their thanks to B.S.Dzhelepov and L.A.Sliv for a number of valuable suggestions and for discussion of the results.

Physical Scientific Research Institute of
Leningrad State University

References

1. J.Jaeger & H.Hulme, Proc. Roy. Soc., A 148, 708 (1935).
2. M.Wang, Nature, 162, 264 (1948).
3. H.Yukawa & S.Sakata, Proc. Phys.-Math. Soc. Japan, 17, 397 (1935).
4. B.Dzhelepov & L.Zyrianova, Tablitsy po β-raspadu (Tables on β-decay), Pub. Leningrad State Univ. L. 1952.
5. M.Rose, Phys. Rev., 51, 484 (1937).
6. L.Sliv, Zhur. eksp. i teor. fiz., 17, 1049 (1947).
7. A.Sakharov, Thesis, Phys. Inst. USSR Acad. of Sci., M. 1947.
8. G.Horton & E.Phibbs, Phys. Rev., 96, 1066 (1954).
9. S.Drell & M.Rose, Progr. Theor. Phys., 7, 125 (1952).

INTERNAL CONVERSION POSITRONS IN THE SPECTRUM OF RADIOACTIVE Sb^{124}

- B.S.Dzhelepov and O.E.Kraft

1. Description of apparatus

A special magnetic spectrometer has been constructed at Leningrad State University for the purpose of studying weak β-radiation of one charge against a strong background of the opposite charge. In this instrument the β-particles moved along helical paths in an uniform magnetic field and were focused three times: 180° after the source the particles are defined by the first slit behind which the first counter is located; 180° further they pass through a second slit located under the first counter; lastly, after another semi-circle they pass through the third slit behind which the second counter is located. A diagram of the instrument is given in Fig. 1.

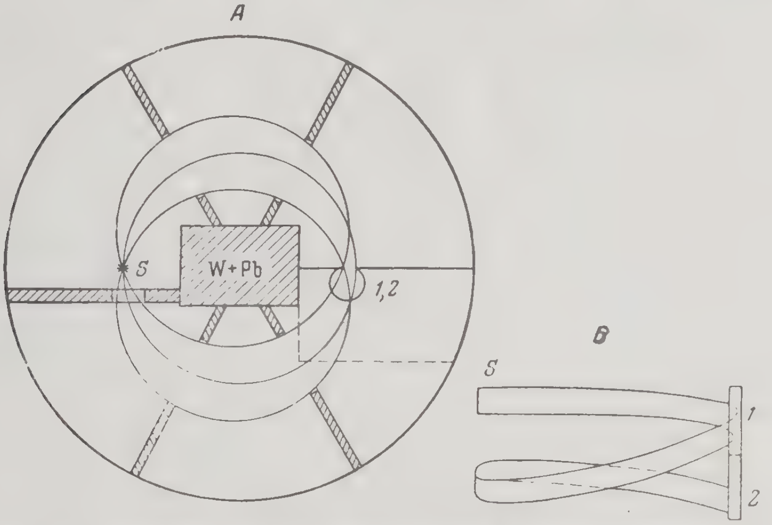

Fig. 1. Diagram of triple-focusing β-spectrometer: A) view from above, B) view of trajectory from the side, 1) first counter, 2) second counter, S) source.

The counters are located one directly under the other and are connected in coincidence. The number of spurious coincidences due to cosmic radiation was 4-6 per hour.

A plate of lead and tungsten is located between the source and the counters to shield the latter from the direct γ-rays. In addition to the above-mentioned slits the instrument has six Plexiglas diaphragms (baffles) whose edges were 1 mm distance from the beam path defined by the slits. There is a "floor" of Plexiglas coated lead between the two sections of the instrument.

The radius of curvature of the instrument is 4.7 cm; the angle of divergence of the beam in the plane perpendicular to the field is 30°; the angle of divergence in the direction of the field is 4°. The solid angle defined by the instrument is $1 \cdot 10^{-2}$ sterad.

The first version of the instrument was constructed by Anton'eva, Shestopalova and Kzhelepov[1] in 1949 who used the spectrometer to investigate the positron spectrum of Br^{80}.

A shortcoming of the first version of the instrument was that it had to be filled with air at a pressure of 10-12 cm Hg. Yet it will be seen that the electron path in the instrument is long: $S = 3\pi\rho = 42$ cm, where ρ is the radius of curvature of particle trajectory. Obviously the trajectories were greatly distorted due to scattering from air.

In a new version of this instrument this shortcoming has been eliminated. The counters have been installed in a chamber separated from the instrument proper by cellophane films 8-10 μ thick; the inside of the instrument is evacuated to $5 \cdot 10^{-2}$ mm Hg.

Even under these conditions the shape of the electronic spectra is reproduced correctly by the instrument only in the region of relatively high energies (>600 kev). Distortion of the spectra in the region of low energies occurs due to scattering of the electrons in the windows of the first counter.

It is obvious that scattering through even a small angle may result in the electrons being deflected out of the beam since the electrons have to travel a large distance ($2\pi\rho \approx 30$ cm) before reaching the second counter. Under conditions of the experiments with Sb^{124} to be described below the deviations from the true shape of the spectrum at 600 kev amounted to not over 5%.

2. Upper limit for the number of positrons in the decay of P^{32}

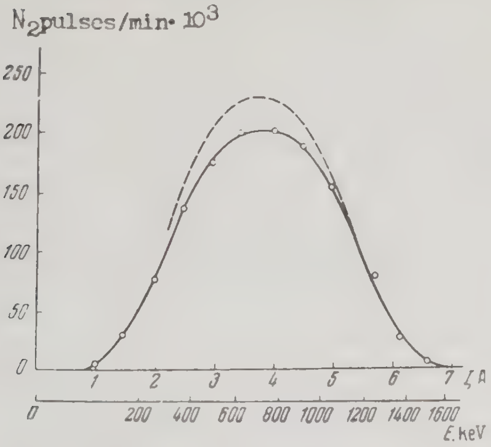

Fig. 2. Electron spectrum of P^{32}: N_2) number of pulses recorded by the second counter per min (background subtracted). Solid line with circles - experimental spectrum. Dash line - shape of spectrum of P^{32} according to Ref. 18.

In the case of our instrument the extent of electron scattering in the instrument is an important factor since the number of main component electrons scattered largely determines the detection threshold for the weak component of opposite charge.

In order to investigate the scattering we undertook a series of experiments with P^{32} (T = 14.3 days) which is a pure electron emitter: the decay sequence in the isobaric chain with mass number 32 is $Si^{32} \rightarrow P^{32} \rightarrow S^{32}$ (Ref. 2). P^{32} emits no γ-rays; the only possible source of positrons is bremsstrahlung in the source material: the β-spectrum of P^{32} has an end-point energy of 1.712 Mev. However, if the source is very thin and contains no heavy nuclei the probability of positron formation is very small. It was established in 1952 that no more than $3 \cdot 10^{-4}$ positrons per disintegration can be formed in the decay of P^{32} (Ref. 3). In 1954 McClure[4] established in experiments with a β-spectrometer having a small radius of curvature that in the 0 to 550 kev energy interval the $N_{e+}/N_{\beta-}$ ratio for P^{32} is less than $8 \cdot 10^{-6}$.

In our experiments we used a P^{32} source having an activity of about 10 mc. The coincidence rates were counted with "negatron" and "positron" fields. The experimental spectrum of P^{32} obtained with negatron fields is shown in Fig. 2; the spectrum obtained with positron fields is shown in Fig. 3. It will be seen that in the case of weak positron fields the number of coincidences falls off with increasing field strength.

The question arises whether despite the unfavorable magnetic field and triple focusing scattered electrons still reach the second counter and produce coincidences? That the answer to this question is negative follows from investigations of the dependence of the counting rate of each of the counters on the intensity of the magnetic field. The counting rate of the first counter falls off with increasing positron field intensity (Fig. 4). This is due to the fact that scattered electrons, which in the presence of a strong positron field are stopped by the "baffles", reach the first counter in the absence of a field or in weak positron fields. The counting rate of second counter remains constant for all values of the positron field.

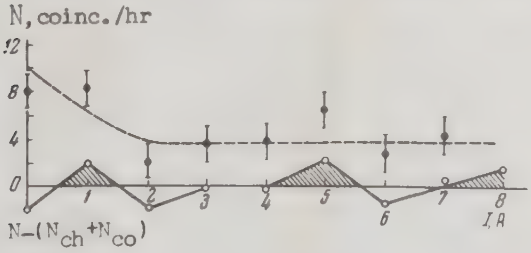

Fig. 3. Results of measurements with P^{32} with positron fields. Solid dots show number of coincidences per hour and the corresponding statistical uncertainties; the dash line shows the variation of the sum $N_{ch}+N_{co}$ computed for the load on both counters with the value of the magnetic field. Open circles indicate the dependence of $N-(N_{ch}+N_{co})$ on the field intensity.

Knowing the number of pulses recorded by the first and second counters and the resolving time of our amplifier ($8 \cdot 10^{-6}$ sec)

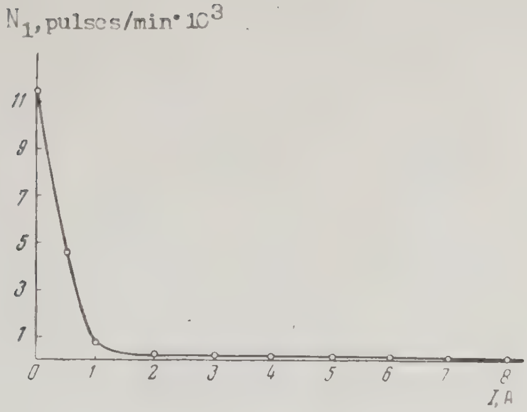

Fig. 4. Variation of the counting rate of the first counter on the intensity of the positron magnetic field.

we could readily evaluate the number of chance coincidences with any magnetic field: the number decreases with increasing field strength. The coincidence rate with any positron field, within the limits of the mean square error equals the sum of the counting rates due to chance and cosmic coincidences, the number of which $(N_{ch}+N_{co})$ is shown by the dash-line in Fig. 3. Thus no positrons were observed in the decay of P^{32}. If we plot the dependence of $N-(N_{ch}+N_{co})$ on the intensity of the field, the area hatched in Fig. 3 may be taken as an index to the statistical accuracy of the measurements. The ratio of this area to the area under the electron spectrum of P^{32} equals $1\cdot10^{-7}$.

It follows from what has been said above 1) that the number of positrons in the radiation from P^{32} is less than $1\cdot10^{-7}$ per disintegration and 2) that for sources having a spectrum of the P^{32} type and not emitting γ-rays the number of electrons scattered in our instrument in positron fields amounts to less than $1\cdot10^{-7}$ per disintegration.

3. Upper limit of the number of positrons per disintegration of Ir^{192}

For what follows it is important to clarify the possibility of detecting positrons in the radiation of sources emitting γ-rays. To this end we investigated the radioactive isotope Ir^{192}.

In addition to β^--decay there is evidence of orbital electron capture in Ir^{192}; β^+-decay has not been detected. The β-spectrum of this isotope comprises a large number of lines, all having energies under 1 Mev. The 1080 and 1910 kev lines are very weak.[5,6] Hence the number of pair-conversion positrons must be very small. Measurements of the number of coincidences with positron fields, similar to the described measurements with P^{32}, yielded an upper limit for the number of positrons or scattered electrons of $1\cdot10^{-6}$ per disintegration. It is difficult to lower this limit since in the case of Ir^{192} the γ-rays impose rather heavy loads on the counters and consequently an appreciable number of chance coincidences occurs.

4. Experiments with Sb^{124}

After preliminary tests of the instrument we investigated the radioactive isotope Sb^{124}; this isotope has a complex decay scheme, a complex electronic spectrum and γ-lines of different energies. It has been studied by many investigators.

We are interested in the possible existence of positrons in the radiation from this isotope. Direct positron decay of Sb^{124} is apparently impossible. Although Sb^{124} has two stable isobars Sn^{124} and Te^{124} and there must consequently occur a $Sb^{124}\to Sn^{124}$ transition the mass difference between Sb^{124} and Sn^{124} is less than $2m_oc^2$ (Ref. 7). Hence the only possible source of positrons in the radiation from Sb^{124} is pair conversion of γ-rays: the γ-spectrum of Sb^{124} includes several lines with $h\nu > 2m_oc^2$.

In 1947 Barber[8] carried out a search for positrons in the decay of a number of radioactive isotopes by means of the "trochoidal" method. Among others he investigated Sb^{124}; no positrons from this isotope were observed. Barber indicates that the upper limit for the ratio of the number of positrons to electrons is

$$N_{e+}/N_{\beta-} < 5\cdot10^{-3}.$$

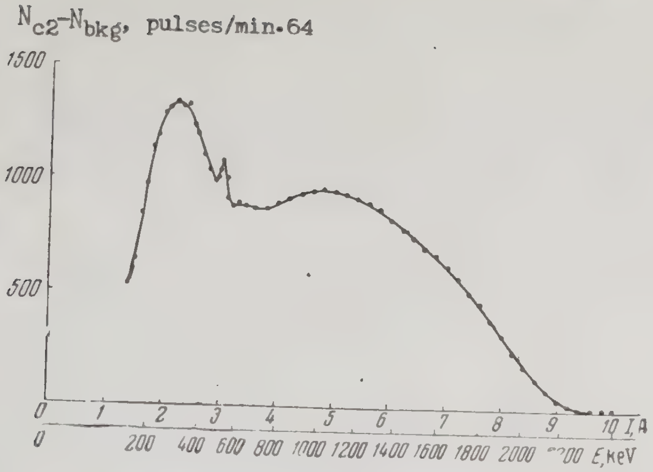

Fig. 5. Experimental β^--spectrum of Sb^{124}.

Nor were any positrons detected in the investigation of Langer et al[9].

We prepared a radioactive antimony source 13 mg/cm^2 in thickness on a Plexiglas backing. The width of the source was 2 mm; the length 12 mm.

The results of our measurements are shown in Figs. 5 and 6. Fig. 5 shows the experimental electron spectrum. The horizontal axis is scaled in current values; the vertical axis in the number of pulses recorded by the second counter with the background subtracted. It was impossible to study the electron spectrum by the coincidence method since the load on the first counter with negatron fields was very high ($>10^6$ pulses/min). The positron spectrum of Sb^{124} is reproduced in Fig. 6. Here the vertical scale is graduated in coincidences per minute; the horizontal scale, as before, in current values and in equivalent energy values. Two positron groups are clearly discernible. The positron spectrum after processing (subtracting background, reduction to uniform energy intervals and corrections for absorption) is shown in Fig. 7 (points and solid line).

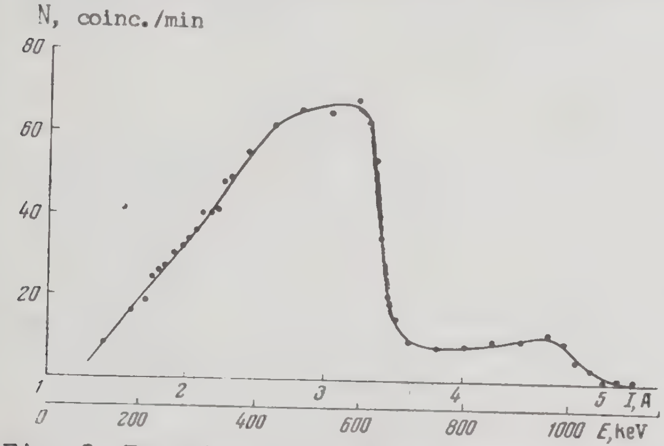

Fig. 6. Experimental internal conversion positron spectrum of Sb^{124} (background subtracted).

The number N_o of coincidences recorded at each value of the positron field was the sum of

1) N_{true} - the number of true coincidences due to positrons of the conversion pairs;

2) N_{ch} - the number of chance coincidences, dependent on the loads on the counters and the resolution of our amplifier;

3) N_{co} - the number of coincidences due to cosmic radiation;

4) N_{pe} - the number of coincidences caused by electrons, knocked out in the vicinity of the second counter and recorded by it, penetrating into the first counter (the positron field is favorable for such electrons).

Thus, we have

$$N_{true} = N_o - (N_{ch}+N_{co}+N_{pe}).$$

N_{ch} can be calculated from the loading and resolving time of the amplifier while N_{co} can be measured by direct experiments with the source removed. In order to determine N_{pe} a shutter was installed in the path of the electron beam immedately after the first diaphragm. This shutter could be opened or closed without disturbing the vacuum in the instrument. We measured the number N' of coincidences with the shutter closed for each value of the positron field:

$$N' = N'_{ch}+N_{co}+N_{pe}.$$

We found $N'_{ch} < N_{ch}$, since with the shutter closed the load on the counters, particularly that on the first, is smaller. However, knowing the load on and the revolv-

ing time of the amplifier we could compute N'_{ch}. It was found that N' and ($N'_{ch}+$ $+N_{co}$) are virtually equal. Hence we assumed that N_{pe} was negligibly small and took

$$N_{true} = N_o - (N_{ch} + N_{co}).$$

The end-point energies of the observed positron groups proved to be 665 ± 20 kev and 1080 ± 50 kev. The spectrum shape and energy values of the positron groups indicate that this positron activity is due to internal conversion of the 1691 and 2088 kev γ-rays from Sb^{124}.

In order to make sure that the observed spectrum is not produced by some spurious side effect, as, for example external pair production, we carried out the following control experiment.

A shutter of Plexiglas was installed in the positron beam near the source. If the observed positron spectrum were due to pair formation somewhere near but outside the source, the spectrum should have persisted under these conditions (i.e., with the Plexiglas shield in place). Measurements showed, however, that the number of coincidences at each field value corresponded to the number of chance coincidences for the given counter loading. Therefore, external conversion in the source proper can be disregarded. It can be safely asserted that the observed positrons are created in the process of internal conversion with pair formation.

5. Determination of the internal pair conversion coefficients

In order to determine the internal pair conversion coefficient $\alpha_p = N_{e+}/N_\gamma$ we must know 1) the ratio of the areas under the positron and electron spectra: $N_{e+}/N_{\beta-}$ and 2) the number of photons per disintegration for the investigated line: $N_\gamma/N_{\beta-}$.

Value of $N_{e+}/N_{\beta-}$. As noted above, our instrument rendered the spectra correctly only in the hard region. Appreciable distortion occurs in the region of low energies due to the use of thick sources and electron scattering in the windows of the first counter. The distortion differs for different counter window films and for sources of different thickness, and even strictly speaking, for spectra of different shape and end-point energy. In order to determine the deviations from the true spectrum shape introduced by the instrument in the low energy region we must in each case compare our spectrum with the spectrum obtained under conditions close to the ideal. We did this for the electron spectrum of Sb^{124}. We compared our Sb^{124} spectrum with the spectrum obtained by A.V.Zolotavin[10] on a double-focusing β-spectrometer. In Fig. 8 our spectrum obtained by means of the second counter is indicated by the solid dots, while the solid line is the spectrum found by Zolotavin.

It will be seen that at high energies ($>$500 kev) the curves coincide, while at energies below 500 kev they diverge. Reducing the β-spectrum of Sb^{124} to its true shape increases the area under the contour by a factor of 1.4. Strictly speaking we should have reduced to its true shape the β^--spectrum of Sb^{124} recorded under the same conditions as the e^+-spectrum of the isotope, i.e., a β^--spectrum recorded by the method of coincidences and at approximately the same counting rates as the e^+-spectrum. This could have been achieved by waiting a sufficient length of time after measurement of the positron spectrum. However, since Sb^{124} has a long half-life ($T \approx 60$ days) this was not expedient. Hence measurements of β^--spectrum of Sb^{124} were carried out using only the second counter with the first counter switched off.

Control experiments showed that the second counter usually records about 5% more pulses than the coincidence circuit (due to "coincidence circuit misses"). Misses of the second counter also did not exceed 5% at the peak counting rate of 80,000 pulses/min. Appropriate corrections were made in the recorded β^--spectrum of Sb^{124}.

As may be seen from the experimental curve the positron spectrum of Sb^{124} separates readily into two components. The positrons of energy above 700 kev are associated with the 2088 kev γ-line. Judging from the β^--spectrum, at $E > 700$ kev,

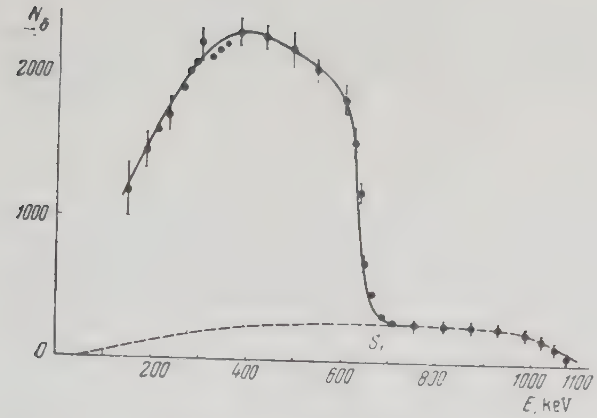

Fig. 7. Internal conversion positron spectrum of Sb^{124}. The points are experimental values with the corresponding uncertainties. The dash-line is the theoretical positron spectrum for the 2070 kev γ-transition in the case of a 0--0 transition (computed taking account of the resolution of the instrument).

the positron spectrum is not distorted by radiation loss and scattering. In order to determine the shape of the curve in the region of low energies we utilized theoretical data on the shape of the positron spectrum.

Zyrianova and Krutov[11] give a calculation for the shape of the internal pair-conversion positron spectrum taking into account the coulomb nuclear field and finite nuclear size for Z = 49. These calculations were carried out for the 0—0 transition. The transitions we are dealing with may be of a different type. However, the shape of the internal conversion positron spectrum is determined primarily by the statistical factor and the influence of the electrostatic fields, and is only weakly dependent - near the boundary - on the type of the transition. Hence, in the first approximation, we can justifiably compare our positron spectrum with the spectrum of Zyrianova and Krutov.

In Fig. 7 the experimental positron is represented by the solid dots; the theoretical spectrum associated with the 2088 kev γ-line taking into account the resolution of the instrument (line half-width - 7%) by the dash line. It will be seen that both spectra are in good agreement over the range from 700 to 1050 kev.

By extrapolating our hard positron spectrum into the region of low energies in conformity with the shape of the theoretical spectrum, we can determine the energy under the contour (S_1 in Fig. 7). The ratio of this area to the area under the electron spectrum was calculated to be

$$(N_{e+}/N_{\beta-})_{2088} = 3.96\cdot 10^{-5}.$$

Let us examine the section of the positron spectrum from 450 to 665 kev. Judging by the γ-ray spectrum given by Gromov et al,[12] positrons of such energies are created wholly at the expense of the intensity of the 1690 kev γ-line. However, before attempting comparison with theory we must correct the experimental spectrum for the distortion due to scattering and bremsstrahlung and subtract the contribution of the positrons from the 2088 kev γ-quanta.

It may be assumed that the relative distortion of the ordinates of the positron spectrum is the same as that of the corresponding ordinates of the electron spectrum; hence the correction factor can be found by comparing the ordinates of the two curves in Fig. 8. In the energy interval in question the factor differs from unity by less than 20%.

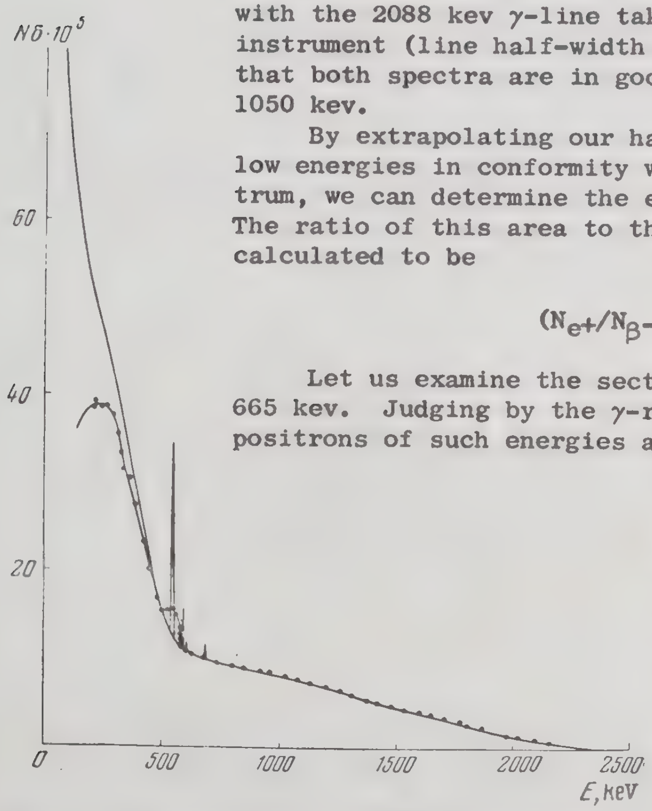

Fig. 8. β^--spectrum of Sb^{124}. The experimental errors lie within the dimensions of the solid points.

After introduction of these corrections, the section of the spectrum was fitted to the theoretical spectrum of Zyrianova and Krutov (Fig. 9). Extrapolating the theoretical spectrum into the region of low energies and comparing its area with the area under the β^--spectrum we found

$$(N_{e^+}/N_{\beta^-})_{1690} = 1.85 \cdot 10^{-4}.$$

It must be noted that after subtraction of the two spectra assigned to the 1690 and 2088 kev lines from the experimental spectrum there remains a number of positrons that appreciably exceeds the experimental error: $0.3 \cdot 10^{-4}$ per disintegration. Part of these positrons may belong to pairs from the γ-lines of energies from 1022 to 1690 kev. According to Gromov et al[12] there are two lines in this interval, having energies of 1047 and 1347 kev, with an intensity of 0.12 quanta per decay. According to Zolotavin et al[13] there are five γ-lines in this interval (1047, 1298, 1326, 1361 and 1370 kev with a total intensity of 0.07 quanta per decay). In either case even if the transitions are E1 the number of positrons produced should not exceed $0.2 \cdot 10^{-4}$ per decay. It appears impossible to explain fully the observed excess of positrons at present.

Value of N_γ/N_{β^-}. The number of γ-quanta of energies 1690 and 2088 kev per decay event in Sb^{124} can be found from a comparison of a) the data on the relative γ-line intensities given in Ref. 12 and b) data on the number of quanta per decay for some one γ-line of Sb^{124}. The ratios of the numbers of quanta per decay for the lines according to Ref. 12 are

$$N_{603} : N_{1690} : N_{2088} = 100 : 65 : 6.5.$$

The most intense line in the spectrum of Sb^{124} is the 603 kev line. The absolute number of 603 kev quanta per decay according to the scheme given by Gromov et al in 1952 is 0.840. In more recent investigations (Refs. 14 & 15) it is shown that 100% of the decays of Sb^{124} pass through the 603 kev level of Te^{124}. The numbers of 1690 and 2088 kev γ-quanta per decay (i.e., the N_γ/N_{β^-} ratios) according to these investigations are 0.65 and 0.065. Accepting the values of N_{e^+}/N_{β^-} and N_γ/N_{β^-} given above we obtain the following pair conversion coefficients:

E, kev	Experimental values of α_π	Transition
1690	$(2.8 \pm 0.7) \cdot 10^{-4}$	E1
2088	$(6.1 \pm 1.8) \cdot 10^{-4}$	E1

If we accept for N_γ/N_{β^-} the values obtained by Zolotavin et al[13], we obtain the following values for the pair conversion coefficients:

E, kev	Experimental values of α_π	Transition
1690	$(3.8 \pm 1.2) \cdot 10^{-4}$	E1
2088	$(5.7 \pm 1.8) \cdot 10^{-4}$	E1

The results of relativistic calculations of internal pair conversion for electric dipole and quadrupole transitions with $Z = 84$ carried out by Jaeger and Hulme[16] for a pure coulomb nuclear field without taking screening into account are shown in Fig. 10. In the same figure we have plotted the pair conversion coefficient curves for electric dipole and quadrupole and magnetic dipole transitions calculated by Berestetski and Shmushkevich[17] in the Born approximation which is valid for small values of Z. It may be assumed that the true curves for $Z = 52$ lie somewhere in the hatched regions. As may be seen in Fig. 10, the experimental values of α_π come closest to the theoretical ones for an E1 transition.

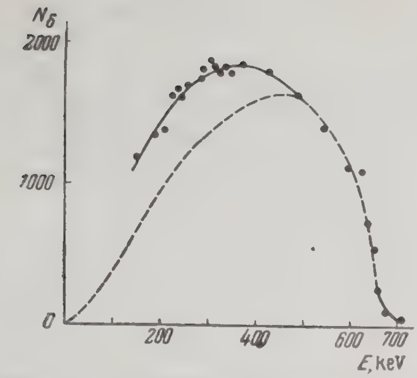

Fig. 9. Internal conversion positron spectrum associated with the 1690 kev γ-line. Solid line with points - experimental data; dash-line - theoretical shape of internal conversion positron spectrum for a 0—0 transition (resolution of instrument taken into account).

The greatest error in determining the pair conversion coefficients of the 1690 and 2088 kev transitions is due to inaccuracies in determining the total number of β^--particles: the shape of the β^--spectrum is such that there are many slow β^--particles, while the conditions of recording them in our experiments are unfavorable. On the other hand there are comparatively few slow particles in the positron spectrum and the error in determining the ratio of the number of positrons from the different lines must be appreciably smaller.

From our experiments it follows that

$$N_{e^+_{1699}}/N_{e^+_{2088}} = 4.7 \pm 0.8.$$

If the 1690 kev transition is really an E1 transition, as follows from our experiments and the measurements of the internal conversion coefficients carried out by Zolotavin et al[13], the 2088 kev transition must also be E1. This can readily be seen from Fig. 10: if the ordinates of all the points are multiplied by an appropriate factor so as to bring the 1690 kev experimental point to the theoretical curve for E1, the ordinate of the point corresponding to 2088 kev will also fall in the region of the curves for the E1 transition within the limits of the experimental error. It may be noted that such processing of the results will reduce the error connected with the 2088 kev γ-line.

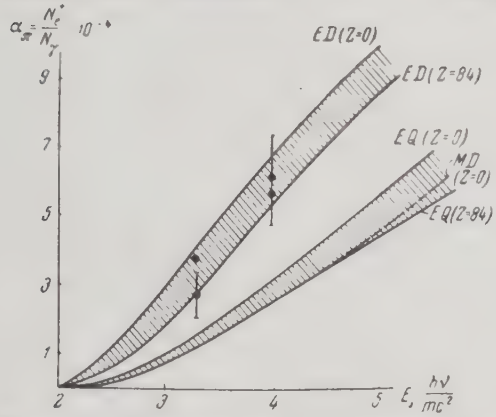

Fig. 10. Theoretical curves for the energy dependence of the internal pair conversion coefficients. Points — experimental values of the coefficients of pair conversion for the γ-transitions of Sb^{124}. Solid circles — values of α_π obtained using the N_γ/N_{β^-} ratios from Ref. 12; open circles sic — values of α_π obtained using the N_γ/N_{β^-} ratios from Ref. 13.

The authors desire to express their thanks to A.K. Gruden' who participated in the work.

Physical Scientific Research Institute of Leningrad State University

References

1. N.Anton'eva, B.Dzhelepov & S. Shestopalova, Doklady AN SSSR, 64, 309 (1949).
2. M.Lindner, Phys. Rev. 91, 642 (1953)
3. G.Groetzinger & F.Ribe, Phys. Rev. 87, 1003 (1952).
4. G.McClure, Phys. Rev., 94, 1637 (1954).
5. M.Johns, S.Nablo, Phys. Rev., 96, 1599 (1954).
6. R.Pringle, W.Turchinetz & H.Taylor, Phys. Rev., 95, 115 (1954).
7. N.Wall, Nucl. Sci. Abs., A6, 203 (1954).
8. W.Barber, Phys. Rev., 72, 1156 (1947).
9. L.Langer, R.Moffat & H.Price, Phys. Rev., 79, 808 (1950).
10. A.Zolotavin, Izv. AN SSSR, Ser. fiz., 18, 127 (1954).
11. A.Zyrianova & V.Krutov, See present issue of Bulletin.

12. K.Gromov, B.Dzhelepov, et al, Doklady AN SSSR, 86, 255 (1952).
13. A.Zolotavin, E.Grigo'ev & M.Abroian, present issure of Bulletin.
14. N.Lazar, Phys. Rev., 95, 292 (1954).
15. D.Lu, W.Kelly & M.Weidenbeck, Phys. Rev., 95, 1533 (1954).
16. J.Jaeger & H.Hulme, Proc. Roy. Soc., A148, 708 (1935).
17. B.Berestetski & I.Shmushkevich, Zhur. eksp. i teor. fiz., 20, 574 (1950).
18. N.Anton'eva, A.Bashilov, B.Dzelepov & V.Orlov, Izv. AN SSSR, Ser. Fiz., 18, 93 (1954).

THE ELOTRON - A MAGNETIC γ-SPECTROMETER WITH IMPROVED FOCUSING

-B.S.Dzhelepov and S.Z.Shestopalova

Introduction

In recent years the γ-spectra of various radioactive substances have been successfully investigated by magnetic analysis of the Compton recoil electrons knocked out of a thin layer of light matter by the γ-rays.

The advantages of this method over other methods of γ-spectrometry such as the scintillation method, for example, are 1) the possibility of attaining a high resolution, 2) the possibility of separating the effects connected with different γ-lines, 3) the possibility of precise calculation of the shape of the spectrum line as well as of the spectral response and other basic characteristics of the spectrometer.

The greatest number of γ-spectra has been investigated by means of the Ritron γ-spectrometer of the Radium Institute of the USSR Academy of Sciences.[1] In this instrument the width at half-height of lines in the 1 Mev region is about 5.5%.

However, in γ-spectra there are frequently encountered lines which differ from each other by less than 10% as regards energy. Such lines cannot be fully resolved even with an instrument resolution greater than 5.5% due to the asymmetric shape of the lines. This reduces the accuracy in determining the relative intensities of close lines. Hence where investigation of γ-spectra is concerned there is an urgent need for increasing the resolving power of spectrometers.

The width of the spectrum lines observed on the Ritron is determined by:

1) inaccurate focusing of the electrons both at the first and the second slits;
2) the geometric dimensions of the slits;
3) scattering and bremsstrahlung of Compton electrons in the target;
4) scattering and bremsstrahlung of electrons in the gas filling the instrument.

It is impossible to eliminate fully the causes of line broadening without changing the principle of operation of the instrument.

Thus, for example, reducing the pressure of the helium filling the instrument to below 30 cm Hg, we decrease the efficiency of the counter system, while at pressures below 5 cm Hg helium-filled counters stop operating entirely.

If the instrument is entirely evacuated a thicker window must be installed over the first counter which results in further broadening of the lines. Scattering and bremsstrahlung in the target can be reduced by using a thinner target but this reduces the coincidence counting rate. The same thing occurs when the slit width is reduced. Experiments showed that as the slit is made narrower the transmission factor of the instrument falls off very rapidly, while the line width decreases comparatively slowly.

However, even at the cost of a great reduction of the transmission factor one cannot make the Ritron spectrum lines very narrow since from a certain point reduction of the radiator thickness, narrowing of the slit and reduction of the gas pressure no longer narrow the line; the attainable narrowing is limited by the inaccurate focusing of the electron beam in the first and second slits of the Ritron. Thus in the Ritron the width of the focus at both the slits is about 1.7 mm and hence there is no advantage in making the slits narrower than 2 mm.

It follows from the above that in order to realize a high resolution instrument it is necessary to improve the focusing of the electron beam.

1. The Elotron

The focusing of the electron beam before the first slit can be enhanced either by using an inhomogeneous field or by curving the target in an appropriate manner. The focusing of the beam between the slits can be enhanced only through the use of an inhomogeneous magnetic field.

In 1953 Dzhelepov, Zhukovski et al[2] published descriptions of two γ-spectro-

meters in which the focusing before the first slit was improved by curving the target while the focusing between the slits was improved by using a magnetic field falling off in intensity along one Cartesian coordinate (a "Ketron" field). Choice of this method of improving the focusing was dictated by the fact that the only magnet available for the work at that time was a C-shaped one with rectangular cross section polepieces. This determined the type of focusing field used and the necessity of employing a curved target. Given a choice of magnets, of course, other variants are possible: one can for example, construct a spectrometer with a field falling off along the radius and employing a flat target.

Below we shall describe a spectrometer constructed in the VNIIM (All-Union Scientific Research Institute of Metrology).

Magnetic field. The magnetic field is produced by an electromagnet with polepieces measuring 320 x 280 mm and a gap of 143 mm.

Current for the magnet windings is supplied by a special storage battery. The current is measured and monitored to within 0.01% by the compensation method by means of a PV-6 potentiometer and a GPZ-2 galvanometer. The light spot of the galvanometer is displaced one division on the scale when the current value changes by 0.02% from the set value.

The current value is set by means of a regulating device designed by Karamian and fabricated by the "Etalon" plant.

The magnetic field intensities were measured by means of a ballistic galvanometer and flip coil. During the measurements the sensitivity of the system was checked by means of a standard inductance.

The calculation of the topography of a magnetic field necessary for precise focusing of a plane beam was carried out by Pavinski in connection with the construction of the Ketron.[3] In order to obtain the specified theoretical distribution of the magnetic field the polepieces of the magnet must be machined to a special shape which depends to an appreciable extent on the design characteristics of the magnet.

In view of the fact that in our magnet the gap between the polepieces is rather large (143 mm), the field becomes inhomogeneous at a distance of only about 100 mm in from the edge of the pole pieces: the intensity of the field begins to fall off towards the edges from this point. The weakening of the field is such that the experimental curve falls off less steeply than the theoretical one (for $\rho = 6.5$ cm) and it is impossible to make the two curves match perfectly. It proved possible, however, by shifting the instrument to obtain an experimental distribution in which the difference between the ordinates at no point exceeded 5% of the field intensity value.

This is the best that could be realized without altering the shape of the polepieces but the quality of the focusing obtained in this case is not high. Since the experimental curve falls off less steeply than the theoretical one, filing down the edges of the polepieces in the Ketron would only increase the divergence between the two curves. It was necessary to take other measures to make the experimental curve fall off more steeply at the gap edges.

We achieved this by means of steel insets applied to the polepieces; the most advantageous shape and location of these were determined experimentally by successive changes in shape and magnetic field topography surveys.

Since the clearance between the cover of the instrument and the polepieces is small it is impossible to attach the insets directly to the polepieces. Hence they were located inside the instrument. However in this case it was difficult to effect the field measurements. In order to be able to study the field topography we substituted brass plates 5 mm thick for the bottom and cover of the instrument. Despite many repeated tests we did not succeed in obtaining for $\rho = 6.5$ cm and a 143 mm gap the sharp bend in the field curve called for by the theoretical one. The best agreement with the theoretical curve was obtained with insets having the forms, sizes and locations shown in Fig. 1. The results of measurements of the field in the central plane are shown in Fig. 2, in which the theoretical curve is

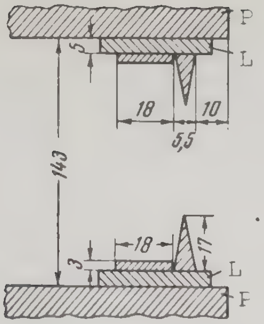

Fig. 1. Shape, size and location of the steel insets by means of which the best agreement was obtained between the experimental and theoretical field distribution curves: P - polepiece of magnet, L - brass plates simulating the bottom and cover of the spectrometer.

shown for comparison. The falling off of the field begins some 5 mm further in the gap than is required by theory but after that point the slopes of the experimental and theoretical curves are very close. The maximum deviation of the experimental field intensity from the theoretical with this arrangement does not exceed ± 1%.

If the actual (experimental) field fails to coincide over any interval with the design (theoretical) field, obviously precise focusing of the flat beam will not be obtained. The quality of focusing or, in other words, the degree of smearing out of the point focus was checked graphically for two positions of the instrument relative to the polepieces. The plot showed that in one of the positions (the one in which the instrument was shifted 5 mm into the region of the inhomogeneous field) the focusing of the beam was such that the width of the focus equalled 0.5 ± 0.1 mm.

It is entirely possible that some other close position (within 1 mm of the above) might have proved to be somewhat more favorable for focusing in the central plane. What is of practical interest, however, is the focusing of the entire steric electron beam and this defies calculation so far. Hence the most favorable location of the instrument in the magnetic field must be sought experimentally by observing a γ-line of known energy with the instrument in different positions.

All the above described results were based on field measurements in the central plane along the line Oy (Fig. 3). However, the field proves to be slightly inhomogeneous in the perpendicular direction as well: there is a noticeable edge effect, i.e., the field falls off towards the edges of the magnet. The maximum weakening of the field, amounting to 1.5% is observed at the points most remote from the center of symmetry line: points a and b in Fig. 3. The quality of focusing was investigated by the semi-analytic method which is a generalization of the Hartree method.[4] According to our calculations the width of the focus equalled 0.35 mm. This result indicates that taking into account the weakening of the field at the edges of the magnet does not lead to any substantial additional smearing-out of the focus.

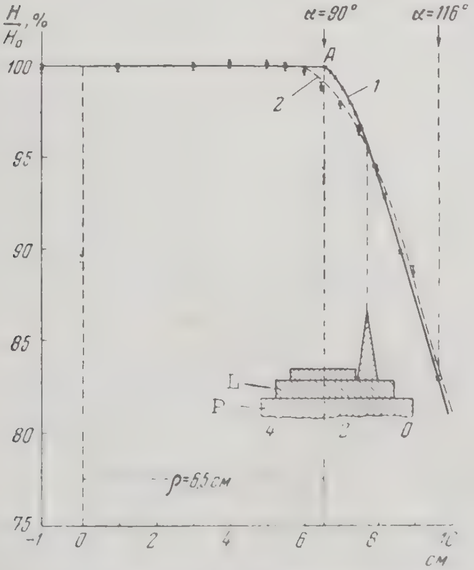

Fig. 2. Results of measurements of the field intensity in the central plane: 1) theoretical data; 2) experimental data.

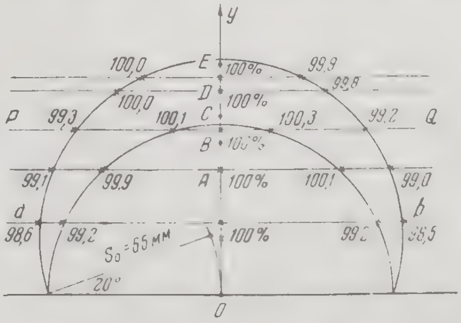

Fig. 3. Results of measurements of the magnetic field intensity along the particle trajectory. Intensity value at the Oy taken as 100%.

The independence of the configuration of the magnetic field on the absolute

value of its intensity was checked by investigating the topography of the field with a current of 1 amp and 2.5 amps through the magnet windings (these values correspond to E_γ = 1715 and 2542 kev, respectively). Within the limits of the measurement error the topography of the field remained constant.

The field intensities 5 mm above and below the central plane proved to be identical with the intensity in the central plane within the limits of the measurement error. At a distance of 15 mm from the central plane the field proved to be symmetric relative to this plane within 0.8% but did not at all points equal the field in the central plane. The greatest rise in the field value was observed near the boundary between the homogeneous and inhomogeneous regions and amounted to 2-3%. Theory predicts an increase in the value of the normal component of the field in going away from the plane of symmetry.[5] In our instrument the heights of the first and second slits are 11 and 15 mm respectively. Therefore, the particle trajectories passing through these slits are never over 7 mm from the central plane. Hence it may be assumed that the electrons travelling along the extreme side paths are also satisfactorily focused; more accurate calculations as regards this are desirable.

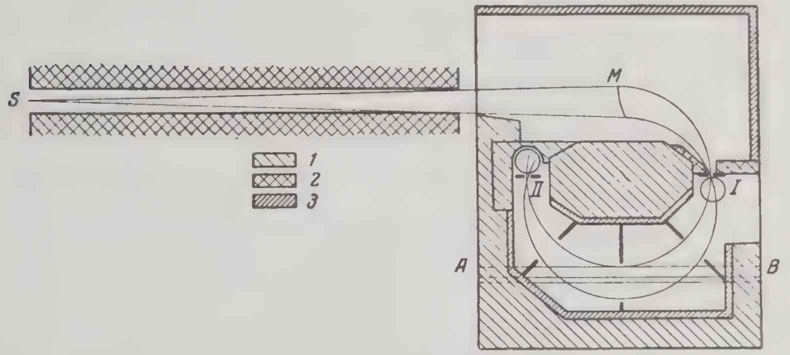

Fig. 4. Cross sectional view of instrument: S) source, M) curved target, I and II) counters. The field above the line AB is homogeneous; below this line the field falls off according to the law deduced by Pavinski[3] 1) tungsten covered with lead, 2) lead, 3) Plexiglas.

Instrument. A cross sectional view of the instrument in the plane of symmetry of the magnetic field is shown in Fig. 4. The spectrometer consists essentially of a brass box 22 x 27 x 14 cm with 10 mm thick walls. Along the path of the γ-ray beam near the entry slit the instrument wall is milled down to 1 mm.

The cover of the instrument is removable. The vacuum seal is provided for by a rubber gasket and plasteline sealant. The counters are mounted on a special stand. The beam is defined by diaphragms located in front of the counters. The width and height of the slits are changed by replacing the metal plates in which the slits are cut. The slit plates are slipped into special grooves in frames m mounted in front of the counters. The distance between the outer edges of the slits is 13 cm. In the interval between the first and second slits there are three radial diaphragms (baffles) of plexiglas 4 mm thick installed at angles of 45, 90 and 135° to the principal focal axis. These diaphragms prevent scattered electrons and electrons of extraneous energies from reaching the second counter. In order to obviate possible scattering, their edges are located 2 mm away from the beam, i.e., they are not defining diaphragms. The diaphragms and the protective shielding plates are fastened to the bottom of the instrument.

Counters. The Compton recoil electrons are recorded by 2 GM counters connected in coincidence. The diameter of each counter is 8 mm, the working length 80 mm. The windows of the first counter were covered with cellophane films about 3 μ thick; the window of the second counter was covered with a 17 μ thick film.

The counters and the instrument chamber are maintained at the same pressure. During the test measurements the instrument was filled with pure helium at pressures ranging from 380 to 120 mm HG. In investigating the γ-spectrum of RaC the instrument was filled with a mixture of helium and methane in the following proportions: He - 165 mm HG and CH_4 - 5 mm HG. The threshold voltage in this case was ~750 v.

During the course of the measurements the operation of the counters was systematically checked. The pulse height was maintained constant by appropriate adjustment of the voltage on the counters. The filament current for the counters was supplied by dry cells. The body of the instrument and counter envelopes were grounded.

Amplifier. The counter pulses were recorded by means of a Rossi coincidence circuit. The resolving time of the circuit was $3 \cdot 10^{-5}$ sec. This was determined by measuring the number of chance coincidences with independent loads on the counters.

Collimator and shielding plates. To shield the counters from the direct γ-radiation from the source, the latter was mounted in a collimator consisting of a 300 mm long lead block with a rectangular cross section channel. This length insures good shielding of the counters from the direct γ-radiation. Thus, for example, with a 4 g Ra sample in the collimator the load on the first counter amounted to 470 ± 13 pulses/min, that on the second - 1510 ± 16 pulses/min. In the case of softer radiation the loads were much smaller. For example with a Cs^{137} source (1.7 curie) the load on the second counter was only 50 pulses/min. In the course of the experiments we used two different collimators. The first, used in the preliminary tests, had entrance and exit apertures of different size: 8 x 6 mm and 15 x 12 mm. The second which was used in measurements of the γ-spectra of RaC, Cs^{137} and Zn^{65} the dimensions of the apertures were equal (height 12 mm, width 15 mm).

In addition to this external shielding, plates of lead sheathed tungsten and of lead were installed inside the instrument chamber. To minimize electron scattering the plates were covered with a 4 mm thickness of Plexiglas.

Target. The target in our experiments was a curved cellophane film. In preliminary investigations the thickness of the film was varied from 5 to 100 μ. In the main measurements (RaC, Cs^{137} and Zn^{65}) the thickness of the target was 35 μ; tests showed that this was close to the optimum thickness for γ-rays of energies above 1 Mev. The target was 21 mm wide and 12 mm high.

The following equation was used to calculate the shape of the target:[6]

$$(x+1)^2 + (1-y)^2 = 2\,\frac{x(L+1) + y + L}{\sqrt{x^2 + (L+y)^2 + z^2}}\,, \qquad (1)$$

where x and y are coordinates of points on the target in the plane perpendicular to the magnetic field and z is the coordinate in the direction of the magnetic field, reckoned from the central plane; L is the distance from the source to the center of the target. All the variables are measured in terms of the radius of curvature ρ.

Calculations using the equation (1) indicate that the shape of the target is closely approximated by a cylindrical surface formed by a generatrix parallel to the z axis. This obviously facilitates forming the target.

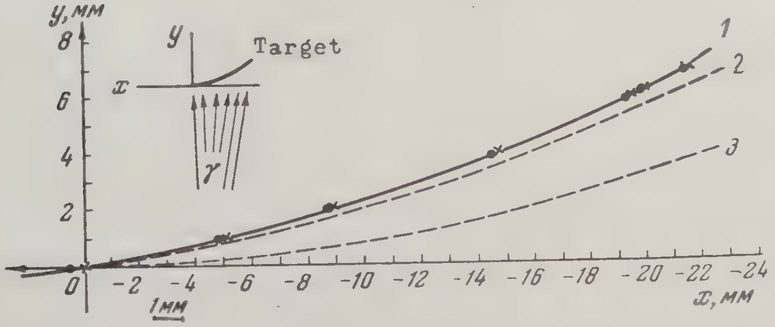

Fig. 5. Results of calculations for the shape of the target according to equation (1) for: 1) L = 41 cm, 2) L = 51 cm, 3) L = ∞, ×) z = ±1 cm, ●) z = ±2cm.

Our target was curved in conformity with a value of L = 41 cm (Fig. 5, curve 1).

The investigated γ-ray sources were obviously not point sources: the value of L differs for different points on the source. Thus, for example, in the experiments with RaC, L ranged from 44 to 57 cm. Hence it was important to determine to what extent the shape of the target is sensitive to

the value of L.

The results of calculations of the target shape for L = 51 cm are shown by curve 2 in Fig. 5. The fact that curves 1 and 2 almost coincide (the maximum divergence at x = -22 mm is 0.7 mm) is very important; the curves show that it is possible to use sources having a length of up to 10 cm without significant sacrifice of the resolution. Experiments with a Co^{60} source confirmed this.

The target was cemented to a Plexiglas frame of sufficiently large dimensions to be wholly outside the collimated γ-ray beam. The upper and lower members of the frame were shaped in conformity with curve 1 of Fig. 5 at z = 0. When cemented to this frame the film acquired the necessary curvature for proper focussing of the electrons. The frame was mounted on a slider by means of which it could be withdrawn from the beam. The target could be positioned with an accuracy of within ± 0.5 mm by means of an indicator located on the wall of the instrument.

2. Investigation of certain characteristics of the Elotron

An important characteristic of any spectrometer is the ratio between the resolution and the transmission. This ratio depends on many parameters and is not easily determined.

We had two problems in mind in testing the Elotron: 1) to determine the best resolution at which it would be possible to investigate sources having an activity of about 1 curie and 2) to realize conditions under which the instrument would have a maximum transmission factor without undue sacrifice of resolution.

It was necessary to carry out several series of experiments to this end; these are described below.

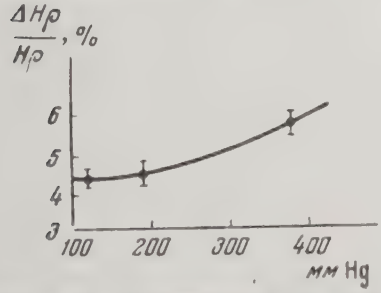

Fig. 6. Dependence of the relative width of the 1171.5 kev γ-line of Co^{60} on the helium pressure in the instrument. Target thickness - 100 μ; slits - 22 x 2 mm and 30 x 2 mm; 17 μ thick cellophane film covering windows of first counter.

Dependence of the relative half-width of lines on the gas pressure in the instrument. We studied the 1171.5 kev γ-line of Co^{60} with different pressures of helium in the instrument: 380, 190 and 120 mm Hg. The other conditions remained the same during these tests: thickness of target 100 μ; first slit 22 x 2 mm, second slit 30 x 2 mm; cellophane film 17 μ thick over the counter windows.

The dependence of the relative half-width of the observed γ-line on the pressure is shown in Fig. 6. The half-width went down from 5.6 ± 0.3% to 4.3 ± 0.3% when the pressure was reduced from 380 to 190 mm Hg. Further decrease of the pressure (to 120 mm Hg) did not further reduce the half-width of the line but at the lower pressure the lines are resolved somewhat better due to reduction of the low-energy tails. The peak intensity falls off in accordance with the decreasing efficiency of the counters.

It follows from these results that in measuring γ-rays of energies over 1 Mev the helium pressure in the instrument can be maintained at about 120 mm Hg.

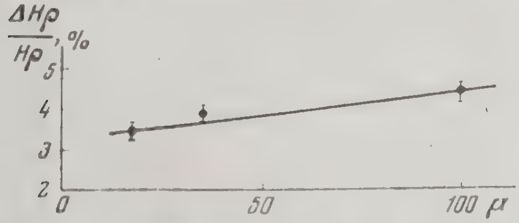

Fig. 7. Dependence of the width of the 1171.5 kev line of Co^{60} on the thickness of the target. Helium pressure - 125 mm Hg; slits - 22 x 2 and 30 x 2 mm; 17 μ thick cellophane film over windows of first counter.

Influence of the target thickness on the the line width. The same γ-line of Co^{60} was studied with targets of different thickness: 100, 35, and 17 μ other conditions remaining the same: p_{He} = 125 mm Hg; slits - 22 x 2 and 30 x 2 mm; 17 μ thick cellophane film over the windows of first counter.

The results of measurements shown in Fig. 7 indicate that under the given conditions the line width cannot be reduced below 3% by decreasing the thickness of the target even to

the ultimate "zero" point. Reducing the target thickness reduces the intensity of the line. Hence at this stage we decided to fix on 17 μ for the target thickness and to study the other causes of line broadening.

Influence of the film covering the windows of the first counter. Scattering of recoil electrons in the windows of the first counter can smear out the line. Obviously this smearing-out will be greater, the thicker the film. We did not investigate in detail the dependence of the line width on the thickness of the window film but immediately replaced the 17 μ films by films 2-3 μ thick. Use of even thinner films would be difficult in view of the rather large dimensions of the counter windows.

As a result of this replacement of the counter window films the intensity at the peak of the 1171.5 kev Co^{60} line increased by a factor of about two and the line became narrower (2.8% instead of 3.5%). These tests confirm the importance of using films of minimal thickness over the windows of the first counter.

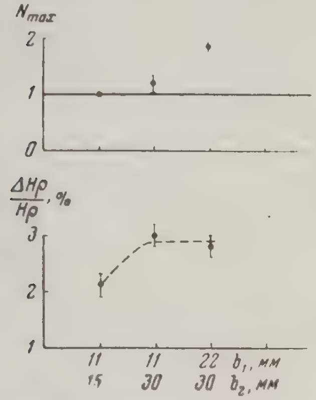

Fig. 8. Dependence of coincidence rate N_{max} at the line peak and relative line-width ($\Delta H\rho/H\rho$) on the height of the slits b_1 and b_2.

All further measurements were made with 2-3 μ thick films over the first counter windows. Since reduction of the thickness of the film over the windows of the first counter altered the operating conditions of the instrument we decided to see how further reduction of the target thickness would effect the resolution of the instrument under these conditions.

Measurements of the 1171.5 kev Co^{60} line with a 5 μ thick target showed that the relative half-width of the line is the same as with the 17 μ thick target (2.8%). This confirms our previous observation that at γ-energies above 1 Mev scattering in the target plays an insignificant part and that the resolution of the instrument is limited by other factors. It was natural to assume that these factors are the height and width of the slits.

Influence of the slit-height on the resolution and transmission of the instrument. We reinvestigated the 1171.5 kev line with different slit heights, keeping the other parameters constant. First, we reduced the height of only the first slit (to 11 mm instead of 22 mm), leaving the height of the second slit at 30 mm. Then we reduced the height of the second slit from 30 to 15 mm.

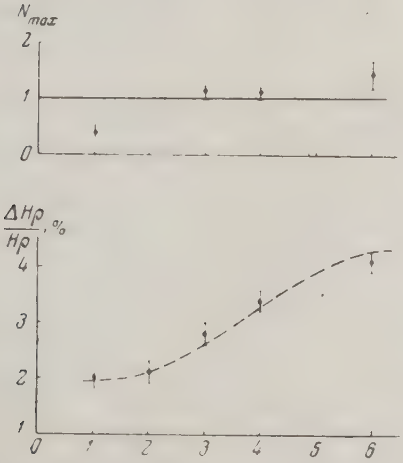

Fig. 9. Dependence of coincidence rate at the line peak and relative half-width on the width a_1 of the first slit with a_2 = 2 mm.

As may be seen from curves shown in Fig. 8, when the height of only the first slit is reduced by a factor of two the resolution of the instrument is not enhanced while the transmission is reduced approximately in proportion to the decrease in slit height. There is an improvement in resolution only when the height of both slits is reduced. In this case when the height of both slits was halved the ratio $\Delta H\rho/H\rho$ was decreased by a factor of 1.4.

Influence of slit-width on the resolution and transmission of the instrument. In these tests the height of the first slit was kept constant at 11 mm, that of the second at 15 mm. The results, given in Fig. 9, show that with the given slit height the most favorable conditions are obtained when both slits are 2 mm wide. The resolution under these conditions equals ~2%.

Summing up, we note that the best resolution we were able to obtain with our instrument is approximately 2% in the 1 Mev energy region. This best value

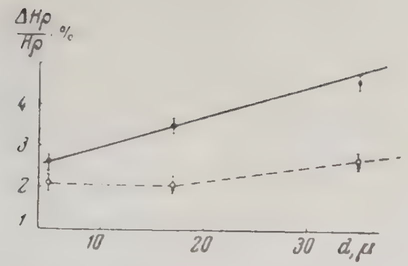

Fig.10. Dependence of relative line width on thickness (d) of the target under the following conditions: slits 11 x 2 mm and 15 x 2 mm; p_{He} = 180 mm Hg; 2-3 μ thick film over windows of first counter. ● - 606 kev Sb^{124}, ○- 1171.5 kev Co^{60}, ▲ - 1690 kev Sb^{124}.

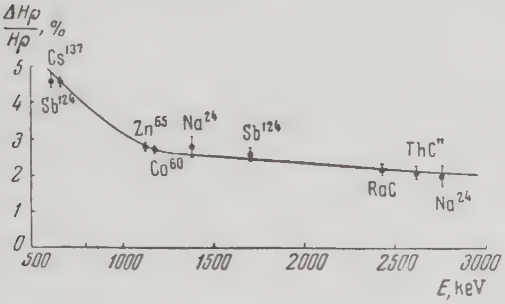

Fig.11. Dependence of relative line widths on the γ-ray energies under the standard conditions: target thickness 35 μ; slits 11 x 2 and 15 x 2 mm; p_{He} = 165 mm Hg; p_{CH_4} = 5 mm Hg.

was obtained with a 5 μ thick target and slits 11 x 2 mm and 15 x 2 mm. We found, however, that the transmission factor of the instrument under these conditions was not particularly high.

Hence we turned to our second problem - that of finding means of increasing the transmission of the instrument without undue sacrifice of the resolution. For this purpose we carried out a series of experiments with the above mentioned slits but with targets thicker than 5 μ.

Influence of target thickness on the resolution and transmission factor of the instrument at different γ-ray energies. These tests were carried out with targets of 5, 17 and 35 μ for the following γ-lines: 606 kev line of Sb^{124}, 1171.5 kev line of Co^{60} and 1690 kev line of Sb^{124}.

Comparison of the results (Fig. 10) shows that in the 1-2 Mev energy region scattering in the target becomes noticeable only with target thicknesses exceeding 17 μ. When the target thickness is increased from 17 to 35 μ the relative line half-width increases from 2.1 to 2.7%. If there were no scattering and radiation loss of the electrons in the target, the counting rate at the line peak should increase linearly with the target thickness. As a result of scattering and radiation loss, however, the counting rate at the line peak increases more slowly in proportion to the target thickness. Thus the counting rate at the peak of the 1171.5 kev Co^{60} line increases only 4 times when the target thickness is increased seven-fold. From this one may conclude that for γ-lines of energies on the order of 1 Mev conditions for measurement with a 35 μ thick target are close to optimal. Any further increase in the target thickness will lead to an increase in the line width, while the coincidence rate will increase more slowly.

At energies above 2 Mev one can use thicker targets without fear of impairing the resolution.

At energies on the order of 600 kev, as might be expected, scattering in the target plays an appreciable role: the line width increases from 2.6% with a 5 μ target to 4.6% with a 35 μ target.

In order to determine the energy dependence of the relative line width with a 35 μ thick target we determined the half-widths of the following γ-lines: 661.6 kev Cs^{137}, 1120 kev Zn^{65}, 1367.9 kev Na^{24}, 2450 kev RaC, 2614.3 kev ThC" and 2753.5 kev Na^{24}. The results (Fig. 11) show that the line half-width changes gradually with the energy. In the 600 to 1200 kev interval the line width goes down from 4.7 to 2.5% and then decreases more slowly (to 2.1% from the 2614.3 kev line of ThC"). The analogous energy dependence of the line width with 5 and 17 μ thick targets is shown in Fig. 12. It will be seen that with these targets the relative line width above 1 Mev is virtually constant and equal to 2.1%. In the 600-1000 kev interval the half-width changes from 2.7 to 2.1% with the 5 μ target and from 3.5 to 2.1% with a 17 μ thick target.

It follows from the curves of Figs. 11 and 12 that at γ-ray energies above 2 Mev one can use targets having a thickness of more than 35 μ.

Effect of changing the composition of the gas filling the instrument and counters. In order to enhance the operating stability of the counters the helium

of the preliminary tests was replaced with a mixture of helium (165 mm Hg) and methane (5 mm Hg). As regards scattering this mixture is equivalent to pure helium at 200 mm Hg. In selecting this proportion of helium to methane we were guided by the considerations noted at the beginning of this section.

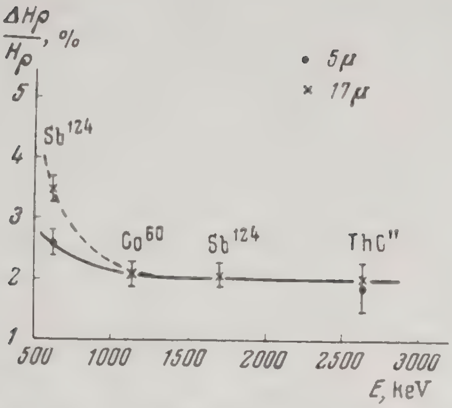

Fig. 12. Dependence of the relative line width on the γ-ray energy with 5 and 17 μ thick targets: slits 11 x 2 and 15 x 2 mm; p_{He} = 180 mm Hg.

The results of investigations of the 1171.5 kev line of Co^{60} with the instrument filled with pure helium at 180 mm Hg (solid dots) and with the helium methane mixture (crosses) are shown in Fig. 13. It will be seen from the figure that in both cases the line half-width is the same and equal to 2.7%.

In all further measurements the instrument was filled with the same helium and methane mixture.

Influence of the shape of the collimator on the resolution of the instrument. The collimator used in all the above described tests had an entrance aperture 8 x 6 mm and an exit opening 15 x 12 mm. Since radioactive materials often have a low specific activity, in studying them it is necessary to use a source having dimensions appreciably exceeding the size of the entrance aperture of the collimator. In this case not all the activity of the material is utilized. We measured the 1171.5 kev line of Co^{60} with two collimators: the one described above and another in which the entrance aperture was of the same size as the exit one. Identical lines were obtained with both collimators when the source was located on the center line of the collimator.

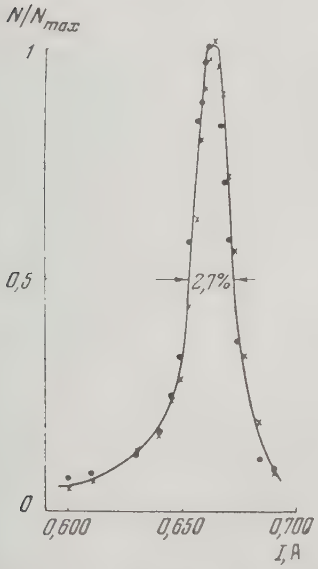

Fig. 13. Effect of the composition of the gas in the instrument on the shape of the 1171.5 kev line of Co^{60}. X - instrument filled with a mixture of helium (165 mm Hg) and methane (5 mm Hg); ● He at 180 mm.

Table 1

Position of source	Height of peak	Position of peak	Line half-width
A	100 %	0,667	2,8±0,2 %
B	93±7	0,666	2,8±0,2
C	91±7	0,667	2,8±0,2
D	89±5	0,666	3,0±0,2
E	83±7	0,666	3,0±0,2

In order to evaluate the influence of the transverse dimensions of the source on the resolution and transmission factor of the instrument we made a series of measurements of the 1171.5 kev line of Co^{60} using a source 4.5 mm in diameter and 8 mm long shifted to different positions relative to the entrance aperture of the collimator.

The results are shown in Table 1 and Fig. 14.

As may be seen from the table when the source is moved from the central A position 5 mm to the side (to positions B and C) the height and half-width of the line peak remained unchanged within the limits of the experimental error. However, when the source was moved up or down 3 mm (positions D and E) the line was somewhat broadened and reduced 10-15% in height.

Influence of the length of the source. We indicated above that the shape of the target in our instrument was calculated for a source-to-target distance of L = = 41 cm. Since it is often necessary to use long sources (up to 10-13 cm), we felt

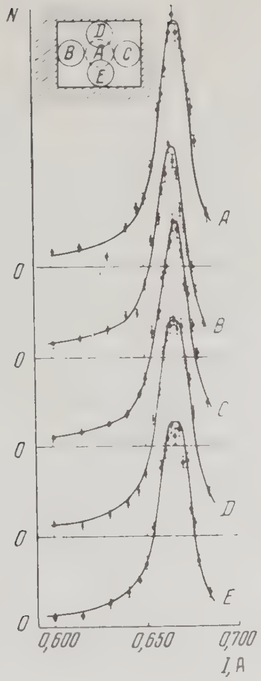

Fig. 14. Influence of the transverse dimensions of the source on the resolution and transmission of the instrument. A, B, C, D and E - positions of source at which measurements were made.

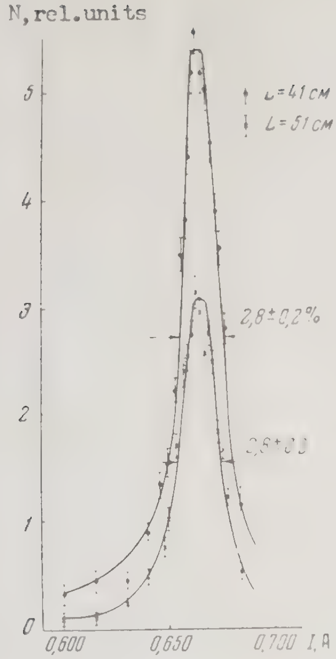

Fig. 15. Results of measurements of the 1171.5 kev Co^{60} line with source-to-target distances of 41 and 51 cm.

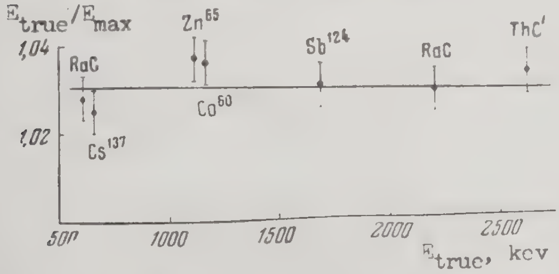

Fig. 16. Results of energy calibration of the Elotron. The calibration was carried out under standard conditions: target 35 μ, slits 11 x 2 and 15 x 2 mm; p_{He} = 165 mm Hg and p_{CH_4} = 5 mm Hg.

it important to determine to what extent changing the source-to-target distance affects the resolution of the instrument. To this end we remeasured the 1171.5 kev line of Co^{60} with the source at a distance of 51 cm from the target.

The results are shown in Fig. 15; it will be seen that the resolution is not changed. Consequently it is feasible to use sources up to about 10 cm long without fear of appreciable line broadening. However, in using a longer source we do decrease the transmission by a factor of $(L_2^2/L_1^2)\cdot(S_1/S_2)$ where S_1 and S_2 are the areas of the target irradiated by direct rays from the source when the latter is at distances of L_1 and L_2 from the target.

In our particular case increasing L from 41 to 51 cm should have reduced the counting rate at the line peak by a factor of 1.66. The experimental factor was 1.7 ± 0.1.

Energy calibration. The primary purpose of the instrument is measurement of the relative line intensities; determination of energies is secondary, hence the instrument was calibrated as regards energy with reference to known γ-lines.

The calibration consisted of plotting an experimental curve relating the "true" energy E_{true} of the γ-rays with the value of E_{max} which corresponds to the experimental location of the line peak and is defined as the abscissa of the point of intersection of tangents to the steepest parts of the line contour on both sides of

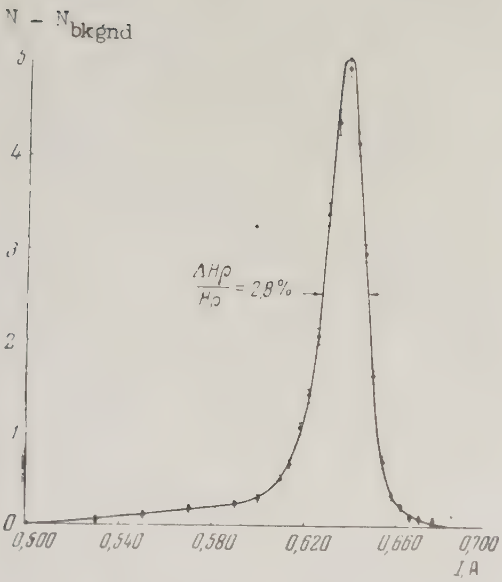

Fig. 17. The single 1120 kev line of Zn^{65} measured under standard conditions.

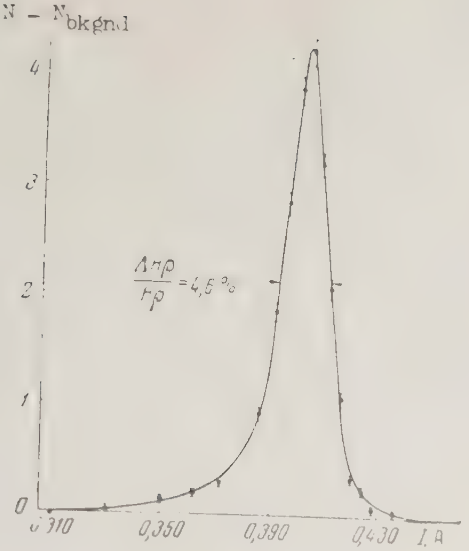

Fig. 18. The single 661.6 kev line of Cs^{137} measured under standard conditions.

the peak. For E_{true} we used the energies of γ-lines known with great accuracy (to within some hundredth of a percent) from observation of conversion electrons or from measurements carried out by means of spectrometers with bent crystals.

Obviously the calibration measurements must be carried out under the same conditions as subsequent investigations of γ-spectra.

The calibration curve is shown in Fig. 16, in the form of a plot of E_{true} vs the ratio of E_{true}/E_{max}. As may be seen the ratio does not exceed 1.03 and remains virtually constant over the entire range from 600 to 2500 kev.

Line shape and the spectral sensitivity of the instrument. In investigating complex γ-spectra it is necessary to know the shape of the lines of different energies in order to be able to separate the effects due to individual lines. Calculation of the line shape for our instrument does not appear to be feasible at present in view of the inhomogeneity of the magnetic field; such calculation is already exceedingly complex even for the Ritron[1] which has a uniform field.

In order to obtain experimental data on line shapes we investigated the single 1120 kev line of Zn^{65} (Fig. 17) and the single 661.6 kev line of Cs^{137} (Fig. 18) under the following "standard" conditions: target 35 μ thick, slits 11 z 2 and 15 x x 2 mm, p_{He} = 165 mm Hg and p_{CH_4} = 5 mm Hg. Unfortunately we had no suitable source materials yielding single lines having energies in the region of 2 Mev, but the 1690 kev Sb^{124} and 2450 kev RaC lines could be investigated over an appreciable range.

If the 661.6, 1120, 1690 and 2450 kev γ-lines are normalized to the same half-width (Fig. 19), the shape proves to be almost identical over most of their extent, the only difference apparent being in the rising portion on the low energy side.

Bearing this, as well as the dependence of the relative half-width on the energy, in mind and making use of linear extrapolation for the rising sections on the low energy side, one can readily deduce the shape of a spectral line of any energy.

In order to determine the relative intensities of the γ-lines recorded one must know the spectral sensitivity or response of the instrument. Until a detailed experimental investigation of the spectral response of our instrument can be made we are using the calculated (theoretical spectral sensitivity) of the Ritron as given in Ref. 1. Provisional use of the Ritron sensitivity values for our instrument is justified by the experiments of Dzhelepov, Zhukovski and Nedovesov who

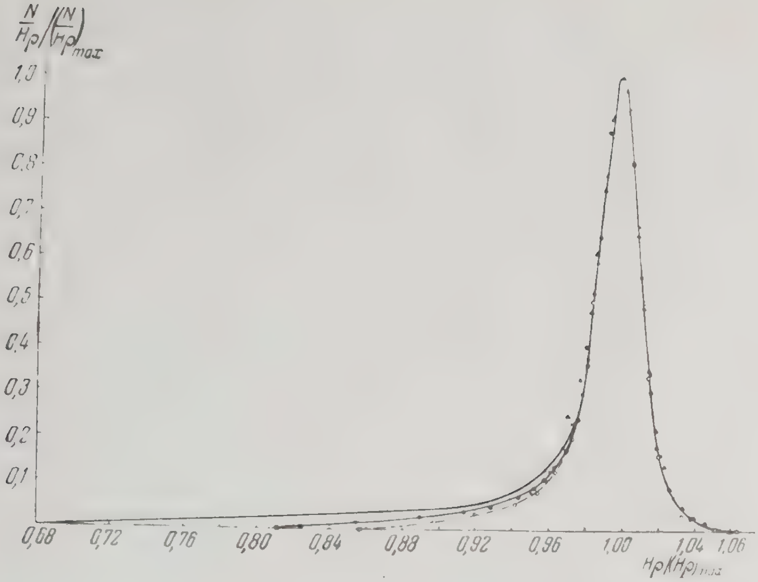

Fig. 19. Shape of the spectral lines reduced to the same coordinates: ▲ - 2450 kev RaC; X - 1690 kev Sb^{124}; ● - 1120 kev Zn^{65}; O - 661.6 kev Cs^{137}.

investigated Eu^{152} and Eu^{154} on the Ritron and on an instrument similar to ours and found that the spectral sensitivities of both instruments were virtually identical.

Conclusion

The above description of the characteristics of the Elotron is obviosly not exhaustive. However, we feel that the data can be helpful in the design and construction of similar spectrometers.

The experiments concerned with the effect of the pressure in the instrument and the thickness of the films over the counter windows were carried out with the aid of A.S.Karamian. Iu. Podkopaev participated in the tests on the effect of slit dimensions. Iu.Starostenko helped in the investigation of the influence of the source size.

All-Union Scientific Research Institute of Metrology.

References

1. B.Dzhelepov, N.Zhukovski & Iu.Khol'nov, Izv. AN SSSR, Ser. fiz., 18, 599 (1954). (Trans. Bulletin Vol. 18, No. 5, p. 285).
2. B.Dzhelepov, N.Zhukovski, A.Karamian & S.Shestopalova, Izv. AN SSSR, Ser. fiz., 17, 518 (1953).
3. P.Pavinski, Izv. AN SSSR, Ser. fiz., 18, 175 (1954).
4. D.Hartree, Proc. Cambr. Phil. Soc., 21, 746 (1923).
5. B.Dzhelepov & A.Bashilov, Izv. AN SSSR, Ser. fiz., 14, 263 (1950).
6. B.Dzhelepov, Doklady AN SSSR, 77, 389 (1951).

INVESTIGATION OF LOW-INTENSITY HARD γ-RAYS BY MEANS OF THE PHOTONEUTRON EFFECT

- B.S.Dzhelepov and I.A.Iaritsyna

Hard γ-rays of low intensity are encountered in the spectra of a number of radioactive substances. Various difficulties are encountered in studying such γ-rays by means of magnetic or scintillation γ-spectrometers. Magnetic γ-spectrometers (such as the Ritron and Elotron) can be used for studying sources emitting not less than $3 \cdot 10^7$ quanta of a given energy per second. On the other hand, when the total activity of the source exceeds several curies work with the instrument becomes difficult. Thus the intensity of the investigated γ-lines must not be less than 10^{-3} quanta per decay.

In the case of scintillation spectrometers the feasibility of studying weak γ-rays is generally limited by the presence of other lines which load the crystal with numerous pulses even when the activity of the source is relatively low. There are no reports in the literature of successful measurment by means of a scintillation spectrometer of any hard γ-rays having an intensity less than $7 \cdot 10^{-4}$ quanta per decay.[1]

In this respect the photoneutron method has a clear advantage: all γ-rays having energies below the photoneutron reaction threshold are effectively cut off, i.e., do not participate in photoneutron production. Since in applying this method one can increase the amount of radioactive material used on the one hand and measure a small number of neutrons on the other, this method permits of detecting high-energy γ-quanta in the amount of only 10^{-5} - 10^{-6} per disintegration.[2-5]

A shortcoming of the method is that the quantity measured is the sum

$\sum_i \sigma_{(h\nu_i)} \gamma_{i(h\nu_i)}$, where γ_i is the number of quanta of energy $h\nu_i$ per disintegration and σ is the photoneutron cross section for quanta of a given energy; the summation is carried out over all quanta of energies above the threshold value. Hence the results of the experiment do not directly indicate the energies and the relative intensities of the different quanta producing the photoneutron effect. The energy of the photons has to be determined by independent experiment or deduced on the basis of assumptions regarding the decay scheme. Having assumed an appropriate energy value and knowing the activity of the source (the number of disintegrations per unit time) one can calculate the number of quanta per decay.

During the past few years the hard γ-rays from a number of sources have been studied by observation of photoneutrons in the laboratory of the All-Union Scientific Research Institute of Metrology. Different methods of recording the photoneutrons were studied. It was found that the most suitable methods where investigation of hard γ-quanta is concerned is the spiral uranium chamber method and the manganese activation method.

In view of the complexity of the systems employed (source, moderator and neutron detector) theoretical evaluations of their efficiency were necessarily approximate. Hence we calibrated our installations with reference to the 2.76 Mev γ-line from an Na^{24} source of known activity.

In our standard geometry photoneutrons from a 1 mc Na^{24} + D_2O source produced 51 ± 1 pulses/hour in the uranium chamber. The photoneutrons from the standard 1 mc Na^{24} + D_2O source activated the calcium permanganate solution so that the precipitated MnO_2 produced $\sim 107 \pm 1$ pulses/min in the β-counter. A 1 mc Na^{24} + Be source under analogous conditions produced 43.2 ± 0.5 pulses/min in the β-counter.

We undertook an investigation of the hard γ-rays in the spectra of Co^{60}, Sb^{124}, Ag^{110} and In^{114} by means of the above mentioned two methods.

1. No hard γ-rays from Co^{60} were detected. Mn^{55}, activated by neutrons from a 1700 mc Co^{60} + D_2O source, produced less than 5 pulses/min in the β-counter; activation with 1700 mc Co^{60} + Be also resulted in a counting rate under 5 pulses/min. In accordance with the generally accepted scheme of decay to Ni^{60} (Ref. 6) there exist $4+ \rightarrow 2+$ (1.17 Mev) and $2+ \rightarrow 0+$ (1.33 Mev) transitions. There is also

reason to assume that a 2.5 Mev crossover transition exists (Fig. 1*). The intensity of this crossover transition, according to our measurements with D_2O does not exceed $4 \cdot 10^{-5}$ quanta per decay. This value is in satisfactory agreement with present day data on the quantum characteristics of the levels of Ni^{60}: the 4+ → 0+ transition must be weaker than the 4+ → 2+ transition by a factor of at least 10^5. It is interesting to note that in the decay of Cu^{60} there is yet another excited level, having an energy of 2.2 Mev. This energy is higher than the threshold for the photoneutron reaction on Be. From our measurements with Be it can be established that the relative intensity of this transition in $Co^{60} \rightarrow Ni^{60}$ decay is less than 10^{-4} quanta per decay. Thus we have the curious fact that the 2.2 Mev level of Ni^{60} is involved in the decay of Cu^{60} but not in the decay of Co^{60}.

2. The γ-rays from Ag^{110} produced a certain number of photoneutrons in the case of interaction with Be, but no detectable neutrons in the case of D_2O. Mn^{55} activated by neutrons from a 400 mc source of Ag^{110} + Be produced 16 pulses/min in the β-counter while the same source in D_2O resulted in less than 5 pulses/min. On the basis of calibration with references to Na^{24} we found that the effect with Be is due to a γ-line having an intensity of $8 \cdot 10^{-4}$ quanta per disintegration, assuming a γ-ray energy of 1.8 Mev. We purified the Ag^{110} source chemically and measured the effect before and after purification. No radioactive impurities were found: the effect was clearly associated with the silver isotope and fell off with a period close to the half-life of Ag^{110}. Thus there can be no doubt that the observed γ-rays are associated with the decay of Ag^{110}.

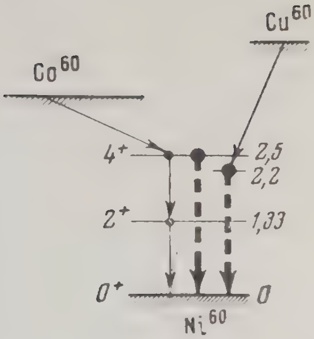

Fig. 1. Decay scheme for Co^{60} and Cu^{60}.

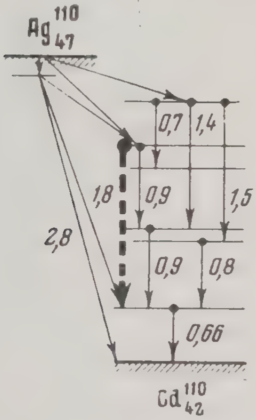

Fig. 2. Decay scheme for Ag^{110}.

However, in this case the nature of the γ-rays could not be determined definitively only from observations of photoneutrons. As may be seen from Fig. 2 (Ref. 7) Ag^{110} emits hard β-rays; the end point of the β-spectrum is 2.8 Mev, i.e., is appreciably higher than the photodisintegration threshold of Be. There is the question whether the observed hard γ-rays are not due in whole or in part to bremsstrahlung in the silver itself.

Calculations of the bremsstrahlung of the electrons from Ag^{110} in the silver showed that the intensity of the hard part of the bremsstrahlung (> 1.67 Mev) amounts to $1 \cdot 10^{-4}$ quanta per disintegration and consequently may be responsible for an appreciable fraction of the observed effect.

In order to determine whether nuclear γ-rays exist we carried out the following experiment: 2 curie of Ag^{110} were dissolved in nitric acid, then the solution of the radioactive silver nitrate was divided into two equal parts, one of these was mixed with finely powdered carbon, the other with an equal amount of lead powder.

The volume of solution was taken so as to completely fill the pores in both the C and Pb powders; after filling, the mixture was carefully dried. Inasmuch as the intensity of bremsstrahlung under these conditions is approximately proportional to Z we should have obtained distinctly different effects with the two sources if the photoneutrons were due to bremsstrahlung. However, the effect proved to be

---

*In the decay schemes the heavy arrows indicate the probable origin of the γ-rays producing the photoneutrons observed in our experiments; dash-line arrows indicate transitions for which the upper intensity limit was determined.

identical in both cases. Hence we are inclined to believe that the observed effect is due primarily to nuclear γ-rays from Ag^{110} rather than to bremsstrahlung.

3. We studied the interaction of the γ-rays from Sb^{124} with D_2O both by the means of the manganese activation method and in the uranium chamber. A photoneutron effect exceeding the background several-fold was observed in both cases. Mn^{55} activated by the neutrons from a 950 mc source of $Sb^{124} + D_2O$ produced 130 pulses/min in the β-counter. Inasmuch as the observed effect fell off approximately in accord with the half-life of Sb^{124} (60 days) it may be assumed that the effect was due to Sb^{124} and not to any radioactive impurities.

According to the most recent decay scheme for Sb^{124} (Fig. 3 - Ref. 8) one may expect to observe 2.3 Mev or 2.7 Mev γ-rays from this isotope. In order to determine the energy of the γ-rays we made a rough measurement of the energy of the photoneutrons produced in our experiments. The photoneutron energy value differs by a factor of almost 7 for alternate γ-ray energy assumptions : $\overline{E}_n = 35$ kev if the photoneutrons are produced by 2.3 Mev γ-rays and $\overline{E}_n = 235$ kev if they are produced by 2.7 Mev γ-rays.

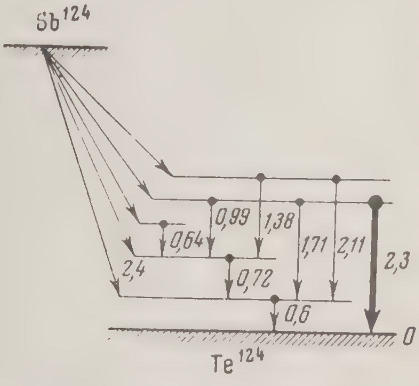

Fig. 3. Decay scheme for Sb^{124}.

In general the neutron energy spectrum is somewhat smeared out due to collisions of neutrons with D or O nuclei; however, there are few neutron-nucleus collisions in our sources and the ratio of the mean energies changes little. Despite the appreciable difference between the photoneutron energies it is impossible to find a substance in which the absorption cross sections at the two energies differ by more than a factor of 4. We elected to use sulfur for which σ_t equals 1 barn for $\overline{E}_n = 35$ kev and 3.5 barns for $\overline{E}_n = 240$ kev.

An 8 cm thick sulfur plate and then a 5 cm thick lead plate were alternately introduced between the uranium chamber and the photoneutron source. The photoneutron source and detector were surrounded by a 1 mm thickness of cadmium.

With the sulfur plate in place the effect from the interaction of Sb^{124} with D_2O virtually did not change, while with the lead plate it fell off almost to the level of the background. Thus for our neu-

Isotope:	Co^{60}		Sb^{124}	Ag^{110}		In^{114}	
Half-life	5,3 years		60 days	250 days		49 days	
Target	D_2O	Be	D_2O	D_2O	Be	D_2O	Be
Energy of hard γ-rays expected from decay scheme, Mev	2,5	2,2	2,3 и 2,7	—	1,8	—	1,85
Experimentally obtained data on the γ-ray energy, Mev	—	—	2,3		$2,23>h\nu>1,66$		$2,23>h\nu>1,66$
Experimentally determined value of $\Sigma\sigma_{(h\nu_i)}\eta_{(h\nu i)}$, barns-quant/decay	$<3,5\cdot10^{-32}$	$<5\cdot10^{-32}$	$1,6\cdot10^{-30}$	$<1,5\cdot10^{-31}$	$7\cdot10^{-31}$	$<7\cdot10^{-32}$	$6\cdot10^{-31}$
Energy value used for computation . . .	2,5	2,2	2,3	2,28	1,8	2,25	1,85
Number of quanta per decay	$<4\cdot10^{-5}$	$<10^{-1}$	$2\cdot10^{-3}$	$<3\cdot10^{-1}$	$<8\cdot10^{-1}$	$<10^{-4}$	$7\cdot10^{-1}$

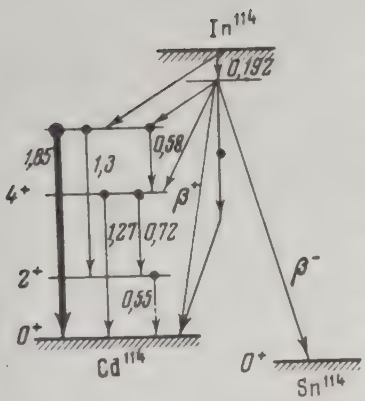

Fig. 4. Decay scheme for In^{114}.

trons σ_t in sulfur is appreciably smaller than in lead. Hence the observed effect can be attributed primarily to the 2.3 Mev transition. In this case the intensity of this hard γ-line amounts to about $2 \cdot 10^{-3}$ quanta per disintegration.

4. The decay scheme for In^{114} (shown in Fig. 4 - Ref. 9) indicates that there may be a hard γ-line having an energy $>$1.66 Mev. A certain photoneutron effect was observed with the In^{114} source placed in a beryllium block; no effect was observed with the source in heavy water. Mn^{55} activated by neutrons from a 900 mc source of In^{114} + + Be produced 33 pulses/min in the β-counter while with the same source interacting with D_2O there were less than 5 pulses per min. The effect fell off with a period close to the half-life of In^{114} (49 days). Assuming an energy of 1.85 Mev, the intensity of this transition amounts to about $7 \cdot 10^{-4}$ quanta per decay.

The principal results of our investigation are summarized in the accompanying table.

All-Union Scientific Research Institute of Metrology

References

1. R.Pringle, W.Turchinetz & H.Taylor, Phys. Rev., 95, 115 (1954).
2. A.Wattenberg, Phys. Rev., 71, 497 (1947).
3. V.Mayers & A.Wattenberg, Phys. Rev., 75, 992 (1949).
4. R.Fluharty & MDeutsch, Phys. Rev., 76, 182 (1949).
5. R.Wilson, Phys. Rev., 79, 1004 (1950).
6. R.Van Lieshout, R.Nussbaum, G.Nijgh & A.Wapstra, Phys. Rev., 93, 255 (1954).
7. J.Hollander, I.Perlman & G.Seaborg, Rev. Mod. Phys., 25, 531 (1953).
8. N.Lazar, Phys. Rev., 95, 292 (1954).
9. J.Prazos & R.Steffen, Bul. Am. Soc., 30, 19 (1955).

TESTS AND OPERATING REGIME OF A SCINTILLATION γ-SPECTROMETER

- A.A.Konstantinov, O.I.Sumbaev & V.V.Chekin

Scintillation counters and spectrometers are finding evermore extensive application in different branches of nuclear physics and technology. However, until now serious difficulties have been encountered in attempting to construct a satisfactory γ-spectrometer using standard, "series-produced" photomultipliers and crystals of domestic (Soviet) manufacture.

We undertook a detailed investigation of those characteristics of FEU-19 type photomultipliers which are important when these are employed in scintillation spectrometers; we also developed a procedure for selecting the best individual photomultiplier tubes.

It was established as a result of tests using short light pulses modulated by a Kerr cell that the principal reasons for the inadequate resolution of scintillation spectrometers is the low sensitivity of the photomultiplier cathode as well as the low and nonuniform (over different parts of the cathode) electron collecting efficiency of the photocathode. We investigated the dependence of the mean collecting efficiency and of the apparent inhomogeneity (as manifested by the nonuniform collecting characteristics) of the photocathode on the voltage distribution between the focusing and multiplying electrodes of the FEU-19 tube. It was established that the mean collecting efficiency can be appreciably increased (by a factor of 2) if the ratio of the voltage between the first & second and second & third dynodes is brought up to 1:4-1:5. On condition of uniform illumination of the entire FEU-19 photocathode, obviating the influence of the apparent inhomogeneity of the cathode, increasing the mean collecting efficiency results in an improvement of the resolution of the spectrometer. By way of scintillator we used a crystal of CsI(Tl) which yields appreciably more intense total energy peaks than the commonly used NaI(Tl) crystals, with insignificantly lower scintillation intensity. Of the 100 FEU-19 photomultipliers tested (with the modified voltage ratio), ten gave a half-width of the total energy peak (at ~1 Mev) less than 10%. With the usually used equal potential differences between the first & second and the second & third dynodes the half-width with the same tubes was always greater than 15%.

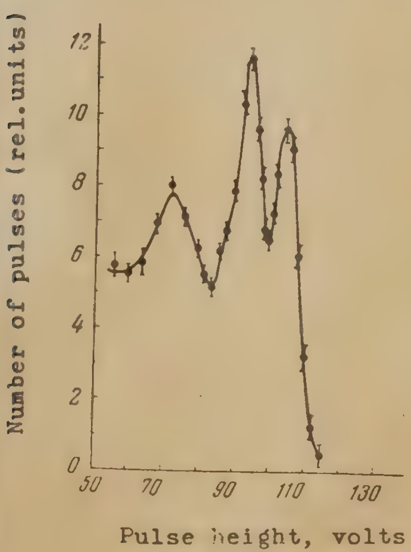

The accompanying figure shows the recorded γ-spectrum of Co^{60} illustrating the operation of our spectrometer. The spectrum was obtained with a CaI(Tl) crystal 30 mm in diameter and 17 mm thick with the following voltage distribution between the dynodes (U_{pc-d} = 200 v, U_{d-1} = 200 v, U_{1-2} = 32 v, U_{2-3} = 135 v, $U_{3-4} = U_{4-5} = \ldots U_{12-13}$ = 40 v, U_{13-14} = 80 v and U_{14-f} = 160 v.

All-Union Scientific Research Institute of Metrology.

DETERMINATION OF THE RELATIVE PROBABILITIES OF K-CAPTURE AND β-DECAY

- A.A.Bashilov, N.M.Anton'eva & B.V.Pshenichnikov

Among the known nuclides there are a number of isobaric triplets in which the two side members are stable while the middle member is radioactive: for example, Os^{192} - Ir^{192} - Pt^{192} and Pt^{198} - Au^{198} - Hg^{198}. In view of the familiar stability conditions for two neighboring isobars, the middle radioactive isobar may be expected to decay to both of the side members. Thus for Ir^{192} the ratio of the probabilities of transformation to Os^{192} (K-capture) to Pt^{192} (β-decay), $K/\beta^- \approx 0.04$. However, K-capture in the case of Au^{198} and certain other isobaric nuclei has not yet been detected. It is of undoubted interest to observe K-capture in similar cases and determine its relative probability with respect to β-decay.

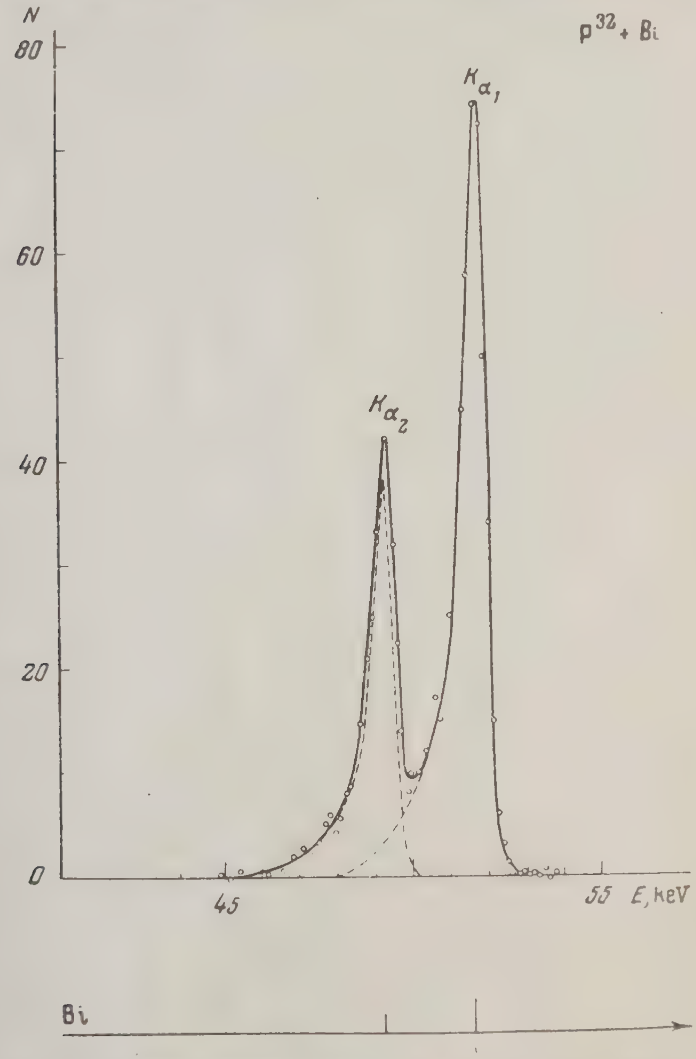

Fig. 1. Experimental spectrum of photoelectrons ejected by Bi $K\alpha_2$ and Bi $K\alpha_1$ x-rays from the silver target 0.5 μ thick (background subtracted). The x-rays of bismuth were excited by β-particles from P^{32}. The expected (theoretical) photoelectron spectrogram is shown schematically under the curve.

The problem of determining the relative probability was solved in the present investigation by observation of photoelectrons from x-rays produced as the result of K-capture and conversion of γ-rays in β-decay. The photoelectron spectrum was studied by means of a magnetic spectrometer. From the photoelectron spectrum one can find the ratio X_K/X_β of the intensities of the K-lines of the x-rays associated with K-capture and β-decay. The examination can be limited to the K_α lines; the K_β lines can be neglected since the quantity $(1 + K_\beta/K_\alpha)$ changes very little in going from Z - 1 to Z + 1. The ratio of the probabilities of K-capture and β-decay is

$$K/\beta^- = (X_K/X_\beta)(W_{Z+1}/W_{Z-1})n_\beta - n_K \qquad (1)$$

where n_β and n_K are the numbers of conversion electrons from the K-shells of the daughter nuclei in β-decay and K-capture, calculated in both cases per β-particle (these numbers are determined directly from the spectrum of the conversion electrons and β-particles) and W_{Z-1} and W_{Z+1} are the fluorescence yields from the K-levels of the daughter nuclei incident to K-capture and β-decay.

By way of illustration of this procedure we shall describe below determination of the relative probability of K-capture in the cases of Ir^{192} and Au^{198}. The photoelectron spectra were measured by means of a magnetic spectrometer with improved focusing - the Ketron.[1] The theoretical line half-width was 0.5% but in practice the lines are somewhat wider due to deceleration of the photoelectrons in the target. The targets

were prepared by vacuum evaporation of silver and had a superficial density of 0.1 and 0.5 mg/cm^2. The film over the counter window passed electrons having energies above 10 kev. A number of supplementary experiments were carried out in order to facilitate interpretation of the observed photoelectron groups.

Supplementary experiments. In the first experiment we studied photoelectrons from x-rays due only to the radiation loss of β-particles in the source material. To this end a homogeneous mixture of bismuth dust and P^{32} was packed in a brass tube; this was wrapped in silver foil and mounted at the focus of the spectrometer. Fig. 1 shows the two distinctive groups of photoelectrons ejected from the K-shells of the silver atoms by the $K_{\alpha 2}$ and the $K_{\alpha 1}$ x-rays from bismuth. The photoelectron groups corresponding to K_β-radiation are located in the region of high energies and are not shown in Fig. 1. The expected spectrogram, calculated on the basis of x-ray data, is shown schematically under the experimental curve. The excellent coincidence between the expected (theoretical) and observed lines confirms our interpretation.

In the second experiment we investigated the photoelectrons from the x-rays emitted in the filling of the K-shells previously made vacant by γ-ray conversion. In these experiments we used the radioactive isotope Hg^{203}. Fig. 2 clearly shows the three groups of photoelectrons ejected from the K-shells by the $K_{\alpha 2}$ and $K_{\alpha 1}$ x-ray radiation of mercury and thallium; the photoelectric lines corresponding to the Hg $K_{\alpha 1}$ and Tl $K_{\alpha 2}$ radiation have merged.

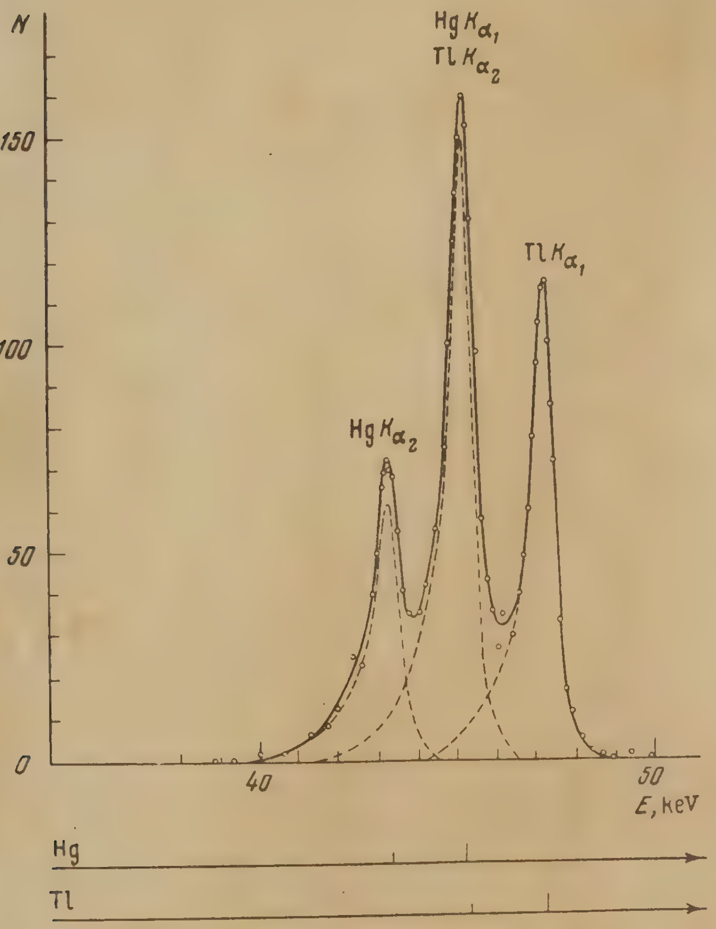

Fig. 2. Experimental spectrum of photoelectrons ejected by the Hg $K_{\alpha 2}$, Hg $K_{\alpha 1}$, Tl $K_{\alpha 2}$ and Tl $K_{\alpha 1}$ x-rays from a silver target 0.5 μ thick (background subtracted). The x-rays are produced in the bombardment of the mercury by the β-particles from Hg^{203} and as a result of the conversion of γ-rays emitted in the $Hg^{203} \rightarrow Tl^{203}$ decay.

In the third experiment of the supplementary series we studied the photoelectrons from the x-rays produced in the filling of the K-shells vacated as a result of K-capture. In these experiments we used a mixture of radioactive isotopes of hafnium: Hf^{175} (K-capture) and Hf^{181} (β^--decay). In the spectrum of Fig. 3 one can distinguish groups of photoelectrons ejected from the K-shells of the silver atoms by the $K_{\alpha 2}$ and $K_{\alpha 1}$ radiation from the lutecium, hafnium and tantallium.

The results of the supplementary experiments clearly indicate how the photo-electron spectra obtained in the subsequent experiments must be interpreted.

Determination of K/β^- for Ir^{192}. The decay of Ir^{192} was investigated by us earlier.[2] We established from the conversion spectrum that part of the γ-quanta are emitted in the decay process with capture of atomic electrons. From the intensity of these γ-lines it was concluded that the relative intensity of K-capture amounts to at least 4%

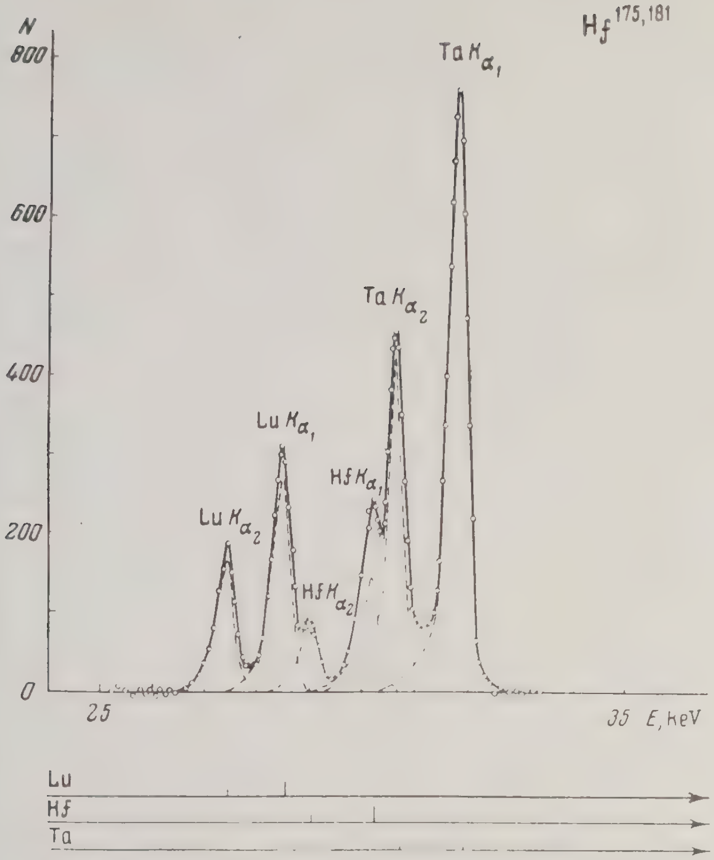

Fig. 3. Experimental spectrum of photoelectrons ejected by the K_{α_2} and K_{α_1} x-rays from lutecium, hafnium and tantallium from a silver target 0.1 μ thick. The x-rays were produced as a result of K-capture (Hf^{175}), bombardment of hafnium with β-particles, and the conversion of the γ-rays emitted incident to the Hf^{181} → Ta^{181} decay.

relative to the β-decay. However, this conclusion was based on certain unverified assumptions regarding the Ir^{192} → Os^{192} decay scheme. In the present investigation we determined the total relative probabilities of K-capture and β-decay using the above-described procedure. In distribution of photoelectrons ejected from the K-shells of silver atoms by K_α x-rays emitted by the Ir^{192} source is shown in Fig. 4. The energy values of the peak and comparison of the spectrum in Fig. 4 with the curves of Figs. 1, 2 and 3 show that in the present case K-capture does occur. Photoelectron groups corresponding to the Os K_{α_2} and Pt K_{α_1} x-ray lines are fully resolved and permit of determining the relative intensities of the of the K_α-radiations of O and Pt. In calculating, by means of equation (1), the numbers of conversion electrons from the K-shells of the daughter nuclei in β-decay and K-capture, n_β and n_K, respectively, we used the data of Bashilov et al[2] regarding the conversion spectrum. We obtained a value of $K/\beta^- = 4.5 \pm 1.0\%$ for the case of Ir^{192}.

This result is in good agreement with the evaluation in Ref. 2.

Search for K-capture in Au^{198}. We had studied the decay of Au^{198} in an earlier investigation.[3] Recently, in addition to the 412 kev line, there have been detected a number of other low-intensity nuclear transitions in Hg^{198} making but an insignificant contribution to the number of conversion electrons. According to the data in the literature[4] the probability of Au^{198} decay atomic electron capture amounts to less than 0.4%.

In the present investigation we made a search for the decay of Au^{198} by electron capture by means of the described procedure. The spectrum of photoelectrons knocked out of the K-shells of silver atoms by K_α x-rays emitted by the Au^{198} source is shown in Fig. 5. The energy values for the three discernible lines indicate that they are associated with conversion in β-decay and with bombardment of the gold by β-particles. Careful examination of the experimental curve shows no signs of photoelectron lines corresponding to K-capture.

Comparing the value of the statistical error of measurement for the section of the curve where the photoelectron line due to Pt K_{α_2} x-rays should appear with the height of the photoelectron peak associated with Hg K_{α_1} we conclude that the upper limit for K-capture in Au^{198} is less than 0.01% ($K/\beta^- < 1\cdot10^{-4}$).

Thus the high sensitivity of our method made it possible to push back appreciably the upper limit for the probability of K-capture in Au^{198}.

Physical Scientific Research Institute
of Leningrad State University

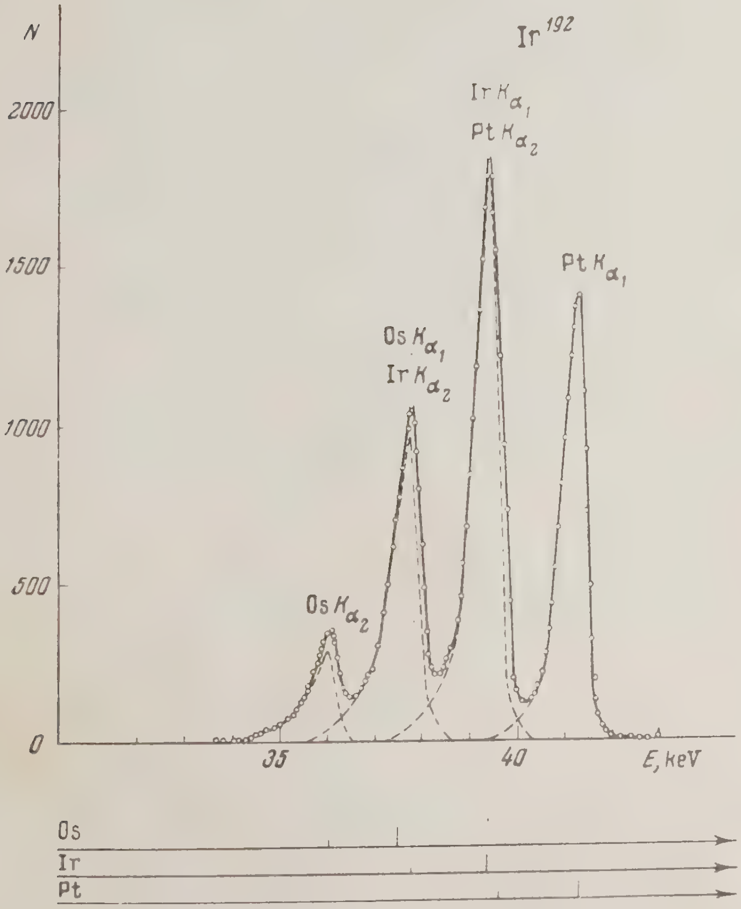

Fig. 4. Experimental spectrum of photoelectrons knocked out of 0.1 μ thick silver target by the K_α x-ray radiation from an Ir^{192} source. The first two peaks on the low-energy side indicate the existence of K-capture in Ir^{192}.

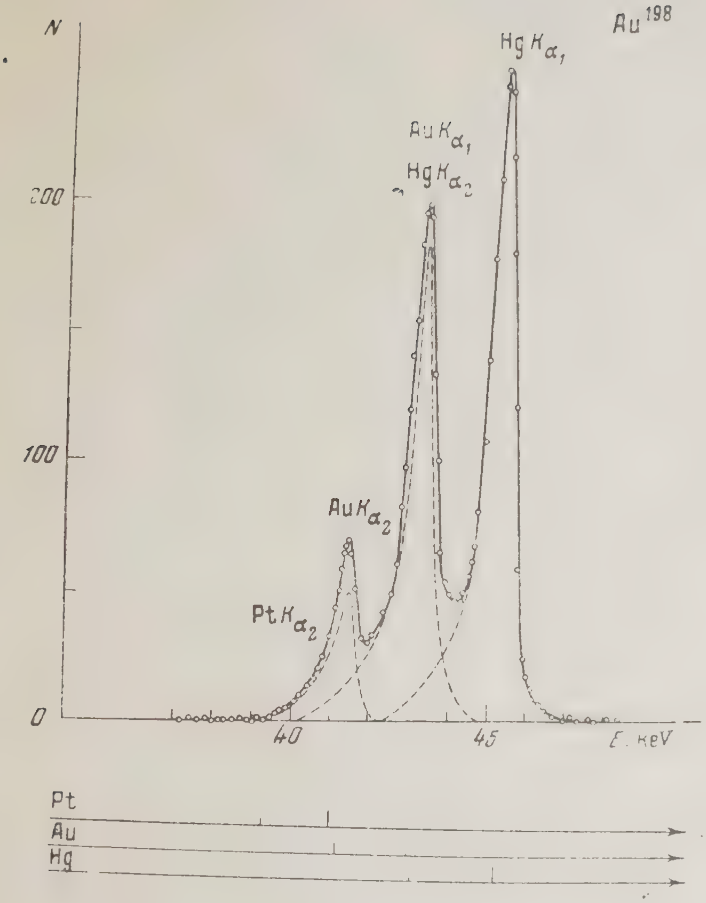

Fig. 5. Experimental spectrum of photoelectrons ejected from a silver target 0.5 μ thick by K_α x-rays emitted from the Au^{198} source. The "Pt $K_{\alpha 2}$" and the marker on the Pt scale below indicate the point at which the photoelectron peak corresponding to K-capture in Au^{198} should appear.

References

1. B.S.Dzhelepov & A.A.Bashilov, Izv. AN SSSR, Ser. fiz., 14, 263 (1950).
2. A.A.Bashilov, N.M.Anton'eva & B.S.Dzhelepov, Izv. AN SSSR, Ser. fiz., 16, 264 (1952).
3. N.M.Anton'eva, A.A.Bashilov, B.S.Dzhelepov & A.V.Zolotavin, Izv. AN SSSR, Ser. fiz., 14, 299 (1950).
4. G.A.Renard, C.R., 226, 1269 (1948).

INHERENT WIDTHS OF THE INTERNAL CONVERSION LINES OF AN ACTIVE DEPOSIT OF RADIOTHORIUM

- G.D.Latyshev, A.G.Sergeev, E.M.Krisiuk,
L.A.Ostretsov, Iu.S.Egorov & N.M.Shirshov

Introduction

It was noted in studies of the internal conversion lines of radiothorium[1,2] that the F line is wider than the I line. These lines are due to conversion of the γ-rays from the 237.9 kev transition on the K- and L-shells, respectively, of the Bi^{212} atom.

Table 1

Half-widths of the internal conversion lines of Th(B + C + C' + C"), after Slätis[3]

Line designation (after Ellis)	Origin of line	Energy, kev	Half-width %	Difference in width
F	*K*	147,8	0,050	
I	L_I	221.8	0,020	3/10000
G	*K*	188,8	0,039	
I_a	L_{II}	224.4	0,012	2,7/10000
H	*K*	209,7	0,041	2,9/10000

Siegbahn, according to a note in Ref. 2, has suggested that the difference in the width of the conversion lines is due to a difference in the inherent widths of the K and L energy levels of the Bi atom. It follows from x-ray data, assuming the Z^4 law to be applicable, that for Z = 83 the width of the K-level must be ~60 ev, while the width of the L-level is ~10 ev.

In the first experimental investigation[3] devoted to this problem the different conversion lines of active radiothorium were measured on a 180° magnetic spectrometer with a permanent magnet, the conversion electrons being recorded photographically. The results of this investigation are shown in Table 1 from which it may be seen that all the lines due to conversion on the K-level have an appreciably greater half-width than the lines from the L-level.

The first quantitative data on the inherent width of the internal conversion lines were given by Mladjenovic[4] who investigated the internal lines of RaB on a double-focusing spectrometer with the electrons being recorded by GM counters. In this work the magnetic field was measured by the compensation method, by means of a coil rotating in the magnetic field. The source material was applied to a tungsten wire 0.21 mm in diameter. The results are shown in Table 2, from which it may be seen that the L-lines have a much greater width than would follow from the x-ray data (~10 ev). Mladjenovic explains part of this divergence by the fact that the topography of the magnetic field in his instrument was dependent on the field intensity; in view of this the measured line width varied with the field intensity. For this reason, the author notes, it was impossible to determine the absolute value of the natural width of the conversion lines: one could only roughly evaluate the difference between the K- and L-conversion lines. The author asserts that the corresponding difference between the levels is 80-100 ev. This is approximately twice as great as the difference deduced from x-ray data, from which it follows that the difference between the inherent widths of the K- and L-levels

Table 2

Inherent widths of the conversion lines of RaB according to the data of Mladjenovic[4]

Line designation (after Ellis)	*A*	*F*	*G*	*Ga*	*H*	*Ha*
Origin of line	L_I	*K*	*K*	L_I	*K*	L_{II}
Energy, kev	36.9	151.5	204.7	225.5	261.3	278.7
Inherent width, ev	90	153	227	126	230	109

of the Bi atom is only ~50 ev.

The author attempts to explain this divergence by the influence of different effects accompanying internal conversion. However, the evaluations of these effects given in the report show that their influence on the inherent width of conversion lines is very minor.

The present investigation was undertaken for the purpose of determining the absolute values of the natural widths of some of the more intense internal conversion lines of active radiothorium.

1. Experimental method

1. Selection of the optimum operating conditions of the Ketron. The Ketron-type magnetic spectrometer shown in Fig. 1 was used for the investigation. The radius of curvature of the electron trajectories in the homogeneous section of the magnetic field was 80 mm. The topography of the magnetic field was adjusted with such precision that, without sacrifice of the 0.4-0.5% line half-width obtainable on the Ketron, it was possible to utilize a divergence angle of 70° in the horizontal plane and a mean divergence angle of 3° in the vertical plane.

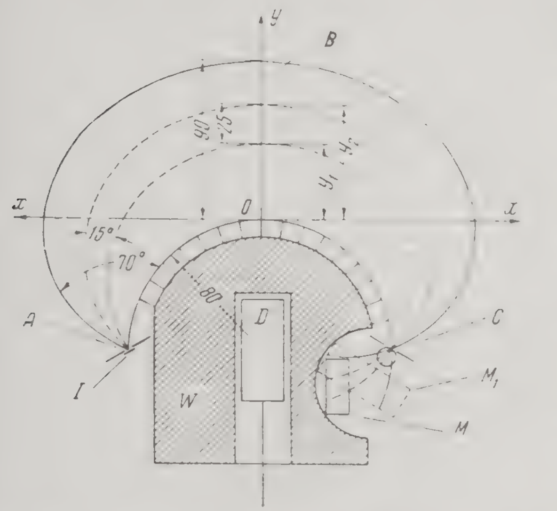

Fig. 1. Diagram of the Ketron type magnetic spectrometer: I) electron source, A) slit defining the effective dimensions of the source, mounted at the first focus, B) position of central diaphragm determining the divergence of the electron beam in the Ketron, C) counter slit mounted at the second focus (A, B & C determine the transmission factor and resolution of the instrument), M_1) location of the second counter (shown by dash lines) when the Ketron is operated for maximum transmission, M) location of second counter in our investigations of the inherent conversion line widths, W) one-piece tungsten block shielding counters from γ-rays from the source, D) magnetic field probe mounted inside the tungsten block in the center of the uniform section of the magnetic field of the Ketron. The solid lines indicate the electron trajectories in the Ketron when the instrument is operated from the maximum transmission factor (angle of divergence in the horizontal plane $\alpha = 70°$; the width of the central diaphragm in this case = 90 mm). The dash lines indicate the electron trajectories in our investigation of the inherent width of conversion lines. The trajectories pass through the section of the field where minimal aberration is observed (angle divergence $\alpha = 15°$; the width of the central diaphragm in this case was 25 mm).

The relative difference between the experimental and theoretical fields in the instrument is shown in Fig. 2. Minor departures of the experimental field from the theoretical distribution lead to aberrations, the magnitude of which depends both on the angle of divergence in the horizontal plane and on the relative location of the working section of the field. In order to find the optimum operating conditions we studied the dependence of the peak of the F conversion line on the position of the narrow diaphragm (Δy = 6 mm) along the y axis.

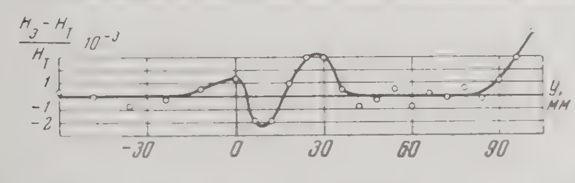

Fig. 2. Relative difference between the values of the experimental and theoretical fields at different points along the y axis.

As a preliminary step we checked the

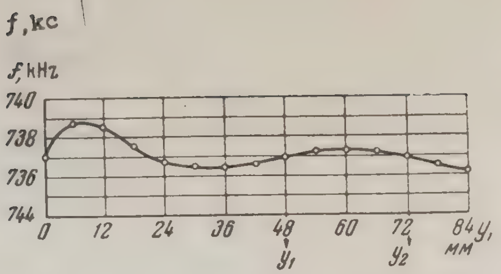

Fig. 3. Dependence of the position of the F-line peak on the location of the diaphragm (Δy = 6 mm) along the y axis. The frequency f, in which the vertical scale is graduated, is proportional to the magnetic field intensity inasmuch as the field was measured by the proton magnetic resonance method; $y_1 - y_2$ is the section of the field which was finally selected for our measurements of the conversion line widths.

reproducibility of the position of the line peak in successive measurements. The reproducibility proved to be better than within 1 part in 10^4. The dependence of the position of the F line peak on the location of the Δy = 6 mm thick diaphragm on the y axis is shown in Fig. 3. This curve permits selecting the section of the field in the horizontal plane necessary for obtaining the desired spectrometer resolution.

In order to determine the optimum height of the diaphragm we investigated the dependence of the conversion line half-width on the height of the diaphragm (in the selected section of the field). The results are shown in Fig. 4 and were used for determining the height of the diaphragm for obtaining the desired resolution.

2. Source. The active deposit of radiothorium was collected on one side of a thin aluminum foil 5 μ thick. The effective dimensions of the source were defined by the slit mounted immediately in front of the activated foil. The edges of the slit, beveled to conform to the shape of the electron beam, were made of gold in order to minimize penetration by extraneous electrons. The width of this slit was varied from 11 to 100 μ; the height from 4 to 6 mm (see column 13, Table 3).

3. Counters. The electrons were recorded by means of two self-quenching GM counters connected in coincidence. The first counter was mounted vertically, the second horizontally. The relative locations are shown in Fig. 1. The thickness of the counter windows was of the order of 50-80 $\mu g/cm^2$.

In front of the counters there was a second diaphragm defining the entrance to the counters. The width of its defining slit was varied from 11 to 100 μ. Usually the width of this slit was made approximately equal to that in front of the source. (See column 14, Table 3).

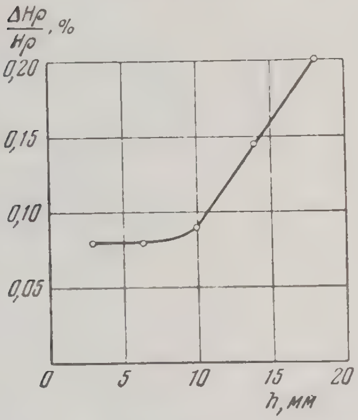

Fig. 4. Dependence of the F-line half-width on the height of the central diaphragm of the Ketron.

4. Shielding against γ-rays. The counters were shielded against γ-radiation from the source by a heavy tungsten block (Fig. 1). The minimal effective thickness of tungsten between the source and the counters was 60 mm.

5. Adjustment of the instrument. All the internal components of the spectrometer (the slit in front of the source and the counters, the source holder and the counters) were mounted on a single heavy base plate which could be set on a large universal measuring microscope; hence we were able to measure accurately the distance between the slits, their widths and heights and to check their parallelism.

The entire assembly, after measurements and verification on the microscope stand, was lowered intact into the magnetic spectrometer; dependence of the F conversion line half-width was investigated with the system in different positions in the magnetic field. The position in which the narrowest lines were obtained was fixed by means of positioning pins. The curves of Fig. 5 clarify the adjustment procedure.

6. The magnet and measurement of the magnetic field. Current for the magnet windings was supplied from two floated storage batteries having a capacity of 400 amp-hours. The current was measured and monitored by means of a PV-6 potentiometer. The current was maintained constant to within 1 part in 10^5.

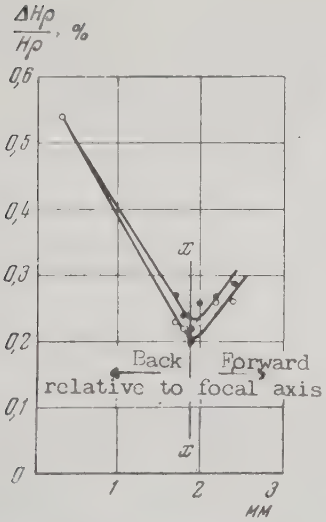

Fig. 5. Dependence of the F-line half-width on the location of the slits relative to the focal line of the Ketron (the position of the origin on the horizontal axis is arbitrary). ●) first counter, ○) counter coincidences.

Prior to each series of measurements the magnet was thoroughly demagnetized. The effectiveness of the demagnetization was checked by means of a flip coil and a ballistic galvanometer. In every case the intensity of the residual field was brought down to under 0.1 oersted.

Studies of the topography of the uniform section of the field showed that in working on the initial magnetization curve the field topography is less dependent on the field strength than in working on a hysteresis loop. A noticeable change in the field topography in the uniform region was observed only for fields under about 100 oersted. In stronger fields there was virtually no noticeable change in the topography. We assumed that in the inhomogeneous regions of the field the topography is also nearly independent of the field intensity in the range from 100-400 oersted. This was subsequently substantiated by our investigation of conversion lines of different energies. The magnetic field was measured by the proton magnetic resonance method. The water volume in the probe was 6 cm^3. The probe was located in the most homogeneous section of the magnetic field in order to obtain the narrowest possible resonance absorption curve.

Initially the frequency of the oscillator was determined with a heterodyne wavemeter; subsequently we used the procedure described in Ref. 5 which insured an accuracy of 1 part $2 \cdot 10^6$ in measuring the frequency.

In the 150-400 oersted field strength interval the accuracy of the relative magnetic field intensity measurements was 1 part in $2 \cdot 10^5$.

2. Experimental data.

As noted in the introduction we investigated the most intense conversion lines of the radioactive deposits: the F, G, H and L lines. Their energies and origins are indicated in Table 3.

In order to reduce the statistical error 10-15 minutes were expended on recording each point; due to the rather short period of the active material (10.6 hours) only two lines could be studied using any one source: one of the K-conversion lines (F, G, H or L) and the I-line (conversion from the L_1 level). Between 5-10 series of measurements were made for each such line. After appropriate processing of the results for each pair of lines we obtained a series of averaged values for all the parameters needed for computing the inherent width of the K-conversion lines.

Particular attention was paid to the F-line. This is the most intense line of the investigated source material. Hence in studying it the transmission factor could be reduced to the greatest extent in order to obtain the maximum resolution. The I-line is also fairly intense. The narrowest F- and I-lines obtained for the same source under identical measurement conditions are shown in Fig. 6. It will readily be seen that the F-line is appreciably wider than the I-line.

Subsequently this line pair was studied with three different resolutions of the instrument. The G and I, H and I, and L and I line pairs were investigated only at one resolving power. These line pairs are

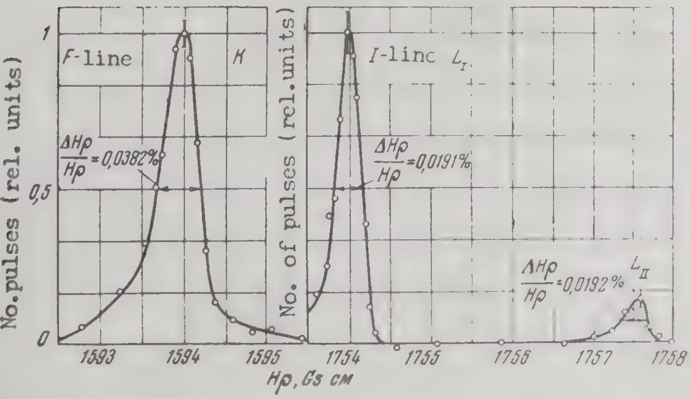

Fig. 6. F- and I-conversion lines.

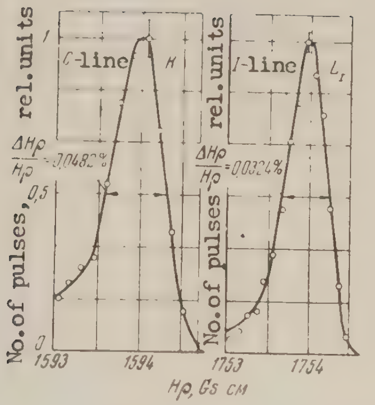

Fig. 7. G- and I-conversion lines.

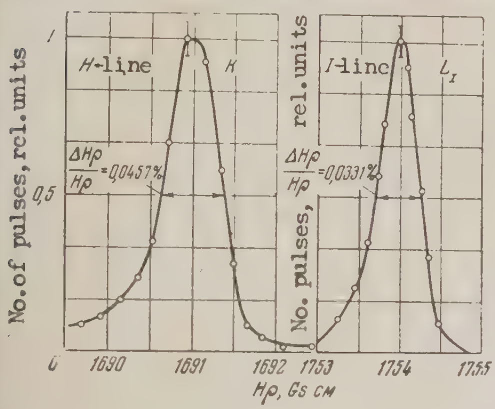

Fig.8. H- and I-conversion lines.

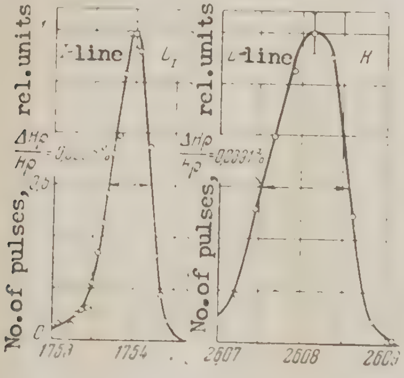

Fig.9. L- and I-conversion lines.

shown in Figs. 7, 8 and 9. In Figs. 6-9 the counter background and the β-spectrum have been subtracted and the curves normalized to the same peak height.

All the principal experimental data and parameters of the instrument are summarized in Table 3.

A noteworthy fact is that as the resolution of the instrument is increased the shape of the F-line approaches the classical dispersion shape (see Fig. 6).

3. Calculation of the inherent line widths

If the conversion line has a natural (inherent) shape $f(x)$, while the instrument yields a shape $\varphi(x)$ for a rigorously monoenergetic line, the shape of the observed line will be described by

$$F(x) = \int_{-\infty}^{+\infty} f(\xi)\,\varphi(x-\xi)\,d\xi. \qquad (1)$$

For the "apparatus" line shape $\varphi(x)$ we can take the shape of the I-line since this line is associated with conversion on the L_I-shell and the inherent width of the L_I-level ($\sim$10 ev) is much smaller than the apparatus width of the line and may therefore be neglected in the first approximation. Equation (1) contains two experimentally obtained functions: $F(x)$ and $\varphi(x)$. To determine the inherent line width we must find $f(x)$ from equation (1).

In our calculations we made the assumption that the natural shape of the K-conversion lines is dispersional:

$$f(x) = \frac{1}{2\pi}\,\frac{\Gamma_K}{x^2+\frac{\Gamma_K^2}{4}}, \qquad (2)$$

where Γ_K is the natural width of the K-conversion line.

To simplify the calculations we replaced the apparatus shape of the line $\varphi(x)$ by a number of rectilinear sections of the form

$$\varphi_i(x) = A_i x + B_i. \qquad (3)$$

Fig. 10 shows that along the sides of the peak the experimental points fit well on the straightline sections.

Substitution of (2) and (3) in (1) gives

$$F(x) = \frac{\Gamma_K}{2\pi}\left\{\sum_{i=1}^{4}\frac{A_i}{2}\ln\frac{(x_{i+1}-}{} + \sum_{i=1}^{4}\frac{2(B_i+A_i x)}{\Gamma_K}\left[\operatorname{arc\,tg}\frac{2(x_{i+1}-x)}{\Gamma_K}\ \operatorname{arc\,tg}\frac{2(x_i-x)}{\Gamma_K}\right]\right\}. \qquad (4)$$

Table 3

Inherent width of K-conversion lines of the active deposit of radiothorium

Line designation (after Ellis)	Level from which conv. occurs	Isotope	Natural width of line Γ_K, ev	Energy E, kev	$H\rho$	$\left(\frac{\Delta H\rho}{H\rho}\right)_K$, %	$\left(\frac{\Delta H\rho}{H\rho}\right)_{L_I}$, %	Effect bkgnd	No. of series avrgd	Angle of divergence		Slit dimensions, mm	
										α	β	Source	Counter
1	2	3	4	5	6	7	8	9	10	11	12	13	14
			67			0,042	0,025	40	10	7°30′	40′	4×0,011	4×0,018
F	*K*	Bi^{212}_{83}	64	148,1	1388,44	0,050	0,034	100	10	15°	1°	6×0,06	6×0,05
			70			0,079	0,065	54	7			6×0,1	6×0,1
G	*K*	Bi^{212}_{83}	70	188,6	~1594	0,047	0,034	5,5	10				
H	*K*	Pb^{208}_{82}	61,5	208,8	~1691	0,044	0,034	7	5	15°	1°	6×0,06	6×0,05
*I**	L_I	Bi^{212}_{83}		222,2	1753,91			35					
L	*K*	Pb^{208}_{82}	66	422,8	2607,17	0,038	0,034	5,5	7				

---

* Values in this row are given to allow comparison of the I-line (L_I) with the other lines as regards energy.

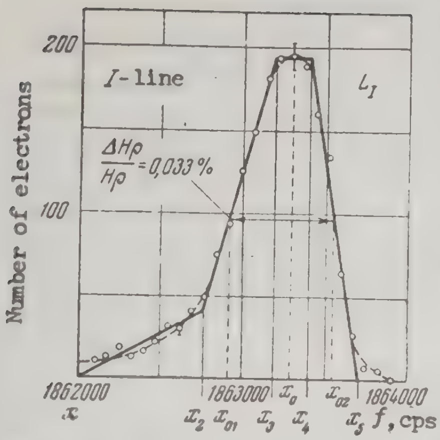

Fig. 10. Replacement of the experimental apparatus line by straightline sections.

The value of Γ_K was found from this equation by trial substitution of different values of Γ_K. It was not necessary to redetermine each time the shape $F(x)$ of the line for the Γ_K and then compare it with the experimental shape; it was sufficient to carry out the calculation for three points: $x = x_0$, the ordinate of the peak of the experimental line, and $x = x_{01}$ and $x = x_{02}$, the half-width points of the experimental line. If Γ'_K was correctly chosen we had

$$F(x_{01}) = F(x_{02}) = \frac{F(x_0)}{2}. \tag{5}$$

If the above equality did not hold another value of Γ_K was selected, larger or smaller, depending on whether $F(x_{01})$ and $F(x_{02})$ were found to be larger or smaller compared with $F(x_0)/2$.

Calculations of the inherent line width at different resolutions of the instrument made it possible to establish a certain regularity for the dispersional additions to the apparatus lines of different widths. By virtue of this it was possible to find the true value of the apparatus line width by introducing an appropriate correction to the natural width of the I-lines (conversion on the L_I-shell). The final calculations of the inherent width of the K-conversion lines were carried out taking this correction into account.

4. Results of calculations

The F-lines were measured with three different resolutions of the instrument. The calculations for the inherent widths of the F-lines were carried out independently for each case. The results are shown in Table 3. All three values of Γ_K are in good agreement within the limits of the experimental error. This substantiates the validity of the method of calculation employed.

In calculating the natural width of the F-lines we proceeded on the assumption that the width and shape of the apparatus line is independent of the line energy. The line shape may be dependent on the energy when

1) the topography of the field changes with its intensity or

2) there is strong scattering in the source backing or in the edges of slit in front of the source.

In order to verify the independence of the shape of the apparatus line on the energy of the conversion electrons we measured and calculated the natural widths of the G, H and L lines. The energies of these lines are 189, 209 and 422 kev, respectively.

If we had obtained increasing values of Γ_K with increasing energy this would indicate that the shape of the apparatus line was dependent on the energy. Results of the calculations are shown in Table 3; it will be seen from these that there are no systematic changes in the value of Γ_K. The inherent widths of all four lines agree within the limits of the experimental error.

5. Evaluation of errors

The overall error in determining the inherent width of the F-line is comprised of 1) the statistical error, 2) the error due to replacement of the experimental line with straightline sections and 3) the error in determining the natural width of the I-line.

1. The statistical error, taken from the three values of Γ_K for different resolutions, amounts to ± 2 ev.

2. The greatest error involved in replacing the apparatus line by straight-line sections apparently occurs in replacing the left tail of the line by one rectilinear section. The magnitude of this error was evaluated in the following manner. We calculated the inherent width of the line for the case when the left tail of the apparatus line is not taken into account. It turned out that neglecting the low energy tail changes the value of $\Gamma_{L_{I}}$ by about 10 ev. In view of the fact that in our approximation the tail is taken into account to the extent of about 40%, the actual error involved in the determination of Γ_K amounts to about 4 ev.

3. There are no experimental data on the inherent width of the L_I-level of Bi. This width may be evaluated in the following manner. It is known (Ref. 6) that the width of the L_I-level of the gold atom (Z = 79) equals 8.7 ev. If we extrapolate this value according to the Z^4 law we obtain $\Gamma_{L_I} \approx 10$ ev for Bi. The error in determining Γ_{L_I} presumably does not exceed ± 5 ev; hence the error in determining Γ_K is ± 2 ev.

The root mean square error $\Delta\Gamma_K = \sqrt{2^2 + 2^2 + 4^2} \approx 5$ ev. Thus we obtain $\Gamma_K = (67 \pm 5)$ ev for the inherent width of the F-line. Since the statistical accuracy in determining the G, H and L lines was somewhat lower, for them $\Delta\Gamma_K \approx 10$ ev.

Conclusions

The F-line of the active deposit of radio thorium, associated with the conversion of γ-quanta on the K-shell of Bi^{212} has an inherent width $\Gamma_K = 67 \pm 5$ ev. Within the limits of the measurement error this, too, is the inherent width of the G-line, also arising from conversion on the K-shell of Bi, and the inherent widths of the H- and L-lines associated with conversion on the K-shell of the P^{208} atom.

There are no direct x-ray data on the inherent widths of the K-levels of atoms with Z = 83. It is known, however, that the inherent widths of the atomic levels obey the Z^4 law which has been verified experimentally up to Z = 79. Extrapolation to Z = 83 yields 61-63 ev for the width of the K-level of Bi.

The inherent width of the K-conversion lines agrees with this value within the limits of the experimental error. This indicates that the inherent width of the conversion lines is determined primarily by the widths of the atomic levels and is virtually independent of effects accompanying internal conversion.

In conclusion we wish to thank B.S.Dzhelepov and A.A.Bashilov who supplied us with the basic data for the construction of the Ketron.

Department of Physics of the
"V.N.Obraztsov" Leningrad Institute of Railway Transport Engineers.

References

1. G.Lindstrom, Ark. F. Fysik, 4, 1 (1952).
2. H.Slatis & G.Lindstrom, G. Phys. Rev., 88, 1429 (1952).
3. H.Slatis, Ark. f. Fysik., 6, 415 (1953).
4. M.Mladjenovic, Ark. f. Fysik, 8, 27 (1954).
5. A.Sergeev, G.Latyshev & V.Leonov, present issue of the Bulletin.
6. E.Ramberg & F.Richtmyer, Phys. Rev., 51, 913 (1937).

INTERNAL CONVERSION ON THE L_I, L_{II} AND M_I & M_{II} SUBSHELLS OF ThC (Bi^{212})

- A.M.Krisiuk, G.D.Latyshev, M.A.Listengarten,
L.A.Ostretsov & E.G.Sergeev

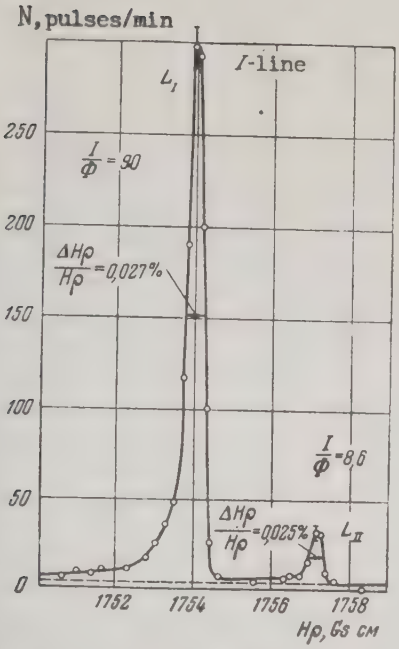

Fig. 1. Internal conversion of the 237.9 kev γ-rays on the L_I and L_{II} subshells of Bi.

1. Experimental data.

In the present investigation we determined the conversion coefficients on the L_I, L_{II}, L_{III} and M_I and M_{II} subshells for the 237.9 kev γ-transition in ThC(bi^{212}). The measurements were made on the Ketron which has been described in Ref. 1. To insure accurate determination of the relative conversion coefficients we strove to obtain complete resolution of the corresponding conversion lines.

For complete resolution of the L_I and L_{II} lines the line half-width must not exceed 0.07%; resolution of the M_I and M_{II} lines requires a line half-width under 0.04%.

The L_I and L_{II} lines were measured 28 times at three different resolving powers of the instrument: 0.066, 0.034 and 0.025%. The results of one series of measurements are reproduced in Fig. 1. The results of all three series of measurements were in close agreement.

The L_I and L_{III} lines were studied separately at an instrument resolution of 0.050%. This is the resolving power at which the most favorable ratio of the height of the conversion peaks to the background is obtained (the background here comprises the continuous β-spectrum). The L_I and L_{III} lines were recorded 11 times. The results of one series of these measurements are shown in Fig. 2. In drawing the curve for L_{III} we took into account the "apparatus" shape of the line, which is known from the curve for L_I (Ref. 1).

The following conversion coefficient ratios were obtained on the basis of data averaged over all the series of measurements:

$$L_I : L_{II} : L_{III} = 1 : (0.116 \pm 0.003) : (0.0066 \pm 0.0004). \qquad (1)$$

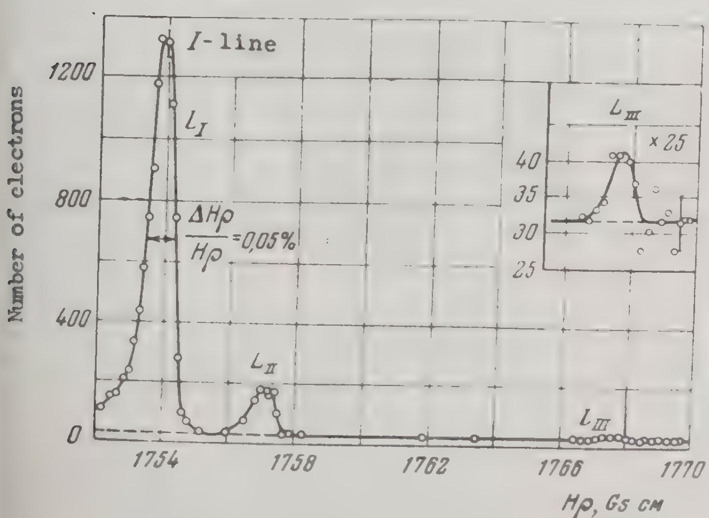

Fig. 2. Internal conversion of the 237.9 kev transition γ-quanta on the L_I, L_{II} and L_{III} shells of Bi.

The M_I and M_{II} lines were measured at a resolution of 0.034%. Six series of measurements were made; the results of one of these are shown in Fig. 3. The ratio based on the averaged value is

$$M_I : M_{II} = 1 : (0.118 \pm 0.003). \qquad (2)$$

These values differ appreciably from the data given in the literature. Shpinel' and Farafontov[2] give $L_I : L_{II} = 1 : 0.05$;

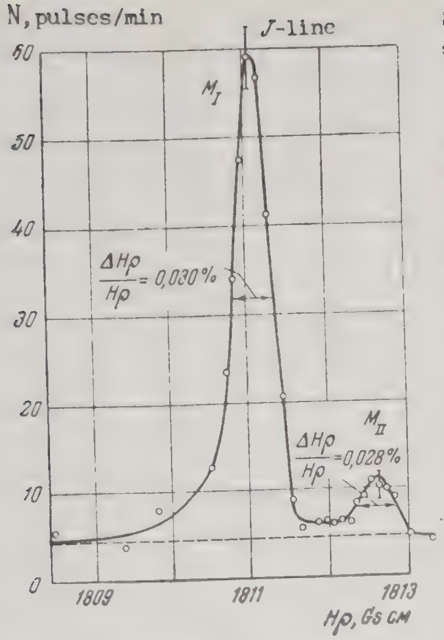

Fig. 3. Internal conversion of the 237.9 kev transition γ-quanta on the M_I and M_{II} shells of Bi.

Silverston[3] gives $L_I : L_{III} = 1 : 0.055$ and $M_I : M_{II} = 1 : 0.23$.

In these investigations, however, the lines were not fully separated and the ratios were found by graphic resolution of the total curve. One of the sources of error inherent in this method is connected with the fact that the lines are assumed to have the "standard" shape of the nearby conversion lines. However, as is known, K conversion lines have a certain inherent width, hence, the shapes of the K and L_I conversion lines are different. A characteristic of the shape of the K conversion lines is the presence of a high-energy tail. This tail is much smaller than the L_I tail. At resolutions at which separation between the L_I and L_{II}-lines becomes noticeable inherent half-width of the K-line already has an appreciable influence on the shape of line.

2. Comparison of experimental and theoretical data.

To obtain the theoretical conversion coefficients for comparison with our experimental values we interpolated in the tables given by Rose and Siegbahn[4]. The theoretical value nearest to our experimental data was that for magnetic dipole radiation:

$$L_I : L_{II} : L_{III} = 1 : 0.091 : 0.0054 \tag{3}$$

(Z = 83, energy = 238 kev); for other multipole orders, the ratios differ radically from the experimental values: 1 : 0.13 : 0.11 for M2; 1 : 0.25 : 0.20 for E1; the difference is even greater for other multipole orders.

It is known, however, that the data of Ref. 4 are not entirely accurate since in calculating the conversion coefficients for heavy nuclei it is necessary to take into account the influence of finite nuclear size.[5] According to Sliv and Listengarten[6] the ratio of the uncorrected conversion coefficient for magnetic dipole radiation on the L_I-shell to the conversion coefficient computed taking into account the finite size of nuclei equals 1.37 for Z = 83 and 238 kev energy. In view of the latest and most accurate values for the electromagnetic radius of the nucleus[7,8] this ratio must be reduced by some 5%; hence the ratio of the uncorrected to the corrected L_I coefficient is about 1.3.

Assuming that the correction for finite nuclear size for the other subshells is negligible we obtain the following theoretical value for magnetic dipole radiation on the L-subshells taking finite nuclear size into account:

$$L_I : L_{II} : L_{III} = 1 : 0.12 : 0.007 \tag{4}$$

Thus taking the finite size of nuclei into account gives closer agreement of experiment with theory.

We note that correction for screening on the L_I-shell in computing the correction for finite nuclear size should also result in a small reduction of the two last terms in (4), which should bring the theoretical and experimental data into even closer agreement.

If we attempt to attribute the difference between the experimental ratio (1) and the theoretical value (3) computed without correction for finite nuclear size, not to the effect of finite size of nuclei but to the influence of some admixture of electric quadrupole radiation we arrive at a contradictory result. Thus designating through f the fraction of electric quadrupole radiation we have

$$\alpha = (1 - f)\alpha_{M1} + f\alpha_{E2} \tag{5}$$

for each of the subshells; finding their ratios we obtain two independent equations for determining f. Since for electric quadrupole radiation $L_I : L_{II} : L_{III} = 1 : 4 : 2$ (Z = 83 energy 238 kev), even a small admixture of E2 will be very noticeable. From the ratio $L_I : L_{II}$ we find $f \approx 5\%$, while from the ratio $L_I : L_{III}$ we obtain $f \approx 0.5\%$. In other words, without correction for finite nuclear size it is impossible to match the experimental values of the ratios $L_I : L_{II}$ and $L_I : L_{III}$.

With corrections for finite nuclear size, it follows independently from both ratios that the transition is pure magnetic dipole and that if there is an admixture of electric quadrupole it does not exceed 0.3%.

There are no dependable theoretical data as yet for the $M_I : M_{II}$ ratio.

The ratio $K : L_I$ cannot be used in this case for evaluating the electric quadrupole contribution f since this ratio with Z = 83 and 238 kev is identical for magnetic dipole and electric quadrupole radiation.

It must be noted that while the relative values of the conversion coefficients taking into account finite nuclear size are in good agreement with the theoretical value for a magnetic dipole transition there is no such good agreement where the absolute values of the coefficients are concerned. According to Martin and Richardson[9] the experimental value of the K-conversion coefficient for the 238 kev ThC line differs appreciably from that predicted by theory for a magnetic dipole transition: $\alpha_K \approx 0.65$ (with correction for finite nuclear size).

Conclusions

It follows from a comparison of the experimentally determined ratios $L_I : L_{II} : L_{III}$ with the theoretical ratios for the 237.9 kev γ-transition in ThC(Bi^{212}) that this is a pure M1 transition.

The results of our investigation show that the accuracy attained in measuring the conversion coefficients on the K-subshells makes this method of determining the multipole order of γ-radiation of nuclei from the $L_I : L_{II} : L_{III}$ ratios the most dependable of all the methods based on measurement of the conversion coefficients; our results also show that it is essential to take into account the finite size of nuclei in order to obtain good agreement of theory with experiment.

In conclusion the authors desire to thank L.A.Sliv for his interest in the work and discussion of the results.

Note added in proof. Wapstra and Nijgh[10] in their report on the strong influence of finite nuclear size on the magnetic dipole conversion coefficient came to conclusions analogous to ours regarding the character of the 238 kev transition in ThC and the necessity of taking into account the influence of finit dimensions of nuclei in this case. These authors also indicate that according to their data the internal conversion coefficient on the K-shell for this line equal 0.66 which is in agreement with the views expressed in this article.

Department of Physics of the
"V.N.Obraztsov" Leningrad Institute of Railway Transport Engineers

References

1. G.Latyshev, A.Sergeev, E.Krisiuk et al, present issue of the Bulletin.
2. V.S.Shpinel' & N.V.Farafontov, Doklady AN SSSR, 72, 49 (1950).
3. D.A.Silverston, Proc. Phys. Soc., A65, 344 (1952).
4. M.E.Rose in K.Seigbahn: Beta- & Gamma Spectroscopy, Amsterdam 1955.
5. L.A.Sliv, Zhur. eksp. i teor. fiz., 21, 770 (1951).
6. L.A.Sliv, M.A.Listengarten, Zhur. eksp. i teor. fiz., 22, 29 (1952).
7. R.Hofstader, H.Fechter & I.McIntyrel, Phys. Rev., 92, 978 (1953).
8. V.Fitch & I.Rainwaters, Phys. Rev., 92, 789 (1953).
9. D.Martin & H.Richardson, Proc. Phys. Soc., A 65, 328 (1948).
10. A.H.Wapstra & G.J.Nijgh, Nucl. Phys., 1, 245 (1956).

INVESTIGATION OF THE A-LINE OF AN ACTIVE DEPOSIT OF RADIOTHORIUM

- E.M.Krisiuk, G.D.Latyshev & A.G.Sergeev

It is known that the A-line of active deposits of radiothorium is complex and should consist of two lines: a line corresponding to the conversion of the 39.9 kev γ-rays on the L_I shell of the thallium atom and a line corresponding to the conversion of the 114.7 kev transition γ-rays on the K shell of the bismuth atom. The purpose of the present work was to resolve this A-line by means of the Ketron.[1] The principal experimental difficulty lay in obtaining a good source. After a number of tests it became clear that the best sources for the investigation of the A-line were obtained when the aluminum foil was activated for a short time (2-3 hours) and the foil shielded by a metallic screen; in the process the radiothorium sample was grounded and a small positive bias was applied to the covering screen. This kept radioactive dust, which is always present in an emanation chamber, from settling on the foil. This radioactive dust consists mainly of minute particles of radiothorium (ejection particles), ejected from the sample into the chamber as a result of α-decay. The collecting potential on the activated foil was 700-800 volts.

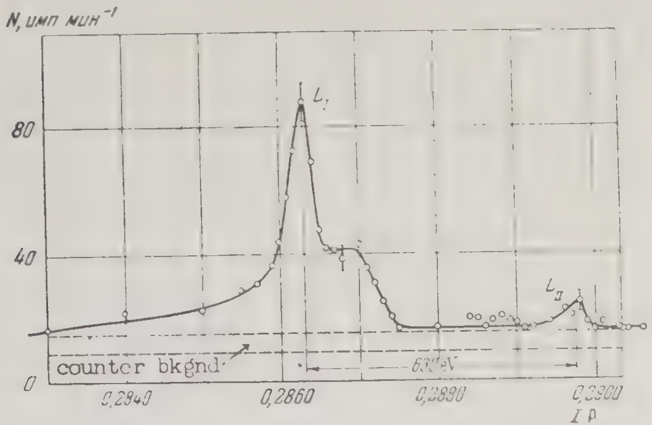

Fig. 1. Internal conversion of the 39.9 kev γ-rays of radiothorium on the L_I and L_{II} shells of thallium.

The results of the experiments are presented in Figs. 1 and 2. The abscissae are the readings of the potentiometer indicating the current through the electromagnet coils; the ordinates are the numbers of electrons recorded by the first counter.

In addition to the A-line, there also appears in Fig. 1 the Aa-line from the conversion of the 39.9 kev γ-rays on the L_{II} shell of Tl. The difference in binding energy between the two subshells L_I and L_{II} for thallium is 630 ev. Using this information we established that the high peak on the low-energy side pertains to conversion of the 39.9 kev γ-rays on the L_I shell, and that the bulge on the high-energy side of the A-line corresponds to conversion of the 114.7 kev transition γ-ray on the K level of the Bi atom. The A-line recorded using a higher resolution, is shown in Fig. 2. Here a partial separation of the L_I and K lines is observed.

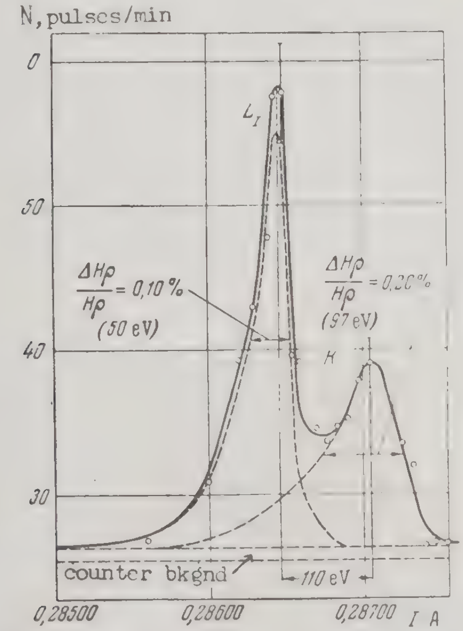

Fig. 2. Complex structure of the A-line.

The separation between the L_I and K lines obtained in our measurements is 110 ev.

Fig. 2 is a good illustration of the inherent widths of conversion lines. Since the L_I and K lines are of almost the same energy (the difference is only 110 ev), the conditions of electron scattering at the baffles, the influence of the source support and other factors must be nearly identical for the electrons of these two lines.

The half-width of the L_I line, as found in the experiment, is 50 ev, while the half-width of the K line is 97 ev. The difference between the half-widths

equals 47 ev, which is in good agreement with the results of the investigation of the natural line width of the conversion lines of the active deposit of radiothorium reported by Latyshev et al[1], according to which the difference between the natural widths of the K and L_I conversion lines of Bi is ~50 ev.

So far we have not yet succeeded in fully separating the K and L_I lines. The problem is complicated by the fact that the K conversion line of Bi has a natural width of 67 ev and the L_I line a width of 10 ev, while the distance between them is only about 110 ev.

The ratio of the intensities of the L_I and K lines, calculated from the contours in Fig. 2 is approximately 1.2.

Physics Department of
"V.N.Obraztsov" Leningrad Institute of Railroad Transport Engineers

References

1. G.D.Latyshev, A.G.Sergeev, E.M.Krisiuk et al, see present issue of Bulletin.

MEASUREMENT OF THE MAGNETIC FIELD INTENSITY IN β-SPECTROSCOPY BY THE PROTON MAGNETIC RESONANCE METHOD

- A.G.Sergeev, G.D.Latyshev & V.D.Leonov

In work with high-resolution β-spectrometers extreme accuracy in measurement of the magnetic field is essential. One of the most accurate methods of magnetic field measurement is that based on magnetic resonance of protons. The difficulty of applying the resonance method in β-spectroscopy stems from the fact that the fields involved are relatively weak ($<$1000 oersteds). Measurement of such weak fields requires the use of large samples in order to obtain an adequate signal. This requirement, together with the condition of high homogeneity of the field in the region of the sample, presents an obstacle to the practical application of the resonance method in β-spectroscopy.

We built an instrument employing proton magnetic resonance which has been successfully used for measurement of the magnetic field in a Ketron type β-spectrometer with $\rho = 8$ cm. The use of the method is predicated on the presence of an homogeneous field region in the Ketron. The probe or source of the signal, which is located in the center of the homogeneous field region in the Ketron, consists of an ampoule, a high frequency coil and two modulating coils. The ampoule is a thin-wall cylinder of acrylic plastic, holding 6 cc of water with ferric chloride dissolved therein. The high-frequency coil is wound in one layer directly on the ampoule. The inductance of the coil is 9 μh; its Q is 100. The modulating coils are wound of single silk covered enameled copper wire 0.31 mm in diameter on acrylic plastic coil forms. They consist of 24 turns each. The conductor is cemented to the coil form in order to obviate vibration of the wires in the magnetic field. The modulating coil forms are firmly attached to the plastic ampoule. The overall dimensions of the assembly are: width 28 mm, height 32 mm and length 60 mm. The amplitude of the modulating field can be varied between 0 and 2 oersted by means of an autotransformer; the frequency of the modulating field is 50 cps (the regular power line frequency).

The oscillator coupled to the high-frequency coil is based on the circuit described in Ref. 1. A variable capacitor (C_{max} = 1000 μμf) is used to provide smooth regulation of the oscillator frequency. The lower limit of the field intensities measurable with a given probe can be extended by adding a constant value capacitor to the variable one. The probe described above was successfully used for measuring fields from 100 to 1300 oersteds, which range corresponds to electron energies from 60 to 2700 kev in the Ketron.

The attainable accuracy of field measurement depends greatly on the width of the resonance peak and on the signal to noise ratio. By finding the most uniform section of the field and through appropriate selection of the ferric chloride concentration we succeeded in reducing the width of the resonance peak to 0.3 oersted and enhancing the signal-to-noise ratio. The signal-to-noise ratio could also be substantially improved by installing a narrow pass-band filter, tuned to 100 cps (the signal frequency) at the output of the last low-frequency amplifier stage. The signal is observed on the screen of an oscilloscope, the sweep of which is synchronized with the modulating voltage. In making measurements, if the total amplitude of the modulating field is large, the frequency of the oscillator must first be slowly adjusted until a trace appears on the oscilloscope screen. Then the modulating voltage is reduced so that the amplitude of the modulating field is several times smaller than the width of the resonance peak. We matched the oscillator and resonant frequencies by the appearance of the oscilloscope pattern, exact coincidence being indicated by a figure eight pattern on the screen.

The oscillator frequency was measured by means of a heterodyne wavemeter which had an accuracy of 1 in $3 \cdot 10^5$. For more precise frequency measurements we used the arrangement shown in the accompanying diagram.

The oscillator signal (i.e., the measured frequency) and pulses from a multivibrator are applied to the mixer stage. The frequency of the multivibrator is controlled by a quartz crystal maintained at constant temperature. The multivibra-

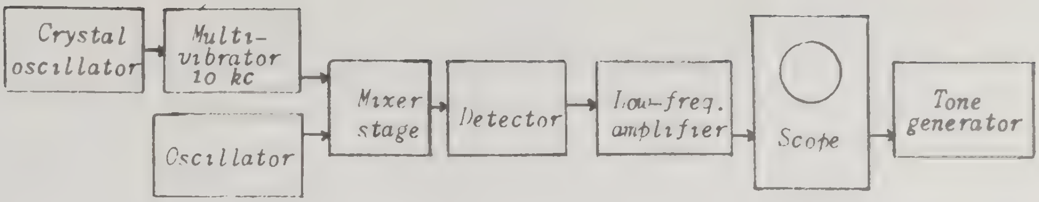

Block diagram

tor pulses are rich in harmonics that are multiples of 10 kc. Beats of these harmonics with the measured frequency appear at the mixer output. The beats go to the detector and the low-frequency amplifier which passes only frequencies in the 50 to 5000 cycle interval and cuts off all frequencies above 5000 cycles. Hence the amplifier puts out only the differential frequency resulting from the mixing of the measured frequency with the multivibrator harmonic closest to this frequency. The differential frequency Δf is measured by means of a tone generator to within 2 cycles.

The number n of the harmonic with which the measured frequency is being mixed can readily be determined by means of a wavemeter or an appropriate indicator linked with the variable capacitor in the oscillator circuit. The frequency being measured is given by $f = 10{,}000\ n \pm \Delta f$. The sign in this expression can easily be determined by slightly increasing the frequency of the oscillator: if the Δf increases the plus sign should be used; if it falls off, the Δf term should be subtracted.

The quartz crystal exciter controlling the multivibrator was tuned to 100 kc with great accuracy with reference to a standard vibrator, the signal from which was brought into the laboratory from the VNIIM by means of a special conductor. The same standard frequency was also utilized in calibrating the tone generator. The accuracy of frequency measurement by the described method is 1 part in $2 \cdot 10^6$. The accuracy of magnetic field measurement in our case is determined primarily by the precision with which the oscillator can be tuned to the frequency of the resonance absorption peak. In the region 150-400 oersted fields the accuracy of relative magnetic field intensity determinations is 1 in $2 \cdot 10^5$ and increases with rising field strength. The described apparatus made it possible to investigate qualitatively the inherent width of the conversion lines of an active deposit of radiothorium.[2]

References

1. R.Pound & W.Knight, Rev. Sci. Inst., 21, 219 (1950).
2. G.Latyshev, A.Sergeev, E.Krisiuk, L.Ostretsov, Iu.Egorov & N.Shirshov, present issue of the Bulletin.

$$A = A'\left(1 - e^{-\frac{\Delta I}{\Delta I_0}}\right).$$

Hence

$$\Delta H = A'\left(1 - e^{-\frac{\Delta I}{\Delta I_0}}\right)\left(1 - e^{-\frac{t}{\tau}}\right). \qquad (2)$$

For our magnet $\Delta I_0 \approx 1$ ma and $A' \approx 0.055$ oersted.

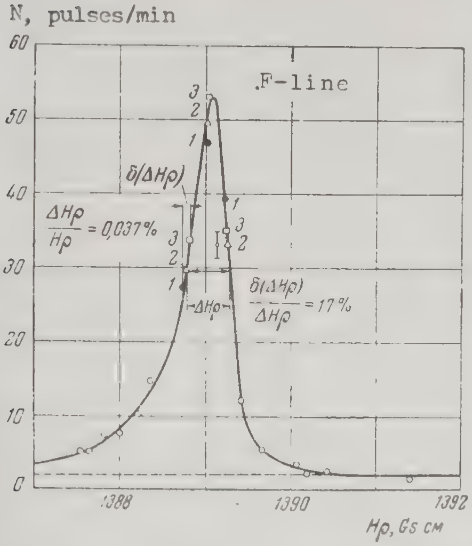

Fig. 3. Illustration of possible error resulting from the magnetic aftereffect.

This shows that in working with magnetic spectrometers having iron components, for accurate determination of the half-width and shape of internal conversion lines it is not enough to simply measure the current supplied to the electromagnet windings. It is essential to make accurate and direct measurements of the magnetic field.

It is particularly important to take the magnetic aftereffect into account in working with spectrometers having a high resolving power, for in such cases the aftereffect can appreciably alter the shape and half-width of the recorded lines. By way of illustration an F line recorded by means of our spectrometer is shown in Fig. 3. Points 1, 2 and 3 were recorded at a constant current value. The quantity $\delta(\Delta H\rho)/\Delta H\rho$ characterizes the error that might be involved in determining the half-widths without taking the magnetic aftereffect into account.

In order to obviate such errors, in the investigation of Ref. 1 we made three measurements of the field intensity at each current setting: at the beginning of the measurement period, in the middle of it and at the end, and then took the average value for the field intensity.

Department of Physics of the
"V.N.Obraztsov" Leningrad Institute of Railway Transport Engineers.

References

1. G.Latyshev, A.Sergeev, E.Krisiuk et al, present issue of the Bulletin.
2. A.Sergeev, G.Latyshev & V.Leonov, present issue of the Bulletin.

IN ELABORATION OF THE CONTRIBUTION[1] "ON THE PROBLEM OF FOCUSING A PLANE BEAM OF CHARGED PARTICLES BY A MAGNETIC FIELD VARYING ALONG ONE CARTESIAN COORDINATE"

- V.P.Saulit

In Ref. 1 we made a particular assumption regarding the expansion into a power series of the function $f(\mu)$. In the present contribution the integral equation in question is solved under a more general assumption regarding this function. In addition we present a general equation for finding the coefficients in the expansion series for the function $f^*(\mu)$, which was omitted from the original contribution.

As we showed in Ref. 1, the problem of focusing a plane beam of charged particles in a magnetic field varying along one Cartesian coordinate reduces to the solution of the integral equation

$$f(\mu) = -4\mu^{3/2} \int_0^{\pi/2} \sqrt{2-\mu\cos^2\varphi}\,\psi_1(\mu\sin^2\varphi)\cdot\sin\varphi\cos^2\varphi\,d\varphi, \tag{1}$$

where $\psi_1(\tau)$ is the sought function and $f(\mu)$ is defined by the expression

$$f(\mu) \equiv x_0 - x_F + \sqrt{1-(\cos\alpha_0-\mu)^2}\,R_0(\cos\alpha_0-1) + \sqrt{1-(\tau_0+1-\mu)^2}\,R_0(\tau_0) + {} + 2\int_{\cos\alpha_0-1}^{0} \sqrt{1-(\tau+1-\mu)^2}\,\psi_0(\tau)\,d\tau + \int_{\tau_0}^{\cos\alpha_0-1} \sqrt{1-(\tau+1-\mu)^2}\,\psi_0(\tau)\,d\tau. \tag{2}$$

In solving equation (1) we assumed that the function $f(\mu)$ can be represented by a series in integral powers of μ:

$$f(\mu) = \sum_{k=1}^{\infty} a_k\mu^k. \tag{3}$$

Actually this is valid only in the case when $\psi_0(\tau) = 0$ (case of the Ketron field - Ref. 2). In the general case, we must write

$$f(\mu) = \sum_{k=1}^{\infty} a_k\mu^{\frac{k+1}{2}}. \tag{4}$$

It might appear that all the terms in (2) could be expanded in series in integral powers of μ; this pertains, in particular, to the expressions under the integral. However, it can be shown that the series in powers of μ, in which the expression under the first integral in (2) was expanded, fails to converge uniformly over the entire integration interval. In view of this the integration of the series proposed in our original contribution is not allowable and leads to erroneous results. Hence it is necessary to make a correction in the solution of (1).

To this end we rewrite the integral $A \equiv \int_{\cos\alpha_0-1}^{0} \sqrt{1-(\tau+1-\mu)^2}\,\psi_0(\tau)\,d\tau$ in the form of the difference

$$A = \int_{\cos\alpha_0-1}^{0} \sqrt{1-(\tau+1-\mu)^2}\,\psi_0(\tau)\,d\tau - \int_0^{\mu} \sqrt{\mu-\tau}\cdot\sqrt{2-(\mu-\tau)}\,\psi_0(\tau)\,d\tau. \tag{5}$$

Introducing a new integration variable into the second term

$$\varphi \equiv \arccos\sqrt{1-\frac{\tau}{\mu}}, \tag{6}$$

we obtain

$$A = \int_{\cos\alpha_0-1}^{\mu} \sqrt{1-(\tau+1-\mu)^2}\,\psi_0(\tau)\,d\tau - 2\mu^{3/2} \int_0^{\pi/2} \sqrt{2-\mu\cos^2\varphi}\,\psi_0(\mu\sin^2\varphi)\cdot\sin\varphi\cos^2\varphi\,d\varphi. \tag{7}$$

The first integral in this equation gives us a series in integral powers of μ, while the second yields an expansion in half-integer powers of μ, i.e., we see that $f(\mu)$ is actually represented not by (3) but by the series (4). Comparing the right-hand parts of (1) and (2), taking (7) into account, we see that the solution of equation (1) can be written in the form

$$\psi_1(\tau) = \psi_0(\tau) + \psi_1^*(\tau), \tag{8}$$

where $\psi_1^*(\tau)$ is the solution of equation (1) in which $f(\mu)$ is replaced by $f^*(\mu)$, here

$$f^*(\mu) \equiv x_0 - x_F + \sqrt{1-(\cos\alpha_0-\mu)^2}\,R_0(\cos\alpha_0-1) + \sqrt{1-(\tau_0+1-\mu)^2}\,R_0(\tau_0) + 2\int\limits_{\cos\alpha_0-1}^{\mu} \sqrt{1-(\tau+1-\mu)^2}\,\psi_0(\tau)\,d\tau + \int\limits_{\tau_0}^{\cos\alpha_0-1} \sqrt{1-(\tau+1-\mu)^2}\,\psi_0(\tau)\,d\tau. \tag{9}$$

In this case $f^*(\mu)$ is actually represented by a series in integral powers of μ:

$$f^*(\mu) = \sum_{k=1}^{\infty} a_k^* \mu^k \tag{10}$$

and, as follows from Ref. 1, $\psi_1^*(\tau)$ has the form

$$\psi_1(\tau) = \tau^{-1/2} \sum_{k=0}^{\infty} c_k \tau^k, \tag{11}$$

where c_k is found by means of the recurrent equations

$$c_k = \left\{ \frac{k!}{(2k)!} \sum_{n=1}^{k} \frac{[(2n)!]^2\,[2(k-n)]!\,(2n+1)}{2^{3n}(n!)^3(k-n)!\,(2n-1)}\, c_{k-n} \right\} - \frac{2^{2k}(k!)^2(k+1)}{\pi\sqrt{2}\,(2k)!}\, a_{k+1}^* \qquad (k = 1, 2, \ldots), \tag{12}$$

and

$$c_0 = -\frac{a_1^*}{\pi\sqrt{2}}. \tag{13}$$

Bearing in mind (8), we have

$$y(\tau) = y_{02} + \int_0^{\tau} R_0(\tau_1)\,d\tau_1 + \tau^{3/2} \sum_{k=0}^{\infty} \frac{4c_k}{(2k+1)(2k+3)} \tau^k. \tag{14}$$

We note that in deducing the solution of (1) we assumed that such a solution exists. Rigorously speaking we should in every concrete case check the solution obtained, i.e., substitute the derived expression for $\psi_1(\tau)$ in equation (1) and show that the equality is satisfied.

The following equation can readily be deduced for finding the coefficients a_n^* in (10):

$$a_n^* = 2f_n + \frac{1}{\pi} \sum_{k=0}^{n} \frac{B(k+1/2,\, n-k+1/2)}{(n+1)[2(n-k)-1](2k-1)\,B(k+1,\, n-k+1)} \times \left\{ \frac{(-1)^k |\sin\alpha_0|\, R_0(\cos\alpha_0-1)}{(1-\cos\alpha_0)^k(1+\cos\alpha_0)^{n-k}} + \frac{\sqrt{1-(\tau_0+1)^2}\,R_0(\tau_0)}{\tau_0^k(2+\tau_0)^{n-k}} + \int\limits_{\tau_0}^{\cos\alpha_0-1} \frac{\sqrt{1-(\tau+1)^2}\,\psi_0(\tau)\,d\tau}{\tau^k(2+\tau)^{n-k}} \right\}, \tag{15}$$

where B is a β-function and

$$f_n \equiv \frac{1}{n!} \left\{ \int\limits_{\cos\alpha_0-1}^{0} \sqrt{1-(\tau+1)^2}\, \frac{d^n\psi_0}{d\tau^n}\, d\tau + \sum_{k=0}^{n-1} \left. \frac{d^k\psi_0}{d\tau^k} \right|_{\tau=\cos\alpha_0-1} \cdot \delta_{n-k-1} \right\}, \tag{16}$$

where, in turn,

$$\delta_n = \frac{|\sin\alpha_0|\, n!}{\pi(1+\cos\alpha_0)^n(n+1)} \sum_{i=0}^{n} \frac{(-1)^i B(i+1/2,\, n-i+1/2)}{(2i-1)[2(n-i)-1]\,B(i+1,\, n-i+1)} \left(\frac{1+\cos\alpha_0}{1-\cos\alpha_0}\right)^i. \tag{17}$$

Physical Scientific Research Institute of Leningrad State University

References

1. V.Saulit, Izv. AN SSSR, Ser. fiz., 18, 233 (1954).
2. P.Pavinski, Izv. AN SSSR, Ser. fiz., 18, 175 (1954).

BULLETIN of the Academy of Sciences of the USSR - Physical Series
Vol. 20, No. 3, 1956 - Transactions of the Fifth All-Union Conference on
Nuclear Spectroscopy (Moscow, 10-14 February 1955)

TABLE OF CONTENTS

	Page	
	Orig.	Trans.
Forbidden β-spectra of Rb^{86}, Sr^{90}, Y^{90} and Tl^{204} - E.E.Berlovich, D.M.Khai and A.V.Savateev	275	259
Radiation of Sb^{124} - A.V.Zolotavin, E.P.Grigor'ev & M.A.Abroian	289	270
On analysis of the shape of the β-spectrum of RaE - L.N.Zyrianova	308	285
Calculation of probability of pair conversion in the case of 0--0 nuclear transitions - L.N.Zyrianova & V.A.Krutov	312	288
Internal conversion positrons in the spectrum of radioactive Sb^{124} - B.S.Dzhelepov and O.E.Kraft	318	293
The Elotron - A magnetic γ-spectrometer with improved focusing - B.S.Dzhelepov and S.Z.Shestopalova	328	302
Investigation of low-intensity hard γ-rays by means of the photoneutron effect - B.S.Dzhelepov and I.A.Iaritsyna	343	314
Tests and operating regime of a scintillation γ-spectrometer - A.A.Konstantinov, O.I.Sumbaev & V.V.Chekin	347	318
Determination of the relative probabilities of K-capture and β-decay - A.A.Bashilov, N.M.Anton'eva & B.V.Pshenichnikov	348	319
Inherent widths of the internal conversion lines of an active deposit of radiothorium - G.D.Latyshev, A.G.Sergeev, E.M.Krisiuk, L.A.Ostretsov, Iu.S.Egorov & N.M.Shirshov	354	324
Internal conversion on the L_I, L_{II}, L_{III} and M_I & M_{II} subshells of ThC (Bi^{212}) - E.M.Krisiuk, G.D.Latyshev, M.A.Listengarten, L.A.Ostretsov & E.G.Sergeev	363	332
Investigation of the A-line of an active deposit of radiothorium - E.M.Krisiuk, G.D.Latyshev & A.G.Sergeev	367	335
Measurement of the magnetic field intensity in β-spectroscopy by the proton magnetic resonance method - A.G.Sergeev, G.D.Latyshev & V.D.Leonov	369	337
Magnetic aftereffect in an iron core electromagnet - Iu.G.Zhukovski, E.M.Krisiuk, G.D.Latyshev & A.G.Sergeev	371	339
In elaboration of the contribution, "On the problem of focusing a plane beam of charged particles by a magnetic field varying along one Cartesian coordinate" - V.P.Saulit	374	341

Translated in 1957 by
Columbia Technical Translations,
5 Vermont Ave., White Plains, N.Y.

Number 4 Volume 20 1956

BULLETIN

of the

Academy of Sciences of the USSR

- Physical Series -

(Izvestiia Akademii Nauk SSSR)
(Seriia fizicheskaia)

Reproduction rights reserved

by

Columbia Technical Translations
5 Vermont Avenue
White Plains, New York

Single Issues

$20

Annual Subscription

$215

OPENING ADDRESS

- V. L. Levshin

The Fourth All-Union Conference on Luminescence, opening today is devoted specifically to problems of molecular luminescence and luminescence analysis.

The three previous conferences on luminescence had a more general program and encompassed all aspects of the subject. However, it became clear at the last conference that the diversity of luminescence studies in the Soviet Union made it impossible to embrace all its branches at a single conference, if they are to be treated with the necessary attention and completeness. Therefore, the Committee on Organization decided that it was necessary to set up separate conferences to deal with each of the two major branches of luminescence: molecular luminescence and crystal phosphors.

This decision serves to emphasize the great importance of molecular luminescence. There was a time when virtually all work on luminescence in the Soviet Union was in the field of molecular and atomic luminescence. Thirty years ago S. I. Vavilov set his group the problem of investigating the light emission of liquids. As investigations of luminescence progressed, and large groups of researchers were involved, the objectives pursued naturally expanded, and ultimately came to encompass all aspects of this field. Furthermore, the center of interest shifted, during the past 15 years, from the luminescence of molecules to that of crystal phosphors. Study of molecular luminescence temporarily became of secondary importance. I say "temporarily", because the problems of molecular luminescence are no less important and no less interesting to investigation of the properties of matter than are studies of crystal phosphors. Moreover, they offer possibilities of the most varied technical applications of luminescence in the national economy.

Permit me to note certain trends in the development of molecular luminescence studies which, to my way of thinking, are of particular importance to the study of the properties of matter.

Molecular luminescence offers a method of probing deeply into the processes occurring within the emitting material: the changes occurring in the molecule incident to absorption of energy, the redistribution of the absorbed energy within the molecule, migration of this energy within the molecule and, finally, the transfer of energy from the molecule to the surrounding medium, to which is related one of the most important problems of molecular luminescence, namely, the question of why certain molecules possess the property of luminescence while others do not. Among the most important questions in the study of luminescent bodies is the investigation of metastable molecular states giving rise to a persistent after glow. The role of metastable states and triplet energy levels in intramolecular processes, and specifically in the processes involved in the transformation of molecular energy, is far from clear.

The question of the interaction of molecules with each other and with the surrounding medium is also of exceptional importance.

The exchange of energy between molecules considerable distances apart and between solvents and solutes lies at the root of many problems related to the energetics of luminescence. These problems have attracted the particular attention of investigators only recently are yet to be solved.

Of no less importance than the study of luminescence per se is the identification through luminescence studies of the properties of materials, the characteristics of emitters and of the surrounding medium. The first stage here is determination of the nature of the emitter. During his last years, Vavilov concerned himself with the characteristics of the elementary emitter and the possibility of representing it in the form of a simplified model of an electric dipole, an electric quadrupole or a magnetic dipole or yet a more complex combination of dipoles and quadrupoles. The feasibility of using the complex

model stems from the existence of separate absorption and emission oscillators and the transfer of energy within the molecule.

Obviously these concepts are only a preliminary stage in the description of molecules. Real molecules are incomparably more complex. However, we now know much about their properties, structure, the positions of their components, and the binding forces acting between these components. Only a few decades ago examination of the effect of the association of luminescent molecules upon luminescence efficiency and the other optical properties of solutions appeared to many to be a purely formal exercise, because it was impossible to determine the actual manner in which molecules combine and what energy transfer processes might occur in such associated systems. At present, however, we have a great deal of specific data on the nature of the forces responsible for association and the ways in which particles can combine. We can now fully and accurately evaluate the effect of such associations on the optical properties of the material.

The employment of luminescence to study the processes of association, dissociation, complex formation, etc., which go beyond the bounds of luminescence itself, offers a powerful tool for the study of states of matter.

Study of molecular luminescence, in addition to helping solve theoretical problems, leads to a variety of applications of luminescence in biology, medicine and the national economy in general. These applications are far too numerous to list here even in the briefest form.

Therefore I shall mention only the new methods of luminescence analysis, which should be introduced into practice, and those fields of application of luminescence analysis which have already gained major importance in scientific research.

In speaking of these new methods, I must draw attention to the need for developing applications of the phosphorescence of organic substances. The phosphorescence spectra of certain organic luminophors are very specific and can serve to identify certain compounds.

A second new method of luminescence analysis may be provided by the study of polarization spectra which make it possible to determine the orientation of the oscillators in molecules and of the molecules themselves.

Among the applications of luminescence analysis that have come into wide use in the USSR, luminescence methods of investigation in biology and medicine deserve particular attention. At the beginning of 1955 the Academy of Sciences and the Ministry of Public Health set up a coordinated plan of work for the purpose of applying luminescence analysis to medical, biological and microbiological objectives. Meetings held for this purpose have shown how broad is the range of medical biological institutions interested in the development of luminescence studies and how important and various are the problems already being solved by this method.

Another significant area of practical application of molecular luminescence is the development of organic luminophors for use in light industry.

Finally, let us note the major significance of luminescence defectoscopy for the metalworking industries.

These applications of molecular luminescence, and many others that I have not mentioned, testify to the high practical value of investigation of this phenomenon and explain the rapid increase in work in this field in the Soviet Union.

The purpose of the present conference is to shed light upon every major aspect of molecular luminescence. The agenda gives prominence to problems of the energetics of molecular luminescence and the physical processes occurring in luminescening molecules. Due attention will be given to the problem of the interaction of molecules with the surrounding medium. We shall hear a number of papers on the methods and results of application of luminescence analysis

in various fields of science and technology.

Our conference is meeting in Minsk. This is the first time that an All-Union Conference on Luminescence has been held outside Moscow. This is quite significant, for it testifies to the importance of the work done by the Byelorussian Academy of Sciences in the field of luminescence.

It is remarkable, too, that our conference is being held in this city of Minsk which was wholly destroyed during World War II. Our conference will be held in newly-erected buildings, and with the cooperation of the newly-established Institute of Physics and Mathematics of the Byelorussian Academy of Sciences. This is testimony to the tremendous attention lavished by the Party and government of our country on the development and progress of science.

The Presidium of the Academy of Sciences of the Byelorussian SSR and our hosts, the physicists of Byelorussia, have gone to great trouble in organizing this Conference. I believe that I am expressing the opinion of all assembled here in expressing our profound gratitude for this effort.

The large number of persons working in the field of luminescence assembled here is evidence of the interest shown in this Conference. I hope our work will prove fruitful.

On behalf of the Organizing Committee, I declare the Fourth All-Union Conference on Molecular Luminescence open.

* * * * * * * * *

INTERMOLECULAR ENERGY TRANSFER MANIFESTED IN SENSITIZED LUMINESCENCE (Abstract*)

-A.N.Terenin and V.L.Ermolaev

The report is devoted to a review and critical discussion of studies of the transport and migration of electronic excitation energy in solutions and crystals of organic compounds. The survey comprises studies published from 1950 to 1954.

The first part of the paper examines the results of studies of radiationless energy transfer between fluorescent molecules in solutions, obtained by various Soviet researchers (Galanin, Frank and Levshin) continuing the classic studies of S.I.Vavilov. Foreign studies of the same question are also treated, including Schmillen's fluorometric measurements on mixed dye solutions and the spectrophotometric measurements of the luminescence yields of various components solutions of mixed aromatic hydrocarbons as a function of the concentration (Bowen, Brocklehurst, Livingston). The second part of the paper discusses the new experimental and theoretical work on energy migration in molecular crystals (Davydov, Schmillen, Zhevandrov, etc.). Much attention is given to investigations of energy transfer in liquid systems subjected to the influence of high-energy particles and quanta.

The third part of the report is devoted to a critical review of the major studies in this field (Kallmann, Fürst, Birks, etc.). The treatments of these phenomena are considered to be inadequate when based either on non-radiative energy transfer alone (Kallmann, Fürst) or on radiative alone (Birks), without taking into account the appearance of excited particles (electrons, radicals, ions) and the associated processes of chemiluminescence. The fourth section is devoted to a discussion of a number of studies of energy migration in frozen solutions and suspensions of aromatic hydrocarbons (Reid, Moody, Faidysh), and presents a more plausible interpretation of the results of these investigators.

The fifth part of the report is concerned with the luminescence of complexes of sym-trinitrobenzene with polycyclic hydrocarbons (Reid, Moody). Sensitized phosphorescence, interpreted as a process of non-radiative energy transfer from a molecule at the triplet level to an unexcited molecule with transition of the latter to the triplet level (Terenin, Ermolaev) is the subject of the sixth part of the report. Finally, the seventh and last part is devoted to spectrophotometric studies of the fluorescence of photosynthesizing pigments in living algae, proving the transfer of electron excitation energy from phycoerythrin to phycocyanin and chlorophyll (French, Young). This section also presents a critique of Bannister's work on the migration of energy in phycocyanin from the albumin to the pigment.

EXCITON STATE OF AN IMPERFECT MOLECULAR CRYSTAL (Abstract**)

- A.S.Selivanenko

A non-localized exciton for a semi-infinite molecular crystal is examined. The boundary is taken as a local perturbation of the lattice. The requirement that the perturbation be small is not imposed. Solution of Schrödinger's stationary state equation yields exciton waves, the wave vector of which is parallel to the crystal boundary. These waves penetrate into the depth of the crystal to the same extent that the perturbation is propagated over the surface, i.e., they are localized on the surface.

The author terms the corresponding model the "surface exciton" model. This surface exciton has levels differing from those of a volume exciton. The number of levels is equal to the number of the lattice constants within the range of the surface perturbation. If the molecule is in the cell α, each of the levels is split into α bands, each of which in turn is characterized by a quasi-continuous structure related to the wave vector.

Experimentally, the surface effect must be observed at low temperatures in powders or crystals with a well developed cell structure. The observed spectra should comprise lines corresponding to the surface levels.

---

*Complete paper published in Usp. fiz. nauk, 58, 37 (1956).

**Complete report scheduled for publication in Zhur. eksp. i teor. fiz., 31, 9 (1956).

TRANSFER OF EXCITATION ENERGY FROM THE SOLVENT TO THE DISSOLVED LUMINOPHOR IN LIQUID AND SOLID SOLUTIONS

-T.P.Belikova, M.D.Galinin & Z.A.Chizhikova

1. Modern resonance energy transfer theory enables us to express the probability of excitation energy transfer in terms of the optical characteristics of the interacting molecules.[1,2] For two molecules M_1 and M_2 at a distance R from each other the transfer probability in the case of dipole transitions is characterized by

$$W(R)=\frac{9c^4}{8\pi n^4}\cdot\frac{1}{\tau_{1e}R^6}\int\frac{\varkappa_2(\omega)f_1(\omega)}{\omega^4}d\omega\cdot|2\cos\vartheta_1\cos\vartheta_2-\sin\vartheta_1\sin\vartheta_2\cos\varphi|^2, \tag{1}$$

where τ_{1e} is the mean "natural" lifetime of the excited state of the M_1 molecules, n is the refractive index of the solvent, $\varkappa_2(\omega)$ is the absorption coefficient of the M_2 molecules (calculated per molecule), $f_1(\omega)$ is the normalized luminescence spectrum of the M_1 molecules, ϑ_1 and ϑ_2 are the angles of the dipoles relative to the direction of R and φ is the difference between the dipole azimuth angles. Whence we can evaluate the characteristic energy transfer range R_o, which can be determined from

$$W(R_0)\quad\frac{1}{\tau_{10}}. \tag{2}$$

Summation and averaging of the transfer probability over all the molecules makes it feasible to determine the dependence of the output B_1 and the mean lifetime τ_1 of the excited state of the M_1 molecules on the concentration N_2 of the M_2 molecules.[2] In the simplest case (when the molecules may be regarded as stationary during the lifetime of the excited state), we have the following expressions:

$$\frac{B_1}{B_{10}}=1-2qe^{q^2}\int_q^\infty e^{-x^2}dx\approx1-\sqrt{\pi}q+\ldots \tag{3}$$

and

$$\frac{\tau_1}{\tau_{10}}=\frac{1+q^2-(3+2q^2)qe^{q^2}\int_q^\infty e^{-x^2}dx}{1-2qe^{q^2}\int_q^\infty e^{-x^2}dx}\approx1-\frac{\sqrt{\pi}}{2}q+\ldots, \tag{4}$$

where

$$q=1{,}55\left(\frac{\bar\lambda}{2\pi n}\right)^2\sqrt{\frac{\tau_{10}}{\tau_{1e}}}\,\bar\varkappa_2N_2, \tag{5}$$

with $\bar\lambda$ and $\bar\varkappa_2$ being defined by the relationship

$$c^4\int\frac{\varkappa_2(\omega)f_1(\omega)}{\omega^4}d\omega=\bar\lambda^4\bar\varkappa_2. \tag{6}$$

Equations (3) and (4) hold in cases where the premises of the theory are valid.[2] There is agreement with experiment both as regards the nature of the dependence on the concentration and the relationship between B_1 and τ_1 and where the absolute value of q is concerned, provided the latter is calculated on the basis of independent experimental data on the overlapping of the spectra.

Thus observation of cases of resonance transfer involving deviation from these regularities may serve as indication of the necessity of taking certain additional factors into account. Two such cases will be examined in the present report.

2. Experiments on the excitation of luminescent solutions by high-energy radiation[3] have established that the above mentioned regularities can be explained only on the assumption that there is a transfer of excitation energy from the solvent to the dissolved luminophor. There are conflicting opinions regarding the transfer mechanism.[4,5] We investigated the process of energy transfer from solvent to solute with excitation by light in the absorption band of the solvent and attempted

to apply the theory of resonance transfer thereto. The experiments were carried out on two typical solutions: terphenyl in xylene and anthracene in toluene.[6]

Our evaluation of the emission efficiency of the pure solvents (about 3% for xylene and 1% for toluene) showed that it is too low to explain the energy transfer simply on the grounds of reabsorption of the emission of the solvent by the luminophor.

For purposes of comparison with the theory of resonance transfer, we measured the relative luminescence efficiencies, the absorption coefficients and the luminescence spectra. Neglecting the luminescence of the solvent, the intensity of emission of the solution can be characterized by the expression

$$I = E\,\frac{K_1}{K_s + K_1}\,\eta_1 + \frac{K_s}{K_s + K_1}\,\eta_1^1\, q_{s1}^t, \qquad (6)$$

where E is the intensity of the exciting light, K_1 is the absorption coefficient of the luminophor, K_s is the absorption coefficient of the solvent, η_1 is the luminescence efficiency of the luminophor under the influence of the incident light, η_1^1 is the luminescence efficiency of the luminophor after the energy transfer and q_{s1}^t is the probability of energy transfer from the solvent to the luminophor.

It was found that for both solutions at a concentration of about 10^{-3} g/ml the value of q_{s1}^t attains about 0.5. With increasing concentration, concentration quenching develops in anthracene, while for terphenyl q_{s1}^t approaches unity at a concentration of $5 \cdot 10^{-3}$ g/ml.

3. Comparison with resonance transfer theory showed that the experimental values of q_{s1}^t are one order of magnitude greater than the calculated ones. It is natural to seek an explanation for this divergence by questioning the validity of the assumption that the molecules are "stationary" during the lifetime of the excited state in solutions having a low viscosity. Thus, the characteristic transfer range R_o as calculated from (2) is appreciably smaller than the mean square displacement r^2 of the molecules due to Brownian movements (diffusion) during the lifetime of the excited state interval.*

In order to evaluate the effect of diffusion, we examined the following model. Let us assume that the transfer occurs with an appreciably high probability (for example, p = 1/2) only when the molecule moves into a sphere of radius R_o. In this case we can apply the quenching theory developed for extraneous quenchers of the type of KI and write

$$q_{s1}^t = 4\pi p R_o \tau_{10} D N_2 \left(1 + \frac{R_o}{\sqrt{\tau_{10} D}}\right) \qquad (7)$$

where D is the diffusion coefficient.

The values of R_o and $\sqrt{r^2}$ as well as the experimental and calculated values of q_{s1}^t are given in the accompanying table.

Characteristic energy transfer ranges R_o, mean displacements $\sqrt{r^2}$ of molecules due to diffusion and the probabilities of energy transfer from the solvent to the luminophor for solutions of terphenyl in xylene and anthracene in toluene.

Luminophor & solvent	R_o, Å	$\sqrt{r^2}$, Å	q_{s1}^t for $C = 5 \cdot 10^{-5}$ g/mole		
			Exper.	Theo. disregarding diffusion	Theo. taking diffusion into account
Terphenyl in xylene	20	75	0.05	0.004	0.06
Anthracene in toluene	17	140	0.07	0.003	0.15

---

*We were unable to measure the lifetime of the excited state directly. It was evaluated from the area under the contour of the first absorption band on the assumption that the quenching reducing the luminescence efficiency is quenching of the second type.

As may be seen from the table the theoretical values calculated taking diffusion into account are in fairly good agreement with the experimental data. Thus, we have here energy transfer by means of "collisions", the cross section for which is determined by the probability of resonance transfer.

4. The other case of resonance transfer investigated by us is that of the sensitized luminescence of naphthacene in anthracene.[8] Despite the great number of investigations of this classical solution, until now no one has compared the results of these investigations with the theory of resonance transfer.

By virtue of transfer of excitation energy from the anthracene to the naphthacene, the lifetime τ_1 of the excited state of anthracene decreases with increasing naphthacene concentration. Having measured τ_1, the luminescence spectrum of the anthracene and the absorption spectrum of the naphthacene, we can attempt to apply the theory of resonance transfer. At a naphthacene concentration of $2.5\cdot10^{-5}$ g per gram of anthracene ($N_2 = 8\cdot10^{16}$ molecules/ml) we obtain the experimental value of $1 - \tau_1/\tau_{10} \approx 0.3$. The calculated value for this concentration is 0.005.

Consequently, in this case we have a very considerable divergence. The reason may be that the theory does not allow for migration of the excitations through the anthracene lattice, although the fact that such migration occurs cannot be doubted. Unfortunately we still know little about the mechanism of this migration at room temperature. According to Davydov[9] both localized and non-localized excitons may exist. The theory does not yield sufficient information for evaluating the possible consequences of the migration of non-localized excitons. Let us assume, therefore, that only localized excitons are involved. The movement of such excitons through the lattice partakes of the nature of diffusion and we have a complete analogy with the transfer of excitation from a liquid solvent, except that instead of the diffusion of molecules we have diffusion of excited states. One can determine from the experimental data what value the diffusion coefficient must have to assure the observed transfer. The evaluation yields $D = 4.5\cdot10^{-4}$ cm^2/sec; whence for the time an exciton remains in an individual molecule we obtain 10^{-12}-10^{-11} sec. On the other hand, from the superposition of the spectra, we can evaluate the probability W of resonance transfer of excitation energy from one anthracene molecule to a neighboring one, also on the basis of the localized exciton hypothesis. This evaluation yields a value of 1/W between $3\cdot10^{-12}$ and 10^{-10} which agrees in order of magnitude with the preceding estimate.

The foregoing is not to be taken as an argument in favor of the hypothesis that the migration of energy through the lattice is accomplished specifically by localized excitons, but the considerations set forth do at least indicate that this hypothesis is not in conflict with the experimental data. At the same time, it must be emphasized that, regardless of the actual nature of the migration mechanism, the existence of migration is substantiated by our data. Thus comparison of experimental data with resonance transfer theory is fruitful and permits of drawing certain physical deductions regarding the characteristics of the energy transfer process.

"P.N.Lebedev" Physical Institute of the
Academy of Sciences of the USSR

References

1. T.Förster, Ann. d. Phys., 2, 55 (1948); ZS. f. Natur., 4a, 321 (1949); D.L.Dexter, Chem. Phys., 21, 836 (1953).

2. M.D.Galanin, Zhur. eksp. i teor. fiz., 28, 485 (1955).

3. H.Kallmann & M.Furst, Phys. Rev., 79, 857 (1950); 81, 853 (1951); 85, 816 (1952).

4. M.Furst & H.Kallmann, Phys. Rev., 96, 902 (1954).

5. J.B.Birks, Scintillation Counters. London, 1953.

6. T.P.Belikova & M.D.Galanin, Optika i spektroskopiia (Optics and spectroscopy), 1, 168 (1956).

As may be seen from the table the theoretical va[illegible]alculated taking diffusion into account are in fairly good agreement with the experimental data. Thus, we have here energy transfer by means of "collisions", the cross section for which is determined by the probability of resonance transfer.

4. The other case of resonance transfer investigated by us is that of the sensitized luminescence of naphthacene in anthracene.[8] Despite the great number of investigations of this classical solution, until now no one has compared the results of these investigations with the theory of resonance transfer.

By virtue of transfer of excitation energy from the anthracene to the naphthacene, the lifetime τ_1 of the excited state of anthracene decreases with increasing naphthacene concentration. Having measured τ_1, the luminescence spectrum of the anthracene and the absorption spectrum of the naphthacene, we can attempt to apply the theory of resonance transfer. At a naphthacene concentration of $2.5 \cdot 10^{-5}$ g per gram of anthracene ($N_2 = 8 \cdot 10^{16}$ molecules/ml) we obtain the experimental value of $1 - \tau_1/\tau_{10} \approx 0.3$. The calculated value for this concentration is 0.005.

Consequently, in this case we have a very considerable divergence. The reason may be that the theory does not allow for migration of the excitations through the anthracene lattice, although the fact that such migration occurs cannot be doubted. Unfortunately we still know little about the mechanism of this migration at room temperature. According to Davydov[9] both localized and non-localized excitons may exist. The theory does not yield sufficient information for evaluating the possible consequences of the migration of non-localized excitons. Let us assume, therefore, that only localized excitons are involved. The movement of such excitons through the lattice partakes of the nature of diffusion and we have a complete analogy with the transfer of excitation from a liquid solvent, except that instead of the diffusion of molecules we have diffusion of excited states. One can determine from the experimental data what value the diffusion coefficient must have to assure the observed transfer. The evaluation yields $D = 4.5 \cdot 10^{-4}$ cm^2/sec; whence for the time an exciton remains in an individual molecule we obtain 10^{-12}-10^{-11} sec. On the other hand, from the superposition of the spectra, we can evaluate the probability W of resonance transfer of excitation energy from one anthracene molecule to a neighboring one, also on the basis of the localized exciton hypothesis. This evaluation yields a value of 1/W between $3 \cdot 10^{-12}$ and 10^{-10} which agrees in order of magnitude with the preceding estimate.

The foregoing is not to be taken as an argument in favor of the hypothesis that the migration of energy through the lattice is accomplished specifically by localized excitons, but the considerations set forth do at least indicate that this hypothesis is not in conflict with the experimental data. At the same time, it must be emphasized that, regardless of the actual nature of the migration mechanism, the existence of migration is substantiated by our data. Thus comparison of experimental data with resonance transfer theory is fruitful and permits of drawing certain physical deductions regarding the characteristics of the energy transfer process.

"P.N.Lebedev" Physical Institute of the
Academy of Sciences of the USSR

References

1. T.Förster, Ann. d. Phys., 2, 55 (1948); ZS. f. Natur., 4a, 321 (1949); D.L.Dexter, Chem. Phys., 21, 836 (1953).
2. M.D.Galanin, Zhur. eksp. i teor. fiz., 28, 485 (1955).
3. H.Kallmann & M.Furst, Phys. Rev., 79, 857 (1950); 81, 853 (1951); 85, 816 (1952).
4. M.Furst & H.Kallmann, Phys. Rev., 96, 902 (1954).
5. J.B.Birks, Scintillation Counters. London, 1953.
6. T.P.Belikova & M.D.Galanin, Optika i spektroskopiia (Optics and spectroscopy), 1, 168 (1956).

7. S.I.Vavilov, Acta physica polonica, 5, 417 (1936); B.Ia.Sveshnikov, Acta Phys.-chem. URSS, 3, 257 (1935); Trudy GOI (Proc. State Optical Inst.) No.108.

8. M.D.Galanin & Z.A.Chizhikova, Optika i spektroskopiia, 1, 175 (1956).

9. A.S.Davydov, Teoriia pogloshcheniia sveta v molekularnykh kristallakh (Theory of light absorption in molecular crystals), Kiev 1949; Symposium "Pamiati S.I.Vavilova"(In memory of S.I.Vavilov), M.-L. 1952.

DISCUSSION

A.N.Terenin: Does not the luminescence spectrum of liquid xylene have similarities with the universal blue luminescence?

M.D.Galanin: No. The universal blue luminescence was also observed but it lay in the region of longer wavelengths.

B.Ia.Sveshnikov: Was the dependence of transfer on the viscosity checked experimentally?

M.D.Galanin: In the case of the investigated solvents the viscosity does not vary sufficiently with the temperature. The theory might be checked using plastics.

M.V.Vol'kenshtein: As I see it, the studies described are of interest from the viewpoint of molecular physics. One of the important problems in modern molecular physics has to do with the structure of liquid and amorphous systems to which statistical concepts are inapplicable, i.e., where kinetic processes are of paramount importance. Here spectroscopy as such holds little promise, whereas investigations of processes of quenching and energy transfer, as we have heard, present the possibility of studying relaxation and other kinetic effects in liquids. In this respect these methods may be compared with the method of nuclear magnetic resonance which also allows of studying relaxation processes. Study of concentration-induced quenching, energy transfer and the like in conjunction with the methods of conventional spectroscopy should lead to a deeper understanding of the essence of such processes as vitrification.

E.V.Shpol'ski: It is possible that some observations I made 30 years ago in studying photochemical reactions under the influence of x-rays may have some bearing on the subject under discussion. At the time I was interested in the Eder reaction, a reaction between aqueous solutions of mercuric chloride and potassium oxalates and ammonia. Both components are transparent and entirely colorless. Normally, the reaction does not occur under the influence of visible light. However, the components are readily sensitized by various agents including fluorescein dyes - fluorescein, eosin and erythrosin. Upon the addition of a small amount of dye solution, the reaction proceeds intensively under the influence of visible light. On the other hand, when the reaction is stimulated by x-rays, the presence of even a minor amount of dye has an entirely different effect: the reaction is de-activated and the flow of energy is reversed. The process depends on the susceptibility of the substance to sensitization: the greater the sensitization to visible light, the stronger the inhibiting effect of x-rays.

CALCULATION OF THE MEAN RADIATIVE LIFETIME OF IMPURITY CENTERS AND LOCALIZED EXCITATIONS IN THE EXCITED STATE

- A.F.Lubchenko

Consistent application of the methods of quantum electrodynamics in the investigation of the optical properties of solutions and molecular crystals makes it possible to determine the shape of the absorption and luminescence bands of impurity centers and localized excitations,[1] their variation with temperature, the symmetry of the bands relative to the electronic transition frequency, as well as the mean radiative lifetime τ of impurity centers and localized excitations in the excited state.

In our calculations of τ we used the method of Weisskopf and Wigner[2] developed for determining the shape of the emission band of a free atom, extending it to the case of impurity centers and molecular crystals. We determined the wave functions of the solutions and the corresponding energy values in the adiabatic approximation, separating out the wave functions corresponding to local oscillations; the wave functions of the molecular crystals, with the positions of the molecules being fixed, were chosen in the form of antisymmetrized products of the wave functions of the molecules comprising the crystal, it being assumed that these functions take into account the mutual polarization of the molecules.

In this approximation the state of the system solution + emission field (crystal + emission field) is described by the set of quantum numbers

$$l_i\,(n_s^i)\,(v_\tau^i)\,\{N_\sigma\},$$

where the l_i's are the quantum numbers characterizing the states of the optical electrons of the impurity center (localized excitation), (n_s^i) and (v_τ^i) are the aggregate quantum numbers of the crystal and local vibrations and N_σ are the quantum numbers of the emission field. The equations for the probability amplitudes for the transition

$$l_1\,(n_s)\,(0)\,\{0\} \to l_0\,(n_s^1)\,(0)\,\{1_\sigma\}$$

have the form

$$i\hbar\dot{b}_{l_0(n_s^1)(0)\{1_\sigma\}} = \left[l_0\,(n_s^1)\,(0)\,\{1_\sigma\}\,|\,\hat{H}'\,|\,l_1\,(n_s)\,(0)\,\{0\}\right] b_{l_1(n_s)(0)\{0\}} \times \\ \times \exp\left\{i\left[\nu_\sigma - \Omega_{l_1 l_0}^{n_s} + \sum_s \omega_s^{l_0}\,(n_s^1 - n_s)\right] t\right\} \tag{1a}$$

and

$$i\hbar\dot{b}_{l_1(n_s)(0)\{0\}} = \sum_{\{n_s^1\}\sigma} \left[l_1\,(n_s)\,(0)\,\{0\}\,|\,\hat{H}'\,|\,l_0\,(n_s^1)\,(0)\,\{1_\sigma\}\right] \\ \times \exp\left\{i\left[\Omega_{l_1 l_0}^{n_s} - \nu_\sigma + \sum_s \omega_s^{l_0}\,(n_s - n_s^1)\right] t\right\} b_{l_0(n_s^1)(0)\{1_\sigma\}}. \tag{1b}$$

Here $\Omega_{l_1 l_0}^{n_s} = \sum_s n_s\,(\omega_s^{l_1} - \omega_s^{l_0})$ is the frequency of a purely electronic transition,[3] $\omega_s^{l_1}$ and $\omega_s^{l_0}$ are the natural vibrational frequencies of the nuclei of the system when the electrons are in states l_1 and l_0 and $(l_1\,(n_s)\,(0)\,\{0\}\,|\,\hat{H}'\,|\,l_0\,(n^1)\,(0)\,\{1_\sigma\})$ is the matrix element of the emission field-molecule interaction energy.

Solving the system of equations (1) by substituting $b_{l_1(n_s)(0)\{0\}} = e^{-\Gamma t}$, where $\Gamma = \frac{1}{\tau}$, we can readily calculate the amplitude $b_{l_0(n_s^1)(0)\{1_\sigma\}}$, the square of the modulus of which determines the probability of the transition and, consequently, the shape of the emission band; the second equation is used to compute Γ. In the case of solutions, we obtain the following.

1. In the limiting case when the excitation of the impurity molecule is not accompanied by a change in the equilibrium positions of the solvent molecules, the

expression for Γ can be written in the form

$$\Gamma = G \frac{\pi}{h^2} \rho(\Omega^{n_s}_{l_1 l_0}) \int \bar{n}^3_{\lambda j} |\hat{H}'|^2 \, d\Omega, \tag{2}$$

where $\int d\Omega$ denotes integration over all directions and summation over the polarizations; $\rho(\nu) = \frac{\nu^2}{(2\pi c)^3}$; $\hat{H}' = (l_0 \{1_\sigma\} | \hat{H}' | l_1 \{0\})$. It follows from (2) that in case the positions of the solvent atoms are rigidly fixed, Γ for an impurity molecule differs from Γ for a free molecule both as regards the frequency entering into the expression for the matrix element $|\hat{H}'|$ and the emission density and as regards the refractivity. With $n_{\lambda j} = 1$ and $\Omega^{n_s}_{l_1 l_0} = \nu_{l_1 l_0}$, expression (2) becomes identical with the expression for Γ of a free molecule.

2. If the electronic transition is accompanied by an appreciable displacement of the solvent atoms from their equilibrium positions, we can write

$$\Gamma = \frac{\pi}{h^2} G \left\{ \rho\left(\Omega^{n_s}_{l_1 l_0} - A_0\right) + \frac{6B_0^2}{(2\pi c)^3} \right\} \sum_{j=1}^{2} \int \bar{n}^3_j |\hat{H}'(\Omega^{n_s}_{l_1 l_0} - A_0)|^2 \, d\Omega, \tag{3}$$

where $\bar{n}_j$ is the mean value of the index of refraction,

$$A_0 = \frac{1}{2} \sum_s \omega_s^{l_0} (\xi_{sl_0} - \xi_{sl_1})^2, \quad B_0^2 = \sum_s (\omega_s^{l_0})^2 \left(\bar{n}_s + \frac{1}{2}\right) (\xi_{sl_0} - \xi_{sl_1})^2,$$

here ξ_{sl_i} are the equilibrium positions of the nuclei of the system when the electrons are in the l_i state. It follows from (3) that the radiative lifetime of the impurity molecules in the excited state depends on the nature of the solvent, the dependence being manifest not only through the refractivity n_j, but also through the coefficients A_0 and B_0. Inasmuch as A_0 is virtually independent of the temperature, disregarding the difference $\omega_s^{l_0} - \omega_s^{l_1}$, we have

$$\Gamma = c_1 + c_2 \sum_s \left\{ \frac{1}{\exp\left(\frac{h\omega_s^{l_0}}{kT}\right) - 1} + \frac{1}{2} \right\}, \tag{4}$$

where c_1 and c_2 are virtually temperature independent. It follows from (4) that if the electronic transition interacts only with the optical vibrations of the lattice, the frequency of which is of the order of 10^{14}, the lifetime of the impurity molecules in the excited state remains practically constant almost up to room temperatures. At more elevated temperatures (when $h\omega_s^{l_0}$ kT) Γ varies linearly with the temperature:

$$\Gamma = c_1' + c_2' T.$$

The coefficient B_0 in (3) is related to the half-width $\Delta\Omega_0$ of the luminescence band by

$$B_0 = \frac{\Delta\Omega_0}{2\sqrt{\ln 2}},$$

consequently, Γ can be expressed in terms of the band half-width:

$$\Gamma = c_1 + c_3 (\Delta\Omega_0)^2, \tag{5}$$

whence it follows that the radiative lifetime of impurity molecules in the excited state decreases with increasing band half-width.

The variation of τ with temperature described by (4) is in qualitative agreement with the experimental data of Galanin,[4] Rau[5] and Gaviola.[6]

3. If the electronic transition is accompanied by only a minor displacement of the solvent atoms from their equilibrium positions, Γ as a function of the temperature can be written as

$$\Gamma = c_4 e^{-g(T)}, \qquad (6)$$

where

$$g(T) = c_5 \sum_s \left\{ \frac{1}{\exp\left(\frac{h\omega_s^{l_0}}{kT}\right) - 1} + \frac{1}{2} \right\}$$

wherein c_4 and c_5 are virtually independent of the temperature.

An increase of τ with the temperature has actually been observed for a solution of anthracene in naphthalene.[7]

The temperature variation of Γ in the case of localized excitations is also determined by the magnitude of the shift of the crystal molecules from their equilibrium positions incident to changes of the quantum state of the system: if the electronic transitions are accompanied by appreciable displacements of the molecules, Γ increases with rising temperature (the dependence is described by expressions analogous to (4) and (5); in the case of small displacements, taking into account the interaction of the electronic transitions with the acoustic vibrations of the molecules, the expression for Γ can be written in the form

$$\Gamma = \left[k_1 + k_2 \sum_s \left(\bar{n}_s + \frac{1}{2}\right)\right] \exp\left\{- \sum_s{}' \left(\bar{n}_s + \frac{1}{2}\right)\left(\xi_{s l_0}^{\tau'} - \xi_{s l_1}^{0}\right)\right\};$$

at high temperatures, when $h\omega_{s l_0}^{v'_\tau} < kT$,

$$\Gamma = k'_1 (1 + k'_2 T) \exp(-k_3 T).$$

Here $\bar{n}_s = \dfrac{1}{\exp\left(\frac{h\omega_{s l_0}^{v_\tau}}{kT}\right) - 1}$ and $k_1, k_2, k'_1, k'_2, k_3$ are positive quantities that are virtually independent of the temperature.

The above expressions for Γ -- both for impurity centers and for localized excitations -- were deduced on the assumption that Γ is determined only by the emission, i.e., that radiationless transitions are absent or negligible. However, the probability of radiationless transitions increases with rising temperature,[8] consequently the above results are no longer valid at elevated temperatures at which radiationless transitions begin to play a substantial role.

I wish to thank A.S.Davydov for his valuable advice and discussion of the work.

Physics Institute of the
USSR Academy of Sciences

References

1. A.S.Davydov, Teoriia pogloshcheniia sveta v molekularnykh kristallakh (Theory of light absorption in molecular crystals), Kiev, 1951.
2. V.Weisskopf & E.Wigner, ZS f. Phys., 63, 54 (1930); 65, 18 (1930).
3. A.S.Davydov, Zhur. eksp. i teor. fiz., 24, 197 (1953).
4. M.D.Galanin, Thesis, Trudy FIAN (Transactions of the Physics Institute of the USSR Ac. of Sc.) 5, 1950; Doklady AN SSSR, 70, 989 (1950).
5. K.L.Rau, Optik, 5, 277 (1949).
6. E.Gaviola, Ann. d. Phys., 81, 681 (1926); ZS. f. Phys., 42, 853 (1927).
7. S.H.Liebson & J.O.Elliott, Phys. Rev., 78, 65 (1950).
8. A.S.Davydov, Zhur. eksp. i teor. fiz., 24, 397 (1953).

LUMINESCENCE OF ORGANIC MATERIALS UNDER THE INFLUENCE OF PARTICLES AND HARD RADIATION

- M.D.Galanin

The years since 1947, when Kallmann[1] first suggested utilizing the luminescence of naphthalene and other organic crystals for observing the scintillation produced by γ-rays by means of photomultipliers, scintillation counter techniques have seen a great development. Scintillation counters are now used for recording all types of particles and have become an indispensable instrument both in the physics laboratory and in many fields of technology. In view of this, study of the excitation of luminescence by charged particles as well as by photons and neutrons has become extremely important.

We do not intend here to give an exhaustive survey of the extensive literature on the subject (see, for example, Refs. 2 and 3). The purpose of this report is to review the more important results and to indicate the current problems in the field.

1. Luminescent materials. The organic substances now used in scintillation counters can be divided into two classes: pure crystals and solutions. The latter include crystals with impurities, liquid solutions and solid solutions in plastics. Most of the crystals used as luminophors in counters are aromatic hydrocarbons: naphthalene, anthracene, stilbene (diphenyl ethylene), tolane (diphenyl acetylene) chrysene, diphenyl, terphenyl, etc. An example of crystals with an impurity is furnished by naphthalene with anthracene. The most effective among liquid solutions have proved to be solutions of terphenyl and diphenyl oxazole in aromatic solvents. The most commonly used plastic is polystyrene into which different luminescent substances are introduced.

2. Emission spectra. It has been shown in a number of studies that the spectra excited by hard radiation generally do not differ substantially from the spectra of photoluminescence. Although trivial in itself this observation is important in that it indicates that the last stage of the process of luminescence excitation is an optical transition from the same excited state as the one attained in photoluminescence.

3. Luminescence yield. The problem of the luminescence yield or efficiency, i.e., the fraction of the energy of the particles transformed into light, is undoubtedly the most important problem where counters are concerned. Where the excitation of crystallophosphors by α-particles is concerned, the problem has been studied experimentally and discussed by many investigators.[5] The luminescence efficiency of organic materials when excited by charged particles (we have in mind here weakly ionizing particles, for example, electrons having energies of the order of 10^6 ev) has been repeatedly determined in recent years and its order of magnitude may be regarded as firmly established even though there are considerable divergences between the data given by different investigators. The values obtained by different investigators for anthracene are listed in Table 1. Furst et al[8] measured the mean light emission intensities; Hopkins[6] and Galanin & Grishin[10] observed individual scintillations. This difference in observation procedures, however, does not explain the great divergence of the results since the fraction of persistent emission from anthracene is relatively small.[11]

The quantum efficiency of photoluminescence of anthracene is close to unity. If the efficiency of excitation of different substances by particles is the same, the quantum output of photoluminescence of a given substance must determine its

Table 1

Luminescence output of anthracene according to the data of different investigators

Efficiency, %	Investigators
1.1 - 1.9	Hopkins (Ref. 6)
4	Harrison (Ref. 7)
8 - 10	Furst, Kallmann & Kramer (Ref. 8)
3.8	Birks & Szendrei (Ref. 9)
1.7 ± 0.7	Galanin & Grishin (Ref. 10)

relative energy output when excited by hard radiation. Chizhikova and the writer[12] have recently compared the relative luminescence outputs of a number of organic crystals incident to γ- and photoexcitation. The ratio of the output with γ-excitation to the quantum yield of photoluminescence proved to be the same within the limits of the experimental error for all the investigated crystals, which substantiates the assumption that the same excitation mechanism is common to all the investigated crystals.

4.Dependence of the luminescence efficiency on the type and energy of the incident particles. The dependence of the scintillation on the energy of the exciting charged particles (electrons, protons, deuterons, α-particles and heavier ions) has been thoroughly studied in a number of investigations. (for example, Ref. 13). For electrons of energies greater than $1.25 \cdot 10^5$ ev the scintillation output is reasonably proportional to the energy. However, for strongly ionizing particles, for example, α-particles or electrons of lower energy there is a marked deviation from linearity. Consequently, the luminescence output for a $5 \cdot 10^6$ ev α-particle is some 10 times smaller than for an electron of the same energy.

An important result of these investigations is that the dependence of the scintillation yield on the energy of different charged particles can be reduced to a dependence on their ionizing power. In order to explain this dependence Birks[14,2] has advanced a theory which is in good agreement with experiment. Birks suggests that the reason for the non-linear dependence of the scintillation on the energy is connected with two factors: the exciton character of the excitation of organic crystals and the formation of "defective" (for example, ionized) molecules incident to the passage of the charged particles. Birks assumes that the capture of an exciton by such defective molecules leads to a radiationless transition. He further assumes that the number of excitons formed incident to the passage of a charged particle is proportional to the energy loss dE/dx of the particle, i.e., that the number of excitons formed is $A \cdot dE/dx$, while the number of damaged molecules is $B \cdot dE/dx$. If the ratio of the probability of capture and quenching of an exciton by a defective molecule to the probability of capture of an exciton and emission by a normal molecule is k, the specific fluorescence dS/dx, i.e., the fluorescence emitted over an element dx of the particle path, will be given by:

$$\frac{dS}{dx} = \frac{A\frac{dE}{dx}}{1 + kB\frac{dE}{dx}}. \tag{1}$$

The constants A and kB can be determined from two experiments with different particles; if this is done it will be found that all results obtained for other particles bombarding the same material fit the resultant curve.

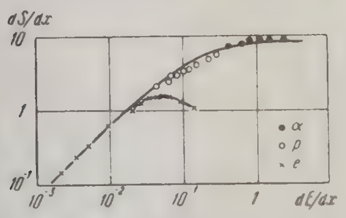

Fig. 1. Dependence of the specific fluorescence of anthracene on the energy-loss of the exciting particles (α-particles, protons and electrons), after Ref. 13.

Birks explains the deviations observed for very short range particles by suggesting that in cases when the exciton free path is comparable with that of the particle the crystal boundary on which the quenching of the exciton may occur plays an important role. The pertinent data (Ref. 13) for α-particles, protons and electrons in anthracene are shown in Fig. 1. The curve was computed according to equation (1). The deviation of the specific fluorescence due to low energy electrons is explained by Birks suggestion.

We note that in his recent publications (Ref. 2) Birks rejects the exciton concepts and speaks instead of "primary photons" (see under 6 below).

5. Duration of scintillation. The short period of scintillation of organic crystals is one of their great advantages as compared with inorganic crystals where use in scintillation counters is concerned. The major portion of the scintillation emission of crystals and solutions has a duration on the order of the lifetime of the excited state in photofluorescence, i.e., about 10^{-8} sec. There are data on

a more persistent low intensity emission from organic crystals.[11]

From the point of view of the theory of the excitation process it is interesting to note that the duration of scintillation, as follows from the data in the literature, in most cases somewhat exceeds the excited state lifetime in photoluminescence. By way of illustration some data from Ref. 15 are listed in Table 2.

Table 2

Duration of scintillation in the luminescence of some organic materials according to Ref. 15.

Material	, 10^{-8} sec	
	UV excitation	γ-excitation
Anthracene	1.7	3.0
Carbazole	0.7	1.3
Chrysene	2.2	2.6
Diphenyl acetylene	0.25	0.4
Stilbene	0.31	0.8

The temperature dependence of the persistence of scintillation is also of interest: the duration of scintillation decreases with decreasing temperature (Ref. 16 & Fig. 2).

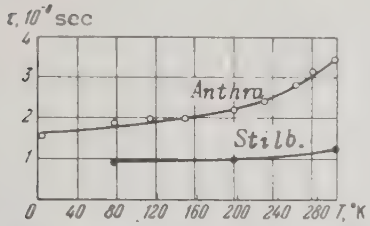

Fig. 2. Dependence of the duration of scintillation of anthracene and stilbene on the temperature according to Ref. 16.

It must be noted that the absorption and emission spectra of all crystals overlap to a certain extent. Hence there is some reabsorption of luminescence with resultant secondary fluorescence which appreciably increases the observed duration of scintillation of thick crystals. However, the difference between photo- and γ-luminescence cannot be attributed solely to the different manifestations of this effect. At the same time it must be noted that the method of measuring the duration of short scintillation pulses is entirely different from the procedure used for determining the duration of photofluorescence (usually measured by phase-shift techniques). So far there has been no thorough analysis of the possible systematic errors introduced by the different procedures. In this connection we note that Liebson, Bishop and Elliot[15] observed that the values of the duration of luminescence under the influence of x-rays as determined by the phase-shift technique agree with the duration of photo-fluorescence rather than with the duration of scintillation.

6. Theory of the scintillation process. The theoretical problem here is to examine in sufficient detail the "mechanism" of scintillation i.e., to determine the contribution of the different processes -- ionization, excitation, formation of excitons -- to the scintillation energy, clarify the role played by primary and secondary particles, elucidate the kinetics of scintillation, etc. In the first place the theory must satisfactorily explain the values of the absolute energy output and the decay time of scintillation.

The theoretical problem is undoubtedly complex. It includes the question of the distribution of the ionization losses of particles between ionization losses proper and losses on excitation and the question of the efficiency of excitation of luminescence incident to ionization and incident to excitation of atoms and molecules. Some of the complexity of the problem stems from the necessity of taking into account secondary low-energy particles. An analogous, much older problem, the problem regarding the number of ions formed by a moving charged particle, has not yet been definitively solved.

Among others, Birks[2] attempted a theoretical examination of the scintillation process. Birks' basic assumption is that in its motion the particle (assumed to have a low specific ionization) produces an excitation as a result of which there is emitted a hypothetical "primary photon" with an energy close to the energy of molecular ionization (8 ev). The energy expended by the particle on the formation of one primary photon is assumed to be equal to that expended on the formation of one ion pair (30 ev), i.e., one primary photon is produced simultaneously with a pair of ions. The decay time $(t_p)_o$ of the primary photon is assumed to be the same

as the molecular decay time $(t_f)_o$ of the usual excited state of the molecule. Increase of the scintillation time $(t_I)_t$ (the "technical" decay time) as compared with $(t_f)_o$ is interpreted as the result of multiple reabsorption and emission in the course of which the emission frequency gradually decreases. The mean number of emission processes:

$$n = (t_I)_t/(t_f)_o \tag{2}$$

while the number of fluorescence photons per primary photon

$$q = q_o^n, \tag{3}$$

where q_o is the quantum output per single excitation.

For anthracene, according to Birks' experimental data, $(t_f)_o = 3.5\cdot10^{-9}$ sec, $(t_I)_t = 27\cdot10^{-9}$ sec, $q_o = 0.9$ which gives $n = 7.7$ and $q = 0.44$. Whence the energy expended by a particle on the formation of one luminescence photon $x/q = 68$ ev/photon; this corresponds to an efficiency of 4.2%, which is in excellent agreement with the experimental data of Birks and Szendrei.[9]

Thus Birks' theory purports to explain two basic quantities: the absolute efficiency and the duration of scintillation. It must be emphasized, however, that the initial assumptions of this theory are somewhat arbitrary and lack independent experimental proof. This applies not only to the quantitative assumptions (for example, that the decay time of the "primary photon" is equal to the fluorescence decay time: $(t_p)_o = (t_f)_o$), but also to the concept of the emission of a primary proton accompanying the formation of each ion pair. All present data on the luminescence of complex organic molecules support the concept that emission always occurs from the first excited electronic level and that the transition to this level from the higher ones is always radiationless.

The problem is hardly as simple as might be supposed from Birks' theory. This follows, in particular, from the considerations set forth in a contribution by Grishin and the present writer[10] in which an attempt was made to analyze the role of so-called far (large impact parameter) collisions in the excitation of luminescence. This analysis was based on the following premises.

The energy losses of a moving charged particle can be divided into ionization losses and excitation losses. Where organic crystals are concerned it is highly improbable that the ionization itself is effective in exciting luminescence, since the existence of recombination processes leading to luminescence of organic materials in the condensed stage is doubtful. In any case the duration of such processes (if they exist) must be greater than the duration of scintillation. Ionization leads to luminescence only insofar as it gives rise to secondary electrons having a certain energy. One can distinguish with little ambiguity between two forms of excitation: excitation in large impact parameter collisions when the molecule is excited as a whole (for example, when the π-electron system of the molecule is excited) and close (small impact parameter) collisions when in the first approximation one may consider collisions with individual atoms of the molecule, neglecting their bonds with the other atoms. The question of whether the excitation of an atom is transferred to the entire molecule remains open. This is one of the important problems arising in the study of scintillation processes.

The excitation in large impact parameter collisions can be evaluated theoretically. We used Fermi's theory[17] for calculating the excitation loss. For particles of less than Cerenkov energy we obtain the following expression for the specific fluorescence excited by a large parameter collision with a particle having a charge e and a velocity $v = \beta c$:

$$\frac{dS}{dx} = \frac{e^2}{v^2}\eta_0\omega_1\int_{\omega_1}^{\omega_2}\frac{\alpha\lambda}{\pi n^2}\left[\ln\frac{4\beta^2}{3{,}17\left(\frac{\rho}{\lambda_0}\right)^2(\beta^2n^2-1)}-\beta^2n^2\right|d\omega, \tag{4}$$

where η_o is the quantum output of fluorescence, ω_1 is the frequency of the longwave

absorption limit, ω_2 is the frequency of the ionization limit, α is the coefficient os absorption, $\lambda\!\!\!^{-}$ is the wavelength divided by 2π, n is the refractivity, ρ is a quantity of the order of the intermolecular distance, demarcating the bound between "far" and "close" collisions. Available experimental data permit of only a rough evaluation of dS/dx. Such an evaluation (Ref. 10) shows that this quantity can attain 1% of the total ionization loss. The question of the contribution made by the secondary particles and particularly the question of the dependence of the distribution of losses between the different processes on the velocity of the particle (the excitation function) require further investigation. There can be no doubt, however, that this approach can lead to a more complete understanding of the scintillation process.

7. Luminescence of solutions. Interpretation of the effect of excitation of solutions by hard radiation is connected with the problem of the transfer of excitation energy from the solvent to the dissolved luminophor.[18] A detailed discussion of this problem lies beyond the scope of the present report and we shall limit ourselves here to a few remarks.

That there is transfer of energy from the solvent to the luminophor follows from experimental data on the excitation of solutions by hard radiation.[18] This deduction is also substantiated by the observed dependence of the scintillation on the concentration of solutions. However, the constants used in the descriptive formulae are empirical. Yet, as has been shown in Ref. 19, it is possible to investigate quantitatively the energy transfer from the solvent to the luminophor in optical excitation in the absorption band of the solvent. Hence the current problem is to establish whether the energy transfer in hard excitation can be attributed to the same mechanism with the same probability of transfer as in optical excitation. Such comparison of the effects observed with optical and hard-radiation excitation should show whether the energy transfer process has any distinctive characteristics in the case of γ-ray excitation.

"P.N.Lebedev" Physical Institute of the
Academy of Sciences of the USSR.

References

1. H.Kallmann, Natur und Technik, July (1947); I.Brose, L.Herforth, H.Kallmann & V.M.Martius, ZS. f. Natur., 3a, 6 (1949).
2. J.B.Birks, Scintillation Counters, London, 1953 (Russian trans.) M. 1955.
3. G.F.Garlick & J.Brit, Appl. Phys., 3, 169 (1952); D.Blanc, J.F.Detoeuf, & P.J.Maignan, phys. et rad., 13, 567 (1952); Nucleonics, 10, 3, 32 (1952); 10, 7, 46 (1952); R.K.Swank, Nucleonics, 12, 3, 14 (1954).
4. J.C.Milton & R.Hofstadter, Phys. Rev., 75, 1289 (1949); W.S.Koski & C.O. Thomas, Phys. Rev., 79, 217 (1950); F.B.Harrison & G.T.Reynolds, Phys. Rev., 79, 732 (1950).
5. G.Born, N.Ril' & K.Tsimmer, Doklady AN SSSR, 59, 1269 (1948); T.V.Timofeeva, Izv. AN SSSR, Ser. fiz., 13, 135 (1949).
6. J.I.Hopkins, Rev. Sci. Inst., 22, 29 (1951).
7. F.B.Harrison, Nucleonics, 10, 6, 40 (1952).
8. M.Furst, H.Kallmann & B.Kramer, Phys. Rev., 89, 416 (1953).
9. J.B.Birks & E.Szendrei, Phys. Rev., 91, 197 (1953).
10. M.D.Galanin & A.P.Grishin, Zhur. eksp. i teor. fiz., 30, 33 (1956).
11. J.A.Jackson & F.B.Harrison, Phys. Rev., 89, 322 (1953); K.P.Meyer & A.Maier, Helv. Phys. Acta, 28, 411 (1953); F.B.Harrison, Nucleonics, 12, 3, 24 (1954)
12. Z.A.Chizhikova & M.D.Galanin, Zhur. eksp. i teor. fiz., 30, 187 (1956).
13. C.J.Taylor, W.K.Jentschke, M.E.Remley, F.S.Eby & P.G.Kruger, Phys. Rev., 84, 1034 (1951).
14. J.B.Birks, Proc. Phys. Soc. A64, 874 (1951).

15. S.H.Liebson, M.E.Bishop & J.O.Elliott, Phys. Rev., 80, 907 (1950).
16. J.O.Elliot, S.H.Liebson & C.F.Ravilious, Phys. Rev., 79, 393 (1950).
17. E.Fermi, Phys. Rev., 57, 485 (1940); P.Budini, Nuovo Cim., 10, 236 (1953).
18. H.Kallmann & M.Furst, Phys. Rev., 79, 857 (1950); 81, 853 (1951); 85, 816 (1952); 96, 902 (1954).
19. T.P.Belikova & M.D.Galanin, Optika i spektroskopiia (Optics and Spectroscopy), 1, 168 (1956).

DISCUSSION

A.M.Bonch-Bruevich: You gave comparative data on the duration of scintillation and the duration of light emission in photoexcitation and, if I understood correctly, you consider the chief reason for the difference between them to be reabsorption. If this is indeed the case, the luminescence decay time should depend substantially on the depth of penetration of the exciting particles; for relatively slow electrons this time should approach the duration of emission in photoexcitation, which is not confirmed by observation. Further, there are data in the literature indicating that the duration of scintillation is shorter than the duration of emission in photoexcitation. This would seem to conflict with your notion of the paramount importance of reabsorption.

M.D.Galanin: I did not make a definite claim. I merely wondered whether it has been actually established that the difference cannot be reduced to the difference in reabsorption.

L.A.Tumerman: In Birks' theory are the "damage" processes reversible or irreversible?

M.D.Galanin: As far as one can judge from the available data, irreversible "damage" to the molecule under the influence of α-particles cannot explain the low yield of α-scintillation.

A.N.Terenin: What is your view regarding the possibility of migration of excitation energy in solvents in which, in contradistinction to aromatic hydrocarbons, the molecules do not form stable excited states as, for example, in water, alcohol or CCl_4?

M.D.Galanin: Aromatic solvents yield a scintillation output appreciably exceeding the output of non-aromatic solvents. The luminescence of non-aromatic solvents is very weak and possibly may be largely due to Čerenkov radiation.

EFFECT OF ASSOCIATION AND OTHER PHYSICO-CHEMICAL FACTORS ON THE LUMINESCENCE AND ABSORPTION OF COMPLEX MOLECULES IN SOLUTIONS

- V.L.Levshin

1. Introduction

Varying the concentration of the luminescing substance in a solution may lead to considerable modification of the optical properties of the solution. The earliest in point of time was the discovery by Stokes of concentration quenching of luminescence.[1] In 1926 we[2] and in 1936 Shaibe[3] discovered the appearance of new luminescence bands incident to an increase in concentration. Weingert and Keppler,[4] Karelli and Pringsheim[5] and ourselves[6], independently, observed the concentration-induced depolarization of the luminescence in dye solutions, which begins at significantly lower concentrations than concentration quenching. Gaviola,[7] Shimanovski,[8] and others, established experimentally the decrease in the duration of luminescence with increasing concentration, which ordinarily occurs more gradually than the decrease in the luminescence efficiency. Finally Soderberg,[9] Van-der Plaats,[10] we[11,12], and Rabinowitch and Epstein[13] discovered large changes in the absorption spectrum of dye solutions with increasing concentration.

These phenomena were initially investigated in isolation from each other. Various physical and physico-chemical hypotheses were proposed to explain them: the hypothesis of association (Stenger[14] and Walter[15]), electrolytic dissociation (Buckingham[16]), collisions of the second kind (Vavilov[17]), inductive quenching (Perrin[18]) and others. Recently attempts were made to interpret the concentration-induced effects from a single point of view: from the viewpoint of association (Levshin[2,11]) or from that of energy transfer in solutions (Vavilov & Galanin[19-21]) (migration theory). Dushinskii[22] made an attempt to combine the two approaches.

The purposes of the present report are 1) to show the diversity of concentration effects and the differences between them, 2) to emphasize the importance of physico-chemical factors in constructing a theory of concentration effects, 3) to demonstrate through examples of different classes of compounds the simultaneous existence and interaction of different factors influencing the development of concentration effects, and 4) to show the role of inactive absorption and of migration of excitation energy in associated solutions on the development of luminescence quenching.

2. Differences in the Development of Concentration Effects, Evidencing the Variety of the Causes Responsible for these Effects.

Changes in the optical properties of solutions occurring as a consequence of increases in concentration in the solution of various substances follow different laws and, not infrequently, proceed in opposite directions. By way of illustration, let us examine some concentration effects.

1. Changes in the luminescence yield. Changes in the yield take place in extremely varied ways. In some cases (for example, in dyes) the output begins to decrease only above a certain "threshold" concentration[17], while in others the decrease begins at the lowest concentrations (uranyl compounds);[23] the concentration dependence of quenching also varies. Further, there are substances[24,25] the quantum efficiency of which does not change over a wide range of concentrations. Finally, there are substances in which an increase in concentration results in the appearance of new emission bands[2] or of luminescence which is not present in dilute solutions.[3]

Examples of such contradictory effects of concentration increases on the luminescence yield are shown in Fig. 1.

Temperature changes also have different effects on the luminescence yield of concentrated solutions. Aside from the normal temperature quenching, temperature stimulation of luminescence is observed in a number of substances (Fig. 2).

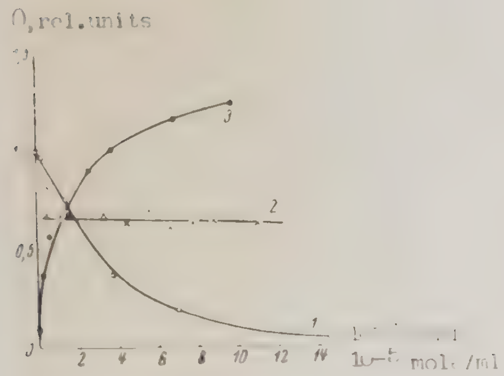

Fig. 1. Dependence of the luminescence yield of various substances on the concentration: 1) NH_4-fluorescein in congealed sugar (after Levshin), 2) solution of anthracene in ethyl alcohol (after Shishlovski), 3) solution of 3,3'-diethylthiocyaninchloride in water, λ_{exc} = 365 mμ (after Derkacheva). The upper abcissa scale pertains to curve 3.

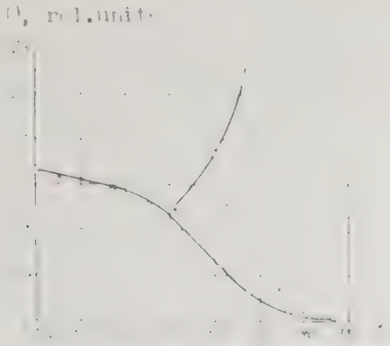

Fig. 2. Dependence of the luminescence yield of dyes on the temperature (after Levshin): 1) solution of rhodamine B extra in glycerin (C = $2\cdot10^{-4}$ gm/ml), 2) solution of red rhoduline in propyl alcohol (C = $9\cdot10^{-5}$ gm/ml, 3) solution of NH_4-fluorescein in water (C = 10^{-2} gm/ml).

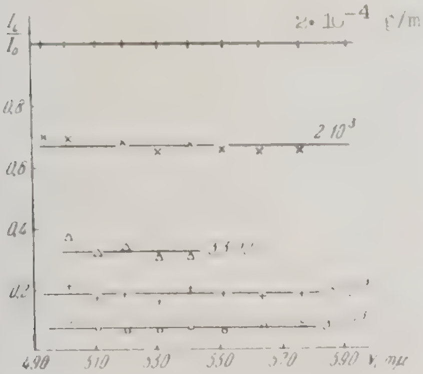

Fig. 3. Ratio of the intensity at a given concentration to the intensity taken as unity (at C = $2\cdot10^{-4}$ gm/ml) in various parts of the luminescence spectrum of solutions of NH_4-fluorescein in water (after Levshin).

2. Absorption and Emission Spectra. The shapes of the luminescence spectra of most substances are independent of the concentration (Fig. 3), indicating stability of the emitting oscillator; however, there are exceptions (Fig. 4).

On the other hand, the absorption spectra of most substances undergo large changes;[11] thus, with increasing dye concentration the longwave peak ordinarily decreases, while, at the same time, a new peak begins to develop on its short wave side; in some cases this new peak attains greater development than the first (Fig. 5).[26]

Heating causes the new bands to fade and the absorption spectra of the concentrated solutions to approach those of dilute solutions (Fig. 6).[26]

The total absorption of a substance in concentrated solutions can be either smaller or greater than the absorption in dilute solutions.

Increasing the concentration tends to shorten the decay time of the excited state and reduce the degree of polarization of the emission. An extremely important factor in considering the kinetics of quenching is that the decrease in the decay time of the excited state with increasing concentration is slower than the decrease in efficiency (Fig. 7).

It is obvious that the frequently contradictory effects of concentration on the various optical properties of luminescent solutions, described above, cannot be related back to a single general cause: it is necessary to admit the existence of various concentration effects, varying in nature, developing with different strengths

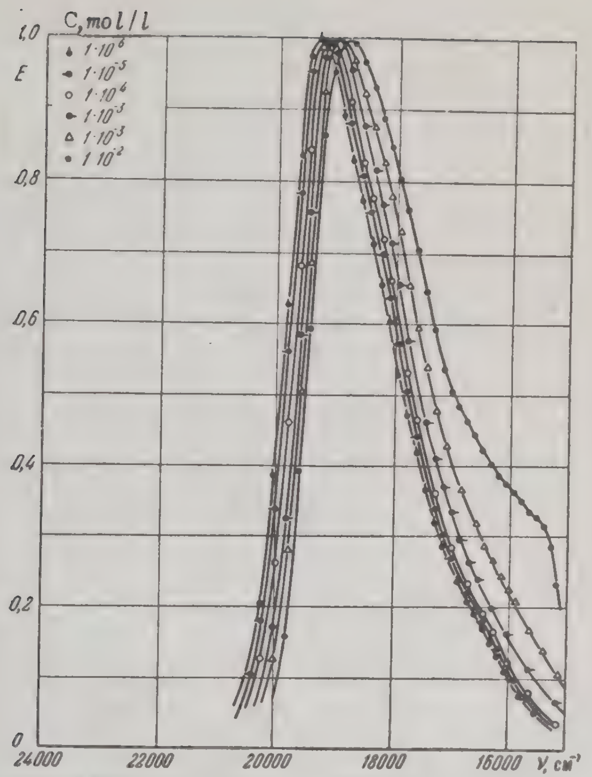

Fig. 4. The effect of changing the concentration from $1\cdot10^{-6}$ to $10\cdot10^{-2}$ mole/liter on the distribution of energy in the cation spectrum of solutions of acridine orange in an ether-alcohol mixture (1:2) (after Zanker[32]).

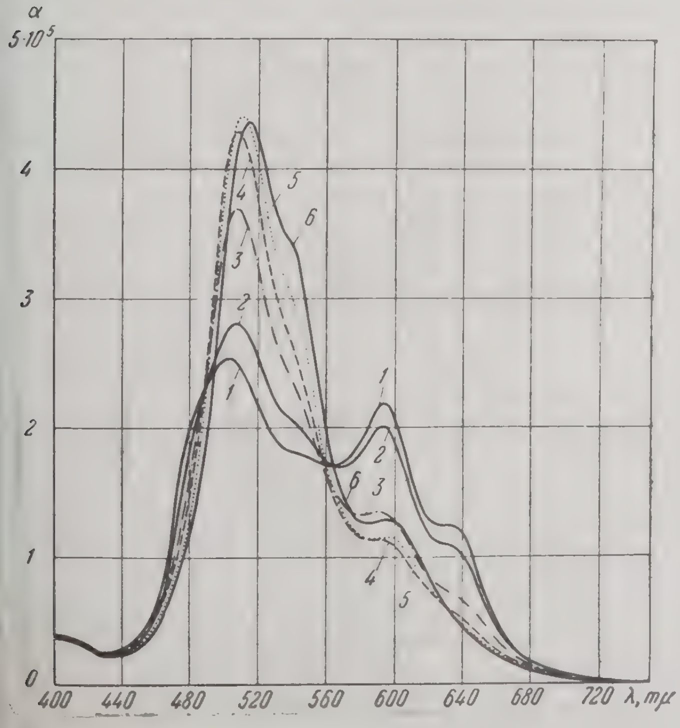

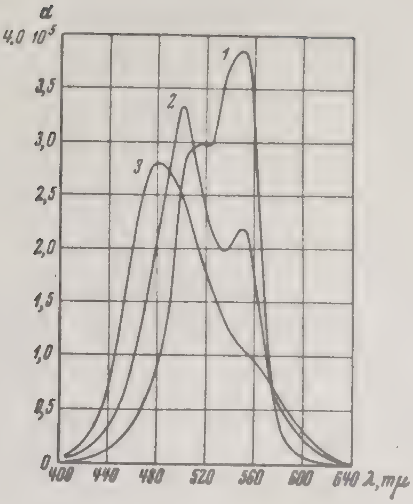

Fig. 5. The effect of concentration on the absorption spectrum of aqueous solutions of 3,3'-diethylcarbothiocyanine chloride (after Derkacheva): 1) $C = 6.6\cdot10^{-6}$, 2) $C = 1.29\cdot10^{-4}$, 3) $C = 2\text{-}13\cdot10^{-3}$ gm/ml.

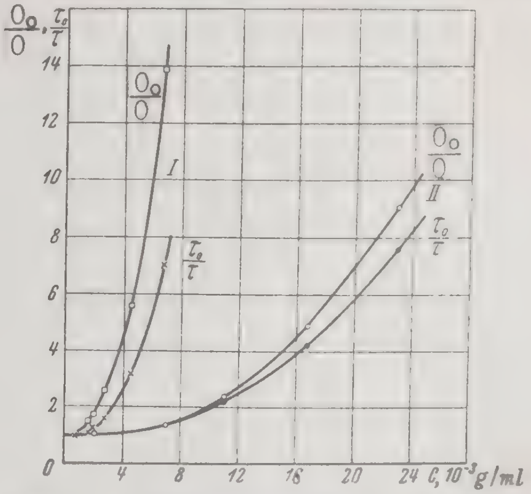

Fig. 7. The dependence of the reciprocal of the relative output and relative duration of luminescence of solutions of fluorescein on the concentration: I) water solutions, II) solutions in ethyl alcohol (after Shimanovski[8]).

--Fig. 6. The dependence of the absorption spectrum of aqueous solutions of pinacyanol ($C = 1.8\cdot10^{-3}$ gm/ml) on the temperature (after Derkacheva): 1) 23.5°, 2) 40.5°, 3) 51°, 4) 60°, 5) 70.5°, 6) 80.5° C.

depending on the properties of the substance and the physical conditions of the medium, and frequently superimposed upon each other.

3. Inadequacy of the Migration Theory for Explaining Concentration Effects

The explanations of concentration effects most common in the literature are based essentially on the idea of inductive transfer of the excitation energy from the excited to the non-excited molecules, a process in which a part of the transfer events lead to quenching. Quenching leads to a shortening of the mean lifetime of the excited state. Transfer of excitation energy to other molecules, differently oriented in space, leads to the depolarization of the emission. This is the way the common physical theory attempts to explain the three effects of concentration: quenching, depolarization and change in the lifetime of the excited state.

In spite of the partial successes of the migration theory, it is not hard to show its inadequacy for explaining all the effects of concentration. Let us note first of all that the quenching effects do not necessarily follow from molecular energy transfer. Thus, experiment shows that the excitation energy unquestionably migrates in crystals of many substances, for example, in anthracene, although quenching is not always observed in such cases.

The migration theory offers an explanation of the decrease in the duration of luminescence and depolarization, yet the change in the duration of luminescence is often more gradual than the change in efficiency. To obviate this difficulty, S.I.Vavilov proposed the hypothesis of a certain minimal volume - "the sphere of action" - in the vicinity of the excited molecule, a volume having the peculiar attribute by virtue of which the presence within it of a second molecule of the luminophor at once results in quenching of the luminescence. The introduction of the concept of a "sphere of action presupposes the existence of another process of quenching superimposed on migration quenching. Förster[27] and Galanin[28] made an attempt to give a physical interpretation of the sphere of action. However, their interpretation is basically applicable only to media characterized by a high viscosity.

The following experimental facts also speak against interpretations based on migration theory alone: 1) the luminescence yield of many concentrated solutions depends on the wavelength of the exciting light; 2) the luminescence efficiency of many concentrated solutions increases with temperature in spite of the fact that there is no basis for expecting a cessation of the independent process of temperature quenching; 3) the increase of concentration in almost all cases produces changes in the absorption spectra, indicating the formation of molecular complexes in solutions (Fig. 5); 4) in some cases changes occur also in the emission spectra (Fig. 4) proving that the emitters are modified.

These experimental facts are not accounted for by present-day migration theory. Accordingly it appears desirable to attempt an explanation of these facts by taking into account the different physico-chemical factors that have received scant attention. As will be evident from the sequel, the processes of quenching and the other concentration effects can be understood only in the light of both the physical and the physico-chemical changes occurring in solutions at high concentrations.

4. Changes in the Physico-Chemical Properties of Luminophors in Concentrated Solutions and Their Influence on the Optical Properties of the Solutions.

An increase in the concentration of the luminescent substance leads to a change of the molecular field of the solution which affects the interaction between the molecules of the solute and of the solvent and thereby produces various physico-chemical changes of the solution. Among such changes may be included: 1) a change in the degree of dissociation of the luminescent substance or an alteration in the equilibrium of the tautomeric forms of the luminescent molecules in the solution, 2) the reversible formation of dimers and polymers, 3) a change in the solvate

envelope of the luminescent molecules, etc.

Where these effects occur they give rise to new possibilities for short range molecular interactions and influence the optical properties of the interacting particles. In addition, with an increase in the concentration, the optical properties of the solution may be modified through direct action of the molecular field of the solution on the emitting particles. There are, as yet, no quantitative calculations for effects of this kind.

Let us examine in greater detail the possible effects of changes in the electrolytic dissociation and the appearance of reversible association, occurring incident to increased luminophor concentration, on the optical properties of luminescent colutions.

Many luminescent substances are electrolytes, the degree of whose dissociation varies with the concentration. In addition to changes in ionization, variation of the pH may lead to an alteration in the ratio of the tautomeric forms, characteristic of the given substance.

A stable state of the solute is observed only within a certain range of concentrations and pH values. In general, a solution can simultaneously contain different forms of the substance, which is evidenced by progressive changes in the absorption and emission spectra with increasing concentration. If one of the modifications of the solute substance does not luminesce, there may be considerable quenching. The change in the lifetime of the excited state occurs in accord with the change in the proportions of various luminescent substances, having different decay times and luminescence intensities, in the solution. A significant effect of a change in electrolytic dissociation in concentrated solutions on the optical properties of the solution may be expected in those cases when artificial alteration of the pH of the medium in dilute solutions results in appreciable modification of their optical properties.

The strong influence of the pH of the medium on the optical properties of acridine compounds was discovered by Ramart-Lucas and co-workers[29] and has been recently studied in detail by Levshin.[30]

Let us turn to an examination of the influence of association of the particles of the luminescent material. Experiment shows that in many cases an increase in the concentration leads to a sharp change in the absorption spectra even though the solution contains an excess of alkali or acid which precludes changes of the charge of the emitting particles. The change in absorption is accompanied by a drop of the luminescence efficiency. Thus even when the solution contains ions of only one kind, quenching develops and the absorption is altered.

Decisive proof of the physico-chemical character of this process is furnished by the effect of an increase in temperature; a temperature rise simultaneously changes the absorption spectra (bringing them closer to the spectra of dilute solutions) and produces a sharp increase in the luminescence efficiency.

The described effects naturally lead to the idea of the formation in high-concentration solutions of unstable aggregates which break up when solutions are diluted or heated.

This process is studied quantitatively by separating the absorption spectra into the spectra of the monomers and dimers (in the absence of more complex associations). Having established the relative concentration of the monomers and dimers from the shape of the spectrum, by using the law of mass action, it is easy to calculate the dissociation constant, and to determine the dissociation energy from the change in spectrum with the temperature. The general equation for the law of mass action for binary solutions of monomers and dimers has the form:

$$(1 - x)K = 2Cx^2. \qquad (1)$$

Here C is the total concentration, x is the fraction of molecules remaining in the monomeric state and K is a constant having the form:

$$K = Ae^{-E/KT}, \qquad (2)$$

where E is the energy of dimer dissociation and A is a constant whose value depends on the properties of the molecules and the temperature and the viscosity of the medium, and is related to the probability of [illegible].

From (2) it follows that

$$\ln K = \ln A - E/kT \qquad (3)$$

If ln K graphed as a function of 1/T turns out to be a straight line, then it is evident that A varies little with temperature and viscosity. The straight line (3) allows the determination of the dissociation energy.

An increase in the temperature results in splitting up of the associated [illegible]. One can judge of the dissociation of associates as well as of the fraction α by the change in the absorption spectra and by the increase in luminescence efficiency of the concentrated solutions if in computing the efficiency, we introduce a correction for the simultaneous development of temperature quenching which, in turn, can be determined independently from the decrease in the luminescence output of dilute solutions with increasing temperature.

The indicated method for finding the degree of dissociation and the heat of dissociation is not applicable when higher polymers form in the solution.

Investigation of absorption spectra shows, however, that in many cases the deformation of the absorption spectrum ceases in a rather wide range of high concentrations; evidently in this range of concentrations the dimers persist as fundamental units of the polymers being formed and, in large measure, act independently. That is, further changes in spectra, corresponding to the formation of polymers with specific optical properties, are observed only at very high concentrations.

The natural question about the character of the forces responsible for the union of ions bearing identical charges is answered at the present time by postulating Van der Waals forces, associated with the interaction of π-electron clouds.

In constructing the appropriate interaction equations dipole-dipole, dipole-quadrupole as well as ordinary nuclear and Coulomb repulsive forces are taken into account.[31]

The dimers and polymers formed may possess different luminescence characteristics. In some cases dimerization leads to quenching, while in others luminescence develops only upon association.

The absorption of dimers can be either larger or smaller than that of the monomers. For the frequency at which the absorption in monomer and dimer spectra is the same, the equality of absorption is conserved at all concentrations and at monomer to dimer ratios and therefore the absorption curves for all concentrations pass through one point. Absorption bands in the ultraviolet region normally change less incident to association than the bands in the visible region. This confirms the assumption that the forces responsible for association are developed as a consequence of the interaction of the electrons responsible for absorption in the visible region, i.e., due to the interaction of π-electron clouds.

Thus association theory explains the development of quenching, the origin of new emission bands in concentrated solutions, alterations of the absorption spectrum, the increase in the output on heating concentrated solutions, and the approach of the shape of concentrated solution spectra to the spectra of dilute solutions. The differences in the absorption spectra of dimers and monomers explain the difference in the variation of quenching when the luminescence is excited by light of different wavelengths.

The emission of concentrated solutions of substances yielding non-luminescing associations is ascribed to residual monomers. For this reason the experimentally observed shortening of the mean lifetime of the emitting state and the depolarization of luminescence must be attributed in the pure association theory of quenching to the specific effect of the change in the molecular field on the excitation of the monomers. Although such an effect is possible, effects of this type are more naturally linked with migration of the excitation energy to the associated particles.

This point of view will be examined in detail below

Table 1

Principal features characterizing the type of process induced by an increase in concentration

Type of Process	Spectra		Luminescence	Decay Time of
	Absorption	Emission	Efficiency	Excited State
Migration of energy	a) does not change, b) changes little with rise in temperature	a) does not change; b) changes with temperature, c) does not depend on λ of exciting light	a) decreases; b) quenching independent of λ of exciting light and increases with the temperature.	a) decreases in proportion to the output b) explanation of the slower decrease requires special hypotheses
Change in pH of medium with increasing concentration	a) changes; b) analogous changes can be obtained with dilute solutions through changes in the pH of the medium; c) the influence of temperature is connected with the change in pH		a) changes; b) with increase in temperature, temperature quenching is observed; c) depends on λ of the exciting light	a) changes in accord with content of various forms of the luminescent material; b) depends on λ of the exciting light
Association of particles of the luminescent substance	a) changes; b) changes cannot be obtained in dilute solutions by changing the pH; c) with increase in temperature the shape of the spectra approaches that of dilute solutions	a) does not change if dimers are not luminescent b) changes if dimers luminesce; c) in the last case depends on λ of exciting light and temperature	a) decreases if dimers do not luminesce; in this case, on heating, temperature quenching is more gradual in concentrated solutions than in dilute ones; stimulation of luminescence is frequently observed; b) efficiency depends on the the λ of exciting light	a) in substances having nonluminescent associations, decreases as a consequence of migration of excitation energy to the associates; b) in the case of luminescent associations, the decay time may change

5. Characteristic features of various types of concentration effects and determination of the nature of these effects.

In elucidating the nature of an observed concentration effect (migration of energy, association of molecules, change in the pH of the medium) reliable deductions can be arrived at only if the characteristic features are considered in the aggregate.

Any particular feature by itself is ordinarily insufficient. The following optical features may serve as indications:

1) Changes in the absorption spectrum: a) with an increase in concentration, b) in concentrated solutions, with changes in temperature, c) in dilute and concentrated solutions with changes in the pH.

2) Changes in the emission spectra: a) with increase in concentration, b) in concentrated solutions when the wavelength of the exciting light is changed, c) in concentrated solutions when the temperature is changed, d) in dilute and concentrated solutions when the pH of the medium is changed.

3) Changes and the rate of change of the luminescence efficiency: a) with increase in concentration, b) with change in temperature, c) with change in the wavelength of the exciting light.

4) Changes in the decay time of the excited state with increase in concentration and in the relationship between the luminescence decay time and efficiency with changes in the concentration.

The characteristic features of various types of concentration effects that are helpful in identification are listed in Table 1.

6. The nature of concentration effects in several classes of luminescent substances

1. Acridine compounds. Concentration quenching in acridine compounds is poorly developed. Many of them luminesce well in the solid crystalline state. Increase in the concentration frequently leads to a large change in the absorption spectrum and alteration of the emission spectrum. These changes are determined primarily by changes in the pH of the medium, although in a number of cases the formation of associates is also observed. The associates formed have their own emission spectrum A significant change in the decay time of the excited state that is not proportional to the change in the efficiency is evidence that migration quenching also exists

2. Xanthene dyes. Dyes of this type exhibit properties indicating the formation of associated groups in concentrated solutions.

However, in xanthene dyes, just as in acridine dyes, quenching is accompanied by a decrease in the luminescence decay time that is not proportional to the change in efficiency. Evidently, in xanthene dyes, too, part of the quenching is connected with migration of energy to the associated molecules.

Förster[27] considers that the nature of quenching in aqueous solutions of xanthene dyes differs from that in alcohol solutions. However, the difference is purely quantitative: the formation of associates takes place at higher concentrations in alcohol and glycerin than in water.

3. Cyanine dyes. The cyanine dyes furnish an especially clear example of concentration effects produced by association. With increasing concentration sharp changes take place in the luminescence and absorption spectra in aqueous solutions Not only dimers but also polymers consisting of enormous numbers of molecules are present in aqueous solutions. In a number of cases an increase in the ability to luminesce develops only at high concentrations. Destruction of associates upon heating and dilution of solutions and the gradual change from higher to lower associations results in complex temperature variation of individual peaks in the absorption spectra. In several cases it is necessary to allow for the possibility of migration quenching. The latter is highly probable in view of the appreciable overlapping of the absorption and luminescence spectra of the polymers.

7. Development of the Association Theory of Concentration Quenching through the Introduction of Concepts Regarding Migration of the Excitation Energy

The basic conclusion to be drawn from our examination of the concentration effects in various types of luminescent substances is that a pure type of concentration influence is not observed in any compound. To a greater or lesser extent

processes of several types are simultaneously involved in every case. With this in view, we will make an attempt to unify theoretically the influence of molecular association and of migration of excitation energy. Let us establish the following premises for our development of the theory:

1) monomers as well as polymers absorb; their absorption spectra are different;

2) absorption of light by monomers leads to luminescence; absorption of light by polymers does not result in luminescence;

3) during the lifetime of the excited state, part of the monomers transfer excitation energy to the polymers, which leads to quenching; in the first approximation, the transfer of energy from monomers to monomers can be neglected.

Analogous concepts were proposed by Dushinski[22]. The difference between our initial polsulates and the assumptions of Dushinski consists in the fact that he did not take into account inactive absorption of the exciting light by associated molecules and assumed the activity of aggregates to be confined to quenching of the excitation energy transferred to them. For this reason in Dushinski's theory, the decay time of the excited statechanges in proportion to the change in efficiency (output), which is in conflict with experiment. Our additional postulates explain the decrease in the lifetime of the excited state with increasing concentration and the fact that the decrease occurs more gradually than the change in efficiency.

Let us examine the problem in more detail. The degree of association is high in aqueous solutions of many dyes at high concentrations; as a consequence associated groups absorb a significant fraction of the energy of the exciting light. This inactive absorption results in strong quenching. The other part of the quenching is due to migration of energy from the excited monomers to non-luminescing polymers. The residual luminescence is that from monomers which emit radiation before they have a chance to transfer energy to the polymers.

The decrease in the luminescence output and in the lifetime of the excited state with increasing concentration under these conditions, in the first approximation, must take place in the following manner

$$\frac{B}{B_0} = \frac{xK_m}{xK_m + (1-x)K_d}(1-p) \qquad (4)$$

and

$$\frac{\tau}{\tau_0} = \frac{\tau_1}{\tau_0 + \tau_1} = 1-p, \qquad (5)$$

where B_0 and B are the luminescence yields of monomers outside the quenching range and during quenching, τ_0 and τ are the lifetimes of the excited states taking migration into account and without it, τ_1 is the average time of energy transfer from excited monomers to associates, K_m and K_d are the absorption coefficients of monomers and associates (dimers and polymers) under monochromatic excitation, x and 1-x are the relative amounts of the dissolved substance (by weight) in the form of monomers and associates, p is the fraction of excited molecules transferring their energy to associates (it is a complicated function of the distance between monomers and polymers in the solution, and, consequently, a function of the concentration). B/B_0 and τ/τ_0 decrease with increasing concentration, while p increases rapidly with the concentration. The total decrease of B/B_0 according to the equation (4) proceeds faster than the decrease of τ/τ_0 since it is due to a considerable extent to direct inactive absorption of associates, which is taken into account by the first factor in equation (4).

In alcohol solutions association is weak and inactive absorption is, therefore, comparatively low. Absorption spectra change noticeably only at high concentrations. Inasmuch as the second term in the denominator of equation (4) remains small compared to the first in a wide range of concentrations, the first factor in the left part of equation (1) is close to unity; B/B_0 and τ/τ_0 vary in practically the same manner. Quenching proceeds more slowly than in water but, nevertheless, does take

place as a consequence of the presence in (4) of the factor (1-p), which takes into account the possibility of energy transfer to the associated molecules.

We did not examine the question of transfer of excitation energy from monomers to monomers. However, the possibility is not excluded that such transfer may lead to additional quenching as well as to a corresponding change in the duration of luminescence. Such a process can easily arise in binary solutions of two substances with overlapping absorption and luminescence spectra and different luminescence capabilities, for example, in aqueous solutions of mixtures of fluorescein and erythrosine.

In closing let us make an evaluation of p and (1-x) for aqueous solutions of fluorescein, making use of data by Shimanovski (Fig. 6) and equations (4) and (5). The values of the probability p of energy transfer from monomers to dimers, computed in this way, are given in Table 2. Further, using the values of p, we calculated, according to (4) and (5), the variation of quenching as a consequence of inactive absorption as determined by the first factor on the right side of the expression (4). These results are listed in the fourth column of Table 2.

If it is assumed that K_m and K_d under Shimanovski's experimental conditions were approximately equal, then the values in the fourth column of Table 2 also represent the values of x, while (1-x) is then the fraction of dimers in the solutions (fifth column). Then C(1-x) will be the concentration of dimers in the solution.

Table 2

Luminescence quenching in solutions of fluorescein due to energy migration to dimers and to inactive absorption

Fluorescein Solution	C, 10^{-3} g/ml	p	Quenching due to inactive absorption (x)	Fraction of dimers (1-x)	$C(1-x)\cdot 10^3$
In water	2	0,27	0,72	0,28	0,55
	4	0,58	0,54	0,46	1,82
	6	0,81	0,52	0,48	2,90
	7	0,87	0,50	0,50	3,50
In alcohol	8	0,33	0,96	0,04	0,32
	12	0,58	0,86	0,14	1,63
	16	0,75	0,90	0,10	1,60
	20	0,83	0,85	0,15	3,00
	24	0,88	0,84	0,16	3,84

It follows from Table 2 that at equal concentrations of dimers in aqueous and alcohol solutions (figures of the last column), the probability p of excitation energy transfer from monomers to dimers is approximately the same in alcohol and in water solutions. This conclusion may be inaccurate because of the assumption regarding the equality of K_m and K_d in Shimanovski's experiments, as well as because of possible experimental errors; however, the reasoning given supplies a method of finding the dependence of p on the distance between monomers and dimers in various media.

The purpose of the present report was to emphasize the important role which physico-chemical factors play in the development of concentration effects. In the three following reports[30, 33, 34], to which ours serves as introduction, this problem will be examined in detail for specific types of luminescent compounds.

The association theory of concentration effects is at the present time still in its infancy. As further developed the theory must enable us, on the basis of the experimentally determined strengths of association forces, to determine their nature and calculate theoretically their magnitudes starting only with the structure of the corresponding molecules. These results will enable us to draw deductions with regard to the kinetics of the exchange of excitation energy between associated molecules and concerning the structure of emitting molecular groups.

The complexity of associated groups forming in solutions and the specific nature of their interactions with the solvent undoubtedly present difficulties where development of the theory is concerned, but these difficulties are not of a fundamental character and will be overcome sooner or later.

The "P.N.Lebedev" Physical Institute of the Academy of Sciences of the USSR
and The"M.V.Lomonosov"State University of Moscow

References

1.G.Stokes, Phil. Trans., 143, 421, 463 (1952).
2.V.L.Levshin, ZS. f. Phys., 43, 230 (1927).
3.G.Scheibe, u. andere, ZS. ang. Chem., 49, 563 (1936).
4. F.Weigert & G.Käppler, ZS. f. Phys., 25, 106 (1924).
5. A.Carrelli & P.Pringsheim, ZS. f.Phys., 18, 317 (1928).
6. V.L.Levshin, ZS. f. Phys., 26, 274 (1924).
7.E.Gaviola, ZS. f. Phys., 35, 748 (1926); 42, 853 (1927); Ann. d. Phys., 81, 681 (1926).
8.W.Szymanowski, ZS. f. Phys., 95, 440 (1935); 95, 460 (1935).
9.B.Söderberg, Ann. d. Phys., 41, 381 (1913).
10.B.Van-der Plaats, Ann. d. Phys., 47, 424 (1915).
11.V.L.Levshin, Zhur. fiz. khim., 6, 1 (1935); Acta Phys. chem. URSS, 1685 (1935)
12.V.L.Levshin, Zhur. fiz. khim., 6, 991 (1935); Acta Phys. chem. URSS, 2, 221(193
13.E.Rabinowitch & L.Epstein, J. Amer. Chem. Soc., 63, 69 (1941).
14.F.Stenger, Wied. Ann., 28, 20 (1886).
15.B.Walter, Ann. d. Phys., 34, 316 (1889).
16.E.Buckingham, ZS. f. phys. Chem., 14, 129 (1894).
17.S.I.Vavilov, ZS. f. Phys., 31, 750 (1925).
18.J.Perrin, C.R., 184, 1097 (1927).
19.F.Perrin, Ann. d. Phys., 17, 283 (1932).
20.S.I.Vavilov, Zhur. eksp. i teor. fiz., 13, 13 (1943).
21.S.I.Vavilov, Mikrostruktura sveta (Microstructure of light), Ch. 3, M.-L. 1950; Collected works, Vol. II, M.-L. 1951.
22.F.Dushinski, Doklady AN SSSR, 14, 73, 179 (1937).
23.S.I.Vavilov & V.L.Levshin, 48, 397 (1928).
24.A.A.Shishlovski, Zhur. eksp. i teor. fiz., 7, 1212 (1937).
25.F.M.Pekkerman, Doklady AN SSSR, 52, 409, 773 (1946).
26.L.D.Derkacheva, Dissertation, Moscow Sate University, 1955.
27.TH.Förster, Naturwiss., 33, 166 (1946); Ann. d. Phys., 2, 55 (1947); Fluoreszenz organischen Verbindungen. -Göttingen, 1951.
28.M.D.Galinin, Zhur. eksp. i teor. fiz., 28, 485 (1955).
29.P.Ramart-Lucas et coll., Mem. pres. Soc. chim., 8, 554 (1946).
30.L.V.Levshin, Present issue of the Bulletin.
31.S.Shapperd, Rev. Mod. Phys., 14, 303 (1942).
32.V.Zanker, ZS. f. phys. Chem., 200, 5/6, 250 (1952).
33. V.L.Levshin & E.G.Baranova, Present issue of the Bulletin.
34.L.D.Derkatcheva, Present issue of the Bulletin.

DISCUSSION

B.La.Sveshnikov: Are you reviving Dushinski's theory in its entirety?

V.L.Levshin: I consider the inherent inactive absorption by dimers, which was formerly the single factor in the association theory of quenching, and the migration of excitation energy to associates, which was suggested by Dushinski.

A.N.Terenin: V.L.Levshin justly raises the question of the limits of applicability of the concept of a transfer mechanism and of the possibility of applying the molecular association hypothesis for explaining concentration quenching and other effects. Concentration quenching, although present in concentrated solutions, is eliminated in some substances (anthracene) upon the formation of crystals. Analogously, in the case of dimers incapable of luminescing, further aggregation having the characteristics of ordering may lead to the reappearance of luminescing power. The second problem I want to mention is the problem of the effect of association of different molecules. To the phenomena of quenching by foreign molecules, which are interpreable by an inductive mechanism, it is possible occasionally to apply the concepts

which were proposed by A.V.Banov for explaining concentration quenching in solutions. He showed that on adding salts to a dye solution, quenching of the dye results because of its aggregation. This factor, that is, the change in the state of aggregation of the solute molecules of the dye upon the addition of another component, has not yet been adequately taken into account.

One can give an example from our experiments on activation of luminescence in solutions of chlorophyll and its analog, magnesium-phtalocyanin, in aromatic hydrocarbons: benzene and others. The luminescence yield in these solutions is comparatively small. However, if one adds even a trace of polar molecules which can form some complex with cyanin and chlorophyll, both the absorption coefficient and the luminescence efficiency increase by about a factor of five. It would seem that in benzene or toluene solutions the dimers or other aggregates with almost identical spectra assume a "monomeric" form as a consequence of union with polar molecules, which results in an increase in efficiency and some change in the absorption coefficient, i.e., in the oscillator strengths.

The problem lies in extending investigations not only to cases of identical molecules (that is, concentration variation) but to cases of molecular association involving distinct species of molecules.

M.D.Galanin: A wide range of concentration effects in the luminescence of solutions is explainable by physico-chemical changes of the dissolved substances. Accordingly such effects cannot be considered as side effects. On the other hand, however, many concentration effects are explained by transfer of excitation energy and we already know the properties of molecules in the presence of which such energy transfers are possible.

Physico-chemical changes are, by their very nature, more complicated and, therefore, we cannot yet say which properties molecules must have so that reversible dimerization or electrolytic dissociation can occur. Unfortunately, almost all investigations of the influence of physico-chemical factors on luminescence have failed to take energy transfer into account.

CONCENTRATION EFFECTS IN SOLUTIONS OF QUINOLINE DYES

-L.D. Derkacheva

An increase in the concentration of dyes in solution is often accompanied by changes in the optical properties: the luminescence efficiency and the decay time of the excited state change, the luminescence is depolarized, the absorption spectra and sometimes the luminescence spectra of the dissolved substances are modified.

The concentration-induced changes in the optical properties of solutions (if we exclude changes due to the formation of new chemical compounds) may be produced by physical or physico-chemical interaction between the molecules or ions of the substance. Changes in the optical properties connected with purely physical interaction have been thoroughly studied both theoretically and experimentally; specifically we have in mind here the resonance energy migration theory developed by Vavilov and his students and substantiated by experimental studies of concentration quenching, depolarization and the decrease in the decay time of the excited state. Changes in the optical properties connected with physico-chemical interaction have been less intensively studied, although they are met with more frequently than the changes due to purely physical factors. The most important physico-chemical process having a strong influence on optical properties, in particular on the luminescence, is association of the molecules and ions of the dissolved substance. Interaction between associating molecules is not an ordinary chemical interaction. Ionic bonds are created between the associating molecules which explains why physicists are interested in the association phenomenon.

The nature of the association of dye molecules can be studied in two ways: 1) by changing the medium in which the association occurs and thus bringing out those properties of the medium which influence the association process and 2) by changing the chemical composition of the substance and relating the associative properties with the molecular structure. We utilized both approaches in our investigation of the association of quinoline dyes.

The question of the role of the medium in association of quinoline dye molecules has been raised before. In his works on the properties of cyanine dyes, Scheibe[1,2] had noted more than once that association of cyanine dye molecules occurs only in water solutions. We attempted to verify this by investigating the concentration-induced changes in the properties of pseudoisocyanine in different solvents.

As Scheibe[2] established, association occurs between like positively charged ions of the dye. Consequently the forces responsible for the association must overcome Coulomb repulsion. The Coulomb repulsion between the dye cations is inversely proportional to the dielectric constant of the solvent. Thus there must be a relationship between the proclivity of the dye to association and the dielectric constant of the solvent: in solutions with a high dielectric constant there must be more active association than in those with a lower constant.

In the light of these considerations we investigated the concentration induced changes in the properties of pseudoisocyanine in solvents having different dielectric constants: water ($\varepsilon = 81$), glycerin ($\varepsilon = 56.2$) and ethyl alcohol ($\varepsilon = 27.8$).

The absorption spectrum (recorded on SF-2M and SF-4 type spectrophotometers) of pseudoisocyanine in ethyl alcohol is shown in Fig. 1. The spectrum remained unchanged as the concentration was increased 300 times. The shape of the spectrum was also unaltered as the temperature was increased from 20 to 60°. This clearly indicates that in ethyl alcohol the pseudoisocyanine molecules remain in the monomer state.

As may be seen from Fig. 2, an entirely different situation obtains when the concentration of pseudoisocyanine in a glycerin solution is changed.* At low concentrations of the dye (curve 1) the absorption spectrum of the solution in glycerin

---

*The glycerin was thoroughly purified by double distillation under vacuum.

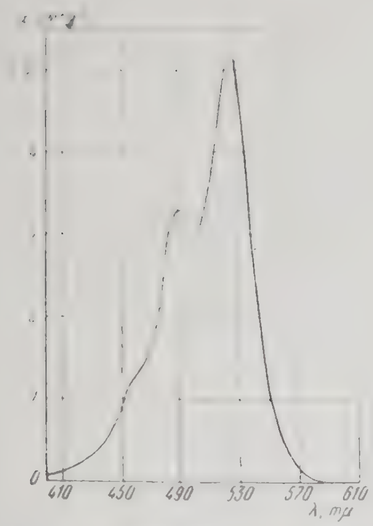

Fig. 1. Absorption spectrum of ethyl alcohol solution of pseudoisocyanine; concentrations: $1.1\cdot10^{-5}$, $2.2\cdot10^{-4}$ and $3.59\cdot10^{-3}$ mole/liter.

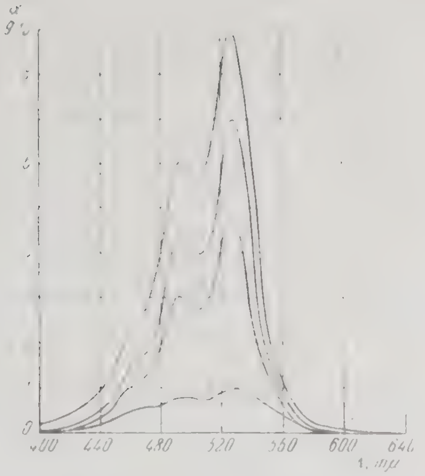

Fig. 2. Variations of the absorption spectrum of glycerin solutions of pseudoisocyanine with changes in the pseudoisocyanine concentration: 1) $C = 6\cdot10^{-6}$, 2) $1.18\cdot10^{-4}$, 3) $1.96\cdot10^{-3}$, 4) $1.1\cdot10^{-2}$ mole/liter.

is identical with the absorption spectrum of pseudoisocyanine in ethyl alcohol. In view of this it may be assumed that in a [illegible] glycerin solution the pseudoisocyanine molecules are monomers. Increasing the pseudoisocyanine concentration in the solution leads to an appreciable lowering of the absorption over the entire spectrum. At still higher concentrations of pseudoisocyanine in glycerin there is a marked change in the shape of the spectrum which can be clearly seen in Fig. 3 where the vertical scale has been increased. Curve 1 in Fig. 3 is the absorption spectrum of the $4.55\cdot10^{-2}$ mole/liter solution of pseudoisocyanine in glycerin. It will be seen that it differs appreciably from the spectrum of the dilute glycerin solution (Curve 3). This substantial change in the absorption spectrum with concentration can be explained by assuming the formation of associated molecular groups, the absorption spectrum of which differs from the spectrum of monomeric molecules. By subtracting the monomeric part (Curve 3, Fig. 3) from the total absorption band of a concentrated solution (Curve 1) we obtained the absorption spectrum (Curve 2) characterizing the molecular associations. The separation was carried out on the assumption that in the vicinity of the principal monomeric peak (528 mμ) the associated groups do not absorb. The absorption spectrum of the associated groups does not change as regards shape over the entire inter-

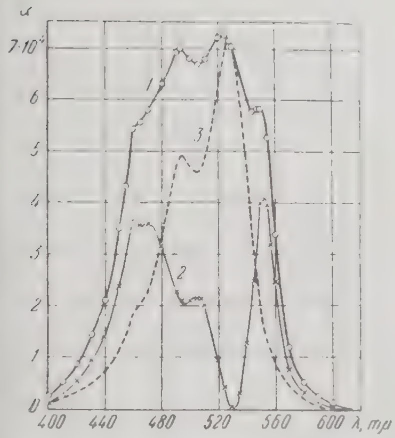

Fig. 3. Resolution of the absorption band of pseudoisocyanine in glycerin at a dye concentration of $4.55\cdot10^{-2}$ mole/liter (Curve 1) into monomeric (Curve 3) and associated (Curve 2) components.

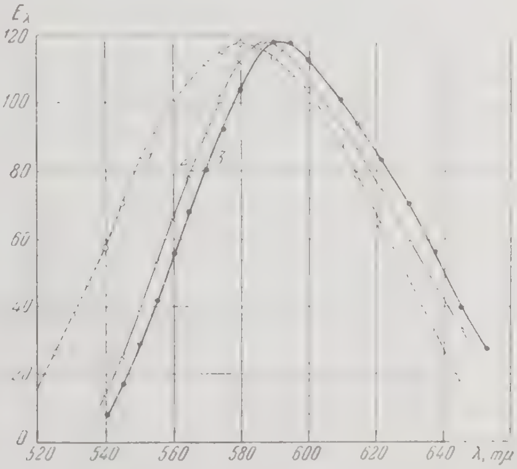

Fig. 4. Variations of luminescence spectrum of solutions of pseudoisocyanine in glycerin with changes in the dye concentration: 1) $C = 9.1\cdot10^{-4}$, 2) $8.3\cdot10^{-3}$, 3) $2.54\cdot10^{-2}$ mole/liter.

val of measured concentrations. It only changes as regards height in view of the increase in the degree of association of the solution. This indicates that only one type of molecular group is present and confirms the validity of our method of separating the absorption spectrum of the associated groups.

The ratio of the areas under the absorption spectra of the monomers and the associated groups shows that the absorption of the associated groups is lower than that of the monomers. Knowing the factor by which the absorbing power decreases, the absorbing power of the monomers and the total absorption of the solution of pseudoisocyanine, we can compute the degree of association of the solution (in percent) at different concentrations. The degree of association can also be computed from the change in coefficient of absorption at the monometric peak at 528 mμ as a function of the dye concentration.* The results of our calculations are listed in the accompanying table.

Degrees of association (in percent) of pseudoisocyanine molecules in glycerin solution calculated by two methods.

Concentration of pseudoisocyanine in the solution, mole/liter	Value computed according to monomer peak	Value obtained by comparing areas under absorption spectra for monomers & associated groups	Average value of degree of association
$5.1\cdot10^{-6}$	0	0	0
$1.18\cdot10^{-4}$	21.2	24.5	22.7
$1.96\cdot10^{-3}$	47.4	50.0	48.7
$1.1\cdot10^{-2}$	88.8	87.9	88.3
$4.55\cdot10^{-2}$	91.5	90.9	91.2

For computing the order of association, i.e., the number of molecules forming an associated group, we made use of the law of mass action:

$$C_M^x = kC_A e^{-Q/RT},$$

where C_M is the concentration of monomeric molecules, $C_A = C - C_M$ is the concentration of associated molecules, x is the association order, k is a proportionality coefficient (equilibrium constant), Q is the heat of dissociation, T is the absolute temperature and R is the gas constant.

At constant T we have:

$$x \log C_M - \log C_A = \text{const.}$$

The mean value of x was found to be 2.1 (accuracy ~15%). Thus as the concentration of pseudoisocyanine in the glycerin solution is increased the dye ions are dimerized.

The fact that a reasonable value is obtained for the degree of association upholds the validity of our method of separating the absorption spectra and substantiates our assumption regarding the absence of absorption by the associated groups at the monomeric peak.

As the concentration of pseudoisocyanine in the glycerin solution is increased, in addition to the noted change in the absorption spectrum, there is also a change of the luminescence spectrum** (Fig. 4). Increasing dye concentration in the

---

*The two methods are not entirely independent. The calculations were carried out by the two methods to enhance the accuracy of the results.

**Appropriate corrections were made for reabsorption.

glycerin solution leads to a shift of the luminescence spectrum to the side of long wavelengths. It may be assumed that the associated molecular formations have a luminescing power of their own with emission in a band shifted to the side of long wavelengths relative to the luminescence spectrum of the monomers. The observed gradual shift of the spectrum may be attributed to the increasing contribution to the luminescence made by the associated groups as the dye concentration of the solution is increased.

Tests showed that not only pseudoisocyanine but also some other dyes of the cyanine series are capable of associating in glycerin. Consequently water is not a unique solvent where association of cyanine dye molecules is concerned: the associative qualities of the molecules are simply more strongly manifested in water. The strong association of pseudoisocyanine molecules in water ($\varepsilon = 81$), their weaker association in glycerin ($\varepsilon = 56.2$) and the absence of association in ethyl alcohol ($\varepsilon = 27.8$) may be connected with the different values of the dielectric constants of these solvents.

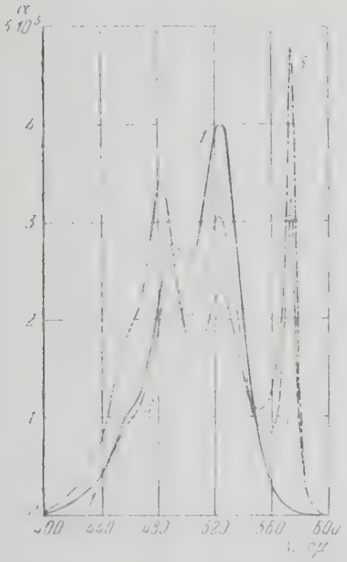

Fig. 5. Variation of the absorption spectrum of aqueous solutions of pseudoisocyanine with increasing dye concentration: 1) $C = 1.38 \cdot 10^{-5}$, 2) $2.7 \cdot 10^{-4}$, 3) $4.46 \cdot 10^{-3}$ mole/liter.

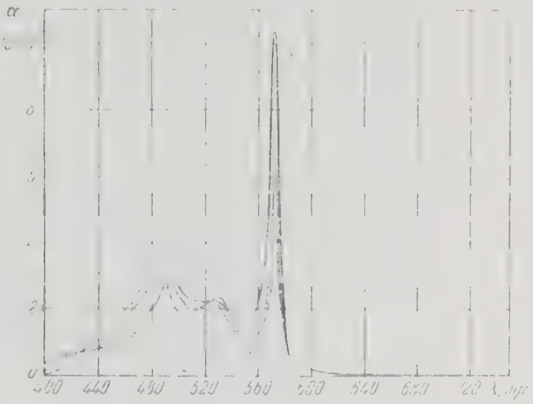

Fig. 6. Variation of the absorption spectrum of aqueous solutions of pseudoisocyanine with increasing dye concentration: 1) $C = 4.46 \cdot 10^{-3}$, 2) $1.1 \cdot 10^{-2}$, 3) $4.84 \cdot 10^{-2}$ mole/liter.

In water association is very intense. The absorption spectrum of aqueous solutions of pseudoisocyanine is shown in Fig. 5. It consists of the principal band and an unusually narrow band which appears when the concentration is increased (in accord [illegible]).

At low concentration (Curve 1) the shape of the absorption spectrum of pseudoisocyanine in water is identical with the shape of the absorption spectrum in an ethyl alcohol solution (Fig. 1). It may be deduced from this that at a given concentration all the molecules [illegible] monomers. As the concentration is increased the peak at 524 mμ is reduced, not to zero but to a certain value [illegible] that remains constant with further increase in concentration up to $4.84 \cdot 10^{-2}$ mole/liter (Fig. 6). This limited decrease shows that the peak at 524 mμ belongs not only to the monomers but also to the aggregations into which the monomer molecules associate as the concentration is increased. From the action law, which in this case may be written in the form

[illegible]

it follows that the decrease in the number of monomers occurs at the expense of formation of dimers. The fact that x remains equal to 2 in the concentration interval from $1.4 \cdot 10^{-5}$ to $1.4 \cdot 10^{-3}$ mole/liter indicates that the error involved in determining the concentration C_A of aggregated groups in equilibrium with the [illegible] as $C_A = C - C_M$, i.e., without taking into account the possibility of a higher degree of association, is not great for concentrations up to [illegible].

However, dimerization alone does not explain all the changes observed in the principal absorption band. As the concentration is increased there appear new additions to the dimer spectrum, features which characterize the formation of other aggregations. The number of molecules in these more complex formations is always a multiple of 2. This is evinced 1) by the fact that the absorption maximum of the dimers is manifest in the absorption spectra of all the complex aggregations (Fig. 3) and 2) by the fact that the decrease in the number of monomers occurs only at the expense of formation of dimers as shown by our calculations of the degree of association.

A feature characteristic of pseudoisocyanine is the appearance of an exceptionally narrow (half-width ~140 cm^{-1}) long wave (λ_{max} = 574 mμ) absorption peak which increases with the concentration and, as Scheibe[2] has established, is indicative of the formation of large polymer groups.

Scheibe's concepts regarding the polymerization of dye solutions and the association of different absorption peaks with definite molecular aggregations is substantiated by the results of our investigations of the reversible effect of temperature on the absorption of pseudoisocyanine, shown in Fig. 7. As the pseudoisocyanine solution is heated the high-polymer absorption peak at 574 mμ falls almost to zero due to the dissociation of the polymers. The absorption peak associated with simpler groups at 482 mμ goes down as a result of the dissociation of these aggregations into dimers and then with further temperature increase into monomers. Absorption at the 524 mμ peak increases with increasing temperature as a result of the increase in the number of monomeric molecules.

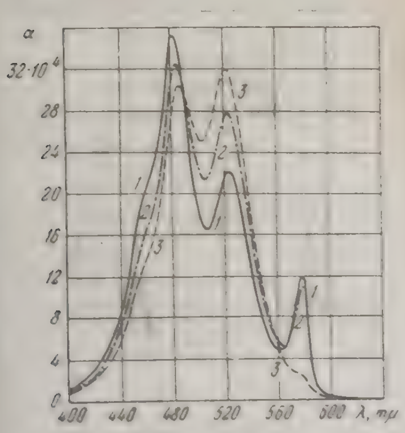

Fig. 7. Variation of the absorption spectrum of an aqueous solution of pseudoisocyanine with temperature: 1) 21°, 2) 50°, 3) 80°.

The heat of dissociation of dimers as computed from the increase in absorption at λ = 524 mμ was found to be 13 ± 2 Kcal/mole.

Absorption measurements at the 574 mμ polymer peak are hampered by the presence of resonance fluorescence at sufficiently high concentrations of the solution. For quantitative measurements of the absorption at the resonance peak we used very thin layers of solution; under 0.01 mm. We also found that the resonance luminescence was quenched by the addition of pyrocatechin.

Our results are at variance with those of Scheibe regarding the concentration at which the narrow long-wave absorption peak appears: according to Scheibe[2] this maximum appears suddenly (unstetig) at a concentration of $7\cdot10^{-3}$ mole/liter. We found that this peak appears at a lower concentration ($2.2\cdot10^{-5}$ mole/liter) and develops gradually with increasing concentration.

The variation of the height of the absorption peak with increasing concentration of pseudoisocyanine is shown in Fig. 8. The curve for α vs log C can be approximated by two straight lines: $\alpha = k \log C + a$ where k has different values befpre and after the break.

The coefficient of absorption α at 574 mμ is proportional to the number of highly polymerized molecules: $\alpha = BN$ (on the assumption that the oscillator strength of the polymer increases in proportion to the number of molecules of which it is comprised). Consequently,

$$N = k_1 \log M + A$$

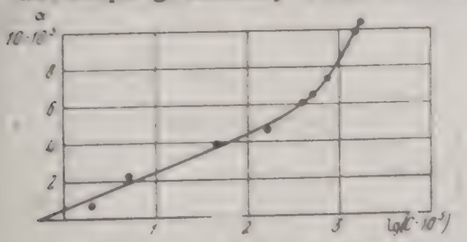

Fig. 8. Variation of the absorption coefficient of aqueous solutions of pseudoisocyanine at the polymer peak (574 mμ) with changes in the dye concentration.

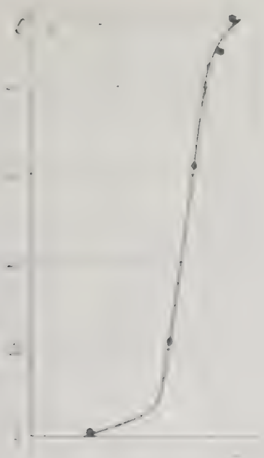

Fig. 9. Variation of the relative luminescence output of aqueous solutions of pseudoisocyanine at the polymer peak with changes in the dye concentration.

where M is the total number of molecules in the solution and N is the number of polymerized molecules.

Thus in the range of concentrations from $2.2 \cdot 10^{-5}$ to $4.8 \cdot 10^{-2}$ mole/liter the number of highly polymerized molecules is a logarithmic function of the number of molecules. The break in the straightline portion of the curve of Fig. 8 occurs in the $6 \cdot 10^{-3}$–$1 \cdot 10^{-2}$ mole/liter concentration interval. In this range of concentrations there is also a marked increase in the viscosity of the solution: up to $6 \cdot 10^{-3}$ mole/liter there is no noticeable change in viscosity, while at $1 \cdot 10^{-2}$ mole/liter the viscosity increases to such an extent that the solution becomes a gel. This appreciable increase in viscosity is evidence of the formation of aggregations comprising very large numbers of molecules.

Coincidentally with the increase in absorption at the polymer peak there is a change in the relative resonance luminescence output. As may be seen from Fig. 9, as the dye concentration is increased there is at first a slow and then a more rapid linear increase in the luminescence output. As we showed above, the number N of polymerized molecules also changes in proportion to log C. Hence, the change in the relative resonance luminescence output may be due to the increase in the number of polymerized molecules.

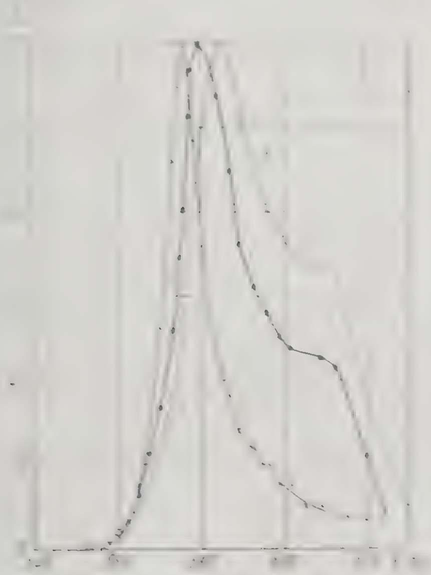

Fig. 10. Variation of the luminescence spectrum of aqueous solutions of pseudoisocyanine with the dye concentration: 1) $C = 7.23 \cdot 10^{-3}$, 2) $1.17 \cdot 10^{-2}$, 3) $6.9 \cdot 10^{-2}$ mole/liter.

The fluorescence* spectrum of the aqueous solution of pseudoisocyanine also changes with increasing dye concentration (Fig. 10). As the concentration is increased above $8 \cdot 10^{-3}$ mole/liter, in the region where the viscosity increases sharply and the solution "gelatinizes", the fluorescence band broadens and shifts somewhat to the long wave side; a new peak begins to appear at 610 mμ. The change in the shape of the fluorescence band with increasing concentration is explained by the fact that in viscous media, in addition to the large polymers, simpler formations begin to luminesce and the spectra of these are shifted somewhat into the long wave region relative to the emission of the polymers. This tentative explanation is based on the above established fact that the monomers and dimers of pseudoisocyanine in a glycerin solution emit luminescence and is substantiated by the nature of the change in the luminescence spectrum with increasing wavelength of the exciting light (Fig. 11). When the viscous concentrated aqueous solution of pseudoisocyanine is excited by light of wavelength in the region of the polymer absorption peak (574 mμ) only the resonance fluorescence band of the polymers is observed. Excitation in the region of absorption of the dimers (excit 560 mμ) leads to broadening of the fluorescence band, with some displacement to the long wave side, and the appearance of a peak at 610 mμ. In the case of excitation by light in the dimer absorption region, in

---

*The fluorescence spectra were investigated on an ISP-51 spectrograph with a PS-381 photoelectric recording attachment.

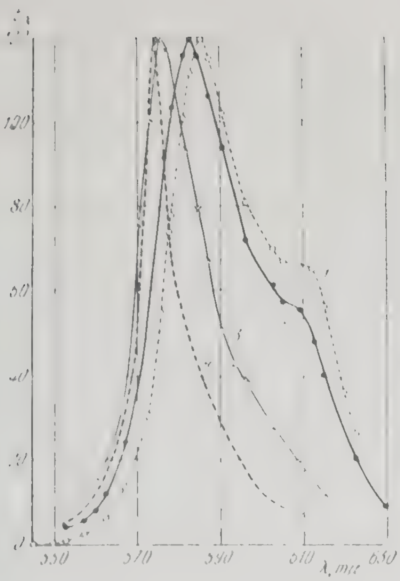

Fig. 11. Variation of the luminescence spectrum of an aqueous solution of pseudoisocyanine with the wavelength of the exciting light (C = $6.9 \cdot 10^{-2}$ mole/liter): 1) λ = 365 mμ, 2) 436 mμ, 3) 558 mμ, 4) 574 mμ.

addition to the polymer luminescence which is excited by virtue of the fact that the dimers are the "structural units" of the polymers, there becomes manifest the luminescence proper to the dimers and other relatively simple groups with a peak at 610 mμ. The gradual change in the shape of the luminescence band as the wavelength of the exciting light is decreased is due to the change in the ratio between the emission of the polymers and the emission of the simpler molecular formations.

The ability of pseudoisocyanine to form complex molecular groups is connected with the peculiarities of its chemical structure. In view of this we felt it would be of interest to study and compare the associative properties of a series of similar dyes in order to clarify the influence of molecular structure on association.

The close relationship between association and absorption effects led Scheibe^2 to suggest that the association of cyanine dye molecules involves the interaction of the absorbing π-electrons. If this is indeed the case, increase of the π-electron cloud should result in enhanced association. We attempted to verify this experimentally. The influence of the size of the π-electron cloud on the association was established by investigating the concentration-induced changes in the optical properties of compounds differing as regards the length of the intermediate chain in the molecule, the presence of additional benzene rings, the presence of naphthalene rings instead of thiazole rings and relative spatial rotation of parts of the molecule. We investigated the associative properties of a series of cyanine dyes which included pseudoisocyanine, pinacyanol, 3,3'-diethylthiacyanine chloride, 3,3'-diethylcarbocyanine chloride, 3,1'-diethylthiaquino-(2')-cyanine chloride, 3,1'-diethyl-6,7-benzothiaquino-(2')-cyanine chloride, 3,1'-diethylthiaquino-(4')-cyanine chloride.

The shape of the absorption spectra of all these dyes in alcohol solutions does not change with increasing concentration from 10^{-6} to 10^{-2} mole/liter or with increasing temperature to 60°C which indicates that their molecules are monomers in the alcohol solution.

In water solutions appreciable changes of the absorption spectra are observed with increasing concentration:

1) In pinacyanol peaks appear at 543, 505, 595 and 635 mμ and the absorption at the 602 mμ peak falls off.

2) In thiacyanine a peak appears at 405 mμ and the absorption decreases at the peak at 425 mμ.

3) In carbothiacyanine the absorption increases at 505 and 486 mμ and falls off at 555 mμ.

4) In thiaquino-(2')cyanine a peak appears at 444 mμ while the initial peak at 486 mμ disappears.

5) In benzothiaquino-(2')-cyanine the absorption falls off at 505 mμ and increases to peaks at 467 and 446 mμ.

6) In thiaquino-(4')-cyanine the absorption at the initial peak at 505 mμ and new peaks appear at 474 and 454 mμ.

The absorption spectra of the aqueous dye solutions change due to the formation at sufficiently high concentrations of associated molecular groups which can be decomposed by raising the temperature of the solution.

Comparison of the relative content of associates in aqueous solutions of

thiacyanine and carbothiacyanine, which differ as regards the length of the intermediate chain, shows that the association process proceeds more actively in carbothiacyanine than in thiacyanine. Thus, for example, at a $4.46 \cdot 10^{-4}$ mole/liter concentration of thiacyanine in the water solution only 44% of all the molecules are in the associated state whereas in a solution of carbothiacyanine, whose intermediate molecular chain is longer, approximately 71% of the molecules are associated at a concentration of $3.24 \cdot 10^{-4}$ mole/liter. In thiacyanine we observed only dimerization, whereas in carbothiacyanine at the same concentrations, in addition to dimers, there are more complex aggregations present.

In aqueous solutions of pinacyanol, the intermediate molecular chain in which is longer than that in pseudoisocyanine, association begins at lower concentrations than in solutions of pseudoisocyanine: at a concentration of $1.6 \cdot 10^{-5}$ mole/liter the dimer spectrum in pinacyanol is well developed whereas in the case of pseudoisocyanine only monomers are present.

In both pairs of substances lengthening of the intermediate chain favors association.

To investigate the influence of replacement of thiazole by naphthalene rings we compared the properties of three dyes: thiacyanine, thiaquino-(2')-cyanine and pseudoisocyanine. At equal molar concentrations of the dyes pseudoisocyanine had the highest and thiacyanine had the lowest percentage of associated molecules: thus, at a concentration of $8 \cdot 10^{-3}$ mole/liter, 88% of all the molecules of pseudoisocyanine were in the associated state in the aqueous solution as against 75% of the thiaquino-(2')-cyanine molecules and 67% of the thiacyanine molecules. Pseudoisocyanine in water forms higher polymers, while the other two dyes at similar molar concentrations form only dimers. Furthermore, the pseudoisocyanine groupings are more stable: the binding energy of the pseudoisocyanine dimers is 13 Kcal/mole, while that of the thiaquino-(2')-cyanine dimers is only 1.1 Kcal/mole.

The addition of a new benzene ring to the molecule also intensifies the association: at a concentration of $3.6 \cdot 10^{-4}$ mole/liter, 66% of all the molecules in a solution of benzothiaquino-(2')-cyanine are in the associated state while in a solution of thiaquino-(2')-cyanine only 46% of the molecules are associated at a concentration of $5 \cdot 10^{-4}$ mole/liter. While in the latter there is only dimerization in the former there is higher polymerization as well. An analogous situation is observed in the case of steric changes resulting in an enlargement of the π-electron clouds. At equal concentrations thiaquino-(4')-cyanine associates more strongly, as regards both degree of polymerization and the number of molecules associating, than thiaquino-(2')-cyanine. For example, at a concentration of about $5 \cdot 10^{-4}$ mole/liter, 81% of the molecules of thiaquino-(4')-cyanine a water solution are associated whereas only 46% of the molecules of thiaquino-(2')-cyanine are aggregated under like conditions. Moreover, the dimers of the former are more stable: the binding energy of thiaquino-(4')-cyanine is 2.9 Kcal/mole while that of thiaquino-(2')-cyanine is only 1.1 Kcal/mole. Thus, increase of the volume of the π-electron cloud no matter how achieved, leads to enhancement of association which is manifested by an increase in the equilibrium constant and the binding energy of the groupings.

In conclusion I wish to thank V.L.Levshin for his guidance and attention.

Physics Department of
"M.V.Lomonosov" Moscow State University

References

1. G.Scheive, A.Maries & H.Ecker, Naturwiss, 25, 474 (1937).
2. G.Scheibe, Kolloid, ZS, 82, 1 (1938).

LUMINESCENCE AND ABSORPTION OF CONCENTRATED SOLUTIONS OF 3,6-DIAMINOACRIDINE

- L.V.Levshin

The optical properties of complex organic molecules are strongly dependent on the concentration of these molecules in solution. We studied these concentration effects in a number of acridine compounds.[1,2] The influence of concentration is particularly strong in solutions of 3,6-diaminoacridine.[3]

All the important optical characteristics of this compound in solution are sensitive to changes in concentration. The shape of the absorption spectrum undergoes considerable changes in going from a dilute to a concentrated solution. In the visible region the absorption peak at 460 mμ falls off while the absorption at 405 mμ increases. No less appreciable changes occur in the ultraviolet absorption band. At the same time the luminescence spectrum is shifted to the side of long wavelengths and changes shape to some extent due to enhancement of its long-wave part. These changes occur not only when the concentration is increased but also when the wavelength of the exciting light is reduced from that at the long-wave absorption peak to that at the short-wave peak. Increasing concentration results in a certain decrease of the emission and of the decay time of the excited state of the molecule. The output and decay time are also dependent on the wavelength of the exciting light. In going from the dilute to the concentrated solution there is an appreciable change in the shape of the polarized emission spectrum which becomes noticeably simpler with increasing concentration. All these changes are reversible: the optical properties are fully reestablished when the concentrated solution is diluted.

The above facts clearly indicate that in concentrated solutions there are formed new distinctive "molecules" having different absorption and luminescence spectra, different efficiencies and a different arrangement of the absorbing and emitting oscillators than the molecules in dilute solutions. By analogy with known data on the effect of concentration on the optical properties of dye solutions;[illegible] it was assumed that the above enumerated effects are due to the formation of associated 3,6-diaminoacridine molecules capable of luminescing.[3] However, further investigations showed that there are two experimental facts which cannot be simply explained on the basis of association of the 3,6-diaminoacridine molecules.

1. In the presence of associated molecules, increasing the temperature of the solution by enhancing the supply of vibrational energy should favor dissociation of the molecules, that is, heating should reestablish the optical properties characteristic of dilute solutions. Experiments, carried out earlier by other investigators with concentrated dye solutions[4,5], showed that heating to 50-70° is commonly sufficient to reestablish the absorption spectrum of the dilute solution. In the case of 3,6-diaminoacridine, however, we found that heating the concentrated solution up to 70-90° results in little change in the absorption spectrum.[3] So great a temperature stability of the associated molecules could obtain in a certain temperature interval only if the association process were highly endothermic. In order to clarify the nature of this phenomenon it was necessary to carry out experiments in a much wider range of temperatures.

2. Investigation of the concentration effects in 3,6-diaminoacridine carried out in different solvents showed that they are strongest in media (dioxane, pyridine, acetone and alcohol) in which the association of dye molecules is weak or entirely absent. It proved impossible to carry out experiments in water (the medium in which association of dye molecules is commonly strongest) due to the weak solubility of 3,6-diaminoacridine. This influence of the solvent is also difficult to interpret if we assume that the concentration effects observed for 3,6-diaminoacridine are due to association.

To clarify the nature of the above mentioned effects we carried out experiments extending over an appreciable temperature range. By way of solvent we used glycerin which permits varying the temperature between wide limits. It should be noted that the effects of temperature manifest themselves in glycerin fully as well as in alcohol solutions.[3]

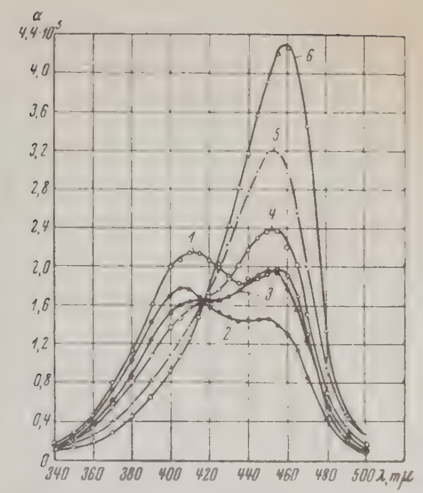

Fig. 1. Temperature dependence of a glycerin solution of 3,6-diaminoacridine ($C = 2\cdot10^{-3}$ g/ml): 1) +20°, 2) +150°, 3) +150° (after 3 hours heating), 4) +150° (after 6 hours), 5) +150° (after 11 hours), 6) +20° (cooled after 11 hours heating).

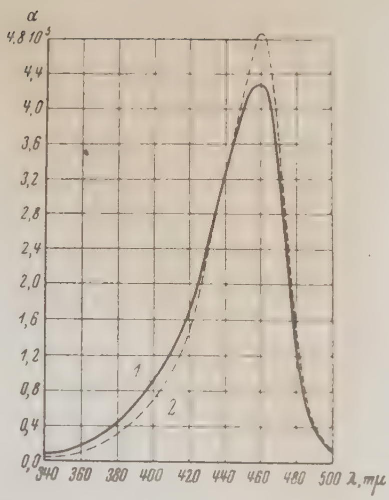

Fig. 2. Comparison of the absorption spectra of a heated and then cooled concentrated solution and of a diluted solution of 3,6-diaminoacridine in glycerin: 1) $C = 2\cdot10^{-3}$ g/ml, 2) $C = 1\cdot10^{-5}$ g/ml.

The temperature dependence of the absorption spectrum of a concentrated solution of 3,6-diaminoacridine in glycerin is shown in Fig. 1. It will be seen that increasing the temperature up to +150° leads to some decrease in absorption at both the long-wave and the short-wave peaks (Curve 2). This effect is apparently connected with reduction of the absorption of both types of molecules (I and II) with increasing temperature.* Where the I molecules are concerned this has been proved by the experiments described in Ref. 3. Prolonged heating at +150° leads to a gradual lowering of the short-wave and a strengthening of the long-wave absorption peaks (Curves 3-5). This effect masks the decrease in absorption in the long-wave part of the spectrum, connected with increased temperature. All these changes occur very slowly and the short-wave peak vanishes almost completely only after 11 hours heating at +150° (Curve 5).

The process proved to be irreversible: when a concentrated solution is cooled after heating not only does the absorption spectrum fail to return to its initial shape, but on the contrary the fading of the short wave peak and the development of the long wave peak continue at an appreciably faster rate than during heating (Curve 6).

As may be seen from Fig. 1 in the case of a concentrated solution heated for 11 hours at +150° and then cooled to room temperature (Curve 6), the short-wave peak virtually vanishes while the long-wave band stands out very clearly. This band as regards both shape and the position of the peak is very similar to the long-wave absorption band observed in very dilute solutions. The long-wave absorption bands of the concentrated solution subjected to prolonged heating and then cooled to +20° (See curve 6 in Fig. 1) and of a dilute solution are juxtaposed in Fig. 2 (Curves 1 and 2, respectively). It will be seen that the two contours are almost identical. The small divergence is presumably due to the fact that the concentrated solution still contains a small amount of II molecules. The similarity of the absorption bands indicates that prolonged heating of the concentrated solution transforms the type II 3,6-diaminoacridine molecules into type I. Certain additional data substantiating this deduction are given below.

Our experiments showed that the absorption spectrum of a concentrated solution of 3,6-diaminoacridine remains virtually unchanged in a wide temperature interval. It is altered only as a result of appreciable heating over a prolonged period.

---

*For the sake of brevity we will designate by I molecules encountered in the dilute solution and by II the molecules appearing in the solution when the concentration is increased.

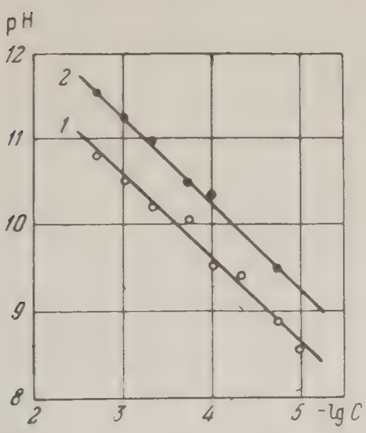

Fig. 3. Variation of the pH with the concentration of 3,6-diaminoacridine: 1) in ethyl alcohol, 2) in pyridine.

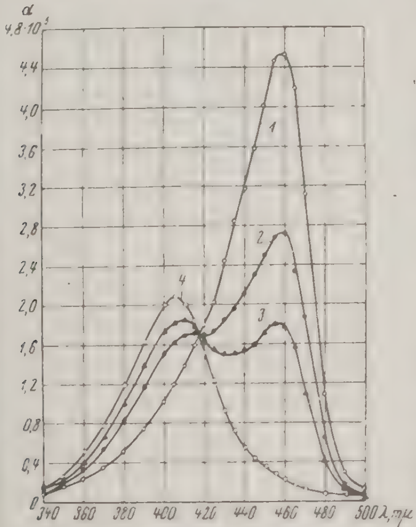

Fig. 4. Dependence of the absorption spectrum of a dilute (C = $2 \cdot 10^{-5}$ g/ml) solution of 3,6-diamino-acridine in ethyl alcohol on the pH: 1) without NaOH(pH = 8.6), 2) with NaOH(pH = 9.1), 3) with NaOH(pH = 9.6), 4) with NaOH(pH = 11.3).

In view of these results it is doubtful whether the concentration-induced changes in the properties of 3,6-diaminoacridine can be explained by molecular association.

Soon after completion of our preliminary experiments we learned of the results obtained by a group of French investigators[7] who indicate that molecules of the 3,6-diaminoacridine type can exist in two differently colored forms, the equilibrium between which depends on the concentration, the solvent and the pH value of the solution.* These investigators were concerned only with data obtained on the basis of the absorption spectra and did not examine the luminescence characteristics of the molecules; they did not investigate the influence of temperature. Moreover, the reasons for the influence of concentration on the equilibrium point between the two assumed forms was not elucidated. The influence of the pH of the medium was not exhaustively studied so that the results are essentially qualitative.

We carried out a detailed investigation of the influence of the pH of the optical properties of solutions. To this end we first studied the concentration dependence of the pH value of 3,6-diaminoacridine solutions. It was found that in the case of ethyl alcohol solutions the pH increases appreciably with the concentration. The variation is shown in Fig. 3 (Curve 1).**

3,6-Diaminoacridine appears to be a rather strong base and the results obtained are indicative of an appreciable dissociation of its molecules in ethyl alcohol. It is highly probable that it is precisely the increase in pH value that is responsible for the change in the optical properties observed at high concentrations. In order to check this, the pH value of a dilute (C = $2 \cdot 10^{-5}$ g/ml) solution was artificially increased by adding different quantities of NaOH. The absorption spectra of the resultant solutions were measured on a SF-4 spectrometer. The results are shown in Fig. 4, from which it will be seen that by increasing the pH value artificially one can obtain the same changes as by increasing the concentration. By sufficiently increasing the pH value of the solution one can obtain the absorption band of the II molecules in the pure form (Curve 4).

By the action of alkali on a concentrated solution of 3,6-diaminoacridine one can consummate the modification of the absorption spectrum, i.e., transform all the I molecules into the II type. It should be noted that these processes are fully reversible: reducing the pH of the solution by dilution one can fully reestablish the initial absorption spectrum. To substantiate further the influence of the solution pH on the optical

---

*M.A.Konstantinova[8] had earlier noted the appreciable influence of the pH on the optical properties of solutions.

**The writer desires to thank P.K.Agosian for making it possible to measure pH values by means of a LP-5 vacuum tube voltmeter. The tests were carried out with a glass electrode.

properties of 3,6-diaminoacridine molecules, we carried out the inverse experiment. Going over from an alkali to an acid medium should reestablish the long-wave absorption band of the concentrated solution, transforming all the II molecules to the I type. The results of this experiment are shown in Fig. 5. In this case small quantities of very dilute hydrochloric acid were added to a concentrated alcohol solution of 3,6-diaminoacridine (Curve 1). It will be seen that decreasing the pH of the solution strongly deforms the absorption spectrum and at pH = 9.0 (Curve 3) the spectrum characteristic of dilute solutions is fully reestablished. The results of our experiments indicate the decisive influence of the pH value of solutions of 3,6-diaminoacridine on the optical properties. The direct role of concentration is limited to changing the pH value of the solution which in turn produces the above described effects.

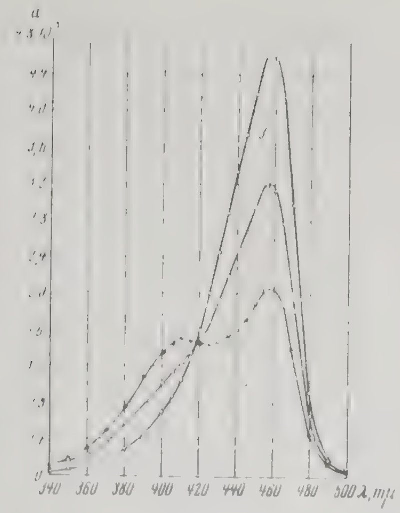

Fig. 5. Dependence of the absorption spectrum of a concentrated ($C = 1\cdot10^{-3}$ g/ml) solution of 3,6-diaminoacridine in ethyl alcohol on the pH value: 1) without HCl (pH = 10.7), 2) with HCl (pH = 9.7), 3) with HCl (pH = 9.0).

In the light of these results we returned to our temperature experiments and were able to obtain certain supplementary data which helped explain the effects occurring in heated, concentrated solutions of 3,6-diaminoacridine. It turned out that when the solution is heated with the consequent decrease in the short-wave and increase in the long-wave absorption peaks there is a simultaneous decrease of the pH value. Thus the pH value of the initial $C = 2\cdot10^{-3}$ g/ml glycerin solution (Fig. 1, Curve 1) is about 10. After prolonged heating and subsequent cooling, i.e., at the point where the long-wave absorption band is obtained (Fig. 1, Curve 6), the pH of the solution is reduced to about 8.4, which is equivalent to the pH value of the dilute $5\cdot10^{-5}$ g/ml solution. In this case the decrease in the pH value of the solution is apparently connected with irreversible changes occurring in the glycerin incident to prolonged heating. This is substantiated by temperature experiments carried out with pure glycerin from which it follows that its pH decreases appreciably in heating (before heating ~6, after heating ~5).

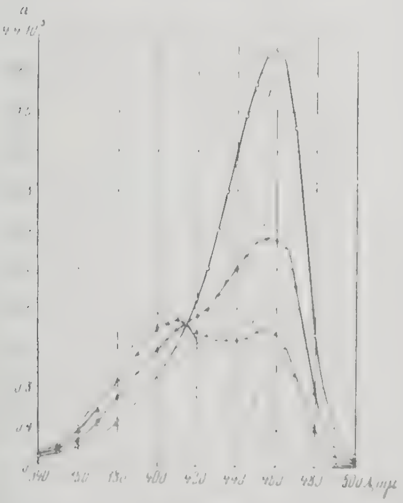

Fig. 6. Dependence of the absorption spectrum of a solution in glycerin ($C = 2\cdot10^{-3}$ g/ml) on the pH value: 1) without NaOH (pH = 8.4), 2) with NaOH (pH = 9.5), 3) with NaOH (pH = 9.9), 4) with NaOH (pH = 10.8).

Further, we investigated the influence of the pH on the long-wave absorption band (Fig. 1, Curve 6) of a concentrated solution subjected to prolonged heating with subsequent cooling. The results of these experiments are shown in Fig. 6 from which it may be seen that as the pH of a solution is increased by the addition of NaOH the long-wave absorption band fades and finally vanishes and at the same time the short-wave band, characteristic of II molecules, appears and develops. Thus we have the same picture as when concentration is increased[3] or the pH of a dilute solution is increased artificially (Fig. 2). In other words the effect which cannot be obtained by cooling a previously heated solution, is observed when its pH is increased.

The results of these experiments substantiate the premise that the form of the molecules observed in the dilute solution is identical with the form of the molecules resulting from prolonged heating of a concentrated solution. The temperature

experiments substantiate our deduction that the observed changes in the optical properties are determined primarily by changes in the pH of the solution. The pH value determines the equilibrium point between the two different forms (I and II) of the 3,6-diaminoacridine molecules.

The second distinctive feature of the concentration effects observed in the 3,6-diaminoacridine solutions is the strong dependence on the nature of the solvent, this dependence being different than that observed in solutions of dyes. The question of the influence of a solvent was not studied in detail in the present investigation; however, the data obtained appear to indicate that in this case also the pH value of the solution has a very considerable influence on the development of the concentration effects. Experiments carried out with pyridine solutions, in which the concentration effects develop more intensely than in alcohol, showed that the pH values of pyridine solutions are appreciably higher than of alcohol solutions at corresponding concentrations (Fig. 3, Curve 2).

In conclusion I wish to thank M.D.Galanin for valuable advice, A.M.Grigorovsky for making the 3,6-diaminoacridine available and A.P.Khobanski and Z.A.Barmin for their help in the work.

Physics Department of the
"M.V.Lomonosov" Moscow State University

References

1. L.V.Levshin, Doklady AN SSSR, 96, 473 (1954).
2. L.V.Levshin, Zhur. eksp. i teor. fiz., 28, 213 (1955).
3. L.V.Levshin, Zhur. eksp. i teor. fiz., 28, 201 (1955).
4. L.V.Levshin, Zhur. fiz. khim., 6, 1 (1935).
5. E.Rabinowitch & L.Epstein, J. Amer. Chem. Soc., 63, 69 (1941).
6. T.P.Kravets, A.L.Pes'kina & Z.V.Zhidkova, Izv. AN SSSR, Ser. fiz., 14, 493 (1950).
7. P.Ramart-Lucas, M.Grumez & M.Martynoff, Mem. pres. Soc. chim., 8,554 (1941).
8. M.A.Konstantinova-Schlezinger, Trudy FIAN (Transactions of the Physical Institute of the USSR Ac. of Sc.), 2, 7 (1942).

CONCENTRATION EFFECTS IN RHODAMINE SOLUTIONS

-V.L.Levshin & E.G.Baranova

1. Introduction

Rhodamines belong in the group of xanthene dyes; their structural formula is

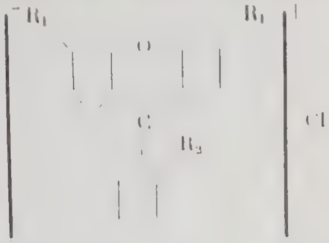

In the rhodamines with which we are here concerned the R_1 designates the radical $N(C_2H_5)_2$ in rhodamine 3B and NHC_2H_5 in rhodamine 6G; in both cases R_2 stands for $COOC_2H_5$.[1]

According to Izmailov and Kremer[2] the absorption spectra in the visible region of solutions of rhodamine B extra ($C = 3 \cdot 10^{-4}$ g/ml) undergo little change in going from alkaline to acid solutions except for a slight increase in intensity and shift to the side of longer wave lengths.

There have been many investigations devoted to rhodamines; below we mention only those closest to our study.

Vavilov[3] investigated the absorption of rhodamine B extra in methyl alcohol and acetone with changes in concentration. He found that in the first approximation the extinction varies as

$$I = I_0 e^{-k(C-C_0)},$$

where C_0 equals $1.0 \cdot 10^{-3}$ g/ml for methyl alcohol solutions and $0.8 \cdot 10^{-3}$ g/ml for acetone solutions.

A detailed study of solutions of rhodamines 6G and G in different solvents was made by one of the present authors (Refs. 4-6); the findings speak in favor of the molecular association theory of quenching. The principal results are the following: the absorption spectra of solutions in isobutyl alcohol are stable at concentrations up to $\sim 10^{-3}$ g/ml; the absorption spectra in aqueous solutions deform beginning with very low concentrations, which is indicative of molecular association; in the process the principal absorption peak in the visible region decreases while a new, second peak appears on the short wave side of the absorption band. When the temperature is increased, with consequent dissociation of the associated groups, the new short wave peak fades and the absorption spectrum of concentrated solutions approaches that characteristic of weak solutions. The influence of concentration on quenching is less pronounced with excitation by light in the region of the long wave monomer maximum and more rapid in the case of excitation by light having a wave length corresponding to the new short wave dimer peak.

Heating of concentrated aqueous solutions of rhodamine 6G led to an increase in the luminescence efficiency due to the break-up of non-luminescing associations, while the heating of weak aqueous solutions, containing only monomers, resulted in little change in the luminescence output; the output of rhodamine G in different alcohol solutions fell off noticeably with heating. Thus all the observed characteristics of the rhodamine G and 6G solutions indicated that the concentration effects in these dyes are connected with molecular association.

The purposes of the present study were:

1) to show that the concentration effects in rhodamines are independent of electrolytic dissociation;

2) to investigate the influence of concentration on the absorption in the ultraviolet region,

3) to obtain more accurate quantitative data on the temperature and concentration effects;

4) to establish the nature of the quenching and the degree of association of the luminescent molecules in solutions at different concentrations on the basis of the concepts and ideas developed in Ref. 7.

2. Influence of pH on the State of the Dye

In order to establish the effect of changes in pH occurring due to increasing the dye concentration, we first measured the pH values of aqueous solutions of rhodamine 3B in the entire attainable range of concentrations. The results are shown in Fig. 1. In the concentration range from $1\cdot10^{-6}$ to $2\cdot10^{-3}$ g/ml the pH changes from 6.9 to 3.4, i.e., in going from low to higher concentrations the initially neutral solution becomes weakly acid. As the next step we added acid to the weak solutions to bring the pH down to about 3 and alkali to concentrated solutions to raise the pH to 6.9. We investigated the influence of acid on the absorption spectra of weak solutions and of alkali on the absorption spectra on the concentrated solutions. The results are shown in Fig. 2 from which it may be seen that the spectra change little with changes in pH value. Consequently the alterations of the shape of the absorption spectra of rhodamines incident to changes of concentration cannot be ascribed to electrolytic dissociation of the dye molecules. The absolute values of the absorption in both cases decreased somewhat with increasing acidity.

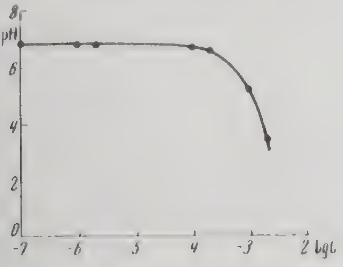

Fig. 1. Variation of pH with the concentration of rhodamine 3B extra in water solutions.

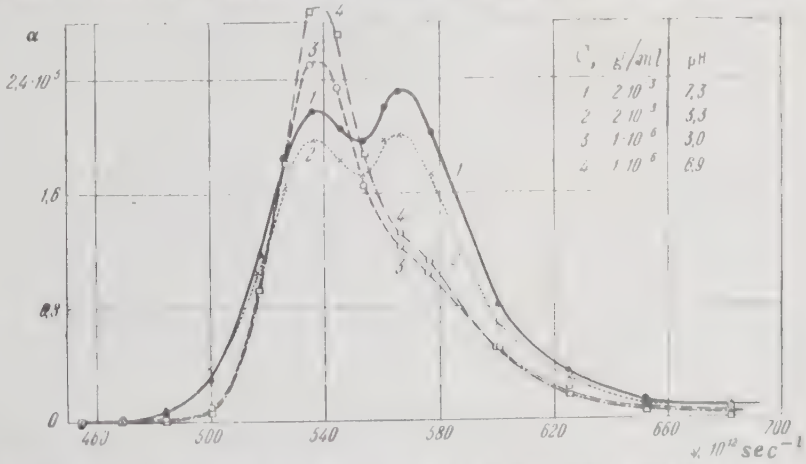

Fig. 2. Influence of the pH value on the absorption spectrum of aqueous solutions of rhodamine 3B extra at different concentrations of the dye.

3. Temperature-Concentration Effects in Rhodamines 3B and 6G Variation of the Absorption Spectra of Rhodamine 6G with Concentration.

Fig. 3 shows the result of our investigation of the absorption of aqueous solutions of rhodamine 6G extra at concentrations from $1.5\cdot10^{-6}$ to $3\cdot10^{-3}$ g/ml. Fig. 3,a shows the spectra in the visible region; Fig. 3,b the spectra in the ultraviolet region. Variation of the concentration of rhodamine 6G extra over the indicated wide range is not accompanied by any noticeable changes in absorption in the ultra-violet region ($750\text{-}1200\cdot10^{12}$ sec^{-1}).

Analogous results were obtained for rhodamine 3B. Hence the molecular association apparently occurs due to interaction of the electrons responsible for absorption in the visible region, i.e., the π-electrons.

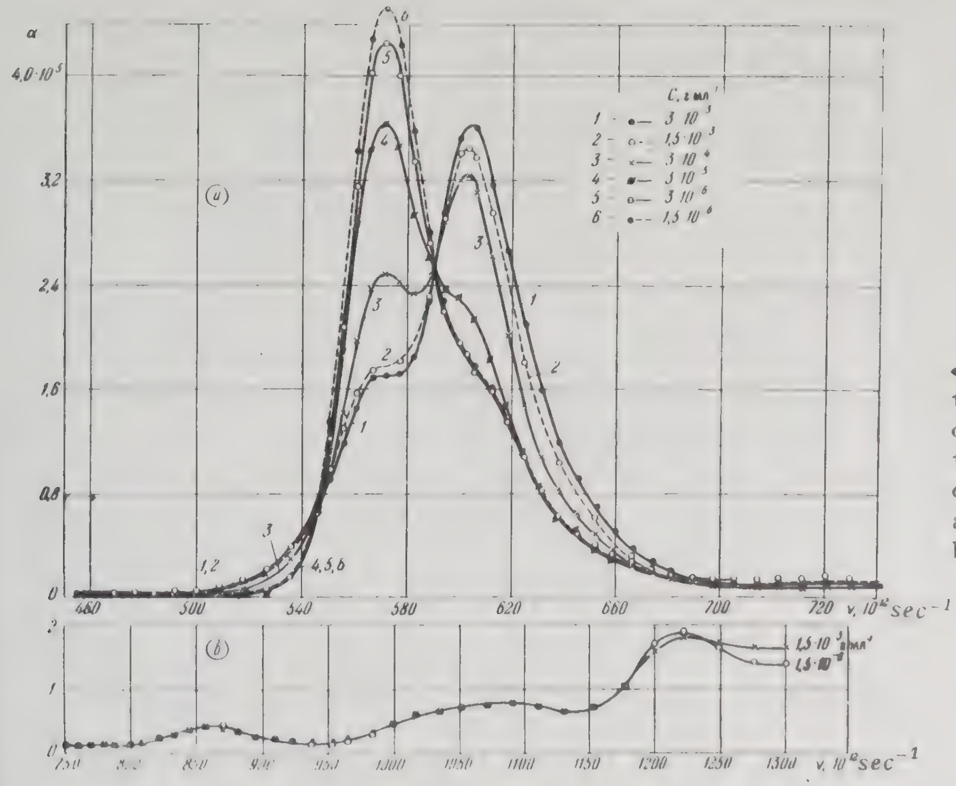

←Fig. 3. Influence of the dye concentration on the absorption spectra of aqueous solutions of rhodamine 6G extra:
a) visible region,
b) ultraviolet region.

Variation of the absorption spectra of concentrated solutions with temperature.

We investigated the absorption spectra of aqueous solutions of rhodamine 3B in the visible region at a concentration of $2\cdot10^{-5}$ g/ml and at the limiting concentration of $2\cdot10^{-3}$ g/ml at 20, 40, 60 and 80°. The results are shown in Figs. 4 and 5.

The spectrum of the $2\cdot10^{-5}$ g/ml solution is almost stable over the entire temperature range. The spectrum of the $2\cdot10^{-3}$ g/ml solution at 20° exhibits a second appreciable peak at $565\cdot10^{12}$ $\sec^{-1}$. When the solution is heated this peak gradually fades and at the same time the absorption at the principal peak ($536\cdot10^{12}$ $\sec^{-1}$) increases.

The appearance of the absorption spectrum of the concentrated solution at 80° (Curve 4) approaches that of the spectrum of a dilute ($2\cdot10^{-5}$ g/ml) solution at the same temperature (Curve 5).

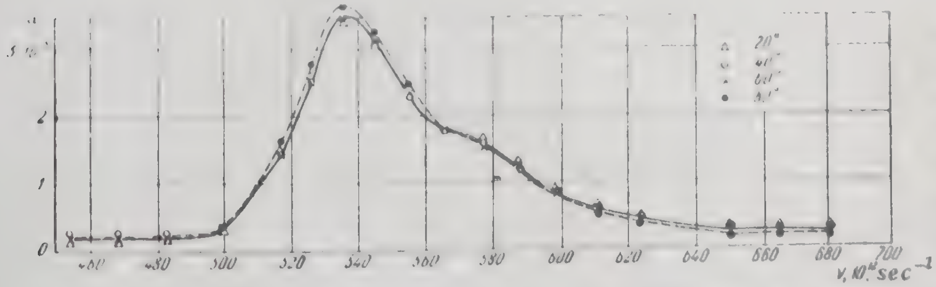

Fig. 4. Influence of temperature on the absorption spectrum of rhodamine 3B extra in water at C = $2\cdot10^{-5}$ g/ml.

The absorption spectra of rhodamine 6G extra in water at 20, 40, 60 and 80° are shown in Fig. 6. The spectra of rhodamine 6G are even more temperature sensitive than the spectra of rhodamine 3B. As the temperature of the concentrated solution is increased the peak

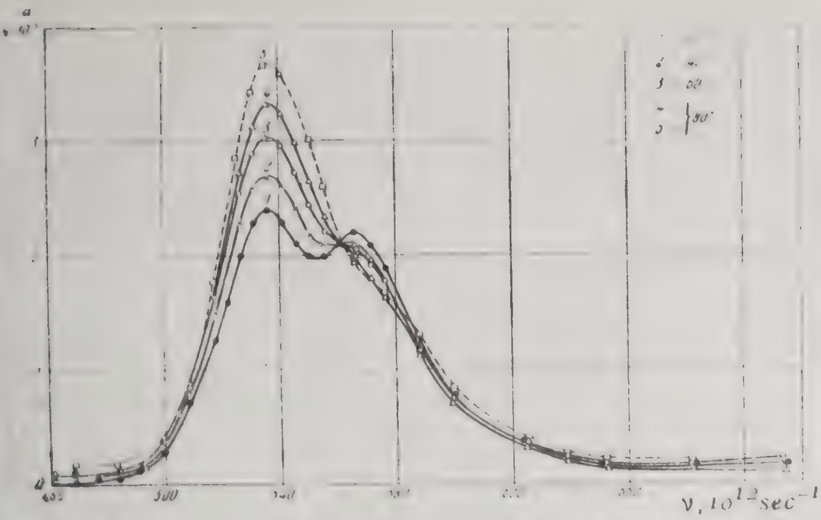

Fig. 5. Influence of temperature on the absorption spectrum of rhodamine 3B extra in water at two different concentrations: 1-4) $C = 2 \cdot 10^{-3}$ g/ml, 5) $C = 2 \cdot 10^{-5}$ g/ml.

at about $565 \cdot 10^{12}$ sec^{-1} is rapidly reestablished while the short wave dimer peak fades slowly.

In conformity with the the results of Ref. 5, our investigation of the emission spectra of rhodamine 6G showed that the shape of the spectrum is independent of the concentration within the limits of the experimental error. This would indicate that the emission is due to non-associated particles.

Measurements of the areas of the absorption curves for rhodamine 3B solutions in water showed that at 20° the total absorption does not change over the entire investigated range of concentrations: 10^{-6}-10^{-3} g/ml (Fig. 7,a).

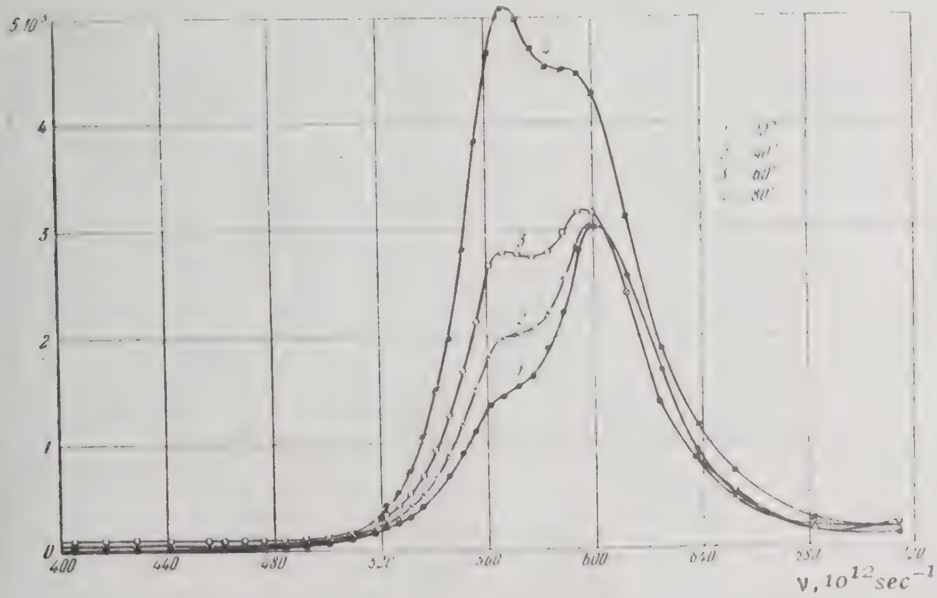

Fig. 6. Absorption spectra of a $3 \cdot 10^{-3}$ g/ml solution of rhodamine 6G extra in water at different temperatures.

Comparison of the areas under the absorption spectra at different temperatures showed that in the case of the $2 \cdot 10^{-3}$ g/ml aqueous solution of rhodamine 3B there is an appreciable increase in absorption (by about 15%) in the 20-80° temperature interval. The absorption of rhodamine 6G begins to increase at a temperature of about 40° and rises to almost 70% above its initial value at 80°. The temperature dependence curves are shown in Fig. 7,b. The reason for the overall increase in absorption with increasing temperature, particularly in the 60 to 80° interval, is still unclear.

Influence of temperature on the emission output of concentrated solutions.

The most convincing proof of dimerization is the increase in luminescence exhibited by concentrated solutions with increasing temperature. This increase is due to the dissociation of the dimers and the formation of monomers capable of luminescing.

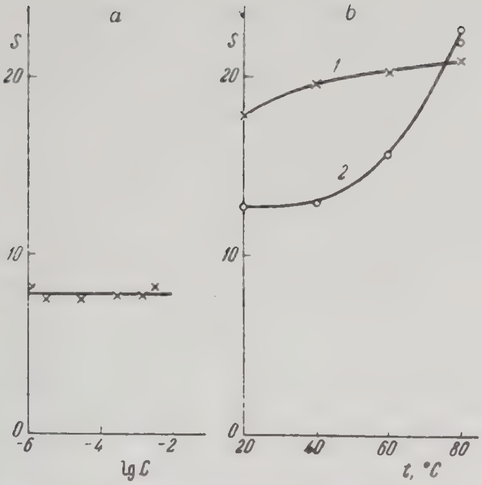

Fig. 7. Dependence of the absorption: a) of solutions of rhodamine 3B extra in water on the concentration at 20° and b) solutions of rhodamine 3B extra (1) and 6G extra (2) on the temperature.

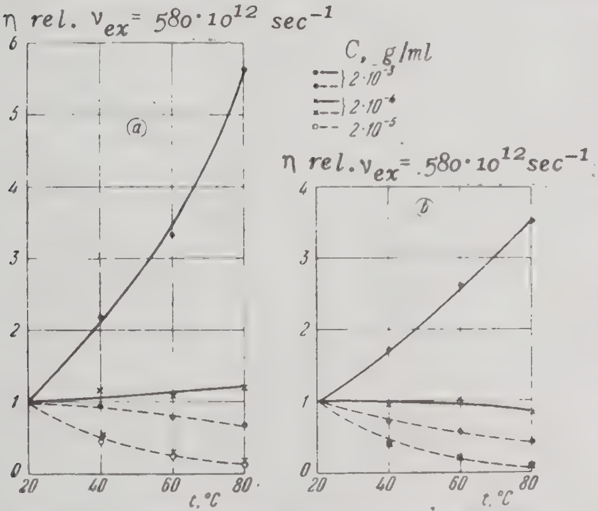

Fig. 8. Temperature dependence of the luminescence efficiency of aqueous solutions of rhodamine 3B extra under excitation by light having a frequency corresponding to the absorption peak of the dimers (a) and the monomers (b). (The solid curves are corrected for the effect of temperature quenching).

The dependence of the luminescence efficiency of aqueous solutions of rhodamine 3B extra on the temperature at concentrations of $2\cdot10^{-5}$, $2\cdot10^{-4}$ and $2\cdot10^{-3}$ g/ml is shown in Fig. 8.

The luminescence was excited by light having a frequency close to the dimer absorption peak - $580\cdot10^{-12}$ sec^{-1} (Fig. 8,a) and close to the monomer absorption peak - $540\cdot10^{12}$ sec^{-1} (Fig. 8,b). The experimentally observed variation in brightness is indicated by the dash curves. In the first case (a) the dissociation of the dimers is obviously more pronounced than in the second (b). The curves characterizing the decrease in efficiency of the $2\cdot10^{-4}$ g/ml solutions when excited by a light of a frequency corresponding to both absorption peaks are parallel (the divergence is within the limits of the experimental error). The emission of the $2\cdot10^{-3}$ g/ml solutions falls off more slowly with increasing temperature.

In order to find the true value of the increase in luminescence efficiency due to dissociation of the dimers incident to heating of the concentrated solutions the observed experimental emission values should be multiplied by a coefficient indicating the factor by which the luminescence of the solution is quenched by the temperature rise. This coefficient can be determined from the temperature vs output curve for the dilute $2\cdot10^{-5}$ g/ml solution. The resultant curves for the luminescence efficiency of the $2\cdot$ $\cdot10^{-4}$ and $2\cdot10^{-3}$ g/ml solutions of rhodamine 3B extra in water obtained after correction for the temperature quenching are shown by the solid lines in Figs. 8,a and b. The luminescence efficiency of the $2\cdot10^{-4}$ g/ml solution excited by light of frequency $\sim580\cdot10^{12}$ sec^{-1} increases by a factor of 1.2 when the solution is heated to 80°; the corresponding factor for the $2\cdot10^{-3}$ g/ml solution is 5.6. When the $2\cdot10^{-3}$ g/ml solution is excited at a frequency of $540\cdot$ $\cdot10^{12}$ sec^{-1} the output at 80° is increased by a factor of 3.5.

Fig. 9 shows the temperature dependence of the luminescence efficiency of aqueous solutions of rhodamine 6G extra at concentrations of $3\cdot10^{-6}$, $1.5\cdot10^{-3}$ and $3\cdot10^{-3}$ g/ml and for two different frequencies of the exciting light: $607\cdot10^{12}$ and $570\cdot10^{12}$ sec^{-1}. The $607\cdot10^{12}$ sec^{-1} frequency corresponds to the dimer peak; excitation by the $570\cdot10^{12}$ sec^{-1} light corresponds to excitation at the monomer peak.

The experimentally observed variation in output is given by the dash lines; the variation taking into account the quenching effect of temperature is indicated by the solid lines.

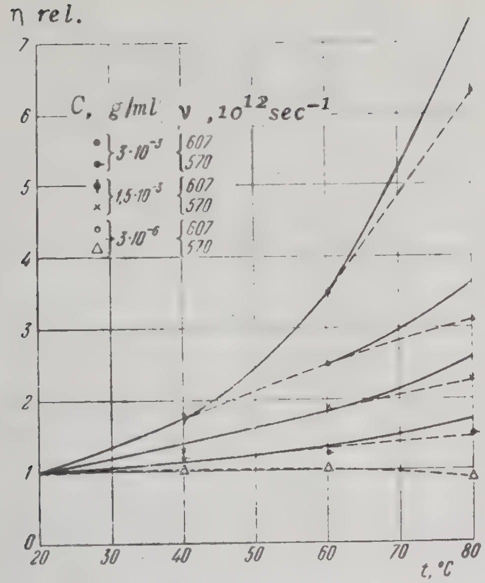

Fig. 9. Temperature dependence of the luminescence efficiency of solutions of rhodamine 6G extra in water (solid lines represent data corrected for the temperature quenching).

Examination of the temperature quenching curve for the $3\cdot10^{-6}$ g/ml solution showed that the emission of rhodamine 6G extra falls off very little with heating to 80°, which might be explained by the stability of the excited rhodamine molecules or by compensation of the temperature quenching by dissociation of the dimers. However, the latter explanation is doubtful since dimerization at concentrations of the order of $3\cdot10^{-6}$ g/ml is very small; this is substantiated both by the closeness of the absorption curves at concentrations of 1.5 and $3\cdot10^{-6}$ g/ml (Fig. 3, Curves 5 and 6) and by the similarity of the temperature quenching curves with excitation by light of frequencies $607\cdot10^{12}$ and $570\cdot10^{12}$ sec^{-1} (Fig. 9). The low value of the dimerization is naturally responsible for the negligible influence of non-active absorption and of migration of excitation energy to the dimers. This is substantiated by the similarity of the temperature variation of absorption in different solvents (Ref. 6) in which the dimerization is obviously not the same. Thus it must be admitted that the excited state of rhodamine 6G extra in the 20-80° temperature interval is stable.

There is a rapid increase in emission when concentrated ($C = 1.5\cdot10^{-3}$ g/ml) solutions of rhodamine 6G extra are heated. With excitation by light corresponding to the frequency at the monomer peak the luminescence is increased by a factor of 2.6 (according to the corrected curves), and with excitation at the dimer peak, by a factor of 7.4. This difference in the rate of increase of luminescence is clearly indicative of the dissociation of the dimers at this concentration and of the enhanced role of monomer excitation.

These effects are repeated at the higher concentration of $3\cdot10^{-3}$ g/ml. However, in this case the emission increases more slowly: under excitation in the region of the monomer peak the efficiency incident to heating to 80° increases by 1.7, while with excitation in the region of the dimer peak, by a factor of 3.6. The slower rate of emission increase as compared with the $1.5\cdot10^{-3}$ g/ml solution shows that by virtue of the great increase in concentration ($C = 3\cdot10^{-3}$ g/ml) the number of dimers at 80° is still appreciable.

4. Determination of the Degree of Association in Rhodamine Solutions

From the absorption spectra at different concentrations (Fig. 3,a), one can evaluate the degree of association in rhodamine 6G extra solutions. To this end let us assume that at a concentration of $1.5\cdot10^{-6}$ g/ml there is no dimerization (this is probably not quite justified) and that at a concentration of $3\cdot10^{-3}$ g/ml all the molecules are polimerized (this is plausible in view of the stability of the spectra). The determination can be carried out both on the basis of the variation of the monomer peak and from the variation of the dimer peak (Ref. 5); the first method is more accurate. The probable values for the degree of association of rhodamine 6G extra in aqueous solutions are given in Table 1. The figures indicate the percent (by weight) of the dye in the associated state. These values refine the data obtained earlier by one of the present writers.[6]

The degrees of association of rhodamine 3B extra in a $2\cdot10^{-3}$ g/ml aqueous solution at different temperatures were evaluated on the basis of the absorption

spectra shown in Fig. 5; for the purposes of the evaluation in the dimer content at a concentration of $2 \cdot 10^{-5}$ g/ml and a temperature of 80° was assumed to be zero (Table 2).

Table 1

Degree of association of rhodamine 6G extra at different concentrations in water solutions.

Concentration, g/ml	$3 \cdot 10^{-6}$	$3 \cdot 10^{-5}$	$3 \cdot 10^{-4}$	$1.5 \cdot 10^{-3}$
Degree of association, %	4	26	76	94

Table 2

Degree of association of rhodamine 3B extra in a $2 \cdot 10^{-3}$ g/ml aqueous solution at different temperatures

t, °C	20	40	60	80
Degree of association, %	100	77	50	24

For determining the degree of association one can also make use of the observed increase in the luminescence efficiency of concentrated solutions incident to heating.

It was established in the experiments that with excitation of the luminescence by light of the frequency absorbed at the dimer peak the luminescence efficiency of rhodamine 3B increases 5.6 times, while with excitation by light of the frequency absorbed at the monomer peak the efficiency increases 3.5 times when the temperature of the solution is raised from 20 to 80°. Let us establish the following designations: x is the fraction of the monomers, α is the coefficient of absorption, the subscripts m and d refer to monomers and dimers, respectively; subscript figures identify the temperature, the prime indicates excitation at a frequency of $580 \cdot 10^{12}$ sec^{-1}, absence of a prime indicates excitation at a frequency of $540 \cdot 10^{12}$ sec^{-1}, $f(C_d)$ designates the probability of the absence of energy transfer from the monomers to the dimers. We then have the following relationships:

$$\frac{\alpha_{m80} x_{80} f(C_{d80})}{\alpha_{m80} x_{80} + \alpha_{d80}(1-x_{80})} : \frac{\alpha_{m20} x_{20} f(C_{d20})}{\alpha_{m20} x_{20} + \alpha_{d20}(1-x_{20})} = 3.5$$

and

$$\frac{\alpha'_{m80} x_{80} f(C_{d80})}{\alpha'_{m80} + \alpha'_{d80}(1-x_{80})} : \frac{\alpha'_{m20} x_{20} f(C_{d20})}{\alpha'_{m20} x_{20} + \alpha'_{d20}(1-x_{20})} = 5.6$$

Assuming that for solutions with $C = 2 \cdot 10^{-3}$ g/ml, $x_{20} \ll 1$, we substitute the values of α from Fig. 5 in the above expressions, taking it for granted that the absorption for individual monomers and non-dissociated dimers changes little with the temperature. Eliminating $f(C_{d30})$ and $f(C_{d20})$, we find $x_{80} \approx 0.80$ or $1 - x_{80} \approx 0.20$ which is in qualitative agreement with the value given in Table 2.

In conclusion the writers desire to thank L.V.Krotov for his assistance in the investigation.

"P.N.Lebedev" Physical Institute of the
Academy of Sciences of the USSR.

References

1. G.Schultz, Farbstofftabellen, Bd. 1., Leipzig, 1931.
2. N.L.Izmailov & V.A.Kremer, Izv. AN SSSR, Ser. fiz., 15, 565 (1951).
3. S.I.Vavilov, ZS, f. Phys., 31, 750 (1925).
4. V.L.Levshin, SZ. f. Phys., 43, 230 (1927).
5. V.L.Levshin, Zhur. fiz. khim., 6, 1 (1935); Acta Phys.-chim. URSS, 1, 685 (1935).
6. V.L.Levshin, Zhur. fiz. khim., 6, 991 (1935); Acta Phys.-chim. URSS, 2, 221 (1935).
7. V.L.Levshin, Present issue of the Bulletin, p.362.

THE INFLUENCE OF CONCENTRATION ON THE LUMINESCENCE OF ALCOHOL SOLUTIONS OF ACRIDINE ORANGE AT -180°C.

-L.A.Kuznetsova and B.Ia.Sveshnikov

S.I.Vavilov's energy migration theory has been repeatedly and successfully invoked to explain concentration-induced depolarization and quenching of the luminescence of solutions at moderately high concentrations of the fluorescing substance.[2] The theory has also been substantiated by experiments on quenching of luminescence by absorbing materials[3] and experiments on sensitized fluorescence[4] and phosphorescence.[5]

Aside from these phenomena, appreciable changes in the absorption and luminescence spectra, increases in the luminescence efficiency incident to heating and a number of other effects are not infrequently observed at high concentrations of the solute. These effects cannot be satisfactorily explained by the energy migration theory but are satisfactorily interpreted by the association theory developed for luminescence phenomena by V.L.Levshin.[6] On the other hand, the association theory cannot explain the effects of concentration-induced depolarization, sensitized luminescence and the decrease in the decay time of the excited state in concentration quenching. There can be no doubt, however, that there must be a connection between the effects observed at moderate and at high concentrations and that in the future the separate energy migration and association theories must be replaced by some unified theory capable of explaining the effects throughout the entire range of concentrations. Development of a common theory of concentration effects would be useful not only where study of luminescence is concerned but also for a better understanding of the mechanism of molecular association processes.

One of the immediate experimental problems in the field is assorting and classifying the various luminescence characteristics invoked in studying association processes. The first investigations along this line are apparently those of Levshin[7] who gave attention not only to the luminescence spectra and efficiency but also to the polarization and time-characteristics of fluorescence in studying association processes.

In the present investigation, in addition to the fluorescence and absorption characteristics, we also investigated the phosphorescence characteristics of associated and non-associated molecules. We studied the influence of dye concentration on the spectrum, the duration and output of the total emission and the phosphorescence of frozen alcohol solutions of acridine orange.

Experimental procedure

All the experiments described hereinafter were carried out with alcohol solutions of acridine orange at the temperature of liquid air. Aside from single or double distillation to obviate blue emission and afterglow no special measures were taken to purify the alcohol. By freezing the material in spherical flasks we were usually able to obtain a fracturefree vitreous solution which remained in this condition during the period of the experiment (20-30 minutes). The dye-acridine orange was used as received from the manufacturer (Meister Lucius).

The total emission spectra were studied by means of a set-up consisting of a Hilger glass monochromator and a photomultiplier and amplifier. The phosphorescence was analyzed by means of a Becquerel phosphoroscope having a rate of disk rotation up to 2500 rpm. The set-up was calibrated with reference to a ribbon filament lamp at two temperatures and the resultant calibration curve was checked by recording a number of luminescence spectra known from the literature. We used the same set-up to determine the phosphorescence efficiency. To this end we determined the ratio of the phosphorescence intensity to the intensity of the total emission for a sufficiently narrow spectral interval lying in the region of the maximum superposition of the two spectra, i.e., the first measurement was made with the openings in both discs of the phosphoroscope in line, the second with the

the openings in the two discs covering each other completely.

As has been shown by one of the present writers (Ref. 8), in order to find the relative phosphorescence yield one must multiply the ratio of the fluorescence light sum to the total emission light sum obtained in this manner by $360/n\alpha$, where n is the number of openings in the discs and α is the size of each opening in degrees.

We studied the concentration dependence of the total emission only in the region of sufficiently high dye concentrations where there was complete absorption of the exciting light; hence in our set-up the excitation was effected and the emission observed from the same side of the set-up with a small angle between the directions of incidence and observation.

The duration of phosphorescence was measured on the phase fluorometer developed by Bonch-Bruevich, Molchanov and Shirokov.* The sensing-recording part of the duration of phosphorescence measurement set-up consisted of a photomultiplier, a short period galvanometer and a kymograph.

Results and Discussion

Spectra of persistent and total emission

The influence of dye concentration on the emission spectra of acridine orange was first studied by Levshin.[9] He studied the emission spectra of this dye in sugar drops at 20° and discovered that when the dye concentration is increased the spectrum changes markedly as regards appearance and position. A similar study was recently carried out by Zanker[10] who studied the influence of concentration on the absorption and luminescence spectra of this dye in a mixture of ethyl alcohol and ether at the temperature of liquid air.

We felt it desirable to supplement Zanker's data by studying the influence of the dye concentration on the spectrum and the duration and output of the phosphorescence of acridine orange. In order to determine the phosphorescence output it was necessary also to repeat Zanker's investigation of the total emission spectra since in studying these Zanker used the method of photographic photometry which is characterized by relatively low accuracy.

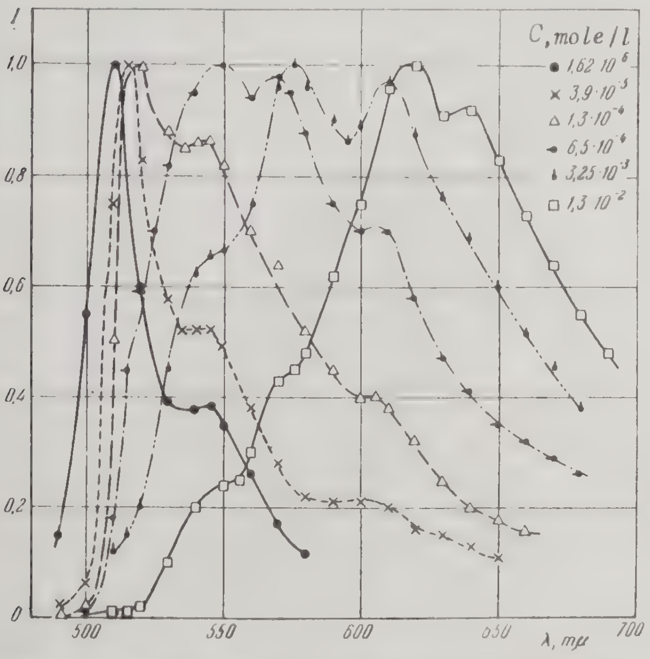

Fig. 1. Total emission spectra of alcohol solutions of acridine orange at T = -183°.

Our spectra of the total luminescence and persistent emission of alcohol solutions of acridine orange with different dye concentrations** at the temperature of liquid air are shown in Figs. 1, 2 and 3. It will readily be seen that as the concentration is increased from $1.6 \cdot 10^{-6}$ to $1.3 \cdot 10^{-2}$ mole/liter the peak of the total emission spectrum is shifted at least 110 mμ and the shape of the spectrum is

---

*We take this occasion to thank them for making the instrument available and for their help in making the measurements.

**In evaluating the concentration we took account of the volumetric contraction at the temperature of liquid air (0.77 the volume at 20°).

altered to such an extent that there is almost no similarity between the two spectra; on the other hand, the persistent emission (phosphorescence) spectrum in this interval of concentrations changes very little: the displacement of the peak does not exceed 10-12 mμ and the spectra at the different concentrations are generally similar.

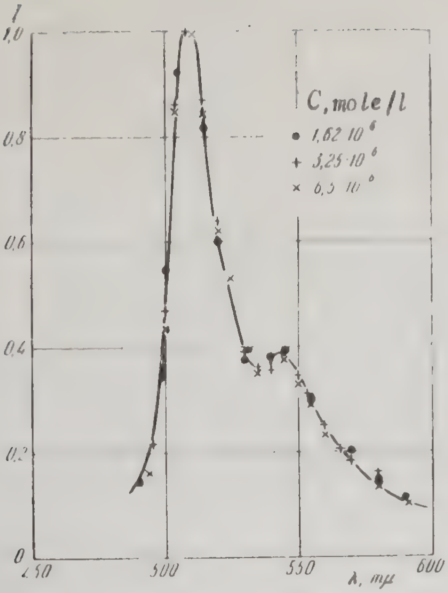

Fig. 2. Total emission spectra of alcohol solutions of acridine orange at very low concentrations of the dye.

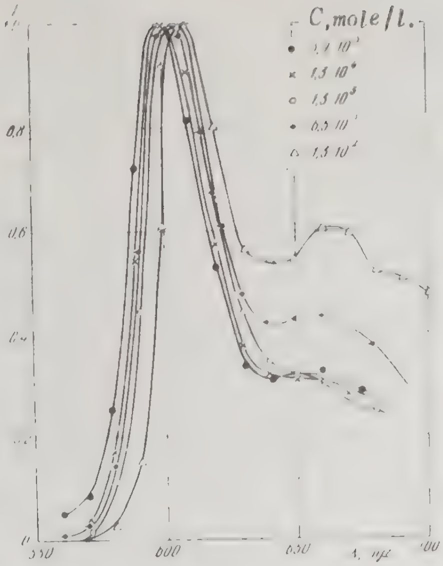

Fig. 3. Phosphorescence spectra of alcohol solutions of acridine orange at T = -183°.

As may be seen from Fig. 2, the total emission spectrum changes very little with concentration at concentrations under $6.5 \cdot 10^{-6}$ mole/liter. From this we conclude that this spectrum belongs to the monomers.* Let us compare the monomer luminescence spectrum with the absorption spectrum obtained by Zanker for a frozen solution with an acridine orange concentration equal to $1 \cdot 10^{-5}$ mole/liter**: according to Zanker's data not less than 97% of the dye molecules are in the form of monomers at this concentration.

As may be seen in Fig. 4, the absorption spectrum 1 and the total emission spectrum 2 approximately satisfy Levshin's[6] mirror symmetry law. The separation of the peaks in the absorption spectrum is 1300 cm^{-1}; the separation in the total emission spectrum*** is 1250-1300 cm^{-1}. Apparently the absorption and emission are associated with the same vibrations**** of the dye molecules and the frequency of this vibration changes little with excitation of the molecules.

It will also be seen in Fig. 4 that approximately the same frequency difference (1300-1400 cm^{-1}) is observed in the phosphorescence spectrum. We consider this re-

---

*Zanker is of the opinion that complete monomerization of the dye in frozen alcohol solutions obtains only at concentrations under $1 \cdot 10^{-7}$ mole/liter. He obtained this result by extrapolation of the curve for the variation of the coefficient of absorption at the peak of the first absorption band with the logarithm of the dye concentration.

**This is the lowest dye concentration for which Zanker investigated the absorption spectrum.

***In Fig. 4 the total emission spectrum is plotted in terms of quanta vs frequencies. Hence in going from Figs. 2 and 3 to Fig. 4 all the ordinates were multiplied by ν^{-3}.

****Zanker, referring to the data of Thompson[11] assumes that these are vibrations of the CN group.

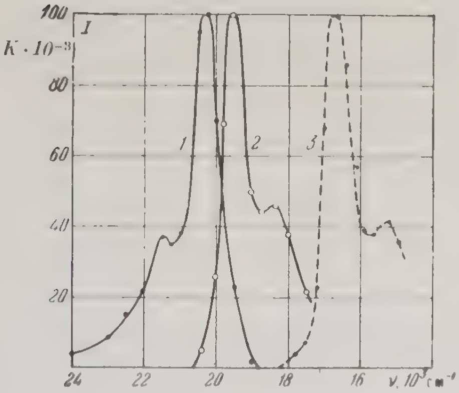

Fig. 4. Spectra of alcohol solutions of acridine orange at T = -183°: 1) absorption, 2) total emission and 3) phosphorescence of the monomer modification.

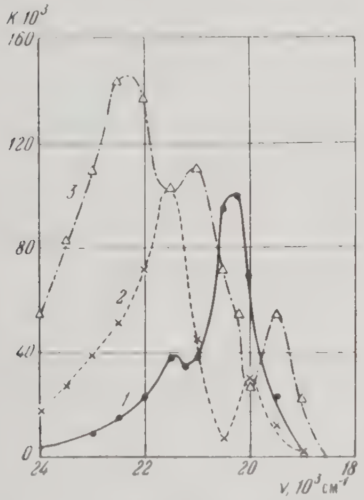

Fig. 5. Absorption spectra of 1) monomers, 2) dimers and 3) tetramers of acridine orange in alcohol solutions at -183°.

sult to be highly significant. According to Zanker's data* the vibrational structure of the phosphorescence spectrum differs markedly from the vibrational structure of the emission and absorption spectra. In the first case, according to Zanker, we have a manifestation of vibrations having a frequency of 450-550 cm^{-1}, in the second case of vibrations having a frequency of about 1300 cm^{-1}. On the basis of this Zanker advances a rather strange hypothesis to the effect that being in a metastable (triplet state) the acridine orange molecule does not return at the instant of emission directly to the normal (singlet) state, but instead first goes over into a special metastable singlet state. This hypothesis is in conflict with a number of facts: for example, the results of analyses of the spectra of benzene and its derivatives[12] and is contradicted by our experimental data. As may be seen from Fig. 4, the phosphorescence spectrm of acridine orange is very similar to the total emission spectrum at low concentrations of the dye; the former is merely shifted about 2900 cm^{-1} relative to the latter.

From the absorption spectra obtained by Zanker for different concentrations of acridine orange and from the table compiled by him giving the concentrations of monomers, dimers, and tetramers for different dye concentrations, one can readily compute the absorption spectra of the dimers and tetramers.** These spectra are given in Fig. 5 with all the spectra being reduced to the same concentrations of the absorbing particles (monomers, dimers, etc.). We computed the dimer absorption spectrum for a concentration of $1 \cdot 10^{-3}$ mole/liter where, according to Zanker, 48% of the total dissolved dye is in the form of monomers, 48% is in the form of dimers and 4% in the form of tetramers. The tetramer absorption spectrum was calculated for a concentration of $1 \cdot 10^{-2}$ mole/liter, where, according to Zanker, 14% of the dye is in the form of monomers, 50% in the form of dimers and 36% in the form of tetramers. Obviously, the accuracy in determining the tetramer spectrum is not very high.

As may be seen from Fig. 5, the absorption spectrum of the dimer has the same two bands as the absorption spectrum of the monomer but the ratio of intensities in the case of the dimer changes in favor of the short-wave band. There might be some doubt about the reality of the small long-wave peak in the dimer spectrum but the following facts speak in favor of its existence:

1) similar peaks have been observed in the dimer absorption spectra of other dyes by a number of investigators*** and

2) with very strong association of the dissolved dye there always persists an

---

*Zanker gives only one phosphorescence spectrum; that for the C = $1 \cdot 10^{-4}$ mole/liter solution.

**Zanker considers that the next stage of association of acridine orange is the tetramer form.

***For example, Kravets, Pes'kina & Zhidkova[13] who computed the absorption spectrum of the dimer of methylene blue.

appreciable absorption in the long wave part of the absorption spectrum.

As has been noted above, the data for the tetramer absorption spectrum are not distinguished by high accuracy: in particular, like Zanker, in compiling the above-mentioned table, we did not take into account the possibility of a shift of the monomer absorption spectrum at very high concentrations of the dye;* still it may be of interest to note that the absorption spectrum of the tetramer consists of three bands, the separation between the peaks in which is also of the order of 1300-1450 cm^{-1}.

The fact that the association of the molecules of acridine orange leads to a considerable weakening of the absorption in the long wave absorption band, which in the first approximation may be assumed to correspond to transitions between purely electronic levels of the molecule, and to an increase in the absorption in the short wave bands, corresponding to transitions to vibrational levels, suggest that where the associated molecules are concerned transitions to the higher electronic state are forbidden in some degree, i.e., that the associated molecules have a higher order of symmetry than the non-associated ones. This hypothesis is based on the assumption that the short wave-band appearing in the monomer absorption spectrum is associated with the same electronic transition as the long-wave band. In favor of this is the fact that an analogous structure is manifest not only in the absorption spectra but also in the fluorescence and phosphorescence spectra at low dye concentrations.

We have already noted that as the concentration is increased the phosphorescence spectrum of acridine orange undergoes far less change than the total luminescence spectrum. The appearance of the phosphorescence spectrum changes very little in the concentration range from $4 \cdot 10^{-5}$-$1 \cdot 10^{-3}$ mole/liter: there is only a small shift to the red side. Yet, according to Zanker's data, obtained on the basis of investigation of the absorption spectra in the indicated concentration interval there is strong dimerization of the dye in this interval. At a concentration of $1 \cdot 10^{-3}$ mole/liter only 48% of the entire dissolved acridine orange is in the monomer form. Whence we must conclude that either the dimers have no phosphorescence at all or, what would appear to be extremely surprising, their persistent emission spectrum is almost identical with that of monomers. In the $1 \cdot 10^{-3}$-$1.3 \cdot 10^{-2}$ mole/liter concentration interval there is a rapid increase of the long wave part of the phosphorescence spectrum. According to Zanker, this is the concentration region in which there is intense formation of tetramers, their concentration increases ten-fold and at a dye concentration of $1 \cdot 10^{-2}$ mole/liter about 40% of the dye is in a tetramer modification. This leads us to believe that the above indicated change in the phosphorescence spectrum is due to the surposition on it of the phosphorescence of the tetramers, which is appreciably displaced towards the long wave side relative to the phosphorescence of the monomers.

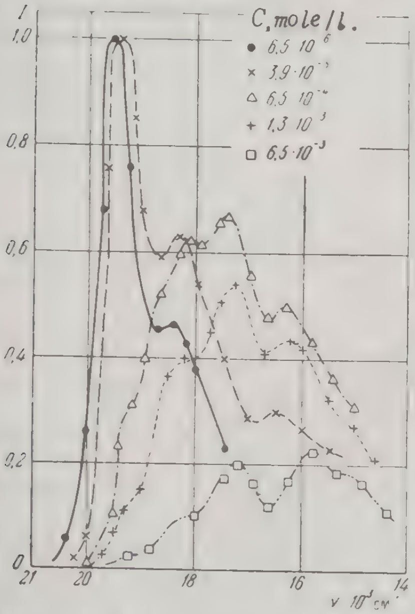

Fig. 6. Fluorescent spectra of alcohol solutions of acridine orange at -183° for different dye concentrations.

The fluorescence spectra can readily be calculated from the total emission and phosphorescence spectra given in Figs. 1 and 3, provided the relative efficiency of phosphorescence is known (see below). The fluorescence spectra computed in this

---

*At very high concentrations it is probably meaningless to speak of an isolated molecule (monomer).

manner are given in Fig. 6; all the spectra are referred to the same vertical scale.* It will be seen from Figs. 6 and 7 (the latter gives the concentration dependence of the total luminescence efficiency) that there is appreciable concentration induced quenching of luminescence. This, as will be shown below, is not connected with the reduction of the decay time of the excited state of the fluorescing molecules and hence cannot be explained from the viewpoint of the energy migration theory. If we accept the hypothesis, widely used to interpret the absorption spectra of association solutions, that an associated solution is a mechanical mixture of separate associated groups and that all the properties of the associated groups of one type are independent of the presence of groups of other types and extend this hypothesis to include fluorescence and phosphorescence, then to explain the appreciable drop in the fluorescence efficiency we must assume that the dimers have an appreciably lower fluorescence efficiency than the monomers.

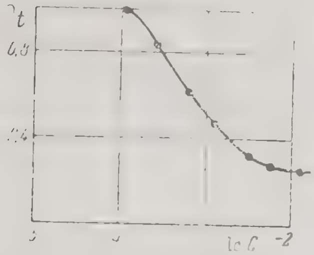

Fig. 7. Concentration dependence of the total luminescence efficiency of alcohol solutions of acridine orange.

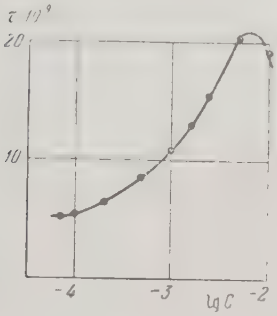

Fig. 8. Concentration dependence of the lifetime of the fluorescent state of acridine orange in alcohol solutions at T = -183°.

At the highest concentrations used in our experiments the contribution of the monomers to the total emission is small in view of their relatively low concentration, their smaller (as compared with the dimers and tetramers) absorption coefficient for the exciting light and secondary absorption of their fluorescence. Hence virtually all the fluorescence observed at the high concentrations is due to the dimers and tetramers.

Influence of the dye concentration on the time-dependent characteristics of acridine orange

As noted at the beginning of this report the purposes of our investigation included determining the time-dependent characteristics of the emission: 1) the lifetime of the excited state as indicated by the absorption at fluorescence, 2) the decay time of the phosphorescence and 3) the probability of transitions from the fluorescent to the metastable state.

The ratio of the strengths of the monomer and dimer oscillators, as determined from the curves of Fig. 5, was found to 1:1.15. From this, bearing in mind that in determining the lifetime of the excited state from the absorption one must keep in mind the ratio of the squares of the frequencies at the peaks of the absorption bands, we find that the lifetimes of the excited states of the monomers and dimers are approximately equal. There is, however, a question of whether it would not be more correct to characterize the associated and non-associated molecules not by the strength of the corresponding oscillators but by the ratio of the strengths of the oscillators to the number of π-electrons as is sometimes done for ring aromatic compounds. If we assume that in a dimer the number of π-electrons capable of participating in absorption is two times greater than in the monomer, the oscillator strength per π-electron in the dimer should be half that in a monomer.

Direct determinations of the lifetime of the excited state of alcohol solutions of acridine orange at the temperature of liquid air were made on the phase fluorometer developed by Bonch-Bruevich. The 435 mμ mercury line was selected for effecting the excitation, while for observation we employed a filter passing the

---

*All the experiments were carried out with complete absorption of the exciting light (435 mμ).

entire visible long-wave region of the spectrum beginning with 540 mμ. The results are shown in Fig. 8. It will be seen from the figure that in going from low to high concentrations the duration of fluorescence (τ_1) increases five times. It is conceivable that in the first stages secondary absorption plays some part in the variation of the fluorescence decay time; however, its contribution to the total effect is probably insignificant since in the investigated concentration interval there is appreciable concentration-induced quenching and in addition, with increasing dye concentration, the absorption coefficients for the 435 mμ mercury line used for excitation increases appreciably while the emission spectrum is shifted to the long wave side.* Thus we come to the conclusion that the associated molecules have a longer lifetime of the excited (fluorescent) state than the non-associated ones.**

While the duration of fluorescence with increasing concentration undergoes so appreciable a change, the duration of phosphorescence appears to be virtually independent of the concentration. The concentration dependence of the lifetime of the fluorescent state of acridine orange in alcohol solutions at -183° is the following:

C,mole/liter	1.3	6.5	1.3	3.2	6.5	13
τ_2, sec	1.65	1.6	1.7	2.0	1.75	1.68

The fact that the degree of association has little influence on the lifetime of the metastable state of acridine orange in frozen alcohol solutions is rather surprising although it is not inconsistent with the weaker concentration dependence of the phosphorescence as compare with the fluorescence.

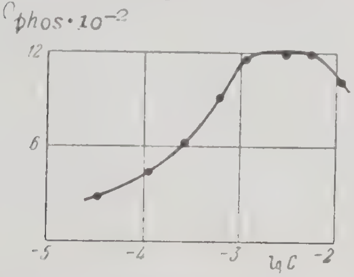

Fig. 9. Concentration dependence of the relative phosphorescence efficiency of acridine orange in alcohol solutions at -183°.

The variation of the relative phosphorescence efficiency with increasing dye concentration is shown in Fig. 9. In the $5\cdot10^{-5}$-$1\cdot10^{-3}$ mole/liter interval, the phosphorescence efficiency quickly increases from 3 to 12%; in the $1\cdot10^{-3}$-$6.5\cdot10^{-3}$ mole/liter interval it remains constant and with further increase in concentration falls off somewhat. In view of the considerations as set forth above in examining the variation of the fluorescence decay time with dye concentration, we believe that only a relatively small portion of the observed variation can be attributed to secondary absorption.

The relative phosphorescence output, as has been shown by one of the present writers (Refs. 8, 15), can be related to the molecular constants by the following expression:***

$$O_{phos} = \frac{r}{p}\pi\tau_2$$

---

*This shift, as we have indicated above, is not due to secondary absorption.

**After completion of the present investigation our attention was called to the data of Schmillen[14] who discovered an increase in the fluorescence decay time with increasing dye concentration in aqueous solutions of acridine orange at room temperature and showed that it is connected with association processes. The decisive argument in favor of our hypothesis was the absence of an increase in the decay time with increasing dye concentration in benzene solutions wherein there is no association. To explain his results Schmillen advances the hypothesis that only the monomers and tetramers fluoresce and that the dimers do not. We cannot agree with this hypothesis since in the concentration interval where there is the greatest change in the decay time tetramers are virtually absent.

***It is assumed that there is no time-independent quenching on the metastable level.

where O_{phos} is the relative phosphorescence output, p and π are the probabilities of transitions with radiation to the ground state from the fluorescent and phosphorescent levels respectively, τ_2 is the decay time of phosphorescence and r is the probability of transition from the fluorescent to the metastable level.

As has been indicated above τ_2 does not change with increasing dye concentration, hence we have no reason to assume that association produces any time-dependent quenching of the metastable molecules, and we can assume, as is usually done ininvestigations of phosphorescence at the temperature of liquid air, that

$$\pi\tau_2 = 1.$$

Then

$$O_{phos} = \frac{r}{p}.$$

Obviously the ratio r/p can increase due either to an increase in r or to a decrease in p. The latter in the first approximation can be assumed to be equal to $1/\tau_1$. In our case, in the concentration interval from $5 \cdot 10^{-5}$-$1 \cdot 10^{-3}$ mole/liter, τ_1 increases by a factor of not more than 2.5, thus it must be assumed that association also leads to an increase in the value of r.

In conclusion we want to emphasize that in this report we have attempted to explain all our results from a unified viewpoint, i.e., from the viewpoint of the hypothesis of the mechanical mixture of different associated groups. This hypothesis is frequently employed in interpreting the absorption spectra of associating dyes. The principal argument in favor of the hypothesis is the intersection at one and the same point of all the absorption curves for different concentrations. In actual fact this is not always the case and the given hypothesis in all probability is only a rough approximation. Nevertheless it is the most suitable hypothesis for attempting the first unified examination and interpretation of the absorption, fluorescence and phosphorescence characteristics of associated solutions.

References

1. S.I.Vavilov, Zhur. eksp. i teor. fiz., 13, 13, (1943).
2. S.I.Vavilov, Sobr. soch, (Collected works) Vol. II, M. -1952; P.P.Feofilov & B.Ia.Sveshnikov, Zhur. eksp. i teor. fiz., 10, 1372 (1940); F.M.Pekerman, Dissertation, 1948; M.D.Galanin, Dissertation,(Transactions of the Physics Ins. of the Ac. of Sc.), 5, 382 (1950).
3. S.I.Vavilov & M.D.Galanin, Doklady AN SSSR, 67, 811 (1949).
4. T.Förster, ZS. Elektrochem., 53, 93 (1949).
5. A.N.Terenin & V.L.Ermolaev, Doklady AN SSSR, 85, 547 (1952).
6. V.L.Levshin, Fotoliuminestsentsiia zhidkikh i tverdykh veshchestv. (Photoluminescence of liquids and solids), M.-L., 1951.
7. V.L.Levshin, Zhur. eksp. i teor. fiz., 28, 201 (1955).
8. B.Ia.Sveshnikov, Doklady AN SSSR, 105, 1208 (1955).
9. V.L.Levshin, ZS f. Phys. 43, 230 (1927).
10. W.Zanker, ZS. f. phys. Chem., 200, 250 (1952).
11. H.Thompson, J. Chem. Soc. (London), 328 (1948).
12. B.Ia.Sveshnikov & P.P.Dikun, Doklady AN SSSR, 65, 637 (1949); Zhur. eksp. i teor. fiz., 19, 1000 (1949); H.Schull, J. Chem. Phys. 17, 295 (1949).
13. T.P.Kravets, A.L.Pes'kina & Z.V.Zhidkova, Izv. AN SSSR, Ser. fiz., 14, 493 (1950).
14. A.Schmillen, ZS. f. Natur., 9a, 1036 (1954).
15. B.Ia.Sveshnikov, Zhur. eksp. i toer. fiz., 18, 878 (1948).

DISCUSSION

M.D.Galanin: Did you exclude reabsorption in measuring the decay times?

B.Ia.Sveshnikov: No. However, it follows from the investigations of Schmillen and Bonch-Bruevich that it is impossible to explain the five-fold increase in duration by reabsorption alone.

M.V.Savost'ianova: Have you any alternatives to offer to the idea of a mechanical mixture of monomers and dimers?

B.Ia.Sveshnikov: If I had anything definite to offer I would have done so. Personally I do not fully approve of the hypothesis that a solution consists of a mechanical mixture of monomers, dimers and tetramers with invariable properties at all concentrations. I think that the monomers cannot remain unchanged when association occurs and that their properties must be altered. In addition to short range action there must also be some long range effects.

V.L.Levshin: It would be desirable to investigate the influence of associated groups on each other and on the monomers. Undoubtedly, the molecular field changes, but these would probably amount to second order changes. First, one must clarify the kinetics of formation of dimers, investigate the stable equilibrium positions and then examine how these more or less permanent formations effect the molecular field.

A.N.Terenin: The speaker has aptly noted that the simple concepts regarding the equilibrium of monomers, dimers and tetramers in concentrated solutions of electrolight are applicable only with certain limitations. Here it might be better to turn to colloidal electrochemistry, the concepts of which investigators working in the field of luminescence have as yet failed to utilize.

INFLUENCE OF ORGANIC IMPURITIES ON THE AGGREGATION OF DYES IN WATER SOLUTIONS

- Kh.L.Arvan

Both the character of the dye itself and the nature of the solvent are important factors in the aggregation of dyes in solution. The influence of the solvent is apparently determined through the degree to which the coupling of the dye molecules is facilitated or, on the contrary, inhibited by the surrounding solvates.

To investigate the influence of the medium on the aggregation of dyes we studied the absorption spectra of solutions of dyes in mixed solvents of different composition. One of the components of the mixture was always water, which, as we know, is the most favorable medium for the association of dye molecules; the second component was an organic solvent. Throughout the variations of the solvent composition the concentration of the dye in the solution was kept constant.

In the investigation we used dyes purified in the Department of Dyestuffs of the Leningrad Textile Institute. The organic solvents were dehydrated and redistilled. The absorption spectra were measured on an SF-4 spectrophotometer.

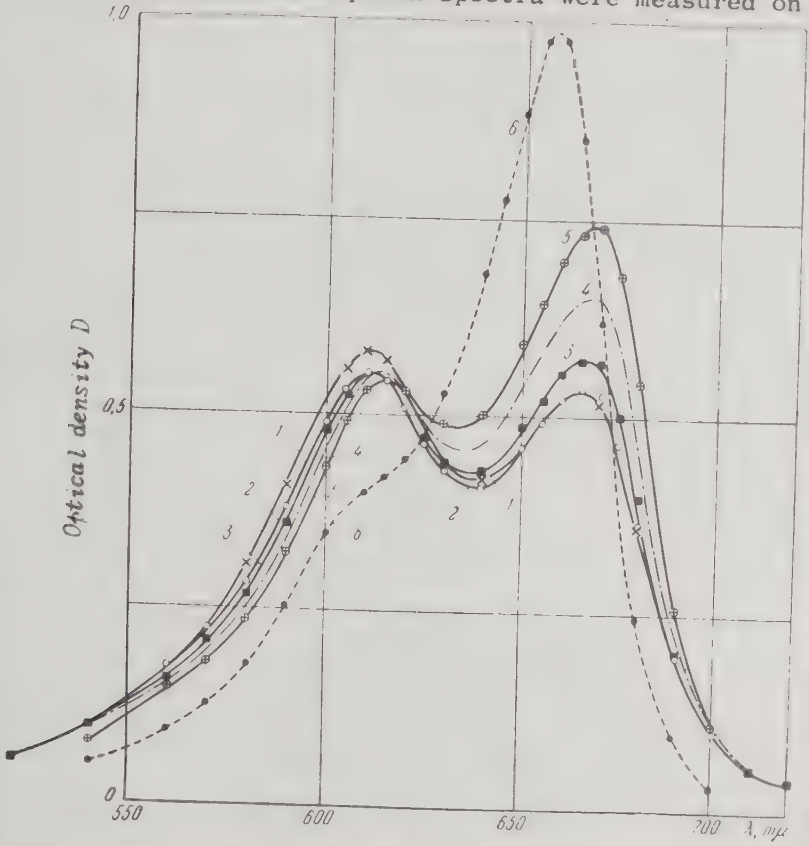

Fig. 1. Variation of the absorption spectrum of methylene blue ($C = 9.0 \cdot 10^{-5}$ g/ml) on the proportion of the components in the isobutyl alcohol - water solvent solution: 1) 0:100%, 2) 1:99%, 3) 2.5:97.5%, 4) 5:95%, 5) 10:90%, 6) 100:0%.

The results of our measurements of a number of strongly aggregating dyes (methylene blue, rhoduline orange NO, etc.) showed that when the composition of the solvent is changed the absorption spectrum of the dye is altered (Fig. 1). To compare the action of different organic solvents we studied the influence of the amount of the organic component of the solvent on the following characteristics:

a) the ratio γ of the heights of the long- and short-wave absorption band peaks, which (in the first approximation) we took as an index to the degree of association of the dye;

b) the position of the long-wave absorption band.

It will be seen from Figs. 2 and 3 which give the dependence of γ on the composition of the solvent that

a) the variation of γ changes in going from one organic component to another;

b) in most cases the variation of γ with the solvent composition is not uniform; at low contents of the organic component γ increases rapidly while at a high content of the organic component the rate of increase of γ falls off; in a number of cases γ approaches a saturation value;*

---

*It must be noted that the value of γ in weakly aggregated solutions can only be determined approximately in view of the absence of a clearcut short-wave peak.

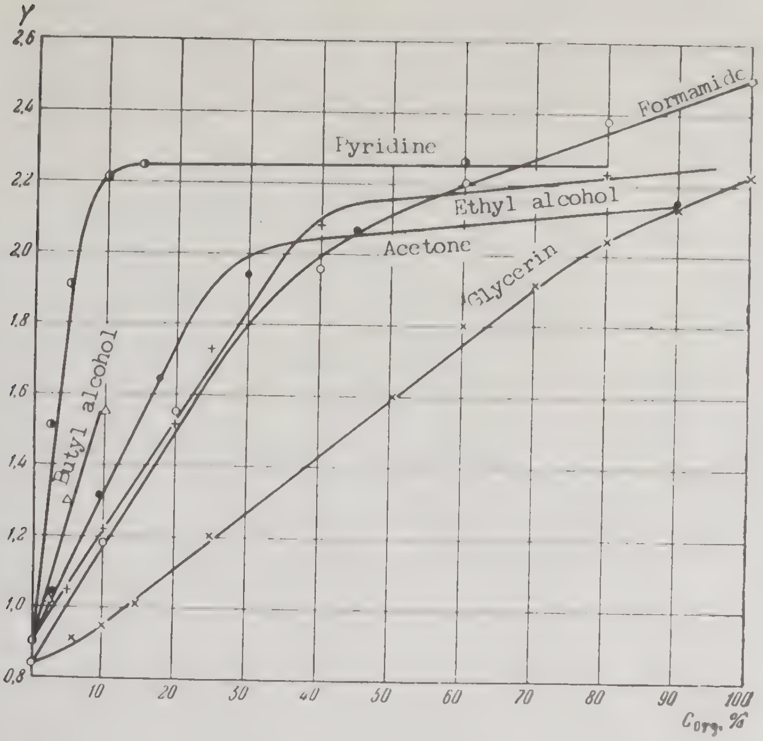

Fig. 2. Dependence of the ratio γ between the heights of the longwave and shortwave absorption peaks of methylene blue ($C = 9.0 \cdot 10^{-5}$ g/ml) on the percentage of the organic component in the water-organic solution.

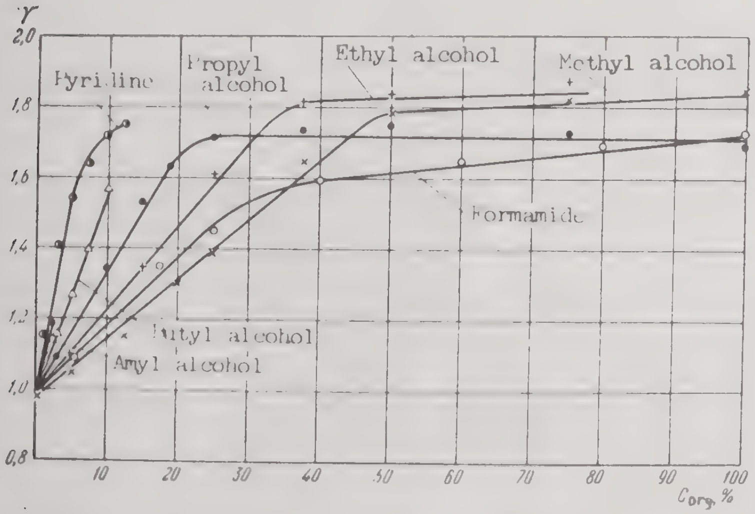

Fig. 3. Same as Fig. 2 but for rhoduline orange ($C = 2.0 \cdot 10^{-5}$ g/ml).

The ratio between the components of the solvent in the region where the slope of the γ curve changes differs for different substances. In a number of cases the absorption spectrum of the dye in complex solvents is shifted somewhat relative to the spectrum in pure solvents to the side of longer wavelengths (Figs. 4 and 5).* The maximum shift of the spectrum occurs at approximately the same composition of the complex solvent at which change in the slope of the γ curve occurs (see Figs. 2 and 4).

The nature of the variation of γ, λ_{max} and S with the concentration of the organic component speaks against the presence of an additive mixture of two types of solvates in the solution.

We assume as a working hypothesis that the formation of compound complexes having a definite composition is possible in the solution. Absorption spectra of the complexes differ from the absorption spectra of the dye in homogeneous solvents. The results of our investigation indicate that the absorption band of such a complex is shifted to the side of longer wavelengths relative to the absorption bands of the dye in pure solvents.

The variation in the slope of the γ curve indicates that complex formation inhibits, to some extent, the aggregation of the dyes in the solution. Water molecules entering into the complexes cannot contribute to the aggregation of the dye.

In the complete absence of aggregation in the mixture (saturation of γ) a convenient characteristic of the rate of formation of the complexes and, consequently, the degree of disaggregation is the slope (tangent) of the initial straightline section of the γ curve.

---

*A similar effect has been observed by Brooker and his co-workers[1] in water-pyridine solutions of different merocyanines.

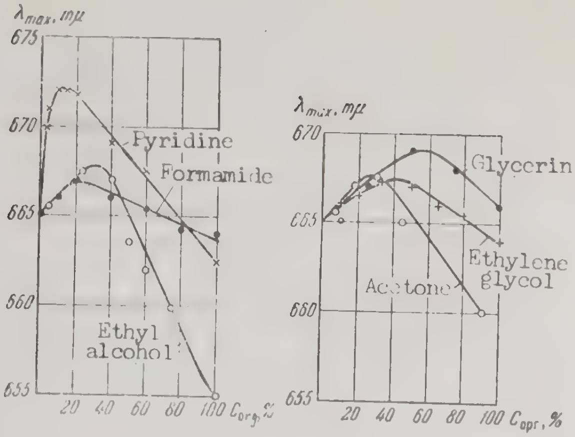

Fig. 4. Variation of the position of the absorption peaks of methylene blue with the percentage of the organic component in the water-organic solvent.

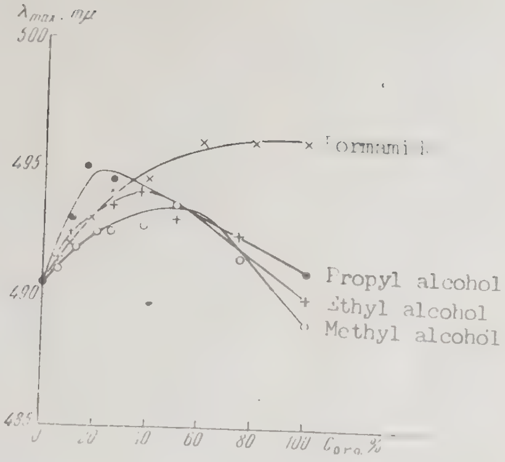

Fig.5. Same as Fig. 4, but for rhoduline orange.

Of the examined compounds the greatest activity as regards the formation of complexes is exhibited by pyridine (next is quinoline). The maximum amount of complexes is formed in a mixture containing approximately 10% pyridine (by volume), i.e., in a mixture in which there is only one molecule of pyridine per 40 molecules of water. This proves sufficient to change appreciably the properties of the solvent determining the position and character of the absorption curves and the aggregation of the dye.

In the alcohol homologous series (as well as in the ketone series) there is an increase of the slope of the γ curve with increasing series number of the alcohol. The iso-alcohols have a weaker effect than the corresponding normal alcohols (see Table): apparently the length of the molecular chain is an important factor.

As the molecular weight of the alcohol is increased the region where the γ curve bends over (and, accordingly, the region of the maximum shift of the absorption curve) is displaced to the side of lower alcohol content in the mixture. As may be seen from Figs. 2 and 3, for some compounds γ has no saturation value. In these cases one must assume either a low probability of complex formation or the absence of a disaggregating effect. Thus, for example, from a comparison of Figs. 2 and 4 it will be seen that the formation of a maximum number of water-glycerin complexes (at 60% glycerin in the mixture) does not terminate the aggregation of methylene blue. Again, there is no discernible shift of the absorption peak in the case of water-glycerin solutions of pyronine G.

Slope of initial sections of the γ curves for solutions of rhoduline orange NO in different alcohol-water mixtures

Type of alcohol	tan α
Methyl	0.80
Ethyl	1.21
Propyl	1.70
Isopropyl	1.35
Butyl	2.77
Isobutyl	1.95
Amyl	5.30
Isoamyl	3.00

Complexes containing formamide exhibit a weak activity as regards destruction of dye aggregations and displacement of the absorption peak.

The reason for the appreciable diversity in the behavior of the different complexes must apparently be sought in the structure of the molecules composing these complexes.

Enhancement of the disaggregating action is observed when the difference between the components of the complex increases (for example, when the number of carbon atoms in the homologous alsohol series increases in the case of combination of alcohol molecules with water molecules). The difference between the values of the dielectric constant of the individual components of the complex also appears to be an important factor. With a few exceptions (dioxane and cyclohexanol) the greatest optical effect is manifested by the complexes which in addition to water ($\varepsilon = 81$) contain molecules with low values of the dielectric constant (pyridine, $\varepsilon = 12.5$, and quinoline, $\varepsilon = 9.0$). The weakest optical effect is characteristic of complexes the molecules of which have a dielectric constant close to that of water (glycerin, $\varepsilon = 56.0$, and formamide, $\varepsilon = 84.0$).

Graduate student Stanevich, under the guidance of N.G.Iaroslavski, carried out a comparison of the proton acceptor properties of a number of organic substances by the method of infrared absorption. The most active in this respect proved to be pyridine and quinoline which is in agreement with their high disaggregating ability. This fact is in accord with the assumption regarding the important part played by hydrogen bonds in the formation of the complexes and if further substantiated, may prove fruitful in clarifying the nature of associations in dye solutions.

The untimely death of T.P.Kravets deprives me of the opportunity of expressing personally my profound gratitude for his great interest in this work. The work was carried out under the guidance of M.V.Savost'ianova whom I wish to thank.

Reference

1. L.G.S.Brooker, G.H.Keves & D.W.Heseltine, JACS, 73, 5350 (1951).

DISCUSSION

V.L.Levshin: Some years ago a similar investigation was carried out in our laboratory; we studied the emission of polyenes. Just as in the reported case the presence of small amounts of impurities was observed to have a marked effect. I explained this at the time by the formation about the polyenes of impurity solvate shells which greatly increased the luminescence of the material.

V.K.Matveev: It seems to me that in continuing the investigation it might be worthwhile to vary the pH of the medium. I think we have a case here where the water interacts with the pyridine. In working with alcohol there must be some change in the pH of the medium although perhaps to a lesser degree.

Kh.L.Arvan: Variation of the pH of the medium for these dyes has been investigated extensively. Deliberate changes of the pH value of dye solutions produced other changes in their spectra.

OBSCURE REACTIONS IN DYES

-A.T.Vartanian

It is commonly known that the spectral absorption curves of aqueous solutions of a number of dyes change with the dye concentration. In the case of some dyes these changes can be explained by differences in the degree of aggregation of the dye ions at different concentrations. There should be aggregates of a high order in solid layers of dyes precipitated from solutions. The absorption spectrum of such precipitated layers usually differs from the spectrum of the solutions. The transition of the dye from the dissolved state to the consolidated one may be accompanied by any of the following spectral changes: a) a shift of the absorption peak to the side of lower frequencies, b) change in the relative heights of the peaks, c) broadening of the absorption bands and d) the appearance of new bands. Furthermore, it has now been established that for solid dye layers the absorption curve may differ, depending on the conditions under which the dye was precipitated.

Water molecules are assumed to play an important part in aggregation effects. Hence we thought it would be of interest to investigate compact dye layers obtained by evaporation under vacuum inasmuch as in this case the conditions for aggregation are less favorable than in precipitation from solutions. Investigation of such layers is also important in view of the fact that vacuum sublimation is sometimes used for thorough purification of some dyes (for example, rhodamine B, phthalocyanines, etc.). Despite this the stability of molecules incident to sublimation of the dye has not so far been studied in detail. In addition to the above two problems, in the present report we shall examine the interaction of water vapor with compact dye layers at temperatures of 120-180°.

Experimental procedure

In preparing the samples a layer of the investigated dye was deposited by precipitation from an alcohol solution on the surface of a quartz "finger". The "finger" was then inserted into a glass jacket connected to a vacuum pump. The quartz plates, onto the surface of which the sublimated dye was to be deposited, were located at a distance of 10 mm from the dye layer on the "finger" inside the glass jacket. The dye deposits obtained by sublimation were fully uniform and homogeneous. They exhibited the selective reflection characteristic of the given dye.

In order to investigate the interaction between water vapor and the dye layer steam at a pressure of 20 mm Hg was injected into the jacket after which the temperature was raised to 120-180°, depending on the dye being investigated. After several hours of such heat treatment the water vapor was drawn off and the resultant product was evaporated in the usual manner. The dye deposits obtained on the quartz plates were then studied on a spectrophotometer.

The dyes investigated were methylene blue, crystal violet and rhodamines B, G and 6G.

Results

Absorption spectra of dye layers obtained by evaporation under vacuum.

1. Methylene blue. The absorption spectrum of the layer of methylene blue obtained by sublimation at 130° is shown in Fig. 1 (curve 1). The curve was recorded immediately after taking the plate from the vacuum jacket since upon prolonged exposure to air the deposit becomes violet (curve 2). The positions and relative heights of the absorption peaks in curve 1 are analogous to the positions and heights of the peaks in the absorption spectrum of an aqueous solution of methylene blue having a concentration of $2 \cdot 10^{-4}$ g/ml (curve 3). In the case of the solution the absorption in the 610 mμ region is due primarily to the dimer ions. Consequently

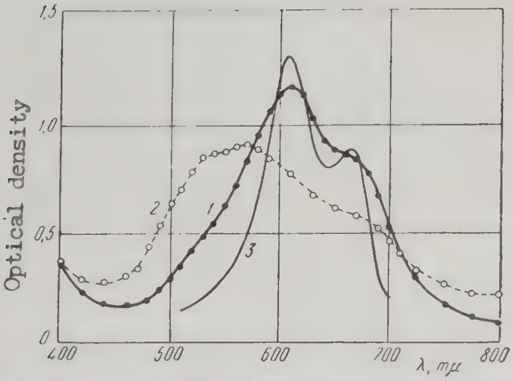

Fig. 1. Spectral absorption curves of methylene blue: 1) solid deposit, evaporated under vacuum at 130°, spectrum measured immediately after extraction of supporting plate from the vacuum jacket, 2) the same deposit after 10 hours exposure to air, 3) water solution; concentration $2 \cdot 10^{-4}$ g/ml.

the absorption of fresh layers of methylene blue obtained by vacuum evaporation is due both to monomers and dimers. Inasmuch as the unit cell of chloride of methylene blue crystals, in addition to four dye molecules, contains 16 water molecules, it may be assumed that the change from the blue coloration of the deposit to violet is connected with the formation of crystals (having a certain orientation) characterized by absorption in the 500 mμ region.

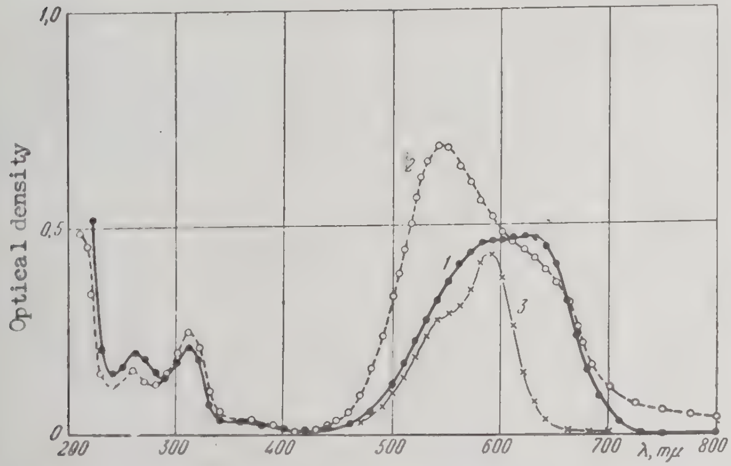

Fig. 2. Spectral absorption curves of crystal violet: 1) solid deposit, evaporated at 150°, 2) solid deposit precipitated from alcohol solution, 3) aqueous solution, concentration $2 \cdot 10^{-5}$ g/ml.

2. Crystal violet. Fig. 2 shows the absorption curves of a deposit of crystal violet obtained by vacuum evaporation (curve 1), precipitation from an alcohol solution (curve 2) and of an aqueous solution having a concentration of $2 \cdot 10^{-5}$ g/ml. It will be seen that curve 1 differs appreciably from curve 2. If we bear in mind that for an aqueous solution of crystal violet the peak at 540 mμ is higher than the peak at 588 mμ we can conclude that the absorption spectrum of the layer obtained by vacuum evaporation is close to the absorption spectrum of solutions but is displaced to the side of lower frequencies by about 1000 cm^{-1}. If this is indeed the case the high peak in the absorption curve of the layer obtained by precipitation from an alcohol solution must have an origin different from that of the peak at 540 mμ in the solution absorption curve. The assumption that the groups responsible for the short wave peak at 540 mμ in the absorption spectrum of crystal violet obtained by precipitation from an alcohol solution are associations of the dye molecules with water is doubtful since prolonged exposure of crystal violet deposits obtained by evaporation under vacuum to an atmosphere of water vapor does not lead to any appreciable alterations of the absorption curve (Figure 3). The only change resulting from exposure to an atmosphere of saturated water vapor is that the peak at 580 mμ becomes somewhat higher than the peak at 630 mμ and is displaced somewhat to the side of shorter wavelengths (to 570 mμ, curve 4). The absorption curve of the deposit precipitated from an alcohol solution and kept under vacuum is similar to the absorption curve of the layer obtained by vacuum sublimation and kept in an atmosphere of water vapor. Consequently, the appearance of the peak at 540 mμ in curve 2 (Fig. 2) can scarcely be due exclusively to the action of moisture. It is possible that the appearance of the peak is also connected with crystallization occurring during precipitation from the solution.

3. Rhodamine B. Our experiments showed that at temperatures above 85° the sub-

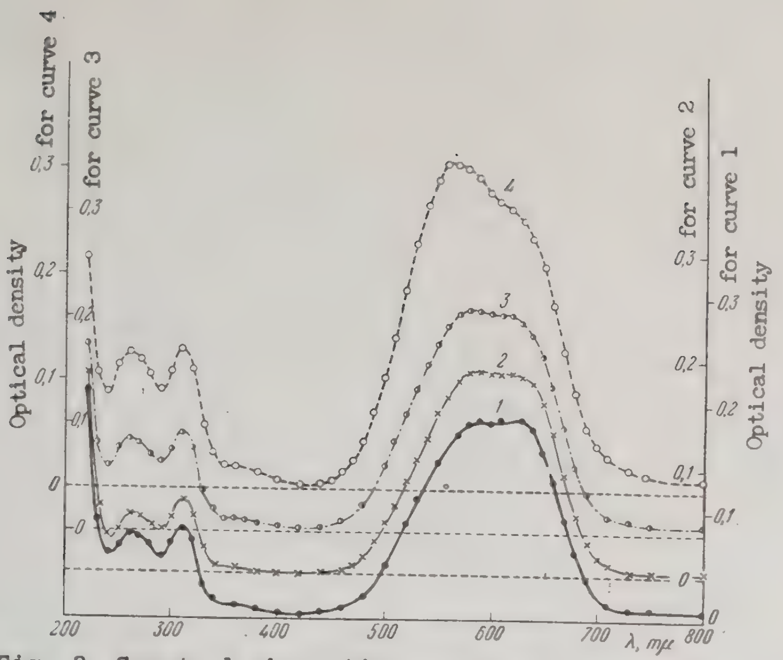

Fig. 3. Spectral absorption curves of layers of crystal violet deposited by sublimation under vacuum: 1) immediately after extraction from the vacuum jacket, 2) 5 hours after removal from the vacuum, 3) after introduction of water vapor (10 mm Hg) into the vacuum chamber, 4) after introduction of water vapor (20 mm Hg) into the vacuum chamber.

limation of rhodamine B, in contrast to the other investigated dyes, is accompanied by the formation of a colorless substance. The absorption curves of the deposits obtained by evaporation under vacuum at 160° (curve 1) and precipitation from an alcohol solution (curve 2) are shown in Fig. 4. The layer obtained by sublimation contains an appreciable amount of some new substance formed as a result of heating the dye.

This new colorless compound has a number of interesting properties. In a water solution this colorless substance transforms back into rhodamine B as may be seen from Fig. 5, since curve 2 here is similar to the absorption curve of aqueous solutions of rhodamine B. It is probably due to this reconstitution of the dye that

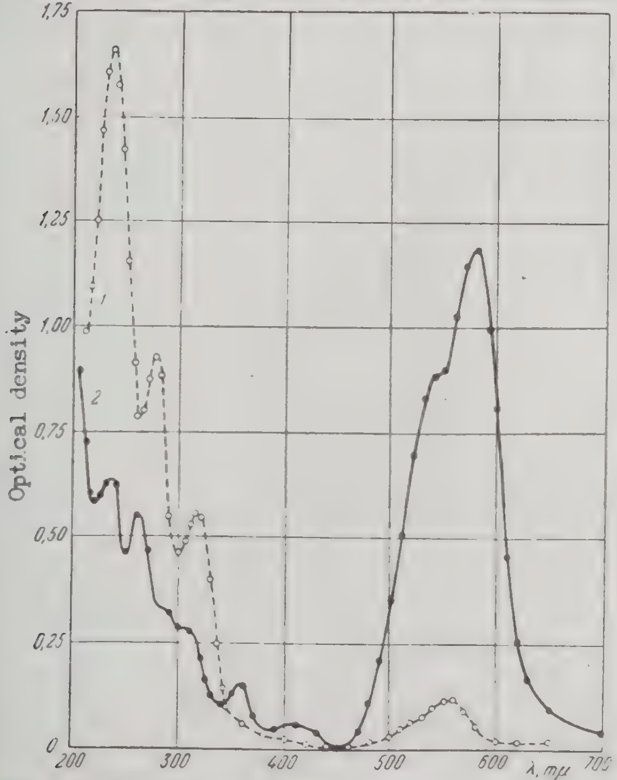

Fig. 4. Spectral absorption curve of rhodamine B: 1) deposit obtained by evaporation at 160°, 2) deposit obtained by precipitation from alcohol solution.

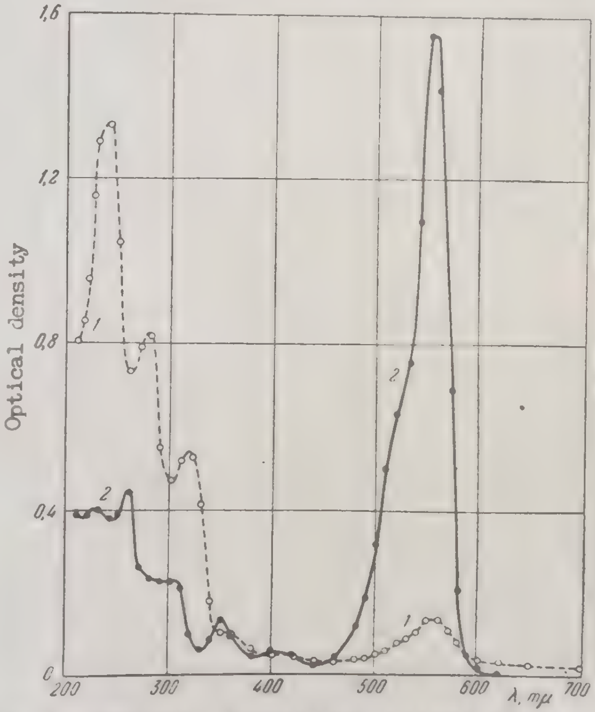

Fig. 5. Spectral absorption curves of rhodamine B: 1) layer obtained by evaporation at 145°, 2) water solution of the same deposit.

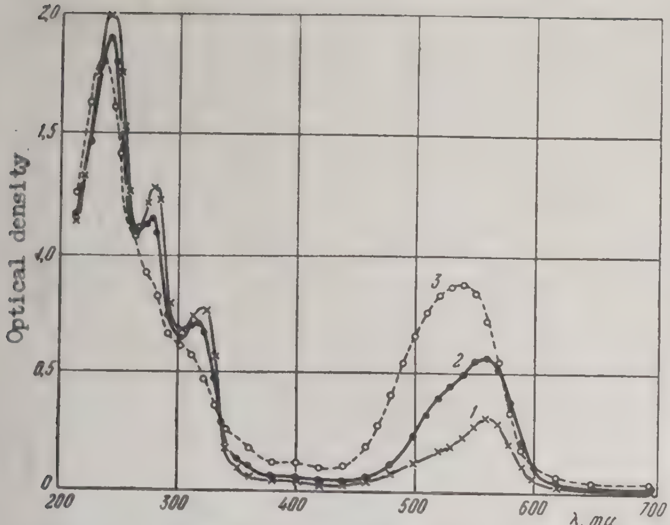

Fig. 6. Influence of illumination on the spectral absorption curves of a deposit obtained by sublimation of rhodamine B at 180° under vacuum: 1) immediately after extraction from the vacuum chamber, 2) after 50 hours exposure to daylight, 3) after 125 hours exposure to light.

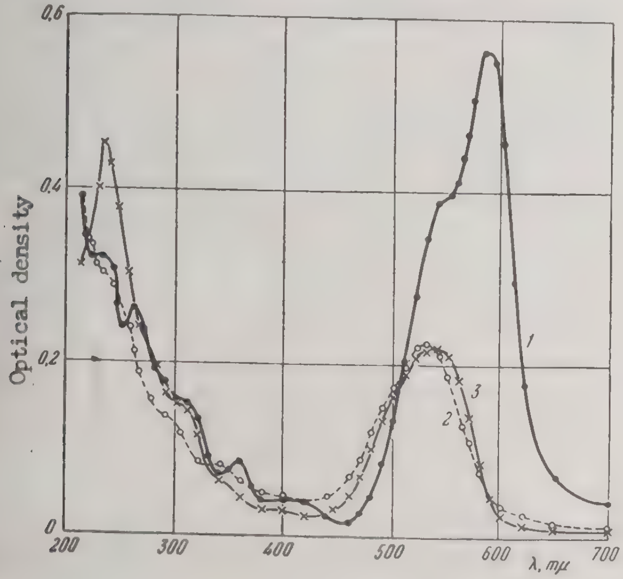

Fig. 7. Spectral absorption curves of deposits of rhodamine B: 1) deposit obtained by precipitation from an alcohol solution, 2) the same deposit after 50 hours exposure to daylight, 3) layer obtained by evaporation after 125 hours exposure to light.

the changes of rhodamine B incident to sublimation have not been noted hitherto. Another important property of the colorless compound is its sensitivity to light. When the colorless substance is exposed to light the dye is regenerated, i.e., the amount of the colorless compound is reduced as is evidenced by the decrease in absorption in the ultraviolet region (Fig. 6), in which the colorless substance is characterized by clearly defined bands with peaks at 318, 277 and 235 mμ.

Concurrently with regeneration on exposure to light the dye also undergoes photo-bleaching as a result of which the absorption curve of rhodamine B is distorted (Fig. 7).

The results obtained for rhodamine B hold in general for rhodamine G. The absorption curves obtained for deposits of rhodamine 6G prepared by evaporation virtually coincide with the absorption curves for layers prepared by precipitation from solution. The difference between the curves obtained for rhodamine G and 6G is probably due to the fact that the molecules of the former contain the replacement group COOH, while in the latter the group is $COOC_2H_5$. It is known that in carboxyl the acid properties of the hydroxyl hydrogen are greatly intensified and that the COOH group imparts distinctly acid properties to any molecule to which it is attached. In this case the appearance of the colorless compound may be explained either by a disproportioning reaction or by a regrouping reaction within the molecule.

Interaction of dye layers with water vapor

4. Methylene blue. When a layer of methylene blue is kept in an atmosphere of water vapor at 135° for several hours bleaching of the dye is observed. The colorless compound formed is readily evaporated and hence can be deposited on a quartz plate in the form of a uniform transparent coating. The absorption spectrum of this colorless substance, shown in Fig. 8 (curve 1), consists of two bands whose peaks at 334 and 265 mμ coincide with the peaks of the leuco base in the solid state that we obtained by reducing methylene blue with gaseous hydrogen sulfide. The other attributes of the

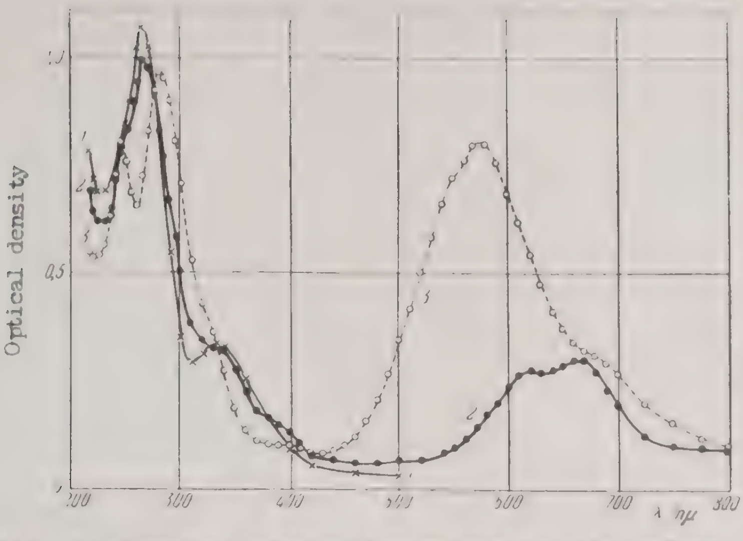

Fig. 8. Spectral absorption curves of the colorless compound formed as the result of the interaction of methylene blue over a period of hours with water vapor (15 mm Hg) at 135° and after subsequent evaporation: 1) immediately after formation, 2) 2 hours after extraction of the deposit from the vacuum chamber, 3) same, after 200 hours.

colorless substance also indicate that it is a compound having the properties of a leuco base. Thus, for example, if a deposit of the colorless compound is kept for a long time in an atmosphere of moist air, at first it acquires a blue coloration (curve 2) and then a violet color (curve 3). As the dye is regenerated the spectrum of the leuco base gradually transforms into the spectrum characteristic of methylene blue. In the visible region of the spectrum the peaks at 665 and 610 mμ (curve 2) coincide with the peaks in the spectrum of the solution. The three peaks in the visible region in curve 3 (colorless substance after 200 hours exposure to air) occupy the same positions as the peaks in curve 2 of Fig. 1.

A water solution of the colorless substance formed as the result of the interaction of methylene blue in the solid state with water vapor is indistinguishable from a solution of the dye, i.e., the absorption spectrum of this solution is identical with the absorption spectrum of an aqueous solution of methylene blue.

When exposed to air the layer of colorless substance formed by the interaction of methylene blue with water vapor gradually colors. The absorption spectrum of an aqueous solution of such a colored layer is also identical with the absorption spectrum of methylene blue solutions.

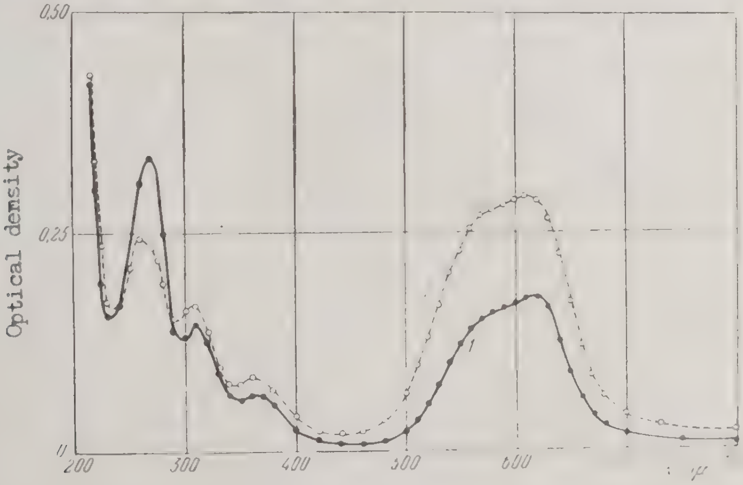

Fig. 9. Spectral absorption of layers of crystal violet deposited on a quartz plate by evaporation in an atmosphere of water vapor: 1) fresh deposit, 2) after 100 hours of illumination by daylight.

To summarize, as a result of the interaction of methylene blue in the solid state with water vapor there is formed at 100° or higher a colorless substance having the properties of a leuco base.

5. Crystal violet. If the crystal violet precipitate is evaporated in an atmosphere of water vapor (20 mm Hg) the deposit formed on the quartz plate contains not only crystal violet but also a colorless compound. The absorption spectrum of the deposit obtained under these conditions is shown in Fig. 9 (curve 1). Whereas in the visible region the absorption spectrum of this layer and that of a layer of crystal violet formed by evaporation under vacuum are identical, the ab-

sorption in the ultraviolet region for the two layers is entirely different (Fig. 2, curve 1). Curve 1 of Fig. 9 shows a strong band with a peak at 270 mμ, characteristic of leuco bases. The band with a peak at 310 mμ may pertain to either the crystal violet or its leuco base, however, it is more characteristic of the dye. As for the band with the peak at 362 mμ it can belong only to the dye.

Under the influence of light the colorless compound in air is gradually transformed to the dye (Fig. 9, curve 2). An increase in the absorption in the visible region is accompanied by a shift of the peak at 270 to 260 mμ, which is characteristic of crystal violet. Hence as a result of interaction of crystal violet with water vapor at temperatures above 100° there is formed a colorless compound having the properties of a leuco base.

It might also be assumed that as a result of the interaction described above, instead of the leuco base, there is formed a carbinol base of the dye inasmuch as it is known that the principal triphenyl methane dyes in aqueous solutions are subject to hydrolysis, in consequence of which there is established a chemical equilibrium, which for crystal violet can be characterized by the following equation:

$$\{[(CH_3)_2N - C_6H_4]_3C\}^+ + H_2O \rightleftarrows \{[(CH_3)_2N - C_6H_4]_3C - OH\} + H^+.$$

The similarity of the leuco base and the carbinol base absorption spectra makes positive identification of the colorless substance difficult; however, since the colorless substance as regards its properties is identical with the compound formed by the reaction of crystal violet with hydrogen sulfide, which is an active reducing agent, we feel that it is reasonable to assume that it is a leuco base.

In the case of methylene blue it is also assumed that in a water solution OH^- groups can become attached to the central nitrogen ion and H^+ ions to the nitrogen atoms of one of the amino groups. A colorless compound must be formed as a result of such hydrolytic association. However, the absorption spectrum of this colorless compound is not known. Inasmuch as the properties of the compound formed as the result of the interaction of methylene blue with gaseous hydrogen sulfide and with water vapor are identical we are inclined to believe that the hard substance formed as the result of the interaction of methylene blue with water is also a leuco form of the dye.

* * * * * * * * * * * * * * * *

REGULARITIES IN THE FLUORESCENCE AND ABSORPTION SPECTRA AND THE ENERGY LEVELS OF COMPLEX MOLECULES

(Abstract*)

-B.S.Neporent

1. The report is concerned with the nature of the intermolecular processes underlying the formation of the different types of continuous spectra characteristic of complex aromatic hydrocarbons.

In 1951 it was established by the author[1] that the character of the spectra of complex aromatic compounds is primarily determined by intermolecular interactions and that the medium plays only a secondary role therein. It was found that in addition to fluorescence and absorption spectra exhibiting mirror symmetry, discovered by Levshin[2], there are also spectra characterized by the width relationship: $\Delta\nu = k\nu_m^2$, where $\Delta\nu$ is the band width, k is a constant coefficient and ν_m is the frequency corresponding to the peak of the absorption band.

Inasmuch as the sole factor determining the band width of a given compound is the position of the bands in the spectrum, in Refs. 1 and 2 it was concluded that the formation of these spectra must be associated with the broadening of the electronic levels due to strong intermolecular interactions. Accordingly, it was suggested that such spectra be called "attenuation spectra".

The concepts regarding the nature of spectra exhibiting mirror symmetry, developed by Levshin[2], presuppose relatively weak coupling between the electronic and vibrational energy in the corresponding molecules; the interaction between the normal vibrations leads, as was shown in Refs. 1 and 2, to a more perfect form of mirror symmetry of the spectra which by classic analogy we suggested calling "modulation spectra".

In the same references we formulated the consequences of the Franck-Condon principle for complex molecules and showed that the width of the modulation spectra as well as the distance between their peaks are determined by changes in the equilibrium configuration of the molecules incident to changes of their electronic state. We also suggested a model describing the formation of modulation spectra by means of a configuration coordinate, which in the simplest cases may be connected with a definite geometric characteristic of the molecule and in more complex cases represents a generalized parameter characterizing the entire vibrational system or that part of the normal vibrations which is associated with the electronic transition in the molecule. Subsequently Stepanov[4], on the basis of analogous concepts, made an attempt to solve the problem of the shape of modulation spectra in a more general form. All these results, naturally, are only approximations and require further elaboration; however, the nature of the physical processes determining the appearance of modulation spectra of complex molecules is now known with fair certainty.

In Refs. 1 and 3 we also made an attempt to define the intermolecular interactions leading to the appearance of the attenuation spectra on the assumption of strong coupling between the electronic and vibrational molecular states. The probability of such energy exchange must have a value on the order of the frequency of molecular vibrations, i.e., 10^{13}-10^{14} sec^{-1}. This assumption, however, encounters certain difficulties which are examined in the present report. In any case the question of the nature of the intermolecular processes leading to the broadening of the electronic levels and the formation of attenuation spectra has not until now been clarified to the same extent as in the case of modulation spectra.

In recent year there have been a number of investigations, the results of which are important in clarifying the problem of the question of complex spectra. For the case of a series of phthalimides, the writer with Klochkov and Zelinski[5,6]

---

*The full survey article will be published in Usp. fiz. nauk; the original part of this contribution was published in Zhur. fiz. khim, 30, 1048 (1956).

established that the transition from modulation spectra to attenuation spectra occurs in parallel with the displacement of the absorption spectrum of the vapor relative to the spectrum of the non-substituted phthalimine to the side of longer wavelengths. This transition is associated with enhancement of the intermolecular interactions under the influence of substituent groups, causing disturbance of the symmetry of the π-electron field relative to the symmetry of the basic molecular structure. Furthermore, it was established[7] that in the same series there is a gradual decrease in the relative phosphorescence efficiency and in going over to substances characterized by attenuation spectra the ability of the molecules to phosphoresce disappears. Investigations[8] also showed that according to the values of the coefficience of absorption, efficiency and duration of emission of the solutions there are no great differences between these two groups of molecules. On the other hand, the luminescence spectra of the vapors of the several investigated derivatives of phthalimide, belonging to different spectral classes, are radically different. In the case of substances exhibiting attenuation spectra the boundary of the anti-Stokes drop in emission is shifted far into the region of the fluorescence spectrum. The results of an investigation by Feofilov[9] indicate that molecules which belong in different spectral classes do not differ substantially as regards the form of their polarization spectra and the value of the limiting polarization, although the orientation of the molecular dipoles determining the electronic transition still remains unclear. It should also be noted that Feofilov and Faerman[10] established that in the case of sharp disturbances of the skeletal symmetry of triphenylmethane dye molecules there also occurs a transition from modulation spectra to attenuation spectra, i.e., that this effect is fairly common.

The attenuation spectra in the investigated cases have a width of the order of 80-90 mμ. Hence, for example, in the case of triphenylmethane dyes, having narrow spectra, the transition to attenuation spectra is accompanied by broadening of the bands, while in the case of phthalimides, whose spectra are very wide, the transition to attenuation spectra despite the complex structure of the molecules leads to a narrowing of the bands. In examining the factors determining the width of the modulation spectra in accordance with Ref. 1, it is shown and illustrated by a number of examples that the configurational distribution may be narrow if in the process of the electronic transition the equilibrium configuration of the molecule changes little or if the configurational changes are such that they lead to little alteration of the reserve vibrational energy of the molecule. Juxtaposition of this result with the fact that the transition to attenuation spectra is accompanied by an increase in the effect of the substituent group on the electronic shell of the molecule leads us to the conclusion that the coupling between the electronic states and the high-frequency vibrations of aromatic groups is disturbed and that strong coupling develops between these states and the deformational vibrations and the mutual vibrations of those parts of the molecule, the interaction between which leads to deformation of its π-electron cloud. These vibrations are characterized by low frequencies and thus enhancement of the intermolecular interactions may lead to narrowing of the configurational distribution which then no longer determines the width of the spectra.

At the same time the increase in the strength of the coupling of the electronic states with those molecular coordinates along which the substituent groups exert their influence on the π-electron system of the molecule (but not all coordinates as was assumed in Ref. 1) leads to broadening of the electronic levels that determine the width of the attenuation spectra. In connection with this we note that Terenin[11] points to the dependence of the position of the electronic levels on the equilibrium spacing or the relative distribution of the parts of the molecule over the examined coordinates. It is not impossible that in the process of an electronic transition in the case of attenuation spectra there occurs an appreciable displacement of the molecular electron cloud.

Further, in contradistinction to the commonly accepted viewpoint, it is assumed that in the examined case the location of the entire system of electronic

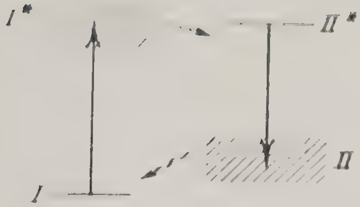

levels depends on the energy state of the whole molecule. This assumption is natural if we take into account the strong coupling of the electronic states with some configurational coordinates of the molecules, a chinge in which incident to excitation of the molecule results in its rearrangement.

Hence, for describing molecules exhibiting attenuation spectra we propose the diagram shown in the accompanying figure, consisting of four levels. After a transition I→I* with absorption of a quantum, the molecule, as a result of rearrangement of its electronic system, goes over into a stable excited state II*. The transition with emission of a quantum occurs to an unstable ground state II, from which the molecule in the process of an inverse rearrangement goes over into the stable state I. The state I* and II are unstable and have short lifetimes; the broadening of the corresponding levels thus determines the width of the attenuation spectra.

The proposed scheme is substantiated by the results of an investigation by Boisevich and the author[12] in which it was shown that in the case of attenuation spectra the absorption peak corresponds to a transition without a change in the vibrational energy reserve of the molecule (I→I* transition). Inasmuch as the fluorescence spectrum is subject to the same regularities as the absorption spectrum, it is natural to associate the maximum of this band with the II*→II electronic transition. This is consistent with the observed shift of the boundary of the anti-Stokes fluorescence output drop into the region of frequencies lower than the frequency of the fluorescence band peak.[8] It is shown that the proposed scheme is consistent with the other experimental data; a possible explanation for the absence of phosphorescence in the case of molecules having attenuation spectra is proposed. The report further examines several variants of the mechanism of shifting of the levels and rearrangement of the molecule and also the difficulties encountered in attempting to apply the proposed scheme.

In conclusion it is shown that in a classical analogy the molecules characterized by attenuation spectra must be compared with nonlinear oscillators with "soft coupling", hysteresis effects in which are analogous to the quantum scheme of four levels. It is also noted that examination of molecular spectra is not limited to relatively simple molecules of fluorescing compounds. Attenuation spectra may prove to be more common than modulation spectra.

References

1. B.S.Neporent, Zhur. eksp. i teor. fiz., 21, 172 (1951).
2. V.L.Levshin, Zhur. fiz. khim., 9, 1 (1937).
3. B.S.Neporent, Izv. AN SSSR, Ser. fiz., 15, 533 (1951).
4. B.I.Stepanov, Present issue of Bulletin.
5. B.S.Neporent, V.V.Zelinski and V.P.Klochkov, Doklady AN SSSR, 92, 927 (1953).
6. V.P.Klochkov, Zhur. fiz. khim, 29, 1432 (1955).
7. B.S.Neporent & A.I.Iniushin, Doklady AN SSSR, 98, 197 (1954).
8. B.S.Neporent & N.A.Borisevich, Doklady AN SSSR, 94, 447 (1954); present issue of the Bulletin; Optika i spektroskopiia (Optics & spectroscopy), 2, (1956).
9. P.P.Feofilov, Dissertation GOI, 1943.
10. P.P.Feofilov & I.G.Faerman, Doklady AN SSSR, 87, 931 (1952).
11. A.N.Terenin, Izv. AN SSSR, Ser. fiz., 9, 305 (1945).
12. N.A.Borisevich, Doklady AN SSSR,99, 695 (1954); N.A.Borisevich & B.S.Neporent, Present issue of Bulletin; Optika i spektroskopiia (Optics & spectroscopy) 4, (1956).

ABSORPTION AND EMISSION BAND CONTOURS OF COMPLEX MOLECULES

-B. I. Stepanov

As is known the spectra of simple systems (atoms, diatomic molecules and simple polyatomic molecules) are highly individual. The spectra of complex molecules may also show a certain degree of individuality: the position of the absorption and emission bands may be different in different spectra. However, the contours of the long-wave absorption band and the luminescence band in many molecules of the same class are identical or nearly identical. According to Vavilov[1] the shape of these bands may be described by a certain more or less universal function applicable to a large number of complex molecules.

Analogous facts are observed as well for simpler emitting and absorbing centers subjected to strong influence of the surrounding medium, for example, for activators in crystal phosphors, for uranyl ions and in a number of other cases. An attempt to deduce an analytic expression describing the band contour, applicable to a given group of substances, was made by Pekar, Krovoviaz, Davydova and Agranovicha[2,3]. These investigators assume, however, that the expressions deduced by them are applicable to complex molecules as well; this is doubtful. Comparing the spectra of solutions with the spectra of vapors Neporent[4] showed that the contours of the absorption and emission bands of complex molecules are determined primarily by the inherent properties of the molecule and are little dependent on the properties of the surrounding medium, which plays only a secondary role.

A different approach to the problem is indicated in the works of Williams and Hebb[5,6], Klick[7] and Neporent[4]. The model selected for the absorbing center is that of a one-dimensional oscillator. The investigations of the first three authors are devoted to crystalline phosphors, hence we will not examine them in detail here. Neporent makes certain very rough approximations and the expression deduced by him does not agree with experiment (gives an excessively strong temperature dependence, two peaks instead of one, etc.).

In the present investigation we also utilize the one-dimensional model of a classic harmonic oscillator. The vibrational energy levels of such a system form a continuous spectrum.[8] It is assumed that the distribution of the molecule over the vibrational energy levels and in two-dimensional phase space has the following form:

$$\rho(E_{vib})\,dE_{vib} = e^{-E_{vib}/kT}\,dE_{vib} \quad \text{and} \quad \rho(q,p)\,dq\,dp = e^{-E_{vib}/kT}\,dq\,dp, \tag{1}$$

where

$$E_{vib} = \frac{1}{2}\varkappa q^2 + \frac{1}{2\mu}p^2. \tag{2}$$

Here $\varkappa$ and μ are two parameters characterizing the system under investigation. The applicability of the one-dimensional model must be substantiated by experiment. The selection of this model is based on the analogy with "gray matter". In a previous contribution by the author[9], devoted to the spectroscopic properties of gray matter, it was shown that in this material of maximum complexity the distribution function $\rho(E_{vib})$ is described by expression (1). Since the interaction of the vibrational degrees of freedom of a complex molecule is very great[8] application of (1) is apparently allowable. This conclusion is substantiated by the experimentally observed simplification of spectra incident to an increase in the number of degrees of freedom as we go from diatomic to more complex molecules and also by the manifestation of universal regularities in all complex molecules, regardless of the number of degrees of freedom.

It is further assumed in the calculations that from a point of view of electronic energy the model fully retains quantum mechanical attributes: the changes in electron energy occur in jumps. The upper electronic state is characterized by

displacement of the equilibrium position ($q'_{equi} = q_{equi} + A$) and a constant value of the potential energy parameters. This assumption is based on experiment and is applicable to molecules exhibiting mirror symmetry of their absorption and luminescence spectra in the frequency scale.[10]

The second fundamental hypothesis assumed in our calculation is the following. According to the Franck-Condon principle the coordinates and momenta of the nuclei do not change in electronic-vibrational transitions. Application of this rule gives good agreement with experiment in the case of diatomic molecules. In the case of complex molecules, however, it is not applicable. Stepanov and Kazachenko[11] carried a special calculation with reference to the one-dimensional model. It turned out that the calculated band width is appreciably smaller than the experimental width and furthermore is strongly dependent on the temperature. In view of this we assume that with regard to electronic-vibrational transitions in the one-dimensional model of a complex molecule one should take into account the possibility of changes of the coordinates q and momenta p.

This assumption is fully justified. In complex molecules the store of vibrational energy is very great and commensurate with the energy of electronic excitation. In view of this an appreciable change in the arrangement of the nuclei may occur in the time necessary for the process of rearrangement of the electron shell during excitation. Neporent[4] also called attention to another important consideration: he notes that each point of the one-dimensional model corresponds to a multiplicity of possible configurations of the nuclei in the actual molecule. This is necessarily manifested in a change in the coordinates of the one-dimensional model incident to optical transitions.

The probability of a transition from point (q,p) of a low-lying electronic state to the phase volume dq'dp' of an upper electronic state is most readily approximated by the equation

$$db = b_0 e^{-\alpha(q'-q)^2} e^{-\xi(p'-p)^2} dq'dp', \tag{3}$$

where α and ξ are constants characterizing the given molecule.

The case when $\alpha = \infty$ and $\xi = \infty$ corresponds to no change in the coordinates and momenta.

In the present investigation we calculated the absorption (and emission) band contours on the basis of assumptions (1) and (3). We assumed at first that p' = p, i.e., that the electronic-vibrational transition is not accompanied by a change in momentum. This made it possible to shorten the calculations appreciably. In the transition from point (q,p) to q',p) there is absorption of radiation of the frequency

$$\nu = \frac{1}{h}(E_{el} + E'_{vib} - E_{vib}) = \nu_{el} + \frac{\kappa}{2h}[(q' - A)^2 - q^2]. \tag{4}$$

This same frequency is involved in transitions from different points q,p to the corresponding points q',p. Integrating (3) over the entire phase space, taking (1) and (4) into account, we obtain the following final expression for the probability of absorption at the frequency ν:

$$a(\nu)\delta\nu = a_0\int\left\{\exp\left[-\frac{\Delta\nu}{kT}y^2 - \beta\left(1 - y - \sqrt{y^2 - \frac{\nu_{el} - \nu}{\Delta\nu}}\right)^2\right] + \exp\left[-\frac{\Delta\nu}{kT}y^2 - \beta\left(1 - y + \sqrt{y^2 - \frac{\nu_{el} - \nu}{\Delta\nu}}\right)^2\right]\right\}\cdot\left(\sqrt{y^2 - \frac{\nu_{el} - \nu}{\Delta\nu} + \frac{\delta\nu}{\Delta\nu}} - \sqrt{y^2 - \frac{\nu_{el} - \nu}{\Delta\nu}}\right)dy. \tag{5}$$

Here we have introduced the following notation:

$$y = \frac{q}{A}, \quad \Delta\nu = \frac{\kappa A^2}{2h}, \quad \beta = \alpha A^2 \tag{6}$$

With $\nu > \nu_{el}$ one must integrate over y from $-\infty$ to $+\infty$, with $\nu < \nu_{el}$ over y

from $-\infty$ to $-\sqrt{\frac{\nu_{el}-\nu}{\Delta\nu}}$ and from $+\sqrt{\frac{\nu_{el}-\nu}{\Delta\nu}}$ to $+\infty$.

The band contour is determined by only two constants: β and $\Delta\nu$. The constant ν_{el} is not connected with the contour and only determines the position of the band in the frequency scale.

Investigation of expression (5) in the general form is extremely difficult hence we carried out a numerical integration. The basic data were obtained for room temperature ($kT = 200$ cm^{-1}). Preliminary calculations showed that the values of the constant $\Delta\nu$ is close to $\nu_m - \nu_{el}$, hence we selected the value $\Delta\nu = 1000$ cm^{-1}, which is frequently encountered in different molecules. The value of β was varied ($\beta = 100$, 20, 10 and 2). The results of our calculation are shown in Fig. 1. The best agreement with experiment is obtained for $\beta = 10$. The value of $\beta = 2$ has no meaning. The values of 100 and 20 do not yield the requisite asymmetry or the correct relationship between $\nu_m - \nu_{el}$ and the half-width of the curve. The value $\beta = 10$ shows that an appreciable change in the arrangement of the nuclei is possible incident to an electronic-vibrational transition. The probability of the transition decreases by a factor of e (compared to the probability of a vertical transition $q' = q$) when $q'-q = A/\sqrt{10}$. The change in the q coordinate attains one third the displacement of the equilibrium position incident to excitation of the electronic shell.

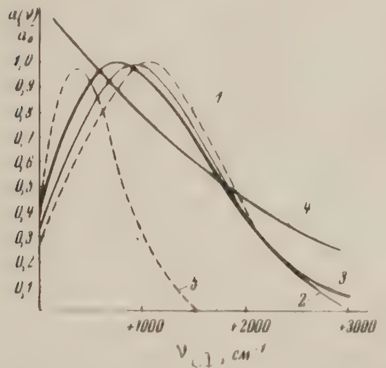

Fig. 1. Dependence of the absorption band contour on the parameter β; 1) $\beta = 100$, 2) $\beta = 20$, 3) $\beta = 10$, 4) $\beta = 2$, 5) computed according to Neporent's equation for $\beta = 10$.

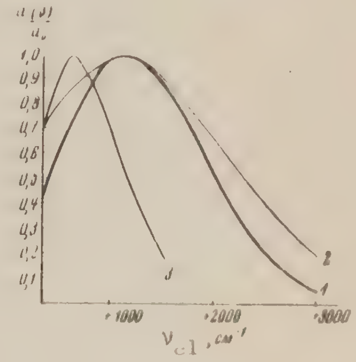

Fig. 2. Dependence of the absorption band contour on the temperature and the parameter $\Delta\nu$ with $\beta = 10$; 1) $\Delta\nu = 1000$ cm^{-1}, $kT = 200$ cm^{-1}; 2) $\Delta\nu = 1000$ cm^{-1}, $kT = 500$ cm^{-1}; 3) $\Delta\nu = 400$ cm^{-1}, $kT = 200$ cm^{-1}.

In order to elucidate the dependence of the absorption band contour on the temperature and the parameter $\Delta\nu$ we calculated $a(\nu)$ for $\Delta\nu = 1000$ cm^{-1}, $\beta = 10$, $kT = 500$ cm^{-1} ($T \sim 750^0$ K) and for $\Delta\nu = 400$ cm^{-1}, $\beta = 10$ and $kT = 200$ cm^{-1}. The shape of the contours in relative units is shown in Fig. 2. When the temperature is increased 2.5 times there is an insignificant displacement of the peak (to the side of ν_{el}) and some broadening of the bands. In the region where $\nu_{abs} < \nu_{el}$ the influence of temperature is appreciably greater. It also follows from Fig. 2 that the half-width of the curve is connected with the separation $\nu_m - \nu_{el}$: a decrease in $\nu_m - \nu_{el}$ is accompanied by some decrease of the half-width although this is slower than the reduction of the level spacing. All these results are fully in agreement with experiment.

The results of the absorption band contour calculations are applicable to the contours of fluorescence bands. If it be assumed that $\varkappa = \varkappa'$, we have full mirror symmetry of the spectra.

We also investigated the dependence of the probability of optical transitions on the transition frequency and on the store of vibrational energy of the initial state. The absorption band contour $a(\nu)$ is related to the investigated probability $a(E_{vib},\nu)$ by

$$a(\nu) = \int \rho(E_{vib})\, a(E_{vib},\nu)\, dE_{vib}. \qquad (7)$$

In order to deduce the expression for $a(E_{vib}, \nu)$, one must take into account all possible transitions with frequencies ν from all points in the phase space of the lower electronic state corresponding to the energy E_{vib}. Solution of the problem is reduced to calculating the double integral with $p' \neq p$ and the integral:

$$a(\varepsilon, \chi)\,\delta\chi = a_{0'} \int\limits_{\varphi} d\varphi \Big[\exp - \{\beta\,[\sqrt{\varepsilon}\cos\varphi - 1 + \sqrt{\varepsilon\cos^2\varphi + \chi}\,]^2\} + \exp\{-\beta\,[\sqrt{\varepsilon\cos\varphi} - 1 - \\ - \sqrt{\varepsilon\cos^2\varphi + \chi}\,]^2\}\ (\sqrt{\varepsilon\cos^2\varphi + \chi + \delta\chi} - \sqrt{\varepsilon\cos^2\varphi + \chi}\,)\Big] \tag{8}$$

with p' = p. Here we have introduced the notation

$$\varepsilon = \frac{E_{vib}}{\Delta\nu}, \quad \chi = \frac{\nu - \nu_{el}}{\Delta\nu}. \tag{9}$$

For $\nu - \nu_{el} > 0$ the integration over φ is carried out from 0 to π; for $\nu - \nu_{el} < 0$ - from $\varphi = 0$ to $\varphi_{sp} = \arccos\sqrt{-\chi/\varepsilon}$ and from $(\pi - \varphi_{sp})$ to π.

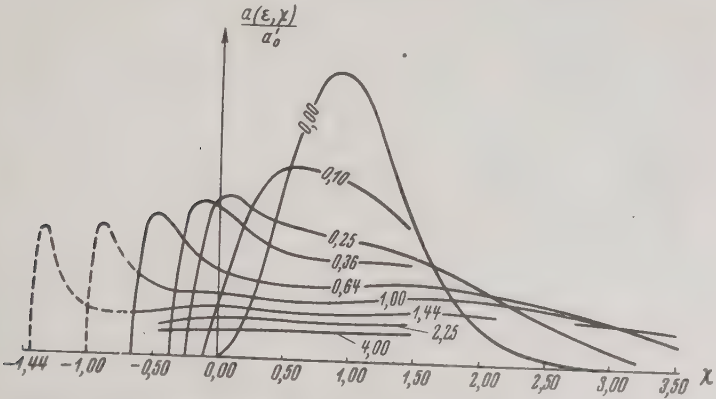

Fig. 3. Dependence of the probability of transitions on χ at the indicated values of ε.

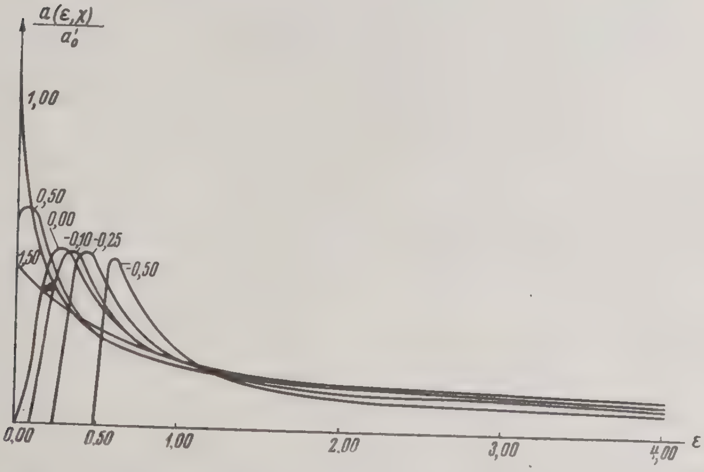

Fig. 4. Dependence of the probabilities of transitions on ε at the indicated values of χ.

Expression (8) was investigated by numerical integration for $\beta = 10$ and $\Delta\nu = 1000$ cm^{-1}. The results of the calculations are given in Figs. 3 and 4. It follows from an analysis of the curves that the probability of the $a(E_{vib}, \nu)$ transition is strongly dependent both on the energy of the initial vibrational level and on the frequency of the absorbed radiation. The dependence on the energy is weak only at large values of E_{vib} ($E_{vib} > 1.5\Delta\nu$). Actually at these high values of E_{vib} the probability of the transition is also virtually independent of ν.

Fig. 3 shows the dependences of the probability a on ν at different given values of ε (these dependences are sometimes called the configurational distribution). They characterize the contour of the absorption band which would be observed if all the molecules had one and the same initial value of the vibrational energy. The character of the configurational distribution is strongly dependent on E_{vib}. The curve for $\varepsilon = 0$ corresponds to the absorption band contour at T = 0. Increasing the temperature increases the contribution of all the other configurational distributions to the absorption band and leads to displacement of the peak and broadening of the band.

The probabilities of transitions with emission from the different vibrational levels of the excited electronic state can be found by the same method. For they are symmetrical with the curves of Fig. 3. Analysis of these curves makes it possible to explain the dependence of the shape of the emission bands of vapors

on the frequency of the exciting light and, in particular, the so-called anti-Stokes cutoff of the bands.

In the present investigation numerical calculations were carried out only for the particular case of constant momentum ($p' = p$ and $\xi = \infty$). It can readily be shown that taking into account the possible changes in momentum leads only to a certain additional broadening of the bands.

Equation (5) is an analytic expression describing the contour of the absorption band. It closely characterizes the experimental curves with the aid of two molecular constants. Unfortunately expression (5) is very cumbersone and not suitable for plotting experimental curves. Further work must be directed towards finding a convenient semi-empirical expression which would make it possible to determine β and $\Delta\nu$ for molecules of different classes.

The aforementioned calculations were carried out by graduate students L.P.Kazachenko and A.M.Samson. A detailed exposition of the computations is given in Refs. 11 and 12.

Institute of Physics and Mathematics of the
Academy of Sciences of the Byelorussian SSR

References

1. S.I.Vavilov, Works, Vol. 1, p. 108, M.L. 1954.
2. S.I.Pekar, Usp fiz. nauk, 50, 197 (1953); M.A.Krivoviaz & S.I.Pekar, Trudy In-ta fiziki (Proceedings of the Physical Inst. AN Ukrainian SSR) No. 4 (1953).
3. A.S.Davydov, Zhur. eksp. i teor. fiz., 24, 197 (1953); V.M.Arganovich & A.S.Davydov, Fizicheskii sbornik (Physics collection) No. 7, Kiev State Univ. 1955.
4. B.S.Neporent, Zhur. eksp. i toer. fiz., 21, 172 (1951); Izv. AN SSSR,Ser. fiz., 15, 533 (1951); Proceedings of the State Optical Inst. (GOI); Meeting dedicated to the memory of Academnician S.I.Vavilov. Oborongiz, 1953.
5. F.E.Williams, J. Chem. Phys. 19, 457 (1951); Phys. Rev., 82, 181 (1951); 83, 877 (1951).
6. F.E.Williams & M.H.Hebb, Phys. Rev., 84, 1181 (1951).
7. C.C.Klick, Phys. Rev., 85, 154 (1952); J. Chem. Phys. 57, 776 (1953).
8. B.S.Neporent & B.I.Stepanov, Usp. fiz. nauk, 43, 380 (1951).
9. B.I.Stepanov, Zhur. eksp. i teor. fiz., 28, 5, 599 (1955).
10. V.L.Levshin, Zhur. fiz. khim., 6, 991 (1935).
12. B.I.Stepanov & A.M.Samson, Izv. AN Byelorussian SSR, Ser. fiz., 1 (1956).

DISCUSSION

V.L.Levshin: Why did you not take into account changes in momentum?

B.I.Stepanov: Only for the sake of simplicity of calculation. Approximate calculations make taking changes of momentum into account showed that the influence of this factor is secondary.

A.T.Vartanian: Does this theory explain the appearance of weak side absorption peaks?

B.I.Stepanov: No. These side peaks are not connected with the principal band contour.

A.N.Terenin: It seems to me one should carry out a systematic analysis of the model with two degrees of freedom.

B.S.Neporent: The presented calculations are undoubtedly a step forward: they generalized the scheme we proposed earlier for all values of the coordinates

and energies of the molecules. I have certain reservations, however, regarding the assumed change in the coordinates of the nuclei in the process of an electronic transition. This assumption is superfluous since in our investigation we showed that invariability of the real coordinates in the assumed scheme requires an alteration of the generalized coordinate. With respect to actual molecules both our results and those examined by the speaker are apparently still very rough approximations.

B. I. Stepanov: Our contribution is a development and generalization of a whole series of investigations by different authors. In his study Neporent correctly formulated the basic method of solving the problem, however, the scheme suggested by him is far too rough and leads to results which are not in agreement with experiment. Obviously our scheme is also imperfect and is at best only a certain approximation. At present we are trying to develop the theory further. The reservation expressed by Neporent is not well founded inasmuch as the possibility of changes of the coordinates of the nuclei in the process of an electronic transition follows from the general premises of quantum theory.

LUMINESCENCE OF URANYL SALT SOLUTIONS

-A.N.Sevchenko & L.V.Volod'ko

It has been known since the time of Stokes[1] and Becquerel[2] that all uranyl compounds in which the uranium is hexavalent emit a highly characteristic and intense yellow-green photoluminescence. Despite the fact that the emission of uranyl compounds has been studied for over 100 years many important problems still remain unsolved today. Judging from the extensive literature[3-9] published in the last decades there is an increased interest in spectroscopic investigation of the properties of uranyl compounds; there are a number of reasons for this.

First, investigation of the emission of uranyl compounds is important from the point of view of developing an accurate and sensitive method of luminescence analysis of an important group of chemical compounds. The electronic spectra of uranyl compounds differ advantageously from the spectra of orgainc dyes in that they are discernibly altered even by minor changes in the chemical composition of the crystals or solutions.

Second, investigation of the electronic-vibrational spectra of uranyl compounds helps understand the properties of electronic energy levels in solutions and amorphous solids. In contrast to the spectra of most other materials in the condensed phase, the spectra of uranyl compounds have an unmistakably discrete structure.

Third, uranyl compounds in crystals, solutions, minerals and glasses have a long lifetime of the excited state and a very high quantum efficiency as compared with complex organic dyes.[10]

Fourth, the photoluminescence of uranyl compounds is anisotropic. Investigation of the luminescence anisotropy of uranyl compounds helps understand the nature of the elementary processes of absorption and emission of radiant energy.[11]

When the temperature is reduced from room temperature to that of liquid air, hydrogen or helium, a large number of additional narrow lines, similar to the lines of atomic spectra, appeared in all the luminescence and absorption bands of uranyl compounds. For example, the luminescence spectra of uranyl crystals at the temperature of liquid air consists of a series of the type $v' = 0, v'' = 0,1,2,3,\ldots$, where v'' are quantum numbers characterizing the change in the vibrational energy in the ground state with a fundamental symmetric vibrational frequency equal to approximately 860 cm^{-1}. The luminescence bands begin in the blue part of the spectrum and extend to the red region.

Immediately next to the short-wave part of the luminescence spectrum there begins the absorption spectrum series $v'' = 0$, $v' = 0,1,2,\ldots$ with the separation between the corresponding lines in the absorption bands being equal to approximately 720 cm^{-1}.

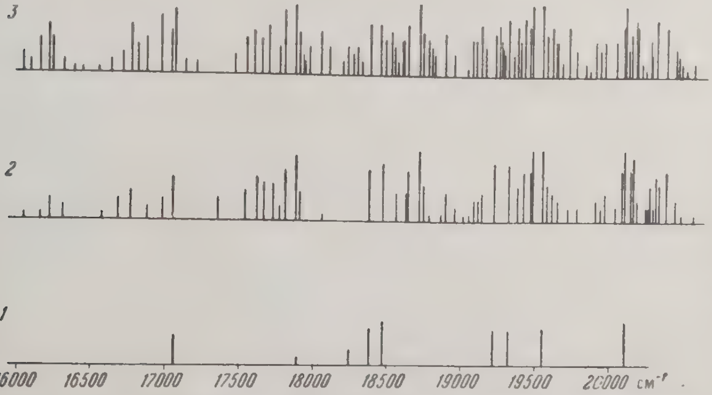

Fig. 1. Distribution of lines in the luminescence spectra of uranyl sulfate crystals with different amounts of water of crystallization: 1) UO_2SO_4, 2) $UO_2SO_4 \cdot 3H_2O$, 3) $K_2UO_2(SO_4)_2 \cdot 2H_2O$.

In spite of the fact that the luminescence spectra of different uranyl crystals lie in the same spectral region, they differ appreciably particularly at the temperature of liquid air. The difference between luminescence spectra is also fairly great for crystals of uranium salts of the same chemical composition but containing different amounts of water of crystallization.[12] For example, if three molecules of water or a second metal anion are added to anhydrous uranyl sulfate the discrete structure of the luminescence spectrum is radi-

cally altered (Fig. 1). Many foreign authors have attempted to explain the diversity of the lines in the absorption and emission spectra of uranyl compounds on the basis of the hypothesis that the fine structure of the spectra is due only to electronic-vibrational levels of the UO_2^{++} ion.[4,13,14] The erroneousness of this hypothesis has been proved by Sevchenko and Stepanov[9,15]: the fine structure of the electronic spectra of crystals of uranyl salts observed at low temperatures is associated primarily with transitions between levels of the crystal lattice and only a small fraction of the lines can be due to transitions between electronic-vibrational levels of the uranyl ion.

One can obtain important information on the interaction of uranyl ions with the surrounding medium in the process of emission and absorption by studying the dependence of the photoluminescence of uranyl solutions on the chemical nature of the solvent and the temperature. It is known that the character of the luminescence spectra of uranyl salt solutions differs radically from the character of the spectra of uranyl salt crystals. The absorption and luminescence spectra of aqueous and acid solutions of uranyl compounds have a diffused character not only at room temperature but at the temperature of liquid air as well.

Pringsheim[16] and Levshin[17] assert that solutions of uranyl sulfates and nitrates are extremely sensitive to the quenching influence of halogen ions and organic compounds, for example, ethyl alcohol and glycerin. Attempts were made to explain the "absence" of luminescence in organic solvents by recourse to different chemical and chemical-physical hypotheses. In particular, Pringsheim suggested that the hexavalent uranyl ion in an organic medium is transformed into a tetravalent uranyl ion that cannot luminesce; Levshin in his monograph[17] wrote that glycerin molecules in solutions act as a quenching impurity and that consequently uranyl salts in glycerin solutions yield no luminescence even at low temperatures. These views are erroneous; we have succeeded in showing that all uranyl salts in organic solvents as well as complex organic salts exhibit photoluminescence but only at very low temperatures.

The various forms of photoluminescence quenching in uranyl compounds are well known. The probability of the quenching process is determined by the duration of emission and depends on the temperature and the chemical-physical properties of the solvent: viscosity, chemical composition and concentration of the quenching molecules. The luminescence of uranyl ions as compared with the photoluminescence of organic dyes has a long duration (of the order of 10^{-4}-10^{-5} sec), consequently the probability of quenching, in general, must be rather high. Hence it is desirable to select conditions under which quenching would be eliminated or at least minimized. A favorable factor in this respect is reducing the temperature. When the solution is cooled to the temperature of liquid air its viscosity is greatly increased. Consequently the thermal motion of the ions virtually stops and transformation of the absorbed excitation energy into heat is almost wholly precluded. Our experiments show that all organic solutions of uranyl compounds emit light at sufficiently low temperatures. All solutions of uranyl nitrate, chloride, sulfate and acetate in alcohols, glycerin, formalin, acetone, butyl acetate, ethyl acetate and other solvents luminesce in the frozen state. The quantum efficiency of luminescence of the solutions is lower than the luminescence efficiency of the corresponding salts in the crystal state. A small increase in temperature above -185° produces a sharp decrease in the quantum efficiency and the lifetime of the excited state. It might be assumed that if the temperature is reduced to -185° microcrystals separate out from the solution and that these crystals are the luminescence carriers in the frozen solutions. In this case the discrete structure or at least some residue of it must persist in each band of the luminescence spectra. To this end we recorded the luminescence spectra of uranyl nitrate dissolved in acetone, glycerin, isobutyl alcohol and formalin. The luminescence spectrum of the alcohol solution of uranyl nitrate (Fig. 2, curve 2) is displaced to the side of shorter wavelengths relative to the spectrum of uranyl nitrate in formalin (curve 1). The photoluminescence spectrum of uranyl nitrate in glycerin exhibits

an anomaly: each emission band shows two peaks; however, we did not detect the discrete structure peculiar to the luminescence of uranyl salts in the crystal state at -185°. The luminescence bands of uranyl nitrate in acetone solutions are less diffused than in solutions in other solvents.

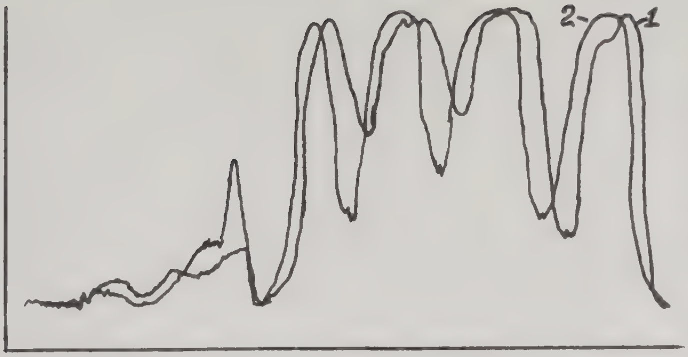

Fig. 2. Microphotograms of luminescence spectra of solutions of uranyl nitrate: 1) in formalin and 2) in isobutyl alcohol.

Fig. 2 shows the microphotograms of the luminescence spectra of solutions of uranyl nitrate in formalin and isobutyl alcohol. Comparison of these microphotograms shows an appreciable redistribution in energy over the spectrum for the different solvents: the spectrum of the solution in formalin has 7 luminescence bands, having peaks at 483, 504, 527, 581, 614 and 646 mμ, while the peaks of the luminescence bands in the isobutyl alcohol solution are located at 480, 508, 533, 559, 585, 605 and 650 mμ.

Nichols and Howes[18] showed that the luminescence spectra of alcohol solutions of uranyl acetate exhibit an anomaly: according to their data these spectra have a discrete structure at the temperature of liquid air. Pringsheim[16] also noted the discrete nature of the luminescence spectra of alcohol solutions of uranyl acetate at low temperatures.

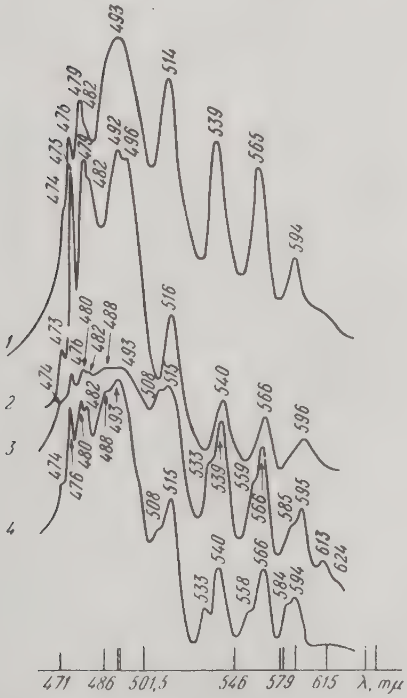

Fig. 3. Microphotograms of the luminescence spectra of solutions of uranyl acetate at -185°: 1) in methyl alcohol, 2) in ethyl alcohol, 3) in isoamyl alcohol, 4) in butyl alcohol.

Until now there has been no systematic investigation of the electronic spectra of organic solutions of uranyl acetate. As a result of our experiments we have come to the conclusion that the assertions of Nichols and Howes and Pringsheim to the effect that the luminescence spectra of alcohol solutions of uranyl acetate at the temperature of liquid air have a discrete structure is erroneous. Our experiments showed that the luminescence spectra of solutions of uranyl acetate of different concentrations in dehydrated organic solvents have the usual band structure characteristic of uranyl compounds in the crystal state at room temperature. Microphotograms of the luminescence spectra of uranyl acetate in methyl, ethyl, isoamyl and butyl alcohols are shown in Fig. 3. The concentration of uranyl in the solutions was taken equal to 0.1N as in the experiments of Nichols and Howes.[18] It is evident from comparison of the microphotograms that the luminescence spectra of alcohol solutions of uranyl acetate at the temperature of liquid air are similar to the emission spectra of uranyl salt crystals at room temperature, i.e., do not exhibit discrete structure in the individual bands. The mean spacing between the peaks of neighboring bands is approximately 860 cm^{-1} and undoubtedly reflects the nature of the vibrational structure of the uranyl ion in the lower electronic state. It is important to note that in all the alcohol solutions the shortwave emission band (473-482 mμ) exhibits four distinct peaks. When observed visually on a

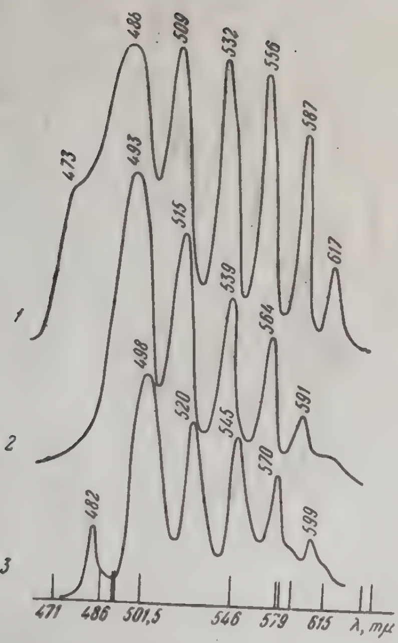

Fig. 4. Microphotograms of luminescence spectra of uranyl acetate: 1) crystalline at +20°, 2) acetone solution at -185° and 3) ethyl acetate solution at -185°.

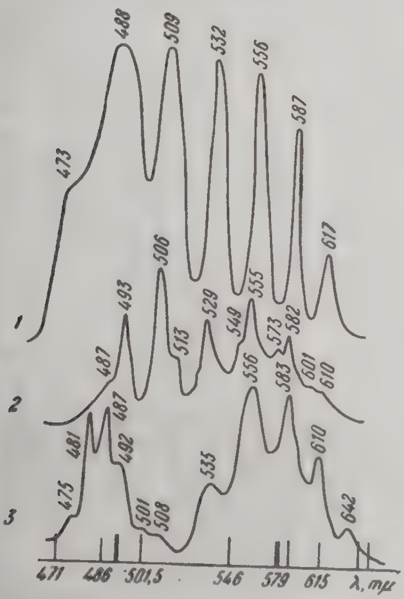

Fig. 5. Microphotograms of luminescence spectra of uranyl acetate: 1) crystalline at +20°, 2) solution in water at -185° and 3) solution in glycerin at -185°.

spectrometer having a low linear dispersion they appear as discrete lines. A certain bifurcation of the long-wave luminescence band in alcohols with a high molecular weight (isoamyl and butyl) is observed.

The most anomalous effect was observed in the photoluminescence spectra of saturated solutions of uranyl acetate in ethyl acetate (Fig. 4, curve 3) and acetone (curve 2) recorded at -185°. Curve 1 in Fig. 4 represents the luminescence spectrum of crystalline uranyl acetate at room temperature. Analysis of the microphotograms shows that the luminescence spectra of uranyl acetate in ethyl acetate and acetone differ as regards their energy distribution not only from each other but also from the emission spectrum of the crystalline salt. The third luminescence band (508 mμ) is virtually absent from the solution in ethyl acetate; in contrast, this emission band has a maximum intensity in the spectra of the crystal material and of the acetone solution. In view of the disappearance of this band the emission energy maximum in the ethyl acetate solution is displaced into the long-wave region (556 and 583 mμ), which explains the yellowish-orange color of the luminescence characterizing this solution (Fig. 4, curve 3). The peaks of the first two short-wave bands (480 and 492 mμ) appear to be doublets with different intensity distributions between the components.

The spectral energy distribution curve of the uranyl acetate solution in acetone differs markedly from the curve for crystalline uranyl acetate (cf. curves 1 and 2 in Fig. 4). The intense short-wave band (473 mμ) appearing in the crystal spectrum is wholly absent from the spectrum of the solution. The other luminescence bands exhibit doublet characteristics. There is a considerable redistribution of energy within the bands.

Fig. 5 shows microphotograms of luminescence spectra of solutions of uranyl acetate in glycerin and in water, recorded at +20°. As in the case of the solvents mentioned above, there is no discrete structure discernible in the individual bands. Going from the crystalline material to water and glycerin solutions there is an appreciable shifting of all the bands to the long-wave side and a considerable spectral energy redistribution within the individual bands.

The fact that the character of the luminescence spectrum of uranyl compounds in organic solutions in the frozen state depends on the nature of the solvent indicates that the solvent molecules participate in the absorption and emission processes. Comparison of the different spectra discloses not only relative displacement of the bands but a

very considerable redistribution of energy within the individual luminescence bands. The character of the spectra of organic solutions at the temperature of liquid air differs from that of the spectra of crystalline uranyl acetate at +20°. The luminescence of uranyl compounds in organic solutions is markedly dependent on the temperature. In most alcohols luminescence is virtually absent at +20°. In glycerin displacement of the bands is observed in the temperature interval from 0 to -185°. There is a pronounced increase in the brightness of the emission in all alcohol solvents as the temperature is decreased from -100° to -185°. Obviously the molecules of the different solvents have different quenching effects on the luminescence of uranyl ions. The marked difference between the luminescence spectra in different organic solvents is indicative of the strong dependence of the interaction between the uranyl ions and the molecules of the solvent on the nature of the latter. If the spectrum were determined primarily by the uranyl ion, the luminescence spectra in different solvents and for different uranyl salts would be similar. The fact that the luminescence spectra of different uranyl solutions have a different temperature dependence also indicates that the emission of the uranyl ion cannot be investigated without reference to the surrounding medium.

In connection with the problem of the interaction of the uranyl ions with the atoms and molecules of the surrounding medium one must mention the investibations of Freymann et al[4,5] on the photoluminescence spectra of organic compounds of uranyl acetate and uranyl nitrate in the crystal state. According to Ref. 5 the luminescence spectra of organic salts of uranyl acetate and nitrate in which the molecules of the water of crystallization have been replaced by molecules of acetone, ether or alcohol are similar to the emission spectra of the corresponding inorganic salts containing water of crystallization molecules. On the basis of their results Freymann et al[5] have advanced the hypothesis that the discrete electronic spectra of uranyl compounds are due primarily to the uranyl ion and that only an insignificant number of the spectral lines are associated with the crystal lattice. In our earlier investigations we showed that the discrete structure in the spectra of uranyl compounds is greatly dependent on the chemical nature of the anion, the second cation and the number of molecules of ordinary or heavy water of crystallization. Consequently the structure of the emission and absorption spectra of organic uranyl compounds in the crystalline state may be expected to be greatly dependent on the organic part of the molecule; this is substantiated by experiment. Our experimental data show that the electronic spectra of uranyl organic salts at low temperatures have a much greater number of discrete lines in both the absorption and emission spectra than the corresponding spectra of inorganic uranyl salt crystals containing water of crystallization. In some cases the number of lines in individual emission and absorption bands of uranyl salts is as great as 50-80.*

Hence replacement of the molecules of ordinary water of crystallization in uranyl compounds by organic molecules brings about a marked change in the discrete structure of the electronic spectra; this directly substantiates our assertion that the structure of the electronic spectra of uranyl compounds is determined primarily by transitions between energy levels of the crystal lattice although individual lines can, of course, be associated with transitions in the uranyl ion or the molecule as a whole. This experimental result invalidates the attempts made by a number of investigators to analyze the discrete structure of the electronic spectra of uranyl compounds on the basis of the hypothesis that the discrete structure of the electronic spectra is due to transitions between different electronic-vibrational levels of the uranyl ion.

The cited experimental data on the spectra of organic uranyl compounds in solutions and crystal form furnish evidence of strong temperature quenching. The character of the temperature quenching of photoluminescence process alters when

---

*Specific data on the spectra of crystals of organic uranyl salts will be presented in a subsequent communication.

the organic part of the molecule is changed and is undoubtedly connected with the chemical nature of the solvent.

Systematic and thorough investigation of organic uranyl compounds should yield important new information on the structure of crystals and solutions.

Institute of Physics and Mathematics of the
Academy of Science of the Byelorussian SSR

References

1. G.Stokes, Phil. Trans., 2, 142, 463 (1852); 3, 143, 385 (1853).
2. H.Becquerel, C.R., 25, 296 (1872).
3. A.N.Sevchenko, Doklady AN SSSR, 42, 349 (1944); J. of Phys., 8, 163 (1944); Izv. AN SSSR, Ser. fiz., 15, 613 (1951).
4. M.Freymann, C.R., 225, 529 (1947).
5. M.Freymann, T.Guilmart, R.Freymann, C.R., 223, 545, 573 (1946); M.Freymann, H.Chantrel, C.R., 227, 1029, 1096 (1948).
6. V.L.Levshin & G.D.Sheremet'ev, Zhur. eksp. i teor. fiz., 17, 204 (1947).
7. B.N.Samoilov, Zhur. eksp. i teor. fiz., 18, 1030 (1948).
8. G.H.Dike & A.B.F.Duncan, Spectroscopic Properties Uranium Compounds.-N.Y. 1949.
9. A.N.Sevchenko & B.I.Stepanov, Zhur. eksp. i teor. fiz., 19, 113 (1949); 21, 213 (1951).
10. M.M.Gurevich & L.Chakhrov, Iav. AN SSSR, OMEN, 509 (1935).
11. A.N.Sevchenko, Izv. AN SSSR, Ser. fiz., 13, 188 (1949).
12. A.N.Sevchenko, M.B.Vdovenko & T.V.Kovaleva, Zhur. eksp. i teor. fiz., 21, 204 (1951).
13. G.H.Dike, Van Heel, Leiden Comm., Suppl., A55 (1925); B55 (1925).
14. D.Pant, Proc. Ind. Acad. Sci., A22, 95, 110 (1945).
15. B.I.Stepanov & A.N.Sevchenko, Trudy GOI, Proceedings of the State Optical Inst., Meeting deducated to the memory of Academician S.I.Vavilov - Oborongiz, 1953.
16. P.Pringsheim, Fluorescence and phosphorescence (in Russ. trans.) M. 1951.
17. V.L.Levshin, Fotoliuminestsentsiia zhidkikh i tverdykh veshchestv. (Photoluminescence of liquids and solids) M.-L. 1951.
18. E.L.Nichols & H.L.Howes, Fluorescence of the Uranyl Salts. - Washington, 1919.

INFLUENCE OF THE SOLVENT ON THE LUMINESCENCE SPECTRUM OF AROMATIC HYDROCARBONS AT LOW TEMPERATURES

-E.V.Shpol'ski & L.A.Klimova

1. At the Second Conference on Luminescence, Il'ina and Shpol'ski[1] reported on the results of their investigation of the fluorescence and phosphorescence spectra of polycyclic hydrocarbons of the pyrene series in frozen solutions at the temperature of liquid air. They used alcohols, benzene and paraffin oil as the solvents. Under these conditions the fluorescence spectra of these compounds consist of narrow bands (100-150 cm^{-1} wide) arranged in regular sequences. The regularities are particularly distinct in the case of 3,4-benzopyrene and 3,4,6,7-dibenzopyrene and its methyl derivative.[2] Subsequently these investigators[3] studied the fluorescence spectrum of yet another polycyclic hydrocarbon -- coronene -- for which the bands are still narrower and the spectrum is even more reminiscent of an atomic spectrum with greatly broadened lines.

Unfortunately we were able to find data in the literature on the fluorescence spectrum in a gaseous state of only one polycyclic hydrocarbon; namely, that of 3,4-benzopyrene.[4] As regards the number and character of the bands, this spectrum was found to be fully analogous to the spectrum of 3,4-benzopyrene observed by us in a frozen solution of paraffin oil; the positions of the band peaks in the wavelength scale for the two spectra are in satisfactory agreement.

The spectra of the above mentioned hydrocarbons in the solid, crystalline state are entirely different. In this case even at the temperature of liquid nitrogen (77°K) the emission is greenish, i.e., shifted to the long-wave side; the emission spectrum is essentially a continuum with a few weak peaks (see Ref. 3 for example).

2. The spectra of the frozen solutions undergo an appreciable change when the solvent is a normal paraffin hydrocarbon.

The fluorescence spectrum of a solution of 3,4,6,7-dibenzopyrene in n-heptane at the temperature of liquid nitrogen is shown in Fig. 1. This spectrum was recorded on a Füss glass spectrograph with a Rutherford prism at a plate factor of 25 A/mm (at 4000 A). As may be seen the spectrum observed in a n-heptane solution consists of sharp lines comparable in width to the atomic lines in gasses.

The fluorescence spectrum of 3,4-benzopyrene in heptane and octane solutions has an analogous appearance. The separation between the fine structure components in this case is 15-20 cm^{-1}.

Even more interesting results were obtained in studying the fluorescence spectrum of coronene in solutions frozen at the temperature of liquid nitrogen.[5]

In oil solutions the bands no longer appear except in the case of pyrene derivatives (see Fig. 1 in Ref. 5), while in normal paraffin hydrocarbon solutions these bands split into narrow "lines" similar to the lines of simple molecules in gases.

The spectral lines may be divided into two groups: one, consisting of bright and sharp lines; the other, equally sharp but much weaker lines; the latter are particularly numerous and virtually constitute a background.

Bowen & Brocklehurst (Ref. 6),* who repeated our experiments and substantiated our results, call attention to the fact that our sample of coronene like the one they used themselves contained a certain admixture of the related substance,

---

*The fluorescence spectrum of coronene in heptane given by Bowen and Brocklehurst agrees with our spectrum as regards wavelengths but differs from it as regards distribution of intensity between doublet components: the intensity relationships are reversed. The intensity distribution shown by Bowen and Brocklehurst is characteristic for hexane but not for heptane solutions. We fail to understand this divergence: we repeatedly photographed and measured the fluorescence spectrum of coronene in heptane and obtained the same distribution of intensities (the inverse of that given by Bowen and Brocklehurst) every time.

1,12-benzoperylene, despite repeated purification by all the available methods (chromatography and vacuum distillation). Using two samples of coronene, one of which contained 40%, while the other contained only 1% of 1,12-benzoperylene and employing two different wavelengths for excitation (3650 and 3135 A), Bowen and Brocklehurst were able to separate the spectra of the two substances. Comparison with our results shows that the multiple weak-line background, mentioned above, and several of the brighter lines are due to the 1,12-benzoperylene.

We made a new series of photographs of the luminescence spectra of coronene in different solvents, exciting the emission by the 3135 A mercury line separated by means of a Zeiss monochromator. According to Bowen and Brocklehurst, the absorption of 1,12-benzoperylene in this region is negligible; hence only the coronene is excited. In this case the above-mentioned multiple weak-line background disappears but the persisting bright lines of coronene are identical as regards both position and distribution of intensities with the lines obtained earlier with the sample excited by the group of mercury lines at 3650 A separated by means of a light filter.

3. In our previous communications [1,3] it was noted that the lines of the fluorescence spectra of coronene form doublets with a constant frequency difference $\Delta\nu$ within the limits of a given spectrum. Comparison of these doublets for different solutions showed that both the value of $\Delta\nu$ and the relative intensities of the components depend on the solvent.

Fig. 2 shows the microphotograms (recorded on a Zeiss microphotometer) of two doublets in the fluorescence spectrum of coronene in a number of different solvents from hexane to nonane. The following features may be noted:

a) in going from hexane to heptane to relative intensities are reversed; it is difficult to compare the spectra in octane and nonane in view of the inadequate resolution of our instruments;

b) the wavelengths of the short-wave component of the doublet and the values of $\Delta\nu$ are indicated in the figure. It will be seen that in going from lighter to heavier solvents $\Delta\nu$ decreases from 84 to 38 cm^{-1}; in the heaviest of the investigated solvents, hexadecane ($C_{16}H_{34}$), the fine structure is altogether effaced: the lines turn into diffuse bands.

4. Hitherto we have been speaking of the fluorescence spectrum proper, i.e., of the emission of short duration ($\tau \approx 10^{-8}$ sec). However, with the exception of 3,4-benzopyrene, all the above mentioned hydrocarbons in solid media, specifically in frozen solutions, emit a more or less bright phosphorescence of considerable duration (τ on the order of several seconds; in the case of coronene τ = 9 sec[7,8]), having a spectrum shifted to the long-wave side relative to the fluorescence spectrum by approximately 6000 cm^{-1}.

In most of the experiments we photographed the phosphorescence spectrum simultaneously with the fluorescence one. Recently, however, the set-up was modified: the Fuss spectrograph was replaced by a three prism ISP-21 spectrograph with a camera having a focal length of 370 mm. In view of the long duration of the emission it was possible to use the simplest phosphoroscope and excite the sample by non-filtered light from a mercury tube thereby greatly reducing the exposure time.

In frozen oil solutions the phosphorescence spectrum consists of a series of bands of approximately the same width as the bands of the fluorescence spectrum. In normal paraffin hydrocarbons each of the bands undergoes further splitting, the character of which (number of components and intensity) depends on the solvent.

Parts of the phosphorescence spectra of 3,4,6,7-dibenzopyrene in n-heptane and n-octane are shown in Fig. 3. It will be seen that in heptane each of the bands is split into three components while in octane only two components can be seen.

An analogous regularity is manifested by the phosphorescence spectra of coronene. The phosphorescence spectra of this hydrocarbon in a number of different solvents are shown in Fig. 4. It will be seen that in paraffin oil the spectrum consists of relatively wide bands (100-150 cm^{-1} wide), constituting of a regular progression of groups of two and three bands; in n-heptane each of the bands undergoes complex splitting, while in n-octane the splitting pattern is simplified:

the number of components decreases (the number of components remains the same in nonane), and finally, in pentadecane the complex structure disappears entirely and we again have wide bands.

Some of the measured frequencies of the lines in the phosphorescence spectrum of the solution of coronene in heptane are shown in Fig. 5. In all, we determined the frequencies of 50 lines.

5. Turning to a discussion of the results let us first summarize the facts that can be regarded as firmly established:

a) polycyclic aromatic hydrocarbons in solutions frozen at 77°K are capable under certain conditions of yielding spectra consisting of narrow lines reminiscent of the atomic lines in gases;

b) the character of the spectrum in each case, namely, the intensity distribution, the degree of splitting and in some cases the number of components as well, depend on the solvent.

Without attempting to develop an elaborate theory, we can indicate qualitatively the causes that play an important part in producing the observed effects.

The salient point of our argument is that at low temperatures the emitting molecules of the aromatic hydrocarbon enter into the crystal lattice of the solvent. The crystallinity of the frozen solution follows a) from the external appearance of the frozen solution (a snowlike mass), b) from the readiness with which normal paraffin hydrocarbons usually crystallize and c) from the experimentally observed fact that the fine structure disappears in media which vitrify in freezing (for example, the well-known "ERA" mixture, which is specially used for obtaining a frozen solution in a form of a transparent vitreous mass, as well as methyl and ethyl alcohols, completely efface the fine structure; the following fact is also of interest: in contrast to n-octane the branched hydrocarbon, isooctane, does not yield a fine structure, which is probably connected with the ability of isooctane to form a glass at low temperatures).

It is important to note that an aromatic hydrocarbon incorporated in the solvent lattice is dispersed molecularly rather than in the form of microcrystals; this follows directly from the fact that in the crystal state the spectrum has a diffused character and exhibits no fine structure. In view of the low concentration of the emitting hydrocarbon its molecules may be regarded as isolated inclusions in the host lattice of the solvent (in the case of coronene solutions there is approximately one molecule of coronene per several million molecules of the solvents).

Fig. 1. Fluorescence spectrum of solution of 3,4,6,7-dibenzopyrene in n-heptane at T = 77°K.

Fig. 2. Influence of the solvent on the principal fluorescence peaks (doublets) of coronene in 1) n-hexane, 2) n-heptane and 3) n-nonane with excitation by 3650 A radiation.

Fig. 3. Part of the phosphorescence spectra of 3,4,6,7-dibenzopyrene in 1) n-heptane, 2) n-octane.

Fig. 4. Phosphorescence spectra of solutions of coronene in different solvents (recorded on an ISP-51 spectrograph with an f = 370 mm camera; excitation by the complete emission of a mercury tube; magnification - 10 X): 1) in paraffin oil, 2) n-heptane, 3) n-octane and 4) pentadecane.

Fig. 5. Frequencies of the lines in the phosphorescence spectrum of a solution of coronene in n-heptane.

Obviously it would be expedient to consider separately the possible influence of the medium on the electronic terms and the vibrational states. The influence on the electronic terms may be due to the molecular Stark effect. In the presence of appropriate degeneration, the effect results in splittings, dependent on the symmetry of the field in which the emitting molecule is located.[9] A similar effect is observed in the spectra of trivalent rare earth ions.[10] It is highly probable that the splittings observed by us may at least partially be explained by an analogous effect. However, the Stark effect cannot afford a full and complete explanation of the observed facts. Thus, for example, in the case of coronene one cannot explain by means of the Stark effect the dependence of the amount of splitting on the solvent in the case of fluorescence and, particularly, the complexity of and the changes in the splitting picture in the case of phosphorescence, inasmuch as the symmetry of the field in all tested solvents remains the same and only the length of the c-axis and the volume of the unit cells changes.

The causes of the fine structure must also be sought in the coupling between transitions in the emitting molecule and the vibrations of the surrounding solvent lattice. The existence of such coupling with the vibrations of the lattice of the emitting substance itself has been established in the investigations of Obreimova, Prikhot'ko and their co-workers. In this case, however, we are dealing with coupling with an extraneous lattice and, consequently, with a new and somewhat different effect. Thus, the coupling between the emitting molecule and the lattice of the solvent may occur due to replacement of one of the paraffin molecules by the emitting molecule in the frozen paraffin lattice. Moreover, there has recently been established the existence of a series with a higher degree of unique, so-called "molecular combinations" in which two types of molecules are firmly bound to each other in the absence of any special attractive forces between them through a process of capture or envelopment of one type of molecule by another (see Ref. 7, p. 256 ff).

In the case of frozen solutions of coronene in normal paraffin hydrocarbons the conditions for "capture" are highly favorable. Thus the maximum dimensions of the coronene molecule in the plane of the σ-bond are 7.1 A, while the dimensions of the c-axis of the unit cell of the paraffins from hexane to nonane vary from 8.57 to 12.8 A.[7] Further, the chain molecules of paraffin in this cell are separated laterally by a distance of 3.6-3.8 A. Hence, on the one hand, there is sufficient space for the coronene molecule in the unit cell of the solvent and, on the other hand, the relationship between the dimensions of the π-electron cloud of this molecule and the lateral distance between one molecule of paraffin and the next is sufficient to insure an adequate bond between the penetrating coronene molecule and the molecules of the solvent. Unfortunately, there are not enough data in the literature on the low-frequency spectra of paraffin hydrocarbons to permit of a complete interpretation of the observed frozen solution spectra. Inasmuch as the frequencies in question lie between 10 and 100 cm^{-1} we are dealing here with the "Gross" frequencies of the slow vibrations of entire large molecules relative to each other,[11] experimental investigation of which is connected with appreciable difficulties.

From this point of view one can also qualitatively explain the effacement of the fine structure in paraffin solvents with a large number of carbon molecules (C_{15} and C_{16}): in such cases the dimensions of the unit cell become so great that the position of the penetrating coronene molecule in the cell becomes indeterminate within rather wide limits.

If the hypothesis formulated above is substantiated, it is possible that investigation of the fine structure of luminescence spectra will open a simple way to determining the low natural frequencies of lattice vibrations.

"V.I.Lenin" Moscow State
Pedagogical Institute

References

1. A.A.Il'ina & E.V.Shpol'ski, Izv. AN SSSR, Ser. fiz., 15, 585 (1951).
2. E.V.Shpol'ski & A.A.Il'ina, Zhur. eksp. i teor. fiz., 21, 142 (1951).
3. E.V.Shpol'ski, A.A.Il'ina and L.A.Klimova, Doklady AN SSSR, 87, 935 (1952).
4. P.Pringsheim, Ann. Acad. Warsaw, 5, 29 (1938).
5. E.V.Shpol'ski & L.A.Klimova, Izv. AN SSSR, Ser. fiz., 18, 673 (1954); (Translation: Bulletin, Vol. 18, No. 6, p. 357).
6. E.J.Bowen & B.Brocklehurst, J. Chem. Soc., London, Nov., 3875 (1954).
7. J.M.Robertson, Organic Crystals and Molecules, Cornell Univ. Press (1953).
8. V.V.Bredel', Thesis, Moscow State Pedagogical Institute, 1953; Doklady AN SSSR, 103, 787 (1955).
9. H.Bethe, Ann d. Phys., 3, 133 (1929).
10. H.Ewald, Ann d. Phys., 34, 209 (1939).
11. E.F.Gross and M.F.Vuks, J. Phys. and Rad., 6, 457 (1935); 7, 113 (1936).

DISCUSSION

B.S.Neporent: I assume that one cannot categorically reject the assumption of possible splitting of the electronic levels of the molecule in the field of the crystal: the consequences of the hypothesis of superposition of such frequencies of the crystal should be apparent in all cases of triplets, inasmuch as the frequencies are not high and the anti-Stokes components must be intense. The same thing applies to the change in the intensity of sometimes the right and again the left component in the case of phosphorescence spectra. This fact may be related to conditions of symmetry of the field which influences a molecule incorporated into the crystal itself.

In hexane the cross section of the molecule coincides with the dimensions of the c-axis, hence there is only one possible cell structure. In the case of octane there are greater possibilities. In this case it is natural to expect splitting into a greater number of components or in any case a change in the relative intensity of the components. Polarization measurements could be decisive in making a choice between the two hypotheses.

E.V.Shpol'ski: B.S.Neporent may be right. A definitive answer can be found only through further investigations, in particular polarization measurements.

Note added in proof. In view of the fact that clarification of certain details of the investigated spectra required a higher resolution than that used hitherto, after the Conference we made and measured new photographs of the spectra of coronene and pyrene using spectrographs with a higher resolving power. We used the ISP-51 three-prism glass spectrograph (similar to the Zeiss spectrograph) with a long focus camera (f = 840 mm; dispersion 6.3 A/mm near 400 A) and a set-up with a plane diffraction grating (dispersion 6.4 A/mm) generously made available for this purpose by P.P.Feofilov. The photographs made on both instruments brought out new details which greatly facilitated interpretation of the results. The photographs and the numerical data will be published in the near future.

Analysis of the results has shown that in the case of fluorescence, as well as in the case of phosphorescence, the observed spectrum consists of a superposition of two spectra repeating each other but shifted a constant distance which is characteristic of the given solvent.

Recently we have learned of a new investigation published by Bowen and Brocklehurst (J. Chem. Soc., London, Dec. 1955, pp. 4320-4331). In this publication the authors explain the anomalous distribution of intensity in the spectra of coronene in heptane obtained earlier by the fact that in this earlier investigation they used insufficiently pure heptane. In addition these investigators have obtained a number of very interesting new results which in general are close to ours. We note however that they photographed their spectra on a one-prism monochromator equipped with a camera. The inadequate dispersion of this instrument explains many of the difficulties encountered by these investigators.

SPECTRA AND ANTI-STOKES AND STOKES FLUORESCENCE YIELDS OF AROMATIC COMPOUNDS

(Abstract*) - B.S.Neporent and N.A.Borisevich

We investigated the spectra and measured the absolute quantum efficiency of the fluorescence of the vapors and solutions of a number of substituted phthalimides with excitation in a wide spectral range, including the anti-Stokes region, at different temperatures and vapor pressures.

In individual cases the fluorescence output of the vapor exceeds the corresponding output of the solution. The spectrum of the vapor, having a downward branch not only in the anti-Stokes but also in the Stokes region, serves to characterize the investigated molecules.

The decrease in fluorescence output in the anti-Stokes region must be associated with intramolecular processes occurring incident to excitation of the molecule, inasmuch as it is observed in rarefied vapors as well and is not accompanied by a decrease in the duration of luminescence. The reduction of fluorescence efficiency is, therefore, connected with quenching of the first kind. These results serve as a further confirmation of Vavilov's law and refute the objections to this law recently raised by Pringsheim. Analysis of the spectra and the temperature dependence of the output show that the excitation of anti-Stokes fluorescence is due to molecules having an excess of vibrational energy, while the general emission is due to molecules with small reserve of vibrational energy.

The decrease in output in the Stokes region is due to the gradual increase in the probability of non-radiative transitions. Equivalence of the thermal and optical methods of increasing the store of vibrational energy of the investigated molecules is evinced under excitation with large quanta. The vibrational specific heats of the investigated molecules were measured by the optical method.

Careful examination of the spectra of the vapors and solutions showed that every change in the efficiency (output) is accompanied by a small but definite change in the shape of the fluorescence spectrum. In the Stokes excitation region this is connected with changes in the vibrational energy of the molecules. With excitation in the anti-Stokes region, the alteration of the shape of the spectrum is connected with the tendency towards a Stokes cut-off of the spectrum, which increases with decreasing temperature.

The results of the work demonstrate again that investigations of fluorescence and absorption spectra and, particularly, the spectra of the fluorescence yield of vapors and solutions of complex organic compounds are important in studying intramolecular energy transformation processes.

DISCUSSION

V.L.Levshin: Were collisions of the molecules with each other a significant factor in your experiments and how do you explain the decrease in output in the ultraviolet region?

N.A.Borisevich: Collisions were a negligible factor because of the low vapor pressure; the decrease in yield is due to non-radiative transitions.

L.A.Tumerman: What is the mechanism of these transitions?

N.A.Borisevich: Either internal conversion of the electron excitation energy or photochemical processes.

B.S.Neporent: The important point is that the probability of radiationless transitions is a monotonic function of the energy store of the complex molecule. This has now been substantiated by many investigations.

B.Ia.Sveshnikov: The difficulties of interpretation where the transition mechanism is concerned are connected with the fact that in going over to excitation in the anti-Stokes region the spectra and the yield change, while the duration of luminescence remains constant. As regards the emission of solutions, it would be desirable to repeat the measurements I made some years ago.

---

*Report published in Doklady AN SSSR, 69,695 (1945) & Optika i spektroskopiia,2(1956).

INFLUENCE OF EXTRANEOUS GASES ON THE SPECTRA AND FLUORESCENCE YIELD OF VAPORS OF AROMATIC COMPOUNDS

(Abstract*) - N.A.Borisevich & B.S.Neporent

Studies of the influence of extraneous gases on the fluorescence of vapors serve as a source of data on intermolecular interactions and, as the results of the present study show, can yield information on the structure of molecular energy levels.

We investigated the influence of extraneous gases (N_2, NH_3 CO_2 and C_5H_{12}) on the fluorescence spectra and efficiencies of a number of substituted phthalimides with excitation in a wide spectral range, including the anti-Stokes region. It was established that as the frequency of the exciting light is reduced the initial increase in the fluorescence of the vapor, due to a decrease in the store of vibrational energy of the excited molecules incident to collisions, becomes a decrease, associated with an increase in vibrational energy. The value of the excitation frequency at which the increase ceases and the decrease in fluorescence begins indicates the frequency of the electronic transitions in the investigated molecules. In the case of molecules characterized by "attenuation spectra" this frequency, in contrast to the case of molecules exhibiting "modulation spectra", lies in the region of the absorption spectrum peak.

The effect of extraneous gases, which is in agreement with results obtained in our earlier investigation (see preceding article in the present issue), substantiates this deduction.

On the basis of the experimental results, we determined the dependence of the mean energy transferred in a collision of an excited molecule with a molecule of the extraneous gas on the vibrational energy of the former. The computed values of the coefficient of accomodation indicate that the energy transfer from the excited to the extraneous gas molecules is far more efficient than the reverse transfer.

The influence of the solvent on the fluorescence of the dissolved substance is not limited to the general and universal effect of accelerating attainment of thermal equilibrium of the system. There is also observed a quenching effect, specific for each solvent. We propose a method for separating the general and specific effects.

Analyisis of the influence of extraneous gases on the yield of anti-Stokes fluorescence of vapors also confirms the conclusions drawn in our earlier (preceding article) investigation.

---

*The complete report will appear in Optika i spektroskopiia, 4, (1956).

ABSORPTION AND FLUORESCENCE SPECTRA AND THE QUANTUM EFFICIENCY OF FLUORESCENCE OF CERTAIN MESO-DERIVATIVES OF ANTHRACENE

- A.S.Cherkasov

1. The absorption and luminescence of meso-substituted derivatives of anthracene have been studied by a number of investigators; however, only a few studies are devoted to an elucidation of the influence of different replacement radicals on the optical properties of the substance.[1-3] In order to clarify the effects and regularities involved we carried out an investigation of the absorption and fluorescence spectra and the fluorescence efficiencies of several compounds of this anthracene series.

2. The absorption spectra were studied on an SF-4 spectrophotometer; the fluorescence spectra were measured by means of a diffraction grating monochromator with a photoelectric recording attachment. The fluorescence was excited by the group of mercury lines at 364 mμ, separated by means of an appropriate filter. The relative fluorescence efficiency was determined on the basis of the ratio of the areas bounded by the fluorescence spectrum contour and the frequency axis. The scale for plotting the fluorescence spectra was determined by measuring the fluorescence intensity at a number of points in the spectra of solutions of the investigated compounds, characterized by the same absorption of light of 365 mμ by an equal thickness of the solution. The solvent used was ethyl alcohol; all measurements were made at about 20°C.

3. The absorption spectra of the alkyl- and aryl-derivatives of anthracene are similar to the spectrum of the unsubstituted hydrocarbon and in the investigated 220-420 mμ wavelength region consist of two well-separated bands, corresponding to different electronic transitions. In 9-phenyl-10-(α-naphthyl)-anthracene and in 9.10-di(α-naphthyl)-anthracene there is also appreciable absorption in the interval between the first and second absorption bands; this absorption is due to the naphthyl chromophores.

Introduction of the alkyl and aryl substituents into the meso-positions in the anthracene molecule leads to a shift of the absorption spectrum to the side of longer wavelengths; in the case of double substitution the displacement is twice as great as in the case of single substitution and amounts to 1200-1600 cm^{-1} and 600-800 cm^{-1}, respectively, for the long-wave band.

The long-wave absorption band is altered greatly by the influence of the amino group: the spectrum of 9-aminoanthracene, for example, is shifted far into the long-wave region and no longer exhibits the distinct vibrational structure characteristic of anthracene (see Fig. 2, curve 1). In the case of acetylation or benzoylation of the amino groups the absorption spectrum is shifted in the opposite direction and becomes similar to the normal spectrum of anthracene.

Measurements of the areas under the absorption spectrum contour showed that the introduction of different substituent groups leads to an increase of the absorption in the region of the long-wave band and a decrease in the region of the short-wave band; the aryl radicals appear to exert a stronger influence than the alkyl radicals.

4. The fluorescence spectra of meso-alkyl-derivatives of anthracene are similar as regards shape to the spectrum of normal anthracene, exhibit a distinct vibrational structure and are mirror images of the absorption spectra (Fig. 1, curve 1). Substitution of aryl radicals leads to diffusion of the fluorescence spectrum (however, the structure persists in the absorption spectrum), partial effacement of the vibrational structure and the appearance of weaker secondary peaks (evinced by inflexions in the curve) in the vicinity of the principal peaks (Fig. 1, curve 3).

The frequency difference between the principal fluorescence peaks changes from 1400±25 cm^{-1} in anthracene and its alkyl-derivatives to 1200-1300 cm^{-1} in the aryl-derivatives.

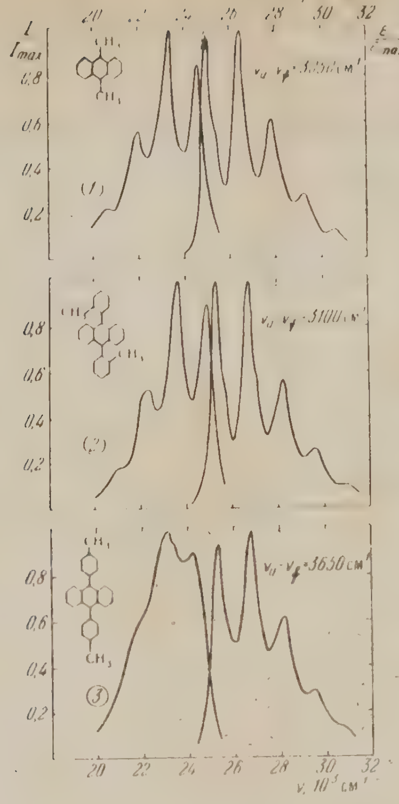

Fig. 1

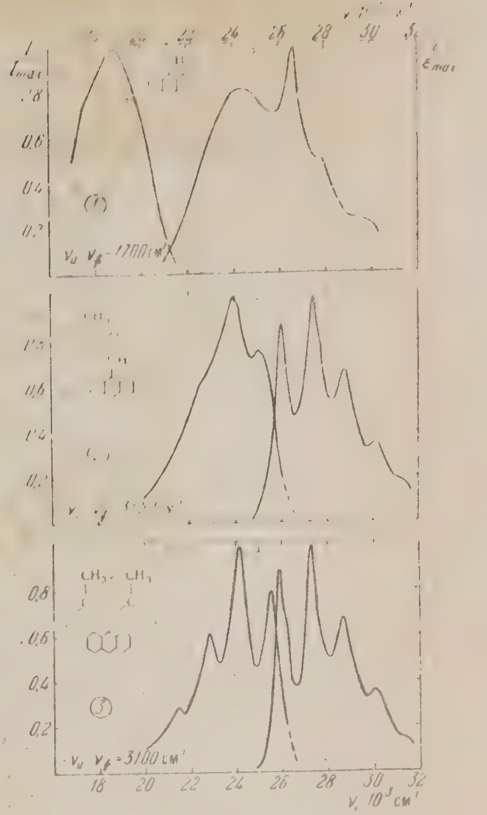

Fig. 2

Fig. 1. Absorption spectra (at right) and fluorescence spectra (at left) of alcohol solutions of 1) 9,10-dimethylanthracene, 2) 9,10-di-o-tolylanthracene and 3) 9,10-di-n-tolylanthracene; $\nu_a - \nu_f$ = frequency difference between principal absorption and fluorescence peaks. Dotted lines indicate positions of the principal absorption and fluorescence peaks of anthracene.

Fig. 2. Absorption (at right) and fluorescence (at left) spectra of alcohol solutions of 1) 9-aminoanthracene, 2) 9-monoacetylaminoanthracene and 3) 9-diacetylaminoanthracene.

The fluorescence spectra of diphenylanthracene and di-m-tolylanthracene are similar to the spectrum of di-n-tolylanthracene (Fig. 1, curve 3), while the spectrum of di-o-tolylanthracene is markedly different in that it has a distinct vibrational structure and is analogous in appearance to the spectrum of anthracene. This may be explained by the fact that the presence of a methyl group in the ortho position prevents (due to steric hindrance) any appreciable deviation of the plane of the benzene rings from the plane perpendicular to the anthracene nucleus. As a result of this "fixing" of the o-tolyl radicals their interaction with the anthracene nucleus must be much weaker than the interaction of such radicals as phenyl, m- and n-tolyl, etc. In the case of the latter any steric hindrance is due to the minor overlapping of the hydrogen atoms of the aryl and anthracene nuclei and hence they can rotate to a position close to the coplanar with the anthracene nucleus. Obviously, the presence in this case of interaction between the benzene rings of the substituent and the anthracene nucleus results in diffusion of the fluorescence spectrum without alteration of the anthracene-like absorption spectrum.

The fluorescence spectra of the meso-aryl and meso-alkyl derivatives of anthracene are displaced to the long-wave side relative to the fluorescence spectrum of anthracene. As in the case of the absorption spectra, the shift for double-

substituted products is twice that for single-substituted derivatives.

In the case of replacement of a hydrogen atom linked to a meso-carbon atom in the anthracene by an amino radical the fluorescence spectrum becomes entirely structureless and is displaced far into the long-wave region (Fig. 2, curve 1). Acetylation of the amino group appreciably reduces the influence of the group on the anthracene nucleus with the result that the fluorescence spectrum is shifted back and again exhibits structure. In monoacetylaminoanthracene the vibrational structure is still weakly evident (Fig. 2, curve 2), whereas the fluorescence spectrum of diacetylaminoanthracene already differs little in appearance from the spectrum of anthracene (Fig. 2, curve 3) and is virtually identical as regards position with the spectrum of monoalkyl derivatives of anthracene.

5. Comparison of the absorption and fluorescence spectra of the meso-substituted derivatives of anthracene and the separations between the principal absorption and fluorescence peaks permits of drawing the following qualitative deduction: the more clearly evident the vibrational structure in the absorption and fluorescence spectra, the smaller the frequency difference between the principal fluorescence peak and the principal absorption peak.

This observation is illustrated by the following examples. Anthracene, monoalkyl- and dialkyl-substituted anthracene, di-o-tolylanthracene and diacetylaminoanthracene all have absorption and fluorescence spectra exhibiting distinct structure; the frequency difference between the principal absorption and fluorescence peaks for all of these is 3000-3100 cm^{-1}. The absorption spectra of diphenylanthracene, di-m-tolylanthracene and di-n-tolylanthracene show structure, but their fluorescence spectra are diffuse and for these compounds the frequency difference increases to 3500-3600 cm^{-1}. In the case of 9-bromanthracene-10-carboxylic acid, which according to Shpol'ski, Il'ina & Bazilevich,[2] has an absorption spectrum exhibiting structure but a continuous fluorescence spectrum, the frequency separation between the principal absorption and fluorescence peaks is 6000 cm^{-1}. Finally, in the case of 9-aminoanthracene, for which not only is the fluorescence spectrum a continuum but the absorption spectrum is very diffuse, the fluorescence and absorption peaks are even further apart (7700 cm^{-1}).

6. We can draw the following deductions from an examination of the measured values of the quantum efficiency of fluorescence of alcohol solutions of the tested meso-derivatives of anthracene (see table):

Fluorescence efficiency of alcohol solutions of meso-derivatives of anthracene

Substance	Quantum efficiency rel.	Quantum efficiency abs.	Substance	Quantum efficiency rel.	Quantum efficiency abs.
Anthracene	1.0	0.22*	9,10-Diphenylanthracene	3.9	0.86
9-Methylanthracene	1.3	0.29	9,10-Di-n-tolylanthracene	3.3	0.76
9-Ethylanthracene	1.35	0.30	9,10-Di-m-tolylanthracene	2.9	0.64
9-n-Propylanthracene	1.4	0.31	9,10-Di-o-tolylanthracene	2.6	0.57
9-n-Butylanthracene	1.6	0.35	9-Phenyl-10-(α-naphthyl)-an.	3.0	0.66
9-Isobutylanthracene	1.75	0.39	9,10-Di(α-naphthyl) anthra.	2.2	0.49
9,10-Dimethylanthra	2.85	0.63	9-Nitroanthracene	0	0
9,10-Di-n-propylanth.	3.45	0.76	9-Aminoanthracene**	1.3	0.29
9-Phenylanthracene	2.05	0.45	9-Monoacetylaminoanthracene	2.0	0.44
9-n-Tolylanthracene	2.0	0.44	9-Diacetylaminoanthracene	1.6	0.35
			9-Benzoylaminoanthracene	0	0

---

* According to Bowen & Norton.[4]

** Aminoanthracene oxidizes rapidly in air; hence the cited value may be somewhat low.

1) alkyl and aryl substituents as well as the amino and acetylamino groups enhance the fluorescence efficiency; 2) in the alkyl derivative series the efficiency increases with the molecular weight of the alkyl radical; 3) the fluorescence yield of dialkyl and diaryl derivatives is approximately twice that of the corresponding mono-substituted derivatives; 4) in the ortho-, meta and paratolylanthracene series the efficiency goes down as the methyl group approaches the anthracene nucleus; 5) acetylation of the amino group leads to an increase in the fluorescence efficiency, while benzoylation of the group, on the contrary, tends to kill the fluorescence entirely.

References

1. R.W.Jones, Chem. Rev., 41, 353 (1947).
2. E.V.Shpol'ski, A.A.Il'ina & V.V.Bazilevich, Izv. AN SSSR, Ser. fiz., 12, 519 (1948).
3. F.I.Polovikov, Doklady AN SSSR, 71, 453 (1950).
4. E.J.Bowen & A.Norton, Trans. Farad. Soc., 35, 44 (1939).

DISCUSSION

V.L.Levshin: I feel that the approach employed in this investigation should be fruitful. Careful study of a large number of anthracene derivatives has enabled the authors to establish a number of regularities in the influence of different radicals on the absorption and fluorescence spectra. It is apparent from the cited data that the substituents have a much stronger effect on the excited level than on the unexcited one. In view of the disappearance of mirror symmetry of the absorption and fluorescence spectra as a result of substitution one can draw certain deductions regarding modification of the electronic levels of the molecules.

E.V.Shpol'ski: This investigation is an example of the desirability of collaboration of physicists and chemists in the field of luminescence.

LUMINESCENCE OF COLOR CENTERS IN FLUORITE CRYSTALS

- G.A.Tishchenko and P.P.Feofilov

It is known that ionic crystals become colored when heated in a metal vapor or irradiated with x-rays or γ-rays. This coloration is connected with the formation of certain structural defects in the crystal lattice, which give rise to wide bell-shaped absorption bands in the longer wave region of the spectrum. Numerous investigations have shown that several types of color center are produced; however, in all cases the formation of the centers is connected with some impairment of the regularity of the ideal lattice. The simplest type of center is the so-called F-center which consists (according to the most plausible De Boer model) of an electron localized at a vacant anion site. In addition to F-centers there may exist more complicated centers extending over several lattice sites.[1]

Whereas the absorption spectra of color centers in ionic crystals have been investigated in great detail, data relating to their luminescence are very scanty and often contradictory. Theoretically, luminescence from F-centers is possible only at sufficiently low temperatures[2], and it is predicted that the emission should occur in the near infrared. In 1952 Ghormley and Levy[3] discovered luminescent bands near $\lambda = 1\ \mu$ in additively colored crystals of KCl and x-rayed crystals of LiF, which they attributed to F-centers. Some recent work of Klick[4] conflicts with these data. Klick investigated colored KCl crystals at liquid helium temperature and established that, contrary to the predictions of theory, F-centers either do not luminesce at all or, if they do, have a very low quantum efficiency.

The luminescence of more complicated formations than F-centers has been proved conclusively. In 1950 Klick[5] attributed luminescence in LiF to color centers which he called M-centers.* In 1953 one of us discovered and investigated the intense luminescence of color centers in NaF and CaF_2.[6] An investigation of the polarization of this luminescence showed that it, like the luminescence of color centers in LiF, could be ascribed to F_2-centers, i.e., pairs of electrons localized at neighboring anion sites.[7]

In the present work we investigated the shapes of the absorption and luminescence bands due to color centers in artificial fluorite.** We have compared the results obtained with the predictions of the theory of impurity absorption developed by Pekar[8]. In addition, by employing the method of luminescence polarization diagrams, we have determined the nature (multipole order) of the elementary emitters of the color centers.

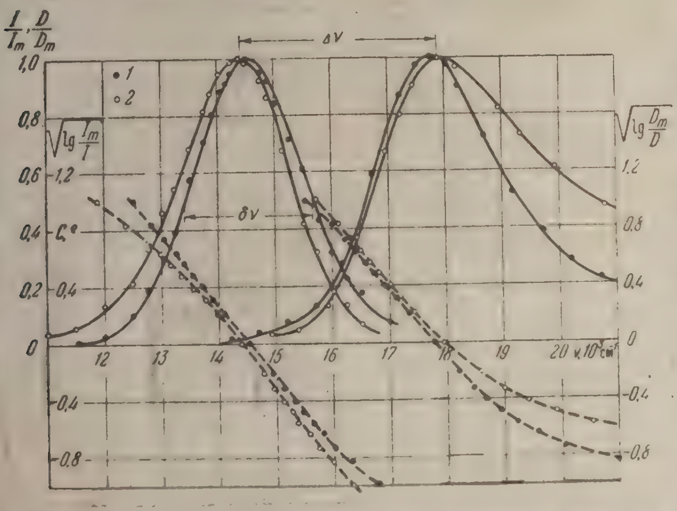

Fig. 1. Absorption and luminescence spectra of additively colored (1) and x-ray irradiated (2) fluorite crystals.

2. Absorption and luminescence spectra. The measurements of the absorption spectra were on an SF-4 spectrophotometer. For the low temperatures work we built a special cryostat which could be placed between the exit slit of the monochromator and the photoelement. The luminescence spectra were measured with the photoelectric apparatus of B.S. Neporent.[9] *** The crystals used

---

*According to Seitz, an M-center is a system consisting of an F-center and two vacancies of opposite polarity.

**Our gratitude to I.V.Stepanov for preparing the crystals and allowing us to use them.

***We desire to thank B.S.Neporent for making available his equipment for our use.

were colored either during their growth (additive coloration), by x-ray treatment, or by irradiation with γ-rays from Co^{60}.

The measurements of the absorption by fluorite crystals containing color centers showed, in agreement with previously published data,[10] that the absorption spectrum consists essentially of two intense bell-shaped bands situated in the visible and near ultraviolet regions (peaks at about 560 mμ and 380 mμ). The general character of the spectra does not depend on the method of coloration; however, the spectra of different samples may differ somewhat in detail. For example, the shape of the long-wave absorption band was appreciably more symmetric in additively colored crystals than in crystals that had been irradiated. (Fig. 1).

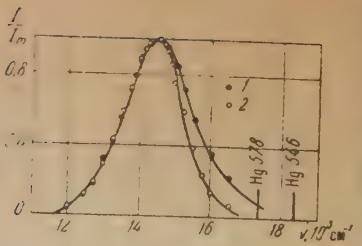

Fig. 2. Luminescence spectra of color centers in fluorite crystals with excitation by light of different wavelengths: 1) 546 mμ; 2) 578 mμ.

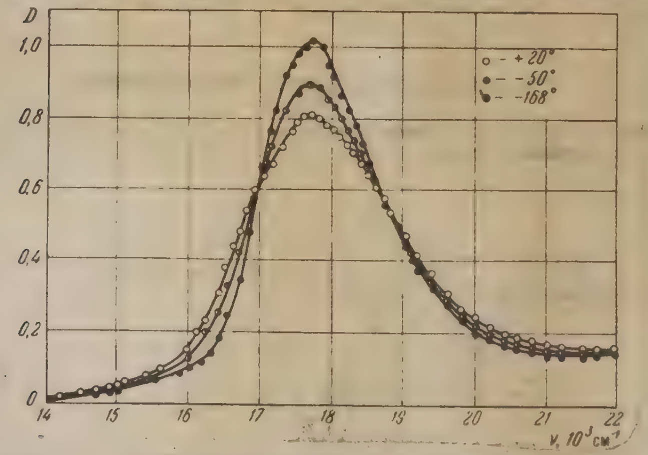

Fig. 3. Influence of temperature on the absorption of color centers in fluorite crystals.

The strong red luminescence of the color centers in fluorite is excited at the same frequencies by light of all wavelengths in the center absorption spectrum, which is a reason for attributing both absorption bands to the same centers. The luminescence spectrum consists of a single bell-shaped band having a peak at about 695 mμ, which is symmetric in additively colored crystals and somewhat more sloping on the long-wave side in the case of crystals colored by irradiation (Fig. 1). The luminescence spectra and the long-wave branches of the absorption bands exhibit mirror symmetry when plotted against frequency. The Stokes shift $\Delta\nu$ of the bands is about 3500 cm^{-1} (0.43 ev). The halfwidth $\delta\nu$ of the luminescence band is about 2200 cm^{-1} (0.27 ev). The luminescence and absorption overlap to an appreciable extent. When the luminescence is excited by 578 mμ light (the yellow line of mercury) the so-called Stokes cut-off is observed, i.e., the relative intensity of the short-wave part of the luminescence spectrum is reduced. (Fig. 2).

On reducing the temperature to 160°C there is a slight narrowing of the absorption and luminescence bands. At the same time the absorption at the peak increases. (Fig. 3). Apparently the area under the absorption curve remains unchanged, which allows us to judge of the band half-width from the absorption at the peak. The effect of temperature is too small to permit an exact determination of the temperature dependence of the half-width, but in the range of temperatures investigated the linear relation $D_m = f(T)$ seems to fit the data better than the relation predicted by the theory: $D_m \approx (\delta\nu)^{-1} \approx T^{-1/2}$ (Fig. 4).

The theory of the absorption of light by impurities[8] shows that in the case of large emission of heat the absorption and luminescence spectra may be described in the first approximation by the Gaussian curve:

$$\frac{D}{D_m} = e^{-\alpha\,|\nu-\nu_m|^2}. \qquad (1)$$

The satisfactory rectification of the curves obtained for additively colored crystals when plotted in terms of $\sqrt{\log\,(D_m/D)} = f(\nu)$ (Fig. 1) is evidence that the theory correctly renders the principal features of the effect. In order to clarify

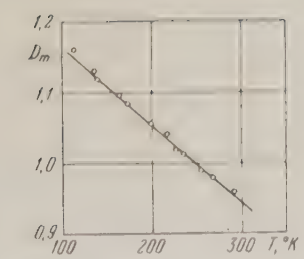

Fig. 4. Temperature dependence of the peak absorption.

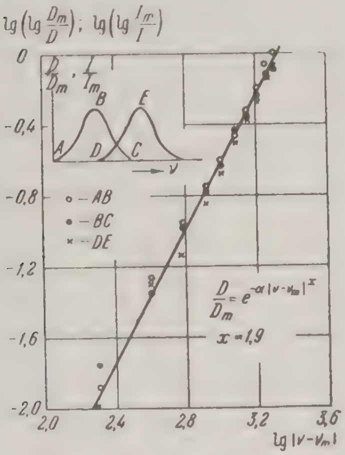

Fig. 5

whether the exponent of $(\nu - \nu_m)$ can be set = 2, we plotted the spectra in the coordinates log(log (D_m/D)) vs log $|\nu - \nu_m|$ (Fig. 5). The reason for this check was the recent work of Hesketh & Schneider[11] in which the results for x-ray irradiated KCl indicated an appreciable deviation of the exponent from 2. According to our data the mean value of the exponent for the different branches of the absorption and luminescence spectra is 1.9, i.e., given the experimental error, is reasonably close to the theoretical value. Attempts to approximate the experimental contours by means of Lorentz dispersion curves yielded significantly inferior results.

An additional criterion for the validity of the theory is furnished by a comparison of the observed half-width $(\delta\nu)$ of the luminescence band with the half-width calculated from the theory of impurity absorption formula:

$$\delta\nu = 2\sqrt{2 \ln 2}\sqrt{\frac{\Delta\nu}{h} kT}. \qquad (2)$$

The value obtained by means of this formula, $\delta\nu \approx 2000$ cm^{-1} = 0.25 ev is in good agreement with the experimental value.

Thus the theory of impurity absorption correctly describes the principal features of the spectra of luminescent color centers in fluorite crystals.

3. The nature (multipolarity) of the elementary emitters. One of us has shown that the luminescence-polarization method of determining the nature of the elementary emitters, proposed by S.I.Vavilov[12] for the case of isotropic media, can be extended to the case of anisotropic luminescent centers oriented along the symmetry axes of cubic crystals. Applying this method we determined the nature of the elementary oscillators in terms of which it is feasible to describe the luminescence of color centers in fluorite.

As was established earlier (Refs. 6 & 7) the anisotropic luminescent color centers in fluorite are oriented along the fourth order symmetry axes.

In connection with this the samples were cut from the crystals containing color centers in such a way that the luminescence could be excited and the emission observed through two mutually perpendicular faces of the cube (the method is described in Ref. 13). The results of the investigation of the dependence of the intensity $I(\eta)$ and polarization $P(\eta)$ on the angle of rotation η of the exciting electric vector in the plane normal to the direction of excitation are presented in Fig. 6. A comparison of the experimental curves with the calculated ones (from Ref. 13) leaves no doubt that for excitation in the first absorption band (546 mμ), the process of absorption and emission may be described by linear electric dipoles (π_e).

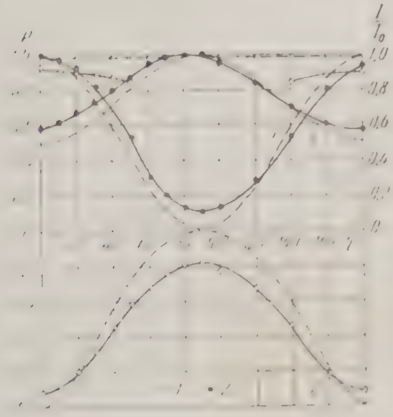

Fig. 6. Dependence of the polarization (1) and intensity (2) of the luminescence from color centers in fluorite crystals on the angle of rotation of the exciting electric vector in the plane perpendicular to the direction of excitation at two wavelengths of the exciting light: I) 546 mμ and II) 365 mμ. The dash lines are the theoretical curves for the cases $\pi_e \rightarrow \sigma_e$ and $\sigma_e \rightarrow \pi_e$.

There is, however, an ambiguity in the interpretation of the results obtained for excitation in the second absorption band (365 mμ): the results can be described with equal success as absorption by a plane-polarized oscillator (π_e) and emission by a circularly-polarized oscillator (σ_c) perpendicular to the former, or vice versa, the absorption may be by σ_e and the emission by π_e. This ambiguity may be resolved if one makes use of data obtained in an investigation[14] of anisotropic photochemical conversion of color centers. It follows from these data that the change in the sign of the polarization in going from excitation in the first absorption band to excitation in the region of the second band must be interpreted as a result of a change in the orientation of the absorbing oscillators. Accordingly, the luminescence process in excitation by the shorter waves must be characterized as absorption by circularly polarized electric oscillators (σ_c) and subsequent emission by plane-polarized electric oscillators (π_e).

The electric dipole nature of the luminescence of the color centers in fluorite crystals, established in the above experiments, is fully consistent with short duration (about 10^{-8} sec) of this luminescence and the large value of the oscillator strengths deduced from the absorption spectra.

4. Discussion of results. Above we have described the principal features of the absorption and luminescence spectra of crystals of fluorite (CaF_2) containing color centers. We obtained analogous results for color centers in lithium and sodium fluoride. Polarization studies lead us to believe that in all the investigated cases we are dealing with more complex formations than F-centers, possibly with F_2-centers, for example. The quantum efficiency of these formations is very high. It is probable that bright luminescence from color centers is not specific to fluorides alone. However, it can readily be shown that in all other alkali halide crystals the emission bands must be located outside the visible spectrum. As Ivey[16] showed, the location of the M-bands is adequately described by the empirical expression

$$\lambda_{max} = 1400\ d^{1.56}\ \text{Å} \tag{3}$$

where d is the lattice constant.

The locations of the bands we observed in crystals of CaF_2 ($d = 2.36$, $\lambda_{max} = 560$ mμ), LiF ($d = 2.01$, $\lambda_{max} = 445$ mμ) and NaF ($d = 2.31$, $\lambda_{max} = 510$ mμ) also fit the curve described by (3). Apparently the centers we investigated are identical with M-centers, although the model we adopted on the basis of our polarization measurements (i.e., the F_2-center model) differs from the M-center model proposed by Seitz. It is impossible to decide at present which model corresponds most closely to the true structure of the centers. If we accept that the Stokes shift is approximately the same for all salts ($\Delta\nu = 0.5$ ev), then already in the case of complex color centers in LiCl crystals ($d = 2.57$, the lowest value for alkali halide crystals other than those we investigated) one should expect to observe luminescence with a peak at 810 mμ. In the other salts (the values of d range from 2.75 in LiBr to 3.66 in CsI) the luminescence should occur at even longer wavelengths.

In BaF_2 the luminescence from the complex color centers might be expected at about 800 mμ. It would be of interest to search for this emission in the near infrared.

References

1. F.Seitz, Rev. Mod. Phys., 26, 7 (1954).

2. N.F.Mott & R.W.Gurney, Electronic processes in ionic crystals, (in Russian trans. M. 1950) Oxford 1948; S.I.Pekar, Zhur. eksp. i teor. fiz., 22, 641 (1952).

3. J.A.Ghormley, H.A.Levy, J. Phys. Chem., 56, 548 (1952).

4. C.C.Klick, Phys. Rev., 94, 1541 (1954).

5. C.C.Klick, Phys. Rev., 79, 894 (1950).

6. P.P.Feofilov, Doklady AN SSSR, 92, 545 (1953).

7. P.P.Feofilov, Zhur. eksp. i teor. fiz., 26, 609 (1954).

8. S.I.Pekar, Usp. fiz., nauk, 50, 197 (1953).

9. B.S.Neporent & V.P.Klotchkov, Izv. AN SSSR, Ser. fiz., 20, 601 (1956). (Translation in the next issue - Vol. 20, No. 5 - of the Bulletin.)

10. E.Mollwo, Gött. Nachr., 1, 79 (1934); R.Herman, S.Silverman, JOSA, 37, 871 (1947); A.Smakula, Phys. Rev., 77, 408 (1950); ZS. f. Phys., 138, 276 (1954); S.Barile, J. Chem. Phys., 20, 297 (1952); F.Lüty, ZS. f. Phys., 134, 596 (1953).

11. R.V.Hesketh & E.E.Schneider, Phys. Rev., 95, 837 (1954).

12. S.I.Vavilov, Zhur. eksp. i teor. fiz., 10, 1363 (1956).

13. P.P.Feofilov, Optika i spektroskopiia, No. 2 (1956).

14. P.P.Feofilov, Doklady AN SSSR, 98, 949 (1954).

15. A.M.Bonch-Burevich, V.A.Molchanov & V.I.Shirokov, Izv. AN SSSR, Ser. fiz., 20, 596 (1956), (Trans. in next issue - Vol. 20, No. 5 - of the Bulletin).

16. H.T.Ivey, Phys. Rev., 72, 341 (1947).

QUANTUM EFFICIENCY OF PHOTOCHEMICAL TRANSFORMATION OF F-CENTERS IN HEATED KCl CRYSTALS

- A.A.Shatalov

In earlier investigations we studied photochemical reactions involving F-centers in KCl crystals.[1,2] In the present report we give the results of measurements of the quantum efficiency of photochemical processes occurring in heated potassium chloride crystals.

The quantum efficiency η of a given photochemical process may be defined[3] as the ratio of the number ΔN of F-centers disappearing from the examined volume of the crystal during a certain time interval Δt under the influence of the incident light to the number ΔM of centers in the same volume absorbing photons during the same interval. It is a simple matter to calculate this quantity on the basis of the fundamental law of photochemical kinetics, written in the form proposed in Ref. 3:

$$-\frac{dN}{N}\cdot\frac{1}{dt}=K\eta\frac{I_0}{h\nu}.$$

Through simple transformations we obtain the following convenient expression for evaluating the quantum efficiency:

$$\eta=\frac{\Delta N}{\Delta M}=\frac{A\delta_F\left(\ln\frac{I_0}{I_1}-\ln\frac{I_0}{I_2}\right)}{\frac{940S}{S_0}\cdot\frac{1}{h\nu_{max\,F}}\cdot\frac{I_0-\overline{I}}{I_0}\Delta t}.$$

Here $A = 1.31\cdot10^{16}$ ev^{-1} ml^{-1} is a constant from the familiar expression for the concentration of F-centers, deduced by Kleinschrod[4] for KCl, δ_F is the half-width of the F-band in ev, I_0 is the intensity of the incident light, I_1 and I_2 are the intensities of the light transmitted through the crystal at the beginning and end of the irradiation interval, respectively, $\overline{I}$ is the mean intensity of the transmitted light during the interval Δt and S and S_0 are the deflections of the galvanometer, respectively, during measurements of the light intensity and during calibration of the thermal column in Hefner candles.

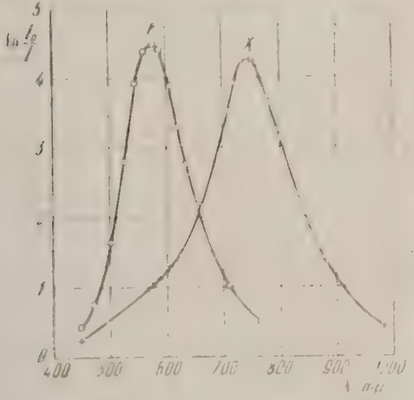

Fig. 1. F and X absorption bands in KCl measured at 280°.

An analogous expression was used by Pick[5] in determining the quantum efficiency of transformation of F-centers into F'-centers.

As may be seen from Fig. 1, the F- and X-bands overlap appreciably. Hence at all times one must add the increasing absorption of the X-centers to the measured value of the absorption at the peak of the F-band. Making use of the expression

$$\tau=\tau_0\exp\left[-\frac{4\ln2\,(h\nu-h\nu_{max})^2}{\delta^2}\right],$$

introduced by Pekar[6] for evaluating the absorption τ corresponding to a given wavelength when the absorption τ_0 at the F-band peak is known, we computed the requisite correction for the overlapping. The final form of the expression used for determining the quantum efficiency was therefore

$$\eta=\frac{A\delta_F\left(\ln\frac{I_0}{I_1}-\ln\frac{I_0}{I_2}\right)\left\{1+\exp\left[-\frac{4\ln2\,(h\nu_{max\,F}-h\nu_{max\,X})^2}{\delta_X^2}\right]\right\}}{\frac{940S}{S_0}\cdot\frac{1}{h\nu_{max\,F}}\cdot\frac{I_0-\overline{I}}{I_0}\Delta t}$$

where δ_X is the half-width of the X-band and $h\nu_{max\,F}$ and $h\nu_{max\,X}$ are the energies of the quanta corresponding to the peaks of the F- and X-bands.

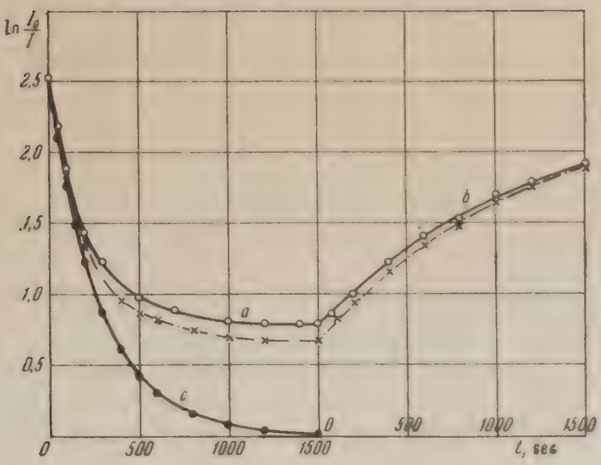

Fig. 2. Time-dependence of the optical density measured at the F-band peak during photochemical disintegration (curve a) and thermal regeneration (curve b) of the F-centers; the calculated variation in optical density in the hypothetical case of absence of thermal disintegration of the F-centers is indicated by curve c. The dash-line curves take into account the overlapping of the F- and X-bands.

At temperatures below 270°, when there is no symmetrical conversion of the F-band to the X-band, the corrections are also simple but must be based on measurements of the absorption at the peak of the new band.

The experiments were carried out on thin samples cut from KCl crystals with uniformly colored (in a homogeneous electric field - see Ref. 7) F-centers, clamped in a special holder mounted in an oven with end windows.

It was most convenient to follow the photochemical transformation of the F-centers by recording at set intervals the indications of a short-period galvanometer connected to a photoelectric cell mounted to receive the monochromated light originating from a 400 watt motion picture projection lamp and passing through the crystal specimen. The monochromator was set for the wavelength of the F-band peak and had a slit width of 0.1 mm. During the measurements with the amylacetate filled thermal column and its calibration in Hefner candles the entire set-up was shielded by means of a large metal box and the light beam utilized was limited by a series of apertures in iron sheets. The temperature of the crystal was gaged by a platinum - platinum+rhodium thermocouple. The overall error did not exceed 20% for the lower quantum efficiency values.

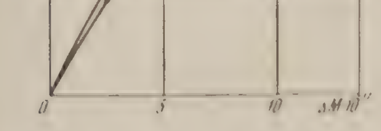

Fig. 3. Curve a - the dependence of the number of centers disappearing as result of irradiation at 280° on number of photons absorbed during the same interval. Curve b - the same dependence computed for case of no thermal disintegration of the F-centers. The slopes of the curves represent the quantum efficiency.

Curves a and b in Fig. 2 show the variation with time of the optical density measured in the course of photochemical decomposition and thermal regeneration of the F-centers. From this data one can calculate the time dependence of the quantum efficiency. Curve a in Fig. 3 shows the variation of the number of centers vanishing under the influence of irradiation at 280° with the number of quanta absorbed during the same interval. Obviously, the slope of this curve represents the quantum efficiency at different times during the process. The initial value, computed for the first 50 sec of irradiation by light, is $\eta_0 = 0.017$.

With time the experimentally determined quantum efficiency falls off, reaching zero at the time the curve representing the photodisintegration of the F-centers becomes parallel to the time axis, although the absorption does not vanish entirely. This paradoxical result is understandable if we recall[1] that there are two opposite processes going on at the same time at 280°: photodisintegration and thermal regeneration of the F-centers; the intensity of these changes with time so that at the end of a certain interval the number of centers destroyed per unit time becomes equal to the number reconstituted. Obviously, we must distinguish

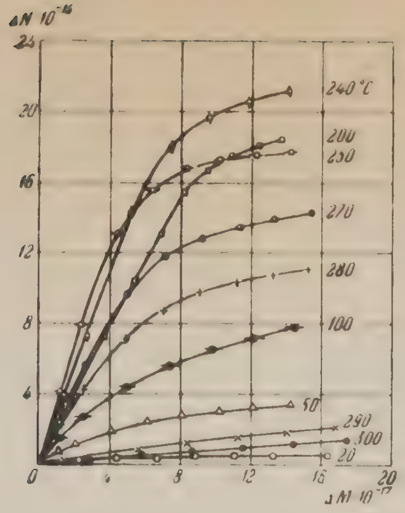

Fig. 4. Dependence of the number of F-centers vanishing on the number of photons absorbed at different temperatures of the KCl crystal.

between two quantum efficiencies, i.e., between the experimentally measured efficiency and the true efficiency characterizing only the actual photochemical activity of the absorbed light without regard to the inverse regeneration process. This true efficiency can be calculated if we can separate the optical and thermal processes.

We attempted to do this in the following manner. Let us assume[1,2] that the photochemical reaction occurring in KCl at temperatures in the 270-300° interval consists in the removal of an electron from an F-center, the formation of an F'-center and the subsequent merging of this center with a halide vacancy, i.e., is schematically described by $2F \rightarrow F_2$, and that it is accompanied by the reverse process of disintegration of F_2-centers. In this case the number of F-centers vanishing from a unit volume of the crystal during a time dt will be given by

$$-dN_F = 2\lambda_F N_F dt - 2\lambda_X N_X dt.$$

where λ_F and λ_X are the respective probabilities of the optical and thermal transformations and N_F and N_X are the concentrations of the F- and X-centers.

Denoting the initial number of F-centers through N_0 and assuming that the electrons remain a very brief time in the conduction band and in the F'-centers, we can write

$$N_F + 2N_X = N_0.$$

These kinetic equations can be readily integrated, taking into account the appropriate boundary conditions. For the process occurring under the influence of light, we obtain

$$N_F = K_F + (N_0 - K_F)\exp[-(2\lambda_F + \lambda_X)t],$$

where $K_F = \frac{N_0\lambda_X}{2\lambda_F + \lambda_X}$.

For the reverse thermal disintegration process, which occurs in the pure form when the incident light is cut off, we obtain

$$N_F = N_0 - (N_0 - K_F)\exp(-\lambda_X t).$$

The resultant time dependences yield curves in quantitative agreement with the curves a and b for the optical densities, reproduced in Fig. 2.* As may be seen from the proportionality between the concentrations and the optical densities, their logarithmic time-dependence curves must be straight lines with corresponding slopes. Hence having determined the slopes $2\lambda_F - \lambda_X$ and λ_X of the straight lines (plotted, for example, on the basis of the dash-line curves in Fig. 2), we can compute the value of $2\lambda_F$, i.e., the constant in the exponent in the expression for the time dependence of the F-center concentration:

$$N_F = N_0\exp(-2\lambda_F t),$$

---

*More detailed information on the kinetics of photodisintegration of F-centers in heated KCl crystals will be published at a later date.

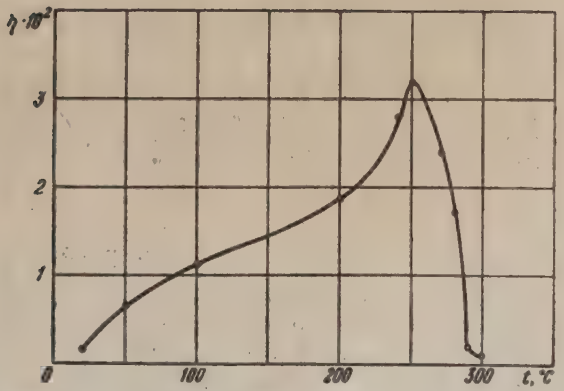

Fig. 5. Temperature dependence of the initial quantum efficiency values as calculated from the initial slopes of the curves of Fig. 4.

which would obtain at the given effectiveness of the incident light provided λ_X were equal to zero, i.e., if there were no reverse temperature disintegration of the X-centers. The calculated dependence is represented by curve c in Fig. 2. Using the optical density values given by this curve we can easily calculate the time dependence of the true quantum efficiency. The ratio of ΔN and ΔM is given by curve b in Fig. 3. The value of the true quantum efficiency for the first 50 seconds of the phototransformation process is $\eta_0 = 0.018$.

With time curve b straightens out relative to curve a, i.e., approaches a linear dependence, corresponding to a constant quantum efficiency.

As is known[1,2] light is capable of effecting the transformation of F-centers in KCl at lower temperatures as well. We carried out measurements of the quantum efficiency at different temperatures. The curves giving the efficiencies, i.e., the ratios of the number of centers undergoing photochemical transformation to the number of photons absorbed, are given in Fig. 4.

The temperature dependence of the initial efficiency values, computed from the slopes of these curves, is shown in Fig. 5, while the numerical values are listed in the accompanying table.

t, °C	$\Delta N \cdot 10^{-14}$	$\Delta M \cdot 10^{-17}$	η_0	t, °C	$\Delta N \cdot 10^{-14}$	$\Delta M \cdot 10^{-17}$	η_0
20	1,83	1,12	0,0016	250	40,3	1,26	0,032
50	7,2	1,09	0,0066	270	32,1	1,34	0,024
100	14,3	1,26	0,0113	280	22,7	1,32	0,017
200	17,8	0,96	0,019	290	2,54	1,41	0,0018
240	39,6	1,42	0,028	300	1,28	1,46	0,0009

The maximum photochemical activity occurs at 250° which is close to the location of the maximum (240°) obtained in the investigation of Ref. 2 for the temperature dependence of the rate of phototransformation in KCl. Just as the rate of transformation, the quantum efficiency falls off rapidly after the maximum due to the enhanced instability of the X-centers, at higher temperatures. At lower temperatures the efficiency (like the rate) is reduced due to decreased ion mobility. The similarity can be readily understood if we recall that there must be a constant proportionality between the rate of a photochemical process at different temperatures and its efficiency.

The low values of the quantum efficiency (under 2-3%) are connected with relatively weak photochemical activity of the absorbed light; apparently in most cases the absorption leads to reverse non-radiative electronic transitions. It is conceivable that the low temperature stability of the F'-centers also plays an important role here (the F'-centers disintegrate before they have a chance to transform to F_2-centers). The question of the return of the electrons from the conduction band to their initial level with radiation requires further investigation.

The difference between the quantum efficiency observed for our photochemical reaction and the much higher (100-fold) efficiency found by Pick[5] in studying the $F \longrightarrow F'$ reaction at low temperatures might be explained by the difference in the mechanism of the transformations (requiring ion mobility in our case) and the

different stability of the F'-centers. Actually, we feel that Pick's round figure of 2 for the efficiency (in KCl) is a gross overestimate. Even if we accept the doubtful assumption that at a certain temperature the electrons excited by the light will go only to other F-centers with the formation of F'-centers (and that none of the electrons will return to their own original holes), the round figure given by Pick is not consistent with uncertainty regarding the value of the constant A in the equation for the F-center concentration.

Summary

1. We describe the measurement procedure and give the results of measurement of the quantum efficiency of the photochemical reversible transformation of F-centers in KCl at 280°.

2. We show the possibility of separating the concurrent, reverse processes of photochemical and thermal transformation and calculate the true quantum efficiency of the photochemical process at the indicated temperature.

3. We determine the temperature dependence of the quantum efficiency of photochemical transformation of F-centers in KCl crystals.

Kiev State University

References

1. A.Shatalov, Doklady AN SSSR, 92, 549 (1953).
2. A.A.Shatalov, Trudy fiz. fak. (Transactions of the Physics Dept. of Kiev State University, 8, 111 (1955).
3. A.N.Terenin, Fotokhimiia krasitelei (Photochemistry of dyes), M.-L. 1947.
4. F.G.Kleinschord, Ann. d. Phys., 27, 97 (1936).
5. H.Pick, Ann. d. Phys., 31, 365 (1938).
6. S.I.Pekar, Issledovaniia po elektronnoi teorii kristallov (Investigations relating to the electronic theory of crystals), M.-L. 1951.
7. A.A.Shatalov, Trudy fiz. fak. (Transactions of the Physics Dept. of) Kiev State University, 6, 43 (1952).

DISCUSSION

A.A.Shiskov: Was photoconductivity observed in the investigated crystals?

A.A.Shatalov: According to our preliminary data, there is photoconductivity.

O.A.Schmidt: To solve problems connected with the structure and arrangement of color centers in the crystal lattice one can use the method of studying photochemical reactions in polarized light, employed by Feofilov in particular. Applying this method to crystals containing F-centers, we detected structural anisotropy which cannot be reconciled with the usual concepts regarding these centers.

LUMINESCENCE EFFICIENCY OF COMPLEX MOLECULES

- B.I.Stepanov

1. According to Vavilov's[1] definition, luminescence is the energy excess radiated by a body over and above the temperature emission where this excess has a finite duration greater than the period of light oscillations. The existence of a thermal background is revealed to some extent in the study of any characteristic of luminescence, including the quantum efficiency. Since the total emission is the sum of two types of emissions, it is necessary to distinguish between the quantum yield of luminescence and the quantum yield of the total emission. The following expression (1) for the quantum yield of the total emission of a system of particles with two energy levels was deduced by us[2]; the expression (2) for the quantum efficiency of luminescence was derived by Alentsev, Antonov-Romanovski, Stepanov and Fok[3]:

$$\beta_{emi} = \frac{An_2'}{B(u_o + S)(n_1' - n_2')} \tag{1}$$

and

$$\beta_{lum} = \frac{(A + Bu_o)n_2' - Bu_o n_1'}{BS(n_1' - n_2')}. \tag{2}$$

Here A and B are Einstein coefficients, while n_1' and n_2' are the numbers of particles on the levels 1 and 2 under constant irradiation and at constant temperature; these numbers depend on the intensity of the incident radiation S, the density of the equilibrium radiation u_o, the ratio $h\nu/kT$ and the probabilities of optical and non-optical transitions between the energy levels.[2]

In the numerator of (2), An_2' is the number of spontaneous 2 → 1 transitions, $Bu_o n_2'$ is the number of 2 → 1 transitions forced by the surrounding thermal radiation u_o. This forcec emission has a certain duration and persists after cessation of excitation to attainment of thermal equilibrium.

Only a part of all the emitted quanta $(A + Bu_o)n_2'$ can be attributed to the luminescence. The radiation detector records only part of these quanta, namely

$$(A + Bu_o)n_2' - Bu_o n_1'.$$

Here $Bu_o n_1'$ is the number of thermal radiation quanta absorbed. The denominator of (2) defines the energy of the external radiation absorbed by the luminescing substance.

Calculation shows that

$$\beta_{lum} = \frac{1}{1 + d/A\ 1 - \exp(- h\nu/kT)}, \tag{3}$$

$$\beta_{emi} = \frac{1 + \dfrac{d\ 1 - \exp(- h\nu/kT)}{A(1 + S/u_o)}}{1 + d/A\ 1 - \exp(- h\nu/kT)}, \tag{4}$$

$$\beta_{emi} \geqslant \beta_{lum}. \tag{5}$$

In contrast with β_{lum}, β_{emi} depends on the density of the incident radiation. At low values of T and large values of ν, equations (3) and (4) go over into the usual equation:

$$\beta_{lum} = \beta_{emi} = \frac{A}{A + d}. \tag{6}$$

At very small values of $h\nu/kT$, β_{lum}, as well as β_{emi}, tends toward unity. Under such conditions the presence of external radiation does not disturb the equilibrium energy distribution over the levels and, consequently, the number of quenchings is equal to the number of non-optical excitations.

2. Most of the luminescence characteristics of complex molecules, including t the quantum efficiency, can be calculated provided the probabilities of transitions with emission $f(E^*)$ and without emission of light $d(E^*)$, as well as the distribution of excited molecules according to their vibrational energy $\rho^*(E)$ are known. The first two quantities are determined by the internal properties of molecules; the function $\rho^*(E)$ depends, in addition, on the excitation conditions and on the nature of the surrounding medium. Investigation of the output of fluorescence and the lifteime of the excited state of substances highly sensitive to various external influences is one of the best means of determining $f(E^*)$ and $d(E^*)$ and clarifying the nature of processes taking place in the excited molecule.

One of the most important laws of luminescence was established by Vavilov[4]: the quantum yield of luminescence by solutions does not depend on the frequency of the exciting light when $\nu_{exc} > \nu_{el}$ and even with $\nu_{exc} < \nu_{el}$ the efficiency continues to be independent up to a certain frequency ν'_{exc}, in the emission band. Above this frequency the quantum efficiency falls off rapidly. The value of ν'_{exc} differs for various molecules: in some cases it is greater than ν_{emi}, in others it coincides with ν_{emi}, and yet in other cases is lower. Vavilov's law is universal; it has been verified for many substances in the solid and liquid states having different degrees of complexity and for different emission mechanisms.[5] The interpretation of Vavilov's law for the case of Stokes excitation is simple; the law takes into account interaction between the excited molecules and the solvent, the transfer of excess vibrational energy developed during the excitation $(h\nu_{exc} - h\nu_{el})$ to the medium, and attainment of the stationary distribution $\rho^*(E^*)$. The exact expression for the quantum output, taking into account energy exchange (but not the thermal background) was deduced by us[7] in the form:

$$\beta = \frac{\bar{f}}{\bar{f} + \bar{d}} = \frac{f(E^*)\rho^*(E^*)dE^*}{f(E^*)\rho^*(E^*)dE^* + d(E^*)\rho^*(E^*)dE^*} \approx \frac{f(\overline{E^*})}{f(\overline{E^*}) + d(\overline{E^*})} . \qquad (7)$$

Here $\bar{f}$ and $\bar{d}$ are the transition probabilities averaged over all values of E^* and characterizing the entire assembly of molecules as a whole. The equation (7) is valid only for Stokes excitation and provided the probability of energy exchange with the solution is much greater than the probabilities $f(E^*)$ and $d(E^*)$ for all values of E^*. In solutions the form of the function $\rho^*(E^*)$ and, consequently, $\bar{f}$, $\bar{d}$ and β are independent of ν_{exc}.

Vavilov formulated his law only for condensed systems. In rarefied vapors exchange of energy with the medium does not occur (during the time τ), and the equation (7) is not directly applicable. It is not surprising that study of the luminescence of vapors (Refs. 7 & 8) led to the discovery of a regularity: as ν_{exc} is reduced within the limits of the Stokes region, the quantum output gradually increases. In passing into the region where $\nu_{exc} < \nu'_{exc}$ it falls off rapidly (just as in solutions). Neporent explained these facts by the hypothesis that the probability d of a non-radiative transition increases with the value of E^*, while the probability f of a radiative transition remains constant.

According to Refs. 7 and 9, for vapors:

$$\beta = \int \frac{f(E^*)}{f(E^*) + d(E^*)} \rho^*(E^*)dE^* = \left\{ \frac{f(E^*)}{f(E^*) + d(E^*)} \right\}_{av} \approx \frac{f(\overline{E^*})}{f(\overline{E^*}) + d(\overline{E^*})} , \qquad (8)$$

where $\overline{E^*}_{(vap)} = \overline{E^*}_{(sol)} + h(\nu_{exc} - \nu_{el})$. If $\partial d(E^*)/\partial E^* > 0$, then, when ν_{exc} increases, E^* increases and, consequently, d decreases.

With increasing temperature, the quantum yield at first remains constant at low temperatures and then drops rapidly at higher temperatures (Refs. 10-12). It follows from this that the probabilities of non-radiative transitions begin to increase at sufficiently large values of E*. That is, temperature quenching is an intra-molecular process; influence of the solvent is secondary.

Neporent[7,8] showed that, at large values of E* enhancement of E* by increasing T or by increasing ν_{exc} have an equal effect on the magnitude of the output. This enabled Neporent to propose a unique optical method for determining the specific heats of excited molecules.

There exists a perfectly definite relationship between the quantum efficiency and the lifetime of the excited state[13,7,9]:

for solutions

$$\frac{\beta}{\tau} = \bar{f} = \int f(E^*)\rho^*(E^*)dE^* \approx f(\overline{E^*}), \qquad (9)$$

for vapors

$$\frac{\beta}{\tau} = \left\{\frac{f(E^*)}{[f(E^*) + d(E^*)]^2}\right\}_{av} : \left\{\left[\frac{f(E^*)}{f(E^*) + d(E^*)}\right]^2\right\}_{av}. \qquad (10)$$

With monochromatic excitation, i.e., provided the maximum of the function $\rho^*(E^*)$ is sufficiently sharp, expression (10) is close to (9). The relationship (9) shows that the ratio β/τ does not depend on the probability of non-radiative transitions. When d is changed by introducing extraneous substances into the solution, the values of β and τ change equally so that their ratio remains constant. In vapors, the ratio β/τ depends on the non-radiative transition probabilities. It follows from (9) that the ratio β/τ for solutions can depend only on the form of the distribution $\rho^*(E^*)$, i.e., only on the temperature. Experiment shows that the ratio β/τ remains constant in a wide temperature range. For solutions of rhodamine B in alcohol or glycerin, for example, it is constant from -50° to +50° (Ref. 12). At sufficiently high temperatures the decrease of τ slows down and the ratio β/τ begins to grow smaller. This proves that at low values of E* the radiative transition probability f does not depend on E*. At higher values of E*, f begins to depend on E* (in the case of rhodamine B, f decreases).

Knowing the forms of the functions f(E*) and d(E*) it is easy to interpret the changes in β and τ produced under the influence of vapors of an extraneous substance[6-8,14,15].

Vavilov[13,16] proposed distinguishing between two types of luminescence quenching. As regards their ultimate results they may be equivalent; the difference between them lies in the nature of the intermediate processes. In the second type of quenching the absorption event is accompanied by transition of the molecule to an excited state. In this case the relations (9) or (10) are applicable. Quenching of the first type takes place in all other cases. This type includes, for example, the weakening of fluorescence with increasing concentration accompanied by molecular association.[10,17,18] It also includes the case of so-called inactive absorption which involves the excitation of very high vibrational levels of the lower electronic state. It is frequently argued that optical transitions within a given single electronic state, associated with large changes in the vibrational energy, are characterized by a low probability. However, this is valid only for simple systems. In complex molecules the anharmonicity of the potential function is extremely great. It is manifested in the redistribution of vibrational energy inside the molecule, the redistribution time being commensurate with the period of vibration. The probability of transitions with a large value of ΔE grows with increasing anharmonicity. In cases of maximal complexity the probability of absorption of a quantum $h\nu = E$ generally no longer depends on the magnitude of the quantum.

When quenching of the first type is taken into account, the equation of the

form (9) becomes (Ref. 16):

$$\beta/\tau = \gamma\beta_0/\tau_0 = \text{const.} \tag{11}$$

Here γ is the fraction of absorption events accompanied by excitation of the electronic state and subsequent fluorescence.

3. The interpretation of various aspects of anti-Stokes fluorescence is the most difficult and controversial part of luminescence studies.

The dependence of the output on ν_{exc} in anti-Stokes excitation is virtually identical in vapors and solutions.[6] This contradicts Pringsheim's[20] view that the anti-Stokes drop in efficiency is associated with the influence of the solvent.

The elementary event of absorption and subsequent emission of light at a frequency $\nu_{exc} < \nu'_{exc}$ is connected with the conversion of thermal energy into radiant energy. This explains the strong temperature dependence of anti-Stokes fluorescence. At T = 0, such fluorescence is impossible. On the other hand, the higher the temperature, the lower the specific requirement for anti-Stokes excitation and the smaller the fall in efficiency.[21] Experimental studies of the influence of temperature (Ref. 22) agree with these basic assumptions.

Sveshnikov[23] and Neporent & Borisevich[6] discovered that the decrease in output with lowering of ν_{exc} is not accompanied by a decrease in the duration of fluorescence. Their data are not altogether reliable and must be checked by observations on a larger number of substances. Nevertheless they point to the special character of the quenching in the case of anti-Stokes excitation.

The decrease in efficiency with anti-Stokes excitation must find an explanation in terms of processes occurring in individual molecules. Difficulties encountered in doing so have led to attempts to develop phenomenological explanations of the decrease in output (Refs. 21, 24 & 25).

The energy and quantum outputs are related by the equation:

$$\Gamma = \beta\bar{\nu}_{emi}/\nu_{exc} \tag{12}$$

If a purely thermodynamic proof of the relationship

$$\Gamma \leqslant 1 \tag{13}$$

could be found, then this would constitute a novel explanation for the decrease of β actually observed. Attempts at such proof have been based on the method of ideal cycles. The most widely discussed is the cycle proposed by Adirovich.[24] Antonov-Romanovski, Stepanov, Fok and Khapaliuk[26] have recently shown that Adirovich's deductions are incorrect. He assumed that there exists a luminophor capable of completely transforming light of frequency ν' into light of frequency ν. Such a luminophor is thermo-dynamically impossible. Moreover, Andirovich does not take into account in his analysis the unavoidable thermal background which leads to a certain transfer of heat from the hot body to the cold and can compensate the reverse transfer involved in the luminescence.

Landau[25] investigated the problem of output taking into account the change in entropy of the radiation. He obtained an upper limit for Γ. However, this imposes virtually no new limitations since at low emission densities the limit itself tends to ∞. Pringsheim[27] has expressed the hypothesis that Γ can exceed unity. He examined a system of three levels (Fig. 1): the first two are vibration levels of the lower electronic state, the third is the upper electronic state. On excitation by a frequency ν_{32} an anti-Stokes line of frequency ν_{31} appears in the spectrum. Assuming that $\beta = 1$, he comes to the conclusion that $\Gamma > 1$. Pringsheim's arguments are not altogether convincing. He fails to take into account non-radiative transitions and the influence of the thermal radiation background.

The extended debate about the validity of the relationship (13) has recently

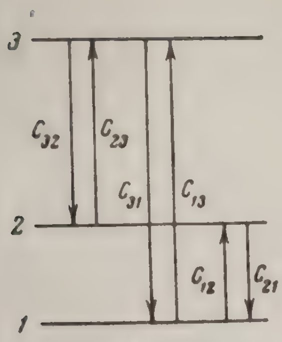

Fig. 1.

been resolved in Refs. 2,3 & 26. The authors of Ref. 26 carried through an exact calculation of the output for the same system of particles, taking into account optical and non-optical transitions between all levels of energy and the thermal radiation in the volume under consideration. The thermodynamic equilibrium is disturbed as a result of the influence of the external radiation of frequency ν_{32}. The spectral composition of the emission becomes rather unique: at the frequencies ν_{31} and ν_{32} there will be an excess over the thermal emission at the temperature T, while at the frequency ν_{21} there be a deficiency. The excess energy at the frequencies ν_{31} and ν_{32} constitutes the ordinary luminescence[1]. The deficit of energy at the frequency ν_{21} has been dubbed the negative luminescence by the authors of Ref. 26. The total energy output is given by

$$\Gamma = 1 - \frac{d_{31}c_{21}\nu_{31}/\nu_{32} + d_{32}[c_{21} + c_{31}\exp(-h\nu_{32}/kT)] - d_{21}c_{31}\nu_{21}/\nu_{32}}{c_{21}c_{32} + c_{21}c_{31} + c_{32}c_{31}\exp(-h\nu_{32}/kT)} . \tag{14}$$

Here c_{ij} is the total transition probability, while d_{ij} is the probability of a non-radiative transition. For certain values of the ratio between these two probabilities the output (efficiency) becomes greater than unity. Such systems are thermodynamically impossible, of course. The entire process reduces to a transfer of energy from the light source at a temperature $T' > T$ to the whole system of particles together with the surrounding medium at the temperature T. A substance for which $\Gamma > 1$ may be likened to the refrigerant in a refrigerating machine.

Let us now examine the intra-molecular "mechanism" of anti-Stokes fluorescence. In the process of excitation the vibrational energy of the individual molecule decreases $(E^* < E)$. However, it does not directly follow from this that $\overline{E^*} < \overline{E}$. If the probability of absorption increased with increasing E, then only the molecules for which $E > \overline{E}$ would participate in the absorption events. For such "hot" molecules the loss of the small amount of energy $h(\nu_{el} - \nu_{exc})$ would be of no particular importance and, therefore, we would have $\overline{E^*} > \overline{E}$. If only "hot" molecules were raised to the excited state, this would open the way to a relatively straightforward explanation of the decrease in output when $\nu_{exc} < \nu_{exc}$. Experiment shows, however, that $\overline{E^*} < \overline{E}$. This was proved by Borisevich[28] who investigated the stimulation and attenuation of fluorescence under the influence of extraneous gases. With $\nu_{exc} > \nu_{el}$ the introduction of extraneous gases increases the output, while with $\nu_{exc} < \nu_{el}$ the yield is decreased. The latter can occur only if $\overline{E^*} < \overline{E}$. This inequality is substantiated by the absence of an anomaly in the variation of the quantum output with ν_{exc} at the point $\nu_{exc} = \nu_{el}$. The anti-Stokes decrease in output begins at lower values of ν_{exc} and is apparently not associated with changes in the vibrational energy store of the molecule.

Under anti-Stokes excitation the decrease in the quantum output is not accompanied by a decrease in τ. Analyzing this fact, Tumerman[22] and Vavilov[29] came to the conclusion that anti-Stokes quenching should be classified as quenching of the first type, and associated with non-exciting absorption. The experiments of Borisevich support this hypothesis.

A fairly reliable picture of the process can be drawn on the basis of the available experimental facts. In Levshin's book[10] an attempt is made to deduce the function $\beta(\nu_{exc})$. The derivation itself is not rigorous but its basic idea, it seems to us, is correct.

Let the system absorb external radiation of frequency $\nu_{exc} > \nu_{el}$. The greatest probability is that the absorption will result in excitation of the electronic shell

and a small increase of E ($E = h(\ _{exc} - \ _{el})$). Much less probable (by several orders of magnitude) are the purely vibrational transitions not accompanied by excitation of the electronic shell. The total number of absorbed quanta is

$$N = N_{el} + N_{vib} = n_1 \int_{E=0}^{\infty} \rho(E) a_{el}(E, \nu_{exc}) dE + n_1 \int_{E=0}^{\infty} \rho(E) a_{vib}(E, \nu_{exc}) dE, \qquad (15)$$

where n_1 is the total number of molecules in the lower electronic state and a_{el} and a_{vib} are the probabilities of the exciting and non-exciting transitions, respectively. With $\nu_{exc} > \nu_{el}$ the second term does not have any effect; the total amount of energy absorbed depends on the properties of the function a_{el}; the yield, on the quenching processes occurring in the excited electronic state.

Different relationships obtain in the region where $\nu_{exc} < \nu_{el}$. Not all molecules but only those for which $E > h(\nu_{el} - \nu_{exc})$ can participate in an exciting absorption event. Hence in this case

$$N_{el} = n_1 \int_{E=h(\nu_{el}-\nu_{exc})}^{\infty} \rho(E) a_{el}(E, \nu_{exc}) dE = n_1 a_{el}(\nu_{exc}). \qquad (16)$$

Here $a_{el}(\nu_{exc})$ is the probability of absorption of the frequency ν_{exc}, averaged over all values of E and measured experimentally. As ν_{exc} decreases (from the point $\nu_{exc} = \nu_{el}$) the value of $a_{el}(\nu_{exc})$ falls off rapidly (especially at low temperatures). At the same time the probabilities of exciting absorption change not at all or very slowly ($a_{vib} \approx$ const.). The corresponding transitions take place from all levels beginning with $E = 0$, regardless of ν_{exc}.

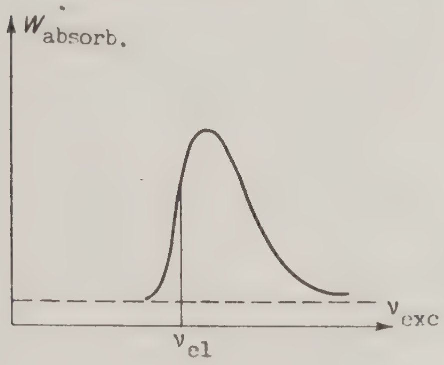

Fig. 2.

The curve giving the dependence of the absorption power W_{abso} on ν_{exc} is shown in Fig. 2. The dash-line indicates the non-exciting absorption power. This can be neglected in the $\nu_{exc} > \nu_{el}$ region in general and in the region $\nu_{exc} < \nu_{el}$ for small departures from ν_{el}. With large deviations from ν_{el}, the non-exciting absorption power becomes noticeable and finally preponderant. As is shown by analysis of the experimental data obtained by various investigators for other purposes, far from ν_{el} the absorption power (coinciding with the non-exciting absorption power) actually depends little on ν_{abso}.

In the presence of non-exciting absorption the quantum output is

$$\beta = \beta' \frac{W_{el}}{W_{vib} + W_{el}} = \beta' \frac{N_{el} h\nu_{exc}}{(N_{el} + N_{vib}) h\nu_{exc}} = \beta' \frac{N_{el}}{N_{el} + N_{vib}}. \qquad (17)$$

In the region where $\nu_{exc} \geqslant \nu_{el}$, $\beta = \beta'$; the magnitude of the yield is determined by the properties of the excited electronic state and, primarily, by the amount of vibrational energy. As ν_{exc} decreases, beginning with ν_{el}, the ratio $N_{el}/(N_{el} + N_{vib})$ for some time remains close to unity in spite of the decrease of N_{el}. Later N_{el} and N_{vib} become comparable, and the quantum efficiency β becomes less than β'. The value of the frequency ν'_{exc}, corresponding to the beginning of the anti-Stokes fall-off in output, depends on the magnitude of N_{vib} and the rate of decrease of N_{el}. In different molecules it can assume different values and is in no way related to the maximum of the emission band. At the very edge of the absorption band the value of N_{el} falls to zero and the absorption is determined by the value of N_{vib}. In this region of the excitation spectrum

$$\beta(\nu_{exc}) = \beta'(N_{el}/N_{vib}) \qquad (18)$$

Since N_{vib} and β' depend relatively little on ν_{exc},

$$\beta(\nu_{exc}) = CN_{el} = C'a_{el}(\nu_{exc}) \tag{19}$$

It follows from (19) that the dependence of the quantum yield of anti-Stokes fluorescence on the frequency of the exciting light coincidences with the frequency variation of the probability of absorption, or (what is equivalent) of the coefficient of absorption. Both have the same temperature dependence. Increase in T leads to an increase in the absorption coefficient (with $\nu_{exc} < \nu_{el}$) and to a proportional increase in the quantum output.

Relationships (17)-(19) are derived here for the first time. They can be readily checked experimentally. Existing experimental data do not allow of an exact quantitative verification of the equations (17)-(19), but are in qualitative agreement with them. The output begins to fall off just where the magnitude of the absorption coefficient becomes very small.

The equations (17)-(19) are applicable not only to complex molecules, but to any system and, in particular, to crystal phosphors.

To explain the details of the effect and to develop a more exact theory of anti-Stokes fluorescence, it is essential to study the shapes of the absorption bands and the fluorescence output jointly.

References

1. S.I.Vavilov, Collected works, Vol. II, pp. 293 & 315, M.-L. 1952.
2. B.I.Stepanov, Doklady AN SSSR, 99, 971 (1954).
3. M.N.Alentsev et al, Zhur. eksp. i teor. fiz., 28, 253 (1955).
4. S.I.Vavilov, Collected works, Vol. I, pp. 150 & 222, M.-L. 1954.
5. M.N.Alentsev, Trudy (Transact. proçeedings) Phys. Inst. of the Ac. of Sc., 5, 499 (1950).
6. B.S.Neporent & N.A.Borisevich, Doklady AN SSR, 44, 447 (1954).
7. B.S.Neporent & B.I.Stepanov, Usp. fiz. nauk, 43, 402 (1951).
8. B.S.Neporent, Zhur. fiz. khim., 13, 965 (1939); ibid, 24, 1219 (1950).
9. B.I.Stepanov, Izv. AN Byelorussian SSR, 5, 65 (1954).
10. V.L.Levshin, Fotoliuminestsentsiia zhidkikh i tverdykh tel (Photo-luminescence of solids and liquids), M.-L. 1951.
11. A.N.Sevchenko, Trudy (Transactions) State Optical Inst., 15, 65 (1941).
12. M.D.Galanin, Trudy (Transac.) Phys. Inst. of the Ac. of Sc., 5, 339 (1950).
13. S.I.Vavilov, Collected works, Vol. I, p. 424 M.-L. 1954.
14. N.A.Borisevich et al, Doklady AN SSSR, 44, 37 (1954).
15. N.A.Borisevich, Doklady AN SSSR, 99, 695 (1954).
16. S.I.Vavilov, Collected works, Vol. II, p.190, M.-L. 1952.
17. V.L.Levshin, Doklady AN SSSR, 1, 474 (1935); Acta Phys. chem. USSR, 2, 221 (1935).
18. V.L.Levshin, Zhur. eksp. i teor. fiz., 28, 201, 213 (1955).
19. B.I.Stepanov, Zhur. eksp. i teor. fiz., 28, 559 (1955).
20. P.Pringsheim, Fluorescence and Phosphorescence (in Russ. trans.) M. 1951.
21. S.I.Vavilov, Collected works, Vol. II, pp. 238 & 246, M.-L. 1952.
22. L.A.Tumerman, Trudy (Transact.) Phys. Inst. of the Ac. of Sc., 4, 77 (1938).
23. B.Ia.Sveshnikov, Trudy (Transact.) State Optical Inst., 12, 108 (1935).
24. A.I.Adirovich, Nekotorye voprosy teorii liuministsentsii (Some problems in the theory of luminescence), M.-L. 1951.
25. L.D.Landau, J. of Phys.USSR, 10, 503 (1946).
26. V.V.Antonov-Romanovski et al, Doklady AN SSSR, 105, 50 (1955).
27. P.Pringsheim, J. of Phys. USSR, 10, 495 (1946).
28. N.A.Borisevich & B.S.Neporent, Present issue of the Bulletin.
29. S.I.Vavilov, Collected works, Vol. I, p. 438, M.-L. 1954.

DISCUSSION

A.N.Terenin: What is your evaluation of the oscillators strengths in inactive absorption?

B.I.Stepanov: Small. Inactive absorption is manifested only in the tail of the absorption band; it is noticeable however and does not drop to zero.

V.L.Levshin: in studying the quantum efficiency, in what specific cases must the thermal background be taken into account?

B.I.Stepanov: In the case of electronic spectra the influence of the thermal background is negligible and may be ignored up to temperatures of 300°. The thermal background becomes important for infrared luminescence and at high temperature.

B.S.Neporent: The hypothesis of inactive absorption in the anti-Stokes region, in my opinion, is correct and is in accord with the views of a number of authors. The conclusions regarding the connection between the point at which the efficiency falls off and region of small values of the absorption coefficient and of the independence of this point of height of the electronic energy level is debatable, however, and is not fully supported by experimental facts.

B.I.Stepanov: Our deduction follows from the basic assumption regarding inactive absorption. One cannot agree with the basic thesis and then question its consequences. Convincing proof is difficult due to the lack of adequate experimental data. We used the values of the efficiency and of the absorption coefficient obtained Neporent and Borisevich and obtained satisfactory results.

G.A.Kundzich: Because the results obtained by us in the laboratory of the Kiev State University relate directly to the subject of the report, I will take the liberty of showing two graphs and making a few remarks.

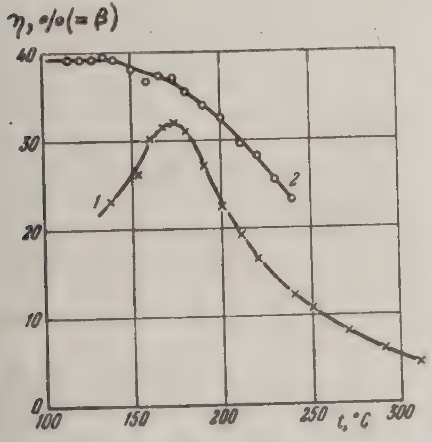

Fig. 1.

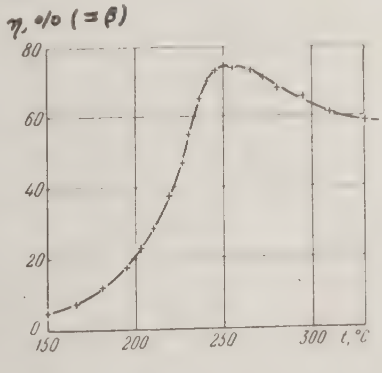

Fig. 2.

Fig. 1. Temperature dependence of the quantum efficiency of luminescence from 3,6-tetramethylaminophthalimide vapor (λ_{exc} = 436 mμ): 1) tetramethylaminophthalimide vapor alone, 2) the same plus ether vapor.

Fig. 2. The same as for Fig. 1, but for 3,6-diaminophthalimide vapor.

The temperature quenching of the fluorescence of vapors of organic molecules has been observed repeatedly. It was observed by us most thoroughly for certain phthalimides. It has an exponential character and, as can be seen from Fig. 1, has different effectiveness for different substances. We were interested in going into the low temperature region, since, by extrapolating temperature quenching curves to this side, we get a value of $\beta_{lum} = 1$ already at sufficiently high values of t (for tetramethylaminophthalimide, at 120-130°) and 2) it was of interest to find the temperature of the transition, predicted by theory, from the

temperature independence β_{lum} to temperature quenching. In doing so we discovered a new effect — temperature stimulation of the fluorescence of the vapors of the two phthalimides studied. The rise in efficiency with t has an exponential character (Fig. 1, curve 1 and Fig. 2). With the addition of a high concentration of ether vapor (of the order of 2-3x10^{20} molecules/ml) to the 3,6-tetramethylaminophthalimide vapor the temperature stimulation disappears (Fig. 1, curve 2); the output at first holds constant and then, at t = 140-150° begins to fall somewhat more slowly than in the case of the pure vapor. In the case of a solution of the given substance in ether, the temperature quenching of the luminescence is also not apparent in going from 20 to 130°. Ether as a solvent is characterized by the fact that in it the luminescence yield of 3,6-tetramethylaminophthalimide is of the same order as the maximum yield in vapors with excitation in the neighborhood of the purely electronic transition (λ = 436 mμ) and even higher, while in all other solvents studied by us the absolute value of the output is lower than from the vapor, that is, ether does not have a quenching effect. In all solvents, except ether, temperature quenching is observed at temperatures above 20°. It is clear, therefore, that temperature quenching in solvents, in that region of temperatures where it does not exist in vapors, is the result of intensification of purely external quenching, i.e., quenching by the solvent, and not the result of internal conversion. This shows that one cannot draw conclusions regarding variation of the probability of non-radiative transitions on the basis of investigations of the temperature dependence of the photoluminescence efficiency.

It is still difficult to give an unambiguous explanation of the observed temperature stimulation of luminescence. It is essential to study the vapor absorption spectra at these temperatures. Possibly molecular association is involved, although no one has so far observed any tendency of the phthalimides to associate under any conditions. Perhaps the effect can be explained by assuming that the excitation and emission processes involve a metastable level and that there is a high probability of non-radiative transitions from the metastable to the ground level.

ABSOLUTE PHOTOLUMINESCENCE EFFICIENCY OF ANTHRACENE AND NAPHTHALENE CRYSTALS

-M.D.Borisov & V.N.Vishnevski

We measured the absolute photoluminescence efficiencies of anthracene and naphthalene crystals by the method of an integrating sphere and photographic plates.

The copper sphere, the bottom part of which terminated in a heavy copper rod, was mounted in a glass cryostat with quartz windows. In photographing the luminescence spectrum at low temperature the cryostat was filled with liquid nitrogen to the level of the bottom of the sphere. The copper rod immersed in the nitrogen insured adequate cooling of the sphere.

The sphere had two openings: the first served to admit the light exciting the luminescence in the crystal suspended approximately at the center of the sphere; the second served for emission of the luminescence, which upon emerging from the sphere was focused on the spectrograph slit. Measurements showed that a crystal suspended in the sphere was cooled to -180° when the cryostat was filled with liquid nitrogen.

The inside walls of the sphere were coated with a layer of magnesium oxide. As a result the luminescence excited in the crystal underwent multiple reflection inside the sphere before emerging from the window. A suitable screen was mounted in front of this second aperture in the sphere to shield the spectrograph slit from direct light from the crystal.

After photographing the luminescence spectrum, a plate covered with magnesium oxide was mounted in place of the crystal and the excitation spectrum was rephotographed in the same manner. In both cases the intensity of the light beamed into the sphere was the same and the same fraction of the total luminous energy inside the sphere fell on the spectrograph slit. If the two fractions are measured in the same units, their ratio will be the value of the absolute technical luminescence efficiency.

Together with the luminescence and excitation spectra we photographed the spectrum of a hydrogen discharge tube having known spectral characteristics on the same photographic plate. The hydrogen tube spectrum was used as the reference in measuring the intensities of the lines in the luminescence and excitation spectra.

The photographic record of the luminescence spectrum obviously also comprises the spectrum of the light incident on the crystal. This spectrum is due to reflection of the light from the surfaces of the crystal. The intensities in this spectrum were measured as described above (i.e., with reference to the hydrogen calibration spectrum). This made it possible to make an appropriate correction for the reflection of light from the crystal. No special correction was made for the variation of the reflecting power of MgO with the wavelength.

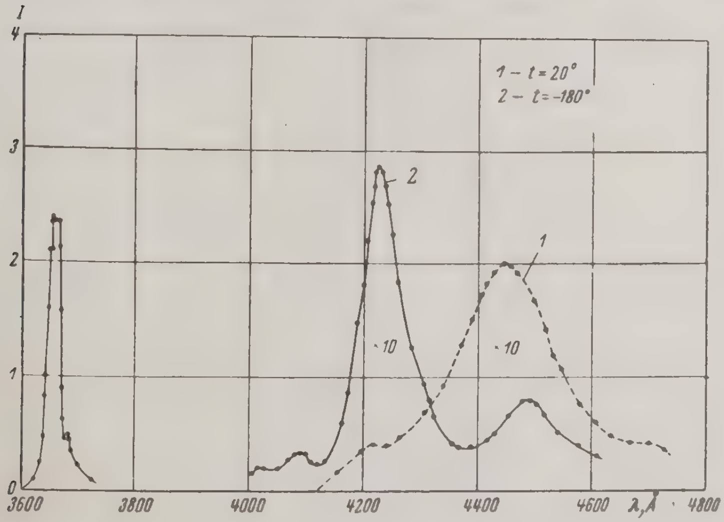

Fig. 1.

For the purpose of the experiments, specimens approximately 1 mm thick were chipped from large crystals of anthracene and naphthalene. In the case of anthracene we also carried out a number of experiments with a single crystal 3μ thick.

The luminescence spectra of the anthracene crystal approximately 1 mm thick at room

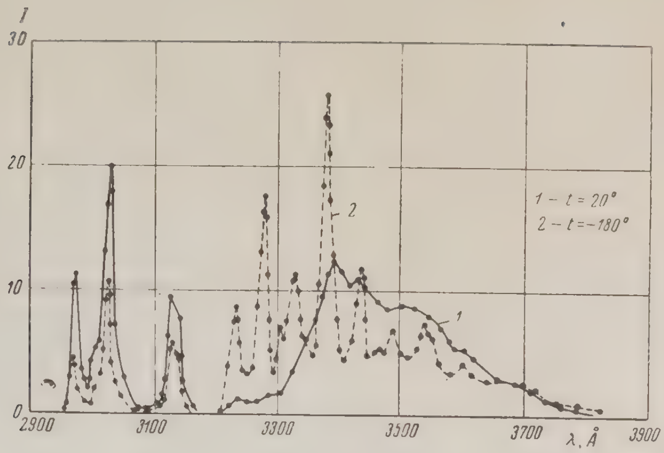

Fig. 2.

Values of the absolute technical and quantum luminescence efficiencies of naphthalene and anthracene crystals at +20 and -180° C

Substance		Crystal		
		Thick		Thin
		+20°	-180°	+20°
Naphthalene	W_t	0.37	0.80	
	W_q	0.42	0.90	
Anthracene	W_t	0.68	0.70	0.70
	W_q	0.83	0.80	0.80

temperature and at -180° are shown in Fig. 1 (the spectrum of the thin anthracene crystal is not shown). The excitation spectrum is given at the left in the figure (on the previous page).

Fig. 2 shows the luminescence spectra of the thick naphthalene crystal at 20 and -180°; again the excitation spectrum is indicated at the left. In both figures the intensity scales of the excitation and luminescence spectra are in the ratio of 1:10.

The values of the absolute technical and quantum luminescence efficiencies obtained from these spectral curves are listed in the accompanying table.

It will be seen from the curves of Fig. 1 that the luminescence spectrum of the thick anthracene crystal is greatly dependent on the temperature. The increase in intensity in the short-wave region with decreasing temperature may be interpreted as the result of reduced overlapping of the absorption and luminescence spectra. It will be seen from the curves in Fig. 1 that the peak in the vicinity of 4450 A falls off sharply in going from room temperature to that of liquid nitrogen. The area under the spectral curve, in contrast, remains virtually constant.

In the luminescence spectrum of the 3μ thick anthracene crystal the intensity of the band at 4450 A at room temperature is already lower than the intensity of the band at 4225 A. The shape of the luminescence spectrum of the thin crystal differs from both of the curves shown in Fig. 1, but the luminescence efficiency is virtually the same as for the thick crystal. It must be concluded therefore that at room temperature we have not simply absorption of the luminescence energy in the short-wave part of the spectrum but also transformation of the absorbed energy into energy at lower frequencies.

Usually the energy of the reabsorbed radiation is transformed into heat; in the case of anthracene, however, non-radiative processes play only a minor role and the absorbed luminescence energy can be re-emitted. After a number of such absorptions and re-emissions the luminescence energy is finally radiated in the long-wave region where there is virtually no absorption.

The fact that the technical luminescence efficiency of the naphthalene crystals at room temperature is relatively small is indicative of the important part played by quenching processes in naphthalene. As may be seen from Fig. 2 there is no evidence of transformation of the reabsorbed energy into lower frequency radiation in the case of the naphthalene crystal. The absence of this effect indicates that in naphthalene there do occur processes resulting in the transformation of the excitation energy into heat.

Our value of the quantum efficiency of the naphthalene crystal at room temperature does not agree with the data of Galanin & Chizhikova[1] and of Bowen et al.[2]

Inasmuch as these investigators worked with naphthalene powder, we also measured the output of powdered naphthalene. At room temperature we obtained for the powder $W_t = 0.33$ and $W_q = 0.37$, i.e., values differing little from those obtained for the crystal.

Physics Institute of the
Academy of Sciences of the Ukranian SSR

References

1. M.D.Galanin & Z.A.Chizhikova, Zhur. eksp. i teor. fiz., 26, 624 (1954).
2. E.J.Bowen, E.Mikiewicz & F.W.Smith, Proc. Phys. Soc., A62, 26 (1949).
3. F.I.Polovikov, Doklady AN SSSR, 71, 453 (1950).

DISCUSSION

M.U.Belyi: What do you understand under the term "technical efficiency"?

M.D.Borisov: This is the efficiency without taking reabsorption into account.

E.V.Shpol'ski: I would like to mention here an investigation carried out some five years ago by Polovikov[3] who measured the quantum efficiency of anthracene and its derivatives by the sphere method employing photoelectric recording. The result for anthracene was the same; in the case of substitution of a chlorine atom in the 9th position the output decreases; in the case of dichlor-substituted anthracene the efficiency increases.

M.D.Galanin: A repetition of our experiments confirmed our original value of about 16% for the quantum efficiency of the photoluminescence of naphthalene. The divergence between our data and that reported by the speaker may be explained by the fact that he did not take into account the decrease in the reflection coefficient of magnesium oxide in the far ultraviolet region.

BULLETIN of the Academy of Sciences of the USSR - Physical Series
Vol. 20, No. 4, 1956 - Transactions of the Fourth Conference on Luminescence

TABLE OF CONTENTS

	Page Orig.	Page Trans.
Opening address - V.L.Levshin	379	345
Intermolecular energy transfer manifested in sensitized luminescence (Abstract) - A.N.Terenin & V.L.Ermolaev	382	348
Exciton state of an imperfect molecular crystal (Abstract) - A.S.Selivanenko	383	348
Transfer of excitation energy from the solvent to the dissolved luminophor in liquid and solid solutions - T.P.Belikova, M.D.Galanin & Z.A.Chizhikova	384	349
Calculation of the mean radiative lifetime of impurity centers and localized excitations in the excited state - A.F.Lubchenko	388	353
Luminescence of organic materials under the influence of particles and hard radiation - M.D.Galanin	392	356
Effect of association and other physico-chemical factors on the luminescence and absorption of complex molecules in solution - V.L.Levshin	397	362
Concentration effects in solutions of quinoline dyes - L.D.Derkacheva	410	374
Luminescence and absorption in concentrated solutions of 3,6-diaminoacridine - V.L.Levshin	419	382
Concentration effects in rhodamine solutions - V.L.Levshin and E.G.Baranova	424	387
Influence of concentration on the luminescence of alcohol solutions of acridine orange at -180°C - L.A.Kuznetsova and B.Ia.Sveshnikov	433	394
Influence of organic impurities on the aggregation of dyes in water solutions - Kh.L.Arvan	443	403
Obscure reactions in dyes - A.T.Vartanian	448	407
Regularities in the fluorescence and absorption spectra and the energy levels of complex molecules (Abstract) - B.S.Neporent	455	413
Absorption and emission band contours of complex molecules - B.I.Stepanov	458	416

Luminescence of uranyl salt solutions - A.N.Sevchenko and L.V.Volod'ko	464	422
Influence of the solvent on the luminescence spectrum of aromatic hydrocarbons at low temperatures - E.V.Shpol'ski & L.A.Klimova	471	428
Spectra and anti-Stokes and Stokes fluorescence yields of aromatic compounds (Abstract) - B.S.Neporent & N.A.Borisevich	476	434
Influence of extraneous gases on the spectra and fluorescence yield of vapors of aromatic compounds (Abstract) - N.A.Borisevich & B.S.Neporent	477	435
Absorption and fluorescence spectra and the quantum efficiency of fluorescence of certain meso-derivatives of anthracene - A.S.Cherkasov	478	436
Luminescence of color centers in fluorite crystals - G.A.Tishchenko & P.P.Feofilov	482	440
Quantum efficiency of photochemical transformation of F-centers in heated KCl crystals - A.A.Shatalov	488	445
Luminescence efficiency of complex molecules - B.I.Stepanov	493	450
Absolute photoluminescence efficiency of anthracene and naphthalene crystals - M.D.Borisov & V.N.Vishnevski	502	459

Translated by
Columbia Technical Translations,
5 Vermont Ave., White Plains, N.Y.

Transactions

# of the

Fourth Conference on Luminescence

(Continued from Vol.20, No. 4)

INVESTIGATION OF THE ABILITY OF COMPLEX ORGANIC MOLECULES TO FLUORESCE AND PHOSPHORESCE

- V.V.Zelinski, M.P.Emets, V.P.Kolobkov & L.G.Pikulik

The fluorescence and phosphorescence yields of substances are the result of competition between different transitions of the excited molecules, the probability of each of which depends in a different manner on the structure and ambient conditions of the molecule.

We investigated the influence of different factors on the probabilities of different transitions of excited molecules:

1) r -- the probability of transition from the labile level to the metastable level;

2) q_1 -- the transition probability from the labile level to the ground level without emission;

3) q_2 -- the transition probability from the metastable level to the ground level without emission;

4) π -- the transition probability from the metastable level to the ground level with emission.

Influence of different factors on the probability r of transitions from the labile to the metastable level. In some cases the value of r is decisive where the quantum yield of fluorescence is concerned.[1] There are a number of facts that indicate that the probability p of radiative transitions from the labile level to the ground level is relatively stable. Hence the dependence of r on different factors can be investigated by measuring the ratio r/p. In the absence of quenching on the metastable level this ratio is equivalent to the ratio of the quantum yields of phosphorescence and fluorescence: Y_{ph}/Y_{fl}.[2]

Influence of temperature on r. Apparently the value of r, just as the probability of a spontaneous transition,[3] is independent of the temperature. The relative yield of short wave phosphorescence of phenanthrene vapor[4] is equal to the yield of long-wave phosphorescence of the compound in a frozen alcohol solution at -196° (Table 1). The ratio Y_{ph}/Y_{fl} also remains reasonably steady in the case of fluorescein in the temperature range from -196° to +20°.

Table 1

Relative phosphorescence yields of solutions and vapors

Substance	At -196°	At higher temperatures
Phenanthrene	0.22 in ethyl alcohol	0.25 in vapor at 300°
Fluorescein	0.4 in sulfuric acid	0.45 in boric acid at 20°

The fact that r remains constant is also indicated by the invariability of the quantum yield of fluorescence in the -196° to +20° range of certain phthalimides having an appreciable value of the r/p ratio.

The quantum yield of fluorescence of 3-acetylamino-N-methylphthalimide in ethyl alcohol equals 0.1 at both 20° and -196°; the yield of 4-acetylamino-N-methylphthalimide at both temperatures is 0.7. At present we can cite no instances of variation of r with temperature.

Influence of the solvent on r. The figures given in Table 1 show the stability of r in certain compounds as regards the medium as well. The ratio of the quantum yields of phosphorescence and fluorescence of phenanthrene is the same in the vapor and the solid solution. In other cases the value of the ratio Y_{ph}/Y_{fl} is markedly dependent upon the solvent. In neutral and weakly polar solvents (n-hexane, carbon tetrachloride, benzene, ether and chloroform) the ratio for most compounds is small.

For many compounds the value of Y_{ph}/Y_{fl} is appreciably greater in polar than in neutral solvents. For 3-acetylamino-N-methylphthalimide Y_{ph}/Y_{fl} equals 0.33

in benzene, 0.37 in hexane, 0.20 in carbon tetrachloride and goes up to 2.2 in methyl alcohol and 3.2 in pyridine. For 3,6-diacetylamino-N-methylphthalimide the value of this ratio in benzene and hexane is under 0.01, while in butyl alcohol it is 0.27 and in pyridine it is 0.17. However there appears to be no direct relationship between the value of Y_{ph}/Y_{fl} and the dipole moment of the medium (Table 2).

Y_{ph}/Y_{fl} rises to an exceptional degree in solvents whose molecules contain bromine (in propyl bromide, ethylene bromide and bromoform). In the case of 3-acetylamino-N-methylphthalimide in ethylene bromide $Y_{ph}/Y_{fl} \geqslant 50$. For 3,6-diacetylamino-N-methylphthalimide in bromoform the ratio equals 0.46 as against 0.16 in methyl alcohol and 0.001 in carbon tetrachloride. The introduction of hydrobromide and hydroiodide salts into the solution also usually results in an increase in Y_{ph}/Y_{fl}. Thus, for example, in the case of 3-acetylamino-N-methylphthalimide in methyl alcohol the value of the ratio rises from 2.2 to over 12 upon the addition of potassium iodide to the solution; in the case of 4-acetylamino-N-methylphthalimide in methyl alcohol the corresponding values are 0.1 and 0.6 (see Table 2).

In order to make sure that the increase in the value of Y_{ph}/Y_{fl} is due to an increase in r rather than to more intense fluorescence quenching, we measured the absolute quantum yields of phosphorescence and fluorescence at -196°. In the case of 4-acetylamino-N-methylphthalimide in methyl alcohol the quantum yield of fluorescence decreases by a factor of 3.7 (from 0.66 to 0.18) with the addition of potassium iodide, whereas the phosphorescence yield increases almost twofold (from 0.06 to 0.11). For β-acetylaminonaphthalene the total luminescence yield at -180° in ethyl alcohol remains virtually unchanged upon the addition of potassium iodide (0.47 and 0.48, respectively). The fluorescence yield at -180° falls from 0.36 to 0.24 as the result of addition of KI; at the same time the phosphorescence yield increases from 0.12 to 0.24. The duration of phosphorescence is somewhat reduced (qualitative observations). The increase in the phosphorescence yield with the introduction of a quencher clearly indicates that r increases. The decrease in fluorescence yield in this case is due entirely to an increase in the probability of transitions to the metastable state.

The decrease and the duration of phosphorescence incident to the addition of the quenching agent is evidence that the quenching occurs on the metastable level of the molecule. Consequently the actual rise in r is even greater than the value computed from the change in the Y_{ph}/Y_{fl} ratio.

Influence of structure on r. In considering the influence of structure we must examine separately 1) the variation of r with the structure of the molecule without regard to the influence of the medium and 2) the sensitivity of r to the influence of the medium in view of or depending upon the structure.

We have seen above that the transition probability from the labile level to the metastable one depends in many cases on the nature of the solvent. It will be seen from the cited examples that the extent to which different compounds are subject to the influence of the solvent varies. Some compounds have low values of Y_{ph}/Y_{fl} in all the investigated solvents. Thus the value of Y_{ph}/Y_{fl} for 3-dimethylamino-N-methylphthalimide, 3-dimethylamino-6-nitro-N-methylphthalimide, 4-oxy-N-methylphthalimide, 3-dimethylamino-6-amino-N-methylphthalimide, 3-acetylamino-6-amino-N-methylphthalimide, para-aminobenzaldehyde, meta-aminobenzoic acid, and oxyquinoline in different alcohols does not exceed 0.01.

The value of Y_{ph}/Y_{fl} for 4-amino-N-methylphthalimide, 3-amino-N-methylphthalimide and 3,6-diamino-N-methylphthalimide in a great number of different solvents (water, alcohols, ether, acetone, benzene, n-hexane, carbon tetrachloride, chloroform, bromoform, propyl and ethylene bromide, pyridine, acetic acid, sulfuric acid and ethyl alcohol containing KI) does not exceed 0.01 (Table 3).

In another group of compounds Y_{ph}/Y_{fl} varies over an extremely wide range. For 3-monoethylacetylamino-N-methylphthalimide Y_{ph}/Y_{fl} varies from 0.52 in sulfuric acid to 12.8 in methyl alcohol; for 3-acetylamino-N-methylphthalimide the ratio

Table 2

Ratios of quantum efficiencies of phosphorescence and fluorescence in different media

$\mu \cdot 10^{18}$*	0	0	0	0,99	1,14	1,15	1,65	1,66	1,67	1,70	1,73	1,75	1,84	2,23	2,73						
Solvent / Substance	n-hexane	benzene	CCl_4	bromoform	ether	chloroform	isopropyl alcohol	butyl alcohol	methyl alcohol	ethyl alcohol	acetic acid	isobutyl alcohol	water	pyridine	acetone	methyl alcohol + KJ	ethyl alcohol + KJ	polymethylmetacrylic plastic	H_2SO_4	propyl bromide	ethylene bromide
3-Monomethylacetyl-N-methylphthalimide			1,6					3,2	13	10	0,52	3	1,95							24,0	
3-Acetylamino-N-methylphthalimide	0,37	0,33	0,20	30	0,72	0,18	3,0	3,5	2,2	3,0	3,6	4,5		8,2	2,1			6,7	0,50	17,5	~50
3-Oxy-N-methylphthalimide								0,08		0,10											
3,6-Diacetylamino-N-methylphthal.	0,01	0,00	0,000		0,01		0,25	0,27	0,16	0,32	0,11	0,25	0,01	0,17	0,03	1,22	1,75			0,11	
4-Acetylamino-N-methylphthamide	0,06	0,10	0,000		0,05		0,15	0,12	0,10	0,12	0,22	0,14	0,01	0,04	0,09	0,61	0,82	0,08		0,17	
3-Acetylamino-6-nitro-N-methylphthalimide								0,16		0,37		0,4									
3-Amino-6-nitro-N-methylphthalim.								0,49		0,37		0,4									
3-Dimethylamino-6-acetylamino-N-methylphthalimide								0,01 : 0,001		0,01 : 0,001		0,01 : 0,001									
4-Oxy-N-methylphthalimide								0,01÷ 0,001		0,01÷ 0,01		0,01÷ 0,001									
3-Dimethylamino-6-amino-N-methyl-phthalimide								0,00		0,000		0,00									
3-Acetylamino-6-amino-N-methylphthalimide	0,00		0,000		0,00		0,000	0,000		0,000		0,000									
3-Amino-N-methylphthalimide							0,000	0,000	0,00	0,000		0,000	0,00		0,00	0,11		0,00			
1-Amino-4-nitro-5-bromonaphthalene									0,06												
α-Acetyl-amino-5-bromonaphthalene																					
1,4-Diamino-5-bromonaphthalene									0,08							0,22					
Naphthalenediamine									0,00							0,06					
β-Naphthaquinone									0,03							0,30					
α-Oxynathphaldehyde									0,05							0,17					
Phenanthrene									0,34	0,22						4,9	0,4				

---

* μ = dipole moment of the medium

Table 3

Examples of substances with low values of r/p in different media

Substance	Solvent											
	water	methyl alcohol	ethyl alcohol	isopropul alcohol	butyl alcohol	isobutyl alcohol	ether	acetone	*n*-hexane	CCl_4	polym. plastic	ethyl alcohol + KI
3-Dimethylamino-6-amino-N-phthalimide			0,000		0,00	0,00						
4-Amino-N-methylphthalimide			0,000		0,000	0.000						0,00
3,6 Diamino-N-methylphthalimide			0,000		0,000	0,000						0,00
3-Amino-N-methylphthalimide	0,00	0,00	0,000	0.000	0,000	0,000	0,00	0,00	0.00	0,000	0,00	<0,01
3-Acetylamino-6-amino-N-phthalimide			0,000	0.000	0,000	0.000						

varies from 0.2 in carbon tetrachloride to 50 or more in ethylene bromide; for 3,6-diacetylamino-N-methylphthalimide, from 0.001 in carbon tetrachloride to 0.46 in bromoform and 1.75 in ethyl alcohol containing KI; for naphthalenediamine it varies from 0.03 to 0.3 in different solvents (see Table 2).

Influence of different factors on the probability q_2 of nonradiative transitions from the metastable to the ground level. In view of the fact that the duration of phosphorescence is virtually the same for compounds of similar structure in different media, we can safely assume that the quenching of phosphorescence is independent of the temperature at the temperature of liquid air.[1,3] This assumption does not extend to media which are fluorescence quenchers, where temperature independent phosphorescence quenching is evinced. The temperature quenching of phosphorescence in a number of organic compounds is very small; some of these exhibit phosphorescence even at 350° (Ref. 4).

The phosphorescence of phthalimides and certain other benzene derivatives is more subject to temperature quenching.[5] We investigated a series of phthalimide derivatives in a large number of solvents that remain solid above 0°C: bromoform, ethylene bromide, acetic acid, polymethylmetacrilic plastic, polyvinyl alcohol, sugar, boric acid, cellophane, cellulose acetate, microporous glass, aluminum oxide, silicagel, monochloroacetic acid, tricholoracetic acid, orthophosphoric acid, metaphosphoric acid, menthol and benzene. None of the investigated phthalimides exhibited phosphorescence above 0° in any of the listed solvents. Temperature quenching of phosphorescence in these media is characterized by a lower probability than the temperature quenching of fluorescence.

As Sveshnikov showed, the probability of quenching of the emission from metastable states by impurities is appreciably lower than the probability of quenching of fluorescence.[6] Analysis of data on concentration quenching of phosphorescence[6] and quenching by oxygen[7] leads to similar results.

One of the principal causes of temperature quenching of phosphorescence is the modification of the state of the medium produced by the temperature change.

As Sveshnikov and Dikun[5] showed, phosphorescence quenching by the medium depends primarily on the viscosity, the actual nature of the medium per se being secondary. Consequently the temperature may indirectly effect the phosphorescence quenching through its influence on the viscosity of the medium.

However, it can be shown that purely temperature quenching of phosphorescence also exists. In a number of phthalimides quenching of phosphorescence begins at

approximately the same temperature in different media. For example, in 3-acetylamino-N-methylphthalimide the decrease in phosphorescence yield begins at -180° in almost all media. Furthermore in almost all the investigated phthalimides the phosphorescence is completely quenched at 0° in all the media. The variation of the rigidity with temperature can hardly be the same in all the different media tested which included plastics, vitreous materials and crystalline substances. Hence the identical change in q_2 with temperature in phthalimide derivatives in different media cannot be ascribed to an equal change in rigidity. Apparently in phthalimides in solid media the increase in q_2 with temperature is due primarily to intramolecular processes. An analogous conclusion follows from the data of Piatnitski[8] who investigated benzene derivatives in crystal form where the change in q_2 with temperature is obviously not due to variations in rigidity.

Influence of different factors on the probability q of non-radiative transitions from the labile to the ground level. There is little information in the literature on the influence of temperature, the solvent and the structure of luminescent substances on q_1. In most investigations only the influence of these factors on the fluorescence yield is considered. Here we shall examine the influence of these factors on q_1 in certain phthalimide derivatives.

We found that in phthalimides, the fluorescence yield of which is strongly dependent on the solvent, there is a connection between the quantum yield of fluorescence of the solution and the position of the fluorescence band. As may be seen from the accompanying figure, the influence of structure in related compounds is secondary, as is the influence of the solvent proper. When the fluorescence spectra of a given substance in different solvents are identical, the quantum efficiencies are also equal. Thus a decisive factor where the fluorescence yield is concerned is the separation between the ground and excited levels.

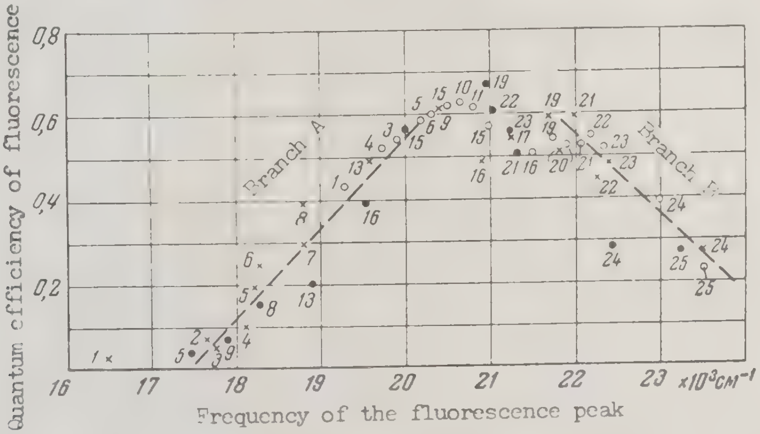

Dependence of the fluorescence yields of solutions of phthalimide derivatives on the location of their fluorescence band. Solvents: 1) water, 2) glycerin, 3) acetic acid, 4) butyric acid, 5) methyl alcohol, 6) ethyl alcohol, 7) cyclohexane, 8) nonylic acid, 9) butyl alcohol, 10) isobutyl alcohol, 11) isopropyl alcohol, 12) acetic anhydride, 13) ethyl acetate, 14) quinoline, 15) pyridine, 16) acetone, 17) chloroform, 18) α-chloronaphthalene, 19) dioxane, 20) anisole, 21) diethyl ether, 22) chlorobenzene, 23) benzene, 24) carbon tetrachloride, 25) n-hexane; x) 4-amino-N-methylphthalimide, ●) 4-methylamino-N-methylphthalimide, o) 3-amino-N-methylphthalimide.

In the general case the curve for the fluorescence yield vs the position of the fluorescence band consists of two branches (A and B in the figure). From this it must be concluded that there are at least two different deactivation processes, the probabilities of which depend in a different manner on the separation between the ground and excited levels.

We found that branch A is determined by the temperature dependence of the fluorescence yield (at -196° the quantum yields of systems pertaining to this branch are almost equal[9]).

Inasmuch as the probability r of transitions to the metastable state is independent of the temperature, branch A is obviously due to changes in the probability q_1. Since at -196° the quantum yield of fluorescence within the range of branch A does not depend on the solvent, it must be assumed that the absorption in the fluorescence band per se does not affect the value of q_1.

The generally observed decrease in the fluorescence yield associated with displacement of the fluorescence band to the side of longer wavelengths could have been predicted on the basis of earlier developed concepts. One of the proposed explanations for temperature quenching of fluorescence is the following. The excited molecule has a certain probability of attaining the energy corresponding to the point of intersection of the potential curves for the ground and excited states. There should then occur a nonradiative transition to the ground state. The probability of this transition obviously increases with the temperature. When the ground and excited levels come closer together the point of intersection of the potential curves is shifted so that the nonradiative transition can occur upon attainment of a relatively lower vibrational level.

We cannot at present say anything definite regarding the quenching process that gives rise to the B branch. We can only note that there are reasons for assuming that the increase in fluorescence quenching accompanying displacement of the spectrum to the short-wave side occurs not as a result of an increase in q_1 but rather as a consequence of a rise in the probability r of transitions to the metastable state with subsequent temperature quenching at this level.

We note that in the absence of quenching on the metastable level it is relatively easy to determine to what extent the different nonradiative transitions participate in the deactivation process. Solution of this problem becomes more difficult when quenching on the metastable level does occur at the temperature under investigation.

References

1. V.V.Zelinski & V.P.Kolobkov, Doklady AN SSSR, 101, 241 (1955).
2. B.Ia.Sveshnikov, Izv. AN SSSR, Ser. fiz., 13, 67 (1949).
3. B.Ia.Sveshnikov, Thesis FIAN (Physics Inst. of the Ac. of Sc.), M. 1951.
4. P.P.Dikun, Trudy GOI (Transac. State Opt. Inst.) M. 1953.
5. B.Ia.Sveshnikov & P.P.Dikun, Doklady AN SSSR, 60, 571 (1948).
6. B.Ia.Sveshnikov, Doklady AN SSSR, 60, 791 (1948).
7. A.V.Kariakin, Zhur. fiz. khim., 23, 1332 (1949).
8. B.A.Piatnitski, Doklady AN SSSR, 62, 59 (1948); Doklady AN SSSR 68, 281, (1949); B.A.Piatnitski & T.P.Vinokurova, Doklady AN SSSR, 68, 483 (1949).
9. V.V.Zelinski & V.P.Kolobkov, Doklady AN SSSR, 106, 1042 (1956).

SENSITIZED PHOSPHORESCENCE OF AROMATIC COMPOUNDS (ENERGY TRANSFER FROM THE TRIPLET LEVEL TO THE PHOSPHORESCENT TRIPLET LEVEL)

-V.L.Ermolaev

In earlier articles by A.N.Terenin and the writer[1,2] there was described a new energy transfer phenomenon involving the transfer of electronic excitation energy in frozen solutions from molecules on the triplet level to non-excited molecules with transition of the latter to a phosphorescent triplet level. This process, which we called sensitized phosphorescence, occurs in naphthalene, for example: visible phosphorescence of naphthalene in an alcohol solution at -180° can be excited by the ~3660 A mercury lines in the spectral region where naphthalene itself does not absorb[3] by adding benzaldehyde or benzophenone, which do absorb in this region, to the solution. Subsequently we detected the same effect in a number of other compounds (Table 1). We observed excitation energy transfer from the donor to the acceptor molecules with excitation only of the former in all binary combinations of any substance in the upper half of the table with any other substance in the lower half of the table. The presence of such transfer was established not only from the appearance of phosphorescence bands of the acceptor material in the emission spectrum but also from the decrease in the lifetime of the donor molecules in the metastable state in the presence of the acceptor substance. In the case of carbazole and diphenylamine as the donors we were able to establish the occurrence of transfer only by the latter effect.[4]

Table 1

Substance	Triplet level, cm^{-1}	τ_0 phosphor., sec	Long-wave absorption edge, cm^{-1}
	Energy donor		
Benzaldehyde	25200	$1.5 \cdot 10^{-3}$	26750
Benzophenone	24200	$4.7 \cdot 10^{-3}$	26000
Acetophenone	25350	$2.3 \cdot 10^{-3}$	27500
Ethylphenylketone	--	$3.7 \cdot 10^{-3}$	27500
o-Oxybenzaldehyde	24600	--	26000
Benzoin	25650	$2\text{-}4 \cdot 10^{-3}$	28000
Diphenylamine	25200*	1.85	31000
Carbazole	24480*	7.25	29500
	Energy acceptor		
Naphthalene	21250	2.3	31000
Diphenyl	22800	4.4	34000
α-Methylnaphthalene	21200*	---	30500
α-Chlornaphthalene	20700*	0.30	---

The energy values of the electronic transitions from the triplet level to the ground level and the lifetimes of the molecules in the triplet state also are listed in Table 1. It will be seen from the table that in all cases of nonradiative transfer the necessary condition that the electronic level of the molecule giving up the energy be higher than the electronic level of the acceptor molecule ($T_D > T_A$) is fulfilled.

One of the objections which might be raised against the explanation of sensitized phosphorescence being due to nonradiative energy transfer is the hypothesis regarding the peculiar effect of aromatic aldehydes and ketones on naphthalene, diphenyl and other acceptors, which is presumably accompanied by removal of the prohibition of transitions from the ground singlet state to the triplet level with the appearance of corresponding absorption in the vicinity of the exciting 3660 A line. If we accept this explanation we must then expect to observe an alteration in the phosphorescence spectra of the molecules participating in the transfer and an appreciable reduction of the duration of phosphorescence of the acceptors (naphthalene, diphenyl, etc.) in connection with the reverse transition from the triplet to the ground state. However, the fact that the sensitized and normally excited phosphorescence spectra of naphthalene and diphenyl are

---

*Data taken from Ref. 5.

identical has been proved photographically by Terenin and the writer.[1,2]

To resolve the question definitively we measured the decay time of the afterglow of naphthalene and diphenyl in alcohol solutions at -180° in the case of excitation in the self-absorption band (in the spectral region under 3200Å) and in the case of sensitized phosphorescence, i.e., in the presence of benzaldehyde and benzophenone with excitation by the mercury lines at 3660 A.

Table 2

Acceptors	τ (sec) phosphor, excited by 3130 A, light	τ (sec) sensit. phosphorescence excited at 3660 A in the presence of	
		benzaldehyde	benzophenone
Naphthalene	2.3	2.3	2.3
Diphenyl	4.4	4.1	4.6

The results of these measurements are summarized in Table 2 from which it may be seen that the lifetime of naphthalene and diphenyl in the triplet state is the same in both cases within the limits of the experimental error. Hence the explanation based on the formation of associated donor-acceptor pairs with removal of the ban on intercombination between the ground and phosphorescent levels must be rejected.

To get a clearer idea of the effect let us picture the electronic levels of the molecules participating in the transfer. In the scheme of Fig. 1 we have shown at the left the ground level S_A, the fluorescent level S^*_A and the lower triplet level T_A of the acceptor molecule and at the right the corresponding levels of the donor; straight lines indicate transitions associated with the emission or absorption of a photon; wavy lines denote nonradiative transitions. Let us introduce the following notation for the transition probabilities: $p(C_A)$ is the probability of nonradiative transfer which is a function of the acceptor concentration π and r are the probabilities of transitions from the triplet level of the sensitizor to the ground level with and without emission, respectively, ρ and q are the probabilities of radiative and nonradiative transitions from the phosphorescence level in the acceptor, respectively. Transitions from T_A to T_D cannot occur since the difference between their energies (8.4 Kcal/mole) is too great for the transition to be realized at the expense of the thermal energy at the temperature of the experiment (-180°).

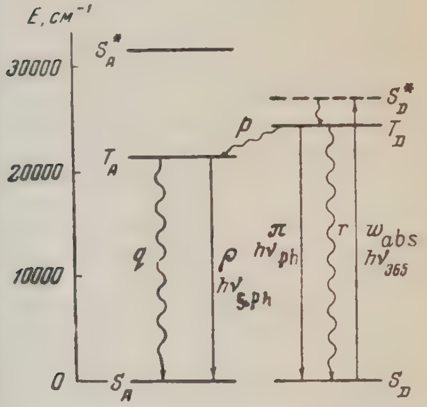

Fig. 1. Scheme of electronic energy levels of the acceptor and donor molecules in sensitized phosphorescence (specifically benzophenone* + naphthalene).

Writing differential equations for the number of excited molecules of one type and the other and solving these equations, we obtain expressions for the number of molecules in the triplet state. Going over to intensities I_A and I_D for stabilized excitation conditions, we obtain the following expression for the ratio of intensities:

$$\frac{I_A}{I_D} = \frac{p(C_A)\rho}{\pi(\rho+q)} ,$$

wherein only $p(C_A)$ depends on the acceptor molecule concentration C_A. Let us term I_A/I_D the relative yield of sensitized phosphorescence. Another quantity that is connected with the probability of nonradiative energy transfer by a simple relationship and can easily be determined experimentally is given by the expression:

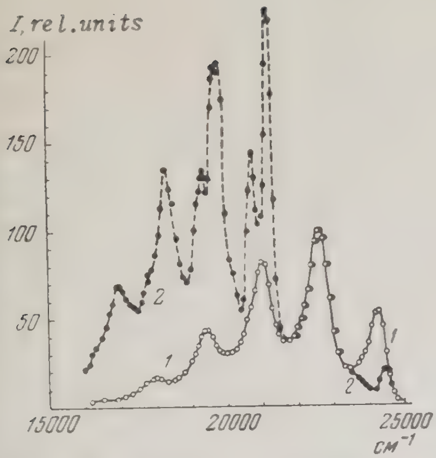

Fig. 3. Luminescence spectra of solutions in a mixture of ether and ethyl alcohol (1:2) at -190° with excitation at 3660 A of 1) benzophenone ($2 \cdot 10^{-2}$ mole/liter) and 2) benzophenone* + naphthalene ($2 \cdot 10^{-2}$ and $6.4 \cdot 10^{-1}$ mole/liter, resp.).

deviation from exponential decay of the donor emission in the presence of an acceptor. The question of deviations from exponential decay of the emission in the case of energy transfer in viscous solutions was recently examined theoretically by Galanin.[8] In the case of emission of a solution of benzophenone alone or benzaldehyde alone, when the decay is exponential, we obtain a virtually straight line on the oscillograph screen. In the presence of α-methylnaphalene and, consequently, in the presence of energy transfer we were unable to obtain a rectified line.

In addition we determined the probability of energy transfer from benzophenone to naphthalene from the relative yield of sensitized phosphorescence (I_A/I_D) as determined from the areas under the phosphorescence quantum yield curves for the acceptor and donor (Fig. 3). Prior to this we investigated the influence of the donor (benzophenone) concentration on the relative yield of sensitized phosphorescence at a constant concentration of the acceptor (naphthalene). The measurements showed that a 100-fold variation of the donor concentration (from $2 \cdot 10^{-3}$ to $2 \cdot 10^{-1}$ mole/liter) has very little effect on the sensitized emission of the naphthalene. The concentration independence of the yield invalidates the hypothesis regarding the indispensability, where energy transfer is concerned, of formation of benzophenone-naphthalene complexes by analogy with the sensitization of emission in complexes, discovered by Reed (see Ref. 9).

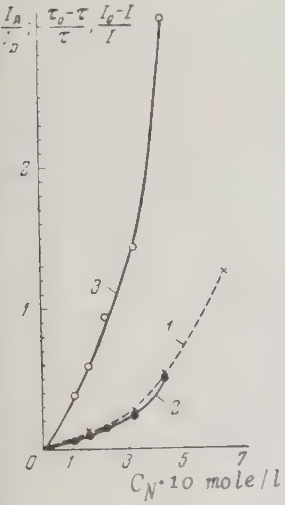

Fig. 4. Relative yield (1), reduction of donor lifetime (2) and quenching of donor phosphorescence (3) in sensitized phosphorescence of the benzophenone* + naphthalene system. Excitation by 3660 A light: t = -190°; solvent = ether + ethyl alcohol (1:2).

Variation of the acceptor (naphthalene) concentration, however, has a strong effect on the value of I_A/I_D. The results of our measurements are given in Fig. 4, where the horizontal scale is laid off in molar concentrations of the acceptor (naphthalene) and the horizontal scale gives the values of I_A/I_D (curve 1), $(\tau_0-\tau)/\tau$ (curve 2) and $(I_0-I)/I$ (curve 3) for benzophenone. It will be seen from Fig. 4 that in this case, as in the case of sensitized fluorescence and quenching by absorbing impurities, quenching develops appreciably more rapidly than the decrease in τ and the increase in the relative yield. This is evidence in favor of the presence of instantaneous quenching processes in the case of energy transfer between triplet levels.

From the reports of Gilmore, Gibson and McClure[10] we know that the quantum yield of phosphorescence of benzophenone in ERA is 0.86. This allows us to determine the absolute quantum yield of sensitized luminescence of naphthalene: the yield is 0.11 at a naphthalene concentration of $3.2 \cdot 10^{-1}$ mole/liter, which is even somewhat higher than the value of the yield of phosphorescence of naphthalene with excitation in its absorption band (0.095, see Ref. 10).

The facts examined above indicate that sensitized phosphorescence is undoubtedly connected with nonradiative transfer of electronic excitation energy between the triplet levels. The mechanism of this transfer is apparently analogous to that of the transfer between fluorescent levels.

$$\frac{\tau_0 - \tau}{\tau} = \frac{p(C_A)}{r + \pi}$$

where τ_0 is the decay time of the luminescence of the donor in the absence of energy transfer and τ is the decay time in the presence of transfer with the probability $p(C_A)$.

Thus in order to determine the probability of energy transfer between the donor and acceptor one must evaluate the relative yield and the phosphorescence decay time as well as the extent of the quenching of the phosphorescence of the donor by the acceptor at different concentrations of the compounds.

The possibility of selective excitation of only the donor and complete absence of reabsorption and secondary luminescence would provide for a more accurate quantitative investigation of energy transfer: however, this is not realizable in the case of sensitized fluorescence in view of the necessity of working with thin layers and the difficulty of evaluating the extent of reabsorption. In the present investigation we carried out measurements of the relative yield, the reduction in τ and the quenching in sensitized phosphorescence as functions of the concentration of the components.

According to the concepts developed by Vavilov[6] there are two processes involved in resonance migration of energy in fluorescing solutions: 1) time dependent resonance interaction between the molecules and 2) static interaction leading to instantaneous energy transfer or expenditure of the energy for thermal vibrations. A consequence of assuming that the first process exists would be reduction of the luminescence decay time of the substance giving up energy, i.e., the donor. Hence a reduction in τ of the donor molecules in our case would indicate that sensitized fluorescence is a resonance effect. We have succeeded in showing on the example of the systems benzaldehyde* + naphthalene, benzophenone* + naphthalene, benzophenone* + α-methylnaphthalene, carbazole* + naphthalene and others that the presence of the acceptor reduces the lifetime of the donor in the phosphorescence state. The measurements of τ were made on a Tolstoi and Feofilov[7] oscillographic phosphoroscope, kindly made available for this purpose by V.A.Arkhangel'skaia.

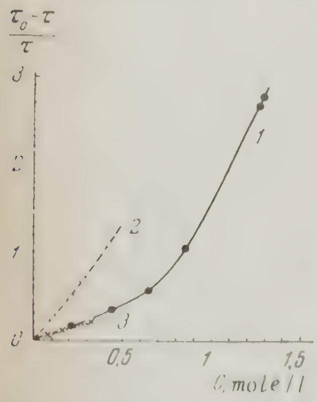

Fig. 2. A reduction in the duration of phosphorescence of donor molecules in the presence of an acceptor: 1) benzophenone* + α-methylnaphthalene, 2) carbazole* + naphthalene and 3) benzaldehyde* + naphthalene.

Curve 1 in Fig. 2 shows the variation of $(\tau_0 - \tau)/\tau$ for the emission of benzophenone (donor) with the concentration of α-methylnaphthalene (acceptor). This quantity is proportional to the ratio of the energy t.e transfer probability to the initial probability of a transition from the phosphorescent to the ground level in the benzophenone molecule. As may be seen from the figure this quantity increases nearly linearly with increasing acceptor concentration in the concentration interval below 0.2 mole/liter; above this concentration the decrease in τ proceeds more rapidly. Curve 2 in Fig. 1 shows the variation of the ratio for the afterglow of carbazole and curve 3 the variation for benzaldehyde with the naphthalene concentration. It is interesting to note that in the case of energy transfer from the different donors listed in Table 1 to α-methylnaphthalene present in the amount of 0.4 mole/liter the value of the relative probability of nonradiative energy transfer $(\tau_0 - \tau)/\tau$ remains of the same order of magnitude for all donors whereas τ_0 varies by three orders of magnitude: from $1.5 \cdot 10^{-3}$ for benzaldehyde to 7 sec for carbazole.

It must be noted that in the course of our measurements on the oscillographic phosphoroscope of the values of τ of aromatic aldehydes and ketones we observed a

However, as has been shown in Ref. 9, a specifically quantum aspect is evinced in the phenomenon inasmuch as the transfer occurs only when the total spin of the components remains unchanged (Wigner's rule).

The present investigation was carried out under the direct supervision of A.N.Terenin whom I wish to thank. I also desire to express my gratitude to B.Ia.Sveshnikov for a number of valuable suggestions.

References

1. A.N.Terenin & V.L.Ermolaev, Doklady AN SSSR, 85, 547 (1952).
2. V.L.Ermolaev & A.M.Terenin, in Sbor. "Pamiati S.I.Vavilova" (Symposium "In Memory of S.I.Vavilov") M. 1952.
3. L.A.Blumenfel'd, Zhur. fiz. khim., 24, 838 (1950).
4. V.L.Ermolaev, Doklady AN SSSR, 102, 925 (1955).
5. G.Lewis & M.Kasha, J. Amer. Chem. Soc., 66, 2100 (1944).
6. S.I.Vavilov, Zhur. eksp. i teor. fiz., 13, 13 (1943); Collected works, Vol. 2, p. 490, M. 1952.
7. N.A.Tolstoi & P.P.Feofilov, Usp. fiz. nauk, 41, 44 (1950).
8. M.D.Galanin, Zhur. eksp. i teor. fiz., 28, 485 (1955).
9. A.N.Terenin & V.L.Ermolaev, Usp. fiz. nauk, 58, 37 (1956).
10. E.H.Gilmore, G.E.Gibson & D.S.McClure, J. Chem. Phys., 20, 829 (1952); 23, 399 (1955).

DISCUSSION

A.N.Sevchenko: Did you observe absorption transitions from the ground level to the triplet level and from the latter to higher levels?

V.L.Ermolaev: Absorption from the ground level to the triplet one was not observed under our conditions. We measured the spectrum of the T*→T transition-absorption of naphthalene (the acceptor); it agreed with the data in the literature.

A.N.Terenin: Sensitized phosphorescence has all the traits of an inductive mechanism, although it is associated with optically forbidden transitions. The degree of forbiddenness is apparently reduced by the fact that the total spin of the system does not change; according to Wigner's rule such transitions have a fairly high probability.

G.A.Sivkova: We investigated the dependence of the initial intensity of the sensitized emission of the host substance on the concentration of the sensitizer. With increasing concentration, the intensity increases, reaches a saturation value and finally falls off rapidly. We also observed deviations from exponential decay which were greatest with the highest transfer probabilities.

V.L.Ermolaev: The decrease in the intensity of sensitized emission at high acceptor concentrations is connected with the presence, in addition to energy transfer, of strong quenching of the donor phosphorescence by the acceptor.

INFLUENCE OF CONCENTRATION AND THE SOLVENT ON THE PHOSPHORESCENCE OF AROMATIC COMPOUNDS AT LOW TEMPERATURES

- P.A.Tepliakov and B.A.Piatnitski

Concentration induced quenching of phosphorescence has been studied by Vavilov & Shishlovski[1] in solid sugar solutions and by Vinokurov & Levshin in boric phosphors. The appreciable decrease in the value of the exponent in the function characterizing the decay of phosphorescence and the decrease in the initial emission intensity with increasing concentration of the activator has been interpreted as quenching of the emission of the molecules in the metastable state. On the other hand, Lewis, Lipkin & Magel[3] concluded that energy exchange is impossible between the unexcited and metastable states of the molecule in organic luminophors. Sveshnikov[4] detected a decrease in the duration of phosphorescence with increasing activator concentration in boric phosphors, solidified sugar and alcohol solutions of benzene at the temperature of liquid air. Concentration induced quenching of phosphorescence in solid alcohol solutions of benzene and its derivatives has also been noted by Zinov'eva[5] and Dikun, Petrov & Sveshnikov[6]. There are data on the influence of the solvent which indicate that varying the solvent has relatively little effect on the basic characteristics of the metastable level. At the same time Terenin[7], Piatnitski[8] and Zinov'eva[5] have demonstrated that the lifetime of the metastable state and the initial emission intensity do change in going from solutions to the pure substances, from alcohol solutions to aqueous ones and from polar solvents to non-polar solvents.

In the present article we report on our investigation of the decay of phosphorescence and lifetime of the metastable state of the molecules of ten aromatic acids and two phenols in different solvents and at different concentrations at the temperature of liquid oxygen. The investigation was carried out by the photoelectric method developed by Piatnitski[9]. The solvents used included purified ethyl alcohol, acetone, and diethyl ether, water and carbon tetrachloride. As a rule the concentration was varied from $5 \cdot 10^{-1}$ M to $5 \cdot 10^{-4}$ M.

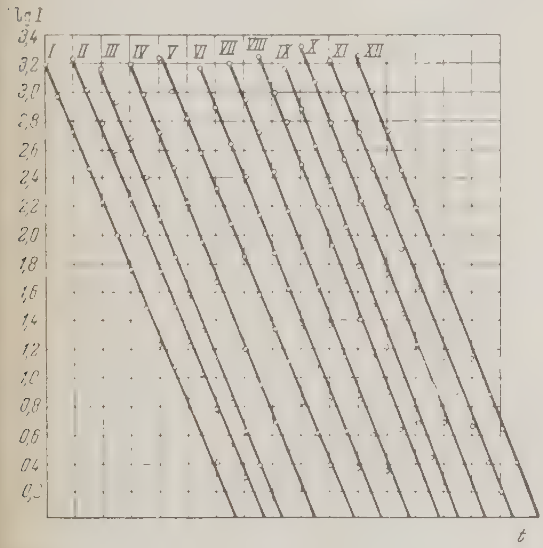

Fig. 1. Phosphorescence decay curves for gallic acid in alcohol at the following concentrations: I - 0.5 M; II - 0.25 M; III - 0.1 M; IV - 0.075 M; V - 0.05 M; VI - 0.025 M; VII - 0.01 M; VIII - 0.0075 M; IX - 0.005M X - 0.0025 M; XI - 0.001 M; XII - 0.0005 M.

1. Influence of concentration

As may be seen from the curves reproduced in Figs. 1, 2 and 3* changes in concentration do affect the lifetime τ of the metastable state and the initial emission intensity I_0.

The decay law was found to be exponential both in the crystalline state and at different concentrations in all solvents where the phosphorescence of benzoic, gallic, cinnamic, salicylic, n-aminobenzoic and anthranilic acid, hydroquinone and resorcinal are concerned. In the case of cinnamic, hydrocinnamic and salicylic acid in alcohol there is evidence that the lifetime of the metastable state is influenced by the concentration.

---

*In all the figures the zero of the time scale is arbitrary; each division on the scale equals 2 sec.

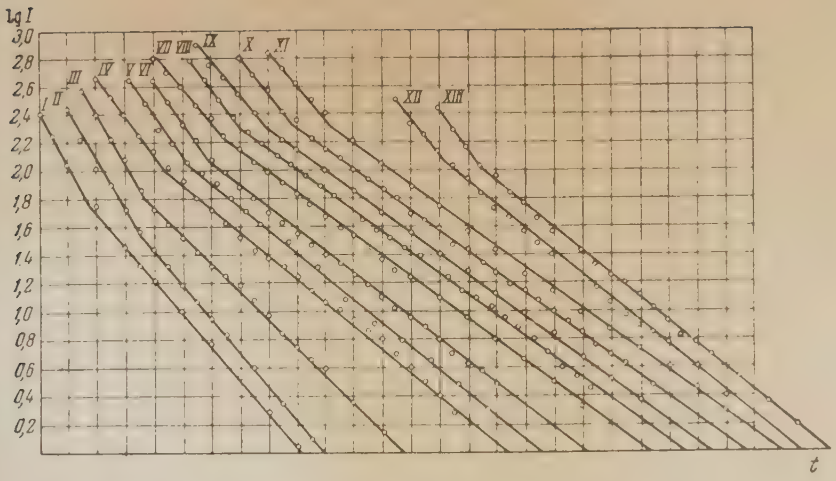

Fig. 2. Phosphorescence decay curves for hydrocinnamic acid in alcohol at the following concentrations: I - 0.75 M; II - 0.5 M; III - 0.25 M; IV - 0.1 M; V - 0.075 M; VI - 0.05 M; VII -)0.25 M, VIII - 0.01 M; IX - 0.0075 M; X - 0.005 M; XI - 0.0025 M; XII - 0.001 M; XIII - 0.0005 M.

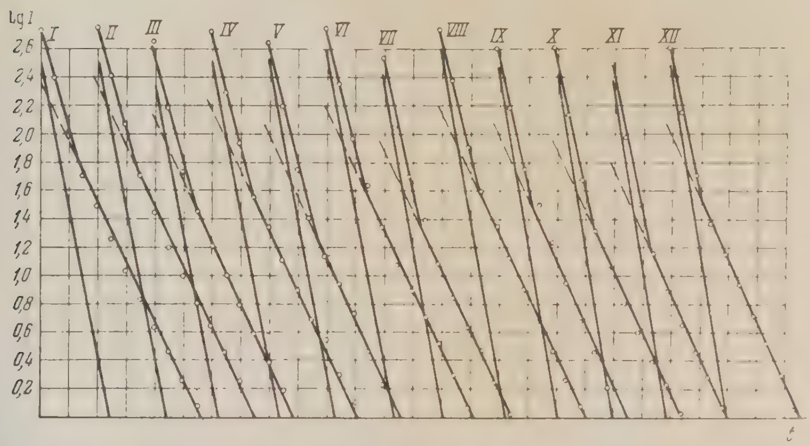

Fig. 3. Phosphorescence decay curves for sulfobenzoic acid in alcohol in the following concentrations: I - 0.5 M; II - 0.25 M; III - 0.1 M; IV - 0.075 M; V - 0.05 M; VI - 0.025 M; VII - 0.01 M; VIII - 0.0075 M; IX - 0.005 M; X - 0.0025 M; XI - 0.001 M; XII - 0.0005 M.

For liquid solutions of dyes Vavilov deduced the following simple equation giving, in the first linear approximation the relationship between the lifetime of the metastable state and the concentration C:

$$\frac{1}{\tau} = \frac{1}{\tau_0} + C\frac{1}{K} \qquad (1)$$

Equation (1) proved to be applicable to alcohol solutions, cinnamic acid and acetone solutions of anthranilic acid but did not hold for alcohol solutions of salicylic and hydrocinnamic acid. For the other aromatic compounds in all solvents and for hydrocinnamic and anthranilic acids in all the other solvents employed the results indicated the absence of concentration quenching at the metastable molecular level, i.e., the lifetimes of the metastable state of all the compounds remain constant over the entire range of concentrations.

Analyzing the values of the initial emission intensity at different concentrations we note the following: for alcohol solutions of gallic, sulfobenzoic and cinnamic acid the initial intensity does not change with the concentration. This fact which characterizes the absence of concentration quenching on the metastable level at the instant of cessation of excitation can also be taken as evidence of the absence of concentration induced changes in the absorption of the exciting light.

In the case of solutions of the other compounds the initial intensity does not remain constant with changes in concentration. The influence of concentration on the initial emission intensity is satisfactorily described by the following empirical expressions:

$$I_{oC} = B \cdot c^{\beta}, \qquad (2)$$

and

$$I_{oC} = A \cdot c^{-\gamma}, \qquad (3)$$

where I_{oC} is the initial emission intensity at the given concentration C; B and A are constants and β and γ are, respectively, indices characterizing the variation in the initial intensity and the quenching at the metastable level. These equations were derived for conditions of complete saturation but without taking into account possible changes in the absorption of the exciting light. They are valid in the case of absence of concentration induced changes in absorption and in the case of linear dependence of the coefficient of absorption of the exciting light on the concentration.

We established deviations from the exponential decay law for solutions of some of the acids. For hydrocinnamic acid in alcohol and bromobenzoic acid in alcohol, acetone, water, and ether the decay is best characterized in the form of two exponential terms:

$$I = I_{01}e^{-\alpha_1 t} + I_{02}e^{-\alpha_2 t}, \qquad (4)$$

where I_{01} and I_{02} are the initial intensities of the short-term and persistent emission, respectively, α_1 and α_2 are the probabilities of transitions from the metastable state for short-term and persistent emission, respectively.

In Fig. 3 the phosphorescence decay curves of alcohol solutions of sulfobenzoic acid have been resolved into components in accordance with equation (4).

2. Influence of the solvent

The data pertaining to the influence of the solvent on the mean lifetime of the metastable state are summarized in the accompanying table. The values for a number of compounds in the crystal state (identified by asterisks) taken from Piatnitski[8], while the data for salicylic acid in water and gallic acid in carbon tetrachloride are due to Zinov'eva[5]. The concentration of all solutions equals 0.05 M.

Lifetimes of metastable states

Substance	Solvent					Crystal state
	alcohol	acetone	ether	water	CCl_4	
Benzoic acid	1.9	2.1	1.8	2.5	2	2.2*
Phthalic acid	2	1	2.2	1.5	1.37	0.99*
Salicylic acid	1.8	1.8	1.8	1.6	1.3	1.2*
Gallic acid	1.8	1.32	--	1.8	1.6	1.5*
Cinnamic acid	1.8	--	--	--	--	1.9*
Hydrocinnamic acid	5.3	2.1	--	--	--	3.7
n-Aminobenzoic acid	2.1	2.2	--	2.2	1.2	1.1
Anthranilic acid	1.5	1.8	--	1	1	1.1
Bromobenzoic acid	2	1.7	2.2	--	1	1
Sulfobenzoic acid	2.1	1.35	--	2.3	--	1.7
Hydroquinone	2.2	2.2	--	--	--	3.03*
Resorcinal	1.8	2.2	--	--	--	1.85*

Gor'ki State Pedagogical Institute

References

1. A.A.Schischloswki & S.I. Wawilov, Sow. Phys., 5, 379 (1934).
2. L.A.Vinokurov & V.L. Levshin, Zhur. fiz. khim., 8, No.2 (1936); Doklady AN SSSR, 2, 4 (1936).
3. G.Lewis, D. Lipkin & T.Magel, J. Am. Chem. Soc., 63, 3005 (1941) & 64, 1774 (1942).
4. V.Ia.Sveshnikov, Doklady AN SSSR, 58, 49 (1947).
5. O.G.Zinov'eva, Doklady AN SSSR, 68, 2 (1949).
6. P.P.Dikun, Petrov & Sveshnikov, Zhur. eksp. i teor. fiz., 21, 150 (1951).
7. A.N.Terenin, Izv. AN SSSR, Otd. khim. nauk, 1, 59 (1940).
8. B.A.Piatnitski, Izv. AN SSSR, Ser. fiz., 15, 5 (1951).
9. B.A.Piatnitski, Doklady AN SSSR, 57, 771 (1947).

TEMPERATURE QUENCHING OF PHOSPHORESCENCE OF CERTAIN AROMATIC ACIDS

- B.A.Piatnitski & M.S.Fadeeva

The luminescence of organic phosphors is generally understood to consist of emission from discrete centers obeying an exponential decay law*, the afterglow being characterized by two distinct spectral bands: a long-wave and a short-wave one.

The theory of metastable states, developed during the thirties, has proved to be the most satisfactory one for interpreting the process of persistent afterglow (phosphorescence) and the origin of the two phosphorescence bands characteristic of organic compounds. It is known that both of the phosphorescence bands of a given substance cannot always be observed. When the material is excited at a low temperature (for example, at that of liquid oxygen) there is observed only a long-wave phosphorescence band which disappears with rising temperature.

The influence of temperature on the luminescence of organic phosphors and, in particular, on their fluorescence has been studied by a number of authors.[3-5] Among the first to investigate the influence of temperature on the phosphorescence was Piatnitski[6-8] who studied the decay in the emission of a number of aromatic acids, benzene and diphenyl in different temperature ranges.

The quenching influence of a temperature increase on the afterglow of aromatic compounds, detected by Piatnitski is interpreted as being due to the initiation at a certain temperature of radiationless activated transitions from the metastable state to the ground state. This leads to a decrease of the lifetime of the metastable state $\tau = 1/\alpha$ and the initial emission intensity I_0. The initial intensity changes with temperature according to the following expression derived by Piatnitski:

$$I_0 = \frac{I_{0max}}{1 + Ce^{-\frac{W}{kT}}}, \qquad (1)$$

where $I_{0\,max}$ is the initial emission intensity at T = 90° and W is the quenching energy.

In the case of low temperatures the variation of the probability $\alpha = 1/\tau$ with the temperature can be described by the expression

$$\alpha = A + \gamma_0 e^{-\frac{W}{kT}}, \qquad (2)$$

where A = const. is the probability of spontaneous radiative transitions from the metastable to the ground state (M→N) and $\gamma = \gamma_0 e^{-\frac{W}{kT}}$ is the probability of activated nonradiative M→N transitions; for the latter to occur the excited molecule must have a certain activation energy (quenching energy) W.

The photoelectric method developed by Piatnitski for investigating the decay law made it feasible to compute the values of I_0, α and W at different temperatures.

Our investigation was carried out using the same method but on other aromatic acids (n-aminobenzoic, anthranilic, n-bromobenzoic, sulfobenzoic, sulfanilic and hydrocinnamic) in the crystal state.

Utilizing the reasoning of Sveshnikov[9] regarding the quenching of phosphorescence of organic phosphors for the case of temperature quenching under the conditions of our experiments, we arrived at the following differential equations characterizing the time dependence of the number of particles at the labile and metastable levels (assuming light saturation of the phosphor and stable excitation):

---

*Cases of deviation from the exponential law are also known.

$$\frac{dn_1}{dt} = -(q_1 + r)\,n_1\,, \tag{3}$$

and

$$\frac{dn_3}{dt} = rn_1 - (\pi + q_2)n_3\,, \tag{4}$$

where q_1 is the probability of quenching on the labile level, r is the transition probability from the labile to the metastable level, π is the crossover transition probability from the metastable to the ground level with emission and q_2 is the probability of quenching on the metastable level.

Solution of the system of equations (3) and (4) taking into account the initial conditions yields

$$n_3 = n_{03}e^{-(\pi + q_2)t}\,, \tag{5}$$

where

$$n_{03} = \frac{r\omega n_0}{(\omega + q_1 + r)(\pi + q_2) + r\omega}\,. \tag{6}$$

here $\pi + q_2$ is the probability of deactivation of the metastable state, ω is the probability of transition from the ground to the labile state and n_0 is the total number of luminescing molecules.

Analysis of (6) makes it possible to evaluate the population of the metastable level at the instant of cessation of excitation (t = 0) and hence the dependence of the initial intensity I_0 on the quenching factors q_1 and q_2, the first of which accounts for quenching on the labile level and the second, on the metastable level.

Obviously the decrease in I_0 with increasing temperature is due to quenching of the excited molecules not only on the metastable but also on the labile level. Experimental proof of this is the fact that the variation of I_0 and τ (the lifetime of a metastable state) is not proportional to the temperature change for all the above enumerated acids. According to (6), the initial emission intensity I_0 varies in conformity with the

$$I_0 = \frac{I_{0\,max}}{1 + a\cdot\alpha}\,, \tag{7}$$

law, where $\alpha = \pi + q_2$ is the probability of deactivation of the metastable state (q_2 is a function of the temperature) and $a = \frac{\omega + q_1 + r}{r\omega}$ depends on the quenching factor $q_1(T)$ at the labile level.

Experiments show that the values of α and a increase with rising temperature, decreasing the relative initial intensity $I_0/I_{0\,max}$. Experiment also shows that for all the investigated acids except m-bromobenzoic acid, the temperature dependence of a is satisfactorily described by

$$a = a_0 e^{-\frac{\Delta E}{kT}}\,, \tag{8}$$

where a_0 and ΔE are empirical constants; ΔE is in a sense the activation (quenching) energy [illegible] at the [illegible] level [illegible] a [illegible] the temperature quenching q_1 at this level.

The value of ΔE (in ev) in any given case can be evaluated from the straight line plotted in log a vs 1/T coordinates on the basis of (8) - see table.

Increasing the temperature leads to a reduction of the mean lifetime τ of the metastable state.

Expression (2) satisfactorily describes the variation of α, the probability of deactivation of a metastable state with the temperature. Solving (2) in terms of W/kT we obtain the linear dependence of log (α - A) on 1/T. The slope

of the line in log $(\alpha - A)$ vs $1/T$ coordinates allows us to determine W for each substance.

The case where W = = 0 over a certain temperature interval (for example, the case of anthranilic and sulphanilic acids) merits particular attention.* This case, which has been detected for the first time in our investigation, obviously indicates that here nonradiative transitions from the metastable to the ground state can occur without absorption of any fraction of the energy of activation (quenching) W. In other words, the nonradiative transition (M⟶N) is realized from a vibrational level of the metastable state of the excited molecule from which transitions to the ground state occur without absorption of energy.

A c i d	Structural formula	Emission interval °K	Quench. temp., °K	Quench. energy W, ev*	ΔE, ev*
Anthranilic	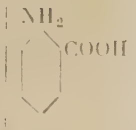	90÷175	110	0,24 0 0,38	0,05
n-Aminobenzoic	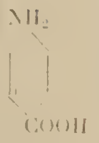	90÷165	110	0,06	0,1 0,02
n-Bromobenzoic	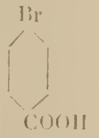	90÷237	104	0,04	0,33
Sulfanilic	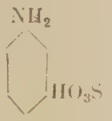	90÷241	110	0,04 0	0,06 0,03
Sulfobenzoic	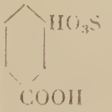	90÷229	137	0,13 0,03	0,125 0,015
Hydrocinnamic	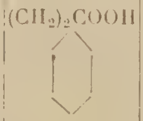	90÷270	234	0,10	0,03

Experience shows that as a rule the values of ΔE and W for the same substance do not coincide (see table) which is indicative of differences in the structure of the vibrational levels and the quenching conditions on the labile and metastable levels. We did not make direct measurements of the lifetime of the excited labile state since in the case of the listed acids raising the temperature does not lead to the appearance of a short-wave phosphorescence band.

Indirect evaluations, through (7), of the relative lifetime of the labile state lead to the following relationship:

$$\frac{1}{\alpha}\left(\frac{I_{0max}}{I_0} - 1\right) = \tau_{10} + \frac{\tau_{10}}{\tau_{11}\omega}, \tag{9}$$

where $\tau_{10} = 1/r$ and $\tau_{11} = 1/(r + q_1)$ are the mean lifetime of the labile state in the absence and in the presence of quenching q_1, respectively.

Bearing in mind that the variation of the relative lifetime in the labile state τ_{10}/τ_{11} may be considered to be proportional to the factor $e^{-\frac{\Delta E}{kT}}$, we obtain

---

*The zero value of W was observed in two diphenols and a number of aromatic acids in solution.

the dependence of τ_{10}/τ_{11} on the absolute temperature with the same value of ΔE as in (7).

The above arguments substantiate our conclusion to the effect that the decrease in the initial intensity I_0 with increasing temperature occurs due to quenching of excited molecules not only on the metastable level but also on the labile level.

Conclusions

1. Increasing the temperature has a quenching effect on the initial intensity I_0 of the long-wave phosphorescence band of aromatic acids.

2. The decrease in I_0 with temperature is described by formula (7) and is the result of quenching of molecules not only at the metastable but also at the labile level.

3. The decrease in the mean lifetime τ of the metastable state is characterized by the following expression

$$\tau = \frac{1}{A + \gamma_0 e^{-\frac{W}{kT}}},$$

proposed by B.A.Piatnitski, wherein W remains constant only in certain temperature intervals and may have one, two or even three different values for one and the same substance in different temperature ranges.

Gor'ki State Pedagogical Institute

References

1. B.A.Piatnitski, Zhur. eksp. i teor. fiz., 9, 1351 (1930).
2. V.A.Iastrebov, Doklady AN SSSR, 90, 1015 (1953).
3. B.S.Neporent, Sb "Pamiati S.I.Vavilova" (Symposium "In Memory of S.I. Vavilov") M. 1952.
4. T.M.Tarasova, Zhur. eksp i teor. fiz., 21, 189 (1951).
5. M.D.Galanin, Trudy FIAN **(Transact.** Phys. Ins. of the Ac. of Sc.) 5,339(1950).
6. B.A.Piatnitski, Doklady AN SSSR, 62, 59 (1948).
7. B.A.Piatnitski, Doklady AN SSSR, 68, 281 (1949).
8. B.A.Piatnitski, Izv. AN SSSR, Ser. fiz., 15, 597 (1951).
9. V.Ia.Sveshnikov, Zhur. eksp. i teor. fiz., 18, 878 (1948).

DISCUSSION

V.Ia.Sveshnikov: The first temperature investigations were made back in 1936 by Vogel and Pringsheim (the report appeared in the J. of Chem. Phys. for 1936); they gave an expression for the temperature dependence but in it did not take into account the probability of spontaneous transitions hence the dependence was not linear. Pringsheim and Vogel actually showed that the α- and β-bands were attenuated in a different manner and that the attenuation constant of the β-band (the long-wave band) is independent of the temperature. We showed, however, that both bands fade with the same decrement.

PARAMAGNETISM OF BORIC PHOSPHORS IN THE PHOSPHORESCENT STATE

- N.A. Lebedev & I.D. Shmerkovich

The question of experimental determination of the paramagnetic susceptibility of dye molecules in the phosphorescent state is not only of theoretical but practical interest. Investigation of paramagnetism throws light on the nature of the metastable state of the excited molecules and makes it possible to evaluate the concentration of excited molecules.

The literature on the subject is virtually limited to the contributions of Lewis and his co-workers.[1-3] Lewis, Calwin and Kasha used a modification of Theorell's method[4]; they found that the molar paramagnetic susceptibility of an acid fluorescent dye in its phosphorescent state in boric acid at 25° agrees, within the limits of the experimental error, with the molar paramagnetic susceptibility of an oxygen molecule in the 3Σ-state. The aforementioned investigation has certain shortcomings both as regards the procedure employed in determining the magnetic susceptibility and the determination of the number of molecules in the metastable state.

In view of this we made an attempt to detect paramagnetism of metastable molecules by the procedure proposed by Zavoiski[5] and developed by the Kazan school.[6-9] This procedure was employed for investigating paramagnetic salts and their solutions. Salikhov[9] believes that under certain conditions paramagnetic absorption must always be observed in solutions of paramagnetics.

Our experiments were carried out on fluorescein and uranyl phosphors in boric acid at room temperature. The samples were placed into the coil of an Esau circuit oscillator, designed about a VT-232 (E-1148) tube and operated at a frequency of $1.2\cdot10^8$ cps. The measuring procedure is described in Ref. 8. We did not succeed in detecting any noticeable absorption. The absorption per molecule may depend on the concentration and increase more rapidly than in proportion to the concentration decrease[10]; for this reason the experiments were carried out in the 10^{-4}-$2\cdot10^{-3}$ g/g concentration range.

Analogous experiments were carried out by Shmerkovich in cooperation with the workers of the Physics Institute of the Kazan Branch of the USSR Academy of Sciences and the staff of Kazan University. Attempts were made to detect the absorption at frequencies of about 10^7 cps by the above mentioned procedure as well as by measuring the derivative of the paramagnetic absorption with respect to the magnetic field intensity (dQ/dH) at 10^8, 10^9, and 10^{10} cps.* In no case was either zero absorption or absorption incident to variation of the intensity of the biasing magnetic field from 0 to about 6000 oersted observed.

One must be very careful in evaluating the negative results of the relaxation experiments inasmuch as observation of the effect may be hampered by a number of factors. For example, great width of the absorption curve would make observation difficult and it is virtually impossible to make any a priori assumptions regarding the width. In addition, observation of the effect may be hindered in view of the familiar theorem of Kramers regarding the removal of the degeneration of levels inasmuch as in a given case the spin assignment for the system is even.

The negative results of the relaxation experiments impelled us to return to conventional magnetostatic experiments since these obviate a number of additional hypotheses.

The method developed by Lewis et al fails to take into account the appearance of additional forces incident to deflection of the pendulum due to dimagnetism of the boric acid. Actually, of course, with the polepiece points located at the center of an ideally homogeneous strip of fluorescein-activated boric phosphor,

---

*The measurements at 10^{10} cps are in need of verification, inasmuch as irradiation difficulties are encountered in working with the klystron.

the phosphor strip will remain in equilibrium when an external magnetic field is applied. However, this will now be unstable equilibrium inasmuch as there develops a null system of forces tending to spread out the projecting parts of the sample in consequence of the dimagnetism of the boric acid and the glass bar to which the phosphor is attached. With deflection of the pendulum the system will become unbalanced since one projecting part of the sample will be elongated and the other shortened. Hence, contrary to assumption of Lewis et al, the restoring force will not be proportional to the deflection of the pendulum. When the field is applied, there will be a new equilibrium position, corresponding to minimal potential energy of the system, to either side of the initial (no field) equilibrium position. It is interesting to note that the additional force due to the dimagnetism of the boric acid acts in the same direction as the paramagnetic force arising due to irradiation of the phosphor.

Instability of the null point in the experiments can be taken as confirmation of the instability of the null point of equilibrium. Unfortunately, Lewis et al do not give the expression characterising the falling off of the field and hence it is impossible to determine the positions of the new equilibrium points and the magnitude of the additional force. However, in view of the calibration experiment data ($F = 0.84\ F_{max}$) and assuming that the magnetic field intensity falls off with distance from the polepieces as H_{max}/x ($x \approx 3$ cm), we evaluate the additional force as amounting to 20% of the paramagnetic force observed by the investigators.

To obviate possible errors due to displacement of the sample, the latter should be located wholly to one side of the magnet. The repulsion due to the dimagnetism of the boric acid in this case can be compensated by a constant force. In our experiments this was achieved by means of a physical pendulum of special design, pictured schematically in the accompanying figure. The pendulum, which was fabricated from thin glass tubes prepared by drawing out 5 mm diameter glass tubing, rests on the corundum pivot points K bearing on the glass supports S. The repulsion due to the dimagnetism of the boric acid is compensated by the weight W riding on the horizontal glass rod. The sample of fluorescein and boric acid is suspended below at O.

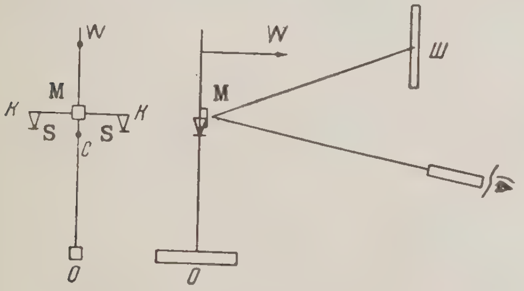

Diagram of pendulum system.

One advantage of this physical pendulum over a mathematical one is that the sensitivity of the system can be increased (theoretically indefinitely) by bringing the center of gravity C closer to the axis of rotation. In practice the sensitivity of the pendulum system is limited by friction at the supports. Furthermore, with this system it becomes possible to utilize an optical "lever" for which purpose a small mirror M, reflecting the scale Ш , is mounted on the pendulum.

Equilibrium conditions of the pendulum are characterized by

$$P a \sin\varphi = f l_{H},$$

where P is the weight of the pendulum, a is the distance from the center of gravity to the axis of rotation and f is the force acting at the end of the lower lever arm of length l_H.

The value of a is found from the expression for the period of oscillation of the physical pendulum which was determined experimentally (for one of the pendulums used, the period was 14 sec.):

$$T = 2\pi\sqrt{\frac{I}{mag}} \quad \text{and} \quad a = \frac{4\pi^2 I}{T^2 mg}.$$

The moments of inertia of the pendulum components were computed using the conventional formulas on the assumption that the glass tubes were of uniform cross section. The overall length of the pendulum was 21 cm. The weight of the pendulum with the phosphor was 0.45 g; the moment of inertia of the pendulum plus phosphor was 46.4 g cm^2; the length of the optical "lever" was 4 meters.

Under these conditions the sensitivity of the pendulum to a horizontal force applied at the end of the lower lever arm amounts to 10^{-4} dynes per mm scale graduation.

Inasmuch as the magnetic field we used was almost 2.5 times weaker than that in the experiment of Lewis et al, the effect should have been some 6.25 times smaller. However, if there were any effect it should have been readily observed in view of the 100-fold reserve of sensitivity.

In order to exclude radiometric and oxygen effects the experiments were carried out under vacuum. The phosphor was irradiated by a 1 kw motion picture projection bulb through a condenser and a heat filter (an aqueous solution of copper sulphate).

No deviation of the pendulum beyond the limits of the experimental error was observed with the phosphor irradiated.

The negative results of the relaxation experiment and our experiments with the physical pendulum can be explained only on the assumption that the value of the paramagnetic susceptibility of fluorescein and boric acid in the phosphorescent state, given by the American investigators, is over-estimated.

"M.V.Frunze"
Crimean State Pedagogical Institute

Note added in proof: Evans, in a contribution (Nature, 176, 777 (1955) which appeared after the Conference, cites evidence of paramagnetism of the metastable states but gives no definitive indication of the value of the molecular susceptibility.

References

1. G.N.Lewis & A.M.Calwin, J. Am. Chem. Soc., 67, 1232 (1945).
2. G.N.Lewis & M.Kasha, J. Am. Chem. Soc. 66, 2100 (1944).
3. G.N.Lewis, M.Calwin & M.Kasha, J. Chem. Phys., 17, 804 (1949).
4. H.Theorell, Arkiv Kemi Mineral Geol., A 16, 1 (1943).
5. S.A.Al'tshuler, E.K.Zavoiski & B.M.Kozyrev, Zhur. eksp. i teor. fiz., 14, 407 (1944).
6. E.K.Zavoiski, Zhur. eksp. i teor. fiz., 16, 603 (1946).
7. B.M.Kozyrev, Scientific Records, Kazan State University, 2, 83 (1948).
8. S.G.Salikhov, Zhur. eksp. i teor. fiz., 17, 1070 (1947).
9. S.G.Salikhov, Doklady AN SSSR, 60, 576 (1948).
10. E.K.Zavoiski, Zhur. eksp. i teor. fiz., 15, 243 (1945).

DISCUSSION

M.D.Galanin: In interpreting these experiments it is essential to evaluate the number of excited molecules present. It may be that only one tenth or one hundredth of the molecules were excited to the metastable state, in which case there is nothing surprising about the negative results obtained.

N.A.Lebedev: The negative results can be explained by a low concentration of molecules on the triplet levels. I believe further experiments to verify the described results are indicated.

Experiments on the quenching of the phosphorescence of fluorescein and trypaflavine by the electrolyte ions showed an interesting variation of quenching.

These substances in solution form a large solvate shell. To obviate this we used formic and acetic acids as the solvents. Solutions of fluorescein and trypaflavine in formic acid at low temperatures exhibit much lower phosphorescence in the presence of paramagnetic ions such as magnesium ions. Magnesium ions produce an appreciable quenching of the phosphorescence and reduce the lifetime of the molecule from 3.7 to 2.4 sec when the concentration is increased from 0.1 to 0.2 mole/liter of Mg. The presence of magnesium ions, however, has virtually no effect on the fluorescence of the solutions. Dimagnetic ions have an inverse effect: the addition of KI or KBr increases the phosphorescence by about 10%. Thus, our experiments are indirect evidence of magnetic interactions of the triplet levels.

A.V.Kariakin: It would be expedient to try pulsed discharge tubes for such experiments; according to recent experiments of Norris & Porter these sources produce a high concentration of molecules on the triplet levels.

CHEMILUMINESCENCE OF LUCIGENINE

- B.D.Ryzhikov

Investigation of chemical reactions accompanied by the emission of light is of great interest to investigators in different fields of chemistry and physics. Despite the fact that there have been numerous attempts to elucidate the emission mechanism involved in chemiluminescence, the nature of this mechanism is still obscure.

In most past researches the approach was that of studying the kinetics of emission as a function of the concentration of the components participating in the reaction. For the most part the investigators determined the time-dependence of the integral luminescence intensity. Many investigators working on chemiluminescence have tended to ignore the question of the nature of the emission, apparently simply assuming that the observed irradiation was chemiluminescence.

Obviously pure chemiluminescence can be observed only when the emission spectrum lies outside the region of absorption of the different molecules in the solution. The presence of absorbing molecules leads to distortion of the chemiluminescence spectrum and, in fact, may give rise to secondary photoluminescence. In such cases the time dependence of the integral emission intensity will be determined not only be the concentration of the chemiluminescing molecules but also by the concentration of absorbing molecules and by quantum efficiency of the fluorescing molecules. Inasmuch as in general the variation with time of each of these quantities is different, one cannot draw any definitive conclusions regarding the kinetics of chemiluminescent reactions on the basis of direct measurements of integral intensity.

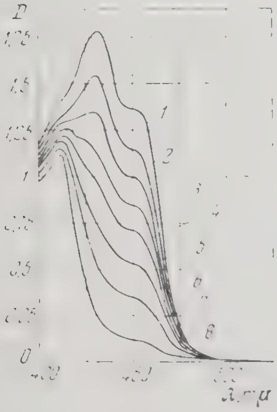

Fig. 1. Variation of the absorption spectrum of an aqueous solution of lucigenine with the reaction time ($C_{luc} = 10^{-4}$ g/cm^3; $C_{NaOH} = 10^{-3}$ g/cm^3; $C_{H_2O_2} = 10^{-3}$ g/cm^3; thickness of absorption cell - 10 mm): 1) t = 0, 2) 2.5 min, 3) 6 min, 4) 11 min, 5) 16 min, 6) 25 min, 7) 39 min, 8) 280 min.

The purpose of our investigation was to evaluate the possibility of energy transfer from the chemiluminescing molecules to the other molecules present in the solution. To this end we studied the absorption and emission spectra of chemiluminescing aqueous solutions of the lucigenine in the process of oxidation by hydrogen peroxide in an alkaline medium.

The absorption spectra (Fig. 1) in the visible region consist of three overlapping bands. During the reaction alterations are observed in only the two bands on the long-wave side. These bands are due to the lucidenine. By resolving the absorption spectra into three bands one can determine the variation in the lucigenine concentration during the course of the reaction.

The emission spectra (Fig.2) are not sensitive to changes in pH. They consist of two parts: an intense green emission with a peak at 496 mμ and a weaker **blue** emission, the peak of which it is difficult to locate precisely.

Comparison of the absorption and emission spectra shows that the green band lies outside the absorption region of the solution; consequently, the intensity of the green emission is proportional to the radiation density in the solution and independent of the variation in absorption. The blue emission, in contrast, occurs in the region of strong absorption and consequently its intensity is determined not only by the radiation density in the solution but also by the varying absorption. The variation of the intensities of the green (496 mμ) and **blue**

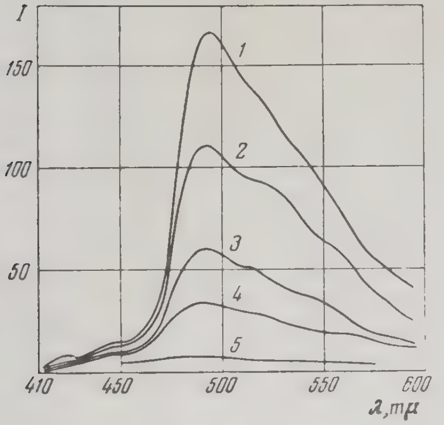

Fig. 2. Variation of the luminescence spectrum of an aqueous solution of lucigenine with reaction time ($C_{luc} = 10^{-4}$ g/cm^3; $C_{NaOH} = 10^{-3}$ g/cm^3; $C_{H_2O_2} = 10^{-3}$ g/cm^3; thickness of absorption cell d = 50 mm): 1) t = 3.5 min, 2) 10.5 min, 3) 24.5 min, 4) 41.5 min, 5) 91.5 min.

(436 mμ) emissions with time is shown in Fig. 3. It will be seen that in the case of the green radiation the intensity falls off rapidly, whereas the intensity of the blue radiation remains virtually constant, falling off only slightly towards the end of the reaction.

It is of interest to determine the true density of the blue emission and to compare it with the density of the green luminescence. To do this one must take into account the absorption in solution. While it is possible to calculate this, the computation is cumbersome. Hence we made only a qualitative evaluation of the ratio. Such an evaluation is necessary to determine what part of the green emission is due to secondary photoluminescence. Assuming that with decreasing absorption the limiting case will represent the true ratio between the densities of the blue and green radiations, we investigated the dependence of the intensity ratio of the green and blue bands on the reaction time, the thickness of the absorption cell and the lucigenine concentration. It will be seen from Fig. 4 that in all cases the intensities of the blue and green emissions finally become comparable as the absorption decreases. It is difficult to extrapolate these curves accurately; it is obvious, however, that the intensity of the blue band must become greater than that of the green one. It may reasonably be assumed therefore that the green band is primarily if not wholly due to secondary photoluminescence. Quantitative determination of the secondary luminescence intensity is somewhat difficult since in addition to the density of the blue radiation one must also know or determine the amount of energy absorbed, the value of which depends on the duration and yield of photoluminescence which also varies with time.

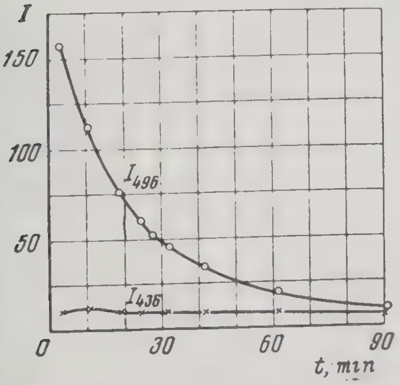

Fig. 3. Variation of the intensity of the blue (I_{436}) and green (I_{496}) **luminescence with the reaction time.**

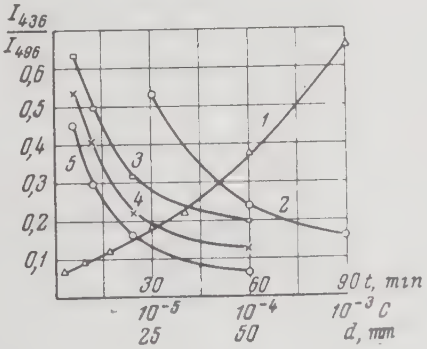

Fig. 4. Variation of the ratio I_{436}/I_{496}: 1) with the reaction time, 2) with the lucigenine concentration and 3-5) with the absorption cell thickness d: 3) t = 35 min, 4) 18 min, 5) 3 min.

Thus we see that in the chemiluminescing solutions in addition to the chemiluminescence proper there is a certain amount of photoluminescence. In consequence of the strong absorption in the blue region of the spectrum the intensity of the chemiluminescent emission is appreciably lower than the intensity of the secondary photoluminescence. In studying the kinetics of chemiluminescent reactions one must take into account the existence of these two types of radiation. Measurement of only the variation in the intensity of total emission will not give

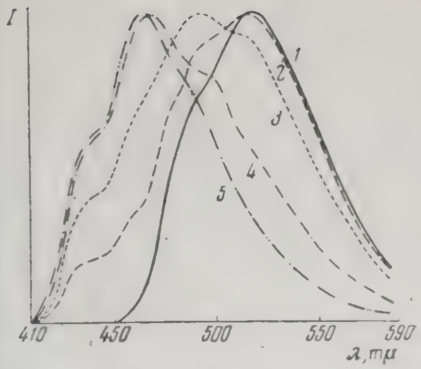

Fig. 5. Fluorescence spectra of the chemiluminescing solution: 1) t = 0, 2) 18 min, 3) 38 min, 4) 90 min, 5) 48 hours.

a true picture of the processes associated with chemiluminescence of lucigenine.

It would be of interest to identify the molecules responsible for the two types of emission. Some indication of the origin of the green and blue radiation may be obtained from a study of the fluorescence spectra. The fluorescence spectra recorded at different instants during the oxidation reaction are shown in Fig. 5. We can draw the following conclusions in view of the fact that during the reaction there are present in the solution two kinds of fluorescing molecules, the emission spectra of which are similar to the fluorescence spectra of the molecules of the initial substances and the end products of the reaction. The chemiluminescence spectrum of lucigenine is similar to the fluorescence spectrum. The small shift of the chemiluminescence spectra to the short-wave side relative to the fluorescence spectra of lucigenine may be explained by the superposition of the spectrum of the blue emission. Apparently the green radiation is due to the lucigenine molecules and molecules formed at the initial stages of the reaction and similar in structure to the lucigenine. The fluorescence spectrum of the final product lies in the blue region. Hence presumably the origin of the blue emission is connected with the formation of the end products of the reaction.

In conclusion I wish to thank V.L.Levshin for valuable suggestions and advice and A.M.Grigorovski for making the chemical reagents available.

Physics Department of
Moscow State University

DISCUSSION

B.Ia.Sveshnikov: To check your hypothesis you could add a small amount of fluorescein, which absorbs blue radiation much better than lucigenine, to the solution. You should then obtain the emission of this added component.

B.D.Ryzikov: Such experiments were made. There is observed an increase in intensity, a narrowing of the bands and shift of the spectrum to the long-wave side relative to the fluorescence spectrum of pure fluorescein.

A.V.Kariakin: What concentrations of hydrogen peroxide did you use? To what can one attribute the blue chemiluminescence?

B.D.Ryzhikov: The hydrogen peroxide concentration was varied between 10^{-4} and 10^{-2} g/cm^3; measurements were made at different ratios of alkali to peroxide. The blue band is apparently connected with the formation of some product of the reaction in the excited state. Further investigation is necessary to identify it.

B.Ia.Sveshnikov: Until now, primarily Drew's hypothesis has been used to explain the mechanism of chemiluminescent reactions: a peroxide of lucigenine or 3-aminophthalohydrazine is first formed and then the oxygen bridge is thrown off and we obtain the lucigenine or hydrazine in the excited state. This hypothesis has been substantiated by investigations of the kinetics of the reaction; moreover, Drew isolated the peroxide compound which decomposed under irradiation. The emission observed by the speaker is perhaps superposed on the chemiluminescence; the experiments appeared convincing. But one must be careful in attempting to interpret the mechanism.

ON THE STRUCTURE OF THE CHLOROPHYLL-PROTEIN-LIPOID COMPLEX

- T.N.Godnev

In recent years there has been convincing proof that the more important components of the photosynthetizing parts of the molecules of chlorophyll a and chlorophyll b couple with the molecules of albumin and lipoids to form a unique complex[1]. On electron diffraction photographs of microsections a few hundredths of a micron thick[2] through chloroplasts of certain plants one can readily discern pigmented protein layers on the chloroplast granules, so that, on the one hand, one can readily evaluate the total surface area of the pigmented layers and, on the other hand, having established the amount of chlorophyll, determine the area on these surfaces occupied by each pigment molecule. If we accept that this area corresponds exactly to the diameter of the phorbin ring of the chlorophyll molecule, there can be no doubt that the chlorophyll molecules are distributed in a single layer over the surface of separation of the protein and lipoid lamina composing the chloroplasts. We can, therefore, now think of the chlorophyll molecule as a sort of two dimensional crystal: monomolecular lamina, the molecules of which are associated through phytol groups with the lipoid molecules (probably phosphatides), and at the same time through phorbin rings with the protein molecules.

Whereas most investigators agree on the nature of the linkages between the phytol groups and the lecithin molecules, there is a difference of opinion as regards the bonds between the phorbin nucleus and the protein molecules.

Liubimenko[3], Hilpert et al[4], and Stoll et al[5] all note the chemical nature of the protein-chlorophyll bonds, assuming the protein-chlorophyll-lipoid complex to be a colored proteid. However, so far, there is no definitive proof of this. Tsvet[6] and Seybold & Egle[7] consider an adsorptive association to be more likely, pointing to analogous chlorophyll adsorbates on different substances with the properties of chlorophyll in choloplasts. Actually, in the light of the latest data it is scarcely correct to attempt a clear distinction between adsorption and chemical linkages, inasmuch as adsorption is frequently realized through the agency of Van de Waals forces, hydrogen bonds and coordinate bonds. All this leads us to believe that the chlorophyll molecules adsorbed on the surface of the protein phase are at the same time joined through the phorbin rings by labile chemical bonds with the protein molecules. We felt it should be feasible to obtain experimental proof of the existence of such linkages and, possibly, some indication of their nature by studying the interaction of chlorophyll with protein molecules and their decomposition products (ammino acids), on the one hand, and with high molecular weight aliphatic acids, on the other hand.

Krasnovski[8], Evstigneev[9], working in Terenin's laboratory, and Livingston et al[10] demonstrated that chlorophyll does form complexes with different polar molecules.

Inasmuch as in our earlier researches we obtained data indicating that the acid proteins group and the basic radicals of the chlorophyll molecules participate in such linkages, we set up experiments to study the influence on chlorophyll (in benzene solution) of stearic and palmitic acid at concentrations not sufficiently high to displace the magnesium from the chlorophyll. An examination of the curves described in Ref. 11 shows that these curves are fully similar to the curves of Krasnovski, Evstigneev and Livingston. This is evidence in favor of the formation of molecular complexes of chlorophyll with high molecular weight aliphatic acids. Such complexes are probably similar to the complex formed by chlorophyll with the acid groups of protein molecules.

Of appreciably greater interest, we feel, is investigation of the interaction of chlorophyll with components of protein molecules and with proteins in general. However, such experiments encounter the difficulty that chlorophyll is soluble only in organic solvents while most proteins and amino acids are readily dissolved

only in water. To eliminate this difficulty instead of chlorophyll we used chlorophyllide a, which differs from chlorophyll a by the substitution of hydrogen for the phytol lipophylic radical $C_{20}H_{39}$. This makes the chlorophyllide, which wholly retains the structure of the phorbin ring, readily soluble in water. The interaction of chlorophyllide with neutral amino acids slightly altered the absorption without affecting the position of the absorption peaks.

Aspartic and glutamic acids at concentrations not causing the removal of the magnesium also fail to change the position of the peaks in the violet and the red region but did reduce the absorption at both these peaks which is probably connected with the formation of labile coordinate bonds.

We use the water soluble albumin M.B. 45000 for the protein in our experiments. The use of chlorophyllide which is molecularly soluble in water instead of chlorophyll thus made it possible to obtain interaction of the phorbin nucleus under conditions not complicated by the polymerization of the pigment molecules with the relatively simple molecules of the protein. At a moderate protein concentration, we observe an appreciable increase in absorption particularly near the peaks at 430 mμ and 660 mμ with a simultaneous small shift of the peaks to the long-wave side which can be explained by the formation of loose linkages between the protein and the pigment.

It is difficult at present to clarify the details of this association. However, since the changes in the spectrum obtained are insufficient to explain the long-wave shift observed in live leaves, we think it possible that the displacement is a consequence both of the aggregation of chlorophyll molecules into monomolecular layers and of chemical interaction with the formation of labile chlorophyll-protein linkages. This assumption is consistent with the data of Meyer[12], who demonstrated a large displacement to the long-wave side in aqueous colloidal suspensions of chlorophyll when the particle concentration attains the level observed in chloroplasts and granules. Our assumption is also substantiated by the experiments of Krasnovski et al on the spectral characteristics of films of chlorophyll and bacterio-chlorophyll, as well as by the results reported by Jacob et al[13] who studied the properties of pure crystalline chlorophyll (phytolchlorophyllide). This hypothesis is also consistent with the above described electron diffraction photographs which show the chlorophyll arranged in thin molecular laminae closely associated with each other and with the protein and lipoid molecules.

Krasnovski and Kosobutskaia[14] note that chlorophyll reforming from protochlorophyll is a monomer. The chlorophyll molecules, being linked to the protein and lipoid, are not associated with each other and form a complex of the chlorophyll-protein-lipoid (C-P-L) type.

In light of the monomolecular chlorophyll film theory (the two dimensional crystal concept) we can sketch the following picture: The initially forming C-P-L monomers are distributed in individual islets on the surface of the protein plate, probably in small embryonic chloroplasts, and then, linking up with similar islets, form regular monomolecular layers, producing the above described laminar chloroplast structure. In light of the experiments of Turchin et al[15] and our researches on the renewal of chlorophyll, this structure does not appear to be stable inasmuch as chlorophyll even when present in a constant amount in the chloroplast is continuously sensitized and decomposed. It is entirely possible that the monomer and the aggregated modifications may dissociate into chlorophyll, protein and lipoid molecules. This is consistent with the partial extractibility of chlorophyll from chloroplasts by entirely inactive solvents (strongest for chlorophyll a) which we observed in a different degree for almost all plant tissue. This can be explained on the assumption that some part of the chlorophyll in process of decomposition or synthesis is molecularly dissolved in the lipoid phase. This apparently serves to explain the weak fluorescence of chlorophyll in live

chloroplasts.

Institute of Physics and Mathematics of the
Academy of Sciences of the Byelorussian SSR

References

1. E.Rabinovich, Fotosinez (Photosynthesis) IL, 1951.
2. J.J.Wolken, F.A.Schwertz, J. Gen. Physiol., 37, 111 (1953).
3. V.N.Liuvimenko, Dnevnik I Vsesoiuznogo s"ezda russkikh botanikov v Petrograde, (Reconrs of the First All Union Meeting of Russian Botanists in Petrograd) 1921.
4. S.Hilpert, H.Hofmeier, A.Woner, Berichte d. Deutsch. Chem. Ges., 64, 2570 (1931).
5. A.Stoll, E.Wiedmann, Atti congr. intern. chim., 10th Congr., Rome, 1938.
6. M.S.Tsvet, Khromatograficheskii adsorbtsionnyi analiz (Chromatographic adsorption analysis) 1946.
7. A. Seybold & K.Eg.e, Botan. Archiv, 41, 578 (1940).
8. A.A.Krasnovski & G.P.Vrin, Doklady AN SSSR, 95, 611 (1954).
9. V.V.Evstigneev, Biokhimiia, 14, 559 (1952).
10. R.Livingston, W.F.Watson & J.McArdle, J. Amer. Chem. Soc., 71, 1542 (1949).
11. T.N.Godnev, R.V.Efremova & L.A.Kravtsov, Present issue of the Bulletin.
12. K.P.Meyer, Helv. Phys. Acta, 12, 349 (1939).
13. E.E.Jacobs, A.E.Valter & A.S.Holt, Arch. of Biochem. and Biophys., 53, 228 (1954).
14. A.A.Krasnovski & L.M.Kosobutskaia, Doklady AN SSSR, 91, 343 (1953).
15. F.V.Turchin, M.A.Guminiskaia & E.G.Plyshevskaia, Iav. AN SSSR, Ser. Biol., 6, 66 (1953).

THE INFLUENCE OF CERTAIN ACID AND BASIC SUBSTANCES ON THE ABSORPTION SPECTRA OF CHLOROPHYLL AND CHLOROPHYLLIDE

- T.N.Godnev, R.V.Efremova and L.A.Kravtsov

According to the theory developed in Ref. 1, chlorophyll molecules are not adsorbed purely physically on the chloroplast stroma but rather form complexes with the protein and lipoids. It is assumed that labile chemical bonds are formed between the chlorophyll molecules on the one hand and the protein and lipoid molecules on the other. Wolken and Schwertz[2] showed that chlorophyll molecules form monomolecular layers on the boundaries of the protein and lipoid phases, being oriented so that the phorbin rings are associated with the active groups of the protein and the phytol parts with the lipoid molecule.

In order to verify this we investigated the spectra of the products of reaction of chlorophyll with proteins and amino acids. As a first step we investigated the absorption spectra of solutions of chlorophyll a in ether and benzene and chlorophyllide in water. The locations of the principal peaks in the absorption spectra of these solutions are listed below **(wavelengths in mμ):**

Solution	Violet	Red
Chlorophyll in ether	429	662
Chlorophyll in benzene	415	658
Chlorophyllide in water	402	656

The chlorophyllide was obtained from a mixture of chlorophyll a and b through the action of the enzyme chlorophylase which led to a loss of phytol by the chlorophyll. It must be assumed that we obtained primarily chlorophyllide a in view of the fact that the content of chlorophyll a in leaves is 3-4 times greater than that of chlorophyll b and the enzyme acts on chlorophyll a more rapidly than on chlorophyll b. Chlorophyllide is readily soluble in water which made it possible to investigate the influence of amino acids that are soluble in water on the basic part of the chlorophyll molecule: the phorbin ring which persists in the chlorophyllide. It is known from Fischer's work that the appearance of the red absorption peak is connected with the hydrogenation of the fourth pyrrole ring of porphin; enhancement of this peak is connected with the replacement of two hydrogen atoms in the pheophytin by magnesium during the formation of chlorophyll; the red peak is shifted to the short-wave side. Formation (or rupture) of the cyclopentane ring (V) leads to a small shift of this peak to the long-wave (or short-wave) side of the spectrum. The violet peak is associated primarily with the conjugate porphin system.[3]

Thus from the changes in the absorption spectra of chlorophyll under the influence of acid or basic substances, we can judge of the transformations that occur in the most characteristic part of the chlorophyll molecule - in the phorbin ring. In view of the fact that in the complexes the phorbin ring is apparently linked to the proteins, we investigated the influence of substances entering the composition of proteins, i.e., amino acids. In addition we investigated the influence of certain other acids and amines. The absorption spectra were recorded (on a SF-4 spectrophotometer) 24 hours after preparation of the solution when the reaction between the chlorophyll and the added substance was assumed to have gone to completion. The absorption figures for the curves shown in the accompanying figures are relative values.

The amino acids used were glutamic, aspartic and aminoacetic acid and cysteine. Inasmuch as chlorophyllide and these acids are all soluble, in water we investigated the influence of different concentrations of the acid on the chlorophyllide.

Glutamic acid ($HOOCCH \cdot NH_2(CH_2)_2COOH$) yields an acid reaction in water; it

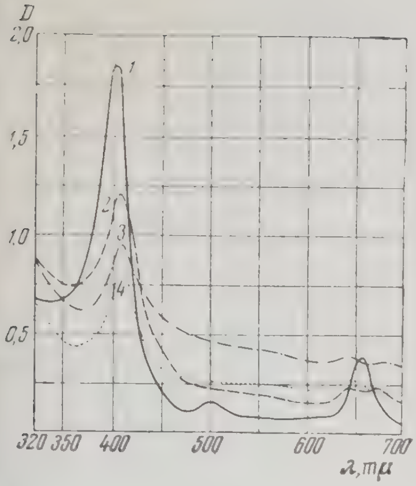

Fig. 1. Influence of glutamic acid on the absorption spectra of aqueous solutions of chlorophyllide: 1) pure solution, 2) 0.01 N acid, 3) 0.1 N, 4) 0.2 N.

is of common occurence in plant proteins. Figs. 1 and 2 show the absorption spectra of chlorophyllide in water with the addition of the following concentrations of glutamic acid: 0.001, 0.01, 0.05, 0.1, 0.2, 0.5 and 1 N. Fig. 1 gives the general absorption spectra in the range from 320 to 450 mμ; Fig. 2 shows only the region of the red absorption peak. The absorption at the violet peak (402 mμ) falls off with increasing concentration of glutamic acid (from 0.01 to 0.2 N). The violet peak is very slightly (4-5 mμ) shifted to the long-wave side. The influence of glutamic acid on the red peak of chlorophyllide can be seen from Fig. 2. With increasing glutamic acid concentration there is observed an alteration in the chlorophyllide molecules: two peaks at 642 mμ and 675 mμ are formed in the absorption spectra. This is evinced initially by the decrease in absorption in the region of the red peak and splitting of the peak at an acid concentration of about 0.001 N. With further increase in acid concentration the absorption in the region of the red peak of chlorophyllide continues to increase in the interval from 0.01 to 0.1 N. The absorption peak at 642 mμ systematically increases while the peak of 675 mμ decreases. Further increase in acid concentration from 0.1 to 1 N leads to destruction of the 675 mμ peak. The peak at 642 mμ becomes sharper although the absorption actually decreases. Apparently a certain amount of pheophorbid is formed; this is also evinced by the increasing displacement of the violet peak to the long-wave side. It is possible that labile complexes of pheophorbid with the still undecomposed chlorophyllide are formed; this is suggested by the formation of the new peak at 675 mμ and its subsequent disappearance.

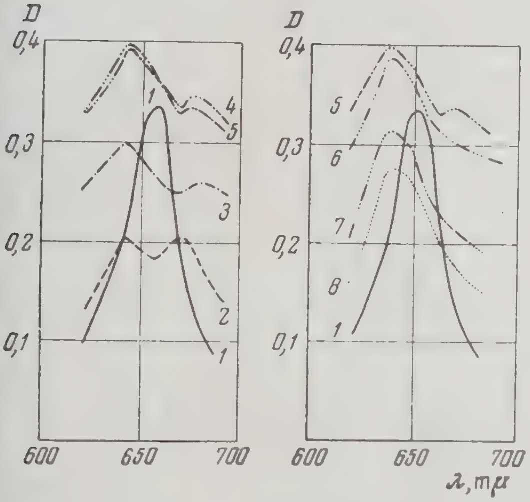

Fig. 2. Influence of glutamic acid on the absorption spectra of aqueous solutions of chlorophyllide (in the region of the red peak): 1) pure solution, 2) 0.001 N glutamic acid, 3) 0.01 N, 4) 0.05 N, 5) 0.1 N, 6) 0.2 N, 7) 0.5 N, 8) 1 N.

Aspartic acid ($HOOCCH\cdot NH_2CH_2COOH$) in aqueous solutions has a pronounced acid reaction. It is found free in plants and is contained in some proteins. We recorded the absorption spectra of chlorophyllide in water with the addition of small quantities of aspartic acid (0.0006, 0.0012 and 0.0024 N). In the violet region we observe the same picture as obtains when glutamic acid is added to an aqueous solution of chlorophyllide, i.e., there is a gradual decrease in absorption and a small shift of a peak to the long-wave side. In the red region there is a shift of the absorption peak similar to that obtaining under the influence of glutamic acid but apparently the formation of the pheophorbid proceeds more rapidly.

Aminoacetic acid (glycine) (H_2NCH_2COOH) has a neutral reaction in water. We recorded the absorption spectra of chlorophyllide with the addition of aminoacetic acid of concentrations ranging from 0.2 N to the saturated solution. These absorption spectra show that aminoacetic acid does not alter the chlorophyllide

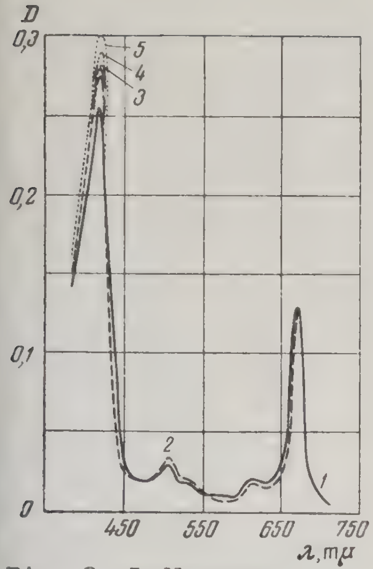

Fig. 3. Influence on acetic acid on the absorption spectra of chlorophyll a in benzene: 1) pure solution, 2) 1/80 N acetic acid, 3) 1/40 N, 4) 1/20 N, 5) 1/10 N.

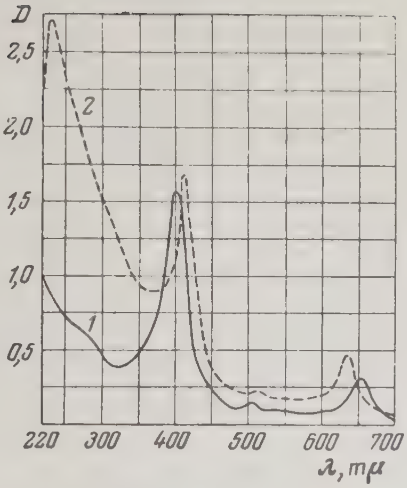

Fig. 4. Influence of diethylamine on the absorption spectra of an aqueous solution of chlorophyllide: 1) pure solution, 2) 1 N diethylamine.

molecule, i.e., that only intermolecular interaction occurs.

The amino acids, cysteine and cystine, also do not produce any great changes in the absorption spectra of chlorophyllide.

The aliphatic acids used in the experiment included acetic, palmitic and stearic. These acids were added to chlorophyll dissolved in benzene and in ether. Their effect amounted to an increase in the violet peak with increasing concentration (Fig. 3). The red peak is displaced some 2-4 mμ to the short-wave side in the case of palmitic acid, some 2 mμ in the case of acetic acid. It should be noted that aliphatic acids enhance the violet peak, while amino acids bring it down.

Thus aliphatic acids behave in a fashion analogous to that observed in the experiments of Krasnovski et al[4] and Livingston et al[5] who investigated the formation of molecular complexes with polar molecules over a wide range of concentrations. The changes in the chlorophyll spectra observed were similar to those described above.

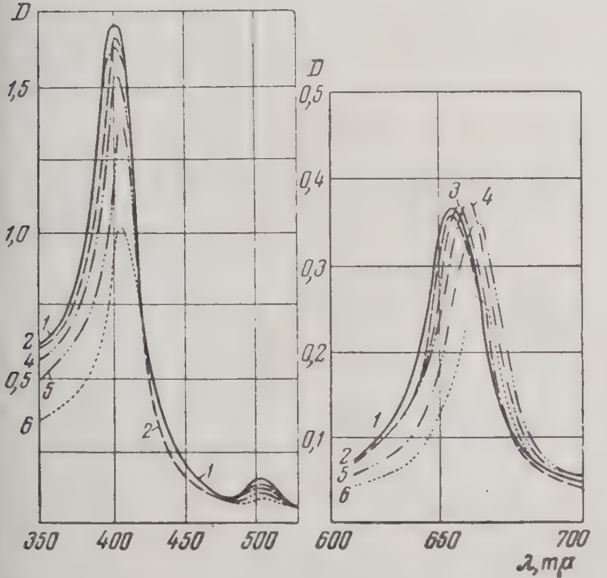

Fig. 5. Influence of pyridine on the absorption spectrum of aqueous solutions of chlorophyllide: 1) pure solution, 2) 0.1 N Pyridine, 3) 0.2N, 4) 1N, 5) 2N, 6) 5 N.

The basic substances investigated included diethylamine $(C_2H_5)_2NH$, dimethylamine $(CH_3)_2NH$, β-naphthylamine $C_{10}H_7NH_2$ and pyridine C_5H_5N. The strongest of these bases -- diethylamine -- displaces both peaks in the absorption spectrum of chlorophyllide towards the middle, i.e., the violet peak, 10 mμ to the long-wave side and the red peak, 20 mμ to the short-wave side (Fig. 4). The medium strength base -- dimethylamine -- shifts only the red peak some 15 mμ to the short-wave side, while the weakest of bases -- β-naphthylamine -- does not shift the absorption peaks and has an effect on the absorption spectra of chlorophyllide in water opposite to that of weak aliphatic acids.

Apparently the influence of bases (amines) leads to disintegration of the cyclopentane ring (V) at high concentrations. The effect of pyridine on the absorption spectra of chlorophyllide in water is the following:

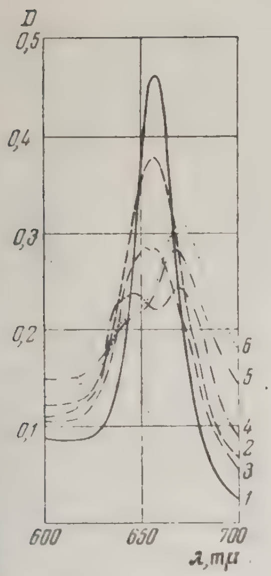

Fig. 6. Influence of hydrochloric acid on the absorption spectrum of aqueous solutions of chlorophyllide: 1) pure solution, 2) 0.0011 N HCL, 3) 0.0013 N, 4) 0.0015 N, 5) 0.0017 N, 6) 0.0030 N.

the absorption at the violet peak is reduced with increasing pyridine concentration (as in the case of amines), while the red peak is displaced to the long-wave side (Fig. 5). Apparently pyridine even at the highest concentration (5 N) does not break up the cyclopentane ring but rather forms complexes.

In addition to the influence of organic acids we investigated the effect of hydrochloric acid on chlorophyllide in water. The effect is most marked in the region of the red peak at 656 mμ in the absorption spectrum of chlorophyllide (Fig. 6). At small concentrations of HCL (0.0011 N) the absorption is reduced. With an increase in concentration to 0.0013 N the red peak begins to split and at a concentration of 0.0015 N two clearly separated peaks of approximately the same height develop at 648 and 670 mμ. Further increase in concentration of HCL leads to destruction of the 648 mμ peak and an increase in absorption at 670 mμ. The red peak at 670 mμ indicates that the magnesium has been eliminated from the chlorophyllide and that pheophorbid is formed. However, this process is probably accompanied by the formation of unstable complexes of pheophorbid with the chlorophyllide that has not had time to decompose.

Thus our experiments indicate the possibility of formation of unstable molecular complexes of chlorophyll with amino groups and other basic groups of protein as well as with carboxyl groups. It is conceivable that these complexes are formed at the expense of additional valences of magnesium as is suggested by Terenin[6] and a number of other investigators.

The acid and, to an appreciable extent, the basic radicals of protein molecules may participate in the formation of these complexes. It is possible that this type of linkage binds the phorbin rings of the chlorophyll molecules on the surface of the protein plates of the chloroplasts.

Institute of Physics and Mathematics of the
Academy of Sciences of the Byelorussian SSR

References

1. T.N.Godnev, Stroenie khlorofilla i metody ego kolichestvennogo opredeleniia (The structure of chlorophyll and methods of its quantitative determination), Minsk 1952.

2. J.J.Wolken & F.A.Schwertz, J. Gen. Physiol., 37, 111 (1953).

3. E.Rabinovich, Fotosintez (Photosynthesis) Vols. I and II, M. 1953.

4. V.B.Evstigneev, A.A.Krasnovski & V.A.Gavrilova, Doklady AN SSSR, 70, 261 (1950).

5. R.Livingston, W.F.Watson & J.McArdle, J. Am. Chem. Soc., 71, 1542 (1949).

6. A.N.Terenin, Fotokhimiia khlorofilla i fotosintez (Photochemistry of chlorophyll and photosynthesis), M. 1951.

DISCUSSION

A.N.Terenin: Which are the most effective acids from the point of view of displacement of the spectrum to the red side, and from the point of view of

development of the red peak? Was there not some elimination of magnesium under the influence of the acids?

T.N.Godnev: At high concentrations there was of course some removal of magnesium. Magnesium pheophorbid has a tertiary nitrogen atom and acids are readily joined to it as to all porphyrins. One peak is explained by the formation of a complex of the acid with the unaffected chlorophyllide, while the second is due to the formation of a complex with pheophorbid. The experiments with hydrochloric acid indicate the point at which removal of the magnesium begins.

V.L.Levshin: How is the behaviour of chlorophyll a different from that of chlorophyll b?

T.N.Godnev: Chlorophyll a is the predominant form and is found in all plants in which the COH group is present; in some plants, for example, algae, chlorophyll b is entirely absent, only chlorophyll a is present. This means that chlorophyll a is the basic and that chlorophyll b is a secondary component, adapted to certain conditions. In shade growing plants the ratio of chlorophyll a to b is about 2:1; in other plants the ratio is 5:1. To start with, we concentrated on chlorophyll a since chlorophyll b complicates the problem. In cases where it was impossible to separate them we took both a and b together.

B.Ia.Sveshnikov: Does chlorophyll in plants fluoresce?

T.N.Godnev: It does, but weakly. One might find a state of aggregation in which chlorophyll would fluoresce better; so far we have not succeeded in realizing this. Noar, for example, has reported on obtaining certain states of chlorophyll in association with protein, but check experiments have not substantiated his findings. It has also been reported that adsorbates on certain aluminates were obtained; this, too, has not been verified. Possibly there is another form of association of chlorophyll with protein and lipoids which may fluoresce; it probably includes free molecules which combine with lipoids to give fluorescent molecules. The whole question is in need of further study.

A.N.Terenin: There are two points of view regarding the anomalously large shift of the red absorption peak of chlorophyll in live leaves as compared with the shift in solutions and in artificial adsorbates: the first is that there are formed complexes with protein through the intermediary of strong acid groups of the protein-lipoid medium in the live leaf and that these complexes are responsible for large displacement which cannot be realized in ordinary solutions or artificial absorbates. It should be noted that chlorophyll, just as its close relative porphyrin, is an acid-base indicator. Hence under the influence of acids and in complexes with them there may be an appreciable displacement of the absorption region. In artificial systems we have not yet detected an appreciable displacement but, on the other hand, in case of aggregation of chlorophyll there is at once manifested a shift to the long-wave side of the same order of magnitude as in live leaves. This gave rise to the second point of view that the shift in the absorption observed in live leaves is due to aggregation, i.e., the presence in chlorophyll of colloidal associations; they are in a sense two-dimensional crystals (not three-dimensional formations) with the chlorophyll molecules arranged in a dense monolayer grid.

Hence we here again have the same questions regarding the migration of energy, the transfer of energy, the behaviour of aggregates, and the changes in spectra that we have already discussed at this conference.

Apparently where the luminescence of live leaves is concerned there is the question of just what fluoresces: free molecules of chlorophyll dissolved in lipoid or aggregated formations. This is a problem very much on the research agenda. It must be said that in the case of leaves, due to reabsorption, it is difficult to establish mirror symmetry between the absorption spectrum and the luminescence spectra, which would immediately resolve the question.

The following experiments were carried out by A.A.Krasnovski. He studied the luminescence and absorption spectra of chlorophyll not in mature leaves but in

eaves which had been kept in the dark and only began to turn green. In such cases we may assume that the chlorophyll will have a low concentration and will not be aggregated to any extent. The absorption peaks proved to be in the shorter wave region of the spectrum as compared with an ordinary solution; as the chlorophyll accumulated the peak gradually shifted to the long-wave side, as usually observed in leaves.

V.L.Levshin: In live leaves fluorescence is very weak and there is a large shift to the red side. Could we not assume that in a live leaf complex organic molecules form a system which shifts the spectrum to a much greater extent than molecular aggregations. We might reason by analogy with polyenes; in the case of polyenes as the chain becomes more complicated, the shift is increased and the luminescence falls off.

L.A.Tumerman: There can be no doubt that the question of just what luminesces - aggregated chlorophyll or free chlorophyll molecules - is important where elucidation of the structure of chloroplast is concerned. It seems to me that the problem could be solved by measuring the decay of luminescence. It is known that the fluorescence efficiency of chlorophyll solutions is high, while in leaves it is very low. Regarding the duration of luminescence of chlorophyll in solution we have indirect data indicating that it is of the order of 10^{-9} sec; regarding the emission of chloroplast we have no information. If we should succeed in measuring the duration of luminescence of chloroplast and it prove to be of the same order as in solution this would prove that the fluorescence is due to free molecules and that the measurement of the fluorescence yield of chloroplast are erroneous because the concentration of the fluorescing molecules was not properly evaluated. On the other hand, if it should prove that both the yield and duration of luminescence change in parallel, decrease in going from solution to chloroplast, this would indicate that chlorophyll aggregations are involved.

SPECTROSCOPIC INVESTIGATIONS OF THE PRODUCTS AND MECHANISM OF OXIDATION OF CELLULOSE BY NITROGEN PEROXIDE

- M.M. Pavliuchenko and I.N. Ermolenko

The product obtained by oxidizing cellulose with nitrogen peroxide is an excellent hemostatic substance capable of being absorbed by tissues without an anaphylatic reaction. It also finds other applications in medicine, for example, as an absorptive carrier in the administration of drugs.

In 1945 a large plant devoted to the production of cellulose oxidized with nitrogen peroxide was opened in the United States[1]. This product is also finding increasing use in textile and other industries. The mechanism of the oxidation reaction, however, has been little studied. We elected to study this reaction using spectroscopic procedures in conjunction with chemical methods. The reaction was carried out according to a procedure developed by us in a specially designed set-up which has been described earlier.[2]

The absorption spectra were recorded by means of a SF-4 quartz photoelectric spectrometer. The cellulose material used was cellophane film. α-cellulose absorbs light only in the far ultraviolet. β-cellulose is known to have an absorption peak at 358 mμ. The aldehydes, ketones and furfural absorb in the same region. γ-cellulose has two peaks, one at 346, the other at 420 mμ which are apparently associated with uronic acids. The absorption of light by cellulose may be due to the chromophore groups CHO, CO, $\mathrm{C}{<}^{\mathrm{O}-}_{\mathrm{O}-}$ and COOH or to impurities.[3]

Cellulose absorbs light only in the ultraviolet and infrared regions. With oxidation by nitrogen peroxide the absorption increases in both regions. In the 320 to 400 mμ interval we detected absorption consisting of a system of bands at 330, 341.5, 355 and 365 mμ as shown in Fig. 1 for cellulose oxidized at 25°. There is also a very intense band in the 230-270 mμ region.

Prolonged extraction under vacuum, heating to 50° and washing with hexane do not reduce the intensity of the observed absorption bands. These tests show that the absorption bands in the spectrum of oxidized cellulose are not due to absorption of light by the adsorbed nitrogen oxides or other by-products of the reaction. To verify this further we investigated the absorption spectra of the different oxides of nitrogen.

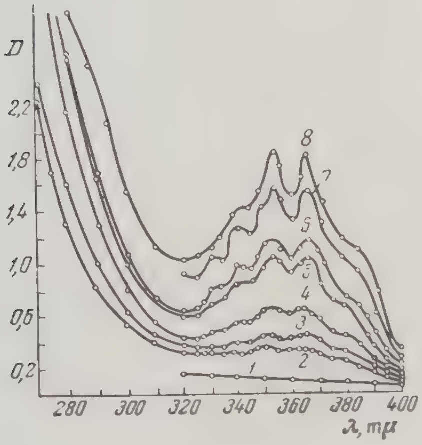

Fig.1. Absorption spectra of cellulose oxidized by nitrogen peroxide for different lengths of time: 1) initial cellulose, 2) 445, 3) 235, 4) 180, 5) 140, 6) 10, 7) 20, 8) 45 min. $D = \log I/I_0$.

It might be assumed for instance, that the absorption is due to nitrogen peroxide adsorbed by the cellulose. We measured the absorption spectrum of gaseous nitrogen peroxide as well as of solutions of the oxide in organic solvents. As is known, in the temperature interval from -11 to + 150° the gaseous phase consists of an equilibrium mixture of $NO_2 + N_2O_4$. The spectra of solutions of N_2O_4 in organic solvents (chloroform, benzene, CCL_4, etc.) have an absorption band at 340 mμ (Fig. 2) and agree as regards appearance with the spectrum for gaseous N_2O_4 as deduced by Hall and Blacet[4], whence it may be concluded that in solutions the nitrogen peroxide is present in the dimer form.

The investigated solvents can be arranged in a series on the basis of the band intensities. The maximum intensity of the band at 340 mμ is observed in CCL_4 and C_6H_6 solutions. The intensity in ethylchloride is lower and that in $CHCL_3$ is still lower.

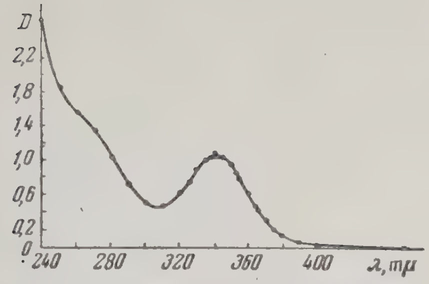

Fig. 2. Absorption spectrum of solution of N_2O_4 in $CHCL_3$.

Thus neither the spectrum of N_2O_4 nor that of NO_2 corresponds to that observed for oxidized cellulose. Another gaseous product that might be adsorbed on cellulose in NO. Nitric oxide is another product of the cellulose exidation reaction. Its spectrum lies in the wavelength region below 280 mμ. At 226 mμ there is a narrow band with a coefficient of absorption at the peak of K = 9.3 ± 0.1. At 280 mμ there is a weak absorption band (K ∼ 0.6). Nitric oxide does not absorb light in the 320-400 mμ interval; hence it is not responsible for the bands observed in the absorption spectrum of oxidized cellulose. In the presence of NO_2, nitric oxide yields nitrogen trioxide; many investigators are of the opinion, however, that N_2O_3 is actually an equimolecular mixture of NO + NO_2. The vapor density of the trioxide corresponds to the formula N_2O_3 only for the dry gas.

In the spectrum of N_2O there is a band at 226 mμ which also appears in the spectrum of NO. A number of bands in the 320-400 mμ interval is connected, we assume, with incomplete drying. The absorption coefficients here are very low (∼ 0.4). It is known that water reacts with N_2O_3, yielding HNO_2. Our assumption is substantiated by the spectrum of N_2O_3 recorded without preliminary drying of the gas. In this case the intensity of the bands in the 320-400 mμ region is appreciably higher.

The absorption of the moist gas is much stronger than that of dry gas, not only in 320-400 mμ interval, but also in the vicinity of 226 mμ. It is not impossible that the large coefficient of absorption at the peak of the 226 mμ band in the case of N_2O_3 as compared with that in the band for NO (11 as against 9.4) is due only to the additional absorption of HNO_2.

According to the data in the literature, the spectrum of N_2O_3 has diffused bands at 3850 Å. Thus the observed spectrum of the oxidized cellulose is not anywhere duplicated by the oxides of nitrogen. Even through careful and prolonged drying it is impossible to eliminate all the moisture from cellulose. On the other hand, water is one of the products of the oxidation reaction. Hence one may expect the formation of nitrous or nitric acid due to the interaction of the oxides with water. Nitric and nitrous oxides absorbed on the cellulose may either themselves absorb light or may form esters absorbing light. The spectrum of HNO_3, which is well known, does not correspond with the observed oxidized cellulose spectrum.

We measured the absorption of nitrocellulose films containing 11 and 12% nitrogen. The absorption curve is shown in Fig. 3. A solution of nitrocellulose in methyl alcohol had an identical absorption spectrum.

The spectra of organic nitrates given in literature are similar to the nitrocellulose spectrum. There is no absorption in the 320-400 mμ interval in the nitrocellulose spectrum. Hence the bands in this region of oxidized cellulose spectrum cannot be due to nitric acid or to a cellulose ester.

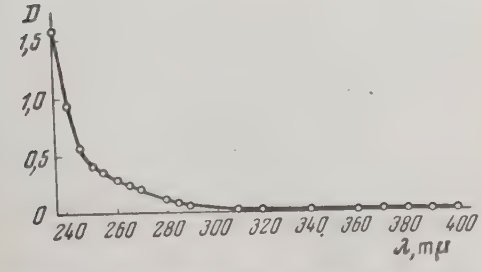

Fig. 3. Absorption spectrum of nitrocellulose.

We also obtained the spectrum of an aqueous solution of HNO_2 in mixture with HNO_3 and NO. The spectrum of nitrous acid is similar to the absorption spectrum of the oxidized cellulose, although the peaks of the absorption band of HNO_2 are displaced somewhat to the long-wave side.

Despite the similarity of the absorption spectra we doubt whether the observed absorption of oxidized cellulose can be due to adsorbed HNO_2. As already noted prolonged extraction under vacuum, heating and a treatment

with a nonaqueous solvent not only does not lead to disappearance of absorption in the 320-400 mμ interval but even does not decrease it noticeably as might be expected in the case of adsorbed acid. Treatment with water on the other hand, even for a brief period, makes the absorption bands disappear.

On the other hand, it is known that in acting on alcohol, nitrogen peroxide or nitrous acid at the instant of formation readily form esters which are readily decomposed under the influence of water.

We assume that in the process of oxidizing the cellulose nitrogen peroxide forms cellulose nitrite which is responsible for the absorption in the 320-400 mμ region. Nitrocellulose film after prolonged exposure to NO_2 and short term extraction under vacuum does not yield absorption bands in the 320-400 mμ region; this is further evidence against firm adsorption of nitrogen oxides or acids by the cellulose. The alcohol groups in nitrocellulose are already esterified and hence no cellulose nitrite forms.

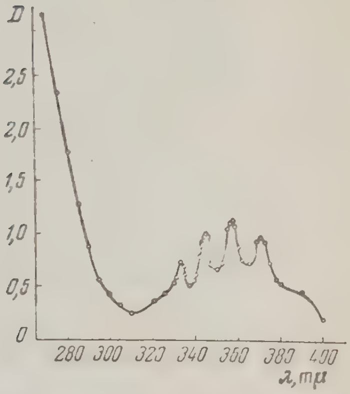

Fig. 4. Absorption spectra of isoamyl nitrite.

The properties of organic nitrites given in the literature readily explain the attributes of oxidized cellulose we observed. It is known that nitrites are often intermediate products in the oxidation of paraffins by nitrogen axides.

We investigated the absorption spectra of the products of interaction of nitrogen peroxide with an excess of the lower alcohols: methyl, ethyl and butyl. The shape of the spectra in the 320-400 mμ region is identical with the shape of the spectrum of the cellulose exidation product. Here, in the case of the lower alcohols acted on by nitrogen peroxide, we have the same esterification of the alcohol groups leading to the formation of a nitrite as in the case of cellulose. This was further substantiated by a study of the analogous spectra of pure nitrites. We recorded the spectrum of isoamyl nitrite and its solution in hexane; this is shown in Fig. 4. This spectrum is identical in shape with the spectra of methyl nitrite, ethyl nitrite, β-octyl nitrite, etc. cited in the literature. Thus the system of bands in the 320-400 mμ interval in the spectrum of the oxidized cellulose may be attributed to the chromophor nitrite group as a whole or possibly only to N=O.

By measuring the absorption spectra of samples of cellulose oxidized for different lengths of time one can follow the changes in the nitrite content in the course of the reaction by the variation of the optical density at the absorption peaks. For our observations, we selected the peak at 365 mμ. The variation of the optical density of oxidized cellulose film measured at this wavelength as a function of the oxidation time at 31° is shown in Fig. 5; it will be seen that the nitrite content attains a maximum value and then falls off.

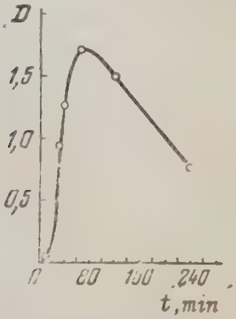

Fig. 5. Variation of nitrite content in the cellulose with the oxidation time at 31°.

The decrease in the nitrite content occurs simultaneously with an increase in the concentration of carboxyl groups. This led us to assume that the cellulose nitrate is an intermediate product of the reaction.

We felt it would be of interest to compare a spectra of organic nitrites, nitrogen oxides and their solutions, and nitrous acid with the spectrum of a salt of nitrous acid. The absorption spectrum of a concentrated aqueous solution of sodium nitrite in the 320-400 mμ region has only one peak (Fig. 6). As may be seen from the curve of Fig. 2, this too is the region of the absorption peak of solutions of NO_2 in a number of solvents. Like absorption in this region is characteristic of a number of organic nitro compounds. The

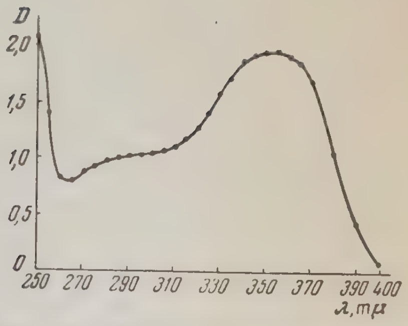

Fig. 6. Absorption spectrum of an aqueous solution of $NaNO_2$.

spectrum of the NO_2 ion as studied by Friedman[5] has in addition to a low intensity band in this region a very intense band at 211 mμ which is associated with the transition of an electron from the NO_2 ion to the solvent molecule.

The absorption spectrum of nitrous acid, as we see, differs from the spectrum of its salts and at the same time is similar to the spectrum of its esters. This is proof that the structure of HNO_2 differs from the structure of its salts and that the acid comprises the same chromophor group as its ester. Consequently nitrous acid must have the structure H-O-N=O. Apparently, the electrons of the chromophor group $N\lessgtr^{O}_{O}$ participate in the absorption of the NO_2 ion. Possibly both chromophors take part in the absorption of nitrous acid.

The absorption of the nitrite in the 320-400 mμ interval consists of four separate bands. On the basis of investigation of the optical anisotropy of these bands in β-octyl nitrite, Kuhn and Lehmann[6] conclude that these bands are associated with different electronic rather than vibrational transitions.

As already noted the absorption band is absent from the spectra of oxidized cellulose recorded after washing with water. Whence it may be concluded that no appreciable quantity of nitro compounds is formed in the oxidation reaction inasmuch as these compounds are not saponified by water.

We attributed the intense absorption band at 210-220 mμ in the spectrum of oxidized cellulose (the band removed by water treatment) and the weak band at 280 mμ to carboxyl and carbonyl groups, respectively, the presence of which in the samples was established by chemical analysis and which according to the data in the literature absorb in these regions. Thus our results show the presence of nitrite groups in the oxidation product. Their content passes through a maximum in the course of the reaction. This permits us to affirm that cellulose nitrite is an intermediate product of the oxidation reaction.

It was of interest both from the practical point of view and for the purpose of clarifying the mechanism of the process to study the character of the reaction at different temperatures. As far as we know ours is the first study of the influence of temperature on the rate of the reaction. By means of our special setup we carried out the oxidation reaction at 25, 31, 44 and 65°.

Determination of the carboxyl groups by the calcium-acetate method shows that the final carboxyl group content decreases with increasing oxidation temperature.

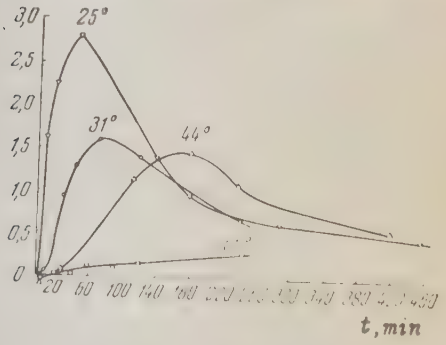

Fig. 7. Variation of the nitrite content in the oxidation product as a function of the oxidation time at different temperatures.

We also carried out a spectroscopic investigation of the nitrite content in the product obtained with different exidation times at different temperatures. As may be seen from Fig. 7, as the temperatures increased the maximum nitrite content decreases and the peak value is attained after a longer oxidation time.

In fact, there is no peak in the nitrite content curve for the experiment at 65°. In the case of oxidation at 25° the maximum content is attained in 45 min, at 31° in 70 min, at 44° in 180 min. Whereas the peak nitrite content decreases with increasing temperature, the final content attained after a prolonged reaction time is virtually independent of the temperature.

Conclusions

1. Spectroscopic investigation of the oxidation of cellulose by nitrogen peroxide showed the expediency of using spectroscopic procedures for investigating the mechanism of the cellulose oxidation reaction. This procedure made it possible to establish the formation of one of the principal intermediate products of the reaction - cellulose nitrate - and to investigate the variation in its content with time and the temperature of the reaction. Hitherto even the existence of the cellulose nitrate had not been established by chemical methods.

2. The spectroscopic procedure makes it possible to follow the formation of carboxyl and carbonyl groups in the course of the oxidation process and also to establish the influence of a number of factors (time, temperature, etc.) on formation of the carboxyl groups.

3. All this helps clarify the mechanism of this highly complex oxidation reaction.

"V.I.Lenin" Byelorussian State University

References

1. R.L.Kenyon, R.H.Hasek, L.G.Davy & K.I.Broadbooks, Ind. Eng. Chem., 41, No. 1, 2 (1949).
2. M.M.Pavliuchenko & I.N.Ermolenko, Uch. Zap. BGU, Ser. Khim. (Scientific Record of the Byelorussian State University, Chemical Series) (1955).
3. E.Freiber, Koll. ZS., 130, 39 (1953).
4. T.C.Hall & F.E.Blacet, J. Chem. Phys., 20, 1745 (1952).
5. H.L.Friedman, J. Chem. Phys., 21, 319 (1953).
6. W.Kuhn & H.L.Lehmann, ZS. Electroch., 37, 549 (1931).

Discussion

A.N.Sevchenko: Do the oxidation products exhibit luminescence? Did anyone study the Raman spectra?

M.M.Pavliuchenko: There are indications that almost any purified cellulose may luminesce. As far as we know there have been no spectral investigations of the products of the oxidation reaction.

V.K.Matveev: Has the presence of nitrogen and nitrous oxide been established chemically?

M.M.Pavliuchenko: Analyses for nitrogen were carried out rather carefully. The analytic procedure is very onerous and each point requires hours of work; scores of hours would have been necessary to construct the requisite curve whereas spectroscopic analysis gives a complete picture in a matter of minutes. The results of chemical analysis are in complete agreement with those of spectroscopic studies. The presence of nitrous acid was determined qualitatively.

A.N.Sevchenko suggested that in the future not only absorption spectroscopy but also Raman and infrared spectroscopy be applied to the study of cellulose.

POLARIZED LUMINESCENCE OF CUBIC CRYSTALS (Abstract*)

(*The complete article appears in Usp. fiz. nauk, 58, 69 (1956).)

- P.P.Feofilov

A distinctive feature of polarized luminescence of crystals of the cubic system is that anisotropic luminescence centers introduced into the optically isotropic cubic crystals or formed therein are oriented along the crystal symmetry axes. The character of the orientation is determined by the crystallochemical structure of the system, the nature of the luminescence centers and the manner in which they enter into the crystal lattice of the host substance. Crystals containing symmetrically oriented anisotropic centers must be regarded as quasi-isotropic systems inasmuch as despite the absence of dichroism and double refraction the degree of luminescence polarization in such crystals is strongly dependent on the position of the plane of polarization of the exciting light relative to the axes of symmetry. By investigating this dependence one can uniquely establish the orientation of the centers and this in turn makes it possible to throw light on the nature of luminescence centers, on the one hand, and to arrive at certain deductions regarding the character of the arrangement of the extraneous atoms and ions in the given crystal lattice, on the other hand.

Investigation of photochemical processes induced by polarized light in ionic crystals containing color centers makes it possible to decide between the alternate variants of the oscillator model describing luminescent color centers.

The fact that the individual luminescent centers are oriented along the axis of symmetry of cubic crystals particularizes the method of polarization diagrams developed by Vavilov for establishing the nature (multipolarity) of the elementary oscillators. Applying the method of polarization diagrams extended to the case of cubic crystals the writer was able to establish the electric dipole character of the luminescent color centers in ionic crystals and to detect in luminescence spectrum of europium ions introduced into the crystal lattice of fluoride lines corresponding to emitters of four different types.

ELECTROLUMINESCENCE OF ORGANIC COMPOUNDS (Abstract)

- L.A.Tumerman

The report reviews the work of Bernanoz and his colleagues who investigated the luminescence of a series of acridine dyes and other substances under direct excitation by an electric field. The effect was observed when an alternating electric field was applied to cellophane film and thin sheets of paper coated with aqueous or alcohol solutions of the different substances. In a number of cases and particularly in that of carbazole, the investigators also observed electrophotoluminescence. In this effect the normal emission brightness induced by the application of an electric field is greatly enhanced when the colored film is f first exposed to daylight or light from a mercury tube. This additional emission, due to preliminary photoexcitation, decays approximately according to the exponential law for some 20-25 minutes down to the usual stable dark value of the electroluminescence.

"P.N.Lebedev" Physical Institute of the
Academy of Sciences of the USSR

POLARIZATION DIAGRAMS OF LUMINESCENCE OF MOLECULAR SINGLE CRYSTALS

- I. D. Zhevandrov

Introduction

Investigation of the polarization of luminescence of molecular single crystals can yield valuable information on the structure and anisotropy of both the crystal lattice and the molecules constituting it. If, in the first approximation, we apply to crystals the oscillator model which has proved helpful in understanding the polarized luminescence of solutions, we can say that the polarization of the luminescence of single crystals is determined by two anisotropy factors: the first is the orientation of the oscillators responsible for the emission relative to the axes of the molecule (i.e., relative to its structural skeleton), the second is the orientation of the molecule itself in the lattice (i.e., the orientation of the molecular axes relative to the crystallographic axes).

Where one of these factors is known from independent data, the other can in principle be determined from the polarization of the luminescence. Thus if the orientation of the molecules in the lattice is known from x-ray data, the polarization of the luminescence can be used to determine the orientation of the emitting oscillator relative to the molecular axes. Results along this line have been obtained by Brodersen[1] for naphthalene, by Pesteil[2] for stilbene, naphthalene, diphenyl, acenaphthalese, fluorene and other compounds and by Ganguly and Choudhury[3] for anthracene, pyrene, phenanthrene and benzyl.

A different approach is feasible. It is possible to establish the orientation of the oscillators responsible for the absorption and emission relative to the structural elements of the molecule from a comparison of the polarization spectra of fluorescing solution with the absorption spectra. We can formulate the problem as follows: given the orientation of the oscillator in the molecule, determine the orientation of a molecule of the substance in the crystal lattice. In solving the problem it is assumed that interaction of the molecules in the crystal does not substantially effect the luminescent properties of the individual molecules and in particular the orientation of the emission oscillators. Optical data on the orientation of the molecules in the crystal lattice obtained in this manner can be of great aid in x-ray analysis, the procedures of which in the case of organic crystals are complex and cumbersome.

Obviously for the purposes in question it is not enough to measure the polarization of the fluorescence in some one direction. It is essential to determine the spatial distribution of the polarization. In some investigations (in particular, in certain investigations dealing with naphthalene), the measurements were made in three directions, perpendicular to the faces of the single-crystal parallelepiped cut so its edges were parallel to the crystallographic axes. This yielded a complete three dimensional picture. Such measurements, of course, require the preparation of appropriate single crystals. Among organic molecular crystals there are many which upon sublimation form thin single-crystal plates. The preparation procedure is facile and simple but in this case it is impossible to make measurements in three mutually perpendicular directions. However, such measurements can be replaced by measurements of the dependence of the polarization of fluorescence on the angle between the direction of observation and the normal to the surface of the plate in the widest attainable range of angles.

Analogous characteristics were studied in the case of fluorescing solutions by Vavilov[4] and Feofilov[5]. In solutions the spatial distribution of the polarization is characterized by two directions: the direction of observation and the direction of the electric vector of the exciting light. In crystals the polarization of a fluorescence is independent of the polarization of the exciting light[6] and is wholly determined by the direction of observation. The variation of the

degree of polarization in the case of crystals with the angle of observation may be termed (as is the usage in working with solutions) the polarization diagram. Obviously the polarization diagrams will be different for different orientations of the crystal itself, i.e., for different angles of rotation of the crystal about the normal to the surface of the crystal plate.

Polarization diagrams of fluorescing solutions are of great interest in that they allow us to determine experimentally the multipole order of the elementary emitters, inasmuch as the diagrams differ for cases of absorption and emission of light by different multipoles (dipoles, quadrupoles, etc.). The situation is somewhat different in crystals. If two oriented media (crystals) consist of emitters characterized by a different distribution of the emission in space but an identical distribution of the polarization, the polarization diagrams of these crystals will be identical whereas the polarization diagrams of solutions in the analogous case will be different.

For example, the emission diagram for an electric dipole and a quadrupole are different. The intensity in a direction forming an angle α with the axis of the multipole for a dipole is proportional to $\sin^2 \alpha$, while for a quadrupole it is proportional to $\sin^2 2\alpha$; the spatial distribution of the polarization emission for the two is identical however. Crystals composed of identically oriented dipoles or quadrupoles will also have identical polarization diagrams (in the expression for the degree of polarization $P = (I_{\parallel} - I_{\perp})/(I_{\parallel} + I_{\perp})$, $\sin^2 \alpha$ or $\sin^2 2\alpha$ will cancel out). The same principle will hold for crystals with any number of different orientations of dipoles and quadrupoles (here the terms $(\sin^2\alpha_1 + \sin^2\alpha_2 + \sin^2\alpha_3 + \ldots)$ or $(\sin^2 2\alpha_1 + \sin^2 2\alpha_2 + \sin^2 2\alpha_3 + \ldots)$ will cancel out). In isotropic solutions, on the other hand, dipoles and quadrupoles yield different polarization diagrams because the fluorescence can be polarized only in the case of anisotropic excitation and dipoles and quadrupoles having a given orientation will be excited unequally and will make different contributions to the total polarization of the emitted radiation. Hence here the difference in the diagrams for dipoles and quadrupoles is important.

Obviously crystals comprised of emitters with different spatial distributions of the polarization will have different polarization diagrams (for example, the diagrams in the case of electric dipoles as against magnetic dipoles will differ).

Thus in the case of crystals, polarization diagrams as a method for determining the multipole order of the emitters are less generally useful than in the case of isotropic media.

However, as was noted above, in the case of crystals they help solve a different problem, that of determining the orientation of the molecules in the lattice.

Feofilov[7] used the method of polarized luminescence to investigate the orientation of the elementary oscillators in crystals of alkali halide compounds of the cubic system. Such crystals are optically isotropic. Organic molecular crystals, as a rule, belong to more complex systems (in many cases to the monoclinic). They are optically anisotropic and in investigating their polarized luminescence double refraction must be taken into account.

1. Subject of investigation

For purposes of investigation it is expedient to start with a material for which we know 1) the orientation of the emission oscillators in the molecules, 2) the optical anisotropy of the crystal (its indicatrix, i.e., the directional dependence of the index of refraction) -- this is necessary in order to be able to introduce the appropriate corrections in the observed polarization of the fluorescence -- and 3) the orientation of the molecule in the crystal lattice as deduced from x-ray defraction or other independent data. The last is desirable for verifying the orientation obtained from measurements of the fluorescence polarization.

For purposes of the present investigation we selected anthracene for which all the above data are known.

The emission oscillator in the anthracene molecule lies in the plane of the molecule and is directed along its transverse axis. This follows from theoretical calculations[8,9] and experimental data, in particular from some investigations of the absorption spectra[10] and polarization spectra of solutions of anthracene[11] and its derivatives.

The indicatrix of anthracene crystals has been studied by Obreimov et al.[13] These investigators measured the index of refraction for different angles in the (010) plane and obtained the corresponding indicatrix sections.

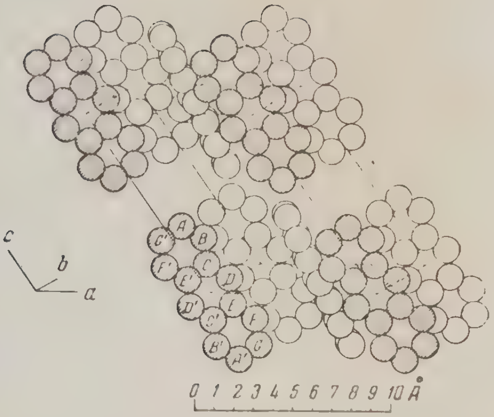

Fig. 1. Arrangement of anthracene molecule in the unit cell.

An x-ray structural analysis of crystalline anthracene was first carried out by Robertson[14] in 1933 and later repeated by his group[15] in 1950. The crystal lattice of anthracene belongs in the monoclinic system. Robertson obtained the following data for the unit cell:

$$a = 8{,}56\,\text{Å},\ b = 6{,}04\,\text{Å},\ c = 11{,}16\,\text{Å},\ \beta = 124°42'.$$

The unit cell contains two molecules. The molecules are located at the lattice sites and in the center of the (001) faces (Fig. 1). The orientation of the molecules differs. Below we list the angles between the molecular axes and the crystal axes. These angles define the orientation of the molecules at the lattice sites in accordance with Robertson's latest data. The values given in (Ref. 15) differ little from the earlier 1933 data.

	L	M	N
a	119°,7	71°,3	36°,2
b	97°	26°,6	115°,5
c'	30°,6	71°,8	66°,2

Here L, M and N are the axes of the anthracene molecule (L is the longitudinal, M the transverse, and N the axis normal to the plane of the molecule), a, b and c' are the axes of the crystal (a and b are the crystallographic axes and c' is the axis perpendicular to the plane ab).

The position of the molecules in the centers of the (001) faces is obtained from the location of the molecules at the sites by means of reflection in the (010) plane or rotation about the b axis and displacement by 1/2 a and 1/2 b. Inasmuch as the emission oscillators are directed along the transverse molecular axis we are primarily interested in the orientation of precisely these axes of the molecule with respect to the lattice. Fig. 2 shows the oscillator scheme of the unit cell of the anthracene crystal.

The emission oscillators 00_1 and $0'0''$ (the transverse axes of the anthracene molecules located at the lattice site and at the center of the face) are oriented at angles $\varphi = 26.6^{\circ}$ and $\Psi = 71.3^{\circ}$ relative to the axes b and a. Both oscillators lie in the plane passing through the b axis and forming an angle η with the ab plane. The angle between the b axis and projection of each of the oscillators on the plane bc' = ξ. The angles η and ξ are readily computed: $\eta = 44^{\circ}$ and $\xi = 19.3^{\circ}$.

Further for such an oscillator diagram we can readily compute the dependence of the degree of polarization $P = (I_{\parallel} - I_{\perp})/(I_{\parallel} + I_{\perp})$ of the emission on the direction of observation, i.e., on the angle χ reckoned from the c' axis in the ac' plane or in the bc' plane.

In the first case (χ in the plane ac'):

$$P(\pm\chi) = \frac{\cos^2\varphi - \sin^2\varphi\cos^2(\eta\pm\chi)}{\cos^2\varphi + \sin^2\varphi\cos^2(\eta\pm\chi)}. \qquad (1)$$

In the second case (χ in the plane bc'):

$$P(\pm\chi) = \frac{2\cos^2\psi - [\sin^2\psi\cos^2(\xi\mp\chi) + \sin^2\psi\cos^2(\xi\pm\chi)]}{2\cos^2\psi + [\sin^2\psi\cos^2(\xi\mp\chi) + \sin^2\psi\cos^2(\xi\pm\chi)]}. \qquad (2)$$

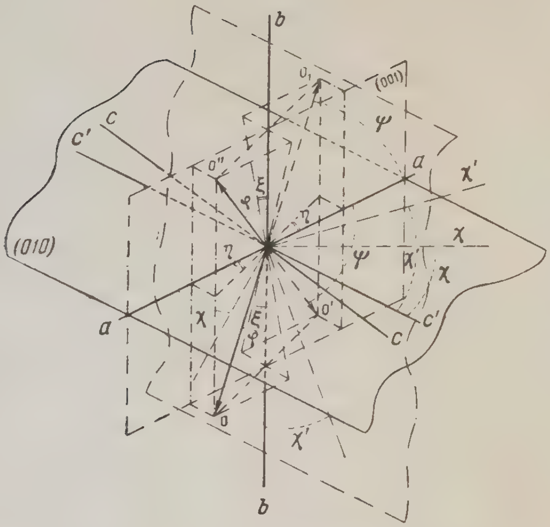

Fig. 2. Oscillator diagram of the elementary anthracene crystal cell.

Substituting the values of the angles φ, η, ψ and ξ in equations (1) and (2) we can compute the polarization diagram for an anthracene crystal for the case when the b axis is parallel to the principal direction of the polarimeter (1) and for the case when the a axis is oriented in this direction (2). The results of such computations are shown in Figs. 3 and 4. In the first case the polarization is positive in a wide range of angles; in the second case negative. Let us make the convention of calling these "positive" and "negative" polarization diagrams.

2. Procedure and experimental results.

The single crystals were prepared by sublimation of purified anthracene in porcelain crucibles. They were obtained in the form of very thin plates (approximately 10 mμ) which could readily be lifted with a needle and set in optical contact with a glass or quartz support. The surface of the plate is the (001) plane. From among the many crystals formed in the sublimation we selected the best, i.e., those formed separately, having a uniform appearance and being free of defects and cracks. It is desirable to diaphragm the edges of the single crystal to eliminate their depolarizing effects.

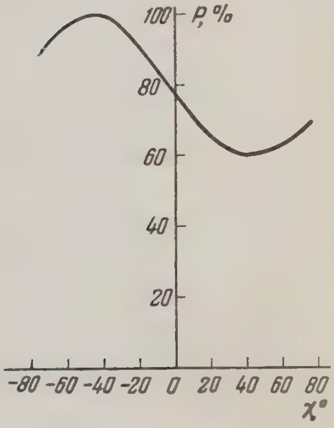

Fig. 3. Positive polarization diagram computed on the basis of x-ray analysis data.

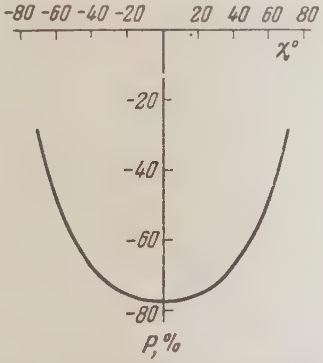

Fig. 4. Negative polarization diagram computed on the basis of x-ray analysis data.

The crystal on its support was mounted on the vertical axis of the goniometer so that the axis lay in the plane of the crystal. The Cornu **polarimeter was** mounted on the goniometer circle with its optical axis passing through the center of rotation. This arrangement made it possible to measure the polarization of the fluorescence at different values of the angle χ. In addition the crystal was also mounted in a special holder with a vertical circle and could be rotated about the horizontal axis passing through the center of the crystal. This was necessary in order to vary the orientation of the crystal.

The fluorescence was excited by light from a mercury tube in the vicinity of the 365 mμ line. The direction and polarization of the exciting light are unim-

portant inasmuch as the polarization of the fluorescence of a single crystal is independent of the anisotropy of excitation. In most cases the fluorescence was excited by nonpolarized light incident along the normal to the surface of the crystal from the side opposite to that of observation. The polarization of the fluorescence obviously depends on the orientation of the crystal. In measurements along the normal to the surface of the crystal polarization of the fluorescence depends on the angle between the projections of the oscillators on the surface, i.e., on the (001) plane. It may be seen from the oscillator scheme these projections are located symmetrically relative to the crystallographic axes a and b; the a axis bisects the obtuse angle between the projections while the b axis bisects the acute angle between them. As the crystal is rotated about the horizontal axis the degree of polarization $P = (I_{\parallel} - I_{\perp})/(I_{\parallel} + I_{\perp})$ along the normal to the crystal will gradually change ($I_{\parallel}$ is the component parallel to the principle direction of the polarimeter and $I_{\perp}$ is the component perpendicular to it). The maximum of the azimuthal dependence of the polarization occurred at the orientation when the b axis was vertical; the minimum when the a axis was vertical.

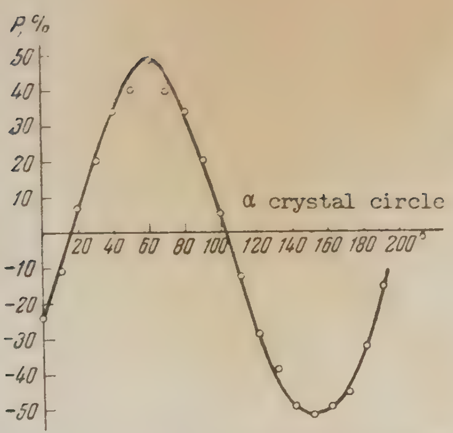

Fig. 5. Azimuthal dependence of the fluorescence polarization of an anthracene single crystal.

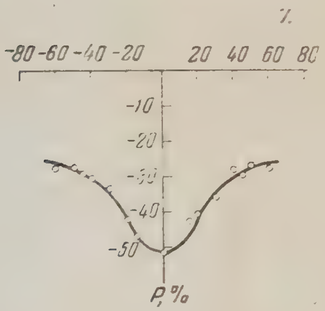

Fig. 6. Experimental negative polarization diagram.

The azimuthal dependence curve of **the fluorescence** polarization of one of the investigated anthracene single crystals is shown in Fig. 5.

The azimuth values corresponding to the maximum and minimum indicate the positions of crystal for which one should obtain the "positive" and "negative" polarization diagrams. Obviously for each diagram of this type there are two positions 180° apart. In order to enhance the accuracy and obviate accidental errors we obtained the diagrams for all four azimuth values.

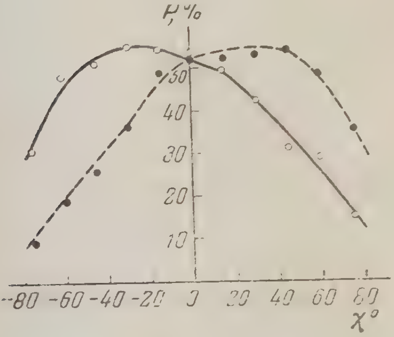

Fig. 7. Experimental positive polarization diagrams of the first type.

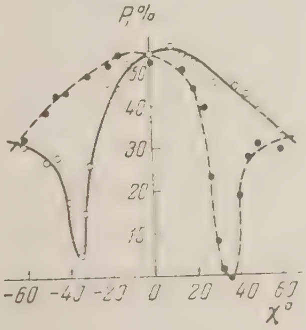

Fig. 8. Positive polarization diagrams of the second type.

Proceeding in the outline manner we investigated an appreciable number (several score) of anthracene single crystals; the following results were obtained.

The negative polarization diagrams for all monocrystals have the same appearance and are in qualitative agreement with the negative diagram plotted on the basis of x-ray data. A typical experimental negative polarization diagram **is shown in Fig.6.** [illegible] value the measured polarization is lower than the theoretical, the difference varying in different crystals. This difference may be attributed to different depolarizing [illegible] factors; in particular, the difference between the abs[illegible] tion of different specimens can be due to the presence in some of them of unnot

cracks, minor surface defects, etc.

The positive polarization diagrams in most cases have the appearance shown in Fig. 7. Here again the observed polarization is less than the theoretical; moreover in this case the angular variation of the curves differs markedly from the variation of the curves plotted on the basis of x-ray data. In the case of some single crystals the absolute value of the polarization at $\chi = 0$ attains 60%, in other cases it is appreciably lower; however, the character of the variation in most cases is similar.

Apparently the depolarization in these cases is also due to imperfections of the single crystals. Thus the polarization of fluorescence can serve as index to the homogeneity and degree of perfection of the specimens.

Aside from the polarization diagrams described, in a few individual cases we obtained positive diagrams of an entirely different type (see Fig. 8). It is worth noting that the negative diagrams for these exceptional crystals have the usual shape.

3. Corrections

Before comparing the experimental data with that computed on the basis of theory we must take certain corrections to account.

In the computed polarization diagrams no allowance is made for the optical anisotropy of the crystal which necessarily affects the light propagated therein. The theoretical calculations are made for a certain orientation of the oscillator system in an isotropic medium. Yet the actual fluorescing molecular crystal is not only an anisotropic emitter but is also essentially a double refracting anisotropic medium for the light, in particular, for its inherent fluorescence radiation.

Anthracene crystals belong to the monoclinic system and are biaxial. In monoclinic crystals, as we know, the crystallographic axis b is perpendicular to the other two axes (a and c), the angle between which differs from a right angle. One of the principal indicatrix axes coincides with the b axis while the other two axes lie on the plane ac, but do not coincide with either a or c, the positions of which are specific for each given substance. The optical axes are perpendicular to the circular sections of the indicatrix and lie in the plane of the major and minor principal axes of the latter.

The fluorescence light emitted by a molecular oscillator having a certain orientation and, consequently, plane polarized with a given azimuth will then be propagated through the crystal in all directions, undergoing double refraction. It will be propagated in each and every direction just as light falling on the crystal from the outside on the point of location of the oscillator and will be polarized in the same manner. For each direction of the wave normal of such incident light there will be two directions in the crystal along which the light will be propagated with different polarizations. In our particular case of a biaxial crystal, the polarization of light (i.e., the direction of oscillation of the induction vector D) in these directions is given by the familiar theorem of Fresnel (Ref. 16).

The oscillation directions lie in the planes bisecting the angles between the planes passing though the direction of the wave normal and the optical axes. In this respect a uniaxial crystal is a particular case. The two optical axes merge into one and, accordingly, one direction of oscillation will lie in the principal plane (extraordinary ray), the second direction in the plane perpendicular to it (ordinary ray).

The ratio of the intensities of differently polarized light in these two directions is determined by the orientation of the electric vector of the incident light relative to the above indicated directions in the crystal. The intensities will be equal when the electric vector of the incident light forms an angle of 45° with these directions and also if the incident light is unpolarized.

On the other hand, if the electric vector of the incident plane polarized

light coincides with one of the directions of oscillation in the crystal (the so-called uniradial azimuths - see Ref. 17) only one ray will be propagated in the crystal, while the intensity of the other will be equal to **zero**.

Thus in effect the incident or emitted light propagating in any direction is essentially split into two beams which fall on the inside face of the crystal at different angles. The linear divergence of the beams will be negligibly small in view of the small thickness of the crystal (for crystal thickness of 10 mμ and an angle of observation of χ = 60°, the linear divergence in anthracene is 1.3 mμ).

These two beams falling at different angles on the exit face of the crystal will also be characterized by different indices of refraction. After refraction they will be parallel in the air but the ratio of their intensities will differ from that obtaining in the crystal since they undergo different reflection losses. In consequence of this the degree of polarization of light emerging from the crystal in a given direction will be different from the polarization of the light emitted inside the crystal in the same direction. In order to determine this true polarization one must introduce an appropriate correction for the reflection loss difference.

To evaluate this correction let us make use of the Fresnel formulas for reflection and refraction of light at the interface between two transparent media. These formulas were deduced for isotropic media but we will use them for the case of anisotropic media separately for the beams of different polarization, taking into account the different indices of refraction in two directions and for the differently polarized beams. The expressions relating the amplitudes of the incident A^E and refracted A^D light for the case when the electric vector lies in the plane of incidence (A_p) and the case when it is normal to the plane (A_s) have the following form:

$$A_p^D = \sigma_p A_p^E \quad \text{and} \quad A_s^D = \sigma_s A_s^E,$$

where

$$\left.\begin{aligned} \sigma_p &= \frac{2\cos\delta\sin\chi}{\sin(\delta+\chi)\cos(\delta-\chi)}, \\ \sigma_s &= \frac{2\cos\delta\sin\chi}{\sin(\delta+\chi)}, \end{aligned}\right\} \qquad (3)$$

here δ is the angle of incidence in the crystal and χ is the angle of refraction into air.

If in the anthracene crystal the light is propagated in the plane ac, we have the case of a "positive" polarization diagram. The optical axes lie in the plane ac inasmuch as the central principal axis of the indicatrix coincides with the crystal axis b. Both planes passing through the wave normal and the optical axes merge into one plane (the ac plane). Consequently, one direction of oscillation of the electric vector coincides with the b axis, while the other is perpendicular to it and lies on the plane ac. The first vector (A_s) is perpendicular to the plane of incidence, the second (A_p) is parallel to it, ($A_s \parallel b$ and $A_p \perp b$). Obreimov et al[13] measured the index of refraction for different directions of light in the ac plane and for different directions of the electric vector ($\parallel$b and $\perp$b). The values of the indices of refraction computed on the basis of the data given in Ref. 13 are shown in Fig. 9.

The principal axes of the indicatrix (except the central one) as well as the optical axes of the anthracene crystal are diffused. The cited data pertained to a wavelength of 436 mμ, which lies near the peak in the luminescence spectrum of crystalline anthracene.[18]

Knowing the values of the indices of refraction we can find the angles δ of incidence in the crystal (different for different directions of oscillation of the electric vector) corresponding to the **refraction angle** χ in air for the case of a "positive" polarization diagram and, consequently, the values of the coefficients σ_p and σ_s. Having these, we can go from the amplitudes A^D of the refract-

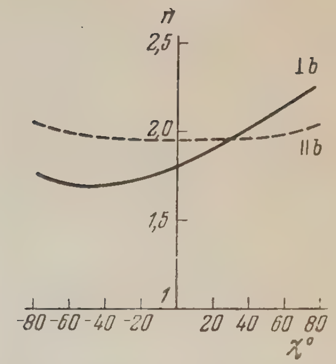

Fig. 9. Dependence of the indices of refraction on the direction of propogation in the anthracene crystal.

ed light, the ratio of which A^D_p/A^D_s is known from the experimentally measured degree of polarization, to the amplitudes A^E of the light incident in the crystal.

In order to go from amplitudes to intensities we must 1) take the squares of the amplitudes, 2) take into account that the energy density in the propogation of light through a material medium is proportional to the square of the index of refraction ($U \approx A^2 n^2$) and 3) allow for the change in the cross section of the incident and refracted beams and the change in the velocity of the light (from conservation of energy considerations, the flux of the incident energy equals the reflected flux plus the refracted flux).

Finally the relation between the intensity I^D of the refracted light and the intensity I^E of the incident light will be given by

$$I^E = I^D \frac{n}{\sigma^2}\cdot\frac{\cos\delta}{\cos\chi}, \qquad (4)$$

where σ, n and δ are, respectively, the Fresnel coefficient, the index of refraction and the angle of incidence for the light (I_s) polarized parallel to b (σ_s, $n_{\parallel b}$ and $\delta_{\parallel b}$) or for the light (I_b) polarized perpendicular to b (σ_p, $n_{\perp b}$ and $\delta_{\perp b}$).

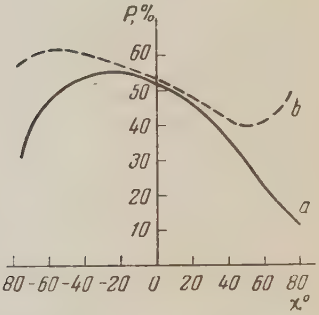

Fig. 10. Positive polarization diagram of the first type: a) experimental, b) corrected.

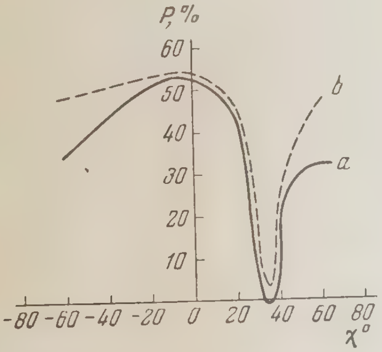

Fig. 11. Positive polarization diagram of the second type: a) experimental, b) corrected.

We used equation (4) to calculate the corrections to the experimentally determined positive polarization diagrams. The results of the diagrams of the first type (shown in Fig. 7) are given in Fig. 10. It will be seen that the corrections are relatively minor for small angles (χ up to about 30°), but become very appreciable at large angles.

The corrections to the negative diagrams were not computed inasmuch as the appropriate index of refraction values were not known.

If we juxtapose the corrected experimental positive polarization diagram (Fig. 10) with the diagram plotted on the basis of x-ray data (Fig. 3), we can say that variations of polarization with angle are in good qualitative agreement. We can hardly expect better agreement if we bear in mind that the calculation of the corrections is based on a number of simplifications and that certain factors were left out of account (for example, dichroism, although apparently it can play an appreciable role due to the relatively small overlapping of the absorption and emission spectra[18]; dispersion of the axes; the influence of light reflected from the back face of the crystal, etc.) and that the juxtaposition is in itself of a qualitative character.

Quantitatively the experimental values are lower than follows from the x-ray data. Thus at χ = 0 the experimental degree of polarization after correction amounts to 53%, while the computed value is 77.5%. One of the reasons for this divergence may be the presence of thermal rotational oscillations of the molecule

leading to partial depolarization.[19] From the fact that the experimental diagram lies below the calculated one while the variations are in qualitative agreement we conclude that the anisotropy of these oscillations is not great.

As for the exceptional positive polarization diagrams of the second type, we must note that introduction of corrections in this case does not lead to agreement with the computed diagrams (Fig. 11). Apparently these cases correspond to a different structure of the lattice and a distinctive orientation of the molecules. One of the possibilities is that in these cases we were dealing with dianthracene or an appreciable admixture of it. The lattice of dianthracene has a different structure than that of anthracene.[20]

"P.N.Lebedev" Physical Institute of the
Academy of Sciences of the USSR

References

1. S.Brodersen, C.R., 233, 1094 (1951).
2. P.Pesteil, C.R., 234, 2532 (1952); 235, 150, 1384 (1952); 237, 235 (1953); 238, 75, 1400, 1789 (1954).
3. S.S.Ganguly & N.K.Choudhury, J. Chem. Phys., 19, 617 (1951); 21, 554, (1953); ZS. f. Phys., 135, 255 (1953).
4. S.I.Vavilov, Zhur. eksp. i teor. fiz., 10, 1363 (1940).
5. P.P.Feofilov, Doklady AN SSSR, 55, 407 (1947).
6. N.D.Zhevandrov, Doklady AN SSSR, 83, 667 (1952); 100, 455 (1955).
7. P.P.Feofilov, Zhur. eksp. i teor. fiz., 26, 609 (1954).
8. C.A.Coulson, Proc. Phys. Soc., 60, 257 (1948).
9. I.V.Vol'kenshtein & L.A.Borovinshii, Doklady AN SSSR, 85, 737 (1952).
10. R.N.Jones, Chem. Rev., 41, 353 (1947).
11. V.I.Gribkov & N.D.Zhevandrov, Doklady AN SSSR, 98, 565 (1954).
12. N.D.Zhevandrov, Doklady AN SSSR, 74, 25 (1950).
13. I.V.Obreimov, A.F.Prikhot'ko & I.V.Rodnikova, Zhur. eksp. i. teor. fiz. 18, 409 (1948).
14. I.M.Robertson, Proc. Roy. Soc., A 140, 79 (1933).
15. A.M.Matheison, I.M.Robertson & V.C.Sinclair, Acta cryst., 3, 245, 251 (1950).
16. M.Born, Optics (in Russian trans.) M. 1937.
17. F.Pockels, Lehrbuch der Kristalloptik., Leipzig-Berlin, 1906.
18. M.D.Galanin & Z.A.Chizhikova, Zhur. eksp. i teor. fiz. 26, 624 (1954).
19. N.D.Zhevandrov, Trudy FIAN (Transactions of the Physics Institute of the USSR, Ac. of Sci., 6, 121 (1955).
20. N.E.Nechaeva, A.N.Faidysh & O.P.Kharitonova, Trudy (Transactions), Physics Inst. of the Ac. of Sc. of the Ukranian SSR., No. 2, 81 (1952).

DISCUSSION

A.F.Lubchenko: In the case of molecular crystals, the dominant factor in absorption is not the dipole moment of an individual molecule but the total moment of the unit cell. Does this also hold in the case of luminescence?

N.D.Zhevandrov: If the predominant role in the polarization of luminescence were played by purely crystal frequencies polarized along the a and b axes, there should be no asymmetry in rotating the crystal to the right or left. Experiment shows, however, that the dominant role is played by purely molecular frequencies. In measurements at low temperature (which we feel would be highly desirable) one might expect to obtain different polarization diagrams for different lines: diagrams of the type we have shown for the molecular lines and diagrams of a simpler symmetric type for the purely crystalline lines.

DETERMINATION OF THE OPTICAL PARAMETERS OF ABSORBING CRYSTALS

- F. I. Fedorov

Absorbing crystals constitute a large and important group in the crystal family. In studying and using absorbing crystals it is important to know the parameters, such as the dielectric constant ε and the conductivity σ, which determine the refractive properties of the crystal and its ability to absorb and reflect light. In absorbing crystals both ε and σ are tensor qualities and it must be noted that in the crystals belonging to the monoclinic and triclinic systems the principal axes of these tensors are not identical. We know that classification of crystals according to their optical properties plays a very important part in modern crystallography and mineralogy. Nevertheless at present crystals having an appreciable absorption have been relatively little studied from the point of view of their optical attributes. For example, we note that the three principal (complex) indices of refraction of a rhombic absorbing crystal (antimony glance or stibnite) were first determined only comparatively recently (1931). We still do not know a single optical parameter of any strongly absorbing crystal in the monoclinic or triclinic syngonies. This is due to the fact that the methods commonly used for determining the optical properties of transparent crystals are not applicable in the case of absorbing crystals unless the absorption is very weak. The principal method applicable in the given case is based on studying the light reflected by the absorbing crystal. This method of determining the optical constants of absorbing crystals was first proposed by Drude[1] and later used by a number of other investigators. However, the potentialities of Drude's method are limited. Its main shortcomings are the following:

1. The method is applicable only to absorbing crystals of the rhombic and middle* syngonies.

2. The method is applicable only provided the reflecting face is parallel to one of the principal planes while the plane of incidence is parallel to another principal plane.

3. Even given the above conditions, the method allows of determining only the principal complex indices of refraction that correspond to the principal axes of the complex permittivity tensor, parallel to the reflecting faces. The third principal index of refraction remains undeterminable.

4. The method is approximate and useful only on the assumption that the principal values in the tensor ε'** (or more exactly their moduli) are large compared to unity. This means that if ε'_i is the principal value, $|1/\varepsilon'_i|$ is negligibly small compared to $1/\sqrt{|\varepsilon'_i|}$

It will be seen therefore that Drude's method is entirely unsuitable for mineralogical analysis on sections cut from a mineral and polished on one or both surfaces, where the arrangement of the reflecting faces is entirely random. Moreover, regardless of any special selection of the reflecting face, the method does not permit determining the optical parameters of monoclinic and triclinic crystals; these are still wholly unknown. This is due to the absence of an adequate theory characterizing the reflection of light from absorbing crystals of the monoclinic and triclinic syngonies. Nor is there any specific theory developed for crystals of other systems (except the cubic) for the case of general orientation of the reflecting planes. This can be attributed to the great complexity of the theory of the optical properties of absorbing crystals developed at the end of the Nineteenth century by Voigt and Drude and based on bringing the complex tensor ε' to

---

*By the middle syngonies we understand the tri-, tetra- and hexagonal symmetry systems; by the lower syngonies we understand the rhombic, monoclinic and triclinic systems.

**The complex tensor ε' is defined by the expression $\varepsilon' = \varepsilon - \frac{2i}{\nu}\sigma$, where ν is the frequency.

the diagonal form by analogy with the theory of transparent crystals. This theory, though still generally accepted, has a number of serious shortcomings.

First, despite the transition to the diagonal form of the tensor ε' the theory remains so complex that Voigt, employing it, could analyse the properties of absorbing crystals and, in particular, determine the direction of the rotary axes only in the case of low absorption and small anisotropy. Only thirty years later was M. Berek able to free the theory of these restrictions and determine the direction of the rotary axes* of a rhombic crystal. For triclinic and monoclinic crystals this problem remained unsolved.

Second, in his development, Voigt did not take into account that complex symmetric tensors do not always reduce to the diagonal form. Hence, contrary to the generally held opinion, the theory of Voigt and Drude is not general: many of the deductions therefrom have a limited validity while others are simply erroneous.

The theory of the optical properties of absorbing (and, of course, transparent) crystals can be developed on the basis of the invariant methods of vector and tensor analysis not based on the utilization of a system of principal axes or some other system of preeminent coordinates. Such a theory had been developed by the writer[2]; it is entirely general and at the same time much simpler than the Voigt-Drude theory. Basic to the new formulation of the theory is the presentation of the reciprocal complex tensor ε'^{-1} in the form

$$\varepsilon'^{-1} = \alpha + \beta\,(\mathbf{c}'\cdot\mathbf{c}'' + \mathbf{c}''\cdot\mathbf{c}'). \tag{1}$$

Here α and β are complex scalar quantities and $\mathbf{c}'$ and $\mathbf{c}''$ are complex vectors; the expression $\mathbf{c}'\cdot\mathbf{c}''$ denotes a dyadic, i.e., a tensor the components of which are described in the condition

$$(\mathbf{c}'\cdot\mathbf{c}'')_{ik} = c'_i\,c''_k. \tag{2}$$

The complex vectors $\mathbf{c}'$ and $\mathbf{c}''$ belong to one of the following three types[3]: linear, if $[\mathbf{c}\mathbf{c}^*] = 0$; circular, if $\mathbf{c}^2 = 0$; or elliptic, if neither of these conditions obtains.

A special significance attaches to the directions in the crystal the unitary vector $\mathbf{n}$ for which satisfies the relation

$$(\mathbf{n}\mathbf{c})^2 = 0, \tag{3}$$

where $\mathbf{c}$ is either of the vectors $\mathbf{c}', \mathbf{c}''$.

It follows from (3) that

$$\mathbf{n} = \frac{\sqrt{\mathbf{c}^2}\cdot\mathbf{c}^* + \sqrt{\mathbf{c}^{*2}}\cdot\mathbf{c} \pm i\,[\mathbf{c}\mathbf{c}^*]}{|\mathbf{c}|^2 + |\mathbf{c}^2|}. \tag{4}$$

The last expression in the case of a linear vector $\mathbf{c}$ determines the optical axis of the crystal, in the case of a circular vector, one rotary axis and in the case of an elliptic vector, two rotary axes. From this and the canonical expression (1) for the tensor ε'^{-1} it follows that rhombic crystals can have either two optical axes or four rotary axes. In the case of monoclinic and triclinic crystals the number of axes in different cases can vary from one to four; one of these (but not more than one) can be an optical axis, the others being rotary axes. Thus the possible optical properties of absorbing crystals prove to be far more

---

*The distinction between an optical axis and a rotary axis in a crystal is that light of any polarization can be propagated along the former while only light circularly polarized in a given sense can be propagated along the latter. In both cases there is no double refraction for these directions, i.e., the refraction index assumes a unique value.

diversified than was assumed in the former theory, according to which it was assumed that all crystals of the lower syngonies must have four rotary axes and cannot have optical axes.

The invariant formulation of the principal relationships of crystal optics makes it possible to solve in general form the problem of the reflection of light from an arbitrarily oriented surface of a transparent as well as an absorbing crystal. Denoting through A and B the complex amplitudes of the electric vector of the incident wave, perpendicular and parallel to the plane of incidence, respectively, and through A' and B' the same amplitudes for the reflected wave, we obtain on the basis of the general interface conditions of electrodynamics linear expressions for A' and B' in terms of A and B:

$$A' = \frac{MA + NB}{\Delta} \qquad \text{and} \qquad B' = \frac{QA + PB}{\Delta}. \tag{5}$$

Here M, N, P, Q, and Δ are functions of the angle of incidence and of the parameters determining the properties of the crystal as well as the orientation of the reflecting plane and the plane of incidence. If the incident light is plane polarized, the ratio A/B is real. Let us introduce the notation

$$\frac{A}{B} = \operatorname{tg} \chi , \tag{6}$$

where χ is the angle between the electric vector of the incident wave and the plane of incidence (azimuth of the oscillations of the incident wave). The corresponding expression for reflected light has a form

$$q = \frac{A'}{B'} = \frac{MA + NB}{QA + PB} = \frac{M \operatorname{tg}\chi + N}{Q \operatorname{tg}\chi + P}. \tag{7}$$

For absorbing crystals M, N, P, and Q as well as q = A'/B' are complex. Consequently in the general case the reflected wave will be elliptically polarized. By means of a suitable compensator and analyzer, we can readily measure the parameters of the elliptic polarization of the reflected wave: the orientation of the major axis of the ellipse and the phase difference between A' and B'; this data gives us the ratio q. Equation (7) can be rewritten in the form

$$\frac{N}{Q} + \operatorname{tg}\chi \frac{M}{Q} - q \frac{P}{Q} = q \operatorname{tg}\chi. \tag{8}$$

If we vary χ, keeping all other conditions the same, q will change, while the ratios M/Q, N/Q and P/Q will remain constant. Thus by taking a number of angles χ_1, χ_2 and χ_3 and determining, through appropriate measurements, the corresponding values of q_1, q_2 and q_3 we can obtain from (8) three equations by means of which we can calculate the ratios M/Q, N/Q and P/Q for any angle of incidence in any plane of incidence. Consequently the values of M/Q, N/Q and P/Q can, on the one hand, be determined experimentally and, on the other hand, theory yields expressions for these quantities as functions of the parameters characterizing the properties and orientation of the crystal. Thus the problem is reduced to computing the parameters of the crystal from the corresponding relationships. The mathematical difficulties encountered in the process stem from the complexity of these relationships.

For the case of transparent uniaxial crystals expressions for M, N, P, Q and Δ were deduced by the writer in the invariant form in Ref. 4. These expressions can be modified for the case of uniaxial absorbing crystals (i.e., crystals of the tri-, tetra- and hexagonal syngonies) if we replace the real permittivity tensor for a transparent crystal $\varepsilon = \varepsilon_0 + (\varepsilon_e - \varepsilon_0)\, c \cdot c$ by the appropriate expression for the complex tensor:

$$\varepsilon' = \varepsilon - \frac{2i}{\nu} \sigma = \varepsilon_0' + (\varepsilon_e' - \varepsilon_0')\, c \cdot c. \tag{9}$$

Here ε is the real permittivity tensor, σ is the real conductivity tensor, ν is the frequency of the light, $\varepsilon_0' = \varepsilon_0 - \frac{2i}{\nu}\sigma_0$ and $\varepsilon_e' = \varepsilon_e - \frac{2i}{\nu}\sigma_e$ are the principal values of the tensor ε' and c is the real unit vector representing the optical axis.

Let us examine the cases when the incident light is plane polarized perpendicularly to the plane of incidence (A = 0) or parallel to it (B = 0). As follows from (7), the reflected light in the general case will be elliptically polarized. However, if the plane of incidence is parallel to the optical axis of the uniaxial crystal, then with A = 0, we will have A' = 0 and with B = 0, we will have B' = 0, i.e., the reflected light will be plane polarized in the same two directions as the incident light. This follows from both the exact equations given in Ref. 4 and from considerations of symmetry. Consequently, if there exists a plane of incidence (one!) for which the conditionsA - A' = 0 and B - B' = 0 are fulfilled, the crystal will be uniaxial, i.e., will belong to the trigonal, tetragonal or hexagonal syngony. For crystals of the cubic system all planes of incidence will possess this property. Thus from this indication we can at once determine whether an investigated crystal belongs to the middle or lower syngony or is optically isotropic.

The method of determining the optical parameters of absorbing crystals of the cubic syngony are the same as those for any isotropic absorbing media (metals). These procedures have long been familiar and are described in many standard texts (see, for example, Refs. 5-7). Where the parameters of uniaxial crystals are concerned, they can be determined by means of the following procedure. First, using the indication described above we find the plane of incidence parallel to the optical axis of the crystal; we will hereinafter refer to it as the principal plane of incidence. Taking another plane of incidence forming an angle θ with the principal plane of incidence and we determine by means of the above described method the complex ratio N/Q. As shown in Ref. 4, the following relationship is valid:

$$\frac{\sqrt{\varepsilon_0' - \sin^2\varphi}}{\sin\varphi}\cos\theta\,\mathrm{tg}\,\psi = \frac{1 - N/Q}{1 + N/Q} = \gamma. \tag{10}$$

Here φ is the angle of incidence and ψ is the angle between the optical axis and the normal to the reflecting plane (it is assumed that the reflection occurs at the interface with air, the index of refraction of which is taken equal to unity). Utilizing the expression (10) for some two suitable angles of incidence in the same plane of incidence we obtain two equations from which we can readily calculate ψ and ε_0'. We thereby determine the orientation of the optical axis of a crystal and the principal value of tensor ε', corresponding to the ordinary wave. We now have only ε_e' to determine. To this end it is sufficient to measure M/P at some angle of incidence in the principal plane for which the relationship (7) assumes the form

$$q = \frac{A'}{B'} = \frac{M}{P}\mathrm{tg}\,\chi. \tag{11}$$

From this, ψ and ε_0' being known, we can readily find ε_e' (see Ref. 4).

Thus the problem of determining all the optical parameters of a uniaxial absorbing crystal can be solved entirely and, in principle, accurately by measuring the elliptic polarization of light reflected from an arbitrarily chosen section of the surface of the crystal. Obviously, we are not here taking into account the possible influence of the surface layer.

The solution of the problem for absorbing crystals of the lower syngonies with an arbitrary orientation of the reflecting face becomes much more complicated. In this case we must determine the six complex or 12 real parameters determining the general complex tensor ε' (1), which enter in an extremely complicated manner into the expressions for the coefficients M, N, P and Q. An exact solution of this problem is hardly realizable; however, by making certain simplifying

assumptions we can arrive at an approximate solution. One assumption is the natural one that the anisotropy of tensor ε' is small, i.e., that the difference between the principal values of the tensor ε_i' is small compared with the values themselves. Where transparent crystals are concerned this is true in the overwhelming number of cases. Further simplification is obtained, if we investigate the reflection at sufficiently small angles of incidence so that $\sin^2\varphi$ will be negligible compared with unity. Under these conditions by measuring the elliptic polarization of the reflected light in three planes of incidence forming angles of 45° with each other (but otherwise arbitrarily oriented) we can obtain a series of relationships from which we can readily determine all the components of the complex tensor ε' (see Ref. 2).

Institute of Physics and Mathematics of the
Academy of Sciences of the Byelorussian SSR

References

1. P.Drude, Wied. Ann., 32, 584 (1887); 34, 489 (1888).
2. F.I.Fedorov, Thesis, 1954.
3. F.I.Fedorov, Doklady AN SSSR, 102, 69 (1955).
4. F.I.Fedorov, Doklady AN SSSR, 84, 1171 (1952).
5. M.Born, Optics (in Russian trans.) M. 1937.
6. P.Drude, Optics (in Russian trans.) M. 1935.
7. C.Schaefer, Theoretical Physics (in Russian trans.) Vol. 3, M. 1938.

DISCUSSION

V.L.Levshin: You stated that this theory is applicable in case the anisotropy is not too great. In what percent of the substances is it low? That is, to how many substances is your theory applicable?

F.I.Fedorov: The theory is entirely general and the assumption regarding low anisotropy is necessary only as regards the problem of determining the parameters with respect to the reflected light. It is hard to say how common are the substances for which this condition holds for the simple reason that strongly absorbing crystals have hardly been studied. We know, however, that for transparent crystals a high degree of anisotropy is rarely encountered. This is probably true for absorbing crystals as well.

M.V.Vol'kenshtein: This contribution is of great theoretical importance because the anisotropy of absorption is interconnected with molecular structure.

One of the weak areas in the classical electromagnetic theory of light is the theory of optically active anisotropic media. Even in Born's monograph where the matter is discussed in greatest detail there are a number of serious errors. I corrected some of these error in my "Molecular Optics"; I did not attempt to give a complete theory for crystals; I merely showed the necessity of taking into account the quadrupole moment. Undoubtedly your mathematical approach would be helpful in solving this problem.

F.I.Fedorov: The described method is fully applicable to optically active crystals as well and simplifies the treatment.

POLARIZATION SPECTRA OF CERTAIN NAPHTHYLAMINES AND POLYENES

- N.D. Zhevandrov

Studies of the correlation between the structure of complex molecules and their optical properties are of interest in that they offer the means of investigating various aspects of molecular structure by optical procedures. The present work is such a study.

The method of polarization spectra allows of studying the anisotropy of molecules and determining the orientation of the virtual absorption and emission oscillators. In the present study we investigated the polarization spectra of certain derivatives of naphthalene and the polyenes.

We used a Kavraiski[1] polariscope with a compensator to measure the degree of polarization of the luminescence. The principal difference between the Kavraiski polariscope and the familiar Savart instrument is that the analyser, instead of being a Nicol prism, is a dividing double-refracting prism (a modification of the Wollaston prism) with a splitting angle equal to the half-width of the interference bands given by the polariscopic assembly. The last also differs from the conventional Savart plate. The splitting produced by a Wollaston prism is very constant for rays parallel to the edge, whereas bands produced by Savart plate are not entirely parallel. In order to obtain a clear interference pattern in a large field of view the Savart plate is replaced by an assembly consisting of two similar quartz plates but oriented in opposite directions (with a half-wave plate between them) instead of being crossed as in the Savart plate. The Wollaston prism differs from the conventional prism in that the optical axes of its components, lying in the planes of the bases, form angles of $\pm 45^{\circ}$ with the refracting edges.

The Kavraiski polariscope has two advantages over the Savart instrument: twice as high a transmission factor and an appreciably greater field of view.

A compensator consisted of a stack of glass plates rotatable about a horizontal and a vertical axis. Thus it was possible to measure both the positive and negative polarization. The compensator was calibrated with reference to a source having a known polarization, that is, diffused light from a lamp, passed through a Nicol prism having a known orientation. The calibration was checked by the method of Weber.[2] The absorption spectrum was measured on a SF-4 spectrophotometer.

Measurement of the polarization spectrum of naphthalene is hindered by the fact that its luminescence spectrum lies in the violet and ultraviolet region and also by the difficulty of obtaining sufficiently viscous solutions of naphthalene in view of its poor solubility.

We investigated a number of naphthalene derivatives, i.e., naphthylamines: phenyl-β-naphthylamine, paratolyl-β-naphthylamine and phenyl-α-naphthylamine. All these substances were dissolved in glycerin (via an alcohol solution). We used double-distilled glycerin, the luminescence of which was negligible compared with the bright blue glow of the solutions. The observed polarization spectra and the absorption spectra are shown in Fig. 1.

Vol'kenshtein and Vorovinski[3] and Davydov[4] give theoretical calculations of levels of the naphthalene molecule and show that the first transition is polarized along a transverse axis of the molecule, while the second and third transitions are polarized along the longitudinal axis. An analogous situation obtains in the anthracene molecule, as is shown by the experimental data for anthracene and its derivatives (in particular, for the derivatives similar to those of naphthalene investigated in the present study).

Brodersen[5] who investigated the polarization of the luminescence of naphthalene single crystals taking into account the x-ray data on the orientation of the naphthalene molecule in the crystal lattice, established that the oscillators associated with the emission bands (and the long-wave absorption band) lie in the

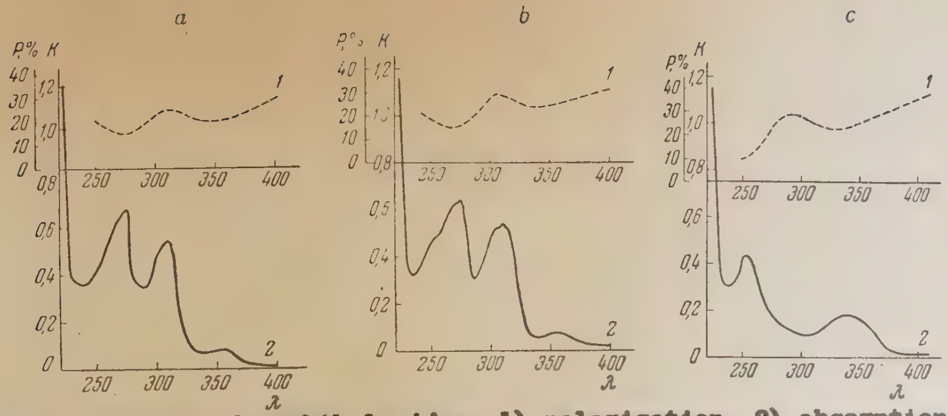

Fig. 1. Spectra of naphthylamides: 1) polarization, 2) absorption; a) phenyl-β-naphthylamine, b) paratolyl-β-naphthylamine, and c) phenyl-α-naphthylamine.

plane of the molecule and are directed along its transverse axis.

Investigation of the polarization spectra of solutions of naphthalene and its derivatives is of interest in that it can help clarify how the oscillators associated with the second and third absorption bands are oriented. As may be seen from Fig. 1, within the region of the first three absorption bands the polarization of the luminescence remains positive, does not change sign and retains the same order of magnitude. As in most cases, interpretation of the structure of polarization spectra is difficult. Further studies at low temperatures are necessary. However, from the fact that the polarization in the entire investigated range does not change sign, one can conclude that the oscillators associated with the second and third absorption bands are directed approximately parallel to the first oscillator, i.e., are also aligned parallel to the transverse axis of the molecule. In this respect the investigated compounds differ from anthracene and its derivatives.

This result is not in agreement with the conclusion of the above mentioned theoretical investigations (Refs. 3 & 4). However, there are other experimental data substantiating our result. These are the data of Borisov[6] on the dispersion of light in naphthalene single crystals. Computation of the ratio of components of the oscillator strength along the crystallographic axes for the corresponding transitions yields agreement with experiment only when it is assumed that all three transitions occur along the transverse axis of the molecule.

We had available only a limited number of polyenes, mainly derivatives of butadiene: tetraethyl butadiene, triphenyl butadiene and tetraphenylmethyl butadiene as well as tetraphenyl propadiene and tetraphenyl ethylene (the emission of the latter was so weak that it was impossible to measure the spectrum in the short-wave region).

Inasmuch as these substances did not dissolve in glycerin they were investigated in solid solutions in polystyrene. Their absorption and polarization spectra are shown in Fig. 2.

The absorption spectra lack a distinct structure. In general terms, they may be described as follows: first a broad diffused long-wave absorption band, then — going to the short-wave side — a certain decrease in absorption and then an intensive increase, obviously tending to a short-wave peak which lies outside the investigated spectral region.

The polarization spectra of the polyenes are also generally similar: there is an appreciable degree of positive polarization in the long-wave region, then some decrease in polarization as we go to the short-wave side and finally again a rise. The structure which appears in the spectra of some of the compounds is

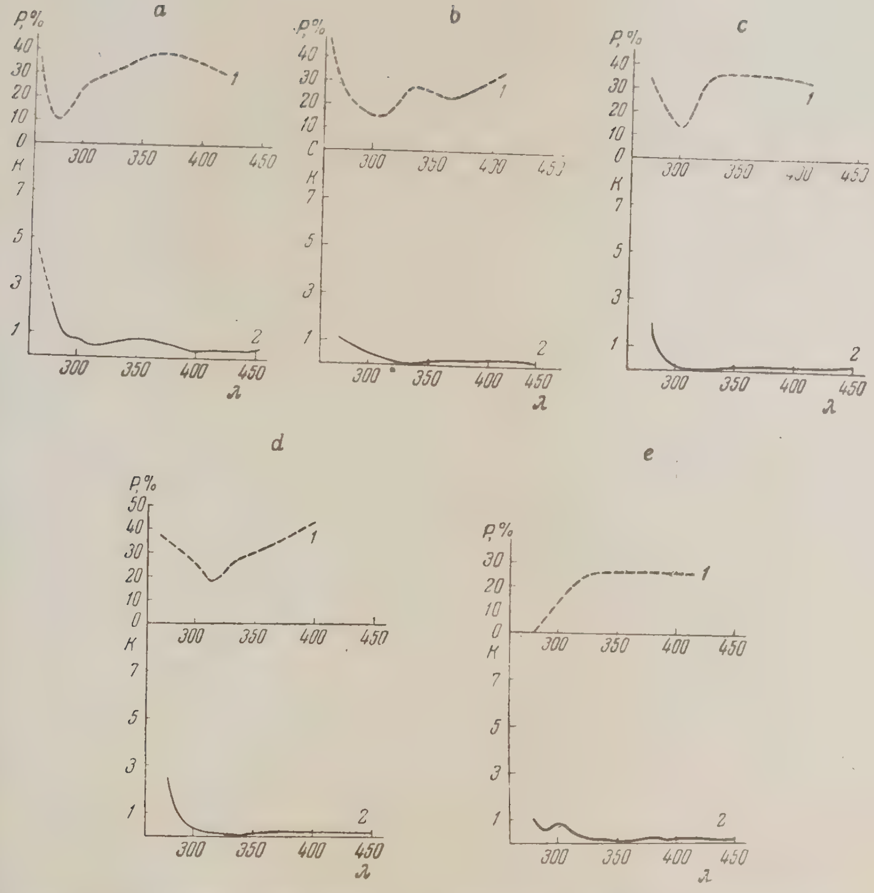

Fig. 2. Polyene spectra: 1) polarization, 2) absorption; a) tetraphenyl butadiene, b) 1, 1, 2-triphenyl butadiene, c) 1, 1, 4, 4-tetraphenyl-2, 3-dimethylbutadiene, d) tetraphenyl propadiene and e) tetraphenyl ethylene.

difficult to interpret in the absence of low temperature measurements. However, qualitatively we can conclude that the oscillators associated with the absorption band in the short-wave region are approximately parallel to the long-wave oscillator.

The spectra of polyenes have been theoretically calculated by different methods. In particular, Kuhn[7] calculated the spectrum of the polyene chain according to classical theory, regarding the oscillations of the electrons in the different rings as being coupled. He obtained good agreement with experiment for the dependence of λ_{max} of the first absorption band on the number of members in the polyene chain. Kuhn also determined the polarization of the electronic transition and showed that it is polarized along the polyene chain. In other words, the oscillators associated with the long-wave absorption are directed along the longitudinal axis of the polyene molecule. This being so it then follows from the polarization spectra that the short-wave oscillator, being approximately parallel to the long-wave one, is also aligned with the longitudinal axis of the polyene molecule.

In the course of this investigation we attempted to determine the possibility of applying the method of polarization spectra to problems of luminescence analysis. Inasmuch as polarization spectra often have a shape peculiar to the given substance - in fact, sometimes more specific for the substance than the luminescence spectra - it should be possible to utilize them for analytic purposes. This approach may be particularly valuable in cases when the luminescence spectrum is less characteristic of the substance than the polarization spectrum.

We compared the polarization spectra of the three grades of adrenaline: good quality (standard), especially purified and substandard (rejected). The solutions were prepared in glycerin with the addition of 10% of a 50% solution of KOH. It should be noted that in glycerin (in contrast to the case in

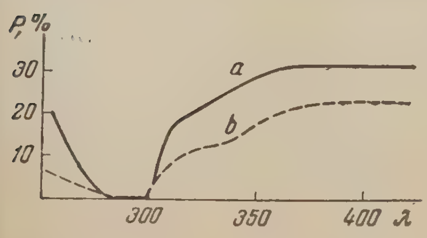

Fig. 3. Polarization spectra of adrenaline: a) pure adrenaline, b) substandard product.

other solvents) adrenaline exhibits a very stable luminescence, i.e., the glow of the solution persists for many days.

The polarization spectra of the purified and substandard adrenaline samples are shown in Fig. 3. The polarization of the latter is lower; however, there is no great difference in the variation with wavelength. It may be concluded that in the given case the proposed method would not be of practical value.

In conclusion I desire to thank B.M.Mikhailov, in whose laboratory (Inst. of Organic Chemistry of the Ac. of Sc.) the investigated substances were synthesized, and graduate student A.F.Serkin for his help in making the measurements.

"P.N.Lebedev" Physical Institute of the
Academy of Sciences of the USSR

References

1. V.V.Kavraiski, Zhur. eksp. i teor. fiz., 20, 619 (1950).
2. G.Weber, Biochem. J., 51, 145 (1952).
3. M.V.Vol'kenshtein, L.A.Borovinski, Doklady AN SSSR, 85, 731 (1952).
4. A.S.Davydov, Zhur. eksp. i teor. fiz., 17, 1107 (1947).
5. S.Brodersen, C.R., 233, 1094 (1951).
6. M.D.Borisov, Trudy (Transactions), Physics Institute of the Academy of Science of the Ukrainian SSR, No. 2, 87 (1952).
7. W.Kuhn, Helv. Chim. Acta, 31, 1780 (1948).

ABSORPTION AND LUMINESCENCE OF FLUORIDE SOLUTIONS OF LEAD AND THALLIUM

- M.U.Belyi and A.A.Shishlovski

Investigation of the luminescence of solutions of electrolytes is important from the viewpoint of physical chemistry since such investigations make it possible to follow the interaction of ions and clarify the nature of the elementary processes occurring in solutions under the influence of light. Unfortunately the number of electrolytic solutions capable of luminescing is very limited. Hence the discovery of new luminescent solutions is of undoubted interest.

The results of our earlier investigations of the absorption and luminescence of chloride, bromide and iodide solutions of lead and thallium[1] prompted us to undertake similar study of fluoride solutions of these heavy metals. Investigation of fluoride solutions is not only of theoretical but of practical interest since fluorine compounds are widely used in industry. Thus, for example, the fluoride of bivalent lead is used as a fluorination agent in the production of carbon fluorides.

The absorption spectra were studied on an SF-4 photoelectric spectrophotometer; the luminescence spectra on a high-transmission quartz spectrograph. It must be noted that the investigation of fluoride solutions presents certain difficulties due to the activity of these solutions where glass and quartz are concerned. Nevertheless by taking appropriate precautions, one can obtain reliable results. The fluorine ions were introduced into solution in the form of KF. The lead and thallium cations were introduced by dissolving the appropriate perchlorate salts.

The variation of the absorption of solutions of $Pb(ClO_4)_2$ + KF with gradually increasing concentration is shown in Fig. 1. It will be seen that the absorption of lead salts in water-fluoride solutions has certain very distinctive characteristics. Whereas in the case of chloride, bromide and iodided solutions of thallium and lead the absorption band of the cation gradually goes over into an appreciably longer wave band of the associate with increasing halide ion concentration, here we see that the absorption spectrum of the Pb^{++} cation at first (at relatively low F^- concentrations -- to 1.41 mole/liter) continues to weaken and at the same time broadens somewhat. With further increase in the F^- ion concentration the position of the absorption band (λ_{max} = 208.5 mμ) and its intensity remains practically unchanged within the limits of experimental error up to a concentration of 4.1 mole/liter. From this

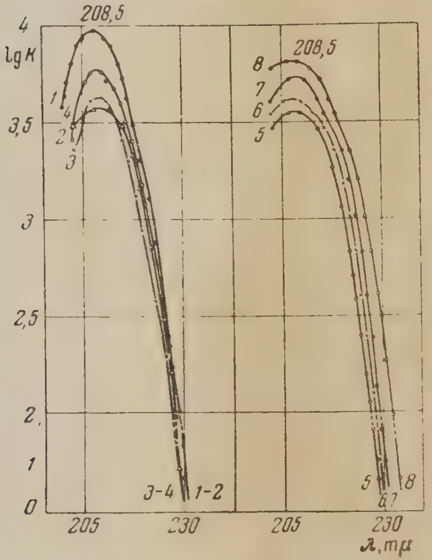

Fig. 1. Absorption spectra of water-fluoride solutions of lead at different F^- concentrations ($C_{Pb(ClO_4)_2} = 1.47 \cdot 10^{-4}$ mole/liter = const.); C_{KF}: 1) 0, 2) $5.06 \cdot 10^{-2}$, 3) $5.06 \cdot 10^{-1}$, 4) 1.42, 5) 4.1, 6) 5.06, 7) 7.1 and 8) 10.1 mole/liter

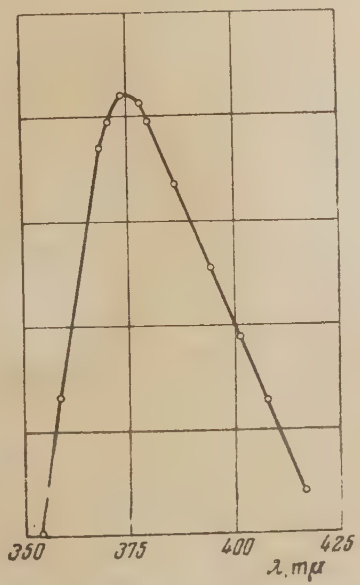

Fig. 2. Energy distribution in the luminescence spectrum of the $Pb(ClO_4)_2$ + KF solution.

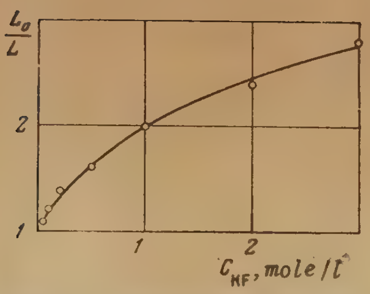

Fig. 3. Quenching of the luminescence of thallium by potassium fluoride.

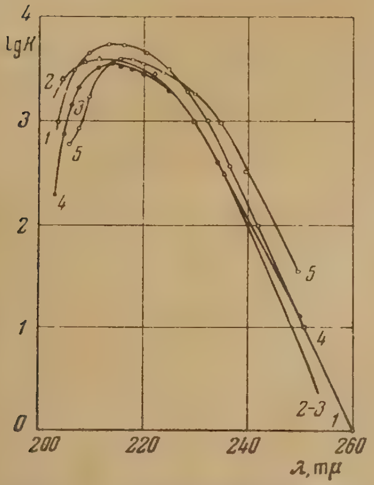

Fig. 4. Absorption spectra of TlCl + KF solutions at different F⁻ ion concentrations ($C_{TlCl} = 5 \cdot 10^{-4}$ mole/liter = const.); C_{KF}: 1) 0, 2) $1 \cdot 10^{-2}$, 3) $1 \cdot 10^{-1}$, 4) 1, 5) 6.8 mole/liter.

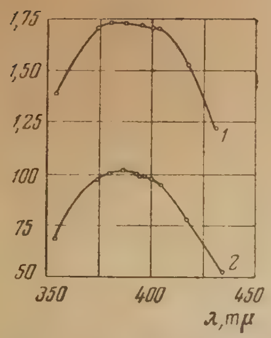

Fig. 5. Plate blackening curve characterizing the luminescence spectra of thallium solutions: 1) aqueous (exposure 1.5 min), 2) water-fluoride solution (exposure 3 min).

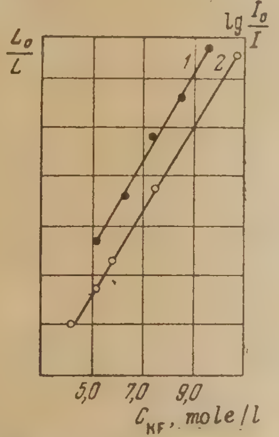

Fig. 6. Dependence of the luminescence efficiency (1) and the optical density of absorption (2) of fluoride solutions of lead on the F⁻ ion concentration.

point on the absorption spectrum increases in intensity, tending to a peak value at the maximum possible concentration of F⁻ ions in the solution. It is interesting to note that it is precisely in this region of high concentrations that the violet glow of lead solutions first appears; this luminescence is further intensified with increasing fluorine ion concentration. The luminescence spectrum of such solutions, as may be seen from Fig. 2, consists of a diffused, structureless band with a peak at about 376 mμ.

The absorption spectra of the hydrolyzed Pb^{++} cation and the $Pb(ClO_4)_2$ + KF solution approximately coincide both as regards position and shape. Nevertheless, as we have indicated, fluoride solutions of lead have the ability to luminesce in contradistinction to pure aqueous solutions of lead perchlorate which exhibit no trace of luminescence. Thus it must be assumed that the coincidence of the bands is fortuitous inasmuch as they associated with different absorption centers; this was substantiated by our further structural investigations.

We note that fluoride solutions kept for a long time (several days) in a silicate container (glass or quartz) exhibit two additional luminescence bands, one in the region of 285-310 mμ, another at 260-280 mμ. These bands apparently are associated with a compound of lead, silicon and fluorine. On the other hand if the solutions are kept in a plastic vessel, the emission always consists of only one band with a peak at 367 mμ.

The behavior of fluoride solutions of thallium is entirely different. As is known in pure water solutions the hydrolyzed thallium ions have a bright violet luminescence. This luminescence is quenched when fluorine ions are introduced into the solution. Fig. 3 shows the dependence of the luminescence on the concentration of the quenching ions (the curve is obtained by a method excluding inactive absorption). Studies show that in the process of quenching there are no substantial changes in the absorption spectrum (Fig. 4) or in the luminescence spectrum (Fig. 5). Using the quenching data and the well known equation of Vavilov[2], characterizing the quenching of luminescence by extraneous substances,

one can show that as a result of quenching the lifetime of the excited state is reduced in the given case by a factor of about 3. This indicates that we here have a quenching of the second kind. Hence we conclude that there are no stable compounds of thallium with fluorine in fluoride solutions of thallium.

In the case of fluoride solutions of lead, in which, as was indicated, luminescence appears at appreciable fluorine ion concentrations, we must assume the formation of some associations, i.e., ion groups responsible for the luminescence. It is possible to deduce the composition of these luminescent centers from the dependences of the intensity of luminescence and the optical absorption density on concentration of the fluorine (Fig. 6) and the lead ions (Fig. 7). In view of the linear character of these dependencies we can affirm that we are dealing here with a luminescing molecular ion of the PbF^+ type. The deviation from linearity in Fig. 7 at high concentrations of Pb^{++} is to be explained by concentration quenching, on the one hand, and, on the other hand, by the inapplicability of the method employed for determining the composition of the complex groups where such high concentrations are concerned.

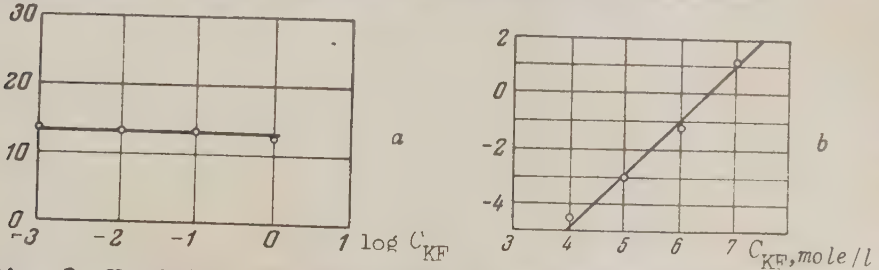

Fig. 8. Variation of the index of refraction of fluoride solutions of lead at different F^- ion concentrations (the index of refraction values are scaled in relative units).

In the interests of a more reliable interpretation of the results of ionic interaction, one of the authors[3] proposed a further study of a number of optical characteristics of the solutions as functions of concentration of the solution components. A study of the refraction in the investigated solutions by the compensation method, as may be seen from Fig. 8, substantiates the conclusions made on the basis of the luminescence and absorption studies. It will be seen that introduction into the lead solution of fluorine ions up to a concentration of 1 mole/liter does not alter the index of refraction (Fig. 8, a); however, beginning with a concentration of 4 mole/liter, i.e., from the concentration at which the luminescence of fluoride solutions of lead begins, the index of refraction changes rapidly (Fig. 8, b). Thus on the basis of these data we can conclude that at high concentrations of KF (4 mole/liter and higher) the structure of the solution changes with a resultant change in the index of refraction. Hence we can safely affirm that in the presence of such high concentrations of fluorine ions in lead solutions there is formed a new compound, the composition of which may be represented by PbF^+.

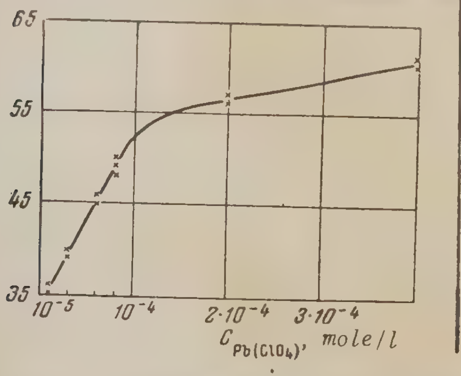

Fig. 7. Dependence of the intensity of luminescence of fluoride solutions of lead on $Pb(ClO_4)_2$ concentration; C_{KF} = const.

Kiev State University

References

1. M.U.Belyi, I.I.Kondilenko & A.A.Shishlovski, in Sb."Pamiati S.I.Vavilova" (Symposium in memory of S.I.Vavilov) M. 1952; A.A.Shishlovski, Doklady AN SSSR, 35, 181 (1942).

2. S.I.Vavilov, Collected Works, Vol. 2, p. 122, M.-L. 1952.

3. A.A.Shishlovski, Izv. AN SSSR, Ser. fiz., 18, 678 (1954). (Translation in Bulletin, Vol. 18, No. 6, p. 362.)

LUMINESCENCE AND ABSORPTION OF SOLUTIONS OF TIN SALTS

- M.U.Belyi and K.F.Gudymenko

The luminescence of tin salt solutions has been known for some time. Shishlovski[1] in 1940 noted that acidified solutions of stannous chloride yield a weak green luminescence. Pringsheim[2] in 1941 described a rather strong glow from tin in hydrochloric acid, noted that the luminescence faded rapidly under the influence of light.

Since the outer electronic shell of bivalent Sn is similar to the shells of Pb^{++} and Tl^{+}, the luminescence of which has been rather thoroughly studied[3], we felt it would be of interest to carry out a detailed investigation of the luminescence of solutions of tin salts.

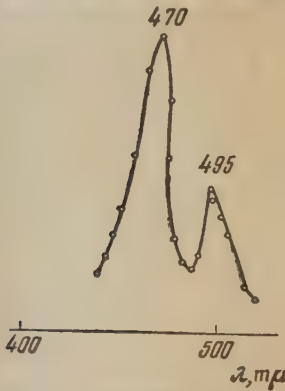

Fig. 1. Energy distribution in the luminescence spectrum of Sn^{++} + HCl.

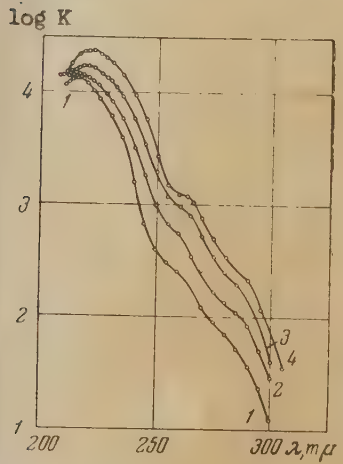

Fig. 2. Absorption spectra of solutions of bivalent tin in hydrochloric acid. $C_{SnCl_2} = 1 \cdot 10^{-3}$ mole/liter; C_{HCl}: 1) 1, 2) 3, 3) 6, 4) 11 mole/liter.

We used C.P. grade reagents (acids and the appropriate tin salts). The excitation source was a high voltage spark between zinc electrodes. The luminescence spectra were photographed on quartz and glass spectrographs having a high transmission factor; the energy distribution was determined by photographic photometry. The absorption spectra were measured on an SF-4 spectrophotometer by the differential method with exclusion of the inherent absorption of the solvent.

Investigation of the luminescence of tin salt solutions in hydrochloric acid at different concentrations showed that the luminescence spectrum of these solutions consists of two bands with peaks at 470 and 495 mμ (Fig. 1), the location of which is independent of both the HCl and Sn^{++} concentration. It must be noted that luminescence is exhibited only by freshly prepared solutions of salts of bivalent tin, for example, $SnCl_2$. In air the bivalent ion of tin undergoes rapid oxidation to the tetravalent form (for example, at an $SnCl_2$ concentration of 10^{-4} mole/liter, the transformation occurs in the matter of a few minutes). The hydrogen sulfide reaction was used to determine the state of oxidation. Solutions containing only tetravalent tin ions do not luminesce in either the visible or ultraviolet regions.

If the fresh $SnCl_2$ solution is immediately sealed in an airtight cell, the ability to luminesce persists indefinitely; moreover prolonged (several hours) irradiation with the spark source does not affect the intensity of the emission.

It must be borne in mind that the bivalent tin ions can go over to the tetravalent form due to the presence of oxygen dissolved in the acid. For this reason the tin concentration in such solutions should be made higher than the oxygen concentration. Aqueous solutions of $SnCl_2$ emit a luminescence of the same color; however, the emission quickly fades because of hydrolysis. The absorption spectrum of bivalent tin in hydrochloric acid differs markedly from that of tetravalent tin: the spectrum of bivalent tin has three peaks (Fig. 2), while the absorption spectrum of tetravalent tin is free of these features (Fig. 3). It should also be noted that all three bands in the spectrum of bivalent tin are luminescently active.

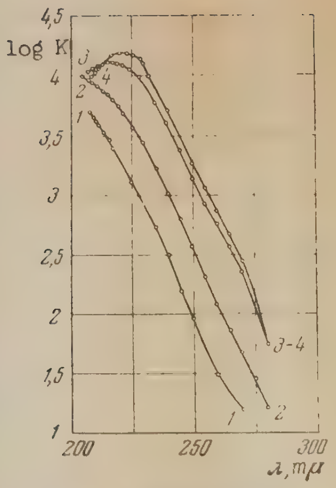

Fig. 3. Absorption spectra of solutions of tetravalent tin in hydrochloric acid (concentrations same as in Fig. 2).

We found that solutions of bivalent tin in sulfuric acid exhibit a very bright luminescence. As may be seen from Fig. 4, the luminescence of these solutions is strongly dependent on the sulfuric acid concentration; at the maximum acid concentration the spectrum consists of a wide band with two peaks at 550 and 615 mμ (Fig. 4, curve 1). As the concentration of H_2SO_4 is reduced, the peak at 550 mμ fades and the second peak at 615 mμ becomes the stronger one (curves 2 and 3). Upon further dilution, luminescence is observed only in the red part of the spectrum and the peak emission lies in the infrared region. In other words, there is a redistribution of energy among the three emission bands as the H_2SO_4 concentration is varied.

The ability of $SnSO_4$ solutions in concentrated sulfuric acid to luminesce is retained in air and under the influence of prolonged exposure to light. Oxidation occurs only when the solution is heated to 100°. Solutions of $SnSO_4$ in diluted sulfuric acid, on the other hand, retain their ability to luminesce only in a sealed container, the $SnSO_4$ oxidizing in air to $Sn(SO_4)_2$ at a rate increasing with decreasing sulfuric acid concentration.

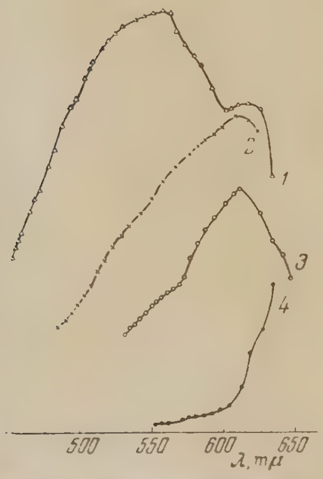

Fig. 4. Energy distribution in the luminescence spectra of solutions of bivalent tin in sulfuric acid. $C_{H_2SO_4}$: 1) 18, 2) 14, 3) 9, 4) 5 mole/liter.

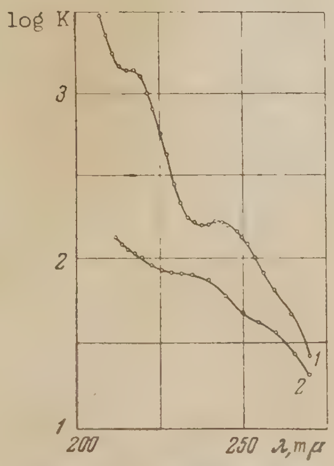

Fig. 5. Absorption spectra of solutions of bi- and tetravalent tin in sulfuric acid. $C_{H_2SO_4}$ = 1 mole/liter; 1) Sn^{++}, 2) Sn^{++++}.

The absorption spectra of solutions of bi- and tetravalent lead in sulfuric acid are analogous to the absorption spectra of the hydrochloric acid solutions (Fig. 5).

The absorption spectrum of bivalent tin has the same structure not only in sulfuric and hydrochloric acids but also in HBr, HI and $HClO_4$ (Ref. 4). Thus it may be asserted that in all these cases we are dealing with identical absorption centers. Apparently both the absorption and luminescence are due to the bivalent tin cation whose excited state is the triplet state ^3P.

If we compare the outer electronic shells of the cations of the heavy metals whose solutions exhibit luminescence, namely Tl^+, Pb^{++} and Sn^{++}, we see that they all have two s-electrons. We thus have reason to assume the luminescence in these cases is always associated with the presence of these s-electrons. We note that the solutions of salts of these elements in which the cations are devoid of outer s-electrons (Tl^{+++}, In^{+++} and Sn^{++++}) do not luminesce.

Kiev State University
and
Kiev Pedagogical Institute

References

1. A.A.Shishlovski, Fizichni zapiski AN USSR, (Physical records of the Ukrainian SSR Academy of Sciences), 9, 19 (1940).

2. P.Pringsheim, M.Vogel, Physica, 7, 225 (1941).

3. I.I.Kondilenko & A.A.Shishlovski, Doklady SSSR, 35, 181 (1942). B.Gordon, Zhur. fiz. khim., 15, 448, (1941).

4. H.Fromherz, H.J.Walls, ZS. f. Phys. Chem., Abt. A, 178, 29 (1937).

DISCUSSION FOLLOWING THE PRECEDING TWO PAPERS

F.I.Fedorov: (question addressed to A.A.Shishlovski): What excitation source did you use and what wave length?

A.A.Shishlovski: The luminescence of the investigated solutions is excited in the short wave region. Hence a mercury tube, the usual source, is unsuitable; one must use a condensed spark or an arc between metal electrodes. We used light in the 2000-2300 A interval. Of course the best wave length in any particular case will depend on the substance studied.

F.I.Fedorov: Did you investigate the influence of impurities?

A.A.Shishlovski: In most cases we would simply have surposition of the absorption of the added impurity on the absorption spectrum of the investigated substance. As a rule there is no effect due to association in the presence of other cations.

LUMINESCENCE OF PLATINOCYANIDE COMPOUNDS

- N.A.Tolstoi, A.K.Trofimov, A.M.Tkachuk
and N.N.Tkachuk

Introduction

The luminescence of platinocyanide salts has long attracted the attention of many investigators. Stokes'[1] classic study (1853) - in which Stokes first proposed the method of crossed light filters that has since become one of the basic procedures in investigating luminescence - is connected with the investigation of the luminescence of platinocyanide salts. During the hundred years since then there have been numerous publications on the luminescence of platinocyanides. However, we still lack reliable systematic data of a phenomenological nature which would serve as an adequate basis for a theoretical interpretation of the luminescence of this interesting and unique class of luminophors. At the same time the great brightness of the emission of these substances, the relative simplicity of their chemical structure, the diversity of their spectra and ensuing feasibility of establishing homologous regularities, all make the platinocyanides an attractive subject for complex investigations of luminescence. The recently renewed interest in the relation between luminescence properties and the crystal structure, stimulated by the publication of a number of important investigations in this field, leaves no doubt that platinocyanides will be the subjects of systematic complex investigations. Such studies must comprise 1) a chemico-preparatory part and 2) an optical part.

In view of the known strong dependence of the properties of platinocyanides on their content of water of crystallization and on their crystalline modification, which are dependent on the preparation procedure, careful determination of the precise physical-chemical characteristics of the investigated samples is essential. The numerous contradictions and discrepancies in the data on the luminescence of platinocyanides are undoubtedly connected with experimental negligence in this respect. We can safely assume that nominally identical samples studied by different investigators were actually of a different physical-chemical nature.

The optical studies proper, which obviously include spectral measurements (absorption and emission), efficiency determinations, polarization studies and finally investigations of the kinetics of the emission, could not until now be phenomenologically complete in view of the impossibility of kinetic measurements. Whereas for the investigation of spectra, efficiency and polarization we have long had well developed procedures, for the study of the kinetics of emission we had only fluorometers ($\tau < 10^{-8}$ sec) and phosphoroscopes (of these for the taumeter $\tau > 10^{-5}$ sec). Experiments show that the relaxation of the emission of the platinocyanides is not susceptible of measurements by either a fluorometer or a taumeter, i.e., falls into the "blind area" (10^{-8}-10^{-5} sec) mentioned by Vavilov back at the Second All Union Conference on Luminescence.

Recently the situation as regards such measurements has greatly improved. Development of the ultrataumeter method[2-4] virtually eliminates the "blind area" in the measurement of the kinetics of luminescence and allows of an all-around complex study of the luminescence of platinocyanide salts. In the present report we shall give the first data on the kinetics of the luminescence of a number of platinocyanide salts synthesized by us.

1. Procedure

The measurements of the luminescence relaxation time were made by means of an ultrataumeter with a mechanical light modulator.[4] Although based on the same

principles as the taumeter[5] the ultrataumeter differs from the latter as regards 1) greatly enhanced steepness of the wave fronts of the square exciting-light pulses, 2) virtually zero inertia of the photomultiplier circuit, attained by the use of cathode followers installed immediately after the photomultiplier tube, and 3) the wide band characteristics of the specially designed cathode-ray oscillograph (2 c to 10 Mc at an amplification factor of about 500). A detailed description of the instrument and measuring procedure will be given elsewhere.

2. Synthesis of the platinocyanide salts

The raw material for preparing the platinocyanide was barium platinocyanide synthesized by the method of Bergsöe.[6] An 8-10% solution of chloroplatinic acid was added to a hot aqueous solution of barium hydroxide taken in the proportion of 1 to 7-8 relative to the $H_2(PtCl_6)$. SO_2 was passed through the continuously heated reagent mixture until the solution became entirely colorless and showed a definite acid reaction. In the process the tetravalent platinum was entirely reduced to the bivalent:

$$H_2[PtCl_6] + 7Ba(OH)_2 + 5SO_2 = PtSO_3 \cdot 3BaSO_3 + BaSO_4 + 3BaCl_2 + 8H_2O.$$

Next the reagent mixture was alkalized by barium hydroxide with litmus as the indicator. The filtered and washed (warm water) white precipitate consisting of $PtSO_3 \cdot 3BaSO_3$, while being heated in a water bath, was treated with a solution of $Ba(CN)_2$ taken in a slight excess over the amount required by the following reaction:

$$PtSO_3 \cdot 3BaSO_3 + 2Ba(CN)_2 = Ba[Pt(CN)_4] + 4BaSO_3.$$

The excess of $Ba(CN)_2$ was removed by passing carbon dioxide through the heated mixture, the reaction resulting in $BaCO_3$ (precipitate) and HCN (gas). After separation of the insoluble barium salts ($BaSO_3$ and $BaCO_3$), the transparent solution was carefully evaporated. Upon evaporation the cold solution yielded yellowish green crystals of $Ba[Pt(CN)_4] \cdot 4H_2O$ characterised by a bluish-violet sheen and a bright blue luminescence.

Preparation of Li, Na, K, Rb, Cs, Mg, Y, La, Pr, Nd, Sm, Gd, Dy, Er, Tu and Yb platinocyanide. The sulphates of these metals are soluble. The platinocyanides were prepared by double exchange in water solution:

$$Ba[Pt(CN)_4] + Me_2SO_4 = Me_2[Pt(CN)_4] + BaSO_4\downarrow.$$

Preparation of Ca and Sr platinocyanide. These platinocyanides were prepared from $K_2[Pt(CN)_4]$, prepared as described above. First we obtained the insoluble copper salt

$$K_2[Pt(CN)_4] + CuSO_4 = Cu[Pt(CN)_4] + K_2SO_4,$$

which was then converted to Ca or Sr platinocyanide according to the following reaction:

$$Cu[Pt(CN)_4] + Ca(OH)_2 = Ca[Pt(CN)_4] + CuO\downarrow + H_2O.$$

All the platinocyanide salts were subjected to repeated recrystallization. The properties and characteristics (including the temperatures of hydrate transformation and color change) of the final products fully corresponded to the pertinant data given in chemical literature. While this freed us of the necessity

of chemical analyses we felt it expedient to verify the chemical composition of the $Ba[Pt(CN)_4]\cdot 4H_2O$. To this end we determined the amount of both Ba and $Pt(CN)_2$. The analysis substantiated the indicated composition. In addition we checked the composition of several of the rare earth platinocyanides. This was done indirectly on the basis of the amount of $BaSO_4$ formed in their synthesis.

As was noted above, the amount of water of crystallization in the platinocyanide salts is a very important factor where their optical properties are concerned. For the sake of definitiveness we generally limited ourselves to the preparation of the crystal hydrates with the maximum H_2O content and the anhydrous salt (except for the Ba and Mg salts for which we prepared certain intermediate hydrates). The highest hydrates were obtained by slow crystallization from the saturated solution with retention of a small amount of the mother liquor. The anhydrous salts were obtained by prolonged heating of the hydrates at the temperatures indicated in the literature.

A number of the platinocyanides exhibit isomorphism. Salts crystallizing from solutions with different pH values form different modifications. We obtained salts of Ca, Sr and Ba of the two different modifications by crystallizing them from a neutral and an alkaline (cyanide) solution.

3. Experimental results

The emission of all the investigated platinocyanides is characterised by the fact that the brightness of the stabilized luminescence is proportional to the excitation intensity E and the fact that the curves characterising the rise and decay of the emission are symmetric and exponential*

$$I_{rise} \approx E(1 - e^{-t/\tau}) \text{ and } I_{decay} \approx Ee^{-t/\tau}$$

The value of τ is independent of E, but does vary with the temperature. We studied most of the salts in a wide temperature range (as a rule from -150°C to the temperature at which loss of water crystallization begins for the given substance). The values of τ for the investigated salts at the lowest temperature of the experiment and at room temperature are summarized in Table 1.

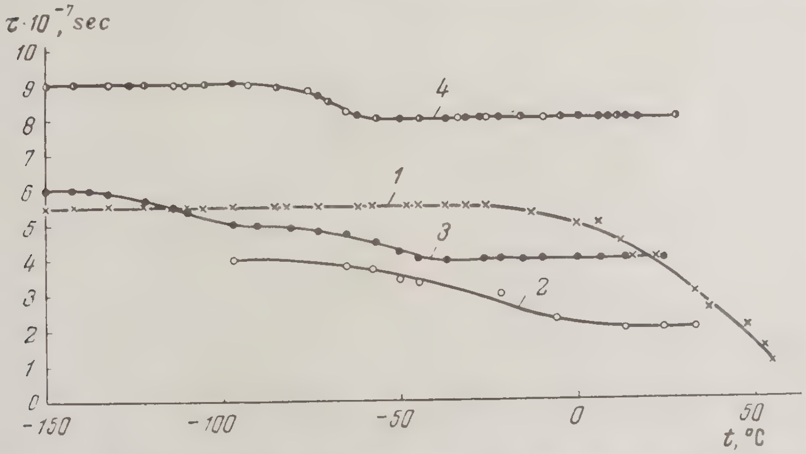

Fig. 1. Temperature dependence of the relaxation time: 1- $Ba[Pt(CN)_4]$, 2- $Ba[Pt(CN)_4]\cdot 2H_2O$, 3- $Ba[Pt(CN)_4]\cdot 4H_2O$ crystallized from a neutral medium, 4- $Ba[Pt(CN)_4]\cdot 4H_2O$ from $Ba(CN)_2$; × and ● - heating, ○ - cooling.

Examples of the complete temperature dependences of τ are given in Figs. 1, 2 and 3.

It follows from Table 1 that the value of τ depends not only on the nature of the cation in the given platinocyanide but also on the amount of water of crystallization, although in general the relaxation time of most of the investigated salts lies between 10^{-6} and 10^{-7} sec.

Fig. 1 shows the temperature dependences of τ for four samples of the barium salts; the anhydrate, a dihydrate and two

---

*Small deviations from exponential decay (for example, the presence of the sum of two exponents with slightly different values of τ cannot as yet be established by our procedure.

tetrahydrates obtained by crystallization from an alkaline and from a neutral solution. It will be seen that the variations of τ with temperature differ for the four samples.

Table 1

Formula	Amount crystlzn. water	t, °C	$\tau \cdot 10^7$, sec	$\tau \cdot 10^7$ sec at $t=20°$	Remarks
Li_2 [Pt $(CN)_4$]	Anhydrous	—150	12	5	
Li_2 [Pt $(CN)_4$]	x H_2O	—150	10	2	
Na_2 [Pt $(CN)_4$]	Anhydrous	—150	10	7	
Na_2 [Pt $(CN)_4$]	3 H_2O	—150	8,5	4	
K_2 [Pt $(CN)_4$]	Anhydrous	—150	6	5	
K_2 [Pt $(CN)_4$]	3 H_2O	—150	9,5	5	
Rb_2 [Pt $(CN)_4$]	x H_2O	—150	8,5	2	
Cs_2 [Pt $(CN)_4$]	x H_2O	—150	Red	2	
Mg [Pt $(CN)_4$]	2 H_2O	—150	9,5	7	
Mg [Pt $(CN)_4$]	5 H_2O	—126	9	5	
Ca [Pt $(CN)_4$]	Anhydrous	—150	9	6	
Ca [Pt (CN_4)]	5 H_2O	—150	5,8	3,5	From neutral medium
Ca [Pt $(CN)_4$]	5 H_2O	—150	8	5,6	From alkaline medium
Sr [Pt $(CN)_4$]	Anhydrous	—150	12,8	10,5	
Sr]Pt $(CN)_4$]	5 H_2O	—150	12,5	3	From neutral medium
Sr [Pt $(CN)_4$]	5 H_2O	—150	7,8	3	From alkaline medium
Ba [Pt $(CN)_4$]	Anhydrous	—150	5,5	4	
Ba [Pt $(CN)_4$]	2 H_2O	—100	4	2	
Ba [Pt $(CN)_4$]	4 H_2O	—150	6	4	From neutral medium
Ba [Pt $(CN)_4$]	4 H_2O	—150	9	8	From alkaline medium
Y_2 [Pt $(CN)_4]_3$	21 H_2O	—183	Red	Red	
Ln_2 [Pt $(CN)_4]_3$	18 H_2O	—183	11	6	
Pr_2 [Pt $(CN)_4]_3$	18 H_2O	—183	<1	<1	
Nd_2 [Pt $(CN)_4[_3$	18 H_2O	—183	4	1—1,5	
Sm_2 [Pt $(CN)_4]_3$	18 H_2O	—183	1	<1	
Gd_2 [Pt $(CN)_4]_3$	18 H_2O	—183	11	6	
Dy_2 [Pt $(CN)_4]_3$	21 H_2O	—183	3	Red	
Er_2 [Pt $(CN)_4]_3$	21 H_2O	—183	3	»	
Tu_2 [Pt $(CN)_4]_3$	21 H_2O	—183	<1	»	
Yb_2 [Pt $(CN)_4]_3$	21 H_2O	—183	7	»	

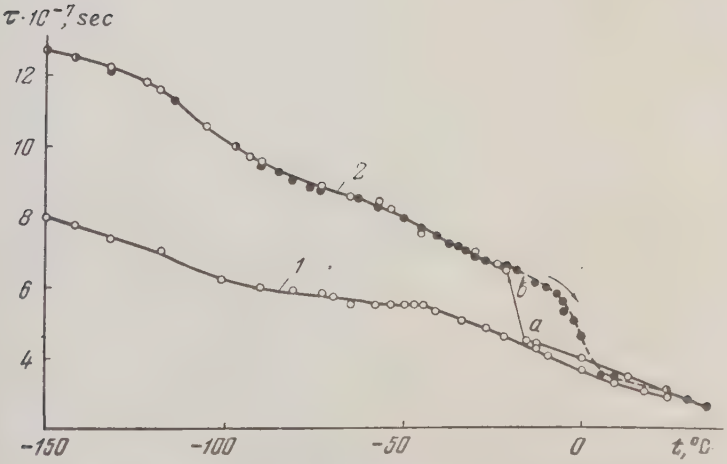

Fig. 2. Temperature dependence of the relaxation time: 1-[Sr Pt$(CN)_4$]·$5H_2O$ crystallized from an alkaline medium, 2- Sr[Pt$(CN)_4$]·$5H_2O$ from a neutral medium; ● - heating, ○ -cooling.

Fig. 2 shows $\tau(t)$ for two strontium platinocyanide pentahydrates (the highest hydrate) also crystallized from a neutral and an alkaline solution. It will be seen that, as in the case of the barium salt, the dependences differ. A noteworthy feature of the curves is the presence of temperature hysteresis. This effect, which is also observed for a number of other salts, is apparently connected with crystallomodificational transitions. The rates of cooling and heating used in our experiments while sufficiently low to permit establishment and maintenance of temperature equilibrium in the region of stability of a given crystal form, were apparently excessively high in the region where one form goes over into another. The effect cannot be explained by a trivial loss of water of crystallization since in a number of cases hysteresis is observed in the interval of rather low temperatures and moreover it is also observed in anhydrous salts. It is interesting to note that in the region of temperature hysteresis there also

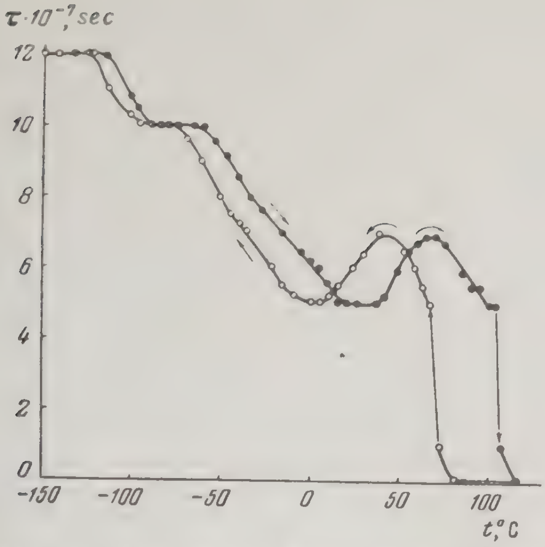

Fig. 3. Temperature dependence of the relaxation time of anhydrous $Li_2Pt(CN)_4$; ● - heating, ○ - cooling.

occur rapid changes in the color of the luminescence. Thus, for example, in cooling from point a to point b (Fig. 2, curve 2) the color of the emission rapidly changes from violet to white.

A very interesting example of a sharp temperature-induced change in the nature of the luminescence is furnished by the anhydrous lithium salt (Fig. 3). At a temperature of about 100° the color of the emission quickly changes from green to light blue and τ falls off from $5 \cdot 10^{-7}$ sec to a value defying measurement ($< 5 \cdot 10^{-8}$ sec). This salt exhibits peculiar features as regards the variation of $\tau(t)$ at other, lower temperatures as well (Fig. 3). Irregular variation of τ (for example, temperature plateaus, increases of τ with temperature, sudden jumps in the value of τ, etc.) are also observed in the case of certain other salts. These irregularities in the variation of τ are often accompanied by changes in the color of the luminescence.

The sodium trihydrate exhibits another distinctive feature: in the interval from about -50 to +20°, in addition to the rapid relaxation process ($\tau = 4\text{-}6 \cdot 10^{-7}$ sec), there is also observed a relatively slow relaxation process ($\tau \approx 10^{-4}$ sec). We did not observe such "tails" in the rise and decay of luminescence curves of any of the other salts so far.

We also carried out a number of experiments with aqueous solutions of the platinocyanides. We mention only the preliminary data here. Liquid solutions yield virtually no luminescence. However, when the aqueous solutions of the barium and potassium salts are frozen a very bright glow appears. This luminescence is still apparent at concentrations as low as 10^{-7} mole/liter. The concentration dependences of the color of the emission are noteworthy. The visually determined variations in the color of the glow at a temperature of about -180° are listed in Table 2 (the concentrations are in mole/liter).

Table 2

Platinocyanide	$5 \cdot 10^{-4}$	$5 \cdot 10^{-5}$	$5 \cdot 10^{-6}$	$5 \cdot 10^{-7}$	$5 \cdot 10^{-8}$
Potassium	whitish	yellow	blue	blue (weak)	no glow
Barium	yellow	yellow	blue	same	same

As the temperature is increased from -180 to 0° the luminescence yield falls off. It is important to note that the glow virtually disappears at temperatures appreciably below 0°; in other words, the quenching is not connected with the melting of the ice. If we assume that with quick freezing of very dilute solutions (the tubes containing the solution were immersed in liquid air) the platinocyanides do not crystallize out, it appears surprising that, given an ionic spacing of the order of 500 A and more, concentrational effects are observed. For not excessively weak solutions ($C \simeq 10^{-5}$ mole/liter) τ can be measured. At $C = 5 \cdot 10^{-5}$, $\tau \approx 2 - 2.5 \cdot 10^{-6}$ sec for the barium and potassium salt solutions at -183°. As the temperature is increased τ falls to $< 10^{-7}$ sec. At lower concen-

centrations (i.e., at the point where the yellow emission begins to turn blue) τ at -183° becomes smaller (about 10^{-6} sec). We feel that the described effects are worthy of further investigation.

In conclusion we give in Fig. 4 approximate data on the luminescence spectra of a number of the investigated salts at room temperature and at the temperature of liquid oxygen or nitrogen.

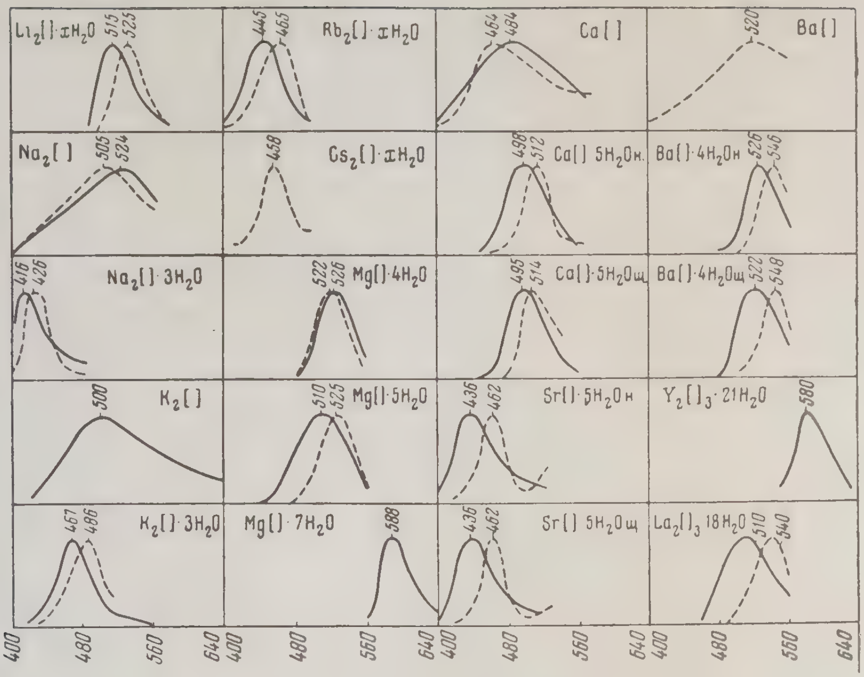

Fig. 4. Luminescence spectra of platinocyanide salts (the brackets in each case denote $Pt(CN)_4$) at 20° (solid line) and at -183° (dash lines). Horizontal scale - wavelengths in mμ; vertical scale - intensities in relative units.

Conclusions

1. The ultrataumeter method now makes it possible to investigate the kinetics of the luminescence of the platinocyanide salt group.

2. Relaxation of the luminescence of the platinocyanide, with some exceptions, is characterized by a time of 10^{-6}-10^{-7} sec.

3. There are salts in this group with a relaxation time measurable by a fluorometer.

4. The kinetics of the emission depend on the complex manner on the nature of the cation, the amount of water of crystallization and the character of the crystal modification.

5. The kinetics of the emission together with the luminescence spectrum may be regarded as a sensitive index to the changes in the state of the crystal lattice of the platinocyanides.

6. The frozen aqueous solutions of the platinocyanides exhibit a bright luminescence having a duration of the same order as the solid salts. The temperature variation of τ, however, differs from that of the salts.

7. The luminescence spectrum of the frozen aqueous solutions shows a certain concentration dependence in a region of very low concentrations.

The new data on the luminescence of platinocyanides described in the present paper are of a preliminary character and our primary aim in presenting them is to draw attention to this very interesting class of substances, further investigation of which may throw additional light on the role of the crystal state in luminescence phenomena. In the future we hope to present the results of more detailed experiments with the platinocyanides.

References

1. G.G.Stokes, Phil. Trans., 143, (1), 1853.

2. N.A.Tolstoi, Trudy GOI (Transactions of the State Optical Institute) Session devoted to the memory of S.I.Vavilov, M. 1953.

3. N.A.Tolstoi & N.N.Tkachuk, Doklady AN SSSR, 95, 65 (1954).
4. N.A.Tolstoi, Doklady AN SSSR, 102, 935 (1955).
5. N.A.Tolstoi, P.P.Feofilov, Usp. fiz. nauk., 41, 44 (1950).
6. P.Bergsöe, ZS. f. anorg. Chem., 19, 319 (1899).

Discussion

V.L.Levshin: The report is of great interest because we have here careful measurements of the variation of the lifetime of excited states in a wide time range and observation of a large number of transitions from one modification to another.

A.N.Sevchenko: Vavilov pointed out repeatedly that many compounds should have a lifetime of the excited state between 10^{-5} and 10^{-8} sec, but unfortunately there were no instruments available for detecting and recording such intervals. Now such an instrument has been developed.

A.A.Shishlovski: It follows from the described experiment that in the case of frozen solutions of platinum and crystalline platinum salts the luminescence characteristics are affected by the short-range order in the vicinity of the platinum ions. This is in agreement with what we have found in our work with thallium and lead salts. Bearing in mind this influence of the short-range order on luminescence, it is strange that in attempting to explain luminescence quenching most investigators consider only the temperature factor. It may be that there is temperature quenching in the case of frozen aqueous solutions of platinum salts but this factor cannot play any significant part in the increase in luminescence in going from liquid to solid solutions.

B.A.Piatnitski: In our experiments with M.S.Fadeeva we observed similar plateaus in the temperature dependence of τ for a number of organic compounds at temperatures near the temperature of liquid air.

N.A.Tolstoi: When we heat a substance, starting from the temperature of liquid air, there occur changes in the thermal motion of the lattice. Perhaps these changes are not gradual but step-like in the sense of "unfreezing" or freeing additional degrees of freedom which then successively exert their effect on the value of τ.

Furthermore there may also occur a modificational rearrangement of the lattice. I believe this is worth further investigation.

I also believe that the conditions under which quenching in liquid aqueous solutions of platinocyanide decreases or ceases (transition to frozen solution or to solid salt) may be connected with an increase in the lifetime due to a change in the degree of forbiddenness of radiative transitions, imposed on the emission centers by the surrounding medium and depending on the temperature and the structure of the medium. This may be the situation in the case of the lithium salt described in our paper.

ON MEASURING THE DURATION OF FLUORESCENCE BY MEANS OF A PHASE FLUOROMETER

- A.M.Bonch-Bruevich

A fluorometer is generally understood to be an instrument for direct measurement of the decay of fluorescence, the persistence of which is about 10^{-8} sec. To this end the investigated substance is irradiated with intensity modulated light E(t) and the time variation of the luminescence intensity I(t) is compared with the law characterising the modulation of the exciting light. If the intensity of the exciting light is varied harmonically, i.e., if

$$E = E_0 (1 + m \cos \omega t),$$

then for spontaneous emission at a time $t \gg \tau$ after the beginning of irradiation the intensity of the luminescence also follows the harmonic law

$$I = I_0 [1 + M \cos (\omega t - \varphi)],$$

where

$$M = \frac{m}{(1 + \omega^2 \tau^2)^{1/2}}, \tag{1}$$

$$\varphi = \operatorname{arc\,tg} \omega \tau. \tag{2}$$

When the exciting light is modulated according to a more complex law than the simple harmonic, expressions (1) and (2) remain valid for each harmonic of the exciting light.

In all fluorometers τ is determined by measuring the phase shift between the luminescence light and the exciting light (2). Depending on the method of measuring this phase shift fluorometers may be classified as photometric (Refs. 1-6), stroboscopic (Refs. 7-12), or phase fluorometers (with direct measurement of the phase displacement) (Refs. 13-19).

The accuracy of measurement on most fluorometers is indicated by the different authors is in the neighborhood of $3 \cdot 10^{-9}$-$6 \cdot 10^{-9}$ sec. However, the scattering in the values of τ given in even the most serious studies goes far beyond these limits. Thus, the values of τ given in the literature vary from $3.1 \cdot 10^{-9}$ to $6 \cdot 10^{-9}$ sec for stilbene, $5.2 \cdot 10^{-9}$ to $13.5 \cdot 10^{-9}$ sec for phenanthrene and $8.8 \cdot 10^{-9}$ to $15 \cdot 10^{-9}$ sec for fluorene etc.

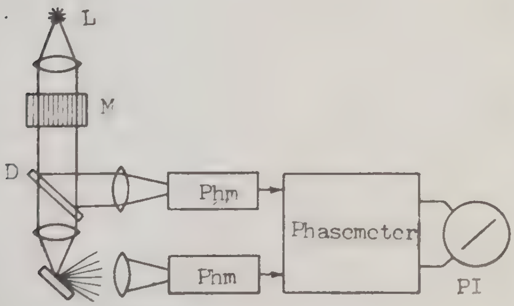

Fig. 1. Diagram of a phase fluorometer: L) light source, M) optical modulator, D) light divider plate, Phm) photomultiplier, PI) phase indicator.

Such divergences in the figures obviously reduce the value of fluorometric measurements. They can be due both to inadequate impurity of the investigated substances and to measurement errors. Measurements made by photometric and stroboscopic fluorometers have been critically evaluated by a number of authors. (Ref. 2, 10, 13). In view of their advantages, phase fluorometers have generally been favored in recent investigations. However, hitherto no one has examined the errors of measurement on such fluorometers or analyzed the sources of possible errors.

The general arrangement of a phase fluorometer is diagrammed in Fig. 1. Measurements of the duration of fluorescence amounts to a two-fold determination of the phase difference between the optical signals in two channels: a) with a scatterer in the

measurement channel (φ_s) and b) with the scatterer replaced by the investigated substance (φ_p). Then $\varphi = \varphi_p - \varphi_s$.

In most fluorometers the measurements are carried out by the null method, for which purpose the circuitry includes an arrangement to introduce an appropriate standard phase shift into one of the channels, while a phase meter is used as an indicator. The resolution $\Delta\varphi_o$ of the latter largely determines the accuracy of measurements. Thus from (2) we find

$$\frac{\Delta\tau}{\tau} = \frac{1+\omega^2\tau^2}{\omega\tau}\, 2\Delta\varphi_0. \tag{3}$$

Fig. 2 gives the generalized curve characterising the relative error in measuring τ

$$\frac{\Delta\tau}{2\tau\Delta\varphi_0} = f(\omega\tau).$$

For $\omega\tau = 1$

$$\frac{\Delta\tau}{\tau} = \frac{\Delta\tau}{\tau}\Big|_{min} = 4\Delta\varphi_0. \tag{4}$$

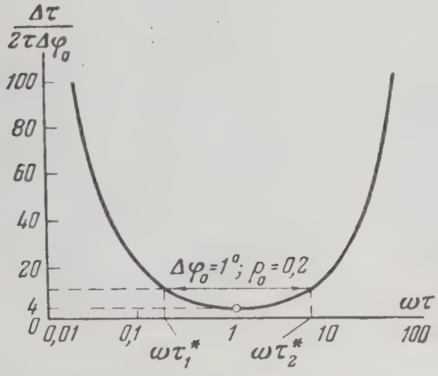

Fig. 2. Generalized curve characterising the relative error in measuring on a phase fluorometer.

Further, the value of φ_o together with the frequency of modulation ω determines the limiting values of τ within which the value of $\Delta\tau/\tau$ does not exceed a given value (p_o). This interval is bounded by the values

$$\overset{*}{\tau}_{1,2} = \frac{p_0}{4\Delta\varphi_0\omega}\left[1 \pm \sqrt{1-16\left(\frac{\Delta\varphi_0}{p_0}\right)^2}\right]. \tag{5}$$

The values of $\omega\overset{*}{\tau}_1$ and $\omega\overset{*}{\tau}_2$ corresponding to $\Delta\varphi_o = 1^\circ$ and $p_o = 0.2$ are indicated in Fig. 2.

The family of curves

$$\omega\overset{*}{\tau}_{1,2} = f(\Delta\varphi_0,\ p_0).$$

is shown in Fig. 3. The ordinate scale, in addition to $\omega\tau^*$, is also graduated in values of (in mμ sec) at a modulation grequency of 10Mc.

The vertical dash line corresponds to $\varphi_o = 1^\circ$. The points of intersection of this line with the curves which correspond to certain definite values of p_o, indicate the effective operating range of the instrument. The resolution of the phase indicator is substantially determined by the fluctuation noise level. Analysis (see Ref. 20 for details) shows that if the noise level remains lower than the level of the useful signal the threshold sensitivity of the set-up is given by the approximate expression

$$\Delta\varphi \approx \Delta\varphi_o + \Delta\varphi_n \approx \Delta\varphi_o + \frac{a u_{no}}{U_c}\sqrt{\Delta f_{pb}}, \tag{6}$$

where a is a coefficient, u_{no} is the effective value of the fluctuation voltage referred to a unit spectral interval and Δf_{pb} is the pass band of the circuit.

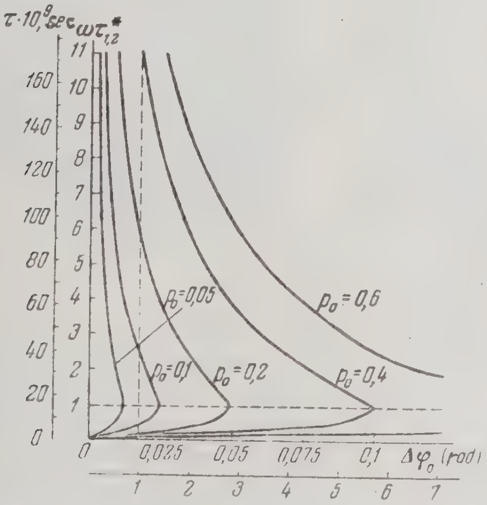

Fig. 3. Family of curves $\omega\tau = \Delta f(\varphi_o, p_o)$ defining the range of values of $\omega\tau$ and τ (at 10 Mc) within which the error of measurement does not exceed certain value. The dash line corresponds to a resolution of the indicator $\Delta\varphi_o = 1^\circ$.

In Fig. 4 we reproduce the photographs of the cathode-ray tube screen obtained in our experiment with $\varphi = 0$ and the indicated values of the resolution $\Delta\varphi_o$ at different values of the ratio

$$\frac{u_n}{U_c} = \frac{u_{no}}{U_c}\sqrt{\Delta f_{pb}}$$

(for our apparatus $\Delta f_{pb} = 5$kc). Using these data and referring to the curve on Fig. 3 we can easily determine to what extent the error in determining τ increases and the effective operating region of the fluorometer employing an oscilloscope is reduced even with a relatively low fluctuation noise level.

As follows from equation (6), one can in principle reduce the value of $\Delta\varphi_n$ as much as desired by narrowing the pass band of the phase meter circuit. However, when the phase meter incorporates a selective electric network, the overall error in measuring the phase shift is given by

$$\Delta\varphi \approx \Delta\varphi_o + \Delta\varphi_n + \Delta\varphi \approx \Delta\varphi_o + \frac{au_{no}}{U_c}\sqrt{\Delta f_{pb}} + x\Delta Q, \qquad (7)$$

where x is a coefficient whose value is determined by the character of the electric network and the width of its pass band and ΔQ is the relative frequency instability of the amplified signals. The greater the selectivity of the electric network, the greater in general will be the value of x so that any effective reduction in the value of $\Delta\varphi_n$ is accompanied by an increase in $\Delta\varphi_\omega$.

Without going into detail we might mention that a satisfactory solution of the problem is achieved by changing from the cathode-ray tube to an inertia phase indicator which in itself has a low sensitivity to fluctuation noise and at the same time does not introduce any phase frequency errors. In fact an inertia phase detector may have a higher resolution than a cathode-ray tube indicator.

The result of fluorometric measurements can be appreciably distorted by systematic errors. There may be a number of sources of such errors.

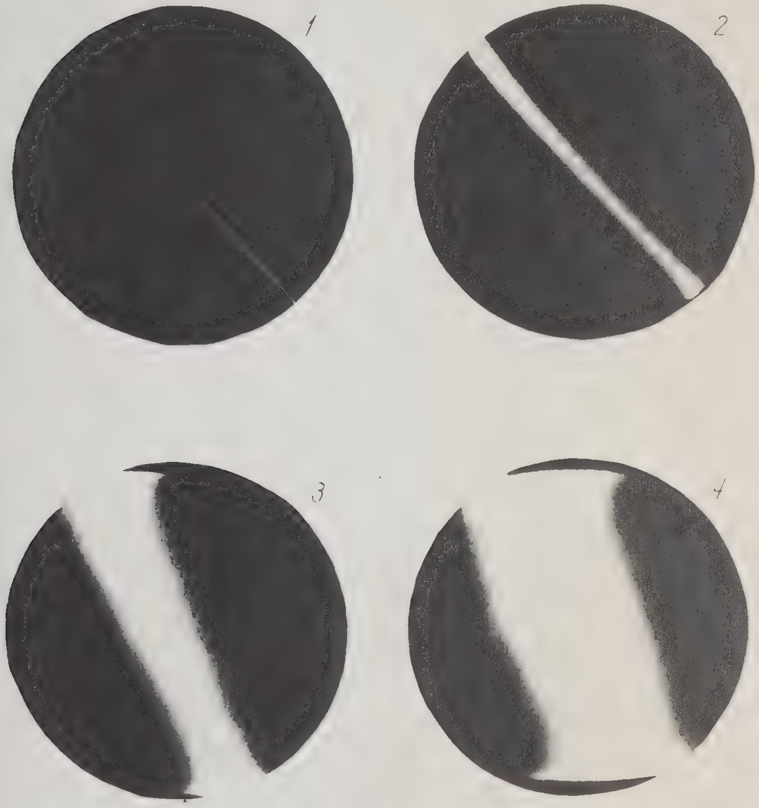

Fig. 4. Oscillograms showing the influence of fluctuation noise in phase measurements by means of a cathode-ray tube and the resultant impairment of the resolution: 1) $u_n/U_c = 0$, $\Delta\varphi_o = 1^\circ$; 2) $u_n/U_c = 0.25$, $\Delta\varphi_o = 4^\circ$; 3) $u_n/U_c = 1$, $\Delta\varphi_o = 15^\circ$; 4) $u_n/U_c = 2.5$, $\Delta\varphi_o = 30^\circ$.

First, the dependence of the electron flight time in the photomultiplier tube on the point of illumination of the photocathode and on the magnitude of the photocurrent (Fig. 5) may lead to an error of the order of several millimicroseconds in determining τ. Changes in the conditions of photocathode illumi-

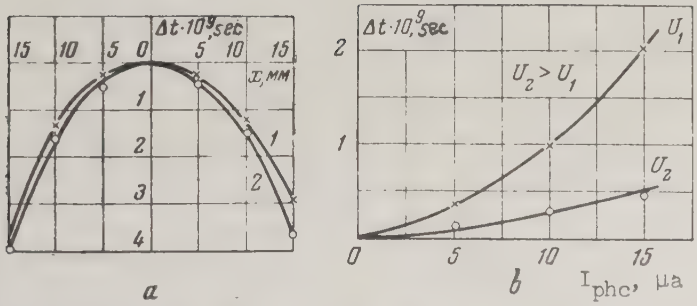

a

b

Fig. 5. Curves showing the variation of the electron flight time (a) in the FEU-19 photomultiplier incident to displacement of the light spot over the photocathode diameter parallel (1) and perpendicular (2) to the generatrix of the dynodes and (b) as a function of the illumination of the photocathode (magnitude of the photocurrent) at different potentials on the photomultiplier tube.

nation can occur a) when the scatterer is replaced by the specimen and b) when the additional phase shift is introduced by changing the length of the optical path in one of the channels. As far as we know, no one hitherto has called attention to these sources of error.

Second, as we discovered in our work with a diffraction modulator*, differences in the modulation phases in different parts of the spectrum and in different sections of the light beam emerging from the optical modulator can be sources of appreciable systematic errors. Hence if different parts (in the geometric or the spectral sense) of the beam are used in measurements with the scatterer and in observing the fluorescence there may occur a systematic error in the determination of of the order of several millimicroseconds.

In addition we note that the differences between the phases of modulation in different parts of the light beam may vary with time which further reduces the accuracy of measurement.

Lastly, considerable systematic errors may be connected with the operation of the vacuum tube part of the fluorometer. The greatest errors may be due to the hitherto ignored amplitude dependence of the time of passage of the signal through the vacuum tube circuit.[20] In consequence, the measured value of τ will depend on the intensity of the fluorescence. In addition to an incorrect value of τ this can lead to appreciable distortions in determining the character of the dependence of the duration of fluorescence on the temperature, the concentration of the investigated substance, the solvent and other factors that influence the intensity of the fluorescence. Such amplitude-phase errors are produced by nonlinear components in the circuit. In order to eliminate such errors special measures - normally unnecessary in designing other measuring instruments - must be taken in designing and constructing the fluorometer. Furthermore in operating the instrument, the noise level must be monitored and the signals from the luminophor and the scatterer equalized insofar as possible.

Thus we have seen that there are sources of appreciable systematic errors in phase fluorometers. The magnitude of these errors can be evaluated if the details of the fluorometer design and its operation are known.

From what has been said above we can conclude that the values of the accuracy of measurement with fluorometers given in the literature are overestimated. The divergences in the value of τ reported for different substances can generally be explained by experimental errors and systematic errors of measurement. Selection of a more reliable value of τ among those given by different authors is difficult in view of the lack of information on the level of fluctuation noise and data on the circuit details which might enable us to evaluate the systematic errors.

---

*For a more detailed description of the diffraction modulator see Ref. 21.

References

1. E.Gaviola, Ann. d. Phys., 81, 681 (1926); ZS. f. Phys., 42, 853 (1927).
2. F.Duschinsky, ZS. f. Phys. 54, 484 (1929).
3. W.Szymanowski, ZS. f. Phys., 95, 440, 450, 460, 466 (1935).
4. L.Brüninghaus, C.R., 204, 118 (1937).
5. L.A.Tumerman & V.V.Shimanovski, Doklady AN SSSR, 15, 325 (1937).
6. J.Birks & W.Little, Proc. Phys. Soc., 66, 921 (1953).
7. O.Mearks, Phys. ZS., 37, 562 (1936); ZS. f. Phys., 103, 598, 685 (1938).
8. W.Kirchhoff, ZS. f. Phys., 116, 115 (1940).
9. L.A.Tumerman, Zhur. eksp. i teor. fiz., 11, 515 (1941).
10. K.Rau, Optik, 5, 276 (1949).
11. M.D.Galanin, Trudy FIAN (Transactions of the Physical Institute of the Ac. of Sc.) 5,341 (1950).
12. W.Hanle, O.Kotschak & A.Scharmann, ZS. f. Naturf., 6a, 202 (1951).
13. L.A.Tumerman, Usp. fiz. nauk., 23, 218 (1947).
14. M.D.Galanin, Doklady AN SSSR, 40, 925 (1950).
15. S.Liebson, W.Bishop & J.Elliot, Phys. Rev., 80, 907 (1950).
16. F.Rohde,ZS. f. Naturf., 8a, 156 (1953).
17. E.Bailey & G.Rollefson, J. Chem. Phys., 21, 1315 (1953).
18. A.Schmillen, ZS. f. Phys., 135, 294 (1953).
19. G.Ravilious, R.Ferrar & S.Liebson, JOSA, 44, 238 (1954).
20. A.M.Bonch-Bruevich & V.I.Shirokov, Zhur. tekh. fiz., 25, 1825 (1955).
21. A.M.Bonch-Bruevich & V.A.Molchanov, Zhur. tekh. fiz., 25, 1653 (1955).

A NEW PHASE FLUOROMETER

- A.M.Bonch-Bruevich, V.A.Molchanov and
V.I.Shirokov

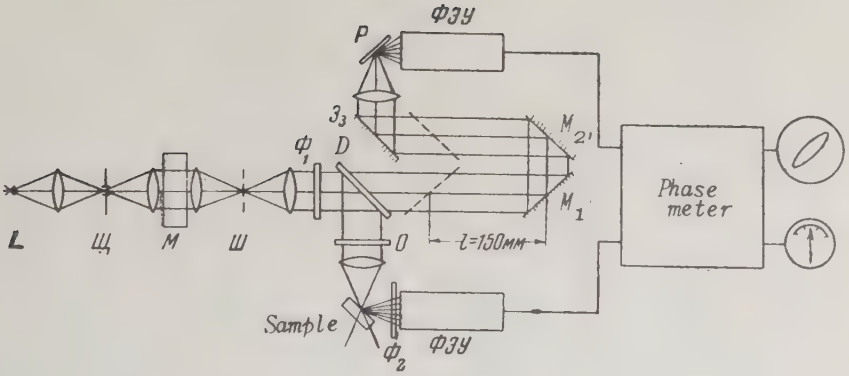

Fig. 1. Diagram of the phase fluorometer: L) light source, Щ, M and Ш) components of the optical modulator, ϕ_1 and ϕ_2) light filters, D) light dividing plate, O) neutral weakener, P) scatterer, M_1 and M_2) system of moveable mirrors, $\phi зу$) photomultipliers.

The new phase fluorometer discussed in this article was built at the end of 1954. The resolution of its phase meter at a low fluctuation noise level is about $2 \cdot 10^{-11}$ sec which is about one order of magnitude better than the resolution of the best fluorometers described hitherto in the literature.[1-3] The accuracy of measurement is accordingly enhanced.[4] The resolution of a fluorometer remains satisfactory even at a relatively high fluctuation noise level. The fluorometer has a number of design features which facilitate work on it, increase the reliability of measurement and make it possible to monitor and control the signal level.

A diagram of the set-up is shown in Fig. 1. The optical part of the instrument includes a light source (an SVDSh-250 lamp), an optical diffraction modulator operating at a frequency of 12 Mc (with separation of side peaks), a light dividing system, an optical line of variable length and FEU type photomultipliers. The instrument also has provision for rapid interchange of the scatterer and investigated sample and for changing the light filters and optical weakeners. The phase meter unit (Fig. 2) comprises two phase indicators: a cathode-ray tube and a special phase sensitive bridge (phase detector) with a pointer indicator, the indications of which depend upon the phase shift between the signals on the two inputs of the phase meter. The duration of fluorescence is determined on the basis of the familiar relationship

$$\tau = \frac{1}{2\pi F} \tan \varphi, \tag{1}$$

where F is the light modulation frequency and φ is the change in the phase of the signal from the photomultiplier in the measurement channel when the scatterer is replaced by the investigated specimen.

The principal indicator - the phase detector - is used in measuring the angle φ; the cathode-ray tube serves for adjustment and monitoring of the operation of the setup as well as for rough measurements and evaluation of the fluctuation noise level. The resolution of the phase detector was selected equal to 0.1° (the order of the zero reading instability of the instrument). The use of an inertia indicator (the phase detector) made it possible to realize a high sensitivity in the presence of fluctuation noise (see table).

Fig. 3 shows the family of curves $\omega\tau = f(\Delta\varphi_o, p_o)$, superimposed on which are straight lines corresponding to the resolution of the indicators for different values of u_n/U_c. The points of intersection of these lines with the corresponding curves indicate the range of values of $\omega\tau$ and τ within which the error of

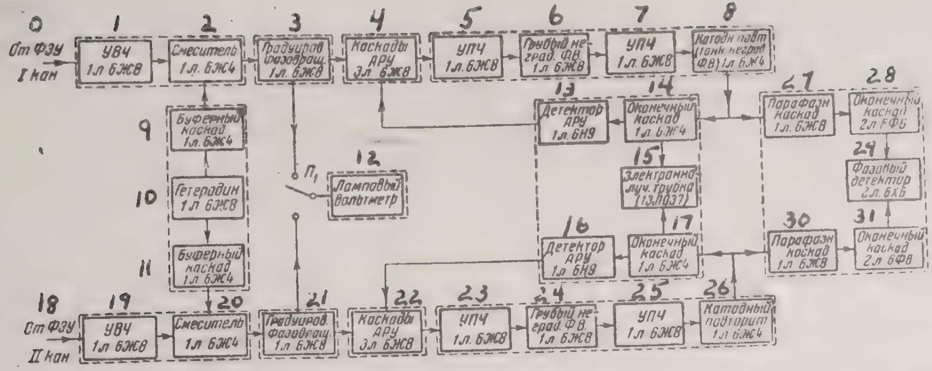
0
От ФЗУ
I кан
1
УВЧ
1л 6Ж8
2
Смеситель
1л. 6Ж4
3
Градуиров фазовращ.
1л. 6Ж8
4
Каскады АРУ
3л 6Ж8
5
УПЧ
1л. 6Ж8
6
Грубый неград. ФВ.
1л 6Ж8
7
УПЧ
1л. 6Ж8
8
Катодн повт (танк неград ФВ) 1л 6Ж4
9
Буферный каскад
1л. 6Ж4
10
Гетеродин
1л 6Ж8
11
Буферный каскад
1л 6Ж4
12
Ламповый вольтметр
П₁
13
Детектор АРУ
1л. 6Н9
14
Оконечный каскад
1л 6Ж4
15
Электронно-луч. трубка
(13ЛО37)
16
Детектор АРУ
1л 6Н9
17
Оконечный каскад
1л 6Ж4
18
От ФЗУ
II кан
19
УВЧ
1л 6Ж8
20
Смеситель
1л 6Ж4
21
Градуиров. фазовращ.
1л 6Ж8
22
Каскады АРУ
3л 6Ж8
23
УПЧ
1л. 6Ж8
24
Грубый неград. ФВ.
1л 6Ж8
25
УПЧ
1л 6Ж8
26
Катодный повторит
1л 6Ж4
27
Парафазн каскад
1л. 6Ж8
28
Оконечный каскад
2л 6Ф6
29
Фазовый детектор
2л. 6Х6
30
Парафазн каскад
1л 6Ж8
31
Оконечный каскад
2л 6Ф8

Fig. 2. A block diagram of the phase meter section of the fluorometer: 0) from photomultiplier of channel I, 1) HF amplifiers, 2 & 20) mixers, 3 & 21) calibrated phase shifters, 4 & 22) automatic signal level controls - ASLC, 5 & 23) IF amplifiers, 6 & 24) rough phase shifters, 7 & 25) IF amplifiers, 8 & 26) cathode followers, 9 & 11) buffer stages, 10) heterodyne, 12) vacuum tube voltmeter, 13 & 16) ASLC detectors, 14 & 17) terminal stages, 15) cathode-ray tube, 18) from photomultiplier of channel II, 27 & 30) paraphase stages, 28 & 31) terminal stages, 29) phase detector. Lower line in each block indicates number of tubes and tube type used in the component.

Relative fluctuation noise level, u_n/U_c	Threshold sensitivity ($\Delta\varphi_o$) and the corresponding error in measuring τ at $\tau=5\cdot10^{-9}$ sec.			
	Cathode-ray tube		Phase detector	
0	1^o	9%	$0^o.1$	1%
0.25	4^o	35%	$0^o.25$	2.5%
1.0	15^o	130%	$1^o.0$	9%
2.5	30^o	260%	$2^o.5$	22%

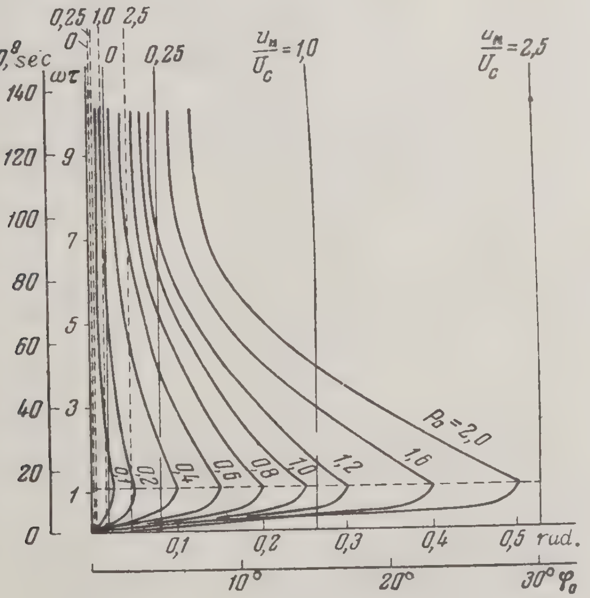

Fig. 3. Family of curves $\omega\tau = f(\Delta\varphi_o, p_o)$ and straight lines corresponding to the resolution of the phase indicators at different fluctuation noise levels (the solid lines pertain to the cathode-ray tube; the dash lines, to the phase detector) at F = 12Mc. The second vertical scale indicates values of τ at a modulation frequency of 12Mc.

measurement does not exceed a given value p_o.[4]

In designing the instrument, a number of special measures were taken to eliminate systematic errors in measuring :

1. Automatic signal level control circuits are incorporated in the amplifier channels. (4 and 22 in Fig. 2.) Each phase meter channel

incorporates three variable low resistance stages with automatic control of their amplification factor without introduction of a parasitic phase shift (this substantially reduced the amplitude-phase error).

2. The set-up incorporates a vacuum-tube voltmeter. Appropriate monitoring of the light signals assures the absence of amplitude-phase errors in the photomultipliers and proper operation of the electronic part of the set-up. Neutral filters are used to equalize the signals from the scatterer and the investigated specimens. By virtue of the measures taken variation of the signal by a factor of 2 cannot lead to an error in the measured value of τ exceeding 10^{-10} sec. Hence in practice there is no need to equalize the signals exactly, which greatly facilitates measurement.

3. The instrument has special provision for equal (both geometrically and spectrally) light division between the measuring and comparison channels.

4. The conditions of illumination of the photomultiplier cathodes remain unchanged when the scatterer is replaced by the investigated specimen and when the length of the optical line in the second channel is varied.

The design of the fluorometer and its phase meter section is such that one can readily check the set-up for proper adjustment and the absence of parasitic effects. This is the only way to insure stability of indication and maximum sensitivity of the instrument.

Measurements are made by the null method with introduction of a known compensating phase shift. To this end the comparison channel incorporates an optical line 30 cm in length by means of which one can introduce a phase shift from 0 to 4.3° (Fig. 1). In addition the instrument has an electric step phase shifter, each step of which is designed to introduce a phase shift of 4.3° (Fig. 2). Thus by appropriate combination of the electric phase shifter step and variation of the line length one can cover the entire range from 0 to 90°, setting the requisite value of φ with the accuracy determined by the resolution of the phase indicator. The comparatively short length of the optical line reduces the danger of errors connected with variation in the illumination conditions on the photocathode in the comparison channel. The presence of two types of phase shifter- optical and electrical - makes it possible to check one against the other which enhances the reliability of measurement.

The duration of the fluorescence of color centers in ionic crystals was measured for the first time by means of this new fluorometer. It proved to be of the order of 10^{-8} to 10^{-9} sec. The fact that the fluorometer retains a relatively high sensitivity even with weak signals made it possible to investigate the concentration dependence of the duration of fluorescence for a number of substances. Investigations of $\tau = f(C)$ for fluorescein showed that in the case of thick layers this dependence is not monotonic (Fig. 4); the nature of the observed dependence is in agreement with the results of Shmillen[2] and Bailey & Rollefson[3]. Comparison of these results with the variation observed for thin layers of fluorescein solution and the data obtained in certain supplementary experiments indicate that the observed increase in the value of τ to the beginning of concentration quenching is connected only with the effect of super absorption. The numerical values for the variation of τ indicate that super-absorption plays a much more important part than might be expected on the basis

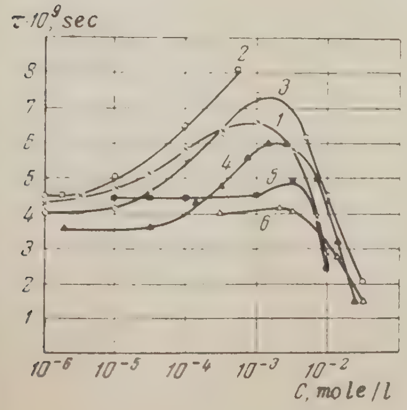

Fig. 4. Variation of τ with concentration for an alkaline solution of fluorescein: 1 & 5) data obtained in the present investigation for a thick and a thin layer of solution, respectively; 2) data of Bailey and Rollefson[2], 3 & 4) data of Schmillen for a thick layer of solution (1953 & 1954 data), 6) data of Schmillen for a thin layer of fluorescein solution.

of earlier investigations (Refs. 1 & 5). Investigation of the concentration dependence of τ for acridine orange (Fig. 5) and comparison of these results with the spectra of solutions leads us to conclude that in this case the duration of fluorescence changes with the formation of associated groups in the solution.[6]

The results of investigation of the concentration dependences of the duration of luminescence of anthracene and diphenylanthracene, polymerized in polystyrene, and comparison of these data with the values of τ for corresponding samples obtained by reprecipitation, substantiates the hypothesis that anthracene does link up with the styrene chains, while diphenylanthracene does not (this hypothesis was advanced by Vol'kenshtein, Koton & Anufrieva; the luminescent samples were prepared by Koton).

The high resolution of the instrument makes it possible to utilize it for studying processes of extremely short duration. Among the more interesting materials already studied is tetraphenyl butadene in xylol, which has a fluorescence decay time of the order of $8 \cdot 10^{-10}$ sec; the decay time is virtually independent of the concentration in the investigated range (Fig. 6).

The measurements already made on the new fluorometer show that the instrument has a number of positive features. In view of this we hope that it will make possible more detailed and extensive investigation of the decay of fluorescence than has hitherto been possible.

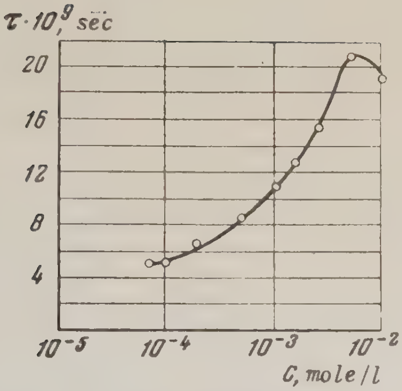

Fig. 5. Dependence of τ on the concentration for acridine orange.

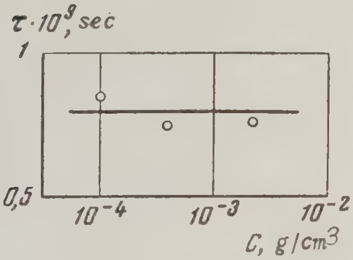

Fig. 6. $\tau = f(C)$ for a solution of tetraphenyl butadene in xylol.

References

1. M.D.Galanin, Doklady AN SSSR, 40, 925 (1950).
2. A.Schmillen, ZS. f. Phys., 135, 294 (1953).
3. E.Bailey & G.Rollefson, J. Chem. Phys., 21, 1315 (1953).
4. A.M.Bonch-Bruevich, Present issue of the Bulletin.
5. M.D.Galanin, Trudy FIAN (Transactions of the Physical Institute of the Ac. of Sci.) 5, 341 (1950).
6. L.A.Kuznechova, B.Ia.Sveshnikov, Izv. AN SSSR, Ser. fiz., 20, 433 (1956); (Translation in Bulletin, Vol. 20, No. 4, p. 394).

DISCUSSION FOLLOWING THE PRECEDING TWO PAPERS

L.A.Tumerman: How do you explain the dependence of the phase shift in photomultipliers on the incident light intensity?

A.M.Bonch-Bruevich: Possibly by the formation of a space charge at some of the photomultiplier electrodes, which substantially changes the configuration of the electric field and consequently the trajectories of the electrons and their flight times through the multiplier.

B.S.Neporent: What is the order of magnitude of the electron flight time through the photomultiplier?

A.M.Bonch-Bruevich: For most multipliers this time is on the order of several 10^{-8} sec. Variations in this time due to fluctuations of the incident intensity and illumination of different points of the photocathode may amount to several times 10^{-9} sec and in individual cases may come to 10^{-8} sec.

A HIGH-TRANSMISSION SPECTROMETRIC SET-UP FOR INVESTIGATION OF LUMINESCENCE

- B.S.Neporent & V.P.Kolochkov

The studies of luminescence spectra in which we have been engaged over a period of years called for the development of a spectrometer* having a high sensitivity together with an accuracy of measurement adequate for detecting small changes in investigated spectra. High sensitivity is required in view of the fact that the substances studied included rarefied gases (pressures down to 10^{-2} mm Hg), the luminescence of which was excited by monochromatic light in the regions characterised by low values of the efficiency (anti-Stokes and far Stokes regions). The set-up herein described was realized as a result of gradual improvement of the equipment operating in our laboratory since 1946 (Ref. 1-4). In developing this spectrometer primary attention was given to obtaining an optical system characterised by high transmission in a wide spectral range.

In the version of the set-up herein described we did not use such means for increasing the sensitivity as cooling the photomultipliers, increasing the response time, utilizing the photomultipliers as quantum counters. All these possibilities were left in reserve.

In contrast to a photographic spectroscopic instrument, the transmission factor of which depends on the relative aperture of the camera, the efficiency of monochromators designed for operation with a photoelectric receiver depends on the dimensions and dispersion of its prism or diffraction grating and the ratio of the slit height to the focal distance of the collimator lenses. This is obvious from the expression characterising the value of the radiation flux leaving the exit slit of the monochromator when the latter separates a spectral interval

$$\Phi_\lambda = B_\lambda \cdot S \frac{d\varphi}{d\lambda} \cdot \frac{h}{F} \cdot (\Delta\lambda)^2 \cdot t_\lambda ,$$

where B_λ is the spectral brightness of the radiation source, S is the effective cross section and $d\varphi/d\lambda$ is the angular dispersion of the diffracting element, h is the height of the slit, F is the focal lens of the collimator lenses, $\Delta\lambda$ is the separated spectral interval and t_λ is the transmission of the monochromator.

The high-transmission monochromator meeting our requirements was designed about a diffraction grating measuring 150 x 120 mm, having 600 line/mm and concentrating 55% of the incident radiation in the maximum reflection region (near 1000 mμ in the first order, near 500 mμ in the second, and 300 mμ in the third). For our purposes a diffraction grating had definite advantages over a prism as regards both acceptable dimensions and angular dispersion.[5] In addition a diffraction grating instrument can be used in a wide spectral range.

A diagram of the monochromator is shown in Fig. 1. The focal distance of the mirror equals 500 mm; the height of the slit, 50 mm. The dispersion of the monochromator which varies slightly with the angle of the grating amounts to 32 A/mm in the first order, 16 A/mm in the second, and 11 A/mm in the third. Having in mind investigation of wide continuous spectra we did not strive to obtain a maximum resolution: the slits were not curved (as suggested by Fastie[6]), the mirror O was not ground with the utmost precision. Nevertheless the instrument clearly resolves in the second order lines only 3-5 Å apart. Use of a more precisely ground mirror and Fastie's arrangement with which all aberrations

---

* We assume that an instrument recording the intensity distribution over the spectrum and characterised by a certain spectral sensitivity curve (a horizontal straight line in the most favorable case) should be called a spectrometer; to make a distinction, a spectrophotometer is an instrument by means of which one can obtain the spectral distribution of some optical characteristics by direct comparison of two fields or two fluxes of radiation.

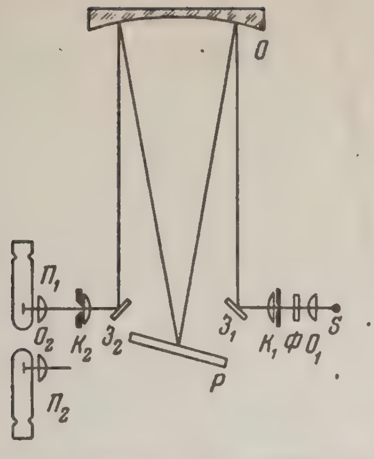

Fig. 1. Optical diagram of the instrument.

except the spherical are compensated would undoubtedly result in appreciably better resolution even with a comparatively large "relative aperture" of the instrument (the ratio of the diagonal of the grating to the focal length of the lenses equals 1:2.5). The grating is rotated by means of a micrometer screw, the knob of which has a wavelength scale.

Filling this instrument with light in view of the height of the slits was somewhat difficult. For the illuminating lens we used a quartz paraboloid O_1 having an aperture of 1:0.67 (D = 45 mm; f = 30 mm). This lens forms a 3x magnified image of the luminescent subject S having a height of up to 15-17 mm, on the entrance slit, the height of which is 50 mm. The collecting lens K_1 together with the mirror O forms an image of the lens O_1 in the plane of the grating P. When the height of the collimator mirror O equals the sum of the heights of the grating and the slit, all the light flux entering the monochromator passes through it without vignetting. In this case the grating serves as the limiting diaphragm of the instrument. In order to reduce the amount of scattered light an appropriate diaphragm was installed over the lens O_1. The arrangement of optical elements forming an image of the exit slit of the monochromator on the cathode of the photomultiplier ($П_1$ in Fig. 1) is symmetric with the illuminating arrangement just described.

We used two photomultipliers in the instrument: an FEU-18 with an uviol (UV transmitting) glass window (sensitivity maximum at about 360 mμ) and an experimental prototype of a cesium oxide photomultiplier (sensitivity maximum in the long wave band near 750 mμ).

The operating conditions of the photomultipliers - the dynode potentials - were selected with a view to obtaining the most advantageous signal to noise ratio. In passing we note that the photomultiplier tubes differ very much from each other as regards noise (dark current fluctuation) which for the FEU-18 is hundreds of times smaller than for the other photomultiplier. The output of the photomultipliers was amplified by a two-stage DC amplifier employing a balanced circuit: the first stage employed 6Zh1Zh (6Ж1Ж) tubes while the second was designed about 6P3S (6П3С) tubes. The amplifiers were supplied from a regular AC line by means of a vacuum tube stabilizer. The photomultipliers were also powered from an electronic stabilizer or alternately from dry cells. An M-91 microammeter (100 μa) and a recording EPP-09 potentiometer were connected in parallel across the output of the amplifier. The maximum gain of the amplifier was sufficiently high for the potentiometer to be able to record the dark current noise of the photomultipliers. Even at this amplification factor the null position of the instruments was not shifted to any appreciable extent. For reasons of convenience and simplicity of operation the photomultiplier was operated at room temperature. The response time of the system was approximately 1 sec.

The wavelength calibration of the spectrometer in the range from 200 to 1300 mμ was carried out in the conventional manner with reference to the visible and ultraviolet lines of standard gas discharge tubes, observed in different orders. The calibration of the instrument as regards spectral sensitivity was carried out by means of a tungsten ribbon filament lamp with a quartz window. The energy distribution in the spectrum of this lamp can readily be computed.[7] The monochromator transmission curve and the sensitivity curves of the photomultipliers have a selective character, stemming from the characteristics of the diffraction grating. In order to obtain the highest sensitivity over the entire wavelength operating range the instrument was calibrated in different parts of the spectrum in dif-

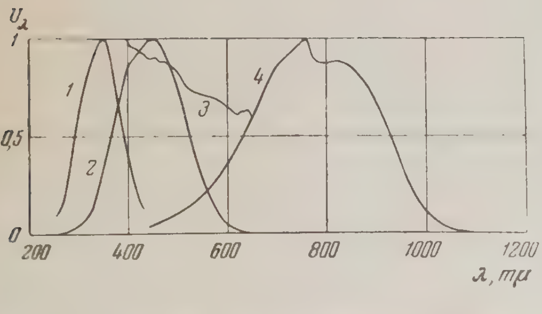

Fig. 2. Curves characterising the relative spectral sensitivity of the spectrometer: 1) third order spectrum, FEU-18 photomultiplier; 2) second order spectrum, FEU-18 photomultiplier; 3) second order spectrum prototype cesium oxide photomultiplier; 4) first order spectrum, cesium oxide photomultiplier.

ferent orders of diffraction selected so as to obtain the maximum amount of reflected light in each case. Each of the photomultipliers was used for recording in two orders. The overlapping of the spectra of the different orders and the interfering effect of scattered light were eliminated by use of appropriate glass light filters (ϕ in Fig. 1). This is particularly important in calibrating the instrument in the ultraviolet region. The spectral sensitivity calibration was carried out at different temperatures of the ribbon filament lamp and with different sets of light filters. The different series of results were in good agreement and are shown in Fig. 2. The relative values of the energy sensitivity of the set-up at approximately the same noise level are characterised by the data in the accompanying table in which we also give the inverse energy values, producing an equal response of the system, for the points corresponding to the peaks of the curves in Fig. 2.

Relative spectral sensitivity of the set-up

Photomultiplier	Order of diffraction	λ_{max}, mμ	Relative sensitivity
Experimental prototype (cesium oxide)	2	394	1
Same	1	754	2.1
FEU-18	3	347	250
FEU-18	2	450	300

Some of the continuous luminescence spectra shown in our recent report (Ref. 4) were obtained on the described set-up. In Fig. 3 and 4 we show samples of records of the luminescence spectra of benzene vapor at room temperature and of a solution of magnesium phthalocyanide in acetone.

Work with the set-up over an extended period of time shows that it is reliable in operation and yields consistent results.

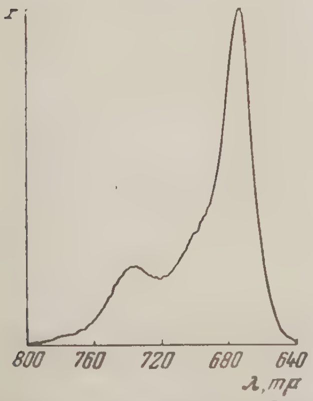

Fig. 3. Record of luminescence spectrum of benzene vapor.

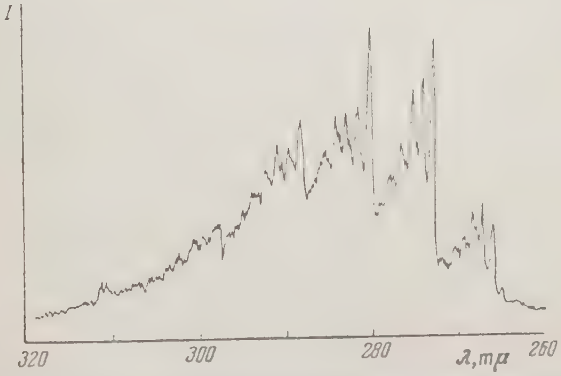

Fig. 4. Record of luminescence spectrum of a solution of magnesium phthalocyanine in acetone.

References

1. B.S.Neporent, Zhur. fiz., khim., 21, 1111 (1947).
2. B.S.Neporent, Zhur. eksp. i teor. fiz. 21, 172 (1951).
3. B.S.Neporent, V.V.Zelinski & V.P.Klochkov, Doklady AN SSSR, 92, 927 (1953).
4. B.S.Neporent, N.A.Borisevich, Doklady AN SSSR, 94, 447 (1954).
5. I.S.Abramson & S.L.Mandel'shtam, Izv. AN SSSR, Ser. fiz., 18, 635 (1954). (Translation in Bulletin, Vol. 18, No. 6, p. 321.)
6. W.G.Fastie, JOSA, 42, 641 (1952).
7. A.Meier, Z.Zeitch, Ul'trafioletovoe izluchenie (Ultraviolet radiation), M. 1952.

Discussion

L.A.Tumerman: Did you try AC amplification with light modulation? Shouldn't the photomultiplier be used as a photon counter?

V.L.Levshin: Would it not be expedient to raise the question of the commercial production of such instruments?

B.S.Neporent: The instrument is relatively simple in design. The only part that cannot be made in the laboratory is the diffraction grating. Further improvement of the sensing-amplifying part and in particular going over to operating the photomultipliers as counters should make it possible to enhance the sensitivity of the set-up further. Under our conditions AC amplifiers have no advantages.

STABILIZATION OF THE EMISSION OF GAS DISCHARGE TUBES

- V.I.Shirokov

Discharge tubes are the most extensively used sources of radiation for exciting luminescence. In measuring luminescence spectra, efficiencies, etc., it is convenient to have a stable excitation source. Stabilization of the light flux may be realized in several ways. The first, indirect method is regulation of the supply voltage or current. In the case of an incandescent lamp it does not matter which is regulated - the current or the voltage - since their interdependence is virtually linear. The situation is different where discharge tubes are concerned for in their case, as follows from their voltage current characteristics, a small change in voltage corresponds to an appreciable change in current. Obviously, with discharge tubes to obtain a given stability of operation the voltage must be regulated more closely than the current. For this reason stabilizers for discharge tubes are designed as current regulators rather than as voltage regulators. Such regulators differ in no way from current regulators utilized for other purposes. A light flux stabilizer for a mercury-vapor discharge tube designed on this principle is described in Ref. 1. A similar regulator is used to stabilize the hydrogen discharge tube used in conjunction with the SF-4 spectrophotometer. However, such stabilization gives good results only in cases when fluctuation of the power supply is the only cause of instability of the light flux. This is actually true only for incandescent lamps, but does not hold for gas discharge tubes. It is known, for instance, that in the case of ultrahigh pressure mercury vapor tubes there occurs displacement (wandering) of the discharge strand relative to the electrodes that is not connected with variations in the supply voltage. When this luminous strand is projected on the entrance slit of an optical instrument its displacement or wandering leads to changes in the illumination of the slit and consequently to changes in the magnitude of the light flux passing through the slit. We know, further, that not all the individual hydrogen tubes intended for use with the SF-4 spectrophotometer operate with the same stability when supplied from a given current regulator, i.e., there are instability causes of "intra-tube" origin. It follows from the above, that in using gas discharge tubes it is more expedient to stabilize the light flux directly rather than the power supply. This is particularly important in the case of set-ups in which it is necessary to stabilize the light flux beyond the entrance slit upon which the source is focused. Such a flux stabilizer is described in Ref. 2; however, this device is intended for an incandescent lamp rather than for a discharge tube. Its use was dictated by the necessity of eliminating the instability due to darkening of the envelope and gradual vaporization of the filament during the period of measurement. An analogous stabilizer for a mercury tube used in photocopying machines is described in Ref. 3. Obviously this installation does not have an entrance slit and apparently in this case direct stabilization of the flux has no advantages over regulation of the current supply.

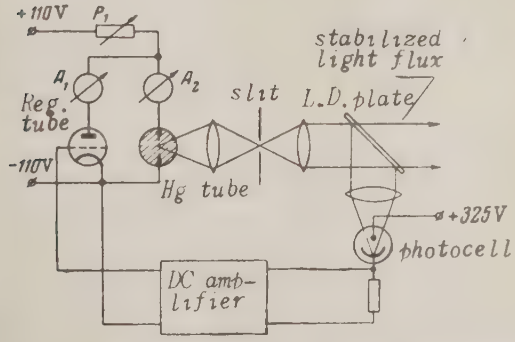

Fig. 1. Diagram of regulator with direct stabilization of light flux.

We constructed a regulator for an SVDSh-250 mercury tube, operated on 110 volts DC, with direct stabilization of the light flux beyond the entrance slit.

The basic diagram of the regulator is shown in Fig. 1. It will be seen that a vacuum tube, which we shall call the regulating tube and which plays the part of an automatic shunt, is connected in parallel with the mercury tube. When the

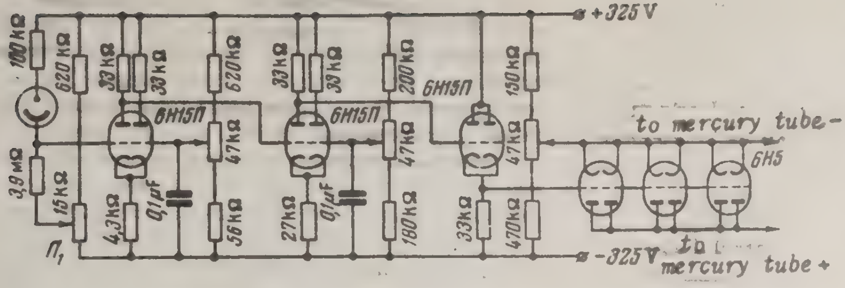

Fig. 2. Diagram of the electronic part of the regulator.

voltage on the tube grid changes, the tube impedence changes and with it the current through the mercury tube. Part of the light flux used for measurement is reflected from the transparent plate π mounted behind the entrance slit of the instrument and falls on the auxiliary photocell PC. The voltage taken off its load resistance is amplified by a DC amplifier and applied to the grid of the regulating tube. The amplifier is designed so that when the light flux increases the voltage on the grid of the regulating tube also increases; thereupon its resistance falls and consequently the current flowing through the mercury tube decreases. Thus the regulation opposes variation in the magnitude of the light flux regardless of the causes producing it.

Such a regulator may be called a stabilizer with a negative feed-back with respect to the light. Its operation is not limited to stabilization of the current supply: when the discharge strand wanders, the illumination of the slit is re-established precisely by adjustment of the current supply.

The electronic diagram of the regulator is shown in Fig. 2. Actually three 6N5S twin triodes connected in parallel are used as the regulating element. The amplifier comprises two cathode-coupled voltage amplification stages and a cathode follower designed about 6N15P twin triodes. A standard vacuum tube voltage regulator is used for the plate supply and a ferro-resonance regulator for the heater supply.

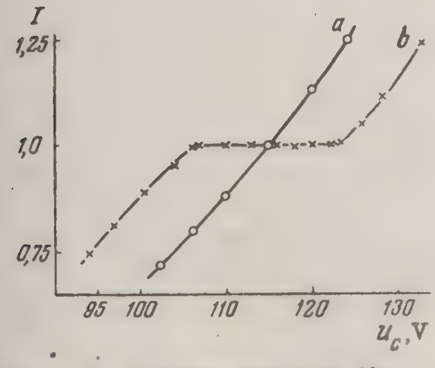

Fig. 3. Curves showing the variation of the light flux I on the supply voltage U_C: a) without regulation, b) with regulation.

Fig. 3 shows the experimentally determined dependence of the light flux I in relative units on the supply voltage U_c without stabilization (curve a) and with stabilization (curve b). Within the stabilization interval a change in the supply voltage of 10 v results in the change in the value of the light flux of only 0.3%. The stabilization coefficient, calculated as the ratio of the slope of curve b to the slope of curve a, is 85. The width of the stabilization interval is determined by the maximum current which the regulating tubes can pass (1.4 amp for the three 6N5S tubes).

The regulator appreciably reduces the magnitude of the variable component in the light flux. Fig. 4 shows oscillograms of the variable components with and without stabilization. It will be seen from a comparison of the oscillograms that the variable component is reduced by a factor of about 50.

The starting operation with the regulator is the following. The potentiometer $П_1$ (Fig. 2) is moved to the extreme lower position (the regulating tubes cut off) and the mercury lamp is started in the usual manner. When the discharge is established, the normal current through the regulating tube, as indicated by ammeter A_1 (Fig. 1), is set by adjusting the potentiometer $П_1$; this should be the current corresponding to the middle of the stabilization region (approximately 0.7 a). At the same time normal current through the mercury tube is maintained by

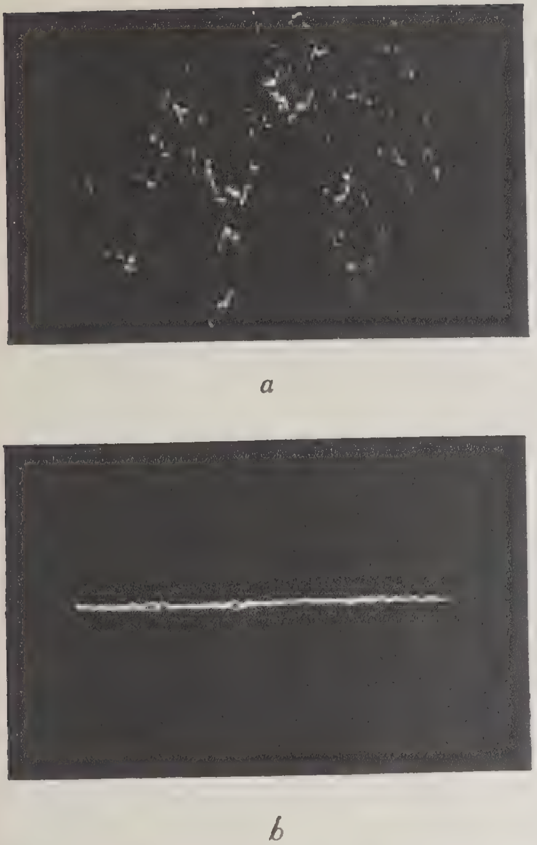

Fig. 4. Oscillograms of the variable components of the light flux: a) without stabilization, b) with stabilization.

adjustment of rheostat P_1. If in a succeeding run (i.e., in resuming operation after the set-up has been shut off) neither the width of the slit nor the setting of potentiometer $П_1$ have been altered, no further regulation in starting is necessary: the value of the light flux will be within 0.5% of the initial value (regardless of the position of rheostat P_1).

Lastly, we must mention one more point in connection with operation of this regulator. In the case of a regulator of this type it is not immaterial whether any light filter used is located before or after the light dividing (reflecting) plate. Obviously, if the filter is located after the light divider the equipment stabilizes the total light flux passing through the slit rather than the spectral interval being used for measurement. Since the regulator does not stabilize the power supply to the tube, the fact that the total flux is constant does not mean that its spectral composition will be constant. Hence it would be more logical to mount the light filter before the light divider. However, this somewhat complicates the procedure since it becomes necessary to readjust the regulator (by means of the potentiometer $П_1$) every time the light filter is replaced by another. In order to determine to what extent the stabilization is impaired when the filter is mounted after the light divider, we check the stability of the light flux passing through a UFS-2 (ultraviolet) filter when a ZhS-4 (yellow) filter was mounted in front of the photocell. In this case one could expect impairment of the stabilization incident to wandering of the discharge strand. The wandering was stimulated by partially covering the slit. No significant lowering of the stability was noticed. Hence, in general, the light filter can be mounted after the light divider plate if desired.

References

1. E.V.Potter & A.Scott, Rev. Sc. Inst., 18, 10 (1947).
2. B.Chance, Electronics, 13, 24 (1940).
3. J.Markus & V.Zeluff, Handbook of industrial electronic circuits (in Russian trans.), M. 1953.

CLOSING ADDRESS

- V.L.Levshin

Comrades! The Fourth Conference on Luminescence has completed its work. It has shown us the great development of luminescence studies in the Soviet Union. The organizational committee's initiative in convening a special conference on molecular luminescence questions has been justified. In five days of arduous work we heard over fifty reports on that subject. The theoretical papers dealt mainly with investigations of luminescence centers, intermolecular energy transfer, the connection between the optical properties of molecules and their structure and, in particular, the causes of persistent afterglow; considerable attention was also devoted to the examination of the interaction of luminescent molecules with the surrounding medium, intermolecular energy transfer and the influence of aggregation (association) on the optical properties of molecules.

The Conference discussed the development of new methods and equipment both for scientific research in luminescence and for practical luminescence analysis. The Conference has also demonstrated that luminescence can be utilized to advantage in many branches of the national economy, in particular, in agriculture, geology, engineering, biology and medicine. The Conference also charted the course to be followed in the future development of molecular luminescence studies.

Owing to the recent emphasis on research into the luminescence of crystal phosphors the study of molecular luminescence has been somewhat neglected. A certain lag was noted in this field, in which the USSR had previously been ahead of other countries. In view of the importance of molecular luminescence as a tool in dealing with problems of molecular energy and molecular structure, steps must be taken to remedy this situation with the utmost speed.

Research into scintillation (of prime importance in the study of various nuclear processes), which has been highly developed abroad, is woefully lagging in the USSR. There has been inadequate application of luminescence analysis, procedures, the value of which in certain branches of science and technology was amply demonstrated in the papers read to us. There can be no doubt that these procedures can yield equally valuable results in other fields of science and technology. In particular, we regret to note that certain simple apparatus developed by our scientists is not yet readily available for general use.

It is to be hoped also that a greater effort will be made to develop new methods of luminescence analysis, such as phosphorescence analysis, the use of polarization spectra, etc. In conclusion, I wish, on behalf of all those present, to express our gratitude to our hosts, A.N.Sevchenko and B.I.Stepanov, active members of the Academy of Sciences of the Byelorussian SSR, for their efforts in organizing this Conference.

BULLETIN of the Academy of Sciences of the USSR - Physical Series
Vol. 20, No. 5, 1956 - Transactions of the Fourth Conference on Luminescence
(Continued from Vol. 20, No. 4)

TABLE OF CONTENTS

	Page Orig.	Page Trans.
Investigation of the ability of complex organic molecules to fluoresce and phosphoresce - V.V.Zelinski, M.P.Emets, V.P.Kolobkov & L.G.Pikulik	507	465
Sensitized phosphorescence of aromatic compounds (energy transfer from the triplet level to the phosphorescent triplet level) - V.L.Ermolaev	514	471
Influence of concentration and the solvent on the phosphorescence of aromatic compounds at low temperatures - P.A.Tepliakov & B.A.Piatnitski	520	476
Temperature quenching of phosphorescence of certain aromatic acids - B.A.Piatnitski & M.S.Fadeeva	524	479
Paramagnetism of boric phosphors in the phosphorescent state - N.A.Lebedev & I.D.Shmerkovich	529	483
Chemiluminescence of lucigenine - B.D.Ryzhikov	533	487
On the structure of the chlorophyll-protein-lipoid complex-T.N.Godnev	537	490
The influence of certain acid and basic substance on the absorption spectra of chlorophyll and chlorophyllide - T.N.Godnev, R.V.Efremova & L.A.Kravtsov	540	493
Spectroscopic investigations of the products and mechanism of oxidation of cellulose by nitrogen peroxide - M.M.Pavliuchenko & I.N.Ermolenko	546	499
Polarized luminescence of cubic crystals (Abstract) - P.P.Feofilov	552	504
Electroluminescence of organic compounds (Abstract) - L.A.Tumerman	552	504
Polarization diagrams of luminescence of molecular single crystals - I.D.Zhevandrov	553	505
Determination of the optical parameters of absorbing crystals - F.I.Fedorov	564	514
Polarization spectra of certain naphthylamines and polyenes-N.D.Zhevandrov	570	519

	Page Orig.	Trans.
Absorption and luminescence of fluoride solutions of lead and thallium - M.U.Belyi & A.A.Shishlovski	574	523
Luminescence and absorption of solutions of tin salts - M.U.Belyi & K.F.Gudymenko	579	526
Luminescence of platinocyanide compounds - N.A.Tolstoi, A.K.Trofimov, A.M.Tkachuk & N.N.Tkachuk	583	529
On measuring the duration of fluorescence by means of a phase fluorometer - A.M.Bonch-Bruevich	591	536
A new phase fluorometer - A.M.Bonch-Bruevich, V.A.Molchanov & V.I.Shirokov	596	541
A high-transmission spectrometric set-up for investigation of luminescence - B.S.Neporent & V.P.Kolochkov	601	545
Stabilization of the emission of gas discharge tubes - V.I.Shirokov	605	549
Closing address - V.L.Levshin	608	552

Translated in 1957 by
Columbia Technical Translations,
5 Vermont Ave., White Plains, N.Y.

Transactions of the Fifth All-Union Conference on the Application of X-rays to the Investigation of Materials

Leningrad 23-29 June 1955

X-RAY DIFFRACTION AND ELECTRON MICROSCOPE STUDIES OF THE AGING OF AN Al-Zn ALLOY

- N.N.Buinov & L.I.Podrezov

The aging of an aluminum alloy containing 25% zinc was studied by the roentgenographic method of coarse-grain specimens[1] and by the electron micrographic method of oxide replicas[2]. The purpose of the investigation was to elucidate the decomposition mechanism in the alloy.

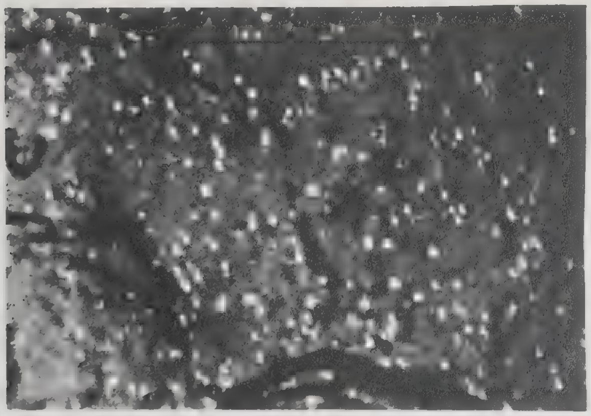

Fig. 1. Electron microphotograph of the Al-Zn alloy aged for six hours at 130° (magnification 50,000 X).

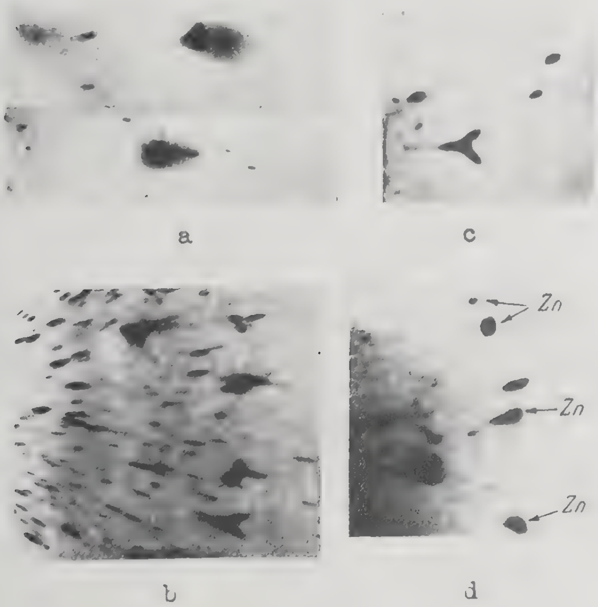

Fig. 3. Effects of anomalous scattering in the x-ray patterns of the Al-Zn alloy (enlarged 1.4 X) after: a) natural aging for 70 hours, b) aging for 1 hour at 200°, c) 3 hours at 200°, d) 5 hours at 200° plus 30 days additional natural aging for b, c and d.

We investigated the states of the alloy after natural and artificial aging (at 100, 130 and 200°). We also studied the state of alloy obtained as a result of artificial (at 200°) followed by natural aging.

After natural aging, light spots are barely discernible in the electron microscope photographs; these spots are so ill-defined that it is virtually impossible to determine their dimensions. After six hours of artificial aging at 130° the electron micrographs show clearly discernible circular spots (see Fig. 1). After aging at 200° for 1-10 hours these spots elongate into streaks. The mean diameter of the circular spots and the width of the streaks remain constant (~ 140 A) in an appreciable range of aging intervals (Fig. 2).

The x-ray patterns of the alloy after natural aging exhibit diffuse spots (Fig. 3, a). The diffuse spot which corresponds to the region of anomalous scattering, coinciding with the points of the reciprocal lattice of the solid solution, is oval in shape. The diffuse spot observed at a smaller angle is also oval, while the spot appearing at a larger angle has a half-moon shape. After artificial aging at 200° (1-5 hours) instead of the spot observed at the smaller angle, we find a two-dimensional effect and instead of the spot observed at the larger angle, a linear image (Fig. 3, b). The diffuse spot closest to the corresponding Laue spot remains unchanged. After aging at 200° for a period of 10 hours the anomalous effects connected with the points of the reciprocal lattice disappear. Diffuse zinc spots appear on the radiograms.

During the investigation we discovered that the Al-Zn alloy after artificial aging at 200° continued

to age at room temperature. After additional natural aging of the specimens first artificially aged at 200° for 1-5 hours, the x-ray patterns exhibit zinc spots in addition to the anomalous effects (Fig. 3, c & d). This additional natural aging is accompanied by an increase in the hardness of the alloy by a factor of about 3; this increase in hardness occurs primarily during the first 5-6 hours, while the zinc spots develop only at the end of some 3-4 weeks. The hardness of the alloy is not reduced when the zinc particles appear. No evidence of change in the electron micrographic structure of the alloy was observed after the additional natural aging.

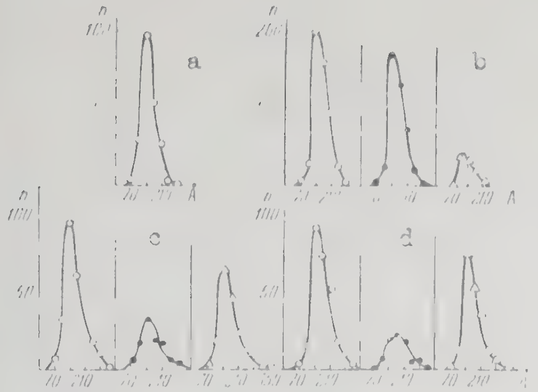

Fig. 2. Distribution of zones and the number (n) of zinc particles according to size (in depth) in aged Al-Zn alloy: a) 6 hours at 130°, b) 1 hour at 200°, c) 5 hours at 200°, d) 10 hours at 200°. In diagrams b, c and d the first curve represents the distribution in depth for all zones; the second only for the equilibrium zones; the third for the lamellar zones.

Discussion of Results

The low contrast and general circular shape of the light spots on the electron micrograph of the naturally aged Al-Zn alloy give reason to assume that in the process of natural aging there develop in the alloy equiaxial zones, relatively little enriched with zinc atoms and having a distorted matrix structure. The x-ray diffraction data of Guinier[3] also indicate that the zones of zinc atom aggregation are approximately spherical in shape. The equiaxial character of the zones and their relatively low enrichment with zinc is in good agreement with the theory of Nabarro[4]. According to this theory particles of equiaxial shape can separate out in an aging alloy when the crystal lattice is coherently coupled with the matrix lattice and the rigidity of the lattices is equal. With a relatively weak concentration of zinc in the zone, according to the data in Ref. 5, the rigidity of the crystal lattice of the zone must differ little from the rigidity of the crystal lattice of the alloy.

Comparison of the electron micrographic and x-ray diffraction data leads us to conclude that the diffuse spot nearest to the Laue spot (originating from the same crystals as the anomalous effects) is a shape effect. It is associated with a dislocation region some 150-200 A in diameter in the crystal. Electron micrograph measurements yield a value of 140 A for the mean dimensions of the zinc enriched regions.

The asymmetry and the nature of the change in shape of the other spots in the process of aging leads us to conclude that the diffuse spot observed at the smaller angle relative to the corresponding Laue spot is associated with a distorted matrix structure in the vicinity of the zones, while the diffuse spot, originally in the form of a half-moon and developing with artificial aging into a linear effect, is associated with the distorted structure of the zones themselves.

The invariance of the zone thickness and of the number of zinc particles in an appreciable interval of aging times is evidence, on the one hand, of the qualitative validity of Nabarro's theory, according to which it is energetically advantageous for the decomposition particles to grow only in diameter and, on the other hand, that there exist stable regions poor in zinc atoms about the zone and particles.

The invariance of the zone thickness and particle number during softening of the alloy (due to the appearance of zinc particles) also indicate that the softening is connected primarily with rupture of the coherent bonds between the decom-

position products and not with coagulation of the zones and zinc particles. In investigating an aluminum-copper alloy, we also found that the zone thickness and the number of metastable-phase particles did not change over an appreciable aging range either in hardening or softening of the alloy (at 150-190°). This is further evidence that the softening is connected primarily not with coagulation but with rupture of the coherent bonds between the dissociation products.

The additional natural aging of the Al-Zn alloy is due to an increase in the concentration of zinc in the zones and their allotropic dissociation into particles. This is evinced by the absence of anomalous diffusion effects associated with the points of the reciprocal lattice of the solid solution, the appearance of zinc spots on the x-ray patterns and the unaltered appearance of the electromicrographs.

According to current concepts, the appearance of particles of a stable phase in the alloy should be accompanied by an appreciable softening. However, actually no softening of the Al-Zn alloy is observed after the additional natural aging. Apparently, incident to the rearrangement of the crystal lattice appropriate to the concentration of the atoms in the zone, there occurs in the zinc lattice not only a relief of strains due to the coherence of the zones and matrix, but also a development of new strains because of "hydrostatic" pressure. This pressure may develop as a result of the fact that in the rearrangement the packing of the atoms in the zones changes from 0.74 (face-centered cubic lattice) to 0.65 (hexagonal zinc lattice). The strains produced by the hydrostatic pressure are stable at low temperatures and impart great hardness to the lattice.

The process determining the aging of the alloy is a process of enrichment of the zones with zinc.

In conclusion we wish to thank A.M.Elistratov for his advice regarding the x-ray diffraction procedure and M.F.Komarova for her assistance in the experimental work.

Institute of the Physics of Metals of the
Ural Branch of the USSR Academy of Sciences

References

1. A.M.Elistratov, Doklady SSSR, 69, 3, 337 (1949).
2. Elektronnaia mikroskopiia (Electron microscopy), A.A.Lebedeva, editor. M. 1954.
3. A.Guinier, Métaux et Corrosion, 18, 209 (1943).
4. F.R.N.Nabarro, Proc. Roy. Soc., A175, 519 (1940).
5. Gmeling, Handbuch der Anorganischen Chemie, 35, Teil A, Lief. 5, 747 (1929).

CHANGES IN THE FINE CRYSTAL STRUCTURE OF AUSTENITIC MANGANESE STEEL DURING PLASTIC DEFORMATION

- O.V.Bogorodski & Ia. S.Umanski

The reasons for the extremely great hardening of austenitic high-manganese steel (Hadfield steel) as the result of cold working are still inadequately known. Niconoff[1] and Goss[2,3] report changes in the intragrain structure incident to cold deformation of this steel; however, their evaluations of both the size of the blocks and the magnitude of the microstrains are qualitative. According to the very rough determination in Ref. 2,the size of the blocks after 80% compression by cold rolling is of the order of 10^{-6}-10^{-7} cm.

In the present investigation we studied the dependence of a) the intragrain structure of the basic solid solution, b) the hardness and c) the period of the austenite lattice on the degree of deformation. In addition we evaluated the variations of the ferromagnetic properties of the steel incident to static compression.

Finally we attempted to establish the causes of the hardening of this steel under plastic deformation in the light of the experimental data.

Materials and procedure

The material investigated was hot rolled steel containing 1.14% C, 12.3% Mn, 0.32% Si, 0.006% S and 0.041% P. The samples measuring 10 x 10 x 2 mm were deformed on a Gagarin compression press at the rate of 3mm/min. Prior to deformation the samples were quenched in water from 1050°. Suitable bars were then cut from the deformed sample and their diameter brought down to 0.3mm by electrolytic etching. The x-ray photographs were made in an RKU camera (85.95 mm diameter) by the K_α line from Fe. The (111) and (222) lines were photometered visually on an MF-4 microphotometer; the blackening was kept between 0.2 and 0.9. The data for each line were obtained by averaging over ten photometric curves. The line width of a tempered sample was used as the standard reference.

The period of the lattice was determined from patterns photographed using Cr K_α radiation; for purposes of computation we used the $(311)_\beta$ line ($\vartheta = 73^\circ$). The hardness was determined with a Vickers indentor and the resultant value transformed to the R_c scale. The ferromagnetic properties were evaluated roughly. After 30% static compression there is appreciable ferromagnetism; at 70% deformation the samples become strongly magnetic and very diffuse lines associated with the α-phase appear on the x-ray patterns of the samples. In the case of compression by rolling even to 80% the samples did not exhibit magnetic properties and no α-phase lines were observed on the x-ray diffraction photographs.

The fine structure was investigated on the basis of the diffusion of the diffraction lines; the calculations of the dimensions of the mosaic blocks and of the micrograins were carried out by two different methods: the first method[4,5], based on the dependence of the broadening of the diffraction line on the Bragg angle, comprises a certain ambiguity as regards selection of the analytic expressions describing the intensity distribution for both the standard (reference) and broadened lines (photometric curves) and for the curve characterizing the broadening due to mosaicity and microstrains; the second method[6] is free of any arbitrary assumptions regarding the shape of the diffraction lines and is based on harmonic analysis of the shape of the "true" broadening curve.

We shall briefly describe both methods as they apply to our case. In using the first method, one must first choose the analytic expression for the standard diffraction line and for the line with the same indices, but at different degrees of deformation.

Choice of the form of the function was effected by the method described in Ref. 5.

The most appropriate proved to be a function of the form

$$I = \frac{I_0}{1+k^2x^2}, \tag{1}$$

where I is the intensity at a distance x from the center of the line, I_0 is the intensity at the center of the line, i.e., at an angle θ_0, k is a coefficient taking into account the broadening of the line contour as a function of the properties of the sample and the geometry of the experiment. With this intensity, the broadening β is given by the expression

$$\frac{\beta}{B} = 0,5\left[\left(1-4\frac{b}{B}\right)+\sqrt{8\frac{b}{B}+1}\right], \tag{2}$$

where b is the width of the standard line and B is the width of the broadened line in radians.

The analytic expressions for the intensity distributions due to mosaicity and microstrains were taken of the same form as (2); consequently, the broadenings due to the former and latter factors were found from solution of the following system of equations

$$\left.\begin{aligned}
\frac{m_1}{\beta_1} &= 0,5\left[\left(1-4\frac{n_1}{\beta_1}\right)+\sqrt{8\frac{n_1}{\beta_1}+1}\right],\\
\frac{m_2}{\beta_2} &= 0,5\left[\left(1-4\frac{n_2}{\beta_2}\right)+\sqrt{8\frac{n_2}{\beta_2}+1}\right],\\
\frac{m_2}{m_1} &= \frac{\cos\vartheta_1}{\cos\vartheta_2},\\
\frac{n_2}{n_1} &= \frac{\operatorname{tg}\vartheta_2}{\operatorname{tg}\vartheta_1},
\end{aligned}\right\} \tag{3}$$

where m_1 and m_2 are the broadenings due to mosaicity for the (111) and (222) lines and n_1 and n_2 are the respective broadenings due to microstrains.

We plotted curves for the dependences

$$\frac{m_1}{\beta_1} = f_1\left(\frac{\beta_2}{\beta_1}\right) \text{ and } \frac{n_2}{\beta_2} = f_2\left(\frac{\beta_2}{\beta_1}\right), \tag{4}$$

from which the values of n_1 and n_2 and m_1 and m_2 were directly determined. In addition, for purposes of verification, we utilized the dependence of mosaicity broadening on the wavelength (photography using radiation from Cr and Mo).

The second method, as already noted, is based on harmonic analysis of the "true" broadening curve. It is known[6] that

$$A_l^{\text{def}} = \overline{\cos 2\pi l z_t}, \tag{5}$$

where A_l^{def} is the coefficient of expansion into a Fourier series of the curve characterising the broadening due to microstrains, z_t is the relative displacement, l is the index of the reflecting plane in the system of reciprocal lattice axes $(00l)$, selected so that l coincides in direction with the normal to the plane, while the two other axes are parallel to it; $a_3 z_t$ is the difference between the displacements in the direction of the normal to the plane for two cells spaced t periods apart (a_3 is the period along the normal to the reflecting plane):

$$l = \frac{a_3}{a_0}\sqrt{h_1^2+h_2^2+h_3^2}, \tag{6}$$

here a_0 is the edge of the cubic cell and h_1, h_2 and h_3 are the indices of the reflecting plane.

$$A_l^{\text{бл}} = \frac{1}{N}\sum_{j=|t|+1}(j-|t|)\,n_j = \frac{1}{N}\int_{j=|t|+1}(j-|t|)\,P(j)\,dj, \tag{7}$$

where A_t^{bl} is the coefficient of expansion into a Fourier series of the curve characterizing the broadening due to mosaicity, n_j is a number of blocks with a number of periods j along the normal to the reflecting plane, N is the total number of cells and P(j) is a function characterizing the distribution of the blocks according to size.

Analysis by this method comprises the following steps.

A. Determination of the coefficients of the series characterizing the "true" total broadening curve (i.e., the total broadening due to the surposition of the two broadening effects); this has been described in detail by Kitaigorodski[6,7].

The values of the series coefficients were calculated using the following equations:

$$F_{\cos} = \frac{H_{\cos}G_{\cos} + H_{\sin}G_{\sin}}{(G_{\cos}^2 + G_{\sin}^2)\,a}\,, \quad F_{\sin} = \frac{H_{\sin}G_{\cos} - H_{\cos}G_{\sin}}{(G_{\cos}^2 + G_{\sin}^2)\,a}\,, \tag{8}$$

where $F_{\cos}$ and $F_{\sin}$ are the coefficients of the series characterizing the expansion of the sought broadening curve; $H_{\cos}$ and $H_{\sin}$ and $G_{\cos}$ and $G_{\sin}$ are the corresponding coefficients for the broadened and the standard curves, respectively.

The changes in the absolute values in the coefficients are of no importance. In order to check whether the values of $F_{\cos}$ and $F_{\sin}$ have been correctly determined, one should synthesize the function on the basis of the series on hand; the same thing should be done for the coefficients G and H at least for a few values of x (x is the interval of expansion of the function into the Fourier series).

In practice the standard and broadened photometric curves are expanded into series by means of strips and templets;[8] the latter are more suitable for this purpose since they permit dividing up expansion intervals into a greater number of parts that are a multiple of the number of parts for which the templet was prepared. In this manner we can obtain intermediate values of the coefficients, which is very important for accurately reproducing the shape of the curve. In our case $F_{\sin}$ was found to be practically equal to zero which is evidence of symmetry of the "true" broadening curve and consequent absence of overall compression or elongation of the crystal lattice.

B. Transformation of the "true" broadening Fourier function. The transformation essentially amounts to plotting the dependence $A_t^{tot} = f(t)$, i.e., the dependence of the value of the coefficients of the "true" broadening curve on the order of the coefficient.

The Fourier transformation in this case is connected with transition to the reciprocal lattice space; however, this operation will not change the shape of the transformed curve inasmuch as the coordinate of the section of the diffused line on the film (x-ray pattern) is proportional to the coordinate of the "diffused" point in the reciprocal lattice. Obviously, it is a matter of the scale of the transformation, which it is more convenient to work out later.

C. Separation of the effects due to mosaicity and microstrains. These effects can readily be separated if there are several orders of reflection from the same plane discernible in the diffraction pattern.[9] However, when the diffraction pattern contains only reflections of the first order or only of first and second orders the scaling method is inapplicable. For such cases there are approximate methods (described by Pines[10]); the one used in the present investigation is based on the assumption that all the blocks are of the same size. This means that

$$\frac{dA_t^{bl}}{dt} = \frac{dA_t^{tot}}{dt}\Big|_{t=0} = k = \text{const.} \tag{9}$$

The first derivative $\frac{dA_t^{tot}}{dt}$ with t = 0 gives the mean size of the blocks; it can readily be found from the curves of Fig. 1 where the dependence of the coefficients A_t^{tot} on t is plotted for different degrees of deformation. Obviously the coefficients of the function characterizing the broadening due to mosaicity

lie on the tangents to the curves $A_t^{\mathrm{tot}} = f(t)$ at the point t = 0. To determine A_t^{def} we invoke the relationship

$$A_t^{\mathrm{tot}} = A_t^{\mathrm{bl}} A_t^{\mathrm{def}}. \tag{10}$$

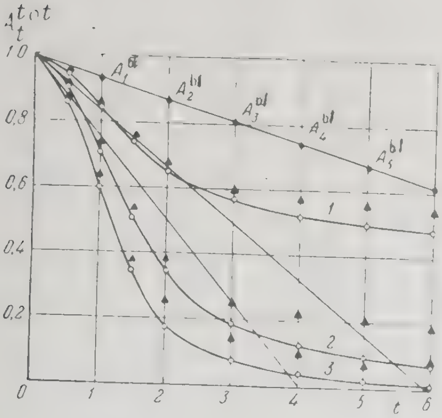

Fig. 1. Dependence of the coefficient A_t^{tot} of the function characterizing the "true" broadening on the order t of the coefficient (transform of the Fourier function of the "true" broadening) at different degrees of deformation (1 - 10%, 2 - 30% and 3 - 50% deformation) for the (222) line. The triangle points denote the same dependence for the (111) line. The straight lines define the coefficients of the function characterizing the broadening due to mosaicity.

D. Calculation of the block size and microstrains. In order to compute the absolute values of the block size and microstrains (in Å) we must go over from the scale of the selected expansion interval $\left(-\frac{a}{2} < x < \frac{a}{2}\right)$ on the photographic film to the scale $\left(-\frac{1}{2} < x < \frac{1}{2}\right)$ of the crystal lattice, although even without this one can readily determine qualitatively how the size of the blocks and the magnitude of the microstrains change with different degrees of deformation inasmuch as the first derivative dA_t^{tot}/dt gives the mean block size in the direction of the normal to the reflecting plane, while $\left.\frac{d^2A_t^{\mathrm{tot}}}{dt^2}\right|_{t=0}$ gives the lower limit of the microstrain.

The conversion is described in detail in Ref. 11; here we will give only the final expressions which we utilized for effecting the conversion:

$$L = t'a_3, \quad t' = \frac{t}{a}l, \quad a' = \frac{2r\,\mathrm{tg}\,\vartheta_0}{l}, \tag{11}$$

where L is the continuous coordinate of the crystal lattice in the direction l, a is the selected expansion interval on the photographic film in mm, a' is the corresponding interval in the reciprocal lattice, r is the radius of the camera, ϑ_0 is the Bragg angle, and t is the order of the coefficient in the expansion in the interval a.

Thus in Fig. 1 we can lay off the scale of the crystal lattice and measure the block size for each case when

$$A_t^{\mathrm{def}} = \overline{\cos 2\pi l z_t} = \exp\left(-2\pi^2 l^2 \overline{z_t^2}\right),$$

$$\ln A_t^{\mathrm{def}} = -2\pi^2 l^2 \overline{z_t^2} = -2\pi^2 \frac{a_3^2}{a_0^2} \sum h_i^2 \overline{z_t^2} = -\frac{2\pi^2}{a_0^2} \sum h_i^2 \overline{\Delta L^2},$$

whence

$$\sqrt{\overline{\Delta L^2}} = \frac{a_0\sqrt{-\ln A_t^{\mathrm{def}}}}{\pi\sqrt{2\sum h_i^2}}, \tag{12}$$

where a is the period of the lattice and h_i are the indices of the reflecting plane.

Experimental results and discussion

Fig. 2 shows the curves characterizing the dependence $\sqrt{\overline{\Delta L^2}} = \varphi(L)$, plotted on the basis of equations (11) and (12) and the curves of Fig. 1 for the (111)

and (222) lines.

From the data of Fig. 2 one can readily plot the dependence of the microstrains:

$$\varepsilon = \frac{\sqrt{\overline{\Delta L^2}}}{L} = \varphi(L). \tag{13}$$

which is shown in Fig. 3.

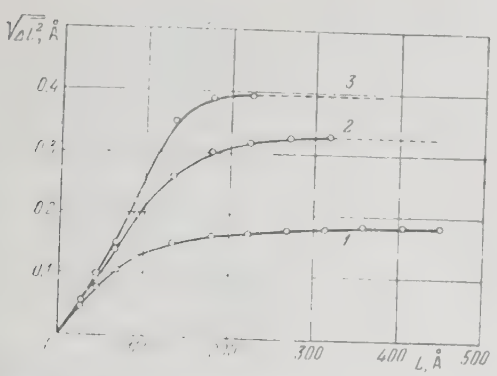

Fig. 2. Distribution of the displacements $\sqrt{\overline{\Delta L^2}}$ along the length L of the crystal lattice at different degrees of deformation: 1) 10%, 2) 30%, 3) 50%.

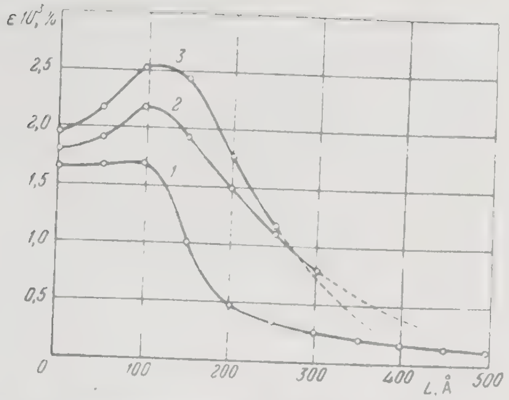

Fig. 3. Distribution of the microstrains ε over the length L of the crystal lattice at different degrees of deformation: 1) 10%, 2) 30%, and 3) 50%.

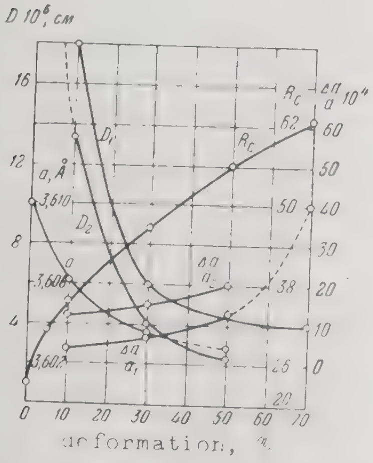

Fig. 4. Dependence of the change in hardness R_C, the block size D_1, and the microstrain $\Delta a/a_1$ computed by the first method and the block size D_2 and the microstrain $\Delta a/a_2$ computed by the second method (harmonic analysis) and the period of the austenite lattice on the degree of deformation.

The results of measurements are summarized in Fig. 4.

The curve showing the variation of the period of the austenite lattice is very characteristic of the material and is similar to the curve for the decrease in block size. The decrease in the period indicates the separation of carbides and enrichment of the austenite lattice with carbon. By virtue of this the α-phase appears at high degrees of deformation. The appreciable fragmentation of the blocks, which is already manifest at relative moderate degrees of deformation, can only be due to the same segregation of the highly dispersed carbide phase.

A like influence of the decomposition of the supersaturated solution on the mosaic structure of the solution has been detected by L'vovskaia and Umanski[12] in a complex titanium-tungsten carbide and by Eliutina and Umanski[13] in beryllium bronze. Umanski[14] has suggested that fragmentation of the blocks incident to decomposition is the principal reason for dispersion hardening. In his hypothesis Umanski utilized Bragg's concepts. Bragg[15] deduced a simple if approximate dependence of the shearing stress σ_τ on the linear dimensions Δ of the blocks.

$$\sigma_\tau = \frac{1}{2} G \frac{a}{\Delta}. \tag{14}$$

where G is the shear modulus and a is the atomic separation in the direction of slip.

Admittedly Bragg's expression is only a rough approximation since it does

not take into account the disorientation angles of the blocks which undoubtedly influence the resistance to plastic deformation or of the presence of particles of a different phase between the blocks. However, taking these factors into account should not alter the basic significance of the formula: the smaller the mosaic blocks, the greater the resistance of the given alloy to plastic deformation.

Conclusions

1. Comparison of the results of the two utilized methods of computing the block size and the microstrains shows satisfactory agreement of the values obtained by both methods.

2. In the light of the experimental results it must be assumed that fragmentation of the mosaic blocks is a determining factor in the hardening of Hadfield steel by cold working.

3. Separation of carbides is the principle reason for the fragmentation of the mosaic blocks and ultimate cause of hardening of the material.

"I.V.Stalin" Moscow Steel Institute

References

1. D. Niconoff, Trans. Amer. Soc. Met., 31, 519 (1941).
2. N.P.Goss, Trans. Amer. Soc. Met., 34, 632 (1945).
3. N.P.Goss, Steel. 120, 29, 74 (1947).
4. L.I.Lysak, in "Voprosy fiziki metallov i metallovedennia" (Problems of metal physics and metallurgy) No. 3, Kiev 1952.
5. Ibid, No. 5, 22, Kiev 1954.
6. A.I.Kitaigorodski, Rentgenostrukturnyi analiz melkokristallicheskikh i amorfnykh tel (X-ray analysis of fine crystal and amorphous solids). M. 1952.
7. A.I.Kitaigorodski, Usp. fiz. nauk., 48, 97 (1952).
8. V.I.Smirnov, Kurs vysshei matematiki (Course in higher mathematics), M. 1949.
9. B.E.Warren, B.L.Averbach, J. Appl. Phys., 23, 3, 497 (1952).
10. B.Ia.Pines, Doklady AN SSSR, 103, 601 (1955).
11. B.Ia. Pines, N.G.Berezniak, Zhur. tekh. fiz., 24, 329 (1954).
12. V.P.L'vovskaia, Ia.S.Umanski, Zhur. tekh. fiz., 20, 1167 (1950).
13. V.I.Eliutina & Ia.S.Umanski, Trudy Moskovskovo instituta stali, (Transactions of the Moscow Steel Institute), Vol. 33, M. 1955.
14. Ia. S.Umanski, in "Primenenie rentgenovykh luchei k issledovaniiu materialov" (The application of x-rays to the investigation of materials) L. 1949.
15. W.L.Bragg, Engineering, 157, 394 (1944).

INVESTIGATION OF EUTECTOID DECOMPOSITION IN A Cu-Sn ALLOY

- M. I. Zakharova & I. B. Mogarycheva

In studying the decomposition of solid solutions the structural changes during the initial stages of the process are of particular interest. In recent years there have been a number of investigations in which the mechanism of decomposition of a supersaturated solid solution was studied through analysis of the anomalous diffuse scattering of x-rays. The diffraction pattern in the initial stages of the separation of a new phase from a supersaturated solid solution is distinguished in the case of certain alloys by the abundance of anomalous diffraction effects.

It was natural to expect that the process of eutectoid decomposition in its initial stages - at the instant of formation of the new phase nuclei - would also be accompanied by anomalous diffused scattering. To check this hypothesis we prepared a copper alloy containing 27% tin in which the β-phase, stable at high temperatures, decomposes at low annealing temperatures into α- and γ-phases. The sequence and nature of phase separation in copper-tin alloys have been investigated in detail by Kudriumov and his co-workers[1-3].

In the present work the eutectoid decomposition of the copper alloy containing 27% Sn was investigated using single crystals grown by the method of slow cooling of the liquid alloy at temperatures of 150, 218, 250, 300 and 350°. The annealing time was varied from several seconds to 60 hours at 218° and to 31 hours at 250°.

The structural changes were studied by the diffraction of monochromatic or unfiltered radiation by a stationary single crystal. The x-ray patterns were recorded using Mo K_α radiation at a voltage of 40 kv. The monochromatic radiation was obtained by reflection from a plane lithium fluoride crystal. To retain the initial orientation of the phases during subsequent annealing the crystal was subjected to heat treatment in a special clamp which during the photography was mounted on the upper sector of the goniometer head.

In the case of a hardened specimen, the pattern recorded with polychromatic radiation showed only β-phase maxima. Investigation of isothermic decomposition at 300° showed that anomalous diffraction effects in the form of non-radial diffuse bands begin to appear on the pattern even after only 6 seconds of heating.

The increase in the intensity of the diffuse bands after annealing for 12 and 24 sec, the appearance of discontinuities and maxima in the bands after heating for 48 sec and the increase in the intensity of the band maxima after heating for 5 minutes, all indicate that these bands are not thermal but structural bands, characteristic of the two-dimensional lattice of lamellar segregations.

Plots of the gnomostereographic projections of the bands appearing in the patterns at different orientations of the crystal show that the projections form large circles, intersecting in bands of the (110) and (100) type. Consequently the lamellae are oriented in the matrix lattice parallel to the (110) and (100) planes.[4]

Similar diffraction patterns are observed after isothermal annealing at 250, 218 and 150°.

At 250° diffuse bands appear after 2 min heating; after 40 min the intensity of their maxima increases and after 2 hours there appear breaks in the bands and many separate diffuse maxima which do not lie on the bands and which do not pertain to the β-phase lattice. The number and intensity of these maxima increase with annealing time up to 19 hours. After annealing for 31 hours the diffuse maxima transform into sharp peaks associated with three-dimensional diffraction of the new phases. The stronger maxima of the β-phase persists against this background of a large number of maxima associated with the new phases. Consequently the eutectoid decomposition of the β-phase in single crystals occurs

non-uniformly over the volume: side-by-side with completely decomposed regions there remain regions of undecomposed solid solution that are responsible for the persistence of the β-phase maxima. Even at the stage when only a small undecomposed region remains in the crystal, two-dimensional nuclei of the new phases first form in this region.

An analogous decomposition picture is observed after annealing at 218°. The anomalous diffraction effects in the form of bands and spots are observed after heating for 3 sec. With increased annealing time the intensity and number of the maxima increase.

At a temperature of 150° such anomalous diffraction effects become relatively intense after 30 sec and still more intense after 2.5 min, while when the decomposition is investigated by method of diffraction in polycrystalline specimens, the beginning of decomposition as evinced by the appearance lines of the new phase, observed at an angle of reflection of 61°10', becomes manifest only after 10 min.

We investigated the eutectoid decomposition at 350° using both unfiltered and monochromatic radiation. In the x-ray patterns obtained with unfiltered radiation diffuse spots and bands appear after 10 sec annealing. When the heating time is increased to 10 min new, additional diffuse spots appear and the intensity of the bands increases. Plots of the gnomostereographic projections of the bands yield the same result as at the other annealing temperatures, namely, they indicate that the lamellae of the new phases are oriented parallel to the (100) and (110) planes of the matrix lattice, but in this case there also appears a large number of short bands for which it is impossible to determine the intersection poles on the projection.

In order to investigate the shape and location of the anomalous scattering regions in reciprocal space we recorded a series of patterns using monochromatic radiation with the stationary "single crystal" turned about the [001] axis in 3-5° steps over a range of 45° (Ref. 5). Fig. 1 shows a radiogram recorded using unfiltered radiation; Fig. 2 is a pattern recorded using monochromatic radiation with the [100] axis of the crystal oriented parallel to the beam, Figs. 3 and 4 are patterns registered with the [110] axis of the crystal parallel to the beam. Plotting of the regions of anomalous scattering with reference to some of the diffuse spots showed that a number of the regions in the direct lattice are laminar in form and are located parallel to the (110) plane of the β-phase; in addition to these, as similar constructions on the basis of other diffuse spots show (Fig. 2), there are regions oriented parallel to the (100) plane. The other diffused spots appear in the patterns only in a narrow range of angular orientations of the crystal and consequently have a very limited extent in the construction in reciprocal space so that it is difficult to determine their orientation.

Conclusions

1. Eutectoid decomposition of the β-phase in copper alloys with 27% Sn at temperatures between 150 and 350° proceeds successively in individual regions of the single crystal.

2. The presence in the single crystal of already decomposed regions does not affect the course of the process in the as yet undecomposed volumes of the solid solution.

3. The decomposition process begins with the formation of two-dimensional lamellae oriented parallel to the (110) and (100) planes of the initial β-phase.

Department of Solid State Physics
of Moscow State University

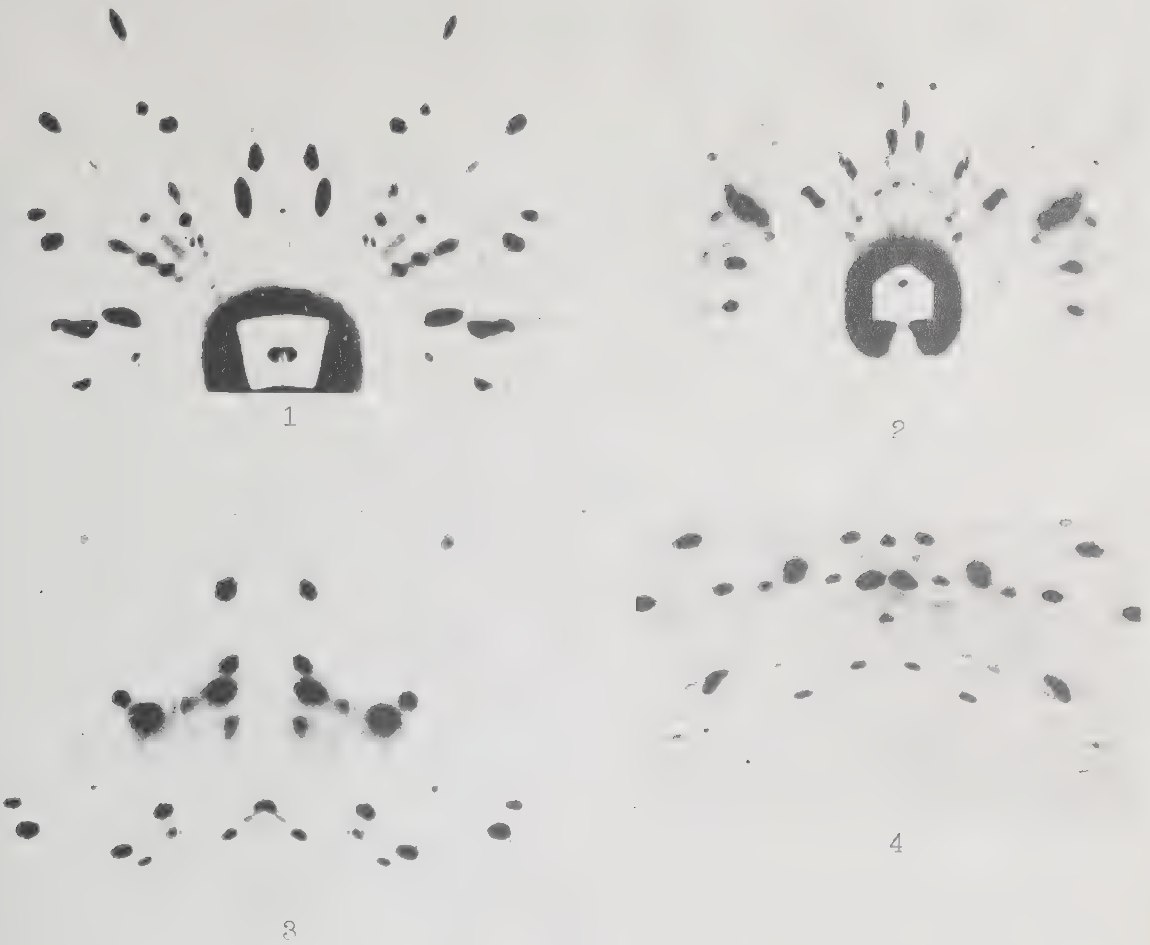

1

2

3

4

Diffraction patterns of the Cu + 27% Sn alloy after annealing at 350° for 2 min: Fig. 1) unfiltered Mo K_α radiation - [100] axis oriented along the beam; Fig. 2) with monochromatic radiation - [100] axis oriented parallel to the beam; Fig. 3) with unfiltered Mo K_α radiation - [100] axis parallel to the beam; Fig. 4) with monochromatic radiation - [110] axis parallel to the beam.

References

1. G.V.Kurdiumov & I.Isaichev, Metallurg (The Metallurgist), 1, 25 (1934).
2. I.Isaichev, Zhur. tekh, fiz., 9, 1868 (1939).
3. I.Isaichev & I.Salli, Zhur. tekh. fiz., 10, 752 (1940).
4. C.S.Barrett, Structure of Metals (in Russian trans. M. 1948).
5. A.H.Geisler, J.K.Hill, Acta Crystallogr., 1, 238 (1948).

ANALYSIS OF STRESSES* OF THE SECOND KIND IN THE α-PHASE OF QUENCHED AND TEMPERED STEEL

- L. I. Lysak

It has been established in a number of investigations that the properties of metals depend to an appreciable extent on the internal stresses (strains). It has been shown that the presence of large lattice distortions of the second and third kinds is characteristic of a state of high strength of the metal. The results of such investigations have stimulated interest in studies not only of the connection between the properties of a metal and its structure but also of the nature of the lattice distortions and their distribution through the volume of the metal.

Kurdiumov and his co-workers[4] arrived at a number of important conclusions regarding the nature of the ordering and disordering processes on the basis of detailed investigations of distortions of the third kind, differentiation between static and dynamic distortions and determinations of the magnitude of such distortions in steel and other hardened or deformed metals. In order to refine further our concepts regarding these ordering and disordering processes we must gain more knowledge of distortions of the second kind, clarify their nature at different stages of the tempering process and determine the influence of alloying elements on the formation and modification of these distortions. In recent years many new experimental facts have been accumulated on stresses of the second kind both in steel and in deformed metals in general.

In the light of the results of extensive studies of 1) the mechanism and kinetics of decomposition of martensite of hardened steel, 2) changes in the fine crystal structure of the α-phase of steel incident to quenching and annealing, 3) the diffuseness of the lines of isolated martensite and 4) the distribution of interference intensities (by means of harmonic analysis), one can propose the following classification of stresses of the second kind and description of the regularities characterizing the changes incident to annealing of hardened steel.

1. Quenching or primary stresses. These arise in the process of quenching during the phase transition due to the difference between the crystal lattices of austenite and martensite and also by virtue of the volumetric changes occurring in the process. The nature of these stresses has been greatly clarified since the Institute of Metal Physics of the Academy of Sciences of the Ukrainian SSR developed an electrolytic method for separating martensite from pieces of hardened steel. It was found that when martensite crystals are freed of the surrounding medium the diffuseness of the martensite lines on the x-ray patterns is greatly reduced. The diffuseness of the lines of non-isolated martensite is proportional to the tangent of the angle of reflection, while the diffuseness of the lines of the same martensite isolated from the surrounding medium is proportional to the secant of this angle. In view of this it was concluded that each martensite crystal in a piece of hardened steel is elastically deformed as a whole; after being freed from the surrounding medium, the martensite crystals "unbend". Studies of the diffuseness of the interference lines led to the conclusion that the dimensions of the martensite blocks are of the order of $2.5 \cdot 10^{-6}$ cm. The results of harmonic analysis of the intensity distribution in the lines showed that the size of individual regions of homogeneous deformation of the crystal lattice of martensite is several times smaller than this. Consequently

---

*X-ray diffraction patterns yield data on the distortions of the crystal lattice. To calculate internal stresses on the basis of this data it is necessary to know the character of the strains of the microvolumes. Hence in the case when we are speaking of direct experimental data it is preferrable to use the term "distortions of the crystal lattice".

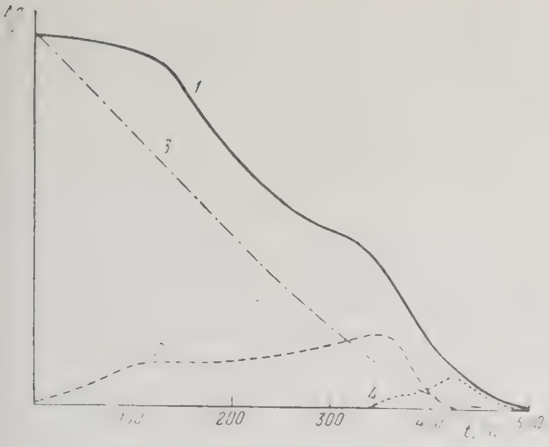

Fig. 1. Probable scheme of changes of lattice distortions of the second kind in the α-phase of hardened U10 steel during annealing: 1) experimentally determined, 2) coherent, 3) quenching and 4) dispersion distortions.

a region of coherent scattering of the x-rays (block) is a volume of metal which is not homogeneously deformed.

Hence distortions of the second kind of the crystal lattice are not a consequence of simple homogeneous elastic compression or extension of the blocks. These distortions are due to flexure or more complex elastic deformation of the blocks.

It is interesting to note that removal of distortions of the martensite lattice by electrolytic separation of the martensite results in an increase in the size of the regions of homogeneous deformation. This would indicate that the removal of distortion occurs through straightening of bent lamellar blocks.

Hardening stresses are maximal in quenched, non-annealed steel. Their magnitude depends on the amount of carbon in the steel. In annealing these stresses are reduced in view of the fact that with increasing temperature the yield point is lowered and the plastic displacements in the microregions of the metal, removing the elastic distortions of the lattice, becomes possible. The variation of these distortions when quenched carbon steel is annealed is shown by curve 3 in Fig. 1.

2. Coherent stresses. During annealing carbide phase nuclei form in the martensite crystals. At the early stages of the decomposition the crystal lattices of the carbide and the α-phase may be linked (coherent) (Fig. 2). Inasmuch as the crystal lattices and the specific volumes of the phases are different, stresses - usually called coherent stresses - develop at the interfaces. These stresses increase as the number and volume of the carbide phase nuclei grow. The maximum value of the coherent stresses depends on the strength of the interatomic bonds.

At temperatures at which the binding of these crystal lattices is weakened (i.e., when the carbide particles separate from the α-phase) the coherent stresses are reduced.

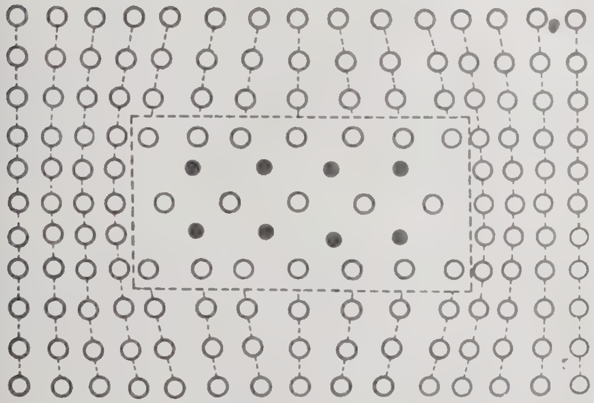

Fig. 2. Probable scheme of distortions of the lattice due to formation of a carbide phase nucleus inside a martensite crystal.

Curve 2 in Fig. 1 shows the suggested change in the coherent (secondary) distortions incident to annealing of carbon steel. These stresses are absent in freshly quenched steel. As the martensite decomposes these stresses increase. The first rise in the curve (to 120-150°) corresponds to the first stage of decomposition of the martensite. This stage consists of the formation of carbide nuclei and their quickly attenuated growth. The kinetics of this stage are determined by the number of carbide nuclei forming in a unit volume per unit time. A product of this stage of decomposition is an α-solid solution still appreciably supersaturated with carbon.[6-9]

The second rise in the curve (in the 120-350° interval) is connected with the end of the second stage of the martensite decomposition consisting of a further separation of carbon from the α-solid solution simultaneously over the entire volume of the specimen. In the process, the tetragonal lattice of martensite approaches the cubic lattice of α-iron. The appreciable decrease of the ratio $\Delta\alpha/\alpha$ (Fig. 1) is connected with the carbide crystals separating out from the α-phase.

During annealing the regions of homogeneous distortions of the lattice increase somewhat in size simultaneously with the increase in the size of the blocks.[10] In the temperature interval (350-350°) of fragmentation of the blocks the size of the homogeneous regions of distortion of the lattice is somewhat reduced. This may be explained by the fact that removal of distortions occurs not through straightening of the bent lamellae, but through plastic deformation, for example, slip over the unstressed zone of the bent lamellae.

At the temperature corresponding to an appreciable decrease in the coherent stresses there is an increase in the number of dispersion stresses due to carbide crystals dispersed inside the α-phase crystals. Inasmuch as the specific volume of the independent, isolated carbide phase differs from the specific volume of both the α-phase and the carbide particles, the lattices of which are linked, an increase in the number of segregated carbide crystals result in an increase of the so-called dispersion stresses (curve 4, Fig. 1).

The experimental facts serving as evidence in favor of the existence of secondary (coherent and dispersion) stresses in steel are the following:

a) the regions of coherent scattering of x-rays (mosaic blocks) are fragmented in precisely the temperature interval in which the decomposition of martensite ends and stresses of the second kind are virtually relieved; the fragmentation of the blocks may be connected with relief of the stresses through plastic displacement in submicroscopic regions;[10]

b) in isolated martensite in which primary stresses are virtually absent, stresses of the second kind are not only not reduced but are increased somewhat in annealing at temperatures up to 350°; above this temperature, however, they fall off sharply.

Thus, quenching (primary) stresses of the second kind are essentially consequences of elastic deformation of each individual martensite crystal as a whole. Secondary stresses, although they produce the same x-ray diffraction effects (diffuse lines) as the primary stresses, differ from the latter in that they are localized inside the martensite crystals and consequently equalize each other within the limits of appreciable smaller volumes of the metal as compared with the former.

It will be seen from the above schemes that the effects of the experimentally determined stresses of the second kind (more accurately, distortions of the crystal lattice) incident to annealing hardened steel may be represented as the result of primary and secondary stresses. The character of the variation of the "resultant" stresses will depend on the relative magnitude of the primary and secondary stresses.

In high-carbon (0.8-1.4% C) steel the quenching stresses are appreciably greater than the secondary ones. Hence the variation of the "resultant" stresses should be similar to that of the quenching stresses. This is evidenced by a comparison of the scheme of Fig. 1 with the experimental curve for the variation of stresses of the second kind incident to tempering of steel with a 1.4% C content.[11]

In low-carbon steel the quenching stresses are small. Hence in this case we may expect the experimentally determined stresses to remain constant or even to increase in the temperature range corresponding to the final stage of cementite formation, i.e., in the temperature interval in which the secondary stresses develop.

In alloy steels, in which, in addition to cementite, special carbides are formed, there may develop additional secondary stress maxima, the number of which

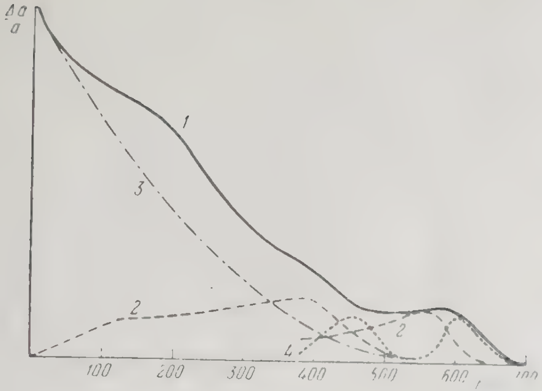

Fig. 3. Probable scheme of variations of distortions of the second kind in the crystal lattice of the α-phase incident to annealing of hardened alloy steel, when cementite and one special carbide form in the steel. Designations same as in Fig. 1.

will depend on the number of carbide transformations. These maxima will appear only in cases when the quenching stresses are not large or when the maxima develop at higher temperatures than the temperature at which the quenching distortions are removed (Fig. 3). Thus the suggested system of classification and scheme of variation of stresses of the second kind occurring during hardening and tempering of steel can be used to interpret the variations in the distortions of the lattice observed not only in carbon steel but in alloy steels as well.

Fig. 4 shows the dependence of changes in distortions of the second kind in the crystal lattice of vanadium steel (0.82% C and 1.07% V) on the annealing temperature.[3] The nature of this curve can be interpreted in the light of the proposed scheme in the following manner. The rapid removal of distortions of the lattice at temperatures up to 450-500° may be explained by a rapid reduction of the quenching stresses, while the subsequent slowing down of strain removal may be attributed to an increase in the secondary stresses due to the formation of a special carbide. It must be noted that it is precisely in the temperature interval where the removal of distortions slows down that secondary hardening of the steel is observed.

Fig. 5 shows the variation of distortions of the lattice during annealing of two die steels, 5KhVS and EI160, and U10 steel.[2] Noteworthy here is the fact that at temperatures above 550° the distortions are greater in the lower alloy 5KhVS steel than in the high-alloy EI160 steel. It has been established that the variation in hardness parallels the changes in the distortions of the lattice.

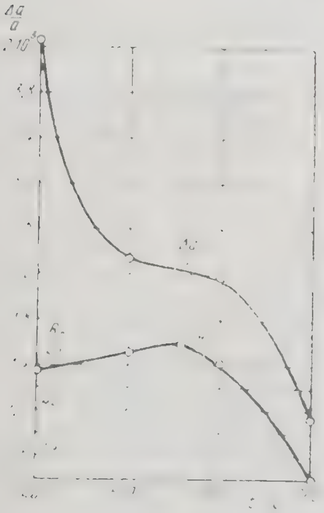

Fig.4. Dependence of changes in the distortions of the second kind of the crystal lattice of the α-phase and of the hardness of vanadium steel on the annealing temperature.

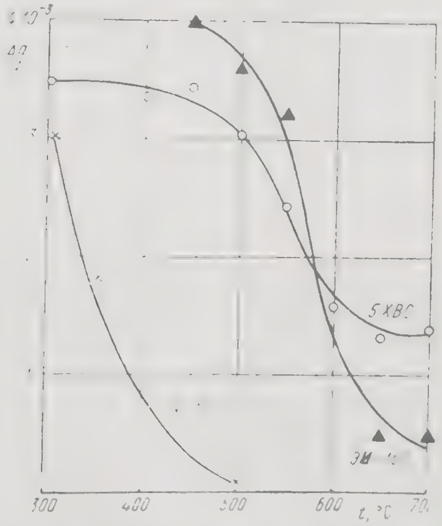

Fig. 5. Variation of distortions of the second kind of the crystal lattice of the α-phase in 5KhVS [5XBC], EI160 [ЭИ160] and U10 [Y10] steels during annealing.

The observed regularity in the variation of the lattice distortion can be interpreted with the aid of the schemes shown in Figs. 6 & 7. Two carbides - cementite and a special carbide - form in the EI160 steel. Hence

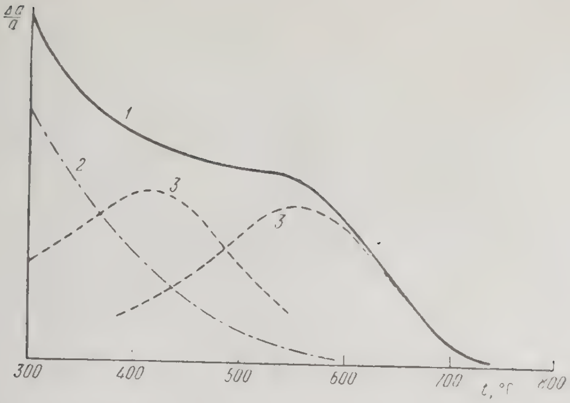

Fig. 6. Probable scheme of variation of distortions of the second kind of the crystal lattice of the α-phase in EI160 [ЭИ160] steel during annealing: 1) experimentally determined, 2) quenching and 3) secondary (coherent and dispersion).

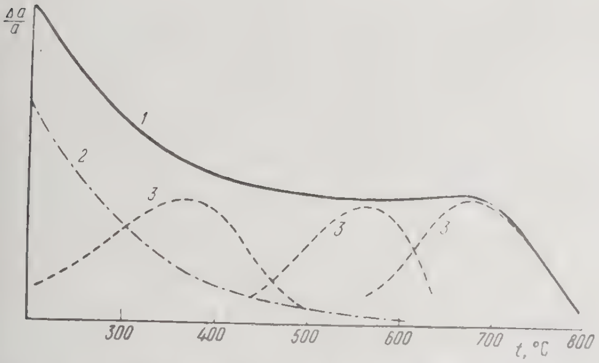

Fig. 7. Same as Fig. 6 but for 5KhVS [5XBC] steel.

there are two secondary stress maxima in curve 3 of Fig. 6. In 5KhVS steel there are successively formed three carbides: cementite and two special carbides; hence there are three secondary stress peaks with the result that the secondary stresses persist to higher temperatures.

The result of our investigation of the internal stress in and hardness of the two die steels points to an important conclusion where the alloying of steels designed to retain a high strength at high temperatures is concerned. Our data indicate that what is important is not the number of alloying elements per se but the matter of taking them in such proportions that there will occur successive changes in the crystal structure of the carbide accompanied by the appearance of secondary stress peaks as the temperature is increased. The higher the temperatures of the successive carbide transformations, the higher will be the temperature to which superior hardness is retained. Obviously in this connection the nature of the alloy elements and the corresponding carbide phases is important.

In conclusion we must note that analysis of distortions of the crystal lattice of α-solid solutions becomes even more complicated when the changes of state occurring incident to the transformation of the residual austentite during annealing are taken into account.

Conclusions

1. We propose that the experimentally determined distortions of the second kind of the crystal lattice of martensite be regarded as the total effect due to

a) quenching distortions, forming during phase transition;

b) coherent distortions, developing inside the martensite crystals during the initial stage of decomposition of the supersaturated α-solid solution;

c) dispersion distortions, also forming inside the martensite crystals, but incident to separation of the carbide phase crystals from the solid solution.

2. On the basis of the results of earlier investigations we give the probable regularity characterizing the variation of each type of lattice distortions during annealing of steel.

Institute of Metal Physics of the
Academy of Sciences of the Ukrainian SSR

References

1. N.N.Davidenkov, in "Primenenie rentgenovykh luchei k issledovaniiu materialov" (The application of x-rays to the investigation of materials), L.1936.

2. L.I.Lysak & E.G.Nesterenko, in "Voprosy fiziki metallov i metallovedennia" (Problems of the physics of metal and metallurgy), Kiev, 1953.

3. L.I.Lysak & L.G.Khandros, Ibid, No. 4, Kiev, 1953.

4. G.V.Kurdiumov, V.K.Krietskaia, V.A.Il'ina & L.I.Lysak, Izv. AN SSSR, Ser. fiz., 17, 297 (1953).

5. M.P.Arbuzov, Doklady AN SSSR, 74, 1085 (1950).

6. G.V.Kurdiumov & L.I.Lysak, Zhur. tekh. fiz., 19, 258 (1949).

7. L.I.Lysak, in Voprosy, etc. (See Ref. 2), No. 3, Kiev, 1953.

8. G.V.Kurdiumov & L.I.Lysak, Zhur. tekh. fiz. 16, 1307 (1946).

9. L.I.Lysak, in Voprosy, etc. (See Ref. 2), No. 2, Kiev, 1950.

10. L.I.Lysak, in Voprosy, etc. (See Ref. 2), No. 3, Kiev, 1952.

11. G.V.Kurdiumov & L.I.Lysak, Zhur. tekh. fiz., 17, 993 (1947).

DETERMINATION OF THE CHARACTERISTIC TEMPERATURE AND DISTORTIONS OF THE LATTICE IN CERTAIN HIGH-MELTING POINT METALLIC COMPOUNDS AND SOLID SOLUTIONS

- S.M.Nikolaeva & Ia.S.Umanski

One of the principal factors determining the resistance of metals and alloys to deformation and destruction under stress, particularly at high temperatures, is the strength of the interatomic bonds in their crystals.

An index to this strength is the characteristic temperature, for the magnitude of the interatomic binding force f is proportional to the square of the characteristic temperature θ:

$$f \approx m\theta^2 \tag{1}$$

where m is the atomic mass.

Among the different procedures for determining the characteristic temperature the roentgenographic is most suitable for brittle metals whose elastic moduli are difficult to determine.

The purposes of the present investigation included determining the characteristic temperature of brittle high-melting point metallic compounds of the NiAl (CoAl and NiAl) and TiC type and solid solutions comprising them, as well as evaluation of the magnitude of the static and dynamic distortions in the crystal lattice of the solid solutions forming by substitution (in the case of solution of Co(Ni) in CoAl(NiAl)) and by "subtraction" (in the case of solution of Al in CoAl and NiAl and in the case of a carbon deficit in titanium carbide).

Our choice of the Co-Al, Ni-Al and Ti-C alloys, aside from their practical importance, was dictated by the fact that with these alloys one can determine how the strength of the bonds and the magnitude of the static distortions changes with the type of solid solution and what influence both these factors have on the hardness of these compounds. We investigated two Co-Al alloys (50 and 55 atomic % Co), two Ni-Al alloys (45.5, 50 and 60 atomic % Ni) and two Ti-C alloys (30 and 50 atomic % C).*

The Co-Al and Ni-Al alloys were prepared by sintering in a TVV-2 furnace under vacuum or in an argon atmosphere. The titanium carbide of stoichiometric composition was obtained by carburization of metallic titanium under vacuum. The low-carbon sample of titanium carbide was obtained by chemical separation from titanium ingots melted in graphite crucibles in an atmosphere of argon.

The characteristic temperatures were determined by the method of measuring the relative intensities of the x-ray interferences at different temperatures following the procedure successfully used by Kurdiumov and Iveronov and their co-workers.[1,2] The interference patterns were recorded at three temperatures - 110, 295 and 473°K - using the K radiation from Mo.

The specimens were prepared by pulverizing sintered briquets in a metallic mortar. The resultant powders were roasted in evacuated quartz tubes at a temperature of 750-900° for a period of one hour to relieve residual stresses of the second and third kind (results of the treatment were monitored by x-ray photography).

From three to eight x-ray patterns were obtained for each specimen at different temperatures. All the roentgenograms were photometered visually on an MF-4 Microphotometer. We compared the integral intensities of the $(200)_\alpha$ and $(510)_\alpha$ lines on the roentgenograms of the Co-Al and Ni-Al alloys and of the $(400)_\alpha$ and $(842)_\alpha$ lines on the x-ray patterns of the Ti-C alloy.

The characteristic temperature was determined from the following relationship

---

*A.N.Litvintsev participated in the investigation of the Ti-C alloys.

$$\psi(\theta, T_1, T_2) = \frac{1}{\theta}\left[\frac{\Phi(\theta/T_1)}{\theta/T_1} - \frac{\Phi(\theta/T_2)}{\theta/T_2}\right] = B\ln\frac{\gamma_1}{\gamma_2}, \qquad (2)$$

where

$$B = \frac{ma^2k}{3h^2(\Sigma l_2^2 - \Sigma l_1^2)},$$

$\Phi(\theta/T)$ is the Debye function, γ_1/γ_2 is the ratio of the intensities of the same pair of lines $(h_1k_1l_1)$ and $(h_2k_2l_2)$ at T_1 and T_2, m is the reduced mass of the alloy, h is the Planck action constant, k is Boltzmann's constant and a is the period of the lattice. The values of γ_1 and γ_2 were determined experimentally.

The characteristic temperature was determined graphically from the calculated value of the function $\psi(\theta, T_1, T_2)$.

The value of the characteristic temperature obtained in the experiments in the two temperature intervals (110-295° and 295-473°K) were consistent; hence for the final value of the characteristic temperature we took the arithmetic mean of the values obtained in the different temperature intervals. The relative error in evaluating θ for the Co-Al and Ni-Al alloys was evaluated to be 6%; that for the Ti-C alloys, 12%.

In order to evaluate the strength of interatomic bonds in the investigated alloys we calculated the magnitude of $m\theta^2$. The values of the characteristic temperatures, $m\theta^2$ and the ratio γ_1/γ_2 are listed in Table 1.

Table 1

Alloy	γ_1/γ_2 at $T_1 = 295°$ & $T_2 = 110°$K	γ_1/γ_2 at $T_1 = 473°$ & $T_2 = 295$ K	θ, K	$m\theta^2 \cdot 10^{8}$, g·deg^2
Co-Al (50)	1,23	1,29	540	17,9
Co-Al (55)	1,30	1,37	480	14,7
Ni-Al (45)	1,45	1,52	420	10,5
Ni-Al (50)	1,28	1,32	500	15,6
Ni-Al (60)	1,35	1,41	450	13,4
Ti-C [illegible]	[illegible]	[illegible]	1130	[illegible]
Ti-C [illegible]	1,15	[illegible]	840	29,6

The mean square deviations of the atoms from the equilibrium positions at 110, 295 and 473° K were computed according to the formula

$$U_0^2 = \frac{9h^2}{3\pi^2 mk\theta}\left[\frac{\Phi(\theta/T)}{\theta/T} + \frac{1}{4}\right]. \qquad (3)$$

The difference $U_1^2 - U_2^2$ characterizing the change in the magnitude of the deviation of the atoms from the equilibrium position in going from T_1 to T_2 was computed directly by means of the formula

$$U_1^2 - U_2^2 = \frac{\ln\gamma_1/\gamma_2}{\frac{4}{3}\pi^2\frac{\Sigma l_2^2 - \Sigma l_1^2}{a^2}} \qquad (4)$$

without intermediate determination of the characteristic temperature.

The values of $\sqrt{U_0^2}$ computed for temperatures of 110, 295 and 473°K and the values of $U_1^2 - U_2^2$ computed for the two temperature intervals 110-295° and 295-473°K are listed in Table 2.

We also measured the magnitudes of the static distortions in the crystal lattices of the solid solutions based on NiAl and TiC. By way of reference samples of an undistorted crystal lattice we used stoichiometric specimens of NiAl and TiC.

To eliminate the influence of extinction on the intensity of the front lines for the relatively coarse-grained samples we utilized the method of photography with a standard (aluminum foil).

We compared the ratio of the intensities of the $(222)_\alpha$ line of NiAl with the $(422)_\alpha$ line of the standard and of the $(511)_\alpha$ line of titanium carbide with the $(422)_\alpha$ line of the standard for ideal and distorted lattices.

Table 2

Alloy	$\overline{U^2_{295°}} - \overline{U^2_{110°}}$, Å²	$\overline{U^2_{473°}} - \overline{U^2_{295°}}$, Å²	$(\sqrt{\overline{U^2_g}})_{110°}$, Å	$(\sqrt{\overline{U^2_g}})_{295°}$, Å	$(\sqrt{\overline{U^2_g}})_{473°}$, Å	$\sqrt{\overline{U^2_{st}}}$, Å	H, Kg/mm²
Co-Al $_{(50)}$	0,0058	0,0072	0,083	0,112	0,141	—	530
Co-Al $_{(55)}$	0,0074	0,0089	0,089	0,125	0,155	—	470
Ni-Al $_{(45)}$	0,0105	0,0118	0,097	0,141	0,176	0,099	400
Ni-Al $_{(50-52)}$	0,0071	0,0079	0,085	0,122	0,151	—	520
Ni-Al $_{(60)}$	0,0085	0,0097	0,091	0,130	0,162	0,077	370
Ti-C $_{(50)}$	0,0018	0,0025	0,073	0,085	0,098	—	2850
Ti C $_{(30)}$	0,0029	0,0043	0,076	0,094	0,112	0,116	1950
Ni-Al $_{(50)}$	—	—	—	—	—	—	540
Ni-Al $_{(55)}$	—	—	—	—	—	—	440

The intensities of the lines were corrected taking into account the difference between the values of certain line intensity factors for the investigated samples and the values of these factors for a sample with an undistorted lattice. The calculated values of $\sqrt{\overline{U^2_{st}}}$ are also listed in Table 2.

We also measured the microhardness of the metallic compound CoAl and NiAl (the results of our tests and the data on the microhardness of TiC alloys given by Koval'ski and Makarenko[3] are listed in Table 2).

The characteristic temperature of the Co-Al alloy containing 50% Co (540°) proved to be higher than that of the alloy with 55% Co (480°). The characteristic temperature of the Ni-Al alloy closer to the stoichiometric and containing 52% Ni (500°) proved to be higher than the characteristic temperature of the extreme solutions of the single-phase β-region of the structural diagram, of the Ni-Al alloy with a maximum (60%) Ni content (450°) and of the alloy with the maximum (54.5%) content of Al (420°).

The characteristic temperature of the Ti-C alloy containing 49% C (1130°) is appreciably higher than the characteristic temperature of the Ti-C alloy containing about 32% C (840°).

Our data on the variation of the characteristic temperature with the concentration in solid solutions are in good agreement with the data on the coefficients of diffusion for Co in Co-Al alloys (Fig. 1).

Calculations of the values of the mean square displacements of the atoms at the three temperatures of the experiment showed that these values increase with the temperature for the extreme alloys appreciably faster than for alloys close to the ideal in composition. The results of calculations of the static distortions in the crystal lattice of solid solutions based on the metallic compound NiAl show that the value of $\sqrt{\overline{U^2_{st}}}$ is higher for the alloy with an excess of aluminum than for the alloy with an excess of nickel (0.099 A and 0.077 A, respectively). Our results are in agreement with the hypothesis that distortions in the crystal lattice of deficiency solid solutions are appreciably greater than in substitutional solid solutions due to the vacancies in the defective structure lattice.

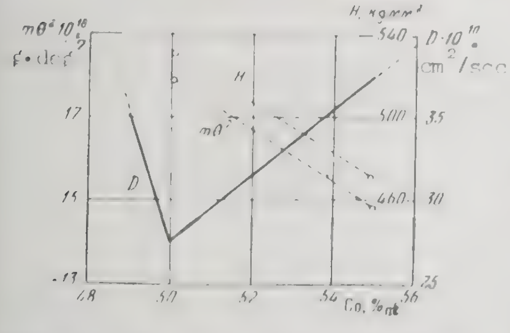

Fig. 1. Dependence of the value of $m\theta^2$, the coefficient of diffusion D and microhardness H of Co-Al alloys on the Co content.

The static distortions in the crystal lattice of low-carbon titanium carbide are very

appreciable (0.116 A).

The curve giving the dependence of the microhardness of NiAl alloys on their composition (Fig. 2) has a maximum corresponding to the 50% Ni alloy (540 Kg/mm^2). The microhardness of the alloys with an excess of nickel (60% Ni) and an excess of aluminum (54.5% Al) is lower than that of the stoichiometric alloy (the respective values are 370 and 400 Kg/mm^2). The microhardness of the Co-Al alloy containing 50% Co (530 Kg/mm^2) is higher than the microhardness of the alloy with an excess (55%) of cobalt (470 Kg/mm^2).

As the investigations of Koval'ski and Makarenko have shown the microhardness of titanium carbide (Fig. 3) increases linearly with the carbon content and is maximal for TiC of ideal composition.

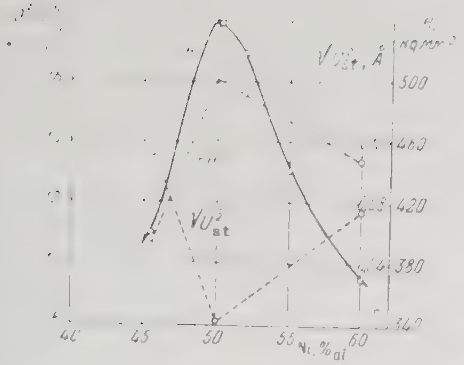

Fig. 2. Dependence of mθ^2, the microhardness H and the static distortions in the crystal lattice ($\sqrt{U^2_{st}}$) of Ni-Al alloys on the Ni content.

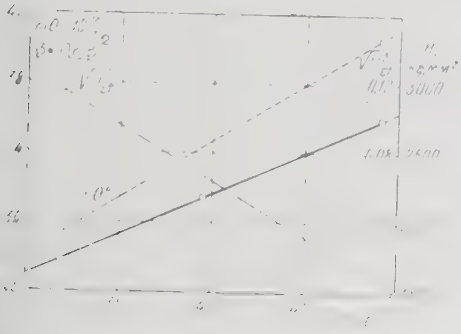

Fig. 3. Same as Fig. 2, but for TiC.

Conclusions

The following conclusions may be drawn in the light of results obtained.

1. Solution of both nickel (or cobalt) and aluminum in the metallic compounds NiAl and CoAl leads to a reduction in the characteristic temperature (and consequently to a decrease in the strength of the interatomic bonds) and to an increase in the static distortions of the lattice and a decrease of the microhardness of the alloy. These effects are more appreciable for solid solutions of the deficiency type than for solid solutions of the substitutional type (Figs. 1 & 2).

2. The interatomic binding forces in the crystal lattice of titanium carbide containing ~ 50 atomic % C are appreciable. Deficit of carbon atoms in the carbide lattice leads to a reduction of the characteristic temperature (and consequently to a reduction of the strength of the interatomic bonds) and an increase in static distortions, and a decrease in the microhardness of the alloys (Fig.3).

3. From a comparison of the character of the static distortions and the values of the microhardness we can conclude that chemical distortions (static distortions connected with formation of a solid solution) cannot in the case of the investigated alloys greatly increase the resistance to plastic deformation inasmuch as the effect of chemical distortions is largely compensated for by the change in the strength of the interatomic bonds.

4. From a comparison of the values of the microhardness of alloys with an excess of aluminum or nickel with the magnitude of the static distortions one can conclude that the distortions of the crystal lattice in a deficiency solid solution exert a greater influence on the microhardness of the alloy than distortions due to substitutions of atoms in the crystal lattice of a substitutional solution.

"I.V.Stalin" Moscow Steel Institute

References

1. V.A.Il'ina, V.K.Krithkaia & G.V.Kurdiumov, "Problemi metallovedenia i fiziki metallov" (Problems of metallurgy and the physics of metals), No.3, M.1952.
2. A.V.Beznosikova & V.I.Iveronova, Zhur. tekh, fiz., 20, 666 (1950).
3. A.E.Koval'ski & T.G.Makarenko, in "Mikrotverdost'" (Microhardness),M.-L.1951.

STRUCTURAL CHANGES IN PURE METALS DURING STRESS RELAXATION

- B.M.Rovinski & V.G.Liuttsau

Earlier, one of the authors[1] showed that stress relaxation in pure metals at room temperature was due primarily to "spontaneous" processes of a translational character. This hypothesis was verified experimentally by x-ray diffraction studies.[2] We investigated the structural changes in aluminum during the process of stress relaxation. In general, these were analagous to changes observed in elastic[3] and ordinary plastic deformation.[4] However, in view of the fundamental character of the hypotheses we attempted to analyze in more detail the structural changes in pure metals in the process of stress relaxation under the conditions of a linearly stressed state.

Description of the experiments

In the present work, we used the procedure described earlier in Ref. 2. This procedure is based on back-reflection registration from large-grain metal. However, in the present experiments the resolving power of the set-up was considerably increased by using a collimating device with narrow cross-shaped and radial slits. The width and length of the cross-shaped slits were 0.02 mm and 3.0 mm, respectively; the width of the radial slit was 0.01 mm; the length, 2.5 mm. The slit to sample distance was 120 mm; the sample to film distance was 240 mm. The film was loaded in a flat film cassette mounted normal to the reflected beam. The x-rays were produced by a copper anode ion tube with a strongly diffused focal spot. We investigated the reflections from the (511) and (333) planes of aluminum and the (420) plane in copper: $\theta_{AL} = 81^\circ 16'$ and $\theta_{Cu} = 72^\circ 17'$ ($K\alpha_1$).

The requisite crystal grain size was obtained by appropriate thermal treatment of the samples in a vacuum oven. The structure was checked by metallographic and x-ray methods.

The samples, which were of pure aluminum (99.99%) and copper (99.92%), were clamped in a special relaxation device mounted on the x-ray camera bench.[2] The accuracy of positioning was checked on the basis of the reproducibility of the x-ray patterns obtained upon re-setting of relaxation device. The relaxation experiments were carried out with an initial elastic longitudinal deformation equal to about 0.1% over a period of about 500 hours. The x-ray patterns were recorded at intervals of one or two days, the first photograph being taken shortly after the loading of the sample. The exposure time for each pattern was about four hours. The films were developed under the same conditions to approximately the same background density.

Results

The nature of the structural changes occurring in a metal in the process of stress relaxation can easily be followed on the diffraction patterns. Fig. 1 shows a time series of the corresponding sections of the x-ray patterns of an aluminum sample recorded during the process of stress relaxation. These patterns (Fig. 1) were obtained with a cross-shaped slit. The upper pattern is of the unstressed sample; the following ones are of the initially elastically strained sample taken 4, 169 and 500 hours after the beginning of the test.

Appreciable changes are noticeable even in the photograph taken four hours from the start of the test. The interference spots marked by arrows in the top pattern either vanished entirely or weakened greatly after the sample was loaded. As was established earlier[2,3] this phenomenon is due to enhanced perfection of the crystals upon stressing in the elastic region. The interference spots reappear in the succeeding patterns. They are all marked with arrows in the last (lowest) pattern.

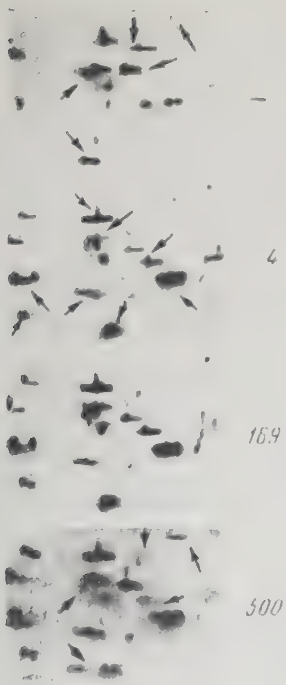

Fig. 1

Fig. 2

Fig. 3

Fig. 4

Fig. 1. X-ray patterns of an aluminum sample during the process of stress relaxation. The numbers indicate the period of loading in hours.

Fig. 2. Changes in structure of cross-slit interference spots. 1.5X enlargement of a section of the pattern for an aluminum sample.

Fig. 3. Changes in structure of radial slit interference spots in the x-ray patterns for a copper sample in the process of stress relaxation. (magnification 6.3X)

Fig. 4. Changes in the relative location of slit interference spots in the x-ray patterns of a copper sample during the process of stress relaxation (magnification 2X).

The structure clearly changes and new spots appear in the process of stress relaxation. The spots identified by arrows in the second-from-the-top x-ray pattern gradually change: their intensity increases as does the width of the vertical and horizontal streaks comprising them; at the same time the number, diffuseness and separation of these component streaks all increase.

Analagous changes in the structure of the cross-shaped interference spots are described in Ref. 5. With a small plastic deformation, the spots in the x-ray patterns change in the same manner as described above. These changes are caused by fragmentation of the crystal grains into finer structural elements (blocks) and their gradual disorientation, i.e., an increase in the mosaicity angles.

The general character of changes in the spot structure is more clearly discernible in Fig. 2 which shows an enlargement of a small section of the x-ray pattern. The spot at the left in Fig. 2 already shows a fairly complex structure in the first (top) pattern. This indicates that the crystallite, whose reflection forms this spot, is composed at least of several fragments, oriented at small angles to each other (<1'). In the process of stress relaxation, the reflection spot gradually diffuses and its structure becomes more complex. It can clearly be seen in the lowest pattern that the spot consists of a series of diffuse horizontal and vertical streaks. The area of the spot and its integral

intensity in this pattern are considerably greater than originally. The spot to the right in Fig. 2 is similar to the one on the left in appearance, but is characterized by a more abrupt fragmentation process and a faster increase in mosaicity.

The changes in the x-ray patterns of the copper samples during stress relaxation are, in general, similar to those in the patterns for the aluminum. Enlarged small sections of the patterns for a copper sample are shown in Fig. 3. These patterns were obtained with a radial slit. The top x-ray pattern is of the initial unstressed sample, while the patterns below were recorded 5 and 97 hours after the start of the test.

Fig. 3 illustrates the increasing complexity of the crystallite structure. The relaxation process is marked by fragmentation of the crystallite and disorientation of its substructure elements. As a result the mosaicity angle increases.

The upper spot in Fig. 3, which is fairly intense in the second-from-the-top pattern, rapidly fades during the process of stress relaxation. This, in our view, is due to an abrupt rotation of the crystallite. In point of fact, in addition to the changes in the structure of the spots in the patterns of Fig. 1, one can readily trace the change in their relative orientations. The change in the relative orientations of the spots is even more clearly evident in the patterns of Fig. 4.

Fig. 4 shows sections of the x-ray patterns of a copper sample (initial and 247 and 503 hours after the start of the experiment). The spot identified by the arrow at the top of the pattern is taken as the reference for position. With respect to it, the spots marked by the arrows at the bottom of the same photograph undergo simultaneous but not identical displacements upward and to the left. Thus, the radial displacement upward of the lower right spot corresponds to 18' rotation of the reflecting crystallite, while the azimuthal displacement, the displacement along the interference ring of reflections from the (420) planes, corresponds to a rotation of approximately 9'.

Simple analysis leads to the conclusion that the displacement of the spots is probably due to rocking of the crystallites during their extremely small relative displacements in the process of stress relaxation.

Conclusions

1. In the process of stress relaxation in aluminum and copper, there arise irreversible structural changes in the crystallites, similar to the changes incident to small plastic deformations.
2. In addition to the changes in the internal structure of the crystallites during the process of stress relaxation at room temperature, there also occur changes in their relative position and orientation.
3. The rotation and the relative displacements of the crystallites as a whole is probably connected with the viscous behaviour of the crystal grain boundaries.

References

1. B.M.Rovinski, Izv. AN SSSR, Otd. tekh. nauk, No. 2, 67 (1954).
2. B.M.Rovinski & V.G.Liuttsau, Izv. AN SSSR, Otd. tekh. nauk, No. 11, 1618 (1954).
3. B.M.Rovinski, Zhur. tekh. fiz., 12, 679 (1942).
4. B.M.Rovinski & L.M.Rybakov, Present issue of the Bulletin.

X-RAY INVESTIGATION OF THE PLASTICITY OF BERYLLIUM SINGLE CRYSTALS

- R.I.Garber, I.A.Gindin, V.S.Kogan
and B.G.Lazarev

The present investigation was carried out on single crystals of beryllium cut in the shape of rectangular parallelepipeds with one of the faces coinciding with the basal plane. The samples were deformed by uniaxial compression at temperatures ranging from -253° (the temperature of liquid hydrogen) to 800° C. The stationary samples were photographed using unfiltered Cu radiation from a sharp focal spot x-ray tube. This choice of radiation was dictated by the fact that for a single crystal of beryllium with the hexagonal axis [001] or the binary axis [120] oriented along the beam, the most strongly reflecting (101) planes are in a position close to that for reflection of the Cu Kα-line. If the scatter in the orientation of these planes, due to plastic deformation of the single crystal exceeds 2°, additional spots lying on the corresponding Debye ring, appear in the Laue pattern. Since such a dispersion of orientations can be caused only by slip, the appearance of these additional spots is a definite indication of plastic deformation.

In conjunction with the x-ray studies of the beryllium single crystals we also carried out metallographic and microinterferometric analyses of their surfaces. As a result, it was ascertained that in a wide temperature interval (-196°C to +800°C) both slipping and twinning occur during plastic deformation of beryllium. These processes are particularly intense at temperatures above 400°C. With the indicated orientation of the crystal axes relative to the axis of compression, the twinning occurs throughout the entire volume of the crystal, which passes into a state characterized by a new orientation, symmetrical with respect to the initial.

This effect is not observed in single crystals of other metals. In this case the reorientation is clearly evident from the Laue patterns. A pattern obtained by photographing perpendicular to the anterior face of the sample after deformation shows that this face coincides with a prismatic face and not with the basal plane as in the case of the undeformed specimens.

Fig. 1 shows the Laue pattern of a deformed beryllium sample. The spots on the (100) and (101) Debye rings show that appreciable slipping has taken place. The crystallographic orientation of the deformed sample, ascertained from juxtaposition of the x-ray patterns with stereographic projections, is shown in the top portion of Fig. 1. The x-ray pattern of Fig. 1,c is the superposition of two Fig. 1,b x-ray patterns, one rotated 60° relative to the other. Obviously, it was recorded from a volume having two systems of twins intersecting at an angle of 60°.

Fig. 1. Laue patterns of beryllium: a) before deformation, b) recorded perpendicularly to the anterior face of the sample after deformation, c) superposition of two (b) patterns rotated 60° relative to each other. Above: the corresponding stereographic projections and crystal orientations.

Fig. 2. Microphotographs of beryllium single crystal: a) dislocation of parts of the single crystal; b) microbreaks along the slip planes.

Fig. 3. X-ray pattern of sample deformed at high temperature (600-800°).

Fig. 4. X-ray pattern of sample weakly deformed at a low temperature (under 200°).

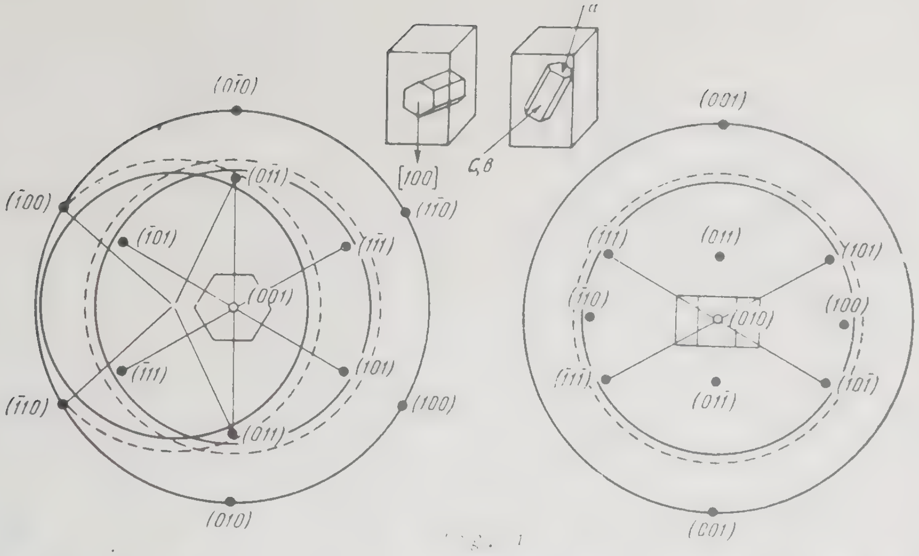
(01̄0)
(1̄00)
(011̄)
(1̄01)
(11̄0)
(11̄1̄)
(0001)
(1̄1̄1)
(101)
(1̄10)
(011)
(100)
(010)
[100]
a
c, b
(001)
(1̄11)
(011)
(101)
(1̄10)
(010)
(100)
(1̄1̄1̄)
(011̄)
(101̄)
(001)

Fig. 1

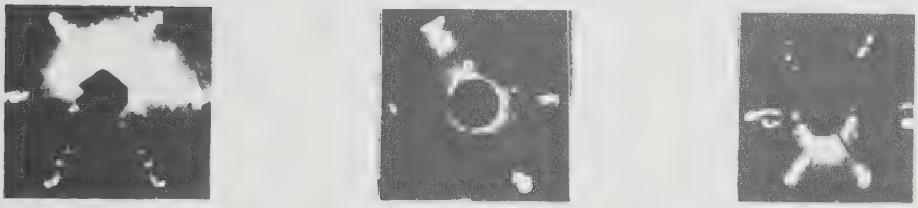

a b c

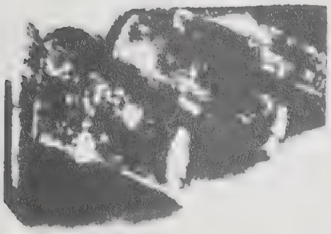

[illegible]

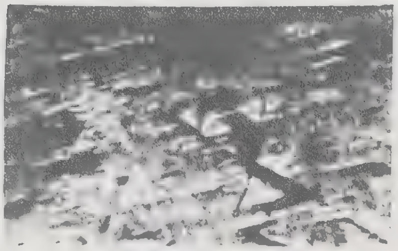

[illegible]

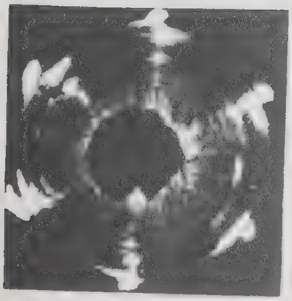

[illegible]

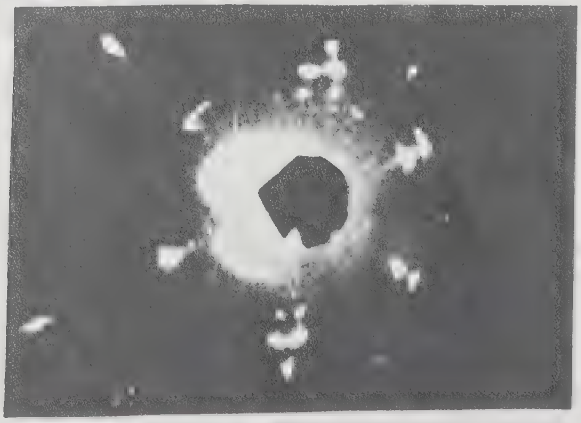

[illegible]

Crystallographic elements of the plasticity of beryllium and the temperatures at which they become manifest

Orientation of the single crystal	Nature of plasticity and its elements						
	Mechanical twinning			Complete re-orientation; axis of symmetry (102)	Slip		
	(101)	(102) [211]	(103)		(001)[100]	(001) [210]	(100) (101) [010]
Binary axis 100 perpendicular to the compression axis	-	-253 - +800	-	400° and over	-	400-800 in twinned regions	200-800 in initial single crystal
Binary axis 100 parallel to the axis of compression	400° and under	-253 - +800°	400° and under	20°C and above	-196-+800° in twinned regions	-	-

In regions where there is only one orientation of the completely twinned crystal (Fig. 1,b), slip develops with particular intensity: entire portions of the single crystal are shifted relative to each other (Fig. 2,a). Simultaneously with such shifts, there occurs healing of dislocations, as a result of which the strength of the sample under static test remains practically unchanged. In the microsection of Fig. 2,b, individual microbreaks are clearly discernible along the slip plane.

In the x-ray patterns of Fig. 1, only reflections due to the Cu Kα-lines appear; Laue spots from the continuous spectrum are absent. This evidently is due to the fact that the slip is accompanied by fragmentation of the microcrystal into separate blocks which retain the crystal's original orientation. Deformation at high temperatures (600° - 800°) causes so considerable a disorientation of the fragmented blocks that the x-ray pattern assumes the appearance characteristic of a textured (fibered) polycrystalline sample. In x-ray patterns of alloy samples which were weakly deformed at lower temperatures (under 200°) there appear both Laue spots and reflections due to the Cu Kα radiation (Fig. 4), the latter being distinguishable from the Laue spots by the fact that upon a small rotation of the sample they are not displaced, but remain on their Debye rings.

The character of the reflection spots due to Cu Kα radiation depends on the slip plane and the direction of slip when the crystal is deformed. From a comparison of the x-ray analysis and metallographic data we were able to establish the crystallographic elements of the plasticity of beryllium and the temperature regions in which they become evident (see table).

Physico-Technical Institute of the
Ukrainian SSR Academy of Sciences

X-RAY INVESTIGATION OF RESIDUAL STRESSES IN ELECTROLYTIC DEPOSITS OF NICKEL

— V.P.Moiseev & O.S.Popova

The present study is part of a series devoted to the study of the nature of electrolytic deposits with a cryptocrystalline structure, carried out in the Structure of Surface Layers Laboratory of the Institute of Physical Chemistry of the USSR Academy of Sciences under K.M.Gorvunova.

Electrolytic deposits of chromium, nickel, manganese and rhenium belong in the category of such deposits. Investigation of the structure and properties of deposits of this type is of interest from the point of view of clarifying their mechanism of formation, a prerequisite for efficient technological control in the production of these metals.

A common trait of all these deposits is the presence of large internal strains, accompanied by distortions of the crystal lattice.

The literature comprises a large number of investigations devoted to the character and origin of stresses and strains in electrolytic deposits.[1-15] In some of these investigations[6-9,15] the strains in electrolytic deposits were studied by the flexible cathode procedure. This method makes it possible to determine the total influence of strains of the first kind (macrostrains) developing in the deposit during its formation. However, this method yields no indication of the microstrains or of the structural transformations occurring in the process of electrocrystallization. Although a number of investigations also give data on x-ray diffraction studies of internal strains,they do not give adequate attention to qualitative characterization of the stressed state. Primary attention is focussed in these investigations on the problem of transformations in the process of electrolysis and in the process of the subsequent heat treatment of the deposits.[2,5,10-13]

In the present investigation we have attempted to use quantitative data to help clarify the reasons for the development of internal strains in the process of electrocrystallization of nickel.

1. Procedure

The subjects of investigation were matte deposits of nickel obtained from a bath made up of 140 g/liter $NiSO_4 \cdot 7H_2O$, 30 g/liter H_3BO_3, 3 g/liter NaCl, and 5 g/liter NaF and bright deposits from the same bath with the addition of 2,6- or 2,7-disulfonaphthalic acid (4 g/liter). The current tensity on the cathode was 1 a/dm^2; the thickness of the deposits was 20 mμ.

Three methods were employed in studying the deposits: 1) the basic method was x-ray diffraction, which allowed of separate determination of the magnitude of the macrostrains and their distribution through the volume of the sample as well as of evaluation of the distortions of the crystal lattice and structural transformations at different temperatures (we also investigated the texture of the deposits); 2) the flexible cathode method was used for determining the total influence of residual macrostrains in the process of electrolysis; 3) the vacuum heating procedure was used to determine the gas content in the deposits and the rate of its evolution at different temperatures.

The internal strains of the first kind were investigated using Cu Kα radiation in a back-reflection KROS camera with a tube operated at a voltage of 30kv and a current of 10 ma; the exposure time was 10 hours. We used a collimator 0.6 mm in diameter and focusing on the (420) line of nickel. The standard was silver foil heated in vacuum at 350° for one hour beforehand (foil thicknesses 0.23 and 0.12 mm). The sample to film distances were 112 and 120 mm.

To evaluate the internal strains of the first kind we utilized the procedure developed by Kurdiumov and his co-workers.[16-18] According to this procedure, to

determine the strains in electrolytic deposits one must record four patterns in order to then determine, with reference to one known principal stress axis, the two other principal axes and the magnitude of the strains. To provide for rotation of the samples we constructed a special holder giving a range of azimuth angles from 0 to 360° and vertical angles from 0 to 180°. The principal stress axis in the deposits was assumed to be oriented in the direction perpendicular to the surface of the deposit; this direction was also that of one of the principle strain axes.

The patterns were photographed on rotating film. The diameters of the $K\alpha_1$-line rings from the (420) plane in the case of nickel and the (511) plane in the case of silver were measured on a comparator, the final values used being the averages for five measurements. The relative error under our conditions was evaluated to be about 8-10%.

The method of a flexible cathode was utilized to investigate stresses in nickel deposits 0.1-3.5 mμ thick. These deposits were obtained on copper plates measuring 0.048 x 6 x 60 mm, coated with insulating BF-2 cement on one side. A series of special tests established that the presence of this cement does not effect the magnitude of the strains or the structure of the deposit.

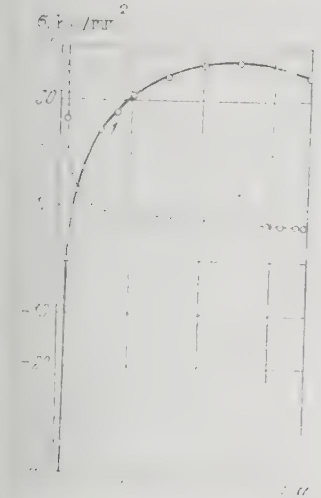

Fig. 1. Variation of stresses in electrolytic deposits of nickel with the thickness of the deposit: 1) bright, 2) matte deposit.

The amount of hydrogen evolved incident to heating of the samples was measured in a vacuum set-up with successive heating of the samples, to 50, 100, 150, 250, 350 and 550°.

2. Results of the investigation

The results of our measurements of internal strains in electrolytic deposits of nickel by the flexible cathode method are presented in Fig. 1. The patterns show that in bright deposits of nickel during the first stage of electrolysis there are appreciable compressive stresses which rapidly decrease; when the deposit reaches a thickness of 0.1-0.2 mμ the stresses change sign, i.e., become tensile. With further increase in the thickness of the deposit the tensile stresses increase in magnitude attaining their maximum value (35-40 kg/mm^2) in the thickness range of 1.5-3.5 mμ, after which they undergo a slight reduction.

In matte deposits of nickel there are appreciable elongating (tensile) stresses at the initial instant of electrolysis; with increasing deposit thickness in the range from 0.1 to 0.5 mμ these decrease rapidly to a value which then remains constant within the limits of the experimental error.

The hydrogen content in these deposits at different temperatures is shown in Fig. 2. For purposes of calculation the total amount of gas liberated from the sample in heating to 550° was taken as 100%. It will be seen from the curves of Fig. 2 that in bright deposits of nickel at room temperature there are 8.3 unit volumes of hydrogen per unit volume of the metal, while in matte deposits there are only 2.2 unit volumes per unit volume of the metal.

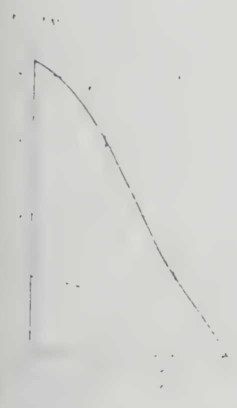

Fig. 2. Dependence of the hydrogen content in nickel deposits on the heating temperature: 1) bright, 2) matte deposits.

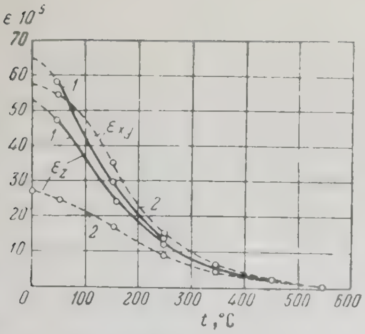

Fig. 3. Temperature dependence of distortions of the crystal lattice in nickel deposits: ε_{xy} - deformations in the plane of the deposit; ε_z - deformations in the direction normal to the surface of the deposit; 1) bright, 2) matte deposit.

The x-ray data pertaining to the strains are shown in Fig. 3, from which it will be seen that all the investigated deposits, both matte and bright, are in a volume-stressed state of tension. The magnitude of the internal strains of the first kind and distortions of the crystal lattice in bright deposits (immediately after their withdrawal from the bath) is so great that it is impossible to catch the reflection from the (420) plane. In matte deposits the magnitude of the deformations is somewhat smaller. In all samples the internal strains exhibit anisotropy, which is more pronounced in the case of matte deposits: in the plane of the deposit there obtain equal stresses (equal deformations ε_x and ε_y); the strains (deformations ε_z) in the direction normal to the surface of the deposit are appreciably smaller. The strain ellipsoid is elongated to a far greater extent in the plane of the deposit than in the direction normal to the surface of the deposit.

The broadening of the lines and the decrease of their intensity are evidence of microstrains and distortions of the crystal lattice. These distortions decrease with increasing temperature during the heating of the specimens, however, the broadening of the lines persist up to 350°. The degree of diffusion of the lines depends on the angle of photographing. This presumably is indicative of the anisotropy of the distortion. At 550° the distortions of the lattice and the internal strains are fully relieved.

A series of special experiments established that all the nickel deposits are fibered (see Fig. 4), although the degree of perfection of orientation varies. In matte nickel deposits the main mass of the crystals is oriented with the (110) plane parallel to the surface of the deposit, while in bright deposits the degree of uniformity of orientation is lower.

Heating of both the matte and bright deposits at 550° for a period of one hour (Fig. 4, b) disorients them somewhat; simultaneously the grain size increases, the increase being greater for matte deposits. It follows that the reduction of the internal strains and distortions of the lattice in electrolytic nickel deposits is due primarily to changes in the content of hydrogen and other impurities and to changes in the degree of dispersion of the deposit with increasing temperature. The anisotropy of the deformation is apparently due to the presence of fibre as well as to the non-uniform distribution of hydrogen and the products of electrolysis over the thickness of the deposit.

The great difference in the character of the stressed state of nickel deposits up to 0.5 mμ in thickness obtained from baths with and without disulfonaphthalic acid (bright and matte deposits - Fig. 1) is apparently connected with the influence of the acid on the process of formation of the deposit at the initial instant of electrocrystallization.

The volume-stressed state of tension with the appreciable stresses involved may be due to a) penetration of hydrogen into the nickel crystal lattice, accompanied by the formation of a solid solution varying in composition over the thickness of the deposits and b) incorporation into the nickel crystal lattice of different impurities (surface active components, the products of their transformation during electrolysis, etc.).

The decrease in the internal strains and reduction of distortions of the lattice with increasing heating temperature may be explained by partial decomposition of the hydrogen-containing solid solution as well as by the segregation of the products of the electrochemical reactions accompanying the process of electro-

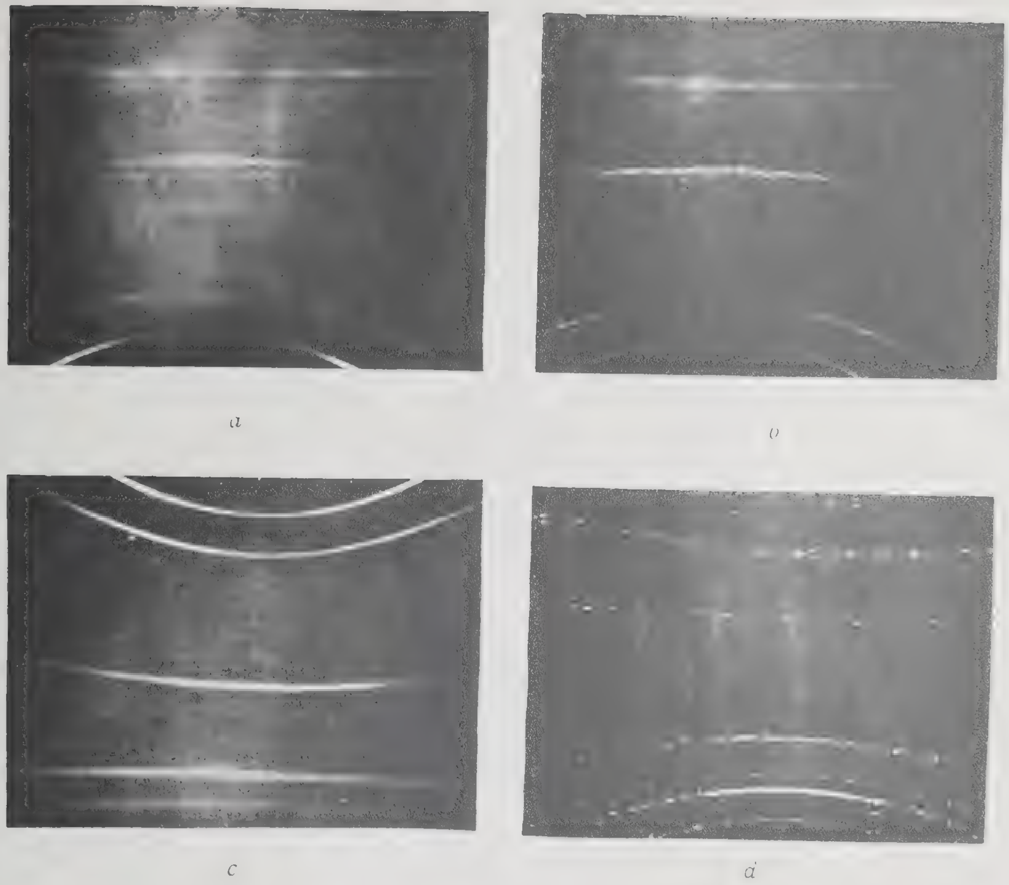

Fig. 4. Texture (fiber) patterns of electrolytic deposits of nickel: a) matte without heating, b) matte after heating to 550°, c) bright without heating, d) bright after heating to 550°.

deposition. However, the fact that heating to 550° fully relieves the internal strains and removes the distortions of the lattice indicates that under these conditions the solid solution decomposes. Despite the fact that, according to the data in the literature, there is presumably a certain quantity of hydrogen remaining in the deposit, our x-ray studies failed to disclose the presence of hydrogen in the heated deposits. The anisotropy of the internal strains and distortions of the crystal lattice, established in our investigation, is undoubtedly due to non-uniform distribution of hydrogen and impurities through the volume of the deposit and is obviously related to the distinctive texture of the deposit (particularly the matte ones).

In view of this anisotropy it is, in principle, incorrect to evaluate the stresses in the deposits on the basis of familiar data on the modulus of elasticity of nickel since in this case the elasticity modulus will be direction-dependent. However, if we provisionally overlook this and assume the value of the modulus for nickel to be $2 \cdot 10^4$ kg/mm^2, we can tentatively evaluate the magnitude of the tensile stresses. Calculated in this way on the basis of the x-ray data shown in Fig. 3, they amount to about 40 kg/mm^2 in bright nickel and 30 kg/mm^2 in matte nickel deposits.

It is of interest to note that the values of the stresses in bright nickel computed from the data based on magnetic measurements carried out in our laboratory by U.M.Polukarov are of the order of 30-28 kg/mm^2 for deposits 20 mμ thick

and 33 kg/mm^2 for deposits 4 mμ thick.

Conclusions

Certain deductions may be drawn regarding the nature of stresses and strains in electrolytic deposits on the basis of results of investigations carried out in our laboratory, investigations establishing correlations between the stressed state of electrolytic deposits and their secondary structure (distortion, texture, etc.), the thickness of the deposits, the nature of the substrate metal and other factors.

1. Our x-ray diffraction studes of electrolytic nickel deposits showed that they are in a volume-stressed state of tension and that there is an appreciable difference between the stresses in the direction normal to the surface and the direction parallel to it.
2. The more pronounced stress anisotropy in matte deposits may be connected with the more perfect texture (fibering) established in these deposits.
3. When the deposits are heated, internal strains are relieved and the distortions of the crystal lattice decrease with simultaneous reduction of the hydrogen content of the deposit; at 550-600° these stresses are completely relieved.
4. Heating of both matte and bright deposits leads to coarsening of the grain and reduction of the degree of perfection of the texture; this process is more intense in the case of matte deposits.
5. The results of the present investigation are in agreement with the hypothesis, advanced on the basis of earlier investigations in our laboratory, that there is formed an interstital solid solution with an inhomogeneous distribution of hydrogen over the depth of the deposit.
6. The results of this investigation furnished additional data which should be of help in clarifying the origin of texture in electrolytic deposits of nickel and its connections with the strained state of such deposits.

We take this opportunity to thank B.M.Rovinski for his kind discussion of the results of the first series of our experiments and valuable advice on the roentgenographic procedures.

Institute of Physical Chemistry of the
Academy of Science of the USSR

References

1. L.S.Palatnik, E.L.Genshtei, I.B.Lukov, Zhur. tekh. fiz., 10, 1756 (1940).
2. A.Krasnikov, Zhur. eksp. i. teor. fiz., 14, 285 (1944).
3. A.Krasnikov, Izv. AN SSSR, Otd. tekh. nauk., 133 (1946).
4. Iu.V.Baimakov & L.M.Evlannikov, Zhur. fiz. khim., 25, 483 (1951).
5. Iu.V.Baimakov, Elektrometallurgiia tsvetnikh metallov, (Electrometallurgy of non-ferrous metals), Leningrad Polytechnical Institute, No.6, 57 (1953).
6. A.T.Vagromian & Iu.S.Tsareva, Doklady AN SSSR, 98, 5, 807 (1954).
7. A.T.Vagramian, Iu.S.Tsareva, V.G.Salokhina & N.T.Kudriavtsev, Zhur. fiz. khim., 29, 166 (1955).
8. A.T.Vagramian & Iu.S.Tsareva, Zhur. fiz. khim., 29, 185 (1955).
9. V.S.Ioffe, Usp. Khim., 13, 48 (1944).
10. M.Kersten, ZS f. Phys. 71, 553 (1931).
11. G.R.Levi & M.Gabet, Atti Academia nazionale dei Lincei, 17,647 (1933).
12. A.Portevin, G.Chaudron & L.Moreau, C.R., 204, 1252 (1937).
13. W.A.Wood, Phil. Mag., 24, 2, 511 (1937); 23, 1, 984 (1937).
14. H.Murback & H.Wilman, Proc. Phys. Soc., 66, 805 (1953).
15. J.B.Kusher, Plating, 41, 1146 (1954).
16. V.Romberg, Zhur. tekh. fiz., 7, 1728 (1937).
17. M.P.Zheldak & G.V.Kurdiumov, Zhur. tekh. fiz., 7, 1719 (1937).
18. M.P.Zheldak, G.V.Kurdiumov & V.Romberg, Zhur. tekh. fiz., 8, 1736 (1937).
19. K.M.Gorbunova & N.A.Shishakov, Izv. AN SSSR, Ser. fiz., 17, 242 (1953).

CHANGES IN THE SUBSTRUCTURE OF ALUMINUM WITH SMALL PLASTIC DEFORMATION AND CREEP

—B.M. Rovinski & L.M. Rybakova

The crystallites in a recrystallized metal consist of a combination of fragments and blocks turned through small angles relative to each other.[1,2] The mosaic formed by these structural elements changes when a load is applied to the metal.[3-7] The nature of the changes in the structure of the crystallites apparently depends on the conditions of deformation. The present report is devoted to the result of a detailed quantitative analysis of the changes in the structure of crystallite or the substructure of pure aluminum in the presence of small residual strains under conditions of simple elongation and creep at room temperature.

1. We investigated specimens of 99.99% pure aluminum. These specimens, 8 mm in diameter and having a gage length of 30 mm, were cut from forged aluminum rod fabricated from cast aluminum. Prior to testing, these specimens with threaded ends were subjected to annealing under vacuum for 1 hour at 500°. The specimens were stretched in a device mounted directly on the bench on the ion x-ray tube. One end of the specimen was screwed into the bottom of a steel cylinder with side slits, while the other end was screwed into a special grip with fine external threads. A spherical nut turned onto this grip bore against the end of the cylinder and when tightened stretched the specimen. Suitable keys passing through the slit in the cylinder prevented the grip from turning and thus obviated torsion of the loaded specimen. The cylinder assembly together with the grips and sample was mounted on three vertical pins screwed into a stand which could be displaced along the rails of the x-ray bench. This stand had provision for locking in the desired position. The cylinder assembly could be raised and lowered on the pins by means of an elevating screw. After appropriate vertical adjustments in the beam by means of the elevating screw, the entire assembly could be lifted off the pins and subsequently replaced with full reproducibility of the x-ray pattern.

The deformation of the specimen effected by turning down the spherical nut was determined directly from the gage length. At first, beginning from 0.19%, the strain was increased in 0.01% steps and then from 0.3 to 1% in 0.1-0.2% steps. The x-ray patterns were photographed after each strain step.

Later the described loading device was used for stretching the specimen under conditions of creep at room temperature. To this end, a bar was screwed into the grip and linked to a 1 to 5 lever by means of which constant loads were applied. The grip was free to move in the guide groove, permitting the specimen to elongate under the influence of the applied load. The creep tests were carried out over a period of about 700 hours with stresses of 1 and 2 kg/mm^2 and corresponding deformations up to 0.23 and 0.71%, respectively.

The variations of substructure with plastic deformations and creep were investigated by study of the interference spots on the x-ray patterns. The patterns were recorded with a collimator in the form of two mutually perpendicular slits, 0.04 mm wide and 4.0 mm long[1], by the method of back-reflection with a specimen-to-film distance of about 195 mm. The source of radiation was an x-ray tube with a cobalt anode yielding a diffused focal spot of about 5.0 x 2.5 mm. The slit assembly was located at a distance of about 200 mm from the specimen and about 30 mm from the anode.

The x-ray patterns were made of the same sections of the surface for which purpose thin lead plates with a rectangular 3 x 5 mm cutout were cemented to the samples. The films were developed under the same conditions to approximately the same background density. After development the second emulsion layer was removed. We studied the spots obtained by reflection from the (420) plane of aluminum at an angle θ equal to 81°40'.

The small slit width and large specimen-to-film distance insured a high resolution (about 1'). It may be noted that with the usually employed photo-

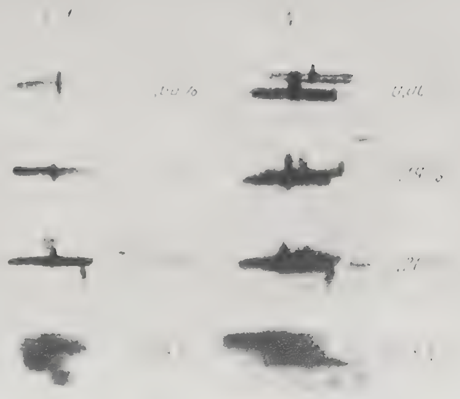

Fig. 1

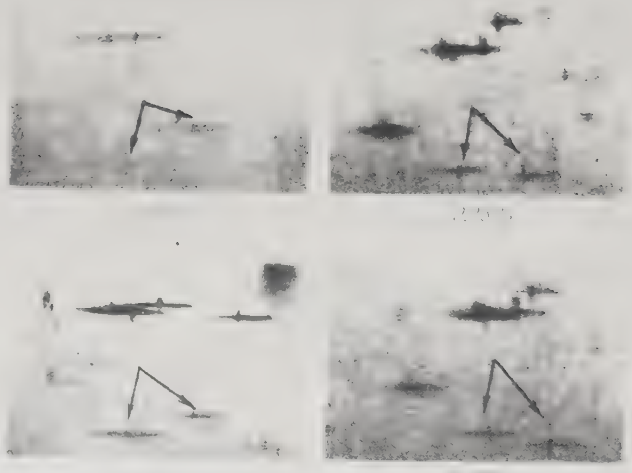

Fig. 2

0 hrs
150 hrs
N°1
1 hrs
660 hrs
N°2

Fig. 3

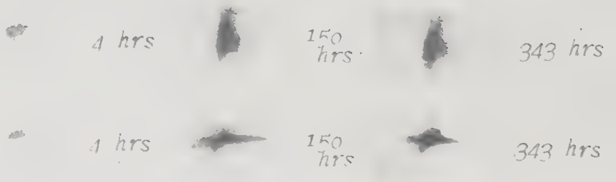
4 hrs
150 hrs
343 hrs
4 hrs
150 hrs
343 hrs

Fig. 4

Fig. 1. Changes in the structure of individual interference spots in the x-ray patterns of aluminum with increasing plastic deformation (magnification 4X).

Fig. 2. Changes in the structure of the interference spots with increasing plastic deformation. Arrows indicate relative displacement of two spots (magnification 3.5 X).

Fig. 3. Changes in the structure of interference spots in the patterns of aluminum in the process of creep at $\sigma = 1$ kg/mm^2 (magnification 4 X).

Fig. 4. Changes in the structure of two spots in the process of creep with $\sigma = 2$ kg/mm^2 (magnification 4 X).

graphic procedures the resolution varies between 30' and several degrees.

2. The x-ray patterns of the annealed aluminum specimen exhibited both simple and structured interference spots similar to those observed in the experiments of Ref. 1. The interference pattern changed discernibly incident to plastic deformation and creep.

Fig. 1 shows a typical sequence of changes in the structure of the interference spots on the x-ray patterns of polycrystalline aluminum samples stressed in simple tension. Interference spot No. 1 of an undeformed aluminum crystallite consists of two low intensity horizontal streaks intersected by two vertical streaks. The separation of the horizontal streaks is approximately 0.3 mm. This indicates that the crystallite in question consists of two blocks rotated approximately 5' relative to each other. At a deformation of 0.19% the spot is transformed into a continuous band and increases in intensity, which is indicative of fragmentation of the crystallite. The mosaicity angle is approximately the same in view of the fact that in the region of elastic deformation it decreased while in the region of plastic deformation it increased only to approximately the initial value.[3] The interference spots before and after deformation by 0.19% have a non-uniform intensity distribution over the length of the streaks: from left to right the intensity falls off. At a strain of 0.20% the distribution of intensity over the length of the spot becomes uniform. With further deformation of the specimen the interference spot broadens, the intensity at the edges decreases, while the integral intensity increases. At the strain of 0.23% the spot breaks up into streaks. With further deformation the number of streaks increases as does the distance between them and the general diffuseness of the spots. The angle of mosaicity at a strain of 0.29% attains 25-30', while the intensity at this strain is somewhat smaller than at 0.23%. The decrease in intensity is due to the fact that the true mosaicity angle is probably greater than the limiting angle of reflection defined by the geometry of the set-up.

The changes in the appearance of interference spot No. 1 are evidence of the breaking up of the crystallite into fragments and blocks, rotated a fraction of a minute (or in any case not more than 1-2') relative to their immediate neighbors, while the total angle of mosaicity is about 0°5'.

The sequence of changes in the case of spot No. 2 is analogous to that for spot No. 1. The detail shows that reflections of two individual crystallites each of which has a complex structure. The upper crystallite consists of two simple fragments or blocks, tipped to an angle of about 5' relative to each other, while the lower crystallite consists of several blocks tipped at angles of less than 1' relative to their neighbors and with a total mosaicity angle of about 5'. At a relative elongation of 0.19% there is obvious rotation of the structural elements inside the grain, just as in the case of spot No. 1. With further deformation, the interference spots diffuse due to fragmentation of the crystallite into blocks and the gradual increase in the angles between neighbors. At the same time there is some rotation of the crystallites themselves. The upper right spot in the pattern for the unstressed sample descends to the level of the left spot and virtually merges with it in an elongation of 0.20%; at a strain of 0.23% it is lower than the left spot and continues to descend further in the patterns for the samples elongated 0.34 and 0.48%. This rotation of one crystallite relative to the other is connected with their mutual displacement.

Mutual displacement is also clearly evinced by the shifting of the interference spots in the patterns of Fig. 2 (the spots indicated by arrows). Changes in the interference spots in this figure are similar to the changes described above.

Thus it will be seen that deformation leads to fragmentation of the crystallite substructure elements and their disorientation. In consequence the appearance of the interference spots becomes more complicated. At the same time in the process of plastic deformation the crystallites as a whole undergo rotation and displacement.

3. The changes occurring in the appearance of the interference spots in the process of creep are shown in Figs. 3 and 4. The initially sharp cruciform interference spot appearing in the first (before application of load) pattern at the end of 4 hours under load has separated into three streaks approximately 0.15 mm apart. Hence the crystallite has broken up into three fragments tipped about 2.5' relative to each other. With the lapse of time under load the number of substructure elements increases as does the angle between neighbors and the total angle of mosaicity: after 660 hours the mosaicity angle is at least 15'. Measurements of the intensity of the spots in successive photographs also bear witness to deterioration of the degree of perfection of the crystallite.

The disappearance of spots and the appearance of new ones on the successive patterns is due to changes in the degree of perfection of the crystallites.[3] Thus in the initial pattern of Fig. 3, there are three interference spots (one strong, two weak); after application of the load the two weak spots vanish. They have not reappeared in the pattern recorded 4 hours after application of the load but after 28 and 150 hours they gradually began to appear in diffused form. These spots become particularly noticeable 245 hours after the start of the test.

The pattern series Nos. 1 & 2 of Fig. 4 show two individual complex interference spots. Both the crystallites whose reflections form these spots are complex formations consisting of a number of blocks and fragments rotated relative to each other. In the process of the creep test the structure of the interference spots changes, which is indicative of changes in the orientation of the elements of the substructure in each crystallite. Spot No. 1 (Fig. 4) appeared in the x-ray pattern only after application of the load, while spot No.2 was present but was very diffuse and of low intensity before the beginning of the test. After application of the load spot No.2 became narrower and sharper. Both spots increased in intensity during the test. This is due to a decrease in extinction effect in consequence of fragmentation and a certain disorientation of the substructure elements.

The interference spots of a sample tested for creep under a load of 1 kg/mm^2 (Fig. 3) exhibit changes similar to those shown by the spots of the sample tested under a load of 2 kg/mm^2 (Fig. 4).

From the changes in the structure of the interference spots in patterns for aluminum samples tested under conditions of creep at room temperatures under tensile loads of 1 and 2 kg/mm^2 in the interval of elongation up to 0.23 and 0.71%, respectively, we can conclude that the structural changes occurring inside the crystallites in the process of creep are qualitatively analogous to the structural changes incident to simple elongation. Application of a load directly enhances the degree of perfection of the crystallite (in the elastic region), but then with time the elements of the crystallite substructure undergo disorientation, fragmentation and relative displacement. Thus the structure of the crystallites becomes more complex, the process as a whole being connected with the development of microstrains.[6,7] At the same time and independent of the structural changes occurring inside the crystallite, the crystallites themselves shift as a whole; this shifting process has the character of viscous flow over the grain boundaries.

Institute of Machine Design of the
Academy of Science of the USSR

References

1. B.M.Rovinski & L.M.Rybakova, Izv. AN SSSR, Ser. fiz., 15, 87 (1951).
2. B.M.Rovinski & L.M.Rybakova, Zhur. tekh. fiz., 24, 1069 (1954).
3. B.M.Rovinski, Zhur. tekh. fiz., 12, 679 (1942).
4. B.M.Rovinski, Izv. AN SSSR, Otd. tekh. nauk., No. 10, 64 (1942).
5. B.M.Rovinski & V.G.Liuttsau, Izv.AN SSSR,Otd.tekh.fiz., No.11,1618 (1953).
6. B.M.Rovinski & L.M.Rybakova, Izv.AN SSSR,Otd.tekh.nauk, No.10,1483 (1952).
7. B.M.Rovinski & L.M.Rybakova, Izv.AN SSSR,Otd.tekh.fiz., No.9,1241 (1953).

X-RAY INVESTIGATION OF RECRYSTALLIZATION OF SOME HIGH MELTING POINT COMPOUNDS

- S.S.Gorelik & Ia.S.Umanski

The increasing use of metallic compounds, in particular carbides, capable of withstanding high temperatures in engineering and technology makes the investigation of softening processes in such compounds extremely urgent. In the present investigation we studied the relaxation and recrystallization of the high-melting point compounds: tungsten carbide WC and the compound NiAl. (R.B. Gutman participated in the experimental work.)

The WC samples were prepared by compressing carbide powder into bars, 7 x 7 x 16 mm, which were then sintered for one hour at 1800°. After sintering the structure of the samples consisted primarily of large crystal grains (grain size 10^{-3}-10^{-4} cm). The spots on the x-ray patterns obtained in a standard camera by Fe Kα radiation were points, which substantiated the coarse-grained character of the original sintered material.

The NiAl powder was prepared by pulverizing the cast alloy to a particle size of 1-4 mμ. Chemical and x-ray analyses showed that the composition of the compound was close to equiatomic.

In view of the extreme brittleness of the investigated phases it was impossible to utilize conventional deformation methods (this is one of the major difficulties encountered in studying relaxation and recrystallization processes in metallic compounds). Hence we used the following methods of deformation which permit using x-ray analysis for investigating relaxation and recrystallization: the tungsten carbide specimens were subjected to surface hardening by grinding on an abrasive wheel; the NiAl powder was hardened directly in the process of grinding the alloy in a ball mill. The lines in the x-ray patterns of both compounds in a deformed state were diffuse.

The influence of different methods of deformation on the temperature of recrystallization was checked using iron. To this end we roentgenologically determined the temperature of the beginning of crystallization in Armco iron after different degrees of deformation by upsetting and after surface hardened by grinding on an abrasive disc.

The temperature of the beginning of recrystallization in the surface layers of iron subject to abrasion proved to be 525-550° (with one hour annealing time) and agreed with the temperature beginning of recrystallization in iron deformed by upsetting (60-70% deformation). In addition we determined the temperature of beginning of recrystallization in electrolytic iron powder work-hardened in a ball mill. This temperature proved to be 550-575°.

Thus these control tests showed that the deformation procedures we employed do give balues of the temperature of beginning of recrystallization approximately equivalent to those obtained with large degrees of deformation (~60%) attained by conventional methods.*

The deformed WC samples were annealed to temperatures of 1000° in a muffle furnace with a hydrogen atmosphere and to temperatures above 1000° in a Tamman graphite lined furnace. The temperature was measured by an optical pyrometer. The temperature fluctuations did not exceed ±15-20°. The samples were placed in a graphite boat and covered with granulated graphite to forestall interaction of the carbon of the carbides with hydrogen.

---

*Attempts to work-harden TiC and Fe_3C by abrasion of the surface layer did not yield positive results. The lines on the x-ray patterns of samples of these compounds after deformation by abrasion remained points just as in the patterns taken before deformation. Obviously, the abrasion method is inapplicable in cases when there is little resistance to tearing off of the surface layers.

The NiAl powder was annealed in a tubular resistance furnace. The temperature fluctuations in this furnace did not exceed ±10°. To prevent oxidation the powder was placed into quartz tubes evacuated to 10^{-2}mm Hg.

The temperature of the beginning of recrystallization was determined from the appearance of the first point interference maxima against the background of the continuous lines. In the case of the WC the photography was effected by Cu K radiation in a 57.3 mm diameter camera (60 kv, 20 ma, 45 min).

Tests showed that the use of these conditions in the case of NiAl is not expedient. Due to the large amount of aluminum with a low absorption coefficient, a large volume of metal participates in the reflection when copper radiation is used. This impairs the resolution so that the initial stage of recrystallization eludes detection. In the case of NiAl we, therefore, used Cr K radiation (35 kv, 10 ma, 5 hours) and a camera having a diameter of 86 mm. This made it possible to detect the first traces of recrystallization at an appreciably earlier stage of the process.

The data on the time of beginning of recrystallization in the process of isothermic annealing at different temperatures for WC and NiAl are listed in Table 1.

Table 1

Dependence of the time of beginning of recrystallization on the annealing temperature

WC	Annealing temperature, °C	1350	1400	1450	1500	1550
	Time of beginning of recrystallization, min	~1100	~40	~30	~10	~5
NiAl	Annealing temperature, °C	700	725	750	775	780
	Time of beginning of recrystallization, min	~60	~35	~15	~10	~4

These data are represented graphically in accompanying figure.

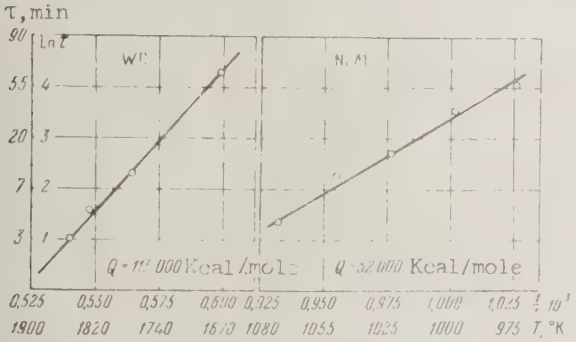

Dependence of the logarithm of time of beginning of recrystallization in WC and NiAl on the absolute temperature (or T^{-1}).

From this dependence of the time of beginning of recrystallization on the annealing temperature and on the basis of the assumption that the time of beginning of recrystallization is proportional to $e^{Q/RT}$ we can determine Q, the nominal* activation energy, by means of the formula

$$Q = \frac{\ln \tau_1 - \ln \tau_2}{1/T_2 - 1/T_1}$$

Calculations yielded a value of Q = 115,000 Kcal/mole for WC and Q = = 52,000 Kcal/mole for NiAl, which values are consistent with the other characteristics of the binding forces in these compounds.

Even in view of the admittedly inadequate accuracy with which the temperature of beginning of recrystallization was determined we can regard it as estab-

---

*Q cannot be regarded as the activation energy of the recrystallization process in the strictly physical sense. The significance of Q here is that it characterizes the temperature dependence of the rate of the process.

lished that the ratio T_{recry}/T_{melt} in the case of the investigated high-melting point compounds (Table 2) is higher than in the case of pure metals, for which as is known, this ratio has a value of 0.2-0.35.

Table 2

Melting points and the temperatures of the beginning of recrystallization for WC and NiAl

Compound	T_{melt}, °K	T_{recry}, °K	$\frac{T_{recry}}{T_{melt}}$
WC	2873	1648	0.57
NiAl	1912	973	0.51

*T_{recry} pertains to an annealing time of 1 hour.

In addition to the temperature of the beginning of recrystallization we also determined the temperature of beginning of intensive relaxation (relief of strains of the second kind) on the basis of the decrease in line breadth. In the case of WC we photometered the (112) line (Fe radiation) and in the case of NiAl the (211) line (radiation from Cr). It was established that, just as in pure metals, relaxation in the investigated metallic compounds begins at temperatures below the temperature of the beginning of recrystallization: in WC relaxation begins after annealing at 900° for 3 hours, while in NiAl it begins after 1 hour annealing at 500°.

"I.V.Stalin" Moscow Steel Institute

CHARACTERISTICS OF RECRYSTALLIZATION OF CERTAIN TWO-PHASE AGING ALLOYS

- S.S.Gorelik

Two processes occur in parallel during the heating of aging alloys following or coincident with their deformation: 1) partial or complete relief of the strains produced by the deformation (relaxation and recrystallization) and 2) decomposition of the supersaturated solid solution and separation of a second phase, usually accompanied by appreciable "phase cold-hardening".

The contribution of Iveronova[1] is virtually the only one in the literature devoted to the influence of decomposition of the solid solution on the recrystallization temperature. It was established in this investigation that the decomposition leads to an increase in the temperature of recrystallization as determined by x-ray analysis. Iveronova is of the opinion that this temperature increase is due to the relaxation of the deformation-induced strains which serve as the nuclei of recrystallization. The relaxation is particularly intense in the process of decomposition of a supersaturated solution or in the process of ascending diffusion.

In the present study we investigated the recrystallization in aging alloys of the Cu-Be system and in nichrome alloys of the following composition:

No. of alloy	Composition,%				No. of alloy	Composition,%	
	Ni	Cr	Al	Ti		Cu	Be
1	>99.0	-	-	-	4	99.8	-
2	Base	13.0	-	-	5	Base	0.54
3	"	13.8	2.18	2.4	6	"	1.05
					7	"	2.33

Alloys Nos. 3, 5, 6 and 7 are two-phase alloys. In the No. 3 alloy the excess phase consists of the compound $Ni_3(Al, Ti)$ with a face-centered cubic lattice, isomorphic with the basic solid solution; in the Nos. 5, 6 and 7 alloys the excess phase is the compound CuBe with a body-centered cubic lattice. The copper and its alloys were deformed by rolling at room temperature. Nickel and its alloys were deformed by upsetting, mainly in the hot state. The x-ray patterns were recorded by Fe Kα radiation in a 57.3 mm diameter camera and partly by Cu Kα radiation in a KROS camera with a flat cassette.

Fig. 1 shows the dependence of the temperature t_r^s of the start of recrystallization of the investigated alloys (as determined by the appearance of point spots on the x-ray pattern lines) on the degree of deformation.

Chromium which forms a solid solution with nickel, greatly increases its t_r^s. This is presumably due to the increase in the strength of the interatomic bonds in the solid solution lattice.[2]

Introduction of aluminum and titanium into the nichrome alloy or beryllium into copper in amounts producing dispersion hardening leads to further increase in the temperature of recrystallization. In the case of the CuBe alloys this increase rises with the beryllium content and the degree of supersaturation of the solid solution, which is in agreement with the data of Iveronova.

The ratio of the absolute temperature of recrystallization (T_r) to the absolute temperature of melting (T_m) in the case of alloys Nos. 3 & 7 attains a value of 0.6-0.65, which is appreciably higher than the values of this ratio for pure metal and one-phase solid solutions. If the abovementioned increases in t_r^s in aging alloys were caused by diffusion relaxation of strains due to decomposition of the solid solution, then in cases where such decomposition is obviated by preliminary aging, recrystallization should begin at a lower temperature. However, tests failed to substantiate this.

Samples of beryllium bronze containing 1.0 and 2.3% beryllium were subjected to deformation with subsequent annealing after preliminary aging at temperatures

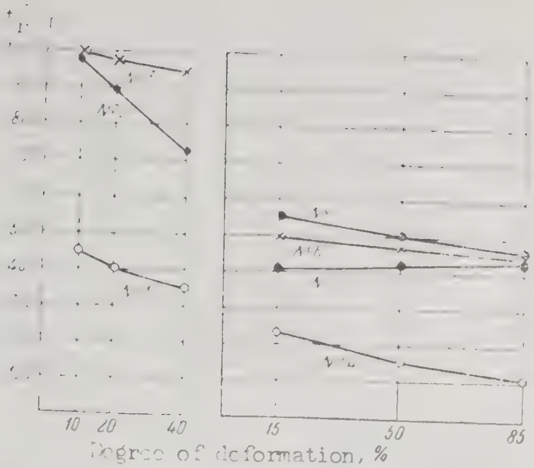

Fig. 1. Dependence of the temperature t_r^s of the start of recrystallization on the degree of deformation; at left- nickel base alloys; at right- copper base alloys. Numbers at curves correspond to alloy Nos. in the table above.

of 300-400°. In the case of the 2.3% beryllium alloy the first traces of recrystallization were detected in the x-ray patterns after 650° (annealing time τ 30 min) for the pre-aged sample as compared with 500° for samples not aged beforehand. After more prolonged annealing (2 hours and more) t_r^s proved to be approximately the same for both types of samples (Fig. 2).

Fig. 3 shows the variation of the hardness of the pre-aged and then deformed sample of the 2.3% beryllium alloy with the temperature of subsequent annealing. It was found that even after heating to 450° for 30 min the hardness became equal to that prior to deformation, i.e., the deformation hardening was removed at a temperature 150-200° lower than the temperature at which recrystallization becomes apparent on the x-ray patterns.

In order to enhance the resolution we photographed patterns by Cu Kα radiation on a flat film located at a distance of 35 mm from the sample with a 0.3 mm diaphragm. The pattern for a sample heated to 450° shows a clearly resolved doublet on the (222) line but the line remains continuous, without points (see Fig. 4).

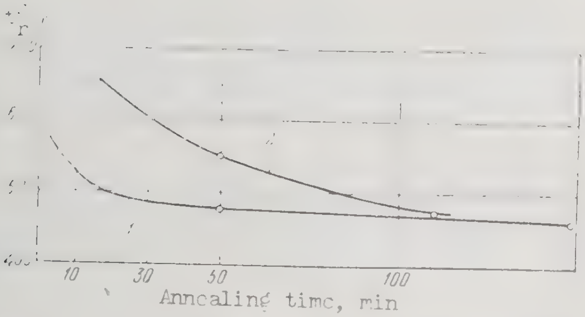

Fig. 2. Influence of preliminary (predeformation) aging on the variation of t_r^s of the Cu-Be (2.3% Be) alloy with the annealing time: 1) without preliminary aging, 2) with aging.

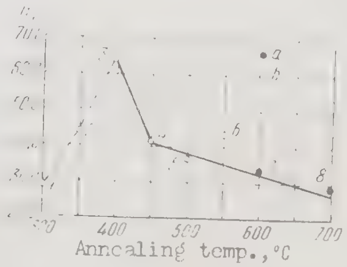

Fig. 3. Dependence of the hardness (1 kg load) of the 2.3% beryllium Cu-Be alloy at annealing temperature: 1) after hardening, 2) after aging, 3) after deformation, 4-8) after annealing; a - indications of recrystallization discernible on the x-ray pattern; b - no traces of recrystallization detected.

We believe this result can be interpreted in the sense that in the investigated alloys the factor retarding recrystallization is the second phase which separates out in large quantity during decomposition. Its retarding role probably consists in inhibiting the growth of recrystallization nuclei forming in the microvolumes, i.e., it holds back agglomerative recrystallization. The following fact also favors this hypothesis. It is known that increasing the degree of deformation generally leads to a reduction of the recrystallization temperature. However, in the No. 5 alloy containing 0.54% Be, we observed the opposite effect (Fig. 1): the values of t_r^s after compression by 15, 50 and 85% by rolling proved

to be 410, 425 and 435°, respectively. To explain this result, the microstructure of the No. 5 alloy sample was examined by means of an electron microscope. The structure of the sample deformed by 15 and 85% and then heated to 410° is shown in Fig. 5. The sample deformed by 15% proved to have a one-phase composition (Fig. 5,a), while in the case of deformation by 85% there is clearly discernible a second phase, segregated along the dislocation lines (Fig. 5, b). The presence of this second phase was probably the reason of retardation of recrystallization. Whether there was recrystallization in the regions of the solid solutions enclosed by the segregations of the second phase we could not establish since the dimensions of these regions average under 1 mμ and obtaining point x-ray patterns would require the use of special methods involving a resolving power appreciably greater than that of the procedures available to us.

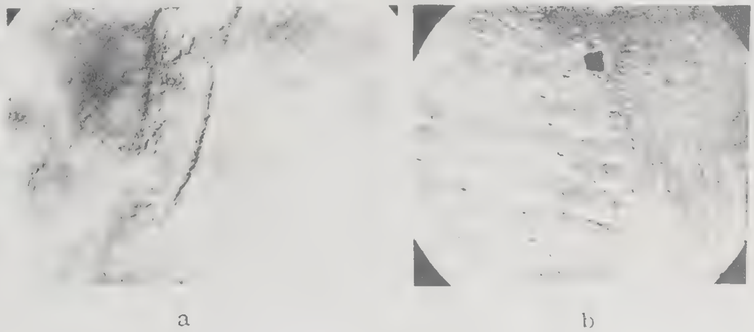

Fig. 4. X-ray pattern of the Cu-Be (2.3% Be) alloy; 50% deformation and annealing for 30 min at 450°.
Fig. 5. Electron microphotograph of Cu-Be (0.5% Be) alloy (magnification 9000 X): a - deformation 15%, b - deformation 85%.

The separation of a second phase with appreciable deformation of the alloy which in the equilibrium state at the given temperature is a one-phase system can be explained by ascending diffusion.[3] In this case increase in the annealing time should lead to solution of the segregated second phase, which is what we observed.

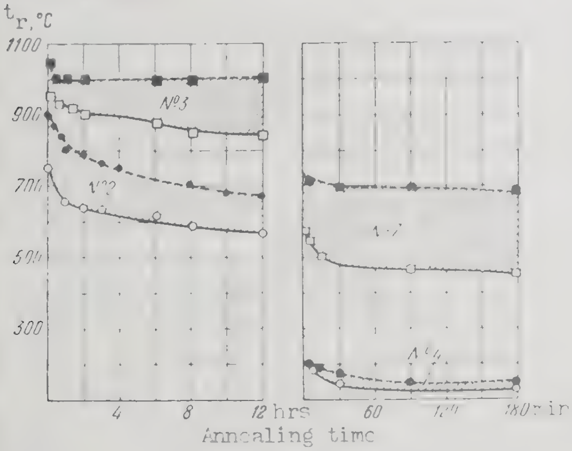

Fig. 6. Recrystallization intervals for copper (No. 4), nichrome (No.2) and aging alloys (Nos. 7 & 3). Dash lines - start of recrystallization; solid lines - end of recrystallization.

The retarding influence of the second phase is also evinced by the great increase in the time to complete recrystallization at annealing temperatures corresponding to the two-phase state of the alloy. The beginning and end of recrystallization* for Cu (No. 4), nichrome (alloy No. 2) and aging alloys based on them (Nos. 7 & 3) are shown in Fig. 6.

For pure copper and the single phase nichrome alloy the temperature t_r^e of the end of recrystallization, like that of the start of recrystallization, depends on the duration of annealing and goes down with the annealing time. In

---

*The end of recrystallization treatment was determined in two ways: from the disappearance of the background consisting of continuous interference lines and from the maximum of the number of point spots on the lines.

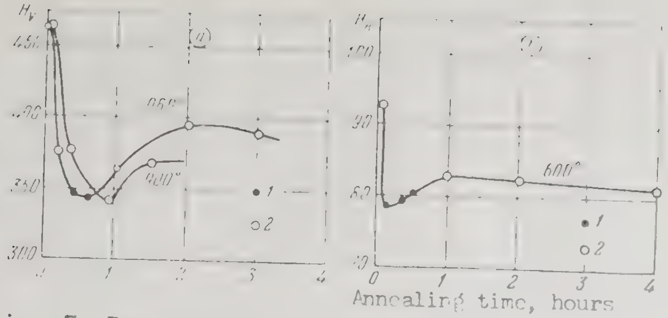

Fig. 7. Dependence of the hardness (with a 5 kg load) of cold deformed aging alloys on the duration and temperature of annealing: a) alloy No. 3, deformation 10%, b) alloy No. 7, deformation 50%; 1) indications of recrystallization detected in x-ray patterns, 2) no signs of recrystallization detected.

the case of the aging alloys t_r^e is virtually independent of the duration of annealing and is approximately equal to the temperature of the transition from the two-phase to the one-phase region. Thus the presence of the second phase even in a relatively small amount retards completion of the diffusion process of recrystallization. If this retardation already occurs at relatively high temperatures and low concentration of the second phase, it will be even more effective at lower temperatures corresponding to the beginning of recrystallization treatment and appreciably larger amounts and greater dispersion of the second phase.

* * *

Further, we established that the intensities of the parallel processes of aging and recrystallization (softening) differ, depending on the temperature of the isothermal annealing and the associated degree of supersaturation of the solid solution as well as on the degree of preceding deformation.

At relatively high annealing temperatures and corresponding low degrees of supersaturation, the softening (recrystallization) is more effective during the initial stage of isothermal annealing. A short term isothermal anneal noticeably reduces the hardness of the alloys (Fig. 7); the lines on the x-ray patterns are narrowed and new crystallization nuclei appear. There is some concurrent decomposition of the solid solution (as evinced by small changes in the period of the solid solution lattice), but the effect of this decomposition is masked by the influence of the reduction or removal of deformation-induced hardening.

Further increase in the annealing time and continuing decomposition of the solid solution stop the formation of new and the growth of earlier formed recrystallization nuclei. The phase hardening resulting from the difference in the specific volumes of the phases leads to an increase in the hardness of the alloy and diffusion of the interference spots associated with the earlier recrystallized volumes, or under certain conditions, to the complete disappearance of the spots.

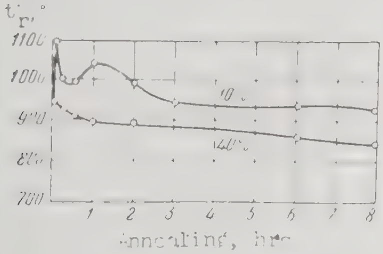

Fig. 8. Dependence of the temperature of the start of recrystallization for aging alloy No.3 on the duration of annealing and the magnitude of deformation.

Further increase in the duration of annealing leads to coagulation of the second phase, reduction of the alloy hardness, narrowing of the lines in the x-ray patterns and to the reappearance of indications of beginning recrystallization.

The above explains the anomalous changes in the temperature of the start of recrystallization as a function of the duration of annealing established for the No.3 nichrome base alloy (Fig. 8). The temperature of recrystallization in this alloy for samples deformed by 10% after annealing for 1 hour proved to be higher than after either 2 hours or 30 min annealing.

With decreasing annealing temperature the relative rates and effects of both processes change. At relatively low temperatures and correspondingly

high degree of supersaturation, aging proceeds at a higher rate and a greater amount of the second phase is segregated. The effect of stresses, developing due to decomposition at the initial stages of annealing, now exceeds the effect of reduction of deformation stresses. The hardness of the alloy quickly increases (Fig. 9). The segregation of the second phase inhibits recrystallization. We cannot yet say whether this inhibiting effect is manifested only in retarding the growth of recrystallization nuclei or in prevention of their formation due to the stability of the phase hardening at the given temperature and duration of annealing.

The rates of both processes are also influenced by the degree of deformation. Increasing the degree of compression in hot deformation has a stronger effect on acceleration of the decomposition process and tends to bring it to completion earlier. The temperature of beginning of recrystallization goes down with increasing degree of deformation to a lesser extent than in the case of pure metals or one-phase solid solutions (see Fig. 6).

Increasing the degree of reduction in thickness in cold rolling leads to the softening process becoming more intense during the initial stages of isothermal annealing (Fig 10).

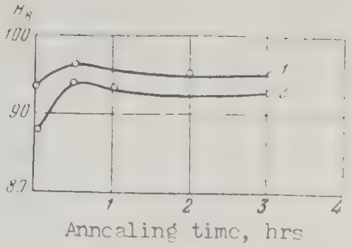

Fig. 9. Dependence of the hardness of deformed alloy No.7 on the duration of annealing: 1) 50% deformation, t = 400°; 2) 15% deformation, t = 450°.

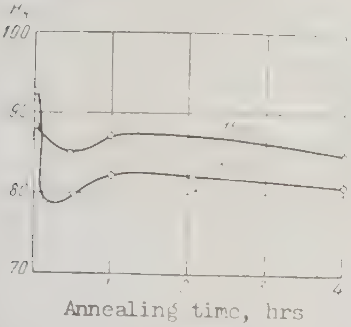

Fig. 10. Influence of the degree of cold deformation on the variation of the softening of aging alloy No.7 with the annealing time at 600° C.

"I.V.Stalin"
Moscow State Institute

References

1. V.I.Iveronova, In "Primenenie rentgenovykh luchei k issledovaniiu materialov" (Application of x-rays to the investigation of materials), L. 1949.
2. G.V.Kurdiumov & N.T.Travina, Doklady AN SSSR, 99, 177 (1954).
3. G.M.Rovenski, Trudy VIAM (Transactions of the All-Union Institute of Aviation Materials), M. 1946.

RESIDUAL CHANGES IN THE INTERPLANAR SPACING IN POLYCRYSTALLINE SPECIMENS AFTER PLASTIC DEFORMATION

- D.M.Vasil'ev & A.F.Erashov

The displacement of x-ray lines lying in the region of diffraction angles near 90° in samples plastically deformed by simple tension or compression was first discovered by Wood[1,2] and has since attracted the attention of many investigators. Analysis of the data in the literature[3-18] shows that to explain the effects occurring during the deformation in thickness of a specimen one must choose between the hypothesis regarding the influence of the anisotropy of the mechanical properties of crystallites and the selective character of diffraction of x-ray in polycrystalline specimens[3] and the hypothesis postulating the development of oriented microstrains[5,19].

The present investigation was undertaken for the purpose of evaluating the validity of these hypotheses and interpreting the observed effects.

We investigated samples of St.25 carbon steel; before cutting out the specimens, the steel billets were normalized with subsequent tempering at 680° followed by slow cooling for the purpose of removing all structural distortions.

For more thorough analysis of all the distortions introduced by plastic deformation we used the method of angular photographs which makes it possible to investigate the process of reflection of x-rays from the family of planes (hkl), forming different angles with the direction of plastic deformation. The angular registration procedure was used earlier[15,18] for flat samples, but led, in a number of cases, to great broadening of the x-ray lines and their displacement due to geometric effects. In order to avoid this we used cylindrical samples cut so that the axis of the cylinder would be perpendicular to the axis of plastic deformation. The specimens were brought to the desired 0.5 mm diameter by electrolytic etching which fully removed the possible structural distortions commonly connected with the mechanical process of machining thin cylinders.

The x-ray patterns were recorded in an axial camera with a sectioned semicircular cassette having provision for obtaining up to five patterns on one film strip. Each series of five patterns included one photograph of an annealed sample which served as the reference standard. The position of the lines was determined relative to the shadow thrown by a thin tungsten wire permanently attached to the screen covering the cassette.

The error in determining $\Delta d/d$ with reference to the strongly diffused lines (plastic deformation about 20%) amounted to $(5-7)\cdot 10^{-5}$ and was somewhat reduced for the less diffused lines (deformation $\sim$5%). An appropriate correction taking into account the apparent change in the interplanar spacing due to diffusion of the Kα-doublet with increasing plastic deformation was made in the experimentally determined values of $\Delta d/d$. The requisite correction was computed according to the formula

$$\Delta(\Delta d/d) = U(\Delta\lambda/\lambda),$$

where $\Delta\lambda$ is the difference between the wave length of the Kα-doublet components and U is a factor characterizing the degree of interaction of the Kα-doublet components (the method of determining this factor is described in Ref. 20). The width of the Kα-doublet components was also determined by the procedure described in Ref. 21.

The dependence $\Delta d/d = f(\psi)$, where ψ is the angle between the reflecting plane and the axis of deformation (Fig. 1), was investigated on samples subjected to preliminary plastic deformations of 0.6, 2.4, 4.9, 9.3 and 14% elongation and 6.4 and 19% compression. In all cases we investigated the positions of the (310) line (Co Kα radiation); in addition, for the samples subjected to 4.9% plastic elongation, we investigated the (220) line. In this case we used the combined

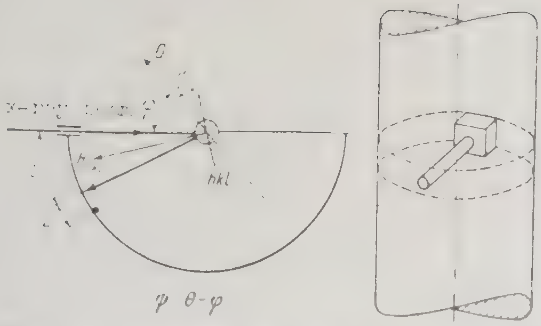

Fig. 1. Diagram of x-ray camera set-up and method of cutting out the samples: ψ - angle between reflecting plane and axis of deformation, θ - Bragg angle, 0 - axis of deformation.

Co-Fe Kα radiation obtained by means of a demountable ion tube with a Co-Fe (60:40) alloy anode.

Each value of Δd/d used for plotting the curves was taken as the average of two values: one corresponding to the given angle ψ and the other corresponding to the angle ψ+180°.

This procedure fully eliminated the possible influence of eccentricity of the sample axis relative to the axis of rotation.

As was noted above, the x-ray specimens had a diameter of 0.5 mm while the initial diameter of the elongated specimen was 14 mm. Obviously the displacement of the lines in the x-ray patterns could be due only to changes occurring in the inner layers of the original specimen (i.e., not at the surface). Thus our procedure fully excluded the influence on the position of the lines of any stresses of the first kind that might have developed in consequence of bending of the specimen during deformation.

The principle experimental data on the dependence Δd/d = *f*(ψ) are shown in Figs. 2 & 3.

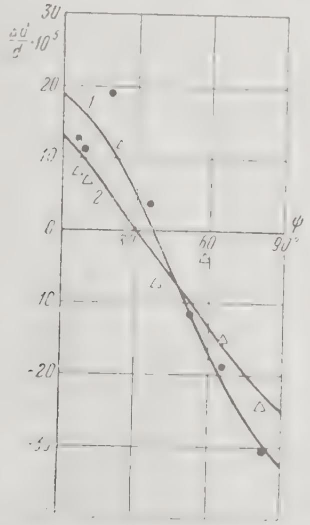

Fig. 2

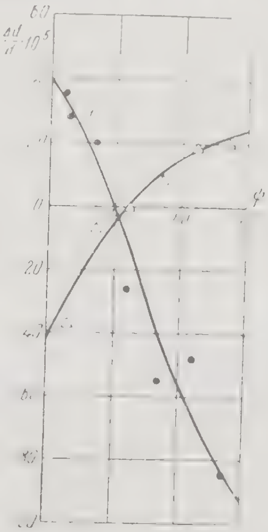

Fig. 3

Fig. 2. Dependence of the relative change in interplanar spacing on the angle between the reflecting plane and the axis of deformation and on the amount of deformation: 1 - (310) line obtained by Co Kα radiation; 0.6% elongation; 2 - same line; 2.4% elongation.

Fig. 3. Same as Fig. 2 but: 1 - 14% elongation; 2 - 19% deformation under compression.

It should be noted that the general character of the dependence Δd/d = *f*(ψ) changes little in going from small to large degrees of plastic deformation. As may be seen from Fig. 4 there is a clear tendency to a monotonous increase in the absolute value of Δd/d with increasing deformation both for ψ = 0° and for ψ = 90°, together with a gradual reduction in the rate of increase of Δd/d. The experimental data graphed in Figs. 2-4 do not agree even qualitatively with the

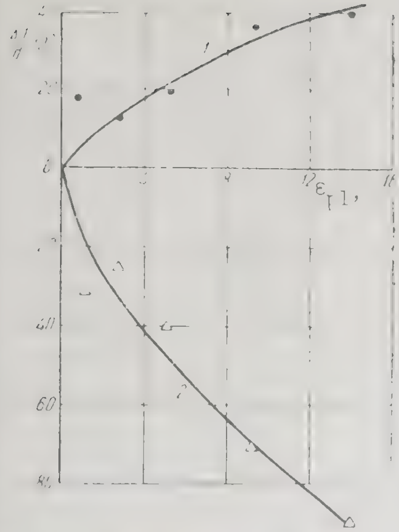

Fig. 4. Dependence of a relative change in the interplanar spacing on the magnitude of the plastic deformation and the angle (elongation, (310) line): 1 - $\psi = 0^{\circ}$, 2 - $\psi = 90^{\circ}$.

theoretical curves computed after Greenough in Ref. 18: the experimental dependence $\Delta d/d = f(\psi)$ is entirely different from the theoretical.

Thus the assertion made in Ref. 18 that Greenough's hypothesis in general correctly describes the nature of the effect is not supported by the facts; a different explanation must be sought at least where specimens of soft steel are concerned.

It can readily be shown that curves similar to those shown in Figs. 2-4 are obtained in the case when there obtains in the specimen after plastic deformation a homogeneous stressed state with principal axis σ_1, σ_2, and σ_3. If σ_1 is directed along the axis of preliminary plastic deformation, obviously $\sigma_2 = \sigma_3$.

Analysis of the curves in Figs. 2-4 shows, first, $|\sigma_1| > |\sigma_2|$ and, second, that $\sigma_1/\varepsilon_{pl} < 0$, so that after preliminary elongation the greatest principal stress acting along the axis of preliminary plastic deformation will be compressive, while that after preliminary compression will be tensile.

In what manner could there develop in the samples a stressed state characterized by the curves of Figs. 2 and 3? Formally, the displacement of the x-ray lines can be explained by the effect of residual macrostresses (residual stresses of the first kind). However, where a specimen not subject to an external load is concerned, it is difficult to conceive of the existence of an equilibrium system of mutually balancing macrostresses, similar to that described above. We can only assume that there exists in the specimen a system of oriented macrostresses (residual stresses of the second kind) acting on the regions of the specimen participating in the formation of the diffraction pattern. This would support the hypothesis advanced in Ref. 5.

In a carbon steel specimen, this system of oriented macrostrains should be balanced by virtue of the presence of regions not participating in the creation of the x-ray lines of ferrite but playing the part of a rigid skeleton and absorbing stresses opposite in sign to those acting on the ferrite.

Such regions can be either cementite grains or nitrides and oxides or transition regions between grains or, finally, parts of crystallites concentrated in the vicinity of slip interfaces, the structure of which is so distorted that they do not participate in the coherent scattering but only increase the background intensity.

While the final choice between the alternative hypotheses can be made only after further experiments, it may be noted that one of the present authors came to the conclusion in Ref. 19 that there exist in plastically deformed carbon steels oriented macrostrains and a rigid skeleton on the basis of an investigation of the aftereffects in deformed samples at elevated temperatures. It was shown in that study by means of dilatometric measurements that plastically stretched low-carbon steel specimens yield a residual increase in length when heated; the results of such experiments with the type of steel employed in the present investigation are shown in Fig. 5. It will be seen readily that the relative residual deformation ε^* obtained in heating to 650° is in close agreement with that measured by means of x-rays.

Comparison of the data obtained from the dilatometric experiments with the results of direct measurements of the changes in volume of specimens during

heating after plastic deformation leads to the conclusion that there develop in a plastically deformed sample oriented microstresses with the result that there act on the ferrite grains stresses, the direction of which is opposite to that of the direction of the preliminary plastic deformation.

These considerations are fully substantiated by the x-ray data obtained in the present investigation.

Thus it may be assumed that at least where carbon steel is concerned the currently accepted concepts regarding the character of microstresses developing after plastic deformation must be somewhat modified: in addition to the disoriented microstresses, responsible for the broadening of the x-ray lines, there apparently also develop microstresses oriented in a definite manner relative to the axis of deformation; these microstresses produce not broadening but displacement of the x-ray lines, which increases with the degree of plastic deformation.

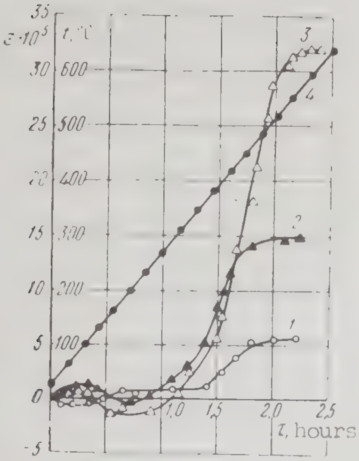

Fig. 5. Dependence of the relative residual strain $\varepsilon^* = \Delta l^*/l$ on the duration of heating of the specimen after work hardening by elongation: 1) 0.4%, 2) 1.4%, 3) 19.3%; 4) rate of temperature change in the dilatometric experiments.

In general, it may be assumed that these oriented microstresses form after plastic deformation whenever there exist in a specimen, in addition to "soft" regions, more "rigid" regions playing the part of a "rigid skeleton". If this assumption is valid, oriented microstresses should be observed not only in carbon steel but in other materials as well.

As the result of our investigation and that of Ref. 22 show, residual changes in the interplanar spacing are manifested in soft steel both after very small plastic deformations (0.6%) and after the material is subjected to a stress not exceeding the macroscopic elastic limit. This gives us reason to assume that the oriented microstresses must play a significant part in processes associated with imperfect elasticity.

From the practical standpoint it may be noted that in x-ray determinations of the residual macrostresses in deformed specimens by the method of oblique angle registration the influence of the effect examined in the present investigation can be taken into account.[23] In more complex cases making the requisite correction becomes difficult since, in addition to knowing the directions of the principal axes of deformation and its magnitude, one must also have evidence of the applicability of the principle of superposition where the microstresses are concerned. Yet the error involved in not taking into account the correction may attain several tens of kilograms per mm^2.

After completion of the outlined experiments we read the contribution of Hauk[24] in which, on the basis of studies of flat specimens by the method of oblique angle registration, he concludes that there exist oriented microstresses in carbon steel and repudiates his former view regarding the validity of Greenough's hypothesis.

The authors desire to thank N.N.Davidenkov for his interest in the investigation.

Leningrad Institute of Railway Transport Engineers

References

1. W.Wood, Phil. Mag., 18, 495 (1934).
2. W.Wood, Phil. Mag., 19, 219 (1935).
3. G.Greenough, Proc. Roy. Soc., A 197, 556 (1949).
4. N.Davidenkov, Zhur. tekh. fiz., 14, 9 (1944).
5. B.Rovinski, Zhur. tekh. fiz., 21, 11 (1951).
6. B.Rovinski, Zhur. tekh. fiz., 17, 10 (1947).
7. G.Greenough & J.Auld, Acta Metall., 2, 209 (1954).
8. L.Glikman, G.Sanfirova & V.Stepanov, Zhur. tekh. fiz., 19, 3 (1949).
9. N.Davidenkov & E.Assur, in "Primenenie rentgenovskikh luchei k issledovaniiu materialov" (Application of x-rays to the investigation of materials)M.1946.
10. G.Greenough, J. Iron & Steel Inst., 169, 235 (1951).
11. N.Davidenkov & M.Timofeeva, Zhur. tekh. fiz., 16, 3 (1946).
12. W.Wood & S.Smith, Proc. Roy. Soc., A 182, 404 (1944).
13. B.Rovinski, Zhur. tekh. fiz., 20, 12 (1950).
14. B.Rovinski & N.Tyzhnova, Zhur. tekh. fiz., 20, 676 (1950).
15. V.Hauk, Naturwiss., 40, 19 (1953).
16. S.Stepkin & L.Kharson, Sb. LIIZhT (Collected Publications, Leningrad Institute of Railway Transport Engineers) 146, 221 (1954).
17. L.Reimer, ZS. angew. Phys., 6, 11 (1954).
18. E.Kappler & L.Reimer, ZS. angew. Phys., 5, 11 (1953).
19. D.Vasil'ev, Dissertation, Leningrad Pedagogical Inst., L. 1951.
20. D.Vasil'ev & Z.Vashchenko, Zhur. tekh. fiz., 25, 4 (1955).
21. V.Vasil'ev, Zhur. tekh. fiz., 25, 11 (1955).
22. R.Garrod, Nature, 165, 241 (1950).
23. E.Kappler & L.Reimer, Naturwiss., 41, 60 (1954).
24. V.Hauk, ZS. f. Metallk., 45, 33 (1955).

X-RAY INVESTIGATION OF PLASTIC DEFORMATION OF METALS UNDER STATIC AND DYNAMIC COMPRESSION

- T.N.Smirnova & Iu.S.Terminasov

Roentgenographic studies of the mechanism of distortion of the atomic crystal lattice of metals subject to deformation under static and dynamic compressive loads carried out by one of the present authors in collaboration with Davidenkov[1] and Gasilova[2] showed that the course of the distortion process differs depending on the rate of deformation. The present investigation is a continuation of these studies.

Experimental Procedure

The investigations were carried out on samples of St.2 and U8 (Y8) steel, commercial grade iron and aluminum. The samples were made in the form of cylinders (15 mm in diameter and 25 mm high). Lines dividing the cylinder into ten equal sections in length were scribed on the sides of the samples.

The specimens were tempered in a vacuum furnace to relieve the work hardening due to fabrication. The iron and steel samples were heated for 1.5-2 hours at 700°; the aluminum specimens, for 1.5 hours at 350°. Slow cooling was assured in all cases by allowing the specimens to cool with the furnace.

The investigated specimens were subjected to static and dynamic compression.

The static deformation was effected on presses: a 60 ton Amsler and a 35 ton Universal press. All the samples except the aluminum ones were subjected to dynamic deformation on a high speed impact machine (pneumatic hammer) designed by Davidenkov, Noskin et al; the rate of deformation attained 120 meters per sec. The deformation was effected by means of blows of the hammer head ejected from the cylinders of the machine at high speed by compressed air. The rate of deformation was assumed to be equal to the speed of the hammer head at the instant of impact.

Under static compression the specimens acquired a symmetric barrel shape. The sections subjected to the greatest longitudinal deformation were the layers adjacent to the end faces. In contrast the specimens deformed dynamically at high speed (about 100 m/sec) were characterized by an asymmetric shape. Commonly in the dynamically deformed samples the zone of maximum convexity was displaced downward (away from the point of hammer impact). At even higher rates of deformation there occurred on the impact side a thickening of the layers adjacent to the end face and the appearance of an incipient zone of minimal deformation between the region near the end surface receiving the impact and the region of maximum lateral bulging, while the sample in general assumed a mushroom shape. The difference in the distribution of deformation in specimens deformed dynamically as compared with those deformed statically is explained by an inertia effect stemming from the inertial resistance of metals.

During compression by impact there was appreciable heating of the samples: at very large deformations temper colors were discernible on the end faces of the samples.

The aluminum specimens were deformed dynamically on an Amsler drop hammer with the specimen held stationary; the weight of the hammer head was 35.2 kg; the maximum drop height was 4 meters. The terminal velocity of the head was computed according to the theoretical formula for free fall; this was also assumed to be the rate of deformation.

The distance between the lines scribed on the sides of the cylinders was measured both before and after deformation by means of a gaging microscope to within 0.01 mm. Thus the degree of deformation was determined separately for each section of the specimen.

The residual distortions of the atomic lattice were studied by the x-ray

method of back-reflection. The usual flat cassette was replaced by a cylindrical cassette designed by one of the authors which had provision for obtaining 11 patterns on one film strip. A special collimator with two 0.6 mm aperture diaphragms was employed in the photography so that the sample was irradiated by a narrow, virtually parallel beam of x-rays. The specimens were rotated during exposure to the Kα radiation of Co.

During the entire investigation all the experimental conditions and factors (operating regime of the x-ray tube, diaphragm to sample distance, processing of the films, etc.) were maintained rigorously constant. X-ray patterns recorded of the different sections of the deformed specimen as well as of the undeformed samples. The x-ray patterns of the annealed non-deformed samples consist of sharp lines with a well defined Kα doublet.

In our work it was essential to obtain two interference lines simultaneously. For the iron and steel samples we obtained the (310) and (220) interference lines. The distance between the film and the sample was 45 mm. Under these conditions the (310) interference line was recorded on flat film while the (220) line was registered on the cylindrical film. In the case of the aluminum samples we recorded the (420) and (331) interference lines. With the same film to sample distance (45 mm) both lines were located in the same plane.

The Kα doublet on the patterns obtained for deformed specimens appears in the form of diffuse interference lines. The greater the degree of deformation of the metal, the greater the diffusion of the lines and the lower their intensity.

The resultant x-ray patterns were photometered on an MF-2 microphotometer. The line width and the areas of the microphotograms were carefully measured on all the patterns to determine the crystallite and elementary distortions of the atomic lattice.

Experimental results

The residual distortions of the crystallites were determined from the width of the interference maxima; the residual elementary distortions of the lattice were found from the ratio of the areas under the photometric curves characterizing the interference lines. The experimental results are shown in accompanying figures. The curves characterizing the change in the crystallite distortions are given in the form of dependence of the line width ΔS on the degree of deformation Δh/h (in percent) of the individual layers. The curves characterizing the changes in the elementary distortions of the crystal lattice are given in the form of the dependence of the intensity ratio of the two interference lines on the degree of deformation.

Aluminum samples. As may be seen from Fig. 1, the width of the interference lines (420) and (331) increases rapidly to a limiting value at about 30% deformation for both static and dynamic compression.

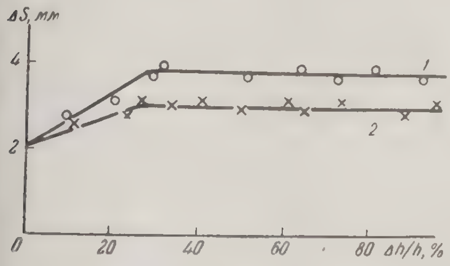

Fig. 1. Dependence of the width of the Kα doublet on the degree of deformation for Al: 1) static deformation, 2) dynamic deformation.

Further deformation of the aluminum specimen produces no additional increase in the width of the interference lines (the curve becomes a straight line parallel to the horizontal axis). Hence we see that the residual distortions of the crystal lattice after having attained a maximum value at about 30% residual deformation increase no further; consequently the process of further deformation of the metal cannot be explained through these distortions.

Comparing the curves for the dependence of the line width on the degree of deformation with static and dynamic compression we see that the curve pertaining to the case of static de-

formation lies entirely above the corresponding dynamic deformation curve.

The maximum width of the interference line for static deformation exceeds the line width in the pattern for the undeformed (annealed) specimen by 94%. In contrast in the case of dynamic deformation this increase in line width amounts to only about 40%. It will be seen from Fig. 1 that the crystallite distortions developing in the metal under dynamic deformation are some 24% smaller than those developing under static deformation. The reasons for this will be suggested below.

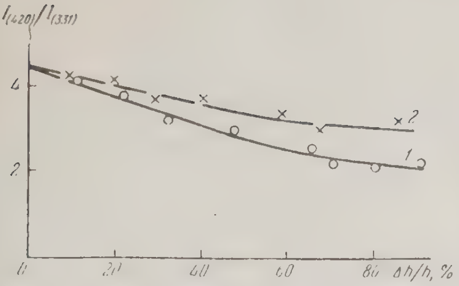

Fig. 2. Dependence of the ratio of the line intensity on the degree of deformation for Al: 1) static deformation, 2) dynamic deformation.

The results of the x-ray determination of the residual distortions of the crystal lattice (elementary distortions) in the statically and dynamically deformed specimens are plotted in Fig. 2.

It will be seen that the elementary distortions of the crystal lattice attain an appreciable magnitude and continue to rise up to 60% deformation, after which their magnitude remains fairly constant. In the case of static deformation the ratio of the interference line intensities I_{420}/I_{331} changed by 40% relative to the initial value for an undeformed specimen. In the case of dynamic deformation the maximum change in the ratio of the intensities is 29% lower than in the case of static deformation. Consequently in aluminum specimens the crystallite distortions and the elementary distortions of the crystal lattice are both smaller in the case of dynamic, as compared with static, deformation.

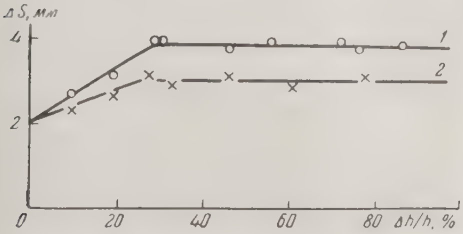

Fig. 3. Dependence of the line width of the Kα doublet on the degree of deformation for St.2 steel: 1) static deformation, 2) dynamic deformation.

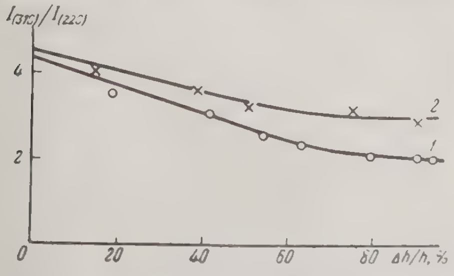

Fig. 4. Dependence of the line intensity ratio on the degree of deformation for St.2 steel: 1) static deformation, 2) dynamic deformation.

St.2 grade steel. Fig. 3 shows the dependence of the interference line width on the degree of deformation for St.2 steel. The crystallite distortions increase up to about 30% deformation, after which point they remain virtually constant. The limiting value of the interference line width exceeds the initial width (for an undeformed specimen) by 110% in the case of static deformation and by only about 56% in the case of dynamic deformation. With dynamic deformation the crystallite distortions are some 26% lower than with static deformation and stabilization of their magnitude begins somewhat earlier (from 25% deformation).

The dependence of the ratio of the interference line intensities I_{310}/I_{220} on the degree of deformation with static and dynamic deformation is shown in Fig. 4. The ratio of the line intensities in the case of static deformation decreases continuously (i.e., the elementary distortions of the crystal lattice increase) to 84% deformation, changing by 53% relative to the initial value. In the case of dynamic deformation the stabilization of the distortions of the crystal lattice begins earlier (from 65% deformation) and

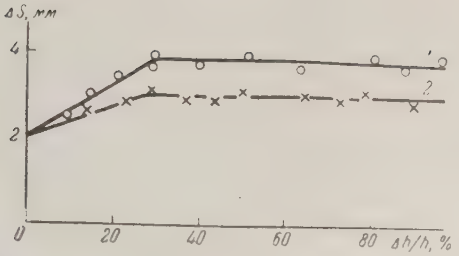

Fig. 5. Dependence of the line width of the Kα doublet on the degree of deformation for U8 steel: 1) static deformation, 2) dynamic deformation.

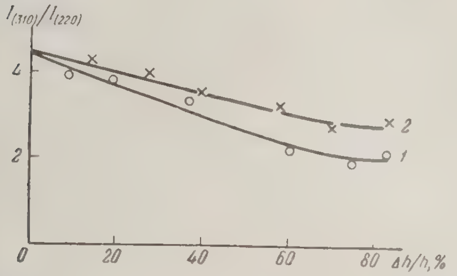

Fig. 6. Dependence of the line intensity ratio on the degree of deformation for U8 steel: 1) static deformation, 2) dynamic deformation.

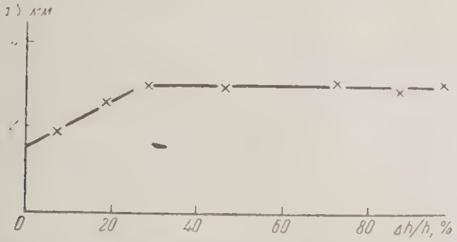

Fig. 7. Dependence of the line width of the Kα doublet on the degree of deformation for dynamically deformed iron.

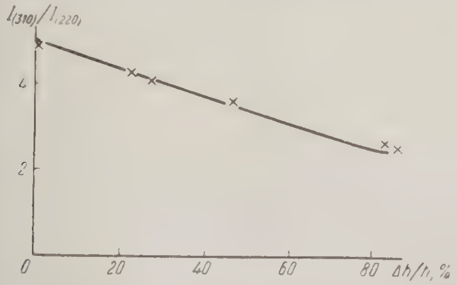

Fig. 8. Dependence of the line intensity ratio on the degree of deformation for dynamically deformed iron.

the stable value of the distortions is some 10% lower than for the case of static deformation.

U8 steel. Fig. 5 shows the dependence of the variation in interference line width on the degree of deformation of U8 steel. It will be seen that the crystallite distortions increase with deformation at low values of the deformation, but beginning with 30-40% deformation tends to stabilize. In the case of static deformation the width of the interference line is some 90% greater than that of the initial line, while in the case of dynamic deformation the increase amounts to only about 50%. It will be seen that the curve for static deformation lies entirely above the curve for dynamic compression and that the maximum value of the line width in the former case is some 26% greater than the maximum value in the latter case.

The dependence of the ratio of I_{310}/I_{220} on the degree of deformation is shown in Fig. 6. It will be seen that at first the ratio decreases in proportion to the degree of deformation and that beginning with about 70% deformation it tends to become stable. The value of this stable ratio for static deformation is 55% under that for the initial state; the corresponding decrease with dynamic deformation is 38%.

The stable ratio with dynamic deformation is 30% higher than the value with static deformation. This indicates that the elementary distortions of the crystal lattice are smaller under dynamic deformation.

Commercial grade iron. The interference line width and intensity ratio curves for dynamically deformed iron are shown in Figs. 7 and 8.

These curves are essentially similar to those given above for steel. The increase in the width of the interference line ceases at about 30% deformation, at which point the width stabilizes at about 175% of the initial value. The ratio of the line intensities also falls off to about 70% deformation. The minimal, stable value of this ratio is 44% lower than the initial value.

One can draw certain general conclusions from the cited results. Thus, it becomes clear that with static deformation the residual distortions increase only up to about 30% deformation; further increase in the static load results in no

further increase of the residual distortions. Hence all microdistortions in the crystallites cease at the indicated deformation and no further microstrains are produced by increasing the external load. Under dynamic deformation, also, there is a limit to the growth of the residual distortions in the crystallite; the growth limit in this case varies between the limits of 25 and 40% residual deformation in different metals. Thus we have shown that the breakdown of metals and alloys cannot be explained directly in terms of distortions of the crystallites. At the same time these distortions create the necessary conditions for the development of distortions of the atomic crystal lattice, the distortions which are largely responsible for the rupture and breakdown of metals. If we compare the maximum diffusion of the interference lines on the x-ray pattern obtained for statically and dynamically deformed samples, we readily note that with dynamic deformation the limiting broadening of the interference lines is some 25-30% less than in the case of static deformation. Consequently with dynamic deformation the crystallite distortions never (even at the greatest degrees of deformation) reach such large values as in the case of static deformation.

This difference can be explained by "thermal relaxation". During the short time of the impact the heat generated and concentrated in the areas of deformation (along the slip planes) cannot be conducted away and hence is expended on partial relief of the distortions arising in the process of deformation. Thus there occurs a unique thermal relaxation of the deformed metal which results in partial removal of the crystallite distortions.

In contrast, in the case of static deformation, which occurs over a longer period of time, the heat generated along the slip planes is easily dissipated so that little or no thermal relaxation occurs.

The elementary distortions of the crystal lattice continue to develop even after cessation of the growth of the crystallite distortions and their stabilization begins only at comparatively great degrees of deformation: in the case of static deformation at about 50-80% and in the case of dynamic deformation at about 50-70% deformation.

It should be noted that the growth of the elementary distortions of the crystal lattice ceases long before destruction of the metal; their stabilization begins when the external deformation is still increasing. Comparison of the rates of growth of the residual distortions of the crystal lattice with static and dynamic deformation for all the investigated metals shows that with dynamic deformation the magnitude of the residual distortions of the crystal lattice is smaller than with static deformation. This result can also be explained by the influence of thermal relaxation. The heat concentrated along the slip planes in the samples deformed by impact inhibits the development of stable distortions of the crystal lattice. The temperature rise in samples subjected to dynamic deformation is substantiated by a number of investigations. Consequently with dynamic deformation there can never be reached the same degree of distortion of the atomic crystal lattice as with static deformation. This fact is of great practical importance.

Conclusions

One can draw the following conclusions on the basis of our extensive experimental material and the deduced regularities characterizing the residual distortions developing in specimens subjected to static and dynamic deformations.

1. Comparison of the curves characterizing the dependence of the residual distortions on the degree of deformation shows that in the case of static deformation the residual distortions both of the crystallite and of the atomic crystal lattice are greater than in the case of dynamic deformation.

2. The lower value of the residual distortions in the case of dynamic deformation may be interpreted as the result of unique "thermal relaxation". In this case, in view of the short period of impact, the generated heat does not have time to dissipate and is expended on relaxation of the deformed metal. In the

case of static deformation, the effect of thermal relaxation is appreciably smaller and the residual distortions attain a larger value.

3. Since the residual distortions of the crystal lattice stop growing long before rupture of the deformed specimen, one cannot regard these distortions as the direct cause of failure of the metal, although they do predispose the metal to failure in so far as they weaken the intercrystalline bonds in the deformed specimen.

"V.M.Molotov" Leningrad Engineering-Economic Institute

References

1. N.N.Davidenkov & Iu.S.Terminasov, Zhur. tekh. fiz., 7-8, 14 (1944).
2. Iu.S.Terminosov & E.B.Gasilova, in "Primenenie rentgenovskikh luchei k issledovaniiu materialov" (Application of x-rays to the investigation of materials.) L. 1945.

X-RAY INVESTIGATION OF EFFECTS ACCOMPANYING PROLONGED EXTENSION OF STEEL AT ELEVATED TEMPERATURES

- M.Ia.Fuks, N.V.Slonovski & L.I.Lupilov

In this investigation we determined microstrains ($\Delta d/d$) and block size in steel stretched to fracture at 20, 300 and 500° under conditions of short-term (i.e., as ordinarily applied on tensile testing machines) and prolonged application of the load (100-200 hours on IP-2 creep test machines). Previously, for the same steel and using the same techniques, an investigation was made of the fracture of specimens subjected to rupture by impact.[1] Thereby it became possible to appraise the importance of microstrain formation and of block fragmentation in predisposing the metal to fracture under various deformation conditions: room temperature and 500°, impact, static and prolonged loading, etc. The investigation of Ref. 2 also forms a part of this series of studies. Similar effects were investigated on the basis of the appearance of spots on x-ray patterns by Wood[3] and Greenough & Smith[4].

It was of interest to clarify what indications on x-ray patterns accompany the reduction in the strength of steel under prolonged loading at stresses above the yield point.

Materials and Procedure

The principal measurements were made on forged 35 KhNM (35 ХНМ) steel; certain additional measurements were made on St. 20 steel. Flat specimens of special shape were prepared for the tests. The average rate of relative elongation was varied from 4 to 0.005% per minute.

The x-ray patterns were recorded without rotation in a 57.3 mm diameter cylindrical camera by Fe radiation and also on flat films by back-reflection using the radiation from Cr and Co. The lines on the patterns of the 35 KhNM steel were continuous.

The influence of geometric conditions was taken into account and the effects of dispersion and microstrains were separated by three methods: a) that of Dehlinger and Kochendorfer[5], b) that of Kurdiumova and Lysak[6], c) harmonic analysis of the intensity curves[7].

Results and Discussion

Carbon Steel. There is correlation between the relative positions of the curves in Fig. 1 and the variation of the mechanical properties of St. 20 steel at elevated temperatures[8].

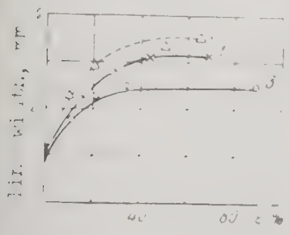

Fig. 1. Dependence of width of the (310) line on the relative deformation ε and the temperature of deformation (short-term tensile loading) of carbon steel: 1) 20°, 2) 300°, 3) 500°.

At 300° the ultimate strength is greater, while the elongation and compression are smaller, than at 20 and 500°. This indicates a greater increase in strength and great structural dislocations. However, even at 500°, a sufficiently high temperature for development of relaxation in carbon steel, short-term elongation results in a noticeable broadening of interference lines. Increasing the duration of loading to some 200 hours at 300° does not lead to marked changes in the patterns as compared with those for short-term loading.

In specimens deformed at 500° for 104 hours, sharp splitting of the doublet was observed all the way to elongations $\varepsilon = 100\%$. Only at $\varepsilon \doteq 130\%$ was weak washing-out of the doublet lines observed. Hence, prolonged deformation of carbon steel at 500° is significantly different from short-term elongation at the same temperature; fragmentation of blocks and microstrains develop only very weakly.

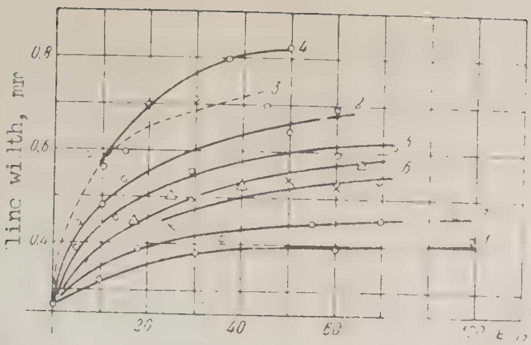

Fig. 2. Dependence of the width of the (220) line on the deformation ε and the temperature of deformation for 35KhNM Steel: 1-4) short-term loading (1 - at 600°, 2 - at 500°, 3 - at 300°, 4 - at 20°): 5-7) prolonged stretching at 500° (5 - 1 hr., 6 - 16 hours, 7 - 96 hours).

35 KhNM Steel. From the results of measurements of the line widths for the different durations of deformation (see Fig. 2), it can be seen how the deformation time at elevated temperatures affects the variation in the width of the (220) line as a function of degree of deformation: the curves are displaced upward with decreasing deformation time.

At a duration close to 100 hours the width of the (110) line does not change, within the limits of the accuracy of measurement, throughout the entire deformation range; the mean linear size of the coherent regions remains equal to that in the initial state.

Microstrains (d/d) are observed even after a deformation time of 96 hours at 500°. It is true, however, that their magnitude is significantly smaller than for short-term deformation and does not exceed 10^{-3}.

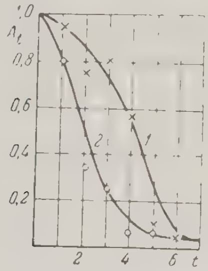

Fig. 3. Results of harmonic analysis based on the (211) line (back-reflection): 1) short-term deformation at 20°, 2) prolonged deformation at 500° over 16 hours.

We carried out our harmonic analysis with reference to the (211) line as recorded by back-reflection of Cr radiation and the (220) line on patterns obtained by Fe radiation for sections with equal values of $\varepsilon = 40\%$.

It can be seen from Fig. 3 that the variation of A_t with t, which, according to the ideas on which the method is based, is supposed to characterize the roles of fragmentation and microstrains, with a deformation time of 16 hours at 500° differs from the variation for short-term elongation to fracture at 20°. In both cases there is superposition of the effects of microstrains and fragmentation of the crystallites, but in the case of prolonged loading at 500°, the role of fragmentation in comparison with that of microstrains is smaller. From the dependence of the root mean square elongation $\sqrt{\overline{\Delta L^2}}$ on the column length L (Fig. 4), it can be seen that over the initial part of the curve the value of $\sqrt{\overline{\Delta L^2}}/L$, characterizing the deformation of the lattice for a specimen subjected to cold fracture, is almost two times larger ($13\cdot10^{-4}$ and $7.5\cdot10^{-4}$) than for specimens subjected to prolonged stretching to fracture at 500°. These values are close to those obtained by the methods of Lysak and Dehlinger.

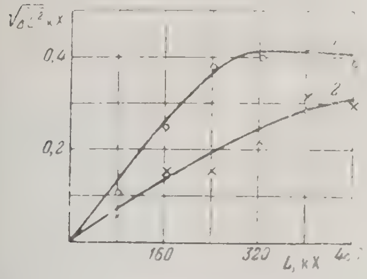

Fig. 4. Dependence of the root mean square displacement on column length L: 1) cold short-term deformation, 2) prolonged deformation at 500°.

The column length L (assumed to be directed normal to the reflecting planes) over which the lattice deformation is uniform ("region of homogeneity" of deformation) is determined in Fig. 4 by the transition point to the horizontal portion of the curve. This length is 300 kX for cold short-term deformation and and 400 kX for a prolonged elongation at 500°. This length is comparable to the dimensions of the coherent regions.

The above-mentioned specimen sections were also x-rayed in a 57.3 mm cylindrical camera by Fe radiation and the resultant patterns were processed by the methods of L. I. Lysak[6] and Dehlinger[5].

Table 1 shows that the presence of microstrains and reduction in the size

Table 1

Dependence of the Dimensions of the Mosaic Blocks and of Microstrains on the Character of the Deformation for Specimens of 35KhNM Steel

Nature of deformation	Calc. acc. to Ref. 5		Calc. acc. to Ref. 6		Harmonic analysis	
	Λ^*, kX	$\frac{\Delta d}{d}\cdot 10^4$	Λ, kX	$\frac{\Delta d}{d}\cdot 10^4$	L with uniform deformation	$\frac{\sqrt{\overline{\Delta L^2}}}{L}\cdot 10^4$
Short-term deformation, 20°	350	6.7	750	18	300	13
500°, 1 hour	380	6.1	510	16	400	9
500°, 16 hours	510	3.8	—	10	400	7

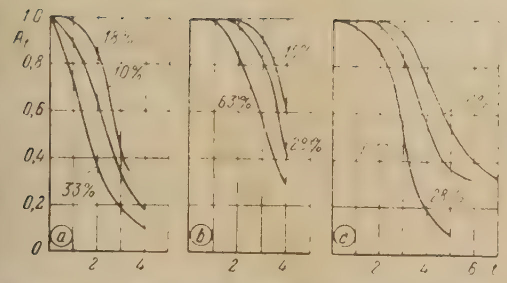

Fig. 5. Results of harmonic analysis based on the (220) line: a) short-term deformation at 20°, b) at 500° for 1 hour, c) at 500° for 96 hours.

of the coherent regions (and the "regions of homogeneity" of deformation), in 35KhNM steel after elongation at 20 and 500° are substantiated by all three methods of processing the x-ray patterns. Dimensions of the "regions of homogeneity" of deformation determined by the method of harmonic analysis are close to the dimensions of the coherent regions evaluated by the method of Dehlinger, as regards both absolute magnitude and the relative differences between specimens. Where the magnitude of microstrains is concerned, the results obtained through harmonic analysis are higher than the results found according to Dehlinger's procedure by a factor of about two, but are somewhat lower than the values obtained by the method of Lysak.*

For every specimen (Fig. 5), as the degree of residual deformation is increased, the A_t curve shifts further down and the derivative [illegible] becomes increasingly different from zero. This indicates an increase in the influence of fragmentation of the coherent regions on the diffraction broadening of the lines. The character of the curves for a specimen subjected to prolonged deformation is basically different from that for a specimen subjected to cold short-term deformation, and indicates the greater importance of microstrains and the smaller role of fragmentation in the observed broadening of the lines. An analogous influence of the temperature and duration of deformation was also noted by Rovinski and Rybakova in studying the creep of EIalT(ЭИ1Т) steel.[2]

Let us recall that the x-ray patterns were recorded after completion of the process of deformation; accordingly, the observed effects are the results of the joint influence of deformation and of prolonged exposure to elevated temperature and, if partial "restoration" of structure does occur, it may elude detection. In view of this it would be of interest to investigate specimens during the process of deformation. However, one can hardly expect that the block size will

---

*The agreement of results obtained by the three methods does not mean that the harmonic analysis was superfluous. The latter leads to new valuable information and brings out more line details than the other two procedures.

increase at 500°; if such an increase does take place, it must be less intensive than the decrease in microstrains (see, for example, Ref. 6 & 9). Moreover, it has been noted that prolonged exposure of bolt steel at 450-500° to stresses below the yield point even to some fragmentation of the block structure. Hence there is reason to assume that the observed differences in the degree of fragmentation reflect actual differences in the mechanisms of short-term and prolonged deformation.

Conclusions

Our x-ray studies show the existence of differences in the fragmentation of the coherent regions, and in the magnitude of microstrains depending on the rate and temperature of deformation.

During short-term plastic extension of St.20 and 35KhNM steels at an average rate of deformation yielding about 4% residual elongation per minute at 20, 300 and 500°, the coherent regions decrease in size and microstrains develop. At 500° these processes are less intense, but still noticeable even in carbon steel.

Going from short-term to prolonged plastic deformation at an average rate of 0.005 to 0.1% per minute shows no effect on the strains in the crystals of carbon steel at 300°, but decreases them significantly at more elevated temperatures. In St.20 steel deformed at 500°, microstrains are not observed even when the residual elongation is 150% and there is no detectable fragmentation of the main mass of the crystallites.

For 35KhNM steel the indicated decrease in the rate of elongation from 4 to 0.01% per minute at 500° results in a decrease in the microstrains by a factor of approximately two. Increasing the temperature to 600° during short-term extension affects the magnitude of the resultant microstrains to a greater extent than the above-mentioned decrease in the rate of deformation at 500°. However, the decrease in the rate of deformation strongly affects fragmentation of the crystallites.

Whereas at a rapid rate of deformation at 20°, and even at 500°, there is observed appreciable, almost uniform fragmentation, while the microstrains decrease with increasing temperature, after prolonged deformation at 500° no fragmentation is observed, while the microstrains, although still appreciable, remain at a lower value than after short-term deformation ($\Delta d/d \approx 10^{-3}$). In contrast, during brittle impact-fracture a considerable fragmentation of the blocks is observed, while microstrains are not detected.[1]

The fragmentation of the blocks and development of microstrains, which "prepare" the metal for fracture under tensile loads, proceed in different ways not only in different materials but even in the same material under different deformation conditions, i.e., at different temperatures and loading times.

It is known that during slow deformation under the influence of stresses exceeding the yield point the strength of metals is appreciably reduced. The fact that under these conditions fragmentation is weak or absent probably indicates that the process of fragmentation of the blocks is responsible for the hardening preceding fracture. Under static loads at room temperature the fragmenta- is considerable even in the inital period of deformation and, in contrast to the case of prolonged loading at elevated temperatures, contributes to enhanced strength.

"S.M.Kirov" Kharkov Turbine Plant

References

1. M.Ia.Fuks & S.S.D'iachenko, Izv. AN SSSR, Ser. fiz., 15, 106 (1951).
2. B.M.Rovinski & L.M.Rybakova, Izv. AN SSSR, Otd. tekh. nauk., No. 9, 1241 (1953).
3. W.A.Wood, W.A.Rachinger, J. Inst. Metals, 76, 237 (1949); W.A.Wood, & R.F.Scrutton, Ibid., 77, 423 (1950); W.A.Wood, C.R.Wilms & W.A.Rachinger, Ibid., 79, 159 (1951).
4. G.B.Greenough & E.M.Smith, J. Inst. Metals, 77, 435 (1950); G.B.Greenough, C.M.Bateman & E.M.Smith, Ibid., 82, 545 (1952).
5. U.Dehlinger & A.Kochendorfer, ZS. f. Metallkunde, 31, 231 (1939).
6. L.I.Lysak, in "Voprosy fiziki metallov i metallovedeniia" (Problems of the physics of metals and metallurgy), No. 3, Ukrainian Ac. of Sci., 1952.
7. B.Ia.Pines & N.G.Berezniak, Zhur. tekh. fiz., 24, 329 (1954).
8. "Konstruktsionnye stali" (Structural Steels)(Handbook), Vol. 1, Ed. by Gudtsova, M. 1947.
9. G.V.Kurdiumov & L.I.Lysak, in "Sbornike nauchnykh rabot laboratorii metallofiziki" (Collected scientific publications of the metal physics laboratory of the Ac. of Sci. of the Ukrainian SSR). 1948.

X-RAY ANALYSIS OF STRUCTURAL CHANGES IN METALS DURING CREEP

- L.M.Rybakova

1. It was shown in an earlier report[1] that broadening of the interference spots and lines is observed in the x-ray patterns of polycrystalline specimens tested for creep. This broadening is indicative of structural changes in the metal and is interpreted as evidence of fragmentation of the blocks and building up of microstrains. In the present investigation we carried out a qualitative x-ray analysis of the structural changes occurring in samples of low-carbon steel tested for creep and elongation at room and elevated temperatures.

2. The tested specimens were prepared of Armco iron of normal chemical composition. The specimens were prepared in the form of cylinders 8-10 mm in diameter and having a gage length of 80 and 180 mm. After fabrication and before testing the specimens were annealed for 2 hours in a vacuum furnace at 800°.

Elongation of the specimens was effected on a 4 ton testing machine at the usual speed (1.2 mm/min) to a deformation of about 12%. One specimen was elongated at room temperature, the others at 450°. After each stage of elongation x-ray patterns were recorded of a section of the surface near the middle of the specimen. The creep tests were carried out on IP-2 testing machine at a temperature of 450° with different loads over periods of 500 or more hours. For these tests we used specimens 10 mm in diameter and 180 mm in gage length. The elongation during creep was evaluated from the readings of the testing machine indicators. The results were plotted in the form of $\varepsilon(t)$ curves. The individual tests were stopped at the point where the curve became a straight line. The specimen was then unloaded and, after cooling with the furnace, x-rayed. After x-raying, the specimen was again clamped in the IP-2 machine and the creep test continued. X-ray patterns were recorded of each specimen prior to the testing and after completion of the entire series.

Lines were scribed on the specimens at the ends of the gage length. The distance between the lines was measured before and after each stage of the elongation. These measurements were used as a check on the readings of the testing machine indicators. In the case of the specimens tested at 450° the oxide surface layer was removed by electrolytic etching prior to x-ray photography.

The x-ray patterns were recorded in a back-reflection camera by the radiation from the cobalt anode of an electron x-ray tube. The x-ray beam was collimated by means of two diaphragms the first with a 0.6 mm diameter aperture, the second with a 1.0 mm diameter aperture. The patterns were recorded on a flat film. Both the specimen and film were kept stationary during the exposure; the distance between them was kept constant (approximately 80 mm). The irradiated area in all cases was kept constant (about 2.5 mm^2). As nearly as possible the same section of the specimen was photographed each time.

3. Fig. 1 shows the x-ray patterns obtained from a specimen of Armco iron elongated at room temperature at the usual rate of deformation. These patterns clearly show that the diffusion of the interference spots increases with deformation and that at an elongation of 10.8% the interference ring becomes almost continuous. It is interesting to note that there is a sudden diffusion of the interference spots at a deformation of about 2.8%. This is in agreement with the experimental data on the jump-like character of the plastic deformation of steel samples at the creep plateau.[2] With further plastic deformation there occurs a gradual diffusion of interference ring.

The x-ray patterns of a specimen stressed at 450° are shown in Fig. 2. The increase in diffusion of the interference ring with increasing deformation at 450° is generally similar to that observed at room temperature. However, one may note the following distinctive features. The pattern of Fig. 2,b shows insignificant diffusion of the interference spots. This indicates that in the elongation of Armco iron at 450° the sudden jump in the diffusion of the interferences is either

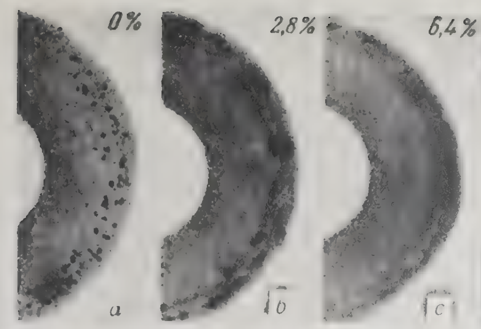

Fig. 1

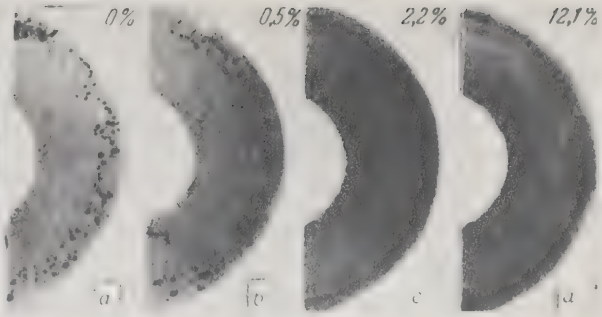

Fig. 2

Fig. 1. X-ray patterns of Armco iron specimen stressed at room temperature to different degrees of elongation.

Fig. 2. X-ray patterns of Armco iron specimen stressed at 450° at different degrees of elongation.

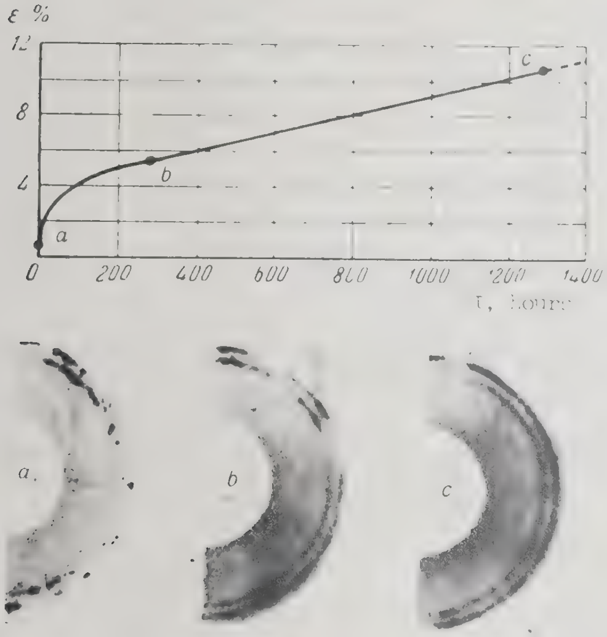

Fig. 3

Fig. 3. X-ray patterns of Armco iron specimen tested for creep at 450° and a stress of 9 kg/mm^2: a) prior to test, b) during test, c) after test. Above: deformation curve; points pertain to the corresponding patterns.

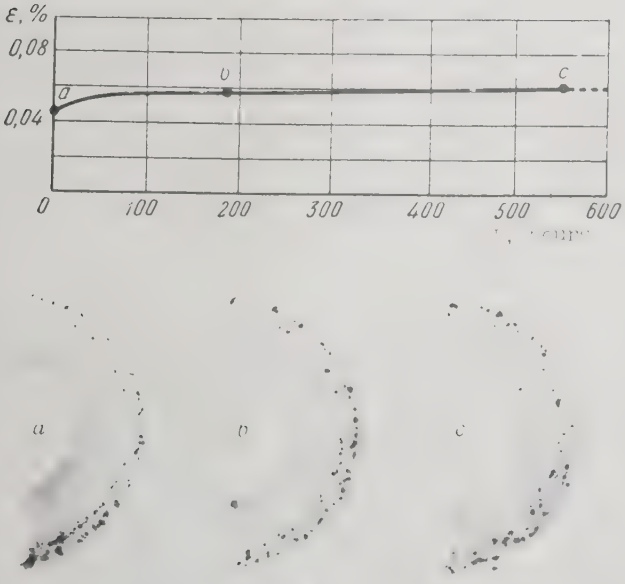

Fig. 4

Fig. 4. Same as Fig. 3 but at a stress of 6 kg/mm^2.

absent or in any case occurs at a deformation above 0.5%.

The overall diffusion of the interference ring is less than that for the specimen stressed at room temperature. Whereas in elongation at 450° to 12.1% (Fig. 2,e) the interference rings are still clearly discernible, in the case of elongation at 20° to 10.8% (Fig. 1,d) the doublet is diffused. Inasmuch as such diffusion of the lines is due to the size of the mosaic blocks and the magnitude of the microstrains, it is apparent that in stretching at the elevated temperature the blocks are broken up into larger fragments while the microstrains are smaller in magnitude at the same deformation of the specimen.[3] Finally we turn to the pattern of Fig. 2,c and compare it with the pattern of Fig. 1,b. The interference rings in the former (2.2% elongation at 450°) are more uniform in intensity than the rings in the latter (2.8% elongation at room temperature). This indicates that fragmentation of the grains during deformation at the elevated temperature leads, even at a 2% residual deformation, to such a disorientation of the blocks that the interference ring becomes equal in intensity to that of the specimen deformed to nearly 3% at room temperature (by disorientation here we understand rotation of the blocks inside the crystal grains and consequently increased mosaicity of the crystallites).

The diagrams of Fig. 3 & 4 show typical deformation curves for the specimens tested for creep at 450° at stresses of 8 and 6 kg/mm^2 for overall periods of 1270 and 560 hours respectively. In the same figures we reproduce the x-ray patterns of these specimens recorded before, during and after the tests.

Let us examine the results and compare them with those for ordinary elongation at room and elevated temperatures. The interference bands on the pattern of Fig. 3,b are diffused, i.e., during the interval from a to b there occur in the specimen during creep processes similar to those taking place during ordinary elongation, at least in so far as one can judge from the diffusion of the interferences. Yet on the x-ray pattern of Fig. 3,b the interference rings are still irregular and of varying intensity although the deformation of the specimen already exceeds 5%.

The interference picture in this pattern corresponds to the picture exhibited by the pattern stretched at 450° at the usual rate and with a residual elongation of about 2.2% (Fig. 2,c). The pattern of Fig. 3,c, obtained after further creep testing to a deformation of 10%, shows a more uniform intensity distribution over the rings. The diffusion of the lines in this pattern is similar to the diffusion in the pattern of Fig. 3,b. Comparing the x-ray pattern of Fig. 3,c with the patterns from the sample elongated at the usual speed at 450° we see that a similar interference picture is observed in the case of approximately 3% residual deformation.

Thus we have shown experimentally that in a certain stress interval there occurs in Armco iron at 450° fragmentation of the blocks and building up of microstrains, i.e., dislocation deformation. However, quantitatively the accumulation of deformations due to dislocation processes during creep amounts to some 30-40% of the mean deformation of the specimen stretched at the usual rate at the same temperature. The residual deformation in the specimen is accumulated apparently as the result of other processes, among the more important of which we feel is the reciprocal shifting of the grains and elements of the substructure, i.e., the process of 'viscous' flow. This is particularly evident in the region of the second section of the creep curve where the uniform intensity ring in the x-ray pattern is evidence of the appreciable displacement of the substructure elements with time. In addition to the mentioned processes, the deformation in creep is probably determined by the influence of relaxation, diffusion and other processes which we have not especially studied and hence will not discuss here.

Fig. 4 shows the x-ray pattern of a sample deformed under creep conditions characterized by a very slow rate of creep. In the x-ray pattern of Fig. 4,b there is apparent a certain reduction in the number of spots as compared with

the pattern for the sample recorded before the test, but the spots are somewhat larger and slightly diffused, though less manifestly so than those in the pattern of Fig. 2,b. With further progress of the creep test this diffusion of the spots decreases somewhat, otherwise there are no noticeable changes in going from 4,a to 4,c. Taken as a group the x-ray patterns of Fig. 4 show that prolonged (400 hours) exposure to a temperature of 450° has no noticeable effect on the structure of Armco iron. As for the structural changes at so low a creep rate they are obviously minor and require the use of more sensitive procedures for their detection.

4. X-ray studies of the structural changes during creep of low-carbon steel at a temperature of 450° and deformation rates of 10^{-2}-10^{-3}% per hour and comparison of these changes with the changes incident to deformation at the usual rate at room and elevated temperatures showed that in creep, particularly in its first stages, there occur processes analogous to those observed during deformation at ordinary speeds. Quantitatively speaking the structural changes,as evaluated from the diffusion of the interference spots,lag behind the progressing creep deformation.

I take this occasion to express my deep gratitude to B.M.Rovinski for his guidance in the investigation.

Institute of Machine Design of the
Academy of Sciences of the USSR

References

1. B.M.Rovinski & L.M.Rybakova, Izv. AN SSSR, Otd. tekh. nauk, No. 9, 1241 (1953).

2. V.S.Ivanova, Doklady AN SSSR, 94, No. 2, 217 (1954).

3. B.M.Rovinski & L.M.Rybakova, Izv. AN SSSR, Otd. tekh. nauk, No. 10, 1483 (1952).

THE INFLUENCE OF TEXTURE ON THE INTENSITY OF INTERFERENCE LINES IN INVESTIGATING LARGE DEFORMED SPECIMENS

- M.Ia.Fuks & G.V.Dobrovol'skaia

Thanks to the pioneering work of G.V.Kurdiumov and his students in recent years there has been an increasing number of investigations of microstrains by the roentgenographic method based on the observation of changes in the intensity of the lines on x-ray patterns. In view of this, it is expedient to evaluate the influence of texture in massive (i.e., not powder) specimens on the relative intensity of the lines even if lines having different indices - for example, (110) and (220) - are being compared. Comparison of these lines is allowable when the width of interference maxima is being observed; in evaluating intensities, however, such comparison is legitimate in one particular case, namely, when the wire specimen has an axial texture with a [110] axis and the registration is effected perpendicular to the fiber axis.

Unfortunately in a number of investigations, including those of Refs. 1 & 2 as well as some of those reported on at the present conference, this circumstance was not taken into account although the influence of texture on the appearance of x-ray patterns is well known. It must be noted that in general rotation of the specimen or of the film does not eliminate the influence of texture.

PROCEDURE

The investigated specimens of chrome-nickel-molybdenum steel were deformed plastically in simple tension at room temperature and at elevated temperatures under conditions of short-term and prolonged loading. Different sections of the specimens characterized by different degrees of residual deformation - up to 150% residual elongation - were studied.

Specimens and deformation conditions

Identification No. of sample	Deformation	Deformation temperature °C	Duration of loading, hours
P-34	Short-term tension	20	-
P-1	Prolonged tension	500	16
P-5	Prolonged tension	500	96

By way of the initial state sample with which all the subsequently deformed specimens were compared we took a non-deformed section near the head end of specimen P-5. The x-ray patterns were recorded by the radiation from iron and chrome anodes, supplied by a sharp focus Pines type tube in a 57.3 mm diameter camera. Iron foil about 0.01 mm thick was cemented over the inner slit of the collimator to obtain iron reference lines for the entire series of patterns. The specimens were mounted in the camera so that the axis of deformation lay in the same plane with the direction of the primary beam and the equator of the film. A number of patterns was also recorded by back-reflection, using chrome radiation and the same reference standard; all the lines on the patterns were continuous. The integral intensity of the lines was evaluated from the ratio of the areas under the photometric curves for the lines of the sample and for the (110) line of the standard ($K\alpha$ or $K\beta$). For the purposes of our investigation we took this ratio as the 'absolute' intensity of the lines. For verification purposes a number of duplicate patterns were registered.

The texture axis and the degree of its perfection (departure from the ideal) were determined by x-raying thin plates by forward transmission using the radiation from molybdenum. These plates were cut from sections of specimens P-34 and

P-5 with a residual elongation of about 50% and etched before x-raying.

Results and discussion

No fiber structure was detected in the initial state. The fiber axis of the plastically elongated specimens has the index [110], which is in agreement with the data in the literature[3] on the texture of drawn metals with a body centered lattice.

The scattering angle of the texture for the cold deformed sample amounted to about ±20°, while the angle for samples elongated over a prolonged period was ±16°. This difference in the degree of perfection of the fibering was substantiated by measurements of the relative intensities of the spots and the intensities of the sections of the (110) line between the spots (at half the annular distance between the spots).

The influence of the recording angle β (i.e., the angle between the surface of the specimen and the primary beam) is shown by the following relative values of the absorption factor (θ is the Bragg angle):—

(hkl).....	(110)	(200)	(211)	(220)
θ.......	28°	42.5°	56°	73°
β = 28°	0.5	0.64	0.68	0.65
β = 90°	---	----	0.27	0.45

Analysis showed that the fragmentation of the crystals in the P-34 specimen produced by intense cold plastic deformation leads to an appreciable change (about 12%) in the coefficient of primary extinction only for the (110) line. For the other lines one cannot expect any noticeable influence where extinction is concerned.

The ratios of the integral intensities of the lines computed taking into account all the intensity factors are in good agreement with the experimental data obtained in photographing the initial (high-annealed) specimen at angles β equal to 28 and 90°. The close agreement is shown by the following data (iron radiation; β = 20°):—

Data	(110)	(200)	(211)	(220)
Calculated	1	0.19	0.52	0.51
Experimental	1	0.19	0.70	0.50

The changes in intensity observed as a result of varying the angle in x-raying the deformed specimen greatly exceeds the values obtained by taking absorption into account.

Changes in the intensity of the lines incident to changes of only the angle of photographing, if the factor of absorption is disregarded, can be explained only by the presence of texture (fiber) in the deformed specimens. Hence x-raying of deformed specimens by the method of back-reflection with the specimen fixed relative to the direction of the primary beam may lead to an incorrect evaluation of the line intensities.

The results of measurement may also depend on the type of deformation and on the radiation used. Thus in photographing our uniaxially elongated specimen by the radiation from a chromium anode with β = 90°, we obtained a lower value of the absolute intensity of the (211) line as compared with that for the initial highly annealed specimen:—

State of specimen	Deformation ε,%	Ratio of intensities; $\frac{I_{(211)}\ \text{specimen}}{I_{(211)}\ \text{standard}}$
Initial	-	0.245
Cold deformed	45	0.10
Deformed for 96 hours at 500°	40	0.17

In the case of rolled iron using an analogous x-ray procedure Sandler[5] observed a more than two-fold increase in the intensity of (211) line. This apparent

inconsistency is explained by the fact that uniaxially elongated specimens have an axial structure with a [110] axis, while in rolled iron one of the possible texture planes has the index (211).

Dependence of line intensities on the degree of deformation for specimens stressed in different ways

Specimen & state	ε, %	Absolute intensity				Relative intensity			
		(110)	(200)	(211)	(220)	(110)	(200)	(211)	(220)
Theoretical	—	—	—	—	—	1	0,19	0,62	0,51
Initial		4,64	0,92	3,3	2,5	1	0,19	0,7	0,5
Specimen P-34	45	3,9	1,25	2,6	2,4	1	0,33	0,66	0,61
Specimen P-1 (500°, 16 hours)	33	4,1	1,2	2,8	2,7	1	0,27	0,69	0,65
	150	2,1	0,84	2,7	1,9	1	0,34	1,14	1,05
Specimen P-5 (500°, 36 hours)	23	3,0	1,05	2,87	2,6	1	0,35	0,96	0,87
	67	2,65	1,3	3,6	2,9	1	0,48	1,2	1,1

It will be seen from the table that with increasing degrees of deformation or in going from short-term to prolonged loading, when the effect of texture increases, the absolute intensity of the (110) line decreases very appreciably, while that of the (220) line falls off very little. Consequently the ratio of the intensities $I_{(220)}/I_{(110)}$ increases markedly.

In view of the fact that the experimental values of the relative intensity of the (110), (200), (211) and (220) lines of the initial specimen are in good agreement with the theoretical calculated values, it may be assumed that the changes in the absolute intensity of the lines for deformed specimens are proportional to the changes in the square of the function of atomic scattering (fe^{-M}). It follows from the plotted f-curve (not reproduced in the present report) that lines having different indices are characterized by different intensity changes and that there is no monotonic decrease in intensity with the increase of $(\sin\theta)/\lambda$ as there should be in the case of distortions of the lattice. Only the presence of fiber could explain the shape of the f-curve obtained.

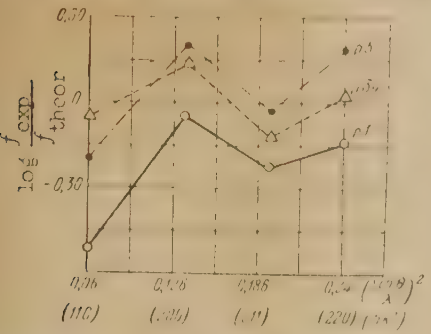

Dependence of the logarithm of the ratio of the experimental to the theoretical function of atomic scattering on the value of $\left(\frac{\sin\theta}{\lambda}\right)^2$

We note that the weakening of the (110) line can be caused not only by the direct influence of texture but also indirectly through secondary extinction. The (110) line being the most intense one will be most noticeably affected by extinction.

Our data were also processed by the method of Iveronova and Katsnel'son[6]. Under the influence of strains of the third kind the points in the graph should fall in a straight line the slope of which characterizes the magnitude of the distortions. With increasing $(\sin\theta)/\lambda$ the above-mentioned intensity ratio should obviously decrease. However, the expected slope of the line was not observed for any of our deformed specimens; on the contrary there is manifest an opposite tendency, i.e., the relative intensity of the (220) line increases with deformation. This indicates the presence of another factor, stronger than distortions of the texture.

Conclusions

Above we described the increase in the relative intensity of the (220) line incident to deformation. On the other hand, there are experimental data showing this intensity decreases in rolling, in the presence of cavitational erosion. This has been noted in a number of reports presented at this conference. This apparent contradiction can be explained if we take into account the fact that the textures in these cases are different than in the case of elongation under simple tensile stress.

It is evident from the experimental results that, in accord with Palatnik's[4] theory, the influence of texture in intensively deformed large specimens is so appreciable and so dependent on the conditions of photographing that the results of determinations of the absolute and relative intensity are highly ambiguous and cannot be considered reliable even in studying the relatively simple case of a uniaxially stressed sample. In the case of shaping by rolling, grinding, turning and so on, the picture becomes even more complicated. This must be taken into account in studying the distortions of the lattice in massive specimens in which one can expect the presence of texture (fibering). One can test for the effect of texture by x-raying the specimens under different angles β, taking into account the influence of the absorption factor.

The suggestion advanced by Iveronova regarding the necessity of reviewing certain studies concerning the intensities in x-ray patterns is also applicable where taking into account the influence of both extinction and texture is concerned.

"V.I.Lenin" Kharkov Polytechnical Institute

References

1. L.Moroz & T.Mingin, Doklady AN SSSR, 91, No.2, 249 (1953).
2. L.A.Glikman, V.P.Tekht & Iu.E.Zobachev, Zhur. tekh. fiz. 25, 280 (1955); L.A.Glikman, In "Korrozionno-mekhanncheskaia prochnost' metallov" (Corrosion-mechanical strength of metals), M. 1955.
3. C.S.Barrett, Structure of Metals (In Russian trans. M. 1948).
4. L.S.Palatnik, Zhur. tekh. fiz., 6, 1624 (1936); Zhur. tekh. fiz., 7, 2109 (1937).
5. N.I.Sandler, In "Tezisy dokladov V.Vsesoiuznogo soveshchaniia po primeneniiu rentgenovykh luchei k issledovaniiu materialov" (Abstracts of reports presented at the Fifth All Union Conference on the Application of X-rays to the Investigation of Materials), L. 1955.
6. V.I.Iveronova & A.A.Katsnel'son, Zhur. tekh. fiz., 25, 696 (1955).

SECONDARY HARDNESS IN STEELS ALLOYED WITH VANADIUM, MOLYBDENUM AND TITANIUM

- L.V.Zaslavskaia, S.T.Kishkin, N.F.Lashko, A.F.Platonova,
N.M.Popova & M.F.Rybina

In certain alloy steels there is observed an increase in hardness - called "secondary" hardness - in the process of annealing at 550-600°C. This effect has been detected in steels alloyed with molybdenum, tungsten, vanadium and titanium. There is also mention in the literature of secondary hardening in steels containing 12-18% chromium.[1] However, we were unable to reproduce the effect in chrome steel containing 0.4%C and 12% Cr.

Most investigators dealing with the subject are of the opinion that the secondary hardness is due to segregation of highly dispersed special carbides. Inasmuch as in many steels exhibiting secondary hardness the segregation of the special carbide in the process of annealing is preceded by the separation of cementite, there naturally arose the question of the role played by cementite in the effect. According to some investigators secondary hardness develops as a result of interaction between metastable cementite and a special carbide.[2] Other investigators have suggested that secondary hardness is connected only with the formation of special carbides.[3] In an investigation of anodic deposits separated from steel no highly dispersed phases are detected by the conventional powder x-ray diffraction method. The special carbides VC, Mo_2C, and TiC were found by this method only after annealing of the steel above 600°, i.e., only above the temperature interval in which the secondary hardness develops. In low carbon steel (0.1% C) it is difficult to detect cementite at any annealing temperature and it has been suggested that cementite does not form in such steels at all.[3]

In the present investigation, devoted to the kinetics of the development of carbides incident to annealing of alloy steel, we employed new methods of differential carbide analysis based on selective chemical solution of the carbides in anodic deposits. The carbides in question, after chemical separation, were subjected to chemical and x-ray analyses; the latter was greatly facilitated by virtue of elimination of the interfering phases.

Two methods of differential carbide analysis were employed for separate determination of carbides: 1) boiling of the carbide deposit with hydrochloric acid which retained the special carbides of vanadium, titanium and molybdenum in the form of a precipitate and brought the cementite into solution[4] and 2) treatment of the carbide deposit with an alcohol solution of hydrogen peroxide which kept the cementite in a solid state and dissolved the special carbides; to insure complete solution of the titanium carbide, fluorine salts were added to the reagent.[5]

For our investigation we used steels containing different amounts of carbon (0.1-0.8%) and alloyed with vanadium (1.0-2.5%), titanium (0.3-0.5%) or molybdenum (1.7%). The heat treatments were carried out in an atmosphere of argon to preclude decarbonization of the surface layers. The steels containing vanadium were quenched from 1350° (15 min) in water; those containing titanium were quenched from 1350° (1 hour) in water; those containing molybdenum were quenched from 1250-1300° (30 min) in water. The quenched specimens were tempered for one hour at 300, 400, 450, 500, 600, 650, 700° and higher.

To separate the carbidesthe specimens were anodically dissolved in 1 N KCl with the addition of 0.5% citric acid at a current density of 0.02-0.03 a/cm^2 and the solution cooled to 0°C. There were no primary carbides in the molybdenum and vanadium steels after quenching, while up to 25-50% of the primary carbides were retained in the titanium steels.

Residual austenite (decomposing at 300-400°) was detected in all the steels by magnetic and x-ray methods.

Two phases were found in the vanadium steel after tempering: Me_3C and VC;

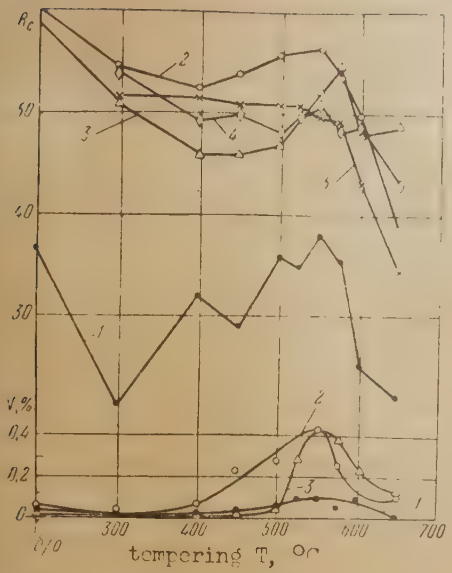

Fig. 1. Dependence of the hardness and the amount of vanadium combined in the highly dispersed carbide on the tempering temperature and composition of the steel: 1) 0.10% C + 1.48% V + 0.94% Mn, 2) 0.38% C + 2.53% V + 1.98% Mn, 3) 0.39% C + 1.42% V, 4) 0.86% C + 0.96% V, 5) 0.42% C + 1.55% V + 4.21 Cr.

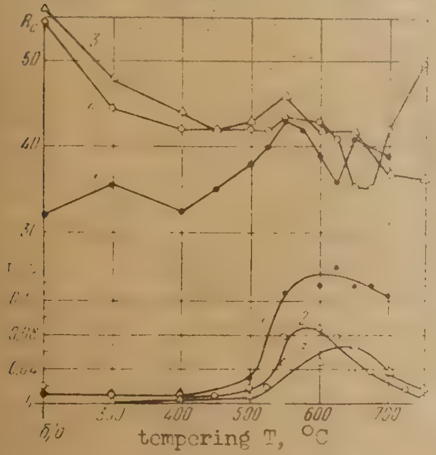

Fig. 2. Dependence of the hardness and the amount of titanium bound in the highly dispersed titanium carbide on the tempering temperature and the composition of the steel: 1) 0.11% C + 0.33% Ti, 2) 0.39% C + 0.35% Ti + 1.98% Mn, 3) 0.53% C + 0.42% Ti.

in the molybdenum steels - Me_3C and Mo_2C; in the titanium steels - Me_3C and TiC. The presence of cementite in the low-carbon steels (0.10% C) was proved by x-ray studies of the anodic deposits purified by chemical elimination of the other carbides.

The special carbides of vanadium, molybdenum and titanium form in appreciable amounts at 450-500° and the amount present increases continuously with the tempering temperature. The special carbides of these elements are partially soluble in hydrochloric acid. The percentage of the acid-soluble component (highly dispersed carbides) can be computed from the difference of the results obtained by the two methods of differential carbide analysis.

Under identical experimental conditions the amount of special carbides going into solution depends on the tempering temperature and may serve as an indication of their degree of dispersion.

The greatest amount of the dispersed VC and TiC is formed at drawing temperatures producing the maximum secondary hardening (Fig. 1 & 2). With increasing temperature the amount of highly dispersed carbides decreases due to segregation of the special carbides. In the case of molybdenum steels, the secondary hardness maximum coincided with the maximum for the amount of highly dispersed Mo_2C only for the low-carbon (0.1% C) steel (Fig. 3). Under the conditions of our experiment the degree of dispersion of the acid-soluble carbides of molybdenum did not correspond with their optimum effect on the development of secondary hardness in molybdenum steels containing over 0.2% C.

Most of the data on the determination of the highly dispersed special carbides in molybdenum, vanadium and titanium steels indicated that the secondary hardness is undoubtedly connected with the formation of these carbides. The behavior of the special carbides (VC, Mo_2C and TiC) in these steels showed that the maximum hardness in aging alloyed steels is connected with the "critical" degree of dispersion of the special carbides.

Cementite in the investigated steels was found in the metastable and stable states. The behavior of the cementite was found to depend on the content of molybdenum, vanadium and titanium in the steel. Where these alloying elements were present in sufficient amounts to combine with all the carbon, the cementite disappeared almost entirely at 650°. Where the amount of the alloying element was insufficient, after a certain amount of solution at 550-600°, the cementite is retained in an equilibrium state with the carbides of vanadium, molyb-

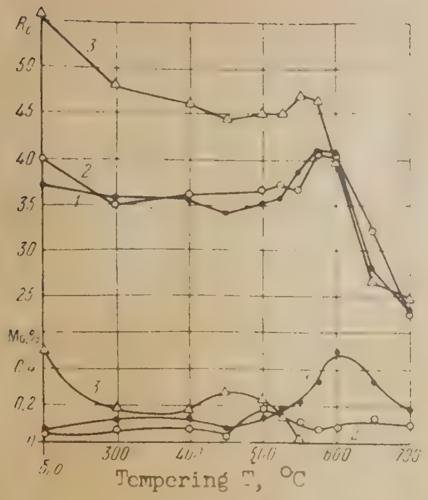

Fig.3

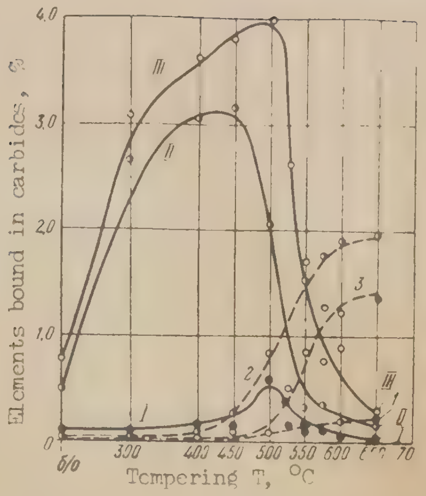

Fig.4

Fig. 3. Dependence of the hardness and amount of molybdenum bound in the highly dispersed molybdenum carbide on the tempering temperature and composition of the steel: 1) 0.10% C + 1.70% Mo, 2) 0.23% C + 1.73% Mo, 3) 0.39% C + 1.72% Mo.

Fig. 4. Dependence of the amounts of iron and vanadium combined in Me_3C and VC on the tempering temperature and composition of steel: I and 1) steel containing 0.10% C + 1.48% V + 0.94% Mn; II and 2) steel containing 0.38% C + 2.53% V + 1.98% Mn; III and 3) steel containing 0.39% C + 1.42% V. The curves identified by Roman numerals give the amount of Fe combined in Me_3C; those identified by Arabic numerals, the amount of V bound in VC.

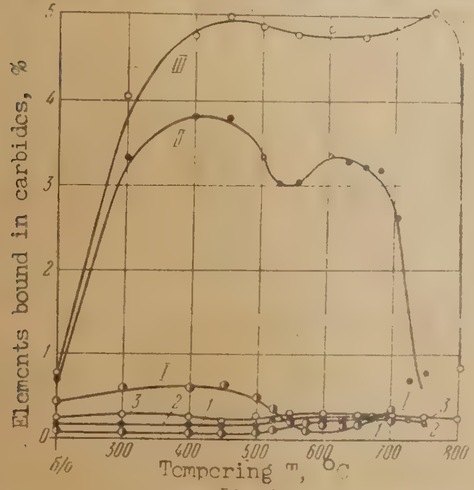

Fig.5

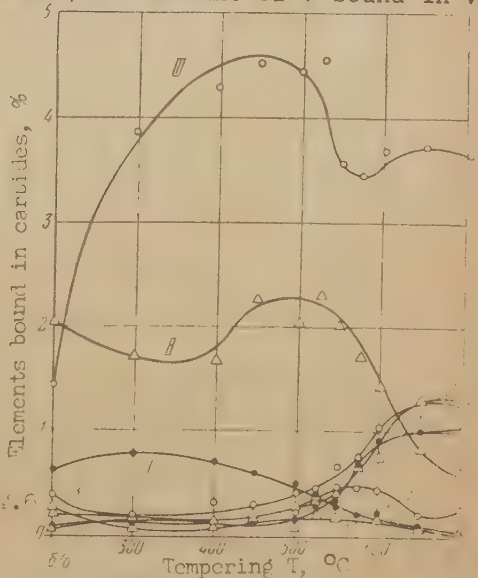

Fig.6

Fig. 5. Dependence of the amounts of iron and vanadium combined in Me_3C and TiC on the tempering temperature and composition of steel: I and 1) steel containing 0.11% C + 0.33% Ti; II and 2) steel containing 0.39% C + 0.35% Ti + 1.98% Mn; III and 3) steel containing 0.53% C + 0.42% Ti. The curves identified by Roman numerals give the amount of Fe combined in Me_3C; those identified by Arabic numerals, the amount of Ti bound in TiC.

Fig. 6. Dependence of the amount of iron and molybdenum combined in Me_3C and Mo_2C on the tempering temperature and composition of steel: I and 1) steel containing 0.10% C + 1.70% Mo; II, 2 and a) steel containing 0.23% C + 1.74% Mo; III, 3 and b) steel containing 0.39% C + 1.72% Mo. The curves identified by Roman numerals give the amount of Fe combined in Me_3C; those identified by Arabic numerals, the amount of Mo bound in Mo_2C; those by letters, the amount of Mo bound in the Me_3C.

denum and titanium. At 550° there appears to be present less cementite than at higher drawing temperatures and a distinct peak appears in the curve showing the development of cementite (Figs. 4-6). This effect can be explained by the higher solubility of cementite in the metastable state as compared with the equilibrium state; upon the attainment of equilibrium some portion of the cementite reseparates from the solid solution.

The variations in the content of the elements combined in cementite found by chemical analysis of the anodic deposits as well as by x-ray diffraction analysis showed that the separation of the special carbides in all the investigated steels is preceded by the formation of metastable cementite (Figs. 4-6), the amount of which increases with increasing tempering temperature to 400° or 450-500° and then decreases. These results are in agreement with the data of other investigators.[6-8]

Secondary hardness appears at tempering temperatures producing solution of the cementite at the maximum rate. The amounts of the special carbides of the MeC and Me_2C type also increase at the maximum rate at these temperatures. Consequently, secondary hardness in these steels develops as the result of redistribution of the carbon between the metastable cementite, the solid solution and the special carbides under the particular conditions characterizing the development of this process; the metastable cementite is a necessary participant in the development of secondary hardness.

As noted above the chemical composition of the carbides was established by means of differential carbide analysis. It was found that titanium does not enter into the composition of the cementite at all; vanadium is alloyed with it in amounts up to 2-3%, while molybdenum is dissolved in varying amounts (2-13%), depending on the annealing temperature. The minimal amount of molybdenum is dissolved in metastable cementite in the 550-600° temperature range.

Chemical analysis of the separated carbides showed that vanadium and titanium carbide contain absolutely no iron. Vanadium carbide can dissolve appreciable amounts of chromium (up to 50%).

We also used the differential carbide analysis procedure to investigate specimens of steel containing 0.40% C, 1.55% V, and 4.21% Cr. Three carbides formed in this steel during annealing: Me_3C, MeC and Me_7C_3. Trigonal chromium carbide appeared in minor amounts at high annealing temperatures (600-650°). The kinetics of the development of cementite and the special vanadium carbide differed little from that in steels not containing chromium. No secondary hardness was observed in this steel. It is possible that this behavior of the steel was connected with the composition of the vanadium carbide which contained up to 50% Cr (the way the carbide is associated with the solid solution depends on the composition of the carbide).

In addition to the phase composition we made a special study of the changes in the degree of dispersion of the cementite and special carbides in the precipitates subjected to selective chemical treatment. The degree of dispersion was determined from the diffuseness of the lines in Debye patterns. Changes in the dispersion of the cementite could be readily detected from the diffusion of the interferences from the (121) and (210) planes as well as from the (113) and (122) planes. In the presence of highly dispersed cementite the interferences from the (121), (210), (113) and (122) planes merge, while in the coagulated phases they are well separated. The ability to segregate depends on the content of carbon and alloying elements. An illustrated example is furnished by the changes in the degree of dispersion of cementite in molybdenum steels. In steel containing 0.1% C and 1.7% Mo, the cementite after annealing at 350° is highly dispersed as is indicated by the diffusion of the lines in the x-ray patterns. The splitting of the lines associated with reflections from the (121) and (210) planes begins with annealing at about 500°. The highest degree of segregation of cementite is obtained after annealing at 525°. Beginning with an annealing temperature of 550° the diffusion of the lines increases, which indicates solution of the cementite.

The splitting of the lines associated with interferences from the (121) and (210) planes in the x-ray patterns of steel containing 0.23% C and 1.7% Mo begins at temperatures above 550°. The sharpness of the lines increases up to an annealing temperature of 700°, which indicates a gradual increase in the mean dimensions of the cementite particles.

In steel containing 0.39% C and 0.7% Mo the degree of segregation of the cementite corresponding to the beginning of splitting of the lines associated with the interferences from the (121) and (210) planes occurs after annealing at 500°. The mean size of the particle increases continuously with the annealing temperature from 300 to 700°.

The gradual increase in the size of the carbide particles with increasing tempering temperature is also observed in steel containing 0.39% C and 1.42% V, as well as in titanium steels containing 0.39% C + 0.35% Ti and 0.53% C + 0.42% Ti.

In vanadium and titanium steels, the degree of segregation of the cementite corresponding to the beginning of the splitting of the lines associated with the interferences from the (121) and (210) planes is reached at 450°. Hence in these steels coagulation of cementite occurs more rapidly than in molybdenum steel. This difference in the behavior of cementite in different alloy steels is connected with processes involved in the distribution of the alloying elements between the cementite and the solid solution.

References

1. W.Bain, Influence of alloying elements on the properties of steel, (In Russian trans. M. 1945).
2. W.Crafts & J.L.Lamont, Metal Technology, 15, No. 6, 1 (1948).
3. G.V.Kurdiumov & M.D.Perkas, Doklady AN SSSR, 67, 41 (1952).
4. N.M.Popova, Platonova et al, The Factory Laboratory, No. 7, 778 (1952).
5. N.M.Popova, A.F.Platonova & L.V.Zaslavskaia, The Factory Laboratory, No. 1, 22 (1955).
6. N.F.Lashko & M.D.Nesterova, Izv. AN SSSR, Ser. fiz., 15, 67 (1951).
7. M.E.Blanter, Zhur. tekh. fiz., 18, 529 (1948).
8. S.Z.Bokshtein, Struktura i mekhanicheskie svoistva legirovannoi stali (Structure and mechanical properties of alloy steels), M. 1954.

X-RAY INVESTIGATION OF THE SURFACE QUALITY OF METALS MACHINED BY GRINDING OR LIGHT-CUT TURNING

- Iu.S.Terminasov, A.G.Iakhontov & A.V.Poltavski

Grinding or finish turning are frequently the final operations in machining important parts. These finishing operations produce a certain quality of the surface layer which may be a deciding factor where the life, performance and other characteristics of the piece are concerned. The quality of the surface layer depends to a great extent on the machining conditions, i.e., on the technology of the final operation.

The present report gives the results of our investigation of the state of the surface layer by x-ray analysis and the method of microhardness. Our purpose was to clarify the dependence of surface hardening on the nature of the finishing operation. We determined the intensity of the cold hardening as well as the distribution of the hardening through the thickness of the surface layer. The degree of hardening was evaluated from the data on the microhardness and the results of x-ray investigation of the crystal and elementary distortions as manifested by the broadening and weakening of the interference lines in x-ray patterns. These distortions are the factors primarily responsible for the hardening of the metal incident to machining.

The experimental procedure and the method of processing the data were the same both for the finish ground and the finish turned samples. For investigating the distortions produced in the process of grinding we selected U8 (Y8) steel and commercial grade iron; for studying the distortions produced by finish turning we used St.40 steel. We studied the effect of 90 different grinding regimes and 24 finish-turning regimes; regime is here understood to mean a particular combination of the different machining factors: depth of cut, cutting speed, rate of rotation of the work and feed.

In view of the minor difference as regards depth of cut between grinding and finish turning it might be assumed that the changes in the surface layer incident to light-cut turning are nearly identical with those produced by grinding. On the whole our findings confirmed this assumption. Both grinding and light cutting produce a hardening of the surface layer as evidenced by an increase of 30-70% in the microhardness, the exact amount depending on the machining regime. At the same time the width of the lines on the x-ray patterns increases by 100-200% and the relative intensity of the interference lines goes down by 40-76%.

It may be assumed that the hardening of the metal, as evaluated by microhardness measurements, is due primarily to elementary distortions of the atomic crystal lattice, connected with displacement of the centers of oscillation of the atoms away from the initial points of the space lattice, and to crystallite distortions of the lattice connected with fragmentation and deformation of the blocks. As a result of the present study we established the dependence of changes in the distortions of the crystal lattice on changes in the grinding or finish-turning regime. In the present report we shall deal only with the results of comparison of these dependences.

The greatest increase in the crystallite distortions in the case of grinding is observed in the range of small depths of cut (5-25 μ). With increasing thickness of the removed metal, the growth of the crystallite distortions slows down and tends to approach a limiting value at a depth of cut of 50-75 μ. In the case of finish-turning increase of the depth of cut by a factor of up to 5-6 leads to no appreciable increase of the crystallite distortions.

An analogous variation is exhibited by the intensity of the interference lines, characterizing the growth of the elementary distortions of the atomic lattice with increasing depth of cut. This type of variation can be explained on the basis of the experimental and theoretical data on the relationship be-

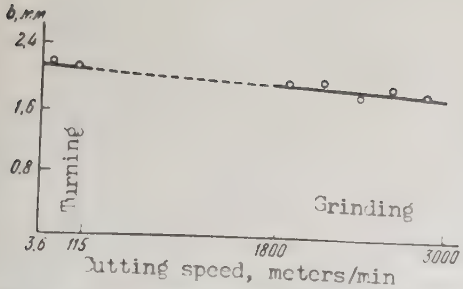

Fig. 1. Dependence of the width of the $K\alpha_1$ interference line on the cutting speed.

tween the depth of cut and the chip thickness[1].

With increasing depth of cut the thickness of the chip obviously increases. At the same time the deforming forces grow, the deformation and fragmentation of the blocks increases and the crystal lattices are deformed to an ever greater extent.

Stabilization of the distortions of the lattice may occur as a result of the softening influence of heat generated in increasing amounts by the cutting as the depth is increased and, also, as a result of attenuation of the growth of deforming forces with increasing depth of cut. From the results obtained with the two different methods of removing metal - grinding and finish-turning - it may be concluded that in general the degree of hardening of the surface layer incident to finishing operations can be controlled by varying the thickness of the layer removed, i.e., the depth of cut.

The curve of Fig. 1 shows the dependence of the line width in the x-ray patterns on the cutting speed. The curve clearly shows that the cutting speed has little influence on the crystallite distortions. An analogous dependence is observed for the elementary distortions of the crystal lattice.

The cutting speed has less influence on the degree of hardening of the surface layer in the case of turning as compared with grinding.

High-speed finish grinding as a rule produces less distortions of the crystal lattice than ordinary grinding. On the basis of comparisons of the results obtained for high speed and ordinary grinding it may be stated that with high speed grinding, which is a more highly productive procedure, there is less deformation of the crystal lattice in the surface layers than in the case of ordinary grinding. This may be explained by the more appreciable generation of heat at the contacting surfaces which results in softening of the metal[2] and by the lesser thickness of the layer removed by the abrasive in high speed grinding.[1]

The influence of feed both in the case of grinding and the case of finish-turning is complex: for certain regimes increasing the feed leads to growth of the distortions; in other cases, to diminution.

For one thing, the feed has an appreciable influence on the thickness of the chip or layer removed. On the other hand, increasing the rate of feed also increases the amount of heat generated. In any specific case the final condition of the surface layer will depend on the resultant influence of these two factors.

The curves of Fig. 2 show the dependence of the width of the interference line on the depth of grinding at different rates of longitudinal feed: in going from a rate of 1 meter per min (curve 1) to 3.75 meters per min (curve 3) the width of the line and, consequently, the crystallite distortions at first increase (curve 2) and then diminish (curve 3). This decrease in the crystallite distortions in going from a longitudinal feed of 1.88 m/min (curve 2) to 3.75 m/min can be explained by the softening effect of the additional heat generated at the faster longitudinal feeds.

The distribution of atomic lattice distortions in depth was also determined by two methods: x-ray analysis and microhardness measurements. To this end successive thin layers were removed from the surface by electrochemical etching and the newly exposed surface investigated between each etching stage.

The two methods of investigation yield results analogous in principle. However, the microhardness method is less sensitive and the actual divergence in determining the thickness of the deformed surface layer is sometimes appreciable (50% or more).

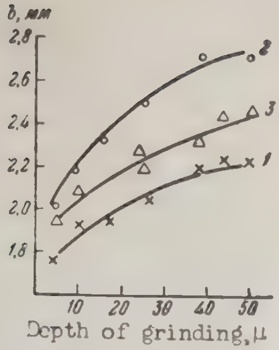

Fig. 2. Dependence of the width of the $K\alpha_1$ interference line on the depth of grinding at different rates of longitudinal feed: 1) 1 m/min, 2) 1.88 m/min, 3) 3.75 m/min.

It was established that the distribution of the crystallite distortions in depth is of the same character as the distribution of the elementary distortions of the atomic lattice. It may be said that in grinding and finish-turning of steel and iron there develop in the metal, as a result of deformation and fragmentation of the blocks, both crystallite and elementary distortions of the atomic crystal lattice.

The depth of work hardening produced by finish-turning is somewhat greater than that produced by grinding. In the case of grinding, the surface zone in the metal having a distorted structure attains a thickness of 120 μ, while in the case of light-cut turning the corresponding thickness may be 200 μ or greater.

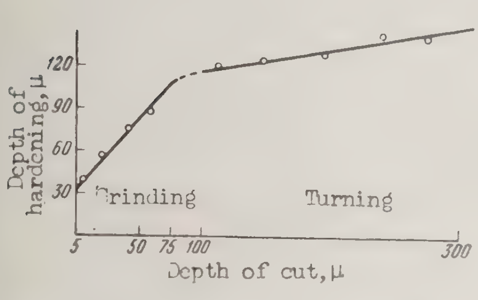

Fig. 3. Variation of the depth of work hardening on the depth of cut.

The variation of the depth of work hardening with the depth of cut is shown in Fig. 3. On the basis of these data and those for the dependence of the crystallite distortions on the depth of cut it may be assumed that the thickness of the layer hardened as the result of cutting is almost linearly related with the maximum hardening on the surface of the metal. This is particularly noticeable in the range of small and medium depths of cut. In the range of greater depths of cut (100-300 μ), wherein the degree of distortion in the surface layer is stabilized, there is observed a certain increase in the thickness of the hardened layer with increasing depth of cut. This is explained by the change in the nature of the distribution in depth of distortions of the crystal lattice with increasing depth of cut: with small depths of cut the distribution of distortions in the surface layer is characterized by a sharp transition from maximal distortion to the undeformed metal; in case of deep cuts there is a more gradual transition from the region of maximum distortion to the undeformed metal.

The following conclusion may be drawn from the results of our investigation: in finish machining metals by grinding and light-turning the degree of hardening and the thickness of the hardened surface layer can be controlled by varying the depth of cut.

"V.M.Molotov" Leningrad Engineering-Economic Institute

References

1. E.N.Maslov, Osnovy teorii shlifovaniia (Fundamentals of grinding theory), M. 1951.

2. N.N.Davidenkov & Iu.S.Terminasov, Zhur. tekh. fiz., 14, 409 (1944).

MECHANISM OF THE INFLUENCE OF MINOR IMPURITIES ON THE FORMATION OF RECRYSTALLIZATION TEXTURE IN METALS AND ALLOYS

– D.I.Lainer & E.I.Krupnikova

All metal products are characterized by a greater or lesser degree of anisotropy of their physical and mechanical properties. In some cases the anisotropy of the properties may be so great that design engineers and technologists have to take it into account.

Design engineers have to take anisotropy into account because in their calculations they must frequently allow for minimal strength or other properties in a given direction. In this connection we would like to draw attention to A.V.Stepanov's observation that materials can often be utilized more efficiently by taking care to load them in the direction of the maximum value of their physical characteristics. When this is done and in cases where particular magnetic properties are required it may be advantageous to strive for maximum anisotropy of properties in question.

Process technologists must take anisotropy of mechanical properties into account in cases, for example, when the metal sheets or bands are intended for deep drawing. In this case pronounced anisotropy of the recrystallized material may result in shells with wavy, split edges or other defects. This both complicates the forming operations and leads to waste.

Whereas in single crystals the anisotropy is connected with the nature of the crystal itself, in polycrystalline solids anisotropy of the physical properties is a function of the degree of perfection of the preferred orientation (fiber or texture). The purpose of the present study was to find methods providing a measure of control over the formation of texture in recrystallization.

It follows from the data in the literature that to obtain a recrystallized material with isotropic properties and a disoriented structure the following technological practices should be followed: a) a minimal degree of deformation between anneals, b) optimal annealing conditions (temperature and time) and c) in case of rolling, changes in the direction of feeding the metal through the rollers.

Data in the literature on the influence of small admixtures on the preferred orientation are scant.

We investigated the influence of a large number of different impurities at different concentrations on the formation of texture of deformation and recrystallization in aluminum, copper, nickel and German silver. By way of initial materials we used high purity metals and employed melting conditions assuring retention of the high purity.

The investigations were carried out by the x-ray method with plotting of pole figures, the method of determining the anisotropy of the elastic and mechanical properties by physical testing of specimens cut at different orientations relative to the direction of rolling and by the "visual" method of observing the degree of fringing at the edges of deep drawn shells.

The extensive experimental material accumulated showed that small amounts of added impurities have little effect on the formation of the texture of deformation but have a pronounced effect on the texture of recrystallization with all the consequences following therefrom. Analogous observations have been reported in the literature. However, most investigators have limited themselves to general remarks. There are no reports of systematic investigations and practical recommendations concerning the expediency of adding a given element to specific metals and alloys.

In our study we established the favorable influence of additions of small amounts of silicon to German silver, antimony to copper, calcium to nickel and zinc to aluminum. These elements, as well as others, added in appropriate concentrations facilitate obtaining rolled stock in a recrystallized state with a

disoriented structure; the rolled sheets are characterized by little or no anisotropy of the mechanical properties. Some of our findings were verified under plant conditions and were found to be highly effective.

We believe that the mechanism of the influence of impurities on the formation of the texture of recrystallization may be pictured as follows. It follows from the Gibbs-Curie-Wolf principle that the direction of development of crystals can be altered by changing the surface energy of the individual crystal faces.

The results of numerous investigations of crystallization from aqueous solutions show that even very minor amounts of impurities have a decisive influence on the shape of the forming crystals. The mechanism of this influence is probably the following: during heating the surface-active impurity particles are adsorbed, in accord with the Gibbs-Curie-Wolf principle and structural correspondence, on certain faces of the recrystallization nuclei. This leads to slowing down of the growth of the crystals in these directions with consequent development of the crystals in the other directions; as a result there is formed a disoriented structure and we obtain a material with isotropic properties.

Thus to be useful the added impurity component must meet the following requirements.

1. The added component must be surface active with respect to the base metal or alloy; otherwise there will be no adsorption on the faces of the crystals during annealing.

2. The added component must not be isomorphic with the base material or alloy; in the case of isomorphism there may be uniform adsorption on all the faces of the recrystallization nuclei; in which case there will only be fragmentation of the structure with retention of the normal crystal habit.

3. The impurities must form a solid solution with the metal or alloy; if the impurity does not enter into solid solution but only forms a mechanical mixture only the usual segregation will occur during annealing.

4. Structural correspondence is a necessary condition for the impurity to have a favorable effect on the texture of recrystallization; depending on the degree of this correspondence the impurities may lead to either a weakening or enhancement of the recrystallization structure.

The above observations have been substantiated by numerous investigations and plant tests.

Scientific Research and Design Institute
for the Processing of Nonferrous Metals

X-RAY INVESTIGATION OF THE INFLUENCE OF HEAT TREATMENT ON PLASTICALLY DEFORMED METALS

- Iu.S.Terminasov and G.A.Feklistov

In recent years there have appeared many papers devoted to x-ray studies of plastic deformation of metals. However, among these there are few papers dealing with the thermal stability of the distortions which atomic crystal lattices undergo during plastic deformation.

This paper is devoted to an x-ray investigation of the mechanism of thermal stability of crystallite and of elementary lattice distortions in plastically deformed metals.

Materials and Procedure

Materials. By way of experimental materials we selected the St.40 steel, aluminum and LS59-1 (ЛС59-1) brass. The specimens were all cylinders 15 mm long and 10 mm in diameter.

To relieve the work hardening due to fabrication the specimens were annealed in a vacuum furnace. After annealing, and x-raying to check the effectiveness of the anneal, the specimens were subjected to compressive deformation in a 60 ton Amsler press.

Deformation at room temperature. The following degrees of deformation were used: a) for steel - 3, 6, 12, 24, 48, and 66%, b) for brass - 3, 6, 12, 24 and 36%, c) for aluminum - 80%.

Special precautions were taken to assure identical test conditions for all samples, to obviate shear and bending and to insure uniform compression. Uniform deformation was assured by careful positioning of the specimens in the test machine and use of a supporting strip with a spherical link, while holding the height of the deformed specimen exactly to the specified value was guaranteed by a specially designed adjustable indicator and signal bell; contacts attached to the struts of this device closed the circuit of the electric alarm bell when the assigned degree of deformation was attained. The degree of deformation was determined by the extent of shortening along the axis of the deformation.

Heat treatment of the plastically deformed specimens. Annealing of all deformed specimens was carried out in a vacuum furnace, the specimens always being loaded into a preheated furnace. This was accomplished by using a specially built vacuum loading flange, which allowed of loading of the specimens at all the temperatures of the experiments. The annealing temperature was recorded by means of a chromel-alumel thermocouple.

The following annealing temperature ranges were chosen for the plastically deformed specimens, the heating period being varied for different specimens: St.40 steel--400-700°; LS59-1 brass--150-300°; aluminum--50-325°.

X-Raying. The x-ray patterns were recorded by the back-reflection method in a KROS camera with a sector cassette.

We used a BSV-4 tube with a cobalt anode for the steel specimens and a BSVL tube for the aluminum and brass specimens. Thus we obtained the (310) and (220) interference lines for steel, the (511) and (422) lines for aluminum and the (420) and (331) lines for brass.

Special arrangements were provided for x-raying the specimen always at the same point on the generatrix. The x-raying and film-processing conditions were strictly identical for all specimens.

Photometry of the patterns and processing of the microphotograms. The x-ray patterns were all analyzed on an MF-2 microphotometer. We employed the procedure of defocusing of the interference line images in the plane of the microphotometer measuring slit. The width of the interference lines was determined as the ratio of the area under the microphotometric curve to the height of this curve; the

distortions of the crystallites were evaluated on the basis of this ratio.

Elementary distortions of the atomic crystalline lattice were determined from the ratio of the intensity of the maximum of the interference line of highest order to the background intensity in the region of small glancing angles where the blackening is greatest.

In addition, the changes in the intensity of the interference lines were determined by the methods of comparing areas under the photometric curves and by the method of comparing the line intensity with the background intensity in the region of reflection angles equal to 75°.

Experimental Results and Discussion

St.40 Steel. In order to investigate the effect of duration of annealing at a given temperature on the mechanism of restoration of the atomic lattice of steel specimens subjected to various degrees of deformation, we annealed the specimens in lots of six, all degrees of deformation being represented in each lot. This was done at all the selected temperatures: 400, 500, 600 and 700°.

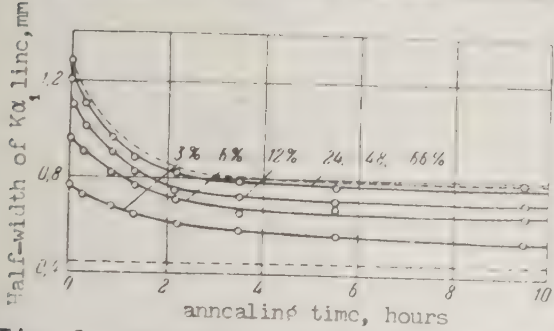

Fig. 1. Dependence of the half-width of the $K\alpha_1$ (310) interference line on the annealing time at 400° for St.40 steel specimens subjected to different degrees of deformation.

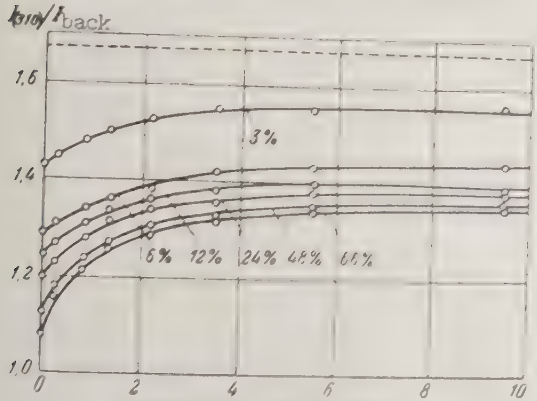

Fig. 2. Dependence of the ratio $I_{(310)}/I_{back}$ on the annealing time at 400° for specimens of St.40 steel subjected to different degrees of compression.

Fig. 1 shows the dependence of the half-width of the (310) interference line on the annealing time at 400° for St.40 steel specimens deformed different amounts, while Fig. 2 shows the variation of the ratio $I_{(310)}/I_{back}$ with the annealing time at 400° temperature.

It is clear from the curves of Figs. 1 and 2 that removal of both the crystallite and elementary distortions occurs most rapidly during the first stages of annealing; then the process slows down and, after reaching a certain value, the residual distortions are stabilized. As is evident from the slopes of the curves, the rate of initial removal increases with the degree of deformation. The general character of the changes in both the crystallite and elementary distortions, however, remains the same for all specimens, regardless of the degrees of deformation.

Annealing of deformed specimens at higher temperatures results in more intensive decreases in crystallite and elementary distortions. Almost complete splitting of the Kα doublet of the (310) line is observed after holding for 50 minutes at 500°. Calculations show that as a result of annealing at this temperature, the crystallite distortions in the deformed specimens are removed to the extent of about 90%; the corresponding average value for the elementary lattice distortions is 60%.

The changes in the ratio $I_{(310)}/I_{back}$ with the annealing time at 600° for specimens subjected to various degrees of deformation are shown in Fig. 3.

The character of the changes observed for deformations of 24-60% differs from that of the changes in the case of 3-12% deformations only in that at the

higher degrees of deformation the beginning is superimposed on the relief of the residual lattice distortions.

LS59-1 brass. Plastically deformed specimens of brass were subjected to heat treatment at temperatures from 150°.

As can be seen from Figs. 4 and 5, after only 30 minutes of heating at 150° there is already an appreciable narrowing of the (420) line and an increase in its intensity. Similar results were obtained for all specimens regardless of the degree of deformation.

Annealing of the plastically deformed brass specimens at the temperatures of 200, 250 and 300° resulted in greater relief of the crystallite and elementary distortions. The greater the degree of distortion of the atomic lattice, the higher is the rate of relief at a given temperature.

To remove fully the distortions of the atomic lattice the annealing temperature must be 250°.

At an annealing temperature of 300°, there is clear evidence of recrystallization of the deformed brass; this process occurred in specimens subjected to all the employed degrees of deformation.

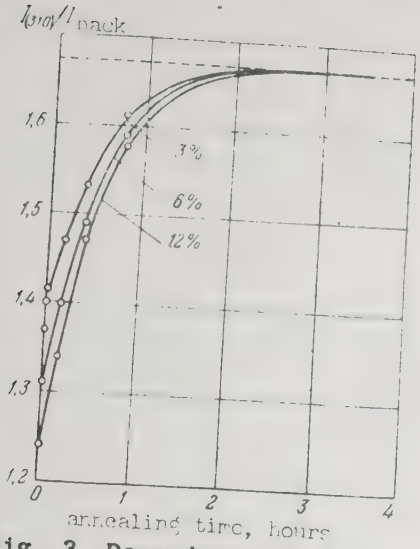

Fig. 3. Dependence of the ratio $I(310)/I_{back}$ on the annealing time at 600° for specimens of St.40 steel subjected to different degrees of deformation.

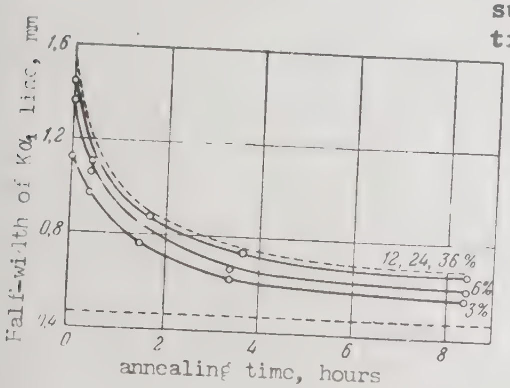

Fig. 4. Dependence of the half-width of the Kα (420) interference line on the annealing time at 150° for LS59-1 brass specimens subjected to different degrees of deformation.

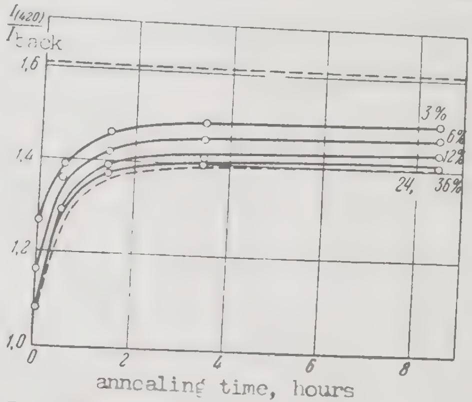

Fig. 5. Dependence of the intensity ratio $I(420)/I_{back}$ on the annealing time at 150°, for specimens of LS59-1 brass subjected to different degrees of deformation.

Aluminum. The aluminum specimens were annealed at temperatures starting with 50°. Holding specimens at this temperature for 127 hours led to a reduction of only 25% in crystallite distortions. No change in the intensity of the (511) line incident to treatment at this temperature was observed. Elementary distortions were also not affected by annealing at 100°, although crystallite distortions are removed more rapidly at this temperature than at 50°. Holding a temperature of 100° for 40 minutes leads to a 47-50% reduction of the crystallite distortions. Annealing at 130° for 25 hours results in a 75-78% relief in crystallite distortions. At this temperature removal of elementary lattice distortions also begins (only about 10-15% relief).

Annealing at a temperature of 190° for 1.5 hours leads to complete removal of crystallite distortions. Under these conditions the elementary distortions are relieved to the extent of 30-35%.

At 210° elementary distortions are removed to the extent of 52-55%.

The general character of the regularities observed during annealing at 210° remains the same as at lower temperatures, but the rate of change in the atomic lattice of the plastically deformed metal and the magnitude of the changes of the residual distortions are appreciably greater than at the lower temperatures. During annealing at 250, 300 and 325° there occurs extremely rapid relaxation of the crystallite distortions, while restoration of the atomic lattice takes place during the initial annealing period.

After annealing at 250°, the elementary distortions are reduced 73-75%. Beginning with a temperature of 300°, recrystallization of the plastically deformed aluminum specimens is observed.

Conclusions

1. The removal of distortions of the atomic crystal lattice under the influence of heat proceeds non-uniformly. Relaxation of elementary and crystallite distortions occurs more intensely during the first moments of heat treatment. With the passage of time the relief process dies down and the residual distortions are stabilized.

2. The nature of the removal of both kinds of distortion depends to an appreciable extent on the initial degree of distortion of the atomic lattice: the greater the initial distortion of the lattice, the more rapid is the process of lattice restoration.

3. For practical purposes it is possible to specify the minimum annealing temperature and holding period necessary for full restoration of the atomic lattice: for the St.40 steel the requisite conditions are heating at 600° for 1 hour 20 minutes; for brass, heating at 250° for 2.5 hours and for aluminum heating at 350° for 1.5 hours.

4. For all of the investigated metals, recrystallization is preceded by the complete removal of the crystallite distortions and appreciable relief of the elementary distortions.

5. The procedure we developed for heating specimens under vacuum allows of loading specimens into the vacuum furnace operating at a stable, constant temperature without disturbing the vacuum.

Department of Experimental Physics at the
"A. I. Gertsen" State Pedagogical Institute of Leningrad

RESIDUAL STRESSES IN METALS AFTER GRINDING

- O.G.Karpinskii & B.M.Levitskii

Grinding is a complex and as yet inadequately studied forming process. Investigation of the stressed state of the surface layer can yield valuable information for clarifying the nature of the grinding process and development of an adequate theory thereof. However, very little is known at present regarding the residual stresses remaining after grinding. This is obvious from the great diversity in the results obtained by different investigators and the fact that there is no general agreement regarding the nature of these residual stresses.

Glikman, Stepanov and Sanfirova[1,2] after grinding specimens of St.20 and EZh2(ЭЖ2) steel detected residual tensile stresses in the surface layer. These investigators are of the opinion that the principal cause of the stresses persisting after grinding is high local heating of the surface layer. An additional factor affecting the development of these stresses may be volume changes connected with phase transformations.

It may be noted that this in general is the most commonly accepted interpretation of the nature of residual stresses left by grinding.

Tensile stresses after grinding have been observed by Almen[3] in annealed spring steel and by Frisch and Thomsen[4] in low carbon steel (S.A.E.1010).

Rovinski[5] detected tensile stresses in aluminum and certain other metals after hand polishing with abrasive paper. He asserts that the residual stresses cannot be regarded as due exclusively to thermal influence to the neglect of mechanical factors.

The present study was devoted to a quantitative x-ray investigation of the influence of the grinding process on the development of residual stresses. The stress state was studied primarily in Armco iron subjected to grinding with KZ-100 water-resistant abrasive paper. The specimens were ground on a machine specially designed for this purpose. The machine was capable of both "directional" grinding in which the "strokes" are parallel to each other and "non-directional" grinding in which there is no favored direction. The grinding speed on this machine was varied from 0.3 to 42 meters/min, while the pressure of the specimen against the abrasive was varied from 1.3 to 5.2 kg/cm^2. Grinding at speeds of 200 to 1400 meters/min was accomplished on a 200 diameter disc faced with abrasive paper.

By appropriate variation in the grinding speed and pressure the specimen could be ground with or without noticeable heating.

In addition Armco iron specimens were ground on a surface grinder with an E60SM$_1$K abrasive wheel.

The residual stresses after grinding where determined from x-ray patterns recorded by the back-reflection method using the Kα radiation of Co.

In order to plot stress distribution curves successive layers of metals were removed from the ground surface. Uniform removal of the layers was assured by electropolishing in a chromium sulfate-phosphate electrolyte. Preliminary tests established that this method of electropolishing does produce any additional stresses in the surface layer. The thickness of the removed layer was measured by means of a Zeiss horizontal optical indicator to within better than 1 μ.

All the x-ray patterns were carefully processed on a photometer and the Kα-doublets were resolved by the method described by Rachinger.[7] In addition to determining the half-width of the diffraction lines, necessary for measuring stresses of the second kind, this method of processing assures a more accurate determination of the position of the maximum for diffused lines and consequently an enhanced accuracy in measuring stresses of the first kind.

We detected high compressive stresses extending to a depth of about 30 μ in Armco iron specimens ground with abrasive paper. After grinding with speeds from 0.3 to 42 meters/min the sum of the principal stresses at the surface attained

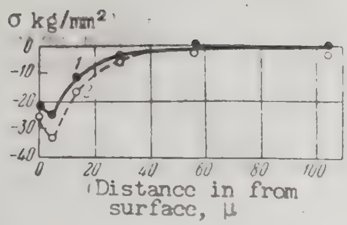

Fig. 1. Distribution of residual stresses in the surface layer of an Armco iron specimen after directional grinding with abrasive paper: 1) stresses parallel to the direction of grinding, 2) perpendicular to the direction of grinding.

as much as 45 kg/mm^2. The curves of Fig. 1 show the distribution in depth of the residual stresses after directional grinding at a speed of 0.3 meters/min and a pressure of 1.3 kg/cm^2.

Increasing the grinding speed from 200 to 1400 meters/min did not change the character of the distribution in depth of the residual stresses but resulted only in the reduction of their absolute magnitude to 20 kg/cm^2.

There is no substantial difference between the distribution of the residual stresses after directional and nondirectional grinding.

In the case of pure commercial grade aluminum we also observed compressive stresses after grinding with abrasive paper.

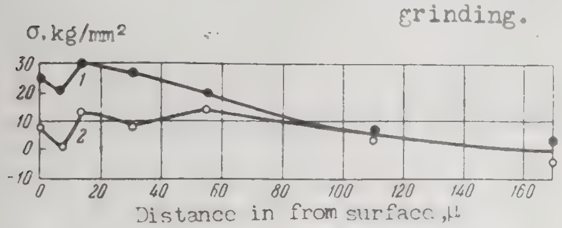

Fig. 3. Distribution of residual stresses of the second kind in the surface layers of an Armco iron specimen after grinding at a speed of a) 5 m/min, b) 650 m/min.

In the surface layer of Armco iron ground on the surface grinder with the E60SM$_1$K wheel (peripheral speed 1800 meters/min, longitudinal feed 2 meters/min, lateral feed 0.005 mm) we found appreciable tensile stresses (Fig. 2). These stresses extend to a depth of the order of 150 µ. The residual stresses in line with and at right angles to the direction of grinding differ appreciably as regards absolute magnitude. It will be seen from Fig. 1 that in grinding with abrasive paper there are also indications of a similar difference, but in this case the difference is of the order of magnitude of the experimental error.

The development of compressive stresses after grinding Armco iron and aluminum with abrasive paper cannot be explained by intense local heating of the surface layer inasmuch as this, as is known, can lead only to tensile stresses. Furthermore, in plastic deformation of the surface layer produced by high heating there could not persist the difference in the magnitude of the principal stresses such as obtained in Armco iron after grinding with the E60SM$_1$K grinding wheel.

These two considerations give reason to assume that the observed residual stresses produced by grinding are due primarily to inhomogeneous plastic deformation.

The results of our investigation of residual stresses of the second kind in Armco iron are shown in Fig. 3. The residual stresses of the second kind were determined from the broadening of the lines in the patterns, since harmonic analysis calculations showed that the line broadening is due primarily to stresses of the second kind. The stresses of the second kind attain their maximum value at the surface of the specimen and penetrate to a depth somewhat inferior to that attained by stresses of the first kind.

In conclusion we desire to thank G.S. Zhdanov for his advice and interest in the work.

Moscow Engineering-Physical Institute

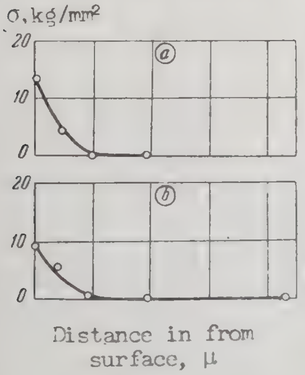

Fig. 2. Same as Fig. 1, but in the case of grinding on a surface grinder with an E60CM$_1$K abrasive wheel.

References

1. L.A.Glikman & V.A.Stepanov, Zhur. tekh. fiz., 16, 791 (1946).
2. L.A.Glikman & T.P.Sanfirova, V.A.Stepanov, Zhur. tekh. fiz., 19, 411 (1949).
3. J.Almen, Mech. Eng., 65, No. 8, 553 (1943).
4. J.Frisch & E.G.Thomsen, Trans. of the ASME, 78, 337 (1951).
5. B.M.Rovinskii, In "Voprocy mashinovedeniia" (Problems of machine design) M.-L. 1950.
6. H.P.Letner & H.G.Snyder, Trans. of the ASME, 75, 873 (1953).
7. N.A.Rachinger, J. Sci. Instr. 25, 254 (1948).
8. B.Ia.Pines & N.G.Berezniak, Zhur. tekh. fiz., 24, 329 (1954).

X-RAY INVESTIGATION OF THE SURFACE QUALITY OF METALS MACHINED BY HIGH-SPEED TURNING

- T.Kh.Chormonov

As Kuznetsov[1] showed machining of metals by cutting is a complex process in which the machined material successively undergoes elastic and plastic deformation. The latter is of course by far the more important where lasting effects are concerned. High-speed turning of metals produces substantial changes in the different physical and mechanical properties of the machined metals.

The present study was devoted to an x-ray investigation of the influence of high-speed turning on the surface quality of metals.

Materials and procedure

By way of the experimental material for investigating distortions of the second and third kinds we selected samples of 38KhMIuA (38XMЮA) and 2Kh13 (2X13) steel as well as of LK80 (ЛК80) brass. The technological variables were the cutting speed, the feed and the depth of cut. The cutting speed was varied between 220 and 600 meters/min; the feed t from 0.1 to 0.2 mm/rev; the other technological factors were: the depth of cut h was kept constant at 2 mm; the plan approach angle was 60°.

The x-ray patterns for determining the distortions of the second and third kind in the specimens were registered by the back-reflection method in a KROS camera by the Kα radiation from a Co anode for the steel and Kα radiation from Cu for the brass specimens.

The operating regime of the x-ray tube, the distance from the collimating diaphragm to the specimen and the conditions of processing the films were maintained rigorously constant throughout the test. An x-ray pattern was recorded for each specimen after turning and then the plastically deformed layer was etched off electrolytically. The thickness of the layer removed by electropolishing was determined to within 2-3 μ by means of an IZV-1 optical indicator.

As is known, the presence of distortions of the second kind in the specimen leads to diffusion of the interference lines in the x-ray pattern. However, the diffusion of the interference lines can also be caused either by the smallness of the regions of coherent scattering of the x-ray or by inhomogeneity of the solid solution. In our experiment the index to the magnitude of distortions of the second kind was the diffusion (broadening) of the Kα-doublet interference lines on the pattern. The index to the magnitude of distortions of the third kind was the decrease in the ratio of the integral intensity of the interference line to the intensity of the diffused background in the pattern: for steel $I_{(310)}/I_{bkgd}$; for brass $I_{(420)}/I_{bkgd}$. In addition the magnitude of strains of the third kind in the steels was evaluated from the magnitude of the ratio of the areas under the photometric curves for the (310) and (220) interference lines:

$$III = I_{(310)}/I_{(220)}.$$

However, the first method proved to be more sensitive than the conventional procedure of comparing two interference line intensities.

Results and Discussion

The variation of the interference lines width with the cutting speed for the steel and brass specimens is shown in Fig. 1.

The results of the x-ray investigation showed that with increasing cutting speed in the range from 220 to 600 meters/min with the other technological factors kept constant, the broadening of the interference lines tends to decrease. Curve 5 in Fig. 1 for brass is similar in shape to curve 4 for the same material. The

distinctive feature of curve 5 compared with curve 4 is only the somewhat greater diffusion of the Kα-doublet, presumably due to doubling the rate of feed. The decrease in the diffusion of the lines with increasing turning speed for the steel and brass is apparently to be explained by the process of relaxation, i.e., relief of strains of the second kind as a result of a rise in temperature in the metal under and behind the tool point.

The curves 6 through 10 in Fig. 1 show the dependence of the relative intensity of the interference lines on the cutting speed. At the lowest cutting speed employed in the experiments there is an appreciable drop in the intensity of the interference lines which indicates the development of appreciable strains of the second kind. As the cutting speed is increased the intensity of the lines in the pattern for the same metals increases, i.e., the distortions of the third kind decrease. A certain amount of heat is generated in cutting metals, the amount generated increasing with the cutting speed. Consequently, in this case we have a unique thermo-relaxation of the plastically deformed metal, which at high-speed turning leads to partial removal of distortions of both the second and third kind.

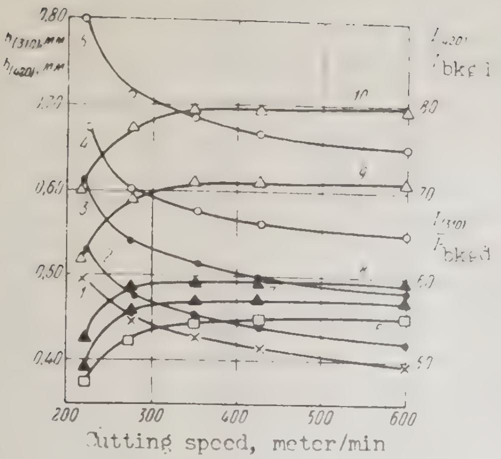

Fig. 1. Dependence of the width of the Kα-doublet (b) and the relative intensity ($I_{(310)}/I_{bkgd}$) of the (310) interference line for 38KhMIuA and 2Khl3 steels and width and ratio of the (420) line for LK80 brass on the cutting speed and feed t: 1 & 6) 38KhMIuA steel; 2,3,7 & 8) 2Khl3 steel; 4,5,9 & 10) LK80 brass; 1,2,3) $b_{(310)}$; 4,5) $b_{(420)}$; 6,7,8) $I_{(310)}/I_{bkgd}$; 9,10) $I_{(420)}/I_{bkgd}$; 2,4,8, 10) t = 0.1 mm/rev; 3,5,7,9) t = 0.2 mm/rev.

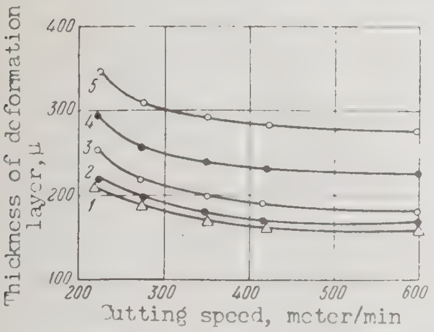

Fig. 2. Dependence of the depth of penetration of plastic deformation in the steels and brass on the cutting speed and feed t: 1) 38KhMIuA steel, t = 0.1 mm/rev; 2) 2Khl3 steel, t = = 0.1 mm/rev; 3) LK80 brass, t = 0.1 mm/rev; 4) 2Khl3 steel, t = 0.2 mm/rev; 5) LK80 brass, t = 0.2 mm/rev.

When deformable metals such as steel and brass are cut, plastic deformation occurs ahead of and under the tool point; this plastic deformation spreads, penetrating to a certain depth below the surface. It will be seen from the curves of Fig. 2 that the penetration of plastic deformation in steel and brass decreases with increasing cutting speed in the 220-600 meters/min range. It was found that when the feed is increased by a factor of 2 (from 0.1 mm/rev to 0.2 mm/rev), the depth of penetration of the plastic deformation increases by about 35-45%.

To investigate the microhardness of the specimens we utilized a PMT-3 hardness tester. We determined the dependence of the microhardness of the 2Khl3 steel and LKh80 brass on the cutting speed. The results of the microhardness determinations for these materials are in accord with the data obtained in investigating the strains.

From the results of our x-ray studies, it may be concluded that the cutting speed as well as the feed and depth of cut have a pronounced effect on the atomic-crystal structure of the surface layers of steel and brass.

Kazakh Mining and
Metallurgical Institute

Reference

1. V.D.Kuznetsov, Fizika tverdogo tela (Solid state physics), Vol. III, Tomsk 1944.

X-RAY INVESTIGATION OF DISTORTIONS OF THE CRYSTAL LATTICE OF MINERAL FIBERS

- E.O.Shvaikovskaia

Distortions of the regular crystal structure and the associated increase in the internal energy of the deformed crystal result in changes in the properties of the crystal. Thus, for example, deformed crystals exhibit an increased resistance to deformation (hardening), an increased resistance to corrosion, an enhanced rate of phase transformations, etc.

In the present study we investigated the influence of the rate of deformation on the plastic deformation. By way of experimental material we used mineral fibers: i.e., asbestos. This choice was dictated by the consideration that as regards structure these fibers approach a one-dimensional chain.

Fibrous materials classed as asbestos, yield x-ray patterns analogous to conventional rotation patterns but obtained without the usual rotation of the crystal.

Just as in conventional rotation patterns, the reflections obtained from fibers are arranged in distinctive layer lines. When the specimen is deformed the usual diffraction picture is altered. Thus the x-ray patterns serve to characterize the state of the fibers.

Experimental procedure

The x-ray patterns were registered using copper radiation by the Laue method in a URS-70 camera (voltage 25 kv, current 18 ma; collimator diaphragm aperture 1 mm dia.). The sample-to-film distance was 4.5 cm; the exposure time 5 hours.

The fibers were first x-rayed in the natural state and were then deformed by bending and also by impact.

The bending was accomplished on a trihedral prism at different rates: slow and fast (the rate of deformation was not determined quantitatively).

Weights and a pendulum were used for applying the impact loads. Different weights weighing from 1 to 10 kg were suspended 20-30 cm above the specimen; the suspending string was then burned and the weight allowed to fall on the specimen positioned on a special stand. One series of experiments was carried out on samples 0.5 mm thick; another series on samples 1 mm thick. The pendulum procedure was similar except that in this case the samples were clamped at both ends in appropriate stands. The pendulum was pulled back with a string which was then burned, allowing the pendulum to swing down and deliver the blow. The samples used had the same thickness (0.5 and 1 mm). The deformed samples were then x-rayed.

The x-ray pattern of a natural (undeformed) fiber is shown in Fig. 1. That of a sample rapidly deformed by bending is shown in Fig. 2. As may be seen from these patterns the structure changes little as a result of rapid bending. In contrast the structure undergoes appreciable alteration in the case of slow deformation by bending; the Debye rings are clearly discernible in Fig. 3. Fig. 4 is the pattern of a sample deformed by impact.

The impact test substantiated the results obtained in deformation by bending. With the exception of a few minor variations the patterns of all the samples subjected to impact were similar to the patterns obtained for the sample deformed by rapid bending.

Thus it was established that the structure of a deformed mineral fiber (asbestos) depends on the rate of deformation: the crystal structure was distorted to a much greater extent when the deformation occurred slowly; in the case of rapid deformation the distortions were negligible.

It may be concluded, therefore, that what is important where distortions of the crystal lattice are concerned is not so much the magnitude of the applied force as the time during which it acts, in other words, the impulse of the force.

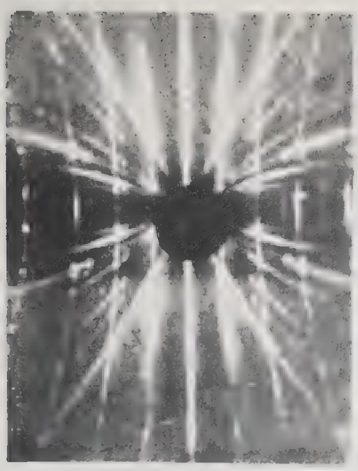

Fig. 1. Pattern of natural fiber.

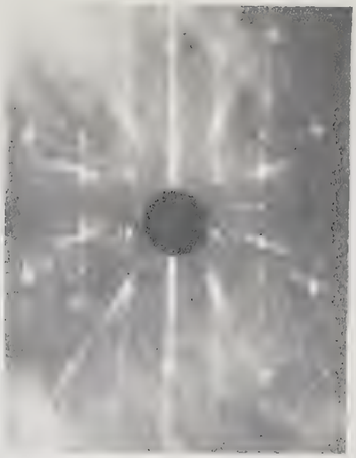

Fig. 2. X-ray pattern of rapidly deformed sample (bending).

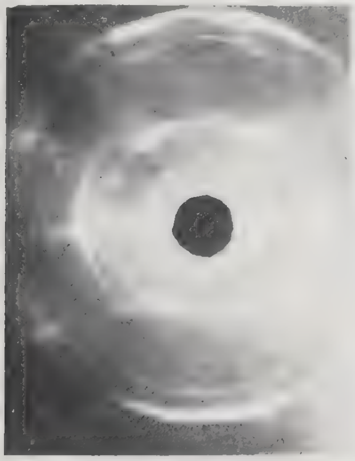

Fig. 3. Pattern of slowly deformed sample (bending).

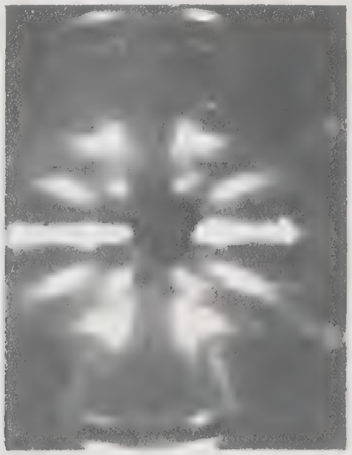

Fig. 4. Pattern of sample after impact tests.

Institute of Mechanical Processing.

X-RAY INVESTIGATION OF COMPOUNDS IN THE Bi-Rh AND Bi-Pd SYSTEMS IN CONNECTION WITH SUPERCONDUCTIVITY STUDIES

- N.N.Zhuravlev and G.S.Zhdanov

In investigating the superconducting properties of alloys of bismuth with rhodium and bismuth with palladium, it was discovered that a given specimen could have either different temperatures of transition to the superconducting state or could lose entirely its capacity to undergo such a transition, depending on the preceding heat treatment. The components of these alloys are not themselves superconductors; it has been established that the superconductivity of such alloys is due to the formation of intermetallic compounds.[1-6] A knowledge of the phase compositions and the atomic crystal lattice structure of the compounds can be of great help in elucidating the reasons for the changes in the temperature (T_k) of transition to the superconducting state and the loss of ability to undergo the transition as a result of heat treatment.

We therefore undertook a microscopic and x-ray investigation of the Bi-Rh and Bi-Pd systems.

Investigation of the Bi-Rh system

The Bi-Rh phase diagram (Fig. 1) was constructed by Rode[7]. Rode notes the existence of three compounds: BiRh, Bi_2Rh and Bi_4Rh.

We made a more profound x-ray and microscopic study of the Bi-Rh system[6-8]. In essential respects, Rode's phase diagram was substantiated by our investigation. The polymorphism of the compounds Bi_2Rh and Bi_4Rh, surmised by Rode, was also confirmed.

Isolated crystals of the three compounds BiRh, Bi_2Rh and Bi_4Rh were produced, with several modifications being obtained of the compounds Bi_2Rh and Bi_4Rh. The following physical properties were determined for all of the separated crystals: density, microhardness, crystal habit, superconducting transition temperature; as well as certain data on the atomic crystal lattice structure. This information is listed in Table 1.

The compound BiRh crystallizes in the hexagonal system and becomes super-conducting at $T_k = 2.06°K$. However, alloys having the composition BiRh exhibit fluctuations in T_k over the interval 2.06-2°K.[2] This fluctuation can be explained by variation in the amount

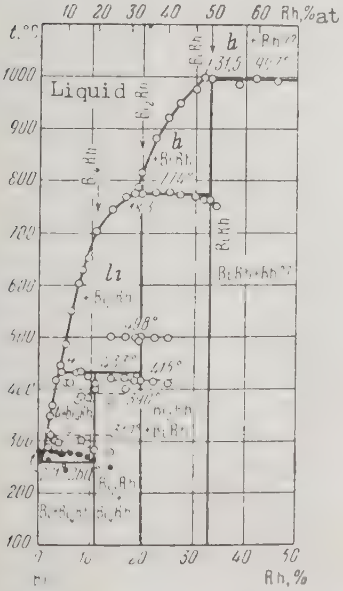

Fig. 1. Phase diagram of the Bi-Rh system.

Table 1

Crystal Structure and Properties of Bi-Rh Compounds

Compound	T_k, °K	Density σ_L	Density σ_X	Mean microhardness kg/mm²	Crystal system	Lattice parameters a, Å	b, Å	c, Å		z
α Bi_4Rh	·	11.0	11.24	105	Cubic	14.928	—	--	—	24
β Bi_4Rh	3.2	10.7	—	65	Rhombic	11.4	4.25	9.0		—
γ Bi_4Rh	2.7	[illegible]	—	40	Hexagonal	—	--	—	—	—
α Bi_2Rh	--	12.2	12	230	Rhombic	5.9	6.8	7.2		4
β-Bi_2Rh	—	11.[illegible]	11,6	45	Monoclinic	16.2	7.0	10.5	92°30′	16
BiRh	2,06	12.5	12.65	410	Hexagonal	4,09	--	5,66	—	2

of the compound present.[9]

Isolated crystals of Bi_2Rh were obtained in two modifications: a high temperature modification and a low temperature one. Crystals of the high-temperture modification belong to the monoclinic syngony and do not undergo superconducting transition down to 1.3°K; crystals of the low-temperature modification belong to the rhomibc syngony and also do not pass into the superconducting state above 1.3°K.

Alloys of the composition Bi_2Rh when cooled slowly, go over into the superconducting state at T_k= 3.2-3.6°K; rapidly cooled alloys have three transition temperatures, 2.2, 2.9 and 3.4°K. The superconductivity in such alloys has been explained by the presence in them of superconducting crystals of the compounds Bi_4Rh and BiRh. Annealed specimens of the Bi_2Rh composition alloy do not transform to the superconducting state.

Crystals of the compound Bi_4Rh were isolated in three modifications: α, β and γ. Crystals of the high-temperature γ-modification belong to the hexagonal system; those of the middle-temperature β-modification - to the rhombic system; those of the low-temperature α-modification - to the cubic system. Crystals of β-Bi_4Rh do not have a superconducting transition down to 0.1°K; crystals of α-Bi_4Rh become superconducting at T = 3.2°K; crystals of γ-Bi_4Rh pass into the superconducting state at T = 2.7°K.

Alloys of the composition Bi_4Rh exhibit an unstable behavior at low temperatures. Annealed specimens do not have superconducting properties. Alloys with different heat treatment histories have different values of T_k.[6] The differences in transition temperature are explained by the presence of varying amounts of the three modifications of Bi_4Rh. The presence in the alloy of two superconducting modifications results in two superconducting transition temperatures. The several tenths of a degree of temperature difference between the values of T_k for the isolated crystals and for crystals of the compound in the alloy may be explained by stresses developing in the heterogeneous alloy in the process of crystallization.

In addition to the above-mentioned modifications (α-, β- and γ-Bi_4Rh, and α- and β-Bi_2Rh) we obtained needle-like crystals similar in crystal habit to β-Bi_4Rh from the alloy with 14% Rh. X-ray investigation of these crystals showed* that they, like β-Bi_4Rh crystals, belong to the rhombic system, but have a smaller unit cell, characterized by $\underline{a}$ = 7.59 ± 0.01 A, $\underline{b}$ = 4.01 ± 0.01 A, $\underline{c}$ = 5.53 ± ± 0.01 A.

The small amount of the crystals precluded determination of their specific gravity, exact chemical composition and superconducting properties.

In our opinion, the location of temperature stagnation points in the Bi-Rh phase diagram (Fig. 1) for alloys in the region of the composition Bi_2Rh allows the drawing of an additional horizontal line at a temperature of about 415°. This line corresponds to still another polymorphic transformation of the compound Bi_2Rh, i.e., the horizontal line at 433° and the polymorphic transformation line at about 415° are very close to each other and Rode did not separate them. Thus, presumably the compound Bi_2Rh can crystallize in three modifications with polymorphic transformation temperatures at 415 and 498°. The crystals investigated belong to the medium-temperature modification of Bi_2Rh. The difficulty in obtaining crystals of the medium-temperature modification suitable for study stems from the peculiar conditions under which this modification forms.

During cooling of the alloy in the solid state the transition from the high-temperature modification of Bi_2Rh to the medium-temperature one (near 500°) is accompanied by a sharp increase in the volume of the alloy, i.e., by a decrease in its density. On the other hand, the density of the low-temperature modification of Bi_2Rh is higher than that of the high-temperature one; for this reason, obtaining well-formed crystals of the medium-temperature modification throughout

---

*R.I.Kuzmin, Thesis, MIFI, 1955.

the whole volume of the alloy is difficult under the given conditions.

Crystals of the medium-temperature modification of Bi_2Rh are formed in the shape of very fine needles in cavities, i.e., under conditions where the volume factor does not interfere with their formation.

Investigation of the Bi-Pd System

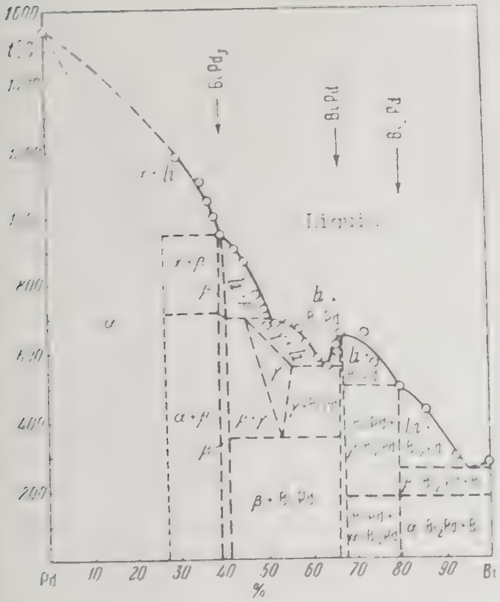

Fig. 2. Phase diagram for the Bi-Pd system.

The preliminary phase diagram of the Bi-Pd system shown in Fig. 2 was constructed on the basis of microscopic and x-ray studies of alloys of bismuth with palladium and determinations of the melting points of a series of alloys.

The following compounds and solid solutions can crystallize out in the Bi-Pd system:

a) Bi_2Pd melts with decomposition at 500° and forms an eutectic mixture with bismuth; it can exist in two modifications with a phase transition temperature of about 200°;

b) BiPd corresponds to the peak in the melting-point diagram; it melts at about 650° and yields an eutectic mixture with the γ-phase (see below); it can dissolve a small quantity of bismuth;

c) $BiPd_3$ (β-phase) melts at about 950°; with an excess of bismuth it forms a solid solution (within narrow limits) and undergoes a polymorphic transformation;

d) in the region of concentrations lying between the composition BiPd and $BiPd_3$ there exists a γ-phase which undergoes eutectoid decomposition into BiPd and $BiPd_3$ (β-phase) in the temperature range from 250 to 400°;

e) in the solid state, palladium is capable of dissolving approximately up to 28% bismuth.

Some of the physical properties of compounds of bismuth with palladium (Table 2) were investigated in the same way as described for the Bi-Rh compounds.

Table 2

Crystal Structure and Properties of Bi-Pd Compounds

Compound	T_c, °K	Density		Mean microhardness kg/mm²	Crystal system	Lattice parameters				
		σ_{exp}	σ_X			a, Å	b, Å	c, Å	β	z
α Bi_2Pd	1,7	11,5	11,58	170	Monoclinic	12,74	4,25	5,665	102°35'	4
β Bi_2Pd	4,25	11,7	11,87	135	Tetragonal	3,362	- -	12,983		12
[illegible]	[illegible]7	12,[illegible]	[illegible]	[illegible]	Rhombic	7,203	8,707	10,662	- -	6

The compound Bi_2Pd can exist in two modifications: a low-temperature (α) modification and a high-temperature (β) one.[10] The low-temperature modification of Bi_2Pd was obtained in the form of a needle with a parallelogram cross section and in the form of a 1-3 mm diameter rod in a quartz capillary tube. It crystal-

lizes in the monoclinic system[10,11] and has a superconducting transition temperature $T_k = 1.7^{\circ}K$.

The high-temperature modification of Bi_2Pd was obtained in a quartz capillary tube by quenching the alloy of composition Bi_2Pd from the liquid state at 18-25° in water. It crystallizes in the tetragonal syngony[10] and becomes superconducting at $T_k = 4.25^{\circ}K$.

Crystals of BiPd were obtained by growing them in a quartz capillary. BiPd crystallizes in the rhombic system[10,12]. The structure of BiPd does not have a center of symmetry. BiPd becomes superconducting at $T = 3.7^{\circ}K$.

The γ-phase and $BiPd_3$ are not superconductors.

If a quenched specimen of β-Bi_2Pd, which becomes superconducting at $T_k =$ $= 4.25^{\circ}K$, is annealed, then after annealing the superconducting transition will occur only at 1.7°K, which is the value of T_k for the monoclinic α-modification. If the specimen which has been annealed is melted and then again quenched, superconductivity will again become manifest at 4.25°K. Thus, specimens of Bi_2Pd behave like those of Bi_4Rh, with the difference that, after annealing, specimens of Bi_4Rh lose their superconducting properties altogether, while those of Bi_2Pd have a substantially lower superconducting transition temperature. It must be noted that if quenching is not sufficiently rapid or if the specimen is not fully annealed, the presence of both phases leads to a situation where the falling off of the resistance begins at 4°K and is completed only at 1.7°K. This great smearing out of the transition curve is probably the consequence of large stresses developing during the cooling of the two phase system.[5]

Alloys having the composition BiPd go over into the superconducting state in the 3.6-3.9°K temperature interval, which can be explained by the low solubility and the presence of stresses.

The superconductivity of alloys richer in palladium than BiPd is explained by the presence in them of BiPd crystals which appear as a consequence of the eutectoid decomposition of the γ-phase.

The compounds of greatest interest in the examined systems are Bi_4Rh and Bi_2Pd. The fact that these compounds form several modifications with differing superconducting transition temperatures is of great interest where interpretation of the nature of superconductivity is concerned.

The compound Bi_4Rh has three monotropic modifications: γ, β and α. The polymorphic transformations $\gamma \rightarrow \beta \rightarrow \alpha$ occur only when the alloy is cooled rapidly from the liquid state. We did not succeed in observing the reverse transformations; crystals of α-Bi_4Rh retain their crystal form up to the temperature of incongruent melting. The two metastable modifications, β- and γ-Bi_4Rh, are both superconducting while α-Bi_4Rh does not exhibit superconductivity down to ultralow temperatures.[4]

Only the atomic crystal structure of α-Bi_4Rh has been fully determined[13] so that comparison of the crystal structures of these modifications is still impossible.

Table 3

Interatomic Distances
and T_k of the Compound Bi_2Pd

Compound	T_K, °K	Interatomic distance, Å		
		Bi—Bi	Bi—Pd	Pd—Pd
α—Bi_2Pd	1,7	3,29	2,78	2,78
β—Bi_2Pd	4,25	3,36	2.97	3,36

In this respect we are more fortunate in the case of Bi_2Pd which has two modifications with different values of T_k. Comparing the minimum interatomic distances for the two modifications of Bi_2Pd (Table 3), we note that the greater interatomic distance in β-Bi_2Pd as compared with α-Bi_2Pd is associated with an increase in the transition temperature T_k from 1.7°K to 4.25°K.

In conclusion it may be said that we have shown for the first time on the example of Bi-Rh and Bi-Pd alloys that a relationship exists

between polymorphic transformations of binary alloys and changes in the temperature of transition to the superconducting state. The appearance, disappearance and variation of the superconducting properties is associated with changes in the atomic crystal structure of the compounds.

The results of our studies also helped clarify the complex phase composition of superconducting alloys which, in turn, made it possible to explain the differences in behavior at low temperatures of alloys subjected to different thermal treatments and to establish the presence of superconducting properties in the different polymorphic modifications in the investigated compounds.

Physics Department of
"M.V.Lomonosov" Moscow State University

References

1. N.E.Alekseevskii, N.B.Brandt & T.I.Kostina, Zhur. eksp. i teor. fiz., 21, 951 (1951).
2. N.E.Alekseevskii, N.B.Brandt & T.I.Kostina, Izv. AN SSSR, Ser. fiz., 16, 233 (1952).
3. N.E.Alekseevskii, Zhur. eksp. i teor. fiz., 23, 484 (1952).
4. N.E.Alekseevskii & Iu.P.Gaidukov, Zhur. eksp. i teor. fiz., 25, 383 (1953).
5. N.E.Alekseevskii, N.N.Zhuravlev, & I.I.Lifanov, Ibid., 27, 125 (1954).
6. N.E.Alekseevskii, G.S.Zhdanov & N.N.Zhuravlev, Ibid., 28, 237 (1955).
7. E.Ia.Rode, Izv. Instituta platiny (Bulletin of the Platinum Institute), 7, 21 (1929).
8. N.N.Zhuravlev & G.S.Zhdanov, Zhur. eksp. i teor. fiz., 28, 228 (1955).
9. V.P.Glagoleva & G.S.Zhdanov, Ibid., 25, 248 (1953).
10. N.N.Zhuravlev,& G.S.Zhdanov, Ibid., 25, 486 (1953).
11. L.S.Zevin, G.S.Zhdanov & N.N.Zhuravlev, Ibid., 25, 751 (1953).
12. D.M.Kheiker, G.S.Zhdanov & N.N.Zhuravlev, Ibid., 25, 621 (1953).
13. V.P.Glagoleva & G.S.Zhdanov, Ibid., 30, 248 (1956).

X-RAY INVESTIGATION OF THE SECONDARY STRUCTURE OF CRYSTALLITES IN RECRYSTALLIZED METALS

- V.N. Shcherbakov

Introduction

The primary purpose of the present investigation was to find answers to the following questions:

1) whether there exist secondary disturbances (mosaic derangement) of the primary atomic structure of the crystallites of polycrystalline materials;

2) in the event that such secondary disturbances of the primary atomic structure do occur, how pronounced they may be and to what degree they depend a) on the type and percent of impurities present and b) on the progress of recrystallization heat treatment;

3) how do these secondary disturbances in the structure of the crystallites and their changes affect the width of both individual interference spots, associated with the diffraction of x-rays by individual crystallites, and of the interference lines as a whole.

The heat treatment conditions were selected so that it would be possible to follow through the entire process from the beginning of treatment recrystallization to the culmination of the process in collective recrystallization.

For the investigation we employed the special procedure developed by the writer in 1950 and described in Ref. 1.

1. Description of the experiments and the basic results

We investigated technically pure aluminum of two grades (Al I and Al II), commercial grade pure copper and α-brass. The data on the impurity content of these materials are summarized in Table 1.

Table 1

Chemical composition of the investigated aluminum, copper and α-brass specimens

Substance	Chemical composition, %									
	Fe	Zn	Bi	Pb	Si	Cu	Mg	Mn	Ni	Al
Al I	traces	—	—	—	0,07	traces				remainder
Al II	0,42	—	—	—	0,28					
Cu	traces	—	0,02	0,01	—	remainder	—	—	—	—
CuZn	0,088	38,062	traces		—	61,85	—	—	—	—

Five specimens in the form of planeparallel plates measuring (0.05-0.1) x (5-8) x (12-17) mm were prepared of each material. The final preparation of the specimen consisted of mechanical deformation (rolling) with a reduction of about 90% followed by recrystallization annealing. The progress of the recrystallization process from the beginning to the termination of the treatment recrystallization stage and from the beginning to complete development of the stage of collective recrystallization was controlled and monitored by counting the number of interference spots on the appropriate interference rings appearing in the series of three Debyegrams recorded for each specimen (under "a series of Debyegrams" here and below we mean three Debye x-ray patterns obtained from the same area of one and the same specimen at three different film-to-specimen distances, other x-raying conditions remaining constant). The data on the heat treatment of the specimens subjected to preliminary 90% reduction by rolling, as well as

the results of counts of the interference spots are listed in Table 2.

Table 2

Data on the heat treatment of the investigated aluminum, copper and α-brass specimens and the number of spots on the interference rings in the series of Debyegrams obtained from the investigated specimens

Substance	Sample No.	Treatment (recrystallization annealing)	Number of interference spots on Debye rings		
			$(111)_\beta$	$(111)_\alpha$	$(002)_\alpha$
1	2	3	4	5	6
Al I	1	350°, 20 sec	41	99	69
	2	350°, 40 sec	89	163	121
	3	350°, 1 min	142	223	154
	4	450°, 1 hr	53	79	57
	5	450°, 36 hrs	23	37	26
Al II	1	300°, 2 min	86	127	89
	2	300°, 10 min	192	293	209
	3	300°, 1 hr	256	363	282
	4	450°, 12 hrs	151	229	162
	5	450°, 36 hrs	49	87	61
Copper	1	270°, 20 sec	19	37	29
	2	270°, 5 min	53	78	59
	3	270°, 25 min	71	104	81
	4	270°, 5 hrs	49	68	51
	5	270°, 48 hrs	34	47	35
α-Brass	1	400°, 20 sec	63	94	71
	2	400°, 10 min	179	276	207
	3	400°, 1 hr	317	647	479
	4	400°, 10 hrs	189	371	271
	5	400°, 48 hrs	127	242	179

As may be seen from Table 2, samples Nos. 1, 2 & 3 represent the beginning, development and culmination of the process of heat-treatment recrystallization, while samples Nos. 4 & 5 represent the beginning and development of the process of collective recrystallization.

The patterns were recorded by the radiation from a demountable ion tube with a copper anode; the diameter of the focal spot was about 7-8 mm. The cameras consisted essentially of an optical bench on which were mounted the holders carrying the collimator, the sample and the film cassette.

The utilized x-ray procedure of determining the angular scattering of mosaic blocks in individual crystallites of the specimens is based on investigating the angles of divergence of interference x-ray beams scattered by these crystallites. In practice the work amounted to determining the variation in the lateral dimensions of the same interference spots on the three Debyegrams of each series.

In the investigation we took into account the influence of the following factors on the broadening of the individual interference spots:

1) the geometric conditions of recording;

2) the character of the relative arrangements of the blocks of the secondary structure within each individual crystallite, i.e., the nature of the mosaic (secondary) structure of the crystallite;

3) the effect of the fineness of the mosaic blocks (the Sherrer effect);

4) the existence of possible residual stresses of the second kind within the boundaries of each individual crystallite;

5) the possible inhomogeneity of the impurity concentrations in the metal specimens and particularly in the alloy specimens;

6) the inherent width of the x-ray spectral lines (in this case the interference spots);

7) for the interference spots due to $K\alpha_1$ and $K\alpha_2$ radiation, the degree of splitting of the doublet.

To eliminate the influence of the second photographic emulsion layer on the width of the spots and interference lines, this layer was removed in processing the film.

To compensate for the influence of the splitting of the $K\alpha_1,\alpha_2$ doublet we

introduced the appropriate corrections calculated according to the following formulas:

for individual spots

$$\Delta r = \frac{\Delta\lambda}{\lambda} \cdot \frac{\operatorname{tg}\theta}{\cos^2 2\theta} D, \tag{1}$$

for the interference lines

$$\Delta r' = 2\frac{\Delta\lambda}{\lambda} \cdot \frac{\operatorname{tg}\theta}{\cos^2 2\theta} D \tag{2}$$

where D is the diameter of the camera.

The corrections for the geometry of the experiment were introduced by the so-called "standard photography" method. The standard sample used for this purpose was finely powdered diamond. The analytic form of this correction was established separately for each experiment in accordance with the procedure developed earlier.[2-4].

No separate account was taken of the influence of the inherent width of the interference spots inasmuch as the influence of this factor was already taken into account in allowing for the influence of the geometric conditions of photography.

Analysis of the influence of the other factors will be given below in discussing the experimental results.

The experimental results are listed in Table 3, first in the form of values of the angles $\delta_{(hkl)}$ of scattering of the interference x-ray beams by the individual crystallites of the samples averaged separately for the $(111)_\beta$, $(111)_\alpha$ and $(002)_\alpha$ interference rings and then in the form of overall averages for each of the investigated specimens. These overall average values of δ were arrived at in the following manner.

Some 30-40 of the most typical spots were chosen and appropriately identified on the three rings of each series of patterns for the given sample. The lateral dimensions of the spots were measured and the determined values used to calculate the angles δ_i of scattering of the interference beams by the individual crystallites. The appropriate corrections for the splitting of the doublet and the geometry of the experiment were then applied to the

Table 3

Averaged values of the angles of scattering of the interference x-ray beams by the crystallites of the investigated diamond, aluminum, copper and α-brass samples (after correction for the influence of splitting of the Cu $K\alpha_1,\alpha_2$ doublet and the geometric conditions of the experiment)

Substance	Sample No.	Averaged values of scattering of the x-ray interference beams			
		$\delta_{(111)_\beta}$	$\delta_{(111)_\alpha}$	$\delta_{(002)_\alpha}$	δ_{averaged}
1	2	3	4	5	6
Diamond	1	1',65	1',75	—	1',70
	1	1',55	1',75		1',65
Al I	1	4',3	[illegible]		[illegible]
	2	4',9	[illegible]		5',2
	3	5',0	[illegible]		[illegible]
	4	6',0	7',1		[illegible]
	5	6',6	8',0		7',3
Al II	1	5',1	5',7	—	5',4
	2	5',2	5',8	—	5',5
	3	5',3	5',9		5',6
	4	5',8	6',8		6',3
	5	6',4	[illegible]		7',0
Copper	1	4',1	[illegible]		[illegible]
	2	4',4	4',9		[illegible]
	3	4',7	5',4		[illegible]
	4	5',6	6',5		6',05
	5	6',4	7',7		[illegible]
α-Brass	1	9',5	10',7	[illegible]	[illegible]
	2	9',2	10',3	11',0	10',2
	3	7',55	[illegible]	[illegible]	8',52
	4	5',6	[illegible]	7',75	6',58
	5	4',2	[illegible]	[illegible]	[illegible]

calculated values of δ_i. These values were then averaged in groups to obtain the mean values of $\delta_{(hkl)}$ for each of the rings. Finally the overall average of these scattering angle values was computed to obtain the listed overall average value of δ for each of the diamond, aluminum, copper and α-brass samples.

2. Discussion of the experimental results

It was necessary to establish which of the other factors (2, 3, 4 and 5 in our list) might be responsible for the determined angular scattering of the x-rays by the crystallites (i.e., for the values listed in Table 3). It is known that the angular spread of x-ray interference beams diffracted by individual crystallites due to the smallness of the linear dimensions of the blocks comprising the secondary structure of the crystallites (the Sherrer effect) is proportional to the secant of the glancing angle θ, while the angular scattering associated with the influence of possible residual internal stresses of the second kind and to inhomogeneity of the impurity distribution is proportional to tan θ.

Bearing this in mind, we proceeded as follows. On the one hand, we found the secants and tangents of the Bragg angles θ for the three interference lines of interest. These data are listed in Table 4.

On the other hand, we computed the ratios of the scattering angles averaged for the individual rings (i.e., the values in columns 3, 4 and 5 in Table 3). The calculated ratios are listed in Table 5.

Table 4

Secants and tangents of the glancing angles and their ratios for the $(111)_\beta$, $(111)_\alpha$ and $(002)_\alpha$ interference rings in the Debye patterns of the investigated samples

Substance	Glancing angles			Values of tan θ and their ratios					Values of sec θ and their ratios				
	$\theta_{(111)_\beta}$	$\theta_{(111)_\alpha}$	$\theta_{(002)_\alpha}$	$\operatorname{tg}\theta_{(111)_\beta}$	$\operatorname{tg}\theta_{(111)_\alpha}$	$\operatorname{tg}\theta_{(002)_\alpha}$	$\frac{\operatorname{tg}\theta_{(111)_\alpha}}{\operatorname{tg}\theta_{(111)_\beta}}$	$\frac{\operatorname{tg}\theta_{(002)_\alpha}}{\operatorname{tg}\theta_{(111)_\alpha}}$	$\sec\theta_{(111)_\beta}$	$\sec\theta_{(111)_\alpha}$	$\sec\theta_{(002)_\alpha}$	$\frac{\lambda_\alpha \sec\theta_{(111)_\alpha}}{\lambda_\beta \sec\theta_{(111)_\beta}}$	$\frac{\sec\theta_{(002)_\alpha}}{\sec\theta_{(111)_\alpha}}$
Diamond	19°45'	22°		[illegible]	[illegible]	—	1,13	—	1,063	[illegible]	—	1,13	
Aluminum	17°25'	19°15'		[illegible]	[illegible]	—	1,12	—	1,048	[illegible]	—	1,12	
Copper	18°30'	21°15'	25°30'	[illegible]	[illegible]	0,477	[illegible]	[illegible]	1,061	[illegible]	1,108	1,13	[illegible]
α-Brass	19°	21°	24°30'	[illegible]	[illegible]	0,456	1,12	[illegible]	1,058	[illegible]	1,099	1,12	[illegible]

Comparing these data we established the following:

1. The fact that the value of the ratios $\frac{\operatorname{tg}\theta_{(111)_\alpha}}{\operatorname{tg}\theta_{(111)_\beta}}$ and $\frac{\lambda_\alpha \sec\theta_{(111)_\alpha}}{\lambda_\beta \sec\theta_{(111)_\beta}}$ were found to be equal to the value of the ratio $\frac{\delta_{(111)_\alpha}}{\delta_{(111)_\beta}}$ for the diamond sample showed that the broadening of the interference spots on the Debyegrams for this sample was presumably due to the combined influence of such factors as possible residual strains of the second kind, possible inhomogeneity of the impurity concentrations and perhaps the smallness of the blocks of the secondary structure of the diamond crystals. The influence of these factors proved to be of the same order of magnitude as the influence of the geometry of the experiment. It follows that the full difference in the lateral dimensions of the spots in the patterns of the standard sample, which we took as the effect of the geometry of the experiment, is in any case not an underestimate where evaluating this correction is concerned.

Table 5

Ratios of the values averaged for the $(111)_\beta$, $(111)_\alpha$ and $(002)_\alpha$ Debye rings of the angles of scattering of the interference beams by the crystallites of the investigated samples of diamond, aluminum, copper and α-brass.

Substance	Sample No.	$\frac{\delta_{(111)_\alpha}}{\delta_{(111)_\beta}}$	$\frac{\delta_{(002)_\alpha}}{\delta_{(111)_\alpha}}$	Substance	Sample No.	$\frac{\delta_{(111)_\alpha}}{\delta_{(111)_\beta}}$	$\frac{\delta_{(002)_\alpha}}{\delta_{(111)_\alpha}}$
1	2	3	4	1	2	3	4
Diamond	1	1,13		Copper			
					1	1,10	
Al I	1	1,09	-		2	1,11	
	2	1,12	-		3	1,15	
	3	1,16	-		4	1,16	
	4	1,18			5	1,20	
	5	1,21		α-Brass			1,05
	1	1,12	-		1	1.13	1,07
	2	1,12	-		2	1,12	1,13
Al II	3	1,11	-		3	1.12	1,21
	4	1,17	—		4	1,14	1,24
	5	1,20	-		5	1.19	

2. For the samples of aluminum, copper and α-brass dominant factor among the last four in our list differs at different stages of the recrystallization process. From a juxtaposition of the data in columns 8, 9, 14 and 15 in Table 4 and columns 3 and 4 in Table 5, we see that at the stages of the process represented by samples Nos. 1 & 2 of Al I and Nos. 1, 2 & 3 of Al III and α-brass the dominating factor is either the residual stresees of the second kind (in not very pure metal and in alloys, the inhomogeneity of the impurity concentrations may also be important) or the Sherrer effect (from the data in column 4 of Table 5 for the α-brass samples, we can state with more certainty that in the stages of the recrystallization process represented by samples Nos. 1 & 2 the dominant factor is the Sherrer effect). In contrast, for the stage of the recrystallization process represented by samples Nos. 4 & 5 of copper and aluminum and No. 5 of α-brass, there are evident more appreciable changes in the angular scattering of the interference beams with changes in the glancing angle θ than can be attributed solely to such factors as stresses of the second kind and possible inhomogeneities of the impurity distribution. Consequently, the predominant factor here can only be pronounced secondary disturbances (mosaic) in the structure of the crystallites.

3. We established that in copper and aluminum (column 6 in Table 3) the angular scattering of the interference beams does not remain constant during the course of the recrystallization process, but rather gradually increases from about 4-5' for the No. 1 samples to 7' or over for the No. 5 samples. We believe this increase is due to the above-mentioned changes in the extent of the influence of the different factors during the course of the recrystallization process. Thus, in the case of the aluminum and copper even at the initial stages of the process, the blocks forming the crystallites already have comparatively large linear dimensions so that the Sherrer effect tends to predominate only slightly if at all over the influence of the other factors. As the recrystallization process proceeds both the crystallites and the blocks composing their secondary structure grow; as a result, when the culminating stages of treatment and collective recrystallization are reached the increasingly dominant effect becomes that due to secondary disturbances or dislocations in the structure of the crystallites (i.e., the influence of the mosaic structure of the crystallites becomes more pronounced).

4. Where the α-brass samples are concerned (column 6 in Table 3) we note that the angular scattering of the interference x-ray beams by the crystallites

of the solid solution having the limiting concentration also changes as the recrystallization proceeds but, in contrast to the case of the technically pure metals or metals with a minor amount of impurities, here (in the case of the solid solution of limiting concentration!) the angular spread of the x-ray beams decreases instead of increasing (drops from 10.5' for sample No. 1 to 5.13' for sample No. 5).

We suggest the following explanation for this effect. As noted above, it follows from comparison of the figures in columns 3 & 4 in Table 5 and columns 8, 9, 13 & 14 in Table 4 that here for the stages of the recrystallization process represented by samples Nos. 1 and 2 of all the factors influencing the scattering angle δ, the dominating one is the Sherrer effect. This in turn means that the crystallites of the Nos. 1 & 2 samples of α-brass consist of blocks characterized by rather small linear dimensions. This smallness of the mosaic blocks is the factor leading to the strong angular scattering of the x-ray beams at the initial stages of the recrystallization process. As the process proceeds through the stage represented by sample No.4 to the stages represented by samples Nos. 4 & 5, both the crystallites and the blocks comprising them gradually increase in size. This in turn leads to weakening of the diffraction effect on the angular spread of the x-ray interference beams and hence to a gradual general decrease of the scattering angle δ. Finally at the stage of the process of recrystallization represented by sample No.5 the clearly dominating factor in the angular scattering of the interference x-ray beams becomes the mosaic disarrangement of the crystallites and we have the lowest value of the scattering angle.

The fact that for the No.5 sample of α-brass the averaged value of δ is somewhat lower than the value for the No.5 sample of copper has a perfectly logical explanation. It follows from the data of columns 5-7 in Table 2 that, whereas on the patterns for the No.5 copper sample there were 34 spots in the $(111)_\beta$ ring, 47 in the $(111)_\alpha$ ring and 35 in the $(002)_\alpha$ ring, on the patterns of the No.5 sample of α-brass there were, respectively, 127, 242 and 179 spots in these rings. Inasmuch as the conditions of x-raying were identical in the two cases, it follows that the crystallites of the α-brass No.5 sample were appreciably smaller than those of the copper sample and in view of this were necessarily characterized by a somewhat less pronounced mosaicity (structural disorientation).

Gor'ki Physico-Technical Research Institute
at Gor'ki State University

References

1. V.N.Shcherbakov, Thesis USSR Ac. of Sc. Crystallography Inst. 1950.
2. F.Jones, Proc. Royal Soc., A 166, 16 (1938).
3. G.Kurdiumov & L.Lysak, Zhur. tekh. fiz., 17, 993 (1947).
4. U.Dehlinger & A.Kochendorfer, ZS. F. Dristallogr., 101, 134 (1939).

BULLETIN of the Academy of Sciences of the USSR - Physical Series
Vol. 20, No. 6, 1956 - Transactions of the Fifth Conference on the Application of X-Rays to the Investigation of Materials (Leningrad, 23-29 June 1955)

TABLE OF CONTENTS

	Page	
	Orig.	Trans.
X-ray diffraction and electron microscope studies of the aging of an Al-Zn alloy - N.N.Buinov & L.I.Podrezov	611	555
Changes in the fine crystal structure of austenitic manganese steel during plastic deformation - O.V.Bogorodski & Ia.S.Umanski	614	558
Investigation of eutectoid decomposition in a Cu-Sn alloy - M.I.Zakharova & I.B.Mogarycheva	621	564
Analysis of stresses of the second kind in the α-phase of quenched and tempered steel - L.I.Lysak	624	567
Determination of the characteristic temperature and distortions of the lattice in certain high-melting point metallic compounds and solid solutions - S.M.Nikolaeva & Ia.S.Umanski	631	573
Structural changes in pure metals during stress relaxation - B.M.Rovinski & V.G.Liuttsau	636	577
X-ray investigation of the plasticity of beryllium single crystals - R.I.Garber, I.A.Gindin, V.S.Kogan and B.G.Lazarev	639	580
X-ray investigation of residual stresses in electrolytic deposits of nickel - V.P.Moissev & O.S.Popova	641	583
Changes in the substructure of aluminum with small plastic deformation and creep - B.M.Rovinski & L.M.Rybakova	646	588
X-ray investigation of recrystallization of some high melting point compounds - S.S.Gorelik & Ia.S.Umanski	650	592
Characteristics of recrystallization of certain two-phase aging alloys - S.S.Gorelik	653	595
Residual changes in the interplanar spacing in polycrystalline specimens after plastic deformation - D.M.Vasil'ev & A.F.Erashov	659	600
X-ray investigation of plastic deformation of metals under static and dynamic compression - T.N.Smirnova & Iu.S. Terminasov	664	605

	Page Orig.	Page Trans.
X-ray investigation of effects accompanying prolonged extension of steel at elevated temperatures - M.Ia.Fuks, N.V.Slonovski, L.I.Lupilov	671	611
X-ray analysis of structural changes in metals during creep - L.M.Rybakova	676	616
The influence of texture on the intensity of interference lines in investigating large deformed specimens - M.Ia.Fuks, G.V.Dobrovol'skaia	679	620
Secondary hardness in steels alloyed with vanadium, molybdenum and titanium - L.V.Zaslavskaia, S.T. Kishkin, N.F.Lashko, A.F.Platonova, N.M.Popova & M.F.Rybina	684	624
X-ray investigation of the surface quality of metals machined by grinding or light-cut turning - Iu.S. Terminasov, A.G.Iakhontov & A.V.Poltavski	689	629
Mechanism of the influence of minor impurities on the formation of recrystallization texture in metals and alloys - D.I.Lainer & E.I.Krupnikova	693	632
X-ray investigation of the influence of heat treatment on plastically deformed metals - Iu.S.Terminasov & G.A.Feklistov	695	634
Residual stresses in metals after grinding - O.G.Karpinskii & B.M.Levitskii	700	638
X-ray investigation of the surface quality of metals machined by high-speed turning - T.Kh.Chormonov	703	641
X-ray investigation of distortions of the crystal lattice of mineral fibers - E.O.Shvaikovskaia	706	643
X-ray investigation of compounds in the Bi-Rh and Bi-Pd systems in connection with superconductivity studies - N.N.Zhuravlev & G.S.Zhdanov	708	645
X-ray investigation of the secondary structure of crystallites in recrystallized metals - V.N.Shcherbakov	714	650

Translated in 1957 by
Columbia Technical Translations,
5 Vermont Ave., White Plains, N.Y.